SCHOLARLY PUBLICATIONS

A CURRENT AWARENESS BULLETIN
OF RESEARCH OUTPUT

@DTU

(47th Edition)

NOVEMBER 2016

BY: CENTRAL LIBRARY

DELHI TECHNOLOGICAL UNIVERSITY
(FORMERLY *DELHI COLLEGE OF ENGINEERING)*
GOVT. OF N.C.T. OF DELHI
SHAHBAD DAULATPUR, MAIN BAWANA ROAD
DELHI 110042

PREFACE

This is the **Forty seventh** Issue of Current Awareness Bulletin started by Delhi Technological University, Central Library. The aim of the bulletin is to compile, preserve and disseminate information published by the faculty, students and alumni for mutual benefits. The bulletin also aims to propagate the intellectual contribution of Delhi Technological University (DTU) as a whole to the academia.

The bulletin contains information resources available in the internet in the form of articles, reports, presentations published in international journals, websites, etc. by the faculty and students of DTU. The publications of faculty and student which are not covered in this bulletin may be because of the reason that the full text either was not accessible or could not be searched by the search engine used by the library for this purpose.

The learned faculty and students are requested to provide their uncovered publications to the library either through email or in CD, etc to make the bulletin more comprehensive.

This issue contains the information published during **November 2016**. The arrangement of the contents is alphabetical. The full text of the article which is either subscribed by the university or available in the web is provided in this bulletin.

Central Library

CONTENTS

1. 5G Millimeter Wave (mmWave) Communications, ***3.S. K. Agrawal*** and ***3.Kapil Sharma***, Computer Engineering, DTU

2. A Feasible Study of Lean Manufacturing: An expert approach, ***3.Dr. A.K. Madan*** and ***6.Er. Sanjeev Jain,*** Production and Industrial Engineering, DTU

3. A New Chaotic-Primitive and its Application in Customizing AES for Lightweight Multimedia Encryption, ***6.Sakshi Dhall,*** Saibal K. Pal and ***3.Kapil Sharma***, Computer Engineering, DTU

4. Algae personification toxicity by GC–MASS and treatment by using material potassium permanganate in exposed basin, Ahmed Aidan Al-Hussieny , Esam Abd Alraheem , Haider Y. Lafta , Mohammed K. Shebli , Mohammed Jassim Obed Alfalahi ***, 3.Allaa M. Aenab*** and ***3.S.K. Singh,*** Environmental Engineering, DTU

5. An Automated Tool for Generating Change Report from Open-Source Software, ***3.Ruchika Malhotra[1],*** Ankita Bansal and Sourabh Jajoria, Software Engineering, DTU

6. An effective collaborative movie recommender system with cuckoo search, ***3.Rahul Katarya*** and ***6.Om Prakash Verma***, Computer Science & Engineering, DTU

7. An Empirical Study to Assess the Effects of Refactoring on Software Maintainability, ***3.Ruchika Malhotra*** and Anuradha Chug, Software Engineering, DTU

8. Analysis of Various I/O Methods for Large Datasets in C++, ***3.Kushaagra Moghe*** and ***3.Hemang Sarkar***, Mathematics and Computing Engineering, DTU

9. Application of Artificial BEE Colony Algorithm Using Hadoop, ***3.Nupur Bansal, 3.Sanjay Kumar*** and ***3.Ashish Tripathi***, Computer Engineering, DTU

10. Automated Classification of Security Requirements, ***3.Rajni Jindal, 3.Ruchika Malhotra*** and ***3.Abha Jain***, Computer Science and Engineering, DTU

11. Auto-Segmentation using Mean-Shift and Entropy Analysis, ***3.Seba Susan*** and ***3.Ankit Kumar***, Computer Science and Engineering, DTU

12. CFD Analysis of Wavy Microchannel Heat Sink with Hemispherical Obstructions and Comparing it with Experimental Results of Rectangular Microchannel Heat Sink, ***7.Rajnish Kumar*** and ***3.M. Zunaid,*** Mechanical Engineering, DTU

13. Clustering based Feature Selection Methods from fMRI data for Classification of Cognitive States of the Human Brain, ***8.Awijit Gupta, 8.Arjun Gupta*** and ***3.Kapil Sharma***, Computer Science and Engineering, DTU

14. Common Threats to Software Quality Predictive Modeling Studies Using Search-based Techniques, ***3.Ruchika Malhotra*** and ***3.Megha Khanna***, Software Engineering, DTU

15. Comparison of Different Topologies of Fuzzy Logic Controller to Control D-STATCOM, ***3.Anuj Varshney*** and ***3.Dr.Rachana Garg***, Electrical Engineering, DTU

16. Comparison studies on mechanical and wear behavior of fabricated aluminum surface nano composites by fusion and solid state processing, ***3.N. Yuvaraj, S. Aravindan*** and ***3.Vipin***, Mechanical Engineering, DTU

17. Conditional Adherence based Classification of Transactions for Database Intrusion Detection and Prevention, ***3.Indu Singh***, ***3.Vaibhav Darbari, 3.Lakshya Kejriwal*** and ***3.Aditya Agarwal***, Computer Science and Engineering, DTU

18. Covariate conscious approach for Gait recognition based upon Zernike moment invariants, ***8.Himanshu Aggarwal 3.Dinesh K. Vishwakarma***, Electronics and Communication Engineering, DTU

19. Design and Experimental Analysis of a 200W Micro Wind Turbine, ***3.Raj Kumar Singh, 6.Sajal Garg and 6.Lohit Gudivada***, Production and Industrial Engineering, DTU

20. Design and Implementation of a Power and Speed Efficient Carry Select Adder on FPGA, ***3.Simarpreet Singh Chawla, 3.Nidhi Goel, 3. Swapnil Aggarwal*** and Mantek Singh Bhatia, Electronics and Communication Engineering, DTU

21. Distributed Data Association Rule Mining: Tools and Techniques, ***3.Manoj Sethi*** and ***3.Rajni Jindal***, Computer Science and Engineering, DTU

22. Dy3þ ions doped single and mixed alkali fluoro tungsten tellurite glasses for LASER and white LED applications, Ch. B. Annapurna Devi, Sk. Mahamuda, M. Venkateswarlu, K. Swapna, ***3.A. Srinivasa Rao*** and G. Vijaya Prakash ,Applied Physics, DTU

23. Effect of number of Passes on mechanical and wear properties of Friction Stir Processed Al 1050 Alloy, ***3.N.Yuvaraj, 6.Vipin*** and ***6.R.S. Mishra***, Mechanical Engineering, DTU

24. Effect of Skin Resistance and Enlarged Base on Pull out Capacity of Modeled Piles***, 7.Ankush Chaudhary, 7.Pankaj Goswami*** and ***3.Dr. A.K. Sahu***, Civil Engineering, DTU

25. Electrochemical performances of Li-rich layered-layered Li2MnO3-LiMnO2 solid solutions as cathode material for lithium-ion batteries, ***6.Rakesh Saroha, Amit Gupta*** and ***3.Amrish K. Panwar***, Applied Physics, DTU

26. Energy Efficient Reactive Protocol for data Aggregation in Wireless Sensor Network, ***3.Rajesh Kumar Yadav, 3.Daya Gupta*** and ***D.K. Lobiyal***, Computer Science and Engineering, DTU

27. Excellent storage stability and sensitive detection of neurotoxin quinolinic acid Ranjana Singh, Sunayana Kashyap, ***3.Suveen Kumar***, Shiju Abraham, Tejendra K. Gupta, Arvind M. Kayastha***, 3.Bansi D. Malhotra***, Preeti Suman Saxena, Anchal Srivastava and Ranjan K. Singh, Biotechnology, DTU

28. Exploratory Test Oracle using Multi-Layer Perceptron Neural Network, Wellington Makondo, ***3.Raghava Nallanthighal***, Innocent Mapanga and Prudence Kadebu, Information Technology, DTU

29. Image coding based on maximum entropy partitioning for identifying improbable intensities related to facial expressions, ***3.SEBA SUSAN, 6.NANDINI AGGARWAL, 6.SHEFALI CHAND*** and ***6.AYUSH GUPTA***, Computer Science and Engineering, DTU

30. Inducing half-metallicity with enhanced stability in zigzag graphene nanoribbons via fluorine passivation, Neeraj K. Jaiswal, ***3.Neha Tyagi***, Amit Kumar and Pankaj Srivastava, Applied Physics, DTU

31. Influence of 100MeV Au+8 ion on photovoltaic response of BiFeO3/BaTiO3 multilayer structures, ***3.Savita Sharma***, Monika Tomar, Ashok Kumar, Fouran Singh, ***3.Nitin K. Puri*** and Vinay Gupta, Applied Physics, DTU

32. MCDM based evaluation and ranking of commercial off-the-shelf using fuzzy based matrix method, Rakesh Garg, R.K. Sharma, ***3.Kapil Sharma*** and R.K. Garg, Computer Science and Engineering, DTU

33. Modeling and Microstructure Study of Thermally Evaporated Nano film Thickness of Gold, ***6.Shailendra Kumar Gaur*** and ***3.R.S. Mishra***, Mechanical Engineering, DTU

34. Novel 4-terminal Perovskite/SiC-based Rear Contact Silicon Tandem Solar Cell With 27.6 % PCE, ***6.Rahul Pandey, 6.Apurva Jain*** and ***6.Rishu Chaujar***, Physics Engineering, DTU

35. Ontology Based Framework for Reverse Engineering of Conventional Softwares, MPS Bhatia, ***3.Akshi Kumar*** and Rohit Beniwal, Computer Engineering, DTU

36. Optimized Sentiment Analysis Tool A Sentiment analysis tool to study cognitive inclinations, Nayonika Sharma, ***3.Dr. s. Indu***, Chetna Sharma and Priyanka Chugh, Electronics and Communication, DTU

37. Performance of Static Sink in Wireless Sensor Networks when Implementing Geographic Routing, Priyankachugh(Shivanka), Abhinav Singh, ***3.Dr.s.Indu***, Anupam Joshi, Rahul Rajpal, Electronics and Communication, DTU

38. Photoacoustic sensor for trace detection of post-blast explosive andhazardous molecules, Ramesh C. Sharma, Subodh Kumar, ***8.1.Surya Gautam***, Saurabh Gupta and Hari B. Srivastava, Electronics and Communication engineering, DTU

39. Prolonging Network Lifetime by Electing Suitable Cluster Head by Dynamic Weight Adjustment for Weighted Clustering Algorithm in MANET, ***3. Vijayanand Kumar and 3.Rajesh Kumar Yadav,*** Computer Sc & Engineering, DTU

40. Quality Issues with Big data Analytics, ***3.Sangeeta*** and ***3.Kapil Sharma***, Computer Engineering, DTU

41. Removal of Baseline Wander from ECG using CEEMD and Adaptive Morphogocial Function, ***3.Mahipal Singh Choudhry*** and ***6.Rajiv Kapoor***, Electronics & Communication Engineering, DTU

42. Repetitive Controller for VSIs in Droop Based AC-Microgrid, ***6.1.Ashutosh Trivedi and 3.Dr. Mukhtiar Singh***, Electrical Engineering, DTU

43. Sensitivity and reliability models of a PV system connected to grid, ***3.Nikita Gupta, 6.Rachana Garga***, and Parmod Kumar, Electrical Engineering, DTU

44. Single VDTA Based Dual Mode Single Input Multioutput Biquad Filter, ***3.Rajeshwari Pandey, 3.Neeta Pandey, and 3.Navin Singhal***, Electronics and Communication Engineering, DTU

45. Skill Development in Solid Waste Management ***6.Shubham Gupta and 3.R.S. Mishra***, Mechanical Engineering, DTU

46. Sorting of Glossiphonia complanata (Linnaeus, 1758) (Rhynchobdellida: Glossiphoniidae) from three aquatic plants in Tigris River within Baghdad city, Manar Dawood Salman, Mohammed K. Shebli, Mohammed Jassim Obed Alfalahi , ***3.Allaa M. Aenab and 3.S.K. Singh,*** Environmental Engineering, DTU

47. Study of Dangerous Voltages in Substation, Different Soil Models and Designing of Grounding System of High Voltage Substation with the help of Computer Program RPDGS Using MATLAB GUI, ***7.1.Rajesh Kumar***, Kamal Bansal, Devender K. Saini and IPS Paul, Electrical Engineering, DTU

48. STUDY ON CHARACTERISATION OF INDIAN DAIRY WASTEWATER, ***3.Rakesh Mehrotra, 3.A. Trivedi*** and ***3.1. S.K.Mazumdar***, Civil Engineering, DTU

49. Survey and Evaluation of Food Recommendation Systems and Techniques, ***3.Akshi Kumar, 3.Pulkit Tanwar*** and Saurabh Nigam, Computer Engineering, DTU

50. SWOT Analysis of Search Based Software Engineering, ***3.Abhilasha Sharma*** and ***6.Yogita Khatri***, CSE, DTU

51. Synchrophasor Based Real Time Monitoring of Grid Events in Indian Power System, K.V.S. Baba, ***8.1 S.R. Narasimhan***, N.L. Jain, Amandeep Singh, Rahul Shukla and Ankit Gupta, Electrical Engineering, DTU

52. Thermodynamic and thermoeconomic analyses of two stage hybrid absorption compression refrigeration system, ***3.Akhilesh Arora***, Mechanical Engineering, DTU

53. Tuning of Software Cost Drivers using BAT Algorithm, ***3.Sanchi Girotra*** and ***3. Kapil Sharma***, Computer Engineering, DTU

54. Using Cell Division for Text to Image Encryption, ***6.Vaishnavikannan*** and ***3. Smita Jhajharia***, DTU

1. *Chancellor*

2. *Pro Vice Chancellor* — ***2.1.*** *Ex Pro Vice Chancellor*

3. *Faculty* — ***3.1.*** *Ex Faculty*

4. *Teaching-cum-Research Fellow*

5. *Alumni*

6. *Research Scholar* — ***6.1.*** *Ex Research Scholar*

7. *PG Scholar* — ***7.1.*** *Ex PG Scholar*

8. *Undergraduate Student* — ***8.1.*** *Ex Udergraduate Student*

5G Millimeter Wave (mmWave) Communications

S. K. Agrawal
Computer Engineering Department
Delhi Technological University, India
Email Id: sachin.ecin@gmail.com

Kapil Sharma
Computer Engineering Department
Delhi Technological University, India
Email Id: kapil@ieee.org

***Abstract* – 5G communication system is attracting researches attention throughout the world for providing seamless user experience in 5G network which can accommodate large number of users in Internet of Things (IoT) environment with a gigabit-per-second (Gbps) data rate in mmWave communications with the consideration of Big-Data (BD). In 5G environment several billions of user devices will be connected seamlessly among each other in mmWave communications along with secure connections. 5G Millimeter Wave (mmWave) communications system proposes mmWave signal transmission along with low latency connection which will offer gigabit-per-second (Gbps) speed. This paper discusses 5G applications and services along with 5G vision and challenges. There are many challenges with the proposed mmWave communications system. 5G mmWave communications system will be revolutionizing for the users.**

Keywords* – *Gigabit-Per-Second (Gbps), Millimeter Wave (mmWave).

I. INTRODUCTION

5G millimeter wave (mmWave) communications system research has been started and there is growth in the system development and research to provide market ready to use system by 2020. Year 2020 5G millimeter wave (mmWave) communications system has clear vision to have user devices in the environment of Internet of Things (IoT) and Big-Data. 5G millimeter wave (mmWave) communications system will provide Big-Data based platform for billions of user connected devices autonomously in a seamless manner . These user devices are interconnected among each other along with the consideration of security. 5G millimeter wave (mmWave) communications system offers low latency high speed data connection with gigabit speed for the billions of users . 5G millimeter wave (mmWave) communications system in mmWave frequency band provides high speed and high bandwidth so that to accommodate Big-Data users . 5G millimeter wave (mmWave) communications system in mmWave frequency band also suffers with wireless channel attenuation due to signal losses [1-16].

5G millimeter wave (mmWave) communications system services, applications, requirements, challenges and standardizations are discussed in this paper. 5G millimeter wave (mmWave) communications system is planned for year 2020 for user usage. There are several challenges for 2020 5G millimeter wave (mmWave) communications system and research is in progress to identify and overcome these challenges by enabling technical solution for 5G mmWave communications systems .There are challenges like radio wave propagation and network related issues [1-5].

II BEGINNING OF 5G MILLIMETER WAVE (mmWave) COMMUNICATIONS SYSTEM

5G millimeter wave (mmWave) communications system research is in progress and standardized definition is progress for 5G, however clear definition is not here at present in literature. 5G millimeter wave (mmWave) communications system still work is in progress and tentatively may be named as "IMT-2020". 5G millimeter wave (mmWave) communications system definition at present can be described as :

- 100 billion devices and more
- 100 Gbps

5G millimeter wave (mmWave) communications system provides enough economic worth and value for the users. As per demand and need for year 2020 , the number of user will increase will a rapid rate by 2020 along with Big-Data requirement and this will be fulfill by the 5G millimeter wave (mmWave) communications system as shown in figure 1. The data demand will be in Exabytes among billions of users [1-5]. .

5G millimeter wave (mmWave) communications system by 2020 will revolutionize the wireless communication system It will also revolutionize the way of interaction among the devices in Big-Data and Internet of Things (IoT) environment. The demand will increase in a rapid manner and 5G millimeter wave (mmWave) communications system will accommodate such demands of large number of users and high speed seamless connection among user devices. 5G millimeter wave (mmWave) communications system in Big-Data and Internet of Things (IoT) environment will provide very low latency in an intelligent and efficient manner [1-5,15-19].

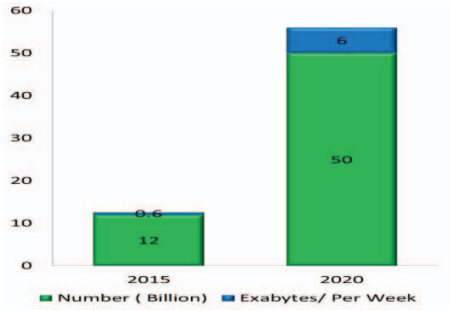

Figure 1: Growth in 5G User Connected Devices and Mobile Traffic (Exabytes)

III 5G SERVICES AND APPLICATIONS

5G millimeter wave (mmWave) communications system is under progress for various services and applications among high speed large

number of users. The list is below for various services of 5G millimeter wave (mmWave) communications system [6-7] :

- Internet of Things
  - Smart Home
  - HealthCare
  - Smart Store
  - Smart Office
  - Connected Car
- Everything on Cloud
- Intuitive Remote Access

Applications of 5G millimeter wave (mmWave) communications system are shown in figure 2 like : driving a car with augmented reality (AR) navigation, watching sport events with virtual reality (VR), ubiquitous health care, wearable device, flexible mobile device, UHD video streaming smart map/navigation, real- time interactive game, mobile cloud and many more [5-10].

Figure 2: Applications of 5G Millimeter Wave (mmWave) Communications System

IV REQUIREMENTS FOR 5G MILLIMETER WAVE (MMWAVE) COMMUNICATIONS SYSTEM

With the explosive research, progress and development for 5G millimeter wave (mmWave) communications system by considering gigabit-per-second (Gbps) data rate among billions of user devices, it is required to have technically rich 5G millimeter wave (mmWave) communications system. Such enhanced, intelligent, technical 5G millimeter wave (mmWave) communications system shall consider the following requirements as shown in figure 3 and discussed below [3-7]:

5G millimeter wave (mmWave) communications system major requirements are High Data Rate, Cell Edge Data Rate, Low Latency, Simultaneous Seamless Connection, Cell Spectral Efficiency & Utilization Optimally, Optimum Cost and Mobility Support . There is need and requirement for seamless billions of user devices connection along with high data rate and low latency [4-9] . billions of user devices in 5G millimeter wave (mmWave) communications system shall also consider Cell Edge Data Rate, Cell Spectral Efficiency & Utilization Optimally, Optimum Cost and Mobility Support [4-7] .

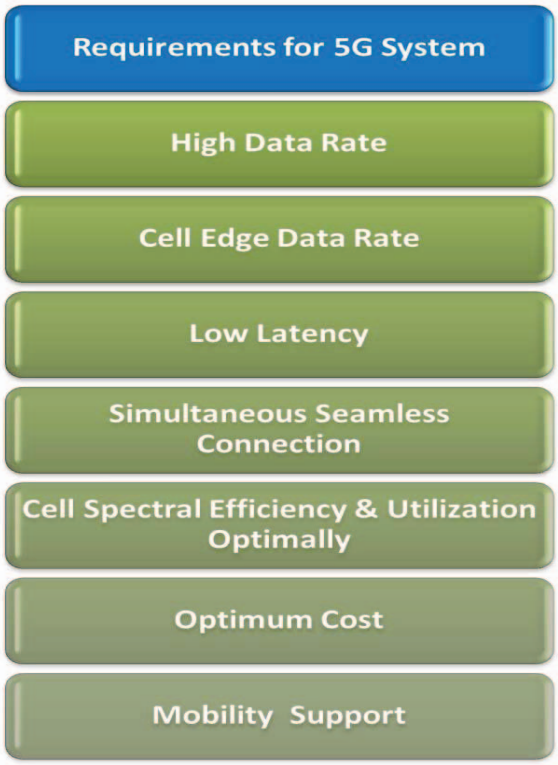

Figure 3: Requirements for 5G Millimeter Wave (mmWave) Communications System

V mmWave FREQUENCIES BENEFITS FOR 5G MILLIMETER WAVE (mmWave) COMMUNICATIONS SYSTEM

5G Millimeter Wave (mmWave) communications system considers frequencies of the mmWave which ranges from 30 GHz to 300 GHz. Considering mmWaves ranging from 30 GHz to 300 GHz has several advantages and benefits to provide high bandwidth and further benefits are [6-9]:

- Big volume of spectrum at mmWave frequencies in 5G Millimeter Wave (mmWave) communications system
- 5G Millimeter Wave (mmWave) communications system mmWaves suffer with high value channel attenuation in wireless channel . 5G Millimeter Wave (mmWave) communications system mmWaves also have penetration. Due to this mmWaves characteristics the frequencess can be can be recycled at a small distance .

5G Millimeter Wave (mmWave) communications system research for mmWave frequencies is in progress for an optimum communication system by 2020 [7-9].

VI CHALLENGES FOR 5G MILLIMETER WAVE (mmWave) COMMUNICATIONS SYSTEM

5G Millimeter Wave (mmWave) communications system shows various Characteristics Challenges. Majorly 5G Millimeter Wave (mmWave) communications system Characteristics Challenges can be classified as shown in figure 4 and figure 5 with following details. 5G Millimeter Wave (mmWave) communications system Characteristics Challenges are mmWave Transmission Characteristics and mmWave communications Network Characteristics [5-11].

5G Millimeter Wave (mmWave) Communications System mmWave communications Network Characteristics challenges are:

- D2D communications
- Heterogeneous Networks
- Small Cell Backhaul

5G Millimeter Wave (mmWave) Communications System mmWave Transmission Characteristics challenges are:

- Channel Characteristics
- Beamforming Technologies due to Channel Propagation Loss and
- Blocking Effect

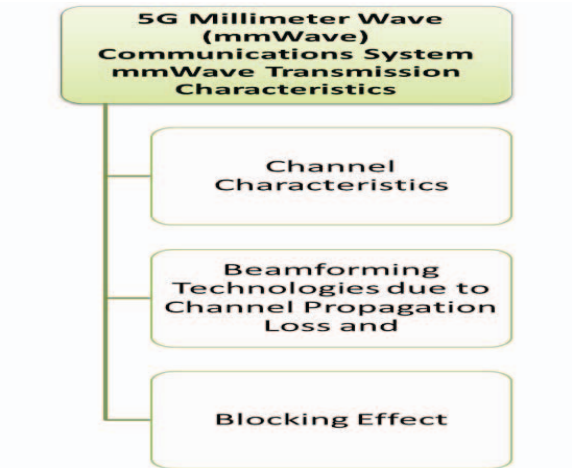

Figure 4: mmWave Transmission Characteristics Challenges

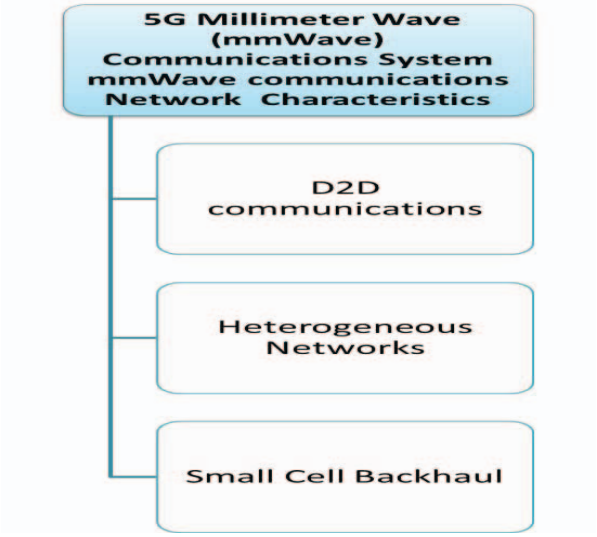

Figure 5: 5G mmWave communications Network Challenges

mmWave 5G communications system will give rich user experience by 2020 and will accommodate large users along with high data connectivity. The challenges are discussed here and the solution, research and development is in progress for the discussed mmWave 5G communications system challenges.

VII STANDARDIZATIONS AND REGULATIONS

5G millimeter wave (mmWave) communications system research is in progress worldwide and various standardization organizations are working with the target of year 2020 for market deployment. Several research organizations are involved in research are as shown in below figure 6 [3-9]:

Figure 6: Global R&D Activities for 5G millimeter wave (mmWave) communications system

Standard Timelines for 5G millimeter wave (mmWave) communications system is shown below in figure 7 for ITU-R and 3GPP standard for 5G millimeter wave (mmWave) communications system is in progress with the aim of year 2020. ITU-R time line considers Vision, requirement, Proposal, Evaluation and Standard Development by 2020. 3GPP standard for 5G millimeter wave (mmWave) communications system is also in progress with the releases in various years on or before 2020 [3-9].

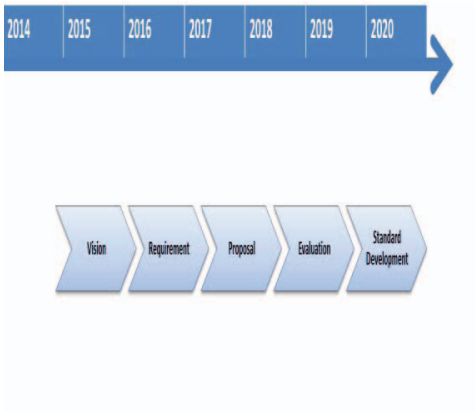

Figure 7: Standard Timelines for 5G millimeter wave (mmWave) communications system

5G millimeter wave (mmWave) communications system standard will incorporate and investigate new mmWave frequency bands. FCC recently has also reported mmWave frequency bands for further system growth. As per viewpoint for 5G millimeter wave (mmWave) communications system , it is planned for commercialization by year 2020 [3-7,19].

IX. CONCLUSION

5G Millimeter Wave (mmWave) communications system research is in progress with common vision of high data speed, high bandwidth, mobility support, rich user experience by 2020 and many more . 5G Millimeter Wave (mmWave) communications system will accommodate large number of users along with high data connectivity. The vision and challenges are discussed in this paper for 5G Millimeter Wave (mmWave) communications system. Various research solutions and technology enablement are in progress worldwide for 5G Millimeter Wave (mmWave) communications system.

ACKNOWLEDGEMENT

This paper is specifically meant for educational purpose for completing Ph.D. degree with Delhi Technological University (DTU), Delhi India. This paper is prepared for submission to under Ph.D. progress. The authors are very much thankful to Samsung Electronics India and Delhi Technological University (DTU) earlier recognized as Delhi-College of Engineering (DCE), New Delhi.

REFERENCES

[1]. Calum Dewar et al., “Understanding 5G: Perspectives on future technological advancements in mobile, ” GSMA Intelligence Report, Dec. 2014.
[2]. Zhouye Pi et al., “An Introduction to Millimeter- Wave Mobile Broadband Systems, ” IEEE Communications Magazine, vol.49, no.6, pp.101- 107, Jun. 2011.
[3]. Andrews J.G. et al., “What Will 5G Be?, ” IEEE JSAC Special Issue On 5G Wireless Communication Systems, May 2014.
[4]. Cheol Jeong et al., “Random Access in Millimeter-Wave Beamforming Cellular Networks: Issues and Approaches, ” IEEE Communications Magazine, vol. 53, no. 1, pp.180-185, Jan. 2015.
[5]. Wonil Roh et al., “Millimeter-wave Beamforming as an Enabling Technology for 5G Cellular Communications: Theoretical Feasibility and Prototype Results, ” IEEE Communications Magazine, vol. 52, no. 2, pp. 106-113, Feb. 2014.
[6]. Samsung, “Technologies for Rel-12 and Onwards, ” RWS-120021, 3GPP TSG RAN Workshop on Rel-12 and Onwards, Jun. 2012.
[7]. Samsung, “5G Vision, ” DMC R&D Center, Samsung Electronics Co., Ltd., Feb. 2015.
[8]. Theodore S. Rappaport et al., “Millimeter Wave Mobile Communications for 5G Cellular: It Will Work!, ” IEEE Access, vol.1, pp.335-349, May 2013.
[9]. Wei L. et. al., “Key Elements to Enable Millimeter Wave Communications for 5G Wireless Systems, ” IEEE Wireless Communications, vol.1, pp.136-143, Dec. 2014.
[10]. Federal Communications Commission: “Evaluating compliance with FCC guidelines for human exposure to radiofrequency electromagnetic fields, ” Washington, DC: FCC. Tech. Rep. Suppl. C to OET Bulletin 65, 2001.
[11]. Taeyoung Kim et al., “Tens of Gbps Support with mmWave Beamforming Systems for Next Generation Communications, ” in Proc. IEEE GLOBECOM’13 Workshop, pp.3685-3690, Dec. 2013.
[12]. Sungnam Hong et al., “Frequency and Quadrature-Amplitude Modulation for Downlink Cellular OFDMA Networks, ” IEEE Journal on Selected Areas in Communication, vol. 32, no. 6, pp.1256- 1267, Jun. 2014.
[13]. S. K. Agrawal and P. Garg, “Calculation of Channel Capacity Considering the Effect of Different Seasons for Higher Altitude Platform System", Wireless Personal Communications, Springer, Wireless Personal Communications: vol. pp-719-729, Issue 4 2010.
[14]. S. K. Agrawal and P. Garg, “Calculation of the Channel Capacity in the Presence of Vegetation and Urban-site Environment for Higher Altitude Platform Communication System", to Wireless Personal

Communications", IET Microwaves, Antenna & Propagation, IET Microw. Antennas Propag., Vol. 3, Iss. 4, pp. 703–713, 2009.
[15]. A. Bhatega, K. Sharma, "Secure Cancelable Fingerprint Key Generation", Power India International Conference (PIICON) IEEE, Dec. 2014, pp-1-3
[16]. S. Dhall Sakshi, K. P. Saibal, K. Sharma, "Cryptographic Primitives for Multimedia Security", INROADS- An International Journal of Jaipur National University, 2014, Volume : 3, pp- 335- 339
[17]. Comments of NYU WIRELESS, Docket 13-84, Jan. 13, 2015. [Online].Available:http://apps.fcc.gov/ecfs/document/view?id=60001013322
[18]. Young-Han Nam et al., "Full Dimension MIMO (FD-MIMO) for Next Generation Cellular Technology, " IEEE Communications Magazine, vol. 51, no. 6, pp.172-179, Jun. 2013.
[19]. Evaluating Compliance with FCC Guidelines for Human Exposure to Radiofrequency Electromagnetic Fields, Federal Communication Commission, OET Bulletin 65, Edition 97-01.

International Journal of Engineering Studies.
ISSN 0975-6469 Volume 8, Number 2 (2016), pp. 107-115
© Research India Publications
http://www.ripublication.com

A Feasible Study of *Lean Manufacturing*: An expert approach

Dr. A.K. Madan[1*] and Er. Sanjeev Jain[2]

[1] *Faculty, Department of Production and Industrial Engineering, Delhi Technological University (Formerly Delhi College of Engineering), Bawana Road, Delhi-110042, E-mail: ashokmadan79@gmail.com*

[2] *Research Scholar, Department of Production and Industrial Engineering, Delhi Technological University (Formerly Delhi College of Engineering), Bawana Road, Delhi-110042*
E-mail: sanjeevjain99@gmail.com

**Corresponding Author; ashokmadan79@gmail.com*

Abstract

James Womack, Daniel Jones, and Daniel Roos coined the term "***Lean Production***" in their 1990 book "***The Machine that Changed the World"*** to describe the manufacturing paradigm established by the Toyota Production System. In the 1950s, the Toyota Motor Company pioneered a collection of advanced manufacturing methods that aimed to minimize the resources it takes for a single product to flow through the entire production process. Inspired by the waste elimination concepts developed by Henry Ford in the early1900s, Toyota created an organizational culture focused on the systematic identification and elimination of all waste from the production process. ***Lean manufacturing*** refers to a manufacturing improvement process based on the fundamental goal of ***Toyota production system(TPS)*** in order to reduce or eliminate waste while improving production flow (Tapping, 2002). Many manufacturing organizations realize the importance of using lean methodology. However, few organizations implement lean concept with the necessary knowledge and proven tools to achieve it. The purpose of this study is to develop a value stream map (VSM) for a manufacturing plant in Manesar, Gurgaon to improve the productivity of line using Lean tool. This particular tool allows the manufacturing plant to document current lead time, inventory levels and cycle times to determine the ratio of value added work to total lead time of the product line being analysed. The first step will be to measure the current state to make a picture of the production flow and understand the

Company's current cycle times, process linkages, and machine equipment capacity. This provides the information needed to produce an improved future state map by creating an ideal value flow. The goal is to identify and eliminate the waste, which is any activity that does not add value to the final product, in the production process which will help to achieve the production capacity as per customer demand through Lean manufacturing techniques.

Keywords: Lean Way; Waste elimination; Value added work; Non-value added work; Productivity; Cycle time; TPS.

1. INTRODUCTION

Manufacturing operations are continually striving to increase productivity and output of their processes. Lean manufacturing or Lean technique is more than a cost reduction project or a problem solving approaches (Tapping, 2002). The main idea is that an efficient production can be achieved by a comprehensive approach to minimize wastes available in production processes. This means eliminating excess production and inventory, movement of material, waiting and delays in production process, over processing, excess worker movement, and the need for rework and corrections in product during or after production. We did the analysis on an assembly line in an automotive product manufacturing company in Manesar to improve assembly line production capacity by using lean manufacturing technique. During this activity we find detect area of improvement and took action to avoid/ reduce possible non value added work and improve current process of assembly line which will help us to meet increased customer demand through reduced working time.

2. WHY LEAN ??

In Manufacturing operations are continually striving to increase productivity and output of their processes. Lean manufacturing or Lean technique is more than a cost reduction project or a problem solving approaches (Tapping, 2002). The main idea is that an efficient production can be achieved by a comprehensive approach to minimize wastes available in production processes. This means eliminating excess production and inventory, movement of material, waiting and delays in production process, over processing, excess worker movement, and the need for rework and corrections in product during or after production. We did the analysis on an assembly line in an automotive product manufacturing company in Manesar to improve assembly line production capacity by using lean manufacturing technique. During this activity we find /detect area of improvement and took action to avoid/ reduce possible non value added work and improve current process of assembly line which will help us to meet increased customer demand through reduced working time.

In Lean, you pursue understanding the source and rooting out the causes of waste. The practice of Lean as the root-cause eliminator of wastefulness is based on a core set of fundamental assumptions. Follow this logic:

>You're in business to sell products and services to customers. The customer has the need and defines the purpose. Everything begins and ends with what the customer requires. Everything else is fluff.
>The customer is the only true arbiter of value. The customer is willing to give you their money for your product or service only when they believe it's a fair exchange of value. It has to be the right combination of quality products and services, in the right place, at the right time and at the right price.

>Value-creation is a process. A combination of steps — such as marketing, design, production, processing, delivery and support — rightly performed, will result in the creation of products and services that the customer will properly value.
>Waste diminishes the process of value creation. Things that naturally creep in and prevent the steps in a process from flowing quickly and effectively will inhibit the creation of customer value.

>A perfect process has no waste. If every step in the process is fully capable, acts only when necessary, flows perfectly, and adapts to perform exactly as needed, the process will develop and deliver products and services without waste.

>Perfect processes maximize customer value. The closer to perfection a process becomes, the more effective the creation of value, the more satisfied the customers and the more successful the endeavour.

No one has ever experienced the perfect process, but Lean continually strives for perfection. Lean is the strategy and approach, and it provides the methods and tools for pursuing the perfect process.
To accomplish this, companies employ a variety of advanced manufacturing tools to lower the time intensity, material intensity, and capital intensity of production. When companies implement several or all of these lean methods, several outcomes consistently result:

- ***Reduced inventory levels*** (raw material available in store, work-in-progress stock at assembly line, finished product available at Finished Goods store) along with associated carrying costs and loss due to damage, spoilage, off-specification, etc.
- ***Decreased material usage*** (product inputs, including energy, water, chemicals, etc. by reducing material requirements and creating less material waste during manufacturing.
- ***Optimized equipment*** as per production process helps to reduced capital cost.
- ***Reduced*** need for ***factory facilities*** by driving down the space required for product production.
- ***Increased production velocity*** (the time required to process a product from initial raw material to delivery to a customer) ***by eliminating*** / reducing process steps, extra movement, **wait times**, and downtime available in production process.

- ***Enhanced production flexibility*** (the ability to alter or reconfigure products and processes rapidly to adjust to customer needs and changing market circumstances) enable the implementation of a pull production, just-in-time(JIT) oriented system which lowers inventory and capital requirements; and
- ***Reduced complexity*** of product (complicated products and processes that increase opportunities for variation and error) by reducing the number of parts/ components and material types in products, and by eliminating unnecessary process steps, movement and equipment with unneeded features.

With the help of all above methods we can achieve the increased profit on product without increase in cost of product as we can understand by Figure 1 & 2. Lean Way not only helps us to gain profit rather than we will achieve customer satisfaction with on time product delivery with right quantity and quality.

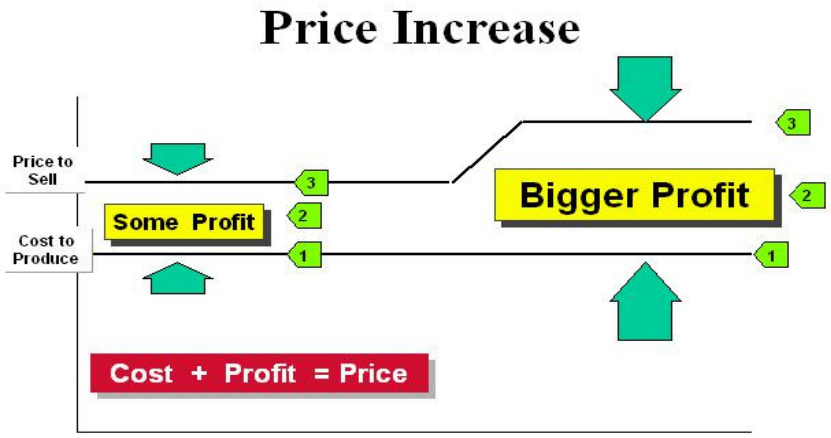

Figure 1. Traditional Way

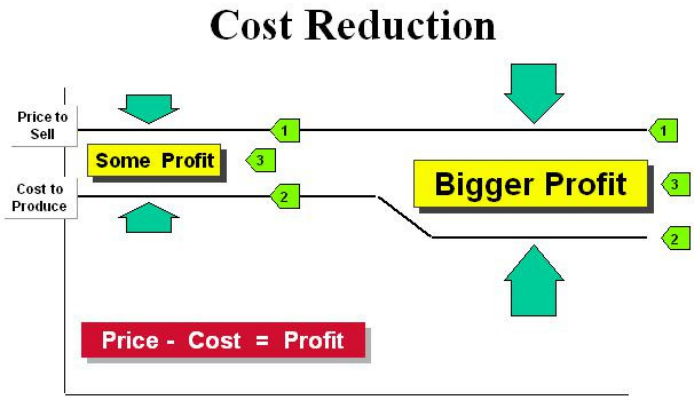

Figure 2. Lean Way

3. WASTE ELIMINATION

To improve the line capacity and its product quality we visited through the assembly line to find out the possible area of improvement through waste elimination.

According to Tapping (2002) "the ultimate lean target is the total elimination of waste. Waste, or Muda, is anything that adds cost to the product without adding value of product" (p. 41).

Sources of waste are available everywhere, we need to focus on production process to find out the available waste in whole Value Stream Mapping. Wastes can be classified into seven categories (Tapping, 2002):

1. ***Waste of overproducing***: Producing components or child parts that are neither intended for stock nor planned for sale immediately will increase only waste.

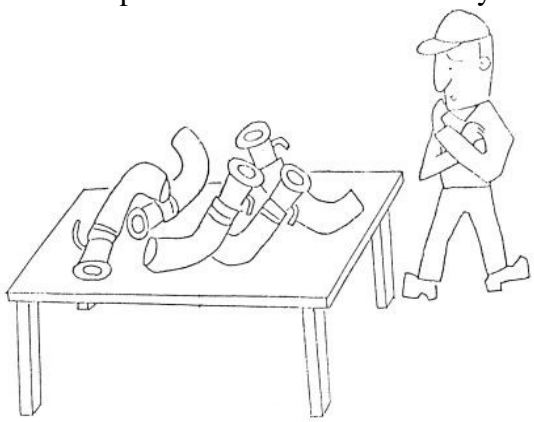

Only one is necessary at one time

2. ***Waste of waiting:*** Refers to the idle time between two operations. We should utilize it.

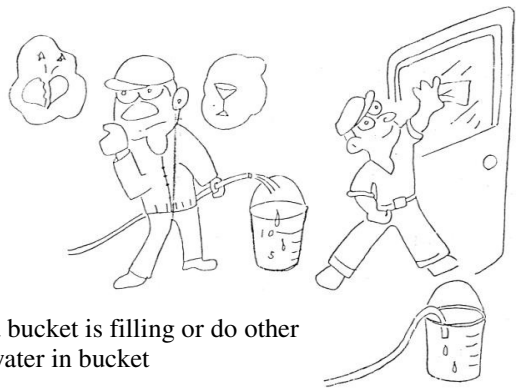

Waiting until a bucket is filling or do other job while fill water in bucket

3. ***Waste of transport:*** Moving material more than necessary will not add any value just un-necessary increase time, cost and fatigue of operator.

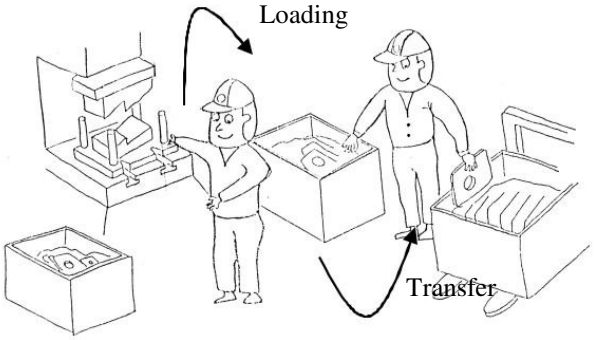

4. ***Waste of processing:*** Doing more to the product than required necessary and the customer is willing to pay. We should focus on all process to eliminate un-necessary work.

5. ***Waste of inventory:*** Excess of stock / more than required stock from raw materials to finished goods always loss for any company.

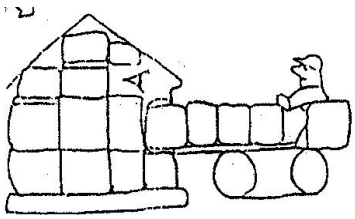

Unnecessary material storage

6. ***Waste of motion:*** Any motion that is not necessary for the completion of a work.

1st Worker go to take a tool repeatedly and 2nd used small bag

7. ***Waste of defects and spoilage:*** Defective parts that are produced and need to be reworked after completion of work.

Based upon the above Waste or Muda's we observed at our assembly line and improve the assembly line to improve the line productivity, to reduce cycle time, to reduce operator fatigue, to improve operator safety and to reduce cost.
During this site visit we found some area of improvement, which we improved at automotive Switch manufacturing assembly line in a company at Manesar, Gurgaon are as follows:

Before: Location of rivet tray at rivet assembly station is left side of fixture.

After: Location of rivet tray shifted at the right side of rivet assembly station which reduces the Waste of Motion.

Before: Location of Insulator at line is also on left side of machine and inside the deep bin.

After: Location of insulator shifted to right side of machine and reduced the depth of bin it reduces Waste of Motion and operator fatigue.

Before: one station uses 2 different type of rivet and always chances of mix up.

After: Location of rivet tray properly identified by colour coding and process defined to use one rivet by left hand other by right hand. It reduces waste of defect.

Before: at spring assembly station operator always faced problem of spring entangled.

After: Spring separator installed at station, now operator can pick one spring easily it reduces Waste of process.

Before: During illumination checking of switch operator have to bend more than normal which caused high operator fatigue and reduced productivity.

After: Illumination checking process improved as per operator height, it reduces operator fatigue and operator can achieve the production as per standard time. It reduces Waste of Motion and Water of Process.

Before: Manual assembly and remove coupler for testing Switch require more time and it became bottleneck process.

After: Automatic assembly and remove coupler machine installed to reduce operation time.

Before: Batch code marking and terminal straightness testing done on two different stations.

After: new modified fixture designed which can do both work at one station. It reduces Waste of Over process.

CONCLUSION

During research, team evaluated where waste occurs in the production process and analyse observations with team to improve the process and achieve customer demand with right quantity and quality, improve employee satisfaction. After all the improvement we achieved:

- ***Cycle time*** reduced from 56.9 seconds to 42.9 seconds. This is ***24.6 % reduction***.
- ***Productivity improved by 38.26%.***
- Able to achieve increased customer demand on time helps us to ***improve customer satisfaction.***
- Knowledge of team for Lean way improved which will be used at other assembly line to improve.
- Operator ***fatigue reduced*** helps to improve employee more adoptable towards changes.
- ***Safety*** of operator ***improved.***
- Team morale improved for new challenges.

REFERENCES

[1] James Womack, Daniel Jones, and Daniel Roos (1990) *The Machine that Changed the World.(Book)*

[2] Ohno, T. (1988). *Toyota production system: Beyond large-scale production.* Cambridge, MA: Productivity Press.(Book)

[3] Womack, J., & Jones, D. (1996). *Lean thinking: Banish waste and create wealth in your corporation.* New York, NY: Simon & Schuster.(Book)

[4] Rachna Shah, Peter T. Ward, "Lean Manufacturing: Context, practices, and performance", *Journal of Operation Management*, 21(2003)129-149 (Article)

[5] J. Ben Naylor, Mohamed M Naim, Danny Berry,"Leagility: Integrating the lean and agile manufacturing paradigms in the total supply chain",Int. *Journal of Production Economics*, 62(1999) 107-118 (Article)

[6] Leonardo Rivera, F. Frank Chen,"Measuring the impact of lean tool on the cost-time investment of a product using cost-time profile", Robotics and computer integrated manufacturing, 23(2007) 684-689 (Article)

[7] Tapping, D., Luyster, T., & Shuker, T. (2002). *Value stream management: Eight steps to planning, mapping, and sustaining lean improvements.* New York, NY: Productivity Press.(Book)

[8] Brandon G. Mabry(Delphi Chassis System), Kenneth R. Morrison : Transformation to Lean Manufacturing by an automotive component supplier.*Computer ind. Engag Vol.31.No.1/2 pp.95-98,1996(Article)*

[9] William G. Sullivan, Thomas N.McDonald, Eileen M. Van Aken : Equipment replacement decision and Lean Manufacturing, *Robotics and Computer Integrated Manufacturing 18 (2002) 255-265(Article)*

[10] *Hitoshi Kume:*A book on Problem Solving Techinique (Book)

[11] *V.* Jayakumar : A book on total Quality Management by Laxmi Publication (Book)

[12] *Jiju Antony and Ricardo Banuelas* : Journal of Key ingredients for the effective implementation of six sigma program Warwick Manufacturing Group, University of Warwick, and Coventry, UK.(Journal)

[13] The six sigma approach, Quality world volume3, march2006.(Book)

[14] Paschal Ugochukwu, Jon Engstrom, Jostein Langstrand: Lean in the Supply Chain: A Literature Review, Management and production engineering review, Volume 3, Number 4, December 2012,pp87-96

A New Chaotic-Primitive and its Application in Customizing AES for Lightweight Multimedia Encryption

Email ID: sakshidhall@gmail.com

Sakshi Dhall
Asst. Prof., Dept. of Mathematics,
Jamia Millia Islamia, New Delhi, INDIA
Research Scholar, Dept. of Computer Engineering, Delhi Technological University, New Delhi, INDIA

Saibal K. Pal
Scientific Analysis Group,
DRDO, New Delhi, INDIA
Email ID: skptech@yahoo.com

Kapil Sharma
Dept. of Computer Engineering,
Delhi Technological University,
New Delhi, INDIA
Email ID: kapil@ieee.org

***Abstract*—Advent of mobile technology and internet in our daily lives has opened up a new dimension to our data exchange requirements. Multimedia like image, video, audio have emerged out be contributing in significant proportions to the data flowing over inherently insecure networks. The traditional encryption schemes which were designed to provide high security to textual data are unable to secure multimedia with similar security levels. The reason is manifolds. Firstly, multimedia is much bulkier as compared to text-based data hence the computational cost incurred in traditional ciphers like AES, DES, IDEA etc… practically becomes unacceptable for multimedia encryption esp. in resource constrained environments like mobiles. Further, multimedia contains significant redundancies which get reflected back in the cipher obtained from traditional schemes. As textual data normally do not contain redundancies hence the traditional schemes never targeted this issue in their design. If redundancy is kept unaddressed, it may act as a point of compromise for security of multimedia. In this light, the paper proposes a lightweight cryptographic primitive based on chaos and its use in customizing the traditional scheme AES to make it applicable for multimedia security. The results show that the customized AES achieves better levels of security, show strong avalanche properties and completely diffuse redundancy in less than 15% time as compared to AES.**

Keywords—image encryption; block cipher; chaos; lightweight; efficiency

I. INTRODUCTION

World of today is witnessing a tremendous upsurge of digitization which has become an integral part of human life in almost every sphere. With the upswing in mobile technology and ubiquitous presence of internet, there has been a stupendous increase in the data transfer requirements in diverse sectors affecting our daily lives like e-commerce, social networking, health-care, entertainment, defense, banking, and the list is endless. But transferring data through inherently vulnerable networks pose security as a big challenge to this ever evolving growth in technology. Addressing this challenge becomes inevitable as its scope is no more confined to few large corporates or government agencies dealing with exchange of sensitive information. Today, technology is touching the lives of common individuals and hence security of transferred data is a concern for larger section of society.

Cryptography [1,2] is the science dealing with designing schemes to ensure that the messages are received securely, without any manipulation, by the intended receiver and exactly no one else. To achieve the purpose, the original information is transformed into a non-perceivable form so that any unauthorized access does not disclose any meaningful information to the adversary.

As highlighted by Shannon [3] confusion and diffusion are two basic properties possessed by any secure encryption scheme. Confusion describes how intricate is the dependency of the cipher on the secret key. Diffusion describes the degree of contribution of each plaintext bits to each cipher text bit thereby ensuring that a change in any of the plaintext bits should result in significant change in the cipher text. To achieve the properties of confusion and diffusion, permutation and substitution steps are commonly incorporated in encryption algorithms. During permutation, the bits/bytes in the plaintext are rearranged and during substitution the bits/bytes are substituted with new bits/bytes and/or are applied on by one or more operations to modify their values. Both these steps can be made key dependent to ensure strong confusion. And to ensure strong diffusion, multiple bits/bytes should contribute in generation for each cipher bit/byte.

With applications like DTH, audio/video-on-demand, biometrics based individual identification etc..., multimedia [4,5] has surfaced as one of the most significant forms of media constituting information stored or communicated over the internet. Securing multimedia [6] is an even stronger challenge as it is intrinsically bulky and contains significant redundancies. Both these characteristics make it unsuitable to use traditional encryption schemes (like AES, DES, IDEA etc...) for securing multimedia which are otherwise suitable for textual data with proven security. Traditional schemes involve

978-9-3805-4421-2/16/$31.00 ©2016 IEEE

high computational cost and also do not take into consideration possible redundancies in the plaintext. If redundancy exists beyond their block size, the cipher will also contain the same redundancy thereby making them vulnerable if directly applied on multimedia. Therefore, it is of utmost importance to cater to both the efficiency and complete removal of redundancy in cipher as the two prime goals for designing algorithms to secure multimedia. This is a major thrust factor motivating researchers to focus research in designing cryptographic primitives dedicated for multimedia security.

The following section gives a brief background by discussing chaos and its properties, AES Block cipher. Section III discusses the details of the proposed chaotic primitive and its application to customize AES. The observations are displayed in Section IV followed by conclusion in Section V.

II. BACKGROUND

A. Application of Chaos in Cryptography

Chaotic functions [7,8,9] have properties that can be appreciably exploited for their use in cryptography. These functions are highly sensitive to their initial conditions and parameters and hence if these initial conditions and parameters could be made key-dependent, significantly different cipher can be obtained with minor changes in the key. Further as the dynamics of chaotic functions has ergodicity and is non-linear, infact random-like, hence presence of chaos increases the strength of the cryptosystem manifolds even with very simple and computationally inexpensive operations like XOR. Their deterministic behavior ensures smooth decryption. Because of these properties chaos based operations have emerged as strong contenders to be included in primitives designed for cryptosystems [10] and customizing existing schemes [11] esp. for securing multimedia. Chaotic maps may be continuous, but they can be discretized for easy application in cryptographical applications as dealing with floating point values has its own limitations. There exist a larger number of 1-D, 2-D, 3-D discrete chaotic maps which are being used by researchers in developing cryptosystems over the past few years now. Logistic map, tent map, sine map are some of the popular 1-D maps while 2-D maps include baker map, cat map, henon map etc…

To demonstrate their high sensitivity to initial condition, the following figure (Fig. 1) displays the plot for logistic map iterated multiple times for slightly modified initial conditions (i.e. r=4, x_0=0.7 (dashed), x_0=0.701(solid)). To observe that the two trajectories do not converge after iterating for sufficient number of times, in this plot, first 900 points have been discarded. Clearly the orbits are still completely uncorrelated showing high sensitivity of logistic map on initial condition.

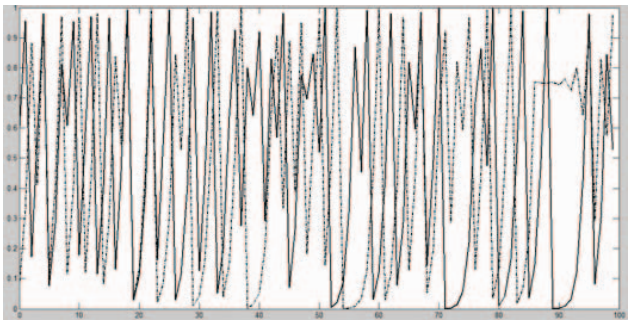

Fig. 1. Plot for Logistic Map, $x_n = rx_n(1-x_n)$

B. AES Block Cipher

Advanced Encryption Standard (AES) [4] is a symmetric block cipher which takes 128 bit plaintext as input, 128, 192 or 256 bit secret key, respectively performs 10,12 or 14 rounds of operations and generates an equal sized cipher. Round keys for each round are generated from the secret key. The plain text is treated as a 4X4 state matrix of bytes. Each round takes the state matrix as input and generates a transformed state matrix which becomes input for the next round until the cipher is obtained. A round of AES scheme is made up of four operations namely – substitute bytes, shift rows, mix columns and add round key.

Substitute byte operation employs an S Box which is a 16X16 byte matrix. Each byte of the state matrix is substituted with a new value using the S Box. For the S Box look-up operation, the higher order nibble is treated as the row number and the lower order nibble is treated as the column number. The value present at the intersection of this row and column is the value being substituted for the original byte of the state matrix.

Shift rows operation circularly left shifts the bytes in the ith row of the state matrix by i elements.

Mix columns operation multiplies the state matrix with a fixed matrix and facilitates diffusion by ensuring multiple bytes contribute in generation of each new byte.

Add round key operation involves simple XOR (Exclusive OR) of the 16 bytes plain text with 16 bytes round key.

III. PROPOSAL

As explained before, due to its high computational requirement and non-addressable of redundancy aspect, traditional block ciphers though has proven strength for textual data yet is not directly suitable for multimedia. To tap and extend their proven strength, we propose a chaotic primitive which can be used to customize them so as to make them suitable for application in securing multimedia.

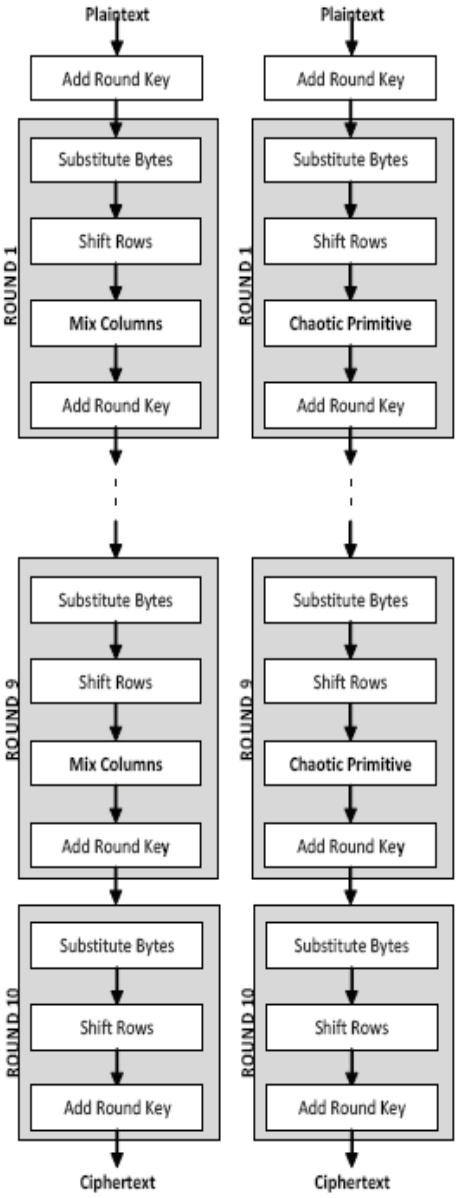

Fig. 2. Comparison between Original and Customized AES

A. Chaotic Primitive

Firstly, a chaotic sequence is generated using a 1-D chaotic map with key-dependent initial condition. This sequence is then transformed into sequence of integer values each value between the range [1, n], where n is the block size in bytes. Further, two values at a time from this discretized chaotic sequence is used in the chaos-based primitive to decide positions of two bytes from the plain text, say *pos1* and *pos2*. Let the two bytes at these locations be represented as *a* and *b*. The higher and lower order nibbles of these two bytes are then rearranged in the following order to create two new bytes say *c* and *d* for positions *pos1* and *pos2* respectively:

$$c_1c_2c_3c_4c_5c_6c_7c_8 = a_5a_6a_7a_8\ b_1b_2b_3b_4$$

$$d_1d_2d_3d_4d_5d_6d_7d_8 = b_5b_6b_7b_8\ a_1a_2a_3a_4$$

Clearly, the operations involved in the chaotic primitive are not bulky thereby making it a very computationally inexpensive primitive to be included in any encryption scheme which shall not add much of computational cost to the overall scheme.

B. Customized Block Cipher

The above explained block cipher can be used to customize traditional block ciphers. In this section, we present customization of AES block cipher. During customization our intent is to increase or at least preserve the strength of the original block cipher, to reduce the computational expense incurred and to ensure that the redundancy existing beyond the block size gets completely removed in the cipher.

To reduce the computational time, we analyzed AES to identify the operation contributing highest to the overall computational cost. The operation Mix Columns is the most expensive operation in the entire scheme and therefore we choose this operation to be replaced by the discussed computationally less expensive chaotic primitive.

The above figure (Fig. 2) presents the block diagram to show comparison between the original and customized AES. The inclusion of this primitive to AES will help us achieve two benefits. Firstly, as the primitive is inherently light hence the computational cost of the customized scheme decreases and secondly as the primitive is key dependent therefore in the customized block cipher there are two key-dependent operations instead of one, thereby strengthening the scheme. Also, to avoid redundancies to propagate to the cipher, the chaotic sequence for the entire image is generated at once at the beginning. Since the chaotic values are highly uncorrelated and random therefore even if the redundancies exist beyond the block size, they get removed completely in the cipher due to the chaotic primitive.

IV. OBSERVATIONS

In this section we present the observations to demonstrate that customizing standard encryption schemes like AES using our proposed chaotic primitive makes it suitable for multimedia applications. To prove the strength of the proposed work, we performed security analysis and few observations taken on 256X256 grayscale Water Lillies image are given as under. Fig. 3 displays the original Water Lillies image along with its histogram and entropy. Fig. 4 shows image encrypted using standard AES algorithm with 10 rounds along with the histogram and entropy of the cipher image. As clearly visible, the cipher image contains textured zones which may be vulnerable to statistical or other cryptanalytic attacks.

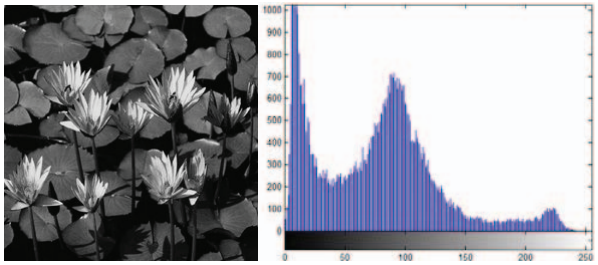

Entropy: 7.2171

Fig. 3. Original Water Lillies Image with Histogram

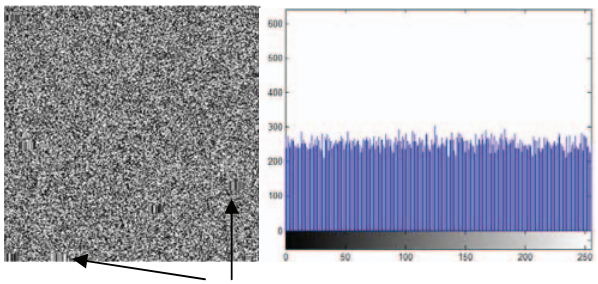

Entropy: 7.9970 Textured Zones

Fig. 4. AES Encrypted Water Lillies Image with Histogram

To study the impact of introduction of chaotic primitive to AES scheme, we took observations using three simple and cost effective 1-D chaotic maps. These include standard logistic map, an improvisation of logistic map proposed by Rui [12] and a hybrid Logistic-Tent map proposed by Zhou et. al [13]. The parameter value used for the Logistic-tent map is 3.6 and that for the other two maps is 4. Further, the initial condition is made key-dependent to ensure that the chaotic primitive operation adds confusion to the overall scheme. Fig. 5 shows the encrypted image, histogram and entropy values obtained using customized AES with these three chaotic maps. As can be seen, the encrypted images obtained using customized AES do not possess textured zones and hence are visibly not vulnerable.

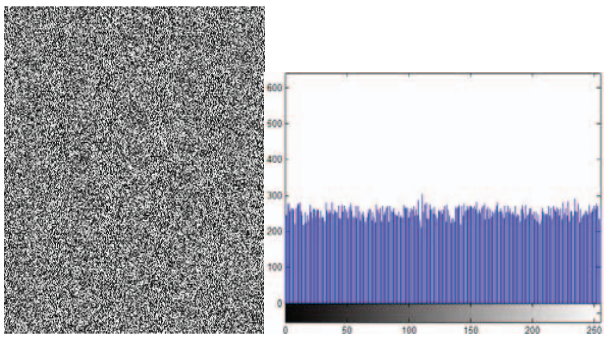

Entropy: 7.9974 No Textured Zones

(a)

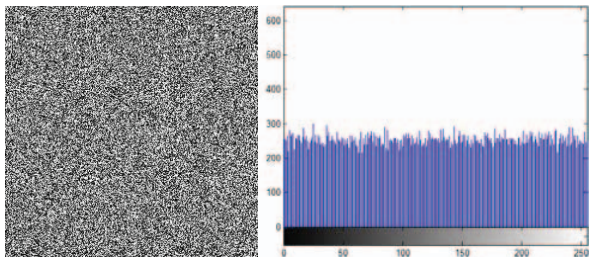

Entropy: 7.9975 No Textured Zones

(b)

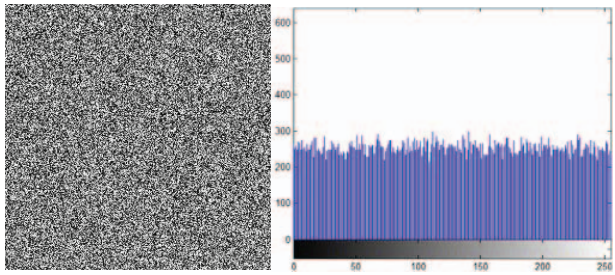

Entropy: 7.9971 No Textured Zones

(c)

Fig. 5. Proposed Customized AES Encrypted Water Lillies Image with Histogram (a) with logistic map (b) with improved logistic map (c) with logistic-tent map

To establish that all color intensities are randomly distributed across the entire image and no portion of the cipher image possesses special color distribution distinguishing it from the other, variation of entropy across the image is observed. For this, the image is treated to be composed of 64X64 blocks and block-wise entropy is plotted as shown in Fig. 6. The plot clearly shows that there is a much smoother or uniform variation of entropy among the different blocks of the cipher obtained using customized AES as compared to standard AES.

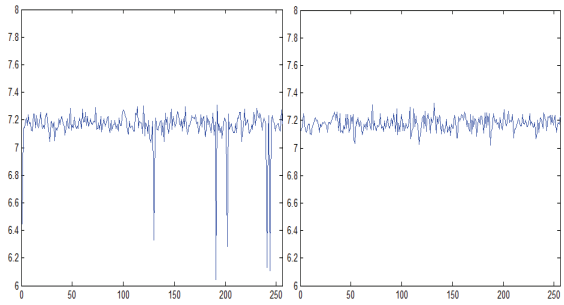

Fig. 6. Block-wise Entopy Plot of Encrypted Image (Water Lillies) with AES vs Proposed Customized AES (with logistic map)

To show that there is complete removal of redundancy in the cipher, observation on plain white image is taken. The cipher image obtained show uniform distribution of the histogram while the plain text contained all identical pixels.

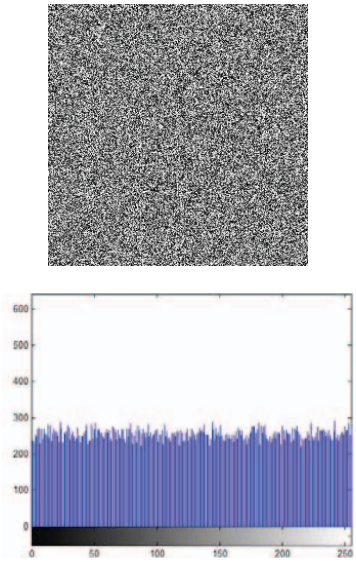

Fig. 7. Encrypted Image and Histogram of Plain White Image encrypted with Proposed Customized AES (with logistic map)

Further, to demonstrate the computational efficacy of the customized cipher, time observations are taken which demonstrate that the use of chaotic primitive inplace of a bulkier operation in the standard scheme reduces the overall cost to less than 15% of the original cost. The following table (Table I) displays the comparison performed on the same machine under identical conditions:

TABLE I COMPARISION OF COMPUTATIONAL COST ON ENCRYPTION OF WATER LILLIES IMAGe

Encryption Scheme	Time (seconds)
AES	104.019
Customized AES (with logistic map)	13.712
Customized AES (with improved logistic map)	13.872
Customized AES (with logistic-tent map)	13.962

The following observations show strong avalanche properties displayed by the proposed customized algorithm. Fig. 8 shows that with a single bit change in the key the cipher image changes by around 50% and this change is persistent for change in any single bit of the key showing that all bits of the key contributes in cipher generation. Fig. 9 demonstrates that for a single bit change per pixel, the cipher again changes by approx. 50% irrespective of the bit position in the pixel.

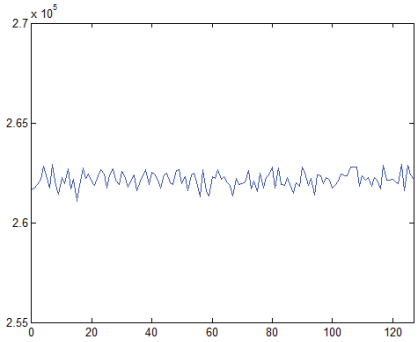

Fig. 8. Avalanche Property – Plot of number of bits changed in the customized AES Encrypted Water Lillies Image (with improved logistic map) with one bit change at each position of the 128-bit key

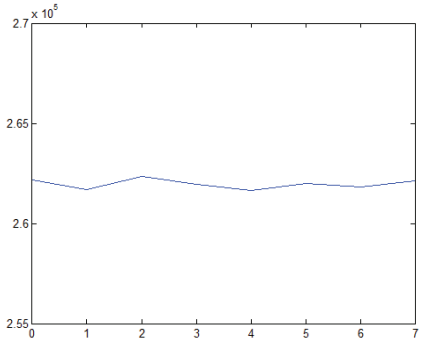

Fig. 9. Avalanche Property – Plot of number of bits changed in the customized AES Encrypted Water Lillies Image (with logistic-tent map) with one bit change per pixel at each of the 8 position

V. CONCLUSION & FUTURE SCOPE

The results of experimental observations show that the proposed chaotic primitive can be incorporated in cryptosystems to provide a cost effective means for securing images and diffuse redundancies completely in the cipher text. The time observations show a sharp dip in the overall computational cost required to obtain the cipher image. With less than 15% cost, the scheme still demonstrates strong avalanche properties and complete removal of textured zones. In fact, a completely uniform histogram is obtained even for plain white image demonstrating strength of the scheme. Though observations have been taken on images but the work can easily be extended to other forms of multimedia. Hence, it is concluded that the proposed primitive can be utilized in encryption schemes for multimedia security and also to customize standard ciphers by replacing their bulkier operations with the proposed chaotic primitive.

In future, we aim to design more cost effective chaotic primitive, to incorporate these primitives to propose new cryptosystems or customize existing cryptosystems for

securing multimedia and to study their strength against statistical and cryptanalytical attacks.

REFERENCES

[1] W. Stallings – *Cryptography & Network Security Principles and Practices*, Third Edition, Pearson Education, 2004.

[2] A. Menezes (ed.) – *Handbook of Applied Cryptography*, CRC-Press, 1996.

[3] C. E. Shannon, "Communication theory of secrecy system", Bell Syst. Techn. J. 28, pp. 656-715, 1949.

[4] B. Furht (ed.) – *Encyclopedia of Multimedia*, Springer, 2005.

[5] R.C. Gonzalez and R.E. Woods – *Digital Image Processing,* Third Edition, Prentice Hall, 2007.

[6] S. Lian, D. Kanellopoulos, G. Ruffo, "Recent Advances in Multimedia Information System Security", Informatica, vol. 33, pp. 3–24, 2009

[7] R. L. Devaney – *An Introduction to Chaotic Dynamical Systems,* Addison-Wesley Publishing, 1989.

[8] G. Alvarez, S. Li, "Some Basic Cryptographic Requirements for Chaos-Based Cryptosystems", International Journal of Bifurcation and Chaos, vol. 16, no. 8, pp. 2129-2151, 2006.

[9] A.N. Pisarchik, M. Zanin, *Chaotic Map Cryptography and Security, Encryption: Methods*, Encryption: Methods, Software and Security, Nova Science Publishers, Inc. pp. 1-28, 2010.

[10] S. Dhall, S.K. Pal, K. Sharma, "Cryptographic Primitives for Multimedia Security", IAET 2014, Jaipur National University, Jaipur, Rajasthan, India, AISC special issue B of INROADS International Journal, Vol. 3, No. 1, Jan-June, 2014, pp-335-339.

[11] S. Dhall, S.K. Pal, K. Sharma, "Improvised block cipher customized for multimedia security", PIICON 2014, Delhi Technological University, Delhi, India, IEEE, DOI 10.1109/POWERI.2014.7117735.

[12] L. Rui, "New Algorithm for Color Image Encryption Using Improved 1D Logistic Chaotic Map", The Open Cybernetics & Systemics Journal, vol. 9, pp. 210-216, 2015.

[13] Y. Zhou, L. Bao, C.L. Philip Chen, "A New 1 D Chaotic System for Image Encryption", Signal Processing, Elsevier, vol. 97, pp. 172-182, 2014.

ARTICLE IN PRESS

Egyptian Journal of Petroleum (2016) xxx, xxx–xxx

HOSTED BY

ELSEVIER

Egyptian Petroleum Research Institute

Egyptian Journal of Petroleum

www.elsevier.com/locate/egyjp
www.sciencedirect.com

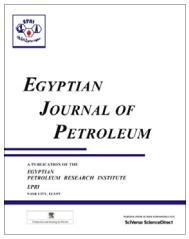

FULL LENGTH ARTICLE

Algae personification toxicity by GC–MASS and treatment by using material potassium permanganate in exposed basin

Ahmed Aidan Al-Hussieny [a], Esam Abd Alraheem [a], Haider Y. Lafta [a], Mohammed K. Shebli [a], Mohammed Jassim Obed Alfalahi [b], Allaa M. Aenab [c,*], S.K. Singh [c]

[a] *Environment and Water Directorate – Ministry of Science and Technology, Baghdad, Iraq*
[b] *Environmental Engineer, Rasan Group Company, Erbil, Iraq*
[c] *Environmental Engineering Department, Delhi Technological University, Delhi, India*

Received 5 June 2016; revised 23 October 2016; accepted 25 October 2016

KEYWORDS

Algal toxins;
Potassium permanganate;
Treatment;
Biomass;
Chlorophyll

Abstract This study was conducted to address algal toxins using potassium permanganate through the control of biomass growth of algae under following conditions value 25 ± 1 °C illumination intensity value 245 microeinstein/m^2/s, using the culture media Chu-10 Modified for the purpose of development algae. We treated algal toxins belonging to groups of Neurotoxins, Hepatotoxins, Pyriproxyfen, Emodin, Brevetoxins-10 (A) and Cytotoxins using concentrations of potassium permanganate represented by 2, 4, 8 and 16 mg/l with alum concentration for each concentration of 30 mg/l, as the removal rate reached to 100% of the toxin blooms in concentrations of 8 and 16 mg/l respectively, through the examination of algal toxins mediated by GC–MASS compared to the standard, which diagnosed a range of algal toxins with $C_2H_3C_{12}NO$ formulas of synthetic $C_9H_{13}NO_2$, $C_{18}H_{27}NO_3$, $C_{11}H_{12}N_2O_6$, $C_{11}H_{17}N_3O$, $C_{10}H_{17}N_3O$, $C_9H_{15}Br_2NO$, $CH_4N_2O_2$, $C_{11}H_{17}NO_2$, $C_{13}H_9BrN_2O_3$, $C_3H_7NO_4S$, $C_{20}H_{29}NO_3$, $C_{15}H_{10}O_5$, $C_4H_8O_2$ and $C_2H_2C_{13}NO$ the concentrations 2 and 4 mg/l turned toxic compounds into non-toxic compounds represented by $C_7H_6O_2$, $C_5H_6N_2O$, $C_{12}H_{11}ClO_4$, $C_6H_6O_2$, $C_{12}H_{10}O_4$, $C_{10}H_{17}N$, $C_4H_6O_2$ and $C_5H_6N_2O$. The results showed reduced primary productivity of algae chlorophyll a result of substance to stop chloroplast for vital activity through the influence of the concentration of potassium permanganate values 0.571, 1.142, 0.583 and 1.713 mg/l respectively, compared to the standard of 114.2 mg/l. As diagnosed types of Algae producing toxins are represented by *Microcystis aeruginosa, Microcystis flosaquae, Oscillatoria amoena, Oscillatoria amphibian, Oscillatoria boryana, Oscillatoria limnetica, Oscillatoria perornata, Phormidium ambiguum, Lyngbya digueti, Lyngbya major, Lyngbya nordgaa-*

* Corresponding author.
E-mail address: allaaaenab@gmail.com (A.M. Aenab).

Peer review under responsibility of Egyptian Petroleum Research Institute.

http://dx.doi.org/10.1016/j.ejpe.2016.10.020
1110-0621 © 2016 Egyptian Petroleum Research Institute. Production and hosting by Elsevier B.V.
This is an open access article under the CC BY-NC-ND license (http://creativecommons.org/licenses/by-nc-nd/4.0/).

Please cite this article in press as: A.A. Al-Hussieny et al., Algae personification toxicity by GC–MASS and treatment by using material potassium permanganate in exposed basin, Egypt. J. Petrol. (2016), http://dx.doi.org/10.1016/j.ejpe.2016.10.020

dii, Lyngbya spirulinoides, Nostoc carneum, Nostoc spongiforme, Anabaena augstumalis, Chroococcus indicus and *Chroococcus minor*, as the dry weight of live Algae producing toxins is 17.342 g/l.

© 2016 Egyptian Petroleum Research Institute. Production and hosting by Elsevier B.V. This is an open access article under the CC BY-NC-ND license (http://creativecommons.org/licenses/by-nc-nd/4.0/).

1. Introduction

Algae are very different and can be found everywhere on the earth. They play a necessary role in many of ecosystems levels, including providing the basis for the hydrous food supply chains supporting all fisher men in the seas, oceans and inland, as well as making about 70% of all the air we breathe [1]. The word Algae represents a big large group of different creatures from different phylogenetic groups, representing many systematic divisions. In general Algae can be referred to as plant-like organisms that are usually photosynthetic and hydrous, but do not have true leaves, roots, trunk, vascular tissue and have simple reproductive formation [2].

Algae are distributed worldwide in the sea, in freshwater and in wet situations on land. Most are microscopic algae, but some of them are so large, also some marine seaweeds that can exceed 50 m in length. The algae have chlorophyll and can make their own food through the steps of photosynthesis.

Recently they are classified in the kingdom of protiste, which include a variety of unicellular and some basic multinuclear and multicellular eukaryotic organisms that have cells with a diaphragm-bound nucleus. Algal poisoning is an intense, often lethal condition caused by high concentrations of toxic blue-green algae (more commonly known as cyanobacteria—literally blue-green bacteria) in drinking water as well as in water used for recreation, agriculture and aquaculture. Severe illness of livestock and Fatalities, birds, pets, fish and wildlife from high growths of cyanobacteria water blooms occur almost in all of the countries in the world. Severe deadly poisonings have also been notarized in people. Poisoning usually comes during warm seasons when the water blossom are more acute and of longer duration. Almost poisonings come among animals drinking cyanobacteria-infested freshwater, but aquatic animals, mostly mariculture fish and prawn, are also affected. The toxins of cyanobacteria comprise six special chemical classes collectively called cyanotoxins [3]. Toxic algae, micro-algal blooms, phytoplankton blooms, red tides, or harmful algae, are all terms for normally occurring phenomena. Around 300 species of micro algae are notify at times to form mass appearance, so called blooms. About one fourth of these species are recognized to produce toxins. The scientific society points out to these events with a generic term, 'Harmful Algal Bloom' (HAB), understanding that, because a wide range of organisms are implicated and some species have toxic impacts at low cell intensity, not all HABs are 'algal' and not all occur as 'blooms' [4]. Many of the organisms in charge for red tides are closely distributed and, in recent years, the organisms appear to be markedly spreading. Natural events such as hurricanes can spread over organisms, and it is doubtful that some organisms may be moved long distances in ship ballast waters. Another factor that may motivate algal proliferation in both freshwater and marine systems is augmentation nutrient loading. Certain algae occur more usually in some areas than others and it is useful to know which ones are problems in particular locations. Good sources of information about algal blooms are the State public health department or the State division of marine resources or marine fisheries [5]. Studies have confirmed the use of UV for removal of all types of microbiology but it is expensive, making it difficult to use on an ongoing basis, while potassium permanganate are a sterile material and removes the microorganisms in addition to not hurting the outer wall of the algae or stopping the process of photosynthesis, causing the need to hold the vital events of moss energy disabled blastids of them, including the reduction in the productivity of material chlorophyll and all pigments in addition to this, it prevents algae toxins out to the outside center 18,6]. So study aims to address the algal toxins using material Potassium Permanganate in the open docks.

2. Materials and methods

2.1. Diagnosis of algae

The non-diatom algae were isolated and diagnosed by microscopic examination, depending on the number of references to classify of non-diatom algae [7–9].

2.2. Method of extract algae toxins Depending on the Reference of WHO [10]

For dried field algae samples certain amount of dry algae powder was added into extracting solution.

2.3. Method of chlorophyll extraction Depending on the Reference of Vollenweider [12]

In order to quantify the amount of chlorophyll in a particular species, the intracellular chlorophyll must first be extracted.

2.4. Examination of algal toxins using GC–MASS Depending on the Reference of Toshihiro et al. [11]

Examination of toxin algal is carried out using Shimadzu-2010 GC–MS.

- Column: 30 m length and 0.25 mm ID.
- Initial temperature: 85 °C.
- Post time: 2 min.
- Ramp: 10 °C/min.
- Final temperature: 340 °C.

2.5. Preparation of potassium permanganate and alum

The proper concentration of potassium permanganate was carried out by dissolving 1 g high purity $KMnO_4$ (99.5% purity)

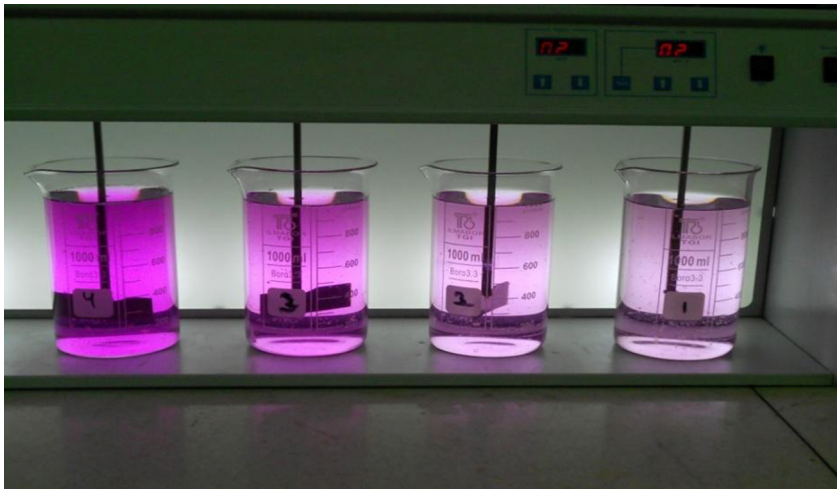

Fig. 1 Streaming device mixer.

in 100 mL distilled water. 2, 4, 8 and 16 mg/l with 30 mg/l of alum solution ($AlSO_4{\cdot}18H_2O$), perfect dose and Coagulant.

Table 1 Numbers of algae toxin-producing, through chlorophyll value of 114.2 mg/l, and dry weight of 17.342 g/L for 100 mL of algal colonies of 100 mL.

Types of algae producing toxins	Numbers of algae (cells/l)	%
Anabaena augstumalis	32	8.48
Chroococcus indicus	26	6.89
C .minor	12	3.18
Microcystis aeruginosa	23	6.10
M. flosaquae	13	3.44
Oscillatoria amoena	24	6.36
O. amphibian	18	4.77
O. boryana	20	5.30
O. limnetica	22	5.83
O. perornata	14	3.71
Phormidium ambiguum	25	6.63
Lyngbya digueti	23	6.10
L. major	17	4.50
L. nordgaadii	27	7.16
L. spirulinoides	16	4.24
Nostoc carneum	18	4.77
N. spongiforme	26	6.89
Westiellopsis prolifica	21	5.57
Total	377	100

2.6. Measuring pH

pH measurement of water samples was directly measured using Boston EXTECH model m 62, calibrated by 4, 7 and 9 pH buffer solutions.

2.7. Mixing potassium permanganate and alum

This process is carried out according to Liang et al. [13] as shown in Fig. 1.

3. Results and discussion

100 mL liquid density of algae growth is spread over all the concentrations of the treated material (potassium permanganate) in addition to the basin control without the impact of any material processing with productivity knowledge Preliminary her through chlorophyll value 114.2 mg/l for the basin control and dry weight of 17.342 g/l. Algae were diagnosed to produce poisons and toxins (see Table 1).

Many researchers used materials to damage growth rates of algae, such as substance use copper sulfate, which led to the rupture of the outer wall of the algae without toxic substance environmental center without affecting the use and this is very dangerous through the algae that carry genes to secrete those toxins including algae blue-greens Division, but for the use of material potassium permanganate, chlorine dioxide and ozone, which are sterile material for many of the germs, we

Table 2 Low initial production of chlorophyll concentration of algae through using of material potassium permanganate and alum solution.

Concentrations (mg/l)	After 5 h	After 24 h	After 48 h	After 72 h
Standard	4.284	44.268	57.1	114.2
2	1.428	31.416	5.285	2.571
4	23.990	21.42	2.426	1.142
8	23.133	1.428	1.142	0.583
16	25.989	7.14	1.713	0.0713

Please cite this article in press as: A.A. Al-Hussieny et al., Algae personification toxicity by GC–MASS and treatment by using material potassium permanganate in exposed basin, Egypt. J. Petrol. (2016), http://dx.doi.org/10.1016/j.ejpe.2016.10.020

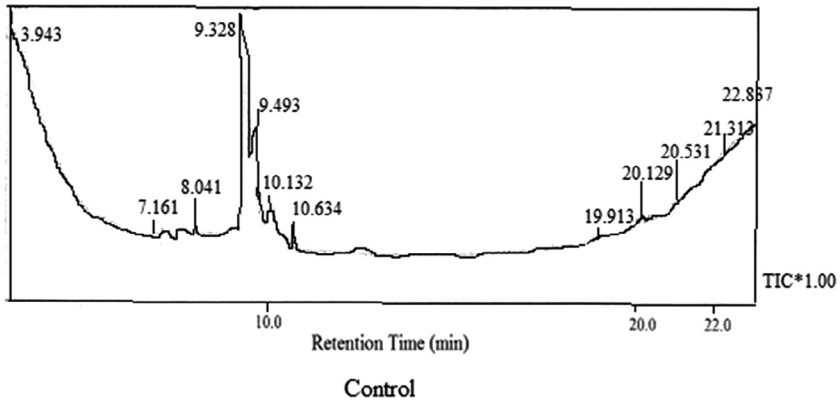

Fig. 2 GC–MASS of algal toxins within the treated standard.

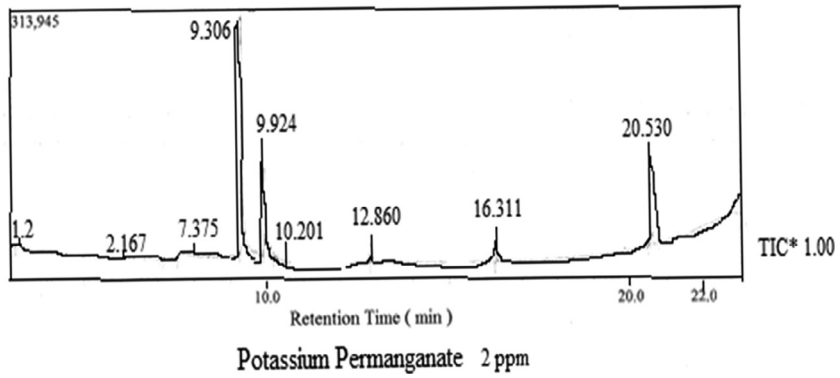

Fig. 3 GC–MASS of algal toxins treated with concentration of 2 mg/l.

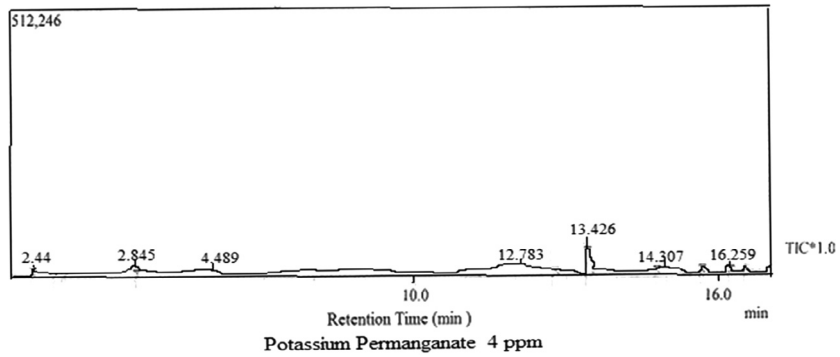

Fig. 4 GC–MASS of algal toxins treated with concentration of 4 mg/l.

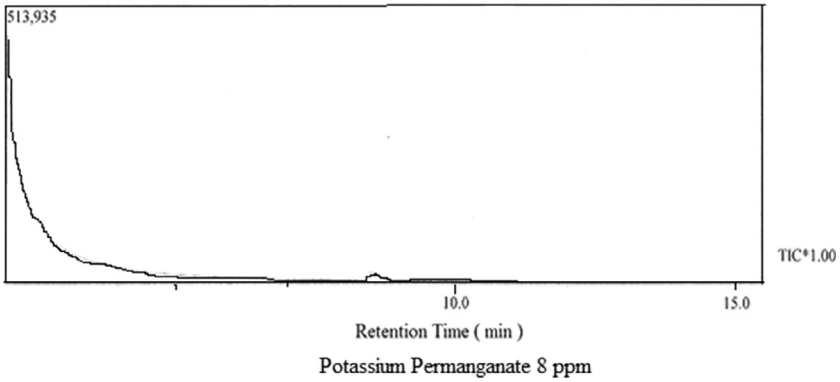

Fig. 5 GC–MASS of algal toxins treated with concentration of 8 mg/l.

Please cite this article in press as: A.A. Al-Hussieny et al., Algae personification toxicity by GC–MASS and treatment by using material potassium permanganate in exposed basin, Egypt. J. Petrol. (2016), http://dx.doi.org/10.1016/j.ejpe.2016.10.020

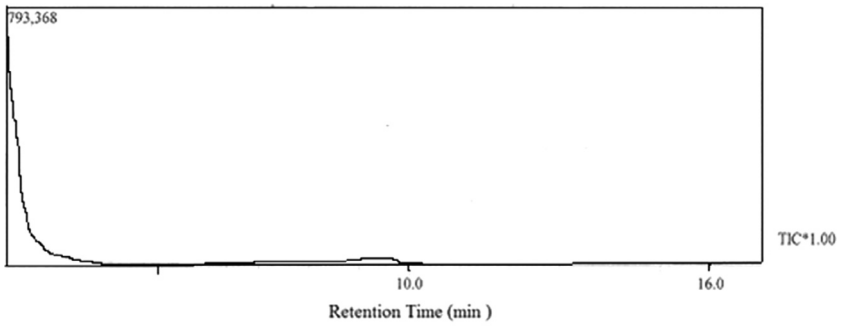

Fig. 6 GC–MASS of algal toxins treated with concentration of 16 mg/l.

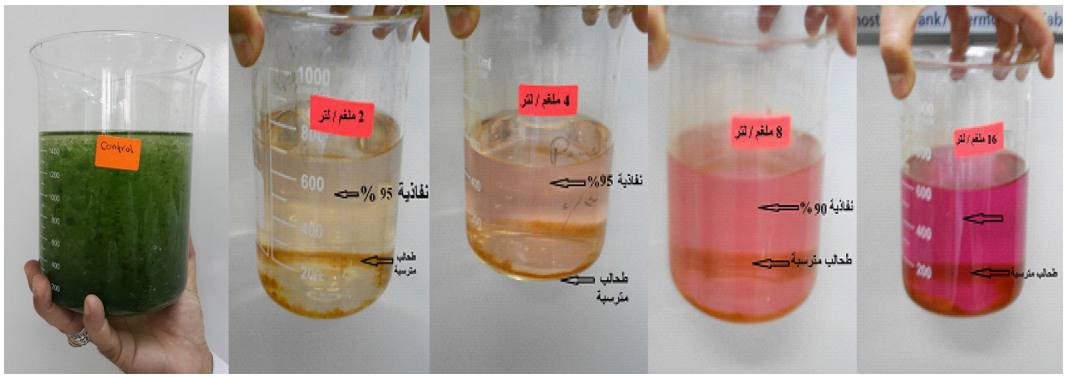

Fig. 7 Concentrations of potassium permanganate and its impact on algae society compared to standard.

Table 3 Treatment of algal toxins of different concentrations of potassium permanganate with chemical formulations statement mediated by GC–MASS.

Algal Toxins	Synthetic version of the toxin	Standard	Concentrations (mg/l)			
			2	4	8	16
1-Neurotoxins						
Antoxin-a	$C_2H_3C_{12}NO$	*	–	–	–	–
	$C_9H_{13}NO_2$	*	–	–	–	–
	$C_{18}H_{27}NO_3$	*	–	–	–	–
	$C_{11}H_{12}N_2O_6$	*	–	–	–	–
	$C_{11}H_{17}N_3O$	*	–	–	–	–
	$C_{10}H_{17}N_3O$	*	–	–	–	–
	$C_9H_{15}Br_2NO$	*	–	–	–	–
Homoanatoxin-a	$CH_4N_2O_2$	*	–	–	–	–
	$C_{11}H_{17}NO_2$	*	–	–	–	–
	$C_{13}H_9BrN_2O_3$	*	–	–	–	–
2- Hepatotoxins						
Microcystin-LA	$C_3H_7NO_4S$	*	–	–	–	–
3-Pyriproxyfen	$C_{20}H_{29}NO_3$	*	–	–	–	–
4-Emodin	$C_{15}H_{10}O_5$	*	–	–	–	–
5-Brevetoxins-10 (A)	$C_4H_8O_2$	*	–	–	–	–
6-Cytotoxins	$C_2H_2Cl_3NO$	*	–	–	–	–

–, Absence of toxins.
* The presence of toxins.

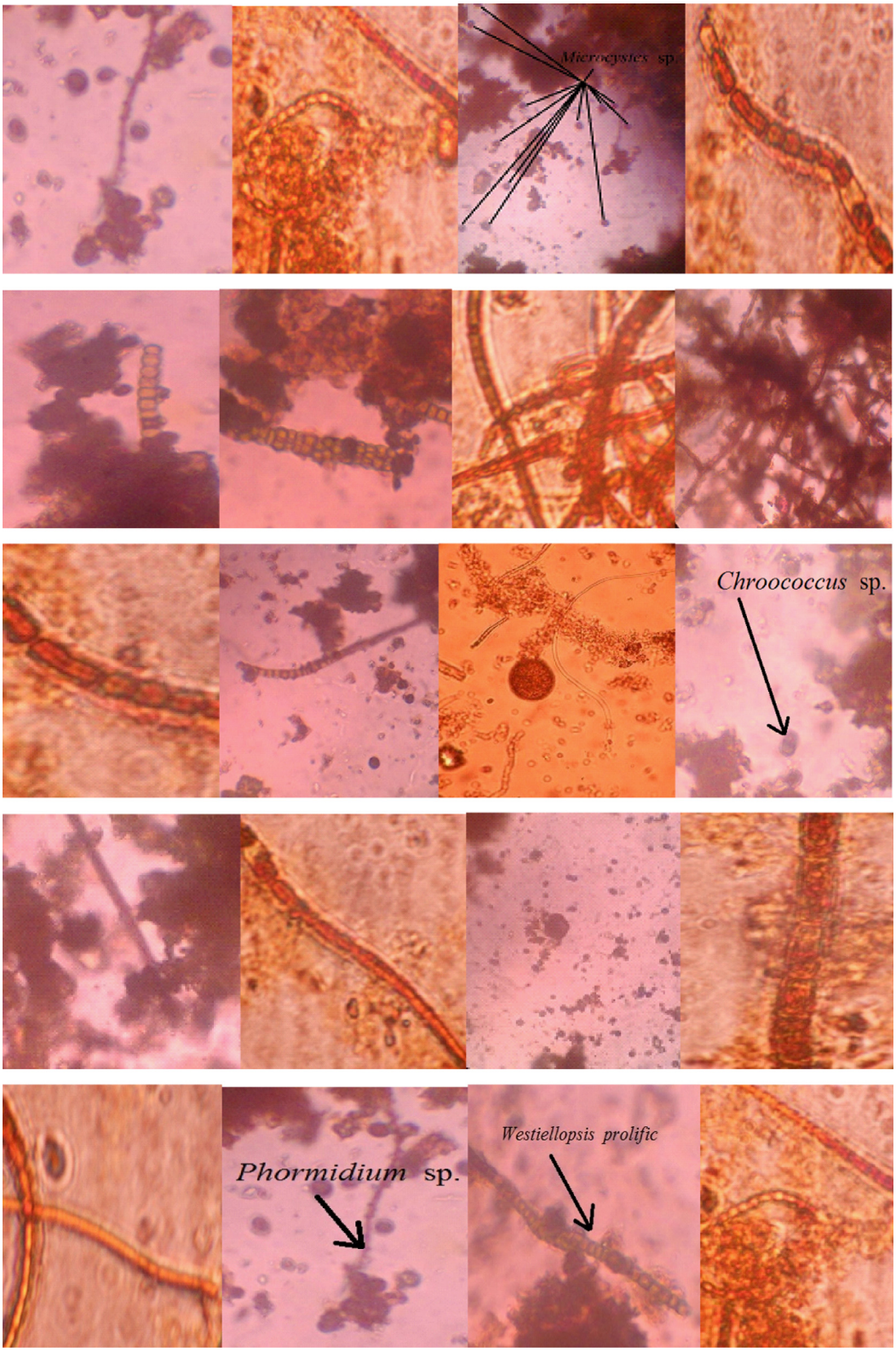

Fig. 8 Algae treated with different concentrations of potassium permanganate without affecting the exterior of the algal cells.

have to be careful to use them in appropriate concentrations in the case of water treatment for human consumption [14].

Tests showed a low concentration of chlorophyll processor permanganate and the use of potassium permanganate blended alum within specific concentrations does not cause any damage through the process of photosynthesis which stops and disables their activity with the presence of alum [14,15], which leads to the deposition of floating masses of algae to the bottom through a stop Productivity initial algae of reducing the concentration of chlorophyll; this means there is

Please cite this article in press as: A.A. Al-Hussieny et al., Algae personification toxicity by GC–MASS and treatment by using material potassium permanganate in exposed basin, Egypt. J. Petrol. (2016), http://dx.doi.org/10.1016/j.ejpe.2016.10.020

decomposition of toxins located inside moss producer of toxins without tearing the outer wall, and Table 2 shows details of the results.

4. Treatment of algal toxins

After decreasing number of algae that causes food to enrich the (excessive growth) using different concentrations of a substance potassium permanganate mixture a concentration of 30 mg/l textured alum as coagulate.

In addition to reducing productivity of initial algae by reducing the concentrations of chlorophyll algal toxins per transaction were examined and compared to standard at the end of the experiment, which lasted for 72 h mediated by GC/MS device. Results showed the presence of toxins' algal belonging to the group Neurotoxins, Hepatotoxins, Pyriproxyfen, Emodin, Brevetoxins-10 (A) and Cytotoxins within the standard treatment, with a note detoxification algal 100% concentrations 8 and 16 mg/l, respectively textured potassium permanganate in comparison with standard, which contained a lot of belonging to the chemical compounds to algal toxins (Fig. 2).

A result of the cessation of photovoltaic installation process stops the outer wall systems (systems enzymatic) to withdraw nutrients that enter into the composition of the algal toxin combination the non-arrival of light to stop light receptors [15], and the concentrations of 2 and 4 mg/l for the same article have some toxic compounds converted into non-toxic compounds and Figs. 3–7 describe them.

Were treated toxins algal belonging to the group Neurotoxins a Besnfein Anatoxin-a, Homoanatoxin-a and the various toxins which is alkaline compounds Alkaloids with effect very quickly called and can be fatal in most cases where the cause muscle surrounding paralysis followed by a respiratory muscle paralysis, which leads to an inability to breathe then death.

As observed in Hepatotoxins group Class Microcystin-LA, these toxins are the most common among toxins Cyanobacteria and have a severe impact, but it takes longer than nerve toxins for death to occur during a period ranging from 5 min to a few days depending on several factors, including weight of the animal and the type of poison and the dosage and others.

Other types of toxins such as Pyriproxyfen, Emodin and Brevetoxins-10 appeared (A) as to remove algal toxins that have emerged within the standard of treatment with 8 and 16 mg/l of potassium permanganate, and Table 3 shows the same.

The concentration of 2 and 4 mg/l of the same material has been converted into non-toxic compounds and toxic compounds as shown in Table 3.

The current study also points to the possibility of potassium permanganate within the concentration of 8 and 16 mg/l, respectively, in the treatment of algal cells by stopping the process of photosynthesis and disables all vital events without tearing the outer wall of moss and then deposition blocs blooms to the pelvic floor and a rise in turbidity levels in the water column compared to the standard that shows a rise in the value of biomass and low turbidity, Fig. 7.

Moreover, all potassium permanganate concentrations 2, 4, 8 and 16 mg/l did not affect the outer wall of the algae within the current study, it did not rupture the out of the cell walls. This is because of potassium permanganate mixture specific concentration of alum led to not tear the outer wall of the algae, which preserves not outer toxins blooms.

It stops the process of photosynthesis, and this contributes to the reduction of primary productivity of algae of chlorophyll, solution Alum is essential for potassium permanganate and it helps the process of sintering and coagulation and sedimentation [17], as shown in Fig. 8.

Additionally, the potassium permanganate affects some algal toxins and do not affect others, as it affects the toxins Anatoxin-a, Cylindrospermopsin and Microcystin and analyses have valued the final removal, while not affecting Saxitoxin toxin, although it is produced by algae greens blue–this is what is confirmed by the organization [16].

5. Conclusions

1. Detection of algal toxins using GC–MS system.
2. Knowledge of the chemical compositions of algal toxins derived from local algae toxin-producing.
3. Algal toxin treatment using potassium permanganate through the use concentrations does not affect the aquatic environment at the same time, a sterile material against germs.
4. Algae die without tearing the outer wall and the preservation of the internal contents without causing environmental pollution in the case of the center, out of their contents to the outside.
5. Photosynthesis of algae process stops and stops the enzymes responsible for the production of algal toxins.
6. Classification of toxic chemical compounds presents in algae extract to the basic varieties of groups toxic algae.

References

[1] Algae Biomass Organization (ABO), 2013. All about algae.com. http://allaboutalgae.com/algae-basics/.
[2] B.V. Lenntech, Algae Description and Types Rotterdamseweg 402 M, 2629 HH Delft, 2014, http://www.lenntech.com/eutrophication-water-bodies/algae.htm.
[3] Wayne W. Carmichael, Overview of Algae Poisoning. Merck Manuals, 2013, http://www.merckvetmanual.com/mvm/toxicology/algal_poisoning/overview_of_algal_poisoning.html.
[4] UNESCO, IOC, Intergovernmental Oceanographic Commission of UNESCO, Harmful Algal Bloom Programme, Project Office for IODE, Oostende, Belgium, 2015, http://hab.ioc-unesco.org/index.php?option=com_content&view=article&id=5&Itemid=16.
[5] Lynn H. Creekmore, Field Manual of Wildlife Diseases: General Field Procedures and Diseases of Birds. USGS science for a changing world. Funded by the U.S. Fish and Wildlife Service, Division of Federal Aid, Administrative Grant No. AP95-017, 2013. http://www.nwhc.usgs.gov/publications/field_manual/chapter_36.pdf.
[6] J. Rositano, B. Nicholson, P. Pieronne, Ozone Sci. Eng. 20 (1998) 223–238.
[7] T.V. Desikachary, Cyanophyta, Indian Council of Agricultural Research, New Delhi, 1959, p. 686.
[8] Edward G. Bellinger, David C. Sigee, Freshwater Algae Identification and Use as Bioindicators Printed in Great Britain by Antony Rowe, Ltd. Chippenham, Wilts, 2010, p. 285.

Please cite this article in press as: A.A. Al-Hussieny et al., Algae personification toxicity by GC–MASS and treatment by using material potassium permanganate in exposed basin, Egypt. J. Petrol. (2016), http://dx.doi.org/10.1016/j.ejpe.2016.10.020

[9] S.A. Felisberto, L. Rodrigues, Braz. J. Biol. 64 (1) (2004) 1–2.
[10] WHO, in: J. Chorus, Bartram (Eds.), Toxic Cyanobacteria in Water, E & FN Spon, an imprint of Toutledge, London, 1999, p. 416.
[11] O. Toshihiro, S. Steffi, K. Ina, B. Susan, S. André, Alisdair R. Fernie, J. Metabolites 3 (2013) 168–184.
[12] R.A. Vollenweider, A Manual on Methods for Measuring Primary Production in Aquatic Environments. Int. Biol. Program Handbook, 12, Black Well Scientific Publication Ltd., Oxford, 1969, p. 225.
[13] Liang Heng, Yang Yanling, Gong Weijia, Li Xing, Li Guibai, Desalination 222 (2008) 74–80.
[14] R.P. Liu, X. Li, Y.L. Yang, H. Liang, G.B. Li, High Technol. Lett. 14 (2004) 90–93.
[15] Ohio Section Technology Committee, White Paper on Algal Toxin Treatment, Environmental Protection Agency, 2011, pp. 1–6.
[16] Ohio Section Technology Committee, Draft White Paper on Cyano Toxin Treatment, Environmental Protection Agency, American Water Works Association Ohio Section Technology Committee, 2015, pp. 1–15.
[17] Ahmed Aidan Al-Hussieny, Elaf Sameer, Reweda Fahim, Zainab Hani, J. Ministry Sci. Technol. 5 (2) (2014) 62–71.
[18] Ahmed Aidan Al-Hussieny, Ahmed Ibrahim Jassim, Haider Y. Lafta, J. Mod. Sci. Heritage 162 (2013) 152 (2)1, www.jmsh.eu.

Please cite this article in press as: A.A. Al-Hussieny et al., Algae personification toxicity by GC–MASS and treatment by using material potassium permanganate in exposed basin, Egypt. J. Petrol. (2016), http://dx.doi.org/10.1016/j.ejpe.2016.10.020

An Automated Tool for Generating Change Report from Open-Source Software

Ruchika Malhotra
Department of Software Engineering
Delhi Technological University
Delhi, India
ruchikamalhotra2004@yahoo.com

Ankita Bansal
Department of Information Technology
Netaji Subhas Institute of Technology
Delhi, India
ankita.bansal06@gmail.com

Sourabh Jajoria
Department of Information Technology
Netaji Subhas Institute of Technology
Delhi, India
sourabhjajoria@gmail.com

***Abstract*— Classes in object-oriented software systems are continuously subject to change. Change prediction is a very important activity in software development. Change data consists of the number of lines of codes added, deleted and modified for each common class between any two versions of a software system. It is important to develop tools to calculate change data and object-oriented metrics that will assist software practitioners in identifying change prone classes in early stages of the software development life cycle. In this paper, we develop a tool, Change Report Generator (CRG) to generate the change report from software source codes of various versions of open-source software. We also extend this tool to automate object-oriented metrics calculation from the source codes of software systems. The generated files store the total number of changes class wise and corresponding values of different object-oriented metrics for each common class between the two versions. This paper gives an overview of some of the applications of the collected data like statistical comparison of two versions and prediction of change-prone classes.**

Keywords*— *Change-proneness; open-source software; correlation feature selection; ensemble learners; cross-validation

I. INTRODUCTION

Changes in software systems are inevitable. Many reasons such as adaptation, bug fixes, enhancements or perfective maintenance lead to changes. Additionally, the requirements of the user may change over time, leading to changes in the software. As software systems are becoming large and complex, maintaining these software systems requires a large amount of effort. About 90% of the total costs of a software system are due to software maintenance [1]. But sometimes resources and time are limited, hence using these limited resources and time effectively is very important. Predicting change prone software components has become a very crucial factor for the maintenance. The likelihood of occurrence of changes in the next version of the software is referred to as change-proneness [2]. Predicting change-prone classes in the early stages of software development can lead to lower cost and effort. There are a large number of classes in an object-oriented software. Classes that are change-prone require more attention because they increase the maintenance cost. Finding the classes which are change-prone can help the developers on focusing preventive actions such as testing, inspections, peer reviews and refactoring on these classes. Also, predicting change-proneness correctly can help developers to allocate resources more appropriately. Besides these advantages, developers also get an insight into the design of the software [3] and developers can alter the design if required.

Increasingly, object-oriented metrics are used for evaluating the quality of software [4]. Researchers have proved that object-oriented metrics are able to predict change-proneness ([5], [6], [7]). Various prediction models have been developed using the source code metrics which can be used to predict change-prone classes [8]. Predictive models can be constructed using the information regarding the number of change between two versions of the software. Change data can be calculated in multiple ways. One of the methods is to compute change as the number of lines of code added, deleted and modified in the recent version with respect to the previous version. The same method to calculate change has been used by other researchers ([6], [7], [9]). Researchers and developers need tools to calculate change data and object-oriented metrics data to make a quality prediction model. There are tools available to calculate metrics data, but there is a shortage of tools to calculate change data. Most of these calculations are done manually. However, manual calculation of change is a cumbersome task due to the presence of a large number of classes in software systems. It is infeasible to manually compare every class of a version with the same class in the next version to find the number of lines of code added, deleted and modified. Hence, it becomes important to automate this process with the help of tools. To the best of the author's knowledge, there are no open source tools available to calculate change data from software source codes. Malhotra et al. developed a tool called CMS to calculate defect and change data from software repositories [10]. Malhotra et al. developed DCRS tool to generate various reports from git based open-source software [11]. In this work, we develop a tool CRG (Change Report Generator) to calculate change data from software source codes. CRG also automates object-oriented

978-1-5090-2029-4/16/$31.00 @2016 IEEE

metrics calculation for software systems which are developed in the Java programming language. The proposed tools by Malhotra et al. use metadata and executable files present in the online repositories for computation, whereas CRG does all the computation from the source code files of open-source software systems. To compute metrics data, CRG automates project creation and metrics computation using Scitools Understand command line tool und [https://scitools.com/support/commandline] via various commands and a Perl script. We generate change report and metrics data for every pair of common classes between two versions of a software system. This data will be used to make prediction models to find change-prone classes therefore the evolutionary process can focus attention on them to develop good quality products with less effort.

The rest of the paper is organized as follows: In Section II, previous approaches on relevant subjects are described. Section III describes the methodology for generating change report and object-oriented metrics data. Section IV provides a demonstration of the tool. Section V gives an overview of the application of the collected data. Finally, Section VI concludes the paper providing some insight into the future applications of the proposed work.

II. RELATED WORK

Software systems can be maintained efficiently with the help of change data. Change-proneness is a software quality attribute. Many researchers have worked on predicting change-proneness in object-oriented software systems. Li et al. studied the relationship between static metrics and maintenance effort [12]. Tsantalis et al. predicted the probability of change in object-oriented systems by calculating the probability that a class will be affected by modifying the functionality of system [2]. Han et al. calculated the Behavioral Dependency Measure (BDM) to predict change-proneness in UML 2.0 models [13]. Khomh et al. studied the impact of Code Smells on software change-proneness [14]. Posnett et al. studied the influence of pattern roles on change-proneness [22]. Malhotra et al. developed a defect collection and reporting system called DCRS for git based open source software [11]. Collecting change data from software source code can help researchers in identifying change-prone components. Malhotra et al. developed a tool called CMS to calculate defect and change data from software project repositories [10]. Zhou et al. calculated change data and object-oriented metrics to examine the effect of class size on the associations between them [9]. Malhotra et al. investigated the relationship between object-oriented metrics and change-proneness [6]. Sharafat et al. analyzed the change history and source code to predict the probability of change in the class [16]. However, very little work has been done on cross-project change prediction. Malhotra et al. used object-oriented metrics for inter-project validation of change-proneness [7]. As software systems are becoming more complex, controlling change is important in software quality management [17].

III. GENERAL ARCHITECTURE

In this section, we provide a detailed description of CRG tool which generates the change report (a report consisting of number of lines of code added, deleted and modified in the recent version with respect to the previous version) and computes object-oriented metrics (of the previous version) by automating Understand tool [https://scitools.com]. The tool then merges them together as shown in Figure 1. Understand project database includes metrics information about all the classes, files, constructors, packages and methods in the software. CRG provides a GUI to give inputs and obtain the output.

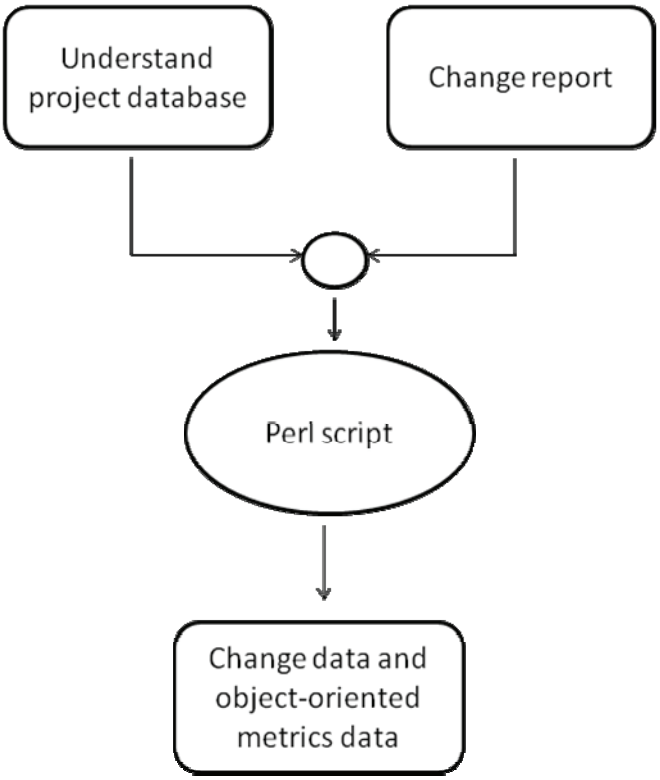

Fig. 1. Change report generator process

A. Change Calculation

The change data is calculated between any two versions of a software system. The inputs to the tool are the path to the source directory of both the versions as shown in Figure 2. In this paper, we define the change data as the number of lines of code added, deleted and modified in the recent version of the software with respect to the previous version. For calculating the change data, we have compared the classes in both the versions. It is logical to only compare the identical classes in both the versions. Thus, before calculating the change data, it is important to obtain a set of comparable classes (or common classes). The output produced from the tool is a file in .csv format (here onwards, referred to as change report) with a total number of changes (number of lines of codes added, deleted and modified) for all the comparable classes between the two

versions. CRG considers all the classes in a Java file and computes the result for each class individually.
CRG generates the change report using the following steps:
Step 1 Extracting Java files from both versions: CRG examines both the versions of the software and all the files having ".java" extension are copied to two separate folders in the working directory. Only Java source code files are considered and other types of files are ignored.

Step 2 Finding Common Java files: CRG compares the lexicographically sorted list of file names from two folders to find the Java files which are common between the two versions. Once the common files are identified, the tool performs preprocessing. Preprocesses involves removing the comments from the code of common Java files. The tool also stores the path to the Java files for the first version in a file as they are needed to create the project database for Understand tool.

Step 3 Extracting Classes: CRG extracts code for each class present in the common files of a version into separate files and stores the files into the classes folder for that version. The same is done for the other version. The tool uses the full name of the classes for naming the corresponding files (i.e. Package name + class name). To do this, the tool scans each Java file line by line and identifies package names and class names using keywords "package" and "class".

Step 4 Finding common classes: Only common classes are comparable between two versions of the software. CRG compares the lexicographically sorted list of class file names from both the class folders to find common classes between the two versions.

Step 5 Calculating changes between common classes: For each common class, the tool identifies the number of added, deleted and modified source code lines using the UNIX diff command (https://en.wikipedia.org/wiki/Diff_utility) to compare two files. The directory path to the two versions of class files is given as input to diff command. Blank lines and white space in the lines are excluded from the change calculation by using "-b" and "-B" options. Each added or deleted line is counted as one change and each line modified is counted as two changes since modification can be treated as line deletion followed by a line addition. Similar counting rules were used by Zhou et al. [9] and Malhotra et al. [10].

Step 6 Storing results: The tool reports the changes between the two versions in a change report with two columns, one column for the class name and other for the total number of changes between the two versions for that class as shown in Figure 3.

Total changes = added lines + deleted lines + (2* modified lines)

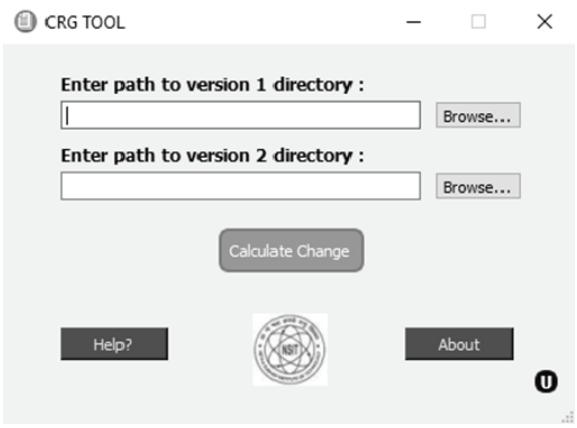

Fig. 2. Change calculation

1	2
javax.faces.FacesException	23
javax.faces.FacesExceptionTest	4
javax.faces.FactoryFinder	62
javax.faces.FactoryFinderTest	0
javax.faces.application.ApplicationFactory	0
javax.faces.application.FacesMessage	7
javax.faces.application.FacesMessage.Severity	0
javax.faces.application.FacesMessageTest	97
javax.faces.application.NavigationHandler	0
javax.faces.application.StateManager	118
javax.faces.application.StateManager.SerializedView	0
javax.faces.application.StateManagerTest	0
javax.faces.application.ViewHandler	65
javax.faces.component.UIColumn	20
javax.faces.component.UICommand	267

Fig. 3. Change report

B. Metrics Calculation

We calculate object-oriented metrics for the first of the two versions of the software. CRG automates project creation and metrics computation using Understand command line tool und which is free for non-commercial use. The inputs to the tool are the path to Understand installation directory, the path to store the output and the output file name as shown in Figure 4. The output produced is a file containing the independent variables (object-oriented metrics) and a dependent variable (indicating whether the class has changed or not) for each class present in the change report. Manually identifying the metrics for each class present in the change report is time-consuming and inefficient as Understand will generate the metrics for all different constructs such as interfaces, constructors, packages, methods, anonymous classes and classes which are not present in the next version of the software.

CRG creates a project database for the first of the two versions providing the following command to und:

create –db database_name.udb –languages java add @files_list.lis analyze

Where files_list.lis is the file containing the list of paths to all the Java files for the first version.

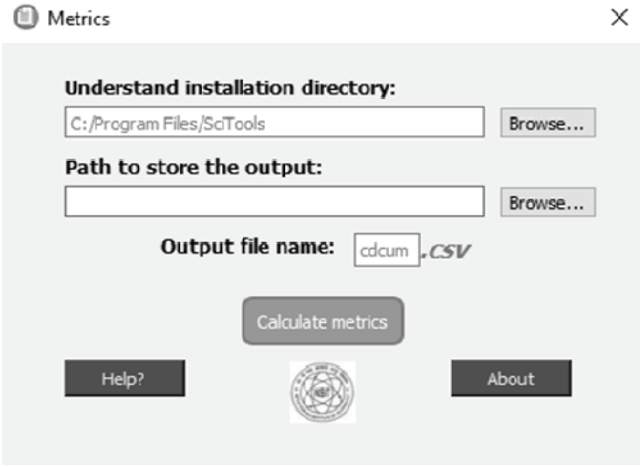

Fig. 4. Metrics calculation

The project database includes metrics information about all the classes, files, constructors, packages and methods in the software. Understand includes a Perl API which allows the user to directly query the Understand database [https://scitools.com/support/perl-api]. We developed a Perl script for Understand Perl API to merge the required object-oriented metrics data for each class with the previously calculated change report between the two versions. The script collects the metrics data only for classes which are present in the change report as we only require metrics for classes which appear in both the versions of the software. The script stores the change value as 'Yes' or 'No' representing whether the class has changed or not between the two versions. If the number of changed reported in the change report is more than zero, the changed value is 'Yes' else it is 'No'. The result is stored in a new file as shown in Figure 5.

CRG runs the Perl script from command line tool und using the following command:

uperl script_name.pl –db database_name.udb

CRG helps the user in automating the process of project creation, metrics computation and merging with the change report for each class present in the change report.

IV. EMPIRICAL DATA COLLECTION

For the demonstration purpose, we have investigated two open source projects which are Myfaces and Struts that are web frameworks of Apache. "A web framework is a software framework that is designed to support the development of web applications including web services, web resources and web APIs" (https://en.wikipedia.org/wiki/Web_framework). In the experiment 3 versions, each of 2 open source projects are investigated. The projects are developed using Java programming language. The source codes of these software systems are available at https://github.com. The details of MyFaces and Struts are provided in Table I.

TABLE I. SOFTWARE DETAILS

Name	Versions	Description
MyFaces	Core-project-1.1.10, 1.2.12, 2.0.2	"Apache MyFaces is an Apache Software Foundation project that creates and maintains an open-source Java Server Faces implementation, along with several libraries of JSF components that can be deployed on the core implementation" [https://en.wikipedia.org/wiki/Apache_MyFaces].
Struts	2.0.0, 2.0.8, 2.1.3	"Apache Struts is an open-source web application framework for developing Java EE web applications. It uses and extends the Java Servlet API to encourage developers to adopt a model–view-controller (MVC) architecture" [https://en.wikipedia.org/wiki/Apache_Struts].

	Name	CBO	NOC	WMC	RFC	NPRM	NPROM	NPM	LOC	DIT	LCOM	Changes
2	com.android.settings.AccessibilitySettings	0	0	10	10	6	3	1	234	2	82	Yes
3	com.android.settings.ActivityPicker	2	1	6	6	0	4	2	262	2	58	Yes
4	com.android.settings.ActivityPicker.EmptyDrawable	0	0	9	9	0	0	8	36	2	66	No
5	com.android.settings.ActivityPicker.IconResizer	1	0	2	2	0	0	2	75	1	9	Yes
6	com.android.settings.ActivityPicker.PickAdapter	1	0	5	5	0	0	5	68	2	50	Yes
7	com.android.settings.ActivityPicker.PickAdapter.Item	1	0	4	4	0	1	0	42	1	54	Yes
8	com.android.settings.AirplaneModeEnabler	0	0	8	8	2	0	6	70	1	62	Yes
9	com.android.settings.ApnEditor	0	0	16	16	7	2	7	346	2	86	Yes
10	com.android.settings.ApnPreference	0	0	11	11	1	0	10	88	2	78	No
11	com.android.settings.ApnSettings	3	0	15	15	6	5	4	244	2	91	Yes
12	com.android.settings.ApnSettings.RestoreApnProcessHandler	1	0	2	2	0	0	2	17	2	0	No
13	com.android.settings.ApnSettings.RestoreApnUiHandler	1	0	1	1	0	0	1	17	2	0	No
14	com.android.settings.ApplicationSettings	0	0	9	9	4	3	2	112	2	78	Yes
15	com.android.settings.AppWidgetPickActivity	2	0	7	13	0	1	2	128	3	68	Yes
16	com.android.settings.BandMode	1	0	6	6	5	1	0	137	2	76	Yes
17	com.android.settings.BandMode.BandListItem	1	0	3	3	0	0	3	12	1	0	No
18	com.android.settings.BatteryInfo	0	0	5	5	2	0	3	133	2	73	Yes
19	com.android.settings.bluetooth.BluetoothDevicePreference	1	0	7	7	0	2	5	55	2	64	Yes
20	com.android.settings.bluetooth.BluetoothDiscoverableEnabler	1	0	9	9	5	0	4	115	1	68	Yes
21	com.android.settings.bluetooth.BluetoothEnabler	2	0	5	5	1	0	4	78	1	36	Yes

Fig. 5. Metrics calculation

Statistical comparison

The change report can be used to analyze the number of changes made between the two versions of software. Table II shows the change data results for MyFaces and Struts.

The results for MyFaces show that 75% of classes changed between version 1.1.10 and version 1.2.12 and 66% of classes changed between version 1.2.12 and version 2.0.2. The results for Struts show that 53% of classes changed between version 2.0.0 and version 2.0.8 and 42% of classes changed between version 2.0.8 and version 2.1.3.

TABLE II. COMPARISON RESULTS

Software	Version 1	Version 2	Total classes	No. of classes changed
MyFaces	1.1.10	1.2.12	302	227
MyFaces	1.2.12	2.0.8	480	315
Struts	2.0.0	2.0.8	681	359
Struts	2.0.8	2.1.3	693	288

V. APPLICATION OF COLLECTED DATA

In this section, we summarize the application of data collected from the developed tool (CRG).

A. Change prediction model

Software systems are continuously subjected to changes. Prediction of change-prone classes can help developers in distributing resources and time effectively. The change data (dependent variable) and object-oriented metrics (independent variables) obtained using the proposed tool (as explained in section III) can be used to develop prediction models for predicting change prone classes in the software systems. For example, the data as shown in figure 5 (obtained from the tool) can be used to develop prediction models which can be used for predicting the change prone classes in the next version of the same software or other similar software. We split this known data set which has known dependent variable into training set and testing test. We train the machine learning or statistical classifier using the training set to create the prediction model. The prediction model is tested on the test set to check the performance of the created model. If the model gives satisfactory results, then it can be used for predicting unknown dependent variable (or identifying change prone classes) for an unknown data set as shown in Figure 6.

B. An Illustration

For the purpose of validation, we have constructed ensemble learner models [18] i.e. AdaBoost, LogitBoost, Bagging and Random forest. The performance of the models is evaluated using three evaluation measures. These three evaluation measures are explained below:

1. **ROC:** Receiver operating characteristics (ROC) curve is drawn by plotting the true positive rate on Y axis and the false positive rate on X axis. The area under the curve (AUC) measures the area under the ROC curve [19]. We have used the AUC value to evaluate performance of the models.

2. **G-Mean:** The g-mean measures the balance between the accuracies of positives and the accuracy of negatives [20]. Mathematically, it is given as:

ACTUAL	CLASSIFIED	
	NEGATIVE	POSITIVE
NEGATIVE	a (True-negative)	b (False-negative)
POSITIVE	c (False-positive)	d (True-positive)

$$i = \frac{d}{c+d}, \quad j = \frac{a}{a+b}$$

$$gmean = \sqrt{i+j}$$

3. **Balance:** The balance measures the balance between the probabilities of true positives and false positives [19]. Mathematically, it is given as:

$$pf = \frac{c}{a+c}, \quad pd = \frac{d}{b+d}$$

$$balance = \frac{\sqrt{(0-pf)^2 + (1-pd)^2}}{\sqrt{2}}$$

We analyzed the consecutive versions of MyFaces data set and collected the data (dependent and independent variables) between MyFaces 1.1.10 and MyFaces 1.2.12 using the tool developed by us. We preprocessed the data by filtering the attributes using Correlation-based Feature Selection (CFS) [21]. We found that out of a total of 7 independent variables, 4 variables are selected using CFS. Thus, only this subset of variables is given as input to construct the models. The results would be highly optimistic if the training and testing are performed on the same data. Hence, we used 10 folds cross-validation [21]. The 10 folds cross-validation breaks the data set into 10 sets of almost equal sizes. The model is trained on 9 sets and then tested on the remaining 1 set. This process is repeated 10 times for all the 10 sets and the mean values of the results are taken. Table III shows the prediction results.

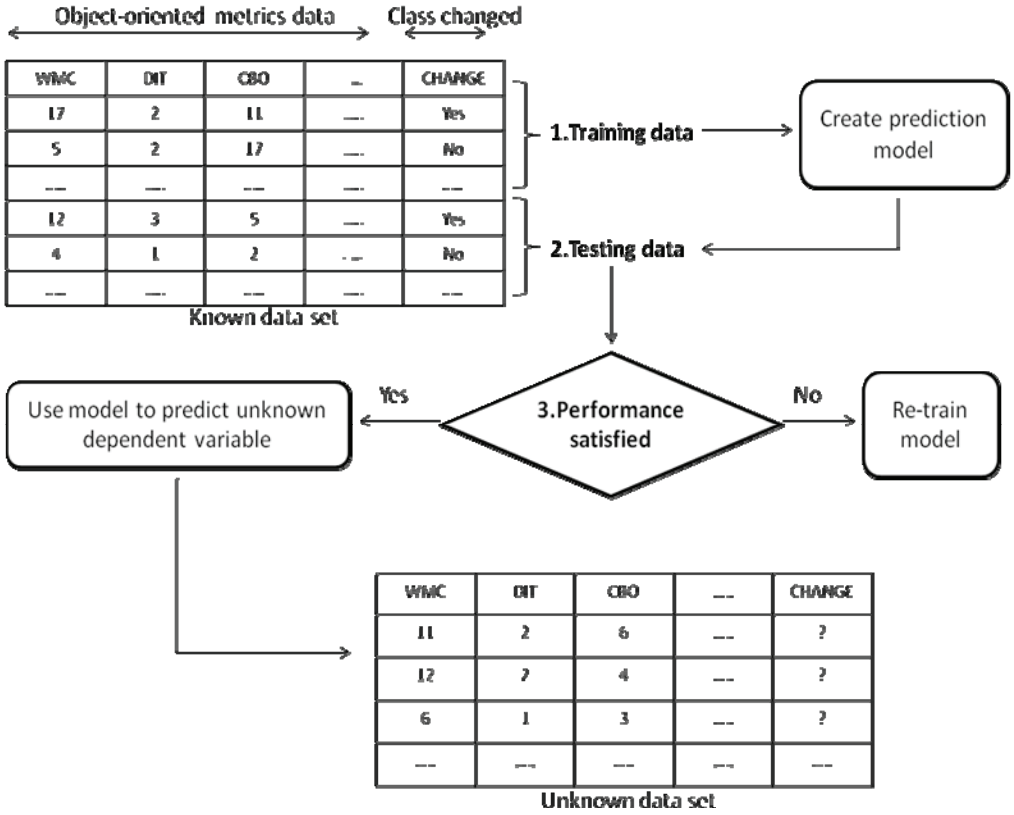

Fig. 6. Change prediction

TABLE III. PREDICTION RESULTS

Classifier	AUC	G-mean	Balance
AdaBoost	0.81	0.66	0.75
LogitBoost	0.81	0.63	0.72
Bagging	0.50	0.43	0.50
Random forest	0.81	0.65	0.73

From Table III, we observe that all the ensemble learners have shown comparable performance except Bagging. Among other models, AdaBoost gives the best results with AUC of 0.81, g-mean value of 0.66 and balance value of 0.75. In other words, it can be used to identify change-prone classes in some future version of the same software or some other similar software.

VI. CONCLUSION AND FUTURE WORK

Change prediction using object-oriented metrics is an important activity that leads to a reduction in maintenance effort. The developers can pay focussed attention on the identified change prone classes. To predict the change prone classes in some future release of software, prediction models are constructed using the historical data (source code of previous two versions) of that software. However, the main challenge is to bring the historical data to a form which can be used for constructing prediction models. Using the source code of both the versions, we need to obtain the number of lines of code added, deleted and modified in the recent version with respect to the previous version (which will constitute the dependent variable). In addition to this, we also need to obtain object oriented metrics for the previous version (which will constitute the independent variables). Using independent and dependent variables, we can develop prediction models to predict change prone classes. In this work, we developed a tool for the collection of dependent and the independent variables from two versions of software using the source codes. We have developed CRG tool to automate the collection of change data (number of lines of code added, deleted and modified) and object-oriented metrics from software source code. The gathered data can be used for statistical comparison of any two versions of the software as well as for constructing prediction models. As discussed, the prediction models constructed can be used by developers in the early stages of software development to predict change-prone classes. The work can be extended for investigating intra-project and cross-project change-proneness prediction. We plan to develop models for cross-project change-proneness prediction to predict change-prone classes of a software version using the CRG tool for software systems having the same application domain, developed by the same company and developed using the same programming language [23].

VII. REFERENCES

[1] Brooks Jr, Frederick P. *The Mythical Man-Month: Essays on Software Engineering, Anniversary Edition, 2/E*. Pearson Education India, 1995.

[2] Tsantalis, Nikolaos, Alexander Chatzigeorgiou, and George Stephanides. "Predicting the probability of change in object-oriented systems." *IEEE Transactions on Software Engineering* 31, no. 7 (2005): 601-614.

[3] Cipolla-Ficarra, Francisco Vicente, ed. *Advanced research and trends in new technologies, software, human-computer interaction, and communicability*. IGI Global, 2013.

[4] Harrison, Rachel, Steve J. Counsell, and Reuben V. Nithi. "An evaluation of the MOOD set of object-oriented software metrics." *IEEE Transactions on Software Engineering* 24, no. 6 (1998): 491-496.

[5] Lu, Hongmin, Yuming Zhou, Baowen Xu, Hareton Leung, and Lin Chen. "The ability of object-oriented metrics to predict change-proneness: a meta-analysis." *Empirical software engineering* 17, no. 3 (2012): 200-242.

[6] Malhotra, Ruchika, and Megha Khanna. "Investigation of relationship between object-oriented metrics and change proneness." *International Journal of Machine Learning and Cybernetics* 4, no. 4 (2013): 273-286.

[7] Malhotra, Ruchika, and Megha Khanna. "Inter Project Validation for Change Proneness Prediction using Object Oriented Metrics." *Software engineering: An International Journal* 3, no. 1 (2013): 21-31.

[8] Subramanyam, Ramanath, and Mayuram S. Krishnan. "Empirical analysis of ck metrics for object-oriented design complexity: Implications for software defects." *IEEE Transactions on software engineering* 29, no. 4 (2003): 297-310.

[9] Zhou, Yuming, Hareton Leung, and Baowen Xu. "Examining the potentially confounding effect of class size on the associations between object-oriented metrics and change-proneness." *IEEE Transactions on Software Engineering* 35, no. 5 (2009): 607-623.

[10] Malhotra, Ruchika, and Anushree Agrawal. "CMS tool: calculating defect and change data from software project repositories." *ACM SIGSOFT Software Engineering Notes* 39, no. 1 (2014): 1-5.

[11] Malhotra, Ruchika, Nakul Pritam, Kanishk Nagpal, and Prakarsh Upmanyu. "Defect Collection and Reporting System for Git Based Open Source Software." In *Data Mining and Intelligent Computing (ICDMIC), 2014 International Conference on*, pp. 1-7. IEEE, 2014.

[12] Li, Wei, and Sallie Henry. "Object-oriented metrics that predict maintainability." *Journal of systems and software* 23, no. 2 (1993): 111-122.

[13] Han, Ah-Rim, Sang-Uk Jeon, Doo-Hwan Bae, and Jang-Eui Hong. "Behavioral dependency measurement for change-proneness prediction in UML 2.0 design models." In *2008 32nd Annual IEEE International Computer Software and Applications Conference*, pp. 76-83. IEEE, 2008.

[14] Khomh, Foutse, Massimiliano Di Penta, and Yann-Gael Gueheneuc. "An exploratory study of the impact of code smells on software change-proneness." In *2009 16th Working Conference on Reverse Engineering*, pp. 75-84. IEEE, 2009.

[15] Posnett, Daryl, Christian Bird, and Prem Dévanbu. "An empirical study on the influence of pattern roles on change-proneness." *Empirical Software Engineering* 16, no. 3 (2011): 396-423.

[16] Sharafat, Ali R., and Ladan Tahvildari. "A probabilistic approach to predict changes in object-oriented software systems." In *11th European Conference on Software Maintenance and Reengineering (CSMR'07)*, pp. 27-38. IEEE, 2007.

[17] Xing, Tao. "Software configuration management of change control study based on baseline." In *Intelligent Control and Information Processing (ICICIP), 2010 International Conference on*, pp. 93-96. IEEE, 2010.

[18] Dietterich, Thomas G. "Ensemble methods in machine learning." In *International workshop on multiple classifier systems*, pp. 1-15. Springer Berlin Heidelberg, 2000.

[19] Menzies, Tim, Jeremy Greenwald, and Art Frank. "Data mining static code attributes to learn defect predictors." *IEEE transactions on software engineering* 33, no. 1 (2007): 2-13.

[20] Shatnawi, Raed. "A quantitative investigation of the acceptable risk levels of object-oriented metrics in open-source systems." *IEEE Transactions on software engineering* 36, no. 2 (2010): 216-225.

[21] Hall, Mark A. "Correlation-based feature selection for machine learning." PhD diss., The University of Waikato, 1999.

[22] Posnett, Daryl, Christian Bird, and Prem Dévanbu. "An empirical study on the influence of pattern roles on change-proneness." *Empirical Software Engineering* 16, no. 3 (2011): 396-423.

[23] Zimmermann, Thomas, Nachiappan Nagappan, Harald Gall, Emanuel Giger, and Brendan Murphy. "Cross-project defect prediction: a large scale experiment on data vs. domain vs. process." In *Proceedings of the the 7th joint meeting of the European software engineering conference and the ACM SIGSOFT symposium on The foundations of software engineering*, pp. 91-100. ACM, 2009.

Egyptian Informatics Journal xxx (2016) xxx–xxx

Contents lists available at ScienceDirect

Egyptian Informatics Journal

journal homepage: www.sciencedirect.com

Full length article

An effective collaborative movie recommender system with cuckoo search

Rahul Katarya *, Om Prakash Verma [1]

Department of Computer Science & Engineering, Delhi Technological University, Delhi, India

ARTICLE INFO

Article history:
Received 21 November 2015
Revised 8 October 2016
Accepted 18 October 2016
Available online xxxx

Keywords:
Recommender system
Collaborative filtering
k-mean
Cuckoo search optimization
Movie

ABSTRACT

Recommender systems are information filtering tools that aspire to predict the rating for users and items, predominantly from big data to recommend their likes. Movie recommendation systems provide a mechanism to assist users in classifying users with similar interests. This makes recommender systems essentially a central part of websites and e-commerce applications. This article focuses on the movie recommendation systems whose primary objective is to suggest a recommender system through data clustering and computational intelligence. In this research article, a novel recommender system has been discussed which makes use of k-means clustering by adopting cuckoo search optimization algorithm applied on the Movielens dataset. Our approach has been explained systematically, and the subsequent results have been discussed. It is also compared with existing approaches, and the results have been analyzed and interpreted. Evaluation metrics such as mean absolute error (MAE), standard deviation (SD), root mean square error (RMSE) and t-value for the movie recommender system delivers better results as our approach offers lesser value of the mean absolute error, standard deviation, and root mean square error. The experiment results obtained on Movielens dataset stipulate that the proposed approach may provide high performance regarding reliability, efficiency and delivers accurate personalized movie recommendations when compared with existing methods. Our proposed system (K-mean Cuckoo) has 0.68 MAE, which is superior to existing work (0.78 MAE) [1] and also has improvement of our previous work (0.75 MAE) [2].

© 2016 Production and hosting by Elsevier B.V. on behalf of Faculty of Computers and Information, Cairo University. This is an open access article under the CC BY-NC-ND license (http://creativecommons.org/licenses/by-nc-nd/4.0/).

1. Introduction

A recommendation system has become an indispensable component in various e-commerce applications. Recommender systems collect information about the user's preferences of different items (e.g. movies, shopping, tourism, TV, taxi) by two ways, either implicitly or explicitly [3–7]. An implicit acquisition of user information typically involves observing the user's behavior such as watched movies, purchased products, downloaded applications. On the other hand, a direct procurement of information typically involves collecting the user's previous ratings or history. Collaborative filtering (CF) is the way of filtering or calculating items through the sentiments of other people [8–10]. It first gathers the movie ratings given by individuals and then recommends movies to the target user based on like-minded people with similar tastes and interests in the past. Additional impression on which some recommender systems are based is clustering. Clustering is a popular unsupervised data mining tool that is used for partitioning a given dataset into homogeneous groups based on some similarity or dissimilarity metric [11–14]. Collaborative filtering and clustering have been discussed in detail in the next section. Hybrid cluster and optimization approach is applied to improve movie prediction accuracy. Such a hybrid approach has been used to overcome the limitations of typical content-based and collaborative recommender systems. For clustering, k-means algorithm is applied and for optimization, cuckoo search optimization is implemented. K-means algorithm is an enormously greater clustering algorithm when compared to other clustering methods in relations of time, complexity or effectiveness for a particular number of

Peer review under responsibility of Faculty of Computers and Information, Cairo University.

* Corresponding author at: Department of Computer Science & Engineering, Delhi Technological University (Formerly Delhi College of Engineering), Shabad Daulatpur, Main, Main Bawana Road, Delhi 110042, India.

E-mail address: rahulkatarya@dtu.ac.in (R. Katarya).

URLs: http://www.dtu.ac.in/Web/Departments/CSE/faculty/ (R. Katarya), http://www.dtu.ac.in/Web/Departments/CSE/faculty/ (O.P. Verma).

[1] Department of Computer Science & Engineering, Delhi Technological University (Formerly Delhi College of Engineering), Shabad Daulatpur, Main, Main Bawana Road, Delhi 110042, India.

http://dx.doi.org/10.1016/j.eij.2016.10.002
1110-8665/© 2016 Production and hosting by Elsevier B.V. on behalf of Faculty of Computers and Information, Cairo University.
This is an open access article under the CC BY-NC-ND license (http://creativecommons.org/licenses/by-nc-nd/4.0/).

Please cite this article in press as: Katarya R, Verma OP. An effective collaborative movie recommender system with cuckoo search. Egyptian Informatics J (2016), http://dx.doi.org/10.1016/j.eij.2016.10.002

clusters [12,15]. Clustering algorithm with a bio-inspired algorithm such as cuckoo search [16–21] delivers optimize results. The cuckoo search has shown best performance when compared with other algorithms such as genetic algorithms and particle swarm optimization. Simulations and comparison of the cuckoo search were greater to these existing algorithms for multimodal objective functions. To find the best results we have to find the most suitable weight among all possible ones. Cuckoo search was also performed well and showed good results that found the appropriate weights [22]. That is why cuckoo optimization algorithm is also used to obtain optimized weight in our work. Besides being one of the most efficient algorithms, it was found that it takes less time than other algorithms applied to the same dataset. The approach of k-means and cuckoo has been applied to the dataset, and the results have been observed regarding evaluation metrics such as mean absolute error (MAE), standard deviation (SD), root mean square error (RMSE) and t-value. These parameters examined and discussed to evaluate the performance of movie recommendation system. Regarding accuracy and precision, the experiment results reflect that the proposed approach is capable of providing more reliable movie recommendations as compared to the existing cluster-based CF methods. In numerous research, the clustering approaches are conducted with the entire dimensions of data which might lead to somewhat inaccuracy and results in more computation time. In general, designing expert movie recommendations is still a challenge, and discovering effective clustering method is a critical problem in this condition. To address aforementioned, a hybrid model- based movie recommendation approach is proposed to alleviate the issues of both extraordinary dimensionality and data sparsity. That is the reason we selected a cuckoo algorithm with k-means for optimization. On the comparison with some other optimization algorithms, the cuckoo was found to perform better than others. The major contributions of this research work are:

- We proposed a novel recommender system with K-means & cuckoo search optimization.
- Our system is innovative and efficient so far, as it employed Cuckoo search algorithm for excellent recommendations for Movielens Dataset.
- Our hybrid model has 0.68 MAE, which is superior to existing work (0.78 MAE).
- Our model also has excellent improvement of our previous work (0.75 MAE).
- The performance with respect to time is also better as compared to already existing systems.
- We used well known Movielens dataset (http://grouplens.org/datasets/movielens/100k/) to analyze the behavior of our proposed system.

The remainder of this article is planned as follows: Section 2 gives a brief explanation of the related work that was carried out on collaborative recommendation systems and clustering-based collaborative recommendation. The proposed approach called as a k-mean-cuckoo approach for movie recommender system is explained in Section 3. In Section 4, experiment results performed on Movielens dataset are described, and finally summarization of this article with future work are highlighted in Section 5.

2. Background and related work

Recommender systems are based on a variety of approaches such as content based [23,24], collaborative approach [9,25–27], hybrid [28,29]. Furthermost movie recommendation systems are centered on collaborative filtering and clustering. In movie recommender systems the user is asked to rate the movies which user has already seen then these ratings are applied to recommend other movies to the user that user has not perceived by utilizing collaborative filtering that is based on similar ratings. Collaborative filtering [9,10,30–32] is tremendously spreading in such a way that this approach influences most of the recommender systems. Collaborative filtering majorly classified into two principal classes such as memory-based collaborative filtering and model based collaborative filtering. Memory-based collaborative filtering [4,5,33] explores for nearest neighbors in the user space for an active user and dynamically recommend the movies. The shortcomings related to this method are computation complexity and data sparsity. Many authors [34] tried to reduce this computational complexity and memory bottleneck issues such as in item based collaborative filtering technique, in which relations between items were computed for neighborhood region around a target object. They showed in their empirical studies that item-based method could decrease the time of computation as well as deliver rationally correct prediction and accurateness. Model-based collaborative technique [3,4,8,33,35] produces a prebuilt model to collect rating patterns based on the database of users and ratings that can treat the issues of data sparsity and scalability. Model-based collaborative filtering is time-consuming and its offline in nature. Clustering based techniques are broadly used in movie recommendation systems to reduce the problem of scalability. Various researchers applied clustering-based methods on recommender systems that delivered expert recommendations [36–41]. The purpose of clustering is to partition objects into groups known as clusters in such a way that two objects within the same cluster have a minimum distance between them to identify similar objects then clustering process is performed offline to build the model. When a target user arrived, the online module allocates a cluster with a substantial similarity weight to the user, and the prediction rating of a specified item is computed based on the same cluster members instead of searching whole user space. The k-nearest neighbor (kNN) algorithm is the orientation algorithm in collaborative filtering recommendation process which is applied in recommendation process [42–45]. kNN based recommender systems for collaborative filtering recommendation process are reliable and with precise recommendations. A bio-inspired algorithm such as cuckoo search has exclusive background sensing abilities and employ a special method to facilitate the evolution of continuing resolutions into novel and quality recommendations by generating clusters with reduced time as discussed in next section.

3. K-means-cuckoo based collaborative filtering framework

To overcome the limitations of a collaborative recommender system, we propose a hybrid cluster and optimization based technique to improve movie prediction accuracy. Our motive is to design a unified model solution that incorporates user ratings from the Movielens dataset for predictions. We use K-means as clustering algorithm and cuckoo search as optimization algorithm and then apply to Movielens dataset for improved efficient recommender systems Initially k-means clustering algorithm is applied to Movielens dataset for clustering of users into different clusters. The clusters are selected randomly at first then users are inspected one by one by calculating the differences in their ratings and the centroid of the clusters, and if their difference is smallest, then the user gets allocated to the cluster to which they are closest. However, at this moment not assure that each user has been assigned to the real cluster with a minimum difference of centroid. So each user's distance is compared to its cluster mean and with other clusters mean and relocate the users according to the smallest distance from any cluster's mean. Now this iterative relocation

Please cite this article in press as: Katarya R, Verma OP. An effective collaborative movie recommender system with cuckoo search. Egyptian Informatics J (2016), http://dx.doi.org/10.1016/j.eij.2016.10.002

would now continue from this new partition until no more relocations occur. After a point, if no more relocations occurred then that point is the point of completion of the clustering process. The K-means algorithm is made of the following steps given in Fig. 1 [12,15,46,47].

Next cuckoo search optimization algorithm is applied to the resultant of the k-means algorithm for optimizing the results. The cluster is prepared with a fitness function that helps in improving the user's centroid distances, whereas fitness function changes previous centroids for a limited number of iteration (i.e. relocation of centroids to users). Then classify the users again by calculating the minimum centroid differences or applying k-means again. Cuckoo Search algorithm may be described using following three idealized rules [16–21]:

(a) Every cuckoo puts one egg at a time and dumps its egg in randomly chosen nest.
(b) The finest nests with the high quality of eggs will carry over to the subsequent generations.
(c) A number of existing host nests is fixed, and the egg laid by a cuckoo is exposed by the hosts birth a probability pa $\in [0,1]$.

For the framework, we considered a correlation where a user is considered as an egg. Each nest can be seen as a cluster. Fig. 2 shows a flowchart that displays the stepwise process that, how cuckoo search algorithm is applied. The procedure commences with the initialization where a random population of n host nests is introduced, and a levy flights behavior equation is obtained then fitness is obtained using the fitness function for obtaining an optimal solution. Levy flights is a random walk in which the step lengths are distributed according to a Levy distribution. The step length and Levy stable distribution can be calculated with the help of Laplace and Fourier transformations. It has been implemented in the cuckoo optimizing algorithm, and the flight length comes out to be $x(N) \sim N1/\alpha$ where $0 < \alpha < 2$, x is the random variable and N is step size. The distance that the cuckoo travels can be calculated using the above equation for each iteration. In order we select a random nest, say j then compared the fitness of the cuckoo egg (incoming new solution) with the fitness of the host eggs present in the nest. In case, the value of the fitness function of the cuckoo egg is less than or equal to the value of the fitness function of the randomly chosen nest, and then the randomly selected nest, j is replaced by the fresh resolution as given in Eq. (1).

$$\text{Fitness function} = \text{Current best solution} - \text{Previous best solution} \quad (1)$$

As the value of the fitness function tends to zero, the deviation between solutions decreases with increasing number of iterations and decision is that if the cuckoo egg is alike to a normal egg, it is difficult for the host bird to distinguish between the eggs. The fitness is the difference in solutions, and the new solution is replaced by the randomly chosen if the fitness of the cuckoo egg is greater than the randomly chosen nest, the host bird can distinguish between the host and the cuckoo egg.

Overall, our approach consists of an advanced k-means clustering technique optimized by a bio-inspired algorithm, cuckoo search. Fig. 3 contains the pseudo-code of the proposed framework. The clusters used to classify the users by interest similarity are analogous to the host bird nest and each egg is analogous to a user in the cuckoo optimization algorithm. The initially classified users are considered as host bird eggs. Some random users are selected to initialize the clusters (nests). The clusters are initialized and k-means is implemented to classify the initially selected users as shown in the algorithm. The users not selected are randomly chosen. For each randomly selected user a cluster is selected randomly and the fitness function. According to the fitness function calculated for that user an egg (user) may be detected by the host bird or it may remain in the nest. Once the cuckoo egg hatches then, it tries to throw other eggs randomly out the nest. This is done in the algorithm if the fitness of the cuckoo egg is better than that a predefined percentage of a number of users already present in the cluster.

Fig. 4 shows the above-described approach applied on the Movielens dataset. The Movielens dataset is recorded by reading the file and dataset is divided into clusters using k-means clustering into k clusters so that each cluster has a centroid. The distance between the user and the centroid is calculated, and the user is placed in the cluster whose centroid is the least distance away from him. When all such users have been relocated, the centroids are relocated and the new positions calculated. Consequently, the estimated rating that the user will give is calculated, and framework is optimized using cuckoo search algorithm. We have calculated various evaluation metrics for predicting the accuracy of recommender system such as: mean absolute error, standard deviation, root mean square error and t-value, which are satisfactory for comparing diverse recommender systems with the framework.

4. Experiment results and analysis

We study the public Movielens dataset to conduct the experiments, which is accessible online, having 100,000 ratings by 943 users or participants on 1682 movies, of scale 1–5. As discussed in the previous section, we presented a hybrid framework of k-means and cuckoo search algorithm to achieve an improved movie recommendation system. Framework mentioned in the previous section is applied to the Movielens dataset where data is considered from u1-u5 and U_a-U_b. The Movielens dataset is divided into different files. The dataset is divided into 80% training data and 20% test data for verification of the result. Movies are classified into 19 types viz. action, animation, horror, comedy, etc. which is also mentioned in 'u.item' file. Information about the user is present in 'u.user' file. To check the performance of recommender system framework, various metrics were calculated which include a MAE, SD, root mean squared error (RMSE) and t-value. Results have been shown in tables and graphs to deliver an enhanced understanding of the relationship between various parameters and the number of clusters which helps us to study the performance of our approach. Detailed analysis & behavior of recommender system framework is given below.

1. Place K points into the space specialized by the users that are being clustered. These points represent an initial set of centroids.
2. Assign each user to the group (cluster) that has the closest centroid.
3. When all users have been assigned, recalculate positions of K centroids for each cluster.
4. Repeat steps two and three till the centroids no longer move. This produces a separation of the users into a group (clusters) from which the metric to be minimized can be calculated.

Fig. 1. K-means algorithm approach.

Please cite this article in press as: Katarya R, Verma OP. An effective collaborative movie recommender system with cuckoo search. Egyptian Informatics J (2016), http://dx.doi.org/10.1016/j.eij.2016.10.002

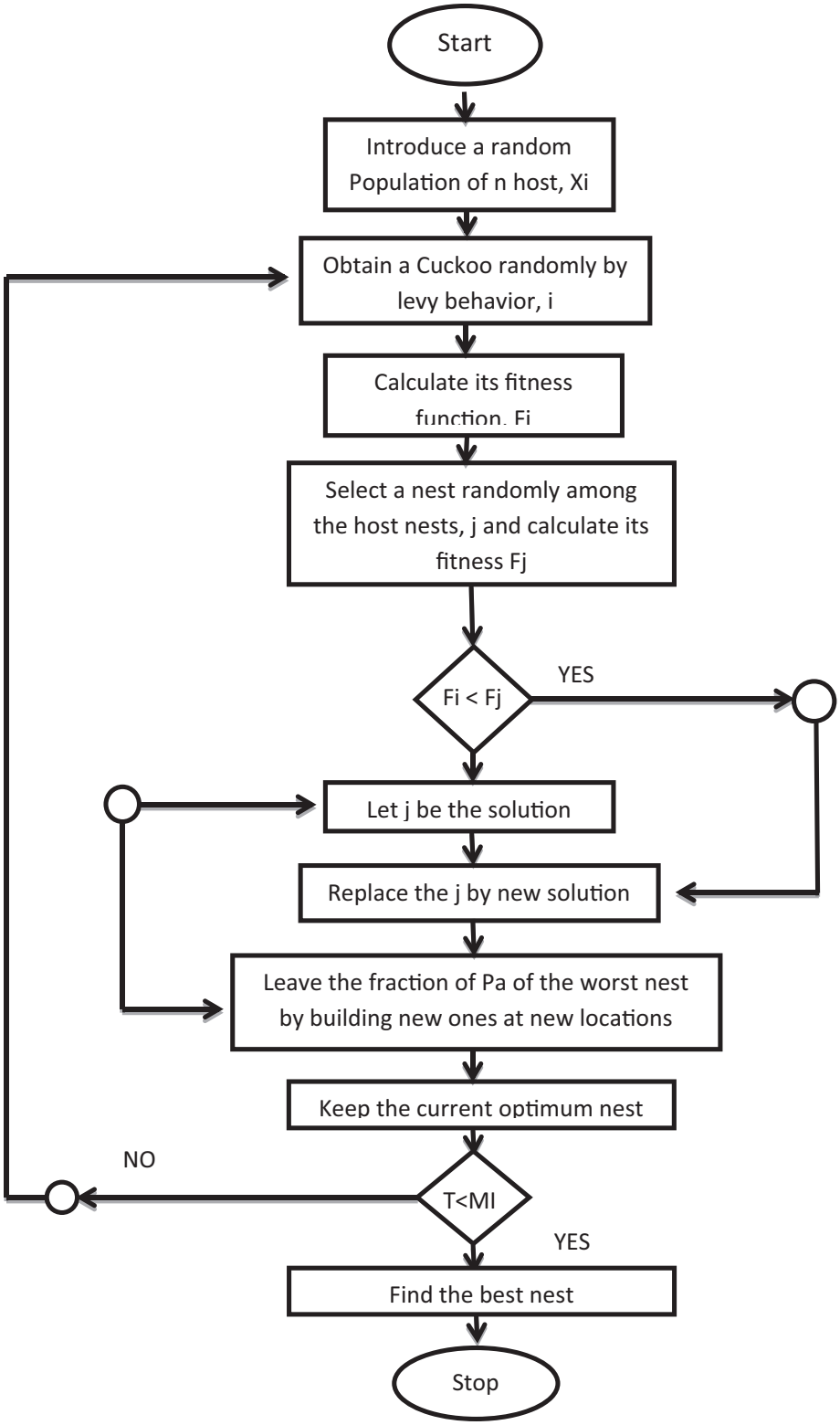

Fig. 2. A flowchart depicting the process involved in the application of cuckoo search algorithm.

4.1. Mean absolute error (MAE)

The mean absolute error is calculated for the Movielens dataset.

$$\mathrm{MAE} = \frac{\sum \left|\widetilde{P}_{i,j} - r_{i,j}\right|}{M} \tag{2}$$

where M is the entire number of expected movies, P_{ij}, represents the predicted value for user i on item j, and rij is the true rating.

$$\mathrm{MAE} = \frac{\mathrm{AE}}{\mathrm{n} * \mathrm{m}} \tag{3}$$

$|e_i| = |f_i - y_i|$, where f_i is the prediction value, and y_i is the true value.

Please cite this article in press as: Katarya R, Verma OP. An effective collaborative movie recommender system with cuckoo search. Egyptian Informatics J (2016), http://dx.doi.org/10.1016/j.eij.2016.10.002

```
Initialization Parameters
k=number of clusters,
n=number of users,
m=number of movies,
itr=number of iterations,
remaining_pool[n]= bool value, remaining_pool[i] representing ith user assigned to any
cluster or not;
no_of_elements_in_clus[i]-number of users present in cluster i
no_of_users_in_remaining_pool=no of users without assigning to any cluster
1. start
2. randomly select some users
3. fill the remaining_poll with the users left
4.  initialize the nests(clusters)
5. for each user i among previously selected
        min_diff=INT_MAX
        for each cluster j
        diff = Euclidian distance between user and cluster
             If diff<min_diff:
                min_diff=diff
                min_index=j
         assign cluster min_index to i
6. while itr>0
       for each cluster i
           For each movie l rated by j
               For each user j belonging to i
                    Calculate mean rating for each movie
7.  For each user i
          For each cluster j
              Calculate diff(i,j)
                Assign user to cluster with min diff
                  Update mean for each movie in assigned cluster
    Itr--
8. from each user in remaining_pool
       Randomly select a user i
           Randomly select a cluster j
              Calculate fitness of the user in that cluster
               If fitness(i,j)>no_of_elements_in_clus(j)*including factor
                   Replace worst fit user with probability p
                    With probability (1-p) add the user to that group without replacing
                       no_of_users_in_remaining_pool--;
9. calculate the predicted rating by each user for each user
10. compare the ratings with actual rating
11. compute the essential factors for efficiency comparison
```

Fig. 3. Pseudo-code of k means-cuckoo search framework.

The MAE has been calculated for different values of k (number of clusters), and the result has been shown in Table 1. It is detected that there is a gradual decrease in the value of MAE as we increase the number of clusters from 4 to 68. When the number of clusters is 4, the MAE is 0.825169 and it drops to 15% as the number of clusters is increased by 64. Thus, we can say that MAE decreases with increase in the number of clusters. The possible description for such behavior is that as we increase the clusters, the closeness between the objects going into the cluster increases. Close elements remain in the same cluster and prediction becomes more and more accurate. As the number of clusters increase, each user gets more choice to be assigned to a cluster, and each cluster may get less number of users assigned to it as the number of clusters increase since the number of users is fixed. The closeness of the user with the cluster assigned to it increases as the number of clusters increase. Hence, the difference between the calculated value and the actual value decrease that decrease the mean absolute error.

4.2. Standard deviation (SD)

The standard deviation is obtained for the Movielens dataset.

$$SD = \frac{\sum_{i=1}^{k}\left\{\sum_{j=1}^{\text{no. of elements in i}}\left(\sum_{l=1}^{m}\sqrt{\frac{(\text{expect l}-\text{mean Kn l})^2}{m}}\right)\right\}}{\text{no. of elements in i}} \quad (4)$$

As the number of clusters increase then standard deviation also decreases in Table 2. At k = 4, the value of standard deviation is 0.235333 which gets approximately halved when the number of clusters is increased by 64. Exceptional performance is observed when standard deviation increases with an increase in the cluster from 28 to 32. Such behavior is attributed to non-uniform nature of the Movielens dataset. As the numbers of cluster increase, each user gets more choice to be assigned to a cluster. Each cluster may get less number of users assigned to it as the number of clusters increase since the number of users is fixed.

4.3. Root mean squared error (RMSE)

The Root Mean Squared Error (RMSE) is a frequently used measure of the deviation between values predicted by a model and the values observed from the environment that is being modeled. The difference between the calculated and observed values are squared

Please cite this article in press as: Katarya R, Verma OP. An effective collaborative movie recommender system with cuckoo search. Egyptian Informatics J (2016), http://dx.doi.org/10.1016/j.eij.2016.10.002

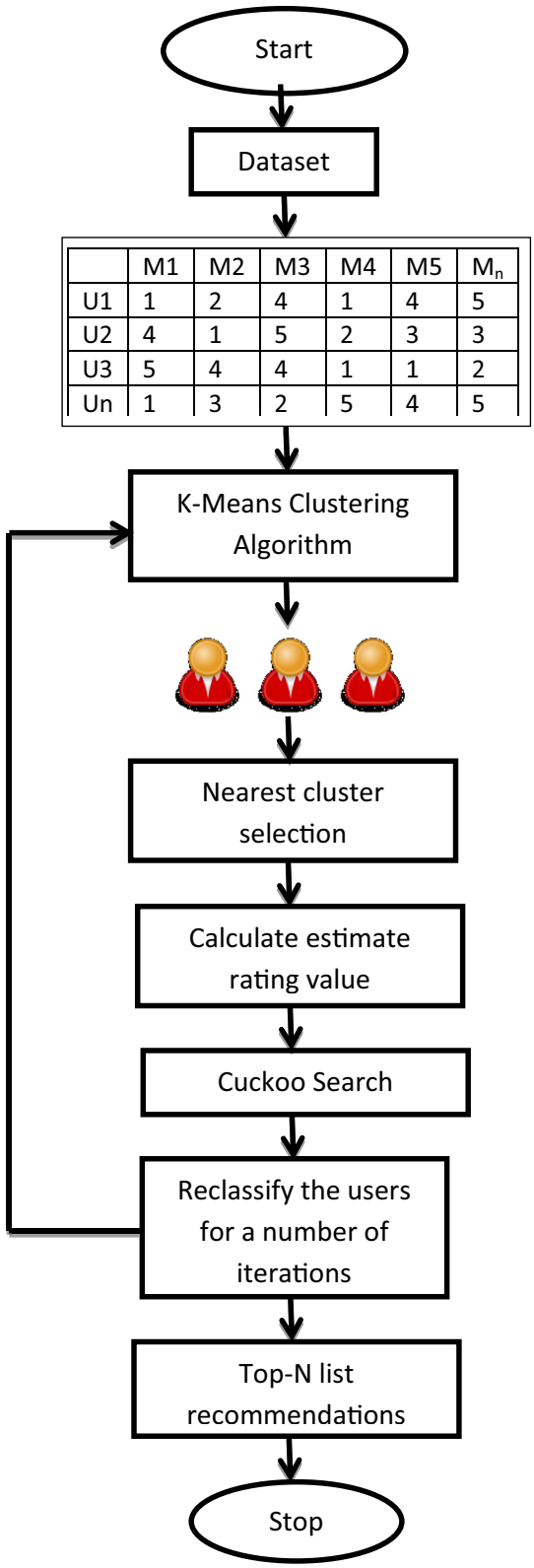

Fig. 4. Movie recommender system framework.

Table 1
MAE for different values of k (number of clusters) between 4 and 68.

S. no.	Numbers of clusters (k)	Mean absolute error
1	4	0.825169
2	8	0.806630
3	10	0.795371
4	12	0.790461
5	16	0.781465
6	20	0.776206
7	28	0.768038
8	32	0.761306
9	36	0.754507
10	40	0.744677
11	44	0.738921
12	48	0.732927
13	52	0.726212
14	56	0.716778
15	60	0.712400
16	64	0.684224
17	68	0.697293

Table 2
Movielens dataset with standard deviation and numbers of clusters.

S. no.	Numbers of clusters (k)	Standard deviation
1	4	0.235333
2	8	0.211460
3	10	0.184073
4	12	0.184289
5	16	0.150996
6	20	0.126688
7	28	0.121020
8	32	0.127900
9	36	0.126319
10	40	0.133401
11	44	0.127355
12	48	0.130083
13	52	0.119024
14	56	0.121663
15	60	0.112847
16	64	0.109447
17	68	0.119283

Table 3
RMSE with numbers of clusters for Movielens dataset.

S. no.	Number of clusters (k)	RMSE
1	4	1.30652
2	8	1.29750
3	10	1.29394
4	12	1.28899
5	16	1.28522
6	20	1.28070
7	28	1.27693
8	32	1.27110
9	36	1.26650
10	40	1.25802
11	44	1.25345
12	48	1.25150
13	52	1.24576
14	56	1.24162
15	60	1.23921
16	64	1.23639
17	68	1.23104

RMSE for each element in test case

$$= \sqrt{\left(\sum(\text{predicted rating} - \text{actual rating})(\textit{predicted rating} - \textit{actual rating})/\text{n}\right)} \quad (5)$$

and then summed n times. n divides the result and then raised to power half. The RMSE of a model prediction on the estimated variable Xmodel is defined as the square root of the mean squared error. Where Xobs has detected values and Xmodel is modeled values at time i.

In Table 3, it is observed that the value of RMSE decreases gradually as we increase the number of clusters. At k = 4, the value of RMSE is 1.3062 which decreases by 6% approx. Such behavior is observed because increasing the number of clusters increase the similarity between the users and the cluster assigned to them.

Please cite this article in press as: Katarya R, Verma OP. An effective collaborative movie recommender system with cuckoo search. Egyptian Informatics J (2016), http://dx.doi.org/10.1016/j.eij.2016.10.002

Table 4
t-value with a number of clusters for Movielens dataset.

S. no.	Numbers of clusters (k)	t-value
1	4	4.12583
2	8	3.99549
3	10	3.36057
4	12	3.39319
5	16	3.39319
6	20	2.81489
7	28	2.79138
8	32	2.79138
9	36	2.81693
10	40	2.81693
11	44	2.81693
12	48	2.81693
13	52	2.81693
14	56	2.81693
15	60	2.81693
16	64	2.81693
17	68	2.81693

Table 5
Comparisons of evaluation metrics with different methods.

Method	Mean	Standard deviation
PCA-SOM	0.98	0.07
SOM-CLUSTER	0.75	0.06
UPCC	0.81	0.11
KMEANS-CLUSTER	0.69	0.10
PCA-KMEANS	0.93	0.12
GAKM-CLUSTER	0.76	0.05
PCA-GAKM	0.98	0.17
K-means-cuckoo (Proposed)	0.68	0.10

4.4. t-value

The t-value for a movie recommendation system is obtained as follows

$$\text{T-value} = \sum_{i=1}^{k}\sum_{j=1}^{k}\left(\frac{\overline{Xi}-\overline{Xj}}{\sqrt{\frac{(SD)^2 i}{(no.\ of\ elements\ in\ i)}+\frac{(SD)^2 j}{(no.\ of\ elements\ in\ j)}}}\right) \quad (6)$$

The t-value depend on upon the values of the mean of different clusters and their standard deviation as shown in Table 4. The change in values of these factors has been explained. The t-value decrease due to the same reasons. However, it is observed to be more or less constant after a fixed number of clusters. The experiment results compared with current existing methods are given in Table 5 [1]. Where all the methods were evaluated on 64 clusters: In PCA-SOM mean value is 0.98. Principal component analysis (PCA) is a scientific procedure that converts correlated variables into a smaller number of uncorrelated variables called principal components. The self-organizing map (SOM) defines a mapping from a higher-dimensional input space to a lower dimensional map space. SOM-Cluster has the mean value as 0.75. UPCC has the average value as 0.81. Kmeans-cluster method has the average as 0.69. PCA with k-means combination as PCA-K-Means has the mean value as 0.93. Genetic Algorithms (GAs) are adaptive heuristic search procedure based on the evolutionary concepts of natural selection and genetics. GAKM-Cluster combination has the mean value as 0.76 and similarly PCA-GA-KM has mean value as 0.98. However, K-means-cuckoo provides best mean as 0.68 when compared to other methods.

As represented in Table 5, it is observed that the mean absolute error is observed to be the least for K-means-cuckoo framework as compared to other methods. Here, a number of clusters used in Table 5 are 64 for every method that was evaluated on Intel i5 processor machine with 4 GB RAM. Thus, the current framework may be used to provide better performance in recommending movies to users. The t-value and RMSE values are significantly low as compared with other approaches thereby proving that the hybrid of k means and cuckoo search algorithm has better performance and accuracy as compared to other methods on Movielens dataset [1]. Table 6 shows the values of mean absolute error obtained by different methods with the various values of k (number of clusters) and Table 7 presents the finish time for various methods.

5. Conclusion and future work

In this article hybrid of k-means and cuckoo search is applied to the Movielens dataset to achieve an improved movie recommendation system. We measured the performance of our approach regarding MAE, RMSE, SD, and t-value. The experiment outcomes on the Movielens dataset discussed indicated that the approach that we discussed provide high performance regarding accuracy and were capable of providing reliable and personalized movie recommendation systems with the specific number of clusters. Evaluation metrics (for a given number of clusters) originated to be lesser than those of other methods. Some limitations of our proposed approach are that if the initial partition does not turn out to work well then, efficiency may decrease. For future work use of various other nature inspired algorithms in place of cuckoo search algorithm can be used. The greatest promising method is the one in which the algorithms used in clustering and optimization provide the best presentation regarding accuracy and speed.

Table 6
MAE values for different approaches for different values of k (number of clusters).

No. of clusters (k)	Mean absolute error (MAE)							
	PCA-GAKM	PCA-SOM	SOM-CLUSTER	UPCC	KMEANS-CLUSTER	PCA-K-MEANS	GAKM-CLUSTER	K-MEANS CUCKOO
8	0.94	1.3	0.78	0.82	0.80	0.92	0.85	0.80
16	0.94	1.1	0.80	0.82	0.77	0.92	0.85	0.78
32	0.94	0.98	0.78	0.80	0.75	0.94	0.86	0.76
64	0.98	0.98	0.75	0.81	0.69	0.93	0.76	0.68

Table 7
Comparison of speed of different approaches for Movielens dataset.

Methods	PCA-GAKM	PCA-SOM	SOM-CLUSTER	UPCC	k-means-Cluster	PCA-K-MEANS	GAKM CLUSTER	K-Means Cuckoo
Speed (in seconds)	29.32	147.73	86.92	179.34	21.25	65.56	325.71	63.22

Please cite this article in press as: Katarya R, Verma OP. An effective collaborative movie recommender system with cuckoo search. Egyptian Informatics J (2016), http://dx.doi.org/10.1016/j.eij.2016.10.002

References

[1] Wang Z, Yu X, Feng N, Wang Z. An improved collaborative movie recommendation system using computational intelligence. J Vis Lang Comput 2014;25:667–75.
[2] Katarya R, Verma OP. A collaborative recommender system enhanced with particle swarm optimization technique. Multimed Tools Appl 2016;75:1–15.
[3] Lu J, Wu D, Mao M, Wang W, Zhang G. Recommender system application developments: a survey. Decis Support Syst 2015;74:12–32.
[4] Bobadilla J, Ortega F, Hernando a, Gutiérrez a. Recommender systems survey. Knowl-Based Syst 2013;46:109–32.
[5] Chen L, Chen G, Wang F. Recommender systems based on user reviews: the state of the art. User Model. User-Adapt Interact 2015;25:99–154.
[6] Konstan Ja, Riedl J. Recommender systems: from algorithms to user experience. User Model. User-Adapt Interact 2012;22:101–23.
[7] Katarya R, Verma OP. Recent developments in affective recommender systems. Phys A Stat Mech Appl 2016;461:182–90.
[8] Isinkaye FO, Folajimi YO, Ojokoh Ba. Recommendation systems: principles, methods and evaluation. Egypt Inform J 2015.
[9] Su X, Khoshgoftaar TM. A survey of collaborative filtering techniques. Adv Artif Intell 2009;2009:1–19. , <http://www.hindawi.com/journals/aai/2009/421425/> [accessed May 21, 2013].
[10] Shi YUE, Larson M, Hanjalic A. Collaborative filtering beyond the user-item matrix: a survey of the state of the art and future challenges. ACM Comput Surv 2014;47:1–45.
[11] Fahad a, Alshatri N, Tari Z, Alamri a, Khalil I, Zomaya a, et al. A survey of clustering algorithms for big data: taxonomy & empirical analysis. IEEE Trans Emerg Top Comput 2014;2. 1–1.
[12] Hartigan Ja, Wong Ma. A K-means clustering algorithm. J R Stat Soc 1979;28:100–8.
[13] Jain aK, Murty MN, Flynn PJ. Data clustering: a review. ACM Comput Surv 1999;31:264–323.
[14] Mukhopadhyay A, Maulik U, Bandyopadhyay S. A survey of multiobjective evolutionary clustering. ACM Comput Surv 2015;47.
[15] Kanungo T, Mount DM, Netanyahu NS, Piatko CD, Silverman R, Wu aY. An efficient k-means clustering algorithm: analysis and implementation. IEEE Trans Pattern Anal Mach Intell 2002;24:881–92.
[16] Yang XS, Deb S. Multiobjective cuckoo search for design optimization. Comput Oper Res 2013;40:1616–24.
[17] Walton S, Hassan O, Morgan K, Brown MR. Modified cuckoo search: a new gradient free optimisation algorithm. Chaos, Solitons Fractals 2011;44:710–8.
[18] Yang X-S, Deb S. Cuckoo search via levy flights, <http://arxiv.org/abs/1003.1594>; 2010.
[19] Yang X-S, Deb S. Cuckoo search: recent advances and applications. Neural Comput Appl 2014;24:169–74.
[20] Yang X-S, Deb S. Cuckoo search via levy flights. Chaos, Solitons Fractals 2013;44:1561–6.
[21] Gandomi AH, Yang X-S, Alavi AH. Cuckoo search algorithm: a metaheuristic approach to solve structural optimization problems. Eng Comput 2013;29:17–35.
[22] Hatami M, Pashazadeh S. Improving results and performance of collaborative filtering-based recommender systems using cuckoo optimization algorithm. Int J Comput Appl 2014;88:46–51.
[23] Lops P, De Gemmis M, Semeraro G. Content-based recommender systems: state of the art and trends. Recomm Syst Handb 2011:1–33. <http://link.springer.com/chapter/10.1007/978-0-387-85820-3_3>.
[24] Pazzani MJ, Billsus D. Content-based recommendation systems 2007:325–41.
[25] Huang Z, Zeng D, Chen H. A comparison of collaborative-filtering algorithms for e-commerce. IEEE Intell Syst 2007;22:68–78.
[26] Ekstrand MD. Collaborative filtering recommender systems. Found Trends® Human-Comput Interact 2010;4:81–173.
[27] Adomavicius G, Tuzhilin A. Toward the next generation of recommender systems: a survey of the state-of-the-art and possible extensions. Adapt Web 2005;69:253–60.
[28] Burke R. Hybrid web recommender systems. Adapt Web 2007:377–408. doi: http://dx.doi.org/10.1007/978-3-540-72079-9_12.
[29] Kim BM. Clustering approach for hybrid recommender system. In: Proc IEEE/WIC Int Conf Web Intell (WI 2003). p. 33–8.
[30] Krzywicki a, Wobcke W, Kim YS, Cai X, Bain M, Mahidadia a, et al. Collaborative filtering for people-to-people recommendation in online dating: data analysis and user trial. Int J Hum Comput Stud 2015;76:50–66.
[31] Xu Y, Yin J. Collaborative recommendation with user generated content. Eng Appl Artif Intell 2015;45:281–94. doi: http://dx.doi.org/10.1016/j.engappai.2015.07.012.
[32] Adomavicius G, Tuzhilin a. Toward the next generation of recommender systems: a survey of the state-of-the-art and possible extensions. IEEE Trans Knowl Data Eng 2005;17:734–49.
[33] Lü L, Medo M, Yeung CH, Zhang Y-C, Zhang Z-K, Zhou T. Recommender Syst 2012:97. , <http://arxiv.org/abs/1202.1112> [accessed August 22, 2014].
[34] Sarwar B, Karypis G, Konstan J, Riedl J. Item-based collaborative filtering recommendation algorithms. Proceedings of the 10th international conference on World Wide Web. ACM; 2001. p. 285–95. doi: http://dx.doi.org/10.1145/371920.372071.
[35] Zhang R, Bao H, Sun H, Wang Y, Liu X. Recommender systems based on ranking performance optimization. Front Comput Sci China 2015;1–11.
[36] Nilashi M, Jannach D, Bin Ibrahim O, Ithnin N. Clustering- and regression-based multi-criteria collaborative filtering with incremental updates. Inf Sci (Ny) 2014;293:235–50.
[37] Guo G, Zhang J, Yorke-Smith N. Leveraging multiviews of trust and similarity to enhance clustering-based recommender systems. Knowl-Based Syst 2014.
[38] Thong NT, Son LH. HIFCF: an effective hybrid model between picture fuzzy clustering and intuitionistic fuzzy recommender systems for medical diagnosis. Expert Syst Appl 2015;42:3682–701.
[39] Kohrs A, Merialdo B. Clustering for collaborative filtering applications. Comput Intell Model Control Autom. IOS Press; 1999. , <http://citeseerx.ist.psu.edu/viewdoc/summary?>.
[40] Xue G-R, Lin C, Yang Q, Xi W, Zeng H-J, Yu Y, et al. Scalable collaborative filtering using cluster-based smoothing. Scalable Collab Filter Using Clust Smoothing 2005:114.
[41] Georgiou O, Tsapatsoulis N. Improving the scalability of recommender systems by clustering using genetic algorithms. Lect Notes Comput Sci 2010;6352:442–9.
[42] Z. Lu, H. Shen, A Security-assured Accuracy-maximised Privacy Preserving Collaborative Filtering Recommendation Algorithm, (2015) 1–9. http://arxiv.org/abs/1506.0001.
[43] Borràs J, Moreno A, Valls A. Intelligent tourism recommender systems: a survey. Expert Syst Appl 2014.
[44] Soares M, Viana P. Tuning metadata for better movie content-based recommendation systems. Multimed Tools Appl 2014:1–22.
[45] Borràs J, Moreno A, Valls A. Intelligent tourism recommender systems: a survey. Expert Syst Appl 2014;41:7370–89.
[46] Ahmad A, Dey L. A k-mean clustering algorithm for mixed numeric and categorical data. Data Knowl Eng 2007;63:503–27.
[47] Pham DT, Dimov SS, Nguyen CD. Selection of K in K-means clustering. Proc Inst Mech Eng Part C J Mech Eng Sci 2005;219:103–19.

Please cite this article in press as: Katarya R, Verma OP. An effective collaborative movie recommender system with cuckoo search. Egyptian Informatics J (2016), http://dx.doi.org/10.1016/j.eij.2016.10.002

An Empirical Study to Assess the Effects of Refactoring on Software Maintainability

Ruchika Malhotra
Department of Software Engineering
Delhi Technological University
Bawana Road, Delhi, India
ruchikamalhotra@dce.edu

Anuradha Chug
School of Information and Communication
Technology GGS IP University
Dwarka, New Delhi, India
anuradha@ipu.ac.in

***Abstract*- Maintenance is the most expensive phase of software and during this process refactoring is performed to improve the code without affecting its external behaviour. This study examines the effects of refactoring on maintainability using five proprietary software systems. Internal quality attributes were measured using design metrics suite whereas external quality attributes such as the level of abstraction, understandability, modifiability, extensibility and reusability were measured through expert opinion. The original versions of software are compared with refactored versions and the changes in quality attributes were mapped to maintainability. The results reveal that refactoring significantly improves the software quality and enhances software life. It was also found that even though refactoring is very tedious and might introduce errors if not implemented with utmost care, it is still advisable to frequently refactor the code to increase maintainability. Results of this study are useful to project managers in identifying the opportunities of refactoring while maintaining a perfect balance between re-engineering and over-engineering.**

Keywords— Refactoring, Software Maintainability, Empirical Validation, Internal Quality Attributes, External Quality Attributes.

I. INTRODUCTION

Maintenance phase starts once the software is delivered to the customer. Software Maintainability is defined as the ease with which the software could be modified. It is measured in terms of Line of Code (LOC) added, deleted and modified in the maintenance phase of SDLC [1]. Software industry today strives hard to find ways and means to improve maintainability of the software's because during the maintenance phase the code is modified many times which results into the deterioration of code quality [12, 13]. Refactoring is a process in which the internal structure of the OO software system is improved and complexity of the code is reduced while ensuring that the external behaviour of the system remains same. There are many methods of refactoring like dead code elimination, clone code removal, extract method, lazy classes, pull up method, push down method, hide methods and renaming method etc. Each method has its effects on the software quality attributes. In this study, we empirically evaluate the repercussions of refactoring on maintainability with the help of their measurable effects on the internal quality attributes as well as the external quality attributes using five proprietary software systems. To the best of the author's knowledge there have been so far no reports to undertake such organized studies which classify various commonly used refactoring methods along with their corresponding quantitative effects on software maintainability. This paper is designed to address this essential and important issue. This study would be beneficial for developers as they can make some reasonable optimized decision regarding the selection of refactoring method. It would also be useful for analysts as before selecting any particular refactoring method and applying it onto the software code, they would be aware about its corresponding enhancement on maintainability. This work would also guide the project managers towards talking an appropriate judgment regarding when to refactor, what to refactor and how much to refactor.

The reminder of this paper is structured as follows: Related work in this field is summarized in Section 2. Section 3 describes the research method adopted in this study. Section 4 described the way internal and external quality attributes are used to assess maintainability. The results are presented in section 5 along with detailed analysis. Validation of the hypothesis presented in section 6 and section 7 concludes the paper with future directions.

II. RELATED WORK

The term Refactoring was introduced by Opdyke [29] in 1990 as the process of restructuring software code in the context of the OO paradigm. Mens et al. [24] compiled a number of empirical studies in which the effects of selected refactoring methods on various software quality attributes were investigated. Bravo et al. [5] developed an automated tool in SOUL (Smalltalk Open Unification Language) which provides an interface and helps developer in identifying bad smells present in the code and subsequently selecting and applying respective refactoring method. Stroggylos et al. [33] studied four open source software and analyzed the effect of refactoring on various software metrics. Ashayeb et al. [3] and Elish and Alshayeb [10] empirically investigated the effects of refactoring on aspect oriented systems. They conclude that although it is expected from refactoring process to improve quality but when it is measured through the OO metrics on real life systems; the results are not as expected. DuBois et al. [8, 9] and Soares et al. [32] proposed the impact of refactoring on quality of the software code and set few guidelines to be considered while refactoring the system. In their study, they observed the effects of refactoring process on cohesion and coupling while adhering to those guidelines. Fowler et al. [12] and [13] have specified 72 different refactoring methods in their book ranging from simple changes such as Extract Local Variable to more complex one such as Extract Class. Kataoka et al. [17] studied effects of refactoring on coupling metrics whereas Geppert et al. [14] empirically investigated the effects

978-1-5090-2029-4/16/$31.00 @2016 IEEE

of refactoring on changeability. Moser et al. [26] strongly recommended refactoring as it improves reusability and validated their statement through an empirical study using XP development environment. Miryung et al. [25] did a field study to explore the challenges faced by the software practioners during implementing the refactoring into the code. Mari et al. [23] argued that there are many dimensions of maintainability and in order to enhance it, each dimension need specific treatment. They promoted the maintainability at three abstraction levels i.e. System, Architecture and Component level. All these studies have not directly evaluated the quantified effects of each refactoring method separately on internal or external software quality attributes; however their cumulative effects have been discussed. In this study, we observed the changes in the internal and external quality attributes due to the application of refactoring and explored the overall impact on maintainability.

III. RESEARCH METHODOLOGY

As shown in Figure 3, in the current study first we selected the refactoring methods based on the bad smell as we did in one of our previous study Malhotra et al. [21]. Values of quality attributes were recorded before and after the refactoring treatment provided into the code. Individual effects of each refactoring method on each of the quality attribute were thoroughly analyzed and cumulative effect of refactoring on maintainability was calculated. Finally Null/Alternate Hypothesis was selected/ rejected based on the cumulative effect of refactoring on quality attributes.

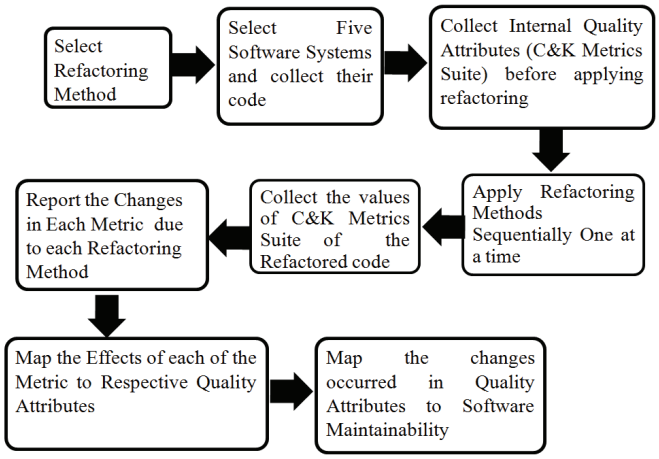

Fig. 1. Research Methodology Adopted

A. Refactoring Methods

Fowler et al. [12, 13] have defined more than 70 methods of refactoring. Few are very simple in nature such as renaming, code extraction or pull-up methods where as few are very complex such as exchanging risky long language idioms with safer alternatives or the code optimization. All refactoring methods were critically examined and following five refactoring methods were selected which either manipulate the methods or redistributes the responsibilities among classes.

- Consolidate Conditional Expression (CCE): This refactoring method combines many consecutive conditional statements into a single statement which contains the corresponding conditional expression.
- Encapsulate Field (EF): If a data field is public and accessed directly in the program it violates data hiding principal of the OO programming. This refactoring process converts public data members in to private data members and provide two extra member functions to get and set their values.
- Extract Method (EM): In this refactoring method first we identify a piece of code that can be grouped together; we extract those groups of statements, put them into a new method and give some name to newly created method.
- Extract Class (EC): If the existing class becomes too complex, this refactoring method creates a new class and move the relevant fields and methods from the source class into the newly created class.
- Hide Method (HM): In this refactoring process, the visibility of member function is changed from public mode to private mode before ensuring that it is not used by any other class in the system.

B. Research Hypothesis

To focus our study on measuring the effects of refactoring methods on maintainability, we set up research hypothesis where H_0 represent Null Hypothesis and H_1 represents alternative Hypothesis. These hypothesizes are further tested for 5% level of significance using two-tail T-Test to ascertain if individual effects of each refactoring methods on internal quality attribute as well as external quality attribute is significant or not.

H_0: A Class on which X refactoring method is applied does not alter its Maintainability.

H_1: A Class on which X refactoring method is applied, its code quality improves which further enhances its Maintainability.

Where X stands for CCE, EF, EM, EC and HM refactoring method.

C. Empirical Data Collection

To analyze the change in values of metrics chosen in this work, their values were computed to validate the hypothesis using five proprietary systems. First two are medium sized and last three are large sized systems. All applications were developed in Microsoft Visual Studio (.NET) software using C# Language as follows:

- FLM is a customize software to handle the File Letter Monitoring System. It is a medium sized software system and consists of 117 classes.
- SMS system is Student Management System which maintains the record of students & teacher for private educational institute. It is a medium sized software system and consists of 129 classes.

- IM System is Inventory Management System which maintains inventory of company at different branch offices in different cities. It is a large sized software system and consists of 143 classes.
- ABP system is Angel Bill Printing software maintains fully editable items list by client itself with generation of a common bill format. It is a large sized software system and consists of 154 classes.
- EASY is a web portal for an Educational Institute which provide study material online. It is a large sized software system and consists of 158 classes.

D. Selection of Internal Quality Attributes

In the current study C&K [6] metrics suite is used for capturing the status of internal quality of the software because it is well established method and this metric suite has also been verified in many empirical studies [1, 2, 4, 6, 11, 19, 20, 22, 34]:

- Weighted Methods per Class (WMC): The WMC metric is calculated as the sum of McCabe's Cyclomatic Complexities of all local methods defined in a class. It is always advisable to have WMC metric value as much less as possible. As suggested by Li and Henry [34] more methods if packed in one class would obviously not only reduce its reuse but the class also becomes more complex which in turn increases maintainability.
- Depth of Inheritance Tree (DIT): The DIT metric measures the maximum inheritance path from any class to the root class. As we increase the depth by implementing inheritance in our code, reusability and maintainability increases only to a certain depth, and beyond certain threshold value of the depth, the code becomes very complex as suggested by Daly et al. [7].
- Number of Children (NOC): The NOC metric is used to measures the breadth present in the class hierarchy. It is counted as the number of immediate child classes derived from the base class. Depth which is measured through DIT metric is always preferred over breadth since it promotes reusability.
- Coupling between Objects (CBO): Used to measure coupling between two classes. Two classes are said to be coupled if methods declared in one class uses methods or instance variables defined in other class. Value of the CBO metric should be kept as lower as possible in order to have a good maintainable system. Sahraoui et al. [30] suggested a maximum CBO metric value to be less than 14 as increased value means there is very high coupling between the classes which would have negative impact on maintainability.
- Response for a Class (RFC): The RFC metric is counted as the number of methods which gets executed whenever a message is communicated to any object of that class. The value of the RFC metric value should be kept as lower as possible to keep the system maintainable. Li and Henry [34] stated that large RFC means more and more methods gets executed in response to any message received by an object of that class and due to this phenomena, tracing an error would be extremely difficult and so the maintenance process.
- Lack of Cohesion of Methods (LCOM): The LCOM metric although named as lack of cohesion but actually measures the cohesiveness present in class. It is calculated by counting the number of disjoint sets of local methods present in the class with respect to the member variables used in each function. As suggested by Basili et al. [4], more cohesive classes are easier to maintain and as the value of LCOM increases, classes become harder to maintain.

It is reported in Singh and Malhotra [31] that all these metrics are negatively correlated with maintainability i.e. less value of the metric means more maintainability in the system.

E. Selection of External Quality attributes

Measuring the external quality attributes are very difficult due to their subjective nature as suggested by Moses et al. [27-28]. However, in the current study following five external quality attributes were carefully selected as they found to be directly correlated with maintainability and measured using expert opinion.

- Understandability: It is measured as the effort required by the developer involved in maintenance activity to recognize the logical concept and applicability of the module. To measure the effect of refactoring on understandability, we noted the time taken (in seconds) by each individual to understand the original code as well as the refactored code. This gives us fair idea about the difference in time taken to understand the original code as well as the refactored code due to application of specific refactoring method. If the time taken by the refactored code after the application of any specific refactoring method is less than the time taken to understand the original code, we claim that the understandability has increased otherwise vise versa.
- Level of Abstraction: It is defined as the amount of complexity by which a software system is viewed. For example the highest level of abstraction is the entire system and lowest level of abstraction is millions of objects, modules, classes etc. To measure this quality attribute, we ask from the participants to rate the effect of specific refactoring on level of abstraction attribute at the ordinal scale of 1 to 10. For example due to the application of CCE, few lines of code are merged into the single line of code and we claimed that level of abstraction has increased.
- Modifiability: It is defined as the efforts required in modifying software during maintenance phase. There are mainly four types of activities (Corrective, Preventive, Perfective and Adaptive) carried out during maintenance phase. The essential difference between maintainability and modifiability is that maintainability is also concerned with the correction of bugs' whereas modifiability is not. Refactoring process is not concerned with correction of bugs as it involves the process of improving only the code quality. To measure

this attribute, participants were asked to judge if the preventive, perfective and adaptive maintenance activity has become easier or difficult due to the application of specific refactoring method and they were asked to rank the change on the ordinal scale of 1 to 10.

- Extensibility: It is defined as the feature that allows its programmers, involved in the maintenance activity to expand or add capabilities with minimal effects on existing system. For example defining new methods, new data types or write new routines to the existing class which is highly coupled with other classes would be extremely difficult. We guided the participants to measure such classes as having very low extensibility and rank them 1 on the ordinal scale of 1 to 10.
- Reusability: It is defined as the ease with which the existing software or class can be used to produce new software systems. For example when we performed extract class refactoring treatment to the existing code, a new class is created which increases the reusability. In an empirical study by Giu et al. [15, 16], extensive guidelines are provided about how to measure and enhance reusability of the code. Participants were asked to give their expert opinion if the reusability has increased or not due to the application of particular refactoring method on the ordinal scale of 1 to 10 for the respective system on which they have been deployed.

IV. Maintainability Assessments

To assess software maintainability, we divided the whole process in to two stages. In first stage, we measured the internal quality attributes as well as external quality attributes. In the second stage final decision about the impact of each refactoring method on maintainability was taken on the basis of the cumulative effects of internal as well external quality attributes as per the framework suggested by Kitchenham et al. [18]. Source codes for the selected software were collected before as well as after refactoring methods were applied which enables us to observe the change in the values of the C&K metrics suite due to the application of specific refactoring method. At a given time only one refactoring method was applied on only one class. The process was repeated each time for all refactoring methods one by one for each system selected in the study. Change in the values of the C&K metrics were further mapped to maintainability using the outcome of existing studies [1, 2, 4, 6, 11, 19, 20, 22, 34]. Roadmap presented in Fig-2 was used to map any change in the values of the C&K metric suite to its subsequent effects on maintainability. In second part, we measured external quality attributes such as Understandability, Level of Abstraction, Modifiability, Extensibility and Reusability through expert opinion. There were 40 individuals who participated in this empirical study for assessing the external quality attributes. Experts were divided into five teams and eight participants were deployed for each of the software. All participants were required to fully understand the functionality of respective software system. They have experts understanding about the nature of external quality attribute under measurements. They were also familiar with the maintenance of the system. They were independently asked to rate external quality attributes on the ordinal scale of 1 to 10.

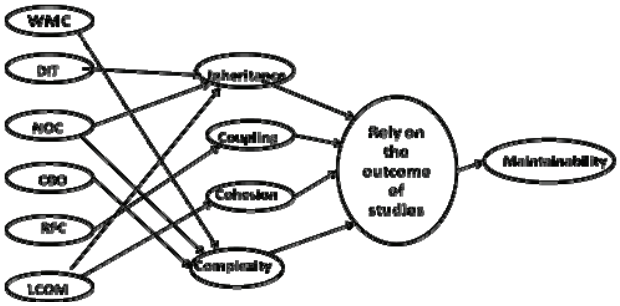

Fig. 2. Roadmap to measure maintainability from the C&K metric suite

Participants were not exposed to any kind of influence, and discussion among themselves were not allowed. For each refactoring method selected in the current study, two sets of each system were made. For example when CCE was applied on FLM system, we get the set as $FLM_{Original}$ and FLM_{CCE}. Similarly, when we applied Extract Method on IM system, we make the set as $IMS_{Original}$ and IMS_{EM} system. We made such set by applying each refactoring method on each system one at a time. In this way we applied each refactoring method CCE, EF, EC, EM, and HM onto each system FLMS, SMS, IMS, ABILL, EASY and we get 25 such pairs of original code as well as refactored code. We seeded eight pre-decided errors (error seeding) into the original code as well as refactored code of each set. The source code of each set was given to respective participants and they were asked to find the errors and rectify them. When they were conquering the problem, their professional behaviour was observed. The starting time and finish time taken by each individual in identifying the problem was noted down in seconds. Difference in the time taken to understand the original code as well as refactored code is considered as understanding Time. The mean change in the value of understanding Time was calculated for each of the refactoring method. Next we noted the time taken to rectify each of the error. Mean Rectifying time for each system was also calculated and considered as Modifiability. At the end, fixed numbers of questions were given to each individual and they were asked to rate the external quality attributes on ordinal scale of 1 to 10 for original as well as refactored code.

V. RESULTS AND ANALYSIS

In this section first we calculate the changes observed in the values of internal quality attributes and re-ascertain ourselves whether the changes are significant at 0.01 and 0.05 level of significance using two-tail T-test. Then we analyse the change in the external quality attributes and check them on 0.01 and 0.05 level of significance using two-tail T-test. Finally we validate the hypothesis defined in section 4.2 on the basis of the cumulative changes observed in the internal as well as external quality attributes due to the application of specific refactoring method.

A. Change in Internal Quality Attributes

Change in the values of each C&K metric for each class corresponding to the application after applying refactoring method was tabulated. A comprehensive report was prepared for each refactoring method to its subsequent effects on each system and presented in Table 1. Mean change in the values of the C&K metrics for each refactoring method was calculated by dividing value of the total change by number of classes in that system. To see whether the changes in C&K metrics due to the application of specific refactoring method are significant or not, the two tail T-test was applied on the final compiled data. Changes in the value of each C&K metrics are divided into five categories i.e. positive significant at 0.01 level, positive significant at 0.05 level, no change, negative at 0.05 level and negative at 0.01 level and presented in Table 2. The up direction of arrow represents the positive effect of refactoring on the C&K metric suite whereas down arrow represents the negative effect of specific refactoring method on the C&K metric suite.

TABLE I. EFFECT OF REFACTORING ON C&K METRICS

Refactoring method	**WMC**	**DIT**	**NOC**	**CBO**	**RFC**	**LCOM**	**LOC**
CCE	↑↑	–	–	–	↑	↓↓	↓↓
EF	↑↑	–	–	–	↑↑	↓↓	↑
EM	↑	–	–	–	↑	↓↓	↑
EC	↓↓	↑↑	↑↑	↑↑	↓↓	↑	↑↑
HM	–	–	–	–	–	–	–

↑denotes change in the metric is significant at 0.01
↑↑ denotes change in the metric is significant at 0.05
– means there is no change is observed in metric
↓↓ denotes significant change in metric at 0.05 in inverse manners
↓ denotes significant change in metric at 0.01 in inverse manners

The following observations were made from Table I.

- CCE method significantly increases the WMC metric and significantly reduces the LOC metric and LCOM metric.
- EF method significantly increases the WMC metric and RFC metric, no change observed on the DIT metric, the NOC metric and the CBO metric. EF method has negative effect on the value of the LCOM metric.
- EM method increases the WMC metric and the RFC metric but significantly reduces values of the LCOM metric. No effects on the value of DIT metric, the NOC metric and the CBO metric were observed.
- EC method significantly increases values of the DIT metric, the NOC metric and the CBO metric.
- HM does not have direct effect on any of the C&K metrics.

B. Change in Internal Quality Attributes

Experts were divided into five teams and eight participants were deployed for each software systems. Each participant was asked to apply one refactoring method at a time on one class of the specific system on which he/she was working. After the application of refactoring method, the participant was asked to compare original code with the refactored code and rate the external quality attribute on the ordinal scale of 1 to 10. The mean change in each external attribute due to the application of each refactoring method was also calculated. To check whether the changes are significant or not, they all were again checked for significance level at 0.01 and 0.05. If the improvement in the external quality attribute was significant, it is marked as positive, otherwise negative. Table 3 presents the mean effect of each refactoring method on each external quality attribute where ↑ represent improvement and ↓ represents deterioration.

TABLE II. EFFECTS OF REFACTORING ON EXTERNAL QUALITY ATTRIBUTE

Refactoring Methods	Under-standability	Level of Abstraction	Modifiability	Extensibility	Re-usability
CCE	↓	↓↓	↑	↑	↑
EF	–	↓	–	↑	–
EM	↑↑	↓↓	↑↑	↑	↑↑
EC	↓↓	↓↓	–	↓↓	↑↑
HM	↑	–	↑	↑	–

↑ denotes change in the metric is significant at 0.01.
↑↑ denotes change in the metric is significant at 0.05.
– means there is no change is observed in metric.
↓↓ denotes change in the metric is significant at 0.05 but in inverse manners.
↓ denotes change in the metric is significant at 0.01 but in inverse manners.

When we map the external quality attributes to maintainability, we noted that the lower the level of extraction, better the maintainability and higher the level of understandability, modifiability, extensibility and reusability, better the maintainability. The following observations were made from Table II.

- CCE method significantly improves all external quality attributes except understandability. It was reported by the participants that when numbers of lines are replaced by single statement, although code becomes compact but understandability suffered.
- EF method has positive effects on extensibility but has no significant effect on understandability, modifiability and reusability. However, the level of abstraction has negative effect.
- EM refactoring process introduces new methods which increases reusability. Abstraction level reduces as one large complex method is converted into smaller one. Code becomes more understandable where improvement on extensibility was observed.
- EC method reduces understandability due to the newly created class which is strongly coupled with existing classes. Abstraction level reduces as two or more overlapping methods are moved up into common method which is shared by them. Adding functionalities becomes more difficult. As anticipated, reusability increases due to the newly created method.
- In HM refactoring process, unnecessary details are hidden which slightly increases understandability as reported in [3]. No effect on abstraction level is observed. Increase in modifiability and extensibility is also observed by the participants.

VI. Validation of Hypothesis

To assess the effects of internal quality attributes on maintainability, we compare the results in this study with the finding of studies [1, 2, 4, 6, 11, 19, 20, 22, 34] and map the changes observed in C&K metrics to maintainability using the outcomes of all these studies. External quality attributes were also given equal weightage to assess final effects of refactoring on software maintainability and depending upon the final scenario based on cumulative effects, Null / Alternate Hypotheses were rejected or accepted.

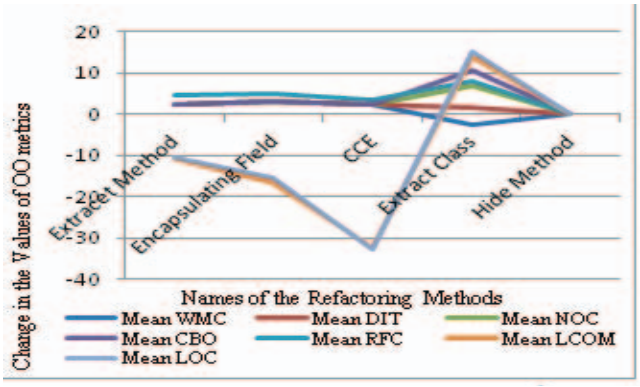

Fig. 3. Affects of Refactoring on C&K metric suite

A. CCE Hypothesis

Effect of the CCE refactoring method on the value of the LOC metric is negative for all systems as visible through Table I. Few previous studies [1, 20, and 34] also found that the LOC metric has direct negative correlation with maintainability i.e. as the LOC metric reduces, the maintainability increases. This newly added method accesses existing instances of data member for FLMS, SMS, IMS, ABILL and EASY systems, which results in reduction of LCOM value by 5%, 10%, 7%, 9% and 3% respectively as the classes becomes more cohesive with an overall increase in maintainability. An increase in the value of WMC the metrics was also observed with regards to all the software systems. For medium systems, more than 2% increase in WMC was observed, whereas less than 1% increase was observed for larger systems. The findings of the previous studies relied by us states that any increase in the value of the WMC metric reduces maintainability. Increase in the value of RFC metric was also observed for all software systems which as per previous studies reduce maintainability. No effect on the mean values of the DIT metric, the NOC metric and the CBO metric was observed. Overall, the WMC and RFC metric reduce maintainability, the LOC and LCOM metric increases maintainability whereas DIT, NOC and CBO does not have any impact due to CCE refactoring method. As far as the external quality attributes are concerned, application of the CCE refactoring method has shown improvement in all of them except understandability. Due to the creation of new method, level of abstraction decreases, class becomes more extensible and more reusable. Participants were of the opinion that although the CCE refactoring method reduces understandability, however, it can be overcome by giving some meaningful self-explanatory name to the newly created method. Rest all external attributes increases maintainability. We reject the Null Hypothesis, accept Alternate Hypothesis and concluded that the CCE refactoring method certainly increases maintainability.

B. EF Hypothesis

The values of DIT, NOC and CBO metrics remains unchanged after the application of EF refactoring method which is visible from Table I. The mean value of the WMC metric was increased by 4.71 %, 2.76%, 2.09%, 1.48% and 2.07% for FLMS, SMS, IMS, ABILL and EASY systems respectively. Values of the LOC and RFC metrics were also increased which is attributed to two newly created methods. Reduction in the value of the LCOM metrics was also observed. Overall, the WMC, LOC and RFC metrics reduces maintainability; the LCOM metric increases maintainability whereas DIT, NOC and CBO do not leave any impact on maintainability due to the application of EF refactoring method. On external quality attributes, small increase in extensibility was observed due to the fact that public data members were converted into private, which are neither visible outside the class nor do they interfere in the event of addition of new functionalities. Level of abstraction reduced due to the creation of two new methods. Even though class becomes secure as public data members are converted into private, no effect on reusability, understandability and modifiability was observed. While evaluating the cumulative effects, we found positive effects of LCOM and negative effects of WMC, LOC and RFC on maintainability. No effect on maintainability was observed due to the DIT, NOC and CBO metrics. Stroggylos et al. [33] also found that if any method is added into a class, it in turn add responsibilities to the class and it further becomes more complex and harder to maintain. There was no significant improvement found in any of the external attributes. Accordingly Null hypothesis was accepted, Alternative hypothesis was rejected with the conclusion that EF refactoring method reduces maintainability. Despite the adverse effects on maintainability, the software practitioners are advised to adopt the EF refactoring method should be adopted whenever there is a requirement of making the class more secure.

C. EM Hypothesis

This refactoring method offers several benefits by decomposing a large method into smaller ones. In this refactoring method no new class is created. No change was observed in the values of DIT, NOC and CBO metrics as revealed from Table 1. Increase in the value of WMC metric was observed due to newly created methods in all systems. For medium systems, WMC was increased by more than 2% whereas for large systems the same was increased by less than 1%. Overall, the WMC, RFC and LOC metrics slightly increases, while the CBO, DIT and NOC metrics remains unaffected and LCOM reduces significantly. Though increased values of the WMC, RFC and LOC metrics reflects

negative impact on maintainability, the LCOM metric makes the class more cohesive and improves the overall maintainability. This can be understood by beautiful example of a house where although walls made in the house consumes space but it clearly separate each room and overall house becomes more organized. The views are further validated through the change in external quality attributes as reported by the participants. The code becomes more readable and the next developer need substantially less time in investigating the existing code before modifying it during maintenance phase. The class not only became understandable, readable and modifiable but newly created methods also increase the reusability of the class. Level of abstraction reduces as one complex object/class/method is replaced by many. An improvement in extensibility was also observed by the participants. Hence we accepted Alternative Hypothesis, rejected Null Hypothesis and concluded that the EM refactoring method increases maintainability.

D. EC Hypothesis

In this refactoring method, a new class is created which moves the relevant fields and methods from source classes into the new class. From Table I it is quite visible that mean values of DIT, NOC and CBO metrics increases. The increase in the mean value of NOC is very marginal for medium as well as for large systems. However, reduction in the values of the RFC, WMC and LOC metrics was also observed. Further, the EC refactoring method increases the coupling between the classes because the extracted class and source class shares same data members. Aggarwal et al. [2] has empirically validated that any increase in coupling would increase complexity, reduce encapsulation, potential reuse and limit the understanding and maintainability of the software systems. Few other studies [20 and 41] also found reduction in maintainability due to the increased values of DIT, NOC and CBO metrics. In this method, common attributes and methods of many classes are extracted into a new class with sole aim to achieve reusability. Overall, reduction in the value of LOC metric was also observed.

As far as external quality attributes are concerned, except reusability, all other suffer badly. In this study, we found a cumulative effect of this refactoring method has adverse effects on maintainability at the cost of gaining reusability. Hence we accepted the Null Hypothesis, rejected Alternate Hypothesis and concluded that EC would certainly have negative effect on maintainability. Because of these observations, the software practitioners are advised to make cautious choice between maintainability versus reusability.

E. HM Hypothesis

This refactoring method only changes the visibility of the member function from public mode to private mode after ensuring that it is not used by any other class. This refactoring method neither creates new classes, nor redistributes responsibilities among classes/methods. Findings of the current study are in full agreement with Elish and Alshayeb [10] that C&K metrics suite was unaffected by the application of this method. Even though this method was found to be un-related to the C&K metric suite and maintainability, yet it is an important refactoring process which ensures that codes follow data hiding principle which is important part of encapsulation. It is always advisable to make use of Hide Method refactoring process frequently to constantly enforce the principle of object oriented paradigm into the code. The internal quality attributes were not affected, however, slight improvements in two external quality attributes were observed. Increase in extensibility was also observed as few methods were made to hide which do not interfere with the new functionalities. Understandability also increases, as unnecessary details were hidden to the programmer due to the application of HM method. Following calculations of the cumulative effects, we rejected the Null Hypothesis; accepted the Alternate Hypothesis and conclude that HM method certainly increases maintainability.

VII. CONCLUSION & FUTURE DIRECTIONS

The effects of few refactoring methods on maintainability have been investigated in the current study. Values of the carefully selected internal as well as external quality attributes were calculated before and after refactoring treatment provided into the code. Changes in the values quality attributes were critically examined and further mapped to maintainability. Five proprietary software systems were used to analyze and empirically validate the effects of refactoring process on maintainability with under mentioned findings:

CCE method increases maintainability with respect to internal as well as external quality attributes. During this refactoring process, understandability suffers badly which can be overcome by giving self explanatory, well understood name to the newly created method. EF method reduces maintainability but make the class more secure as the public data members are converted into private however, practitioners should make cautious choice between securities versus maintainability. In EM refactoring, classes becomes clearer, crisper and organized with associated increase in software maintainability. In EC refactoring method, newly created class is highly coupled with existing class which deteriorates the code quality and maintainability of the system, however achieves substantial improvement in reusability. The practitioners are advised to make cautious choice between reusability and maintainability. Although, HM method does not change any internal quality attribute, slight improvement in external quality attributes were observed which further improves the maintainability. Additionally, this refactoring process is always advisable as OO principles are injected into the code.

Programmers cannot blindly apply refactoring each and every day; instead enough time should be spent to find pros and cons of refactoring process before final call is made. We would also like to mention very interesting observation that decision about refactoring should not be made only on the basis of changes in the values of the C&K metrics. Instead, while calculating the final impact of refactoring on software maintainability, both internal as well as external quality attributes should be given equal weightage. The current study is carried on two medium and three large sizes proprietary software. As part of future work we would like to verify the

results on number of large open source large systems. In the current work, we have applied one refactoring method at a time and observed its effect. A possible future direction could be to apply two or more refactoring methods simultaneously and observe its collective effects on various quality attributes. The task becomes more challenging if the refactoring methods are conflicting in nature, for example Pull-Up Method increases reusability and maintainability but at the cost of augmented testing efforts. Reengineering is always advisable as it has many advantages but over-engineering has its own repercussions such as management of conflict, code reviews becomes difficult, code churns, and adverse effects on quantitative values of design metrics. In today's fast competing world there is a strong urge to draw a fine line between reengineering and over–engineering.

REFERENCES

[1] Aggarwal, K.K., Singh, Y., Kaur, A. and Malhotra, R. Empirical Study of Object-Oriented Metrics, Journal of Object Technology, 5(8), 149-173, 2006

[2] Aggarwal, K.K., Singh, Y., Chandra, P., and Puri, M., Measurement of Software Maintainability Using a Fuzzy Model, *Journal of Computer Sciences,* 1(4), 538-542

[3] Alshayeb, M., Jamimi H.A., Elish M.O. Empirical taxonomy of refactoring methods for aspect-oriented programming, *Journal of Software Maintenance and Evolution : Research and Prectice, Wiley Online Library*, 1-25

[4] Basili, V.R, Briand, L. and Melo, W.L. A Validation of Object-Oriented Design Metrics as Quality Indicators, *IEEE Transaction on Software Engineering, 22*(10), 751-761.

[5] Bravo, F. A Logic Meta-Programming Framework for Supporting the Refactoring Process, *Master Thesis*, Vrije University, Brussel, 2003

[6] Chidamber, S. and Kemerer, C. A Metrics Suite for Object Oriented Design, *IEEE Transactions on Software Engineering, 20*(6). 476-493.

[7] Daly, J., Brooks, A., Miller, J., Roper, M., and Wood, M., An empirical study evaluating depth of inheritance on the maintainability of object-oriented software, Empirical Studies of Programmers: Sixth Workshop (Alexandria, Virginia, 1996), 39-58.

[8] DuBois, B., Demeyer, S. and Verelst, J. Refactoring- Improving Coupling and Cohesion of Existing Code, *Proceedings of 11th Working Conference on Reverse Engineering* (Neatherland, 2004), 144-151.

[9] DuBois, B., and Mens, T., Describing the impact of refactoring on internal program quality, *Proceeding of International Workshop on Evolution of Large-scale Industrial Software Applications,* Netherlands, 2003, 37-48.

[10] Elish K.O. and Alshayeb, M. Investigating the Effects of Refactoring on Software Testing Effort, *Proceedings of Asia-Pecfic Software Engineering Conference APSEC*, (Penang, 2009). 29-34.

[11] Elish, M.O. and Elish, K.O. Application of TreeNet in Predicting Object-Oriented Software Maintainability: A Comparative Study, *European Conference on Software Maintenance and Reengineering, (*Kaiserslautern, Germany, 2009), 69-78.

[12] Fowler, M. *Refactoring: Improving the Design of Existing Code,* Addison-Wesley Longman Publishing Co., Boston, MA, USA, 1999.

[13] Fowler, M., Refactoring Home Page at URL refactoring.com Hosted by ThoughtsWorks

[14] Geppert, B., Mockus, A. and Robler, F. Refactoring for Changeability: A way to go?," Proceeding of 11th IEEE International Software Metrics Symposium (Como, Itly, 2005),2013.

[15] Gui, G., Scott, P.D.: Measuring Software Component Reusability by Coupling and Cohesion Metrics. Journal of Computers, 4(9): 797-805, (2009) doi:10.4304/jcp.4.9.797-805

[16] Gui, G., Scott, P.D.: Ranking reusability of software components using coupling metrics. Journal of Systems and Software, 80(9),1450-1459 (2007),

[17] Kataoka, Y., Imai, T., Andou, H. and Fukaya T., A Quantitative Evaluation of Maintainability Enhancement by Refactoring, *Proceedings of International Conference on Software Maintenance,* (Montréal, Canada, 2002), 576-585.

[18] Kitchenham, B., Pfleeger, S.L. and Fentom, N.E., Towards a framework for software measurement validation, *IEEE transction on Software Engineering*, 21(12), 929-944.

[19] Koten, C.V., Gray, A.R., An application of Bayesian network for predicting object-oriented software maintainability, *Information and Software Technology*, 48(1), 59-67.

[20] Malhotra, R. and Chug, A. Software Maintainability Prediction using Machine Learning Algorithm, *Software Engineering : An International Journal, 2*(2), 19-36.

[21] Malhotra, R. Chug, A. and Khosla *P*. Prioritization of classes for refactoring:A step towards improvement in software quality. *In Proceedings of the Third International Symposium on Women in Computing and Informatics* (2015), pp. 228–234, Kotchi, India.

[22] Malhotra, R. and Chug, A Bench-marking Framework for Maintainability Prediction of Open Source Software using Object Oriented Metrics, *International Journal of Innovative Computing, Information and Control,* 12(2), (2016), pp.615-634.

[23] Mari, M. and Eila, N. The Impact of Maintainability on Component-based Software Systems, *Proceedings of 29th Euromicro Conference* (Antalya, Turkey*, 2003)*, 25-32.

[24] Mens, T. and Tourwe, T. A Survey of Software Refactoring, *IEEE Transactions on Software Engineering, 30*(2). 126-139

[25] Miryung, K., Zimmermann,T. and Nagappan,N., A Field Study of Refactoring Challenges and Benefits, *In Proceedings of the 20th International Symposium on Foundations of Software Engineering* (Cary, North Carolina, 2012), 978-989

[26] Moser, R., Sillitti, A., Abrahamsson, P. and Succi, G. Does refactoring improve reusability?, *Proceeding of 9th International Conference on Software Reuse* (Torino, Italy, 2006), 287-297.

[27] Moses, J. Bayesian probability distributions for assessing subjectivity in the measurement of subjective software attributes *Information and Software Technology*, 2000, 42(8): 533‑546

[28] Moses, J. and Malcolm, F. Tests for consistent measurement of external subjective software quality attributes*, Empirical Software Engineering,* 2008, 13(3): 261-287, http://dx.doi.org/10.1007/s10664-007-9058-0

[29] Opdyke, W. Refactoring: A Program Restructuring Aid in Designing Object-Oriented Application Frameworks, *PhD Thesis,* Univ. of Illinois at Urbana-Champaign, 1992.

[30] Sahraoui, H.A., Godin, R. and Miceli, T. Can metrics help to bridge the gap between the improvement of OO design quality and its automation, Proceedings of International Conference Software Maintenance, (San Jose, CA, 2000). 154-162.

[31] Singh, Y. and Malhotra, R. *Object Oriented Software Engineering*, PHI Learning Private Learning Limited, New Delhi, India, 2012.

[32] Soares, G., Gheyi, R., Serey, D. and Massoni, T., Making program refactoring safer, *ICSE '10 Proceedings of the 32nd ACM/IEEE International Conference on Software Engineering* (Cape Town, South Africa, 2010), 521-522

[33] Stroggylos, K. and Spinellis, D. Refactoring - Does it improve software quality?, *Proc. 5th International Workshop on Software Quality*, (Ho Chi Minh City, Vietnam, 2007), 10-16.

[34] Wei, Li. and Henry, S. Object Oriented Metrics Which Predict Maintainability, *Journal of Systems and Software, 23(*2), 111-12

International Research Journal of Engineering and Technology (IRJET) e-ISSN: 2395 -0056
Volume: 03 Issue: 07 | July-2016 www.irjet.net p-ISSN: 2395-0072

Analysis of Various I/O Methods for Large Datasets in C++

Kushaagra Moghe[1] and Hemang Sarkar[2]

[1,2]*Mathematics and Computing Engineering, Delhi Technological University, New Delhi, 110042, India*

Abstract - *As the size of a dataset increases, the selection of suitable input and output methods for reading and writing the data becomes more and more important. This is mainly on account of the variations in the speeds at which different I/O methods function in C++. The Operating System and the processor of the machine substantially affect these speeds too. In this paper, the variations due to the OS (Windows or Linux) and the size and type (numbers or characters) of the dataset are analysed. The analysis is done on very large random text files generated by using a PRNG (pseudo random number generator). When dealing with huge datasets, time becomes an important constraint and so using the results of this analysis, a suitable input/output method can be selected depending on the type of the file (numeric or character), the operating system of the machine and the size of the data set.*

Key Words: ASCII, CLOCKS_PER_SEC, freopen, PRNG, stdin, stdout

1. INTRODUCTION

C++ is a cross-platform object oriented programming language and has ubiquitous uses in a lot of facets of the modern tech world. Reading from a file and writing to a file are one of the most used features in any programming language, thus minimising the time taken in these two is of immense importance.

2. I/O IN C++

Due to its backward compatibility with C, we can use the various cstdio functions for reading and writing in C++ too. In the experiments performed, we compare the speeds of the functions in cstdio and the iostream objects in C++. We also incorporate custom Fast I/O functions in the analysis.

2.1 Input methods

The standard input stream is the default pre-connected communication channel for data. This input stream is known as stdin and by default is directed from the keyboard. In our experiments, we redirect stdin using the freopen function to access the data files within the system.

In this paper, we compare the speeds of the various input methods for reading numbers and characters from a file.

2.2 Output methods

The standard output stream is the default communication channel for rendering output from the computer program. This output stream also known as stdout directs the data to the text console. We use freopen to redirect this data stream to write directly to data files.

In this paper, we compare the speeds of the various output methods for writing numbers and characters to a file.

2.3 Fast Input/Output methods

1. **Fast cin and cout-** By default iostream objects and cstdio streams are synchronized and this makes cin and cout comparatively slower than scanf and printf. To resolve this we toggle this synchronization off using:

```
std::ios::sync_with_stdio(false);
```

This considerably improves the speed performance of cin and cout.

2. **Custom fast input/output functions-** By using getchar and putchar, we can make custom I/O functions which have extremely good speed performances. This function for reading numbers is:

```
long long int fast_input(void)
{
    char t;
    long long int x=0;
    long long int neg=0;
    t=getchar();
    while((t<48 || t>57) && t!='-')
        t=getchar();
    if(t=='-')
        {neg=1; t=getchar();}
    while(t>=48 && t<=57)
    {
        x=(x<<3)+(x<<1)+t-48;
        t=getchar();
    }
    if(neg)
        x=-x;
    return x;
}
```

The corresponding function for printing numbers is:

```
void fast_output(long long int x, int mode)
{
    char a[20];
    long long int i=0,j;
    a[0]='0';
    if (x<0) {putchar('-'); x=-x;}
    if (x==0) putchar('0');
    while(x)
    {
        a[i++]=x%10+48;
        x/=10;
    }
    for(j=i-1;j>=0;j--)
    {
        putchar(a[j]);
    }
    if (mode==0) putchar('\n');
    else putchar(' ');
}
```

We have an option of using getchar_unlocked which is faster than scanf and getchar but is deprecated in Windows. It is a thread unsafe version of getchar and there is no input stream lock check in this.

3. EXPERIMENT

We perform the experiment on two different machines with the following specifications:

1. Intel i5-3230M CPU @ 2.60 GHz with 8.00 GB RAM and x64 based processor running Windows 10 Professional edition.
2. Intel i5-4210U CPU @ 1.70 GHz X4 with 4.00 GB RAM and x64 based processor running Ubuntu 16.04 LTS.
3. Compiler used- GNU GCC following the C++11 ISO C++ standard on Code Blocks IDE version 16.01.

3.1 Random Datasets

We use rand( ) function defined in the header <cstdlib> which is a PRNG (pseudo random number generator). We write the text generated to .txt files. The rand( ) function needs to be seeded in order to produce better results. This is done as:

```
srand(time(NULL));
```

The time( ) function is defined in the header <ctime> which returns the current calendar time and this current time is used as a seed to the rand( ) function.
For writing to text files, we use the freopen( ) function as:

```
freopen("output.txt", "w", stdout);
```

For reading from text files, we use the freopen( ) function as:

```
freopen("input.txt", "r", stdin);
```

The freopen function with mode “w” (for writing) redirects whatever we print to the file specified as the first argument instead of the text console.

Similarly, if we specify the second argument as “r” (for reading), stdin is redirected to take data from the file specified as the first argument instead of the keyboard.

For the numeric text files, we generate random numbers between 0 and 10^{18} digit by digit and store them in an appropriate sized array. For the character text files we generate random characters whose ASCII values lie between 32 and 122.

3.2 Time measurement

To accurately measure the time taken to only read or write (and not include the time taken to open the file and other parts of the code), we use:

```
clock_t t;
t = clock();
for(int j = 1; j < 1000000;j++)
    printf("%lld ",a[j]);
t = clock() - t;
printf ("%.9lf\n",((double)t)/CLOCKS_PER_SEC);
```

clock_t is a clock type which represents clock ticks of the processor. The clock( ) function returns the approximate processor time used by the process. We make two calls to this function- once before we start printing and once after the printing is done. The difference between these values instances gives us the approximate processor time consumed for printing to the file.

CLOCKS_PER_SEC is a constant macro which gives us the number of processor clock ticks per second. We need to divide the processor time consumed by CLOCKS_PER_SEC to get the time taken to execute the for loop (in seconds). The resultant double value thus printed gives us the approximate time duration of the printing process in seconds.

In a similar way, we can find the time taken to read values from a .txt file.

3.3 Results

To get substantially accurate results, we measure the time taken in five different instances and then calculate their

average. We perform this for each input and output method in both Windows 10 and Ubuntu 16.04.

We tabulate and graphically present the results below:

3.3.1 Reading Numbers

Table -1: Comparison of reading speeds of numbers in Windows

Input size	Time (in seconds)			
	cin	Fast I/O	scanf	Fast cin
50,000	0.26180	0.01520	0.01820	0.04640
1,00,000	0.31740	0.08380	0.03080	0.09660
5,00,000	1.46340	0.06840	0.16340	0.48400
1,000,000	2.83500	0.12460	0.35280	0.99340
2,500,000	8.05340	0.30620	0.69700	2.24140
5,000,000	13.48620	0.58080	1.38120	4.44400
10,000,000	26.83980	1.14980	2.65400	8.44820

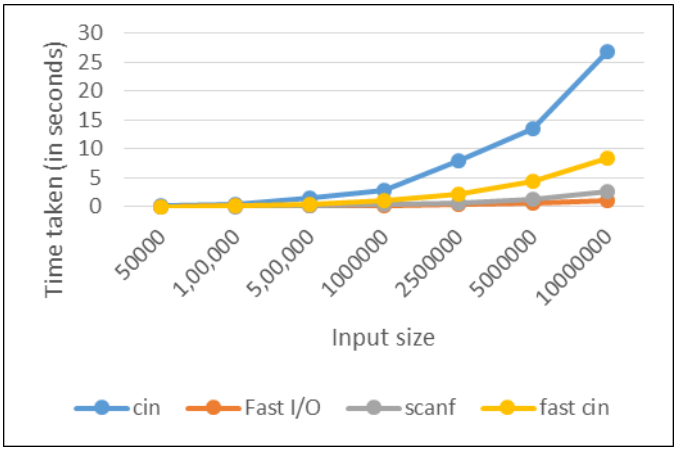

Chart -1: Comparison of reading speeds of numbers in Windows

Table -2: Comparison of reading speeds of numbers in Ubuntu

Input size	Average Time (in seconds)			
	cin	Fast I/O	scanf	Fast cin
50,000	0.03178	0.00860	0.01298	0.00868
1,00,000	0.05862	0.01516	0.02344	0.01986
5,00,000	0.24178	0.07120	0.10752	0.07958
1,000,000	0.46200	0.13656	0.19674	0.14560
2,500,000	1.09602	0.31594	0.44304	0.32644
5,000,000	2.16820	0.59710	0.85402	0.62276
10,000,000	4.31768	1.18746	1.70668	1.22172

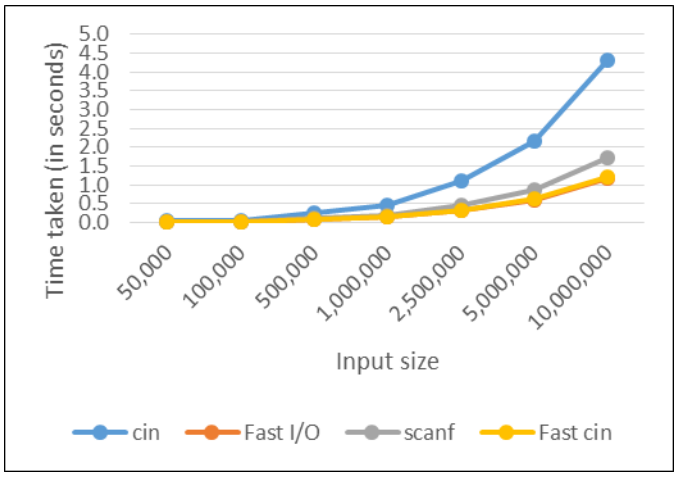

Chart -2: Comparison of reading speeds of numbers in Ubuntu

3.3.2 Printing Numbers

Table -3: Comparison of printing speeds of numbers in Windows

Input size	Time (in seconds)			
	cout	printf	Fast I/O	Fast cout
50,000	0.0402	0.0158	0.0220	0.0534
1,00,000	0.0812	0.0406	0.0406	0.1092
5,00,000	0.3962	0.1782	0.1826	0.4878
1,000,000	0.7940	0.3728	0.3640	0.9254
2,500,000	1.8974	0.8912	0.9066	2.6892
5,000,000	3.8000	1.7842	1.8094	5.0388
10,000,000	7.5390	3.5684	3.5592	9.8254

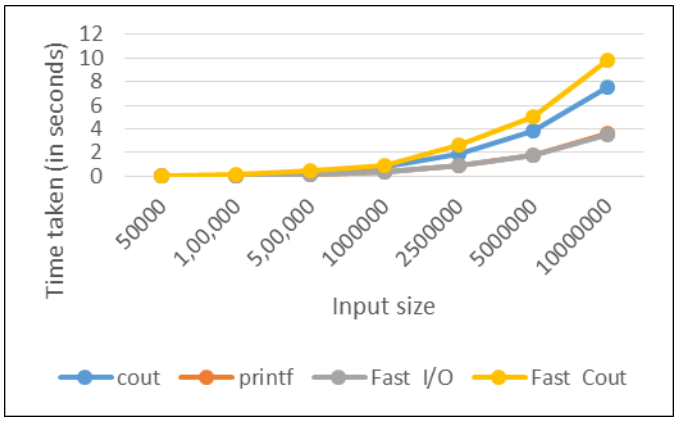

Chart -3: Comparison of printing speeds of numbers in Windows

Table -4: Comparison of printing speeds of numbers in Ubuntu

Input size	Time (in seconds)			
	cout	printf	Fast I/O	Fast cout
50,000	0.00878	0.00838	0.01114	0.01014
1,00,000	0.01658	0.01484	0.02332	0.01710
5,00,000	0.06052	0.05684	0.09102	0.05960
1,000,000	0.11642	0.11220	0.17912	0.11554
2,500,000	0.28018	0.27194	0.43306	0.28312
5,000,000	0.56304	0.53592	0.87418	0.55424
10,000,000	1.13344	1.08044	1.72802	1.13020

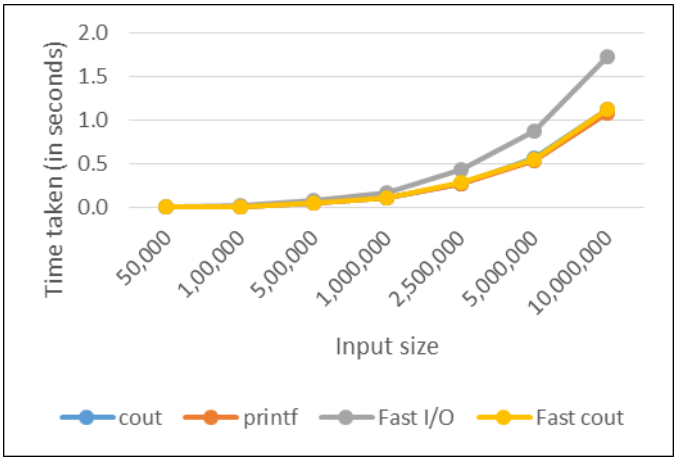

Chart -4: Comparison of printing speeds of numbers in Ubuntu

3.3.3 Reading Characters

Table -5: Comparison of reading speeds of characters in Windows with input size in millions

Input size	Time (in seconds)				
	cin	Fast cin	scanf	cin.get	getchar
1	0.553	0.363	0.213	0.447	0.010
5	2.698	1.703	0.842	2.245	0.037
10	5.440	3.317	1.570	4.572	0.088
25	13.966	8.223	3.188	11.399	0.232
50	31.330	15.386	6.322	25.218	0.457
75	45.039	22.096	9.515	33.317	0.631
100	62.577	29.921	12.654	47.396	0.940

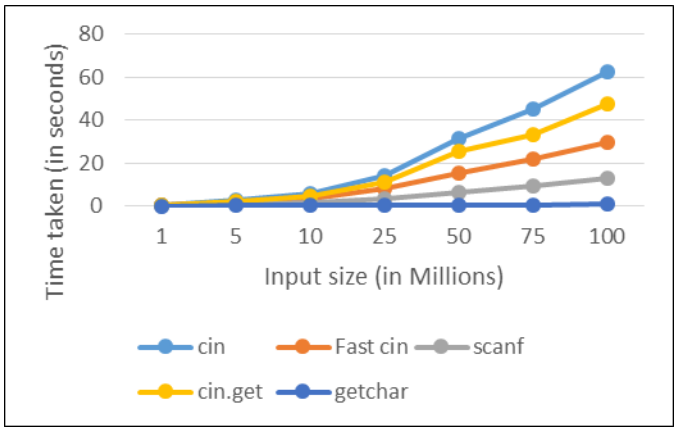

Chart -5: Comparison of reading speeds of characters in Windows

Table -6: Comparison of reading speeds of characters in Ubuntu with input size in millions

Input size	Time (in seconds)				
	cin	scanf	getchar	cin.get	Fast cin
1	0.117	0.053	0.014	0.049	0.019
5	0.503	0.207	0.055	0.199	0.085
10	0.977	0.391	0.107	0.382	0.168
25	2.503	0.913	0.235	0.979	0.413
50	4.666	1.824	0.453	1.858	0.812
75	7.144	3.708	0.650	2.838	1.194
100	9.672	5.778	0.868	3.631	1.637

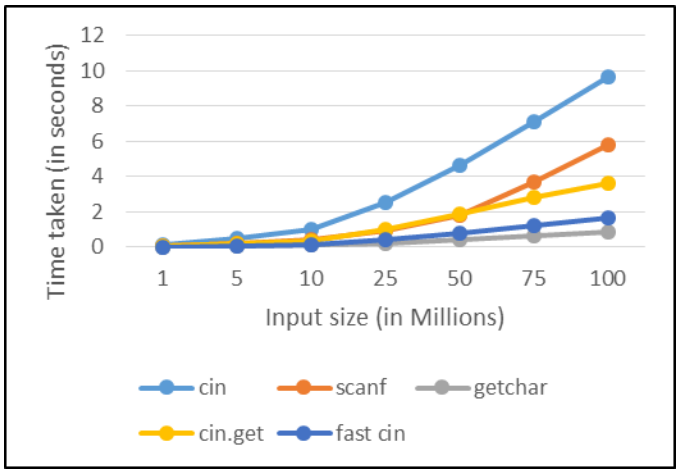

Chart -6: Comparison of reading speeds of characters in Ubuntu

3.3.4 Printing Characters

Table -7: Comparison of printing speeds of characters in Windows with output size in millions

Input size	Time (in seconds)			
	cout	fast cout	printf	putchar
1	0.294	0.209	0.081	0.034
5	1.355	1.250	0.437	0.184
10	2.911	2.481	0.898	0.384
25	8.082	6.030	2.097	0.915
50	17.179	11.312	4.178	1.810
75	24.263	16.032	6.211	2.824
100	34.057	20.139	8.199	3.584

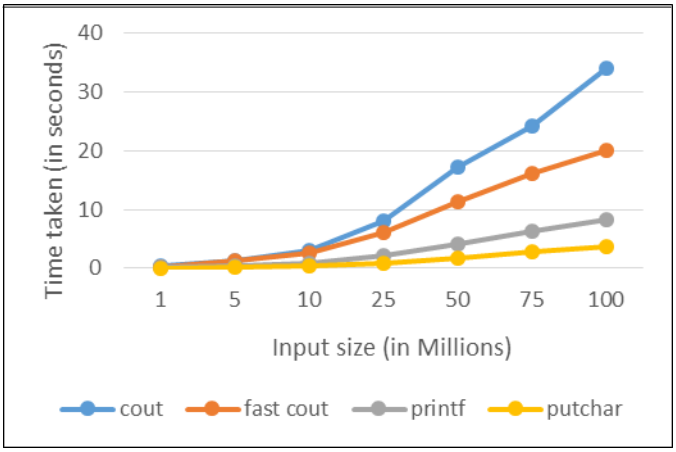

Chart -7: Comparison of printing speeds of characters in Windows

Table -8: Comparison of printing speeds of characters in Ubuntu with output size in millions

Input size	Time (in seconds)			
	printf	putchar	cout	fast cout
1	0.0378	0.0123	0.0378	0.0335
5	0.0508	0.0502	0.1601	0.1336
10	0.0995	0.0967	0.3234	0.2621
25	0.2445	0.2391	0.7992	0.6460
50	0.4890	0.4936	1.5468	1.3183
75	0.7228	0.7111	2.3009	1.9275
100	0.9642	0.9400	3.0448	2.5274

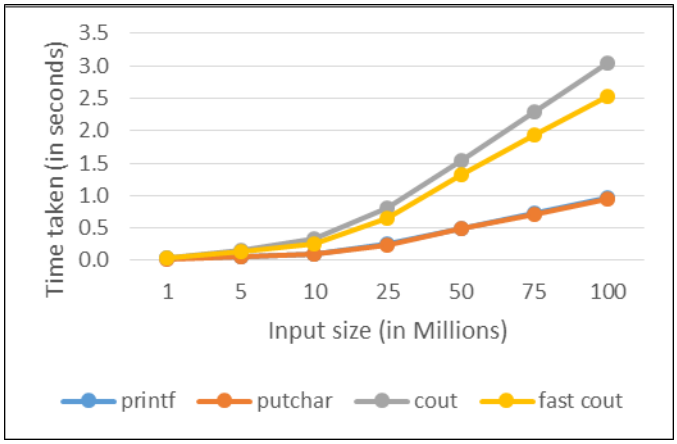

Chart -8: Comparison of printing speeds of characters in Ubuntu

4. INFERENCE ANALYSIS

From the results we observe that scanf and printf are faster than cin and cout respectively. This is mainly because the iostream I/O functions maintain synchronization with the C I/O functions. This synchronization can be toggled off and that has been done in the case of Fast cin and Fast cout which considerably improves the performance.

We also infer that getchar and putchar are faster than scanf and printf respectively. Due to this, the custom Fast I/O functions which are implemented using getchar and putchar become very fast themselves.

The relationship between the size of data and the time taken to read/write it does not exactly follow a linear relationship. Counterintuitively, the relationship seems to be of exponential type as the size of the data set increases.

In general, we observe that Ubuntu has a better I/O speed in C++ than Windows. cin and cout in Ubuntu outperform cin and cout in Windows by a huge margin. Since Ubuntu is more lightweight than Windows, this gives it an edge in terms of speed. Windows tends to have additional codes to support legacy software so that it retains backward compatibility with older versions of itself.

The running time of a program depends on how much of the processor is being currently occupied by other processes. This plays a major role in deciding the speed at which programs execute.

5. CONCLUSIONS

Based on the experiments performed, we have basis to decide upon proper I/O methods as per need. When dealing with characters only, getchar( ) and putchar( ) will always give best speeds. In case of numbers, custom Fast I/O functions implemented using getchar( ) and putchar( ) give the best results and should be preferred over other I/O methods.

REFERENCES

[1] Bjarne Stroustrup, The C++ Programming Language, 3rd edition, Addison-Wesley Pearson Education, 2002.

[2] Brian Kernighan, Dennis Ritchie, The C Programming Language, 2nd edition, Pearson Education, 2015.

[3] Standard C++ Library reference: http://www.cplusplus.com/reference/ Cpp Reference Documentation.

[4] C++ reference: http://en.cppreference.com/w/ Cpp Reference Documentation.

Application of Artificial BEE Colony Algorithm Using Hadoop

Nupur Bansal
Department of Computer Engineering
Delhi technological University
Delhi,INDIA
Email Id:nupur8121991@gmail.com

Sanjay Kumar
Department of Computer Engineering
Delhi technological University
Delhi,INDIA
Email Id:nupur4work@gmail.com

Ashish Tripathi
Department of Computer Engineering
Delhi technological University
Delhi,INDIA
Email Id:mail2ashish07@gmail.com

***Abstract* – Big Data is the latest buzzword in IT industry especially for the last couple of years. Initially this word was used by organizations which had to deal with speedy growth of data such as web data, data which comes from scientific and business simulations or any other data resource. The Google File System and MapReduce Architecture have been the result of the pressure to handle continuously growing amount of data on the web (Ghemawat, Dean, & Sanjay, 2008). Evolutionary Computing (EC) is a stream of Computer Science that adapts the theory given as Darwinian evolution which is used to optimize many computing problems (Eiben & Smith, 2003). The concept of EC revolves around various natural evolution processes such as competition, reproduction, preying and random variation. Since evolution itself is an optimization process, thus the process of EC is applicable to a huge range of problems. One evolutionary algorithm is the Artificial Bee Colony (ABC) which is simple and effective, but this algorithm may take long hours or days to optimize difficult deceptive and/or expensive objective functions. ABC can be expressed naturally in Google's MapReduce framework (Ghemawat, Dean, & Sanjay, 2008) to develop a simple and robust implementation which is parallel as well that includes communication, fault tolerance and load balancing. Since this implementation is flexible it is easy to do some modifications to it, which can improve optimization of objective functions and also improve parallel performance. In this paper, we propose and realize an approach to implement Artificial Bee Colony Algorithm in a parallel manner and use it to compute the effort of COCOMO Model. The population of the bee here are in the form of big data are stored in Hadoop Distributed File System (HDFS) on Hadoop to have better fault tolerance and to store large amount of data in distributed manner.**

Keywords – Big Data ; Artificial Bee Colony algorithm; Hadoop ; COCOMO Model ; Optimization.

I. INTRODUCTION

Over the last few years, Meta-heuristic (discover solution by trial and error) approximation algorithms have been used to solve many continuous and combinatorial optimization problems. It often finds good solution with less computation effort than exhaustive, iterative and simple heuristic methods. Some of the proposed meta-heuristic algorithm are particle swam optimization PSO, genetic algorithm, cuckoo search etc. These algorithms are problem independent thus suit many optimization problems. Artificial Bee Colony (ABC) Algorithm is a swarm intelligence based algorithm inspired by nature which has been proposed by Karaboga in 2005 (KARABOGA). ABC has been successfully applied on many continuous optimization problems such as the minimum routing spanning tree cost, for solving dynamic optimization problem, graph coloring problem etc. and it has shown better convergence to optimal solution than other meta-heuristic algorithms. But ABC takes reasonable amount of time to solve problems involving large volumes of data (big data), involving huge fitness computation or having large number of dimensions. One solution would be to parallelize ABC algorithm and scale it to large number of processors. But after program is successfully parallelized, we must still focus on different issues such as how to parallelize computation, distribute data and how to handle various failures. In order to deal with these concerns, a new abstraction was designed by Google called MapReduce that provides a parallel design pattern for simplifying application development for distributed environments i.e. allows expressing the simple computation in that design model while hiding messy details of data distribution, fault-tolerance, parallelization and load balancing. This abstraction was inspired by map and reduce primitives which are present in Lisp and in various other functional languages. Hadoop MapReduce has successfully parallelized many optimization algorithms like PSO, genetic algorithm and has effectively reduced the running time of algorithm for complex problems like stock trading Strategy (PRS), job shop scheduling problems, k-mean clustering etc. This paper makes the following research contributions:

1. Demonstrates a transformation of artificial bee colony algorithms into the map and reduce primitives
2. Proposes a model of parallel artificial bee colony algorithm.
3. Implements the model on effort estimation problem and also demonstrate whether it is scalable to large problem sizes.

II. LITERATURE REVIEW

978-9-3805-4421-2/16/$31.00 ©2016 IEEE

Graph coloring is a challenging problem of coloring the nodes of any graph by using the least possible number of colors and on the same time we have to ensure that no two adjacent nodes gain same color. Ranjeet singh tomar, Sonali Singh, shekhar Verma, Geetam Singh Tomar (Tomar, Singh, Verma, & Tomar, A Novel ABC Optimization Algorithm for Graph Coloring Problem, 2013) have proposed a novel Artificial Bee Colony (ABC) optimization algorithm for graph coloring problem. In this paper the proposed algorithm has been analyzed and compared with three other graph coloring algorithms.

In the paper, "An Artificial Bee Colony Algorithm for Solving Dynamic Optimization Problems", the authors, (Kojima, Nakano, & Miyauchi, 2013) proposed an ABC algorithm that could be used to solve dynamic problems for optimization with a very simple procedure. For various dynamic optimization problems, the proposed method provides fast solution search. And this method is also very effective in the numerical simulations.

In the paper by Alok Singh and Shyam Sundar (Singh & Sundar, 2011), they have proposed an Artificial Bee Colony Algorithm (ABC)-based approach to solve the minimum routing cost spanning tree (MRCST) problem. They used four best methods – a stochastic hill climber, two genetic algorithms, and a perturbation-based local search and compared all these methods against their approach. And ABC proves its superiority over other approaches by obtaining better quality solution.

In the paper, "A Novel Parallel Approach of Cuckoo Search using MapReduce", authors (Xu, Ji, Yuan, & Liu, 2014) invent a novel approach which can be used to accommodate cuckoo search for the analysis of big data by using MapReduce paradigm. As the backend MapReduce engine, they use HADOOP platform during the implementation of their method. Processing large dataset their approach has much better runtime performance.

In the paper, "Parallelization of the Artificial Bee Colony (ABC) Algorithm", authors (SUBOTIC, TUBA, & STANAREVIC) proposed some modifications to the Artificial Bee Colony algorithm that introduced how to parallelize the standard ABC algorithm. Since multiple processors can be better utilized parallelization allow faster execution. This approach has been used in many optimization problems.

In the paper, "A MapReduce Based Ant Colony Optimization Approach to Combinatorial optimization Problems", authors (Wu, Wu, & Yang, 2012) proposed an Ant Colony Optimization approach based on the MapReduce framework and they also showed how ACO algorithm can be modeled into this framework. They also described the implementation and algorithm design of Ant Colony Optimization approach on Hadoop.

In the paper, "Parallel K-PSO Based on MapReduce", (Wang, Yuan, & Jiang, 2012) parallel K-PSO which is an improved method of Particle Swarm Optimization (PSO) with K-means based on MapReduce is proposed. To improve the global search capability of this new algorithm the approach takes advantage of PSO and then to enhance its capability of processing massive data it makes K-means algorithm parallel with MapReduce.

III. ARTIFICIAL BEE COLONY ALGORITHM

The Artificial Bee colony algorithm is a recent population-based approach which takes motivation from the foraging behaviour of honey bee swarm. This algorithm was introduced by Karaboga in 2005 and was further developed by Karaboga and Basturk in 2006 and by Singh in 2009.

In ABC, there are three classes of the foraging bees—employed bees, onlooker bees and scout bees.

1. Employed bees - Employed bees are those bees that tap a rich artificial food source. The employed bees bring loads of nectar from the rich food sources to the hive. They also share the information about those food sources with onlooker bees.
2. Onlooker bees – These bees wait in their hive for the employed bees to come and share information about the food sources with them.
3. Scouts bees – The scout bees presently look for new sources of food near their present hive.

There is a common area in the hive which is called the dance area. The employed bees dance in this area and share information about food sources with the onlookers. The nectar content of the food source that is being tapped by the dancing bees determines the nature and duration of the. Onlooker bees choose a food source after observing a large number of dances. The nectar content of a food source also determines which food source is chosen by the onlooker bees. The probability of a food source being chosen is proportional to its nectar content. Thus, good food sources tend to attract more bees than the bad food sources. Whenever a bee finds a food source, it becomes employed not considering if it was scout or onlooker earlier. Whenever a food sources becomes completely exhausted, all the employed bees which had been associated with it, leave it, and are free to become either scouts or onlookers. Thus it can be seen that the scout bees are performing the task of exploration while the employed and onlooker bees are performing exploitation.

IV. IMPLEMENTATION OF PROPOSED WORK

This section demonstrates the parallel implementation of Artificial Bee Colony algorithm with its application to find the effort of a project using COCOMO Model. ABC has a bottleneck for mathematically expensive functions and thus needs to be parallelized for more efficiency.

The steps of the algorithm that can be parallelized are:

1. Each iteration of ABC algorithm can be executed in parallel.
2. Position of food source can be updated parallely.

But the iterations in ABC can‘t be parallelized as there is an issue of message passing among the particles in each iteration. The results of previous iteration must be preserved and utilized

in next iteration. Thus to transform ABC in parallel fashion following issues needs to be considered:

1. Determine the input to MapReduce architecture.
2. Determine the jobs of mapper and reducer tasks.
3. Exchanging information between mapper tasks.

A large number of initial random populations are provided as input to the MapReduce framework, which is then split into chunks and distributed across various mappers. Each food source is represented as a key-value pair as:

Key K1 : bee_id

Value V1 : set of attributes representing the food source like position, fitness, probability, etc.

A. Creating initial population

A large number of initial random population is created, which is provided as input to the MapReduce framework. The population created is in the form of tuples containing following information: bee_id, position of food source, fitness, probability.
Here, the position of food source is taken in the form of (a,b), where a and b are the coefficients of the COCOMO model used to compute effort as:
Effort (E) = a $(LOC)^b$. The steps are:

1. Generating food source

   $x_{i,j} = (x_{max} - x_{min}) * rand(0,1) + x_{min}$

   Where , i = 1,2,3,.....FS

   J =1,2,.....D

   x_{max} and x_{min} denote the maximum and the minimum of each design variable.

2. Calculate the fitness fit_i based on the objective function value in each food source.

$$fit_i = \begin{cases} 1/(1+f(x_i)) & f(x_i) \geq 0 \\ 1+|f(x_i)| & otherwise \end{cases}$$

   Assuming initial probabilities as 0

3. Writing these attribute using string representation into a file as:
   Food source, fitness, probability

B. Map Function

In Parallel ABC Algorithm, the map function is called once for each particle. The key is the offset of the tuple which represents the food source and the value is the state string representation of the food source (particle).

Steps are:

map (key, value, context)

a) Employed_Bee_Face()

1. Calculate candidate positions vector V_i to each current food source as:

$$V_{i,j} = \begin{cases} x_{i,d} + \phi(x_{i,d} - x_{k,d}) ... if (j=d) \\ x_{i,j} \end{cases}$$

2. Calculate the fitness as

$$fit_i = \begin{cases} 1/(1+f(v_i)) & f(V_i) \geq 0 \\ 1-|f(v_i)| & otherwise \end{cases}$$

3. Apply greedy selection by comparing fit and fit'.
4. Update the food source as

$$x_{i,j} = \begin{cases} V_{i,j} ....if ..f(V_i) \geq 0 \\ 1+|f(V_i)| ..otherwise \end{cases} \quad prob_i = fit_i / \sum_{i=1}^{NS} fit_i$$

b) Onlooker_Bee_Phase()

1. Determine the relative probabilities of each food source

$$prob_i = fit_i / \sum_{i=1}^{NS} fit_i$$

C. Reduce Function

The reduce function in this model receives a key and a list of all associated values. Here, we have explicitly defined the key as 1 so as to run a single reducer to reduce overhead. In reduce phase the global best of all the particles is calculated and this position of global best obtained is stored.

reduce (key, value_list, context)

a) Scoute_Bee_Phase()

1. Compare relative probability of food source with a random probability.
2. Select the food souce if its probability if greater than random probability

   Else make it abundant.

3. Check if the food source is abundant for a fixed number of cycle, then update the food source using initialization phase.
4. Check for best food source.

Repeat this cycle of map-reduce task for a fixed number of iterations or till we have converged to an optimal solution. The best solution obtained will represent the optimal value of the coefficients a and b.

V. RESULTS

In this paper, optimization of Basic COCOMO model parameters (a,b) has been done, such that calculated effort approximates to the actual effort for NASA 63 project dataset.
Formally, this problem can be described as finding parameter X= {x1, x2}, with xi ∈ {0,5} that minimize the following equation:

$$MMRE = [Actual - x1(KLOC)^{x2}] / Actual$$

Here MMRE - Mean Magnitude of Relative Error used as evaluation criteria for assessment of optimized parameters. And since parameters x1 and x2 are specific to project mode therefore we execute program for each mode separately.
Here, the model has been implemented on Hadoop (2.6 version) and run on a Hadoop cluster with three nodes. Taking from previous works done for extension of genetic algorithms on Hadoop, each node of the cluster runs a two dual Intel Quad cores, 4GB RAM and 250 GB hard disks. The nodes are integrated with Hadoop Distributed File System (HDFS) yielding a potential single image storage space of 2 *52/3 = 34.6TB (since the replication factor of HDFS is set to 3). Each node can parallely run 5 mappers and 3 reducers.
Three tests have been performed and the following results obtained:

A. *Comparison between actual effort and computed effort*

In this experiment the population size of 2 lakhs has been taken and performed 3 iterations to obtain the result in each case.

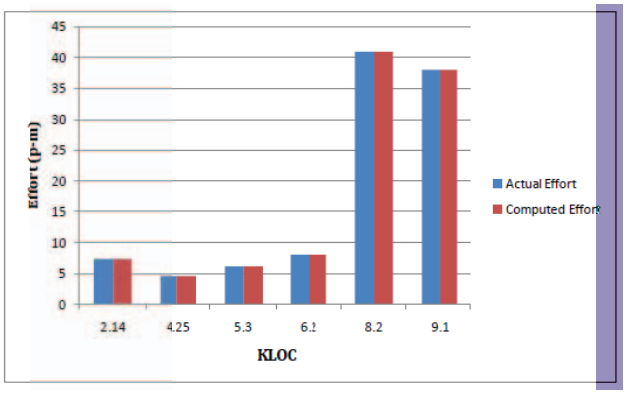

Fig. 1. Graph obtained between Effort Vs KLOC for 1st case

A. *Variation of execution time with different block size*

Taking the population size of 2 lakhs and performing 3 iterations a measurable variation in execution time has been observed while changing the block size of Hadoop resulting in different number of mapper tasks in each iteration.

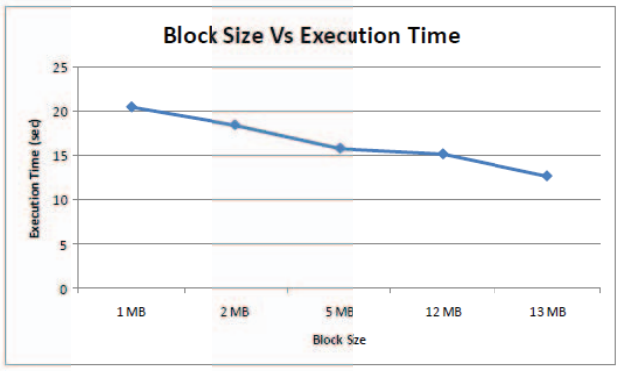

Fig. 2. Graph obtained between Block Size Vs Execution Time

B. *Variation of execution time with number of iterations*

The execution time also varies greatly with different number of iteration. Again while performing this experiment population size of 2 lakhs and block size of 3MB has been kept.

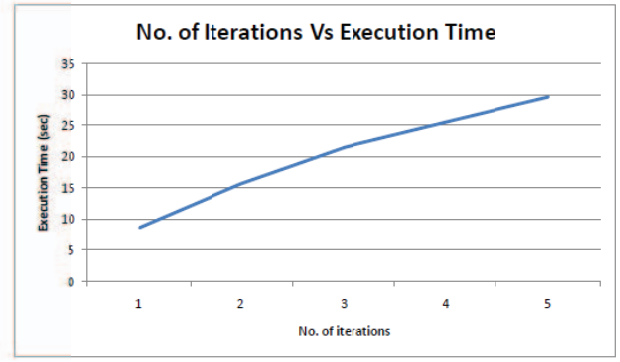

Fig.3. Graph obtained between No. of Iterations Vs Execution Time

VI. CONCLUSION AND FUTURE SCOPE

The Artificial Bee Colony algorithm can easily be parallelized using MapReduce architecture to solve the optimization problems involving large search space. The problem of large search space could be easily tackled by generating a large number of populations so that each particle in the population needs to search a comparatively smaller search space and can thus find the solution more efficiently in less time.
It has been seen that lot of communication, task start up overhead is associated with Hadoop MapReduce Architecture thus is not suitable for problems having small search space with less computation.
Results of the experiments performed show that the proposed model can have better convergence than its serial implementation for intensively expensive computation functions. This model would be really efficient if we deal with solving the problem involving a large number of dimensions. In

such case it would be beneficial to use this parallel implementation for faster convergence to an optimal solution.

The proposed model for parallel ABC can use a large population but could not be applied to a big dataset due to the fact that the particles keep on updating themselves in each iteration. So, a further detailed study is required to modify the algorithm in such a way so that it could be applied to big data to conclude with some meaningful information out of it.

In future work the proposed model should be modified such that it could work upon a big dataset involving large number of dimensions. Also some work could be done in order to improve the execution time of the algorithm examining other features of MapReduce architecture like partitioner, combiner etc. which may reduce the processing.

REFERENCES

[3]. Tomar, Singh, Verma, & Tomar, "A Novel ABC Optimization Algorithm for Graph Coloring Problem", 2013.

[4]. Kojima, Nakano, & Miyauchi, "An Artificial Bee Colony Algorithm for Solving Dynamic Optimization Problems", 2013.

[5]. Xu, Ji, Yuan, & Liu, "A Novel Parallel Approach of Cuckoo Search using MapReduce", 2014.

[6]. Subotic, Tuba, & Stanarevic, "Parallelization of the Artificial Bee Colony (ABC) Algorithm".

[7]. Wang, Yuan, & Jiang, "Parallel K-PSO Based on MapReduce", 2012.

[8]. Wu, Wu, & Yang, "A MapReduce Based Ant Colony Optimization Approach to Combinatorial optimization Problems", 2012.

[9]. Aridhi, Lacomme, Ren, & Vincent, "A MapReduce-based approach for shortest path problem in large-scale networks", 2015.

2016 Intl. Conference on Advances in Computing, Communications and Informatics (ICACCI), Sept. 21-24, 2016, Jaipur, India

Automated Classification of Security Requirements

Rajni Jindal, Ruchika Malhotra, Abha Jain

Department of Computer Science and Engineering, Delhi Technological University
Shahbad Daulatpur, Main Bawana Road, Delhi- 110042, India

rajni.jindal@yahoo.co.in
ruchikamalhotra2004@yahoo.com
me_abha@yahoo.com

***Abstract*— Requirement engineers are not able to elicit and analyze the security requirements clearly, that are essential for the development of secure and reliable software. Proper identification of security requirements present in the Software Requirement Specification (SRS) document has been a problem being faced by the developers. As a result, they are not able to deliver the software free from threats and vulnerabilities. Thus, in this paper, we intend to mine the descriptions of security requirements present in the SRS document and thereafter develop the classification models. The security-based descriptions are analyzed using text mining techniques and are then classified into four types of security requirements viz. authentication-authorization, access control, cryptography-encryption and data integrity using J48 decision tree method. Corresponding to each type of security requirement, a prediction model has been developed. The effectiveness of the prediction models is evaluated against requirement specifications collected from 15 projects which have been developed by MS students at DePaul University. The result analysis indicated that all the four models have performed very well in predicting their respective type of security requirements.**

***Keywords*— Non-functional requirements, Text mining, Machine learning, Security requirements, Requirement engineering, Requirement elicitation, Receiver Operating Characteristics**

I. INTRODUCTION

Security is the most crucial non-functional attributes that need to be focused on with caution and care, apart from various others like availability, usability, look-and-feel, maintainability, performance etc. [1]. Thus, security requirements should be elucidated in Software Requirement Specification (SRS) document with high clarity and understandability [2]. But it has been seen that the stakeholders and requirement engineers are not able to state them as clearly as they should be stated [3]. They intend to specify descriptions of the security requirements without specifying the type of these requirements. As a result of this, these requirements are not taken into account at the right time by the software developers and therefore they go unidentified when developing the actual software. The consequence is that the security aspect of the software is ignored and software developed lacks the basic security feature. This causes great difficulty for the software developers to deliver reliable and secure software free from the threats of virus and cyber terrorism.

Therefore, in this paper, we intend to mine the descriptions of the requirements that pertain to security- related issues specified in SRS document and classify them into their respective categories of security requirements. The descriptions of the security requirements are classified into four types viz. authentication-authorization, access control, cryptography-encryption and data integrity. Text mining steps are employed to mine the descriptions. Mining the descriptions would result in retrieval of some keywords pertaining to each type of security requirement. With the help of these keywords, we would then be classifying the descriptions into their respective types of security requirements. J48 decision tree method has been used for classification of the requirements into their respective security types. Corresponding to each of the four security types, a prediction model is developed and the performance of all the four models is evaluated and compared using performance measures obtained from ROC analysis.

Identification of the keywords specific to each type of security requirement would be highly beneficial in ensuring that the software developed is meeting the security aspect. This is so because in future, we would be able to develop the SRS document in such a way so that it includes the maximum number of keywords pertaining to security requirements. Thus, the proposed methodology will enable software practitioners to classify the security requirements in the very initial phases of Software Development Life-Cycle (SDLC) process i.e. requirement and analysis phases. This would be highly beneficial to the software developers as they can incorporate the security requirements in the software before the actual design and implementation phases begin [4]. The earlier the requirements are identified, the easier is their incorporation in the software. Not only this, determining the adequacy and consistency of the security requirements provides a fundamental basis for estimating costs, defining the scope of the project, constructing the design and testing specifications, and helping in understanding the possible consequences of either a successful or unsuccessful deployment of the system [5]. Thus, the security type requirements must be carefully looked into with caution and care for the overall development of secure and reliable software.

The paper is sub-divided into the following sections: Section 2 provides an overview of the current literature followed by section 3 which describes the methodology

978-1-5090-2029-4/16/$31.00 @2016 IEEE

conducted in order to achieve the classification of security requirements. Section 4 elaborates on the research background that explains the Info-Gain measure used for feature selection and the machine learning method used for the classification. The section concludes by explaining the model assessment parameters. Section 5 presents the analysis of results. Finally, Section 6 provides a summary of the paper.

II. LITERATURE REVIEW

In today's scenario where there are threats of cyberterrorism, development of software that meets the security issues is the main concern. However, security is often thought as an after development concern by the stakeholders [6, 7, 8]. This can prove to be very harmful as once the software is developed and becomes live in the market, it is difficult to remove any kind of virus or vulnerabilities that might have been introduced in the software during its development process. Thus, it is highly beneficial if the security problems are understood in the early phases of SDLC process, especially during the requirement and analysis phases so that the software developed incorporates the security issues [9]. Therefore, capturing the security requirements at the right time is the main issue that needs to be dealt with seriously. Till date, there are only a few authors who have worked on eliciting security requirements in an organized and a systematic way during the requirement engineering process. The aim is to ensure how can the concept of reusable knowledge be incorporated to manage security requirements [10, 11]. The authors Hadary et al. [12] have proposed a technique for elicitation of security requirements based on problem frames. The concept of abuse frames was used to represent the threats, whereas security problem frames were used to represent requirements pertaining to security. Similarly, the authors Lin et al. [13, 14] have also used the concept of abuse frames in order to analyze the security threats and thereby derive the security requirements using Jackson's Problem Frames [15]. The paper by Sindre et al. [16, 17, 18, 19] have extended the traditional use case approach that is one of the most commonly used requirement elicitation technique to cover misuse cases in order to include other types of extra-functional requirements beyond security. They intend to determine the security vulnerabilities in order to analyze security problems. The approach is a combination of misuse cases and use cases. Similar to the above paper, the authors [20, 21] have also used the concept of misuse cases in order to model the negative requirements, that is, the requirements that are not needed in the system. Much similar to the above work, the authors McDermott et al. [22] adapted a object-oriented technique in order to analyze the security requirements and called that adaptation as an abuse case model that is relatively simple to understand from a user perspective. Fewer Authors [23, 24, 25, 26] have proposed a framework to address malicious obstacles i.e. the anti-goals with the help of the threat trees whose leaf nodes represented the software vulnerabilities. Haley et al. [27] presented a framework demonstrating the constraints as security requirements and thereby developing satisfaction arguments for their validation. Also, the authors Haley et al. in another paper [28] studied the effect of security requirements on the functional requirements in order to ensure that the system developed meets the needs of the stakeholders. They represented the security threats as crosscutting concerns and then listed the threats corresponding to the assets.

The work presented in this paper is quite different as we are not focusing on requirements elicitation techniques, but intend to mine the descriptions of security requirements that are specified in the SRS documents during the requirement engineering process and thereafter classify them into their respective categories of security requirements.

III. PROPOSED METHODOLOGY

This section discusses the methodology that has been used in the work for classifying the security requirements based on their descriptions. As depicted in Figure 1, there are three steps used to accomplish the classification and thereby develop the prediction models. The steps have been elaborated in the subsequent sub-sections.

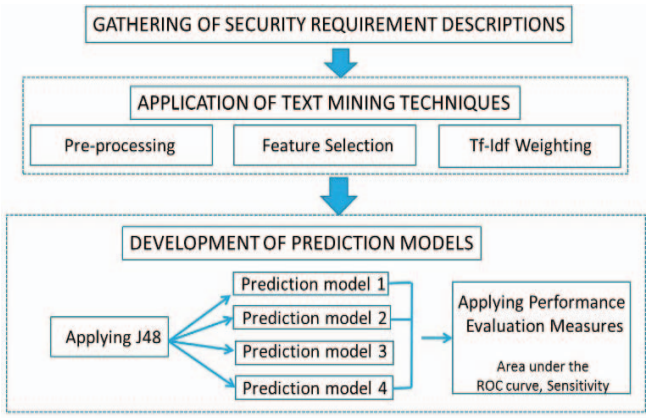

FIG 1. FRAMEWORK USED FOR CLASSIFYING SECURITY REQUIREMENTS

A. Gathering of Security Requirement Description

The descriptions of the security requirements have been gathered from the dataset which is publicly available on an open source PROMISE software engineering repository (http://promisedata.org/repository). The dataset consists of requirements specifications collected from 15 projects which have been developed by MS students at DePaul University. This dataset has been collected and used by the authors Huang et al. in their papers [1, 3] which deal with detecting and classifying the non-functional requirements (NFRs). The dataset consists of a total of 326 NFRs specifications classified into 9 NFR types viz. availability, look-and-feel, legal, maintainability, operational, performance, scalability, security and usability. These are the qualities which play a crucial role in designing the architectural view of the system and therefore should be stated in the SRS document with high clarity. But, it has been observed that NFRs are scattered throughout the SRS documents in an unorganized manner as the stakeholders are not able to define and state such kind of

NFRs clearly [3]. Among all the NFR types, the most critical is the security attribute. Figure 2 depicts the percentage of security requirement descriptions present in each of the 15 projects. There are a total of 58 security- based specifications present in all the 15 projects out of 326 NFRs specifications. Project P11 has the highest percentage of security requirement descriptions, i.e. 30%, followed by projects P3 and P4 which contains 28.5% of the security requirement descriptions. There are no security requirements present in project P9. The task is to carefully read the SRS documents and select only those requirement descriptions that pertain to security related issues. A lot of harm can be caused to the software once it goes live in the market if the security descriptions are not identified properly. Thus, dealing with security requirements is the necessity in today's computer age era where cybercrimes, virus alerts, malicious crackers are increasing at an exponential rate [5]. The selected security requirement descriptions are then further analyzed by applying a series of text mining steps.

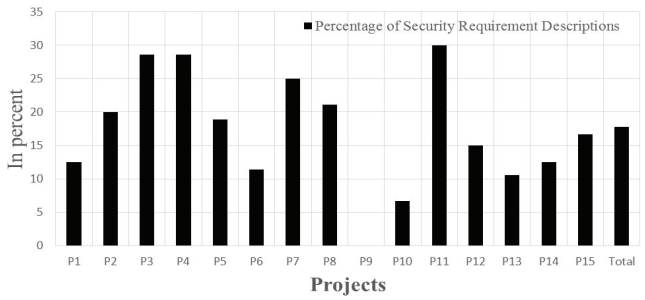

FIG 2. PERCENTAGE OF SECURITY REQUIREMENT DESCRIPTIONS IN EACH OF THE 15 PROJECTS

B. Application of Text Mining Techniques

Here, the analysis of security-based descriptions extracted from the SRS documents are done after an extensive and thorough understanding of the document. The task is to convert the unstructured textual data into a structured format suitable for carrying out data analysis. As can be seen from Figure 1, we have applied text mining techniques viz. pre-processing, feature selection and TF-IDF weighting. As an initial step, the prerequisite activities of pre-processing like tokenization, stop words removal and stemming are carried out in order to remove the words that are not relevant [29]. Tokenization deals with the conversion of a sequence of characters into a group of tokens. This is followed by the removal of stop-words from the document as per the list of stop words mentioned in a standard English dictionary. Finally, the most crucial pre-processing step is performed, i.e. stemming which is concerned with removing the words having the same stem and retaining thereby the stem as the feature. For example, the words like "teach", "teaching", "teaches" are all replaced with a single word as "teach". All such pre-processed words are called as 'features'. It has been observed that despite performing all these pre-processing tasks, the feature set size is very huge consisting of a large number of words, which is unsuitable for performing any kind of data analysis. Thus, as the second step of text mining, we intend to further reduce the size of the feature set by applying a suitable feature selection method. In this work, we have used Info-Gain measure which is based on ranking all the selected features retrieved from pre-processing and thereafter selecting the top 'N' features on the basis of the rank. As the final step of text mining, TF-IDF (Term Frequency Inverse Document Frequency) weighting approach is used to assign an appropriate weight to all 'N' ranked features. The first value, i.e. the term frequency is the number of times the jth term is occurring in a particular document say i. It is represented as 't_j'. The second value, i.e. inverse document frequency is defined by log (n/n_j). Here, n_j represents the documents having the term t_j and n represents all the documents.

C. Development of Prediction Models

Here, the task is to develop the prediction models using a suitable machine learning method that would then be used to classify the security- based descriptions into their respective types of security requirements. We have used J48 decision tree method and have classified all the 58 security- based descriptions into four types of security requirements viz. authentication-authorization (AA), access control (AC), cryptography- encryption (CE) and data integrity (DI). Table I depicts the number of requirement specifications in each type of security requirement. Corresponding to each type of security requirement, a prediction model has been developed. As can be seen from Figure 3, there are in total four prediction models developed specific to each type of security requirement. For instance, prediction model 1 classifies the requirements that are specific to 'authentication-authorization' (AA). Prediction model 2 classifies the requirements that are pertaining to 'access control' (AC) and similarly prediction models 3 and 4 classify the requirements specific to 'cryptography-encryption' (CE) and 'data integrity' (DI). Each of the prediction model is considered as a 'binary model' wherein the value of the dependent variable (security type) could be either 1 or 0. For instance, prediction model 1 will have the value of the dependent variable as 1 for all the instances that are pertaining to 'AA' type of security requirements and value of 0 for all the other remaining instances. Similarly, prediction model 2 will have the value of the dependent variable as 1 corresponding to the instances where the requirements pertain to 'AC' security type and 0 for all the other remaining instances. Similarly, we construct prediction models 3 and 4. Finally, the performance of all these four models is evaluated and compared using the evaluation measures derived from ROC analysis**.**

TABLE I. NUMBER OF SECURITY REQUIREMENT SPECIFICATIONS BELONGING TO EACH TYPE OF SECURITY REQUIREMENT

Security Requirement Type	**# Security Requirement Specifications**
Authentication-Authorization	18
Access Control	12

Cryptography- Encryption	13
Data Integrity	15
Total	**58**

S.No.	Security Requirement Descriptions	Security Requirement Types
1	The product shall ensure that it can only be accessed by authorized users.	AA
2	All authorized users once authenticated must be able to logon to the Disputes System.	AC
-	-	-
-	-	-
58	The system shall be free of computer viruses	CE

Application of Text Mining Techniques

Model 1

S.No	Top 100 words	AA type
1	-	1
2	-	0
-	-	
58	-	1

Model 2

S.No	Top 100 words	AC type
1	-	1
2	-	0
-	-	
58	-	1

Model 3

S.No	Top 100 words	CE type
1	-	1
2	-	0
-	-	
58	-	1

Model 4

S.No	Top 100 words	DI type
1	-	1
2	-	0
-	-	
58	-	1

FIG 3. PREDICTION MODELS DEVELOPED USING TEXT MINING TECHNIQUES

IV. RESEARCH BACKGROUND

In this section, we will be focusing on the research background that is required for the accomplishment of the proposed methodology. Firstly, we will explain the concept behind Info-Gain measure that has been used in our work for feature selection. Thereafter, an overview of learning technique which has been used for performing classification is provided. Finally, the performance evaluation measures are described.

A. Info-Gain Measure

It is the popularly used feature selection method that is concerned with identifying a set of words from a given document that tends to simplify the target concept [30]. The number of bits needed to encode a particular class distribution C_0 is H (C_0). It is as follows:

$$N = \sum_{c \in C} n(c) \quad (1)$$

$$p(c) = {}^{n(c)}/_{N} \quad (2)$$

$$H(C) = -\sum_{c \in C} p(c) \log_2 p(c) \quad (3)$$

The number of bits for coding a class is as follows:

$$H(C|A) = -\sum_{a \in A} p(a) \sum_{c \in C} p(c|a) \log_2(p(c|a)) \quad (4)$$

Where, A is a set of attributes

Now, the attribute obtaining the highest Info-Gain denoted by A_i. is said to be the highest ranked attribute.

$$\text{Infogain}(A_i) = H(C) - H(C|A_i) \quad (5)$$

B. Model Prediction using J48 Decision Tree

J48 decision tree method is one of the simplest algorithm that is used to handle the classification problems [31]. Using J48, two types of trees are created viz. pruned tree and unpruned tree. The type of tree depends on the algorithm implemented. J48 decision tree method provided by the WEKA software provides pruned tree as the output. The idea behind pruning is that, pruning removes the additional nodes/branches without affecting the performance too much. Also, apart from making the tree easier to understand, pruned tree reduces the risk of overfitting to the training data. After the tree is built, it is applicable for classifying every row of the dataset [32, 33]. J48 is the most effective classification technique that performs classification either by constructing decision trees or with the help of generated rules.

C. Performance Evaluation Measures

The performance evaluation measures used are:

1) Sensitivity

It is defined as the percentage of documents that are correctly classified as belonging to the category say 'A' [34].

2) Receiver Operating Characteristics (ROC) curve

It is one of the significant characteristic of ROC analysis, which depicts the performance of the model in a visual manner, i.e. in the form of a graph where x-axis and y-axis represents '1-specificity' and 'sensitivity' respectively at varying cut-off points [35]. The most desirable cut-off point is that which maximizes the values of sensitivity as well as specificity. The area under the ROC curve, known as AUC depicts how accurately the model performs for the new instances. Its value lies between 0 to 1.

3) Validation method used

In this study, each of the four binary models constructed above are validated using k- fold cross validation technique which partitions the entire dataset of 58 security descriptions into k equally sized parts. One of the parts is used for validation and other remaining parts for training [36]. This process is repeated k times such that each data point gets validated once and all the k outcomes are merged to generate the final output. In our study, the value of k is taken as 10. This technique provides accurate estimation.

V. VALIDATION RESULTS

In this section, we highlight the performance of all the four models developed J48 decision tree method. As already specified, model 1 corresponds to 'authentication-authorization' type of security requirements, model 2 classifies 'access control' requirements, model 3 classifies 'cryptography-encryption' requirements and model 4 classifies 'data integrity' requirements. Their performance is evaluated and compared using AUC value, sensitivity value and the cut-off point. Table II depicts the results with respect

to top-100 words sorted by Info-Gain measure corresponding to each model. Table II shows that the model 4 has outperformed all the other models in identifying the data integrity type of security requirements having AUC as 0.83 and the corresponding sensitivity value as 80%. The performance of models 1 and 2 is moderate with the values of AUC being 0.72 and 0.77 respectively. Performance of model 3 is not very good in predicting security requirements as is evident from the AUC value that is 0.69.

Apart from comparing the performance of all the four models with the help of measures derived from ROC analysis, J48 decision tree method also provides pruned tree as the output. The J48 pruned tree corresponding to all the four models is depicted in Figure 4-7. The specific numbers in the tree have a particular meaning. The first number signifies the total number of instances reaching the leaf node. The second number signifies the number of those instances that are mis-classified.

TABLE II. RESULTS OF J48 DECISION TREE TECHNIQUE

	AUC	Sens (%)	Cut-Off
Model 1	0.72	65.00	0.12
Model 2	0.77	75.00	0.41
Model 3	0.69	69.20	0.07
Model 4	0.83	80.00	0.05

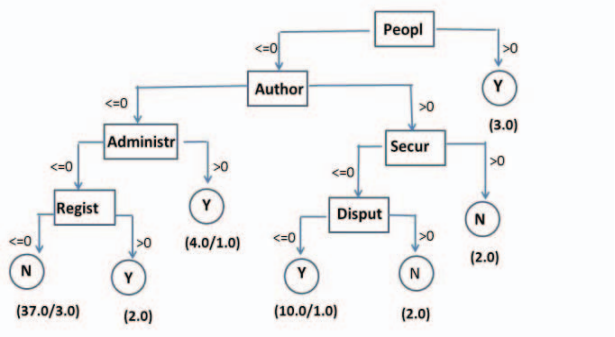

FIG 4. J48 PRUNED TREE CORRESSPONDING TO MODEL 1

The classification rules derived from the above decision tree (figure 4) having the maximum support of the instances are:
if ((people<=0) and (author>0) and (secur<=0) and (disput<=0)) then it is a security requirement of type 1 i.e. authentication- authorization with the support of 9 instances
else if ((people<=0) and (author<=0) and (administer<=0) and (regist<=0) then it is not a security requirement of type 1 with the support of 34 instances

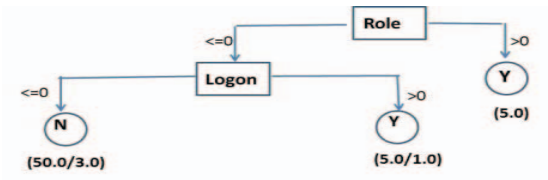

FIG 5. J48 PRUNED TREE CORRESSPONDING TO MODEL 2

The classification rules derived from the above decision tree (figure 5) having the maximum support of the instances are:
if (role>0) then it is a security requirement of type 2 i.e. access control with the support of 5 instances
else if ((role<=0) and (logon<=0)) then it is not a security requirement of type 2 with the support of 47 instances

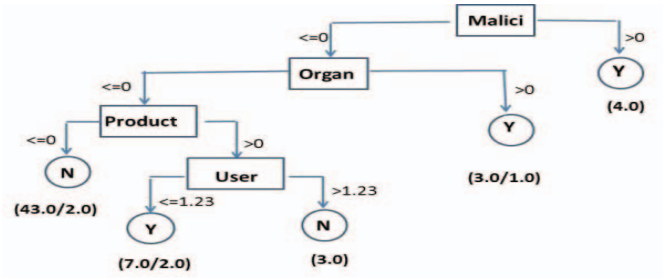

FIG 6. J48 PRUNED TREE CORRESSPONDING TO MODEL 3

The classification rules derived from the above decision tree (figure 6) having the maximum support of the instances are:
if ((malici<=0) and (organ<=0) and (product>0) and (user<=1.23)) then it is a security requirement of type 3 i.e. cryptography-encryption with the support of 5 instances
else if ((malici<=0) and (organ<=0) and (product<=0)) then it is not a security requirement of type 3 with the support of 41 instances

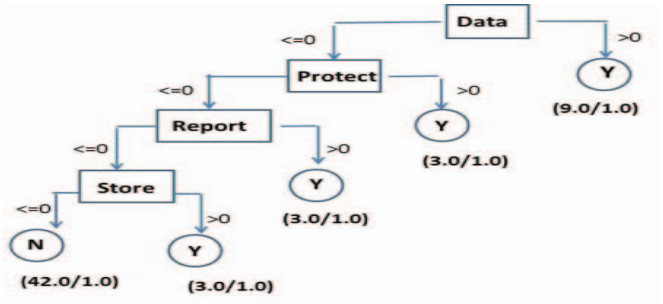

FIG 7. J48 PRUNED TREE CORRESSPONDING TO MODEL 4

The classification rules derived from the above decision tree (figure 7) having the maximum support of the instances are:
if (data>0) then it is a security requirement of type 4 i.e. data integrity with the support of 8 instances
else if ((data<=0) and (protect<=0) and (report<=0) and (store<=0) then it is not a security requirement of type 4 with the support of 41 instances

VI. CONCLUSION

Classification of security-based descriptions scattered throughout the SRS document into their respective types of security requirements is crucial for an overall benefit of the software product. Security related issues must be looked into with caution to ensure the development of the software that is meeting the customer's needs. Thus, we analyze the security-based descriptions that are stated by the stakeholders in the SRS document during the requirement elicitation process.

Text mining steps were used to mine the descriptions followed by the application of J48 decision tree method to classify them into their respective types of security requirements. The predicted models and the proposed framework can be used by the software practitioners and software engineers in classifying security requirements during early phases of software development. The prediction models developed, indicate an overall good performance in classifying the security requirements in terms of the value of AUC obtained from ROC analysis. The best performance is indicated by model 4 while predicting data integrity type of security requirements.

In future, we plan to replicate this work on classifying various other non-functional requirements as these requirements contribute to the overall development of the software and any kind of software application development requires far more than just engineering the functional requirements.

REFERENCES

[1] Cleland-Huang, J., Settimi, R., Zou, X., and Solc, P. 2007. Automated Classification of Non-Functional Requirements. *Requirements Eng*. 12:103–120.

[2] Zowghi, D. Resources: Collection of Software Requirements Specifications. http://www.research.-it.uts.edu.au/re/cgibin/resources_srs.cgi

[3] Cleland-Huang, J., Settimi, R., Zou, X., and Solc, P. 2006. The detection and classification of non-functional requirements with application to early aspects. *IEEE international conference on requirements engineering*, Minneapolis, MN, pp 39–48.

[4] Artelsmair, C., and Wagner, R. 2003.Towards a Security Engineering Process. Orlando, Florida, USA.

[5] Firesmith, D.G. 2003. Engineering Security Requirements. *Journal of Object Technology*. Vol. 2, No. 1.pages 53-68.

[6] Amoroso, E. G. 1994. Fundamentals of Computer Security Technology. Prentice-Hall, ISBN: 0-13-305541-8.

[7] Moffett, J.D., Haley, C.B., and Nuseibeh, B. Core Security Requirements Artefacts. Technical Report number 2004/23. Department of Computing, The Open University, UK, ISSN 1744-1986.

[8] Moffett, J.D., and Nuseibeh, B. 2003. A Framework For Security Requirements Engineering, Department of Computer Science, YCS368. University of York, UK.

[9] Farkhani, T.R., and Razzazi, M.R. 2006. Examination and Classification of Security Requirements of Software Systems. *Information and Communication Technologies,* Vol 2, PP- 2778 – 2783.

[10] Souag, A., Mazo, R., Salinesi, C and Wattiau, I.C. 2105. Reusable knowledge in security requirements engineering: a systematic mapping study. *Requirements Eng*. DOI 10.1007/s00766-015-0220-8, Springer-Verlag London.

[11] Firesmith, D.G. 2003. Analyzing and Specifying Reusable Security Requirements. *RE'03, International Workshop on Requirements for High Assurance Systems*, USA.

[12] Hadary, H.E., and Kassas, S.E. 2014. Capturing security requirements for software Systems. *Journal of Advanced Research*. PP: 463–472.

[13] Lin, L., Nuseibeh, B., Ince, D., Jackson, M., and Moffett, J. D. 2003. Introducing abuse frames for analyzing security requirements. *11th IEEE international requirements engineering conference (RE'03)*. USA.

[14] Lin, L., Nuseibeh, B., Ince, D., Jackson, M., and Moffett, J. D. Analysing Security Threats and Vulnerabilities Using Abuse Frames. Technical Report No: 2003/10. Department of Computing. United Kingdom.

[15] Jackson, M. 2001. Problem Frames: Analysing and structuring software development problems, Addison Wesley.

[16] Sindre, G., Firesmith, D.G., and Opdahl, A.L. 2003. A Reuse-Based Approach to Determining Security Requirements. *9th international workshop on requirements engineering: foundation for software quality.*

[17] Sindre, G., and Opdahl, A.L. 2005. Eliciting Security Requirements with Misuse Cases. *Requirements Eng*, 10(1):34–44.

[18] Sindre, G., and Opdahl, A.L. 2000. Eliciting Security Requirements by Misuse Cases. *37th International Conference on Technology of Object-Oriented Languages and Systems.*

[19] Sindre, G., and Opdahl, A.L. 2001. Templates for misuse case description. *Seventh International Workshop on Requirements Engineering: Foundation of Software Quality (REFSQ'2001)*. Switzerland.

[20] Whittle, J., Wijesekera, D., and Hartong, M. 2008. Executable Misuse Cases for Modeling Security Concerns. *30th International Conference on Software Engineering*. Leipzig, Germany.

[21] Alexander, I.F. 2003. Misuse cases: use cases with hostile intent. *IEEE Software.* 20(1): 58-66.

[22] McDermott, J., and Fox, C. 1999. Using Abuse Case Models for Security Requirements Analysis. *Annual Computer Security Applications Conference*. USA.

[23] Lamsweerde, A.V. 2004. Elaborating Security Requirements by Construction of Intentional Anti-Models. 26th Int'l Conf Software Eng (ICSE 04). IEEE CS Press.

[24] Lamsweerde, A.V., Hermoye, L.A., Perry, D.E. 2006. A Reuse-Based Approach to Security Requirements Engineering.

[25] Lamsweerde, A.V., and Letier, E. 2000. Handling Obstacles in Goal-Oriented Requirements Engineering. *IEEE Transactions on Software Engineering, Special Issue on Exception Handling.* 26(10): 978-1005.

[26] Lamsweerde, A.V., Brohez, S., Landtsheer, R.D., and Janssens, D. 2003. From System Goals to Intruder Anti-Goals: Attack Generation and Resolution for Security Requirements Engineering. *RHAS-03 Workshop, RE'03*. USA.

[27] Haley, C.B., Moffett, J.D., Laney, R., and Nuseibeh, B. 2008. Security Requirements Engineering: A Framework for Representation and Analysis. *IEEE Trans Software Eng*. 34(1):133–53.

[28] Haley, C.B., Laney, R., and Nuseibeh, B. 2004. Deriving Security Requirements from Crosscutting Threat Descriptions. *Third international conference on aspect-oriented software development*. Lancaster, UK.

[29] Sebastiani, F. 2002. Machine Learning in Automated Text Categorization, *ACM Computing Surveys*, Vol. 34, No.1.

[30] Menzies, T., and Marcus, A. 2008. Automated Severity Assessment of Software Defect Reports. *IEEE International Conference on Software Maintenance (ICSM)*.

[31] Patil, T.R., and Sherekar, S.S. 2013. Performance Analysis of Naïve Bayes and J48 Classification Algorithm for Data Classification. *International Journal Of Computer Science And Applications.* Vol. 6, No.2.

[32] Danham, M.H., and Sridhar, S. 2006. Data mining: Introductory Advanced Topics. Person education , 1st Ed.

[33] Sharma, A.K., and Sahni, S. 2011. A Comparative Study of Classification Algorithms for Spam Email Data Analysis. *IJCSE*. Vol. 3, No. 5, pp. 1890-1895.

[34] Jiang, Y., Cukic, B., and Ma, Y. 2008. Techniques for evaluating fault prediction models. *Empirical. Software. Engineering*. Vol.13, No. 15, PP. 561-595.

[35] Emam, K.E., Benlarbi, S., Goel, N., and Rai, S. 1999. A validation of object-oriented metrics. *NRC Technical report ERB-1063*.

[36] Stone, M.1974. Cross-validatory choice and assessment of statistical predictions. *Journal Royal Stat. Soc*. [online]. *36*, pp.111-147.

Auto-Segmentation using Mean-Shift and Entropy Analysis

Seba Susan
Department of Computer Science & Engineering,
Delhi Technological University, New Delhi, INDIA
Email ID: seba_406@yahoo.in

Ankit Kumar
Department of Computer Science & Engineering,
Delhi Technological University, New Delhi, INDIA

Abstract— **In this paper we discuss the automization of the mean-shift clustering algorithm which is dependent on user-defined parameters for its efficiency. We propose that the optimum solution of mean-shift corresponds to the maximum entropy of the mode-probabilities which assume the form of a uniform probability distribution for the meaningful segmentation of a scene. The experimentation on the benchmark Berkeley segmentation database shows high accuracy for the automated mean-shift as compared to the baseline method. The Non-extensive entropy with Gaussian gain gives highly meaningful segmentation that agrees with human perception as compared to the extensive Shannon entropy.**

Keywords- Mean-Shift algorithm; Maximum entropy framework; Color Image Segmentation; Non-extensive entropy with Gaussian gain

I. INTRODUCTION

The segmentation of colour images has wide applications in diverse fields such as medical image analysis [1], video-surveillance and decoding human behaviour [2], object or person tracking and recognition [3] and remote sensing [4]. There are several well known approaches for color image segmentation such as clustering [5], Markov Random Fields (MRF) fields [6], Gaussian Mixture Models (GMM) [7], region-based approaches such as seeded region growing [8] and morphological operations [9]. The fuzzy co-clustering for images (FCCI) [5] is a recent development in this field with most accurate color clustering and differentiation ability. However on comparison, the segmentation by mean-shift clustering algorithm developed by Comaniciu *et. al.* in [10], was found more comprehensive in terms of human understanding as proved by its higher NPR index with respect to ground-truths for many images. Its disadvantage however is the user-defined color bandwidth parameter which is image-specific. There are several works which tried to work around this problem. In [11] Comaniciu himself suggested a technique for optimizing the bandwidth by testing for the most stable combination of mean and covariance of each mode by minimizing Jensen-Shannon divergence between neighbouring distributions. In our work we follow this trail and assume that for a human comprehensive image segmentation solution, the modes corresponding to different image segments would tend to be equally likely and the mode probabilities would approximately form a uniform distribution. A simple entropy analysis determines the optimum solution for mean-shift from the mode-probabilities. The paper is organised as follows. The proposed automization of the mean-shift algorithm is proposed in Section II. The experimental results are discussed in Section III and the overall conclusions are drawn in Section IV.

II. AUTOMIZING THE MEAN-SHIFT ALGORITHM BY ENTROPY ANALYSIS

The Mean-shift algorithm

The mean-shift algorithm [12] moves each seed point $\boldsymbol{x}$ to the average of its neighbors till convergence point is reached. It finds the dominant mode or peak from the gradient of the probability distribution. The mean-shift procedure involves two steps. The first step is the successive computation of the mean-shift vector $\boldsymbol{m}_{H,G}(\boldsymbol{x})$,

$$\boldsymbol{m}_{H,G}(\boldsymbol{x}) = \frac{1}{2} h_r^{\,2} c \frac{\nabla f_{H,K}(\boldsymbol{x})}{f_{H,G}(\boldsymbol{x})} \tag{1}$$

Equation (1) implies that the mean-shift vector $\boldsymbol{m}_{H,G}(\boldsymbol{x})$ at location $\boldsymbol{x}$ computed with kernel G is proportional to the normalized density gradient estimate $\frac{\nabla f_{H,K}(\boldsymbol{x})}{f_{H,G}(\boldsymbol{x})}$ obtained with kernel K. The mean-shift vector thus points to the maximum increase in density. h_r is the range or color bandwidth and the only unknown parameter in (1) that is user-defined. c is the normalization constant which integrates the kernel K to 1 at location $\boldsymbol{x}$. The second step in the mean-shift procedure is the translation of the kernel window $G(\boldsymbol{x})$ by $\boldsymbol{m}_{H,G}(\boldsymbol{x})$. In the image segmentation using mean-shift clustering algorithm [10], the steps would be to iteratively run the mean-shift procedure for each seed pixel $\boldsymbol{x}$ and store the filtered result as $\boldsymbol{z}$ and delineate clusters by merging together all $\boldsymbol{z}$ which are closer than h_r, and finally use the clusters that converge to a stationary point to label each pixel with the cluster number to which it belongs using the computed mode-probabilities. The mode probabilities are computed for the set of F dimensional data points $\{\boldsymbol{y}_i\}, i = 1, 2, .., N$ as

978-9-3805-4421-2/16/$31.00 ©2016 IEEE

$$\hat{f}(\boldsymbol{x}) = \frac{1}{N{h_r}^F} \sum_{i=1}^{N} K\left(\frac{\boldsymbol{x}-\boldsymbol{y}_i}{h_r}\right) \quad (2)$$

The user-defined parameters here are the color bandwidth h_r and the total number of initial random seed pixels $S = \{\boldsymbol{x}\}$. The choice of these parameters affects the clustering results and they are image-specific.

Automizing the Mean-shift

For efficient segmentation comprehensive to the human eye, the regions segmented should be continuous and form large chunks of meaningful information. To achieve this, the computed mode-probabilities, denoted by $\left\{\hat{f}(\boldsymbol{x})\right\} = \{p(\boldsymbol{x})\}$ such that $\sum_{\boldsymbol{x}} p(\boldsymbol{x}) = 1$, should approximate a uniform probability distribution for a human-comprehensive scene segmentation. A measure of how close a distribution approximates a uniform distribution is reflected from the entropy value of the distribution defined below. The entropy is highest when all the modes are equally likely and have equal mode probabilities.

Entropy is the uncertainty in a distribution and is defined as the expected value of information gain. If the information gain is logarithmic, we have the extensive Shannon entropy [12] defined by

$$H_s = -\sum_{\boldsymbol{x}} p(\boldsymbol{x}) \log p(\boldsymbol{x}) \quad (3)$$

If the information gain is Gaussian we have the non-extensive entropy with Gaussian gain [13] given by

$$H_{Next} = \sum_{\boldsymbol{x}} p(\boldsymbol{x}) e^{-p^2(\boldsymbol{x})} \quad (4)$$

Shannon entropy being logarithmic is additive. It is sensitive to noise since it adds up the contributions of all components including noisy pixels in an image which constitute the background clutter. The advantage of the use of the (exponential) Non-extensive entropy with Gaussian gain in the maximum entropy framework is that it is non-additive and hence less sensitive to noise in its additive form, which results in the formation of fewer number of clusters in an image that is conducive to the human eye. The noise-immunity and non-additivity feature of the entropy in (4) was utilized for monitoring crowd motion in videos [15] and for the steady, automatic growth of the hidden layer in dynamic neural networks [16] for incremental learning. In our work we perform an exhaustive search for the optimum parameters $\{h_r, S\}$ for which the entropy of the mode-probabilities attains a maximum value.

The proposed methodology for entropy-based optimization of mean-shift clustering is given below.

Step 1: Convert the color image data into an $N \times F$ array where, N is the number of pixels and F is the number of features with $F = 3$ for R,G,B color dimensions.

Step 2: Set the initial color bandwidth h_r to 0.01 and number of initial seed points S to 2. Let the initial clustering result of size $1 \times N$ be all zeros and let the initial entropy value be zero.

Step 3: Find the mean-shift modes for the given parameters.

Step 4: Find the mode-probabilities using Eq. (2) and normalize the probability distribution to 1.

Step 5: Calculate the entropy of the modes using Shannon entropy in Eq. (3) and also the Non-extensive entropy with Gaussian gain in Eq. (4). For both cases, if the entropy is more than that in the previous iteration, replace the entropy with the current entropy value and replace the (labels) clustering result with the current one.

Step 6: Repeat steps 3-6 for color bandwidth values in the range of [0.01, 1.5] with intervals of 0.01 and the number of initial seed points varying from 2 to 10.

Step 7: The optimum solution to mean-shift clustering is the one retained till the end for which the entropy is maximum for the mode probabilities generated by mean-shift.

III. EXPERIMENTAL RESULTS AND DISCUSSIONS

The experiments are performed on 100 images of the Berkeley segmentation database [17] which contains natural color images supplemented by (multiple) human-annotated ground-truth images. The software platform is MATLAB 7.10 and the execution time is a few seconds per image on a 2.8 GHz PC. The segmentation is carried out as per the procedure described in the previous section for automated color image segmentation by mean-shift. The mean-shift modes are computed and mode-probabilities are used to compute the entropy. The maximum entropy indicates the optimum clustering result. Fig.1 shows the segmentation results for the baseline mean-shift with color bandwidth fixed to 0.8 which gave good results in [5] and the proposed mean-shift automization using both the entropies in (3) and (4), for some example images from the database. The corresponding segmentation evaluation results in terms of Precision, Recall and F-score are summarized in Table 1 (shown here for the first ground-truth image provided with each image). It is observed that the non-extensive entropy based mean-shift gives the best segmentation results (maximum F-score) with least number of clusters and clutter in segmentation, agreeing best with human judgement. The results in Fig. 1 depict visually meaningful segmentation for the same. Examples 4,6,7,9,10 in Fig. 1 show the object clearly for proposed method (d) based on the non-extensive entropy with Gaussian gain. Especially the segmentation of the two polar bears in image 9 in Fig.1 is done very neatly by the proposed non-extensive entropy based mean-shift with no clutter at all. Both entropies give comparable results for images containing distinct colors

indicating unambiguous color probability distributions, as observed from examples 2 and 6 in Fig. 1 and Table 1. On examining the Recall values in Table 1 we see that the non-extensive entropy gives higher values for the same while the Precision is same for both entropies. This indicates more clutter in the segmentation by Shannon entropy based mean-shift due to false alarms. The result for the entire dataset of 100 images of the Berkeley segmentation database averaged for all ground-truths is summarized in Table 2 and reflects the same trend as that in Fig. 1 and Table 1. The proposed automization of mean-shift thus provides a solution to the user-defined parameters in the baseline method and also depicts a higher accuracy in the segmented results that agree with human perception. Replacing the exhaustive search in our method by optimized search techniques forms the future scope of our work.

IV. CONCLUSION

A solution to automizing the mean-shift algorithm is proposed in this work which aids in automatic image segmentation, with the segmentation results most comprehensive to the human eye. This is achieved by checking for the maximum entropy of the mode-probabilities which attains a maximum value for ideal segmentation. The non-extensive entropy with Gaussian gain being non-additive by nature, gives semantically meaningful clusters with less cluster for the proposed method. Experiments on the benchmark Berkeley segmentation dataset clearly highlight the usefulness of the proposed technique in terms of both high accuracy and automatic segmentation.

REFERENCES

[1] Pham, Dzung L., Chenyang Xu, and Jerry L. Prince. "Current methods in medical image segmentation 1." *Annual review of biomedical engineering* 2, no. 1 (2000): 315-337.

[2] Weinland, Daniel, Remi Ronfard, and Edmond Boyer. "A survey of vision-based methods for action representation, segmentation and recognition." *Computer Vision and Image Understanding* 115, no. 2 (2011): 224-241.

[3] Raja, Yogesh, Stephen J. McKenna, and Shaogang Gong. "Tracking and segmenting people in varying lighting conditions using colour." In *Automatic Face and Gesture Recognition, 1998. Proceedings. Third IEEE International Conference on*, pp. 228-233. IEEE, 1998.

[4] Meinel, G., and M. Neubert. "A comparison of segmentation programs for high resolution remote sensing data." *International Archives of Photogrammetry and Remote Sensing* 35.Part B (2004): 1097-1105.

[5] Hanmandlu, Madasu, Om Prakash Verma, Seba Susan, and Vamsi Krishna Madasu. "Color segmentation by fuzzy co-clustering of chrominance color features." *Neurocomputing* 120 (2013): 235-249.

[6] Deng, Huawu, and David A. Clausi. "Unsupervised image segmentation using a simple MRF model with a new implementation scheme." *Pattern recognition* 37, no. 12 (2004): 2323-2335.

[7] Ribeiro, Hebert Luchetti, and Adilson Gonzaga. "Hand Image Segmentation in Video Sequence by GMM: a comparative analysis." In *Computer Graphics and Image Processing, 2006. SIBGRAPI'06. 19th Brazilian Symposium on*, pp. 357-364. IEEE, 2006.

[8] Jain, Puneet Kumar, and Seba Susan. "An adaptive single seed based region growing algorithm for color image segmentation." In *India Conference (INDICON), 2013 Annual IEEE*, pp. 1-6. IEEE, 2013.

[9] Höhne, Karl Heinz, and William A. Hanson. "Interactive 3D segmentation of MRI and CT volumes using morphological operations." *Journal of computer assisted tomography* 16, no. 2 (1992): 285-294.

[10] Comaniciu, Dorin, and Peter Meer. "Mean shift: A robust approach toward feature space analysis." *Pattern Analysis and Machine Intelligence, IEEE Transactions on 24, no. 5 (2002): 603-619.*

[11] Comaniciu, Dorin. "An algorithm for data-driven bandwidth selection.″ *Pattern Analysis and Machine Intelligence, IEEE Transactions on 25*, no. 2 (2003): 281-288.

[12] Cheng, Yizong. "Mean shift, mode seeking, and clustering." *Pattern Analysis and Machine Intelligence, IEEE Transactions on* 17, no. 8 (1995): 790-799.

[13] C.E.Shannon, "A Mathematical theory of communication", *The Bell system Technical Journal,* Vol.27, pp.379-423 July,1948.

[14] Seba Susan, Madasu Hanmandlu, "A Non-Extensive entropy feature and its application to texture classification", *Neurocomputing,* Volume 120, November 2013, pp. 214–225.

[15] Susan, Seba, and Madasu Hanmandlu. "Unsupervised detection of nonlinearity in motion using weighted average of non-extensive entropies." *Signal, Image and Video Processing* (2013): 1-15.

[16] Susan, Seba, and Mayank Dwivedi. "Dynamic Growth of Hidden-Layer Neurons Using the Non-extensive Entropy." In *Communication Systems and Network Technologies (CSNT), 2014 Fourth International Conference on*, pp. 491-495. IEEE, 2014.

[17] The Berkley Segmentation Database and Benchmark. [online] http://www.eecs.berkley.edu/-search/Projects/CS/vision/bsds/

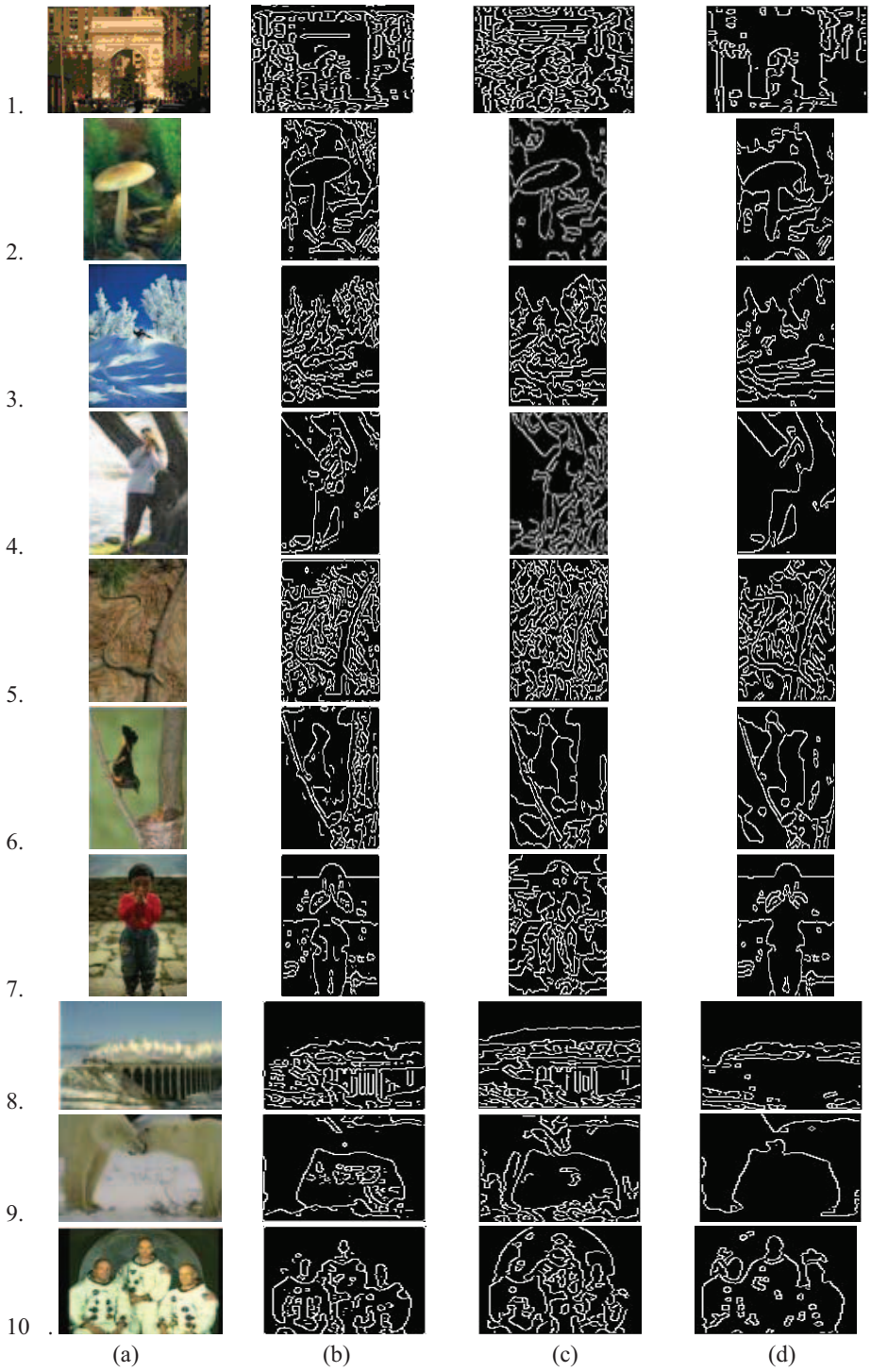

Fig.1. Segmentation results shown for ten of the Berkeley images (a) Original images (b) Baseline mean-shift results (c) Results of Proposed automization using Shannon entropy (d) Results of Proposed automization using Non-extensive entropy with Gaussian gain

TABLE 1: THE SEGMENTATION EVALUATION FOR THE EXAMPLES OF BERKELEY DATASET [17] SHOWN IN FIG. 1 FOR DIFFERENT METHODS (IN TERMS OF PRECISION: PRE, RECALL: REC, F-SCORE)

Image Sample	Baseline Mean-shift algorithm [12]			Proposed automization using Shannon entropy			Proposed automization using Non-extensive entropy with Gaussian gain		
	Pre	*Rec*	*F-score*	*Pre*	*Rec*	*F-score*	*Pre*	*Rec*	*F-score*
1	0.928	0.894	0.910	0.928	0.974	0.950	0.928	0.982	0.954
2	0.892	0.845	0.867	0.892	0.983	0.935	0.892	0.984	0.936
3	0.950	0.926	0.937	0.950	0.988	0.968	0.950	0.990	0.970
4	0.934	0.906	0.919	0.934	0.984	0.958	0.934	0.989	0.961
5	0.919	0.880	0.899	0.919	0.968	0.942	0.919	0.972	0.945
6	0.927	0.895	0.910	0.917	0.988	0.951	0.927	0.989	0.957
7	0.939	0.912	0.925	0.939	0.985	0.961	0.939	0.989	0.963
8	0.939	0.911	0.924	0.939	0.987	0.962	0.939	0.991	0.964
9	0.954	0.934	0.943	0.954	0.993	0.973	0.954	0.995	0.974
10	0.947	0.924	0.935	0.947	0.990	0.968	0.947	0.992	0.969

TABLE 2: THE SEGMENTATION EVALUATION FOR THE 100 IMAGES OF THE BERKELEY DATASET [17] FOR DIFFERENT METHODS (IN TERMS OF MEAN F-SCORE AVERAGED OVER ALL 100 IMAGES FOR ALL AVAILABLE GROUND-TRUTH ANNOTATIONS)

Method	*Mean F-score*
Baseline Mean-shift algorithm [12] (Bandwidth=0.8)	0.9192
Proposed automization of Mean-Shift using the extensive Shannon entropy	0.9540
Proposed automization of Mean-Shift using Non-extensive entropy with Gaussian gain	0.9582

CFD Analysis of Wavy Microchannel Heat Sink with Hemispherical Obstructions and Comparing it with Experimental Results of Rectangular Microchannel Heat Sink

Rajnish Kumar[1], M. Zunaid[2]

[1]*M. Tech Scholar, Department of Mechanical Engineering, Delhi Technological University, New Delhi-110042, India*

[2]*Assistant Professor, Department of Mechanical Engineering, Delhi Technological University, New Delhi-110042, India*

Abstract: **In the present analysis of fluid flow, there are two cases. In first case, CFD Analysis of wavy microchannel heat sink with hemispherical obstructions is done in Ansys CFX package and the simulation results are obtained for pressure drop and heat transfer characteristics for single phase laminar flow. For this analysis the geometry of the channel has been made wavy edge with rectangular entry and exit. Then the obstructions with hemispherical shape have been put at the particular wavelength. Water is taken as coolant and cooper is used as a sink material. The main aim of changing the geometry of the straight channel to wavy channel with the inclusion of hemispherical obstructions is to increase the surface area and contact time of coolant with the heated surface to increase the temperature rise by decreasing thermal resistance. In the second case, comparison of simulation results of the first case with experimental results of rectangular microchannel obtained by Weilin Qu and Issam Mudawar. Both the micro-channels have a width of 0.23mm and height of 0.71 mm. The aspect ratio (ɣ) and the length of both the channels is kept same as 0.32 and 44.7mm respectively. The diameter of hemispherical obstruction is taken as 0.22 mm. The analysis for both the micro-channels is done for five sets of Reynolds number which are 400, 600, 800, 1000 and 1200 respectively. The two values of heat flux used are 100W/cm^{2}and 200W/cm^2.After constructing the geometry in solid works and partially in the Design Modular, the simulation is done on ANSYS CFX.**

I. INTRODUCTION

Micro-channel heat sink-

Micro-channels have become very popular in applications where very high heat transfer rates are necessary. Its development trend as electronics equipment becomes more advanced and smaller in size with continuing innovations. It faces thermal engineering challenges from the high level of heat generation and the reduction of available surface area for heat removal. In the absence of sufficient heat removal, the working temperature of this component may exceed a desired temperature level which then increases the critical failure rate of equipment. Therefore, advanced electronic equipment with high heat generation requires an efficient and compact device to provide proper cooling operation. In order to meet the cooling requirement, needs to increase the product of heat transfer coefficient (h) and heat transfer surface area (A) for a device. Since heat transfer coefficient is related to the channel hydraulic diameter. The heat transfer surface area can be increased by incorporating micro channels on the device surface. One promising solution to the problem is liquid cooling incorporating on micro-channels. Micro-channel heat transfer has the potential of cooling high power density microchips. One can expect that as the size of the channel decrease, the value of convective heat transfer coefficient(h) becomes increasing in order to maintain a constant value of the Nusselt number (hD_h/kf). These chips have machined micro-channels through which cooling fluid like water is circulated. The cooling liquid removes heat by single phase forced convection. Flow within the micro-channel is considered as fully developed laminar flow with constant heat flux. Therefore, heat sinks with larger extended surfaces, highly conductive materials and more coolant flow are key parameters to reduce the base temperature.

Straight Microchannel

In Today's world the basic requirement in the field of heat transfer is compact heat exchanger, for cooling of electronic chips, micro level biological instruments etc. As we are having fixed surface area so, the solution is to vary the surface properties by having surface obstacles (delta-wings), surface indentation (dimples), surface channels (wavy, zigzag channel).

The major advantages of straight channels includes, increased surface area for heat flow, better flow mixing at curved portion results in better distribution of heat, and effective cooling . In normal heat flow as in straight channel same molecule remains in contact with the surface throughout the flow causes poor heat transfer, but in wavy or zig-zag channel, due to the phenomenon known as boundary layer regeneration fluid particle from free layer gets chance to come in contact with the surface which enhances the heat transfer characteristics. But its disadvantage is that it causes pressure

drop. But the value of effectiveness of channel is greater than one which shows that heat transfer enhancement is more as compared to pressure drop.

Wavy Microchannel

In Today's world the basic requirement in the field of heat transfer is compact heat exchanger, for cooling of electronic chips, micro level biological instruments etc. As we are having fixed surface area so, the solution is to vary the surface properties by having surface obstacles (delta-wings), surface indentation (dimples), surface channels (wavy, zigzag channel).

The major advantages of wavy channels includes, increased surface area for heat flow, better flow mixing at curved portion results in better distribution of heat, and effective cooling . In normal heat flow as in straight channel same molecule remains in contact with the surface throughout the flow causes poor heat transfer, but in wavy or wavy channel, due to the phenomenon known as boundary layer regeneration fluid particle from free layer gets chance to come in contact with the surface which enhances the heat transfer characteristics. But its disadvantage is that it causes pressure drop. But the value of effectiveness of channel is greater than one which shows that heat transfer enhancement is more as compared to pressure drop.

NOMENCLATURE

A_c Cross-sectional area of channel (m^2)
C_p Specific heat at constant pressure (J/kg-K)
D_h Hydraulic diameter of channel perimeter (m)
H Height of micro-channel heat sink (m)
H_{ch} Height of micro-channel (m)
H_{w1} Substrate thickness on insulated side of microchannel heat (m)
H_{w2} Substrate thickness on heated side of microchannel heat sink(m)
K Thermal conductivity (W/m-K)
L Length of microchannel heat sink (m)
P Pressure (Pa)
q Heat flux (W/m^2)
Re Reynolds number based on channel hydraulic diameter
R_{th} Thermal resistance (m-K/W)
T Temperature (K)
T_{in} Fluid inlet temperature (K)
T_{bm} Fluid bulk temperature (K)
W Width of micro-channel heat sink unit cell (m)
W_{ch} Width of micro-channel (m)
W_{w1}, W_{w2} Half-thickness of wall separating micro-channels (m)
ɣ aspect ratio

Greek symbols

μ dynamic viscosity ($N\text{-}s/m^2$)
ρ density (kg/m^3)

II. MATHEMATICAL FORMULATION

In the present study the single phase model of computational fluid dynamics is used for the purpose of computing and solving the problem of particular category. This single phase model will solve and calculate one transport equation for continuity and one for momentum for each phase, and after this the energy equations are solved for studying the fluid and thermal performance of the system. The simulation for this single phase model is done using ANSYS CFX.

The equations used in this model include the equation of momentum, equation of continuity and energy equation (ANSYS CFX). The use of energy equation is done for finding out temperature distribution on the wall. The equation for conservation of mass, continuity equation, can be written as follows:

Mass conservation equation

The equation for conservation of mass, or continuity equation, can be written as follows:

$$\frac{\partial \rho}{\partial t} + \nabla.(\rho \vec{v}) = S_m$$

The equation written above is a general equation for conservation of mass. Here S_m is the mass added from any user defined sources.

Momentum conservation equation

Momentum conservation in a reference frame which is non accelerating can be written as

$$\frac{\partial}{\partial t}(\rho \vec{v}) + \nabla.(\rho \vec{v}\vec{v}) = -\nabla p + \nabla.(\bar{\bar{\tau}}) + \rho g + \vec{F}$$

Where,

p is the static pressure ,τ is the stress tensor
F and ρg are the external forces on body and gravitational force on body.

Energy equation-

ANSYS CFX solves the energy equation in the following form:

$$\frac{\partial}{\partial t}(\rho E) + \nabla.(\vec{v}\,(\rho E + p)\,) = \nabla.\left(k_{eff}\nabla T + \sum_J h_j \overrightarrow{J_J} + \overline{\overline{\tau_{eff}}}.\vec{v}\right) + S_h$$

Where,
k_{eff} is the effective conductivity ($k+k_t$), where k_t is the turbulent thermal conductivity, defined on the basis of turbulence model being used, and J_j is the diffusion flux of species J . On the right-hand side of the equation the first

three terms represents energy transfer due to species diffusion, conduction, and viscous dissipation, respectively, S_h denotes the chemical reaction heat, and some other sources of heat.

Standard relations and associated equations

The bulk mean temperature, T_{bm} and the wall temperature, T_{wx} with distance x from the micro-channel entrance can be obtained by doing the thermal energy balance around the micro-channel which is given by the following equations.

$$T_{bm} = T_{in} + \frac{q\pi Dhx}{mCp}$$

Where,

T_{bm} is the bulk mean temperature.
T_{in} is inlet temperature.
q is the heat flux.
D_h is hydraulic diameter of channel.
m is mass flow rate across channel.

The relation between the hydraulic diameter and Reynolds number in a channel is given by

$$Re=\rho v D_h/ \mu$$

Where,
ρ is density
v is average velocity.
μ is dynamic viscocity.
D_h is hydraulic diameter of channel

III. METHODOLOGY

Straight rectangular micro-channel heat sink

In this chapter a three dimensional CFD simulation is done for the heat transfer and pressure drop characteristics of rectangular micro-channel. Material used for heat sink construction is copper. The experimental set up shown in figure was developed by Mudawar and Qu (2002).

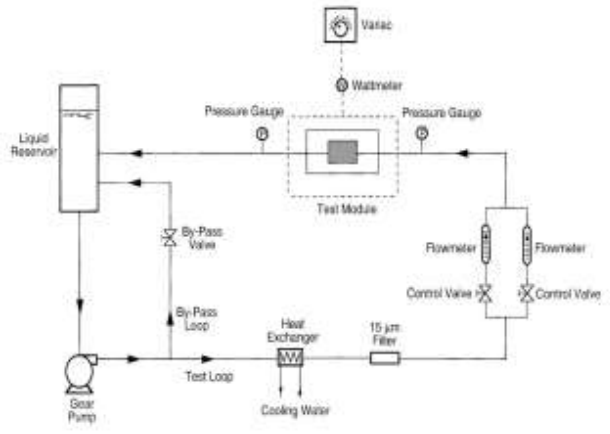

Figure 4.1: Schematic diagrams of flow loop [1]

Description of problem

The experimental work done by Qu and Mudawar, (2001) on the test apparatus is modelled and simulated in this present study. Water is moving through a straight rectangular smaller scale channel implanted in a test module. 21 rectangular smaller scale openings were machined into micro- channel surface by an accuracy machining procedure. The miniaturized scale openings were equidistantly divided inside of the 1-cm heat sink width and had the cross-sectional measurements of 231 μ m wide and 712 μm profound. There are 21 parallel rectangular small scale directs in the module. Figure shows the flow loop that was constructed to supply deionized water to the heat sink at the desired pressure, temperature, and flow rate. The water was pumped from a liquid reservoir and circulated through the flow loop by a gear pump. Upon exiting the pump, a portion of the flow, controlled by a by-pass valve, entered the test loop containing the heat sink, while the remaining portion returned to the reservoir though a by-pass loop. The test loop water first passed through a heat exchanger where the water was cooled to the desired inlet temperature. The water then passed through a 15 lm filter to prevent any solid particles from blocking the heat sink micro-channels. After exiting the filter, the water was routed to one of two rotameters for volume flow rate measurement. The water then entered the micro-channel heat sink test module where the electric power supplied to the heat sink was removed by the water. Leaving the test module, the water returned to the reservoir where it mixed with the bypassed flow.

Geometry of the rectangular microchannel heat sink

In the present analysis, only one micro channel of the remaining 21 micro-channels is considered as a computational domain. Figure shows the micro-channel heat sink with single unit cell used for simulation.

Table 4.1: Dimensions of the rectangular channel unit cell used for simulation

W_w (μm)	$W_{channel}$(μm)	H_{w1} (μm)	H_{ch} (μm)	H_{w2} (μm)	L (mm)
118	231	12700	713	5637	44.7

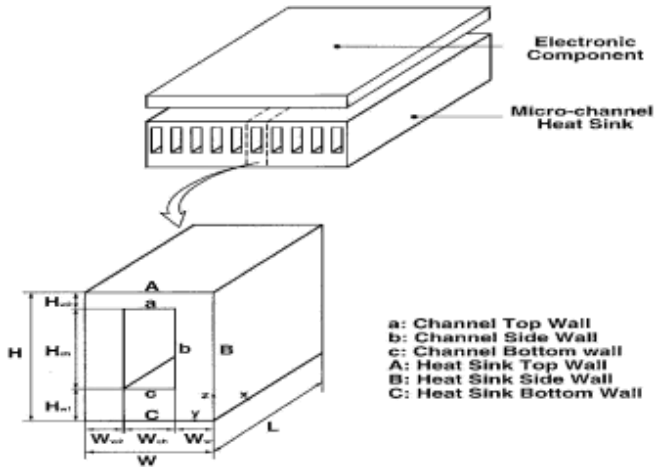

Figure 4.2: Schematic diagram of rectangular microchannel unit cell [1]

Experimental Results

Pressure drop for heat flux value=100W/cm^2

Reynolds number	Experimental pressure drop (bar)
400	0.10
600	0.17
800	0.23
1000	0.32
1200	0.41

Pressure drop for heat flux value=200W/cm^2

Reynolds number	Experimental pressure drop(bar)
400	0.08
600	0.15
800	0.21
1000	0.30
1200	0.40

Temp rise for heat flux value=100W/cm^2

Reynolds number	Experimental temp rise (°C)
400	22
600	16
800	10
1000	8
1200	6

Temp rise for heat flux=200 W/cm^2

Reynolds number	Experimental temp rise (°C)
400	44
600	31
800	22
1000	18
1200	15

CASE-1

Simulation of Wavy edge type rectangular micro-channel heat sink with hemispherical obstructions by taking water as a coolant and cooper as a sink material

In this chapter a three dimensional CFD simulation is done for the heat transfer and pressure drop characteristics of wavy edge rectangular micro-channel heat sink. Material used for heat sink construction is copper.

Problem description-

Water is moving through a wavy edge rectangular smaller scale channel heat sink assembly. In this analysis a design for wavy edge type of micro-channel heat sink is constructed. The dimensions of the micro-channel assembly are same as that of the rectangular micro-channels used in the experiments, the only difference being the length is made wavy along with hemispherical obstruction.

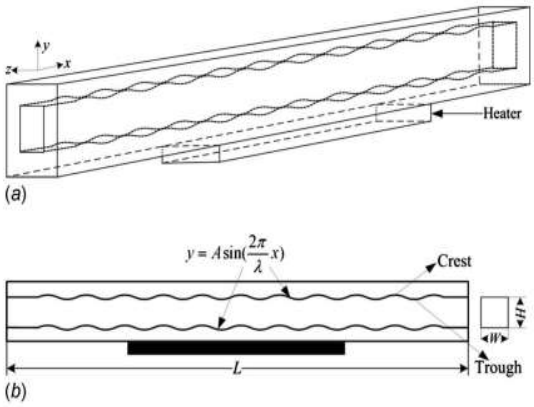

Figure: Schematic diagram of wavy microchannel heat sink.

Table: Dimensions of the wavy channel unit cell used for simulation

W_{wall} (µm)	W (µm)	H_{wall2} (µm)	H (µm)	H_{wall1} (µm)	L (mm)
118	231	12700	713	5637	44.7

In this analysis the only the length of the micro-channel heat sink is made wavy and the pressure drop and heat transfer characteristics are simulated.

Wave equation used- In this analysis, for the construction of geometry a sine wave is used which has the following equation.

$$y = Asin(2\pi x/\lambda)$$

Here, A is wave amplitude and λ is the wavelength.

Geometry construction-

For the analysis of computational fluid dynamics problem, the geometry of the heat sink was constructed using solid works, and was imported to ANSYS workbench CFX for further meshing and CFD simulations.

For creating geometry, first the heat sink was made in solid works as per the dimensions given in table. The wave dimensions were given according to the length of the channel which is 44.7 mm. A sinusoidal wave was assumed and constructed in the solid heat sink. The amplitude of the wave was taken as 0.15 mm while the wavelength was taken as 2 mm, and at a particular wavelength a hemispherical obstruction is made on the wavy edge and repeated to get fully along the channel. However, fluid channel was created in the design modular of Ansys CFX and not in the solid work as it was easy to make in the design modular and also it is made of the same dimensions as of the wavy rectangular slot along the

length of heat sink with hemispherical depression for proper mating and was given the name of fluid part.

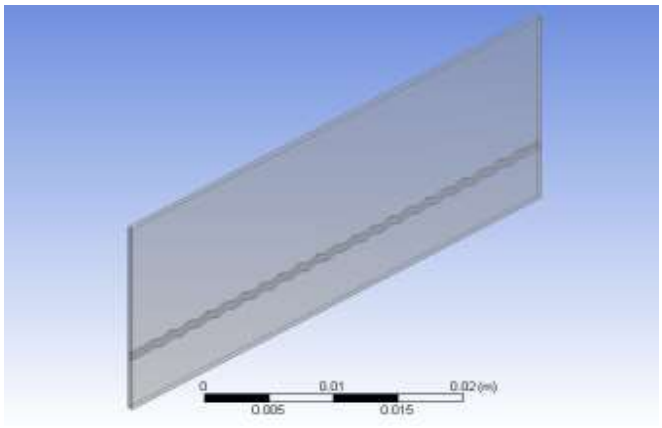

Figure: Geometry of wavy micro-cannel heat sink used in simulation

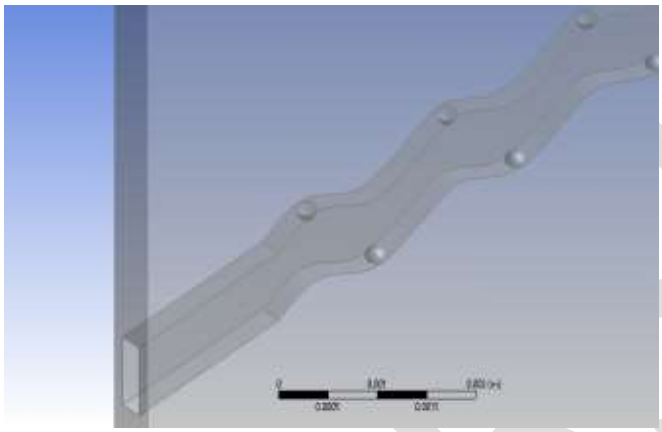

Figure: Detailed view of wavy micro-cannel heat sink with hemispherical obstructions

Meshing-

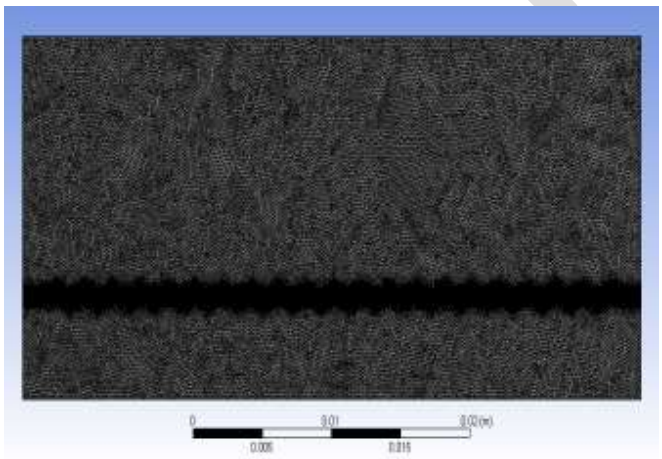

Figure: Meshing of geometry in ANSYS CFX

Table: Mesh details-

Physics preference	CFD
Solver preference	CFX
Smoothing	Medium
Transition	Slow
Transition ratio	0.77
Minimum size	1.2e-5
Maximum face size	1.21e-3
Maximum size	2.42e-3
Nodes	631403
Elements	3125145

Boundary conditions-

1. No slip on the surface.
2. Uniform inlet temperature and static pressure were given at the entry of the channel.
3. Outlet of the channel is based on mass flow rate.
4. A uniform heat flux of 100W/cm^2 and 200 W/cm^2 at the bottom wall of the heat sink for two separate cases was applied.

Table: Zone specification

Front wall of solid heat sink	Wall
Top wall of solid heat sink	Wall
Back wall of solid heat sink	Wall
Bottom wall of solid heat sink	Heat flux
Heat sink right wall	Wall
Heat sink left wall	Wall
Channel entry	Static pressure
Channel exit	Mass flow rate
Default Interface	Wall

Table: Solver settings

Following are the solver settings which are to be used in simulation.

Min. Iterations	1
Max. Iterations	250
Residual type	RMS
Residual target	1E-4
Time scale control	Auto time scale

IV. SIMULATION RESULTS

In the following computational fluid dynamics analysis the results are plotted for temperature rise and heat transfer in wavy edge type rectangular microchannel for two different values of heat fluxes applied at the bottom of the heat sink for varying set of values of Reynolds number. The value of heat flux used in the analysis are 100W/$cm^2$and 200W/cm^2. Five values of Reynolds number are taken for the analysis which are 400, 600, 800, 1000 and 1200 respectively

Results for heat flux= 100W/cm^2 for different sets of Reynolds number

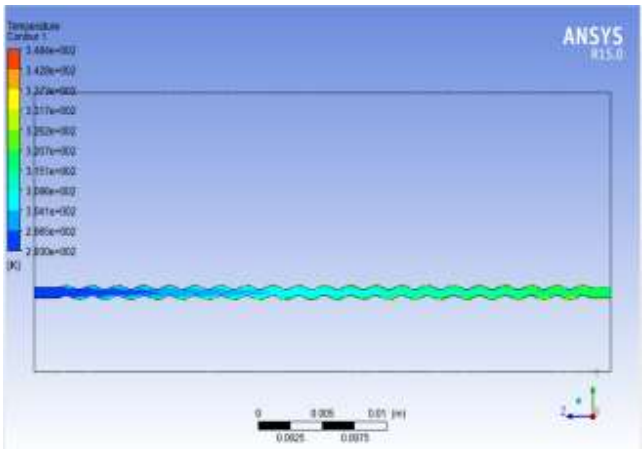

Figure: Temperature contour of water along wavy channel at Re=400

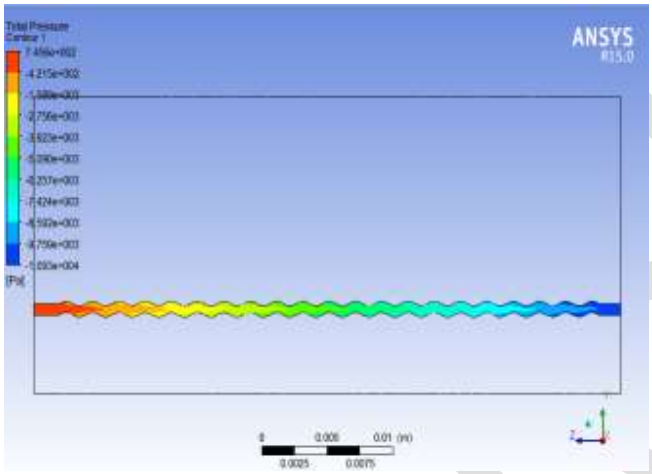

Figure: Pressure contour of water along wavy channel at Re=400

Results for heat flux of 200 W/cm^2 and different sets of Reynolds number

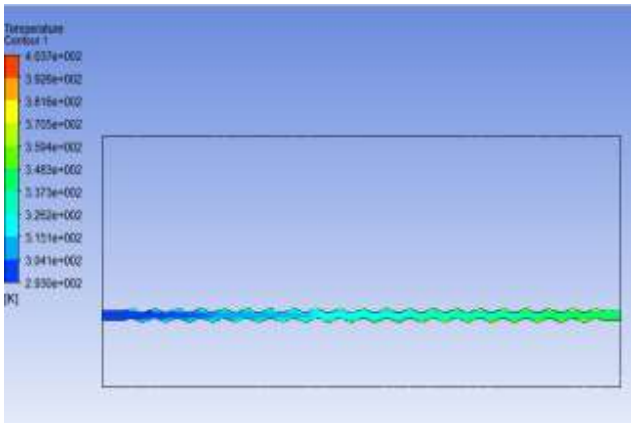

Figure: Temperature contour along wavy channel at Re=400

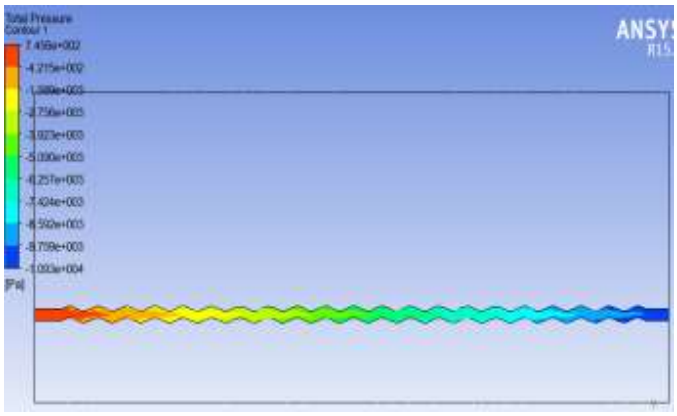

Figure: Pressure contour along wavy channel at Re=400

In the above figures, contours for temperature rise and pressure drop along the channel has been shown at Reynolds number 400 for bottom wall heat flux at 100 W/cm^2 and 200 W/cm^2 respectively. Similarly all the contours for Reynolds number 600, 800, 1000 and 1200 at heat flux 100 W/cm^2 and 200 W/cm^2 are obtained and put in the table in the form of numerical values.

Table: Computational Temperature Rise for heat flux=100W/cm^2

Reynolds number	**Computational temperature rise(°C)**
400	27
600	23
800	21
1000	19
1200	18

Table: Computational Temperature Rise for heat flux =200W/cm^2

Reynolds number	Computational temperature rise (°C)
400	55
600	47
800	43
1000	40
1200	38

Table:Computational pressure drop for heat flux =100W/cm^2

Reynolds number	**Computational Pressure Drop(bar)**
400	0.116
600	0.183
800	0.255
1000	0.344
1200	0.418

Table: Computational pressure drop for heat flux =200W/cm^2

Reynolds number	Computational Pressure Drop(bar)
400	0.115
600	0.181
800	0.254
1000	0.341
1200	0.416

CASE-1

Comparison of simulation results of the Wavy microchannel with hemispherical obstructions with experimental results of rectangular microchannel obtained by Weilin Qu and Issam Mudawar

Table: Temperature Rise for different Reynolds number for heat flux=100W/cm^2

Reynolds number	Experimental Temperature Rise(°C) (rectangular)	Computational Temperature Rise(°C) (wavy)
400	22	27
600	16	23
800	10	21
1000	8	19
1200	6	18

Table: Temperature Rise for different Reynolds number for heat flux=200 W/cm^2

Reynolds number	Experimental Temperature Rise(°C) (rectangular)	Computational Temperature Rise(°C) (wavy)
400	44	55
600	31	47
800	22	43
1000	18	41
1200	15	38

Table: Pressure Drop for different Reynolds number for heat flux=100 W/cm^2

Reynolds Number	Experimental Pressure Drop(bar) (rectangular)	Computational Pressure Drop(bar) (wavy)
400	0.10	0.116
600	0.17	0.183
800	0.23	0.255
1000	0.32	0.344
1200	0.41	0.418

Table: Pressure Drop for different Reynolds number for heat flux=200 W/cm^2

Reynolds Number	Experimental Pressure Drop(bar) (rectangular)	Computational Pressure Drop(bar) (wavy)
400	0.08	0.115
600	0.15	0.181
800	0.21	0.254
1000	0.30	0.341
1200	0.40	0.416

GRAPH-

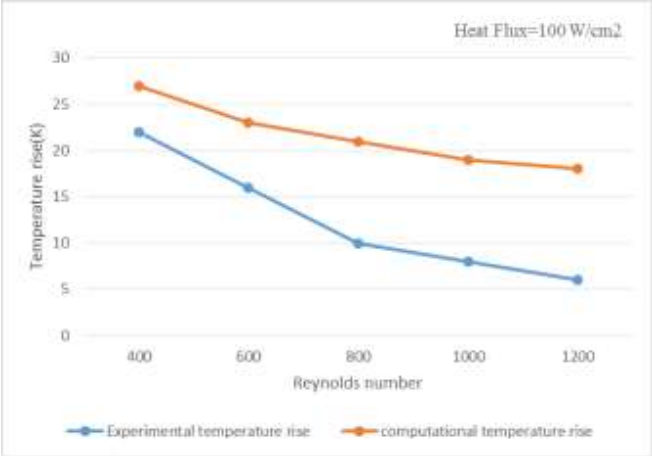

Figure: Temperature rise vs Reynolds number (Heat flux=100 W/cm^2)

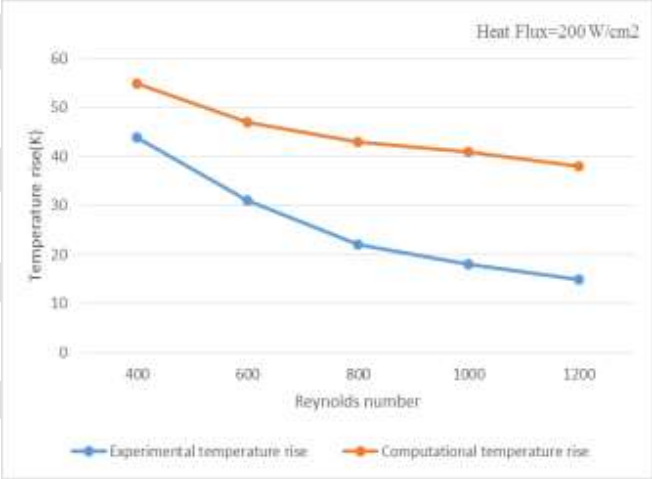

Figure: Temperature rise vs Reynolds number (Heat Flux=200 W/cm^2)

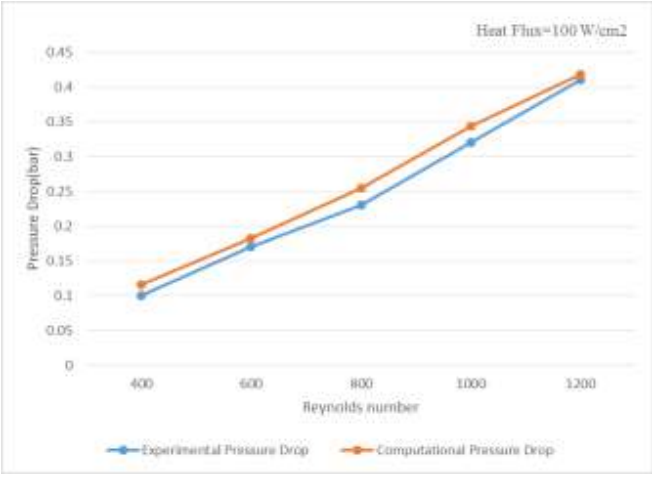

Figure: Pressure Drop vs Reynolds number (Heat Flux=100 W/cm^2)

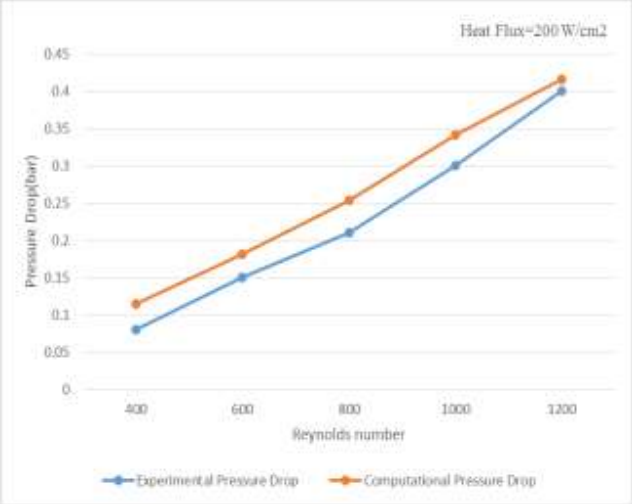

Figure: Pressure Drop vs Reynolds number (Heat Flux=200 W/cm^2)

V. CONCLUSION

Based on the numerical study on both straight and wavy edge type micro-channel with hemispherical obstructions the following conclusions can be made-

- Water temperature rise is more at the outlet of wavy edge type of micro-channels with hemispherical obstructions in comparison to straight micro-channels for same values of Reynolds number and heat flux.
- From the above results both for straight rectangular micro-channel and wavy edge type micro-channel the thermal performance of wavy edge micro-channel is found to be better in comparison to that of straight micro-channel of same hydraulic diameter.
- With the inclusion of hemispherical obstructions in wavy channel, surface area as well as contact time of fluid with heated surface increases due to which thermal resistance decreases which ultimately increases the heat transfer as a result, we get the higher temperature rise of the fluid.
- Pressure drop is found to be more in wavy edge micro-channels in comparison to that of straight micro-channels, however the loss in pressure is compensated by the better heat transfer characteristics of the wavy micro-channel.
- Velocity of water decreases along the flow direction in wavy micro-channels due to loss in energy of fluid while travelling along wavy channel with hemispherical obstructions.
- As the value of heat flux in wavy type of channel is increased from 100W/cm^2 to 200W/cm^2 there is an increase in the outlet temperature of water, however the pressure drop along the channel decreases. But the difference in pressure drop is very less.

REFERENCES

[1] I. Mudawar, W. Qu, Experimental and numerical study of pressure drop and heat transfer in a single-phase micro-channel heat sink, Int. J. Heat and Mass Transfer 45(2002) 2549-2565.

[2] G.M. Mala, D. Li, J.D. Dale, Heat transfer and fluid flow in micro-channels, International Journal of Heat and Mass Transfer 40 (1997) 3079-3088.

[3] L.T. Yeh, Review of heat transfer technologies in electronic equipment, ASME J. Electron. Packag. 117 (1995) 333–339.

[4] D.B. Tuckerman, R.F.W. Pease, High-performance heat sinking for VLSI, IEEE Electron. Dev. Lett. EDL-2 (1981) 126–129.

[5] I. Mudawar, M.B. Bowers, Ultra-high critical heat flux (CHF) for subcooled water flow boiling —I: CHF data and parametric effects for small diameter tubes, Int. J. Heat Mass Transfer 42 (1999) 1405–1428.

[6] I. Mudawar, W. Qu, Analysis of three dimensional heat transfer in micro-channels, Int. J Heat and Mass Transfer 45 (2002) 3973-3985.

[7] K. Kawano, K. Minakami, H. Iwasaki, M. Ishizuka, Micro channel heat exchanger for cooling electrical equipment, Application of Heat Transfer in Equipment, Systems and Education, ASME HTD-361-3/PID-3, 1998, pp. 173–180.

[8] A. Bejan, A.M. Morega, Optimal arrays of pin fins and plate fins in laminar forced convection, ASME J. Heat Transfer 115 (1993) 75–81.

[9] A.G. Fedorov, R. Viskanta, Three-dimensional conjugate heat transfer in the microchannel heat sink for electronic packaging, Int. J. Heat Mass Transfer 43 (2000) 399–415.

[10] X.F. Peng, G.P. Peterson, Convective heat transfer and flow friction for water flow in microchannel structures, Int. J. Heat Mass Transfer 39 (1996) 2599–2608.

[11] K.K. Ambatipudi, M.M. Rahman, Analysis of conjugate heat transfer in microchannel heat sinks Numer. Heat Transfer A, 37 (2000), pp. 711–731.

[12] Y. Sui, C.J. Teo, P.S. Lee, Y.T. Chew, C. Shu, Fluid flow and heat transfer in wavy micro-channels Int. J. Heat Mass Transfer, 53 (2010), pp. 2760–2772.

[13] P. Gunnasegaran, H.A. Mohammed, N.H. Shuaib, R. Saidur, The effect of geometrical parameters on heat transfer characteristics of micro-channels heat sink with different shapes Int. Commun. Heat Mass Transfer, 37 (8) (2010), pp. 1078–1086

[14] E. Utriainen, B. Sunden, Numerical analysis of primary surface trapezoidal cross wavy duct Int. J. Numer. Method Heat Fluid Flow, 10 (6) (2000), pp. 634–648.

[15] S. Kandlikar, S. Garimella, D. Li, S. Colin, M.R. King, Heat Transfer and Fluid Flow in Minichannels and Microchannels, Elsevier, USA, 2005.

[16] E. Utriainen, B. Sunden, Numerical analysis of primary surface trapezoidal cross wavy duct, Int. J. Numer. Method Heat Fluid Flow 10 (6) (2000) 634–648.

[17] W. Yang, J. Zhang, H. Cheng, The study of flow characteristics of curved microchannel, Appl. Therm. Eng. 25 (2010) 1894–1907.

[18] R.K. Shah, A.L. London, Laminar Flow Forced Convection in Ducts, Academic Press, New York, 1978.

[19] S.G. Kandlikar, W.J. Grande, Evaluation of single phase flow in microchannels
for high heat flux chip cooling – thermohydraulic performance enhancement and fabrication technology, Heat Transfer Eng. 25 (8) (2004) 5–16.

[20] S.V. Garimella, C.B. Sobhan, Transport in microchannels – a critical review, Annu. Rev. Heat Transfer 13 (2003) 1–50.

Clustering based Feature Selection Methods from fMRI data for Classification of Cognitive States of the Human Brain

Awijit Gupta
B.Tech, Computer Science Engineering
Delhi Technological University
Delhi, India
awijitgupta@gmail.com

Arjun Gupta
B.Tech, Computer Science Engineering
Delhi Technological University
Delhi, India
arjun220394@gmail.com

Kapil Sharma
Computer Science and Engineering
Delhi Technological University
Delhi, India
kapil@ieee.org

***Abstract*—Functional Magnetic Resonance Imaging (fMRI) is a neuroimaging technique that has proven to be useful for decoding and analyzing cognitive states of the human brain. It generates 3D images with high spatial resolution resulting in high dimensional images. In order to avoid curse of dimensionality, we need good feature selection techniques. Through this paper, we propose a two phase algorithm for finding a small subset of relevant and non-redundant voxels for classification of cognitive states in a human being. In the first phase, the entire feature set is clustered using normalized cut with maximal information compression index as the similarity. The most informative voxel is selected from each cluster using t-statistics and a pool of k voxels is created. In the next phase, a wrapper based sequential forward feature selection technique is used to obtain the optimal voxels for a given classifier.**

I. INTRODUCTION

The advent of FMRI has made it possible to analyze a person's cognitive state based on his neural activity. FMRI measures the ratio of oxygenated hemoglobin to deoxygenated hemoglobin in the blood with respect to a control baseline, at many locations within the brain. The fundamental idea is that when a stimulus is presented to a subject, he consciously thinks about it and that leads to changes in the Blood Oxygen Level Dependent (BOLD) signals [1]. These changes encode the representation of the stimulus in the brain [2]. A common application as well as the case study discussed in this paper is the sentence vs picture study. In this study, using the data taken in trials, we try to predict whether the subject is reading a sentence or looking at a picture.

A typical FMRI image consists of tens of thousands of voxels. A series of these images is used to represent a cognitive state thus taking the feature set to the size of hundreds of thousands. Moreover, due to small sample size, it is safe to say that FMRI dataset suffers the curse of dimensionality[3]. Although, all of the scanned voxels are not activated for every stimulus. Using this information we can effectively reduce the size of the data set to achieve higher accuracy by avoiding over fitting of the classifier.

In this paper, we propose an algorithm which has been used for extracting relevant genes for cancer cells classification [4]. This method for feature selection aims at two main points. Firstly, the features have to be relevant to the classification and secondly, there should be minimum redundancy in the information provided by the features. This algorithm is executed in 2 phases. In the first phase, the correlated voxels are grouped into clusters and from every cluster, the most relevant voxel is selected and placed into a pool of non-redundant voxels. Then, a Sequential Forward Feature Selection (SFFS) method is applied to select a smaller set of discriminatory voxels which can provide maximum classification accuracy for a given classifier [4].

This paper is organized as follows.First we take a look at the work done in the past two decades in this field and other fields where the problem of high dimensionality exists. Then we describe the dataset used for the experiment and discuss the methods applied for preprocessing and readying the data. Following that, we explain the various concepts used in the algorithm and finally present the algorithm. We then present the results and compare it with other techniques and methods previously applied in this area.

II. RELATED WORK

Classification of high dimensional fMRI data is a problem that needs a combination of neuroimaging and machine learning techniques to solve. Applying standard classifiers directly on the large amount of data leads to overfitting of the data and hence reduced accuracy. In order to achieve high accuracy, a smaller subset of discriminatory voxels are to be selected without losing much information. In literature, many feature selection methods have been proposed which are based on some sort of ranking based on relative strength of the voxel [4]. This strength may be defined as the ability to discriminate one class from another or the rate of change of activity when compared with an idle state. These classifiers return a set of top ranked features and a classifier is built on them.

To reduce the dimensionality of the fMRI dataset, [5] selected voxels based on their activity when compared to an idle state. Reference [6]applied Ensemble based techniques, [7] evolutionary algorithm based, [8] mutual information based, [9]

978-9-3805-4421-2/16/$31.00 ©2016 IEEE

ANOVA based and [10] t-test based. These feature selection techniques have shown promising results.

Multivariate techniques such as principal component analysis [11], independent component analysis [12], and canonical correlation analysis [13] have also been applied and have shown better results in some cases. Instead of using voxel activity as a criteria, these methods used the correlation between voxels and the collective effect of multiple voxels.

All the methods listed above work well for classification on a single subject. For classification over multiple subjects, a representation that is comparable across subjects is required and univariate techniques are preferred. Reference [14] indicates the use of genetic algorithms to find the most discriminating voxels.Methods applied in other similar areas of problems facing the curse of dimensionality also have shown some useful results. A closely related study on gene classification for detecting cancer cells also uses highly dimensional data of small sample size. The method proposed in this paper has been applied for relevant gene selection to detect cancer cells and the results obtained have inspired the proposal of the experiment conducted in this paper [4].

Reference [15] has used the Fisher Discriminant Ratio to find the most active voxels from the various Regions of Interests to use for classification purpose. This method has obtained a very high accuracy rate of 96.45 % using the Gaussian Naïve Bayes Classifier, solidifying the premise that it is indeed possible to classify the cognitive states of the brain using fMRI data with efficient feature selection methods.

III. DATA DESCRIPTION, ACQUISITION AND PREPROCESSING

The data used for the study in this paper is publicly available fMRI data made public by [16]. This data was collected from normal students from the university community in California. Out of multiple subjects' data, the least noisy subset was selected for further preprocessing. Artifacts created due to signal drift, head motion and other sources were removed using the FIASCO program [17]. In the dataset, all voxel activity values are represented by the percent difference from their mean value during rest conditions. Further preprocessing included temporal filtering and motion correction.

The data per subject consists of 54 trials where in each trial, an image was captured every 0.5 seconds. In 10 out of these, the subject was simply looking at a blank screen which we will be referring to as fixation trials. In 40 of them, a subject looked at a sentence and a picture for 4 seconds each and the remaining time was spent looking at a blank screen. In these trials, the subject was shown the first stimulus for thefirst 4 seconds followed by a blank screen for another 4 seconds. Then, the second stimulus was shown for 4 seconds again followed by a blank screen for 15 seconds. The total trial lasted for 27 seconds. In these 40 trials, the first stimulus was a picture for 20 trials and for the remaining 20, the first stimulus was a sentence. Hence, the classes are equally distributed with 40 examples of each class.

Previous research has identified regions of interest in the brain where most of the voxel activity takes place for different stimuli [18] and [19]. The regions of interest that we are concerned with are 'CALC', 'LIPL', 'LT', 'LTRIA', 'LOPER', 'LIPS' and 'LDLPFC' [20].

IV. FEATURE SELECTION

The proposed algorithm performs clustering of the data set using Normalized Cut clustering algorithm.This clustering technique was proposed by Shi and Malik [21] and it is based on graph theoretic approach for image segmentation [4]. The normalized cut criteria ensure that the voxels have high level of correlation within the clusters and low correlation among clusters. The distance measure used is Maximal information compression index which measures the dependency between 2 random variables. NCUT is a top down hierarchical clustering algorithm based on graph theory. After the first two clusters are formed, representative entropy is used to decide which cluster is to be partitioned next. These concepts are explained in detail here and they are followed by the two phase algorithm.

A. Maximal Information Compression Index

The similarity measure used for determining the correlation and redundancy between two voxels is given by the maximal information compression index [24]. Given 2 random variables $x_1$and x_2, the index $\lambda(x_1, x_2)$ is defined as:

$$\lambda(x1, x2) = \frac{\sigma_1+\sigma_2-\sqrt{((\sigma_1+\sigma_2)^2-4\sigma_1\sigma_2(1-\rho(x_1,x_2)^2)}}{2} \quad (1)$$

whereσ_1, σ_2 are the variance of $x_1$and $x_2$respectively and $\rho(x_1, x_2)$ is the correlation between $x_1$and x_2.

The lower the value of λ, the higher the correlation. This measure possesses propertiessuch as symmetry, sensitivity to scaling and invariance to rotationwhich are not present in standard distance measures like Euclidean distance, correlation coefficient [5].

B. Entropy measure

Among the partitioned clusters, the next cluster to be partitioned is chosen using the Representative Entropy measurewhich measures the redundancy among voxels in a given cluster. The Representative Entropy H_R of a single cluster is calculated as:

$$H_R = -\Sigma_{l=1}^{p}\overline{\lambda_l}\log\overline{\lambda_l} \quad (2)$$

where$\overline{\lambda_l} = \frac{\lambda_l}{\Sigma_{l=1}^{p}\lambda_l}$ and $\lambda_l, l = 1, 2, \ldots\ldots, p$ are the Eigen values of the matrix Σ. The matrix Σ is the covariance matrix of a cluster containing *p voxels.*

Higher the value ofH_R, lower the redundancy within the cluster. Hence, we select that cluster for partitioning which has highest value of H_R as it contains the most non-redundant genes. The minimum value of H_R can reach zero only when all the eigenvalues except one are zero. This happens when all the information is present along a single direction. $H_R$is maximum when eigenvalues are equally distributed among the voxels.

C. The Algorithm

The feature set is grouped into k clusters using Normalized Cut clustering algorithm. The algorithm initializes with a graph G=(V,E), where $v_i \epsilon$ V represents a voxel and $e(v_i, v_j) \epsilon$ E represents similarity between the two voxels. This graph is then partitioned into two clusters using the NCUT evaluation function. The clusters thus formed are such that the correlation between voxels within a cluster is maximum and that between clusters is minimum.

Among the partitioned clusters, the next cluster to be partitioned is selected using the representative entropy of the clusters. The cluster with the maximum representative entropy is further portioned into two more clusters. The next partition is then selected among the total clusters and this process is repeated until a pre-decided number of clusters is formed.

After the creation of distinct clusters each containing multiple voxels, a t-statistics test against the fixation period was applied to each cluster and the voxel with the highest t-statistic was chosen from every cluster resulting in a pool of k non-redundant voxels. This process was repeated for every trial and a rank matrix was generated which contained the number of times a voxel was selected for the pool of non-redundant voxels. Using this matrix, the top k voxels were finally selected for the second phase.

In the second phase, a Sequential Forward Feature selection (SFFS) method was applied to the above mentioned pool of voxels to select a smaller set of discriminatory voxels which provided maximum accuracy [4]. The Gaussian Naive Bayes classifier was used to measure the accuracies in SFFS.

V. EXPERIMENTAL SETUP AND RESULTS

The classification function used for our study is of the following form:

f: fmri-sequence (t1, t2) → cognitive state

Previous studies [5] have shown that stimulus related activity stays in the brain for another 8 to 10 seconds even after the stimulus is taken away from the subject. This indicates that a few seconds after the stimulus subjection should also be considered for classification. Thus, we take 4 seconds extra per stimulus in our feature set. Hence, (t1, t2) represents a time period of 8 seconds and t1 is always such that it represents the beginning of the stimulus.

Classification of the stimuli was done using Gaussian Naive Bayes Classifier. The accuracy of the learning algorithm was measured as follows. For every run, one example each from both the sentence and picture classes was left out of the training data and cross validation was done with these left out examples. Out of the 40 examples for each class, each one was left at a single run resulting in 40 runs of the classifier. The final result for a given number of clusters k and top n voxels were calculated by averaging the accuracy rates of these 40 trials.

This entire process is repeated for all the six subjects and error rates are averaged out for different values of k in order to make a comparison profile as shown in Table 1.

TABLE 1. CLASSIFICATION ACCURACY RATES FOR DIFFERENT CLUSTER SIZES

Features	Average	A	B	C	D	E	F
All	75	52.55	68.75	97.45	72.15	78.45	80.05
300	81	58.25	77.75	96.25	82.45	85.5	85.95
600	79	56.75	74.75	97.05	79.45	81.25	83.55
900	86	70.05	81.65	97.85	85.55	88.85	92.35
1200	82	68.65	75.85	94.55	82.25	87.95	84.35

A comparison with other methods for this study is plotted in the graph shown in fig. 1. The first bar represents the accuracy obtained by using the entire dataset. The next 2 bars represents the best accuracies obtained by using univariate methods in [5]. The fourthbar represents the usage of k-means clustering with Euclidean distance and the last set represents the algorithm explained in this paper.

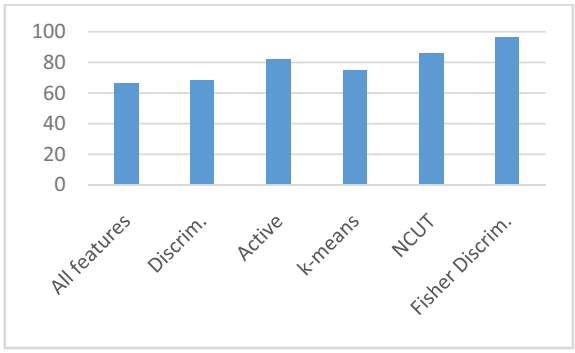

Fig. 1 Accuracy rates comparison with other feature selection techniques

It is observed that NCUT clustering with maximal information compression index of the feature set provides higher accuracy rates as compared to other univariate feature selection techniques but pales in comparison to the Fisher Discriminant ratio technique used in [24].

VI. CONCLUSION

In this paper, we have proposed a reasonably efficient two phase algorithm for finding a small set of features responsible for classification from an otherwise high dimensional data set. We have observed that this high dimension indeed causes over fitting and most of the voxels scanned through fMRI are redundant and/or irrelevant for the classification of cognitive states. Using NCUT clustering with maximal information compression index as the similarity measure has resulted in a

small pool of voxels which are sufficient for decoding whether a person is looking at a picture or reading a sentence.

We compared the results of this process with other previously applied feature selection techniques and observed that it outperforms all the univariate techniques used in [7] but fails to perform better than the Fisher discriminant ratio method used in [24]. Although this method may not have worked very well with this particular study but the experiment shows promising results which can be further exploited to achieve greater results in this field or any other where there is a problem of high dimensionality and irrelevant features.

VII. ACKNOWLEDGMENT

We are grateful to our friends and colleagues Akshay Uppal and Deepankar Anil Kumar for helping us optimize the code and Suhail Ahmed, Bhawani Bhandari and Nikil James Paul for many useful observations and suggestions during the course of this work. We are also grateful to Mr. Ashish Tripathi for his continuous support and proofreading of this paper.

REFERENCES

[1]. Anderson, J. R. et al. (2004). An information-processing model of the BOLD response in symbol manipulation tasks. Psychonomic Bulletin and Review.

[2]. S. A. Huettel, A. W. Song, and G. McCarthy, Functional magnetic resonance imaging. Sinauer Associates Sunderland, 2004, vol. 1.

[3]. Bellman, R.: Adaptive Control Processes. A Guided Tour. Princeton University Press, Princeton (1961)

[4]. Bala, Rajni, R. Agrawal, and Manju Sardana. "Relevant gene selection using normalized cut clustering with maximal compression similarity measure."*Advances in Knowledge Discovery and Data Mining* (2010): 81-88.

[5]. T. M. Mitchell, R. Hutchinson, R. S. Niculescu, F. Pereira, X. Wang, M. Just, and S. Newman, "Learning to decode cognitive states from brainimages," Machine Learning, vol. 57, no. 1-2, pp. 145–175, 2004

[6]. B. Jin, A. Strasburger, S. J. Laken, F. A. Kozel, K. A. Johnson, M. S. George, and X. Lu, "Feature selection for fmri-based deception detection," BMS bioinformatics, vol. 10, no. Suppl 9, p. S15, 2009.

[7]. M. B. ˚ Aberg, L. Löken, and J. Wessberg, "An evolutionary approach to multivariate feature selection for fmri pattern analysis." in BIOSIGNALS (2), 2008, pp. 302–307.

[8]. V. Michel, C. Damon, and B. Thirion, "Mutual information-based feature selection enhances fmri brain activity classification," in Biomedical Imaging: From Nano to Macro, 2008, ISBI 2008.

[9]. B. Thirion, E. Duchesnay, E. Hubbard, J. Dubois, J. B. Poline, D. Lebihan, and S. Dehaene, "Inverse retinotopy: inferring the visual content of images from brain activation patterns," Neuroimage, vol. 33, no. 4, pp. 1104–1116, 2006.

[10]. S. Balci, M. Sabuncu, J. Yoo, S. Ghosh, S. Whitfield-Gabrieli, J. Gabrieli, and P. Golland, "Prediction of successful memory encoding from fmri data," in Medical image computing and computer-assisted intervention: MICCAI...International Conference on Medical Image Computing and Computer-Assisted Intervention, vol. 2008, no. 11. NIH Public Access, 2008, p. 97.

[11]. J. Mourao-Miranda, K. J. Friston, and M. Brammer, "Dynamic discrimination analysis: a spatial–temporal svm," Neuroimage, vol. 36, no. 1, pp. 88–99, 2007.

[12]. M. J. McKeown, L. K. Hansen, and T. J. Sejnowsk, "Independent component analysis of functional mri: what is signal and what is noise?" Current opinion in neurobiology, vol. 13, no. 5, pp. 620–629, 2003.

[13]. D. R. Hardoon, J. Mourao-Miranda, M. Brammer, and J. Shawe-Taylor, "Unsupervised analysis of fmri data using kernel canonical correlation," NeuroImage, vol. 37, no. 4, pp. 1250–1259, 2007.

[14]. Accamma I.V., , Suma H.N., and Dakshayini M.. "A Genetic algorithm based feature selection technique for classification of multiple-subject fMRI data", 2015 IEEE International Advance Computing Conference (IACC), 2015.

[15]. Do, Luu-Ngoc, and Hyung-Jeong Yang. "A Robust Feature Selection Method for Classification of Cognitive States with fMRI Data." In Advances in Computer Science and its Applications, pp. 71-76. Springer Berlin Heidelberg, 2014.

[16]. Gold, Sherri, Brad Christian, Stephan Arndt, Gene Zeien, Ted Cizadlo, Debra L. Johnson, Michael Flaum, and Nancy C. Andreasen. "Functional MRI statistical software packages: a comparative analysis." *Human Brain Mapping* 6, no. 2 (1998): 73-84.

[17]. N. Kanwisher, J. McDermott, and M. M. Chun, "The fusiform face area: a module in human extrastriate cortex specialized for face perception," The Journal of Neuroscience, vol. 17, no. 11, pp. 4302–4311, 1997.

[18]. N. Kriegeskorte, M. Mur, D. A. Ruff, R. Kiani, J. Bodurka, H. Esteky, K. Tanaka, and P. A. Bandettini, "Matching categorical object representations in inferior temporal cortex of man and monkey," Neuron, vol. 60, no. 6, pp. 1126–1141, 2008.

[19]. K. Grill-Spector, Z. Kourtzi, and N. Kanwisher, "The lateral occipital complex and its role in obejct recognition," Vision research, vol. 41, no. 10, pp. 1409–1422, 2001

[20]. Ramasangu, Hariharan, and Neelam Sinha. "Cognitive state classification using transformed fMRI data", 2014 International Conference on Signal Processing and Communications (SPCOM), 2014.

[21]. Shi, J., Malik, J.: Normalized Cuts and Image Segmentation. IEEE Transactions on Pattern analysis and machine Intelligence 22(8), 888–903 (2000)

[22]. Mitra, P., Murthy, C.A., Pal, S.: Unsupervised feature selection using feature similarity. IEEE Trans. Pattern Analysis and Machine Intelligence 24(3), 301–312

[23]. D. D. Cox and R. L. Savoy, "Functional magnetic resonance imaging (fmri) "brain reading": detecting and classifying distributed patterns of fmri activity in human visual cortex," Neuroimage, vol. 19, no. 2, pp. 261–270, 2003.

[24]. J. D. Haynes and G. Rees, "Predicting the orientation of invisible stimuli from activity in human primary visual cortex," Nature neuroscience, vol. 8, no. 5, pp. 686–691, 2005.

2016 Intl. Conference on Advances in Computing, Communications and Informatics (ICACCI), Sept. 21-24, 2016, Jaipur, India

Common Threats to Software Quality Predictive Modeling Studies Using Search-based Techniques

Ruchika Malhotra
Department of Software Engineering
Delhi Technological University
Delhi-110042, India
ruchikamalhotra2004@yahoo.com

Megha Khanna*+
*Delhi Technological University, India
+Sri Guru Gobind Singh College of Commerce,
University of Delhi, India
meghakhanna86@gmail.com

***Abstract*—Development of Software Quality Predictive Models (SQPM) is an important research area as it helps in effective use of project resources and assures a good quality software product. A number of studies in literature have developed successful SQPM using search-based techniques which are meta-heuristic in nature. However, in order to perform a successful empirical study which develops SQPM using search-based techniques, it is essential to consider various probable sources of threats to the empirical study so that the developed models are realistic and efficient. This study reviews and analyzes 33 empirical studies in literature which have successfully used search-based techniques for prediction of two common software quality attributes i.e. fault-proneness and change-proneness in order to comprehensively present various probable threats to such studies. The study also proposes remedial actions to mitigate these threats and presents an analysis of the most common threats which are missed by researchers.**

Keywords—Empirical Validation; Search-based Techniques; Software Quality Predictive Modeling; Threats to Validity.

I. INTRODUCTION

Software quality is an important concern for software practitioners and its prospective users in order to sustain a successful product market and user's satisfiability. Thus, development of Software Quality Predictive Models (SQPM) which efficiently predict various software quality attributes by using a number of software metrics as predictor variables are very useful. These models are useful in planning proper resource allocation in a project, in optimizing schedule and costs of a project and in developing a good quality maintainable software product [1]. SQPM models are developed with the help of classification techniques which use historical data for training these models and therefore predict the quality of forthcoming versions of the software product.

A number of techniques are available for developing an efficient SQPM which includes statistical techniques, machine-learning techniques and the recently explored search-based techniques. Search-based techniques are capable of finding a robust and optimal solution from a number of possible solutions [2]. The optimality of a solution is assessed by evaluating a function which indicates the fitness/goodness of the solution. Previous studies by Harman [3-5] have proposed the application of search-based techniques for developing effective predictive models. Also, these techniques are good at handling noisy data and perform a global search for optimal solution rather than getting stuck up in local optima [2,4]. However, the special nature of search-based techniques necessitates that the empirical studies which use these techniques should be carried out carefully for development of practical models.

In order to develop practical models, the researchers should take into account the various probable sources of threats to the study which mitigate the validity of the obtained results. Hence, a researcher should analyze probable threats in the design phase of an experiment so that proper experimentation set up can be provided and should also list these threats in the study so that the readers can comprehend the limitations of the research results. The unique nature of search-based techniques necessitates proper study design and an analysis of threats of the study so that valid and reliable results can be obtained. This study states the various probable threats to empirical studies which use search-based techniques and categorizes these probable threats into four dimensions namely conclusion validity threats, internal validity threats, construct validity threats and external validity threats. The study explores the following Research Questions (RQ's):

RQ1: What are the possible sources of threats in SQPM studies which use search-based techniques?

RQ2: What are the possible remedial actions which increase the validity of SQPM studies which use search-based techniques?

RQ3: Which threats have not been properly addressed in literature by researchers while developing SQPM?

In order to answer the above RQ's, threats were analyzed from 33 empirical studies which were published from January 1992 to December 2015 and develop SQPM for fault-proneness prediction and change-proneness prediction. The results indicate that while certain threats are completely addressed by almost all the studies, but there are still few experimental gaps due to which certain threats are ignored by majority of the studies. Future research should compulsorily pay attention to these threats in order to develop effective SQPM.

978-1-5090-2029-4/16/$31.00 @2016 IEEE

The organization of the paper is as follows: Section II states the four broad categories of threats in an empirical study. Section III states a brief introduction of the various software quality attributes which have been analyzed in this work along with a brief description of the collected studies. Section IV states the discussion and answers to various research questions of the study. The conclusions of the study and the future research directions for conducting effective empirical studies using search-based techniques is reported in Section V.

II. Threat Categorization In An Emirical Study

This section briefly describes the four possible categories of threats to a study as suggested by Cook and Campbell [6].

A. Conclusion Validity

An empirical study explores the relationship between various independent variables and a specific dependent variable. All those factors which may lead to an incorrect conclusion of an association between the independent and the dependent variables are said to affect the conclusion validity of the study [7]. Therefore, all such concerns should be verified appropriately. It is also termed as statistical conclusion validity as it concerns itself with the statistical relationship between the independent and the dependent variables. For example, if an experiment is not formally verified by developing hypothesis and using an appropriate statistical test then there is a probable threat to conclusion validity in the study.

B. Internal Validity

Apart from the independent variables, there can be other factors, also called the confounding factors which can lead to change in the dependent variable. These factors cannot be controlled by the researchers and should be accounted for their effect on the dependent variable [8]. Internal validity is concerned with all those factors which can lead to changes in the dependent variable except the independent variables. It is also termed as "causal validity" as it demonstrates that the change in the dependent variable is caused only by the independent variables. In case other extraneous variables are responsible for change in the dependent variable, it is a termed as an internal validity threat to the study [7-8]. For example, an extraneous variable size may affect the relationship between Object-Oriented (OO) metrics and change in a class and may lead to an over-estimation of this relationship. Thus, the confounding effect of the class size needs to be evaluated in order to reduce internal validity threats.

C. Construct Validity

Construct validity evaluates whether the metrics used in the study are efficient representatives of the concepts they propose to measure [9]. For example, it is important to use realistic measures for measuring structural properties of a class and therefore it should be assessed whether OO metrics such as Depth of Inheritance Tree (DIT) and Number of Children (NOC) actually measure the reusability and inheritance attributes of a class.

D. External Validity

External validity is concerned with the generalizability of the study's results. It evaluates whether the results of the study can be efficiently used in scenarios or settings which are not accounted for in the study [7,9]. For example, if the data sets used in the study are all developed using C++ programming language, then are the results of the study valid in the context where data sets which are developed using the Java programming language are used.

III. Study Design And Data Collection

This section describes the collection of primary studies which have been assessed to identify various threats to validity in a study which develops SQPM using search-based techniques. We collected empirical studies which use search-based techniques for predicting fault-proneness and change-proneness modules/classes. These quality attributes can be defined as follows:

a) Fault Proneness: It indicates the likelihood that a particular class or module would be detected with a fault in the upcoming version of the software product i.e. after the product has been released.

b) Change Proneness: It indicates the likelihood that a particular class or module would change in the upcoming version of the software product i.e. after the product has been released.

Both these attributes are binary in nature and a number of studies in literature have developed classification models for analyzing these attributes [10-12]. However, the use of search-based techniques for developing such models is relatively new. We collected studies from the period January 1992 to December 2015 as the first use of a search-based technique in a software engineering domain (software testing) was done in 1992 [13]. In order to collect the desired studies, we searched various important databases such as IEEEXplore, Science Direct, ACM digital library, Wiley and some specific search-based avenues such as proceedings of conference on Genetic and Evolutionary Computation Conference (GECCO), Symposium on Search Based Software Engineering (SSBSE) etc. The quality of all the collected studies was also analyzed using a quality questionnaire similar to the one used by Malhotra [10]. A total of 33 studies [14-45] were selected after quality analysis and are called the primary studies. These studies are reported in Table I along with a unique study identifier, author name, study title and year of publication.

IV. Results And Discussion

This section states the results of the study and discusses the answers to the various RQ's of the study.

All the 33 selected studies [14-45] were thoroughly analyzed in order to determine all possible sources of threats in these studies. The identified threats were categorized according to the four dimensions stated in Section II. Furthermore, each study was analyzed to assess how well they have addressed a particular threat to mitigate it. Three possible scores could be

TABLE I. POSSIBLE THREATS WITH CATEGORIZATION

Threat Category	Threat Description	Possible Threat Mitigation
Conclusion	C1: Are the threats statistically verified?	Use of formal hypothesis and an appropriate statistical test for validation of results.
	C2: Does the study use an appropriate statistical test?	Careful selection of a statistical test which is appropriate for validating the given scenario.
	C3: Are all assumptions of statistical tests verified?	Checking all statistical test assumptions on the underlying data before application of these tests or use of non-parametric test which do not need fulfilment of data assumptions.
	C4: Does the study conduct appropriate number of runs to account for stochastic nature of search-based techniques?	Search-based techniques should be run multiple (at least 10) number of times and then the average or median of these results should be analyzed in order to reduce the randomness in results due to stochastic nature of search-based techniques.
	C5: Does the study account for validation bias?	Careful use of appropriate validation technique such as ten-fold cross validation so that validation bias is reduced.
Internal	I1: Are the parameter settings of search-based techniques clearly stated?	Reporting of all parameter settings used in a technique.
	I2: Are the parameters of search-based techniques properly tuned?	Adjusting or tuning the parameters in order to yield optimum results.
	I3: Is the fitness function clearly stated?	Reporting the fitness function used in the study.
	I4: Does the study appropriately use different data for training and validation?	Use of an appropriate validation technique.
	I5: Does the study appropriately handle noisy and inconsistent data?	Application of data cleaning techniques which removes noisy and inconsistent data.
	I6: Does the study use well known methods for attribute selection?	Use of efficient and well known methods for attribute selection in order to reduce model bias.
	I7: Does the study account for confounding nature of extraneous variables?	Account for the confounding nature by controlling the extraneous variable and analyzing its effect on the relationship between the dependent and independent variable.
Construct	CN1: Are the independent variable measures effective representatives of the concepts being studied?	Use of well established, well-known and previously validated metrics as independent variables and use of public data sets which are well known.
	CN2: Are the performance metrics efficient representatives of the effectiveness of the developed models?	Use of well-established performance metrics in literature.
	CN3: Does the study account for unfair comparison amongst different algorithms?	Use of effective performance evaluators such as comprehensibility of the developed model etc. as a comparison parameter to conduct a fair comparison.
	CN4: Does the study account for improper data collection methods or human errors in data collection?	Use of automated or semi-automated tools for data collection which are also manually verified or use of public data sets which are already verified.
External	E1: Does the study use real industrial data sets for experiment?	Use of industrial data sets so that the practical usefulness of the results can be assessed.
	E2: Does the study use appropriate number of data sets for experiment?	Use of an appropriate number of data sets in order to strengthen the generalizability of results.
	E3: Is the data set size used for empirical validation in the study appropriate?	Use of medium/large sized data sets so that efficient prediction models can be developed.
	E4: Are the data sets used for empirical validation in the study developed using varied programming languages?	Use of data sets with varied programming languages such as C++ and Java.
	E5: Are the data sets of the study representative of different companies/domains?	Use of multiple data sets belonging to different domains and companies.
	E6: Are the data sets used by the study publicly available?	Use of publicly available datasets in order to increase replicability of the study.

given to a study corresponding to a specific threat: (i) the study could have completely ignored the threat (N) (ii) the study could have completely addressed the threat (C) or (iii) the study could have partially addressed the threat (P).

RQ1: What are the possible sources of threats in SQPM studies which use search-based techniques?

Table II lists down all the probable sources of threats extracted from the 33 primary studies [14-45]. These threats were categorized according to four dimensions. As stated in Table II each threat category has a few questions associated with the possible cause of threat. A brief description of possible threat sources in an empirical study which uses search-based techniques is as follows:

a) Conclusion Validity Threats

As conclusion validity deals with statistical evaluation of the conclusions of the study, this threat is associated with the proper statistical verification of the results of the study and proper use of statistical tests. Also, it should be noted that search-based techniques have stochastic nature. Thus, these techniques should be run multiple times (at least ten times) [46] and an average or median of results should be evaluated to give realistic estimates of the technique's capability. Finally, this threat dimension should also account for validation bias of the results.

b) Internal Validity Threats

The internal validity threat deals with experimental settings such as proper reporting and tuning of parameters of search-based techniques, specification of fitness functions and appropriate model training and validation. This validity also deals with appropriate attribute selection methods, pre-processing techniques to remove noisy and inconsistent data and accounting for confounding effect of extraneous variables.

c) Construct Validity Threats

The construct validity evaluates the appropriateness of the chosen independent variables and performance metrics in order to evaluate the gap if any in theoretical concepts and practical aspects. This dimension also accounts for unfair comparison amongst different algorithms and improper data collection methods.

d) External Validity Threats

As external validity deals with the generalizability of results, thus this threat evaluates the choice of subjects used in the study so as to determine the applicability of results to domains which are varied in nature and to diverse programming languages. Also the size, number, nature and origin of the datasets are validated to evaluate the generalizability of the obtained results.

RQ2: What are the possible remedial actions which increase the validity of SQPM studies which use search-based techniques?

Table II lists down possible remedial actions for each identified threat. These remedial actions are important to mitigate threats to SQPM studies which use search-based techniques. A well designed study should incorporate these actions in order to yield practical and reliable results. The remedial actions range from clear reporting of experimental settings of the study to use of appropriate number and sized data sets. However, certain remedial actions cannot be easily implemented. For example, in order to account for confounding nature of extraneous variables, it is important to conduct highly controlled experiments [47]. However, such experiments are difficult to implement in practice.

RQ3: Which threats have not been properly addressed in literature by researchers while developing SQPM?

In order to answer this question, each primary study was categorized as N, C or P for each threat depending on whether the study has not addressed, completely addressed or partially addressed a particular threat. Figures 1-4 report the percentage of studies which have completely, partially or not at all handled a particular threat across each dimension.

According to figure 1, 60%-70% of the studies did not perform proper statistical verification of results either by not using a statistical test at all or by choosing an inappropriate statistical test whose assumptions on underlying data have not been properly verified. Only 50% of studies performed sufficient number of runs to account for the randomness of search-based techniques. Similarly, only 45% of studies completely accounted for validation bias by using ten-fold cross validation or leave-one out cross validation techniques. Use of hold-out validation only partially deals with validation bias.

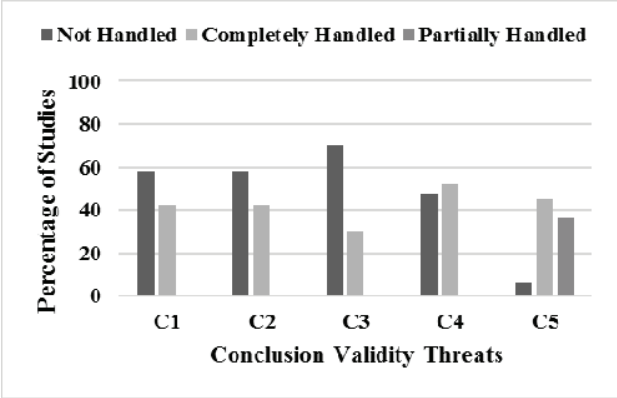

Fig. 1. Addressing Conclusion Validity Threats

Figure 2 states the breakup of how the 33 collected primary studies deal with internal validity threats. According to figure 2, 82%-85% of studies competently report the fitness functions and parameter settings of search-based techniques. This practice also aids the easy replicability of the study. Also, almost all the studies used different data for training and validation by using an appropriate validation method or using a different test set. Approximately 50% of the studies use well-known methods for attribute selection which leads to removal of noisy and redundant attributes. However, only 6% of studies use appropriate pre-processing techniques for handling noisy and inconsistent data. Similarly, very few studies (only 9%) performed proper parameter tuning which gives optimum results. It may be noted that a specific threat which was not

addressed by any study was accounting for the confounding effect of extraneous variables.

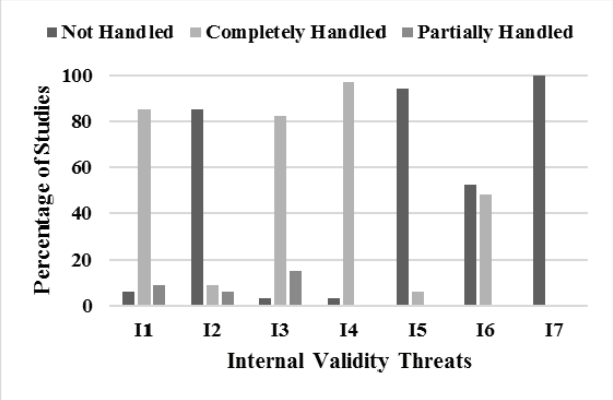

Fig. 2. Addressing Internal Validity Threats

The results in Figure 3 show how well construct validity threats have been addressed in literature. As shown in figure, majority of the studies use effective indicators of independent variables and performance metrics as they choose those variables which have already been well established in literature. Since, the data collection process of public data sets have already been verified in literature and majority of these studies use public data sets, the errors due to improper data collection methods have been minimized. However, no study accounts for the unfair comparison amongst different techniques. Different evaluators should be assessed for a fair comparison amongst different algorithms as each algorithm has unique characteristics which may affect results. However, evaluation of such characteristics such as model comprehensibility for a fair comparison amongst algorithms is difficult.

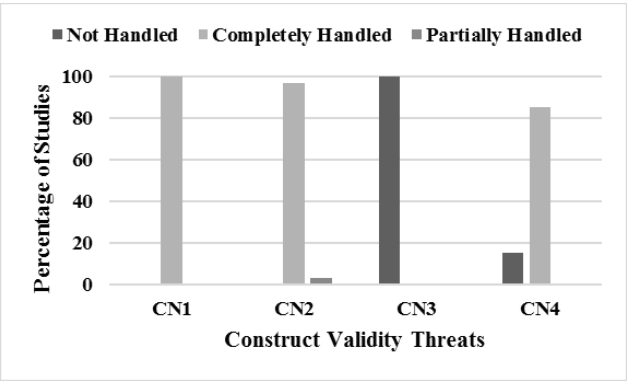

Fig. 3. Addressing Construct Validity Threats

Figure 4 reports the addressing of external validity threats by 33 selected primary studies. As shown in figure, all the studies use industrial real world data sets which have appropriate sizes. However, only 48% of studies use appropriate number (more than 2) of data sets for empirical validation. This needs to be increased in order to assess the generalizability of the obtained results. 60% of the studies have not evaluated their results on different programming languages or different domains. This factor limits the usefulness of the obtained results. However, majority (85%) of studies used public-domain data sets instead of private data sets. This trend increases the possibility of efficient replication of results by other researchers.

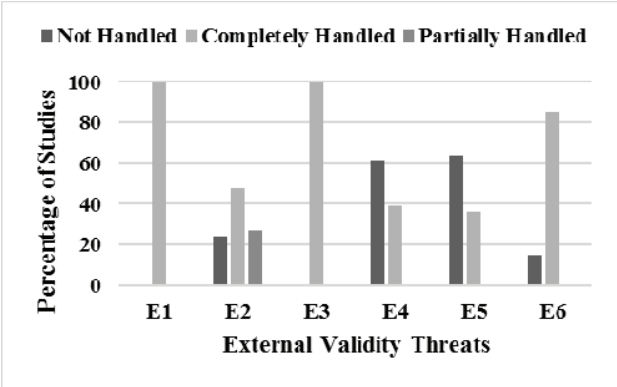

Fig. 4. Addressing External Validity Threats

Thus, after analyzing figures 1-4, we state the following threats which have been commonly ignored by researchers while developing SQPM using search-based techniques:

- Studies have not statistically verified their results by using appropriate statistical tests.
- Studies have ignored the stochastic nature of search-based techniques by not performing multiple runs.
- Studies have not validated the confounding effect of extraneous variables.
- Majority of studies do not perform proper parameter tuning to obtain optimized results.
- Studies have ignored removing noisy and inconsistent data before developing SQPM.
- Studies in literature have not accounted for unfair comparison amongst algorithms.
- Studies have generally validated mono-programming data sets which reduces the applicability of results to other programming languages.
- Studies have ignored the validation of results on data sets from different domains.

V. Conclusions And Future Research Directions

This study analyzes 33 primary studies from January 1992 to December 2015 which use search-based techniques for developing fault-proneness prediction and change-proneness prediction models in order to extract various probable threats which jeopardize the validity of results of such studies. The study categorizes all the possible extracted threats on four dimensions namely conclusion, internal, construct and external validity. Furthermore, the study also reports and proposes possible actions which can be taken to mitigate threats and identifies those threats which have been ignored by researchers in such studies. Addressing the identified threats appropriately

leads to a well-designed experiment which generates reliable results. The results indicate that though, a number of studies effectively address conclusion, construct, internal and external validity threats, there is still a need for more effective addressing of these threats in order to yield practical and reliable results. Thus, the study proposes the following future research directions for an effective experiment design which improves the quality of SQPM studies which use search-based techniques.

- All future studies should formally state their hypothesis and verify its results by using appropriate statistical tests. Studies can use non-parametric tests for doing so, as these tests do not require any stringent data assumptions before application of statistical test.
- Studies should perform at least more than 10 runs so that the non-deterministic nature of search-based techniques is taken into account. Moreover, validation bias should be accounted for in the studies by using different combinations of testing data for validation. Cross-validation techniques such as ten-fold cross validation efficiently account for validation bias.
- Future studies should clearly state the parameter settings and fitness functions used by search-based techniques. Also, steps should be taken to efficiently tune the parameters of an algorithm. However, care should be taken so that the parameters are not over tuned.
- Studies should use effective methods for reducing noisy and redundant features and separate data should be used for training and validation of the models.
- Future studies should aim to explore the confounding effects of various extraneous variables on the relationship between metrics and software quality attributes.
- Studies should carefully select their independent variables and the performance metrics on which SQPM are adjudged. Also, the use of improper data collection methods should be avoided.
- Future studies should aim to explore comprehensibility of the developed models in order to perform a fair comparison of different algorithms.
- Future studies should examine data sets from different programming languages and domains in order to validate the generalizability of the results. It should also be noted that studies should choose appropriate number of real industrial data sets which are appropriately sized in order to yield results which can be effectively utilized in the software industry.

REFERENCES

[1] R. Malhotra and M. Khanna, "Software Engineering Predictive Modeling using Search-based Techniques: Systematic Review and Future Directions, In Proceedings of *North American Search Based Software Engineering Symposium (NASBASE 2015)*, pp. 1-16, 2015.

[2] M. Harman and B.F. Jones, "Search based Software Engineering," Information & Software Technology, vol. 43, no. 14 , pp. 833-839, 2001.

[3] M. Harman, "The relationship between search based software engineering and predictive modeling," *In Proceedings of the 6th International Conference on Predictive Models in Software Engineering*, 2010.

[4] M. Harman, P. McMinn, J. Teixeira de Souza and S. Yoo, S, "Search based software engineering: techniques, taxonomy, tutorial*," Empirical Software Engineering and Verification, Lecture Notes in Computer Science*, vol. 7007, pp. 1-59, 2012.

[5] M. Harman, S.A. Mansouri and Y. Zhang, "Search-based software engineering: trends, techniques and applications," ACM Computing Surveys, vol. 45, no.1, pp. 11, 2012.

[6] T.D. Cook and D.T. Campbell, *Quasi-experimentation – design and analysis issues for field settings*, Houghton Miffin Company, Boston, 1979.

[7] R. Malhotra, *Empirical Research in Software Engineering: Concepts, Analysis and Applications*, CRC Press, 2016

[8] A.A. Neto and T. Conte, "A conceptual model to address threats to validity in controlled experiments," *In the proceedings of the 17th International Conference on Evaluation and Assessment in Software Engineering*, pp: 82-85, 2013.

[9] M. de Oliveira Barros and A.C.D. Neto, "Threats to validity in search-based software engineering empirical studies," UNIRIO- Universidade Federal do Estado do Rio de Janeiro, Tech. Rep. TR 0006/2011, 2011.

[10] R. Malhotra, "A systematic review of machine learning techniques for software fault prediction," *Applied Soft Computing*, vol. 27, pp. 504-518, 2015.

[11] Y. Zhou, H. Leung and B. Xu, "Examining the Potentially Confounding Effect of Class Size on the Associations between Object Metrics and Change proneness," *IEEE Trans. Softw. Eng.*, vol. 35, no. 5, pp. 607-623, 2009.

[12] R. Malhotra and M. Khanna, "Investigation of Relationship between Object-oriented Metrics and Change Proneness," *Int. J. Mach. Learn. & Cyber.*, 4, pp. 273-286, 2013.

[13] S. Xanthakis, C. Ellis, C. Skourlas, A.L. Gall, S. Katsikas, K. Karapoulis, "Application of genetic algorithms to software testing," *In Proceedings of 5th International conference on Software Engineering and its Applications,* pp. 625-636, 1992.

[14] R. Hochman, T. M. Khoshgoftaar, E. B. Allen and J. P. Hudepohl, "Using the genetic algorithm to build optimal neural networks for fault-prone module detection," *In Proceedings of 7th International Symposium on Software Reliability engineering*, pp. 152-162, 1996.

[15] R. Hochman, T. M. Khoshgoftaar, E. B. Allen, J. P. Hudepohl, "Evolutionary neural networks: a robust approach to software reliability problems," *In Proceedings of 8th IEEE International Symposium on Software Reliability Engineering,* pp. 13-26, 1997.

[16] T. M. Khoshgoftaar and Y. Liu, "Genetic programming model for software quality classification," *In Proceedings of 6th International symposium on High Assurance Systems Engineering*, 127-136, 2001.

[17] T. M. Khoshgoftaar, N. Seliya and Y. Liu, "Genetic programming-based decision trees for software quality classification," *In Proceedings of 15th IEEE International Conference on Tools with Artificial Intelligence*, pp. 374-383, 2003.

[18] Y. Liu and T. M. Khoshgoftaar, "Reducing overfitting in genetic programming models for software quality classification," *In Proceedings of 9th IEEE International Symposium on High-Assurance Systems Engineering,* pp. 56-65, 2004.

[19] A. Tsakonas and G. Dounias, "Application of Genetic Programming in Software Engineering Empirical Data Modeling," *In 3rd International Conference on Software and Data Technologies,* pp. 295-300, 2008.

[20] A. Tsakonas and G. Dounias, "Predicting defects in software using grammar-guided genetic programming," *Artificial Intelligence: Theories. Models and Applications*, vol. 5138, pp. 413-418, 2008.

[21] O. Vandercruys, D. Martens, B. Baesens, C. Mues, M. De Backer and R. Haesen, "Mining software repositories for comprehensible software fault

prediction models," *Journal of Systems and Software*, vol. 81, no. 5, 823-839, 2008.

[22] C. Catal and B. Diri, "Investigating the effect of dataset size, metrics sets, and feature selection techniques on software fault prediction problem," *Information Sciences*, vol. 179, no. 8, 1040-1058, 2009.

[23] Y. Singh, A. Kaur and R. Malhotra, "Prediction of software quality model using gene expression programming," *Product-Focused Software Process Improvement*, vol. 32, pp. 43-58, 2009.

[24] W. Afzal, "Using faults-slip-through metric as a predictor of fault-proneness," *In Proceedings of 17th Asia Pacific Software Engineering Conference*, pp. 414-422, 2010.

[25] A. B. De Carvalho, A. Pozo and S. R. Vergilio, "A symbolic fault-prediction model based on multiobjective particle swarm optimization," *Journal of Systems and Software*, vol. 83, 868-882, 2010.

[26] C. Jin, E-M Dong and L-Na, "Software fault prediction model based on adaptive dynamical and median particle swarm optimization," *In Proceedings of 2nd International Conference on Multimedia and Information Technology*, pp. 44-47, 2010.

[27] Y. Liu, T. M. Khoshgoftaar and N. Seliya, "Evolutionary optimization of software quality modeling with multiple repositories," *IEEE Transactions on Software Engineering,* vol. 36, no. 6, pp. 852-864, 2010.

[28] P. C. Pendharkar, "Exhaustive and heuristic search approaches for learning a software defect prediction model," *Engineering Applications of Artificial Intelligence*, vol. 23, pp. 34-40, 2010.

[29] N-H Chiu, "Combining techniques for software quality classification: An integrated decision network approach," *Expert Systems with Applications*, vol. 38, no. 4, pp. 4618-4625, 2011.

[30] S. Di Martino, F. Ferrucci, C. Gravino and F. Sarro, "A genetic algorithm to configure support vector machines for predicting fault-prone components," *Product-Focused Software Process Improvement*, vol. 6759, pp. 247-261, 2011.

[31] L. Yu, "An evolutionary programming based asymmetric weighted least squares support vector machine ensemble learning methodology for software repository mining," *Information Sciences*, vol. 191, pp. 31-46, 2012.

[32] D. Rodriguez, R. Ruiz, J. C. Riquelme and J. S. Aguluir-Ruiz, "Searching for Rules to Detect Defective Modules: A Subgroup Discovery Approach," *Information Sciences*, vol. 191, pp. 14-30, 2012.

[33] F. Sarro, S. Di Martino, F. Ferrucci and C. Gravino, "A further analysis on the use of genetic algorithm to configure support vector machine for inter release fault prediction," *In Proceedings of 27th Annual ACM Symposium on Applied Computing*, pp. 1215-1220, 2012.

[34] H. Can, X. Jianchum, Z. Ruide, L. Juelong, Y. Qiliang and X. Liqiang, "A new model for software defect prediction using particle swarm optimization and support vector machine," *In Proceedings of 25th Chinese Control and Decision Conference*, pp. 4106-4110, 2013.

[35] G. Canfora, A. De Lucia, M. Di Penta, R. Oliveto, A. Panichella and S. Panichella, "Multi-objective cross-project defect prediction," *In Proceedings of 6th International Conference on Software Testing, Verification and Validation*, pp. 252-261, 2013.

[36] G. Abaei and A. Selamat, "A survey of software fault detection based on different prediction approaches," *Vietnam Journal of Computer Science*, vol. 1, pp. 79-95, 2014.

[37] M. Harman, S. Islam, Y Jia, Leandro L. Minku, F. Sarro and K. Sirivisut, "Less is more: temporal fault predictive performance over multiple hadoop releases," *In Proceedings of 6th International Symposium on Search Based Software Engineering,* pp. 240-246, 2014.

[38] L. Kewen, C. Chenxi., L. Wenying., F. Xianghua. and L. Qinghua, "Software defect prediction using fuzzy integral fusion based on GA-FM," *Wuhan University of Natural Sciences*, vol. 19, no. 5, pp. 405-408, 2014.

[39] R. Malhotra, "Comparative analysis of statistical and machine learning methods for predicting faulty modules," *Applied Soft Computing*, vol. 21, pp. 286-297, 2014.

[40] O. F. Arar and K. Ayan, "Software defect prediction using cost sensitive neural network," *Applied Soft Computing*, vol. 33, pp. 263-277, 2015.

[41] C. Jin and S-W Jin, "Prediction approach of software fault-proneness based on hybrid artificial neural network on quantum particle swarm optimization," *Applied Soft Computing*, vol. 35, pp. 717-725, 2015.

[42] D. Azar and J. Vybihal. "An ant colony optimization algorithm to improve software quality prediction models: case of class stability," *Information and Software Technology*, vol. 53, no. 4, pp. 388-393, 2011.

[43] R. Malhotra and M. Khanna, "The ability of search-based algorithms to predict change-prone classes, *Software Quality Professional*, vol. 17, no. 1, pp. 17-31, 2014.

[44] R. Malhotra and M. Khanna, "A new metric for predicting software change using gene expression programming," *In Proceedings of 5th international Workshop on Emerging Trends in Software Metrics*, pp. 8-14, 2014.

[45] R. Malhotra and M. Khanna, "Mining the impact of object oriented metrics for change prediction using machine learning and search-based techniques," *In Proceedings of Advances in Computing, Communications and Informatics,* pp. 228-234, 2015.

[46] Ali, S., Briand, L.C., Hemmati, H. & Panesar-Walawege, R.K. (2010). A systematic review of the application and empirical investigation of search-based test case generation, *IEEE Trans. Software Eng*., 36(6) , 742-762.

[47] L. Briand, J. Wust, and H. Lounis, "Replicated case studies for investigating quality factors in object oriented designs," *Empirical Software Engineering Journal*, vol. 6, no.1, pp. 11-58, 2001.

Comparison of Different Topologies of Fuzzy Logic Controller to Control D-STATCOM

Anuj Varshney
Department of Electrical Engineering
Delhi Technological University, New Delhi-110042
Email ID: varshney.anuj@yahoo.com

Dr.Rachana Garg
Department of Electrical Engineering
Delhi Technological University, New Delhi-110042
Email ID: rachana16100@yahoo.co.in

***Abstract* - This paper demonstrates the controlling of D-STATCOM using fuzzy logic control technique, and different topologies of fuzzy logic controller with proportional plus integral control. The value of energy loss (e_{dc}) at VSC is found out from a rule-base specified on error (e) and change of error (Δe) of the operated variable. All topologies are tested for different loads (non-linear& unbalanced linear load). Performance comparison between the PI-like FLC, PI gain scheduled FLC and Hybrid FLC-PI controller are realized in terms of various performance criteria such as peak overshoot, settling time(t_s) and rise time(t_r) of the DC link voltage.Under all the three topologies, THD of the grid side current is well within the IEEE standards and UPF at grid side is maintained.**

Keyword: DSTATCOM; Fuzzy Logic Controller;DC link voltage;THD; PI-Fuzzy topologies.

I INTRODUCTION

DSTATCOM is a shunt connected FACTs device, used in distribution system to deal with the unwanted component of load currents like harmonics, reactive power requirement and unbalancing due to various linear and nonlinear loads in day to day use [1]. The system explaining the connection of DSTATCOM to a three phase three wire distribution system is shown in Fig. 1. DSTATCOM is built using a 3-phase Voltage source converter and a capacitor to maintain constant voltage at the DC terminal of the converter circuit. To get 6-gating pulses for VSC a controller based onSRF theory with conventional controller (PI) has been proposed in [2], this control scheme is to control the DSTATCOM to compensate all unwanted components of load currents in a distribution system.The scheme consists of two feedback loops: innermost loop is to calculate the reference current generation and the outermostloop is to control DC voltage at the VSC terminals using aconventional PI controller. Thedisadvantages of using a conventional controller are fixed K_p and K_i gains, and the performance of the PI controllers are influenced by parameter fluctuations, load disruptions and unbalancing of load [3].

For obscure or difficult system model, FLC has been found especially helpful for controller design. It does not require complete process model, and doesn't need any numerical model and is established on the linguistic rules acquired from the knowledge of the system decision maker. FLCs have been demonstrated to be efficient w.r.t.perturbations, huge uncertainties and transients in the process behavior [4].Under steady state conditions,FLCs have performed inferior as compared to PI controller. The benefits of both fuzzy & PI controllers can be incorporated using Fuzzy and PI controller in a combination of series or parallel connection [5]. Fuzzy-PI control has been generally examined and different types of Fuzzy-PI controllers has been proposed. They can be sorted into two noteworthy classifications asindicated by their development [6].

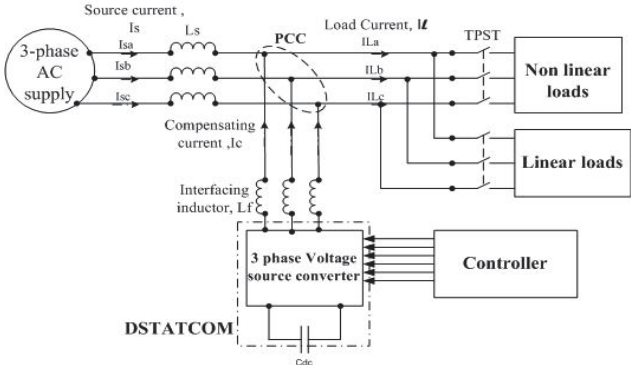

Fig. 1. DSTATCOM shunt connected to the three phase three wire distribution system

First classification is PI-like Fuzzy controllers, comprises of regular FLC, built as an arrangement of heuristic control principles. The control signals is constructed as a nonlinear function of the error (e) and change of error (Δe), where fuzzy reasoning is used for nonlinear function deduction. There are no corresponding k_p and integral gain (k_i) expressly; rather the control signal is specifically deducted from the information base and fuzzy reasoning.This controller structure corresponds to PI type controller hence these are referred as PI-like Fuzzy controllers [7].

Second classification is built using the conventional PI controller in alignment with a set of FLCs, and fuzzy inference mechanism is used to tune the PI gains (k_p& k_i) on line [8]. To employ this class of Fuzzy-PI control, it requires the ultimate gain (k_u) and the ultimate time period (T_u) of the system. Thus designing of this class of Fuzzy-PI controllers demands more observational experience with the system. There is this third category of Hybrid Fuzzy-PI controller,in addition to above two categories, in which under dynamic

978-9-3805-4421-2/16/$31.00 ©2016 IEEE

conditions, theFLCoutput is more than the PI controller output and vice-versa under steady state conditions [9].
In this paper authors have developed and simulated PI-like FLC controller, PI gain scheduling using Fuzzy controller and a Hybrid Fuzzy-PI controller on MATLAB Simulink environment and their performances are compared.

II CONTROL TOPOLOGIES FOR DSTATCOM

A Pi-Like Fuzzy Control

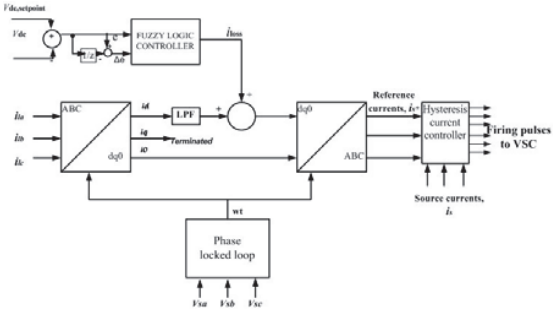

Fig. 2. PI-like Fuzzy Logic control scheme for DSTATCOM

In this part, the design of PI like FLC to control the DSTATCOM for UPF operation is presented in the block diagram as presented in Fig.2. This PI-like FLC system has two I/Ps, error (*e)* and change of error (*Δe*), which are expressed by eqn. (1) &(2),

$$e = V_{dc,set} - V_{dc}^{*} \quad (1)$$

And, $\Delta e = e(n) - e(n-1)$ (2)

Where $V_{dc,set}$and V_{dc}* are the applied set point input (750V) and DC terminal measured voltage across DSTATCOM. The output of the FLC isi_{loss} stands for differential energy (Δe_{dc}) demanded for a self-supporting DC bus voltage for the DSTATCOM and to provide the losses in VSC power circuit [10]. The factor$i_{loss}$is given by eqn, (3)and differential DC energy (Δe_{dc}) by eqn. (4),

$$i_{loss} = \frac{2}{3} * \frac{\Delta e_{dc}}{V_{sm} * T_x} \quad (3)$$

$$\Delta e_{dc} = e_{dc}^{*} - e_{dc} = \frac{1}{2} * C_{dc} * \left[\left(V_{dc,set}\right)^2 - (V_{dc}^{*})^2 \right] \quad (4)$$

And V_{sm} is the voltage magnitude of the system and T_x is the one sixth of the time constant of the supply voltage and given by eqn. (5),

$$T_x = \frac{1}{6} * T_s = \frac{1}{6} * \frac{1}{f_s} \quad (5)$$

All MFs for the FLC's *i/p* and*o/p* are specified on the basic standardized space [-1, 1] and are symmetric triangles with equivalent base and half coverwith adjacent Membership Function, as appeared in Fig.3 The MFs are designated as(*NB, NM,NS,ZE,PS,PM and PB*), which stands for -*ve* Big, -*ve* Medium, -*ve* Small, Zero, +*ve* Small, +*ve* Medium, +*ve* Big, respectively.
The DC energy loss current component (i_{loss}) is computed using the fuzzy logic rule base shown in Table. I; this is anevery now and again utilized rule base designed with a 2-D phase plane [11]. The control rules depend on the qualities of the reaction as though the $V_{dc}$is digressing far from the set point, a large output current is required to draw it towards the set point, while a little current is required when $V_{dc}$is close and drawing closer the set point.

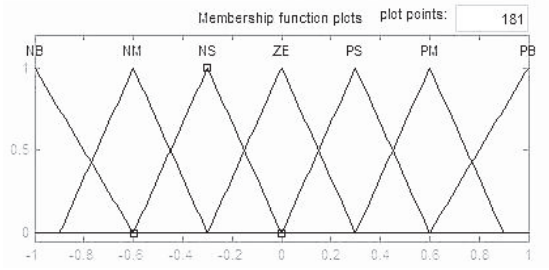

Fig. 3. MFs of *e, Δe* and i_{loss}

TABLE I. FLCs RULE BASE FOR CALCULATION OF I_{LOSS}

Δe / e	NB	NM	NS	ZE	PS	PM	PB
NB	NB	NB	NM	NM	NS	NS	NS
NM	NM	NM	NS	NS	NS	ZE	ZE
NS	NM	NS	NS	NS	ZE	ZE	ZE
ZE	NS	NS	ZE	ZE	ZE	PS	PS
PS	ZE	ZE	PS	PS	PS	PM	PM
PM	ZE	ZE	PS	PS	PM	PM	PM
PB	PS	PS	PS	PM	PM	PB	PB

After designing MFs and rule bases for PI-like FLC controller, the scaling elements are tuned. Studies have been done to see the effect of scaling factors over closed loop system and their tuning procedure.The scaling elements required for standardization of inputs and de-standardization of output assumes critical part for controller stability and performance as in an ordinary controller,as they are the source of conceivable instability, oscillations, and crumbled damping effects [12]. Various expressionsrelating the scaling factors K_e, $K_{\Delta e}$ and $K_{iloss}$and the input &output variables of the FLC are expressed in eqn. (6),

$$e_N = K_e * e \quad ; \quad \Delta e_N = K_{\Delta e} * \Delta e; \quad i_{loss,N} = K_{iloss} * i_{loss} \quad (6)$$

Suitable benefits of scaling components are chosen taking into account master learning about the system to be controlled, and through experimentation.

B Pi Gain Scheduling Using Flc

PI-like FLC controller might bring in steady state errors in light of the fact that the system does not have an inbornintegrator to minimize this error. In this design both fuzzy logic controller and PI controller are utilized to consolidate the benefits of both the controllers into one system. In literature, some other configuration of fuzzy PI controller has also been used in which the tuning of gains (K_p& K_i) have been done using the FLC [13].
Under the transient conditions for higher order process, Fuzzy-PI type controller is known to give poor performance. In this paper authors have used FLC to control the K_p and

$K_i$gains' output based on the input error and change of error as shown in Fig (3). These output gainscontrols the PI-controller, which is tuned firstly based on Ziegler Nichols tuning method [14]. Here the initial values of the gain parameters are modified on line using fuzzy rules defined on *e and Δe*. The eqn. (7) shows the relationship of loss current required and the gains.

$$i_{loss} = u * \left[k_p + \frac{k_i * T_s}{z-1}\right] \qquad (7)$$

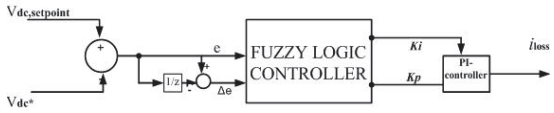

Fig. 4. Fuzzy PI on-line tuning system

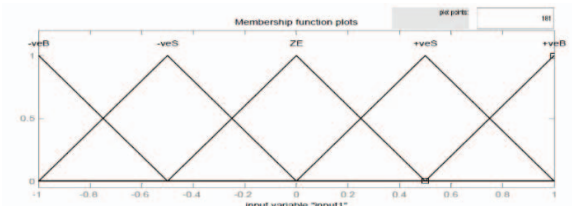

Fig. 5. Membership function *e*, *Δe* and i_{loss}

For gain scheduling of PI controller, all MFs of the FLC are defined on the common normalized domain [-1, 1] and symmetric distribution of triangular MFs with 50% overlap is shown in Fig. 4. The MFs are denoted as *-veB, -veS, ZE, +veS* and *+veB* which stands fornegative big, negative small, zero, positive small and positive big respectively.

The rule base is designed using the prior knowledge of the system response as if the V_{dc} is deviating far away from the set point, a large output current is required to pull it towards the set point, whereas a small current is required when $V_{dc}$is near and moving towards the set point. The rule base is shown in Table. II

TABLE II. FLCS RULE BASE FOR COMPUTATION OF K_P AND K_I

Δe / **e**	***-veB***	***-veS***	***ZE***	***+veS***	***+veB***
-veB	-veB	-veB	-veS	-veS	ZE
-veS	-veB	-veS	-veS	ZE	+veS
ZE	-veS	-veS	ZE	+veS	+veS
+veS	-veS	ZE	+veS	+veS	+veB
+veB	ZE	+veS	+veS	+veB	+veB

C Hybrid Flc-Pi Configuration

In this design a hybrid model of FLC and PI is created in which the output of FLC and PI controller is added to deliver the DC loss component of current (i_{loss}). The performance of FLC, when compared to customary PI controller is prevalent under transient conditions. The benefitsof FLC and PI controller are acquired by executing a Hybrid Fuzzy-PI controller for DC terminal voltage control. In literature Hybrid fuzzy-PI controller is utilized for the control of induction motor by actuating the PI controller at the steady state conditions and FLC when transient and oscillations are detected [15]. The schematic block diagram of Hybrid Fuzzy-PI arrangement is shown in the Fig.5.

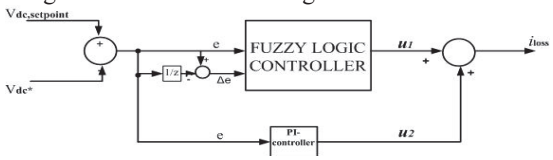

Fig. 6. Hybrid Fuzzy-PI control system

The error (*e*) and change (*Δe*) in error are the two inputs used to produce FLC output, while error only is fed to PI-controller to produce the output .both the outputs are added to produce the loss component of current (i_{loss}) to regulate the DC terminal voltage.

The membership functions and rule base are same as discussed in section. II.A of this paper.

III SIMULATION & RESULTS:

Simulations have been carried out for three topologies discussed above with the non-linear unbalanced load connected to three phase three wire distribution system as given in Appendix. Simulations results with different topologies are as follows,

A. PI like Fuzzy logic controller:

The regulated DC terminal voltage is shown in Fig.6. The DC link voltage has small rising time and settles within 0.0264 sec to the set point of 750 V, with negligible steady state error and overshoot of 1.8%. At 0.2 sec a nonlinear load is inserted into the system which caused the Vdc to decrease for a short period and again maintained at 750V, while at 0.5sec the nonlinear load is disconnected from the system which gives overshoot in the DC link voltage response. The overshoot at this time is of 12.73%. And undershoot at time of inserting the nonlinear load is 8.06%.

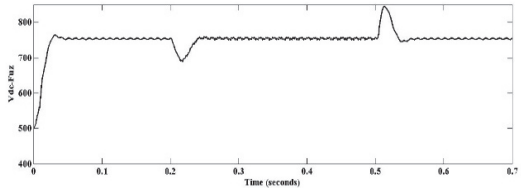

Fig. 7. Regulated DC terminal Voltage using PI like Fuzzy controller

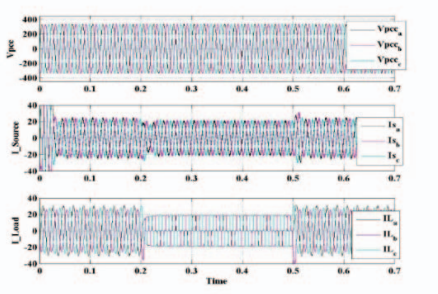

Fig. 8. Voltage at PCC, Grid side current, and Load side current respectively

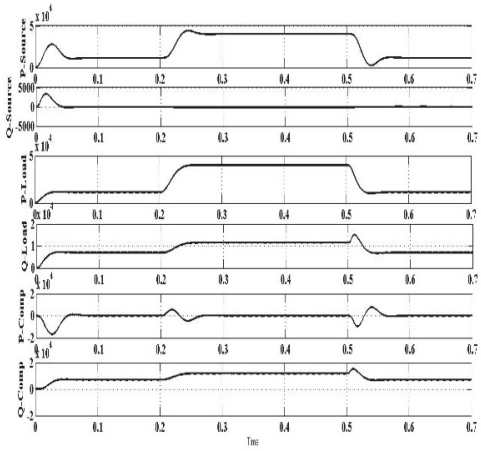

Fig. 8. Active and Reactive powers from Grid, Load and Compensator

Total harmonic distortion in all three phases is calculated using FFT analysis tool in MATLAB and given in Table.III,

TABLE III. TABLE. III THD OF CURRENTS ON GRID SIDE AND LOAD SIDE

	i_{grid}	i_{load}
Phase A	2.92%	16.97%
Phase B	3.16%	18.29%
Phase C	3.04%	19.18%

The THD analysis shows that the harmonic distortion is well below the prescribed standards IEEE-519[14]. Active and Reactive powers from the grid (P_Source & Q_Source), at load end (P_load & Q_load) and from compensator (P_comp & Q_comp) are shown in Fig. 8. And it can be seen that all the reactive power is transmitted to load from compensator for UPF operation of grid, while minimizing the transmission losses.

B. PI Gain scheduling Fuzzy Controller:

DC terminal voltage across the DSTATCOM is shown in Fig.9. The result shows some overshoot at starting of the system and while disconnecting heavy nonlinear load (i.e. 0.5 secs), the overshoot % at these two points are 4.06% and 9.93% respectively. While at the time of inserting non-linear heavy load caused the DC link voltage to drop and undershoot is of 4.467% can be seen in Fig. 9.Due to integral component involved at the output of fuzzy controller, provides negligible steady state error.

The voltage at PCC and current on grid side and load side are shown in Fig. 10.

The FFT analysis of these currents produces the results of harmonic content on the grid side currents and the load side currents respectively, the results of this analysis is tabulated and given in Table. IV. Harmonic content of these currents are well within the boundary of 5% as per IEEE-519 standards. The active and reactive powers from source load and compensator are shown in Fig.11, from this it can be deduced that grid is feeding to a UPF load, while the required reactive power is compensated from DSTATCOM.

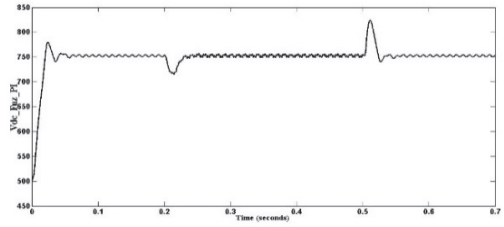

Fig. 9. Regulated DC terminal Voltage using Gain Scheduled Fuzzy PI controller

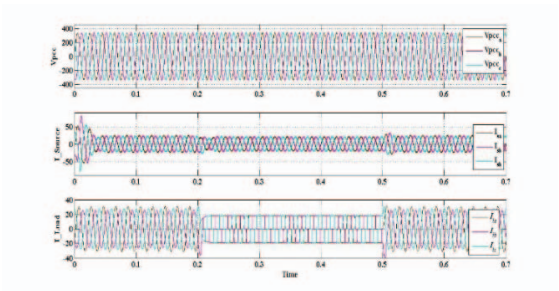

Fig. 10. V_{pcc}, Grid side current (i_{grid}) and load side current (i_{load}) respectively

TABLE IV. TABLE. IV THD OF CURRENTS ON GRID SIDE AND LOAD SIDE

	i_{grid}	i_{load}
Phase A	2.79%	16.97%
Phase B	3.17%	18.29%
Phase C	3.08%	19.18%

The regulated DC voltage due to the Hybrid Fuzzy PI controller is shown in Fig. 12. The overshoot percentage at starting and at 0.5 secs are 6.96% and 8.56% respectively, while the rise time of the response has improved as well as the steady state error is reduced to zero. Undershoot at time 0.2 secs (i.e. due to insertion of nonlinear load into the system) is 3.8%. The PCC voltages and currents on grid side and load side are shown in Fig. 13, FFT analysis is performed to calculate the THD content of these currents.

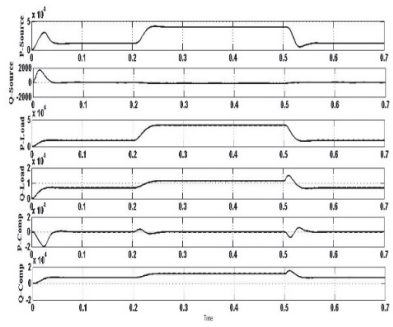

Fig. 11. Active and Reactive powers from Grid, Load and Compensator

C. Hybrid Fuzzy PI Controller:

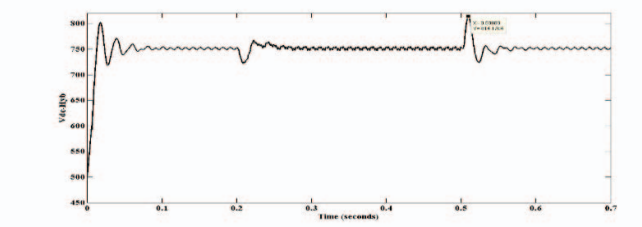

Fig. 12. Regulated DC terminal voltage using Hybrid fuzzy PI controller

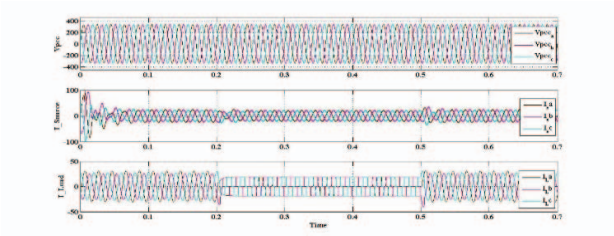

Fig. 13. V_{pcc}, $i_{grid}$and i_{load} respectively

Harmonic content in $i_{grid}$and $i_{load}$is tabulated in Table. V,

TABLE V. TABLE. V THD VALUES ON GRID SIDE CURRENT AND LOAD SIDE CURRENTS

	i_{grid}	i_{load}
Phase A	2.96%	16.97%
Phase B	3.13%	18.29%
Phase C	3.09%	19.18%

The grid side currents have harmonic content well below the permissible limit of 5% as per IEEE-519 standards. The active and reactive powers from the source, load and DSTACOM are shown in Fig. 14, for the UPF operation of the source, all the reactive power demand of the load is met by DSTATCOM.

The results due to three topologies, for regulation of DC terminal voltage V_{dc}, are combined here on one axis for comparison and can be seen in Fig. 12. The three names given to discriminate the responses are '*Vdc fuz*' stands for PI like fuzzy control response, '*Vdc fuz PI*' stands for the response of PI gain scheduled Fuzzy controller and last is '*Vdc hyb*' stands for the response of hybrid fuzzy PI controller.

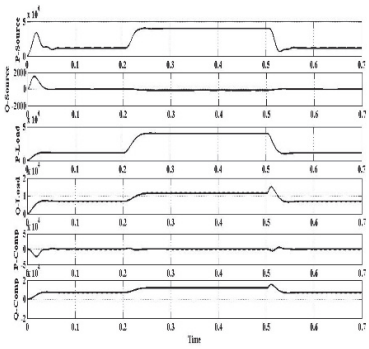

Fig. 14. Active and Reactive powers from Grid, Load and Compensator

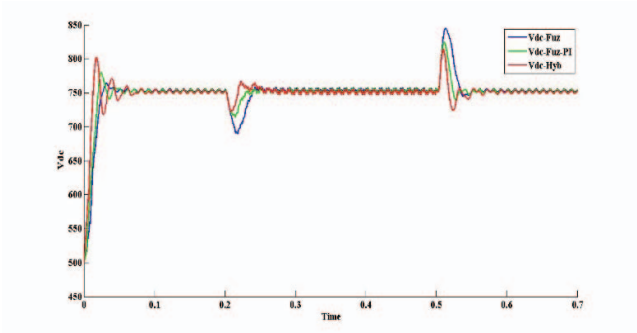

Fig. 15. Performance of different topologies to regulate DC voltage

The results are compared on the basis of simple observations of rise time, overshoot, oscillations, settling time and steady state error. The comparison is given in the Table. VI

TABLE VI. TABLE. VI COMPARISON OF THREE TOPOLOGIES ON VARIOUS PARAMETERS

Topology / Parameters	PI-Like Fuzzy controller	PI gain scheduled Fuzzy controller	Hybrid fuzzy PI controller
Rise Time (secs)	0.0264	0.0201	0.0131
%Overshoot	1.8%	4.06%	6.96%
Settling time	0.045 sec	0.05 sec	0.06 sec
Steady state error	≈ 0 %	≈ 0%	0%
THD of grid current	Lowest (within IEEE standard)	Lower (within IEEE standard)	Low (within IEEE standard)

IV CONCLUSION

DSTATCOM is controlled using PI-like Fuzzy controller, PI gain scheduled Fuzzy controller and Hybrid Fuzzy PI controller. All the 3 controllers are capable of regulating DC link voltage while keeping the source current THD within IEEE- 519 standards under non-linear and unbalancedlinear load conditions. Also the reactive power of the load is supplied by DSTATCOM to maintain the unity power factor operation of the source. PI like fuzzy controller has less settling time then other two while it's rise time is more also

steady state error is in the response which contributes to extra losses and power demand rises. PI gain scheduled Fuzzy controller has fast rise time with some oscillations and overshoot. The settling time is more than PI like fuzzy controller and steady state error is also higher. While the Hybrid Fuzzy PI controller is having fastest rise time but high overshoot and oscillations, compensator is in par with PI like fuzzy controller.

V APPENDIX

TABLE VII. SYSTEM SPECIFICATIONS AND CIRCUIT PARAMETERS

System voltage (V_{ac})	415 V (RMS L-L)	
System Frequency (f_s)	50 Hz	
Grid side Inductance (L_g)	0.06mH (Each Phase)	
Non Linear Load	3-φ diode bridge with 10Ω, 100mH on DC side	
Linear Load (Balanced)	10kVA, 0.8pf (lag)	
Linear Load (unbalanced)	Phase A	25Ω, 0.05H
	Phase B	44Ω, 0.08H
	Phase C	50Ω, 0.021H
Coupling inductor (L_c)	3.5mH (Each Phase)	
DC capacitor (C_{dc})	2500μF	

REFERENCES

[1]. A.Ghosh and G. Ledwich, *Power Quality Enhancement using Custom Power Devices*, Kluwer AcademicPublishers, London, 2002.

[2]. Anuj Varshney, Rachana Garg," SRF Theory based control of DSTATCOM for linear and Non Linear loads" in IJSTM, ISSN online: 2394-1537, vol no. 4, special issue no. 1, March 2015.

[3]. R. Prajapati and Shailendra sharma," Fuzzy Logic Controller based Distribution Static Compensator", IEEE students' conference on electrical electronics and computer science, Pages 1-6: 2014.

[4]. M.sugeno, "Industrial Applications of fuzzy control", Elsevier Science, Amsterdam, 1985.

[5]. J.Xu, C.C.Hang and C.Liu, "Parallel structure and tuning of a fuzzy PID controller," Automatica, Vol.36, pp. 673-684, 2000.

[6]. Y. Zhao, E.G. Collins Jr., "Fuzzy PI control of an industrial weigh belt feeder", proc. of American control conf., Anchorage, AK, May 2002.

[7]. C.S. Sai Pratyusha, K. Harinath reddy, P.Suresh Babu," Power quality enhancement in distribution system using D-STATCOM with fuzzy controller", *Vol.9*, *Issue* 9 (*Jan*. 2014), *PP. 24-29, IJERD, e-ISSN*: 2278-067*X*.

[8]. Mohamed Khaleel, Md. Adam Faraj," Modelling and control of a D-STATCOM with sugeno fuzzy controller and mamdani fuzzy controller for voltage sag mitigation", 2nd ICETET'2014, May 30-31, 2014,London (UK).

[9]. P.P.Shimmeer and A.B. Beevi," Performance Analysis of a Hybrid DSTATCOM Topology as an Effective Solution in Distribution Systems", IEEE-AICERA-ICMMD; pages 1-5: 2014.

[10]. B.N.Singh, P.Rastgoufard, B.Singh, A.Chandra and K.L.Haddad,"Design,simulation and implementation of Three/four pole topologies for active filters," IEE proc.-Electr., Power Appl., Vol. 151, No.4, July 2004.

[11]. Zhen-Yu Zhao, "Fuzzy Gain Scheduling of PID controllers", IEEE transactions on systems, MAN. And cybernetics, Vol. 23, no. 5, sep/oct 1993.

[12]. Vicente Milanés, Jorge Villagrá, Jorge Godoy, and Carlos González," Comparing fuzzy and intelligent PI controllers in stop and go manoeuvers", IEEE transactions on control system technology, vol. 20, no. 3, May 2012.

[13]. Bao-Gang Hu, George K.I. Mann and R.G. Gosine, "A systematic study of fuzzy PID controllers-function based evaluation approach," IEEE Trans. On fuzzy systems, Vol. 9, No. 5, OCT 2001.

[14]. Ziegler and Nichols, " Frequency Response Method," in Astrom & Hagglund, 1995

[15]. Amit V. Sant and K.R. Rajagopal, " PM synchronous motor speed control using hybrid Fuzzy PI with novel switching functions," IEEE Trans. On magnetics, Vol. 45, no. 10, Oct 2009.

Accepted Manuscript

Comparison studies on mechanical and wear behavior of fabricated aluminum surface nano composites by fusion and solid state processing

N. Yuvaraj, S. Aravindan, Vipin

PII: S0257-8972(16)31208-7
DOI: doi:10.1016/j.surfcoat.2016.11.076
Reference: SCT 21822

To appear in: *Surface & Coatings Technology*

Received date: 7 September 2016
Revised date: 20 November 2016
Accepted date: 21 November 2016

Please cite this article as: N. Yuvaraj, S. Aravindan, Vipin, Comparison studies on mechanical and wear behavior of fabricated aluminum surface nano composites by fusion and solid state processing, *Surface & Coatings Technology* (2016), doi:10.1016/j.surfcoat.2016.11.076

This is a PDF file of an unedited manuscript that has been accepted for publication. As a service to our customers we are providing this early version of the manuscript. The manuscript will undergo copyediting, typesetting, and review of the resulting proof before it is published in its final form. Please note that during the production process errors may be discovered which could affect the content, and all legal disclaimers that apply to the journal pertain.

ACCEPTED MANUSCRIPT

Comparison studies on Mechanical and Wear behavior of fabricated Aluminum surface nano composites by fusion and solid state processing

N. Yuvaraj[a], S. Aravindan[b]*, Vipin[a]

[a] Department of Mechanical Engineering, Delhi Technological university, Delhi 110 042, India.
[b] Department of Mechanical Engineering, Indian Institute of Technology, Delhi 110 016, India.

N.Yuvaraj
Department of Mechanical Engineering, Delhi Technological University, Delhi 110 042, India
e-mail: yuvraj@dce.ac.in

S.Aravindan (*corresponding author)
Department of Mechanical Engineering, Indian Institute of Technology, Delhi 110 016, India
email: aravindan@mech.iitd.ac.in, Tel.: +91 11 26596350; fax: +91 11 26582053

Vipin
Department of Mechanical Engineering, Delhi Technological University, Delhi 110 042, India
e-mail: vipin@dce.ac.in

Abstract

By way of increasing the wear resistance, the service life of the industrial components can be enhanced. Nowadays fabrication of surface composites plays a vital role in improving wear resistance. This study attempts to fabricate such surface composites by way of incorporating nano particles of Boron carbide into the Aluminum 5083 alloy by Tungsten Inert Gas (TIG) arc process (liquid state) and friction stir (solid state) process. Microstructural studies were carried out on the processed region to analyze the dispersion of reinforcement particles. Hardness survey and dry sliding wear tests at different sliding loads (30N, 60N &120N) were carried out to investigate the effect of reinforcing particles. The hardness and wear resistance of the fabricated surface composite by both the processes are found to be higher than the base material. Friction stir processed surface composites are possessing higher hardness and wear resistance than that of TIG arc processed composites. The worn out surfaces of the composites and wear debris were analyzed through SEM studies to understand the wear mechanisms.

ACCEPTED MANUSCRIPT

Keywords: Friction Stir Processing; TIG arc surfacing, Boron Carbide (B_4C); Wear

1 Introduction

Aluminum matrix composites are finding high technology applications owing to their excellent mechanical, wear and corrosion resistance properties [1-2]. The useful service life of the components depends on the surface [3-5]. Ceramic particles were reinforced into the matrix by utilizing various techniques such as coating, hard surfacing, cladding, and electron beam irradiation [6-7]. Choo et al. [8] have deposited TiC particles on the plain carbon steel plate using high energy electron beam irradiation technique for producing the surface composite. This composite exhibited 3 to 4 times higher hardness than the base alloy due to the presence of TiC hard particles. These processes create an excellent bond between the substrate and the composite. Dubourg et al. [9] have modified the surface by addition of copper and iron powders on the Aluminum surface by laser cladding. The hardness of Al/38Cu-11Fe(wt%) hardness was 550 $Hv_{0.2}$ whereas the hardness of the non treated sample hardness was 20 $Hv_{0.2}$. Presence of intermetallic compounds, grain refinement and hardened surface of the Al matrix improve the hardness of the composite. TIG arc surfacing is a cost effective process. It produces high thickness surface composite layer which comprises of intermetallic compounds. Metallurgical bonding nature is the specific advantage of TIG arc surfacing [10-11].

Recently Gandra et al. [12] have fabricated SiC composite on the AA2024-T3 substrate by employing AA6082-T6 aluminum alloy consumable rods by friction surfacing process. Faying surface of the consumable aluminum rod has been provided with a 2 mm diameter hole to a depth of 20 mm. SiC particles were packed in the hole for reinforcement during frictional surfacing. The hardness of the composite coating was 110 Hv which is 30% higher than the base alloy. Friction surfacing leads to grain refinement due to continuous and discontinuous recrystallization process. The SiC particles strengthened the coating with improved hardness and reduced wear. Jiguo et al. [13] have used TIG arc source with Ni and Al powder preplaced on the Q235 steel plate to prepare the surface with Ni-Al intermetallics. Islak et al. [11] have fabricated AISI 1060 steel/B_4C surface composite by TIG arc method. Microhardness of the composite was

ACCEPTED MANUSCRIPT

4-5 times higher than the base material. Similarly TIG arc source was used with Ti & Al powder preplaced on the Titanium substrate to form the titanium aluminide intermetallic compounds [14]. The hardness and wear resistance of the coated surface was improved about 3-4 times than base material. In another study conducted on AISI 8620 steel, SiC/C particles diffused on the surface by TIG arc method. The hardness and wear behavior of the modified surface was significantly improved [15].

In order to fabricate surface composite by solid state processing method, recently well known Friction Stir Processing (FSP) technique is used [16]. The composite processed through FSP can have thickness in the range of microns to several millimeters. The reinforcement particles are incorporated in the matrix by mechanical mixing without melting the substrate. Several investigators have produced the surface composite by FSP. Compared to other surface modification techniques, FSP provides better grain refinement and uniform dispersion of reinforcement particles in the matrix [17]. The reinforcement particles are preplaced in the grooves/holes on the surface of the metallic substrate plate and then processed with the FSP tool to form the surface composite [18].Various second phase hard particles such as SiC, ZrO_2, CNT, TiC, Si_3N_4, TiO_2, B_4C and Al_2O_3 were used as a reinforcement in FSP [19-20]. The thermal stability of the Aluminum alloy was improved by the addition of SiC into matrix [21]. The hardness and corrosive behavior of Al5083 alloy were greatly improved by the addition of SiC/CNT and CeO_2 particles. The higher percentage of cerium oxide improves the corrosive resistance of Aluminum alloy [22-23]. Soleymani et al. [24] have reported that there is a significant effect on the wear properties of the Al5083 based MoS_2 reinforced composites.

Increase in number of FSP passes increases the uniform distribution of particles in the matrix and reduces the clustering effect with enhanced mechanical and wear properties [25-26]. The application of B_4C is used in the surface modification processes extensively especially to develop Al based composites. B_4C has its low density (2.52 g/cm^3), high hardness and excellent thermal stability. Owing to its specific properties, it finds specific applications such as neutron absorption; high wear resistance, high impact resistance, etc. [27-28]. The present work aims to fabricate the Al/B_4C surface composite by TIG arc and FSP method. The microstructural characteristics, microhardness and wear properties of the fabricated surface composites were

ACCEPTED MANUSCRIPT

compared. The friction and wear behavior of the composite at different sliding loads (30N, 60N & 120N) were investigated and the results were compared with the base material.

2 Materials and Methods

Aluminum alloy of 5083-O plate with a thickness of 8mm having chemical composition of 4.1%Mg, 0.06%Cr, 0.5%Mn, 0.19%Fe, 0.02%Zn, 0.2%Si, 0.04%Ti (all in weight %) was used. A groove size of 1mm width and 3mm depth was created in the middle of the Aluminum plate for TIG arc surfacing. The same groove size was used for friction stir processing also to have a same volume fraction of particles. Prior to the process, the surfaces of the aluminum plate were cleaned with acetone. To prevent the escape/loss or depletion of particles from the grooves by the flow of shielding gas, B_4C particles were mixed with acetone and then packed on to the groove. The substrates were then dried at 50^oC temperature for 30 min. The average B_4C particle size of 30-60nm with a purity of 99.5% was used. The SEM micrograph of the B_4C nano particles is shown in Fig. 1. TIG arc surfacing process was carried out with straight polarity using a pulse DC TIG machine and the process parameters are presented in the Table No. 1.

Table No. 1 TIG arc surfacing process parameters

S No	**Operation parameters**	
1	Electrode	Zirconated Tungsten Electrode
2	Shielding Gas	99.95 argon
3	Electrode diameter	2.4 mm
4	Gas flow rate	7L/min
5	Current	130A
6	Voltage	20.4
7	Speed	1.25 mm/sec
8	Nozzle to plate distance	5 mm

The dimensions of the groove for both the processes (TIG arc and FSP) were of similar in size so that the same volume of reinforcement particles could be filled. Probe less tool was used initially to prevent the escape of the particles during processing. H-13 hardened tool with 18mm

ACCEPTED MANUSCRIPT

shoulder diameter, cylindrical threaded pin diameter of M6x1.0 and pin length of 5mm was used for processing. The specimens were mounted on a hydraulic fixture of FSW machine capacity of 11 kW & 40kN, to fabricate the surface composites. Tool parameters were fixed at constant tool rotational speed (1070 rpm) and transverse speed of 40 mm/min and the samples were subjected to four FSP passes. After completing each pass, the specimens were allowed to cool to the ambient temperature and then the subsequent passes were carried out.

In order to have uniformity in processing for the second and fourth passes the specimens were changed their orientation from advanced side to retreating side. Fig. 2 (a) and (b) show the experimental setup used for TIG arc surfacing and friction stir processing respectively. The samples were taken from the cross section of the processed region for microstructural and hardness studies. The transverse sections of the processed composite were polished and then examined through optical and Scanning Electron Microscope (SEM) (Hitachi S3700), Field Emission Gun Scanning Electron Microscope (FEG-SEM) (FEI QUANTA 3D FEG). XRD (BRUKER D8 ADVANCE) was used to identify the presence of phases in the stir zone of the surface composite. The micro hardness (Leica VM Auto) values of the surface composite and base alloy were measured along the cross section of the processing direction at the load of 100g with a dwell time of 10s.

Dry sliding wear tests were conducted using a pin on disc tribometer (DUCOM) as per ASTM G99-04 standard. A schematic showing pin on disc set-up is shown in Fig. 3. Cylindrical wear test pins of 8 mm diameter were extracted from the middle of the processed region by wire EDM. Wear test specimens tested against EN-24 steel hardened to 55-58 HRC, ground to a surface roughness (Ra) of 0.2µm. Wear tests were carried out at a constant sliding speed of 1 m/s and normal loads of 30, 60 and 120N with a constant sliding distance of 3000m. A constant track diameter 100mm was used in all the tests. Before each wear test, the pin surface was polished with 1600 grit emery paper. Specimens and discs were cleaned with acetone before and after the wear test. The pin specimens and disc were weighed to an accuracy of 0.01mg by an electronic weighing balance. All wear tests were repeated three times to ensure repeatability. The coefficient of friction between the composite and the hardened disc was measured from the recorded frictional force and applied load. The worn surfaces and wear debris were examined by SEM with Energy Dispersive Spectrometer (EDS) to understand the wear mechanisms. The wear behavior of surface composite was compared with the wear behavior of the base material.

ACCEPTED MANUSCRIPT

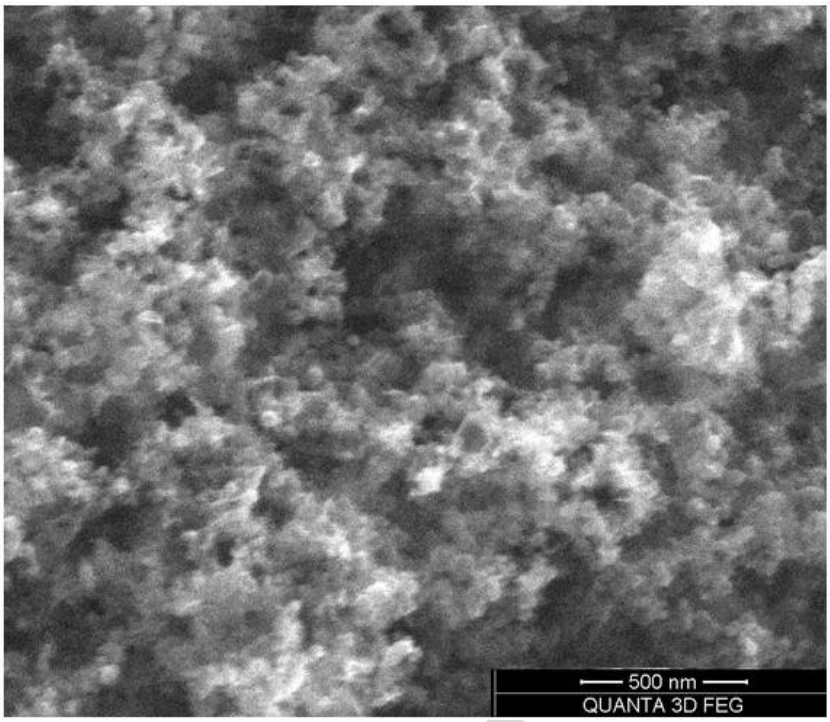

Fig. 1 SEM micrograph of B_4C nano particles

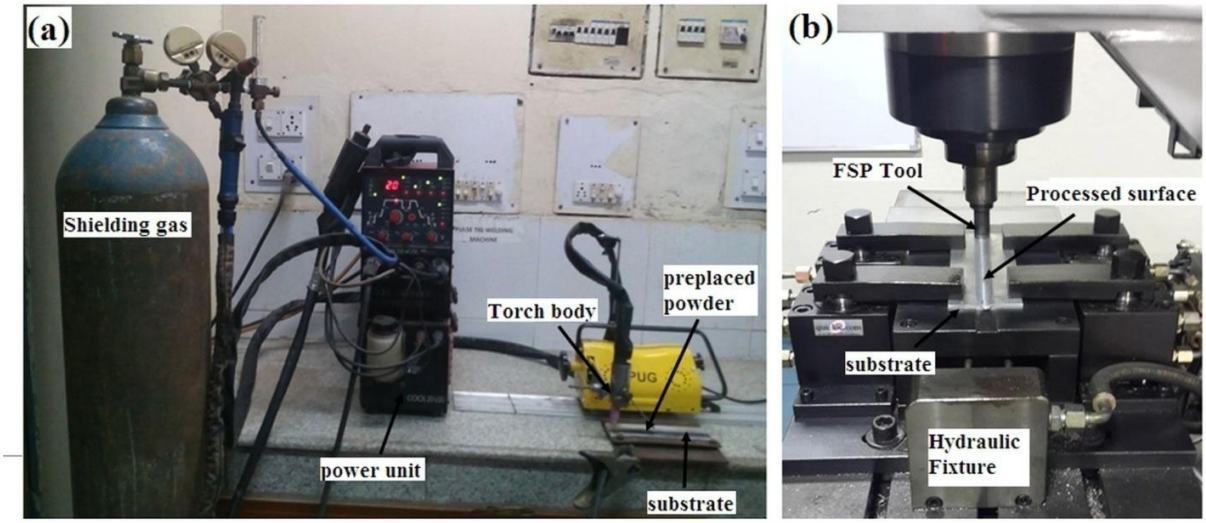

Fig. 2 Experimental set-up (a) TIG arc surfacing (b) friction stir processing

ACCEPTED MANUSCRIPT

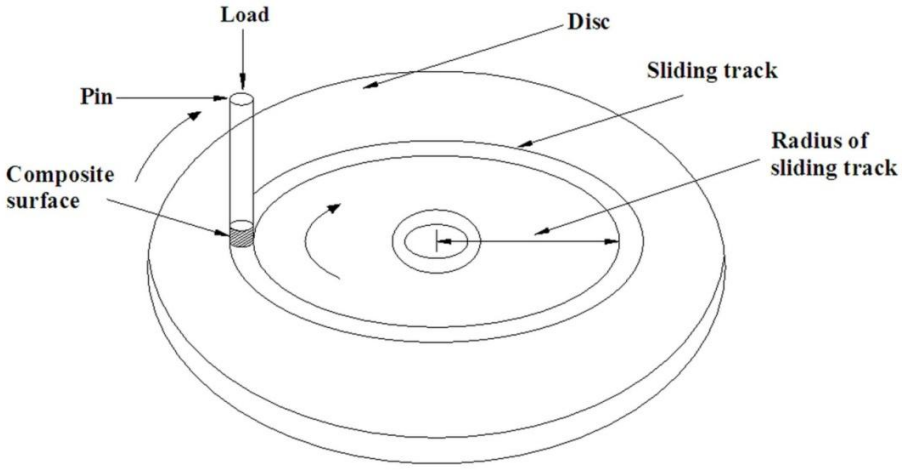

Fig. 3 Schematic diagram of pin on disc set-up

3 Results and discussion

Fig. 4 shows macro images of the composite surface specimens prepared by (a) TIG arc method and (b) FSP method respectively. After a number of preliminary trials, the TIG arc surfacing process parameters were fixed. In the FSP, the tool parameters such as tool traverse speed and rotational speed are the key parameters pertaining to the material flow [29]. Heat generation during FSP in the stir zone is directly related to rotational speed and inverse of traverse speed [30]. T_{max} (maximum temperature) occurs during FSP is an important key factor for determining the mechanical and wear properties of the material surface it affects microstructure and grain size [31]. Excess amount of heat generation during FSP has an adverse effect like coarsened grain structure and it may also lead to melting of the material. On the other hand, low heat generation is insufficient to form the surface composites [32]. Grain refinement may not occur due to insufficient heat input. The defects like tunnel defect and lack of fill will result at the processed surface owing to less heat input. Optimum tool parameters and processing parameters are their necessary.

Cross sectional macrostructures of the composite surface prepared by (a) TIG arc method (b) FSP method are shown in Fig. 5. It clearly shows the defect free composite region processed

ACCEPTED MANUSCRIPT

by both the methods, and the composite produced by the FSP method has a larger thickness (wider and deeper) when compared to the TIG arc method. It has also been observed that the melting of the material occurs in the TIG arc method upto 4 mm in the depth direction. The composite produced by FSP is extending approximately to 5.5mm depth which is slightly higher than the pin length of the FSP tool. The threaded tool provides adequate flow of material around the pin from retreating side to the advancing side. It also facilitates uniform mixing of material in vertical directional also and hence the particles are incorporated in the complete length of the pin. Similar results are reported by Bauri et al. [33] for the fabrication of Aluminum/Tungsten composite by FSP process.

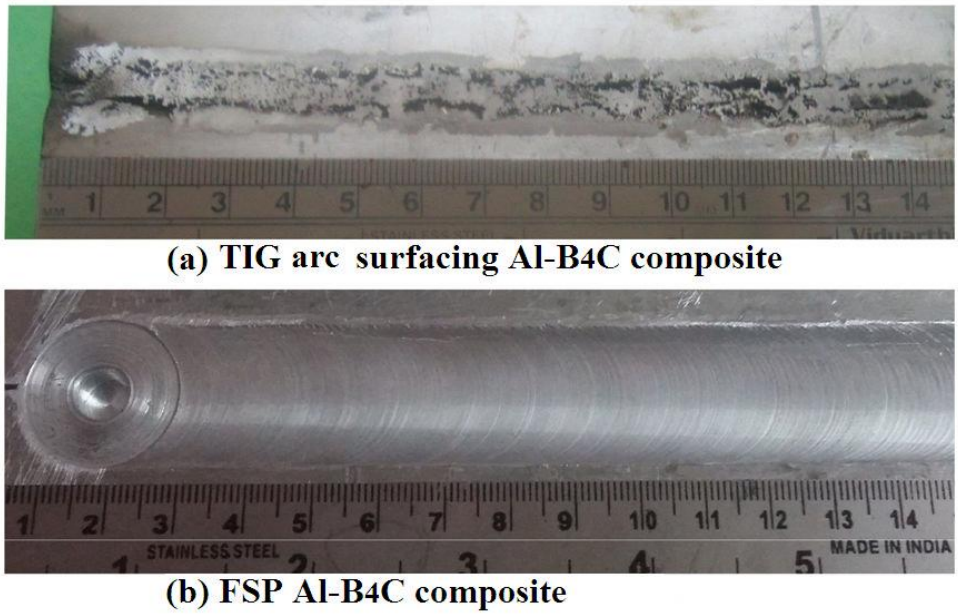

(a) TIG arc surfacing Al-B4C composite

(b) FSP Al-B4C composite

Fig. 4 Macro images of the composite surfaces prepared by (a) TIG arc method (b) FSP method

ACCEPTED MANUSCRIPT

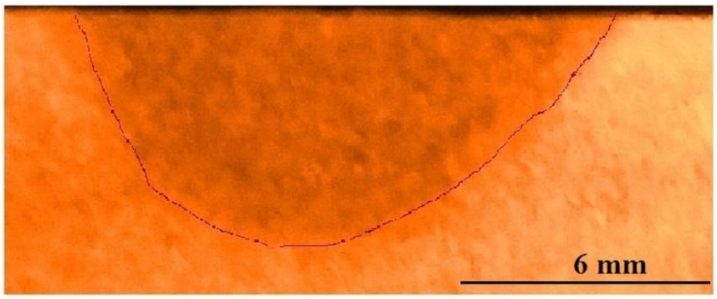

(a) TIG arc composite surface

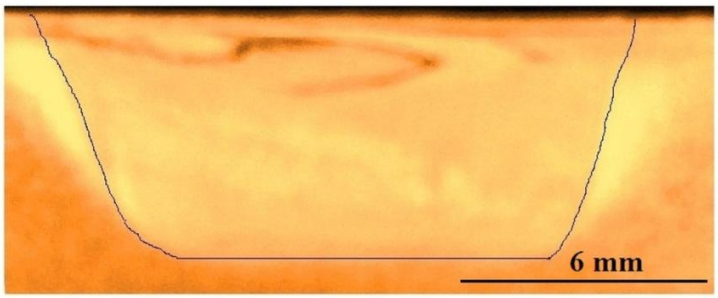

(b) FSP composite surface

Fig. 5 Cross sectional macrostructure of the composite surfaces prepared by (a) TIG arc method (b) FSP method

ACCEPTED MANUSCRIPT

ACCEPTED MANUSCRIPT

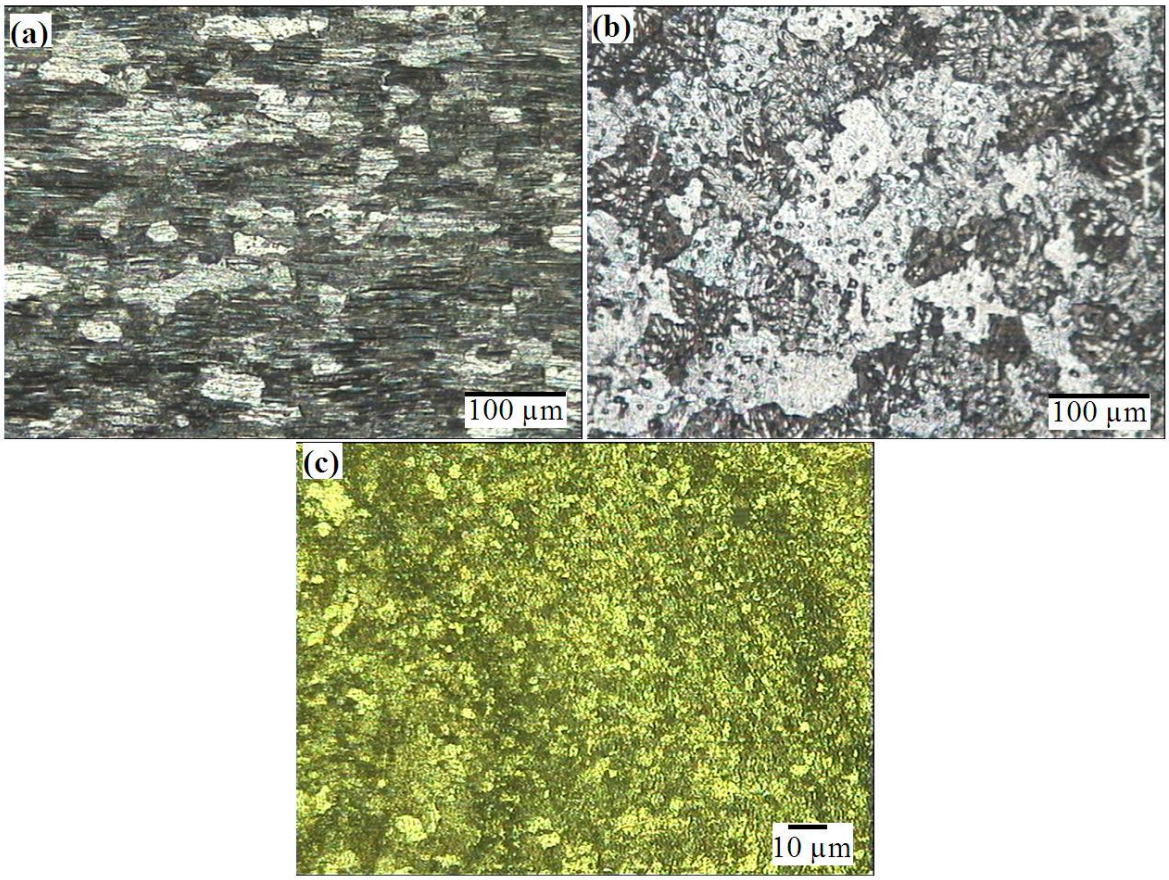

Fig. 6 Optical micrographs of (a) base material (b) TIG arc composite surface (c) FSPed composite surface

3.1 Microstructure

Fig. 6 shows optical micrographs of (a) base material (b) TIG arc surface and (c) FSP composite surface. The temperature of the TIG arc surface material was measured using the thermal imaging camera (Fluke Ti400), and the temperature was approximately 950^{o}C. Due to TIG arc heat, grain coarsening is observed at the surface. The substrate material is melted and mixed with particles and forms the composite. The possible stable phases of the reaction between liquid B_4C and Al may be Al_4C_3, Al_3BC, Al_3B_{48}, Al_3BC_3 and B_4C according to ternary phase diagram [34]. Zhang et al. [35] have fabricated Al-10%B_4C-0.67%Ti composite by stir casting method at 730±2^{o}C. The microstructure of the composite was reported to be consisting of B_4C particles and phases of Al_3BC, AlB_2 and TiB_2. Shorowordi et al. [36] has revealed that Al-B_4C composite casting has better interfacial bonding than Al-SiC and Al-Al_2O_3 composite. B_4C has

ACCEPTED MANUSCRIPT

more wetability and better particle distribution with aluminum when compared with SiC. At the temperature range 868^{o}C, B_4C particles reacted with liquid aluminum and the products formed as ternary carbide Al_3BC and diboride AlB_2. The phases such as Al_3BC and AlB_2 are observed below 868^{o}C. Lee et al. [37] have fabricated Al5052-B_4C composite by pressureless infiltration method and the reaction products were identified as Al_3BC, $AlB_{10,}$ and β-$AlB_{12.}$ Viala al. [38] have reported on the chemical reactivity of B_4C with aluminum. Around 660^{o}C reactivity is very slow and the reaction products are ternary carbide (Al_3BC) and diboride (AlB_2). At the high temperature range of 868^{o}C, Al_3BC is formed and β-AlB_{12} is replaced with $AlB_{2.}$ The average grain size of the base material is about 49.5µm. After four passes of FSP, the composite the grain size is reduced to 3µm.The grain size reduction of the composite sample is due to dynamic recrystallization and the addition of hard nano reinforcement particles prevents the grain growth of the matrix material.

3.2 XRD and EDS analysis

The SEM image of Al-B_4C TIG arc surface is shown in Fig. 7(a) and its XRD pattern shows (Fig. 7(b)) the various elements of the composite. The EDS is taken at the point B, of the composite and the same is presented in the Fig. 7(c) and the results show the presence of boron and carbon in the composite. Fig. 7(d) shows the FE-SEM higher magnification image of TIG arc composite. The isothermal ternary diagram of 1000^{o}C of Al-B-C system is shown in Fig. 8. TIG arc surfacing temperature is around 1000^{o}C and hence this ternary diagram is chosen. The expected phases are to be Al_3BC, $B_2O_{3,}$ and B_4C. The XRD pattern shows the phases of Al_3BC, $B_2O_{3,}$ and B_4C. The optical micrograph also revealed that there might Al-B_4C phases in the dark and white region interface.

ACCEPTED MANUSCRIPT

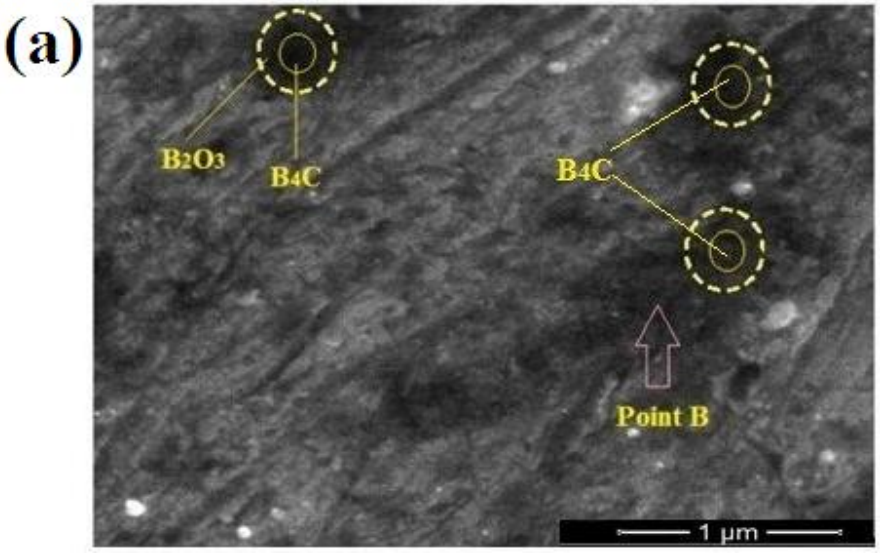

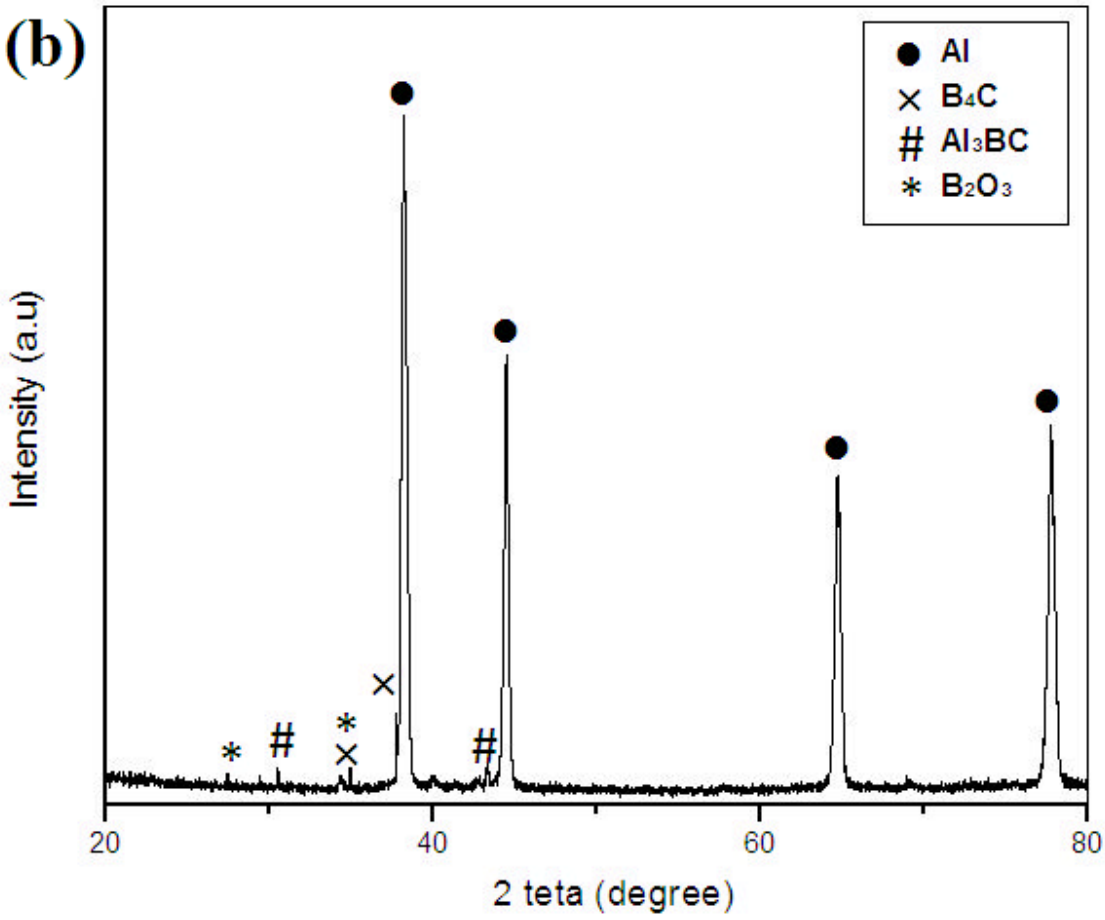

ACCEPTED MANUSCRIPT

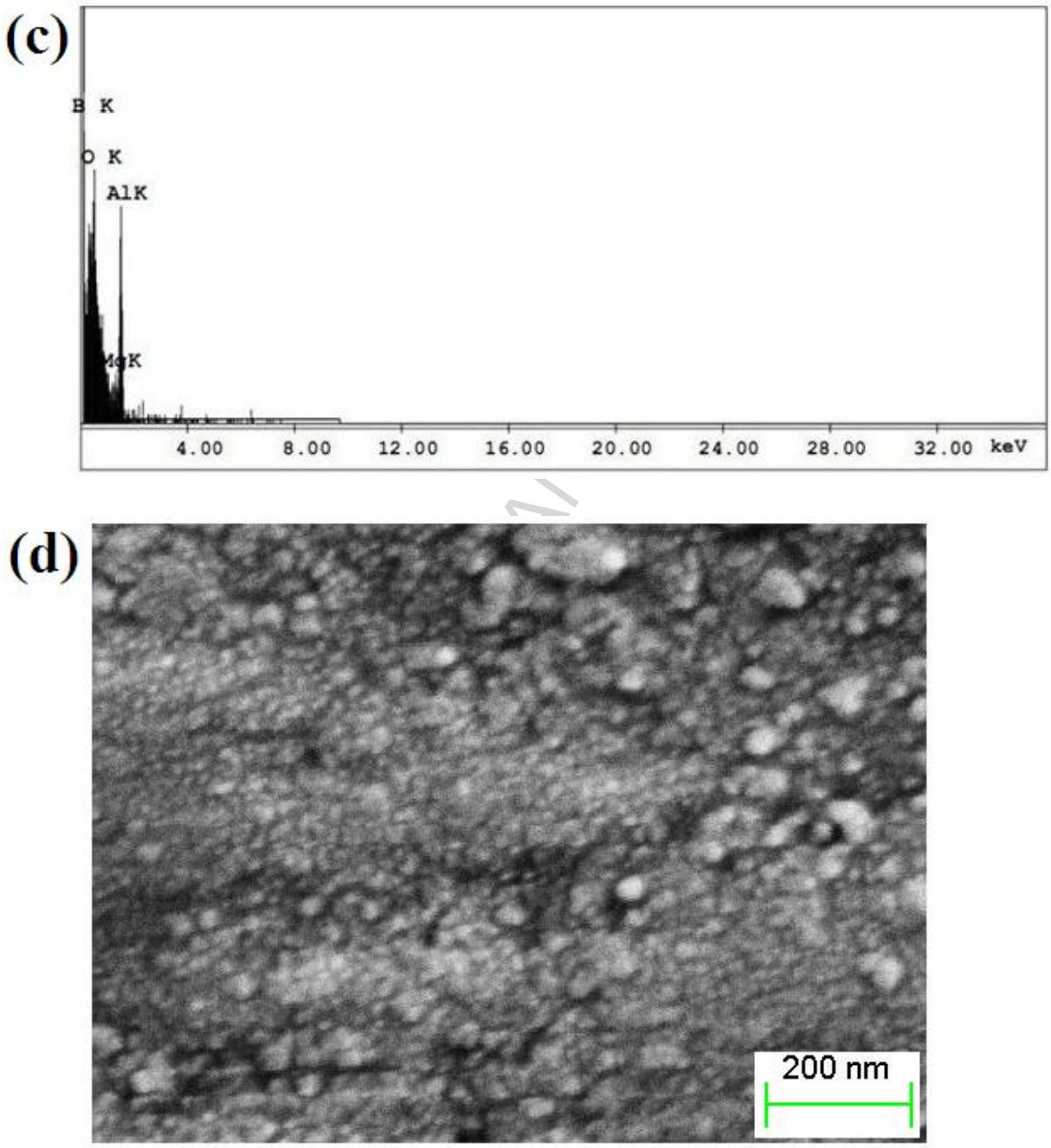

Fig. 7 (a) SEM micrograph of cross section of Al-B_4C composite surface prepared by TIG arc method (b) XRD pattern for Al-B4C composite prepared by TIG arc (c) EDS profile shows the elements present in Point B of the SEM image (d) FE-SEM image of TIG arc composite

ACCEPTED MANUSCRIPT

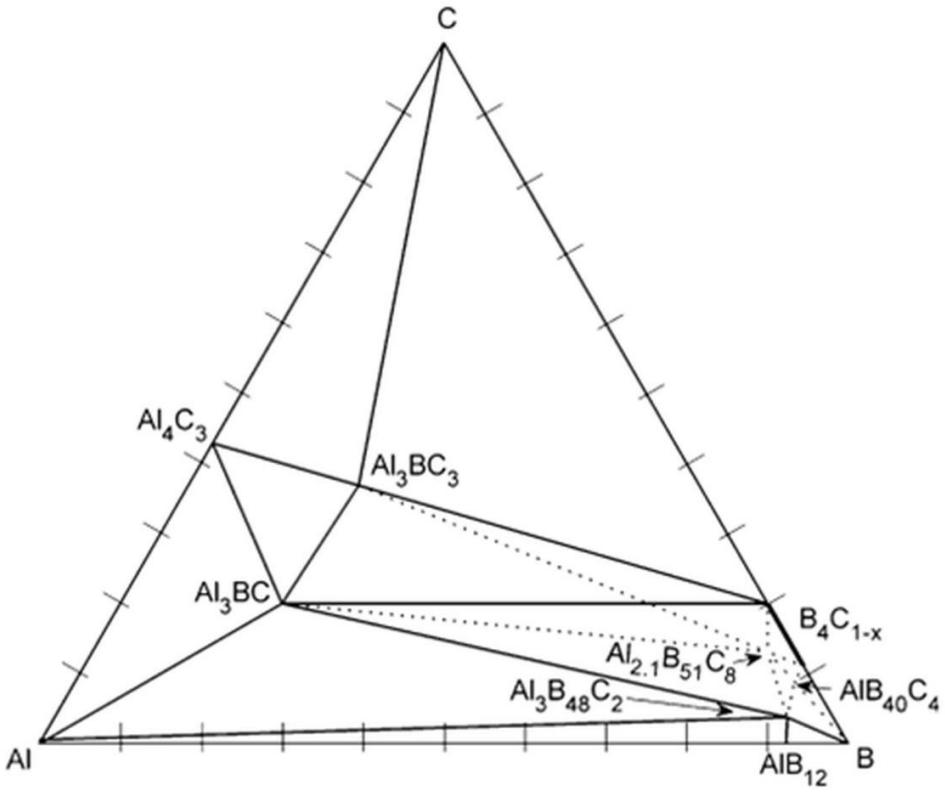

Fig. 8 Isothermal ternary diagrams at 1000°C of Al-B-C system [34]

ACCEPTED MANUSCRIPT

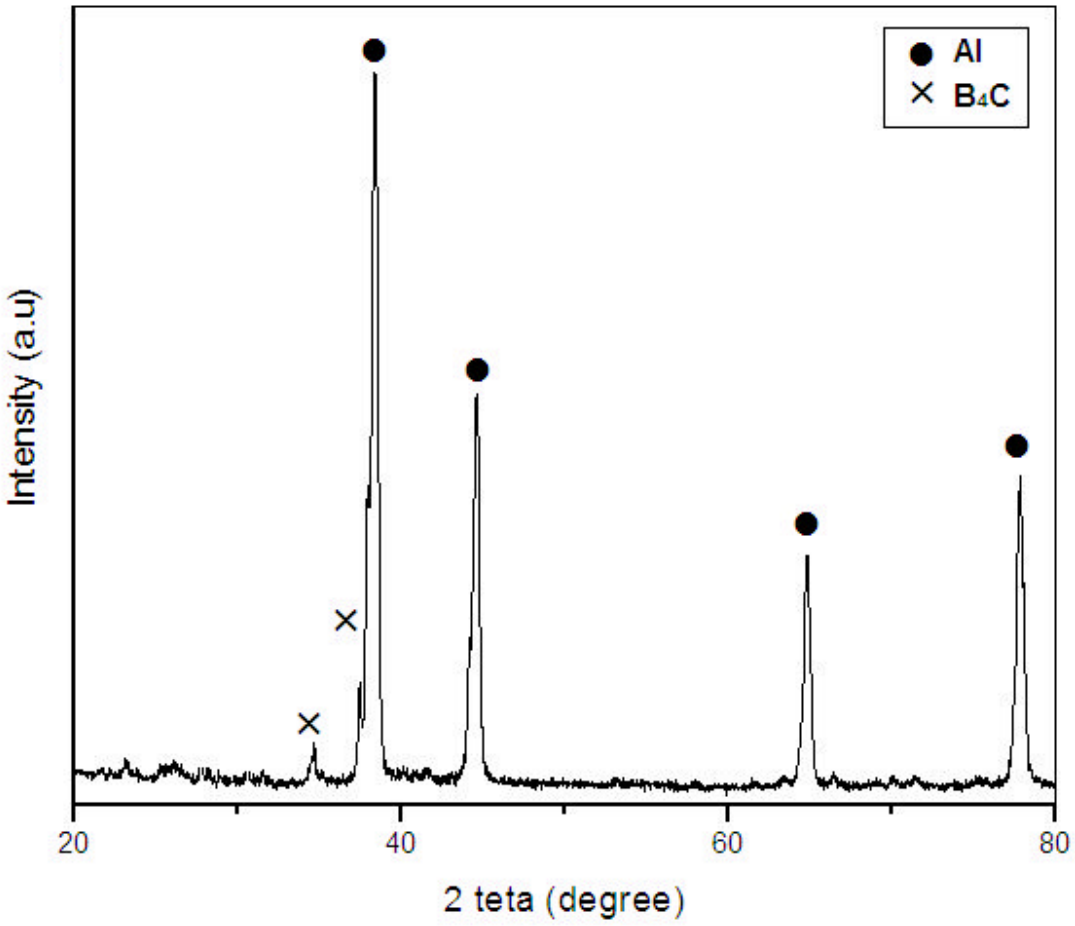

Fig. 9 XRD patterns for Al-B_4C composite prepared by FSP method

Typical XRD patterns for the Al-B_4C FSPed surface composites are presented in Fig. 9. The clear peaks of aluminum and marginal peaks of B_4C are observed, and no intermetallic elements were detected. Fig. 10(a) shows the SEM micrograph of cross section of Al-B_4C composite surface prepared by FSP method and Fig. 10(b) EDS profile shows the elements present in Point C of the SEM image. The elemental composition mapping of processed composite is depicted in Fig 10(c), and Fig 10(d) shows the FE-SEM image of FSPed composite. During FSP the stir zone temperature reaches in the range of 400-450^{o}C. This temp is only (0.17-0.20) T_m of B_4C and this temp is insufficient to melt the B_4C particles and to cause any significant reaction of B_4C particles with Aluminum and as a result no intermetallics are observed in the Al-B_4C composite.

ACCEPTED MANUSCRIPT

(a)

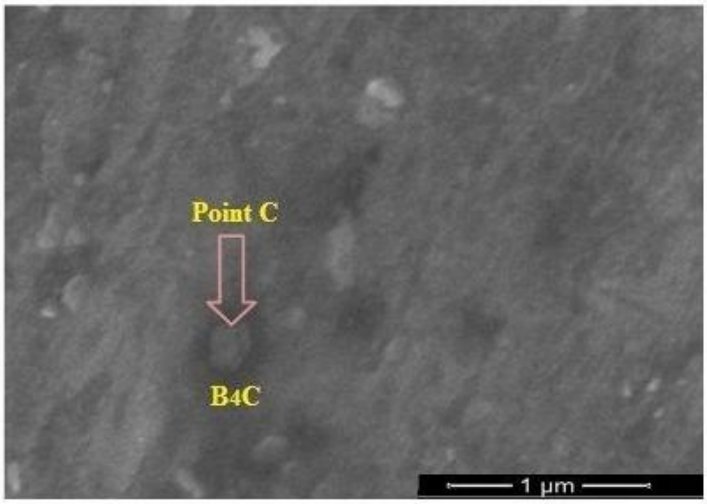

(b)

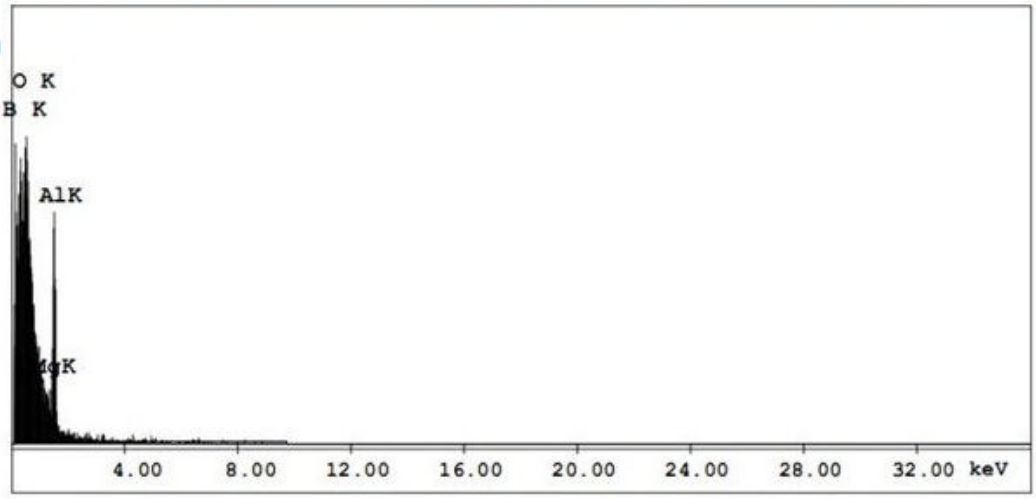

(c)

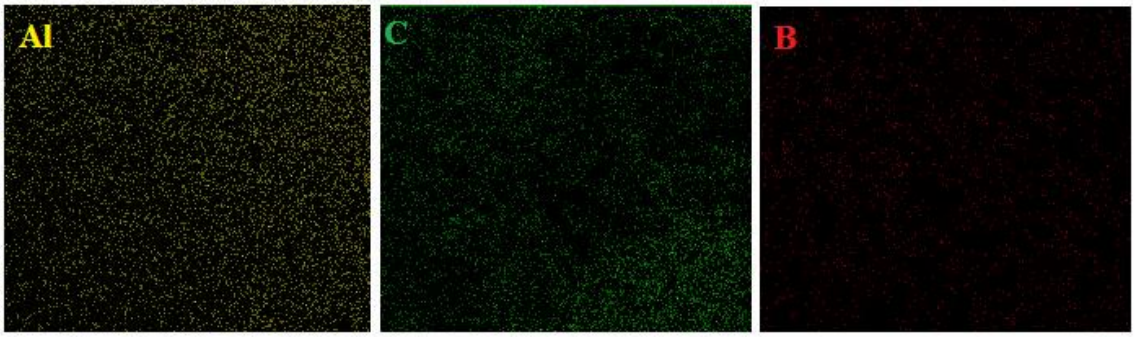

ACCEPTED MANUSCRIPT

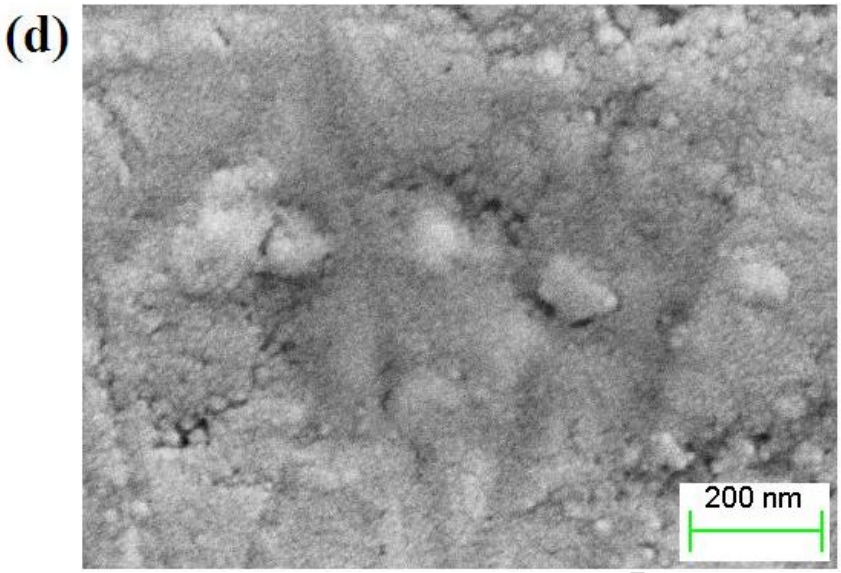

Fig. 10 (a) SEM micrograph of crossed section of Al-B_4C composite surface prepared by FSP method (b) EDS profile shows the elements present in Point C of the SEM image (C) The elemental composition mapping of processed sample (d) FE-SEM image of FSPed composite

3.3 Hardness

Fig. 11 shows the hardness profile of the cross section of the composite surface. The hardness measurement of the cross section of the composite was taken at 1 mm below from the upper part of the processed surface. The average of three hardness measurement was taken for all the samples. The hardness of the TIG arc surface is higher than base material. TIG arc composite surface exhibited an increase in hardness by 32%, and the base material hardness is 83±2 Hv. The hardness profile of the FSP and TIG arc composite specimen along the depth direction are presented in Fig. 12. The depth of the TIG arc composite surface is around 4mm.The enhancement in hardness is uniform throughout the depth of the composite, and an average hardness value of 108±3Hv is observed. After that, the hardness is observed to be decreased and reaches to base material hardness. The depth of the FSP composite is 5.5mm, which is higher than the TIG arc method. The average hardness value of is of 127±2Hv.

The hardness value of the TIG arc surface is increased due to the formation of intermetallic phases and the hard B_4C nano particles with aluminum matrix. The SEM

ACCEPTED MANUSCRIPT

micrograph of the TIG arc surface shows the good bonding of B_4C particles with the matrix. Also, Orowan strengthening mechanism and load bearing effect of ceramic particles are the reasons for the increase in hardness of the TIG arc surface composite. FSPed composite surface exhibited the increase in hardness of 50%. During FSP, severe plastic deformation and grain refinement occurs due to dynamic recrystallization. As per Hall petch relationship smaller grain size of the matrix has higher the hardness [39]. The relationship states that

$H_v=H_o+K_Hd^{-1/2}$ ------- (1)

Where d is the grain size, H is the hardness and $H_{o,}$ and K_H is Hall-Petch constants. With an increase in the number of passes and change in tool direction between the passes promotes good bonding of ceramic particles with matrix. The reinforcement particles are uniformly distributed in the matrix which is also responsible for the enhancement in hardness. Similar results are reported by other researchers on different aluminum alloys and reinforcements. Zhao et al. have [40] reported that the hardness value of FSPed Al6061/B_4C composite is 98Hv which is much higher than base alloy hardness value of 51-57Hv. Similarly, Sahraeinejad et al. [41] have reported that FSPed 5059/B_4C composite is possessing higher hardness when compared to other Al-Al_2O_3, Al-SiC surface composite. From the literature and the findings of present work, the following major mechanisms are contributing to enhancement of hardness of FSPed composite surface [23, 42].

1. Orowan strengthening mechanism - Fine and uniform dispersion of nano particles of reinforcement particles in the matrix.
2. Grain refinement.
3. Load transfer strengthening mechanism - Effective load transfer from softer Aluminum matrix to hard reinforcement particles.
4. Dislocation strengthening mechanism - The difference between the coefficient of thermal expansion of Al matrix ($23.1x10^{-6}$ k^{-1}) and B_4C particles ($5x10^{-6}$ k^{-1}).

ACCEPTED MANUSCRIPT

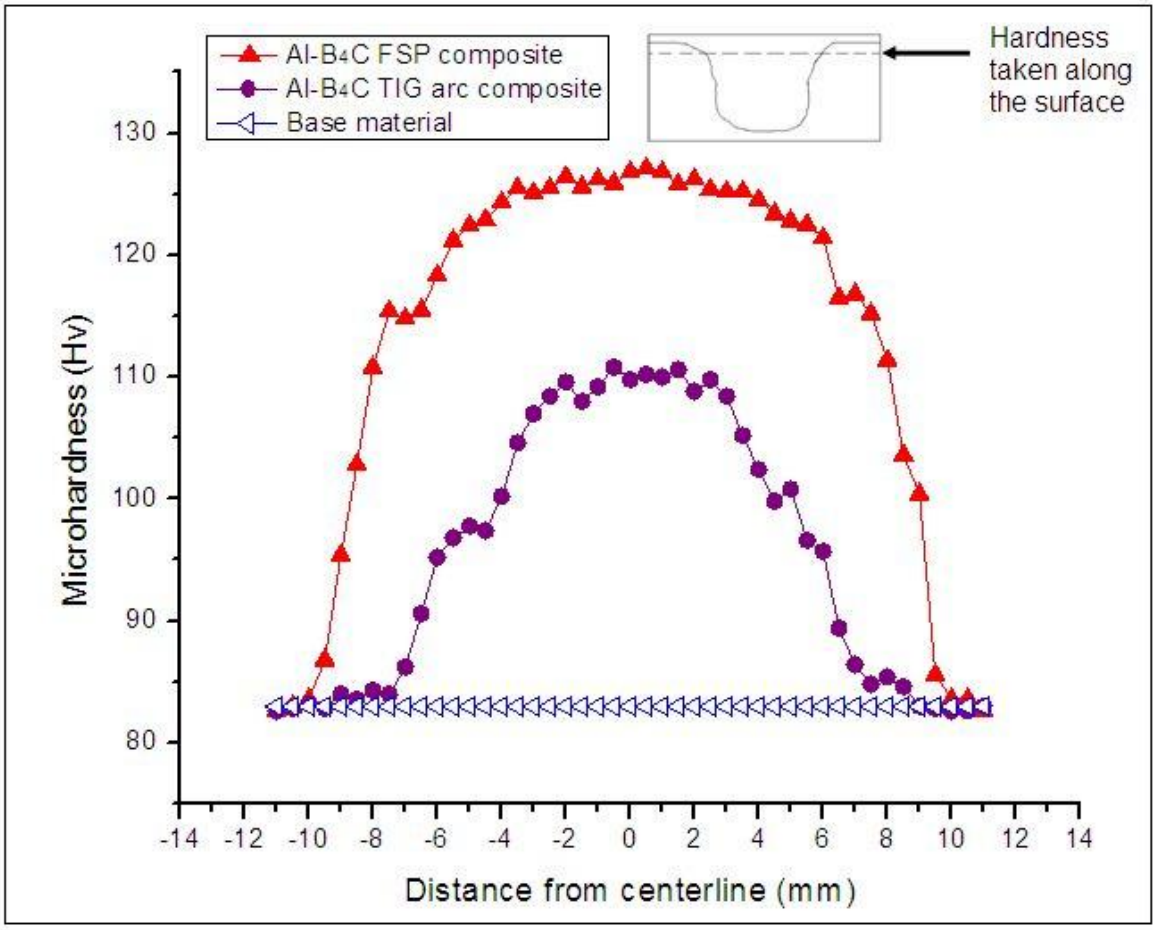

Fig. 11 Micro hardness profiles of TIG arc and FSPed surface composite at the top surface

ACCEPTED MANUSCRIPT

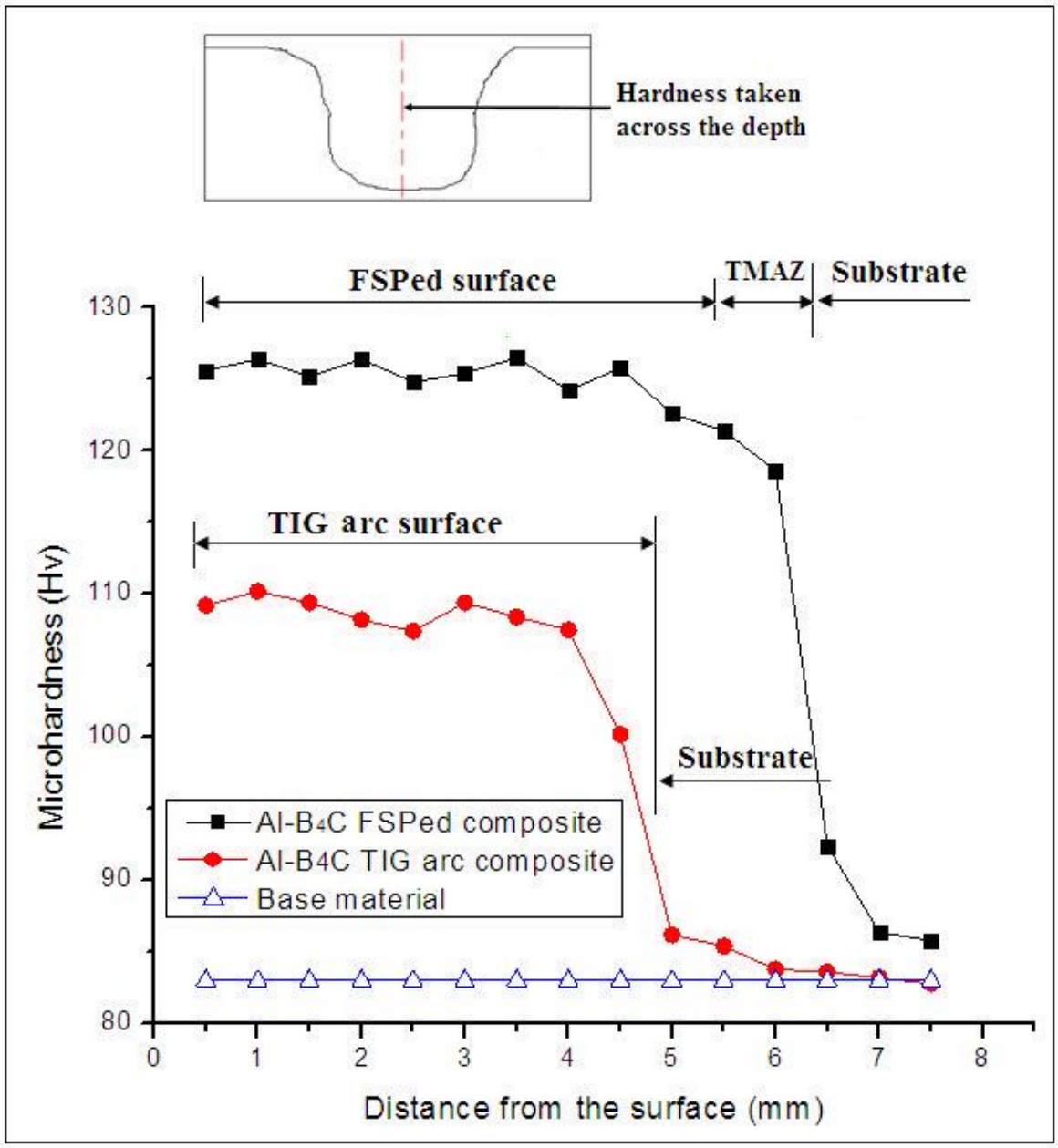

Fig. 12 Micro hardness profiles of TIG arc and FSPed surface composite of the cross section

ACCEPTED MANUSCRIPT

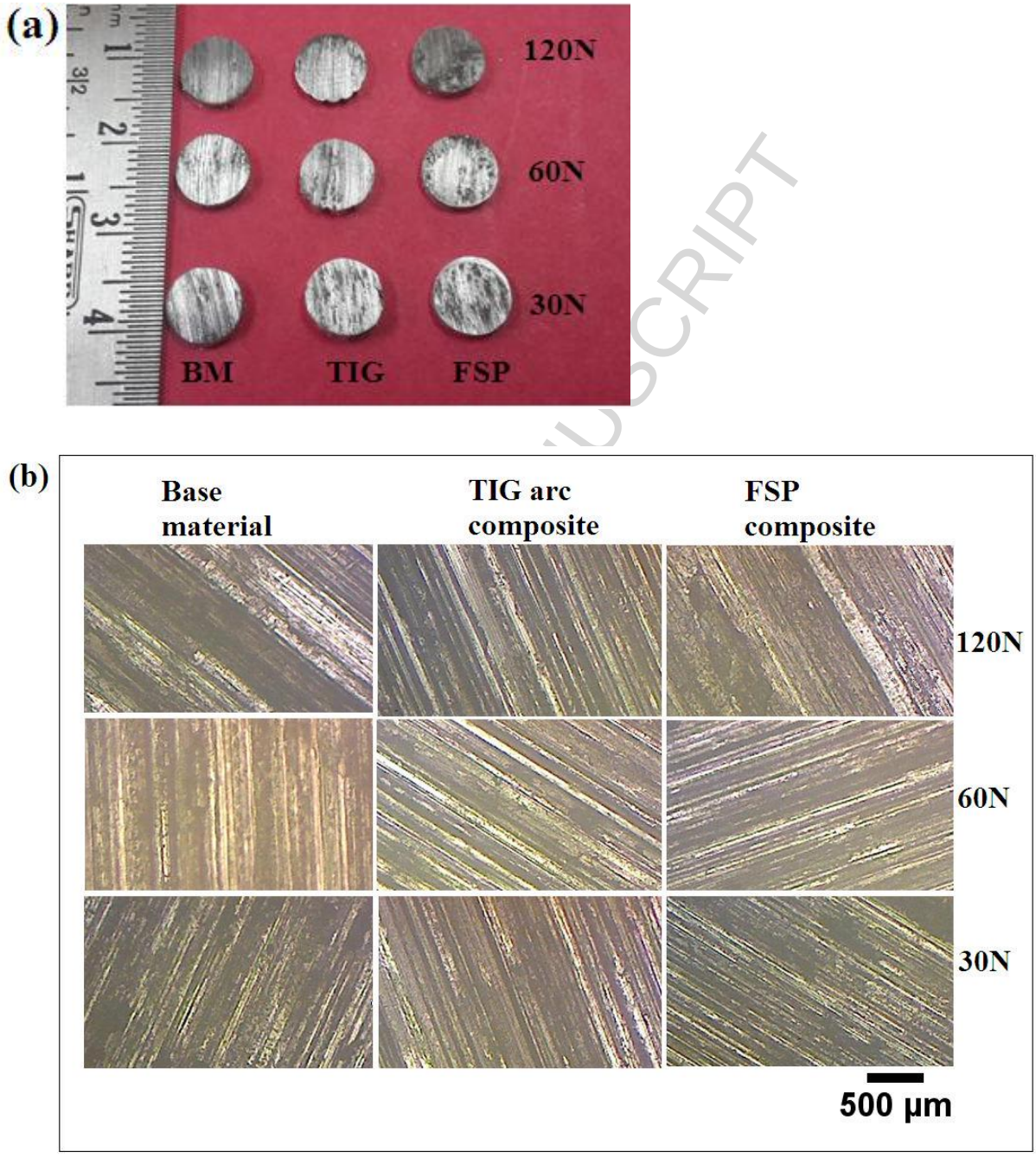

Fig. 13 The worn surface of tested samples (a) macro image (b) micro image

ACCEPTED MANUSCRIPT

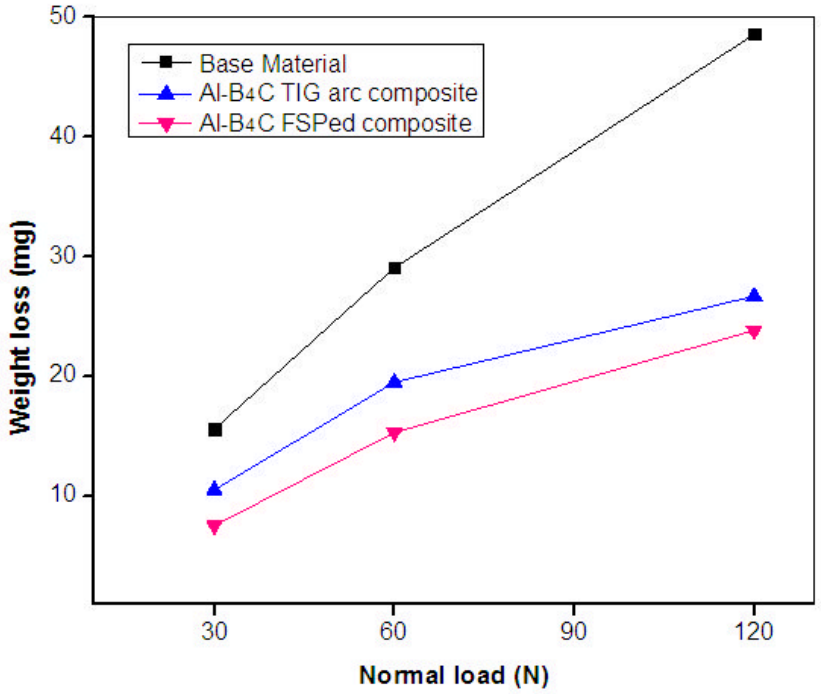

Fig. 14 Effect of applied load on wear resistance

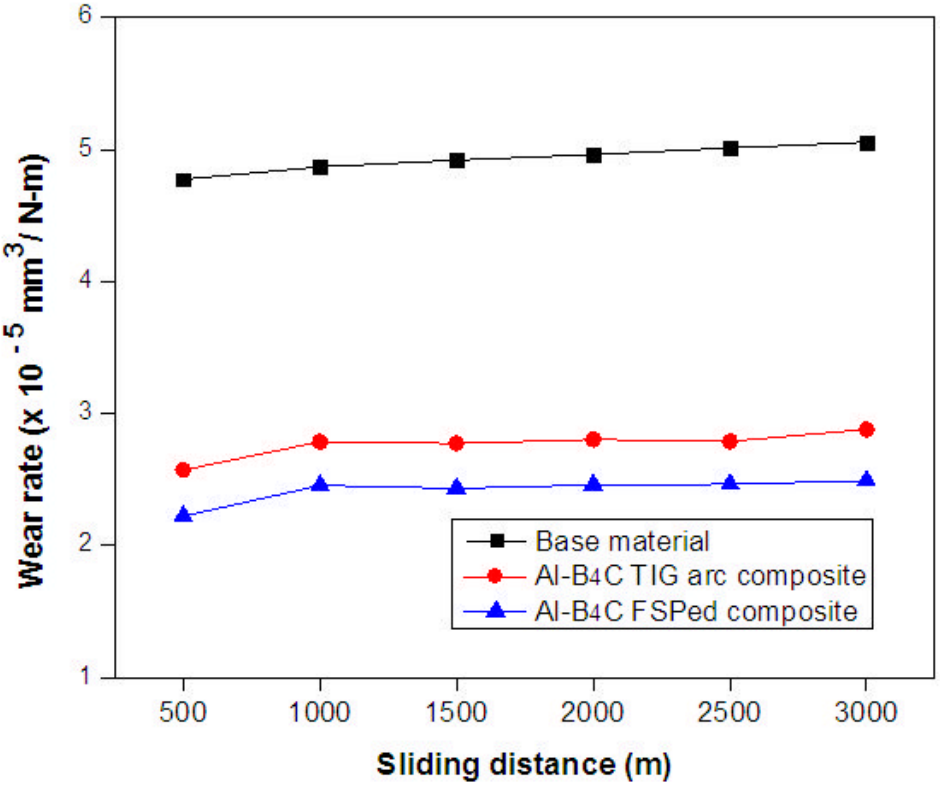

ACCEPTED MANUSCRIPT

Fig. 15 Variations of wear rate with the sliding distance for base metal and composite specimens

3.4 Wear Properties

Fig. 13 (a) and (b) show the macro and micro images of wear tested base material, TIG arc and FSPed composite specimens at different loads. The weight loss of the wear tested specimens as a function of different applied normal loads is depicted in Fig. 14. The variation of wear rate with the sliding distance of the base material and composite specimens tested at 120N normal load is presented in Fig. 15. The weight loss increases with increase in loads for all the samples. However, the weight loss of the base material is higher than composite specimens. These results are supported by various researchers [43-44]. The main wear mechanisms observed at lower load 30N of the base material is oxidation and abrasive wear. The SEM image (Fig. 16(a)) shows the oxide and abrasive marks in the sliding direction of the base material. No excessive surface damage is seen at the worn surface and some areas cracks and damaged pits are observed along the sliding direction. At a normal load of 60N, base material has wider and deeper grooves. Small sized subsurface pits or craters are observed at the surface. At higher loads of 120N (Fig 17(a)), the wear type is changed from mild to severe wear and excess of temperature is generated between the sliding surfaces. Due to frictional heat generated between the sliding surfaces the matrix is softened and more material is removed from the wear specimen. SEM micrographs show the shape and size of wear debris collected at 120N normal load of base material (Fig 18(a)). The wear debris of the base material is in a larger size and irregular shapes of different dimensions. The EDS profile of wear debris of base material confirms the iron content which is transferred from the steel disc to the surface, however, which is lesser than the composite samples. The base material wear specimen is having less hardness than the composite specimen, and severe wear occurs on the base material specimen due to adhesion of aluminum matrix to the harder disc material.

The wear rate of TIG arc composite is lower than base material due to the higher hardness, and the same is related to the Archard's wear equation [45]. The presence of hard B_4C nano particles strengthen the material, and nano particles have a good interface between matrix, load bearing effect and formation of Al_3BC and B_2O_3 resists the wear rate and reduces the detachment of material from the wear specimen. The FSPed composite surface has the lowest

ACCEPTED MANUSCRIPT

wear rate due to higher hardness of the material. Fig.16 (b) &(c) show the SEM micrographs of worn surfaces of TIG arc and FSPed composite wear specimens at 30N. At lower loads (30N) the wear mechanisms observed in both the composites are oxidization and plastic deformation. Iron rich material is observed at the pin surface which confirms the transfer of material from the disc to pin surface, due to the harder B_4C particles.The SEM image [Fig. 16(b)] shows visible micro cracks and oxide traces on the surface which confirms the oxidation and abrasive wear mechanisms. At 60N load oxidation and abrasive wear mechanisms are observed. The iron rich material from the hard steel disc is transferred to the composite surface helps to protect the breaking of B_4C particles. At 60N load, both the composite specimens have deeper grooves and cracks along the sliding direction. The wear damage is the lowest for the FSPed composites among the tested composites and base material.

In order to designing a material for anti-wear applications, the critical load is an important factor and the change in wear occurs rapidly at this critical load. The wear of the composite specimen changes from mild to severe wear at 120N load. During wear process, excessive heat generation between the sliding surfaces and large hydrostatic pressure exists on the wear specimen and deformation continues. Due to this cracks and surfaces damage occur and extensive pits are formed at the surface. Further sliding induces continues loading on the damaged surface which in turn results in deeper and wider surface cracks. This can form also subsurface damages.

Similar results are reported by Abdollahi et al. [46] for Al2024-5/B_4C nanocomposite produced by mechanical milling and hot extrusion. The delamination, abrasive and severe wear are observed at the surface of the composite wear specimen tested 120N as shown in Fig 17(b) & (c). The wear debris of the FSP composite specimen is in smaller and uniform size mixed with oxides protecting the detachment of the material from the composite surface (Fig. 18(b)). The wear debris size of TIG arc surface is smaller than the base material, however, larger than FSP specimen. In base material, the majority of wear debris are in larger lumps of metal, which confirms more wear loss of metal (Fig. 18(c)).The EDS profile of the FSP and TIG arc composite shows the presence of dominant peaks of Fe confirms the transfer of material from the disc as wear debris. The higher amount of iron confirms that the direct contact between counterpart disc and uniform dispersion of hard nano reinforcement particles in the matrix. High

ACCEPTED MANUSCRIPT

hardness of the composite specimen protects the softer matrix material removal from the surface. EDS profile of base material is having comparatively lower intensity peaks of Fe.

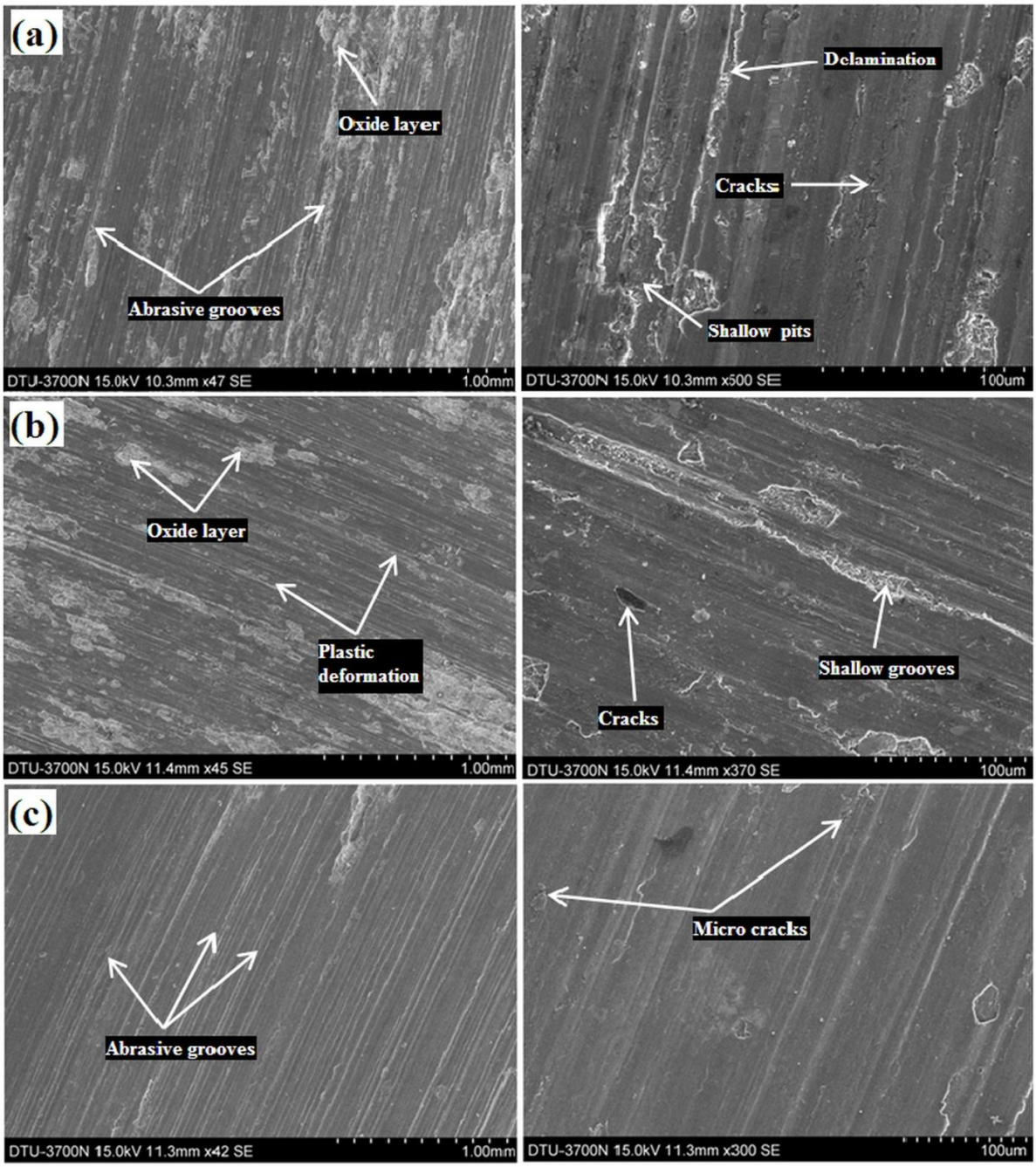

Fig. 16 SEM micrographs of worn surface of the sample tested with 30N and at a sliding speed of 1m/s of : (a) Base material (b) TIG arc composite and (c) FSPed composite ***(Right column micrographs are higher magnification micrographs of respective left column)***

ACCEPTED MANUSCRIPT

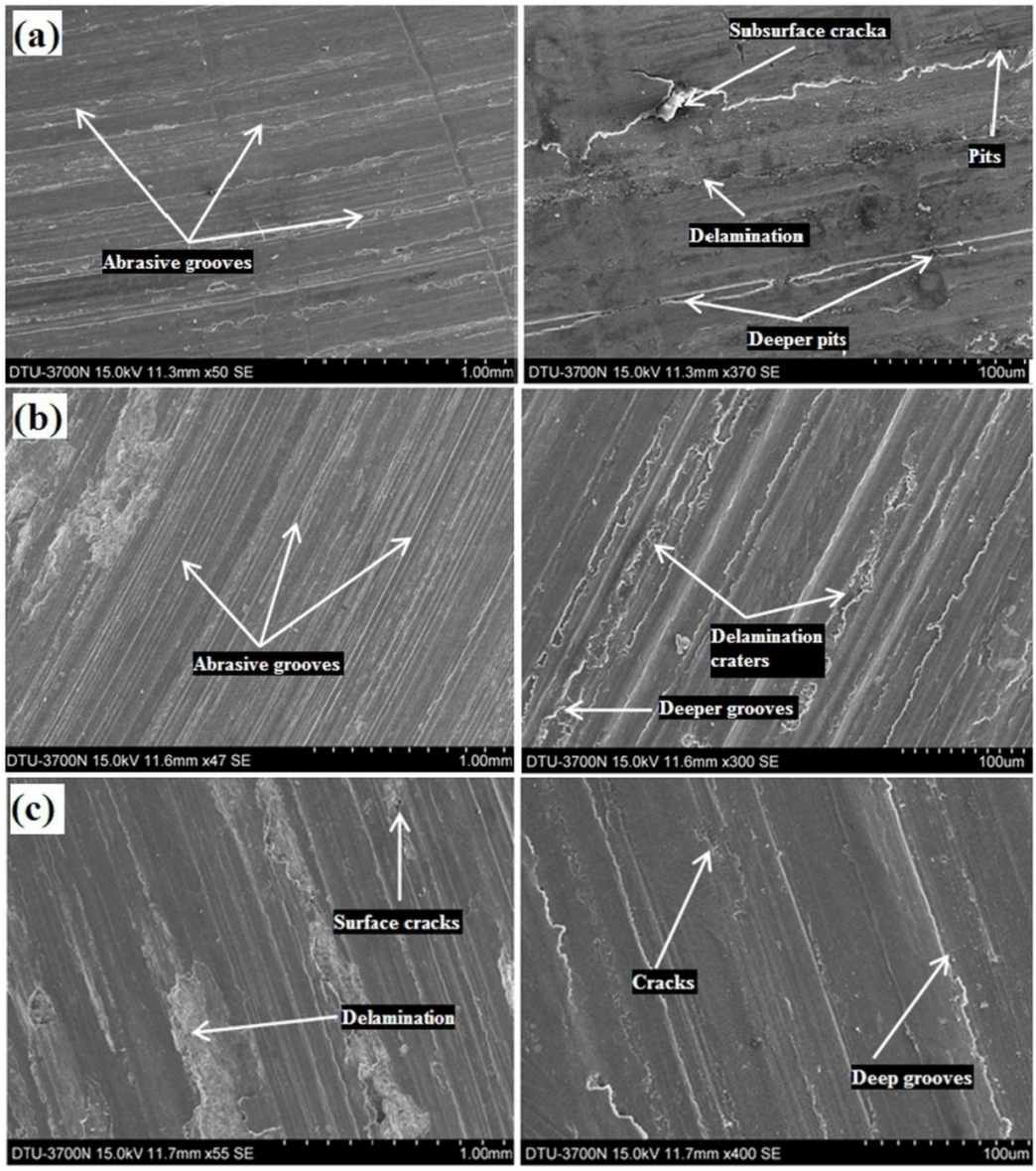

Fig. 17 SEM micrographs of worn surface of the sample tested with 120N and at a sliding speed of 1m/s of : (a) Base material (b) TIG arc composite and (c) FSPed composite ***(Right column micrographs are higher magnification micrographs of respective left column)***

ACCEPTED MANUSCRIPT

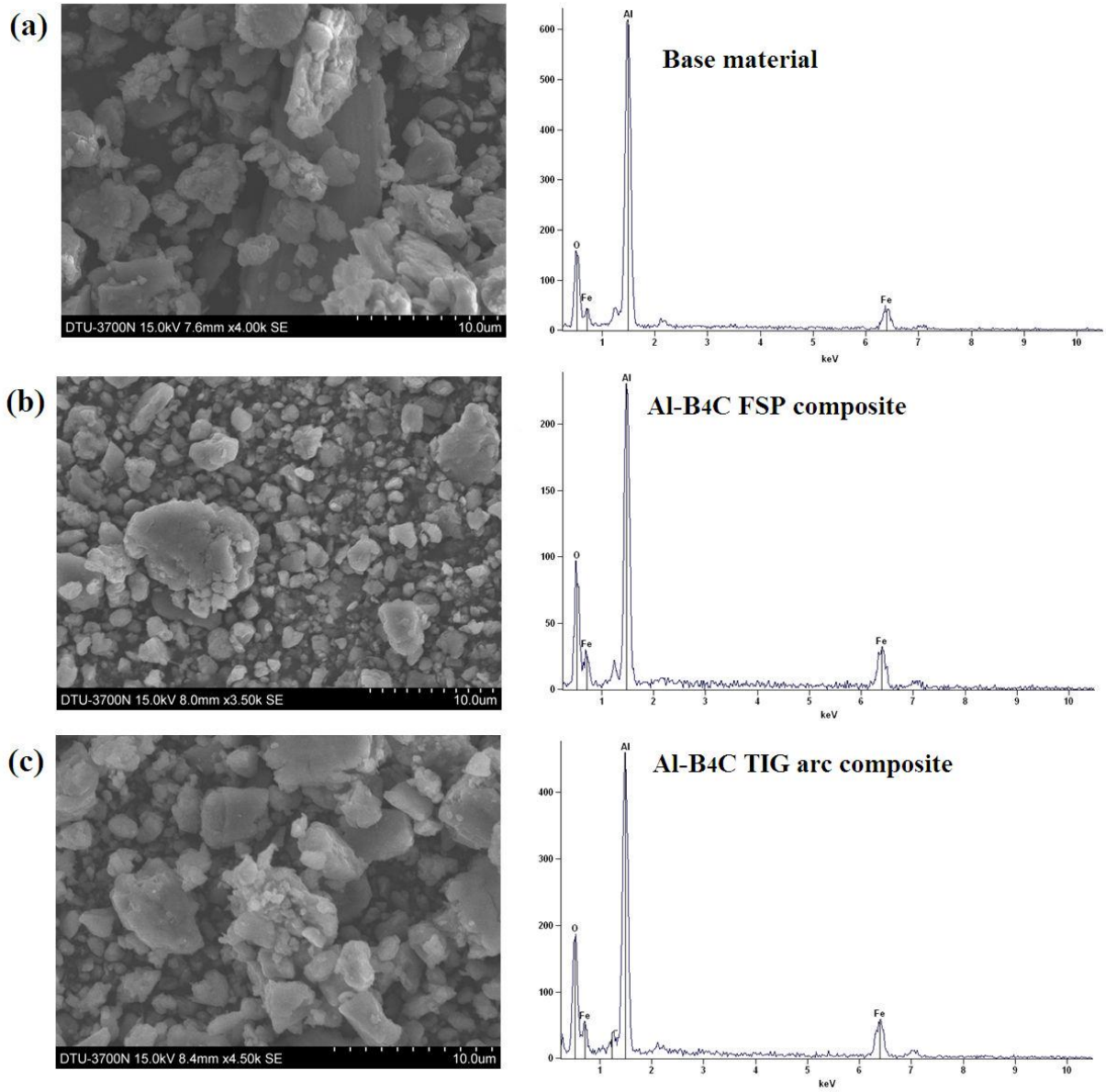

Fig. 18 Typical SEM micrographs showing the wear debris of 120N Normal load wear test specimens and EDS profile of (a) base material (b) Al-B_4C FSP composite and (c) Al-B_4C TIG arc composite

ACCEPTED MANUSCRIPT

3.4 Coefficient of friction

Fig. 19 shows the variation of the friction coefficient of the base material and composite samples under three normal sliding loads. At lower load (30N) a similar type of friction is observed on the TIG arc and FSPed composite samples. The friction coefficients of composite samples were lower than the base material in all sliding loads. The typical variations of the friction coefficient for the base material, TIG arc composite, and FSPed composite surface samples as a function of 120N load and at sliding distance of 3000m is displayed in Fig. 20. In the base material the friction coefficient is gradually increasing up to 100m and then slightly decreases and reaches to a steady value of (0.65) till 1500m sliding distance and again it marginally increases to 0.7 till the completion of sliding wear test. An irregular friction coefficient value with fluctuation is observed. In the case of TIG arc composite specimens, the friction coefficient is lesser till 200m and reaches to the steady state approximately in the range of 0.5 for the entire sliding distance, and some fluctuations are observed. FSPed composite specimen shows the smooth flow of friction coefficient for the entire sliding distance with a lower value in the range of 0.48. The formation of mechanically mixed layer which contains iron oxide protects the surface of the composite specimens at lower and middle range loads. The pull out iron particles from the hard surface and mixed with ceramic particles forms tribo layer, which acts as solid lubricant and insulation between the pin and disc for reducing the friction coefficient of the composite samples. The EDS profile of the composite confirms the higher content of iron on the surface when compared to the base material.

ACCEPTED MANUSCRIPT

ACCEPTED MANUSCRIPT

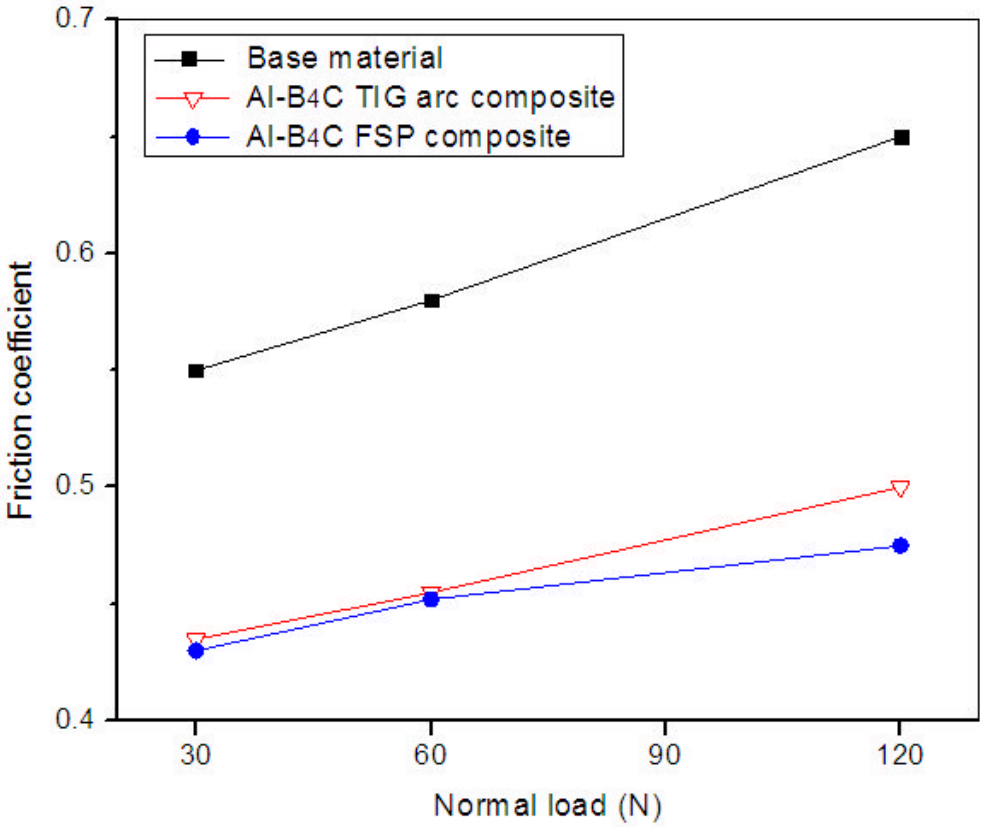

Fig. 19 Variation in the friction coefficient with normal load

ACCEPTED MANUSCRIPT

ACCEPTED MANUSCRIPT

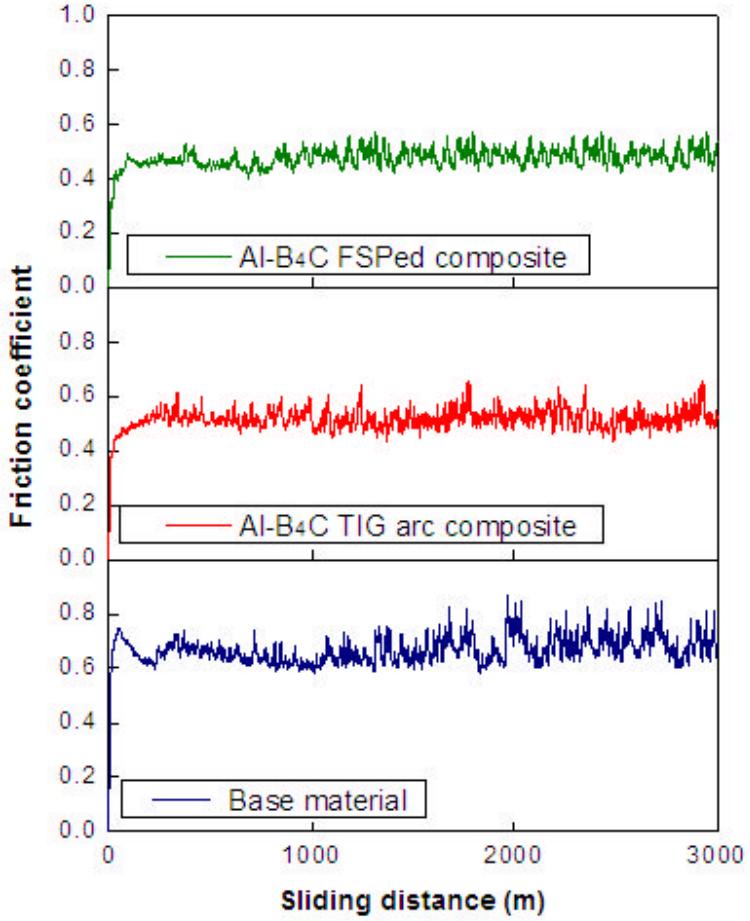

Fig. 20 Friction behavior of composite samples and base material: (samples were tested at normal load of 120N and at 1 m/s sliding velocity)

4 Conclusions

The Al-B_4C nano surface composites were successfully fabricated by using TIG arc and FSP methods. The hardness and wear related properties of the composites were evaluated.

- The metallographic evaluation revealed the uniform dispersion of nano B_4C particles in the fabricated composites.
- The composites produced by FSP method is having larger thickness (wider and deeper composite) when compared to TIG arc method. FSPed composites exhibited higher hardness and wear resistance than TIG arc surface composites.

ACCEPTED MANUSCRIPT

- The microhardness of TIG arc surface and FSPed surfaces are about 108±3 and 127±2Hv respectively, whereas base material has a hardness of 83±2Hv.
- Uniform dispersion of reinforcement particles and grain refinement are responsible for the enhancement of wear resistance of FSPed composite.
- The wear resistance of the friction stir processed surface composite (wear rate =3.8 x 10^{-5} mm^3/N-m @ 60N normal load) was superior to the composite fabricated through TIG arc surface (wear rate =4.05 x 10^{-5} mm^3/N-m @ 60N normal load) method.
- TIG arc surfacing is easier to achieve surface composites. FSPed method is better than TIG arc surface method to produce sound and larger thickness of composite surface.

References

[1] D.B. Miracle, Comp. Sci. Technol. 65 (2005) 2526.
[2] S. Das, Trans. Indian Inst. Met. 57 (2004) 325.
[3] S. V. Prasad, R. Asthana, Tribo. Let. 17 (2004) 445.
[4] C. Garcia-Cordovilla, J. Narciso, E. Louis, Wear. 192 (1996) 170.
[5] M. Rosso, J. Mater. Process. Technol. 175 (2006) 364.
[6] O. Verezub, Z. Kálazi, A. Sytcheva, L. Kuzsella, G. Buza, N.V. Verezube, A. Fedorov, G. Kaptay, J. Mater. Process. Technol. 211 (2011) 750.
[7] A.V. Muley, S. Aravindan, I.P. Singh, Manufacturing Review. 15 (2015) 1.
[8] S.H. Choo, S. Lee, S.J. Kwon, Metall. Mater. Trans. A 30A (1999) 3131.
[9] L. Dubourg, F. Hlawk, A. Cornet, Surf. Coat. Technol. 151-152 (2002) 329.
[10] K.C. Antony, J. Glenny, J.E. Northwood, Hardfacing, Welding, Brazing and Soldering, 9th ed., Vol 6, ASM International, USA, 1983.
[11] S. Islak, S. Buytoz, M. Karagoz, Ind. J. Eng. Mater. Sci. 19 (2012) 253.
[12] J. Gandra, P. Vigarinho, P. Pereira, R.M. Miranda, A. Velhinho, P. Vilaca, Mater. Des. 52 (2013) 373.
[13] S. Jiguo, D. Wei, T. Wenda, Z. Di, R. Jialie, Front. Mech. Eng. 2 (2007) 20.
[14] S. Mridha, H.S. Ong, L.S. Poh, P. Cheang, J Mater. Process. Technol. 113 (2001) 516.
[15] O.N. Celik, M. Ulutan, H. Gasan, U. Er, S. Buytoz, Surf. Coat. Technol. 206 (2011) 1423.
[16] R.S. Mishra, Z.Y. Ma, Mater. Sci. Eng. R 50 (2005) 1.
[17] M.K. Besharati Givi, P. Asadi, Advances in Friction-stir welding and processing, Woodhead Publishing, Cambridge, 2014.
[18] M. Narimani, B. Lotfi, Z. Sadeghian, J. Mater Process. Technol. 285 (2016) 1.
[19] V. Sharma, U. Prakash, B.V.M. Kumar, J. Mater. Process. Technol. 224 (2015) 117.
[20] H.S. Arora, H. Singh, B.K. Dhindaw, Int. J. Adv. Manuf. Technol. 61 (2012) 1043.
[21] M.S. Khorrami, M. Kazeminezhad, A.H. Kokabi, Mater. Des. 80 (2015) 41.
[22] S.A. Hosseini, K. Ranjbar, R. Dehmolaei, A.R. Amirani, J. Alloys comp. 625(2015) 725.
[23] M. Amra, K. Ranjbar, R. Dehmolaei, J. Mater. Eng. Perform. 24(2015) 3169.
[24] S. Soleymani, A.A. Zadeh, S.A. Alidokht, Wear 278-279 (2012) 41.

ACCEPTED MANUSCRIPT

[25] A.S. Zarghani A, S.F.K. Bozorg, A.Z. Zarei, Wear 270 (2011) 403.
[26] N. Yuvaraj, S. Aravindan, Vipin, J. Mater. Res. Technol. 4 (2015) 398.
[27] M. Khakbiz, F. Akhlaghi, J. Alloys comp. 479 (2009) 334.
[28] D. Jianxin, S. Junlong, Ceramics Inter. 35 (2009) 771.
[29] S. Shahraki, S. Khorasani, R.A. Behnagh, Y. Fotouhi, H. Bisadi, Metall. Mater. Trans. B 44 (2013) 1546.
[30] O. Frigaard, O. Grong, O.T. Midling, Metall. Mater. Trans. A, 32A (2001) 1189-1200.
[31] M.A. Moghaddas, S.F.K. Bozorg, Mater. Sci. Eng. A 559 (2013) 187.
[32] J. Jafari, M.K. Besharati Givi, M. Barmouz, Int. J. Adv. Manuf. Tech. 78 (2015) 199–209.
[33] R. Bauri, D. Yadav, C.N.S. Kumar, B. Balaji, Mater. Sci. Eng. A 620 (2015) 67.
[34] M.T. Agne, B. Anasori, M.W. Barsoum, J. Phase Equil. Diff. 36 (2015) 169.
[35] Z. Zhang, X.G. Chen, A. Charette, J. Mater. Sci, 44 (2009) 492.
[36] K.M. Shorowordi, T. Laoui, A.S.M.A. Haseeb, J.P. Celis, L. Froyen, J. Mater. Process. Technol. 142 (2003) 738.
[37] K.B. Lee, H.S. Sim, S.Y. Cho, H. Kwon, Metall. Mater. Trans. A 32A (2001) 2142.
[38] J.C. Viala, J. Bouix, G. Gonzalez. C. Esnouf, J. Mater. Sci. 32 (1997) 4559.
[39] H. Izadi, R. Sandstrom, A.P. Gerlich, Metall, Mater. Trans. A 45A (2014) 5635.
[40] Y. Zhao, X. Huang, Q. Li, J. Huang, K. Yan, Int. J. Adv. Manuf. Technol. 78 (2015) 1437.
[41] S. Sahraeinejad, H. Izadi, M. Haghshenas, A.P. Gerlich, Mater. Sci. Eng. A 626 (2015) 505.
[42] C.N.S. Kumar, R. Bauri, D. Yadav, Tribol. Int. 101(2016) 284.
[43] N. Kumar, G. Gautam, R.K. Gautam, A. Mohan, S. Mohan, Tribol. Int. 97 (2016) 313.
[44] N. Yuvaraj, S. Aravindan, Vipin, Trans. Ind. Inst. Met. (2016) DOI10.1007/s12666-016-0905-9.
[45] R.L. Deuis, C. Subramanian, J.M. Yellup, Comp. Sci. Technol. 57 (1997) 415.
[46] A. Abdollahi, A. Alizadeh, H.R. Baharvandi, Mater. Des. 55 (2014) 471.

ACCEPTED MANUSCRIPT

ACCEPTED MANUSCRIPT

Highlights of this paper

1. Surface modification through TIG arc and Friction Stir Processing (FSP) method.
2. Enhanced hardness and wear resistance of the surface composite layer.
3. Selected regions can be suitably modified to have improved wear resistance property.
4. Easier and faster process compared to conventional heat treatment methods.
5. Effect of various applied load (30N, 60N and 120N) on the base Al5083 alloy, Al-B_4C FSP composite Al-B_4C TIG arc composite were evaluated during wear test.
6. The Al-B_4C FSP composite wear specimen found to be having higher hardness and wear resistance when compared to TIG arc method.

ACCEPTED MANUSCRIPT

2016 Intl. Conference on Advances in Computing, Communications and Informatics (ICACCI), Sept. 21-24, 2016, Jaipur, India

Conditional Adherence based Classification of Transactions for Database Intrusion Detection and Prevention

Indu Singh
Department of Computer Science and Engineering
Delhi Technological University
Delhi, India
indu.singh.dtu14@gmail.com

Vaibhav Darbari, Lakshya Kejriwal, Aditya Agarwal
Computer Science and Engineering
Delhi Technological University
Delhi, India
vaibhavdarbari@gmail.com, lakshya5340@gmail.com,
adiagarwal0396@gmail.com

Abstract*— In recent times, database security has become a major concern of organizations and protection against privilege abuse has gained pivotal importance. We present a novel approach for classification of database transactions based on association rules and cluster analysis (CDTARCA) which detects and prevents malicious transactions from modifying any sensitive information in a database. Association rules are obtained by mining user data access patterns and role profiles are generated by clustering the user activity parameters from database logs. The extent of adherence to the mined rules along with membership of the current user profile in the aforementioned role profile clusters are used to classify the transaction as either malicious or non-malicious. The classification procedure uses adherence as the metric since the real world transactions are never fully compliant to the existing user behavior patterns. Our experimental evaluation on the typical data-set of a bank shows that our CDTARCA algorithm works effectively in detecting and preventing malicious transactions in database systems.

Keywords*— Database Intrusion Detection; Association Rule Mining; Fuzzy Clustering ; Naïve Bayes Classifier;

I. INTRODUCTION

With the increased usage of networked systems and tremendous growth of the Internet, systems are becoming more vulnerable to malicious attacks not only from external agents but also from internal sources such as employees abusing their privileges. Data security breaches arise due to improper data modification, unauthorized data observation and data unavailability. So data protection must meet three key requirements: confidentiality, integrity and availability.[1] Unauthorized access of database launched by one or more insiders [2] can result in significant losses for organizations and individuals, therefore for protection of user information, intrusion detection has become vital part of information security.

An Intrusion Detection System (IDS) is a popular mechanism for dealing with most of the imminent threats. The basic ideology behind it is to check for deviations in the usage of the data resources on the host system [3]. The traditional signature based database IDSs work well for known attacks but are susceptible to novel attacks. They also require updating signatures on a regular basis which is not a trivial task. Thus new attacks are detected by deploying anomaly based IDSs. Also, to handle masqueraded intruders, these anomaly based IDSs employ access control by obtaining user access patterns using data mining techniques. Hu et al. [4] provided a sequential pattern mining technique and identified a new transaction as malicious if it is non-compliant to the mined data dependencies. The method faced limitation in the cases of malicious read operations and the sensitivity of the attributes was also not taken into account.

Our focus in this paper remains on detection and prevention of all types of malicious database transactions. Most of the authentication systems are designed to cater to external attacks but, in this paper, we present a novel approach of classification of database transactions based on association rules and cluster analysis (CDTARCA) to detect and prevent insider abuse of privileges as well. In our approach data dependency rules are obtained by mining user data access patterns and role profiles are obtained by clustering the user activity parameters from database logs. The new transactions are checked before execution with a detection algorithm, and alarm is generated if the transaction is classified as malicious thus preventing them from modifying any sensitive database information. The main advantage of CDTARCA lies in its lower sensitivity to changing user access patterns and its adeptness at detecting abuse of user privileges.

The rest of the paper is organized as follows. Section II describes past efforts related to database security and IDS. In Section III, we explain our proposed algorithm and architecture. Section IV presents the experimental results of our approach. Section V offers conclusions of the paper.

II. RELATED WORK

Several research works have been proposed that apply data mining for network intrusion detection. But there exist relatively few research works that focus on database IDSs. Malicious behaviors on such host systems can be detected at either query level, transactional level or user function level. Some also have detection procedures for SQL injection attacks.

One of the early works in this field is a database misuse detection system. Chung et al. [5] presented a misuse detection

978-1-5090-2029-4/16/$31.00 @2016 IEEE

system for relational database systems called DEMIDS. It used audit log data to derive profiles describing user access patterns. Distance metrics were then used for identifying data items referenced together and for describing the working extent of users. The drawback of such an approach is that when the number of users for a database system becomes quite large, maintaining profiles becomes difficult. Moreover, it assumed domain knowledge about a given database schema.

The proposed method of Srivastava et al. [6] modified the sequential mining algorithm and made it sensitive sequential mining by introducing weights for each attribute based on the sensitivity level. The main disadvantage of this approach was the non-optimal procedure for selection of the weights for the sensitive attributes. Kamra et al. [7] built user profiles by mining database traces that were stored in log files. It used a Naive Bayes clustering method on the RBAC enabled training log file. The RBAC enabled system helped to detect insider attacks by identifying users who have a different behavior from the role assigned to that user. But this method was sensitive to the change of user behavior and database transactions.

Hashemi et al. [8] concentrated on two aspects of database transactions: (1) dependencies among data items in every transaction of the database with a similarity measure introduced to reduce the false positive rate of detection and (2) the change of each individual data item represented as time series data. The anomaly analysis of this data lead to detection of malicious transactions. Hu et al. [9] improved the approach by Hu et al. [4] by clustering transactions to facilitate the mining of data dependencies and write sequences at the inter-transactional level. This technique took care of a malicious group of transactions which individually appear normal.

Doroudian et al. [10] demonstrated a hybrid approach for detecting intrusion at both transaction and inter-transaction level. At transaction level it used a specification based method where the expected transactions of the system were specified and at inter transaction level anomaly based detection was used where sequential rule mining was used to find the relations among identified transactions. Rao et al. [11] enhanced the intrusion detection rate by providing flexibility in profile matching constraint and allowing subset of attribute access pattern in new transaction as a valid user profile. These reduced both false positive and false negative errors.

Frequent association rule mining based IDSs in the past have had the limitation that the sequences with frequency lower than the minimum support threshold were ignored. Thus sequences which were infrequent but of great interest never contributed to any rule. This limitation of the data dependency miner lead to fall in the True Positive Rate. Also, the minimum support, minimum confidence and other parameters were experimentally set and for a certain value of a parameter many important associations were overlooked. Sohrabi et al. [12] introduced a new algorithm ODADRM and overcame these limitations by not using support measure and extracting rules for the lower frequency item-sets too. The rules were generated by using leverage as the rule value measure. This reduced the uninteresting data dependencies, increased the True Positive Rate and decreased the False Positive Rate.

III. Proposed Approach

We propose an intrusion detection system CDTARCA that uses rule mining and clustering in the initial training phase and then classification. The advantage of our methodology is in its lower sensitivity to change in user patterns and its ability to tackle novel attacks.

The algorithm extracts the existing transactions from transaction logs. These are then pre-processed into a form that prevents generation of undesirable rules. In the first part of learning phase, sequential patterns and then data dependencies are generated from the pre-processed transaction logs using PrefixSpan [13] algorithm. Classification rules above certain confidence values are generated pertaining to the mined data dependencies. In the second part of learning phase, role profiles (clusters) are generated from defined parameters after analysis of database logs. It is assumed that only legitimate transaction logs and database logs are provided in this phase.

In the detection phase, the new SQL transaction is parsed and matched against stored rules. The extent of adherence to the mined rules along with membership of the current user profile in the aforementioned role profile clusters are used to classify the transaction as either malicious or non-malicious. We consider adherence as the classification metric because there may be some deviation from the stored rules in a real world scenario.

A. System Architecture

The proposed IDS works as an independent unit and enhances the security of the system without hampering the functioning of the database management system (DBMS). The system is designed to identify and abort malicious transactions submitted to the DBMS by the attacker who has managed to bypass the preliminary security of the database system. The scenario may arise due to a compromised legitimate account, web portal susceptible to SQL injection, abuse of user privileges. In all these cases the attacker can get access to the database by submitting transactions manually or through an application.

The architecture of the proposed system consists of two modules, the *Learning Phase module* along with the *Detection and Classification module*. The proposed architecture is shown in the figure 1.

B. Learning Phase Module

In this phase, transaction logs are utilized for the extraction of data dependencies by the rule generator which are then stored for the adherence computation in later phases. Parallel to adherence estimation database logs are used for analyzing the user access patterns which are then clustered into role profiles. These role profile clusters and generated rules are then passed onto detection phase.

***Transaction Pre-Processor*:** Transaction pre-processor module specifies identified transactions in a desirable form. Each transaction can be represented as a set of queries (Select, Insert, Delete or Update). Each query can then be represented as a sequence of operations (Read or Write) on item-sets. Individual items in an item-set are lexicographically sorted to avoid multiple representations for the same query.

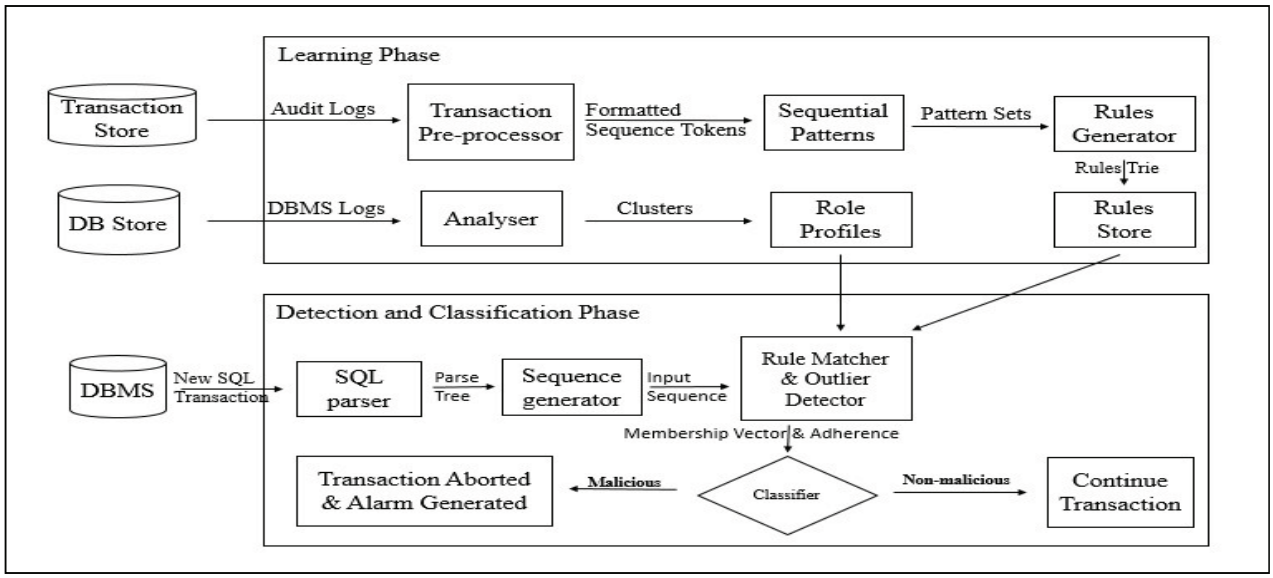

Figure 1. Architecture of Proposed IDS

- Each transaction starts with begin transaction and ends with commit/rollback.
- We denote a transaction T as $< q_1, q_2, q_0, \dots, q_n >$ where $q_i \in Q(s)$. $Q(s)$ is the set of queries.
- We denote a query q_i as $< op_1(D_1), op_2(D_2), op_3(D_3), \dots, op_n(D_n) >$. Where $op_i \in [R, W]$ and D_i represents an item-set $< d_1, d_2, \dots, d_k >$ lexicographically sorted.
- The transaction is represented as queries in a sequential order. For each such query, sub query (if any) is represented first. Clauses like while, order by etc. are evaluated before the SQL statement type (Select, Update, Insert or Delete).

For example consider the following transaction:-

acc_no=select acc_no from customer where cust_name='abc' and cust_id=12345;

update account set balance =balance+1000 where acc_no=accno;

The output after preprocessing is of the form

T_{id} { $R < cust_id, cust_name >, R < acc_no >,$

$R < acc_no >, W < balance >$ }.

Here T_{id} is the unique transaction id.

***Sequential Patterns*:** A sequence is an ordered list of operations. Sequential patterns are those elements which occur simultaneously, in the same order multiple times in the data. The data dependencies are symbolized as read sequences and write sequences.

- **Definition 1:** A **read sequence** $RdSq(a)$ for a particular element a is defined as $< R(a_1), R(a_2), \dots, R(a_i), O(a) >$ where $a_1, a_2, \dots, a_i$ represent all the elements that need to be read before any operation $O \in [R, W]$ can be performed on a.
- **Definition 2:** A **write sequence** $WrSq(a)$ for a particular element a is defined as $< O(a), W(a_1), W(a_2), \dots, W(a_i) >$ where $a_1, a_2, \dots, a_i$ represent all the elements that need to be updated after any operation $O \in [R, W]$ on a before the completion of transaction.
- **Definition 3: Sensitive elements** are defined as those elements which are either updated in the transaction or belong to restricted access groups. Sensitivity of an element is determined by its weight in the transaction. An element can be classified as either highly sensitive (HS), sensitive(S), low priority (LP). Weights of HS, S and LP are in the ratio 4:2:1 for our system.
- **Definition 4: Confidence** for a given sequence (read or write) is given as the ratio of weighted count of occurrence of the sequence for a given sensitive element a_i to the weighted count of occurrences of the sensitive element a_i. We give a formal definition of confidence for a read sequence below. Confidence for a write sequence follows similarly.

$$Confidence\big(RdSq(a_i)\big) = \frac{Count\big(RdSq(a_i)\big)}{Count(a_i)} \quad (1)$$

We made use of PrefixSpan algorithm for mining sequential patterns from transaction logs. PrefixSpan was chosen because of its superior performance and less overhead in comparison to other algorithms like GSP [14] and AprioriAll [15]. Read and write sequences are generated from sequential patterns obtained from PrefixSpan in which the minimum support value is taken as 0.25.

***Rules Generator*:** Data dependency rules are generated from the obtained read and write sequences. All sequential patterns in the read sequence set are transformed into rules of the form $R(a_1), R(a_2), \dots, R(a_i) \rightarrow O(a)$. If such a rule has

confidence greater than the minimum required value, it is included in the read rule set $RR\{\}$. The rule defines all elements $a_1, a_2, \dots, a_i$ that should be read before any operation is performed on a. Similarly, all sequential patterns in the write sequence are represented as $O(a) \rightarrow W(a_1), W(a_2), \dots, W(a_i)$. All such rules with sufficient confidence are included in the write rule set $WR\{\}$ and define that elements $a_1, a_2, \dots, a_i$ be updated after operation on a. We now describe the rule mining phase for the CDTARCA algorithm.

Algorithm 1: Data Dependency Miner

Input: σ = minimum support, min_conf = minimum confidence

Output : Rd_TRIE =read rule TRIE, Wr_TRIE =write rule TRIE

Initialization
1 $RdSqSet \leftarrow \emptyset$
2 $WrSqSet \leftarrow \emptyset$
3 $Rd_TRIE \leftarrow \emptyset$
4 $Wr_TRIE \leftarrow \emptyset$
5 S_p = mined sequential patterns with support 'σ'

Extract Read and Write Sequences
6 **for** each sequential pattern S in S_p **do**
7 **if** there exists a sensitive element in S **then**
8 **for** each sensitive element a in S **do**
9 **if** $RdSq(a) \notin RdSqSet$ and $RdSq(a) \neq \emptyset$ **then**
10 add $RdSq(a) \rightarrow RdSqSet$
11 **end if**
12 **if** $WrSq(a) \notin WrSqSet$ and $WrSq(a) \neq \emptyset$ **then**
13 add $RdSq(a) \rightarrow RdSqSet$
14 **end if**
15 **end for**
16 **end if**
17 **end for**

Generate Dependency rules
18 **for** each $RdSq(a)$ in $RdSqSet$ **do**
19 **if** $confidence(RdSq(a)) > min_conf$ **then**
20 add $RdSq(a) \rightarrow Rd_TRIE$ with key $O(a)$
21 **end if**
22 **end for**
23 **for** each $WrSq(a)$ in $WrSqSet$ **do**
24 **if** $confidence(WrSq(a)) > min_conf$ **then**
25 add $WrSq(a) \rightarrow Wr_TRIE$ with key $O(a)$
26 **end if**
27 **end for**

Steps 1 to 4 initialize the read/write sets and the read/write rule hashed TRIE. Hashed TRIEs were chosen to store and retrieve generated rules as they are more efficient and have lower time complexity than other data structures for storage of strings with common prefix. In step 5, using PrefixSpan algorithm, we mine sequential patterns containing operations on data elements and having support greater than minimum threshold (σ). In steps 6 through 17 we extract read and write sequences for every sensitive element found in the mined sequential patterns. For every such unique read/write sequence found, we add it to the read/write sequence set. In steps 18 to 27, read/write sequences with confidence above a certain threshold (min_conf) are selected for a given sensitive element a and stored in read/write TRIEs as data dependency rules (with $O(a)$ as key). These are then used in the detection phase.

***Analyzer*:** In order to make the system less vulnerable to change in user patterns and prevent privilege abuse, role profiles are generated. The analyzer module uses the existing user activity parameters from database logs to generate the role profiles. For this, vectors are defined for each transaction in the database logs and the defined vectors are clustered using the method defined below.

Fuzzy c-means clustering [16] is used to create clusters such that every vector belongs to every cluster to a certain degree μ in the range (0, 1). The objective function that is minimized to create clusters is defined as:

$$\sum_{i=1}^{N} \sum_{j=1}^{C} \mu_{ij}^{m} \left\| V_i - c_j \right\|^2 \quad (2)$$

Where m is any real number such that $1 \leq m < \infty$, μ_{ij} is the numerical value that tells the degree to which V_i belongs to the cluster j, V_i is the i^{th} measured data, c_j is the center of the cluster, $|| * ||$ is an expression measuring the similarity between the vector and the cluster center.

The resulting k clusters are labelled to give the role profiles, RP. After clustering the vectors using the above method, the role profiles generated are then used by the detection and classification module. For the analyzer module of our system $k = 6$.

C. Detection and Classification Module

In this phase, raw user queries entered by the active user are parsed and the sequence of operations so generated is compared against rules obtained from the learning phase. Also the current user profile is compared with RP and its membership to each RP is grouped into a vector. The adherence value and membership values vector are then passed onto the classification phase. If the query is found malicious then the transaction is rolled back and an alarm is generated otherwise the transaction is continued.

***SQL parser*:** This module takes raw user queries as input. There are syntax differences between Database SQL dialects. The query is analyzed for tokens on the basis of these differences and a source token list is generated. If no error is found, a query parse tree is generated. The top level node for this parse tree is the type of SQL statements like: Select, Update, Delete etc. These nodes lead to sub trees with its children pointing to tables whose children in turn point to attributes. The query parse tree is built in a recursive manner, with sub query processed before primary query.

Sequence Generator: The parse tree generated in the previous phase is the input for this module. The parse tree is analyzed for the sequence in which different attributes are accessed, just as in transaction pre-processor. This list of attributes and operations is stored as input sequence list. For each subsequent query in the transaction the input sequence list is expanded.

***Rule Matcher*:** The input sequence list generated at run time is compared with data dependency rules generated for every

sensitive element present in the list. Accordingly, adherence to each rule is computed.

- **Definition 5: Adherence** to a particular rule for a given sensitive element is defined as the extent to which the input sequence list complies with the rule. For Read rules, it is defined as the extent to which the rule matches with the read operations before the given sensitive element, in the input sequence list. For Write Rules, it is defined as the extent to which the rule matches with the write operations after the given sensitive element, in the input sequence list. The metrics considered for computing adherence are Jaccard Index and Overlap Coefficient. Jaccard index has been chosen because of its dependence on union set of the two inputs. This ensures that if the attacker attempts to satisfy the dependency rules by randomly including operations, then the value of adherence decreases. Overlap Coefficient was chosen as it gives a more precise of estimate of the extent to which the sequence matches read/write rule.

Let, Input Sequence list be $S_I\{\}$, Output sequence list be $S_O\{\}$, read rule and write rule for a sensitive element be $RR\{\}$ and $WR\{\}$. Then Jaccard Index J is given as

$$J(S_I, R_d) = \frac{|S_I \cap R_d|}{|S_I \cup R_d|} \quad (3)$$

$$J(S_O, W_r) = \frac{|S_O \cap W_r|}{|S_O \cup W_r|} \quad (4)$$

Overlap Coefficient is given as

$$O(S_I, R_d) = \frac{|S_I \cap R_d|}{|R_d|} \quad (5)$$

$$O(S_O, W_r) = \frac{|S_O \cap W_r|}{|W_r|} \quad (6)$$

And read and write adherences, R_{Adh} and W_{Adh} are given as

$$R_{Adh} = Adh(S_I, R_d) = \frac{K_j J(S_I, R_d) + K_o O(S_I, R_d)}{K_j + K_o} \quad (7)$$

$$W_{Adh} = Adh(S_O, W_r) = \frac{K_j J(S_O, W_r) + K_o O(S_O, W_r)}{K_j + K_o} \quad (8)$$

Where K_j and K_o are weights assigned to the respective metrics.

Outlier Detector: The fuzzy clusters of role profiles generated in the analyzer module are such that each vector belongs to all the clusters and the membership to each cluster is given by μ_{ij}, where i represents the vector V_i and j represents the cluster c_j.

$$\mu_{ij} = \frac{1}{\sum_{k=1}^{c} \left(\frac{\|V_i - c_j\|}{\|V_i - c_k\|} \right)^{\frac{2}{m-1}}} \quad (9)$$

The vector defined for the input transaction is used to calculate the membership value for each RP and is grouped in a separate vector V_k which is illustrated in Table 1. The vector V_k, is updated for each query executed in the transaction.

User Id	RP_1	RP_2	RP_3	RP_4	RP_5
UID1	0.6	0.3	0.02	0.06	0.01
UID2	0.05	0.9	0.01	0.01	0.03
UID3	0.1	0.03	0.03	0.7	0.14

Table 1. Membership value of role profiles for users

We now formally define the detection phase algorithm.

Algorithm 2: Detection Phase Algorithm

Input: Rd_TRIE, Wr_TRIE , V_k=membership vector

Output: R_{Adh}= Read Adherence, W_{Adh}= Write Adherence

Initialization
1 Transaction T = new SQL Transaction
2 $Rd_Queue \leftarrow \emptyset$
3 $S_I \leftarrow \emptyset$
4 $Wr_Stack \leftarrow \emptyset$
5 $S_O \leftarrow \emptyset$

During Transaction
6 **for** each query Q in T **do**
7 **if** ($Q \rightarrow cmd_type \neq commit$) **then**
8 parse tree = $SQL \rightarrow parse(Q)$
9 Seq = SeqGen(parse tree)
10 **for** each read operation $R(Di)$ in Seq **do**
11 $Rd_Queue \rightarrow push_back(R(Di))$
12 **end for**
13 **for** each write operation $W(Di)$ in Seq **do**
14 $Wr_Stack \rightarrow push(W(Di))$
15 **end for**
16 **for** each sensitive element a in Seq **do**
17 S_I += $Rd_Queue \rightarrow pop()$ till a
18 $RR = Rd_TRIE \rightarrow get(O(a))$
19 $R_{Adh} = Adh\ (S_I, RR)$
20 $V_k = update(V_k)$
21 C = Classify(V_k, R_{Adh})
22 **if** (C = malicious) **then**
23 cmd → rollback
24 **else**
25 continue
26 **end if**
27 **end for**
28 **else if** ($Q \rightarrow cmd_type == commit$) **then**
29 **while** Wr_Stack is not empty **do**
30 $a = Wr_stack.pop()$
31 S_O += a
32 **if** a is a sensitive element **then**
33 $WR = Wr_TRIE \rightarrow get(O(a))$
34 $W_{Adh} = Adh(S_O, WR)$
35 $V_k = update(V_k)$
36 C = Classify(V_k, W_{Adh})
37 **if** (C = malicious) **then**
38 cmd → rollback
39 **else**
40 commit
41 **end if**
42 **end if**
43 **end while**
44 **end if**
45 **end for**

In steps 1 to 5 we initialize read queue, input sequence, write stack and output sequence. Next, in step 7, we check whether the input query statement is a commit statement. If it is not, then a parse tree is generated in step 8. In step 9, sequence generator represents the parse tree in the form of a sequence of operations on data elements. In steps 10 to 15, for each read operation the data element being read is inserted into the read queue. Similarly for every write operation data element is pushed into the write stack. A queue is used for read operations as the read rules are evaluated for read operations occurring before the required sensitive data element while a stack is used for write rules as these rules are evaluated on every write operation occurring after the given sensitive data element. In steps 16 to 19, for each sensitive data element found in sequence of operations the input sequence is augmented with read operations occurring before the data element. The read rule if any is fetched from the read TRIE and adherence to the rule is computed. In steps 20 to 27, adherence and profile membership vector are sent to the classifier to determine if the transaction is malicious or not. If not malicious then the next statement in transaction is executed otherwise the transaction is rolled back and terminated. Similarly in steps 28 to 44, if the command type is commit then the adherence to write rules is computed and these along with the updated profile membership vector are passed to the classifier. If transaction is found malicious it is rolled back otherwise it is committed.

***Naïve Bayes Classifier*:** The Naïve Bayes classifier is a probabilistic classifier based on the Bayes model. It operates under strong (Naïve) independence assumptions. This implies that the presence (absence) of one attribute of a class has no effect on the probability of occurrence of any other. Bayes Theorem is expressed as:

$$P(H|X) = P(X|H) * P(H)/P(X) \qquad (10)$$

Where X represents the data record, H is the hypothesis being tested. For classification we have to determine $P(H|X)$, which gives the probability that hypothesis H holds given the data record X. $P(H)$ is the probability that hypothesis H holds independently i.e. the prior probability. $P(X|H)$ is the probability of occurrence of X conditioned on H.

In the Naïve Bayes classifier, the training dataset is used to estimate $P(X|H)$ and $P(H)$. $P(H|X)$ is determined by applying Bayes rule on the estimated values for the given data record. The error in Naïve Bayes Classifier is primarily a result of three factors: variance, training data noise and bias. Training data noise can be reduced by selection of proper dataset. Bias and variance are a result of improper grouping of dataset and can be corrected accordingly.

UID	T_Id	Role Profile	# of records with Adh<='x'	# of records in the cluster	$P(X\|Ci)$
UID1	T_1	RP1	2519	2738	0.92
		RP2	1742	2176	0.797
		RP3	2290	3418	0.67
		RP4	4413	5449	0.81
		RP5	1191	1567	0.76

Table 2. Snapshot of Naïve Bayes Learning Table for Adherence 'x'=0.84

Table 2 gives an illustration of the learning phase computation of $P(X|Ci)$ for a transaction T_1 by user UID1. The adherence to the current rule for the given transaction by UID1 is 0.84. From table 1 and table 2, we see $max(P(Ci|X))$ occurs when user profile of the current user belongs to RP1 and is equal to 0.636.

The formal definition of the classification algorithm follows next.

Algorithm 3: Classification Algorithm

Input: $V_k, R_{Adh}, W_{Adh}, RP$

Output : C_{NB} = Class (Malicious or non-malicious)

Initialization
1 D = Dataset having n inputs
2 C = set of Role Profile Clusters (RP)
3 X = record with adherence not greater than 'x'
4 H = hypothesis (that X is classified into C)

Learning Phase
5 **for** i ← 1 to number of Clusters **do**
6 C_i → count = number of Di where D_i → Cluster_label = i
7 **for** each discretized adherence value x_i in X **do**
8 x_j → count = number of records with x_j in C_i
9 $P(X|Ci) = xj \rightarrow count / Ci \rightarrow count$
10 **end for**
11 **end for**

Classification Phase
12 **for** i ← 1 to number of Clusters **do**
13 $P(Ci|X) = P(X|Ci) * P(Ci)/P(X)$
14 **end for**
15 C_{NB} = max($P(Ci|X)$)
16 **if** ($C_{NB} < \delta$) **then**
17 C_{NB} → malicious = true
18 **else**
19 C_{NB} → malicious = false
20 **return** C_{NB}

In steps 1 to 4, we initialize the training dataset and role profile clusters. In steps 5 to 11 we calculate the probability of different adherence values for the given rule for each cluster. In steps 12 to 15 we calculate the posterior probability of a record belonging to a cluster given its adherence. Here $P(Ci)$ is given by membership value of the record to that cluster. $P(X)$ is the probability that adherence is not greater than 'x'. $P(X|Ci)$ is obtained from the learning phase for that particular adherence value. The maximum of these values is then used for classifying the record as malicious or non-malicious in steps 16 to 20. Here $'\delta'$ is defined as the control factor. If C_{NB} is less than control factor then the transaction is classified as malicious else it is classified as normal transaction.

IV. Results And Experiments

In order to analyze the performance of the proposed method, several experiments were performed on a typical bank database. To evaluate our system three different types of logs were considered. The first log consisted of malicious transactions generated by random modification of a few attributes in a normal transaction, assuming that the attacker has no

information about the structure of the database. We define such intrusions as external attacks. The second log consisted of transactions specifically designed to fulfil the data dependencies to some (variable) extent thus simulating abuse of user privileges. The third log consisted of normal user transactions. In total 20,000 transactions were generated from the three logs defined above in which the proportion of transactions between the logs was varied from $10:10:80$ to $20:20:80$ respectively.

The performance evaluation of the system was carried out in terms of recall, false positive rate (FPR) and precision. Recall refers to the ratio of attacks caught by the system (TP) to total number of attacks on the system (TP+FN). Similarly, false positive rate refers to ratio of number of normal transactions classified as malicious (FP) to total number of normal transactions (FP+TN). Precision gives the measure of true alarms (TP) to total alarms generated by the system (TP+FP). The database logs comprising malicious transactions were utilized for evaluating the true positives (TP) and false negatives (TN). The log containing normal user transactions was utilized for evaluating the false positives (FP) and true negatives (TN).

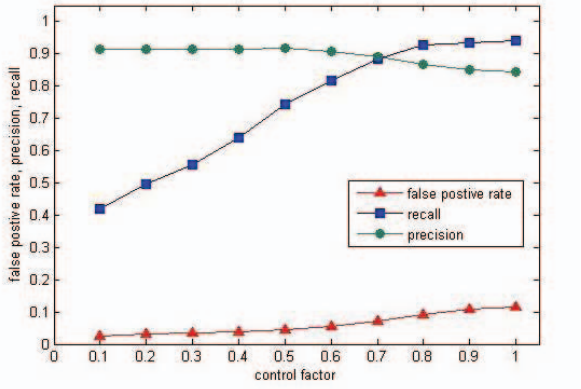

Figure 2. Relation between precision, recall and false positive rate with control factor

Figure 2 depicts the precision, recall and false positive rate of the proposed CDTARCA algorithm for different control factor values. It is observed that the recall increases as the control factor is increased and the false positive rate also increases as the control factor is incremented. As the control factor is varied from 0.2 to 0.8, the recall increases from 0.5 to 0.92 and the false positives increases from 0.05 to 0.11. It can be observed that the recall has a higher value than false positive rate for all values of control factor. Hence, the proposed system raises true alarms more than the false alarms in all cases. Therefore, the system has high accuracy and effectiveness in detecting malicious transactions. A slight dip in precision from 0.91 to 0.86 is also observed as control factor is gradually increased from 0.2 to 1.This could be attributed to the fact that as the control factor approaches 1, the system becomes less tolerant to deviation in user access patterns. After considering the tradeoff between precision and recall, it is seen that the optimum value for control factor lies between 0.7 and 0.8.

Another criterion used for evaluation of the system in terms of real time performance was latency. It is taken as the additional delay in execution of the transaction due to the incorporation of CDTARCA intrusion prevention layer to the DBMS. Two configurations were considered in the evaluation of the latency: 1) Baseline (DBMS without CDTARCA); 2) Proposed System (DBMS with CDTARCA). Figure 3 gives a comparison for the two configurations with increasing number of transactions. It is observed that the average latency in milliseconds (ms) is 49.5 when the number of transactions is increased from 0 to 400. For 400-800 transactions, the average latency is observed to be 67.6 ms and on increasing the number beyond 800, the latency becomes almost constant, averaging to 88.3 ms.

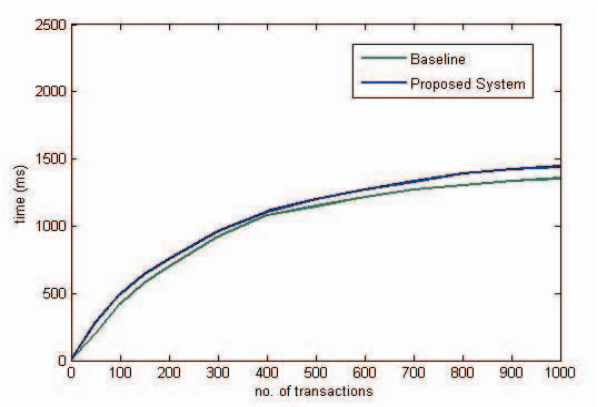

Figure 3. Latency of the proposed system

Technique	Reference	Elements analysed			Intrusion Preventi-on Capabilit y	Performa-nce
		Command Syntax	Accessed Columns	Proce -ssed Rows		
Integrated Dependency with Sequence Alignment Analysis	Hu et al. [4], 2004	X	X	X	Partial	Recall= 0.90
	Srivastava et al. [6], 2006	X	X	X	Partial	Precision =0.80
	Sohrabi et al. [11], 2014	X	X	X	Partial	Recall= 0.65, Precision= 0.77
Inter-transaction Dependency Analysis	Doroudian et al., 2014	X	X	X	Partial	Recall= 0.77, Precision= 0.78
CDTARCA	-	X	X	X	Yes	Recall= 0.92 Precision= 0.89,

Figure 4. Performance comparison of the proposed system

Figure 4 gives a comparison between different techniques on the basis of algorithm used, the intrusion prevention capability and the performance metrics (precision and recall). For each

technique considered, the performance was evaluated for different support values and maximum values for precision and recall were taken. The performance values prove that our algorithm outperforms alternative methods. These improvements can be ascribed to low sensitivity of our algorithm to change in user patterns due to our consideration of relative adherence to data dependencies. This is reflected from the real world transactions where the transactions are never fully compliant with the data dependencies. We are able to minimize both false positive and false negative errors as our algorithm combines the merits of both statistical based detection and anomaly based detection methods.

V. CONCLUSION

In this paper, a new innovative data mining based approach CDTARCA has been proposed for detecting and preventing intrusive transactions in database systems. The proposed system focuses on extracting data dependency rules from existing transactions and generating role profiles by clustering user activity parameters from database logs. The extent of adherence to the mined rules along with membership of the current user profile in the role profile clusters are used to classify the transaction as either malicious or non-malicious. The experimental results on synthetic dataset illustrates that our proposed system works effectively in detecting malicious transactions in database systems.

REFERENCES

[1] E. Bertino and R. Sandhu, "Database Security Concepts, Approaches, and Challenges," IEEE Transactions on Dependable and Secure Computing, Vol. 2, No. 1, pp. 2-19, 2005

[2] Khanh Viet, Brajendra Panda and Yi Hu Korea, “Detecting Collaborative Insider Attacks in Information Systems”, IEEE International Conference on Systems, Man, and Cybernetics COEX, Seoul, 2012

[3] D.E. Denning, “An Intrusion-Detection model,” IEEE Transactions on Software Engineering, Vol. SE-13, pp. 222-232, Feb. 1987

[4] Y. Hu and B. Panda, "A data mining approach for database intrusion detection," in Proceedings of the ACM Symposium on Applied Computing, pp. 711-716, 2004

[5] Christina Yip Chung, Michael Gertz and Karl Levitt, “DEMIDS: a misuse detection system for database systems”, Integrity and internal control information systems: strategic views on the need for control, Kluwer Academic Publishers, Norwell, MA, 2000

[6] Abhinav Srivastava, Shamik Sural, A. K. Majumdar, “Weighted intra-transactional rule mining for database intrusion detection”, Proceedings of the 10th Pacific-Asia conference on Advances in Knowledge Discovery and Data Mining, Singapore, 2006

[7] E. Bertino, A. Kamra, E. Terzi and A. Vakali, "Intrusion detection in RBAC administered databases, " in Proceedings of the Applied Computer Security Applications Conference (ACSAC), 2005

[8] S. Hashemi, Y. Yang, D. Zabihzadeh, M. Kangavari, Detecting intrusion transactions in databases using data item dependencies and anomaly analysis. Expert Systems, 25(5), 460–473, 2008

[9] Y. Hu, B. Panda “Mining inter-transaction data dependencies for database intrusion detection”. In Proceedings of innovations and advances in computer sciences and engineering. Springer 2010.

[10] M. Doroudian and H.R. Shahriari, “A hybrid approach for database intrusion detection at transaction and inter-transaction levels”, 6th Conference on Information and Knowledge Technology (IKT), pp. 1-6, 2014

[11] U. Rao, N. Singh, A. Amin, K. Sahu, “Enhancing detection rate in database intrusion detection system”, Science and information conference (SAI), pp. 556–563, 2014

[12] Mina Sohrabi, M.M.Javidi, S.Hashemi “Detecting intrusion transactions in database systems: a novel approach” J Intell Inf Syst 42:619-644 DOI 10.1007 Springer 2014.

[13] J. Pei, J. Han, B. Mortazavi-Asl, H. Pinto, Q. Chen, U. Dayal, M-C. Hsu, PrefixSpan: Mining sequential patterns efficiently by prefix-projected pattern growth. In Proc. 2001 Int. Conf. Data Engineering (ICDE'01), Heidelberg, Germany, pp. 215–224, 2001

[14]Ramakrishnan Srikant , Rakesh Agrawal, Mining Sequential Patterns: Generalizations and Performance Improvements, Proceedings of the 5th International Conference on Extending Database Technology: Advances in Database Technology, pp. 3-17, March 25-29, 1996

[15]Rakesh Agrawal, Ramakrishnan Srikant, Mining Sequential Patterns, Proceedings of the Eleventh International Conference on Data Engineering, pp 3-14, March 06-10, 1995

[16]J.C. Bezdek, R. Ehrlich, and W. Full, "FCM: The fuzzy c-means clustering algorithm", Comput. Geosci., vol. 10, no. 2&ndash,3, pp. 191-203, 1984

Covariate conscious approach for Gait recognition based upon Zernike moment invariants

Himanshu Aggarwal, *Student Member, IEEE* & Dinesh K. Vishwakarma, *Member, IEEE*

***Abstract*— Gait recognition i.e. identification of an individual from his/her walking pattern is an emerging field. While existing gait recognition techniques perform satisfactorily in normal walking conditions, there performance tend to suffer drastically with variations in clothing and carrying conditions. In this work, we propose a novel covariate cognizant framework to deal with the presence of such covariates. We describe gait motion by forming a single 2D spatio-temporal template from video sequence, called Average Energy Silhouette image (AESI). Zernike moment invariants (ZMIs) are then computed to screen the parts of AESI infected with covariates. Following this, features are extracted from Spatial Distribution of Oriented Gradients (SDOGs) and novel Mean of Directional Pixels (MDPs) methods. The obtained features are fused together to form the final well-endowed feature set. Experimental evaluation of the proposed framework on three publicly available datasets i.e. CASIA dataset B, OU-ISIR Treadmill dataset B and USF Human-ID challenge dataset with recently published gait recognition approaches, prove its superior performance.**

***Index Terms*— Human gait recognition, Gait biometrics, Average energy silhouette image, Zernike moment invariants, Spatial distribution of oriented gradients, Mean of directional pixels.**

I. Introduction

BIOMETRIC have become a common sight these days. While fingerprint scanner, iris scanner, palm scanner etc. are being extensively used in offices, banks, legal organizations; yet there are some biometric methods whose usage in daily lives has still been much constricted.

Individual recognition on the basis of gait is one such domain. The domain exploits the notion that every individual has its own idiosyncratic way of walking. Also, gait data collection being non-intrusive, contact-free and taking into account its easy availability, owing to the widespread usage of surveillance cameras, make gait biometrics a very promising field. However the efficiency of gait recognition algorithms do suffer from presence of some external factors such as covariates like clothing, footwear, bags, etc. This makes gait biometrics a challenging task but nevertheless useful.

Gait recognition approaches can be classified into broadly two categories: Model based approach and Model-free (Appearance based) approach. Model based approach [1] [2] [3] [4] [5] employ modelling of human body structure and local movement patterns of different body parts. The parameters of the models, like knee position, pelvis to knee distance, hip position etc. are mostly learnt by processing the gait sequence. Model based approach is generally view and scale invariant. However, the performance of this approach is highly dependent on the quality of extracted human silhouettes, low quality of which can lead to inaccurate and incorrect parameter estimation resulting in plummeting of the performance. On the other hand, Model free approach [6] [7] [8] [9] [10]is not explicitly based on structural information. This approach works on temporal and shape information. Compared to model-based approach, model-free approach is computationally less expensive and use of temporal information results in much better recognition performance. Furthermore, model-free approach is more robust to noise and has thus become the preferred approach in research.

One of the primary challenge for vision based gait recognition techniques is to disentangle the identity-unrelated factors which yet alter gait appearances drastically. Though existing works [6] [7] [10] [11] [12] [13], give satisfactory performance in normal walking conditions taken under controlled environment, these methods are sensitive to silhouette distortion which occur due to the presence of covariates. A representative gallery set is required for such metrics to perform effectively. In real-world scenarios such an assumption does not hold true. Since the conditions in which a query gait sequence is collected is mostly unknown, a gallery set encapsulating entire population cannot be obtained.

To address these problems, a unified covariate cognizant approach to gait recognition has been proposed in this paper. The method works on spatio-temporal image representation of gait named AESI [14]. AESI is a compact representation of gait which preserves the necessary shape and temporal information of the gait sequence. Furthermore, the presented framework employ two stages. The first stage involves detection of anomalies due to presence of covariates. Zernike invariant moments [15] are used for this purpose. The moments are computed for the AESI and then the distance

Himanshu Aggarwal is working as an Associate Software Engineer in the Division of Computer Vision at Qualcomm Incorporated, Hyderabad, India (e-mail:hiaggarw@qti.qualcomm.com, himanshub43@gmail.com)
D.K. Vishwakarma is working as an Assistant Professor in the Department of Electronics and Communication Engineering, Delhi Technological University, Delhi, India-11042 (e-mail: dinesh@dtu.ac.in, dvishwakarma@gmail.com).

between the moments is used as a comparison metric. Thereafter, second stage involve feature extraction from parts of AESI devoid of any anomalies as decided by the comparison in the first stage. For this, Spatial distribution of gradients (SDOG) [14] is employed. SDOG calculates local orientation of gradients over the silhouette image (AESI) and its sub-pyramids creating feature set that encapsulates both local and global information about the image. In addition to SDOG, MDPs are computed and integrated in the feature set. MDPs show distribution of the MDPs in x direction, the direction in which walking motion is most prominent [16]. MDPs are computed only in regions of high temporality, typically the limb and neck area, and preserve structural information in these regions. As a result the final formed feature set has extensive distinguishing capability, in addition to being low dimensional, resulting in optimal recognition performance. Moreover, the classical approach employed in existing works [6] [7] [17] is to use Principal component analysis(PCA) and Multiple Discriminant Analysis(MDA) approach for feature set dimension reduction obtained from direct matching on various kinds of spatio temporal representations of gait. Our method intrinsically generate a reliable and compact feature set, thus making the use of these approaches superfluous.

Experimental results on three popular gait datasets demonstrate the efficacy of our approach. Our method achieved an overall recognition accuracy of 72.7% on OU-ISIR Treadmill B dataset [18], this is better than recent GII-SF approach [19] by 11.5%. For CASIA B dataset [20], the improvement is even more, where our method achieved overall accuracy of 91.47% which is nearly 19% better than the GII-SF. We also achieved accuracy of 72.53% on the USF Human-ID challenge dataset [21] which slightly outperforms the very recent clothing and carrying condition invariant rotation forest approach [22]. The key contributions of this work are as follows:

- The study of a novel consolidated approach to gait recognition that is capable of detecting covariates and minimize their repercussions by employing AESI, ZMIs, SDOGs and MDPs.
- Employment of AESIs that effectively represents temporal and shape information by fusing gait silhouette images using reference point alignment and forming a single image template .
- Introduction of a novel method for determination of presence of covariates by segmenting AESI into multiple parts and using ZMIs as a comparison metric.
- Use of SDOGs method for defining gait characteristics, that is based on local gradient orientation for feature extraction from gait template and provides low dimensional feature set that encompass both local and global viable information.
- A novel MDPs method that extracts structural information from high temporal regions by studying variation of MDPs in horizontal direction, the direction in which gait motion is most prominent.

The remainder of the paper is organized as follows: A brief survey of the existing popular gait recognition techniques is done in Section 2. Section 3 discusses the pipeline of the proposed approach and details the various modules of the pipeline. A detailed analysis of the performance of the proposed technique is performed in Section 4, alongside comparisons with existing similar state-of-the-art methods. Section 6 concludes the paper.

II. RELATED WORK

In recent years, several techniques have been devised for the recognition of individuals through their gait. As already discussed two approaches to gait recognition exist -Model based approach and Appearance based approach. In model based approach human body structure is modelled through various geometrical shapes. Johansson *[1]* introduced Moving light display i.e., MLD, a unique technique for gait recognition. MLD involved fastening of bright markers to human clothing in order to capture gait motion of subject. Ben Abdelkader et al. *[2]* argued that gait stride and cadence can be used for identification of individuals. The method estimated stride length using a calibrated camera and then used Bayesian classifier for identification. Johnson and Bobick *[3]* inspected a method to recognize people using static body parameters like height of individual, distance between head and pelvis, distance between pelvis and left foot, and distance between right and left foot. Liu and Sarkar *[23]* proposed averaging of silhouette frames for determination of gait characteristics of an individual. The method then used Euclidean distance between averaged silhouettes for classification. Lee et al *[24]* proposed Shape Variated-based frieze pattern (SVB-frieze pattern) representation for gait. SVB-frieze pattern was formed by projecting difference frames onto 1 dimension, the projected values of difference frames were then summed over a gait cycle to obtain the frieze pattern. Nixon et al *[4] [25]* presented automatic gait recognition involving estimation of rotation pattern of hips and modelling of leg movement using a pendulum model. K-nearest neighbor classifier was then used for classification.

Model free approaches involve period based methods. These methods provide compact representation of gait by extracting features from a single image obtained from one gait cycle. Chai et al. *[26]* introduced Perceptual Shape Descriptor (PSD) that encompassed shape information of walking silhouettes. The formed PSDs were then accumulated over time to form Perceptual curve, which was used for gait recognition. Tan et al. *[27]* formed frieze pattern by projecting normalized silhouettes along four directions- vertical, horizontal and two diagonals. The resultant feature set was dimensionally reduced using PCA. A Mahalanobis distance based nearest neighbour method was then used for classification. Han and Bhanu introduced concept of Gait energy image (GEI) *[6]*, which involved averaging of binary silhouette images over a gait cycle to form single image. GEI still remains one of the most popular technique for gait recognition and numerous works use GEI as underpinning. Tao et al. *[11]* used Gabor functions over GEI for image understanding and employed a General Tensor Discriminant

Analysis for recognition. A matrix based Marginal Fisher analysis (MFA) was presented by Xu et al. *[10]* ,that produced a compact feature set, to address problem of gait recognition. Gait flow image(GFI) which represented motion information in a gait cycle by optical flow. Recently, Parul et al. proposed Gait Information image (GII) *[19]*, a technique based on

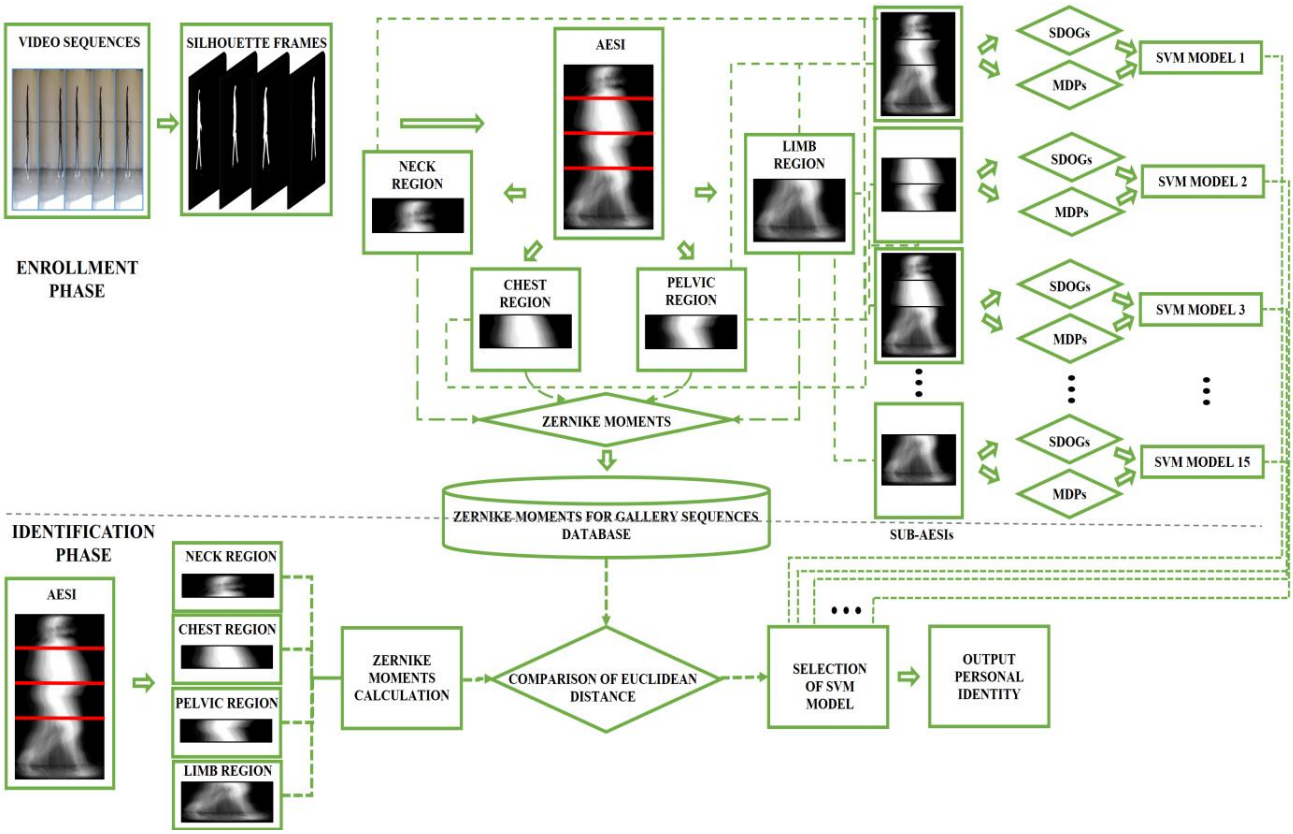

Fig.1. Work flow diagram of the proposed framework

Liu et al. *[28]*modelled human gaits using population Hidden Markov Model (pHMM) and calculated distance between sums of normalized gait stances to identify individual identity. Wang et al. *[7]* introduced a novel template named Chrono-Gait Image (CGI). CGI encodes variation in averaged images into multiple channels thereby effectively preserving the temporal information of gait motion. One of the principal challenge in gait recognition is dealing with intra-class variations spawning from clothing variations and carrying conditions. Several techniques have been studied to reduce adverse effects of these variations. Bashir et al. *[9]* proposed Gait Entropy image (GEnI). GEnI calculates entropy for each pixel in GEI and then segments high temporal regions from regions of low temporality. The regions of high temporality are argued to be devoid of covariate conditions and thus are more relevant to gait recognition. Bashir et al. *[8]* used optical flow fields to capture motion intensity and motion direction. Dupuis et al. *[29]* selected relevant features from GEI by using Random Forest feature rank algorithm. Jeevan et al. *[30]* presented novel temporal template named Gait Pal and Pal Entropy (GPPE) Image. Kusakunniran *[31]*, *[32]* proposed Space Time interest points (STIPs) descriptor to extract gait features directly from raw video. Rokanujjaman et al. *[33]* introduced a novel discrete fourier transform based entropy representation of gait named EnDFT. Lam et al. *[17]* proposed information set theory which involve features derived from Hanman-Anirban entropy function. GII have two features-energy feature (GII-EF) and sigmoid feature (GII-SF). Guan et al. *[34]* proposed a classifier ensemble method based on the random subspace method (RSM) and majority voting (MV). Very recently, Choudhury and Tjahjadi *[35]* introduced averaged gait key-phase image (AGKI) which use rotation forest ensemble learning technique to distinguish individuals and recognize intra-class diversity, leading to good results even in presence of covariates.

III. Proposed Covariate Conscious Framework

The covariate conscious gait recognition approach can be understood in two phases: Enrollment phase and Identification phase as outlined in Fig. 1.

In Enrollment phase, AESI is formed for each of the gallery gait sequence. The formed AESI is segmented into 4 parts according to human body geometry namely neck region, chest region, pelvic region and limb region. Each region is termed as part-AESI. Zernike moments are then calculated for each of the part-AESI and added in '*Zernike moments for gallery sequences*' database. In parallel, sub-AESIs are formed by arranging part-AESIs into all possible combinations resulting in a total of $2^4 - 1 = 15$ sub-AESIs. Features are then

extracted from each of the sub-AESI using SDOGs and MDPs methods. Finally, a linear SVM classifier is trained on the obtained feature set.

In Identification phase, AESI is formed from the probe gait sequence. Similar to enrollment phase, part-AESIs are constructed and Zernike moments are computed for each of the part-AESI. The presence of covariates is then decided by comparison of the computed moments of a part-AESI with the moments stored in '*Zernike moments for gallery sequences*' database for the corresponding part. As decided by the comparison, parts devoid of any covariates are used to form a sub-AESI which is later classified using the corresponding SVM classifier trained during the enrollment phase.

A. *Construction of AESI*

AESI [14] preserves shape and temporal information that is representative of gait motion in a convenient 2D template. AESI use binary silhouettes as basis and its formation is a two-step process. The first step involves extraction of human silhouettes from image frames and calculation of gait period. The second step involves summation and normalization of the obtained silhouettes.

The extraction of binary silhouettes is performed using background subtraction technique. Background subtraction is a challenging task owing to the highly dynamic nature of the background, at the same time, quality of the extracted silhouettes is critical for the performance of the whole gait recognition algorithm. This makes effective modelling of background imperative. This work employs textual feature based background subtraction approach proposed by Chua et al. [36] for foreground segmentation. The approach reckons entropy as an important texture information parameter, which is defined as:

$$\mathcal{E} = \sum_i \sum_j \mathcal{F}(i,j) \log \mathcal{F}(i,j) \quad (1)$$

where $\mathcal{F}(i,j) = \frac{\mathcal{M}(i,j)}{\sum_{i,j} \mathcal{M}(i,j)}$, is the probability density function and, i and j are indices to co-occurrence matrix $\mathcal{M}$. Once the binary images are formed, the silhouettes are obtained by scanning the image row-wise and column-wise. The extreme white pixels are then determined to get the desired bounding box.

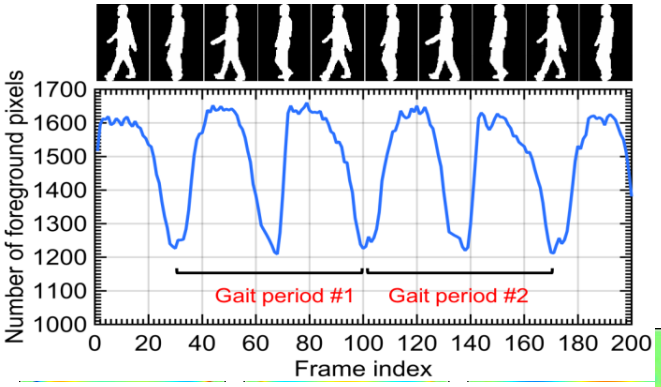

Fig.2. Determination of gait period from variation of foreground pixels

One key step in formation of AESI for gait sequence is determination of gait period. Gait period is defined as the number of frames over which two consecutive walking cycles span. One walking cycle is completed when a person moves from mid-stance position (position where legs are closest) to double-support position (legs are farthest apart) and then back to mid-stance position. The gait period can be computed simply by counting the number of foreground pixels in the lower half [21]. At the mid-stance position the number of foreground pixels attains a local minima, while at double-support position the number attains a local maxima. Therefore, the analysis as shown in Fig. 2 of these local minima and maxima can give the estimate of the gait period.

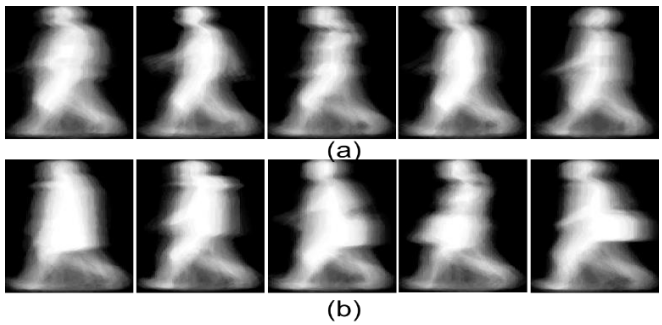

Fig.3. Formed AESIs (a) Normal Walking (b) Clothing and carrying

Once the gait period is determined, the binary silhouettes over that period are aligned using reference point and then fused into a single template on incremental basis [37]. One of the key strengths of AESI is the degree of compression it offers, an entire gait sequence, typically 40-70 silhouettes, is compressed into a single template. AESI fails to maintain the chronology thus loosing on some of the temporal information, however, it has adequate shape information thus making it apposite for the task of gait recognition. AESI is defined as:

$$AESI(x,y) = 1/n \sum_{\tau=1}^{n} |\mathfrak{S}(x,y)_\tau|^2 \quad (2)$$

where 'n' is the number of silhouettes in a gait period and '$\mathfrak{S}(x,y)_\tau$' is the binary silhouette at time instant 'τ'. The salient characteristic of AESI is that the degree of temporality in a region is manifested as intensity variation in AESI. Examples of generated AESIs for normal walking and covariate conditions is shown in Fig. 3.

B. *Covariate detection using ZMIs*

The presence of covariates can significantly alter the shape of human silhouettes. While even though this is one of the prime reason for drop in performance of gait recognition systems, this information could actually be leveraged in order to filter out the regions of the silhouettes affected by such distortion. In this paper, we use Zernike moment based shape

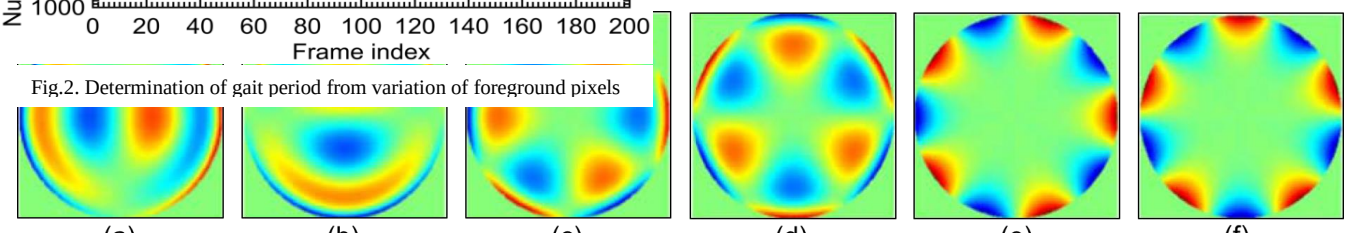

Fig.4. Plot of Zernike Basis function $\mathcal{V}_{nm}(\rho,\theta)$ for order $n = 5$ (a) Re($\mathcal{V}_{5,1}$) (b) Im($\mathcal{V}_{5,1}$) (c) Re($\mathcal{V}_{5,3}$) (d) Im($\mathcal{V}_{5,3}$) (e) Re($\mathcal{V}_{5,5}$) (f) Im($\mathcal{V}_{5,5}$)

descriptors for the purpose. The incentive to using Zernike moments is that they are invariant to position, size and orientation. Teh et al. [38] demonstrated the efficacy of Zernike moments as shape descriptors among other many moment-based descriptors. Zernike polynomials are a set of complex polynomials forming an orthogonal basis, which are defined in the interior of unit circle $x^2 + y^2 \leq 1$. Zernike basis function $\mathcal{V}_{nm}(\rho,\theta)$ of order n and repetition m is defined in polar coordinates as:

$$\mathcal{V}_{nm}(x,y) = \mathcal{V}_{nm}(\rho,\theta) = \mathcal{R}_{nm}(\rho)e^{jm\theta} \quad \text{for } \rho \leq 1 \qquad (3)$$

where '$\mathcal{R}_{nm}(\rho)$' is a radial polynomial defined as:

$$\mathcal{R}_{nm}(\rho) = \sum_{s=0}^{\frac{n-|m|}{2}} (-1)^s \frac{(n-s)!}{s!\left(\frac{n+|m|}{2}-s\right)!\left(\frac{n-|m|}{2}-s\right)!}\, \rho^{n-2s} \qquad (4)$$

Here, n is a non-negative number and m is integer satisfying conditions: $n-|m|$ is even and $|m| \leq n$. The set of basis functions $\{\mathcal{V}_{nm}(\rho,\theta)\}$ is orthogonal, i.e.

$$\int_0^{2\pi}\int_0^1 \mathcal{V}^*{}_{nm}(\rho,\theta)\, \mathcal{V}_{pq}(\rho,\theta)\rho d\rho d\theta = \frac{\pi}{n+1}\delta_{np}\delta_{mq} \qquad (5)$$

where $\delta_{xy} = \begin{cases} 1, & x = y \\ 0, & otherwise \end{cases}$.

The 2-dimensional Zernike moments for continuous image function $\psi(\rho,\theta)$ are defined as:

$$Z_{nm} = \frac{n+1}{\pi}\int_0^{2\pi}\int_0^1 \psi(\rho,\theta)\mathcal{V}^*{}_{nm}(\rho,\theta)\, \rho d\rho d\theta \qquad (6)$$

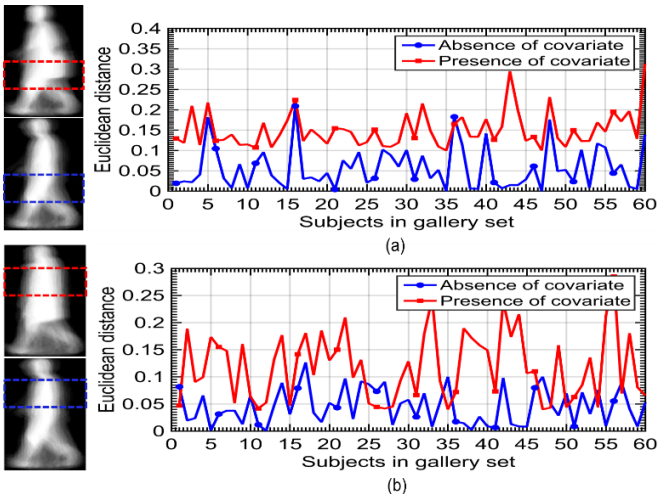

Fig.5. Variation of Euclidean distance between Zernike moments in presence and absence of covariates for two instances (a) and (b). From figure it can be seen that the mean of Euclidean distance does serve as a reliable metric to detect the presence of covariates

$$= \frac{n+1}{\pi}\int_0^{2\pi} e^{-jm\theta}\int_0^1 \psi(\rho,\theta)\mathcal{R}_{nm}(\rho)\, \rho d\rho d\theta$$

The 2-dimensional Zernike moments for discrete digital image function $\psi(x,y)$ are defined as:

$$Z_{nm} = \frac{n+1}{\pi}\sum_x\sum_y \psi(x,y)\, \mathcal{V}^*{}_{nm}(x,y), x^2+y^2 \leq 1 \qquad (7)$$

As stated before, the AESIs of both the gallery and probe gait sequences are partitioned into 4 segments called part-AESIs. This is done in order to restrict the extent of discarded region of AESI to a minimum, and thereby preserving viable information as much as possible. Since the AESIs are size normalized, the same segmentation scheme is followed for all the images. An AESI of height H is segmented based on human body anatomy [39] and scheme is given in Table I.

TABLE I
AESI SEGMENTATION

Body Part	Height
Neck region	1H - 0.80H
Chest region	0.80H - 0.55H
Pelvic region	0.55H - 0.30H
Limb region	0.30H - 0H

Once the partition is done, Zernike moment invariants are calculated for each part-AESI formed for the gallery sequences, and are stored in '*Zernike moments for gallery sequences*' database. To detect the presence of covariate in incoming part-AESI P_i (i = 1,2…4) of probe gait sequence, we compute mean Euclidean distance D_{Pi} between its Zernike moments and the moments stored in '*Zernike moments for gallery sequences*' database for the corresponding part. In our empirical testing we found Zernike moments of order $n = 5$ and repetition $m = 1, 3 \text{ and } 5$ to be efficient for the comparison. Fig. 4 shows plots of real and imaginary part of these moments. D_{Pi} is defined as:

$$D_{Pi} = \frac{1}{N}\sum_{k=1}^{N}\sqrt{\sum_{n=5}^{m=1,3,5}|Z_{nm}^{Gki} - Z_{nm}^{Pi}|^2} \qquad (8)$$

where N is the total number of gallery sequences and G_{Ki} is i^{th} part –AESI of K^{th} gallery sequence.

A part-AESI is declared to infected with covariate if:

$$D_{Pi} \geq \mu_i + 3\sigma_i \qquad (9)$$

where:

$$\mu_i = \frac{1}{N^2}\sum_{j=1}^{N}\sum_{\substack{k=1\\k\neq j}}^{N}\sqrt{\sum_{n=5}^{m=1,3,5}\left|Z_{nm}^{Gji} - Z_{nm}^{Gki}\right|^2} \qquad (10)$$

$$\sigma_i = \frac{1}{N}\sum_{j=1}^{N}\left(\sum_{\substack{k=1\\k\neq j}}^{N}\sqrt{\sum_{n=5}^{m=1,3,5}\left|Z_{nm}^{Gji} - Z_{nm}^{Gki}\right|^2} - \mu_i\right) \qquad (11)$$

It should be noted that computation of μ_i and σ_i is an offline process, and needs to be executed only once, when the database is constructed. This work considers the prevalent scenario where gallery is formed of normal walking sequences and probe sequences involve presence of covariates. However, the same proposed algorithm can be used in the hypothetical opposite scenario as well, since covariate detection works only on relative distance between probe and gallery sequences.

Fig. 5 demonstrates variation of Euclidean distance for infected and non-infected part-AESIs for two instances. It can be discerned from the figure that the mean Euclidean distance does serve as a suitable metric for the detection of covariates.

The added advantage of using ZNIs on AESI rather than on binary silhouettes themselves is AESI's immunity to noise. Since, AESI is formed by fusing multiple silhouettes; the effect of noise in any one silhouette becomes negligible and hence does not perniciously influence the performance of Zernike shape descriptors.

C. Computation of SDOGs shape features

SDOG [14] extracts textural information from images by binning the intensity of image gradients according to their orientation in the image. These characteristics are computed at various decomposition levels (sub-regions) of the AESI, and hence encapsulate both coarse and fine details. The SDOGs computation for K orientation bins at decomposition level v results in a feature vector of length $K\sum_v 4^v$. In this work, we apportion gradient orientations into 9 bins each spanning 20

degrees and a total of 3 decomposition levels ($\upsilon = 0, 1, 2$) are employed. The process to compute SDOG is delineated in Algorithm1 and Fig. 6.

The reason why SDOG particularly complements AESI as a feature extraction method is its fixation to image gradients. Since, AESI manifests both temporal and shape information of gait sequence as intensity variation, it's the AESI's gradients which possess the needed information for optimal recognition performance.

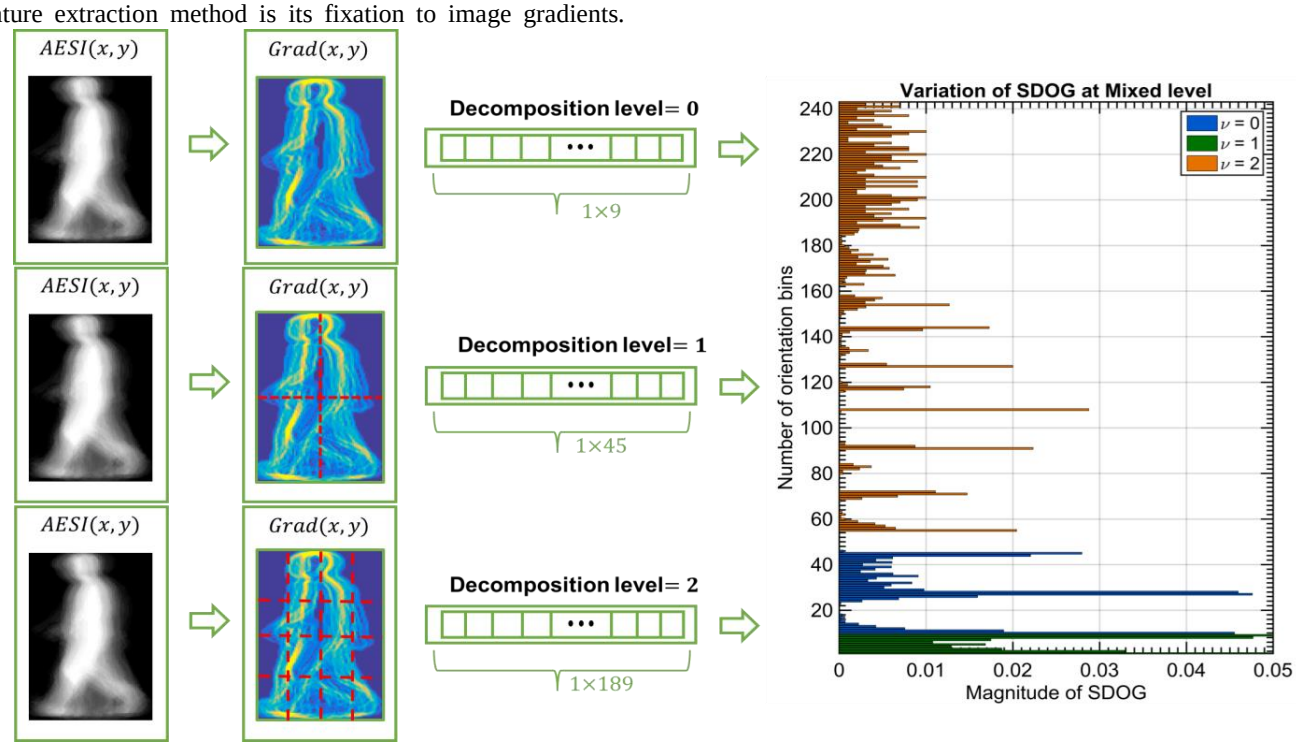

Fig. 6. Representation of decomposition levels and their spatial distribution, involved in calculation of final SDOG feature vector

Algorithm 1: Computation of SDOGs

Input. $AESI(\mathrm{x}, \mathrm{y})$ of gait sequence computed using Eq.2.

Step1. Decompose $AESI(\mathrm{x}, \mathrm{y})$ into sub-regions.

Step2. Determine the magnitude and orientation at each pixel of gradient image $Grad(\mathrm{x}, \mathrm{y})$ at multiple decomposition levels (v) using $\mathcal{H}(x, y) = \sqrt{Grad_x(x, y)^2 + Grad_y(x, y)^2}$ and $\emptyset(x, y) = \tan^{-1}\left[\frac{Grad_y(x,y)}{Grad_x(x,y)}\right]$.

Step3. Apportion the computed magnitude of gradients at different levels (v) into K- orientation bins.

Step4. Aggregate all the sub-regions at level (v) $\mathrm{f_{SDOGs}} = \mathrm{K}\sum_{\mathrm{v}} 4^{\mathrm{v}}$

Step 5. Concatenate all the levels (0, 1, 2) of SDOGs to form a final SDOGs feature vector defined as: $\mathrm{f_{SDOGs}} = \mathrm{K}\left(\underbrace{\sum_{\mathrm{v}} 4^{\mathrm{v}}}_{\text{level v=0}} ; \underbrace{\sum_{\mathrm{v}} 4^{\mathrm{v}}}_{\text{level v=1}} ; \underbrace{\sum_{\mathrm{v}} 4^{\mathrm{v}}}_{\text{level v=2}}\right)$.

Output: The histogram of SDOGs feature vector of dimension 1×189.

D. MDPs calculation

Human gait motion is attributed more to horizontal motion than vertical motion [16]. To exploit this, we introduce MDPs features, and append these with SDOGs to form the final feature set. MDPs treat each row of AESI as an individual feature element, and compute the mean of pixel intensity in individual rows. To keep the dimension of the resulting

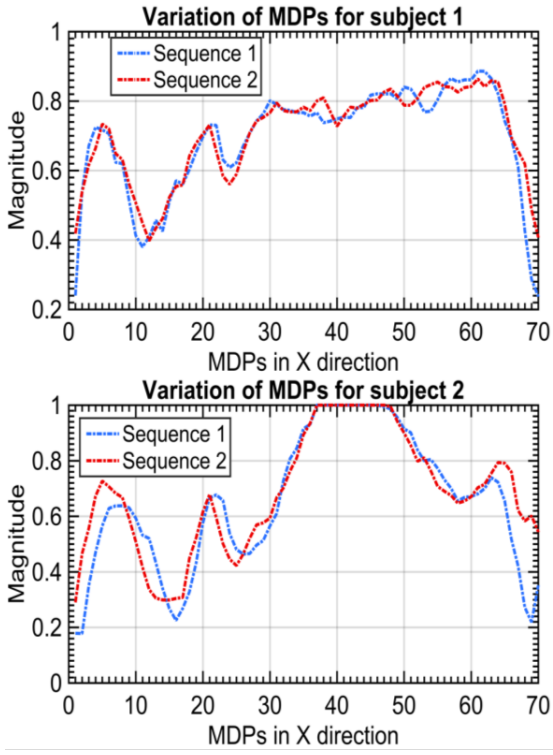

Fig.7. Variation of MDPs for two subjects. The figure illustrates the intra-class similarity and inter-class distinguishing ability possessed by MDPs.

feature set low, only the rows of AESI which belong to high temporal regions, are included in the computation. High temporal rows in AESI can be identified from the variance of intensity values in that particular row.

For AESI of dimension $m \times n$, $MDP(i)$ for row vector i is defined as:

$$MDP(i) = \frac{1}{n}\sum_{k=1}^{n} AESI(i,k) \quad (12)$$

In this work, only $m/2$ MDPs corresponding to most intensity variable rows, are calculated for a $m \times n$ $AESI$.

It should be noted that since the number of rows vary for different part-AESIs, the length of resulting feature set varies as well. Fig. 7 demonstrates the variation of MDPs for two subjects with two sequences each. It can be studied from the figure that MDPs possess remarkable inter-class distinguishing ability while at the same time have the needed intra-class similarity.

IV. Experimental Results

In order to test the performance of proposed framework, an experiment is conducted on three publicly available human gait dataset sets. These datasets are CASIA Dataset B [20], OU-ISIR Treadmill Dataset B [18] and the USF Human-ID gait challenge Dataset [21]. Performance of the algorithm is measured by calculating the correct class recognition rate (CCR) in percentage using support vector machine (SVM) as linear kernel in leave-one-out cross validation scheme. The CCR is determined using Eq. 14 and defined as:

$$CCR = \frac{TP+TN}{TP+TN+FP+FN} \times 100\ (In\ Percentage) \quad (14)$$

where TP, TN, FP, and FN are true positive, true negative, false positive, and false negative respectively. To evaluate the effectiveness of the proposed algorithm, the highest CCR achieved through the proposed algorithm is compared with the others similar state-of-the-art.

A. CASIA Dataset B

CASIA dataset B [20] is a multi-view dataset comprising of 124 subjects. The gait motion is captured from 11 cameras placed 18 degrees apart. There are 10 sequences of each subject which include 6 normal walking sequences (CAS-A), and 2 each with carrying conditions (CAS-B) and clothing

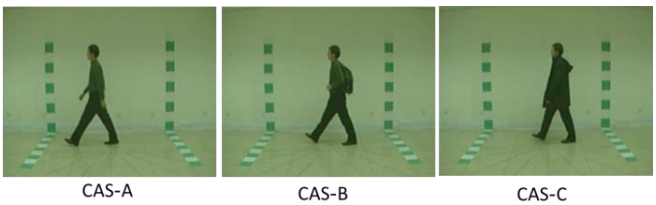

Fig.8. Probe sequences in CASIA B dataset

variation (CAS-C).

For evaluation, only sequences under 90 degrees' view angle have been considered. The first 4 sequences of CAS-A are used as gallery sequences while the remaining 2 along with sequences of CAS-B and CAS-C form the probe set. The AESIs of all the gait sequences are size normalized to 136×72 pixels.

The highest CCR achieved in each probe of the dataset is compared with the others similar state-of-the-art and as presented in Table II and Fig. 9.

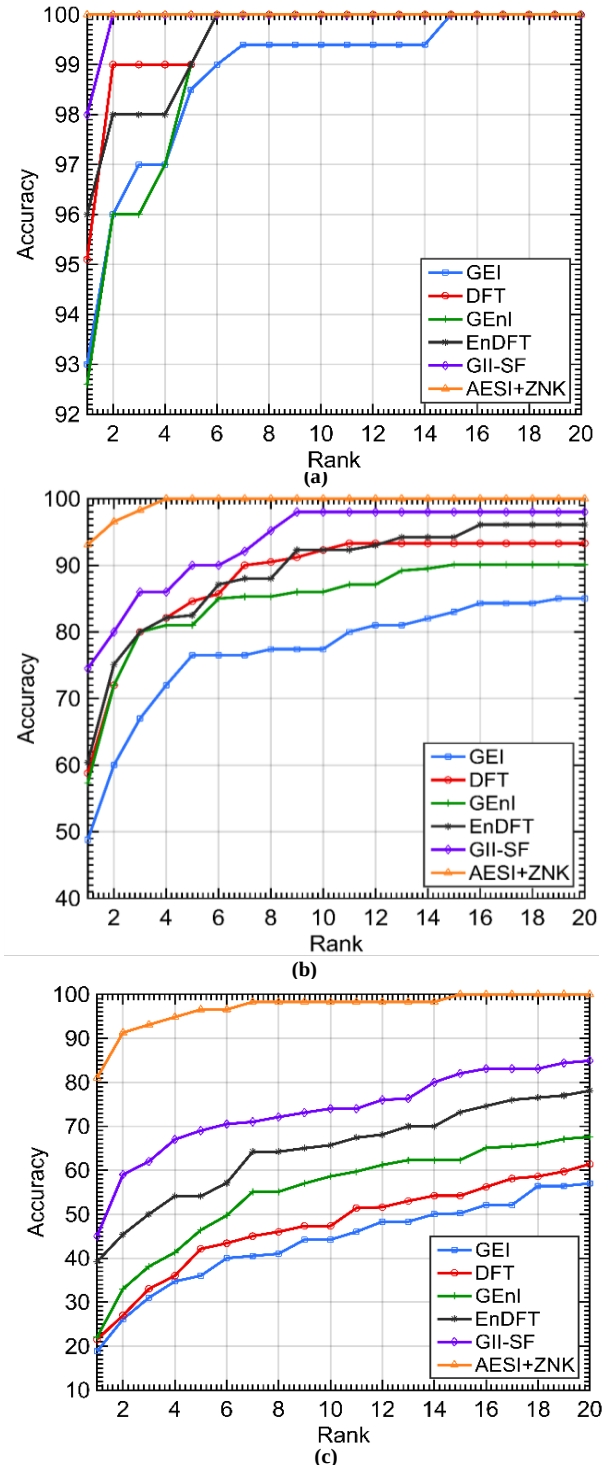

Fig. 9. Depiction of accuracy vs Rank curve for different approaches on three probe sequences of dataset (a) CAS-A, (b) CAS-B (c) CAS-C

Table II, compares the performance of the proposed method with various existing algorithms in terms of average CCR for three different probe of CASIA dataset. From Table II, it can be observed that the proposed algorithm performs admirably

well in presence of covariates (i.e. CAS-B and CAS-C), where it achieves 93.1% accuracy for sequences having carrying conditions (CAS-B). This is 9.5% better than the existing state-of-the-art, Flow Field which achieved recognition accuracy of 83.6%. For sequences having clothing variations (CAS-C), difference is even more drastic. Our method achieved accuracy of 81.3%. This is 17.6% better than the existing Random forest approach, which achieved recognition accuracy of 63.7%. Fig. 9 show Cumulative Match Characteristic (CMC) curve for all three probe sequences, and it can be considered an exhaustive comparison of accuracy because it is achieved through the variation of Rank. In all these cases the CMC curves shows better accuracy. Hence, it can be said the proposed algorithms perform well in comparison with many such existing approaches.

TABLE II
COMPARISON OF CCR WITH THE SIMILAR STATE-OF THE-ART ON CASIA DATASET B

Method	CAS-A	CAS-B	CAS-C	Average
GEI [6]	93.1	48.8	18.8	53.56
GEnI [9]	92.6	57.3	22.0	57.30
DFT [40]	95.1	58.8	21.5	58.46
EnDFT [33]	96.0	60.4	39.2	65.20
CGI [7]	**100**	64.2	43.6	69.26
Flow Field [29]	97.5	83.6	48.8	76.63
Random Forest [29]	98.8	73.8	63.7	78.76
GPPE [30]	93.6	56.1	22.4	57.36
STIP [32]	95.4	60.9	52	69.43
GII-SF [19]	98.0	74.5	45	72.5
AESI+ZNK	**100**	**93.1**	**81.3**	**91.47**

B. OU-ISIR Treadmill Dataset B

OU-ISIR Treadmill B [18] dataset comprises of large clothing variations. The dataset consists of 68 subjects with up to 32 possible variations in clothing from 15 different kinds of clothes such as half shirt, full shirt, baggy pants, hat, cap etc. Fig. 10 shows different gait sequences in the dataset. Table III show clothing combinations for each of the gait sequence.

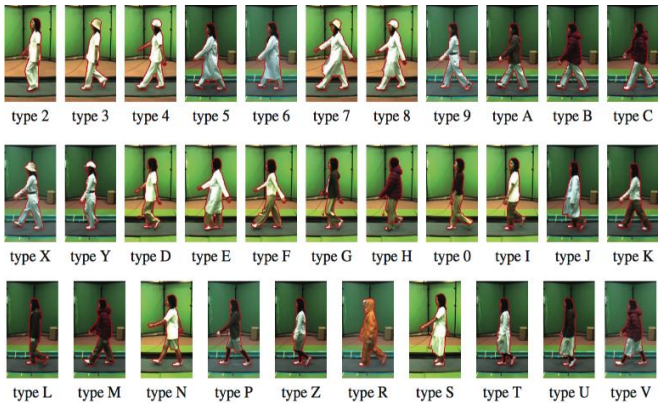

Fig. 10. Gait sequences in OU-ISIR Treadmill Dataset B

The dataset is partitioned into 3 segments- Gallery set, Training set and Probe set. The gallery set comprises of 48 subjects with one standard combination of clothing (Sequence type 9). The training set consists of 446 sequences of 20 subjects with all possible clothing combinations. The set is provided for tuning of model parameters. Since, its unlikely in real world to know the type of covariate variations beforehand, the training set is not used in this evaluation in any manner. The probe set comprises of 856 sequences of the same 48 subjects as in gallery set with all possible clothing combinations, except type 9. The OU-ISIR dataset itself provide extracted silhouettes size normalized to 128×88 pixels, therefore the formed AESIs are of the same size (128×88).

TABLE III
CLOTHING COMBINATIONS INCLUDED IN THE OU-ISIR B DATASET. KEYS FOR CLOTHES: RP-REGULAR PANTS; BP-BAGGY PANTS; SP-SHORT PANTS; SK-SKIRT; CP: CASUAL PANTS; HS-HALF SHIRT; FS- FULL SHIRT; LC-LONG COAT; PK-PARKER; DJ-DOWN JACKET; CW-C

Type	S_1	S_2	S_3	**Type**	S_1	S_2	**Type**	S_1	S_2
3	RP	HS	Ht	**0**	CP	CW	**F**	CP	FS
4	RP	HS	Cs	**2**	RP	HS	**G**	CP	Pk
6	RP	LC	Mf	**5**	RP	LC	**H**	CP	DJ
7	RP	LC	Ht	**9**	RP	FS	**I**	BP	HS
8	RP	LC	Cs	**A**	RP	Pk	**J**	BP	LC
C	RP	DJ	Mf	**B**	RP	DJ	**K**	BP	FS
X	RP	FS	Ht	**D**	CP	HS	**L**	BP	Pk
Y	RP	FS	Cs	**E**	CP	LC	**M**	BP	DJ
N	SP	HS	-	**P**	SP	Pk	**R**	RC	-
S	Sk	HS	-	**T**	Sk	FS	**U**	Sk	PK
V	Sk	DJ	-	**Z**	SP	FS	-	-	-

The Table IV compares the rank 1 and rank 5 performance of the proposed method with the similar state of the art. Fig.11 shows the comparison of CMC on similar state-of-the-art methods and higher accuracy can be comprehend by the proposed approach AESI+ZNK.

The results are depicted using CMC curve in Fig. 12. shows the CMC curve for all the probe sequences in the OU-ISIR Treadmill B dataset achieved by our algorithm.

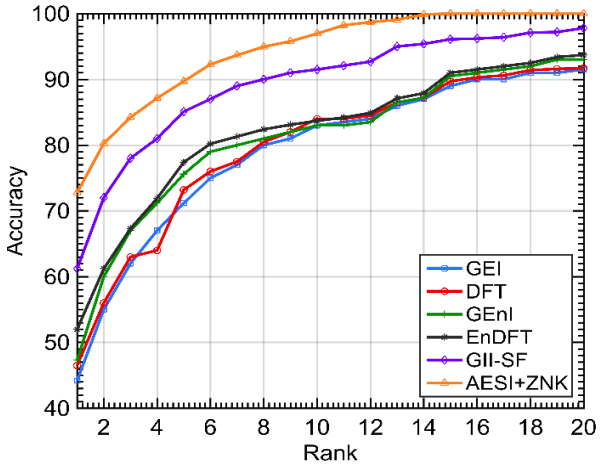

Fig. 11 Comparison using CMC on OU-ISIR Treadmill B dataset

TABLE IV
COMPARISON OF CCR WITH THE SIMILAR STATE-OF THE-ART ON OU-ISIR TREADMILL DATASET B

Method	**Rank 1 CCR**	**Rank 5 CCR**
GEI [5]	44.2	71.2
GEnI [9]	47.3	75.6
DFT [37]	46.6	73.2
EnDFT [32]	52.0	77.4
GII-SF [18]	61.2	85.1
AESI+ZNK	**72.7**	**89.7**

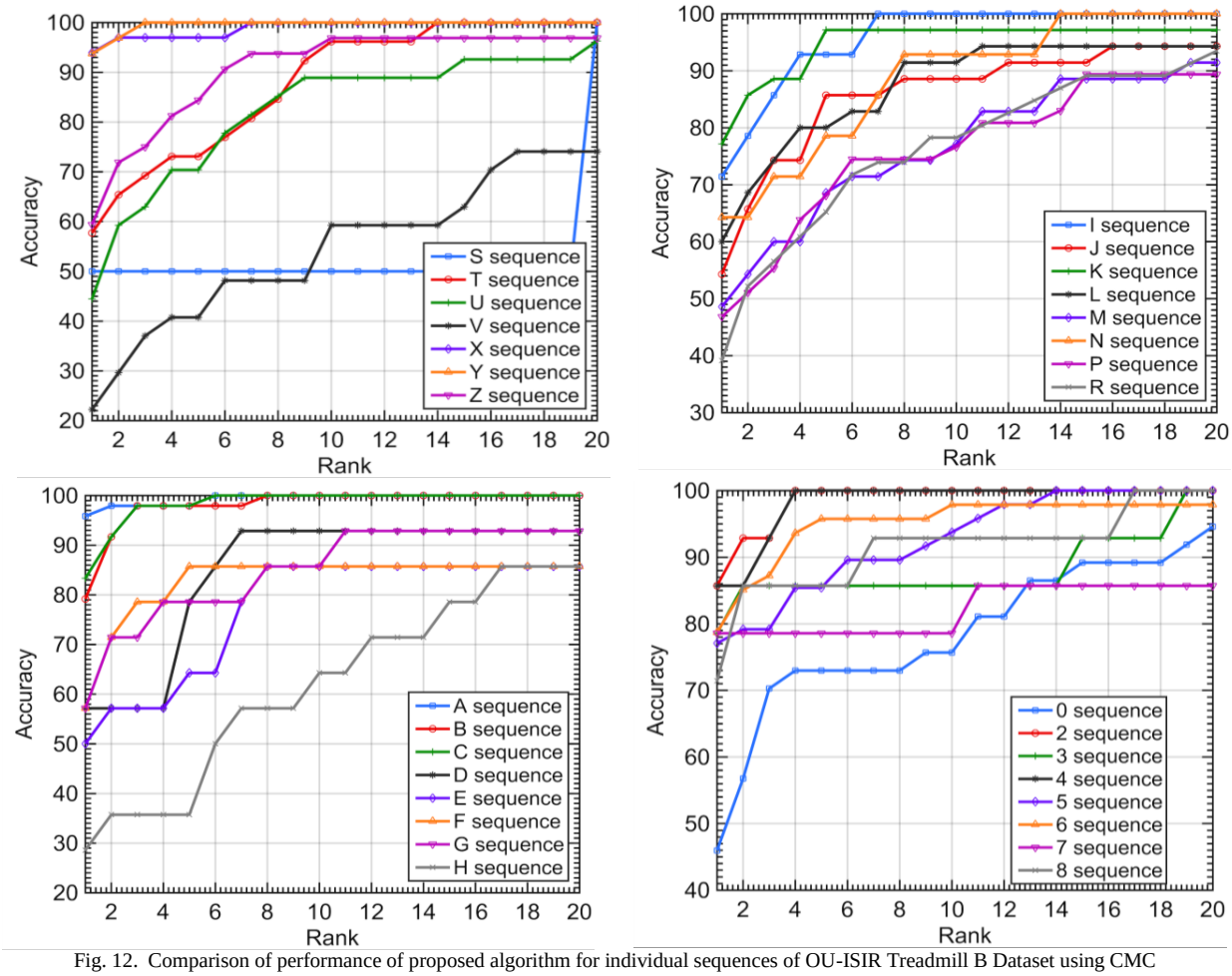

Fig. 12. Comparison of performance of proposed algorithm for individual sequences of OU-ISIR Treadmill B Dataset using CMC

It is clear from Table IV that the proposed approach outperforms existing methods in robustness to distortion by presence of covariates. The recognition accuracy achieved by the proposed algorithm is 72.7%, which is 11.5% better than the existing state-of-the-art, GII-SF that achieved 61.2% recognition accuracy.

From Fig. 12 it can be seen that the recognition accuracy achieved is highest for probe sequences A, X and Y. This is understandable since these sequences have less drastic variations in clothing compared to gallery set. On the contrary, the proposed algorithm fared worst for sequences V and H. This can be attributed to minimal commonality between these sequences and the gallery set.

C. USF Human-ID Gait Challenge Dataset

Finally, the performance of the proposed work is evaluated on USF Human-ID dataset [20]. The dataset is shot in outdoor environment (Fig. 13) and comprises of five variations-concrete or grass surface, presence or absence of briefcase, shoe variation (Type A or Type B), right or left view and variation in elapse time.

The USF Human-ID gait challenge dataset contains a total of 1870 gait sequences of 122 human subjects. The dataset provides a predetermined experimental setup and is segmented into 13 subsets out of which 1 forms the gallery set and the remaining 12 form the probe sets (A-L). As in the case of OU-ISIR dataset, the USF Human-ID dataset also provides size-normalized silhouettes of 128×88 pixels. Therefore, the formed AESIs are of the same size i.e. 128×88 pixels.

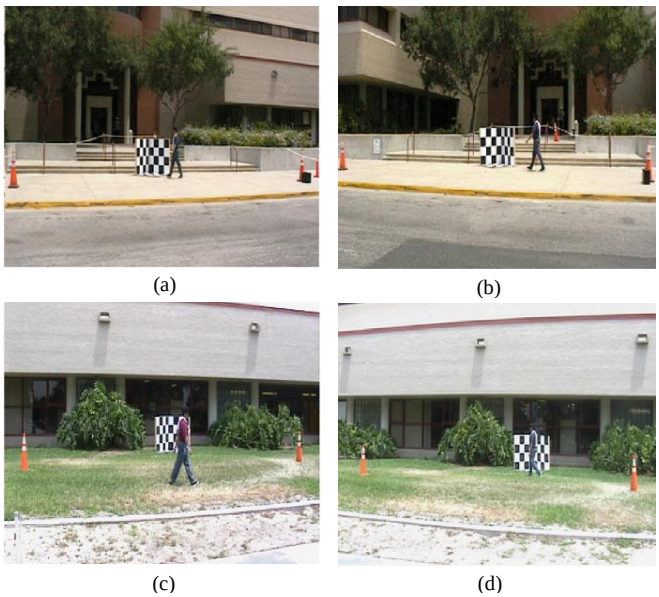

(a) (b) (c) (d)

Fig.13. Sample images of USF Human-ID gait challenge dataset: (a, b) left and right of camera view on concrete surface,(c, d) left and right camera view on grass surface

Table V informs about the covariate variations in all the probe sets (A-L) along with the number of sequences in each set. The table also demonstrates the achieved overall accuracy of the proposed algorithm and similar state-of-the-art for individual probe sets.

TABLE V
COMPARISON OF CCR WITH THE SIMILAR STATE-OF THE-ART ON USF HUMAN-ID GAIT DATASET AT RANK 1 AND RANK 5. KEY FOR COVARIATES -V - VIEW; H - SHOE; S - SURFACE; B - BRIEFCASE; T - TIME; AND C - CLOTHES

Probe Set	A	B	C	D	E	F	G	H	I	J	K	L	Avg.
Probe Size	122	54	54	121	60	121	60	120	60	120	33	33	-
Covariates	V	H	VH	S	SH	SV	SHV	B	BH	BV	THC	STHC	-
Rank 1 CCR													
GEI [5]	90	91	81	56	64	25	36	64	60	60	6	15	57.66
CGI [7]	91	93	78	51	53	35	38	84	78	64	3	9	61.69
GTDA [10]	91	93	86	32	47	21	32	95	90	68	16	19	60.58
GPDF [38]	95	93	89	62	62	**39**	38	94	91	78	21	21	70.07
VI-MGR [34]	95	96	86	54	57	34	36	91	90	78	31	28	68.13
AGKI [21]	96	96	90	62	63	37	**39**	94	**93**	80	**41**	**32**	71.74
AESI+ZNK	**97**	96	**93**	**68**	64	34	37	**96**	92	**86**	27	24	**72.53**
Rank 5 CCR													
GEI	94	94	93	78	81	56	53	90	83	82	27	21	76.23
CGI	97	96	94	77	77	56	58	98	97	86	27	24	79.12
GTDA	98	99	97	68	68	50	56	95	99	84	40	40	77.58
GPDF	99	94	96	**89**	**91**	64	64	99	98	92	39	45	85.31
VI-MGR	100	98	96	80	79	66	65	97	95	89	50	48	83.75
AGKI	100	98	97	88	85	68	**68**	98	95	91	**57**	**54**	84.46
AESI+ZNK	100	**100**	**98**	81	83	68	60	**99**	**98**	**94**	42	36	**84.67**

It can be studied that the proposed algorithm achieved an overall CCR of 72.53% for Rank 1 evaluation. This is highest among all the compared methods. For Rank 5 evaluation, the proposed method achieved CCR of 84.67%, which again is highest among all the existing methods. This proves the efficacy of our approach. The achieved CCR is particularly high for probe sets A, C, D, H and J. However, the approach doesn't offer improved performance for probe sets K and L over the existing state-of-the-art. This shows that while the use of Zernike moments can effectively handle and iron out covariates affecting the shape information, it understandably doesn't offer much immunity from temporal covariates.

V. Conclusion and Future Work

In this paper, a covariate cognizant approach to gait recognition has been presented. A single spatio-temporal template called AESI is formed to represent the gait motion. After which, Zernike moment based shape descriptors are used to detect the presence of covariates. An effective segmentation technique is used which discards the parts of AESI deemed infected by covariates. For feature extraction, SDOGs and MDPs methods are employed. SDOGs method provides a reliable and compact feature set by exploiting gradient information in the AESI. MDPs is a new feature extraction method, adapted specifically for gait motion and extracts information about the horizontal movement, which characterize the gait sequence. The efficacy of the presented approach is evaluated on three publicly available datasets. On all the three datasets our approach showed promising results and outperformed the existing state-of-the-art.

For future studies, an extension of the proposed approach, which is multi-view invariant, can be developed. We will also explore how to improve the representation of temporal information for gait sequences. In addition, we will consider employing the presented approach to the domain of medical prognosis. Since many ailments causes substantial change in walking pattern of an individual, it would be interesting to explore if the technique could help in diagnosis of such ailments.

References

[1] G. Johansson, "Visual Perception of Biological Motion and a Model for Its Analysis," *Attention, Perception, & Psychophysics*, vol. 14, no. 2, pp. 210-211, 1973.

[2] C BenAbdelkader, R Cutler, and L Davis, "Person identification using automatic height and stride estimation," in *International Conference on Pattern Recognition*, Quebec, 2002, pp. 377-380.

[3] A Bobick and A Johnson, "Gait recognition using static, activityspecific parameters," in *IEEE International Conference on Computer Vision Pattern Recognition (CVPR)*, 2001, pp. 423-430.

[4] C. Y. Yam and M. S. Nixon, "Model-based gait recognition," *Encyclopedia of Biometrics*, 2009.

[5] I Rida, X Jiang, and G L Marcialis, "Human Body Part Selection by Group Lasso of Motion for Model-Free Gait Recognition," *IEEE Signal Processing Letters*, vol. 23, no. 1, pp. 154-158, 2016.

[6] Ju Man and Bir Bhanu, "Individual recognition using gait energy image," *IEEE Transactions on Pattern Analysis and Machine Intelligence*, vol. 28, no. 2, pp. 316-322, Feb 2006.

[7] C Wang, J Zhang, L Wang, J Pu, and X Yuan, "Human identification using temporal information preserving gait template," *IEEE Transactions on Pattern Analysis and Machine Intelligence*, vol. 34, no. 11, pp. 2164-2176, Dec. 2011.

[8] K Bashir, K Xiang, and T Gong, "Gait representation using flow fields," in *British Machine Vision Conference*, 2009, pp. 1-11.

[9] K Bashir, T Xiang, and S Gong, "Gait recognition without subject cooperation," *Pattern Recognition letters*, vol. 31, no. 13, pp. 2052-2060,

2010.

[10] D Xu, S Yan, D Tao, S Lin, and H J Zhang, "Marginal fisher analysis and its variants for human gait recognition and content-based image retrieval," *IEEE Transactions on Image Processing*, vol. 16, no. 11, pp. 2811-2821, 2007.

[11] D. Tao, X. Li, X. Wu, and S. J. Maybank, "General tensor discriminant analysis and gabor features for gait recognition," *IEEE Transactions on Pattern Analysis and Machine Intelligence*, vol. 29, no. 10, pp. 1700-1715, 2007.

[12] Dong Xu et al., "Human gait recognition with matrix representation," *IEEE Transactions on Circuits and Systems for Video Technology*, vol. 16, no. 7, pp. 896-903, 2006.

[13] X. Li, S. Lin, S. Yan, and D. Xu, "Discriminant locally linear embedding with high-order tensor data," *IEEE Transactions on Systems, Man, and Cybernetics, Part B (Cybernetics)*, vol. 38, no. 2, pp. 342-352, 2008.

[14] Dinesh Kumar Vishwakarma and Kuldeep Singh, "Human Activity Recognition based on Spatial Distribution of Gradients at Sub-levels of Average Energy Silhouette Images," *IEEE Transactions on Cognitive and Developmental Systems*. [Online]. http://ieeexplore.ieee.org/xpls/abs_all.jsp?arnumber=7486058&tag=1

[15] F.Zernike, *Physica*, vol. 1, p. 689, 1934.

[16] J. P. Foster, M. S. Nixon, and Adam Prügel Bennett, "Automatic gait recognition using area-based metrics," *Pattern Recognition Letters*, vol. 24, no. 14, pp. 2489–2497, 2003.

[17] Toby Lam, K H Cheung, and James N K Liu, "Gait flow image: A silhouette-based gait representation for human identification," *Pattern Recognition letters*, vol. 44, no. 4, pp. 973-987, 2011.

[18] Y. Makihara et al., "The ou-isir gait database comprising the treadmill dataset," *IPSJ Transactions on Computer Vision and Applications*, vol. 4, pp. 53-62, 2012.

[19] Parul Arora, Madasu Hanmandlub, and Smriti Srivastavaa, "Gait based authentication using gait information image features," *Pattern Recognition Letters*, vol. 68, no. 2, pp. 336-342, June 2015.

[20] S. Yu, D. Tan, and T. Tan, "A framework for evaluating the effect of view angle, clothing and carrying condition on gait recognition," in *International Conference on Pattern Recognition*, vol. 18, 2006, pp. 441–444.

[21] S. Sarkar et al., "The humanID gait challenge problem: data sets, performance, and analysis," *IEEE Transactions on Pattern Analysis and Machine Intelligence*, vol. 27, no. 2, pp. 162-177, 2005.

[22] Sruti Das Choudhurya and Tardi Tjahjadib, "Clothing and carrying condition invariant gait recognition based on rotation forest," *Pattern Recognition Letters*, vol. 80, no. 1, pp. 1-7, May 2016.

[23] Z Liu and S Sarkar, "Simplest Representation yet for Gait Recognition: Averaged Silhouette," in *IEEE International Conference Pattern Recognition*, vol. 4, 2004, pp. 211-214.

[24] S Lee, Y Liu, and R Collins, "Shape variation-based frieze pattern for robust gait recognition," in *IEEE Conference on Computer Vision and Pattern Recognition (CVPR)*, 2007, pp. 1-8.

[25] Imed Bouchrika and Mark S Nixon, "Model-based feature extraction for gait analysis and recognition," in *Proc. Int. Conf. Comput. Vis./Comput. Graph. Collab. Tech. Appl.*, 2007, pp. 150-160.

[26] Y Chai, Q Wang, R Zhao, and C Wu, "A new automatic gait recognition method based on the perceptual curve," in *IEEE Region 10 Conference on TENCON 2005 - 2005*, Melbourne, 2005, pp. 1-5.

[27] Daoliang Tan, Kaiqi Huang, Shiqi Yu, and Tieniu Tan, "Uniprojective features for gait recognition," in *International Conference on Biometrics*, Seoul, 2007, pp. 673–682.

[28] Zongyi Liu and Sudeep Sarkar, "Improved gait recognition by gait dynamics normalization," *IEEE Transactions on Pattern Analysis and Machine Intelligence*, vol. 28, no. 6, pp. 863-876, July 2006.

[29] Y Dupuis, X Savatier, and P Vasseur, "Feature subset selection applied to model-free gait recognition," *Image Vision Computating*, vol. 31, no. 8, pp. 580-591, 2013.

[30] M Jeevan, N Jain, M Hanmandlu, and G Chetty, "Gait recognition based on gait pal and pal entropy image," in *IEEE International Conference on Image Processing (ICIP)*, 2013, pp. 4195–4199.

[31] W. Kusakunniran, "Recognizing gaits on spatio-temporal feature domain," *IEEE Transactions on Information Forensics and Security*, vol. 9, no. 9, pp. 1416-1423, 2014.

[32] W. Kusakunniran, "Attribute-based learning for gait recognition using spatio-temporal interest points," *Image and Vision Computing*, vol. 32, no. 12, pp. 1117-1126, 2014.

[33] Md Rokanujjaman et al., "Effective part-based gait identification using frequency-domain gait entropy features," *Multimedia Tools Applications*, vol. 74, no. 9, pp. 3099-3120, 2013.

[34] Y. Guan, C.-T. Li, and F. Roli, "On reducing the effect of covariate factors in gait recognition: a classifier ensemble method," *IEEE Transactions on Pattern Analysis and Machine Intelligence*, vol. 37, no. 7, pp. 1521-1528, 2015.

[35] S. D. Choudhury and T. Tjahjadi, "Robust view-invariant multiscale gait recognition," *Pattern Recognition Letters*, vol. 48, no. 3, pp. 798-811, 2015.

[36] T. W. Chua, Y. Wang, and K. Leman, "Adaptive Texture-Color based Background Subtraction for Video Surveillance," in *IEEE International Conference on Image Processing (ICIP)*, Orlando, 2012.

[37] D. K. Vishwakarma and Rajiv Kapoor, "Integrated Approach for Human Action Recognition using Edge Spatial Distribution, Direction Pixel, and R -Transform," *Advanced Robotics*, vol. 29, no. 23, pp. 1551-1561, June 2015.

[38] C H Teh and R T Chin, "On image analysis by the methods of moments," *IEEE Transactions on Pattern Analysis and Machine Intelligence*, vol. 10, no. 4, pp. 496-513, 1988.

[39] R Drillis, R Contini, and M Bluestein, "Body segment parameters: A survey of measurement techniques," *Arti/icial Limbs*, vol. 2, no. 1, pp. 44-66, 1966.

[40] Y. Makihara, R. Sagawa, Y. Mukaigawa, T. Echigo, and Y. Yagi, "Gait recognition using a view transformation model in the frequency domain," in *Computer Vision–ECCV*, Florida, 2006, pp. 151-163.

[41] Dinesh Kumar Vishwakarma and Rajiv Kapoor, "Hybrid classifier based human activity recognition using the silhouette and cells," *Expert Systems with Applications*, vol. 42, no. 20, pp. 6957-6965, 2015.

Himanshu Aggarwal received his B.Tech. degree in Electronics and Communication Engineering from Delhi Technological University in 2016. Presently, he is working as Associate software engineer in Computer Vison department of Qualcomm Incorporated, Hyderabad, India. His current interest includes human activity recognition, egocentric visual odometry and algorithmic design.

Dinesh Kumar Vishwakarma received his B.Tech. from Dr RML Avadh University, Faizabad, Uttar Pradesh, India, in 2002, M.Tech. from Motilal Nehru National Institute of Technology, Allahabad, Uttar Pradesh, India in 2005, and Ph.D. in Computer Vision from Delhi Technological University, Delhi, India in 2016. Presently, he is working as Assistant Professor, in the Department of Electronics and Communication Engineering, Delhi Technological University, Delhi, India-110042. His research interest includes human action and activity recognition, hand gesture recognition and machine learning.

Volume 4, Issue 2 (2016) 381-384 ISSN 2347 - 3258
International Journal of Advance Research and Innovation

Design and Experimental Analysis of a 200W Micro Wind Turbine

Raj Kumar Singh*, Sajal Garg, Lohit Gudivada
Department of Production and Industrial Engineering, Delhi Technological University, New Delhi, India

Article Info

Article history:
Received 25 January 2016
Received in revised form
20 February 2016
Accepted 28 February 2016
Available online 15 June 2016

Keywords
Wind turbines, blade velocity, NACA 2212

Abstract

Majority of the regions in India are characterized by moderate and low wind regimes. These regions have variable and gusty winds. Our low-wind energy turbine addresses this problem and is capable of providing power to millions of people not connected to the grid in low wind conditions.

Our objective is to design a suitable wind turbine applicable in low speed regions extracting maximum power output. Our team aims to take on the challenge of improving wind turbine efficiencies, at low to medium wind speeds, to reduce environmental impact and encourage adoption of wind energy at domestic and commercial building rooftops and small distributed systems.

Blade Element Momentum theory was adopted to find the suitable parameters at the required wind speeds. Tools like Q-Blade and X-foil were used to optimize the CAD model of the blade.

A customized Wind tunnel was fabricated by the team to validate the practical results against the theoretical ones. Rapid Prototyping technique of 3-D printing was used to manufacture the blades.

Final results establish a close relationship between the theoretical and experimental values.

1. Introduction

For the solar and wind industries of the world, it has been a long-held dream: to produce energy at a cost equal to conventional sources like coal and natural gas.

With humongous subsidies being provided by government agencies like the United States Environment Protection Agency (USEPA) and in India's context the Ministry of New and Renewable Energy (MNRE) to implement such technologies, and projects being done by technical institutions like IEEE and The Energy and Resources Institute (TERI), that dream appears to be coming close to reality. The global energy sector is experiencing a push towards the adoption of renewable energy generation over conventional sources.

Now that we're reaching a point where we can compete with conventional sources of energy, it is becoming increasingly important to not just pit unconventional sources of energy against conventional sources of energy, but also to pit one renewable source of energy against another.

In present times, the debate is largely whether to choose Solar PV over Wind or the other way round. The present trend, very rightly, is to have a resource assessment study done at a particular place, and use solar or wind depending on which is more economical to set up. But in doing so, one important factor is left out, i.e. the relative environmental impact of each technology.

Our aim is to increase the penetration of small and distributed wind. Majority of the small rooftop turbines presently used in India are imported and are designed for high wind regimes. Hence in Indian conditions these have a high cut-in wind speed and poor low wind performance.

Corresponding Author,
E-mail address: rajkumarsingh@dce.ac.in
All rights reserved: http://www.ijari.org

This calls for an indigenously designed small wind turbine with optimal low wind performance and the ability to capture gust energy. Gusts are typically short blasts of wind which blow for a very short period of time. Capturing this energy calls for high starting torque and low rotational inertia so that the rotor blades of the turbine can respond quickly to the fluctuations in wind. [1]

Optimizing each technology is a challenge in its own. Our team aims to take on the second challenge of improving wind turbine efficiencies, at low to medium wind speeds, to reduce environmental impact and encourage adoption of wind energy at domestic and commercial building rooftops and small distributed systems.

This paper is divided into 3 sections:

- Blade Element Momentum Review
- Design of the Blade
- Experimental Results

2. Blade Element Momentum Review

Blade element momentum (BEM) theory is one of the oldest and most commonly used methods for calculating induced velocities on wind turbine blades. This theory actually originates from two different theories: blade element theory and momentum theory.

Blade element theory [2] assumes that blades can be divided into small elements that act independently of surrounding elements and operate aerodynamically as two-dimensional airfoils whose aerodynamic forces can be calculated based on the local flow conditions. These elemental forces are summed along the span of the blade to calculate the total forces and moments exerted on the turbine.

The momentum theory [3] assumes that the loss of pressure or momentum in the rotor plane is caused by the work done by the airflow passing through the rotor plane on the blade elements. Using the momentum theory, one can calculate

the induced velocities from the momentum lost in the flow in the axial and tangential directions. These induced velocities affect the inflow in the rotor plane and therefore also affect the forces calculated by blade element theory. This coupling of two theories ties together blade element momentum theory and sets up an iterative process to determine the aerodynamic forces and also the induced velocities near the rotor.

In practice, BEM theory is implemented by breaking the blades of a wind turbine into many elements along the span. As these elements rotate in the rotor plane, they trace out annular regions, across which the momentum balance takes place. These annular regions are also where the induced velocities from the wake change the local flow velocity at the rotor plane. BEM can also be used to analyze stream tubes through the rotor disk, which can be smaller than the annular regions and provide more computational fidelity.

The generation of rotational kinetic energy in the wake results in less energy extraction bythe rotor than would be expected without wake rotation. In general, the extra kinetic energy inwind turbine wake will be higher if the generated torque is higher. Thus, as will be shownhere, slow-running wind turbines (with a low rotational speed and a high torque) experiencemore wake rotation losses than high-speed wind machines with low torque.

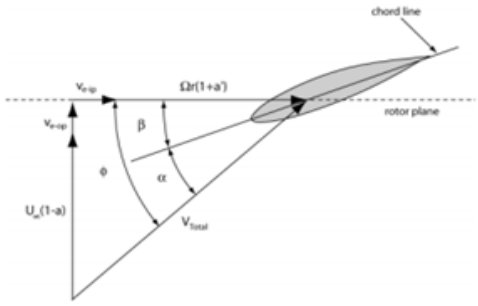

Fig 1: Local Elemental Velocities

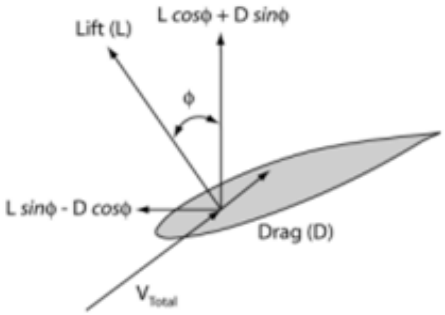

Fig 2: Local Elemental Forces

As we are required to obtain the angle of attack to determine the aerodynamic forces on an element, we must first determine the inflow angle based on the two components of the local velocity vector. Assuming that the blade motion is very small, the resulting equation is dependent on the induced velocities in both the axial and tangential directions as well as the local tip speed r_a

$$tan\phi = \frac{U_\infty(1-a)}{\Omega r(1+a')} = \frac{1-a}{(1+a')\lambda_r} \quad [1]$$

However, if the blade motion is significant we must include the local velocities in the calculation of the inflow angle, as follows:

$$tan\phi = \frac{U_\infty(1-a)+v_{e-op}}{\Omega r(1+a')+v_{e-ip}} \quad [2]$$

This equation holds for all elements of the blade along the span, although typically the inflow angle changes with element location. The induced velocity components in Equations 1 and 2 are a function of the forces on the blades and we use BEM theory to calculate them. A thorough derivation of these equations can be found in most wind turbine design handbooks. From blade element theory, the thrust distributed around an annulus of width dr is equivalent to

$$dT = B\frac{1}{2}\rho V_{total}^2(C_l\cos\phi + C_d\sin\phi)cdr \quad [3]$$

and the torque produced by the blade elements in the annulus is equivalent to

$$dQ = B\frac{1}{2}\rho V_{total}^2(C_{;}\sin\phi - C_d cos\phi)crdr \quad [4]$$

Now, to relate the induced velocities in the rotor plane to the elemental forces of equations, we must incorporate the momentum part of the theory, which states that the thrust extracted by each rotor annulus is equivalent to

$$dT = 4\pi r\rho U_\infty^2(1-a)adr \quad [5]$$

and the torque extracted from each annular section is equivalent to

$$dQ = 4\pi r^3\rho U_\infty\Omega(1-a)a'dr \quad [6]$$

Thus, when we include two-dimensional airfoil tables of lift and drag coefficient as a function of the angle of attack, α, we have a set of equations that can be iteratively solved for the induced velocities and the forces on each blade element. However, before we solve our system of equations, we would like to take into account several corrections to the BEM theory. These corrections include tip- and hub-loss models to account for vortices shed at these locations, the Glauert correction to account for large induced velocities (a >0.4), and the skewed wake correction to model the effects of incoming flow that is not perpendicular to the rotor plane.

3.1 Design of the blade

NACA 22112 [3] was chosen for a few prominent reasons. The large relative thickness can accommodate the root tube easier than thinner profiles. Initial profiles should have a high cross-sectional stiffness to limit overall blade weight and tip deflection. The in board profiles should maximize lift while having a high lift-drag ratio is of less importance [4]. In other words, the inboard profiles, which are the profiles that are closer tothe root, are chosen based on a structural design requirement while trading off optimum aerodynamic properties. The relative large thickness of the airfoil allows these requirements to be met.

3.2: Chord and Twist Distribution

Airfoil data after being generated from XFOIL was fed into a BEM analysis program called Q Blade which utilizes the Blade Element Momentum theory to generate optimal

distributions of chord and twist distribution. [5]Often these values are not practical enough to manufacture, hence the program allows you to modify these values to a manufacture able scale and then give you the performance analysis due to modifications done. The two figures below compare the values of optimal, fitted and practical distributions of chord and twist.

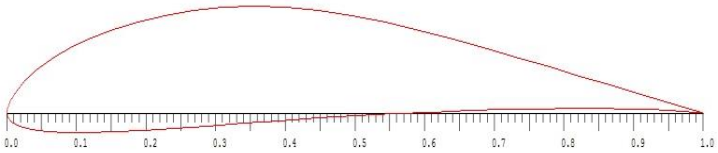

Fig. 2.1 design of Blade

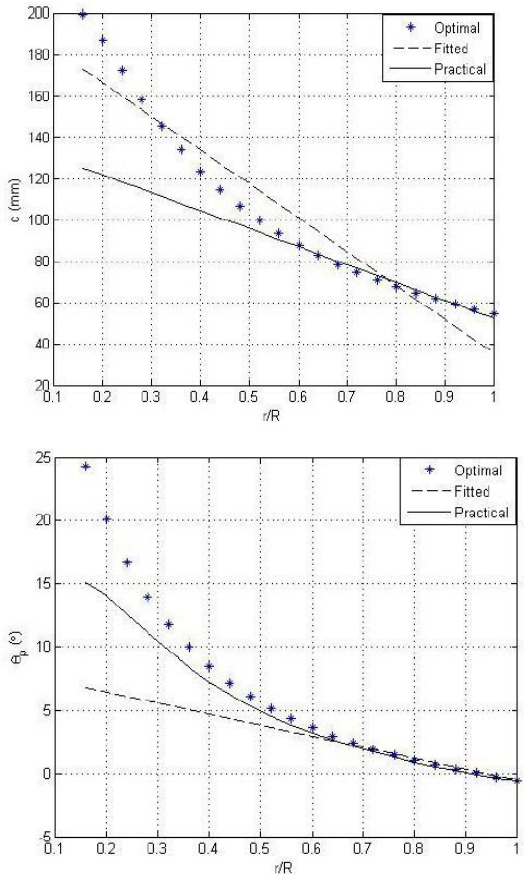

Graph 1*:* Values of Chord and Twist

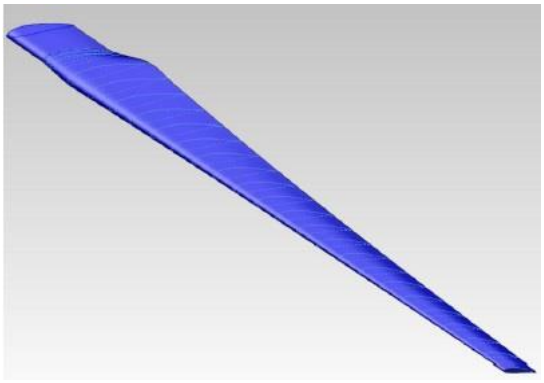

Fig 3: Complete CAD Model of Blade

4 Results

The results are summarized below in the form of comparison between theoretical and measured values of the blade values. The results were obtained on a custom designed wind tunnel with a test section of 1mx1m and maximum air velocity of 14m/s.

Fig 4: 3-D Printed Blades in wind tunnel

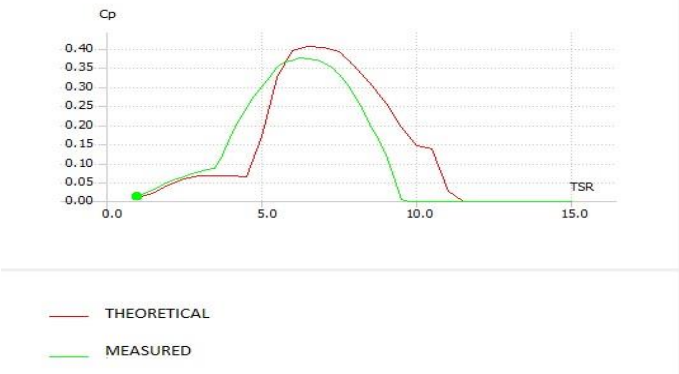

Graph 2: Comparison between theoretical and experimental values of Cp

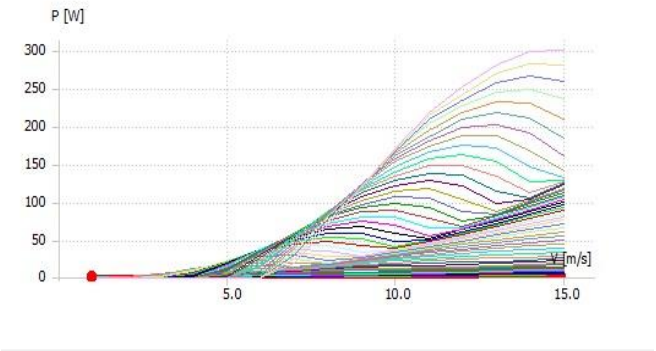

Graph 3: Experimental Power vs. Velocity

The simulated power coefficient curve is not very smooth at some points, especially in the tip speed ratio range of 5 to 6. There must be a trade-off between these two opposing influences that results in an overall reasonable power output. The method of calculating wake factor influences in the BEM simulation has a noticeable impact on the results.

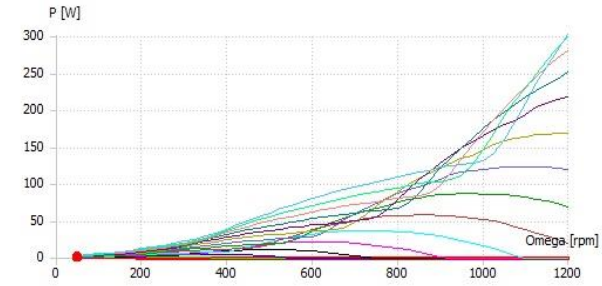

Graph 4: Experimental Power vs. RPM

The BEM process includes iterative solving of sets of equations. The numerical stability of the iteration process depends on the properties of the lift and drag coefficient functions. For this blade, angle of attack along the span varies significantly, and plays a very important role. When local angle of attack is around stall point or becomes negative, getting the BEM code toconverge can become difficult. Sometimes the local power coefficient close to the tip becomes negative.

5 Conclusions

NACA 2212 can accommodate the root tube easier than thinner profiles due to its large relative thickness and hence is a good choice for use as an initial profile.

Buhl method was found to be better than the Glauert and Wilson-Walker methods for calculating the wake factor for the case of this turbine.

The simulated power coefficient curve is not very smooth at some points, especially in the tip speed ratio range of 5 to 6. This is because when the tip speed ratio increases, the local power coefficient at the tip will decrease and local power coefficient close to the root increases.

The differences in the observed and theoretical values of power were found to be within acceptable limits.

References

[1] [Manwell et al. Manwell, J., McGowan, J., and Rogers, A. (2009). Wind Energy Explained. Wiley, second edition.

[2] Haans, W. (2011). Wind turbine aerodynamics in yaw: unravelling the measured rotor wake. PhD thesis, Delft University of Technology.

[3] [Hansen, 2008] Hansen, M. O. (2008). Aerodynamics of Wind Turbines.Earthscan, second edition.

[4] Hageman, A. (1980). Catalogue of aerodynamic characteristics of airfoils in the reynolds number 104-106. Laboratory of fluid dynamics and heat transfer, department of physics, university of Technology, Eindhoven.

[5] Jones, R. (1990). Wing Theory.Princeton University Press.

[6] Kragten, A. (2011). KD 467: Calculations executed for the 2-bladed rotor of the VIRYA-3B2 windmill (d = 6.5, steel blades).

Design and Implementation of a Power and Speed Efficient Carry Select Adder on FPGA

Simarpreet Singh Chawla
Dept. of Electronics and Communication Engineering, Delhi Technological University (Formerly DCE), INDIA
Email ID: chawla.simarpreet@gmail.com

Swapnil Aggarwal
Dept. of Electronics and Communication Engineering, Delhi Technological University (Formerly DCE), INDIA
Email ID: swapnil.aggarwal.in@ieee.org

Nidhi Goel
Dept. of Electronics and Communication Engineering, Delhi Technological University (Formerly DCE), INDIA
Email ID: nidhi.iitr@dce.ac.in

Mantek Singh Bhatia
Dept. of Computer Science and Technology, Amity University, Noida, INDIA
Email ID: mantekbhatia93@yahoo.co.in

***Abstract* — Adders are one of the most common unit in digital systems. The speed, power and area occupied by an adder play a vital role in Digital Signal Processing system, Image Processing system, etc. Hence, they play an important role in deciding the time period of the clock, the place and route of various units comprising of the system and total power consumed by the system. In this paper, we propose a new architecture for a modified sequential high speed carry select adder. We have given emphasis on optimizing the time period of the clock and power consumed, by using the carry ahead generation technique of Carry Look Ahead Adder (CLAA) and multiplexing technique of Carry Select Adder (CSA). The proposed CSA was implemented on Virtex-7 and results were calculated using Vivado Design Suite 2014.4.**

Keywords—Carry Look Ahead Adder (CLAA); Carry Select Adder (CSA); Arithmetic and Logic Unit (ALU); Multiplexer (MUX).

I. INTRODUCTION

The rapid developments in real time processing, communication systems have led to an increase in the need for faster processing and energy efficient systems. In today's world, a digital circuit is expected to have low computation time and power consumption.

Hence, one of the most basic unit in a system is an Arithmetic Logic Unit (ALU) which forms the basic component in microprocessors and microcontrollers. An ALU performs all the basic operations of the processor. Hence, all the performance parameters of a system can be optimized with optimization of the ALU. Moreover, with the increase in complex functions, the computation speed and power consumed has been increased drastically. This has augmented the effort on decreasing the power consumed, area and computational time of a digital circuit [1-3].

An adder is the fundamental unit of an ALU. Hence, with optimization of an adder can result into optimization of an ALU or the whole circuit. Most of the adders emphasize only on one performance parameter (area, timing or power), from which one can use particular type of adder for optimizing a single performance parameter. Hence, there is a need of improving two or more performance parameters for the overall betterment of the system.

We propose a new architecture for Carry Select Ahead (CSA) combining the advantages of both CSA and Carry Look Ahead Adder (CLAA) resulting in optimized power consumption with decrease in time period of the clock time with only a small increase in area. The proposed CSA has been implemented on Virtex-7 and the results were calculated using Vivado Design Suite 2014.4.

II. RELATED WORK

The time critical applications use CLAA to derive fast results. In CLAA, for every single bit, sum and carry is independent of the previous bits. This eliminates the ripple effect making it faster than RCA but it also lead to increase in area. CLAA is fast for a design having less input bits, for higher number bits it shows the worse delay [4]. Several modifications/improved versions have been proposed and implemented to further improve the performance of carry look ahead adders [5]-[9]. In contrast, a Carry Skip Adder (CSKA) uses a carry skip scheme to reduce the additional time taken to propagate the carry signal in RCA. Thus, CSKA is faster than RCA at the expense of a few simple modifications.

Another adder SCBCLA [10], which is a self-time implementation of CLAA adders based on the 'section-carry', has also been implemented via a semicustom ASIC-based design flow targeting a 130nm bulk CMOS standard cell library [11]. Unlike CCLA, SCBCLA need not compute bit-wise look-ahead carry signals for each and every adder stage. Instead SCBCLA produces the look-ahead carry signal corresponding to a 'section' or 'group' of adder inputs. An SCBCLA adder contains three constituent blocks: SCBCLA unit, full adder, and sum logic. Two different topologies of SCBCLA have been suggested based on the utilization of modules– either solely or in conjunction with a ripple carry adder (RCA) section in the least significant adder stage [11].

To mitigate linear dependency of carry propagation delay, a CSA has been proposed that including parallelism by anticipating both possible values of the carry input i.e. 1 or 0 and evaluates the result in advance. The final sum and carry is

978-9-3805-4421-2/16/$31.00 ©2016 IEEE

chosen using multiplexers after the knowledge of real value of the carry. The carry-out bit of the preceding block of the adder acts as the select signal to the multiplexer. Though, the use of two adders and final selection multiplexers consumes more area, reduction in carry propagation delay is substantial. Thus CSA proves to be a compromise between RCA (small areas but longer delay) and CLAA (larger area with shorter delay) [9]. This has led to research in the field of CSA and varied versions of CSA have been proposed in the literature [13]-[16].

In contrast to CSA, a Carry Select Adder with Sharing (CSAS) has been proposed that uses of a fast incrementer circuit instead of adders to increment the interim sum when the input carry is obtained as logic 1 [17]. This performs each of the two additions in half of the clock cycle by using few latches. Iterative use of this concept can lead to efficient trade off of area for delay. More specifically, the delay of the proposed adder is O (2n) while its area is O ((1+α) n), where α<1.

To reduce area and power consumption with small speed penalty, a Modified Carry Select-Adder (MCSA) design has also been proposed, that uses a single RCA and Binary to Excess-1 Converter (BEC) instead of using dual RCAs [18]. Since BEC designing takes less number of logic gates than RCA design, reduction in area for MCSA and total power consumption is achieved.

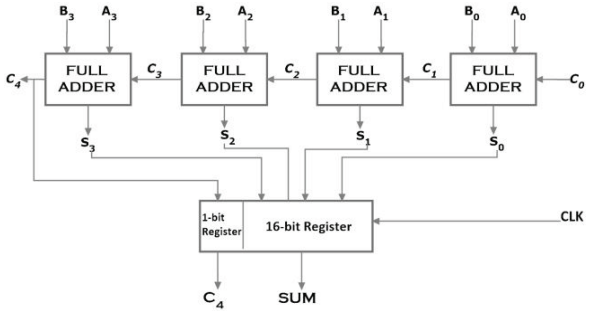

Fig. 1. 4-bit Sequential Ripple Carry Adder [30]

Sequential adder circuits are very important in the design of high performance microprocessors and DSP processors (DSPs), as well as in the critical path of processors, such as memory address calculation, ALU (Arithmetic Logic Unit) evaluation and floating-point computation, etc. Sequential circuits, that are often pipelined, result in a faster implementation of the same adder with a smaller addition latency that depends upon the highest operable frequency. The architectures of [19] - [28] show a wide variety of such implementations. The most popular implementation is by using CLAA as the main architecture [19], [21], [23], [25], [26], [27] and [28]. Pipelined implementations of the same is proposed in [23] and [24]. An 8 bit, adiabatic CLAA [23], which exhibits a conversion efficiency of 77% at 10 MHz operating frequency on 0.6 um CMOS technology. An 8-bit CLAA utilizes 'fine-grain' pipelined Carry-Increment Full Adders (CIFA) [24] with a maximum operating frequency of 800 MHz, which falls down to 480 MHz when optimized for power. A negative logic based 16-bit CLAA [21] on 0.25 um Ga-As HJFET CMOS technology operates at a maximum frequency of 1.67 GHz. The area, too, is optimized to 1.6 mm^2 by using NOR gates. A 32-bit CLAA based on Non-Full Voltage Swing True-Single-Phase-Clocking Logic (NSTSPC) and True-Single-Phase-Clocking Logic (TSPC) is proposed in [19]. Using 0.35 um CMOS technology, the maximum operating frequency reaches 500 MHz. An 8-bit, 64-bit and 8-bit CLAA is proposed in [25], [27] and [28] respectively, however each of these undergo a different mode of operation. [25] uses a 5 bit CSKA with a maximum operating frequency of 19.66 MHz, [27] uses a Race Logic Architecture (RALA) with 1.11 GHz (0.9 ns) maximum frequency and [28] uses a adiabatic quantum-flux-parametron (AQFP) logic, which achieves an energy dissipation of 16.4 aJ per clock cycle at 5-GHz operation. Apart from CLAA, a 32-bit CSA employing 5-stage pipelined architecture on 0.25 um technology [20] achieves a maximum frequency of 1.67 GHz and utilizes 276 registers. Finally, a full adder circuit utilizing a TSPC logic [22] achieved a maximum frequency of 290 MHz on 0.8um standard CMOS technology.

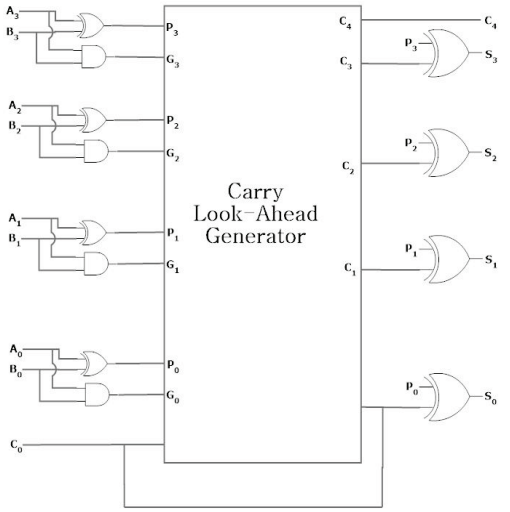

Fig. 2. 4-bit Carry Look-Ahead Adder [30]

The present paper proposes a novel parallel prefix adder that takes the advantage of both carry generating circuit of CLAA and multiplexing of CSA in the sequential sense. The proposed CSAA uses the MUXs which preselect the next four sum bits and their corresponding carry output. The proposed CSAA decreases the time delay without the use of parallel multiplier circuits. A reduction in time delay has been achieved mainly due to addition of four bits simultaneously instead of bit wise addition, as well as the sequential nature of the circuit. Analysis indicates that the performance of proposed CSAA improves with increase in number of bits. Further, the performance improvement has been achieved without making any changes in the structure of conventional logic gates. The next section gives a brief overview of the three basic sequential adders. Section IV presents the proposed adder and its result analysis. Finally, section V concludes the proposed work.

III. PRELIMINARIES

The smallest unit of an adder is a half adder (HA) [31]. An HA takes in two 1-bit input and consists of an AND gate and a

Fig. 3. *16-bit Sequential Carry Select Adder [30]*

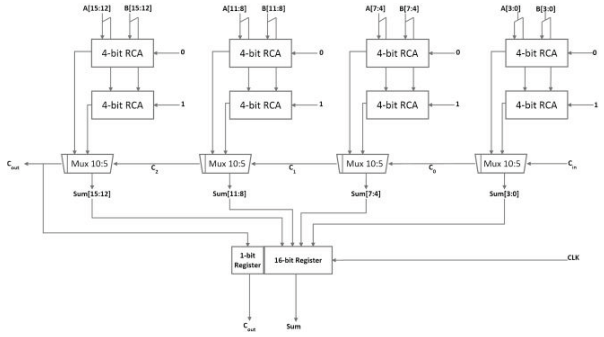

XOR gate. The output of the XOR gate and the AND gate gives the sum and carry of the addition operation respectively. Two HAs combined together along with a XOR gate form a Full Adder (FA) [28]. A FA takes in three 1-bit input and computes the sum and carry output of the respective addition of the three inputs.

The most common type of adder is RCA. A sequential block diagram of RCA is shown in Fig. 1. A 4-bit RCA [31] consists of four FAs joined together by output carry and input carry lines. The output carry of the first adder is input to the second adder, whereas output of the second adder is input to the second as the initial carry and so on. RCA consumes a lot of time in computing the sum of the two numbers as the second FA has to wait for the first FA to compute the sum, whereas the third FA waits for the second FA to compute the sum and so on. Hence, RCA has a large computation delay.

To overcome the disadvantage of RCA, CLAA [31] is used. CLAA generates all the output carries before computing the sum which reduces the waiting time of the adders. The equations of CLAA are given as follows:

$$Gi = Ai.Bi$$

To determine whether a bit pair will propagate a carry, either of the following logic statements work:

$$Pi = Ai \oplus Bi$$

Where Ai and Bi are the 4-bit inputs to the adder,

$$C1 = G0 + P0.C0$$

$$C2 = G1 + P1.C1$$

$$C3 = G2 + P2.C2$$

$$C4 = G3 + P3.C3$$

Substituting C1 into C2, then C2 into C3, then C3 into C4 yields the expanded equations:

$$C1 = G0 + P0.C0$$

$$C2 = G1 + P1.G0 + C0.P0.P1$$

$$C3 = G2 + P2.G1 + G0.P1.P2 + C0.P0.P1.P2$$

$$C4 = G3 + P3.G2 + G1.P2.P3 + G0.P1.P2.P3 + C0.P0.P1.P2.P3$$

Hence, with the reduction of the waiting time of the initial carry, the time period required for the clock also reduces. But for the generation of all the carries before the computation of the sum requires additional hardware which results larger area and more power consumption. The block diagram of CLAA is shown in Fig.2.

Another type of adder, CSA [26] takes advantage of the multiplexing action of multiplexers. A CSA pre-computes the

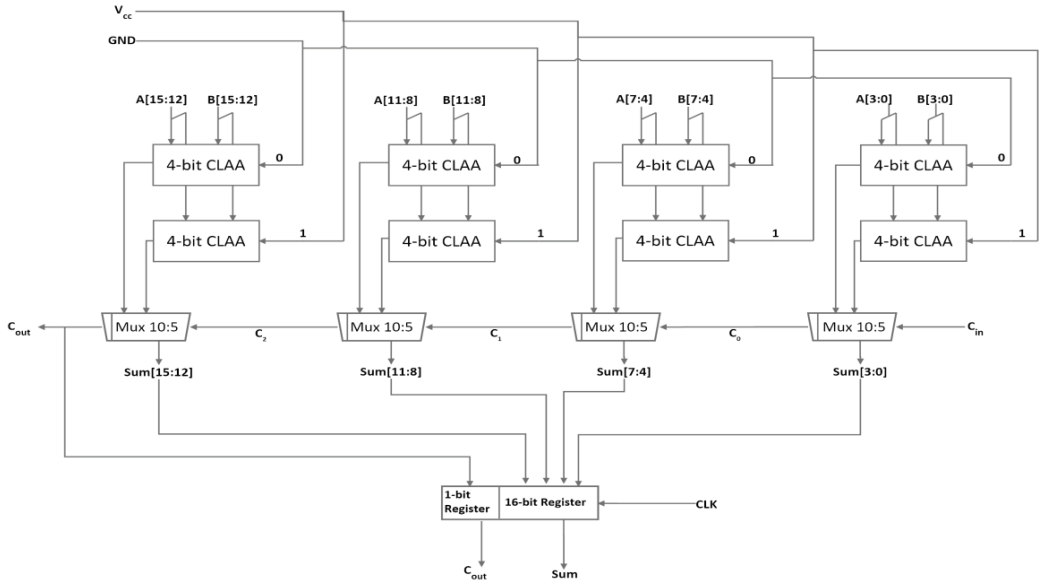

Fig. 1. *Proposed 16-bit Sequential Carry Select Adder*

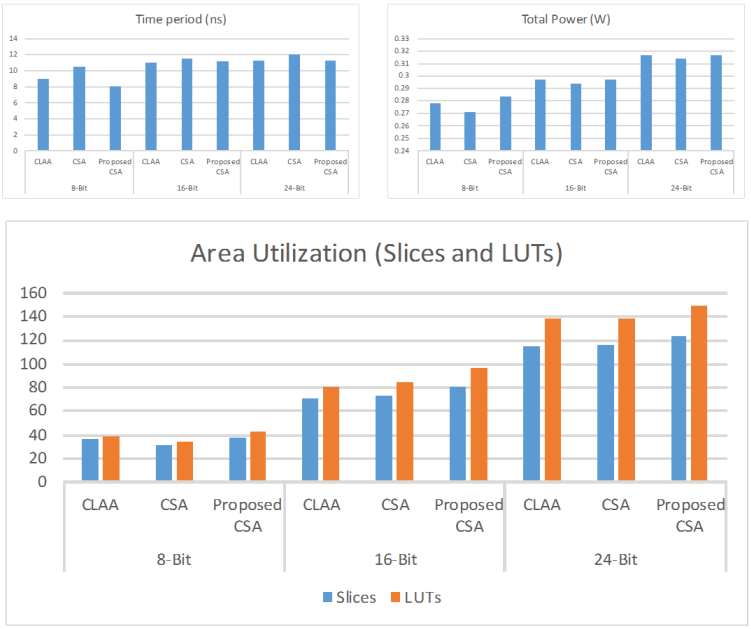

Fig. 5. Timing, Power and Area Parameters comparison among the adders

sum using all the possible combinations i.e. computes the sum for both 0 and 1 as input carries. When value of the original carry is known, it selects the appropriate sum and its output carry using a multiplexer. Area occupied by a CSA is equivalent to two RCAs and a multiplexer of the same number bits as that of the RCAs. A 16-bit sequential CSA can be created taking 4-bits a time, using eight 4-bit RCAs and three 10:5 MUX as shown in Fig. 3. The following section IV explains the architecture and working of the proposed adder, whereas section V and VI presents results and comparison.

IV. PROPOSED CSA

In the proposed CSA, several modifications have been done to decrease the combinational delay, time period of the clock and power consumed by the adder. In the present work, we have exploited the advantages of both CLAA and CSA by using CLAA's ability to generate carry bits before computing the sum and the multiplexing ability of CSA. In a conventional CSA where RCAs are used the multiplexer waits for the RCA to compute the sum and carry bits which then selects the next appropriate sum using the multiplexers. This renders the RCAs containing high order bits inactive as they have to wait for the carry which leads to increase in combinational delay and time period of the clock and also the dynamic power of the adder. The carry ahead generating capability of CLAA helps the RCAs to function simultaneously without waiting for the previous RCAs to compute the sum resulting in decrease in computational delay and dynamic power consumed.

TABLE I . COMPARISON OF ADDERS FOR AREA, POWER AND TIMING

Number of bits	Adder Type	Time period (ns)	Slices	LUTs	Total power (W)
8-Bit	CLAA	8.995	36	39	0.278
	CSA	10.49	32	34	0.271
	Proposed CSA	8.039	38	43	0.284
16-Bit	CLAA	10.966	71	81	0.297
	CSA	11.481	73	84	0.294
	Proposed CSA	11.171	81	97	0.297
24-Bit	CLAA	11.235	115	138	0.317
	CSA	12.004	116	138	0.314
	Proposed CSA	11.231	124	149	0.317

The proposed adder is similar to a traditional CSA. Fig 4 depicts the structure of 16-bit proposed CSA. The operations are divided by taking 4-bits at a time. A 16-bit proposed CSA consists of eight CLAAs and four 10:5 MUXs. The initial carry bit in four CLAA is connected to V_{cc} (+5V) and the remaining

four CLAA is connected to the ground (0V), and each output carry and sum computed by the CLAA is connected as the input of a 10:5 multiplexer, which is then selected by the output carry of the previous stage. In the 16-bit proposed CSAA, the first 2 CLAAs, which only differ in the initial carry bit i.e. 1 or 0, are used for adding the first four bits b(3)-b(0). The sum and the output carry of both CLAA is selected by the input carry of that stage using 10:5 Mux. Similarly, the output carry generated in this stage is used for selecting the output carry and the sum of the next two CLAAs which computed the addition of the next four bits b(7)-b(4). This same procedure takes place for the remaining sets of bits, which are, b(11)-b(8) and b(15)-b(12) and the output carry of the b(15)-b(12) bits is the output carry the whole 16-bit proposed CSA. Similarly, this same procedure can be extended for the required number of bits, taking any number of bits at a time.
A digital schematic for the proposed CSA is shown in fig. 6.

V. RESULTS AND COMPARISON

The architecture of the proposed CSA for 8-bit, 16-bit and 24-bit variants has been designed taking Verilog as the primary HDL and has been implemented on Virtex-7 using Vivado Design Suite 2014.4. For comparison, the 8-bit, 16-bit and 24-bit variants of CLAA, CSA and proposed CSA are also designed.
The following parameters of the circuit are taken into consideration and presented in Table 1:

1) *Time Period –: Units: ns (10^{-9} Seconds)*
2) *Slices*
3) *LUTs*
4) *Total Power –: Units: W (Watt)*

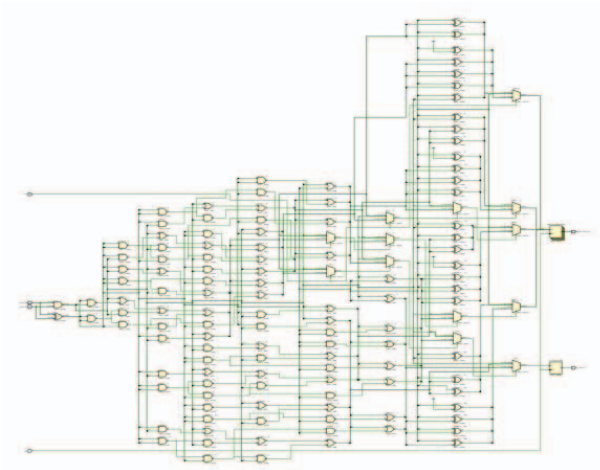

Fig. 6. Digital Schematic for the Proposed 16-bit CSA

Based on the above performance parameters, comparison analysis of the proposed CSA has been done with CSA and CLAA as shown in Table 1 and graphically depicted in Fig. 5. The result analysis clearly indicates the computation time achieved by proposed adder in its 8 and 24-bit variants in lower when compared to its conventional variant CLAA and CSA owing to the carry ahead generation technique of CLAA and multiplexing technique of CSA.
As is evident from Table 1 that the time period of the 8-bit variant of the proposed adder is 10.63 % less than the 8-bit variant of CLAA. However, on increasing the bits from 8 to 16, the timing performance of the proposed adder degrades when compared with the 16-bit variant of CLAA. On further increasing the number of bits to 24, the proposed CSA's timing performance improves and consumed 0.036 % lesser time period than the 2-bit variant CLAA. Moreover, all three variants of proposed CSA take 23.36 %, 2.7 % and 6.44 % lesser time period than the respective variants of CSA.
For the comparison in terms of power consumption, the performance of the proposed CSA increases with increase in the number of bits. The 8 and 16-bit variants of proposed CSA consume 2.16 % and 0 % more power than the 8 and 16-bit variants of CLAA. However, both 24-bit variants of proposed CSA and CLAA consume the same amount of power. On comparison with CSA, all the three variants of the proposed CSA consume more power than the three variants of CSA respectively.

VI. CONCLUSION

Adders are a key component in digital image processing, digital signal processing applications and general purpose microprocessors. The present paper proposes an architecture of adder that combines the multiplexing ability of CSA and CLAA's ability to generate carry bits before computing the sum to optimize the power consumed and computation time. Hardware for the proposed adder has been created taking Verilog as the primary language. Thorough simulation and analysis it can be said the proposed adder is efficient in terms of power and timing indicating the superiority of the proposed adder over conventional adders. The proposed adders find its applications in the areas where computation time and power consumed play an important role.

REFERENCES

[1] S.F. Oberman, "Design issues in high performance floating point arithmetic units," TR CSL-TR-96-711, Computer System Laboratory, Stanford University, 1996.

[2] M.J. Flynn, S.F. Oberman, "Advanced Computer Arithmetic Design," Wiley, New York, 2001.

[3] B. Parhami, "Computer Arithmetic. Algorithms and Hardware Designs," Oxford University Press, Oxford, 2000.

[4] Behnam Amelifard, Farzan Fallah, Massoud Pedram, "Closing the Gap between Carry Select Adder and Ripple Carry Adder: A New Class of Low-power High-performance Adders," Proceedings of the Sixth International Symposium on Quality Electronic Design (ISQED), 2005.

[5] G.A. Ruiz, "New static multi-output carry look ahead CMOS adders," IEE Proc. Circuits, Devices and Systems, vol. 144, no. 6, pp. 350-354, 1997.

[6] J.B. Kuo, H.J. Liao, H.P. Chen, "A BiCMOS dynamic carry look ahead adder circuit for VLSI implementation of high-speed arithmetic unit," IEEE J. of Solid-State Circuits, vol. 28, no. 3, pp. 375-378, 1993.

[7] G. Yang et al., "A 32-bit carry look ahead adder using dual-path all-N logic," IEEE Trans. on VLSI Systems, vol. 13, no. 8, pp. 992-996, 2005.

[8] C.-C. Wang et al., "A low power high-speed 8-bit pipelining CLA design using dual-threshold voltage domino logic," IEEE Trans. On VLSI Systems, vol. 16, no. 5, pp. 594-598, 2008.

[9] R. Zlatanovici, S. Kao, B. Nikolic, “Energy-delay optimization of 64-bit carry-look ahead adders with a 240ps 90nm CMOS design example,” IEEE J. of Solid-State Circuits, vol. 44, no. 2, pp. 569-583, 2009.

[10] K. Preethi, P. Balasubramanian, “FPGA Implementation of Synchronous Section-Carry Based Carry Look-ahead Adders,” 2nd International Conference on Devices, Circuits and Systems (ICDCS), 2014.

[11] P. Balasubramanian, D.A. Edwards, W.B. Toms, “Self-timed section carry based carry look ahead adders and the concept of alias logic,” Journal of Circuits, Systems and Computers, vol. 22, no. 4, pp. 1350028-1 – 1350028-24, April 2013.

[12] Y. Kim and L. S. Kim, “64-bit carry-select adder with reduced area,” Electron. Lett., vol. 37, no. 10, pp. 614–615, May 2001.

[13] Tyagi, “A reduced area scheme for carry-select adders,” IEEE Trans. on Computer”, IEEE Transactions on Computers, vol. 42, pp. 1163-1170, October 1993.

[14] G. A. Ruiz, M. Granda, “An area-efficient static CMOS carry-select adder based on a compact carry look-ahead unit,” Microelectronics Journal, vol. 35, no. 12, pp. 939-944, 2004.

[15] Y. He and C. H. Chang, “A Power-Delay Efficient Hybrid Carry-Lookahead/Carry-Select Based Redundant Binary to Two's Complement Converter,” IEEE Trans. Circuits Syst. I, Reg. Papers, vol. 55, no. 1, pp. 336 - 346, Feb. 2008.

[16] Neve, H. Schettler, T. Ludwig and D. Flandre, “Power-delay product minimization in high-performance 64-bit carry-select adders,” IEEE Trans. Very Large Scale Integration (VLSI) Systems, Reg. Papers, vol. 12, no. 3, pp. 235 - 244, March. 2004.

[17] Samiappa Sakthikumaran, S. Salivahanan, V. S. Kanchana Bhaaskaran, V. Kavinilavu, B. Brindha, C. Vinoth, “A Very Fast and Low Power Carry Select Adder Circuit,” 3rd International Conference on Electronics Computer Technology (ICECT), 2011.

[18] Shivani Parmar, Kirat Pal Singh, “Design of high speed hybrid carry select adder,” 3rd IEEE International Advance Computing Conference (IACC), 2012.

[19] Kuo-Hsing Cheng,Wen-Shiuan Lee and Yung-Chong Huang, “A 1.2V 500 MHz 32-bit Carry-Lookahead Adder,” 8th IEEE International Conference on Electronics, Circuits and Systems, 2001.

[20] Youngjoon Kim, Ki-Hyuk Sung, and Lee-Sup Kim, “A 1.67 GHz 32-bit Pipelined Carry-Select Adder Using the Complementary Scheme,” IEEE Symposium on Circuits and Systems (ISCAS), 2002.

[21] T. Enomoto, A. Hirobe, T. Satoh, M. Fujii, N. Yoshida, S. Wada and M. Tokushima, “A high-speed, low-power 16-bit 0.25 μm GaAs binary look-ahead carry (BLC) adder based on NOR gates for wireless video communication,” 1999 IEEE MTT-S International Topical Symposium on Technologies for Wireless Applications.

[22] Volker Schindler, “A Low-Power True Single Phase Clocked (TSPC),” Proceedings of the 22nd European European Solid-State Circuits Conference (ESSCIRC), 1996.

[23] H.Mahmoodi-Meimand, A.Afzali-Kusha and M.Nourani, “Adiabatic carry look-ahead adder with efficient power clock generator,” IEE Proceedings on Circuits, Devices & Systems, 2001.

[24] Robert Rogenmoser and Qiuting Huang, “An 800-MHz 1-pm CMOS Pipelined 8-b Adder Using True Single-phase Clocked Logic-Flip-Flops,” IEEE Journal of Solid-State Circuits, 1996.

[25] S. M. Rezaul Hasan and Chakaravarty D. Rajagopal, “Low Voltage Dynamic BiCMOS CLA circuit with Carry Skip Using Novel Full-Swing Logic,” IEEE Journal of Solid State Ciruits, 2002.

[26] M. Chanda, S. Naha, S. Manna, A. Dandapat and H. Rahaman, “Implementation of Ultra Low-Power 8 Bit CLA Using Single Phase Adiabatic Dynamic Logic,” 2010 International Conference on Advances in Recent Technologies in Communication and Computing (ARTCom).

[27] Se-Joong Lee and Hoi-Jun Yoo, “Race Logic Architecture (RALA): A Novel Logic Concept Using the Race Scheme of Input Variables,” IEEE Journal Of Solid-State Circuits, Vol. 37, No. 2, February 2002.

[28] K. Inoue, N. Takeuchi, Y. Yamanashi, N. Yoshikawa, “Simulation and Implementation of an 8-bit Carry Look-Ahead Adder Using Adiabatic Quantum-Flux-Parametron,” 2013 IEEE 14th International Superconductuve Electronics Conference (ISEC).

[29] Michael D. Ciletti, “Advanced Digital Design with the VERILOG HDL,” 2003.

[30] Samir Palnitkar, “Verilog HDL,” 2nd ed., IEEE 1364-2001 Compliant, 2003.

M. Morris Mano and Michael D. Ciletti, “Digital Design,” 4th ed.

Distributed Data Association Rule Mining: Tools and Techniques

Manoj Sethi
Department of Computer Science and Engineering,
Delhi Technological University (formerly DCE),
Shahbad Daulatpur, Delhi-110042, INDIA
Email ID: manojsethi@dce.ac.in

Rajni Jindal
Department of Computer Science and Engineering
Delhi Technological University (formerly DCE) Shahbad
Daulatpur, Delhi-110042, INDIA
Email ID: rajnijindal@dce.ac.in

***Abstract*-Distributed data mining (DDM) has become important research area with the increase in large distributed transactional databases and need to investigate important patterns in such databases. DDM may increase the processing capabilities but it increases communication and storage cost. Many algorithms and tools for mining association rules in distributed databases are proposed in literature. This paper illustrates some of the DDM algorithms and also tools proposed in literature for mining association rules in the distributed environment.**

Keywords-- frequent pattern; association rule; distributed data;

I. INTRODUCTION

The use of distributed database environment in place of centralised databases is increased, in which database is partitioned and stored at different locations, share the resources and perform parallel processing. A number of algorithms are available for association rules mining centralised databases but a few for distributed data mining. These algorithms which are available for the centralised database mining can't be used directly for distributed Data Mining (DDM). DDM requires local processing at all the sites to find the local frequent itemsets, communication between the sites and finally finding frequent global itemsets. This requires huge storage space, communication, synchronization and processing capabilities and trade-off between them.

II. LITRATURE SURVEY

A lot of research papers have been published in the area of DDM. In the Literature review on DDM for finding association rules, more than 35 research papers are reviewed and algorithms their variant and issues are studied. In the literature survey the algorithms for the distributed data mining for mining association rule were studied. The survey includes detailed study of the algorithms, tools, data sets, Issues and challenges in developing the algorithms in this area.

Distributed data may be incompatible [29] and DDM based on the extension set can solve this problem. An optimum solution is obtained [26] from DDM as it is done in parallel. The issues are Load Balancing, Minimizing communication and overlapping communication and computation. DDM pays important role [5] in bioinformatics where database is heterogeneous in the distributed environment. A grid can provide accurate representation of available resources [8] and it is future of DDM [6] and effective computational support [24, 32] for DDM where users have options to choose the resources. As the XML system is more complex [28], DDM is more challenging. In E-business lots of heterogeneous data is generated and are distributed [21] in data mining, Rough set theory is a powerful approach [13, 14] and can be used for decision making. Bin Liu [8] proposed a DDM architecture based on the grouping similar data source to reduce communication. DDM systems can be classified[7] based on (i) parallel data mining agents to enhance working efficiency (ii) meta learning to improve the quality of selection of data mining algorithm and (iii) grid to mine in geographically distributed environment. An efficient data structure [9] is required to store the information in mining tasks based on the algorithms. Frequent closed enumeration table (FCET) structure can save storage space and speed up producing the generalized association rules. The information is collected through e-CRM system which is mined by DDM and used for business decisions. The data streams mining [18] is more challenging in the distributed environment. The distributed mining has advantage in terms of degree of parallelism and scalability. ODAM algorithm proposed by [22] which is improved version of Apriori and based on CD and FDM algorithm. In which candidate support counts are not generated from the raw data set after the first pass. It removes infrequent itemsets, and places new transactions into memory. It reduces the transaction length and also data set size significantly. The distributed simulations are available and their acceptance is very much dependent on their methods and tools [2].

Approaches in Large-scale Data Analysis [3] are (i) MapReduce and (ii) Parallel DBMS. MapReduce is easy, more fault tolerance, but large performance panality as compared to parallel DBMS.

The algorithms proposed in the literature addressing different issues for DDM are given below. Moreover, some other findings in this domain are as follows.

III. RESEARCH ISSUES AND CHALLENGES

Issues in designing the DDM algorithms for mining association rules in the distributed data environment are to be

978-9-3805-4421-2/16/$31.00 ©2016 IEEE

addressed which are evaluated due to the distributed nature of the database. Algorithm addressing these issues and improving costs and performance etc, keeping tradeoff between them, is required to suit a particular distributed scenario. Following tables summerise the litrature survey.

Table 1 (a) shows distributed Data Association Rule Mining Issues addressed in litrature. These issues and challenges are not independent of each other. There are relationships between these issues in the sense that some are directly propotional and some are inversely propotional to with each other. On the basis of the size of the database, number of partitions, communication bandwidth availability, processing power and availible resourses the trade-off between them are required. Accoudingly the Inversely propotional issues are listed in table 1(b) and dicectly propotional issues are in table 1(c).

TABLE 1(A). DISTRIBUTED DATA ASSOCIATION RULE MINING ISSUES

Issues	**Descriptions**
Number of data scans[27]	Number of data scans require to find frequent itemsets and support count and it effects the performance
Number of candidate sets	Generated for finding frequent itemsets. Reduce number of candidate sets will reduce the communication overhead
Communication cost	Sites communicate FI and support counts. Reducing the number of messages between nodes will reduce the communication cost
Memory requirement	To store the local and global FI, transactions, support counts
Pruning	Prune out not frequent candidate sets
Synronisation	Needs between the nodes
Work load balancing at various nodes	One or all nodes participate in computing frequent itemsets to balance load
Rule redundancy	Only one node is finding FI for each itemset evenif some of the itemsets are frequent at more than one node
Scalability	Some of the algorithms are good for small database only and do not scale-up well
Skeness[23]	Data skewness may improve the performance by reducing communication
Data decomposition among nodes	May reduce the candidate sets and redundancy
High Dimensionality[25]	Handling the increase of number of dimension or items

TABLE 1(B). INVERSELY PROPOTIONAL ISSUES

Number of data scans	Memory /storage requirement
Skewness	Pruning
Pruning	candidate sets
Work load balancing	Communication, skewness

TABLE 1(C). DIRECTLY PROPOTIONAL ISSUES

Number of candidate sets	Communication
Communication	Synronisation
Rule redundancy	Communication
Good Data decomposition among nodes	Candidate sets, redundancy

Table 2 gives the Distributed data Association rule mining Algorithms along with their features, advantages and shortcomings. This survey also summarizes the list of activities (not-disjoint) which may be involved in distributed data mining in table 3. Lastly table 4 gives brief introduction of some of the widely used Data Mining Tools & Software available for researchers.

IV. CONCLUSION AND FUTURE SCOPE

This paper illustrates some of the algorithms proposed in the literature for mining association rules in distributed data mining domain and proposed solutions to some of the DDM issues. Apriori algorithm is the most popular algorithm for the centralized database. Most of the proposed algorithms used the concept of Apriori, CD algorithms and their variant for finding local frequent itemsets at different sites and used different techniques for further improvement in reducing data scan, storage cost and communication cost. Some of the algorithms and proposed techniques for reducing such costs are illustrated in the paper. In different implementations, resources like storage, processing capabilities, communication bandwidth, data volume varies and the challenge is to find the best suited algorithm and tradeoff between them for a particular distributed scenario. For mining data, different data mining tools are available that have implementation of different data mining algorithms.

The future works concentrate on implementing DDM algorithms on a cluster and also on Map-Reduce technology. Different data structures can be implemented to test the performance of the algorithms.

REFERENCES

[1] Ailing Wang(2009), "Research on Mining Association Rules in Distributed System", International Conference on Business Intelligence and Financial Engineering (IEEE), pp. 472-475, DOI: 10.1109/ BIFE.2009.113, 2009.

[2] Alois Ferscha, Janes Johnson and Stephen J. Turner(2001), "Simulation Performance data Mining", Elsevier : Future Generation Computer Systems 18 pp. 157-174, DOI:10.1016/S0167-739X(01)00050-4, 2001.

[3] Andrew Pavlo, Erik Paulson, Alexander Rasin, Daniel J. Abadi, David J. Dewitt, Samuel Madden, Michael Stonebraker(2009), "A Comparison of Approaches to Large-Scale Data Analysis", Proceedings of the 35th SIGMOD International Conference on Management of Data, (SIGMOD '09), pp. 165-178, DOI:10.1145/1559845.1559865, July 2009.

[4] Assaf Schuster and Ran Wolff(2001), "Comunication-Efficient Distributed Mining of Association Rules", Proceedings of the 2001 ACM SIGMOD international conference on Management of data (SIGMOD '01) pp.473-484, DOI:10.1023/B:DAMI. 0000015870. 80026.6a, May 2001.

[5] Azra Shamim, Maqbool Uddin Shaikh, Saif Ur Rehman Malik(2010), "Intelligent Data Mining in Autonomous Heterogeneous Distributed Bio Databases", Proceedings of the ICCEA 2010: Second International Conference on Computer Engineering and Applications, IEEE Computer Society Washington, DC, USA, Vol. 1 pp. 6-10, DOI: 10.1109/ICCEA.2010.9, 2010.

[6] Bagrudeen Bazeer Ahamed and Shanmugasundaram Hariharan(2011), "A Survey On Distributed Data Mining Process Via Grid", International Journal of Database Theory and Application, Vol. 4, No. 3, September, 2011.

[7] Bin Liu, Shu-Gui Cao, Qing-Chun Li and Qi Li(2011), "A Hierarchical Distributed Data Mining Architecture", IEEE Proceeding of the 11th International Conference on Machine Learning and Cybernetics (ICMLC), (IEEE) Guilin, Vol. 1, pp.40-44, DOI: 10.1109/ICMLC.2011.6016720, July 2011.

[8] Bin Liu, Shu-Gui Cao, Xiao-Li Jia Zhao-Hua Zhi(2010), "Data Mining in Distributed Data Environment", Proceeding of the Ninth International Conference on Machine Learning and Cybernetics (ICMLC), IEEE, pp. 421-426, DOI: 10.1109/ICMLC.2010.5581024, July 2010.
[9] Chieh-Ming Wu and Yin-Fu Huang(2008), "An Effective Data Structure for Mining Generalized Association Rules", IEEE Fifth International Conference on Fizzy Systems and Knowledge Discovery, DOI: 10.1109/FSKD.2008.609_, 2008.
[10] Chunhua Ju and Dongjun Ni (2008a), "Mining frequent Closed Itemsets from Distributed Dataset", International Symposium on Computational Intelligence and Design, IEEE Computer Society, DOI: 10.1109/ISCID.2008.24_, 2008.
[11] Chunhua Ju and Dongjun Ni (2008), "Distributed Mining Model and Algorithm of Association Rules for Chain Retail Enterprise", IEEE: ISECS International Colloquium on Computing, Communication, Control, and Management, DOI: 10.1109/CCCM.2008.129, 2008.
[12] Chunhua Wang Houkuan Huang and Honglian Li (2000), "A Fast Distributed Mining Algorithm for Association Rules With Item Constraints", IEEE International Conference on Systems, Man, and Cybernetics, Nashville, TN, DOI: 10.1109/ ICSMC.2000.886390_, 2000.
[13] Dan Hu, Xianchuan Yu and Yuanfu Feng (2008a), "Distributed Mining Core of Attributes on Horizontally Partitioned Data", IEEE Pacific-Asia Workshop on Computational Intelligence and Inductrial Application, DOI: 10.1109/PACIIA.2008.114, 2008.
[14] Dan Hu, Xianchuan Yu and Yuanfu Feng (2008b), "Distributed Mining Reducts of Attributes on Horizontally Partitioned Data",IEEE Second International Symposium on Intelligent Information Technology Application IITA, DOI: 10.1109/ IITA.2008.398_, 2008.
[15] David W. Cheung, Jiawei Han, Vincent T. Ng, Ada W. Fu and Yongjian Fu(1996), "A Fast Distributed Algorithm for Mining Association Rules", Proceedings of the fourth international conference on Parallel and distributed information systems, IEEE Computer Society Washington, DC, USA, pp. 31-43, DOI: 10.1109/PDIS.1996.568665_, 1996.
[16] David W. Cheung, Vincent T. Ng, Ada W. Fu and Yongjian Fu(1996a), "Efficient Mining Of Association Rules In Distributed Databases", IEEE Transactions On Knowledge And Data Engineering, Vol. 8, No, 6, Digital Object Identifier: 10.1109/69.553158, December 1996.
[17] Dennis Wegener, Michael Mock, Deyaa Adranale and Stefan Wrobel (2009), "Toolkit-based high-performance Data Mining of Large Data on MapReduce Clusters", Proceeding ICDMW '09 Proceedings of the 2009 IEEE International Conference on Data Mining Workshops, pp. 296-301, DOI: 10.1109/ICDMW.2009.34 , 2009.
[18] Eugenio Cesario, Antonio Grillo, Carlo Mastroianni and Domenico Talia(2011), "A Sketch-based Architecture for Mining Frequent Items and Itemsets for Distributed Data Streams", 11th IEEE/ACM International Symposium on Cluster, Cloud and Grid Computing, DOI: 10.1109/CCGrid.2011.45, 2011.
[19] J. Arokia Renjit and K. L. Suunmuganathan(2010), "Mining the Data from Distributed Database Using and Improved Mining Algorithm", (IJCSIS) International Journal of Computer Science and Information Security, Vol.7 No.3, March 2010.
[20] Lijuan Zhou, Shuang Li and Mingsheng Xu(2010), "Research on Algorithm of Association Rules in Distributed Database System", 2nd International Asia Conference on Informatics in Control, Automation and Robotics (IEEE) pp. 216-219, DOI: 10.1109/ CAR.2010.5456669, 2010.
[21] Longyi Li and Lihua Tao(2009), "Study of e-CRM based on Distributed Data Mining", International Conference on Management and Service Science, MASS 2009. IEEE Computer Society, DOI: 10.1109/ICMSS.2009.5302106, 2009.
[22] Mafruz Z. Ashrafi, Taniar, D. and Smith, K.(2004), "ODAM: An Optimized Distributed Association Rule Mining Algorithm" Distributed Systems Online, IEEE, Vol.5, Issue: 3, DOI: 10.1109/MDSO.2004.1285877, 2004.
[23] M. E. Otey C. Wang S. Parthasarathy, A. Veloso and W. Meira Jr.(2003), "Mining Frequent Itemsets in Distributed and Dynamic Databases", Proceedings of the Third IEEE International Conference on Data Mining (ICDM'03), Nov. 2003.
[24] Mario Cannataro, Antonio Congiusta, Andrea Pugliese and Domenico Talia(2004), "Distributed Data Mining on Grids: Services, Tools and Applications", IEEE Transactions on Systems, Man, and Cybernetics, Part B: Cybernetics, Vol.34, No.6, DOI: 10.1109/ TSMCB.2004.836890, 2004.
[25] Mohammed J. Zaki(1999), "Parallel and Distributed Association Mining: A Survey", Journal of IEEE Concurrency, Vol. 7 Issue 4, pp. 14-25, October 1999. Digital Object Identifier: 10.1109/4434.806975
[26] Pallavi Dubey(2012), "Association Rule Mining on Distributed Data" International Journal of Scientific & Engineering Research, Vol. 3, Issue 1, January 2012
[27] Sotiris Kotsiantis and Dimitris Kanellopoulos (2006), "Association Rules Mining: A Recent Overview", GESTS International Transactions on Computer Science and Engineering, Vol.32 (1), pp. 71-82, 2006.
[28] Sujni Paul(2010), "An Optimized Distributed Association Rule Mining Algorithm in Parallel and Distributed Data Mining with XML Data for Improved Response Time", International Journal of Computer Science and Information Technology, Vol.2, No.2, 2010.
[29] Vuda Sreenivasarao, Rallabandi Srinivasu, Prof. G.Ramaswamy, Nagamalleswara Rao Dasari and Dr. S Vidyavathi (2010), "The Research of Distributed Data Mining Knowledge Discovery Based on Extension Sets", International Journal of Computer Applications (0975 – 8887) Vol.8– No.2, DOI: 10.5120/1187-1658, October 2010.
[30] Wang Ailing(2011), "An improved Distributed Mining Algorithm of Association Rules", Journal of Convergence Information Technology, Vol. 6, No. 4, DOI:10.4156/jcit. Vol 6. Issue4.14, April 2011.
[31] Wei Fan and Albert Bifet (2013), "Mining Big Data: Current Status and Forecast to the Future", ACM SIGKDD Explorations Newsletter, Vol. 14 Issue 2, pp. 1-5, DOI:10.1145/2481244.2481246, December 2012.
[32] Wu-Shan Jiang and Ji-Hui Yu(2005), "Distributed Data Mining on the Grid", Proceedings of the fourth International Conference on Machine Learning and Cybernetics, IEEE, DOI: 10.1109/ ICMLC.2005.1527275_, 2005.
[33] Xindong Wu, Xingquan Zhu, Gong-Qing Wu and Wei Ding (2014), "Data Mining with Big Data", IEEE Transactions on Knowledge and Data Engineering, Vol. 26, No. 1, DOI: 10.1109/TKDE.2013.109_, January 2014.

TABLE 2. DISTRIBUTED DATA ASSOCIATION RULE MINING ALGORITHMS

AlgorithmName	Based on Basic mining	Important features	Advantages	Shortcomming / future work
AprTidRec[1,30]	Apriori	A record structure TidRec for each candidate frequent itemset Only joint step, no pruning Junk mail database(ordinal) Data source http://www.ics.uci.edu/~mlearn	scan local database only once I/O spending is saved Efficiency is improved short time complexity (less run time) reduced commu. Cost When support is decreased, runtime improves	Large memory space required when database is large To be tested on non-isomorphic data sources How to balance between time and space complexity
Fast Distributed Mining of	Apriori, CD	Users relationships between locally large and globally large	Small no. of candidate sets Reduces the no. of messages	Not effective for large partition

Association Rules (FDM),FDM-LP, FDM-LUP, FDM-LPP[15]		itemset Polling site for every locally large itemset is responsible for finding globally large itemset Three optimization – local purning, global pruning and count polling	O(n) for support counts exchange Less communication cost More effective when scale-up Effectice pruning technique	Overhead of Parallel Virtual Machine needs more synchronization skewness may improve the performance relationship between candidate sets and pruning
CD [20]	Apriori	Parallelization of Apriori Assumes datasets are horizontally fragmented Generate candidate sets at every site using apriori Broadcast local support count to all sites	Local support count of every candidate itemset is broadcast from every site to every site Only one synchonization per iteration needed	Not scalable to large no. of partitions Does not use memory effectively No. of message required for count exchange $O(n^2)$ High no. of candidate sets
DD [22]	Apriori	candidate set are evenly distributed among nodes uses total system memory generates disjoint candidate sets full database exchange per iteration	reduce no. of candidate set to be scanned when nodes increases utilizes memory efficiently	more traffic between nodeslong high communication overhead performed poorly as compared to CD
Distributed Mining of Association Rules (DMA)[16]		Optimization technique used to eliminate the duplication form the candidate sets. no scan the partition for support count	DMA performed better when the number of nodes are higher	Only Nodes having having identical schemas used Storage for message and support counts reqd
Distributed Decision Miner -DDM [4]	Apriori, CD	Unskewed data It verifies that an itemset is large before collecting its support counts from all nodes	Scaleable Data skew robustness less communication	more storage,
Distributed Mine Closed Itemsets DMCI[10]	FCIM	Small subset of FI but represent same knowledge all candidate sets are closed non-closed itemsets are pruned	communication load between different sites is small reduce problem complexity find non-redundant association rule	time consuming several data scans
Chain Retail Enterprise based on Massed Learning CREMLM Algorithm[11]		Large-scale retail chain enterprises many branch stores large communication bandwidth transaction data is low globally frequent prune on one store brach stores don't communicate with each other	Low communication frequency Communication frequency complexity is O(n)	High data scans Low local mining efficiency Perform better than CREDLM when minsup is high
Chain Retail Enterprise based on Dispersed Learning CREDLM Algorithm [11]		Small-scale retail chain enterprises few branch stores small communication bandwidth transaction data is large globally frequent prune on many stores	low communication load	High data scans Not scale up with no of sites as communication load increases Communication frequency complexity is $O(n^2)$ Perform better than CREMLM when minsup is low
DMCA[12]	FDM	integrates the item constraints into the mining process saves the local counts in hash tables	execution time improves as compared to FDM reduces data set scans and communication cost	tested on boolean constraints only
LMatrix[19]	Apriori, FDM	creates the local LMatrix to calculate local support A pre-fix tree structure FP-tree is used reduces size of transaction and datasets stores transactions in binary matrix	saves time to scan reduces communication cost reduces size of messages	consumes more memory execution time increases when data size increases and minimum support threshold decreases

TABLE 3. LIST OF ACTIVITIES (NOT-DISJOINT) IN DISTRIBUTED MINING

Activity	Definition
Local frequent itemset (FI)	The itemsets that meet a user-specified minimum support at each node. A frequent itemset is maximal if it is not subset of any other frequent itemset.
Local purning	Removing the infrequent itemsets from candidate sets at each node Reduces number of candidate sets, cut communication cost
count polling	A polling site is assigned to itemsets X independent of the site where X is locally large. Polling site responsibility to find whether X is globally large. It broadcast requests to collect local support counts for X and compute global support count.
Skewness	Distribution of itemsets among the various partitions A database's total data skewness is the sum of the skew of all itemsets weighted by their supports. Most algorithms require low data skewness for good load balancing.
Catedate set generation	Candidates are generated in parallel. Each processor generates its own local set
Communicating Local FI	Communication between sites or central site with other sites sending FI by message passing
Data scanning	scanning transactions in the database to compute FI
Data storage	Storage is required on each site for storing local support counts, transactions, FI etc
Global pruning	Additional pruning is being done to global frequent itemsets. The efficiency of local pruning can be enhanced by global pruning
Finding Association rule	According to the global frequent itemsets and minimum support, association rules based on the global database can be acquired

TABLE 4. DATA MINING TOOLS & SOFTWARE

Mining tool	Features	Techniques/Tools
Weka [17]	Based on Parallel & Map Reduce Memnory limitation with large dataset Visualization Open source Good for developing new machine learning schemes	Association, Clustering, Classification, Regression, Pre-processing
Apache Hadoop[31,33]	Single mining task is split into many small tasks. Each task runs on on one or many computing nodes Batch-oriented parallel computing model require Sun JDK	Based on MapReduce
RapidMiner	Open source data mining tool Transparent data handling Scripting language based on XML Run on Every major platform	classification, regression, deviation detection, clustering, association, sequential Pattern analysis
Oracle Mining	operate on relational tables multidimansional data analysis	Association, Clustering, Classification, Prediction, Regression, deviation detection
IBM SPSS Modeler / Clementine	visual programming or *data flow* interface Commercial software Graphical interface can access both structured and unstructured data	Association, Clustering Classification, Prediction
IBM Intellegent Miner	Tightly integrated with IBM DB2 DBMS Scalable Visualization	Association, Clustering, Classification, Prediction, Regression, sequential Pattern analysis
MOA	large data mining open source software use simple XML	classifcation, regression, clustering and frequent item set, frequent graph mining

Optical Materials xxx (2016) 1–9

Contents lists available at ScienceDirect

Optical Materials

journal homepage: www.elsevier.com/locate/optmat

Dy^{3+} ions doped single and mixed alkali fluoro tungsten tellurite glasses for LASER and white LED applications

Ch. B. Annapurna Devi [a], Sk. Mahamuda [a], M. Venkateswarlu [a], K. Swapna [a], A. Srinivasa Rao [a, b, *], G. Vijaya Prakash [c]

[a] Department of Physics, K.L. University, Vaddeswaram 522 502, Guntur (Dt), A.P., India
[b] Department of Applied Physics, Delhi Technological University, Bawana Road, New Delhi 110 042, India
[c] Nanophotonics Lab, Department of Physics, Indian Institute of Technology, Hauz Khas, New Delhi 110016, India

ARTICLE INFO

Article history:
Received 3 August 2016
Received in revised form
17 October 2016
Accepted 12 November 2016
Available online xxx

Keywords:
Dysprosium
Tellurite glasses
Radiative properties
Photoluminescence
Quantum efficiency

ABSTRACT

A new-fangled series of Dy^{3+} ions doped Single and Mixed Alkali Fluoro Tungsten Tellurite Glasses have been prepared by using melt quenching technique and their spectroscopic behaviour was investigated by using XRD, optical absorption, photoluminescence and lifetime measurements. The bonding parameter studies reveal the ionic nature of the Dy–O bond in the present glasses. From the absorption spectra, the Judd-Ofelt (J-O) intensity parameters have been determined and in turn used to determine various radiative properties for the different emission transitions from the $^4F_{9/2}$ fluorescent level. The photoluminescence spectra of all the glasses exhibit two intensified peaks in blue and yellow regions corresponding to the transitions $^4F_{9/2} \rightarrow {}^6H_{15/2}$ (483 nm) and $^4F_{9/2} \rightarrow {}^6H_{13/2}$ (575 nm) respectively. From the photoluminescence spectra, it is observed that the luminescence intensity is maximum for Dy^{3+} ion doped potassium combination of tungsten tellurite glass (TeWK:1Dy). The highest emission cross-section and branching ratio values observed for the $^4F_{9/2} \rightarrow {}^6H_{15/2}$ and $^4F_{9/2} \rightarrow {}^6H_{13/2}$ transitions suggest the possible laser action in the visible region from these glasses. By correlating the experimental lifetimes (τ_{exp}) measured from the decay spectral features with radiative lifetimes (τ_R), the quantum efficiencies (η) for all the glasses have been evaluated and found to be maximum for potassium combination tungsten tellurite (TeWK:1Dy) glass. The CIE colour chromaticity coordinates (x, y), (u, v), colour correlated temperature (CCT) and Y/B ratio were also estimated from the photoluminescence spectra for different compositions of glasses. The chromaticity colour coordinates evaluated for all the glasses fall within the white light region and white light emission can be tuned by varying the composition of the glass. From all these studies, it was concluded that 1 mol% of Dy^{3+} ions doped TeWK glass is more suitable for lasing and white-LED applications.

© 2016 Elsevier B.V. All rights reserved.

1. Introduction

Rare earth ions doped glasses are exhibiting applications in diversified fields of science and technology such as bulk lasers, optical fiber amplifiers and waveguide lasers. In recent times, the applications possessed by rare earth doped glasses are not only confined to infrared optical devices, but also spread in the area of visible optical devices, especially for white light emitting diode (w-LED) applications such as indicators, back light, automobile headlights and general illumination [1]. In the current research, white light emitting diodes (w-LEDs) which are also known as next generation of solid state lighting (SSL) technology has become very popular because of their potential applications in diversified fields [2]. The wide spread of SSL is of great importance to reduce significantly the global electricity consumption and the usage of fossil fuels [3]. The w-LEDs have several superior features such as high luminous efficiency, long operation lifetime reliability, safety and environmental friendly characteristics when compared with other conventional sources such as incandescent and fluorescent lights [4]. Currently, these w-LEDs are made up of by the combination of blue light emitting diode (LED) (GaN-blue chip) chip with yellow phosphor (yellow YAG: Ce^{3+} phosphor) [5]. In this method,

* Corresponding author. Department of Applied Physics, Delhi Technological University, Bawana Road, New Delhi 110 042, India. Tel.: +91 85860 39007; fax: +91 01127871023.
E-mail address: drsrallam@gmail.com (A. Srinivasa Rao).

http://dx.doi.org/10.1016/j.optmat.2016.11.016
0925-3467/© 2016 Elsevier B.V. All rights reserved.

Please cite this article in press as: C.B. Annapurna Devi, et al., Dy^{3+} ions doped single and mixed alkali fluoro tungsten tellurite glasses for LASER and white LED applications, Optical Materials (2016), http://dx.doi.org/10.1016/j.optmat.2016.11.016

the desired white light can be produced by exciting the yellow phosphor with blue LED. Due to lack of red component in their spectra, these w-LEDs possess low colour rendering index (CRI) (R_a = 60–75 range) and high correlated temperature (CCT ~ 7750 K). To improve the CRI to the acceptable range (>80) and the light conversion, a small amount of red phosphor will be introduced (YAG:Ce) [6–8]. But, the individual degradation rates of the blue LED chip and the phosphors coated on the chip would cause chromatic aberration and poor white light performance. To overcome this difficulty, it is necessary to develop novel materials which can emit bright white light by ultraviolet (UV) excitation [9,10]. At present w-LEDs, were constructed by mixing the phosphor powder with an epoxy resin that enables its coating on the chip. Due to the large difference between the refractive index of the phosphors and the epoxy resins, the scattering of light becomes high and heat resistance becomes very low which in turn leads to decrease in luminous intensity and a change of luminescence colour over a period. Not only this, the lifetime of LEDs also decreases due to the aging of organic epoxy resins under the long-term irradiation of UV light [11–13]. To overshoot the aforementioned problem, quite recently, the trivalent rare earth ions doped luminescent materials such as glasses and glass-ceramics have been synthesized and tested as an alternative for phosphor powders, since they can be suitably prepared in a plate like shape to ensure the direct encasement of the UV chip [14]. Apart from this, rare earth doped glasses are capable to showcase their superior nature from the perspective of homogeneous light emitting capacity, simple manufacturing procedure, lower production cost and excellent thermal and mechanical stability when compared with their conventional phosphor counterparts such as Li-α-SiAlON:Eu^{2+},Ca-α-SiAlON:Eu^{2+}, $Ba_3MgSi_2O_8$:Eu^{2+}, Mn^{2+} used in w-LEDs [1]. The aforementioned scientific patronages offered by rare earth doped glasses in the field of optoelectronics devices prompted us to take up the present investigation.

Fluoro Tungsten Tellurite glasses with alkali content in mixed and unmixed form were chosen with different compositions as our host glass material because of the unique properties of tellurium, tungsten and alkali fluorides (KF, LiF and NaF) as network modifiers.

The additions of mixed alkalies to these glasses are responsible for the non-linear variation of properties. This is really a remarkable change in the properties related to alkali ion transport. Due to the addition of mixed alkalies internal friction, dielectric loss, viscosity and glass transition etc also varies [15]. Now a days, tellurite glasses become more attractive because of their special physical properties such as high dielectric constant, low melting point (800 °C) and low phonon energies (780 cm^{-1}) [16]. In addition to the above, they are non-hygroscopic in nature and transparent from visible to IR regions. They are also used as nonlinear optical materials due to the unusual glass forming properties of tellurium dioxide (TeO_2). Even it is a four-coordinate; it is only a conditional glass former and by itself it doesn't form any glass but the addition of MO (M = Pb, W, Nb, Zn, Ba, etc.) increases the glass forming ability along with stability. The addition of alkali fluorides to TeO_2-WO_3 glass decreases the phonon energies by modifying the glass structure and by increasing the mechanical strength of the glass.

Among all the trivalent rare earth ions, the luminescent properties of Dy^{3+} ions have attracted special attention because of the interesting wavelengths produced by transitions between its intra 4f levels. The Dy^{3+} doped materials (glasses/phosphors) gained so much of interest among the researchers as it capable of giving two intense emission bands; one in blue (483 nm, $^4F_{9/2} \rightarrow {}^6H_{15/2}$) and the other one in yellow (574 nm, $^4F_{9/2} \rightarrow {}^6H_{13/2}$) region [17]. White light emission is possible with the suitable adjustment of the Y/B luminescence intensity ratio by changing the content of Dy^{3+} and/or composition of the host material [17]. The transition $^4F_{9/2} \rightarrow {}^6H_{13/2}$ (electric dipole) is a hypersensitive transition ($|\Delta L| \leq 2$ and $|\Delta J| \leq 2$) and its intensity depends upon the host material whereas the intensity of the transition $^4F_{9/2} \rightarrow {}^6H_{15/2}$ (magnetic dipole) is less sensitive to the host environment. In the present work, spectroscopic properties of different compositions of single and mixed alkali fluoro tungsten tellurite glasses doped with dysprosium were studied to check the suitability of these glasses for laser emission and white light generation.

2. Experimental

The glass samples used in the present work were prepared by conventional melt quenching technique with the following compositions.

TeWLi: $59TeO_2 - 20WO_3 - 20LiF - 1Dy_2O_3$

TeWNa: $59TeO_2 - 20WO_3 - 20NaF - 1Dy_2O_3$

TeWK: $59TeO_2 - 20WO_3 - 20\ KF - 1Dy_2O_3$

TeWLiNa: $59\ TeO_2 - 20WO_3 - 10LiF - 10NaF - 1Dy_2O_3$

TeWNaK: $59TeO_2 - 20WO_3 - 10NaF - 10KF - 1Dy_2O_3$

TeWLiK: $59TeO_2 - 20WO_3 - 10LiF - 10KF - 1Dy_2O_3$

Analar grade chemicals such as TeO_2, WO_3, LiF, NaF, KF and Dy_2O_3 were used as the starting materials to prepare the glasses used in the present work. All the chemicals were weighed as per the composition given above and trampled in an agate mortar until a smooth and homogeneous mixture was obtained. Further such homogeneous mixture collected into a silica crucible was heated at 750 °C in an electric furnace for about 30 min to obtain bubble free homogeneous melt. Such melts were then quenched suddenly on a pre-heated brass mould and pressed quickly by another brass mould. The glass samples thus prepared were subsequently annealed at 400 °C for 4 h to remove thermal strains/cracks produced inside and then allowed to cool down to the room temperature. The glass samples prepared thus are polished to a higher degree smoothness before going for the spectral measurements. The densities were measured by employing the Archimedes method using water as an immersion liquid. The refractive indices of these glasses were measured by Brewster's angle method using He–Ne laser (650 nm line) as the source. The optical absorption spectra of the samples were recorded at room temperature in the spectral wavelength range covering 800–2000 nm with a spectral resolution of 0.1 nm using a JASCO model V-670 UV–vis–NIR spectrophotometer. The photoluminescence excitation and emission spectra for all the glasses were recorded using RF-5301PC Spectrofluorophotometer at room temperature. The time-resolved photoluminescence (PL) measurements were carried out using home-built setups with 445 nm (CW laser) laser as an excitation source. The emission from sample was coupled into a monochromator (Acton SP2300) coupled to CCD (charge coupled detector) through the appropriate lenses and filters. For time-resolved photoluminescence, a frequency generator (5 Hz), lock-in amplifier, digital storage oscilloscope and a monochromator (Acton SP2300) coupled to a photomultiplier tube (PMT) were employed.

3. Results and discussion

3.1. XRD spectral analysis

XRD studies have been carried out to differentiate the crystalline

Please cite this article in press as: C.B. Annapurna Devi, et al., Dy^{3+} ions doped single and mixed alkali fluoro tungsten tellurite glasses for LASER and white LED applications, Optical Materials (2016), http://dx.doi.org/10.1016/j.optmat.2016.11.016

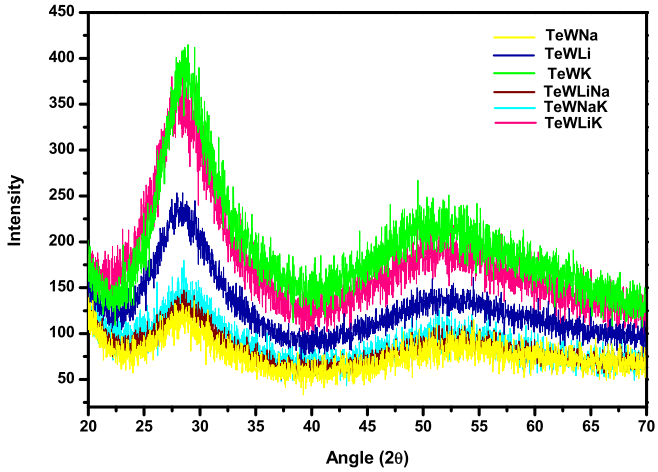

Fig. 1. X- Ray diffraction profiles of Dy^{3+} ions doped single and mixed alkali fluoro tungsten tellurite glasses.

and non-crystalline nature of the as prepared glasses. All the XRD profiles illustrate the similar patterns for all glass samples and are shown in Fig. 1. In Fig. 1 no distinguishable intensity peaks were observed, but at low scattering angles a broad dispersion was observed, which is an indication of the glassy/amorphous nature of the prepared glass systems.

3.2. Physical properties

To study the structural modifications of the glass network, the two important necessary parameters are density and refractive index. The measured values of density and refractive indices with the variation of alkali and mixed alkalis are shown in Fig. 2. By using these parameters, different physical properties were measured like average molecular weight, Dy^{3+} ion concentration, Mean atomic volume, dielectric constant, optical dielectric constant, reflection losses, molar refraction, polaron radius, inter atomic distance, molecular electronic polarizability, field strength and optical basicity and are given in Table 1. In the present glasses, TeWNa glass possesses maximum value of refractive index because of high polarzability value which causes the non linearity behaviour in materials. The maximum value of density and molar volume indicate that the non-bridging oxygen (NBOs) increases in the glass network. The variations in electronic polarizabiltiy values are responsible for the variation in dielectric and optical dielectric constant values [18]. The optical basicity [19] indicates the average electron donating power of the medium to the oxide atoms present in that medium. Among all the glasses TeWK glass possesses maximum value of optical basicity which is an evidence for the strong covalency in the cation-oxygen bonding.

3.3. Absorption spectral analysis (oscillator strengths-nephlauxetic ratio-J-O parameters)

The absorption spectra recorded for all the glasses in the wavelength range 600–2000 nm are shown in Fig. 3. As shown in Fig. 3, the absorption spectra of all the glasses show six well resolved absorption peaks obtained from the ground state $^6H_{15/2}$ to various exited states $^6F_{3/2}$ (~755 nm), $^6F_{5/2}$ (~806 nm), $^6F_{7/2}$ (~909 nm), $^6H_{7/2}$ (~1095 nm), $^6H_{9/2}$ + $^6F_{11/2}$ (~1282 nm), $^6H_{11/2}$ (~1684 nm). Though all the glasses were prepared with different compositions, they appeared same in their peak positions with little variation in their intensities. All the peak positions of glasses are given in Table 2. These peaks are identified mainly based on the Carnall et al. [20]. Using these values, bonding parameters of all the

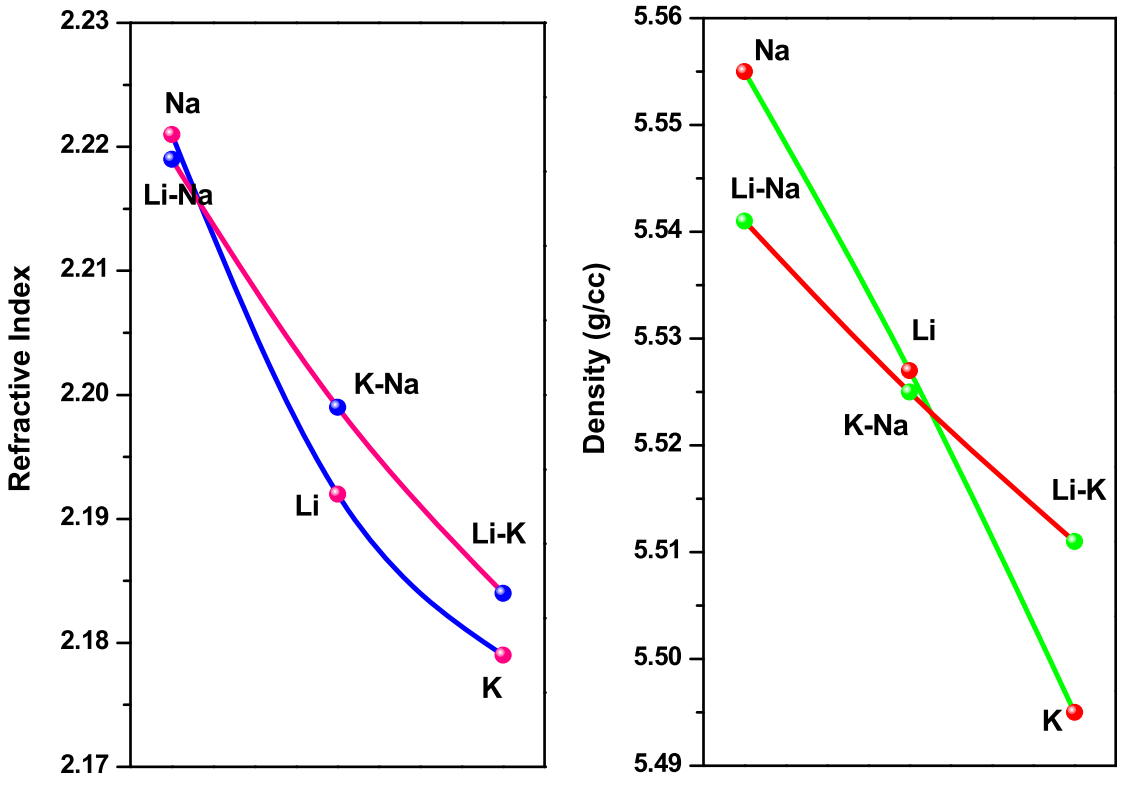

Fig. 2. Variation of densities and refractive indices of Dy^{3+} ions doped single and mixed alkali fluoro tungsten tellurite glasses.

Please cite this article in press as: C.B. Annapurna Devi, et al., Dy^{3+} ions doped single and mixed alkali fluoro tungsten tellurite glasses for LASER and white LED applications, Optical Materials (2016), http://dx.doi.org/10.1016/j.optmat.2016.11.016

Table 1
Physical properties of Dy^{3+} ions doped single and mixed alkali fluoro tungsten tellurite glasses.

Physical property	TeWNa	TeWLi	TeWK	TeWLiNa	TeWNaK	TeWLiK
Refractive index (n_d)	2.221	2.192	2.179	2.219	2.199	2.184
Density, d (gm/cm^3)	5.555	5.527	5.495	5.541	5.525	5.511
Average molecular weight, $\overline{M}$(g)	152.7	149.5	155.8	151.1	154.3	152.7
Dy^{3+} ion concentration, N (10^{22} ions/cm^3)	2.191	2.227	2.123	2.209	2.157	2.174
Mean atomic volume (g/cm^3/atom)	9.100	8.950	11.480	9.027	9.246	9.173
Optical dielectric constant ($p\partial t/\partial p$)	3.933	3.805	3.748	3.924	3.836	3.770
Dielectric constant (ε)	4.933	4.805	4.748	4.924	4.836	4.769
Reflection losses (R%)	0.144	0.139	0.138	0.143	0.140	0.138
Molar refraction (R_m) (cm^{-3})	15.59	15.12	15.75	15.45	15.66	15.43
Polaron radius (r_p) (Å)	1.4399	1.4321	1.4552	1.436	1.4476	1.444
Inter-atomic distance (r_i) (Å)	3.574	3.554	3.612	3.564	3.593	3.583
Molecular electronic polarizability α ($10^{-23}cm^3$)	0.618	0.5997	0.622	0.613	0.621	0.612
Field strength,F ($10^{15}cm^{-2}$)	14.47	14.63	14.17	14.55	14.32	14.39
Optical basicity, (Λ_{th})	0.497	0.506	0.518	0.470	0.480	0.470

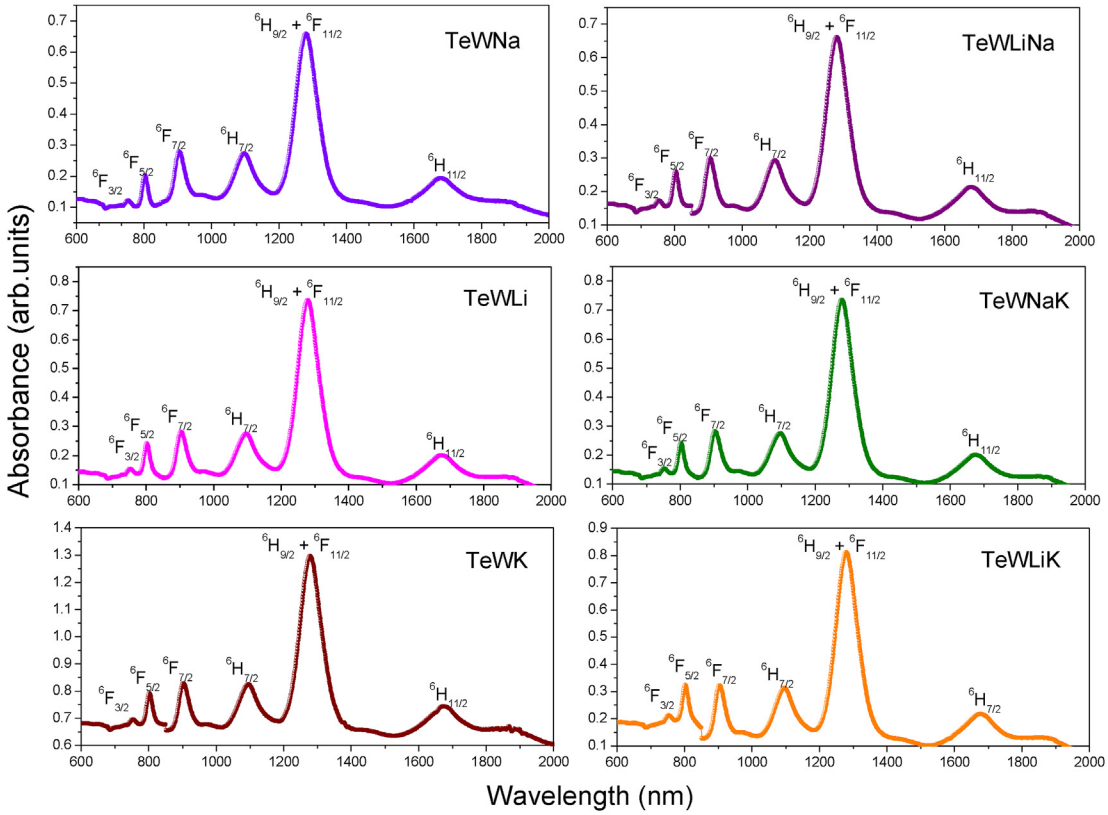

Fig. 3. Optical absorption spectra of Dy^{3+} ions doped single and mixed alkali fluoro tungsten tellurite glasses.

glasses are evaluated and are given in Table 2. From Table 2, it is observed that the bonding parameters are found to be negative i.e., the present glasses are ionic in nature. In the present work, the ionic nature is found to be maximum for TeWK glass when compared with Li and Na containing glasses. In case of mixed alkali glasses, the tungsten tellurite glass in combination with LiK possesses maximum value of bonding parameter when compared with LiNa and NaK glasses. Hence in the present work among all the

Table 2
Transitions, energy values (cm^{-1}) and bonding parameters (β and δ) of Dy^{3+} ions doped single and mixed alkali fluoro tungsten tellurite glasses.

Transition	TeWNa	TeWLi	TeWK	TeWLiNa	TeWNaK	TeWLiK
$^6F_{3/2}$	13245	13297	13245	13245	13227	13315
$^6F_{5/2}$	12406	12422	12469	12422	12422	12422
$^6F_{7/2}$	11001	11049	11061	11049	11049	11049
$^6H_{7/2}$	9132	9124	9124	9099	9124	9132
$^6H_{9/2}$ + $^6F_{11/2}$	7800	7800	7800	7806	7800	7800
$^6H_{11/2}$	5938	5952	5973	5948	5952	5952
$\overline{\beta}$	1.0053	1.0071	1.0079	1.0060	1.0063	1.0075
δ	−0.0052	−0.0070	−0.0078	−0.0060	−0.0062	−0.0075

Please cite this article in press as: C.B. Annapurna Devi, et al., Dy^{3+} ions doped single and mixed alkali fluoro tungsten tellurite glasses for LASER and white LED applications, Optical Materials (2016), http://dx.doi.org/10.1016/j.optmat.2016.11.016

Table 3
Experimental ($f_{exp} \times 10^{-6}$) and calculated ($f_{cal} \times 10^{-6}$) oscillator strengths and rms deviation of Dy^{3+} ions doped single and mixed alkali fluoro tungsten tellurite glasses.

Transitions from $^6H_{15/2}$→	TeWNa		TeWLi		TeWK		TeWLiNa		TeWNaK		TeWLiK	
	f_{exp}	f_{cal}	f_{exp}	f_{cal}	f_{exp}	f_{cal}	f_{exp}	f_{cal}	f_{exp}	f_{cal}	f_{exp}	f_{cal}
$^6F_{3/2}$	0.277	0.820	0.360	1.631	0.510	2.140	0.250	1.220	0.350	1.864	0.290	2.334
$^6F_{5/2}$	1.080	0.435	1.840	0.864	3.650	1.134	1.360	0.646	2.440	0.988	1.549	1.237
$^6F_{7/2}$	3.120	2.437	4.870	3.744	5.580	4.303	4.302	3.009	4.890	3.816	5.709	4.211
$^6H_{7/2}$	2.902	3.225	3.990	4.481	5.340	4.811	3.130	3.717	3.840	4.310	3.841	4.403
$^6H_{9/2} + {}^6F_{11/2}$	15.46	15.430	23.18	23.15	26.59	26.52	20.51	20.46	21.34	21.31	23.54	23.55
$^6H_{11/2}$	1.010	1.237	1.890	2.092	2.069	2.566	1.433	1.764	1.890	2.089	2.592	2.482
δ_{rms} ($\times 10^{-6}$)	±0.472		±0.828		±1.370		±0.772		±0.984		±1.067	

glasses under investigation, the tungsten tellurite glass with potassium combination is more ionic in nature.

The absorption bands in the ultraviolet and visible regions were disappeared due to the strong absorption of the host material. From the absorption spectra it is observed that, one peak ($^6H_{15/2} \rightarrow {}^6H_{9/2} + {}^6F_{11/2}$) is having highest intensity compared to other peaks ($^6H_{15/2} \rightarrow {}^6F_{3/2}$, $^6H_{15/2} \rightarrow {}^6F_{5/2}$, $^6H_{15/2} \rightarrow {}^6F_{7/2}$, $^6H_{15/2} \rightarrow {}^6H_{7/2}$ and $^6H_{15/2} \rightarrow {}^6H_{11/2}$). The corresponding transition to this peak $^6H_{15/2} \rightarrow {}^6H_{9/2} + {}^6F_{11/2}$ is known as hypersensitive transition. This transition obeys the selection rule $\|\Delta S\| = 0$, $\|\Delta L\| \leq 0$ and $\|\Delta J\| \leq 0$ which is very sensitive to the host environment [21]. The experimental spectral intensities (f_{exp}) of all the absorption bands of Dy^{3+} doped glasses under investigation are estimated by measuring the integrated area of the observed absorption bands using the equation given in literature [22] and are presented in Table 3. The calculated spectral intensities (f_{cal}) are measured using the J-O theory [23,24] and are also given in Table 3. The quality of the fit between the experimental and calculated spectral intensities is evaluated by the root mean square deviation method. These values are also presented in Table 3 along with the experimental and calculated spectral intensities. From Table 3, it can be observed that, among all the single alkali glasses, the potassium combination glass (TeWK) possesses maximum values of spectral intensities and among the mixed alkali glasses, TeWLiK glass possesses higher values of spectral intensities. If we compare the spectral intensities of these two glasses again, single alkali metal containing i.e., potassium combination glass possesses higher values of spectral intensities. The same thing is observed in the case of hypersensitive transition ($^6H_{15/2} \rightarrow {}^6H_{9/2} + {}^6F_{11/2}$) which depends upon the local surroundings in the glass.

The J-O intensity parameters were evaluated by using J-O theory and are presented in Table 4 along with the other reported values [25–36]. From the J-O values reported in Table 4, it is observed TeWK glass among single alkali glasses (TeWK > TeWLi > TeWNa) and TeWLiK glass among mixed alkali glasses (TeWLiK > TeWNaK > TeWLiNa) have the highest values of J-O parameters. Among these two, single alkali glass (TeWK) possesses maximum values of J-O intensity parameters than mixed alkali glass (TeWLiK). The variation in the values of J-O intensity parameter with the single alkali and mixed alkali combination are also shown in Fig. 4. Hence in the present investigation, all glasses predominantly show ionic nature, out of which potassium combination tungsten tellurite glass (TeWK) is less ionic than others. The J-O parameters in all these glasses are following the same trend ($\Omega_2 > \Omega_4 > \Omega_6$). Relatively higher magnitude obtained for Ω_2 J-O parameter indicates that the present glasses are more covalent in nature.

Table 4
Judd-Ofelt Parameters ($\Omega_\lambda \times 10^{-20} cm^2$) of the Dy^{3+} ions doped single and mixed alkali fluoro tungsten tellurite glasses.

Glass system	Ω_2	Ω_4	Ω_6	Trend	Reference
TeWNa	6.853	6.718	0.623	$\Omega_2 > \Omega_4 > \Omega_6$	Present work
TeWLi	11.58	9.058	1.268	$\Omega_2 > \Omega_4 > \Omega_6$	Present work
TeWK	14.31	9.427	1.682	$\Omega_2 > \Omega_4 > \Omega_6$	Present work
TeWLiNa	10.36	7.482	0.927	$\Omega_2 > \Omega_4 > \Omega_6$	Present work
TeWNaK	10.48	8.359	1.441	$\Omega_2 > \Omega_4 > \Omega_6$	Present work
TeWLiK	12.70	8.202	1.827	$\Omega_2 > \Omega_4 > \Omega_6$	Present work
$LiNbO_3$	5.42	1.14	2.51	$\Omega_2 > \Omega_6 > \Omega_2$	[25]
Phosphate	5.5	1.31	1.88	$\Omega_2 > \Omega_6 > \Omega_2$	[26]
NaTFP	5.53	2.13	0.88	$\Omega_2 > \Omega_4 > \Omega_6$	[27]
Lead Borate	4.90	0.94	2.07	$\Omega_2 > \Omega_6 > \Omega_2$	[28]
CFBDY10	5.98	2.33	2.33	$\Omega_2 > \Omega_6 = \Omega_2$	[29]
Tellurite	3.80	4.94	4.54	$\Omega_4 > \Omega_6 > \Omega_2$	[30]
$PdF_2 - WO_3$ - TeO_2	5.19	1.93	1.07	$\Omega_2 > \Omega_4 > \Omega_6$	[31]
Nd:LiLTB	5.27	3.92	6.09	$\Omega_6 > \Omega_2 > \Omega_4$	[32]
CBNNd10	4.37	4.50	6.48	$\Omega_6 > \Omega_4 > \Omega_2$	[33]
Fluorogermanate	5.41	1.89	1.92	$\Omega_2 > \Omega_6 > \Omega_4$	[34]
Barium fluoroborate	2.90	1.09	0.98	$\Omega_2 > \Omega_4 > \Omega_6$	[35]
$PbO - PbF_2$	2.13	2.10	1.00	$\Omega_2 > \Omega_4 > \Omega_6$	[36]

3.4. Investigation of luminescence spectra and estimation of various radiative properties

The excitation spectrum of TeWK:Dy glass recorded in the wavelength range 350–500 nm by fixing the emission wavelength at 575 nm is shown in Fig. 5. The excitation spectra has four excitation bands at wavelengths approximately 388, 428, 454 and 474 nm corresponding to the transitions $^6H_{15/2} \rightarrow {}^4F_{7/2}$, $^4G_{11/2}$, $^4I_{15/2}$ and $^4F_{9/2}$ respectively. Among all these transitions, a transition at 454 nm is identified as intense peak and this wavelength is used as an excitation source to record the emission spectra. Fig. 6 shows the luminescence spectra recorded at an excitation wavelength 454 nm in the wavelength range 460–620 nm for the TeWK:1Dy glass and the inset figure shows the luminescence spectra of all the single and mixed alkali combined glasses. The luminescence spectra of all the glasses consist of two peaks; one in blue and the other one in yellow regions corresponding to the transitions $^4F_{9/2} \rightarrow {}^6H_{15/2}$ (483 nm) and $^4F_{9/2} \rightarrow {}^6H_{13/2}$ (575 nm) respectively. Among these two peaks observed, yellow peak (electric dipole) is more intense than the blue peak (magnetic dipole) [37]. The various radiative parameters have been evaluated for the above said peaks for all the glasses and are given in Tables 5 and 6. Table 5 consists of experimental, radiative branching ratios (β_{exp} & β_R), total transition probabilities (A_T) and radiative lifetime (τ_R) values for all the glasses. From Table 5, it can be seen that, TeWK:Dy glass possesses highest values of experimental and radiative branching ratios when compared with single and mixed alkali glasses. It is well known that, a transition with branching ratio more than 0.50 is best suited for potential lasing action [38]. Table 6 consists of emission peak wavelength (λ_P), effective band widths ($\Delta\lambda_P$), transition probabilities (A_R), stimulated emission cross-sections (σ_{se}), gain band width ($\sigma_{se} \times \Delta\lambda_P$) and optical gain ($\sigma_{se} \times \tau_R$) for the two emission transitions $^4F_{9/2} \rightarrow {}^6H_{15/2}$ (483 nm) and $^4F_{9/2} \rightarrow {}^6H_{13/2}$ (575 nm) of 1 mol% of Dy^{3+} ions doped single and mixed alkali glasses. All these parameters are evaluated by using the equations available in the literature [38]. From Table 6, it is observed that, in the series of single alkali glasses, the

Please cite this article in press as: C.B. Annapurna Devi, et al., Dy^{3+} ions doped single and mixed alkali fluoro tungsten tellurite glasses for LASER and white LED applications, Optical Materials (2016), http://dx.doi.org/10.1016/j.optmat.2016.11.016

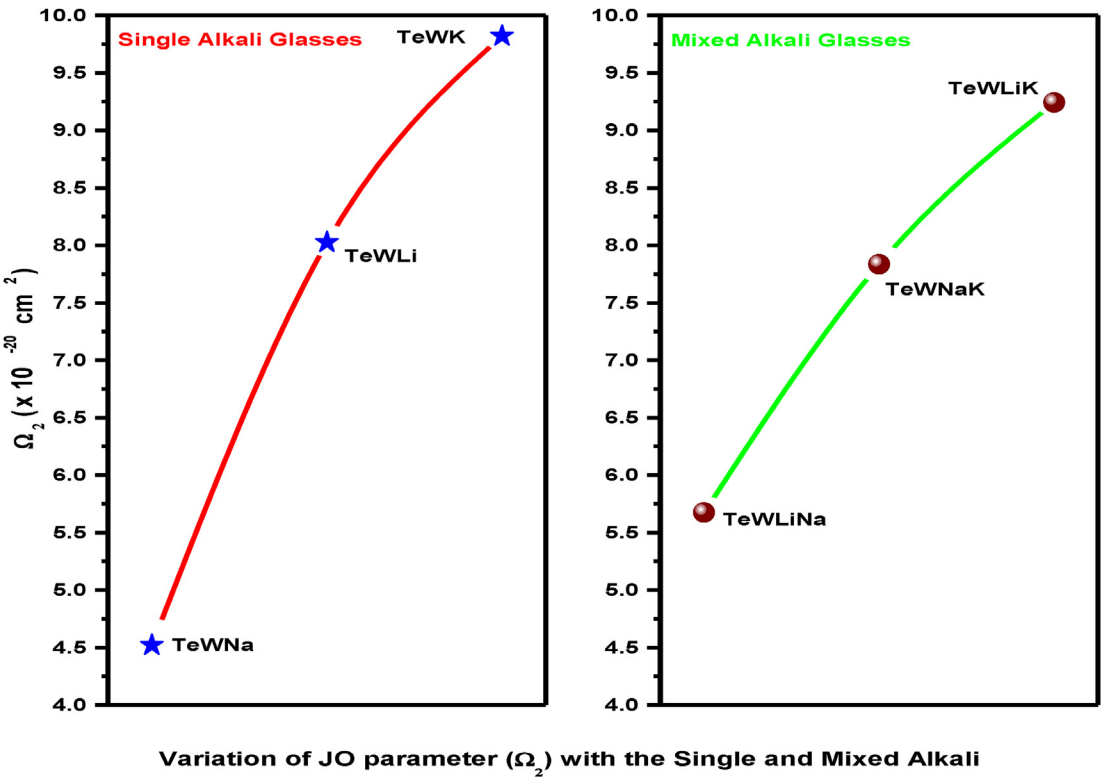

Fig. 4. Variation of J-O Intensity parameter of Dy^{3+} ions doped single and mixed alkali fluoro tungsten tellurite glasses.

TeWK glass possesses more values for stimulated emission cross-section (σ_{se}) than TeWLi and TeWNa glasses. In the series of mixed alkali glasses, the TeWLiK glass possesses more values of stimulated emission cross-section (σ_{se}) than other two glasses. When we compare the stimulated emission cross-section values of TeWK and TeWLiK glasses, the single alkali glass (TeWK) has higher values of stimulated emission cross-section (σ_{se}). Hence from the values obtained, it can be suggested that the TeWK glass doped with 1 mol% of Dy^{3+} ions is preferred as good lasing host to emit the laser in yellow region (575 nm). Similar kind of trend is observed for the optical gain parameters also. The luminescence mechanism possessed by these glasses can be understood from the energy level diagram shown in Fig. 7.

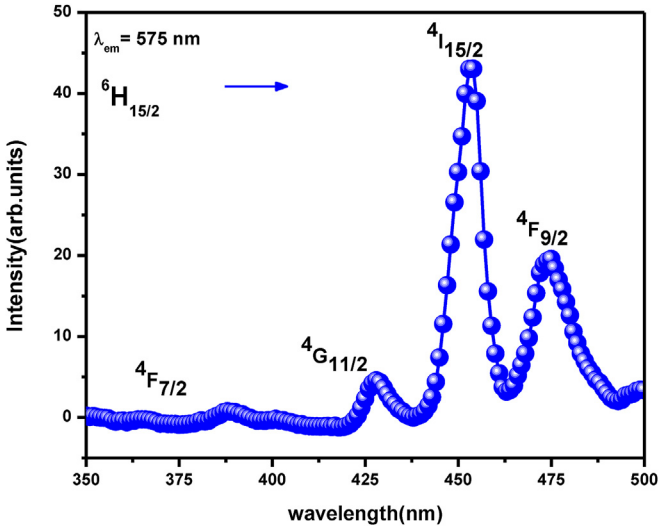

Fig. 5. Excitation spectra for TeWK:Dy glass monitored at an emission wavelength 575 nm.

3.5. Decay analysis

The lifetime spectra of $^4F_{9/2}$ luminescent level measured for all the glass samples under 445 nm excitation wavelength is shown in Fig. 8. The experimental lifetimes (τ_{exp}) of the $^4F_{9/2}$ luminescent level has been measured by taking first e-fold times the decay curves. These experimental lifetimes (τ_{exp}) are given in Table 7 along with the radiative lifetimes (τ_R), quantum efficiencies, non-radiative decay rates (W_{NR}) and other reported values [39–48]. The experimental lifetimes are found to be 102, 157, 153, 97, 137 and 156 μs for 1 mol% of Dy^{3+} doped TeWNa, TeWLi, TeWK, TeWLiNa, TeWNaK and TeWLiK glasses respectively, and they are all nearly single exponential in nature. Considerable discrepancy observed between radiative (τ_R) and experimental (τ_{exp}) lifetimes of $^4F_{9/2}$ level indicates the possibility of non-radiative decay contributions. The quantum efficiencies for all the glasses are found to be 38 (TeWNa), 87 (TeWLi), 95 (TeWK), 48 (TeWLiNa), 72 (TeWNaK) and 92% (TeWLiK).

3.6. Colour chromaticity and colour tunability of single and mixed alkali glasses

The colour of any luminous material can be easily represented by using a point, marked on a colour chromaticity diagram through its colour coordinates. These colour coordinates are evaluated from the luminescence spectra with the help of colour matching functions $\bar{x}(\lambda)$, $\bar{y}(\lambda)$ and $\bar{z}(\lambda)$. The colour co-ordinates (x, y), (u, v) and colour correlated temperature (CCT) values are evaluated from the equations available in the literature [49–52] and are given in

Please cite this article in press as: C.B. Annapurna Devi, et al., Dy^{3+} ions doped single and mixed alkali fluoro tungsten tellurite glasses for LASER and white LED applications, Optical Materials (2016), http://dx.doi.org/10.1016/j.optmat.2016.11.016

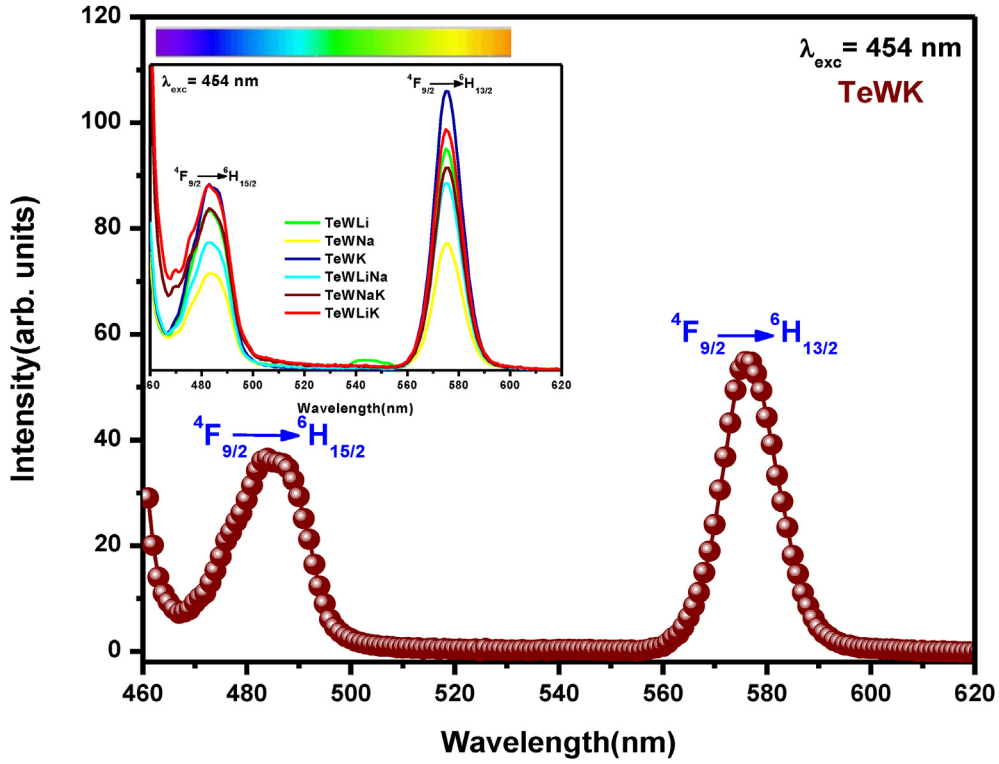

Fig. 6. Luminescence spectra of Dy^{3+} ions in TeWK glass in visible region. Inset shows the luminescence spectra of Dy^{3+} ions doped single and mixed alkali fluoro tungsten tellurite glasses excited at a wavelength of 454 nm.

Table 8. The colour co-ordinates of all the glasses fall in white light region as shown in Fig. 9. Among all the glasses, the CIE coordinates of potassium combination tungsten tellurite glass (TeWK) exactly falls in the white light region. In general, white light can be obtained by mixing the yellow and blue colour lights which can be accomplished by varying the composition of glass or by varying the excitation wavelengths [53]. The luminescence spectra of present glasses have two intensified peaks, one is in yellow region (electric dipole transition) and other is in blue region (magnetic dipole transition). It is well known that the intensity ratio between electric dipole and magnetic dipole transitions gives the Y/B intensity ratio. To get the exact white light, the Y/B intensity ratio must be unity. For the present series of glasses the Y/B intensity ratio values are above one as shown in Table 8. The variation of Y/B values clearly shows that it is possible to vary its values by changing the local environment around Dy^{3+} ions. This is maintained by the fact that when Dy^{3+} ion is located at a lower symmetry local site (without an inversion centre), yellow emission transition is often stronger in its emission spectra [54]. CCT is another important property of visible light and having significant applications in lighting industry. This can be distinguished in two ways. CCTs over 5,000 K are known as cool colours (bluish white), while lower colour temperatures (2700–3000 K) are known as warm colours (yellowish white through red) [55]. For the present series of glasses, the CCT values

Table 5
Radiative and experimental branching ratios (β_R & β_{exp}), total transition probability (A_T) (s^{-1}) and radiative (τ_R) (μs) lifetimes for the emission transitions of Dy^{3+} ions doped single and mixed alkali fluoro tungsten tellurite glasses.

Transition	β_R	β_{exp}	A_T	τ_R
TeWNa				
$^4F_{9/2} \rightarrow {}^6H_{15/2}$	0.1156	0.4179	3675	272
$^4F_{9/2} \rightarrow {}^6H_{13/2}$	0.6430	0.4921		
TeWLi				
$^4F_{9/2} \rightarrow {}^6H_{15/2}$	0.1179	0.5140	5509	181
$^4F_{9/2} \rightarrow {}^6H_{13/2}$	0.6676	0.5160		
TeWK				
$^4F_{9/2} \rightarrow {}^6H_{15/2}$	0.1158	0.5087	6187	161
$^4F_{9/2} \rightarrow {}^6H_{13/2}$	0.6789	0.5912		
TeWLiNa				
$^4F_{9/2} \rightarrow {}^6H_{15/2}$	0.1065	0.4654	4966	201
$^4F_{9/2} \rightarrow {}^6H_{13/2}$	0.6727	0.5346		
TeWNaK				
$^4F_{9/2} \rightarrow {}^6H_{15/2}$	0.1271	0.4946	5249	190
$^4F_{9/2} \rightarrow {}^6H_{13/2}$	0.6586	0.5054		
TeWLiK				
$^4F_{9/2} \rightarrow {}^6H_{15/2}$	0.1246	0.4551	5889	169
$^4F_{9/2} \rightarrow {}^6H_{13/2}$	0.6713	0.5449		

Table 6
Emission peak wavelength (λ_P) (nm), effective band widths ($\Delta\lambda_P$) (nm), Transition probabilities (A_R) (s^{-1}), stimulated emission cross-sections (σ_{se}) (cm^2), gain band width ($\sigma_{se} \times \Delta\lambda_p$) ($cm^3$) and optical gain ($\sigma_{se} \times \tau_R$) ($cm^2$ s) for the emission transitions of Dy^{3+} ions doped single and mixed alkali fluoro tungsten tellurite glasses.

Spectral parameters	TeWNa	TeWLi	TeWK	TeWLiNa	TeWNaK	TeWLiK
$^4F_{9/2} \rightarrow {}^6H_{15/2}$ (Blue)						
λ_P	483	483	483	483	483	483
$\Delta\lambda_p$	15.47	14.56	14.11	15.47	14.56	13.65
A_R	424	645	739	529	667	733
σ_{se} ($\times 10^{-22}$)	4.01	6.66	7.97	5.02	6.84	8.13
$\sigma_{se} \times \Delta\lambda_p$ ($\times 10^{-28}$)	6.21	9.69	11.2	7.76	9.96	11.1
$\sigma_{se} \times \tau_R$ ($\times 10^{-25}$)	1.09	1.21	1.24	1.01	1.30	1.37
$^4F_{9/2} \rightarrow {}^6H_{13/2}$ (Yellow)						
λ_P	575	575	575	575	575	575
$\Delta\lambda_p$	12.74	12.74	12.968	12.74	12.74	12.74
A_R	2363	3677	4336	3340	3457	3954
σ_{se} ($\times 10^{-21}$)	5.45	8.71	10.2	7.72	8.14	9.44
$\sigma_{se} \times \Delta\lambda_p$ ($\times 10^{-27}$)	6.95	11.1	13.2	9.84	10.4	12.0
$\sigma_{se} \times \tau_R$ ($\times 10^{-24}$)	1.48	1.58	1.59	1.55	1.55	1.60

Please cite this article in press as: C.B. Annapurna Devi, et al., Dy^{3+} ions doped single and mixed alkali fluoro tungsten tellurite glasses for LASER and white LED applications, Optical Materials (2016), http://dx.doi.org/10.1016/j.optmat.2016.11.016

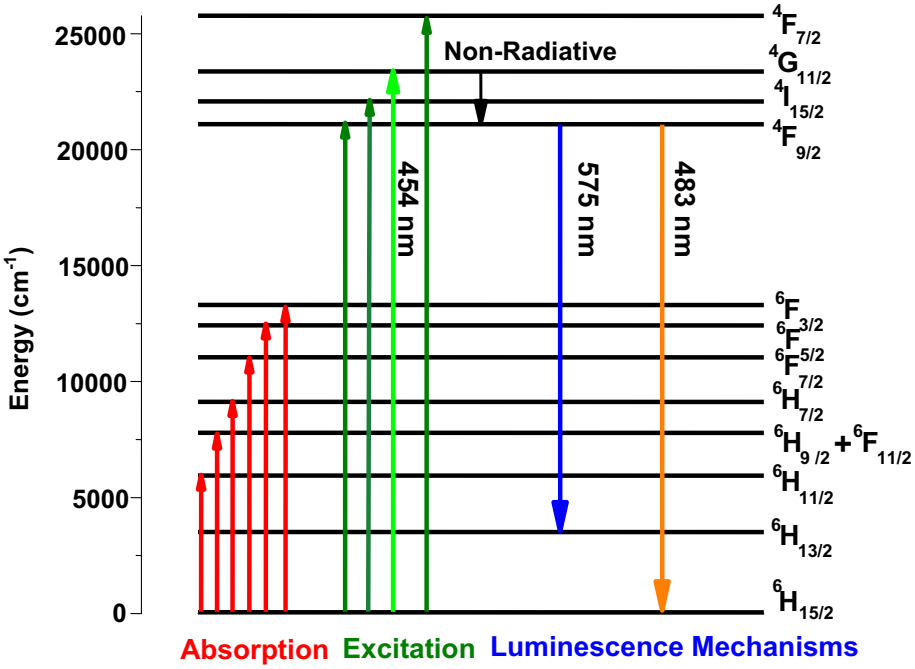

Fig. 7. Energy level diagram of Dy^{3+} ions doped single and mixed alkali fluoro tungsten tellurite glasses with absorption, excitation and luminescence mechanisms.

are in the range of 4900–5600 K. All the glasses are near to the cool colours. Among all the glasses TeWK:1Dy glass has highest value of CCT and is quite suitable to use as a luminescent source in working places. The comparison values of CCT are also shown in Table 8.

4. Conclusion

1 mol% of Dy^{3+} ions doped Single-Alklai and Mixed-Alkai fluoro tungsten tellurite glasses have been prepared using melt quenching technique and their spectroscopic behaviour was studied by XRD, optical absorption, photoluminescence and lifetime measurements. The photoluminescence spectra of all the glasses have shown two sharp peaks; one in blue and the other one in yellow region corresponding to the transitions $^4F_{9/2} \rightarrow {}^6H_{15/2}$ (483 nm) and $^4F_{9/2} \rightarrow {}^6H_{13/2}$ (575 nm) respectively. Among all the glasses, TeWK: 1Dy glass is showing maximum values of emission cross-section, branching ratio and quantum efficiency values for $^4F_{9/2} \rightarrow {}^6H_{13/2}$ (575 nm) transition. The CIE colour chromaticity coordinates (x, y), (u, v), colour correlated temperature (CCT) and Y/B ratio were also evaluated from the luminescence spectra for all the glasses. The colour chromaticity coordinates fall within the white light region and the white light can be tuned by varying the composition of the glass. Among all the single alkali and mixed alkali glasses, the CIE co-ordinates of TeWK:1Dy glass falls in white light region and CCT values for this glass is near to the cool colour. Contemplating on all the studies, we conclude that 1 mol% of Dy^{3+}

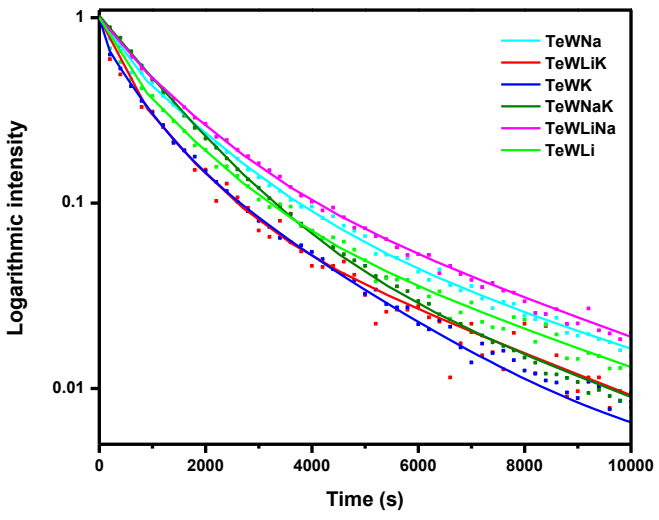

Fig. 8. The decay curves for $^4F_{9/2} \rightarrow {}^6H_{13/2}$ (575 nm) emission of Dy^{3+} ions doped single and mixed alkali fluoro tungsten tellurite glasses when excited at 445 nm.

Table 7
The Experimental (τ_{exp}) (μs), radiative (τ_R) (μs) lifetimes, quantum efficiencies (η) and non-radiative decay rates (W_{NR}) for Dy^{3+} ions doped single and mixed alkali fluoro tungsten tellurite glasses excited at a wavelength of 454 nm.

Glass	τ_{exp}	τ_R	η	W_{NR}	Reference
TeWNa	102	272	38	6127	Present work
TeWLi	157	181	87	845	Present work
TeWK	153	161	95	324	Present work
TeWLiNa	97	201	48	5334	Present work
TeWNaK	137.	190	72	2036	Present work
TeWLiK	156	169	92	493	Present work
$LiNbO_3$:Dy	270	390	69	–	[25]
BPAWDy10	470	630	74	–	[28]
PKABFAD	660	750	88	175	[28]
1.0%Dy:CFB	518	873	59	785	[29]
Fluorogermanate	470	920	52	–	[34]
PKAZFDy10	610	–	90	164	[39]
0.05DPTFB	635	–	94	96	[40]
GPbPbFDy	470	930	50	–	[41]
PKBAD	660	790	83	230	[42]
BLNDy10	410	430	95	–	[43]
PTBDy10	62.0	98.0	63	–	[44]
LBZLFB	320	489	66	1080	[45]
TZPPN	335	374	90	–	[46]
TWZDy10	140	270	52	–	[47]
BPA0.5D	403	666	61	979	[48]

Please cite this article in press as: C.B. Annapurna Devi, et al., Dy^{3+} ions doped single and mixed alkali fluoro tungsten tellurite glasses for LASER and white LED applications, Optical Materials (2016), http://dx.doi.org/10.1016/j.optmat.2016.11.016

Table 8
The chromaticity colour co-ordinates (x,y), (u,v) co-ordinates, CCT and Y/B ratio values of Dy^{3+} ions doped single and mixed alkali fluoro tungsten tellurite glasses excited at a wavelength of 454 nm.

Sample	Colour coordinates (x,y)	Colour coordinates (u,v)	CCT (K)	Y/B ratio
TeWLi	(0.34, 0.39)	(0.194, 0.201)	5261.01	1.45
TeWNa	(0.33, 0.37)	(0.195, 0.327)	5599.23	1.37
TeWK	(0.34, 0.34)	(0.213, 0.319)	5177.98	1.29
TeWLi Na	(0.34, 0.38)	(0.198, 0.331)	5247.75	1.29
TeWNaK	(0.35, 0.39)	(0.201, 0.335)	4947.20	1.49
TeWLiK	(0.34, 0.38)	(0.198, 0.331)	5247.75	1.24

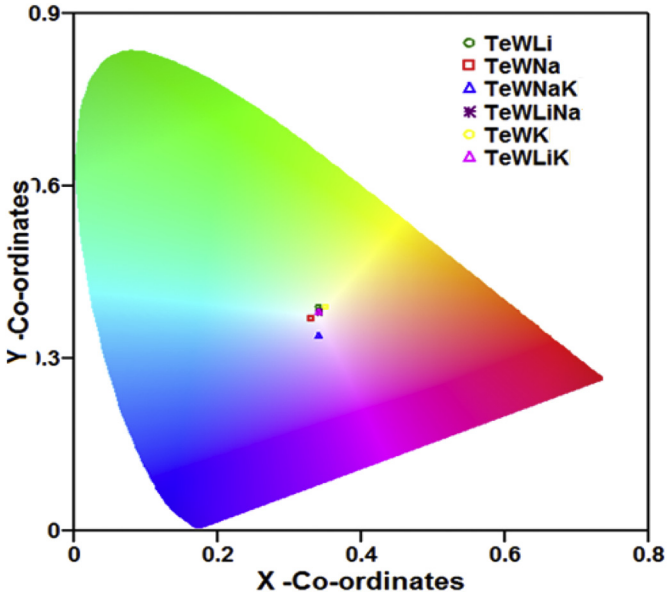

Fig. 9. CIE chromaticity co-ordinates diagram of various Dy^{3+} ions doped single and mixed alkali fluoro tungsten tellurite glasses by 454 nm excitation.

ions doped TeWK glass is quite suitable for visible lasing action and White-LED applications.

Acknowledgments

This work is partly supported by High-impact Research initiative of IIT-Delhi, UK-India Education Research Initiative (UKIERI) and Department of Science and Technology (DST), Govt. of India, New Delhi.

References

[1] Shimin Liu, Gaoling Zhao, Xiaohua Lin, Hao Ying, Junbo Liu, Jianxun Wang, Gaorong Han, J. Solid State Chem. 181 (2008) 2725–2730.
[2] S. Nakamura, G. Fasol, The Blue Laser Diode: GaN Based Light Emitters and Lasers, Springer, Berlin, 1997.
[3] The Promise of Solid State Lighting for General Illumination Light Emitting Diodes and Organic Light Emitting Diodes, Optoelectronic Industry Association, Washington, DC, 2001.
[4] C.C. Lin, R.S. Liu, Y.S. Tang, S.F. Hu, J. Electrochem. Soc. 155 (2008) J248–J251.
[5] J.K. Park, M.A. Lim, C.H. Kim, H.D. Park, J.T. Park, S.Y. Choi, Appl. Phys. Lett. 82 (5) (2003) 683.
[6] C.J. Summers, B. Wagner, H. Menkara, Solid state lighting: diode phosphors, Proc. SPIE 5187 (2004) 123–132.
[7] D.A. Steigerwald, J.C. Bhat, D. Collins, R.M. Fletcher, M.O. Holcomb, M.J. Ludowise, P.S. Martin, S.L. Rudaz, Illumination with solid state lighting technology, IEEE J. Sel. Top. Quantum Electron 8 (2) (2002) 310–320.
[8] C.-H. Chiu, C.-H. Liu, S.-B. Huang, T.-M. Chen, J. Electrochem. Soc. 154 (7) (2007) J181–J184.
[9] C.H. Liang, Y.C. Chang, Y.S. Chang, Appl. Phys. Lett. 93 (2008) 211902.
[10] C.K. Chang, T.M. Chen, Appl. Phys. Lett. 91 (2007) 081902.
[11] T. Nakanishi, S. Tanabe, Phys. Status Solidi A 206 (5) (2009) 919–922.
[12] Z. Shan, D. Chen, Y. Yu, P. Huang, H. Lin, Y. Wang, J. Mater. Sci. 45 (2010) 2775–2779.
[13] S. Fujita, S. Yoshihara, A. Sakamoto, S. Yamamoto, S. Tanabe, Proc. SPIE 5941, Fifth International Conference on Solid State Lighting (2005) 594111.
[14] S. Tanabe, S. Fujita, S. Yoshihara, A. Sakamoto, S. Yamamoto, Proc. SPIE 5941 (2005) 594112.
[15] R.P. Sreekanth Chakradhar, B. Yasoda, J.L. Rao, N.O. Gopal, J. Non Cryst. Solids 353 (2007) 2355–2362.
[16] L. Huang, S. Shen, A. Jha, J. Non Cryst. Solids 345–46 (2004) 349–353.
[17] Jia-li Cai, Ruo-ying Li, Chong-jian Zhao, Shao-long Tie, Xia Wan, Jun-ying Shen, Opt. Mater. 34 (7) (2012) 1112–1115.
[18] R.P. Sreekanth Chakradhar, K.P Ramesh, J.L. Rao, J. Ramakrishna, J. Phys. Chem. Solids 64 (2003) 641–650.
[19] J.A. Duffy, M.D. Ingram, J. Inorg. Nucl. Chem. 37 (1975) 1203.
[20] W.T. Carnall, P.R. Fields, K. Rajnak, J. Chem. Phys. 49 (1968) 4424.
[21] C.K. Jorgensen, B.R. Judd, Mol. Phys. 8 (3) (1964) 281–290.
[22] P. Babu, C.K. Jayasankar, Opt. Mater. 15 (1) (2000) 65–79.
[23] B.R. Judd, Phys. Rev. 127 (3) (1962) 750–761.
[24] G.S. Ofelt, J. Chem. Phys. 37 (1962) 511–520.
[25] G. Dominiak-Dzik, W. Ryba-Romanowski, M.N. Palatnikov, N.V. Sidorov, V.T. Kalinnikov, J. Mol. Struct. 704 (2004) 139–144.
[26] R.M. Vazquez, R. Osellame, M. Marangoni, R. Ramponi, E. Dieguez, M. Ferrari, M. Mattarelli, J. Phys. Condens. Matter 16 (2004) 465.
[27] M. Jayasimhadri, L.R. Moorthy, K. Kojima, K. Yamamoto, Noriko Wada, Noriyuki Wada, J. Phys. D. Appl. Phys. 39 (2006) 635–641.
[28] Joanna Pisarska, J. Phys. Condens. Matter 21 (2009) 285101–285106.
[29] J. Suresh Kumar, K. Pavani, A. Mohan Babu, Neeraj Kumar Giri, S.B. Rai, L. Rama Moorthy, J. Lumin. 130 (10) (2010) 1916–1923.
[30] E. Pecoraro, J.A. Sampaio, L.A.O. Nunes, S. Gama, M.L. Baesso, J. Non Cryst. Solids 277 (2000) 73–81.
[31] A. Mohan Babu, B.C. Jamalaiah, J. Suresh Kumar, T. Sasikala, L. Rama Moorthy, J. Alloys Compd. 509 (2) (2011) 457–462.
[32] S.S. Babu, P. Babu, C.K. Jayasankar, A.S. Joshi, A. Speghini, M. Bettinelli, J. Non Cryst. Solids 353 (2007) 1402–1406.
[33] R. Reisfeld, C.K. Jorgensen, Lasers and Excited States of Rare Earths, 1, Springer, Berlin, 1977, pp. 1–63.
[34] W. Ryba-Romanowski, G. Dominiak-Dzik, P. Solarz, R. Lisiecki, Opt. Mater. 31 (2009) 1547–1554.
[35] Y. Dwivedi, S.B. Rai, Opt. Mater. 31 (2009) 1472–1477.
[36] P. Nachimuthu, R. Jagannathan, V. Nirmal Kumar, D. Narayana Rao, J. Non Cryst. Solids 217 (1997) 215–223.
[37] Ligang Zhu, Chenggang Zuo, Zhiwei Luo, Anxian Lu, Phys. B Condens. Matter 405 (21) (2010) 4401–4406.
[38] Sk. Mahamuda, K. Swapna, M. Venkateswarlu, A. SrinivasaRao, Suman Shakya, G. Vijaya Prakash, J. Lumin. 154 (2014) 410–424.
[39] W.T. Carnall, P.R. Fields, K. Rajnak, J. Chem. Phys. 49 (1968) 4412–4423.
[40] S. Arunkumar, G. Venkataiah, K. Marimuthu, Spectrochim. Acta Mol. Biomol. Spectrosc. 136 (2015) 1684–1697.
[41] B. Kilmesz, G. Dominiak-Dzik, M. Zelechower, W. Ryba-Romanowski, Opt. Mater. 30 (2009) 1587–1594.
[42] S. Surendra Babu, P. Babu, C.K. Jayasankar, Th. Troster, W. Sievers, G. Wortmann, Opt. Mater. 31 (2009) 624–631.
[43] I. Arul Rayappan, K. Marimuthu, S. Surendra Babu, M. Sivaraman, J. Lumin. 130 (2010) 2407–2412.
[44] M.V. VijayaKumar, B.C. Jamalaiah, K. Rama Gopal, R.R. Reddy, J. Lumin. 132 (2012) 86–90.
[45] Sd.Z.A. Ahamed, C.M. Reddy, B.D.P. Raju, Opt. Mater. 35 (2013) 1385–1394.
[46] Kamel Damak, El Sayed Yousef, Christian Russel, Ramzi Maalej, J. Quant. Spectrosc. Radiat. Transf. 134 (2014) 55–63.
[47] G. Venkataiah, C.K. Jayasankar, J. Mol. Struct. 1084 (2015) 182–189.
[48] M. Vijayakumar, K. Marimuthu, J. Alloys Compd. 629 (2015) 230–241.
[49] N. Ohta, A.R. Robertson, Colorimetry: Fundamentals and Applications, John Wiley & Sons, Ltd., 2005.
[50] D.L. MacAdam, J. Opt. Soc. Am. 32 (5) (1942) 247–274.
[51] J. Schanda, CIE Colorimetry – Colorimetry: Understanding the CIE System, Wiley, 2007.
[52] S.M. Berman, M. Navvab, M.J. Martin, J. Sheedy, W. Tithof, Light. Res. Technol. 38 (1) (2006) 41–49.
[53] J. Kuang, Y. Liu, J. Zhang, J. Solid State Chem. 179 (1) (2006) 266–269.
[54] F. Gu, S.F. Wang, M.K. Lu, G.J. Zhou, S.W. Liu, D. Xu, D.R. Yuan, Chem. Phys. Lett. 380 (1–2) (2003) 185–189.
[55] I.T. Kim, A.S. Choi, J.W. Jeong, Build. Environ. 57 (2012) 302–312.

Please cite this article in press as: C.B. Annapurna Devi, et al., Dy^{3+} ions doped single and mixed alkali fluoro tungsten tellurite glasses for LASER and white LED applications, Optical Materials (2016), http://dx.doi.org/10.1016/j.optmat.2016.11.016

Volume 4, Issue 2 (2016) 469-473 ISSN 2347 - 3258
International Journal of Advance Research and Innovation

Effect of number of Passes on mechanical and wear properties of Friction Stir Processed Al 1050 Alloy

N. Yuvaraj*, Vipin, R. S. Mishra
Department of Mechanical Engineering, Delhi Technological University, Delhi, India

Article Info

Article history:
Received 20 January 2016
Received in revised form
10 February 2016
Accepted 28 February 2016
Available online 15 March 2016

Keywords
Aluminum,
Frictions stir processing,
Single and Multiple Passes,
Hardness & Wear Analysis

Abstract

Friction stir processing Technique is used to modify the surface layer and improves the micro-structural modification and enhances the mechanical & wear properties of the material. In this study the effect of number of FSP passes on the Aluminum 1050 alloy was studied. The grain refinement of the matrix was obtained after each FSP pass. With increase in FSP passes decreases the grain size of the matrix alloy and more homogeneous grain refinement occurs on the stir zone. The hardness, tensile strength and wear rate of the processed region was evaluated and found that enhancement of hardness, tensile strength and wear resistance of the samples with increase in passes due to finer refinement of the grain size in the stir zone.

1. Introduction

Aluminum alloy is widely in automobile, aircraft and structural applications due to their excellent mechanical properties and low weight to strength ratio. Most of the engineering components depend upon the surface of the material[1].The surface layer of the material can be improve by various techniques like Equal channel angular processing (ECAP), High pressure Torsion (HPT), Cyclic channel die compression (CCDC), Accumulate roll bonding and Friction Stir Processing [2-3]. Recently great attention is given to the FSP Technique for surface modification due to simple process and the thickness of the surface can be obtain in several millimetres. The specially designed rotating non consumable hardened tool with shoulder and a pin is plunging in the workpiece and tool is traversed along the length. The friction between the tool shoulder and the material causes localized heating and softens the material on the processed region. The pin causes the stirring of the material and forms equiaxied region [4].

Rao et al. [5] studied the effect of multi-pass FSP of hypereutectic Al–30Si alloy and found that the corrosion resistance of the material was decreased due to the reduction of grain size and silicon particle sizes and increase in homogeneity of microstructure. Fadhalah et al. [6] studied the effect of overlapping of the Al6063 by multi pass FSP and found that with increase in passes improves the mechanical properties of the Al alloy. Barmouz et al. [7] fabricated the Cu/SiC composites by multi pass friction stir processing and found that the grain size of the copper matrix was reduced with increase in FSP passes. The mechanical properties of the composite were enhanced due to uniform dispersion of reinforcement particles in the matrix due intense stirring of the material. Balasubramanian et al. [8] studied the effect of tool pin profile and shoulder diameter on the Friction Stir Welded Al6061 aluminium alloy and found that square pin profiled tool produced defect free Welded joint with higher tensile properties. Vijayavel et al. [9] studied the influence of shoulder diameter to pin diameter (D/d) ratio on tensile strength and ductility of friction stir processed LM25Al -5% SiC metal matrix composite. The D/d ratio 3 is produced defect free processed region with enhanced hardness and tensile strength in compare to other D/d ratio composites. The optimum D/d ratio breakups the SiC particles in the finer and equal size and distributed uniformly in the matrix. In this present work FSP is used to modify the surface layer of Al1050 alloy. The effects of number of passes on the mechanical properties and wear resistance were investigated.

Corresponding Author,
E-mail address: yuvraj@dce.ac.in
All rights reserved: http://www.ijari.org

2. Materials and Methods

Aluminium 1050 alloy with 10mm thickness was used for FSP. A hardened tool made of H-13 with a shoulder of 18mm diameter with square pin profile and the pin length of 5mm was used for FSP. Fig. 1(a) shows the dimensions of the FSP tool and Fig. 1(b) show its schematic diagram of the tool. The FSW machine with the capacity of 11 kW and 40kN was used to modify the surface layer of the material. The workpiece materials were clamped on the specially designed hydraulic fixture. After number of preliminary trials the tool rotational speed and traverse speed were fixed at 1000rpm and 40mm/min respectively. Three different specimens namely one pass, two pass and three pass were prepared. For multi passes the advancing and retreading side of the workpiece was changed after every pass. For each pass the work piece was allowed to cool to the room temperature. After the FSP, the cross sections of the specimens were examined through optical microscope. The samples were polished with different grades of emery sheets and etched with keller's reagent and examined the stir zone of the processed layer.

The micro hardness values of the cross section of the stir zone of FSPed regions were measured using a load of 100g with dwell time of 10s. The tensile specimens were prepared along FSP region by wire cut EDM as per ASTM standard. Fig. 2 shows the tensile test specimen dimensions. Tensile specimens were examined through computer controlled tensile testing machine at speed of

1mm/min. To evaluate the wear behaviour of the processed samples pin on disc tribometer (make DUCOM) was used. Cylindrical wear test specimens of 10mm diameter were cut from the middle of the processed region and the wear tests were conducted as per ASTM G99-04 standards. The wear tests were performed against hardened EN-24 steel disc at an ambient temperature. Before each wear test specimen and the disc were cleaned with acetone. The sliding velocity and normal load kept constant at 1.5m/s and 40N respectively at the sliding distance of 3000m. At 500m interval the wear test samples were weighed to an accuracy of 0.01mg. Wear rate were calculated as a ratio of weight loss to sliding distance. The coefficient of friction between pin and disc was determined by measuring the frictional force with stress sensor. The wear samples are examined through SEM for understanding the wear behavior of the processed surface layer and compared with base material.

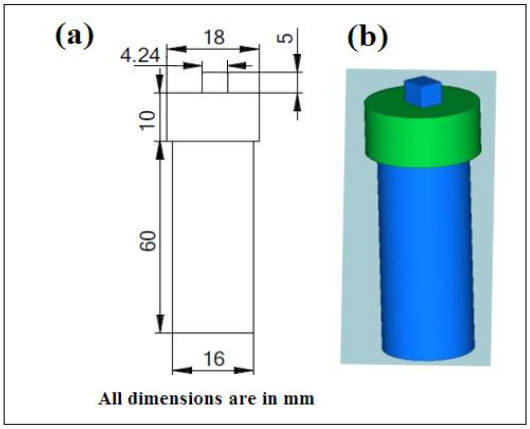

Fig: 1. (a) Dimensions of FSP Tool (b) Schematic diagram of the Tool

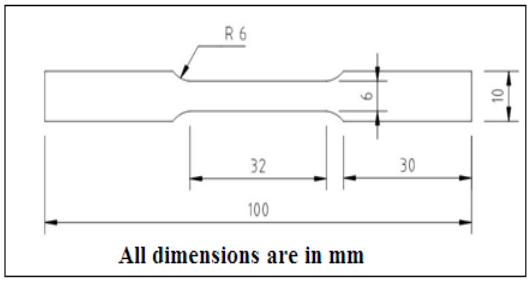

Fig: 2. The Tensile Test Specimen Dimensions

3. Results and Discussions

3.1. Hardness and Tensile Strength

During FSP the tool pin the intermixing and refinement of the grain size in the matrix. The material in moving towards advancing side of the stir zone and the shoulder provides sufficient frictional force for heat generation. Further increase in FSP pass the grain size of the material was reduced. During the second pass the tool rotational direction was changed for uniform refinement of grains. The average grain size of the base material was approximately 54µm. After one pass the grain size of the specimen was reduced about 16µm. After three pass the grain size was reduced about 11µm. Fig. 3 shows the Optical micrograph of stir zone of three pass FSP sample. It clearly seen that the uniform refinement of the grains. The hardness mainly depends upon grain size, microstructural factors and dispersion strengthening. In addition hardness also depends upon in the FSPed Al alloys were FSP process parameters, number of passes and tool shoulder to pin diameter ratio. The hardness of base alloy and processed samples are shown in Fig. 4. The average of three hardness value was taken for experimental purpose. As per Hall-petch relationship the hardness of the material is increased due to finer grain size. Similar results reported by Mahmoud [10] for increase in hardness of FSPed A390 Al alloy.

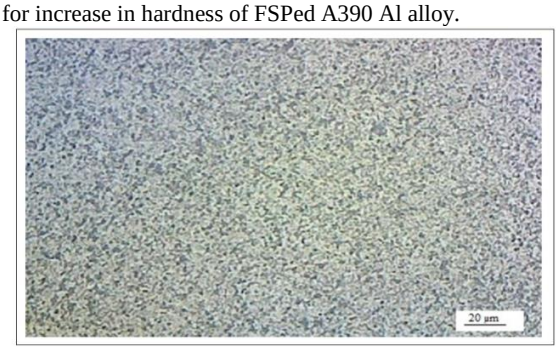

Fig: 3. Optical Micrograph of stir zone of three pass FSP Sample

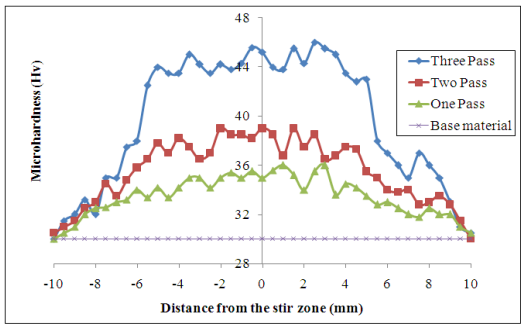

Fig: 4. Microhardness of the stir zone of the Processed Samples

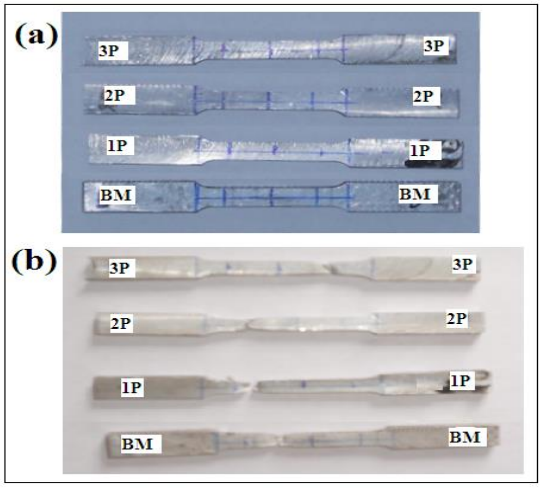

Fig: 5. Tensile specimens (a) Before test (b) After test

The tensile specimens before and after testing are shown in Fig.5 (a) and (b) respectively. The Ultimate tensile strength (UTS) of the three pass FSP specimen was improved about 37%. The base material Ultimate tensile strength was about 90±2Mpa.The detailed tensile strength of the FSPed samples are displayed in the Fig. 6. The tensile strength of the processed samples mainly depends upon the grain refinement and dislocation strengthening mechanisms.

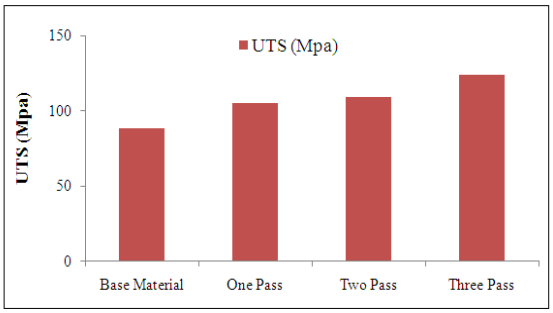

Fig: 6. Tensile Test Results

The maximum tensile strength was achieved in the three pass sample. Tensile properties are mainly depends upon the grain size of the material. As per Hall-petch relationship the tensile strength of material is inversely proportional to grain size. The relationship of the tensile strength and grain size states that

$\sigma_s=\sigma_o+K_y d^{-1/2}$ ------- (1)

Where σ_s and σ_o are constants, d is the average grain size. Fig. 7 shows the fracture surfaces of tested tensile specimens. In all the samples ductile fracture was observed. FSPed samples observed that finer dimples and uniform size, which reveals that uniform elongation. However three pass samples shows the very finer dimples which indicate that refined grain size of the material. Similar results reported by Yadav and Bauri of FSPed Aluminium [11].

3.2. Wear Properties

Fig. 8 shows the schematic diagram of pin on disc experimental set-up. The macro image of the wear test specimens are extracted from the processed region is shown in Fig.9.The wear rates of the processed samples and base material are shown in Fig. 10. This reveals that the wear resistance of the processed samples is higher than base material. Three pass wear sample has highest wear resistance than one pass and two pass samples. Hardness of the processed samples is higher than base material. As per Archard relation harder materials has lesser wear rate than softer materials at same frictional condition. Archard's equation states that [12]

Q=kW/H ---- (2)

Where Q is volume of material removed, W is the applied load and H is the hardness. Fig.11 shows the relationship between hardness and wear rate. It clearly shows that increase in hardness of the material reduces the volume of material from the surface. The enhancement of wear resistance of the FSPed composite samples is due to finer refinement of grain size. Fig. 12 shows the typical variation of friction coefficient with sliding distance of base material and stir zone of the processed material. The average friction coefficient of the base material was to be 0.55 and the fluctuations absorbed throughout the sliding distance. The friction coefficient of three pass wear specimen exhibited to be 0.35, which is lower other samples. Which it is indicated that with increase number in FSP passes lowers the friction coefficient and the low fluctuation curves observed when compare to base material. The worn surface of the base material shows that the abrasion marks, delamination marks, cracks and deeper surface pits (Fig. 13(a)). In the three pass sample SEM image shows that plastic flow lines, delamination wear and traces of oxidation wear (Fig. 13(b)). The material removed from material is entrapped in between pin and the disc causes the two body wear mechanism to three body wear mechanism which results in reduction of friction coefficient of the three pass specimen.

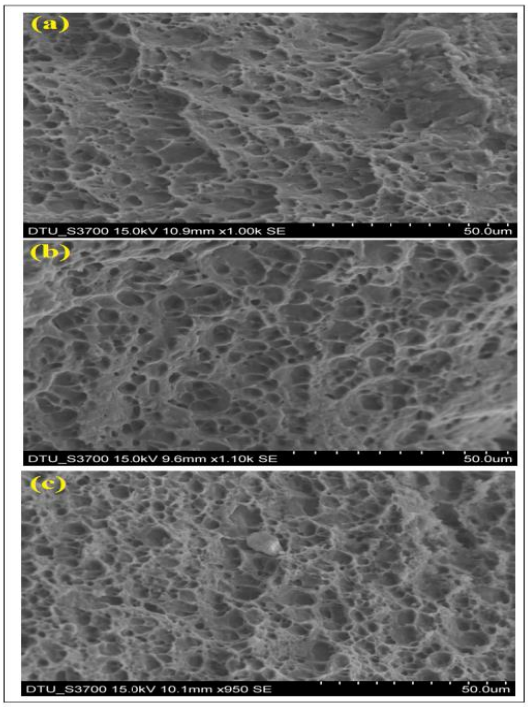

Fig: 7. Tensile fractographs (a) Base Material (b) one pass specimen (c) Three Pass specimen

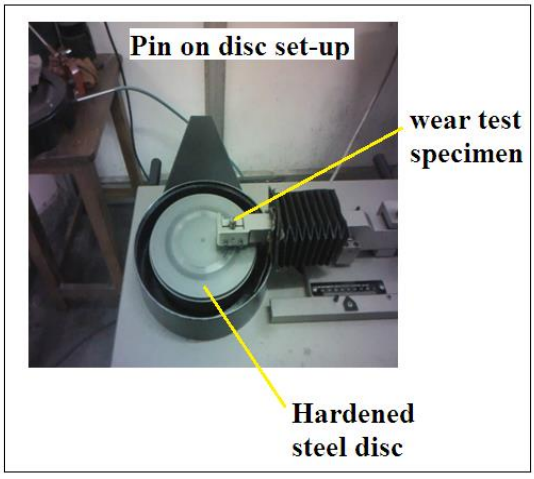

Fig: 8. Typical Pin on disc wear test set-up

Fig: 9. Typical wear Test Specimens Extracted from the Processed Surface Layer

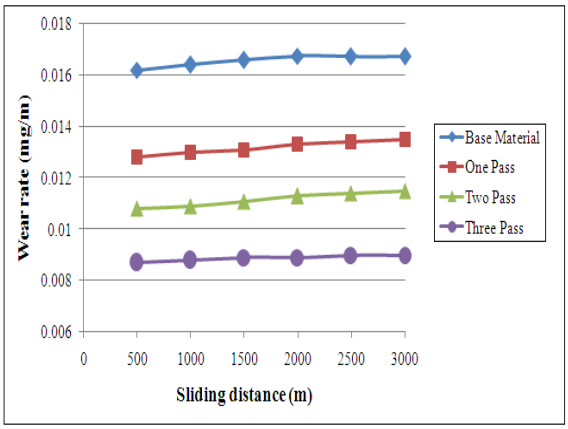

Fig: 10. Change in wear rate with Sliding Distance of Base Material and FSPed Samples

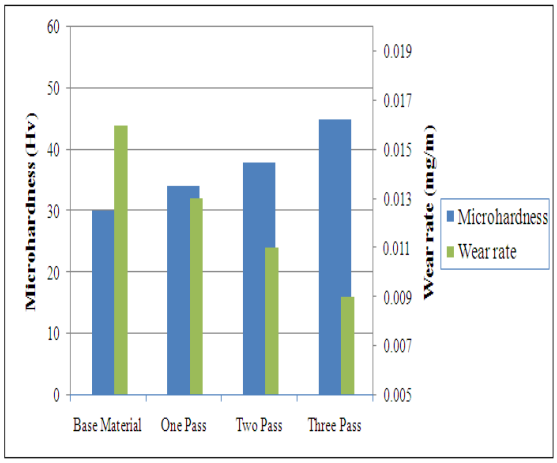

Fig: 11. Change in wear rate of base material and FSPed samples Vs Microhardness

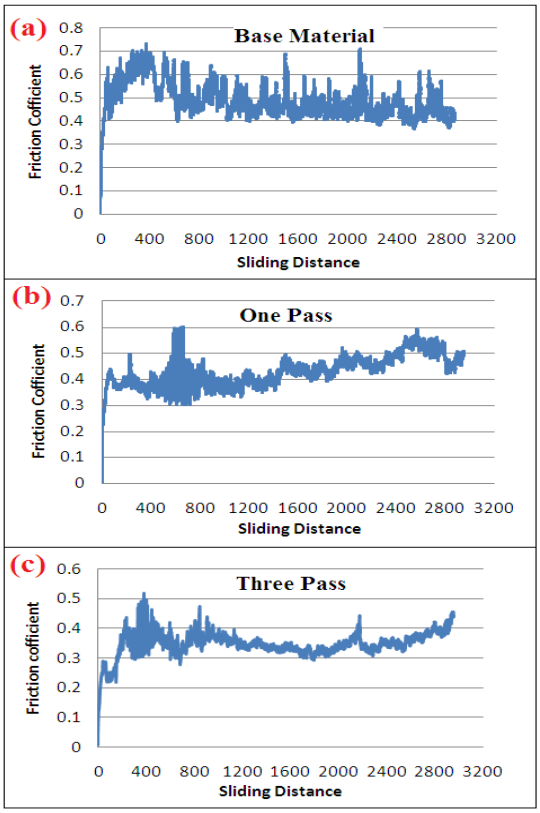

Fig: 12. Varation of friction coefficient Vs sliding distance in (a) Base Material (b) FSPed One Pass sample (c) FSPed Three pass sample

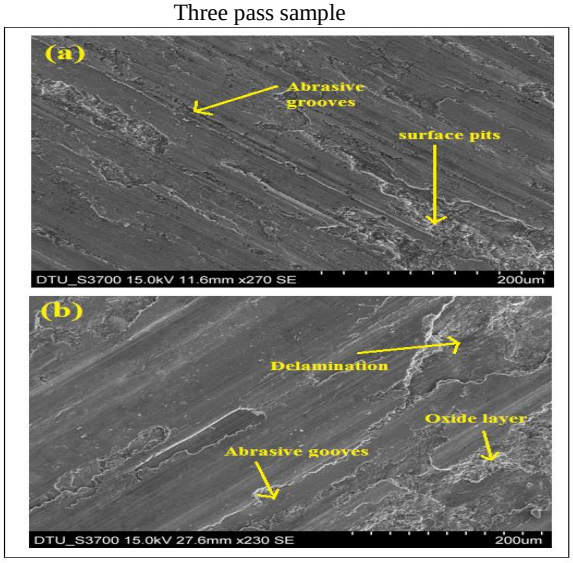

Fig: 13. SEM image of worn out surface of (a) Base Material (b) FSPed three pass specimen

4. Conclusions

In this present investigation an attempt has made to study the effects of FSP passes on mechanical and wear

properties of the FSPed Al alloy were investigated and the following conclusions are derived.

1. Friction stir processing Technique is an effective Technique to modify the surface layer of the material.
2. By increasing the FSP passes the stir zone of the processed material exhibited finer and homogeneous grain size.
3. The FSPed samples exhibited better hardness and tensile strength than base material.
4. The maximum microhardness and ultimate tensile strength of three pass specimen was achieved in stir zone were 45±22 Hv and 124±2 Mpa respectively. The wear behaviour of the FSPed samples significantly improved.
5. The three pass sample exhibited lower friction coefficient with improved mechanical properties.

References

[1] JR Davis, Properties and selection: nonferrous alloys and special-purpose materials. ASM International 1990

[2] A. Azushima, R. Kopp, A. Korhonen, D. Y. Yang, Y. Micari, GD Lahoti, P Groche, J Yanagimoto, N Tsuji, A Rosochowski, A Yanagida, Severe plastic deformation (SPD) processes for metals, CIRP Annals - Manufacturing Technology, 57, 2008, 716–735

[3] RS Mishra, ZY Ma, Friction stir welding and processing, Materials Science and Engineering R 50, 2005, 1–78

[4] N. Yuvaraj, S Aravindan, Vipin, Fabrication of Al5083/B_4C surface composite by friction stir processing and its tribological characterization, Journal of Materials Research and Technology, 4, 2015, 398-410

[5] AG Rao, BRK Rao, VP Deshmukh, AK Shah, BP Kashyap, Microstructural refinement of a cast hypereutectic Al–30Si alloy by friction stir processing, Materials Letters, 63, 2009, 2628–2630

[6] KJA Fadhalah, AI Almazrouee, AS Aloraier, Microstructure and mechanical properties of multi-pass friction stir processed aluminum alloy 6063, Materials and Design, 53, 2014, 550–560.

[7] M Barmouz, MKB Givi, Fabrication of in situ Cu/SiC composites using multi-pass friction stir processing: Evaluation of micro-structural, porosity, mechanical and electrical behavior, Composites: Part A 42, 2011, 1445–1453.

[8] V. Balasubramanian, K Elangovan, Influences of tool pin profile and tool shoulder diameter on the formation of friction stir processing zone in AA6061 aluminium alloy, Materials and Design, 29, 2008, 362–373

[9] P Vijayavel, V Balasubramanian, S Sundaram, Effect of shoulder diameter to pin diameter (D/d) ratio on tensile strength and ductility of friction stir processed LM25AA-5% SiCp metal matrix composites, Materials and Design 57, 2014, 1-9

[10] TS Mahmoud, Surface modification of A390 hypereutectic Al–Si cast alloys using friction stir processing, Surface & Coatings Technology, 228, 2013, 209–220

[11] D. Yadav, R. Bauri, Effect of friction stir processing on microstructure and mechanical properties of aluminium, Materials Science and Engineering A. 539, 2012, 85–92

[12] RL Deuis, C Subramanian, JM Yellup, Dry sliding wear of Aluminium Composites-A Review, Composites Science and Technology, 57, 1997, 415-435

Accepted Manuscript

Electrochemical performances of Li-rich layered-layered Li_2MnO_3-$LiMnO_2$ solid solutions as cathode material for lithium-ion batteries

Rakesh Saroha, Amit Gupta, Amrish K. Panwar

PII: S0925-8388(16)33679-9

DOI: 10.1016/j.jallcom.2016.11.199

Reference: JALCOM 39696

To appear in: *Journal of Alloys and Compounds*

Received Date: 19 September 2016

Revised Date: 12 November 2016

Accepted Date: 15 November 2016

Please cite this article as: R. Saroha, A. Gupta, A.K. Panwar, Electrochemical performances of Li-rich layered-layered Li_2MnO_3-$LiMnO_2$ solid solutions as cathode material for lithium-ion batteries, *Journal of Alloys and Compounds* (2016), doi: 10.1016/j.jallcom.2016.11.199.

This is a PDF file of an unedited manuscript that has been accepted for publication. As a service to our customers we are providing this early version of the manuscript. The manuscript will undergo copyediting, typesetting, and review of the resulting proof before it is published in its final form. Please note that during the production process errors may be discovered which could affect the content, and all legal disclaimers that apply to the journal pertain.

ACCEPTED MANUSCRIPT

Electrochemical performances of Li-rich layered-layered Li_2MnO_3-$LiMnO_2$ solid solutions as cathode material for lithium-ion batteries

Rakesh Saroha[a], Amit Gupta[b] and Amrish K. Panwar*[a]

[a]*Department of Applied Physics, Delhi Technological University, Delhi-110042, India.*

[b]*Department of Mechanical Engineering, Indian Institute of Technology Delhi, New Delhi-110016, India.*

ABSTRACT

In this work a series of Li-rich layered-layered solid solution of Li_2MnO_3-$LiMnO_2$ [$Li[Li_{(1-x)/3}Mn_{(x+2)/3}]O_2$; x=0.0, 0.1, 0.3 and 0.5] nanocomposite structure were successfully synthesized using sol-gel technique. All the synthesized compositions exhibit the main characteristics peaks of m-Li_2MnO_3 and could be indexed to the *C2/*m space group except some weak diffraction peaks located around 20-30° which can be attributed to the superlattice structure originate due to the ordering of Mn ion into Li-Mn layers and are typically observed for Li-rich based materials. CV results show that pristine LMO possesses weak anodic peak around 4.7 V and no symmetric cathodic peak in the voltage window of 2.0-4.8 V. Among all the synthesized compositions, x=0.3 (LMO3) delivers highest specific discharge capacity and best rate and cycling performances at all values of current densities. The LMO3 composition delivers an initial discharge capacity of 177±5 $mAhg^{-1}$ at a current density of 10 mA/g in the voltage range of 2.0-4.8 V and holds nearly 97% of the initial discharge capacity after 120 charge/discharge cycles at the same current density.

Keywords: Layered-layered nanocomposite; Sol-gel; Electrochemical performance.

1. Introduction

Single layered-type transition metal oxide cathode materials such as ABO_2/AB_2O_3, spinel-type cathodes such as AB_2O_4 and olivine-type cathodes materials such as $ABXO_4$ (A=Li, B=transition metal, X=P, Si, etc.) have been extensively studied in order to have high energy density electrode[1] material. Apart from advantages possesses by these materials their disadvantages are also evident. For ABO_2-type cathode materials such as $LiCoO_2$ and $LiNiO_2$, higher cost, toxic nature and poor thermal stability remain important points of concerns [1, 2]. In AB_2O_4-type cathodes such as $LiMn_2O_4$,

*Corresponding author. Amrish K. Panwar, Tel: +91-9891778307
E-mail address: panwaramar@gmail.com

capacity fading due to the dissolution of manganese ions and Jahn-Teller distortion hindered their widespread applications [3, 4]. Furthermore, poor electronic conductivity and sluggish lithium ion diffusion in olivine-type cathode materials such as $LiFePO_4$ restrict their use in automotive industry [5-7]. Layered-layered solid solutions of type AB_2O_3-ABO_2 have become attractive cathode materials for lithium-ion batteries due to their high reversible capacity of 250 $mAhg^{-1}$ with lower cost, structural stability and better safety as compared to the currently used commercial $LiCoO_2$ cathode [8]. Layered oxide $Li[Li_{1/3}Mn_{2/3}]O_2$ (commonly written as Li_2MnO_3) possess AB_2O_3-type monoclinic structure (*C2/m* space group) and high theoretical capacity up to 458 $mAhg^{-1}$ [9-11]. However, it is electrochemically inactive in the typical voltage range 2.2-4.4 V *vs.* Li^+/Li as all Mn atoms exist in +4 valence. Due to this, it is hard to oxidize beyond Mn^{4+} in an octahedrally coordinated environment and therefore, no lithium can be easily removed from the Li_2MnO_3 phase [2, 3, 8, 9, 11]. Furthermore, it requires a high cut-off voltage (~4.8 V *vs.* Li^+/Li) during the initial charging process to activate Li_2MnO_3 by removing Li_2O from the electrode active material according to the following reaction [2, 9, 10, 12, 13]:

$$Li_2MnO_3 \rightarrow xLi_2O + (1-x)MnO_2 \quad (1)$$

Li_2MnO_3 also shows poor cycling performance which is due to the structural transition from layered structure to the spinel structure during charging/discharging process [14]. Therefore, rigorous research efforts are on-going to find optimized electrode materials containing Li_2MnO_3 along with two or three components [2, 3, 8-12, 15-19]. In this work, Li_2MnO_3 has been integrated with another Mn-based layered cathode $LiMnO_2$ in order to have lithium rich layered-layered solid solutions. $LiMnO_2$ crystallizes in two forms: orthorhombic (*o*-$LiMnO_2$, *Pmnm* Symmetry) and monoclinic (*m*-$LiMnO_2$, *C2/m* Symmetry) and shows a high theoretical capacity of around 290 $mAhg^{-1}$ and better cyclability when operated between 2.0 and 4.5 V *vs.* Li^+/Li [9, 14, 20].

The motive behind the present work is to study the physicochemical and electrochemical performances of the lithium rich Mn-based layered-layered solid solutions of Li_2MnO_3-$LiMnO_2$. The research work reported on solid solution in this investigation has not been explored in the past. Although, there are reports on various solid-solution system which have been investigated previously like Li_2MnO_3-$LiMO_2$ ($M=Ni_{1/3}Mn_{1/3}Co_{1/3}$, $Ni_{1/2}Mn_{1/2}$) [21], $Li_{1+x}(Ni_{0.3}Mn_{0.7-y}Ti_y)_{1-x}O_2$, $0<x<1/3$, $y=0$,

0.1, 0.2 [22], $x$$Li_2MnO_3$-(1-$x$) $LiNi_{2/3}Co_{1/6}Mn_{1/6}O_2$ [23], $0.5Li_2MnO_3$-$0.5Li(Mn_{0.375}Ni_{0.375}Co_{0.25}O_2)$ [24] etc. Apart from these reported works several attempts has also been made to synthesize and study electrochemical performances of some Li-rich manganese-based compositions using different methods [25, 26] and morphology [27-29] etc. All the synthesized compositions in this work have been prepared using the sol-gel route and were examined using X-ray diffraction (XRD) for phase analysis, scanning electron microscopy (SEM) for microstructural investigation and Fourier-transform infrared spectroscopy (FTIR) for vibrational modes analysis. Electrochemical characterizations of as-prepared compositions were carried out to study electrochemical performance and lithium ion kinetics.

2. Experimental

2.1. Material preparation

Stoichiometric amounts of lithium acetate dihydrate ($CH_3COOLi.2H_2O$, Sigma-Aldrich, ~99%) and Manganous acetate ($(CH3COO)_2$ $Mn.4H_2O$, Fisher Scientific, 99%) were used as precursors for the development of solid solutions of Li_2MnO_3-$LiMnO_2$ [$Li(Li_{(1-x)/3}Mn_{(x+2)/3})O_2$; x= 0.0, 0.1, 0.3 and 0.5] using sol-gel technique. Citric acid (Sigma-Aldrich, ≥99.5%) was used as a chelating agent. A dispersed solution of all the precursors in deionized water was prepared with continuous stirring and then added to citric acid solution one by one. The pH value of the resulting solution was maintained between 6 and 7 using ammonia solution. The resulting solution of citric acid and precursors was heated at 70 ºC at 400 rpm with continuous stirring until a transparent gel was obtained. The gel thus obtained was dried at 120 ºC for 5 h in a vacuum oven to obtain xerogel. The yielded powders were reground together using pestle mortar and again heated at 600 ºC for 3 h in air and then finally calcined at 900 ºC for 12 h in air and then allowed to cool normally up to room temperature. The powders thus obtained for x=0.0, 0.1, 0.3 and 0.5 were abbreviated as LMO, LMO1, LMO3 and LMO5, respectively. The heating rate of the furnace was kept at 5 ºC min^{-1}.

2.2. Material characterization

Synthesized samples were characterized using RIGAKU make X-ray diffractometer coupled with $CuK_{\alpha 1}$ radiation (λ=1.540 Å) for quantitative analysis of crystal structure and phase composition of the synthesized structures. The XRD data was collected over an angular range of 10-70º with a step

size of 0.02º. Rietveld refinement of LMO sample was performed using 'X'pert high score plus' software in order to obtain quantitative information about structural parameters. The microstructural characterization of the prepared samples was carried out using HITACHI make S-3700N scanning electron microscope working at 15 kV. The as-synthesized samples were mixed with 2.5 wt.% of polyvinyl alcohol (PVA) binder, pressed into round pellets with 10 mm diameter by applying pressure of 5 tons using a hydraulic press and then heated at 250 ºC for 2 h in air to remove PVA. In order to make electrical contacts, silver (Ag) paste was applied on both sides of pellets and then dried at 150 ºC for 1 h in air to remove moisture content. A two-point probe setup (AGILENT 4284A) was used to calculate the electronic conductivity of the synthesized samples. Conductivity measurements were done at a bias voltage of 1.0 V and the frequency range was kept from 20 Hz-1 MHz. The electronic conductivity (σ) can be calculated using the following equation;

$$\sigma = \frac{1}{R}\left(\frac{L}{A}\right) \quad (2)$$

Where R is the resistance of the sample (**Ω)**, L and A is thickness (cm) and cross-sectional area (cm^2) of the circular disc, respectively.

2.3 Electrode preparation and electrochemical characterization

For the electrochemical studies, two electrode coin half-cells (CR2032) were assembled. The working electrodes were prepared by dissolving 70 wt.% active material, 15 wt.% super P as a conductive carbon and 15 wt.% polyvinylidene difluoride (PVDF) as a binder in N-methyl-2-pyrrolidinone (NM2P) as a solvent. This results in the uniform mixing of the active materials which were stirred for 10 h. Thus obtained slurry was uniformly coated on Al foil current collector using the "doctor blade" technique and further dried out at 80 ºC in a vacuum oven for overnight to evaporate the solvent. Then circular electrodes with diameter 19 mm were punched and weighed. The electrodes were then dried up under vacuum at 60 ºC and finally brought inside the Mbraun make glove box having O_2 and H_2O level ≤ 0.5 ppm. The coin cells (CR2032) were assembled for electrochemical studies of the synthesized samples with metallic lithium as both counter and reference electrode and a microporous polypropylene sheet Celgard 2400 used as a separator. The electrolyte used was 1 M $LiPF_6$ in EC: DMC 1:1 v/v. Cyclic voltammetry (CV) experiments were carried out over the potential

range of 2.0-4.8 V (*vs.* Li/Li^+ metal). The galvanostatic charge/discharge (GCD) performance test, rate capability at different C-rates and Electrochemical Impedance Spectroscopy (EIS) using an AC voltage pulse of 5 mV in the frequency range of 10 mHz-10 kHz were performed. All the electrochemical tests were performed using EZstat-pro Nuvant systems Inc. (U.S.A) cell test system at 298 K.

3. Results and discussion

3.1 Structural and morphological analysis

The XRD patterns of the as-synthesized compositions are shown in Fig. 1. The pristine Li_2MnO_3 (LMO) shows diffraction peaks which correspond to the *m*-Li_2MnO_3 and could be assign to *C2*/m space group (Reference Code: 01-084-1634). The sharp and intense peaks indicate the crystalline nature of all the synthesized compositions. Even composite solid-solutions i.e. $Li[Li_{(1-x)/3}Mn_{(x+2)/3}]O_2$ (x=0.1, 0.3 and 0.5) still shows the main characteristics peaks of *m*-Li_2MnO_3, indicating that the layered structure of the synthesized samples is still preserved. The (001) diffraction peaks of the synthesized compositions (shown in the magnified XRD image) clearly shows slight shifts towards higher 2θ angle suggesting a minor shrink of the unit cell and decrease in lattice parameters. On the other hand, weak diffraction peaks located around 20-30° can be attributed to the superstructure ordering of the lattice which is caused by the arrangement of Mn ion into Li-Mn layers and are observed for Li-rich based materials [1, 28, 30-32]. However, the intensity of these superlattice peaks become weaker on changing the value of x from 0.1 to 0.5 which indicates that the local ordering of Li/Mn has been reduced. In addition, the peak around 37° splits into two peaks i.e. $(\bar{2}01)$ and (130), which can also be indexed to *C2/m* space group with a high degree of crystallinity. Similarly, the peak around 45° also depicts the same results. However, the intensity of these doublets gets faded with an increase in x. The splitting of peaks located at 59° and 65° for all values of x has also been noticed which indicates the presence of spinel phase [15]. Rietveld refinement was performed for the pristine LMO synthesized sample to obtain quantitative structural information of the crystal lattice structure using 'X'pert high score plus' software. The observed XRD pattern along with calculated and difference pattern for original LMO sample are shown in Fig. 2. No background subtraction and data smoothening were done before refinement. The starting atomic position coordinates for pristine LMO

were taken from somewhere else [33]. The structural refinement results indicate that the goodness of fitting factor i.e. χ^2 for primitive LMO is around 4.5% which demonstrates that the results are reliable. The crystal structure generated after refinement has been displayed in the inset of Fig. 2 where Li and Mn atoms are surrounded by O atoms to form LiO_6 and MnO_6 octahedra. The lattice parameters obtained from refinement for bare LMO are: a = 4.928 Å, b = 8.522 Å and c = 5.022 Å. The average crystallite size for pristine LMO was calculated to be 54 nm using Scherrer's formula $d= k\lambda/\beta \cos\theta$, where d is the mean crystallite size, k is the constant parameter of shape factor (0.94), λ is the wavelength of X-ray (0.154 nm), β is the full-width half maximum corresponding to (001) peak and θ is the corresponding angle of Bragg diffraction. These results suggest that the variation in x not only increase the crystallinity of the synthesized samples but also induce phase transformation to some extent.

The effect of variation in x value on the morphologies of $Li[Li_{(1-x)/3}Mn_{(x+2)/3}]O_2$ (x= 0.0, 0.1, 0.3 and 0.5) composites are shown in Fig. 3(a)-(d). All prepared samples display nearly same morphology with plate-like and relatively spherical grains. The average grain size of LMO, LMO1, LMO3 and LMO5 composites were found to be around 0.45, 0.3, 0.5 and 0.45 µm, respectively. Therefore, the average grain sizes of the composites were distributed in a range of 300-450 nm. SEM images also show that the synthesized nanocomposites possess dispersed grains with little aggregation.

Among all synthesized samples, the pristine LMO and LMO3 compositions are chosen to investigate the morphological properties further. Fig. 4(A)-(B) shows the TEM/HRTEM images of the LMO and LMO3 synthesized samples. TEM image of pristine LMO (Fig. 4(A)) sample indicates that the particles are homogeneously distributed with little agglomeration. It can also be observed from TEM image that the particles are nearly spherical and possess nearly uniform size. The average particle size was calculated using ImageJ software and observed to be 170 nm for LMO composition. HRTEM image (inset of Fig. 4(A)) clearly indicates that the sample is well crystalline with uniformly spaced lattice fringes. The interlayer spacing of pristine LMO sample was observed to be 0.472 nm which corresponds to (001) plane of the monoclinic structure of synthesized LMO composition. Likewise, TEM image oF LMO3 composition (Fig. 4(B)) also reveals the spherical morphology of the synthesized composition with slight agglomeration. The average particle size for LMO3 composition

was calculated to be 220 nm. HRTEM image (inset of Fig. 4(B)) for LMO3 composition also reveals the crystalline nature of the sample with uniformly spaced lattice fringes. The interlayer spacings of LMO3 composition were found to be 0.470 and 0.475 nm which again corresponds to (001) plane of the monoclinic structure. The obtained TEM/HRTEM results are well synchronized with XRD and SEM results.

3.2 Cation environment study-FTIR

FTIR spectroscopy proves to be an appropriate and dominant technique for the structural evaluation and to study local environment of the cations in the crystal lattice of close-packed oxygen atoms. Vibrational modes are generally assigned to the motion of cations with respect to an oxygen atom. The local cation environment of synthesized compositions in the range of 400-600 cm^{-1} has been studied using FTIR spectroscopy and results are displayed in Fig. 5. It can be observed from FTIR graph that the spectrum of all synthesized samples shows nearly similar features. In the spectrum of LMO, four bands located around 520 cm^{-1} (weak band), 465 cm^{-1} (slightly broad peak), 430 cm^{-1} (sharp band) and at 417 cm^{-1} (less intense band) can be observed. These four IR active modes are assigned to the stretching and bending vibrations of octahedrally coordinated molecule of MnO_6 in $Li[Li_{(1-x)/3}Mn_{(x+2)/3}]O_2$ matrix [32, 34]. The weak band located at 520 cm^{-1} slightly moves towards higher wavenumber side for LMO1, LMO3 and LMO5 compositions which may be attributed to the variation in Li and Mn amount in $Li[Li_{(1-x)/3}Mn_{(x+2)/3}]O_2$ solid solution which induces a difference in the local cation environment. Similarly, the band at 412 cm^{-1} shift towards lower wavenumber side for LMO3 and LMO5 which confirms that the local environment of the cations has been changed.

3.3 Electronic conductivity measurements

Electronic conductivity gives the direct measurement of the electron kinetics and hence, the electrochemical properties of the material. Fig. 6 displays the AC electrical resistance measurement for the as-synthesized compositions. The frequency range for the data collection was kept from 20 Hz-1 MHz. From Fig. 6 it can be seen that all the compositions display depressed semicircle whose intercept at x-axis gives the AC resistance of the cathode active material. It can be seen that excluding LMO3 sample all the compositions have AC resistance in megaohm. The AC conductivity values for the samples LMO, LMO1, LMO3 and LMO5 were found to be $10.1x10^{-9}$, $10.8x10^{-9}$, $1.65x10^{-7}$ and

194 $9.36x10^{-9}$ S/cm, respectively. Therefore, among all the synthesized samples LMO3 shows the highest
195 AC conductivity and hence, superior electrochemical performances are expected from LMO3
196 composition as compared to other synthesized samples.

197 *3.4 Electrochemical performance of* Li_2MnO_3-$LiMnO_2$ *solid solutions*

198 Cyclic voltammetry measurements give an insight into the electrochemical reactions taking place
199 during the charging-discharging process. Fig. 7 displays the CV results of the as-synthesized samples
200 in the voltage window of 2.0-4.8 V. The data for the CV measurement was collected at a scan rate of
201 $0.05mVs^{-1}$. It can be observed from Fig. 6 that pristine LMO possess weak anodic peak around 4.7 V
202 and no symmetric cathodic peak. It indicates the loss of lattice oxygen along with lithium extraction
203 from monoclinic crystal structure as given by eq. (1) [33]. Therefore, CV result indicates that the
204 activation of primitive LMO will take place at 4.7 V and this process will not be reversible. However,
205 for LMO1, LMO3 and LMO5 compositions the intensity of the peak at 4.7 V decreases significantly
206 which indicates that the redox reaction mechanism is different from LMO. Moreover, MnO_2 obtained
207 in eq. (1) is assumed to be electrochemically active and formed spinel structure during Li-
208 intercalation. The samples with $x>0$ i.e. LMO1, LMO3 and LMO5 shows a redox couple around
209 3.0/2.8 V, 4.1/4.0 V and anodic peak around 2.1 V. The redox couple at 4.1/4.0 can be attributed to
210 insertion of lithium ion at vacant *8a* tetrahedral sites of the spinel structure formed by MnO_2 [9].
211 Likewise, the emergence of redox couple at 3.0/2.8 V is due to intercalation of Li-ion at *16c*
212 octahedral sites of the spinel structure [33]. The origin of anodic peak around 2.1 V can be attributed
213 to structural modification of the material which generally take place due to high upper voltage limit
214 and can be assigned to spinel Mn^{4+}/Mn^{3+} redox couple [35]. When charged at higher voltage,
215 transition metal dissociation takes place which leads to phase transformation from layered to spinel
216 structure. However, the intensity of these redox couples was found to vary with *x*. This phenomenon
217 may be correlated to the manganese dissolution which originated due to Jahn-Teller distortion and
218 leads to change in oxidation state of Mn in the composition [9]. The average oxidation states of Mn in
219 LMO, LMO1, LMO3 and LMO5 were calculated to be 4.0, 3.85, 3.61 and 3.40, respectively
220 according to the redox titration method [27]. As average oxidation state of Mn changes from 4.0 to
221 3.4, Jahn-Teller distortion leads to dissociation of Mn^{3+} to Mn^{4+} and Mn^{2+} which results in active mass

loss and a decrease in intensity [9]. This change of oxidation state is generally expressed in terms of the transformation of the layer-to-spinel structure as predicted by XRD (splitting of peaks at 2θ = 59° and 65°). The presence of shoulder peaks at 4.04, 3.98, 3.93 and 3.96 V also indicates the existence of small spinel phase due to electrochemical active MnO_2. Therefore, the above results clearly indicate the coexistence of spinel structure along with layered structure while the redox process observed at 2.8 V and 4.1 V for LMO1, LMO3 and LMO5 samples will lead to stable capacity and cyclic performances.

Fig. 8 shows the initial charge-discharge capacity curves of $Li[Li_{(1-x)/3}Mn_{(x+2)/3}]O_2$ (x=0.0, 0.1, 0.3 and 0.5) solid solution at a current density of 10 mA/g and in a voltage window of 4.8-2.0 V. The initial discharge capacities for composites LMO, LMO1, LMO3 and LMO5 were found to be 81±5, 97±5, 177±5 and 71±5 $mAhg^{-1}$, respectively. It can be observed that as x value increases capacity increases, goes maximum for LMO3 and then decreases for LMO5. For all composite samples, a sloping voltage plateau above 4.5 V can be seen in the charging curves. However, no discharge plateau was observed above 4.5 V for the composite samples which is associated with the oxidation of O^{2-} ions and electrochemical activation of Li_2MnO_3 by irreversible removal of oxygen from the lattice. Moreover, the charge-discharge profile of the LMO1, LMO3 and LMO5 samples exhibits three voltage plateaus around 4.25V, 2.87 V and 2.25 V. The voltage plateaus around 4.25 V and 2.87 V originate due to change in oxidation state of Mn ion during charging-discharging. The length of voltage plateau at 4.25 V, 2.87 V and 2.25 V increases with increase in the value of x, reaching a maximum for LMO3 and then decreases for LMO5 which is possibly due to Jahn-Teller distortion as predicted in CV results. Among all the four samples, the LMO3 composition gives the highest discharge capacity and the composition LMO5 delivers the least charge-discharge capacity. These results indicate superior lithium ion kinetics and excellent reactivity for LMO3 sample. Fig. 9(a)-(d) shows the charge/discharge capacity curves of LMO, LMO1, LMO3 and LMO5, respectively for 1^{st}, 2^{nd}, 10^{th} and 50^{th} cycle at 10 mA/g. From Fig. 9(a), it can be observed that discharge capacity of LMO composition at the 50^{th} cycle is much greater as compared to 1^{st} cycle. This is due to activation of LMO compound due to the removal of O^{2-} along with lithium extraction which causes an increase in the length of voltage plateau around 3.2 V. However, for LMO1 (Fig. 9(b)), LMO3 (Fig. 9(c)) and

LMO5 (Fig. 9(d)) compositions the charge/discharge profiles for 1st, 2nd, 10th and 50th cycle remains nearly same. These results indicate that the integrity of the synthesized compositions remains unchanged during cycling.

Fig. 10(a)-(d) shows the charge/discharge curves of the synthesized samples at different current densities (10–1000 mA/g) for the initial cycle. It can be observed from the Fig. 10 that among all the synthesized samples LMO3 (Fig. 10(c)) delivers the highest specific discharge capacity at all current densities. LMO3 shows an initial discharge capacity of 177 (±5) mAh/g at 10 mA/g and delivers nearly 37% of the capacity at a high current density of 1 A/g. On the other hand, LMO5 (Fig. 10(d)) shows the least specific discharge capacity at all current densities because of its low conductivity.

Fig. 11(a) shows the stepwise rate performance of the $Li[Li_{(1-x)/3}Mn_{(x+2)/3}]O_2$ compositions at current densities of 10-1000 mA/g (10 mA/g= 0.05C). It can be observed that the composition LMO3 delivers the highest discharge capacity at all current densities. The initial discharge capacities for composites LMO, LMO1, LMO3 and LMO5 were found to be 81±5, 97±5, 177±5 and 71±5 $mAhg^{-1}$, respectively at 10 mA/g. However, the discharging capacity values for LMO were found to increase continuously from 81 $mAhg^{-1}$ for the 1st cycle to 133 $mAhg^{-1}$ for 5th discharge cycle which is due to the activation of Li_2MnO_3 as given by eq. (1). Moreover, LMO5 composite possesses the lowest discharge capacities even at low current densities but delivers fairly better discharge capacity values at high current rates as compared to the pristine LMO and LMO1 composites. Table 1 compares the discharge capacity values at each current density with respect to 10 mA/g rate. LMO3 displays highest discharge capacity and retains ~37% of its capacity value even at the high current rate of 5C (1A/g). The loss of capacity at high current densities can be linked to the large polarization effects of the composites which hindered lithium ion kinetics. Fig. 11(b) displays the cycling stability of the synthesized composites at 10 mA/g current density for 120 charge-discharge cycles at room temperature. It is evident from the Fig. 11(b)) and Table 1 that except for LMO3 composite sample, discharge capacity at 120th cycle comes out to be more as compared to 1st cycle for LMO, LMO1 and LMO5 composition. LMO3 shows an initial discharge capacity of 177(±5) $mAhg^{-1}$ at 10 mA/g and retains nearly 97% of its capacity after 120 charge/discharge cycles at same current density.

Fig. 12 depicts the dependence of the rate performance on the variation of *x*. From the Figure, it can be observed that at low C-rates, the difference in electrochemical properties is mainly due to the change in oxidation state of Mn ion which subsequently leads to manganese dissolution and inferior capacity performance. Under high C-rates, the alteration in discharge capacities is predominantly due to increase in polarization potential of the cathode active material which leads to poor discharge capacity values.

EIS of the fresh cells was also performed to study the variation in electrode reaction impedance of the prepared composition. Fig. 13(a) demonstrated the EIS curves of $Li[Li_{(1-x)/3}Mn_{(x+2)/3}]O_2$ compositions in the frequency range of 10 mHz-10 kHz using an AC voltage pulse of 5 mV amplitude. It can be observed from the Fig. 13(a) that all the EIS curves of the composites samples enclose a depressed semicircle lies in the high-frequency region and a straight line falls in the low-frequency region. The intercept by the semi-circle at the real axis in the high-frequency region gives the ohmic resistance (R_s) of the cell which usually represents the resistance of the electrode material and the electrolyte. The part of semicircle lies in the middle-frequency range is mainly attributed to the electrochemical reactions taking place at the electrode and electrolyte interface and named as charge transfer resistance (R_{ct}). The 45° inclined line with the x-axis in the low-frequency region signifies the Warburg impedance (Z_w) which is related to Li-ion diffusion in the electrolyte solution. The values of lithium ion diffusion coefficient in the bulk electrode materials can be calculated using the following equation [36]:

$$D = \frac{0.5R^2T^2}{A^2F^4C^2\sigma_W^2} \quad (3)$$

Where D is Li-ion diffusion coefficient, R is gas constant, T is absolute temperature, A is electrode area, C is the lithium-ion concentration, F is the faraday constant and σ_W is the Warburg factor which is given by the following equation:

$$Z' = R_s + R_{ct} + \sigma_W \omega^{-0.5} \quad (4)$$

Z' is real part of the impedance and the Warburg factor can be obtained from the slope of Z' and $\omega^{-0.5}$ curve in the low-frequency region. Fig. 13(b) demonstrates the plot between Z' and $\omega^{-0.5}$ in the low-frequency region for all the synthesized composites samples and their values are listed in Table 2.

From the EIS plot and Table 2, it is clear that LMO3 has minimum charge transfer resistance and therefore, highest lithium ion diffusion coefficient ($7.75x10^{-16}$ cm^2s^{-1}) among all the compositions confirming the CV and charge/discharge results. However, as compared to other manganese-based cathode materials, the lithium ion diffusion coefficients are found to be low [37, 38]. This may be due to the presence of $LiMnO_2$ component. $LiMnO_2$ undergo irreversible structural changes from layered to spinel as given by equation (5) [14]:

$$3LiMnO_2 + \frac{1}{2}O_2 \rightarrow LiMn_2O_4 + Li_2MnO_3 \quad (5)$$

Spinel material possesses low discharge capacities and small lithium ion diffusion coefficient as compared to the *o*-$LiMnO_2$ [16, 39]. Therefore, the presence of small traces of spinel phase induced by *o*-$LiMnO_2$ might be the possible reason for low lithium ion diffusion coefficient and hence, relatively poor electrochemical performances. Also, the lithium- ion diffusion coefficient was found to be minimum for LMO5 composition and therefore, it possesses inferior electrochemical performances. The EIS results clearly indicate that the LMO3 composition possesses the lowest charge transfer resistance due to which it delivers the highest discharge capacities among all the synthesized samples.

4. Conclusions

A series of solid solution of layered-layered composites $Li[Li_{(1-x)/3}Mn_{(x+2)/3}]O_2$ (x=0.0, 0.1, 0.3 and 0.5) were successfully synthesized using sol-gel technique. XRD results confirm the coexistence of layered structure along with spinel structure. Microstructural investigations reveal that the average grain size of all the compositions lies in a range of 300-450 nm. Among all the synthesized compositions LMO3 shows the best rate and cycling performances. It delivers an initial specific discharge capacity of 177±5 $mAhg^{-1}$ at a current density 10 mA/g. The better charge/discharge profiles and highest rate and cycling performances of the LMO3 composition can be attributed to highest electronic conductivity ($1.65x10^{-7}$ S/cm) and maximum lithium-ion diffusion coefficient ($7.75x10^{-16}$ cm^2s^{-1}) factor.

Acknowledgments

ACCEPTED MANUSCRIPT

Authors are thankful to SERB and FIST, Department of Science and Technology (DST), New Delhi for financial support to carry out this work under the project grants Nos.: SR/FTP/PS-039/2011 and SR/FST/PSI-164/2011(C), respectively.

ACCEPTED MANUSCRIPT

References

[1] Y. Sun, Y. Shiosaki, Y. Xia, H. Noguchi, The preparation and electrochemical performance of solid solutions $LiCoO_2$–Li_2MnO_3 as cathode materials for lithium ion batteries, J. Power Sources 159 (2006) 1353-1359.

[2] D. Kim, J. Gim, J. Lim, S. Park, J. Kim, Synthesis of $xLi_2MnO_3 \cdot (1-x)\ LiMO_2$ (M= Cr, Mn, Co, Ni) nanocomposites and their electrochemical properties, Mater. Res. Bull. 45 (2010) 252-255.

[3] C. Park, S. Kim, I.R. Mangani, J. Lee, S. Boo, J. Kim, Synthesis and materials characterization of Li_2MnO_3–$LiCrO_2$ system nanocomposite electrode materials, Mater. Res. Bull. 42 (2007) 1374-1383.

[4] M.M. Thackeray, Y. Shao-Horn, A.J. Kahaian, K.D. Kepler, E. Skinner, J.T. Vaughey, S.A. Hackney, Structural Fatigue in Spinel Electrodes in High Voltage (4 V) $Li/Li_xMn_2O_4$ Cells, Electrochem. Solid-State Lett. 1 (1998) 7-9.

[5] J. Li, Q. Qu, L. Zhang, L. Zhang, H. Zheng, A monodispersed nano-hexahedral $LiFePO_4$ with improved power capability by carbon-coatings, J. Alloys Compd. 579 (2013) 377-383.

[6] Q. Liu, W. Liu, D. Li, H. Chen, Z. Wang, $LiFe_{1-x}(Ni_{0.98}Co_{0.01}Mn_{0.01})_xPO_4/C$ (x= 0.01, 0.03, 0.05, 0.07) as cathode materials for lithium-ion batteries, Electrochim. Acta 184 (2015) 143-150.

[7] S.-X. Zhao, H. Ding, Y.-C. Wang, B.-H. Li, C.-W. Nan, Improving rate performance of $LiFePO_4$ cathode materials by hybrid coating of nano-Li_3PO_4 and carbon, J. Alloys Compd. 566 (2013) 206-211.

[8] Y. Wu, A. Manthiram, Structural stability of chemically delithiated layered $(1-z)Li[Li_{1/3}Mn_{2/3}]O_2$–$zLi[Mn_{0.5-y}Ni_{0.5-y}Co_{2y}]O_2$ solid solution cathodes, J. Power Sources 183 (2008) 749-754.

[9] Q. Zhang, T. Peng, D. Zhan, X. Hu, Synthesis and electrochemical property of $xLi_2MnO_3 \cdot (1-x)LiMnO_2$ composite cathode materials derived from partially reduced Li_2MnO_3, J. Power Sources 250 (2014) 40-49.

[10] D. Mori, H. Sakaebe, M. Shikano, H. Kojitani, K. Tatsumi, Y. Inaguma, Synthesis, phase relation and electrical and electrochemical properties of ruthenium-substituted Li_2MnO_3 as a novel cathode material, J. Power Sources 196 (2011) 6934-6938.

[11] S. Kim, C. Kim, J.-K. Noh, S. Yu, S.-J. Kim, W. Chang, W.C. Choi, K.Y. Chung, B.-W. Cho, Synthesis of layered–layered $xLi_2MnO_3 \cdot (1-x)LiMO_2$ (M= Mn, Ni, Co) nanocomposite electrodes materials by mechanochemical process, J. Power Sources 220 (2012) 422-429.

[12] W. West, R. Staniewicz, C. Ma, J. Robak, J. Soler, M. Smart, B. Ratnakumar, Implications of the first cycle irreversible capacity on cell balancing for Li_2MnO_3–$LiMO_2$ (M= Ni, Mn, Co) Li-ion cathodes, J. Power Sources 196 (2011) 9696-9701.

[13] J. Li, S. Jeong, R. Kloepsch, M. Winter, S. Passerini, Improved electrochemical performance of $LiMO_2$ (M= Mn, Ni, Co)–Li_2MnO_3 cathode materials in ionic liquid-based electrolyte, J. Power Sources 239 (2013) 490-495.

[14] J. Molenda, M. Ziemnicki, J. Marzec, W. Zając, M. Molenda, M. Bućko, Electrochemical and high temperature physicochemical properties of orthorhombic $LiMnO_2$, J. Power Sources 173 (2007) 707-711.

[15] C. Yu, G. Li, X. Guan, J. Zheng, L. Li, T. Chen, Composites $Li_2MnO_3 \cdot LiMn_{1/3}Ni_{1/3}Co_{1/3}O_2$: optimized synthesis and applications as advanced high-voltage cathode for batteries working at elevated temperatures, Electrochim. Acta 81 (2012) 283-291.

[16] Z. Su, Z. Lu, X. Gao, P. Shen, X. Liu, J. Wang, Preparation and electrochemical properties of indium-and sulfur-doped $LiMnO_2$ with orthorhombic structure as cathode materials, J. Power Sources 189 (2009) 411-415.

[17] K.G. Gallagher, S.-H. Kang, S.U. Park, S.Y. Han, $xLi_2MnO_3 \cdot (1-x)\ LiMO_2$ blended with $LiFePO_4$ to achieve high energy density and pulse power capability, J. Power Sources 196 (2011) 9702-9707.

[18] J.-H. Lim, H. Bang, K.-S. Lee, K. Amine, Y.-K. Sun, Electrochemical characterization of Li_2MnO_3–$Li[Ni_{1/3}Co_{1/3}Mn_{1/3}]O_2$–$LiNiO_2$ cathode synthesized via co-precipitation for lithium secondary batteries, J. Power Sources 189 (2009) 571-575.

[19] H. Shu, X. Wang, Q. Wu, B. Hu, X. Yang, Q. Wei, Q. Liang, Y. Bai, M. Zhou, C. Wu, Improved electrochemical performance of $LiFePO_4$/C cathode via Ni and Mn co-doping for lithium-ion batteries, J. Power Sources 237 (2013) 149-155.

[20] E.M. Jin, B. Jin, Y.-S. Jeon, K.-H. Park, H.-B. Gu, Electrochemical properties of $LiMnO_2$ for lithium polymer battery, J. Power Sources 189 (2009) 620-623.

[21] L. Song, Z. Tang, Y. Chen, Z. Xiao, L. Li, H. Zheng, B. Li, Z. Liu, Structural analysis of layered Li_2MnO_3–$LiMO_2$ (M= $Ni_{1/3}Mn_{1/3}Co_{1/3}$, $Ni_{1/2}Mn_{1/2}$) cathode materials by Rietveld refinement and first-principles calculations, Ceram. Int. 42 (2016) 8537-8544.

[22] M. Tabuchi, H. Kageyama, K. Takamori, Y. Imanari, K. Nakane, Synthesis and electrochemical characterization of Ni-and Ti-substituted Li_2MnO_3 positive electrode material using coprecipitation–hydrothermal–calcination method, Electrochim. Acta 210 (2016) 105-110.

[23] J. Shojan, V.R. Chitturi, J. Soler, O. Resto, W.C. West, R.S. Katiyar, High energy xLi_2MnO_3–(1−x) $LiNi_{2/3}Co_{1/6}Mn_{1/6}O_2$ composite cathode for advanced Li-ion batteries, J. Power Sources 274 (2015) 440-450.

[24] J. Patra, P.P. Dahiya, C.-J. Tseng, J. Fang, Y.-W. Lin, S. Basu, S.B. Majumder, J.-K. Chang, Electrochemical performance of $0.5Li_2MnO_3$–$0.5Li(Mn_{0.375}Ni_{0.375}Co_{0.25})O_2$ composite cathode in pyrrolidinium-based ionic liquid electrolytes, J. Power Sources 294 (2015) 22-30.

[25] C. Hou, Y. Oaki, E. Hosono, H. Lin, H. Imai, Y. Fan, F. Dang, Bio-inspired synthesis of xLi_2MnO_3-(1−x)$LiNi_{0.33}Co_{0.33}Mn_{0.33}O_2$ lithium-rich layered cathode materials, Materials & Design 109 (2016) 718-725.

[26] A. Vu, Y. Qin, C.-K. Lin, A. Abouimrane, A.K. Burrell, S. Bloom, D. Bass, J. Bareño, I. Bloom, Effect of composition on the voltage fade phenomenon in lithium-, manganese-rich $xLiMnO_3$·(1−x)$LiNi_aMn_bCo_cO_2$: A combinatorial synthesis approach, J. Power Sources 294 (2015) 711-718.

[27] F. Yang, Q. Zhang, X. Hu, T. Peng, Synthesis of layered xLi_2MnO_3·(1−x)$LiMnO_2$ nanoplates and its electrochemical performance as Li-rich cathode materials for Li-ion battery, Electrochim. Acta 165 (2015) 182-190.

[28] B. Li, Y. Yu, J. Zhao, Facile synthesis of spherical xLi_2MnO_3·(1−x)$Li(Mn_{0.33}Co_{0.33}Ni_{0.33})O_2$ as cathode materials for lithium-ion batteries with improved electrochemical performance, J. Power Sources 275 (2015) 64-72.

[29] G. Xu, J. Li, X. Li, H. Zhou, X. Ding, X. Wang, F. Kang, Understanding the electrochemical superiority of $0.6Li[Li_{1/3}Mn_{2/3}]O_2$-$0.4Li[Ni_{1/3}Co_{1/3}Mn_{1/3}]O_2$ nanofibers as cathode material for lithium ion batteries, Electrochim. Acta 173 (2015) 672-679.

[30] M. Tabuchi, Y. Nabeshima, T. Takeuchi, K. Tatsumi, J. Imaizumi, Y. Nitta, Fe content effects on electrochemical properties of Fe-substituted Li_2MnO_3 positive electrode material, J. Power Sources 195 (2010) 834-844.

[31] C. Miao, P. Bai, Q. Jiang, S. Sun, X. Wang, A novel synthesis and characterization of $LiFePO_4$ and $LiFePO_4$/C as a cathode material for lithium-ion battery, J. Power Sources 246 (2014) 232-238.

[32] X. Dong, Y. Xu, L. Xiong, X. Sun, Z. Zhang, Sodium substitution for partial lithium to significantly enhance the cycling stability of Li_2MnO_3 cathode material, J. Power Sources 243 (2013) 78-87.

[33] S. Basu, P.P. Dahiya, M. Akhtar, S.K. Ray, J.K. Chang, S.B. Majumder, High energy density layered-spinel hybrid cathodes for lithium ion rechargeable batteries, Mater. Sci. Eng. B (2016).

[34] Y. Li, Y. Makita, Z. Lin, S. Lin, N. Nagaoka, X. Yang, Synthesis and characterization of lithium manganese oxides with core-shell $Li_4Mn_5O_{12}$@Li_2MnO_3 structure as lithium battery electrode materials, Solid State Ionics 196 (2011) 34-40.

[35] J. Pires, L. Timperman, A. Castets, J.S. Peña, E. Dumont, S. Levasseur, R. Dedryvère, C. Tessier, M. Anouti, Role of propane sultone as an additive to improve the performance of a lithium-rich cathode material at a high potential, RSC Advances 5 (2015) 42088-42094.

[36] J. Lin, D. Mu, Y. Jin, B. Wu, Y. Ma, F. Wu, Li-rich layered composite $Li[Li_{0.2}Ni_{0.2}Mn_{0.6}]O_2$ synthesized by a novel approach as cathode material for lithium ion battery, J. Power Sources 230 (2013) 76-80.

[37] P. Suresh, A.K. Shukla, N. Munichandraiah, Characterization of Zn-and Fe-substituted $LiMnO_2$ as cathode materials in Li-ion cells, J. Power Sources 161 (2006) 1307-1313.

[38] K.M. Shaju, G.V.S. Rao, B.V.R. Chowdari, EIS and GITT studies on oxide cathodes, O_2-$Li_{(2/3)+x}(Co_{0.15}Mn_{0.85})O_2$ (x= 0 and 1/3), Electrochim. Acta 48 (2003) 2691-2703.

[39] H. Zhao, S. Liu, X. Liu, M. Tan, Z. Wang, Y. Cai, S. Komarneni, Orthorhombic $LiMnO_2$ nanorods as cathode materials for lithium-ion batteries: Synthesis and electrochemical properties, Ceram. Int. 42 (2016) 9319-9322.

ACCEPTED MANUSCRIPT

Tables

Table 1. Electrochemical performance of synthesized compositions at different C-rates and cycling capability at 0.05C-rate (10 mA/g).

Samples	**R[a] (%)**						**0.05C (±5) ($mAhg^{-1}$)**		
	0.05C (±5) ($mAhg^{-1}$)	**0.1C**	**0.25C**	**0.5C**	**2.5C**	**5C**	**1st**	**120th**	**R[b] (%)**
LMO	81	144.4	128.3	116.0	55.5	6.1	81	144	177.7
LMO1	97	84.5	81.4	72.1	32.9	20.6	97	105	108.2
LMO3	177	84.7	70.6	62.1	50.8	37.2	177	172	97.1
LMO5	71	98.8	90.1	78.8	83.0	67.6	71	72	101.4

[a] Capacity retention ratios of samples at different C-rates as compared to 0.05C

[b] Capacity retention rates of samples compared to the 1st cycle at 0.05C

Table 2. Electrode kinetic factors for synthesized solid solution compositions.

Sample	**R_e (Ω)**	**R_{ct} (Ω)**	**σ_w ($\Omega\ s^{-0.5}$)**	**D** (cm^2s^{-1})
LMO	16.30	177.09	210.10	$5.76x10^{-17}$
LMO1	10.46	71.08	92.53	$2.97x10^{-16}$
LMO3	13.58	50.54	57.26	$7.75x10^{-16}$
LMO5	9.06	1059.6	837.09	$3.63x10^{-18}$

ACCEPTED MANUSCRIPT

Figure Captions

Fig. 1. XRD patterns of solid solution compositions of Li_2MnO_3-$LiMnO_2$.

Fig. 2. Rietveld refined XRD pattern of pristine Li_2MnO_3 (LMO).

Fig. 3. SEM micrographs of Li_2MnO_3-$LiMnO_2$ synthesized compositions (a) LMO; (b) LMO1; (c) LMO3; (d) LMO5.

Fig. 4. TEM and HRTEM images of the synthesized compositions (A) LMO; (B) LMO3.

Fig. 5. FTIR spectrum of the synthesized compositions in the wavenumber range of 400-600 cm^{-1}.

Fig. 6. AC conductivity measurements of synthesized solid solutions in the frequency range of 20 Hz-1 MHz.

Fig. 7. Cyclic Voltammograms of the $Li(Li_{(1-x)/3}Mn_{(x+2)/3})O_2$ samples at a scan rate of 0.05 mVs^{-1}.

Fig. 8. 1st charge/discharge curves of solid solution samples at a current density of 10 mA/g (i_{charge} = $i_{discharge}$).

Fig. 9. Charge/Discharge profiles of the prepared compositions for 1st, 2nd, 10th and 50th cycle at 10 mA/g: (a) LMO; (b) LMO1; (c) LMO3; (d) LMO5.

Fig. 10. Initial charge/discharge curves of the synthesized compositions at various current densities: (a) LMO; (b) LMO1; (c) LMO3; (d) LMO5.

Fig. 11. Performance of $Li(Li_{(1-x)/3}Mn_{(x+2)/3})O_2$ solid solution samples: (A) Rate performance at different current densities (i_{charge} = $i_{discharge}$); (b) Cycling performance at current density of 10 mA/g for 120 charge/discharge cycles.

Fig. 12. Rate capability of the synthesized compositions as a function of *x* in $Li(Li_{(1-x)/3}Mn_{(x+2)/3})O_2$.

Fig. 13. (a) Impedance spectra of synthesized compositions measured at AC pulse of amplitude 5 mV; (b) Relationship plot between Z' and $\omega^{-0.5}$ in low-frequency region.

515 **Figures**

516

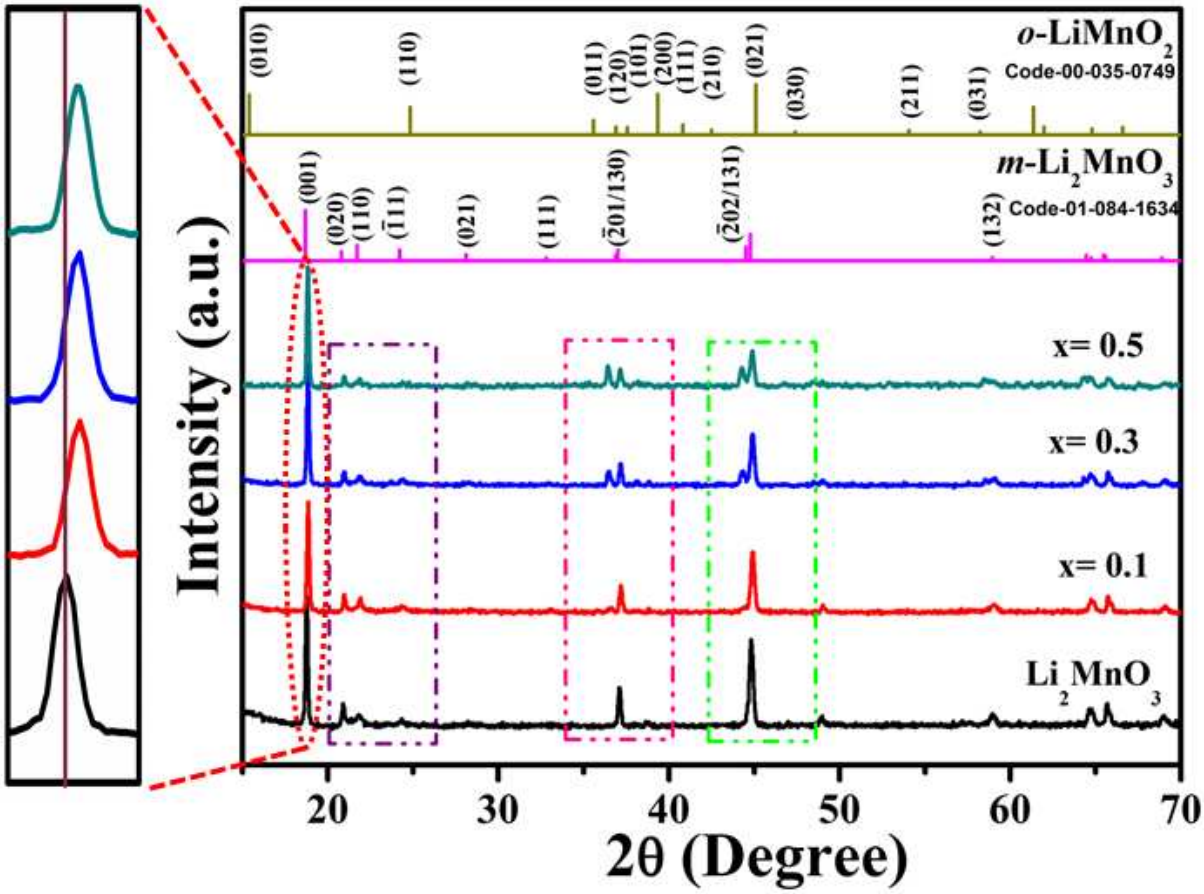

517

518 **Fig. 1**

ACCEPTED MANUSCRIPT

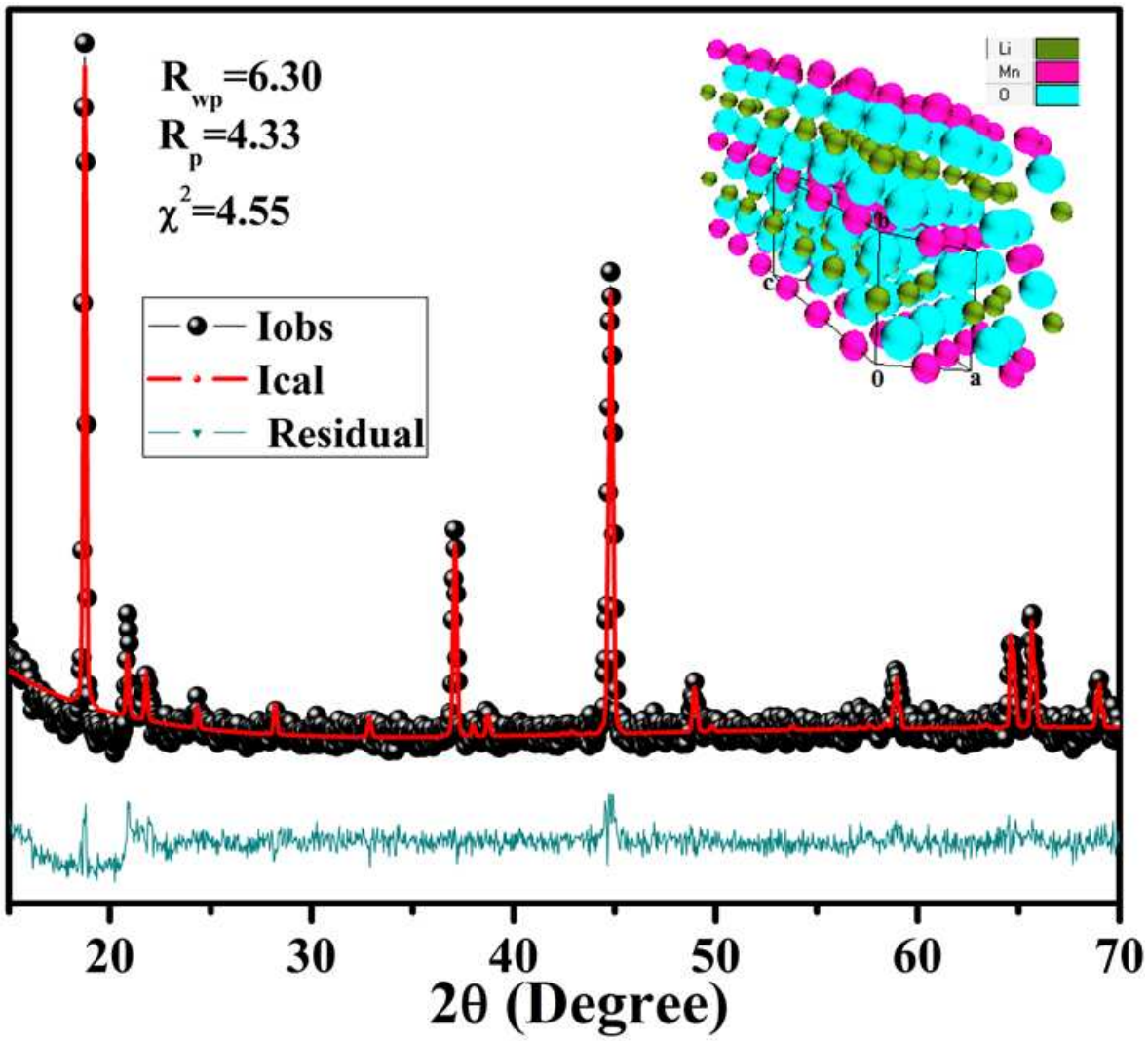

Fig. 2

ACCEPTED

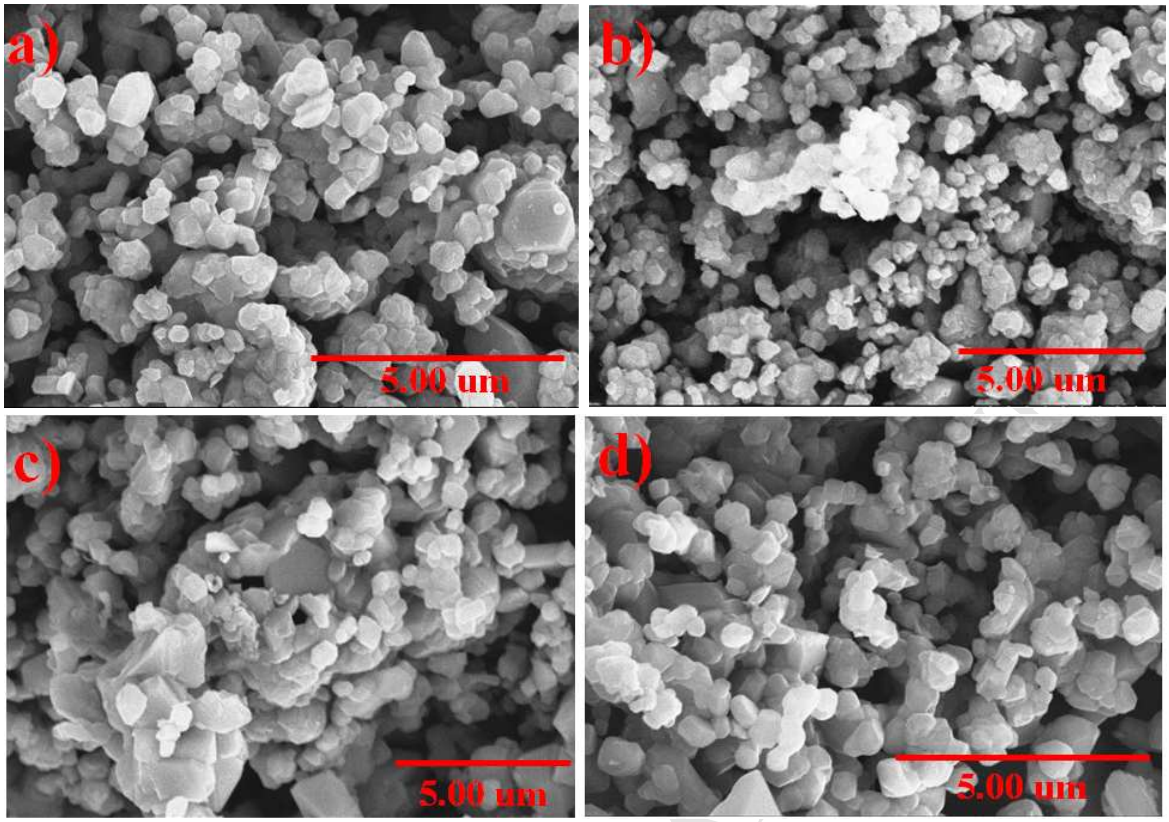

Fig. 3

ACCEPTED MANUSCRIPT

543

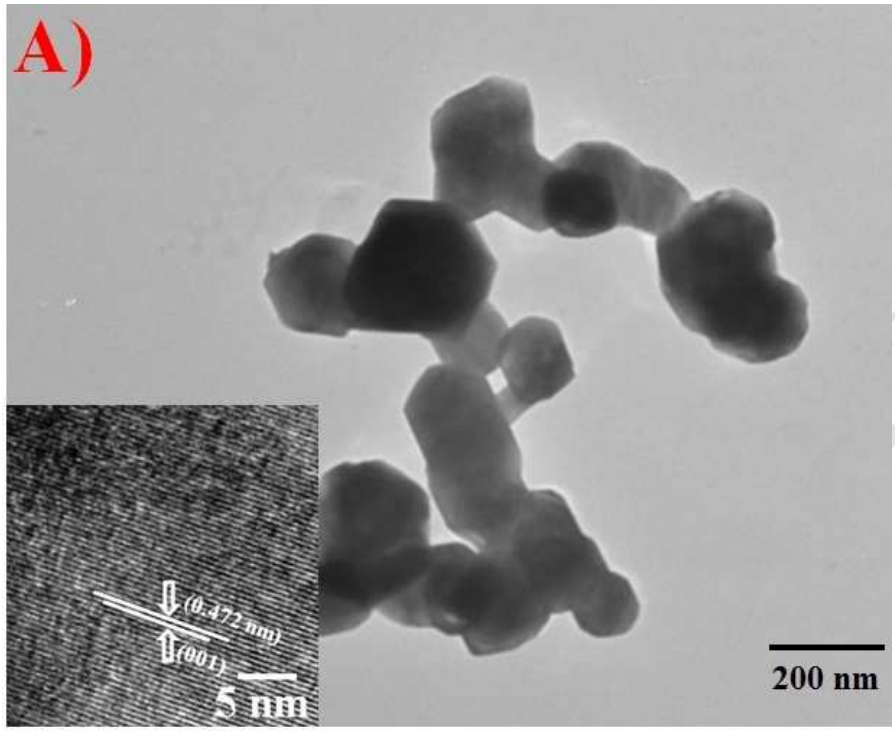

544

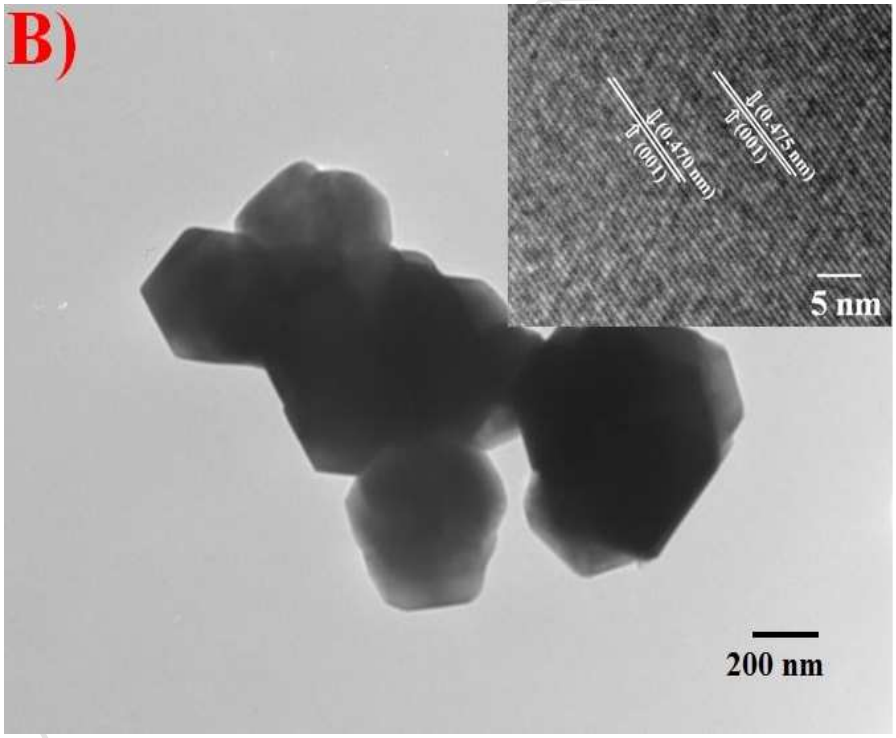

545 **Fig. 4**

546

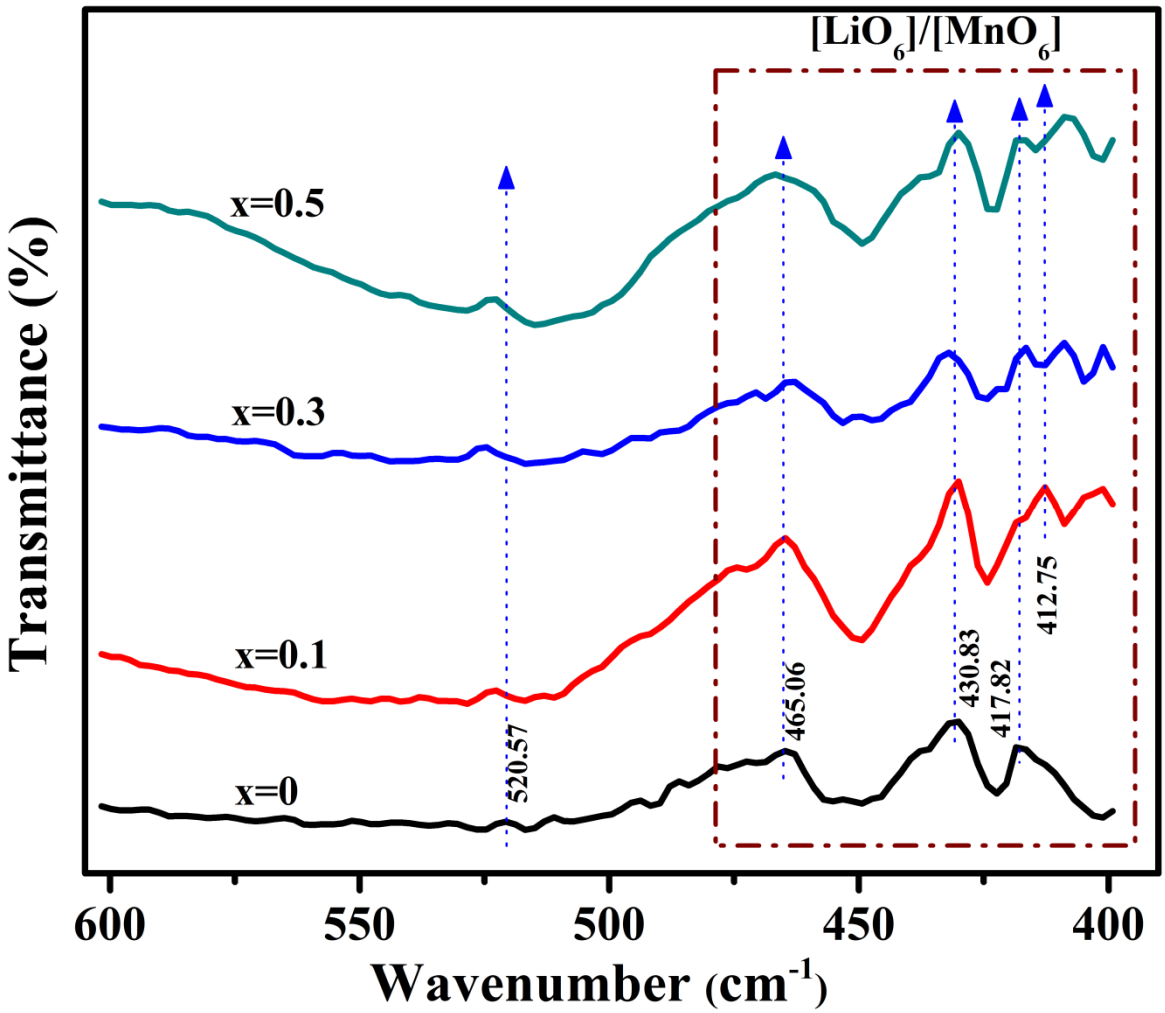

Fig. 5

ACCEPTED

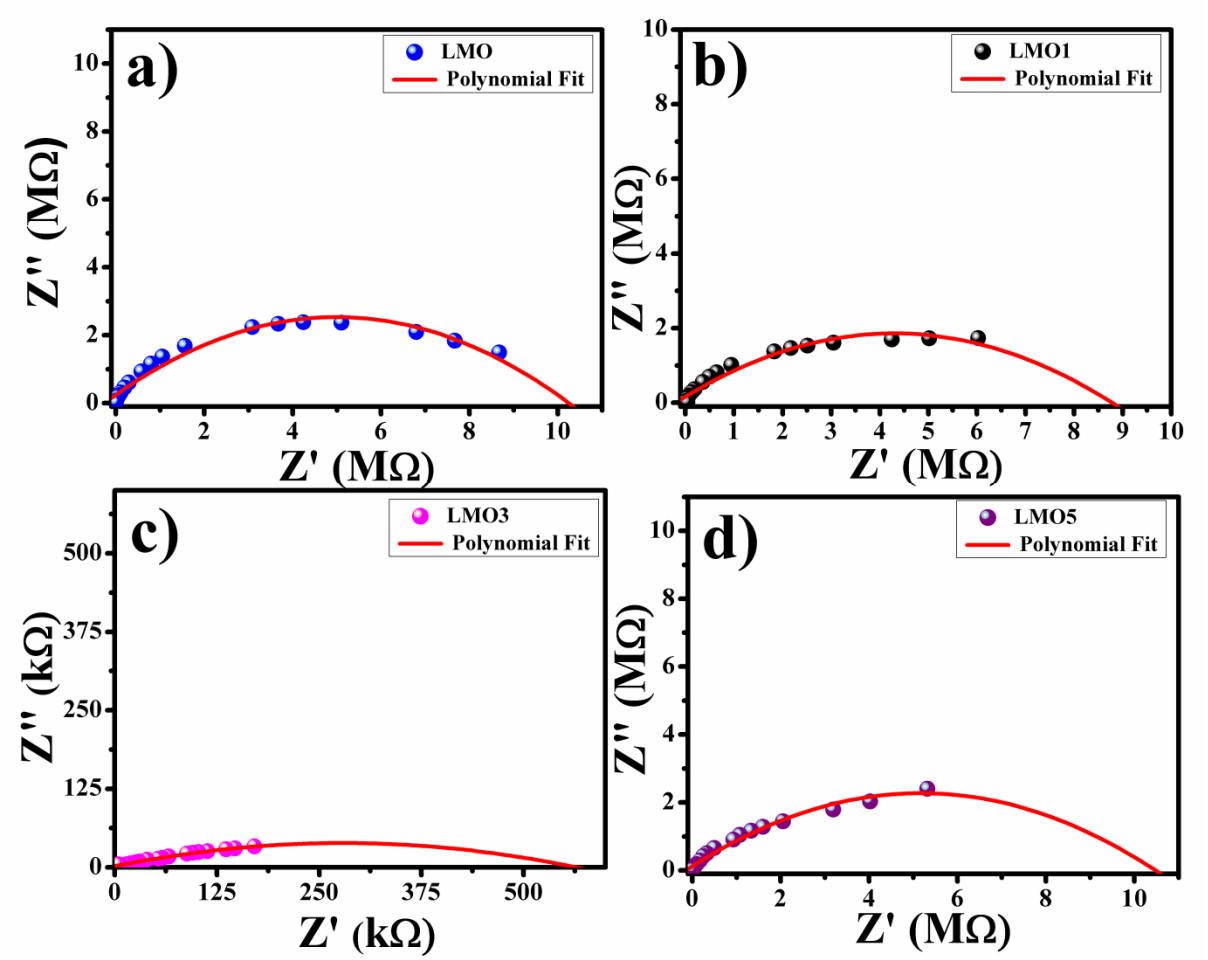

Fig. 6

ACCEPTED

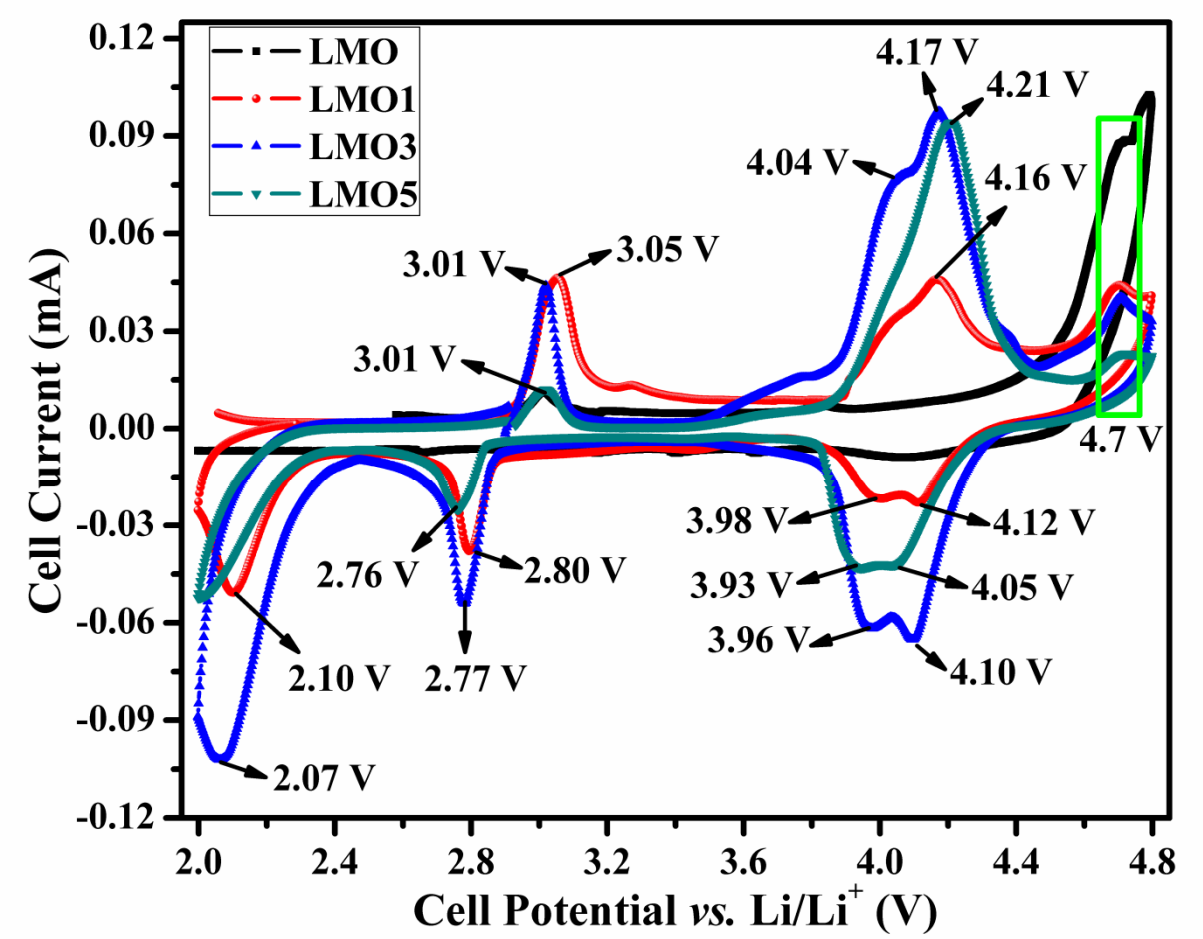

561

562 **Fig. 7**

563

ACCEPTED

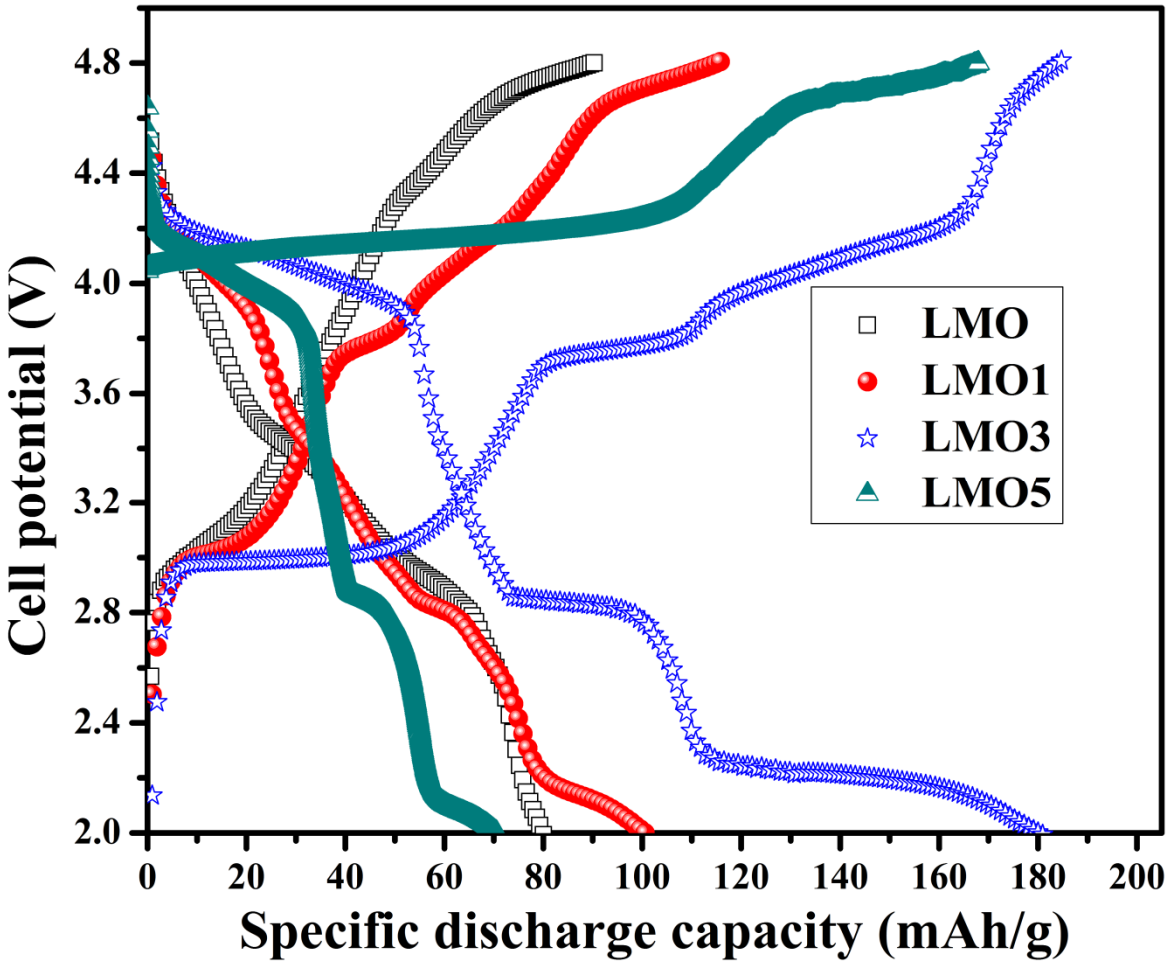

Fig. 8

ACCEPTED

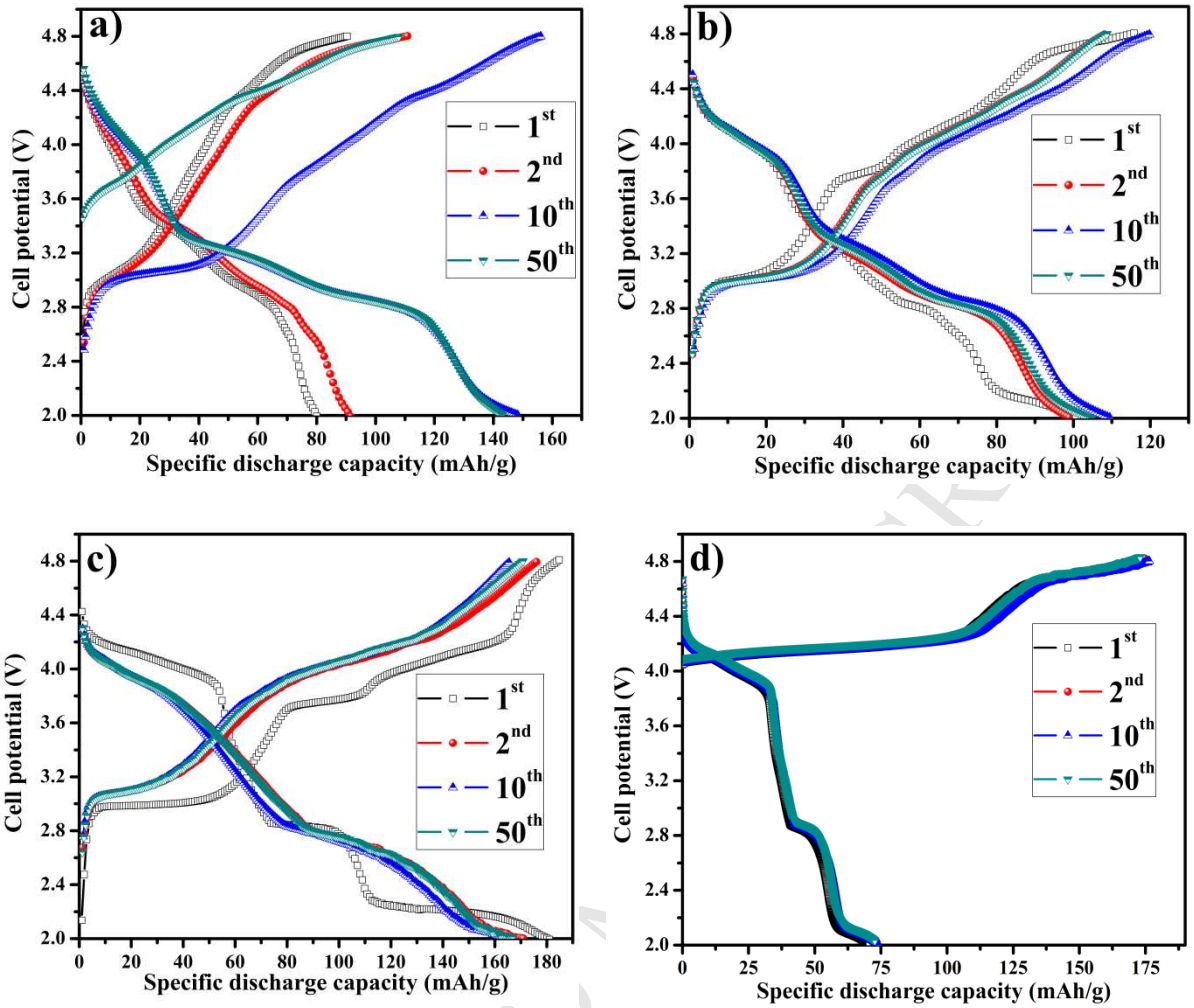
a)
b)
c)
d)
Cell potential (V)
Specific discharge capacity (mAh/g)
1st
2nd
10th
50th

Fig. 9

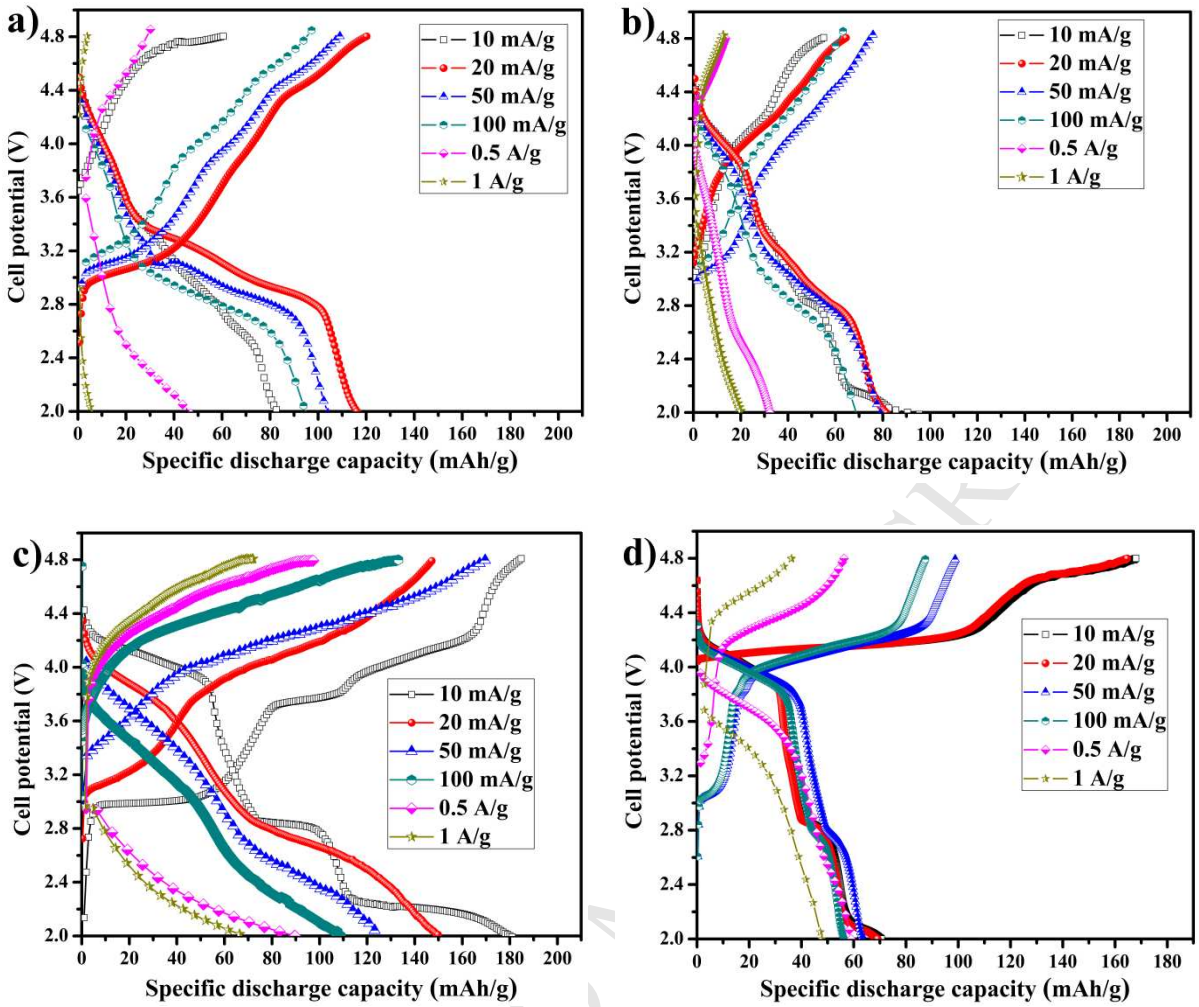

586

587

588 **Fig. 10**

589

590

591

ACCEPTED MANUSCRIPT

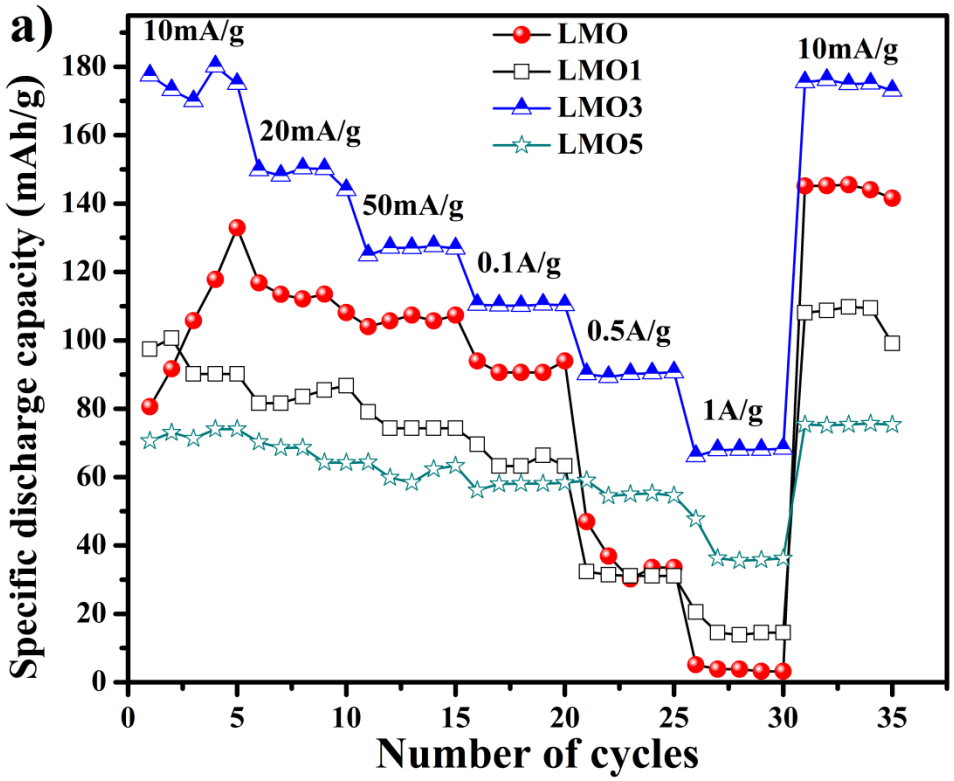

592

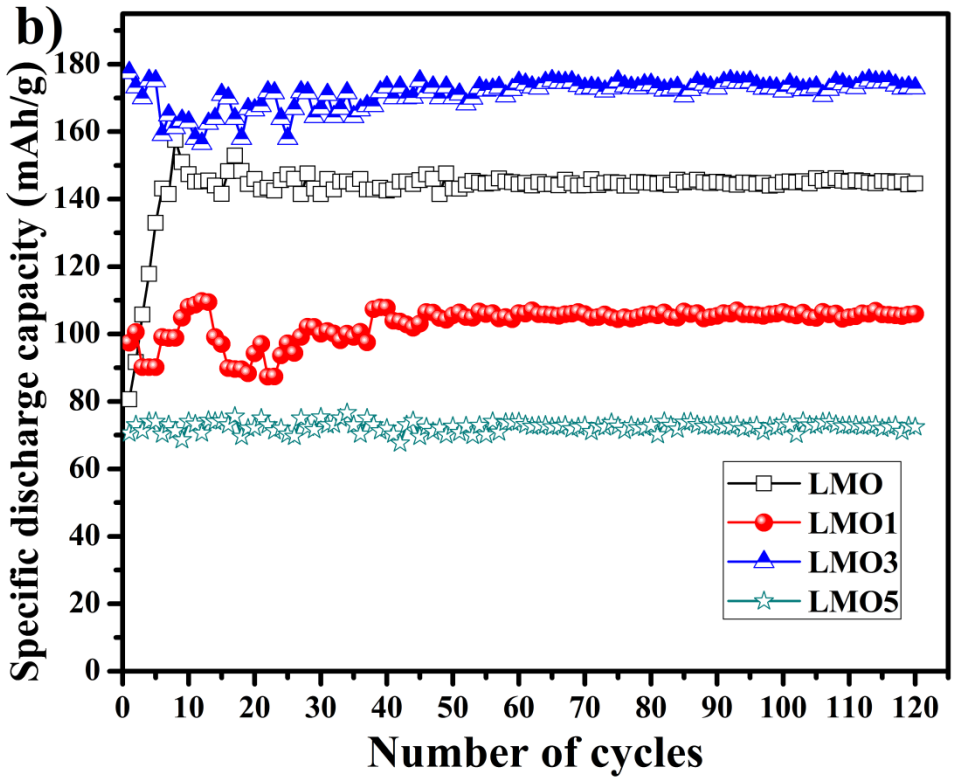

593

594 **Fig. 11**

595

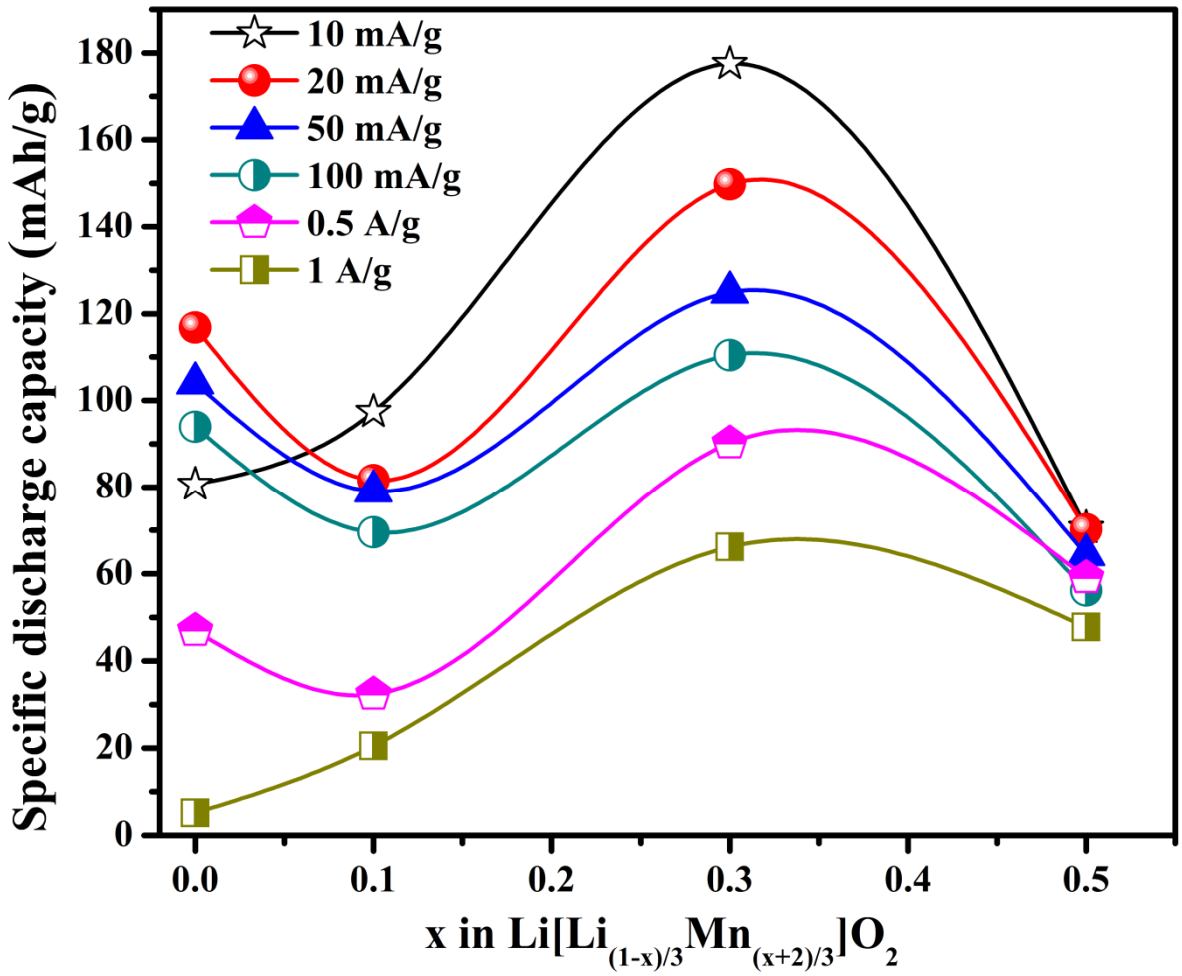

Fig. 12

ACCEPTED

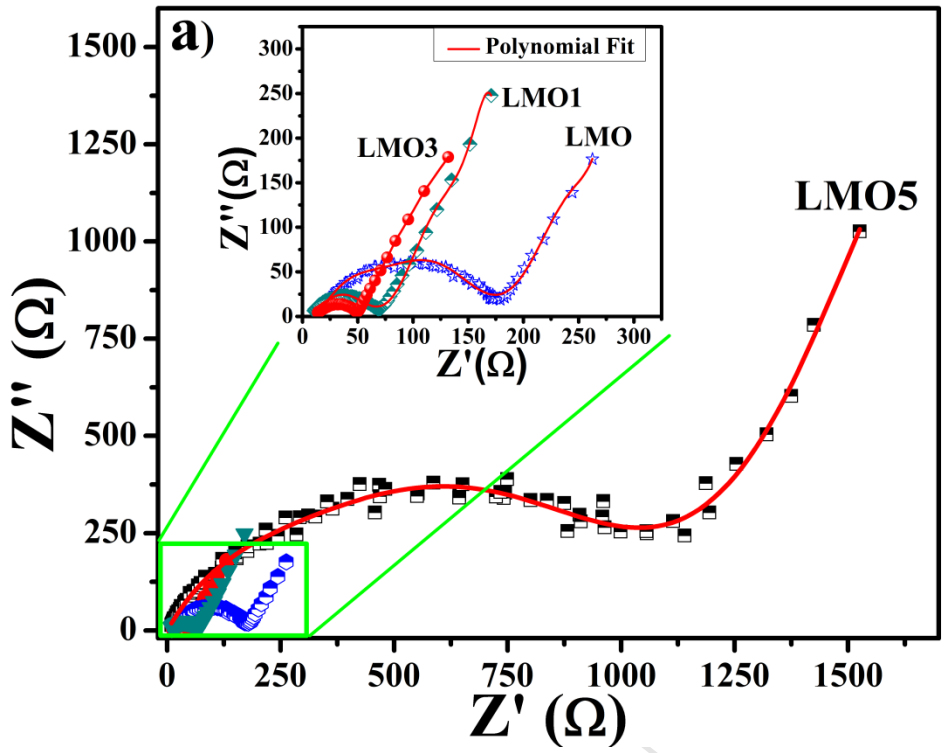

607

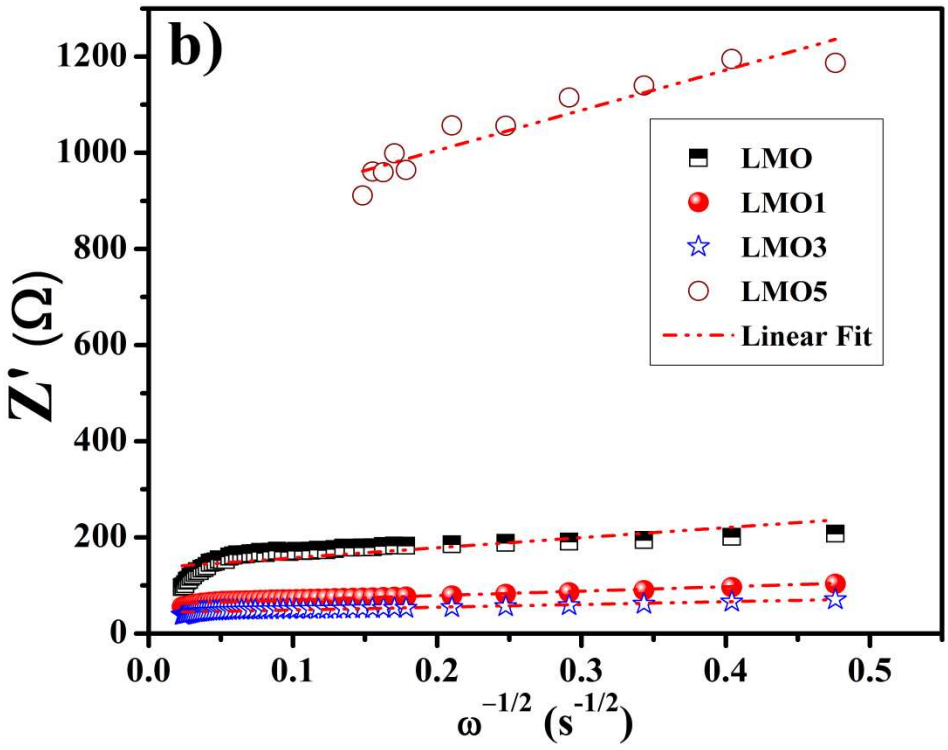

608

609 **Fig. 13**

Highlights

ACCEPTED MANUSCRIPT

- Synthesis of Novel Li-rich [$Li[Li_{(1-x)/3}Mn_{(x+2)/3}]O_2$; $0 \leq x \leq 0.5$] nanocomposite.
- Spherical morphology with slight agglomeration observed for the composition.
- Electronic conductivity increases to the 10^2-10^3 orders for LMO3 composition.
- LMO3 delivers best rate and cycling performances at all C-rate.

ACCEPTED MANUSCRIPT

Energy Efficient Reactive Protocol for data Aggregation in Wireless Sensor Network

Rajesh Kumar Yadav
Department of Computer Sc & Engineering
Delhi Technological University
Delhi, India
rkyadav@dce.edu

Daya Gupta
Department of Computer Sc & Engineering
Delhi Technological University
Delhi, India
dgupta@dce.ac.in

D. K. Lobiyal
School of Computer & System Sciences
Jawaharlal Nehru University
Delhi, India
lobiyal@gmail.com

Abstract: Wireless Sensor Networks (WSNs) are composed of a huge number of small sensors which are effective for gathering data in a variety of environments. Sensor nodes are usually battery powered so energy aware data transfer is required to maximize the network lifetime. In this paper we have introduced an energy efficient reactive protocol for data aggregation (EERPDA) for homogeneous sensor network which gives priority to Critical information and is also adaptive in nature. Here we propose the concept of the average distance of node from all its neighboring nodes and its distance from the Base Station(BS) for the cluster head selection, it helps in improving network lifetime. Moreover, cluster head (CH) selection also depends on the current energy of the sensor node. The proposed protocol compared with the existing protocols such as LEACH, ELEACH and I-LEACH using MATLAB simulation tool which reflects that the proposed protocol significantly improves the network lifetime and throughput in practical operational environments.

Keywords—Network lifetime, Energy efficient, Cluster head, Base station, Critical information

I. INTRODUCTION

Wireless Sensor Network is growing field as it uses the sensor technology and it is used in various application of day to day life.The main application of WSN [1][2] :- military surveillance, environment monitoring, agriculture, medical and health care applications includes blood pressure and oxygen measurement, used in smart phones, industrial application includes factory progress control and automation and in vehicle tracking systems etc.

But these networks have certain drawbacks such as limited battery source, network lifetime, energy efficiency [2][3]. To overcome these drawbacks the concept of clustering in terms of LEACH algorithm was proposed [4][5][6]. According to clustering, the nearby sensors form a cluster among them and then elect one among them as CH for that cluster. All the members send their sensed information to the CH, which act as aggregation points and communicate it to the sink node [1][2][3]. WSNs are classified into two different categories, based on the applications for which they are used:

Proactive: In this type of network the sensor nodes send information at regular intervals of time to cluster head or the Base Station. They are used in the applications which requires periodic monitoring [7][8][9].

Reactive: In this type of network the sensor nodes sense information on a regular basis, but only transmits the information to cluster head or the Base Station when it observes a huge change in the current sensed information and the previously send information, this makes it reactive in nature as it react to the situation and not on a regular basis [7][8][9].

This paper is organized as follows: Section II explains the background detail. Section III provides the proposed work. Section IV and V provide the simulation results and conclusion respectively.

II. BACKGROUND DETAIL

Clustering protocols are divided into two types in terms of sensor node's initial energy. In the homogeneous network every sensor node is given same initial energy. Whereas in heterogeneous network there can be more than two sets of nodes with different energy given to each set. But we are dealing with homogeneous networks. Some of the algorithms are described below:

LEACH [6] algorithm, is one of the famous clustering algorithm. It is a proactive protocol, which main concern is saving energy. In this distributed technique, the node makes a decision without central control. LEACH algorithm has two phases: Cluster forming phase, in which CH selection is done on the basis of threshold value T(n). Each node n compares a random number between 0 and 1. Now, the generated number is compared with the T(n) value for that particular node. The T(n) value is given by:

978-9-3805-4421-2/16/$31.00 ©2016 IEEE

$$T(n) = \begin{cases} \frac{P_{CH}}{1-P_{CH} \times (r \bmod \frac{1}{P_{CH}})} & \\ 0 & otherwis \end{cases} \quad (1)$$

If the generated number is less than this random value, then this node is considered as CH for that particular round ‚r'. Where, P_{CH} is a desired probability of CH in the network, G be the set of nodes that have not been CH in last $1/P_{CH}$ rounds.

The next phase is a Steady-State phase in which each node transfer its data to the CH and CHs send these data to sink. As the Non-CH node will send data via CH, it increases the network's lifetime. Although this protocol has certain drawbacks: Changing of CH is probabilistic in LEACH, which become its drawback as the low energy node has the same chance as that of the high energy node. Since it is proactive protocol, its attributes cannot be changed in between rounds and makes it not suitable for time critical applications.

LEACH-C [4], in which there is a central body (BS) to control the CH selection in each round. Each sensor nodes have to transmit its local data to the sink node and it will decide whether the node can become the cluster head (CH) or not. The centralize control is the drawback of this protocol. **ELEACH** [10], in this algorithm current energy of the nodes is given the preference for CH selection. The count of CH in each round is fixed.

In each round sensor node with maximum energy will become the CH for that particular round. **LEACH-D** [5], this considers into account the node density for the selection of CH, which means node having high density have more probability to become the CH. And also in cluster formation phase, Non-CH nodes join the cluster by considering CH's energy and distance from CH.

I-LEACH [11], is an improvement of LEACH which takes into account the remaining power of a node, the neighborhood of a node and distance of a node from the sink node in CH selection. Also during the cluster formation this algorithm gives more preference to distance between the BS and CH and not to the distance between the node and CH. Its drawback is that it is proactive in nature.

I. PROPOSED ALGORITHM

Here we have proposed a reactive algorithm for homogeneous networks, which is more energy effective than the other described algorithms. The proposed algorithm increases the network lifetime by considering various concepts. The proposed algorithm assumes following specifications in term of network deployment.

- Sensor node's position is static and they are distributed randomly over the whole network area.
- All the sensor nodes have limited battery and their battery cannot be charged again, once they are over with their battery they are supposed to be dead.
- All the nods are at same energy level initially
- Every node is given a unique identity and has the information about its current energy level.
- Each node can obtain sensory data and send it via cluster head or directly to the sink node.

The proposed algorithm is given below:

A. Cluster Head (CH) Selection phase:

In this proposed algorithm, the CH node is selected by considering some important factors, like current energy of each sensor node, average distance of a node from all its neighboring nodes and relative distance of a node from the Base Station. Also the node sensing Critical information in particular round will not take part in CH selection procedure for that round.

In this phase, every sensor node generates a random value in between 0 and 1. Now, this value is then compared with the improved threshold value T(n). If it is less than T(n), then node is taken as cluster head node for that particular round and leave the set G to prevent it from reelection in next $1/P_{opt}$ rounds. The threshold value is given by:

$$T(n) = \begin{cases} \frac{P_{opt}}{1 - P_{opt}(r \bmod (\frac{1}{P_{opt}}))} X \frac{E_{cur}}{E_{avg}} X \frac{d_{toCHavg}}{S_{avgdistonbr}(n)} X \frac{|d_{max} - d(n,\ BS)|}{d_{toBSavg}} & \\ 0 & otherwise \end{cases} \quad (2)$$

Where ‚r' is ongoing round, G is a set of sensor nodes which have not been selected as a cluster head node in last $1/P_{opt}$ rounds, E_{cur} is the current power of the sensor device, E_{avg} is the average power of all the sensor devices in the network, $S_{avgdistonbr}$ is the average distance of particular node ‚n' from all the neighboring nodes, $d_{toCHavg}$ is the average distance of CH from all the nodes inside its cluster, $d_{toBSavg}$ is the average distance of the sensor nodes from the BS, d(n, BS) is the distance between given node ‚n' and BS and d_{max} is the maximum distance from BS.

P_{opt} is the desired percentage of CH, is given by:

$$P_{opt} = \frac{k_{opt}}{N'} \quad (3)$$

Where N' is the number of sensor devices in the network and k_{opt} is the optimal amount of clusters and is given by:

$$k_{opt} = \left(\sqrt{\frac{N'}{2\pi}}\right) * \left(\sqrt{\frac{\epsilon fs}{\epsilon mp}}\right) * \frac{M}{(d_{toBSavg})^2} \quad (4)$$

$d_{toCHavg}$, $d_{toBSavg}$ and d_{max} is given by:

$$d_{toCHavg} = M/\sqrt{2k_{opt}\pi} \quad (5)$$

$$d_{toBSavg} = \frac{1}{N}\sum_{i=1}^{N} d(i, BS) \quad (6)$$

$$d_{max} = \sqrt{\left(\frac{M}{2}\right)^2 + \left(\frac{M}{2}\right)^2} \quad (7)$$

$S_{avgdistonbr}(n)$ is calculated by considering the radius of a neighborhood of a sensor node ‚n'. The nodes which come inside this radius are considered to be the neighbor of a node ‚n' and their distance from the node ‚n' is then calculated, $S_{avgdistonbr}(n)$ is the average distance of all these neighborhood nodes and is given by:

$$S_{avgdistonbr}(n) = \frac{1}{N_{nbr}}\sum_{j=1}^{N_{nbr}} dis(n, j) \quad (8)$$

Where, N_{nbr} is given by set of neighborhood sensor nodes of a given sensor node ‚n'. The radius of the neighborhood(Rch) is given by:

$$R_{ch} = \sqrt{\frac{M\ X\ M}{\pi\ X\ k_{opt}}} \quad (9)$$

Where M × M is the area covered by the network.

Moreover, this algorithm considers the current energy of sensor node for its selection as CH node, which means the more the current energy of a node more its probability to become the CH for that particular round.

B. Cluster Formation Phase:

During this phase, the Non-CH nodes have to decide which cluster head they belong to form the cluster. The decision taken by Non-CH node depends upon some parameters. The sensor node will join to the CH node for which the output of the given equation (10) produces minimum value.

$$\frac{d_{toBsc} * \sqrt{d_{toCHn}}}{(E_{cur}(n) * E_{cur}(CH))} \quad (10)$$

Where d_{toBsc} is the distance between the cluster head node and the Base Station, d_{toCHn} is the distance of Non-CH node ‚n' from the CH node, $E_{cur}(n)$ is the current energy of the node ‚n' and $E_{cur}(CH)$ is the current energy of that particular CH node. Here the node which is sensing Critical information will not take part in cluster formation phase.

C. Data Sensing and Transmission Phase

The BS broadcasts the following parameter in the given network area:

1. Hard Value Threshold [7][9] (Hv): It is an absolute value which allows the sensor node to transmit the sensed data when the sensed value is greater than or equal to ‚Hv'. If the sensed value is less than ‚Hv' then that particular sensor node will not transmit information to the CH in that round.
2. Soft Value Threshold [7][9] (Sv): It is an absolute value which will be compared with the difference between the current sensed value and the previously sensed value of the particular sensor node. If the difference is more or equal to that value, in that case the sensor node can send data to CH node.
3. Critical Value Threshold (Cv): There are applications which require sensor to sense some Critical information like temperature or military applications at certain times. This value marks the point at the sensed data value range, that if the sensor node sensed data having value above this point then that node is considered as Critical node for that particular round. Critical node need not to send its data to CH node as it sensed the data of utmost priority. So in that case it will directly transmit data to the BS and also not take part in CH selection and cluster formation phase.
4. Adaptive Meter [9] (Adm): As the proposed algorithm is reactive in nature, there come times when the sensor node is not sending data consecutively for too many rounds, which make Base Station clueless about its existence. To felt its existence to Base Station we have proposed Adaptive meter in a new way:

$$Adm\ \ \alpha\ \frac{1}{P_{opt}} \quad (11)$$

$$Adm\ = \frac{\lambda}{P_{opt}} \quad (12)$$

Where λ = 1, when the number of rounds reach to this Adm value for a particular sensor node, then that node will start its transmission without considering its threshold value and inform the Base Station about its existence.

These parameters make a sensor node to send data only when its sense something new and reduce the energy consumptions. Also, the nodes which are closer to the BS than that of their cluster head will directly transmit information to the BS.

II. EVALUATION OF PROPOSED ALGORITHM

A. Energy Model

We have used same energy model as in [11][6][12][13][14] algorithms. The model which we used is first order radio energy model. Energy dissipated by the sensor node for transmission of ‚m' bits data to the other node at a distance ‚d' from it, is given by:

$$E_{Tx}(m, d) = \begin{cases} mE_{elec} + m\epsilon fs\, d^2 & , d < do \\ mE_{elec} + m\epsilon mp\, d^4 & d \geq do \end{cases} \quad (13)$$

E_{Tx} is the energy required for transmission and it is directly proportional to m and d. d_o is the optimal distance and is given by:

$$do = \sqrt{\frac{\epsilon fs}{\epsilon mp}} \quad (14)$$

To receive ‚m' bits data, the energy expels by the node is given by:

$$E_{Rx}(m) = mE_{elec} \quad (15)$$

E_{Rx} is the energy required for reception. E_{elec} is the energy consumed in an electronic circuit.

B. Simulation Setup

To analyze the outcome of our proposed algorithm MATLAB used as a simulation tool. Table 1 describes the network parameter used in simulation. In the simulation we have compared the LEACH[6], ELEACH [10] and I-LEACH[11] with our proposed algorithm in terms of throughput, energy and network lifetime. Metrics, which are used to measure the performance, are given below:

1. Alive Nodes: Number of alive nodes after each round.
2. Throughput: Number of packets sent to the Base Station by each CH in every round.
3. Average Energy: Provide the average remaining energy of the network after every round.

C. Result and Analysis

The proposed algorithm is compared with some of the known algorithms working on the similar concept as ours. The LEACH[6] algorithm is the base for clustering algorithms. The other algorithms are I-LEACH[11] and ELEACH[10]. There are 200 homogeneous nodes deployed randomly over the network field of 200m * 200m area. These sensor nodes are sensing temperature in the range of (50^o, 200^o).

Table 1

NETWORK PARAMETERS

parameters	value
Network size (M * M)	200m *200m
Number of nodes (N)	200
Initial energy (E_o)	0.5 J
Electronic energy (E_{elec})	50 nJ/bit
Aggregation energy (E_{DA})	5 nJ/bit/message
Free space (єfs)	10 pJ/bit/m^2
Multipath fading (єmp)	0.0013 pJ/bit/m^4
Data packet size (m)	4000 bits
Critical sense value (Cv)	180^o

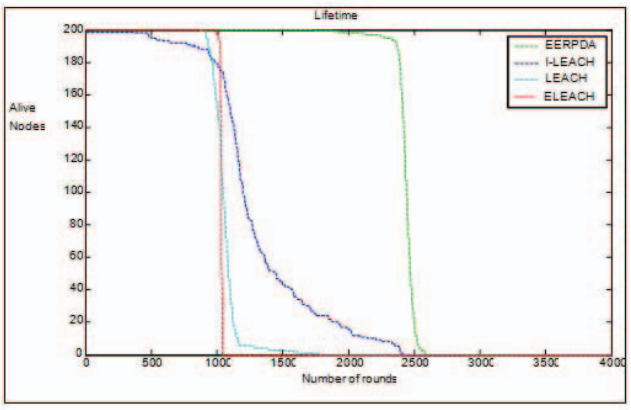

Figure.1 Network Lifetime

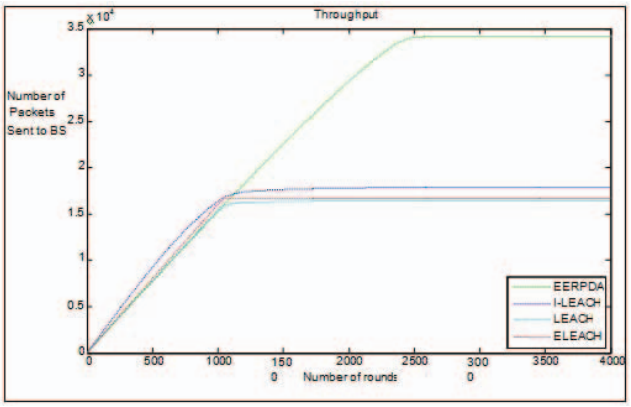

Figure 2: No. of packets sent to BS from CHs

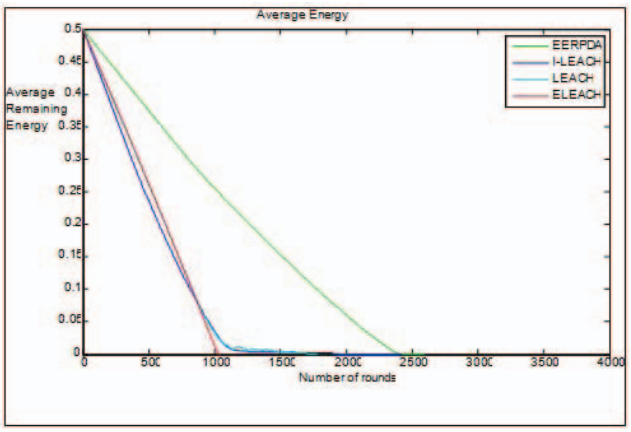

Figure 3: Average Energy

Figure.1 shows the network lifetime of all the algorithms which are compared. In case of LEACH[6] the first node dies after 881 rounds and the last node dies after 2007 round, which shows that there is no transmission after 2007 rounds in this

algorithm. But in case of ELEACH[10] the first node dies after 1052 rounds and the last node dies after 1076, which can be seen as a setback of this algorithm. Only the I-LEACH algorithm gives better result in terms of the last node dead (after 2088 rounds) but its first node dies very early after 239 rounds. Our algorithm gives better result than these three in both the areas, its first node dies even after the last node die of the ELEACH algorithm (after 1881 rounds) and its last node dies after 2591 rounds in the simulation of 4000 rounds.

Figure.2 shows the throughput of all the algorithms in terms of number of packets sent to BS from CHs. The number of packets sent to BS in case of LEACH[6] is 16700 and ELEACH[10] is somewhere 17200 at the end of 4000 rounds. In case of I-LEACH[11] it increases to 17500 at the end of the simulation. But in case of our algorithm the number of packets sent is almost double of all the three algorithms, it is around 34130 at the end of the simulation.

Figure.3 shows that total energy consumption is managed optimally in our algorithm, as it considered energy as a huge factor in terms of CH selection and cluster formation. Hence, taking energy as a factor, in all the three phases of the algorithm helps us in increasing the overall performance.

III. CONCLUSION

In this paper we have introduced, an Energy Efficient Reactive Protocol for data Aggregation which acts on Critical information and is also Adaptive in nature while being reactive. The overall result reflects that the proposed protocol significantly improves the network lifetime and throughput in practical operational environments.

REFERENCES

1. P. Kumarawadu, D.J. Dechene, M.Luccini, A.Sauer, " Alogrithm for Node Clustering in Wireless Sensor Network: A Survey", in IEEE, pp. 295-300, 2008.
2. K. Karenos, V. Kalogeraki, S. Krishnamurthy, " Cluster-based Congestion control for sensor network", ACM Transaction on Sensor Networks, pp. 1-39, 2008
3. I.F Akyildiz, Wireless Sensor Network: A survey, Computer networks 38 (2002) 393-422.
4. W.Heinzelman, A. Chandraksan and H. Balakrishnan,, "An Application-Specific Protocol Architecture for Wireless Microsensor Networks", IEEE Transaction on Wireless Communication, October, 2002.
5. Y. Liu, Z. Luo, K. Xu and L.Chen, " A Relaible Clustering Algorithm base on LEACH protocol in Wireless Sensor Networks", in ICMET pp. 692-696, September 2010.
6. W.Heinzelman, A. Chandraksan and H. Balakrishnan, "Energy-Efficient Communication Protocol for Wireless Micro Sensor Networks", Proceeding of the 33rd Hawaii International Conference on System Science, pp. 2-10, 2000.
7. A. Kashaf, N. Javaid, Z. A. Khan and I. A. Khan, "TSEP: Threshold-sensitive stable election protocol in wireless sensor network", *10th IEEE Int. Conf. on Frontiers of Information Technology,* 2012.
8. A.Sinha and D.K.Lobiyal, "A Multi-Level Strategy for Energy Efficient Data Aggregation in Wireless Sensor Networks", *Wireless Personnel Communication*, pp.1513-1531, 2013.
9. R.K Yadav, Arpan Jain, "Critical Heterogeneous Adaptive Threshold Sensitive Election Protocol for Wireless Sensor Networks", ICACCI , 2014.
10. Fan Xiangning, Song Yulin, "Improvement on Leach Protocol of wireless sensor networks", International Conference on Sensor Technologies and Applications, 2007.
11. Z. Beiranvand, A. Patooghy, M. Fazeli, " I-LEACH: An Efficient Routing Algorithm to Improve Performance & to reduce Energy Consumption in WSN", in IEEE pp. 13-18, 2013.
12. J. Gnanambigai, N. Renugarajan, K. Anbukkarasi, "LEACH and Its Descendant Protocol: A survey", ISSN 2278-9723, pp. 15-21, IJCCTS, September 2012.
13. Keerti Naregal, Anand Gudnavar, " Improved Cluster Routing Protocol for Wireless Sensor through Simplification", in IEEE, pp. 1-3, January 2012.
14. V. Loscri, G. Morabito, S. Marano, "A Two-Level Hierarchy for Low- Energy Adaptive Clustering Hierarchy", Proceeding of Vehicular Technology Conference 2005, vol3, 1809-1813.

Biosensors and Bioelectronics 90 (2017) 224–229

Contents lists available at ScienceDirect

Biosensors and Bioelectronics

journal homepage: www.elsevier.com/locate/bios

Excellent storage stability and sensitive detection of neurotoxin quinolinic acid

Ranjana Singh[a], Sunayana Kashyap[b], Suveen Kumar[c], Shiju Abraham[a], Tejendra K. Gupta[a], Arvind M. Kayastha[d], Bansi D. Malhotra[c], Preeti Suman Saxena[b,*], Anchal Srivastava[a,*], Ranjan K. Singh[a,*]

[a] Department of Physics, Institute of Science, Banaras Hindu University, Varanasi 221005, India
[b] Department of Zoology, Institute of Science, Banaras Hindu University, Varanasi 221005, India
[c] Department of Biotechnology, Delhi Technological University, Main Bawana Road, Delhi 110042, India
[d] School of Biotechnology, Institute of Science, Banaras Hindu University, Varanasi 221005, India

ARTICLE INFO

Keywords:
Quinolinic Acid
QPRT
Enzyme
Neurotoxin
Bio-electrodes

ABSTRACT

Quinolinic acid (QA) is a metabolite of tryptophan degradation obtained through kynurenine pathway, produced naturally in the mammalian brain as well as in the human cerebrospinal fluid. The presence of QA ~10–40 μM is a clear indicator of many neurological disorders as well as deficiency of vitamin B_6 in human being. In the present work; rapid, sensitive and cost-effective bio-electrodes were prepared to detect the trace amount of endogenous neurotoxin (QA). Cyclic voltammetry (CV) and differential pulse voltammetry (DPV) studies were carried out to measure the electrochemical response of the fabricated bio-electrodes as a function of QA concentrations. These devices were found to exhibit desirable sensitivity of ~7.86 mA μM^{-1} cm^{-2} in wide concentration range (6.5 μM-65 mM). The lower detection limit of this device is as low as 6.5 μM and it has excellent storage stability of ~30 days. The capability of the proposed electrochemical bio-sensor was also checked to detect QA in the real samples (human serum). These results reveal that the use of this electrochemical bio-sensor may provide a potential platform for the detection of QA in the real samples for the prior detection of many diseases.

1. Introduction

Quinolinic acid (pyridine 2,3-dicarboxilic acid, hereafter referred as QA) (Heyes et al., 1992) occurs naturally in the mammalian brain in nano-molar as well as in the human cerebrospinal fluid in several nano-molar to micro-molar amounts (Heyes et al., 1992; Chen et al., 2009; Schwarcz and Pellicciari, 2002). The presence of QA is found below 100 nM, whereas the increased level of this molecule (10–40 μM) can be detected in pathological conditions (Guillemin, 2012; Leipnitz et al., 2005). The increased level of this molecule is known to be responsible for many neurological disorders such as Alzheimer, (Guillemin and Brew, 2002) Huntington disease (Schwarcz et al., 2010) and HIV associated dementia (HAD) (Guillemin et al., 2004). The presence of QA also affects the function of neurons by the activation of *N*-methyl-D-aspartate (NMDA) receptors (Birley et al., 1982; Stone and Connick, 1985). Apart from these effects, its elevated level (30–164 μM) has also been recognized as a clear indicator of deficiency of vitamin B_6 in the human being (Brown et al., 1965). All these reports reveal that the elevated level of QA can be used to detect the presence of many diseases (Guillemin, 2012; Leipnitz et al., 2005; Guillemin and Brew, 2002; Schwarcz et al., 2010; Guillemin et al., 2004; Birley et al., 1982; Stone and Connick, 1985; Brown et al., 1965). Hence there is urgent need to fabricate; rapid, cost-effective, durable and sensitive sensor that can be used to detect the trace amount of QA for the early detection of many diseases as mentioned above (Guillemin, 2012; Leipnitz et al., 2005; Guillemin and Brew, 2002; Schwarcz et al., 2010; Guillemin et al., 2004; Birley et al., 1982; Stone and Connick, 1985; Brown et al., 1965).

Several detection techniques such as gas chromatography, mass spectrometry (During et al., 1989; Shoemaker and Elliott, 1991) liquid-chromatography (Patterson and Brown, 1980), thin layer chromatography (Taguchi et al., 1983), radio enzymatic assay (Foster et al., 1986) and capillary electrophoresis-mass spectrometry (Wang et al., 2013) can be utilized to determine the trace amount of QA in the biological samples. All these reported methods are time consuming as well as suffer from lack of selectivity, sensitivity and stability. Liquid

* Corresponding authors.
E-mail addresses: pssaxena@rediffmail.com (P.S. Saxena), anchalbhu@gmail.com (A. Srivastava), ranjanksingh65@rediffmail.com (R.K. Singh).

http://dx.doi.org/10.1016/j.bios.2016.11.053
Received 26 October 2016; Accepted 22 November 2016
Available online 23 November 2016
0956-5663/ © 2016 Published by Elsevier B.V.

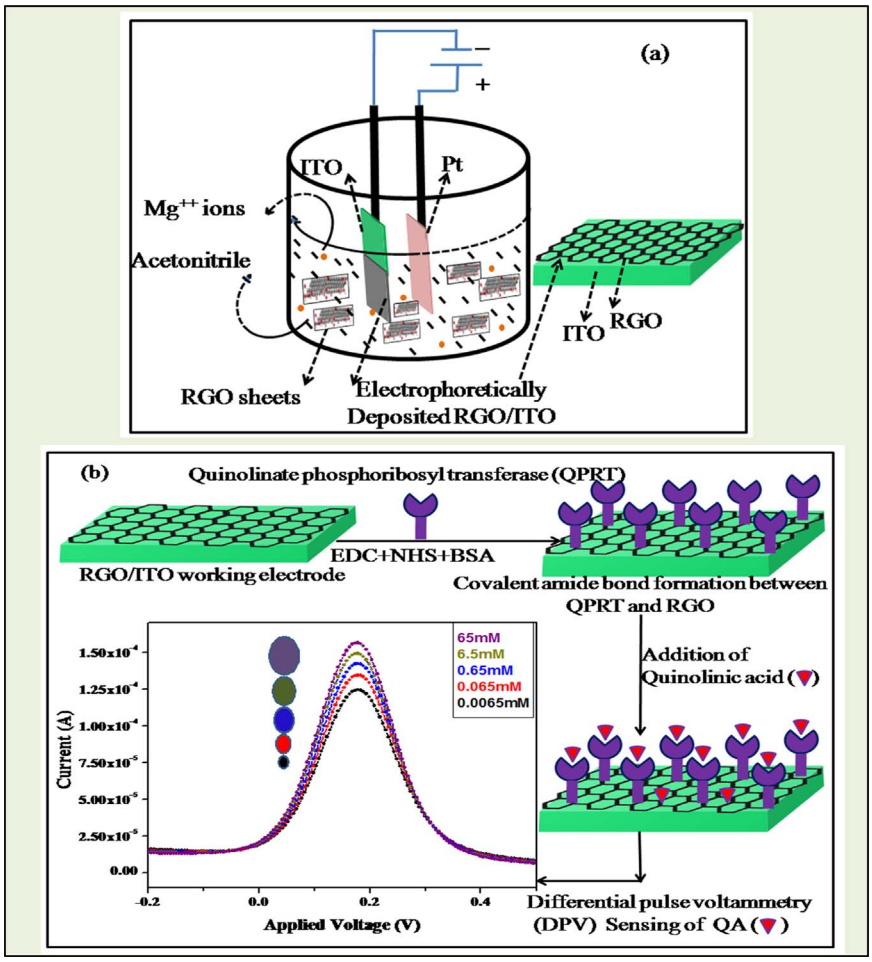

Fig. 1. Schematics for the (a) Fabrication of working electrode RGO/ITO by using electrophoretic deposition (EPD) technique and (b) immobilization of quinolinate phosphoribosyl transferase (QPRT) on working electrode RGO/ITO treated with EDC/NHS and BSA and sensing of QA via differential pulse voltammetry (DPV) technique.

chromatography with fluorimetric detection (Mawatari et al., 1995) has been reported to determine the trace amount of QA. However, this method suffers from certain limitations such as tedious procedure to handle the sample, to protect it from light and lack of selectivity. Fluorimetric detection of QA, based on catalytic activity of horseradish perioxidase (HRP) (Odo et al., 2009) in presence of hydrogen peroxide (H_2O_2) has been available to determine trace amount of QA. In this method; QA acquires fluorescing property but some reducing and oxidizing substances were found to affect the fluorescent derivatization of QA with HRP in presence of H_2O_2. Although sensitivity associated with this method is high but lack of selectivity, stability and time consuming procedure has remained as a challenge. Hence to remove all these short-comings, fabrication of such a sensing device having excellent storage stability and quick response is highly desirable for the early detection of the trace amount of QA.

Electrochemical bio-sensors have become more powerful sensing devices in recent years (Chikkaveeraiah et al., 2009) because of its quick response, sensitivity, simplicity, reproducibility and selectivity. These sensing devices require low reagents consumption, ease of fabrication, miniaturization and continuous monitoring of the analytes (Srivastava et al., 2011). As synthesized reduced graphene oxide (RGO, derivative of graphene) has become a promising material for biosensing applications recently in comparison to the graphene oxide (GO), (Srivastava et al., 2011; Schwierz, 2010; Park et al., 2012; Han et al., 2007; Pumera et al., 2010; Pumera, 2011; Huang et al., 2010, 2011; Srivastava et al., 2013). Chemically active RGO has large surface area, sufficient functional groups, potential to facilitate electron transfer from enzymes and proteins, cost-effective and easy to handle which are the essential properties of the electrochemical bio-sensors (Pumera et al., 2010; Pumera, 2011; Compton et al., 2011).

We have fabricated the cost-effective bio-sensor to detect the trace amount of QA. Various parameters (reproducibility, selectivity, magnitude of currents, linear coefficient and standard deviation) have been calculated for these devices. These bio-electrodes have good sensitivity of 7.86 mA μM^{-1} cm^{-2} with a wide range (6.5 μM– 65 mM) responses. It has good selectivity and excellent storage stability of ~30 days. The observed properties of the present bio-sensor are exciting and it can be useful to develop electrochemical bio-sensor for the early detection of QA. In the present work, we report results of the studies relating to the development of an electrochemical bio-sensing technique differential pulse voltammetry (DPV) to detect the trace amount of endogenous neurotoxin QA in the real samples (serum) also.

2. Experimental section

2.1. Materials

Quinolinate phosphoribosyl transferase (QPRT) enzyme was procured from KrishgenBiosystems, New Delhi India. Quinolinic acid (QA), 2, 6 pyridine di-carboxylic acid (PD), graphite flakes, acetonitrile, magnesium nitrate, sodium citrate, *N*-hydrooxysuccinimide (NHS), *N*-ethyl-*N*-(3-dimethylaminopropyl) carbodiimide (EDC), bovine serum albumin (BSA) and other analytical grade chemicals used in this work were procured from Sigma-Aldrich, India. All these materials were used without further purification.

2.2. Synthesis of reduced graphene oxide (RGO)

Graphene oxide (GO) was prepared by chemical route using Hummer's method (Marcano et al., 2010) and reduced graphene oxide (RGO) was obtained by reduction of GO with sodium citrate (Zhang et al., 2011). In this method, 100 mg sodium citrate was added into 10 ml aqueous suspension of GO (1 mg/ml) and the solution was stirred magnetically at 60 °C for ~6 h. Change in color from brown to black clearly indicates the reduction of GO to RGO. The RGO was treated in the following sequence; cooled down to room temperature, centrifuged at 10,000 rpm, washed with triple distilled water repeatedly and finally dried in the oven. The dried RGO powder was dispersed into water and acetonitrile for further use.

2.3. Preparation of RGO/ITO electrodes

Electrophoretic deposition (EPD) (Srivastava et al., 2013, 2012) technique was employed to fabricate RGO films on indium tin oxide (ITO) coated glass plate with sheet resistance ~30 Ω cm^{-1}. In this method, ITO-coated glass substrate acted as cathode and a platinum (Pt) foil (1 cm×2 cm) acted as an anode. These electrodes were kept parallel separated by 1 cm in a colloidal suspension of RGO prepared in acetonitrile (0.5 mg dl^{-1}). The 10^{-4}-10^{-5} M solution of Mg $(NO_3)_2 \cdot 6H_2O$ was added to the RGO suspension to enhance the deposition rate of RGO sheets on the cathode (ITO) (Wang et al., 2009; Compton et al., 2011). During the EPD process, DC voltage (150 V) was applied for two minutes. All these process involved in the preparation of working electrode has been depicted schematically in Fig. 1(a).

2.4. Immobilization of QPRT enzyme onto the RGO/ITO electrodes surface

An enzyme QPRT was covalently attached to RGO/ITO electrode. Prior to covalent attachment of the enzyme, COOH group of RGO was activated using EDC as a coupling agent and NHS as an activator. The COOH groups of RGO activated by following EDC/NHS chemistry (Srivastava et al., 2013; Sarkar and Nicholson, 1996) bind to the NH_2 groups of QPRT which results into the covalent amide bond (CONH) formation between RGO and QPRT. During the process of covalent attachment of QPRT to RGO/ITO electrode, 10 µl of QPRT enzyme (concentration 300 µg/ml) was freshly prepared in Tris HCl buffer (PH 8.0) and it was uniformly spread on the EDC/NHS activated RGO/ITO electrode [see Fig. 1(b)]. This electrode; immobilized with QPRT was incubated in humid chamber at room temperature for ~6 h. Since QPRT consisted of amino acids residues having NH_2 groups hence the formation of covalent immobilization was proposed via interaction between NH_2 functional groups of QPRT and COOH groups of RGO. Non-specific sites of the bio-electrodes were blocked by using bovine serum albumin (BSA). The amide bond formation was experimentally verified by FTIR spectra of QPRT/RGO. Schematic of immobilization of QPRT on working electrode RGO/ITO treated with EDC/NHS and BSA along with sensing of QA via differential pulse voltammetry (DPV) technique has been shown in Fig. 1(b).

3. Characterization

Structural and morphological characterizations were carried out using scanning electron microscopy (SEM, Philips XL 20), transmission electron microscopy (TEM-FEI Tecnai G2 electron microscope) and X-ray diffraction (XRD, Rigakuminiflex II). Raman (In-via Raman spectrometer, Renishaw), FTIR (Spectrum 65 FT-IR spectrometer, Perkin Elmer), UV–Visible (Lambda 25 UV–Visible spectrometer, Perkin Elmer) spectroscopic techniques were employed to characterize the as synthesized RGO. All the electrochemical measurements such as cyclic voltammetry (CV) and differential pulse voltammetry (DPV) were carried on Auto lab Potentiostat/Galvanostat (Eco Chemie, Netherlands) using three electrode cell configurations. Bio-electrode (QPRT/BSA/RGO/ITO), platinum foil and Ag/AgCl electrodes were used as working, counter and reference electrodes, respectively. The mixture of 5 mM $Fe(CN)_6^{4-}$ (Ferrocynide) and 5 mM $Fe(CN)_6^{3-}$ (Ferricynide) was used as the redox probe.

4. Results and discussion

4.1. Microstructural studies of RGO

SEM images of RGO shown in Fig. S1(a) indicates the uniform and sheet like morphology which is extended to several micrometers. Further, it is clearly visible that the thin layered RGO sheets consist of several wrinkles and folds. These wrinkles and folds might have developed due to defects and functional groups present in the carbon lattice. Fig. S1(b) shows TEM micrograph of RGO, which reveals a few layers of RGO sheets along with wrinkles and folds. HRTEM images in the inset of Fig. S1(b) indicates that the average inter-planar spacing of the lattice fringes of RGO is found to be ~3.5 Å.

The Raman spectrum of RGO has been shown in Fig. S1(c) containing four Raman bands observed at 1352, 1595, 2708 and 2930 cm^{-1}. The most prominent Raman band observed at 1352 cm^{-1} is assigned as D band which is attributed to the disorder present in the RGO. This structural disorder may be correlated to the oxygen functional groups as well as point defects present in the system. The Raman band centered at 1595 cm^{-1} is a well-defined; G band which represents the presence of sp^2 bonded carbon atoms. Overtone of D band i.e. 2D band is found at 2708 cm^{-1}. The presence of this overtone is clearly related to the dispersive nature as a function of frequency (Srivastava et al., 2012).

The X-ray diffraction (XRD) pattern of RGO which has been used as a working electrode for electrochemical bio-sensing studies recorded in the range of 10–75° is shown in Fig. S1(d). In the XRD pattern of RGO, an intense and broad peak with a 2θ value at around 25.28° is observed and assigned to the (00.2) (Srivastava et al., 2013) reflection plane corresponding to an inter-planner spacing of 0.352 nm, which is in good agreement with the HRTEM study [discussed in inset of Fig. S1(b)]. In addition to this, another peak of lower intensity is found at ~43.3° which is assigned to the (00.1) reflection plane of RGO (Srivastava et al., 2013). UV–Visible absorption spectrum of chemically synthesized RGO is shown in Fig. S1(e) where triple distilled water was taken as reference to record UV–Vis spectrum of RGO. The absorption peak at 268 nm can be assigned as π-π* transition of aromatic C=C bonds (Srivastava et al., 2013). Figs. S1(a), S1(b), S1(c), S1(d) and S1(e) have been provided in the Supplementary material.

4.2. FTIR spectroscopic studies of RGO, QPRT and QPRT/RGO electrodes

The IR spectra of RGO, QPRT and QPRT/RGO have been shown by (A), (B) and (C), respectively in Fig. 2(a). The IR bands observed at 1650 and 1400 cm^{-1} are attributed to stretching and bending mode vibrations of C=O and O-H bonds of carboxyl groups present in the RGO respectively. The COH and C=C stretching mode of vibrations are obtained at 1110 cm^{-1}, 1631 cm^{-1}, respectively. A broad band observed at 3453 cm^{-1} is assigned to stretching vibration of OH group. It is important to note that the IR spectra were taken in aqueous medium. The OH bonds of water strongly absorb at ~3453 cm^{-1} which overlaps with OH absorption of RGO. The OH stretching band of RGO is sharp. The OH stretching band of water being broad and strong hides the OH stretching band of RGO. New IR band of QPRT/RGO is obtained 985 cm^{-1} due to OH bending vibration of carboxylic group. While stretching vibrational mode corresponding to CN becomes prominent and is observed at 1215 cm^{-1}. The intensity of stretching mode of C=O in QPRT/RGO is found to be enhanced and blue shifted which confirms the amide bond formation between carboxylic and amino group of RGO

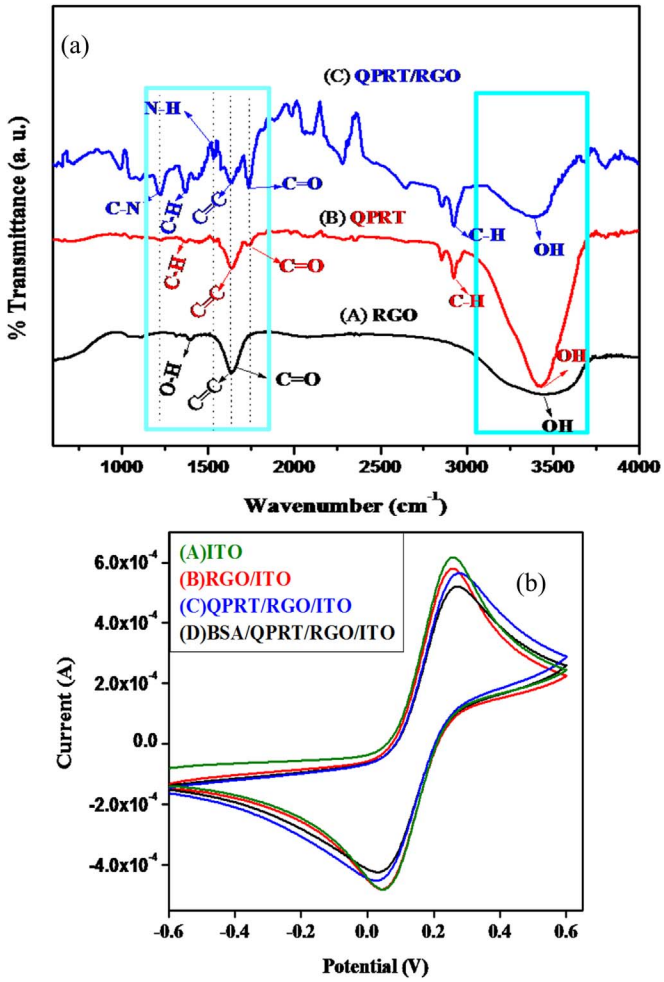

Fig. 2. (a) FT-IR spectrum of (A) RGO (B) QPRT and (C) QPRT/ RGO 3(b) CV curves of (A) ITO (B) RGO/ITO (C) QPRT/RGO/ITO and (D) BSA/QPRT/RGO/ITO electrodes.

and QPRT, respectively.

4.3. Electrochemical studies

The cyclic voltammetry (CV) studies of the fabricated electrodes were conducted in phosphate buffer solution (PBS) of pH 7.0 containing 0.9% NaCl and 5 mM solution of $[Fe(CN)_6]^{3-/4-}$. Fig. 3(b) shows cyclic voltammetry (CV) studies of ITO, RGO/ITO, QPRT/RGO/ITO and BSA/QPRT/RGO/ITO electrodes. It was found from the [Fig. 2(b)]

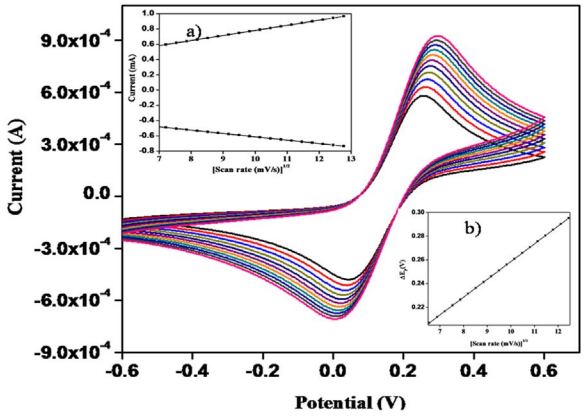

Fig. 3. Scan rate studies of RGO/ITO [Inset (a) magnitude of oxidation and reduction current generated as response of square root of scan rate (mV/s), Inset (b) potential as function of square root of scan rate] electrodes.

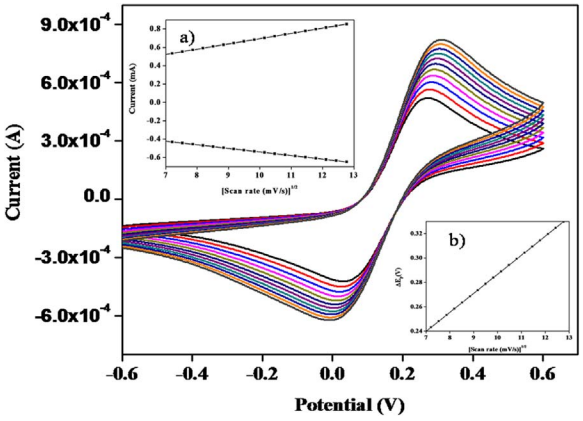

Fig. 4. Scan rate studies of BSA/QPRT/RGO/ITO [Inset (a) magnitude of oxidation and reduction current generated as response of square root of scan rate (mV/s), Inset (b) potential as function of square root of scan rate] electrodes.

that the magnitude of current for RGO/ITO electrode (Peak current 0.580 mA) is lower than that of bare ITO electrode (Peak current 0.616 mA), which indicated the reduction in electron transfer between solution and RGO/ITO interface. The immobilization of QPRT onto the RGO/ITO electrode further lowers the magnitude of peak current (0.565 mA) as compared to that of the RGO/ITO electrode. Bovine serum albumin (BSA) has been used for blocking of non-specific sites of QPRT/RGO/ITO bio-electrode. It was observed that magnitude of the peak current decreased again to 0.521 mA after coating of BSA on the surface of QPRT/RGO/ITO electrode. This reduction in peak current can be assigned due to adsorption of BSA on RGO/ITO sites of the QPRT/RGO/ITO immunoelectrode. To investigate the interfacial kinetics of the fabricated electrodes and bio-electrodes (RGO/ITO and BSA/QPRT/RGO/ITO) scan rate studies were conducted through CV. Fig. 3 and Fig. 4 show the observed CV response of RGO/ITO and BSA/QPRT/RGO/ITO electrodes respectively as a function of the scan rate (50–150 mV/s). A shift was observed in the redox peaks with increase in scan rate. It was also observed that cathodic (Ipc) and anodic peak (Ipa) currents both vary linearly with square root of the scan rate [insets (a) in Fig. 3 and Fig. 4], which indicated that the electrochemical reaction was a diffusion-controlled process (Kumar et al., 2015). The slopes and intercepts for the bio-electrodes RGO/ITO, and BSA/QPRT/RGO/ITO can be given by Eqs. (1–4):

$$I_{pc(RGO/ITO)} = [0.066\ mA(s/mV) \times (\text{scan rate}(mV/s))^{1/2}] + 0.119\ mA,\quad R^2 = 0.999,\ SD = 7.26 \times 10^{-3} \tag{1}$$

$$I_{pa(RGO/ITO)} = -[0.044\ mA(s/mV) \times (\text{scanrate}(mV/s))^{1/2}] - 0.175\ mA,\quad R^2 = 0.999,\ SD = 5.51 \times 10^{-3} \tag{2}$$

$$I_{pc(BSA/QPRT/RGO/ITO)} = [0.058\ mA(s/mV) \times (\text{scanrate}(mV/s))^{1/2}] + 0.120\ mA,\quad R^2 = 0.999,\ SD = 5.13 \times 10^{-3} \tag{3}$$

$$I_{pa(BSA/QPRT/RGO/ITO)} = -[0.039\ mA(s/mV) \times (\text{scan rate}(mV/s))^{1/2}] - 0.152\ mA,\quad R^2 = 0.999,\ SD = 4.45 \times 10^{-3} \tag{4}$$

The difference of cathodic (E_{pc}) and anodic (E_{pa}) peak potentials ($\Delta E_p = E_{pc} - E_{pa}$) and square root of scan rate for RGO/ITO and BSA/QPRT/RGO/ITO electrodes exhibit a linear relationship and follow Eqs. (5) and (6). A good linear relationship indicates the facile electron transfer from medium to the electrodes [inset (b) in Figs. 3 and 4].

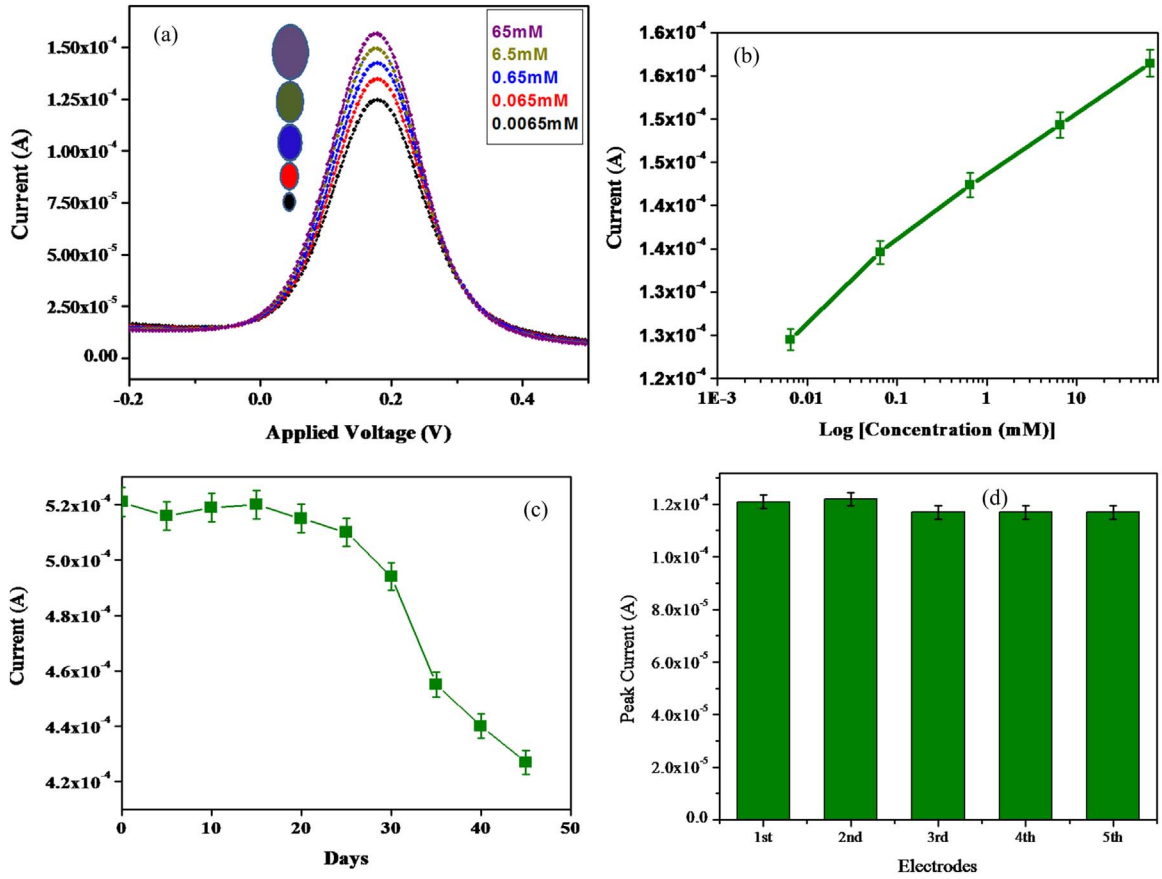

Fig. 5. (a) Electrochemical current response studies (differential pulse voltammetry, DPV) of BSA/QPRT/RGO/ITO electrode as a function of QA concentration [ranging from 6.5 μM to 65 mM] (b) Linearity between peak current of the bio-electrode measured by differential pulse voltammetry (DPV) and QA concentration has been shown on Log scale (c) Electrochemical current response studies (cyclic voltammetry, CV) of BSA/QPRT/RGO/ITO electrode as a function of time (days) and (d) Electrochemical current response studies (differential pulse voltammetry, DPV) of five different bio-electrodes BSA/QPRT/RGO/ITO fabricated via same set of procedure.

$$\Delta E_p(\mathrm{V})_{(\mathrm{RGO/ITO})} = [0.015\ \mathrm{V}(s/\mathrm{mV}) \times (\text{scan rate}(\mathrm{mV}/s))^{1/2}] + 0.11\ V,$$
$$R^2 = 0.999,\ \ SD = 1.31 \times 10^{-3}$$
$$\Delta E_p(\mathrm{V})_{(\mathrm{BSA/QPRT/RGO/ITO})} = [0.016\ \mathrm{V}(s/\mathrm{mV}) \times (\text{scanrate}(\mathrm{mV}/s))^{1/2}] + 0.13\ V, \quad (5)$$

$$R^2 = 0.998,\ \ SD = 1.78 \times 10^{-3} \quad (6)$$

where R is the correlation coefficient and SD is the standard deviation.

The diffusion coefficient (D) of bio-electrode BSA/QPRT/RGO/ITO was calculated using Randle Sevick equation (Kumar et al., 2016) (Eq. (7)) and found to be 0.31 $cm^2\ s^{-1}$.

$$I_p = (2.69 \times 10^5)\ n^{3/2} A\ D^{1/2} C\ \upsilon^{1/2} \quad (7)$$

where Ip is the peak current of immunoelectrode, n is the number of electrons (1) transferred, A is the active surface area of the immunoelectrode (0.25 cm^2), D is the diffusion coefficient, C is the concentration of redox species (5 mmol cm^{-2}) and υ is the scan rate (50 mV/s). Surface concentration (γ) of BSA/QPRT/RGO/ITO electrode was determined by using Laviron's theory (Sharma et al., 2012) given by

$$I_p = n^2 F^2 \gamma A \upsilon (4RT)^{-1} \quad (8)$$

where I_p represents the peak current of electrode, n is the number of electrons (1) transferred, F is the Faraday constant (96485 C mol^{-1}), γ is the surface concentration of the absorbed electro-active species, A is the surface area of the electrode, ν is the scan rate (V/s), R is the gas constant (8.314 J $mol^{-1}\ K^{-1}$) and T is room temperature (25 °C or 298 K). The Eq. (8) yields Υ to be 4.42×10^{-8} mol cm^{-2}.

4.4. Differential pulse voltammetry measurements

Differential pulse voltammetery (DPV) studies were carried out to measure the electrochemical response of the fabricated bio-electrodes (BSA/QPRT/RGO/ITO) as a function of QA concentration varying from 6.5 μM to 65 mM in PBS (pH 7.0, 0.9% NaCl) containing 5 mM $[Fe(CN)_6]^{3-/4-}$ [Fig. 5(a)]. It was observed that the magnitude of current increased with increase in concentration of QA which can be attributed to the formation of enzyme-ligand complex at the electrode surface. This process of complex formation leads to electron release at the electrode surface. QPRT; a member of the phosphoribosyl family of enzymes has been recognized to catalyze the formation of nicotinic acid mononuleotide from QA and substrate 5-phosphoribosyl-1-pyrophosphate (Bello and Grubmeyer, 2010). In this process, QA binds first to QPRT which may cause release of electron at the electrode surface. In the present work this process was monitored through differential pulse voltammetry measurements. Furthermore, a linear correlation was obtained in the wide concentration range of 6.5 μM to 65 mM (R^2 =0.993, SD =4.71×10^{-4}) and follow Eq. (9). Linearity between peak current of the bio-electrodes measured by differential pulse voltammetry (DPV) and QA concentration shown on log scale has been depicted in Fig. 5(b). The sensitivity of the electrode is found to be 7.86 mA $\mu M^{-1}\ cm^{-2}$.

$$I_p(\mathrm{mA}) = 7.86\ \mathrm{mA}\ \mu M^{-1} \mathrm{cm}^{-2} \times \log[\text{concentration}\ (\mu M)] + 0.143\ \mathrm{mA},$$
$$R^2 = 0.993,\ \ SD = 4.71 \times 10^{-4} \quad (9)$$

Several studies on different sensing techniques and sensing characteristic of the proposed electrochemical bio-sensor BSA/QPRT/

Table 1
Sensing characteristics of the proposed electrochemical bio-sensor BSA/QPRT/RGO/ITO summarized along with some results reported in the literature.

Detection techniques of quinolinic acid (QA)	Detection range	Detection limit	Sensitivity	Stability (days)	References
Radio enzymatic assay for quinolinic acid	–	2.5 pmol	–	–	Kumar et al. 2015
Capillary electrophoresis-mass spectrometry	0.4–40 μM	–	–	–	Kumar et al. 2016
Liquid chromatography with fluorimetric detection	0.36–68.8 nmol ml^{-1}	–	–	–	Leipnitz et al. 2005
Fluorimetric detection of quinolinic acid by catalytic activity of horseradish peroxidase	0.1–5 nmol ml^{-1}	0.04 nmol ml^{-1}	–	–	Mawatari et al. 1995
Electrochemical bio-sensor	**6.5 μM–65 mM**	**6.5 μM**	**7.86 mA $\mu M^{-1} cm^{-2}$**	**30**	**Present work**

RGO/ITO discussed above have been compared and summarized in Table 1.

The stability of the BSA/QPRT/RGO/ITO electrode was determined by CV studies at a regular interval of 5 days up to 45 days [Fig. 5(c)] and stored at 4 °C until further use. It was observed that magnitude of the peak current exhibited 95% response upto 30 days and there after the peak current decreased and reached to 80% at the end of 45 days. It indicates that the stability of the fabricated BSA/QPRT/RGO/ITO bio-electrode is upto ~30 days. In order to ensure reproducibility, five different bio-electrodes of constant surface area were prepared under similar conditions and their electrochemical responses were investigated by DPV studies. These bio-electrodes exhibit good reproducibility. Mean value of the current was found equal to ~119 μA. Each measurement was repeated for three times for each electrode and error bar was included accordingly. The relative standard deviation (RSD) for each bio-electrode was less than ~5% which showed the reproducibility of the fabricated bio-electrodes is high [Fig. 5(d)]. DPV measurements have also been carried out for the detection of QA in the real sample (serum) as shown in Fig. S3.

5. Conclusions

Early detection of endogenous neurotoxin, quinolinic acid may be helpful to the patients suffering from many neurological disorders such as Alzheimer's, Huntington's and HIV associated dementia (HAD) as well as deficiency of vitamin B_6. In this work selective, stable and reproducible bio-electrodes have been fabricated to detect quinolinic acid. The proposed bio-sensor based on electrochemical sensing may provide potential platform for the sensitive and selective detection of QA which can be used for the early detection of the neurological disorders and other diseases in the real samples in future.

Conflict of interests

The authors declare no competing financial interest.

Acknowledgements

Ranjana Singh is grateful to UGC, New Delhi, Govt. of India for providing financial support in terms of BHU research fellowship. One of the authors (TKG) is grateful to UGC for providing the research grant under the UGC Dr. D. S. Kothari Post-Doctoral Fellowship Scheme [No. F. 4-2/2006 (BSR)/PH/13–14/0108]. RKS is grateful to AvH Foundation, Germany, DST and CSIR, New Delhi, Govt. of India for support to procure Micro-Raman setup. AS is thankful to DST India (Project Code: DST/TSG/PT2012/68 & DST PURSE SCHEME 5050) and CAS-UGC, (Grant No. [F.530/7/CAS-V/2015/(SAPI)); Departmental Programme for providing financial assistance.

Appendix A. Supporting information

Supplementary data associated with this article can be found in the online version at doi:10.1016/j.bios.2016.11.053.

References

Bello, Z., Grubmeyer, C., 2010. Biochemistry 49, 1388–1395.
Birley, S., Collins, J.F., Perkins, M.N., Stone, T.W., 1982. Br. J. Pharmacol. 77, 7–12.
Brown, R.R., Yess, N., Price, J.M., Linkswiler, H., Sawan, P., Hankes, L.V., 1965. J. Nutr. 87, 419–422.
Chen, Y., Meininger, V., Guillemin, G.J., 2009. Cent. Nerv. Syst. Agents Med. Chem. 9, 32–39.
Chikkaveeraiah, B.V., Liu, H., Mani, V., Papadimitrakopoulos, F., Rusling, J.F., 2009. Electrochem. Commun. 11, 819–822.
Compton, O.C., Jain, B., Dikin, D.A., Abouimrane, A., Amine, K., Nguyen, S.T., 2011. ACS Nano 5, 4380–4391.
During, M.J., Freese, A., Heyes, M.P., Swartz, K.J., Markey, S.P., Roth, R.H., Martin, J.B., 1989. FEBS Lett. 247, 438–444.
Foster, A.C., Okuno, E., Brougher, D.S., Shwarcz, R., 1986. Anal. Biochem. 158, 98–103.
Guillemin, G.J., 2012. FEBS J. 279, 1356–1365.
Guillemin, G.J., Brew, B.J., 2002. Redox Rep. 7, 199–206.
Guillemin, G.J., Kerr, S.J., Brew, B.J., 2004. Neurotox. Res. 7, 103–123.
Heyes, M.P., Saito, K.J., Crowley, S., Davis, L.E., Demitrack, M., Der, A.M., Dilling, L.A., Elia, J., Kruesi, M.J.P., Lackner, A., Larsen, S.A., Lee, K., Leonard, H.L., Markey, S.P., Martin, A., Milstein, S., Mouradian, M.M., Pranzatelli, M.R., Quearry, B.J., Salazar, A., Smith, M., Strauss, S.E., Sunderland, T., Swedo, S.W., Tourtellotte, W.W., 1992. Brain 115, 1249–1273.
Huang, Y., Dong, Shi, X., Li, Y., Li, C.M., Chen, L.-J.P., 2010. Nanoscale 2, 1485–1488.
Han, M.Y., Oezyilmaz, B., Zhang, Y., Kim, P., 2007. Phys. Rev. Lett. 98, 206805–206809.
Huang, X., Yin, Z., Wu, S., Qi, X., He, Q., Zhang, Q., Yan, Q., Boey, F., Zhang, H., 2011. Small 7, 1876–1902.
Kumar, S., Kumar, S., Tiwari, S., Srivastava, S., Srivastava, M., Yadav, B.K., Kumar, S., Tran, T.T., Dewan, A.K., Mulchandani, A., Sharma, J.G., Maji, S., Malhotra, B.D., 2015. Adv. Sci. 2 (8), 1500048.
Kumar, S., J.G, Maji, S., Malhotra, B.D., 2016. Biosens. Bioelectron. 78, 497–504.
Leipnitz, G., Schumacher, C., Scussiato, K., Dalcin, K.B., Wannacher, C.M.D., Wayse, A.T.D., Dutra, C.S., Wagner, M., Latini, A., 2005. Int. J. Dev. Neurosci. 23, 695–701.
Mawatari, K.-I., Oshida, K., Iinuma, F., Watanabe, M., 1995. Anal. Chim. Acta 302, 179–183.
Marcano, D.C., Kosynkin, D.V., Berlin, J.M., Sinitsakii, A., Sun, Z., Slesarev, A., Alemany, L.B., Lu, W., Tour, J.M., 2010. ACS Nano 4, 4806–4814.
Odo, J., Inoguchi, M., Hirai, A., 2009. J. Health Sci. 55, 242–248.
Pumera, M., Ambrosi, A., Bonanni, A., Chng, E.L.K., Poh, H.L., 2010. Trac-Trend Anal. Chem. 29, 954–965.
Pumera, M., 2011. Mater. Today 14, 308–315.
Park, S.J., Kwon, O.S., Lee, S.H., Song, H.S., Park, T.H., Janng, J., 2012. Nano Lett. 12, 5082–5090.
Patterson, J.I., Brown, R.R., 1980. J. Chromatogr. 182, 425–429.
Schwarcz, R., Pellicciari, R., 2002. J. Pharmacol. Exp. Ther. 303, 1–10.
Schwarcz, R., Guidetti, P., Sathyasaikumar, K.V., Muchowski, P.J., 2010. Prog. Neurobiol. 90, 230–245.
Stone, T.W., Connick, J.H., 1985. Neuroscience 15, 597–617.
Shoemaker, J.D., Elliott, W.H., 1991. J. Chromatogr. 562, 125–138.
Srivastava, S., Solanki, P.R., Kaushik, A., Ali, M.A., Srivastav, A., Malhotra, B.D., 2011. Nanoscale 3, 2971–2977.
Schwierz, F., 2010. Nat. Nanotechnol. 5, 487–496.
Srivastava, S., Kumar, V., Ali, M.A., Solanki, P.R., Srivastava, A., Sumana, G., Saxena, P.S., Joshi, A.G., Malhotra, B.D., 2013. Nanoscale 5, 3043–3051.
Sarkar, P., Nicholson, P.S., 1996. J. Am. Ceram. Soc. 79, 1987–2002.
Srivastava, R.K., Srivastava, S., Narayanan, T.N., Mahlotra, B.D., Vajtai, R., Ajayan, P.M., Srivastava, A., 2012. ACS Nano 6, 168–175.
Sharma, A., Pandey, C.M., Sumana, G., Soni, U., Sapra, S., Srivastava, A., Chatterjee, T., Malhotra, B.D., 2012. Biosens. Bioelectron. 38 (1), 107–113.
Taguchi, H., Koyama, S., Shimabyashi, Y., Iwai, K., 1983. Anal. Biochem. 131, 194–197.
Wang, X., Davis, I., Liu, A., Miller, A., Shamsi, S.A., 2013. J. Chromatogr. A 1316, 147–153.
Zhang, Z., Chen, H., Xing, C., Guo, M., Xu, F., Wang, X., Gruber, H.J., Zhang, B., Tang, J., 2011. Nano Res. 4, 599–611.

Exploratory Test Oracle using Multi-Layer Perceptron Neural Network

Wellington Makondo
Department of Information Technology
Harare Institute of Technology
Harare, Zimbabwe
wmakondo@hit.ac.zw

Raghava Nallanthighal
Department of Information Technology
Delhi Technological University
New Delhi, India
nsraghava@gmail.com

Innocent Mapanga
Department of Computer Science
Harare Institute of Technology
Harare, Zimbabwe
imapanga@hit.ac.zw

Prudence Kadebu
Department of Software Engineering
Harare Institute of Technology
Harare, Zimbabwe
pkadebu@hit.ac.zw

***Abstract*—In the context of exploratory testing (ET), human knowledge and intelligence is applied as a test oracle. The exploratory tester designs and executes the tests on fly and compares the actual output produced by the application under test with the expected output in the testers' mind. The shortcoming of human oracle is that they are fallible, that is exploratory testers do not always detect a failure even when a test case reveals it. Depending on a human tester to evaluate program behaviour has also some problems such as cost and correctness. Therefore, in this paper an effort has been made to explore the feasibility of using a multilayer perceptron neural network (MLP-NN) as an exploratory test oracle. The MLP-NN was improved by adding another weight on each connection to perfectly generate reliable exploratory test oracles for transformed different data formats.**

Keywords: **Test Oracle, Software Testing, Multilayer Perceptron Neural Network, Software under Test.**

I. INTRODUCTION

Software testing has always been a crucial phase in the software development life cycle. The previous studies has witnessed many software projects failures that result from lack of proper testing. Software that has been improperly tested can easily break a company's reputation. A better relationship between testing and requirements would finally result in enhanced tests and better-quality software [1]. Consequently, test methods were established to mitigate this limitation [2].

When the flow of requirements is parallel to the development phase, the systematic test case based approach is considered difficult to use owing to the constant requirement change while designing tests [3]. Hence, an approach such as ET can be worthwhile for such environments, where the requirements elicitation has not been completed early in the software development process.

ET is a software testing approach, at times called ad-hoc testing [4] which is not dependent on test cases documentation prior to execution. Today, most researchers defined ET as an activity where a tester learns, design and execute the tests simultaneously [4]. To summarize, this means the tester is discovering the application, studying its functions and running tests based on his/her knowledge. There is no logical method followed as in scripted testing that guides the tester the test steps to run the tests. The tester himself controls the test designs while running and studying the application under test. This supports designing effective test cases while exploring unrealized parts of the software.

In modern days, this approach has gained attention and reputation particularly among professional software testers [5]. The ET term was initially coined by Bach and Kaner in 1983 and it was adopted by many professional testers [6]. ET is used in combination with other testing techniques in industry [6] which includes, Risk Based Testing, Cross functional testing, Requirements based testing, Pair wise testing, Acceptance testing, Checklist based testing, Scripted Testing, Usability Testing, Security Testing and Boundary Value Analysis.

Exploring means focused wandering, navigating through a space with a general assignment, but without a pre-defined route. Exploration encompasses on going studying and execution of tests [7].

In the context of ET, human knowledge and intelligence is applied as a test oracle. A test oracle is defined as a technique used to differentiate an accurate result from an inaccurate result during testing [8]. The challenge of finding a reliable oracle is referred to as "the oracle problem."

In practice, the identification of failures is left to be decided by a human tester [9]. Therefore, the oracle problem is very important in ET and solved using the tester's knowledge and skills. The shortcoming of human oracle is that humans are fallible, that is exploratory testers do not always detect a failure even when a test case reveals it. Depending on human testers to evaluate program behaviour has also some problems such as cost and correctness. How could this be tackled with some subroutines to do such work?

The motivation for work done in ET is its exponential adoption by many software development firms. ET has been recommended as a worthwhile approach due to numerous advantages it has [6], [7]. The quality of the software under test (SUT) is highly dependent on the ability of the tester. The exploratory tester may not properly understand the requirements and specifications of the software and consequently endangers the quality of the product by judging correct results as wrong or wrong results as correct. Sometimes

978-1-5090-2029-4/16/$31.00 @2016 IEEE

the tester may not be able to conclude whether the result is correct or not.

Our research goal is to apply artificial neural networks in a simulated application under test to predict the test oracle of the executed tests. MLP-NN has not been applied to deal with different data formats in software development to facilitate learning and make decisions on test combinations executed.

In our study, we used MLP-NN and evaluated different parameters that gives good results. Although not explicitly stated in the studies, partial knowledge of the internal functionality of the software under test need to be possessed by the exploratory testers. The expected outputs generated by the MLP-NN allows the exploratory tester to judge the test results correctly.

II. Literature survey

The test oracle research literature is comparatively very small in software testing. A test case comprises of a set of inputs and their corresponding expected outputs for the SUT. Automatic generation of test inputs is fairly stress-free, but generation of expected results is a relatively difficult task. Testers cannot have confidence to do automated testing without expected outputs. A test oracle is a trustworthy source of expected results. It can be a program specification or simply the developer's knowledge that verifies the way a program operates. A correct oracle would behave equally the same way with the SUT and absolutely trusted. The SUT would accept all input specified and correct result would always be produced. Recent dynamic software testing approaches rely on the presence of test oracle, i.e., an instrument for proving that the SUT has correctly performed on a certain execution [10].

A partial test oracle [11] was suggested to prove the correctness of observed results in XML data. The SUT considered was a query program which takes XML document as input acquired from an XML repository of any form and produces XML data as a result. The oracle automatically provide a response about the accuracy of the module being tested with a certain degree of accuracy at feasible cost.

Other test oracle methods exploited artificial intelligence and pattern recognition techniques. These approaches involve writing additional program with the similar specifications as well as using pattern recognition and artificial intelligence based oracles [12]. In the application of a typical pattern recognition based oracle, the unit emulates human tester's knowledge and decision making process. The oracle imitates an accurate version of the module tested and make use of a distance measure to check the distance between the tested module output patterns and output patterns of oracles.

The oracle problem exist when either the oracle does exist or not but very expensive to be used. Metamorphic testing [13] uses metamorphic relations, properties of the SUT represented in form of relations amongst the inputs and the outputs of multiple executions, in order to aid validate the perfection of a program. This approach was used to lessen the oracle problem in numerous systems and to improve numerous software examination and testing methods. The authors witnessed that identification of an adequate amount of suitable metamorphic relations for testing by naïve testers was feasible with minimum training. Besides, the approach is cost-effectiveness and could be enhanced using more diverse metamorphic relations.

Currently machine learning methods [14] have been employed in the software engineering specifically in software testing field. However, the algorithms are difficult to discover the faults in certain applications as it is hard to find the test oracle to be used for computed outputs verification. A novel functional testing approach was attempted to verify the test oracles. The expected execution output for a given application is produced and verified by the oracle whether the SUT behaved correctly or not and issues a pass or fail verdict.

Techniques for automatic generation and execution of test cases were reported to improve coverage of many conditions without the increase of significant costs. Yet, one problem of automatically generating and executing test cases is the oracle problem. A model based oracle generation method [15] for unit testing belief desire intention agents was presented. A fault model was developed based on features of the main components to record the kinds of defects that may be faced, and describe how to generate automatically a passive, partial oracle from the agent design models.

Search based test generation method can output enormous volumes of test inputs automatically. Though, it is tough to define the test oracle for every test input. A mining approach [16, 17] was presented to build a decision tree model allowing generation of test inputs from the Java bytecode. Java bytecode was converted into Jimple representation. The resulting extracts predicates derived from the control flow graph of the Jimple code are used as attributes for organizing training data to form a decision tree. Faults were injected to assess the performance of the technique.

III. Proposed methodology

Our proposed methodology employs MLP-NN to facilitate learning of executed test cases and hence classify them as reliable test oracles. The multilayer perceptron neural (MLP) network model was simulated using MATLAB software where the network has one hidden layer containing one or more neurons and one output layer with only one neuron. Ideally, a MLP network that performs best normally uses selected parameters from the experiments.

A. Architecture of Proposed Exploratory Test Oracle

The test oracle requires a simulated model of the application under test that imitates its behavior, and it should produce accurate expected results automatically for all input combination. Figure 1 shows the procedure of using the proposed automated exploratory test oracle.

Test inputs are first passed to the simulate model for compliance then mapped to numeric data to be handled by MLP-NN, then the MLP-NN is trained. The trained MLP-NN becomes usable for generating reliable exploratory test oracles. Testing follows using the trained MLP-NN generating partial test oracle. The same inputs are given to the application under test (AUT) and actual outputs are produced. Based on the actual outputs and expected outputs, the exploratory tester determine whether the test passed or not.

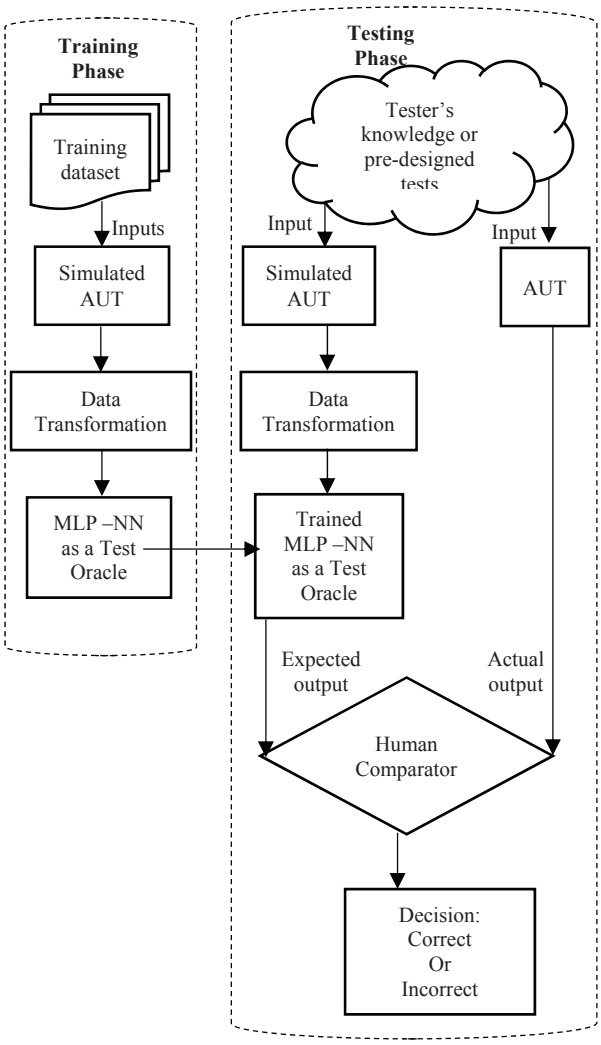

Figure 1: Proposed Exploratory Test Oracle Architecture

The number of inputs of AUT would be equal to the number of inputs defined in the MLP parameters. The AUT is simulated by defining the input data types, length (min and max) and range (min and max) for numerical inputs.

In order to train the MLP-NN, we have created a real test case training dataset. The tool works by taking a 2 dimensional array of test cases in CSV file format. The test case data comprises of different data types, i.e. string, alphanumeric, integer or other forms. Before using test dataset directly in training MLP-NN, extra work must be done. It is essential to map the data into input space of MLP-NN since MLP-NNs can only learn from numerical values.

All data types were mapped into numeric domain by converting to ASCII equivalence values. Each character is converted to its ASCII equivalence, but the ANN cannot handle all these values once as a single input. So, we summarized the ASCII codes to be taken as a single input.

B. Feedforward MLP-NN

A MPL-NN consists of layers of nodes in a directed graph, with each layer connected to the next one. Each node in hidden layer and also output layer is associated with an activation function. There is one layer placed between the input and output layers. The design of feed forward network is such that the signals are fed straight forward throughout the entire network. In figure 2 below, there is no back-feeding of signals into the previous layers.

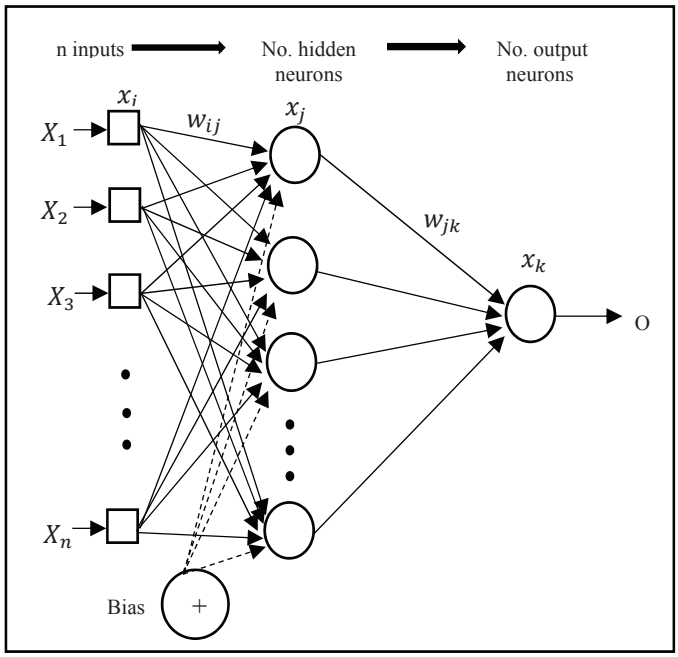

Figure 2: Multi-layer Perceptron Neural Network

This type of network consists of input layer, one hidden layer and output layer. Input layer is represented by one or more input nodes in the multilayer architecture. At every moment there is an activity denoted by x_i in each neuron. Neurons are connected by directed connections that are denoted by w, which is a weight or strength. When node i is connected with node j, then the connection weight is denoted as w_{ij}.

Inputs or other elements are converted into signals and correspondingly strengthened by the weights. In the inside of a neuron, all incoming signals are summarized in equation (1). The inner sum corresponds to:

$$x_{ij} = \sum_{i=1}^{n} x_i \, w_{ij} + w_0 \qquad (1)$$

where w_0 is bias weight.

The summarized input is taken as an argument by the activation function and gives the result or output value of the node. The activating function is denoted with *f* in equation (2) and the resulting activity with x_j.

$$x_j = f(\overline{x_j}) \qquad (2)$$

and equation (3) shows a comprehensive formula with summarized activity.

$$x_j = f\left(\sum_{i=1}^{n} x_i \, w_{ij} + w_0\right) \qquad (3)$$

C. Activation functions

Activation functions decides how the neurons and the network should process signals. The function determine when the neuron should be active depending on the given threshold when reached or not. We applied linear, sigmoid and hyperbolic tangent activation functions. For training process, experiments were carried out to evaluate the activation functions that address the problem better.

A sigmoid activation function uses a sigmoid function and is defined as follows:

$$f(x) = \frac{1}{1+ e^{-\bar{x}}} \quad (4)$$

The hyperbolic tangent activation function is defined as follows:

$$f(x) = \frac{e^{2x}-1}{e^{2x}+1} \quad (5)$$

A linear activation function is perhaps the least used activation function. We considered experimenting to check whether it gives good results or not. The Equation (6) shows the linear function.

$$f(x) = x \quad (6)$$

The output neurons are activated and provide the entire network's result to the outside world, which can be the next neural network or the human user. Output layer in this multilayer architecture is represented by one output node.

Network neurons are numbered starting with $x_{i,}$ $x_{j,}$ and x_k indicating the activities in input layer through hidden layer to output layer. If the desired output for a given input vector x is $d_k = (d_{k1}, d_{k2,} d_{k3})$ and the observed or actual output is $x_k = (x_{k1}, x_{k2}, x_{k3})$. Then the measure of error for this is given below

$$E_k = (d_{k1} - x_{k1})^2 + (d_{k2} - x_{k2})^2 + (d_{k3} - x_{k3})^2 \quad (7)$$

and in general, if we had m outputs, the measure of error would be:

$$E_k = \sum_{i=1}^{m}(d_{ki} - x_{ki})^2 \quad (8)$$

The sum of squared differences between desired and actual outputs of all the *m* output nodes are defined. So, to obtain the overall difference for the whole data set means that we are summing the output over all input vectors where the number of inputs is denoted by *p*.

$$E_k = \sum_{k=1}^{p}\sum_{i=1}^{m}(d_{ki} - x_{ki})^2$$

$$E_p = \sum_{p}(d_k - x_k)^2 \quad (9)$$

Considering the error as a function of the weights in the network and take a closer look at the partial derivatives with respect to weights. The output obtained is clearly determined by the inputs, weights and thus the error too. Suppose we have *n* weights, the error will be denoted by:

$$E = f(w) = f(w_{1,}w_2, \ldots, w_n) \quad (10)$$

As the error *E* is a function of all weights, we need to consider, how a single weight *w* change affects the error *E*. If *f* is a differentiable and continuous function, this is the same as observing the partial derivative of *E* with respect to w_i, $\partial/\partial w_i$ in the point *w*.

Therefore, to find the gradient vector, an error term $\bar{\epsilon_i}$ for node *i* is defined as

$$\bar{\epsilon_i} = \frac{\partial^+ E_p}{\partial \bar{x}_i} \quad (11)$$

Applying the chain rule, the recursive formula for $\bar{\epsilon_i}$ can be written as

$$\bar{\epsilon_i} = \begin{cases} -2(d_i - x_i)\dfrac{\partial x_i}{\partial \bar{x}_i} = -2(d_i - x_i)x_i(1 - x_i) & \text{if node } i \text{ is a output node} \\ \dfrac{\partial x_i}{\partial \bar{x}_i} = \sum_{j,i<j} \dfrac{\partial^+ E_p}{\partial \bar{x}_j}\dfrac{\partial \bar{x}_j}{\partial x_i} = x_i(1 - x_i)\sum_{j,i<j} \bar{\epsilon_j} w_{ij} & \text{otherwise,} \end{cases} \quad (12)$$

Where w_{ij} is the weight connection from node *i* to *j;* and w_{ij} is zero if there is no direct connection. Then the weight update w_{ki} for online, pattern by pattern learning is

$$\Delta w_{ki} = -\eta \bar{\epsilon_i} x_k \quad (13)$$

where η is the learning rate that affects the convergence speed and stability of the weights during learning.

Training data is processed till the error rate is reached. When training completes all the data connections in the network will be saved in the weight matrix. Different elements in input vectors have imbalanced contributions for ANN. Uniform transformation is needed for equalization impaction of all input variables. The principle of executing a test follows that all inputs given to the software under test must be valid to be considered as successful. Otherwise, if the graphical user interface of software under test have one wrong input, the test is considered as invalid or failed.

So it is difficult to differentiate summarised ASCII values that are valid from invalid ones. Therefore, the ANN also fails to classify such data. We then considered the validation aspect of software under test that is, the valid inputs must be associated with weights that differ from weights associated with the invalid inputs. This has given rise to the modification of MLP neural network to Two Weighted MLP-NN.

A larger weight is selected when the input is valid in order to approximate towards the desired class 1 and smaller weight when input is invalid. This allows the ANN to be able to classify invalid and valid input combinations. A combination of valid inputs should be classified as correctly executed, class 1 and

invalid inputs or combination of valid and invalid inputs should be classified as wrongly executed in class 0.

Moreover, the decision of the structure of ANN is a more challenging problem. How many neurons in hidden layer are required for specific problem requires cautious analysis. This process could not be implemented entirely automatically. To find the appropriate parameters, a number of experiments were carried out varying the parameters.

Also, training set is very important for supervised ANN learning. Selection of training set from predefined test cases is another main problem that requires to be addressed carefully. After attaining the expected MLP-NN, it could be used in predication for new input data.

D. Testing Phase

After the MLP-NN is properly trained, it becomes feasible to use it as automated exploratory test oracle. The process of using the MLP-NN based test oracle is as follows: the logical component under test is executed using the inputs provided by the test case, while the trained MLP is given the same inputs. Observed outputs which must be evaluated are produced by the SUT and the expected outputs by the MLP-NN. Human intelligence is employed as a comparator to compare the results, and any deviation is reported as possible SUT defect. This procedure may be automated with little human intervention in preparing the environment and the required dataset.

E. Summary of Exploratory Test Oracle

Exploratory test oracle was summarized in the following steps.

Step 1: Construct neural networks and initialize the weight.

Step 2: Simulate application under test.

Step 3: Load test cases for training.

Step 4: Perform data transformation i.e. map non-numeric data into numeric.

Step 5: Perform feedforward pass in the MLP

Step 5: Using back propagation algorithm to train neural networks in the training sets.

Step 7: When the stopping criterion is not satisfied, repeat step 5 and 6 until all inputs of the AUT are fed to the MLP, otherwise keep the weights and go to step 8.

Step 8: Get testing inputs of AUT and input it to neural networks. Obtain the approximate output from neural networks. Determine if the test oracle is a failure or not by the result.

Step 9: If you need to test a different module, go to step 1. Otherwise, the process finishes.

F. Test cases

A dataset with 160 test cases was created to be used in the MLP-NN based on AUT specifications. It comprises of invalid test cases that fall in class 0 and valid ones that fall in class 1 as shown in Table I. Each data set has four features and its corresponding class. The AUT used for experimenting is user interface for adding a user in a system with four input boxes namely, Username, Password, Employee id and security access level.

The dataset was divided into 60 for training and 100 for testing. This datasets contains 50% valid test cases and 50% invalid test cases.

TABLE I: SAMPLE TEST CASES

	Username	Password	Emp_ID	Access Level	Class
2	welshl	welsh1244	99.231	12	0
3	welshl	welsh1245	99.231	8	0
4	welshl	welsh1246	99.231	`1	0
5	sandeeplean	sandeep1234	98343	2	1
6	prashitlean	prashit1234	99827	1	1
7	sanchitlean	sanchit1234	98943	4	1

IV. EXPERIMENTAL RESULTS

The main objective of this study was to predict the exploratory test oracle using MLP-NN. In order to choose optimal parameters that gives good results, experiments were done differing parameters values and evaluate the results. The excellent networks, are the ones that give the highest correct classification percentage and outputs that are close to 0 or 1, if the test failed or passed respectively. Such a network will be a chosen MLP network for the system. The network would be stopped from training once the error threshold value converged and all training datasets have been applied to the network. Accuracy of MLP networks was evaluated to determine the best parameters that suited the network to perform correct classification of test oracles.

A. Changing Activation functions

Table II shows a summary of the outputs of combinations of activation functions at hidden layer and at output layer.

TABLE II. MLP PERFORMANCE OF TEST ORACLE CLASSIFICATION FOR VARIOUS ACTIVATION FUNCTIONS

No. Code	Network Code	Class 0		Class 1	
		Min	*Max*	*Min*	*Max*
1	sig-sig	0.09107	0.1754	0.8583	0.8786
2	sig-tanh	0.01454	0.0437	0.9171	0.9395
3	sig-pul	Infinite training			
4	pul-pul	Infinite training			
5	Pul-sig	Infinite training			
6	pul-pul	Infinite training			
7	tanh-tanh	0.007612	0.08501	0.9291	0.953
8	tanh-pul	0.06734	0.09352		
9	tanh-sig	0.073464	0.41424	0.86547	0.89706

The results have shown that using sigmoidal activation function at hidden layer and hyperbolic tangent activation function at output layer yields the best results. Pure linear resulted in infinite training execution. It executed finitely when the network code was tanh-pul but classified all test oracles in failed class. Therefore, in the subsequent experiments sigmoid activation function at hidden layer and hyperbolic tangent activation function at output layer were used.

B. Changing Number of Neurons in Hidden Layer

Few neurons gives desirable outputs but the network learns very slowly. Many neurons results in outputs with large error but learns much faster. We therefore choose to use 4 neurons in hidden layer. Since we are predicting the test oracle, we are expecting an output from a single pass as passed or failed; that is why we have one output neuron at output layer.

C. Error Threshold Variations

Based on the different error threshold values that were experimented with, a higher error threshold value results in few iterations executed to reach a shopping criteria and a higher percentage of true error estimate. The highest true error estimate 19.272% was obtained when error threshold was 0.1 and the least number of epochs 6 while with the smallest error threshold 0.001, the MLP-NN performed 50 iterations to reach the stopping criteria while the true error estimate was 3.0756%. Therefore, 0.1 error threshold was chosen to be used in the MLP network.

D. Learning Rate variations

The higher the learning rate (maximum of 1.0) the faster the network is trained. Though, the network has a higher chance of being trained to reach a local minimum solution, which is a point at which the network become stable on a solution that is not the most optimal global solution. Therefore, 0.3 was chosen as the learning rate for our MLP network as it provides optimum performance and has a better chance to stabilize at the most optimal global solution.

V. Conclusion and Future Work

The current work has been focused on application of multilayer perceptron neural network as an exploratory test oracle to generate expected output of the AUT. AUT with different data types was used for experimental purposes and showed that it cannot learn properly from summed ASCII codes as correct and wrong inputs cannot be realized easily by the MLP-NN. This is because the value of the correct and wrong can be similar or they may be more or less the same or fall in the same range.

The normal MLP-NN with one weight on each connection failed to classify the transformed data correctly and hence modified to two weighted MLP-NN. The improved MLP-NN with two weights on each connection perfectly generated reliable exploratory test oracles. The exploratory testers tests the AUT to produce actual outputs while the exploratory test oracle produce the approximate or partial expected outputs. Using tester's knowledge and interpretation, the expected and actual outputs are compared and a fault report is produced.

References

[1] Fewster, M., Graham, D., 1999. Software test automation. Addison-Wesley Harlow, Essex, UK.

[2] Everett, G., McLeod, R., 2007. Software testing: testing across the entire software development life cycle. Wiley-IEEE Computer Society Pr.

[3] Itkonen, J., Rautiainen, K., 2005. Exploratory testing: a multiple case study. In: Empirical Software Engineering, 2005. 2005 International Symposium on. p. 10 pp.

[4] Bach, J., 2000. Session-based test management. Quardev Laboratories.

[5] Itkonen, J., Mantyla, M., Lassenius, C., 2007. Defect detection efficiency: Test case based vs. exploratory testing. In: Empirical Software Engineering and Measurement, 2007. ESEM 2007. First International Symposium on. pp. 61–70.

[6] Naseer, A., Zulfiqar, M., 2010. Investigating exploratory testing in industrial practice, Blekinge Institute of Technology, COM/School of Computing.

[7] Tinkham, A., Kaner, C., 2003. Exploring Exploratory Testing. In: STAR East conference, www.testingeducation.org.

[8] A. Abran, J. W. Moore, P. Bourque, R. Dupuis, and L. L. Tripp, Guide to the Software Engineering Body of Knowledge 2004 Version. Los Alamitos, CA, USA: IEEE Computer Society, 2004.

[9] L. Baresi and M. Young, "Test oracles," University of Oregon, Dept. of Computer and Information Science, Eugene, Oregon, U.S.A., Tech. Rep. Technical Report CISTR- 01-02, Aug. 2001.

[10] Itkonen, J.; Mantyla, M.V.; Lassenius, C., "The Role of the Tester's Knowledge in Exploratory Software Testing," Software Engineering, IEEE Transactions on , vol.39, no.5, pp.707,724, May 2013

[11] Kim-Park, D.S.; de la Riva, C.; Tuya, J., "A Partial Test Oracle for XML Query Testing," Testing: Academic and Industrial Conference - Practice and Research Techniques, 2009. TAIC PART '09. , vol., no., pp.13,20, 4-6 Sept. 2009.

[12] I. Gondra, "Applying machine learning to software fault-proneness prediction," J. Syst. Softw., vol. 81, no. 2, pp. 186–195, Feb. 2008.

[13] Huai Liu; Fei-Ching Kuo; Towey, D.; Tsong Yueh Chen, "How Effectively Does Metamorphic Testing Alleviate the Oracle Problem?," Software Engineering, IEEE Transactions on , vol.40, no.1, pp.4,22, Jan. 2014.

[14] Monisha, T.R.; Chamundeswari, A., "Automatic verification of test oracles in functional testing," Computing, Communications and Networking Technologies (ICCCNT),2013 Fourth International Conference on , vol., no., pp.1,4, 4-6 July 2013.

[15] Padgham, L.; Zhiyong Zhang; Thangarajah, J.; Miller, T., "Model-Based Test Oracle Generation for Automated Unit Testing of Agent Systems," Software Engineering, IEEE Transactions on , vol.39, no.9, pp.1230,1244, Sept. 2013.

[16] Weifeng Xu; Tao Ding; Hanlin Wang; Dianxiang Xu, "Mining Test Oracles for Test Inputs Generated from Java Bytecode," Computer Software and Applications Conference (COMPSAC), 2013 IEEE 37th Annual , vol., no., pp.27,32, 22-26 July 2013.

[17] Weifeng Xu; Hanlin Wang; Tao Ding, "Mining Auto-generated Test Inputs for Test Oracle," Information Technology: New Generations (ITNG), 2013 Tenth International Conference on , vol., no., pp.89,94, 15-17 April 2013.

Sādhanā
DOI 10.1007/s12046-016-0559-7

© Indian Academy of Sciences

Image coding based on maximum entropy partitioning for identifying improbable intensities related to facial expressions

SEBA SUSAN*, NANDINI AGGARWAL, SHEFALI CHAND and AYUSH GUPTA

Department of Computer Science and Engineering, Delhi Technological University, Delhi 110042, India
e-mail: seba_406@yahoo.in

MS received 26 October 2014; revised 2 April 2015; accepted 31 May 2016

Abstract. In this paper we investigate information-theoretic image coding techniques that assign longer codes to improbable, imprecise and non-distinct intensities in the image. The variable length coding techniques when applied to cropped facial images of subjects with different facial expressions, highlight the set of low probability intensities that characterize the facial expression such as the creases in the forehead, the widening of the eyes and the opening and closing of the mouth. A new coding scheme based on maximum entropy partitioning is proposed in our work, particularly to identify the improbable intensities related to different emotions. The improbable intensities when used as a mask decode the facial expression correctly, providing an effective platform for future emotion categorization experiments.

Keywords. Variable length coding; Huffman coding; Shannon–Fano coding; entropy coding; maximum entropy partitioning; facial expression recognition; non-extensive entropy with Gaussian gain.

1. Introduction

Facial expression analysis has assumed great significance in the recent advances made in human–machine interaction. The facial expressions depict various human emotions such as pain, surprise, sorrow and happiness [1, 2] which if interpreted correctly by machine learning algorithms can be of immense practical use, such as for the assistance of elderly [3] and infants [4], providing medical aid to patients in pain who are unable to communicate [5–7], or devising modern day gadgets and applications that react to human emotions [8], a few examples being humanoid robots that recognize faces and facial expressions [9, 10], expression glasses for facial expression recognition [11], adaptive music controller [12], household gadgets, etc. Some online facial expression recognition applications include the FaceReader [13] and LAFTER [14]. However these are limited to certain range of emotions only such as a positive or negative emotion, whether the person is laughing or not, etc. which reduces emotion recognition to a binary problem. In the actual scenario, decoding the human emotion is a most complex task due to the complex state of the human mind, and the presence of mixed emotions both positive and negative cannot be entirely ruled out. The studies linking facial expressions to human psychology and behavior span back to several decades [4, 7, 15, 16]. Since then, several researches have been directed towards developing more efficient machine learning algorithms for deciphering human emotions from facial expressions [17]. Automated facial expression analysis usually proceeds by segmenting the skin pixels, locating the eye, nose or mouth coordinates, and cropping the face followed by normalization to a standard size [18–24]. Automated face cropping tools such as the Viola Jones Face detector [25] are readily downloadable from the web. The cropped and normalized face is subjected to feature-extraction and subsequent categorization into classes, be it the class of the subject (face recognition) or the class of the emotion (emotion recognition/facial expression analysis). The facial features extracted play a great role in the accuracy of the classification. Texture features are more than often used for representing faces, examples being the local binary pattern (LBP) for images/video frames [26] and the hybrid local binary pattern along three orthogonal planes (LBP-TOP) for video blocks [27]. Texture cues are particularly suited for the face and facial expression recognition problem since they represent patterns directly associated with the shape and structure of a person's face or dynamic patterns in subsections of the face associated with some emotion, such as the shape or appearance of the mouth and lips, or the creases in the forehead or near the eyes and the crinkling of the nose [28–31]. Grid-based facial expression analysis using localized texture cues and a normalized similarity index for matching decodes human emotions successfully and detects the presence of mixed, compatible emotions [32]. Similar lines of reasoning have been used by several face models such as the extended Active Shape Model [33] for locating landmark points in an upright face.

*For correspondence
Published online: 19 November 2016

In this paper, we seek to highlight the improbable, imprecise and indistinct image intensities that are indicative of the emotion being portrayed in the cropped facial image. We achieve this by devising a novel image coding scheme based on maximum entropy partitioning which assigns longer codes to those low probability symbols/intensities that are difficult to distinguish from others in terms of their probabilities of occurrences and lack a proper definition. The paper is organized as follows: section 2 reviews the conventional Huffman and Shannon–Fano image coding schemes, section 3 outlines our overall methodology for locating improbable intensities related to emotions by information-theoretic coding, section 4 discusses the new image coding scheme for identifying improbable intensities based on the maximum entropy based partitioning. Section 5 analyzes the experimental results and section 6 draws the overall conclusions.

2. Huffman and Shannon–Fano coding of images: a basic review

We start by discussing the two most important and popular information-theoretic coding techniques. The Huffman [34] and Shannon–Fano coding schemes [35] construct optimal codes for a set of symbols $\{x\}$ and their probabilities $\{p(x)\}$. Compared to Shannon–Fano coding, the Huffman coding is more efficient in terms of the average code-length generated. However the Shannon–Fano codes are within one bit of their ideal theoretical length of $-\log p(x)$ [36]. The two techniques are now described in detail.

The Huffman coding algorithm is a source encoding technique used for unequal length coding. It is described in the context of images [37] below.

Step 1 Construct a tree based on the gray-level frequencies obtained from the image histogram. This is achieved using the following steps:

i. Sort the probabilities from the image histogram in the descending order.
ii. Add the two lowest probabilities to form a node at the higher level.
iii. Repeat until the highest node is a single node.

Step 2 Assign binary codes to each gray level/node as follows:

i. Assign null code to the highest node
ii. Whenever a node splits into two, assign a '0' to the left child and a '1' to the right child.
iii. Repeat until the terminal nodes are reached.

Huffman coding is an example of unequal length coding [38] where the histograms of the symbols are peaked. It is also an efficient coding technique which assigns the shortest codes to the most probable intensities and the longest codes to the least probable intensities. It is stated to have the highest efficiency and the shortest average code-length [39]. Huffman coding is popularly used for image cryptography [40] and image steganography [41] in which the constructed binary codes are assigned to image intensity levels. In our work we further investigate its use for decoding facial expressions by highlighting the low probability facial intensities related to emotions.

The Shannon–Fano coding scheme constructs sub-optimal codes which are not as nearly efficient as that of Huffman codes. The steps for constructing Shannon–Fano codes are described below.

Step 1: Given a list of symbols with their probabilities, arrange them in the decreasing order of the probabilities.

Step 2: Divide this list into two partitions such that the sum of probabilities in one partition roughly equals the sum of probabilities in the other.

Step 3: Assign a '0' to the first partition and a '1' to the second partition.

Step 4: Repeat steps 2 and 3 iteratively on each partition created, until only one symbol is left in each partition and all symbols have been assigned codes.

The above coding scheme works best when the symbols are more or less equally likely and a single bit is sufficient to divide them into two partitions. An example of an application is text compression where Shannon–Fano coding is more useful than Huffman and Arithmetic coding [42]. A reason why Shannon–Fano coding is otherwise almost never used is its low efficiency when the mismatch between the sums of the probabilities of the two partitions is high, as often happens with real-world images having peaked histograms or intensities with unequal probabilities.

3. Locating improbable intensities in an image by information-theoretic coding

In this section we first describe pixel masking based on the thresholding of code-length. The K symbols for image coding are the gray-level intensities in the image quantized to K bins. The overall methodology for selective pixel masking based on the longer length of the codes assigned is given below.

1. Apply Information-Theoretic coding (such as Huffman and Shannon–Fano coding) to generate separate codewords for each intensity value.
2. Check the length of the codewords assigned to each intensity value.
3. Map the code-length back to each pixel position by closest bin matching with pixel intensity. Plot the histogram of the code-lengths associated with the pixels in the image.
4. Determine the optimal threshold value of the length of codewords *t_len* from the histogram of code-lengths.

5. For each pixel

   If (length(codeword)) $\leq$ *t_len*
   Assign 0 (color code for black) to the corresponding pixel
   else if (length(codeword)) $>$ *t_len*
   Assign 1 (color code for white) to the corresponding pixel.

6. The image so constructed is a binary mask which highlights the improbable intensities in the image that are assigned longer code-lengths by information-theoretic coding and are indicative of the specific emotion being portrayed.
7. Alternatively, substituting the 0's in the above result with the original image intensity values and substituting the 1's with 0's would yield the masked original image devoid of any emotions.

The selective pixel masking procedure outlined above is demonstrated for Huffman coding of two real-world images in figure 1, with threshold $t_len = 8$ arbitrarily selected for best results for a 256-bin histogram ($K = 256$).

In figure 1(b), the image intensities excluding the improbable ones are shown. The missing portion includes parts of the face of the person in the picture which is significant information. In figure 1(d) the faces of the two girls in the picture are low probability intensities as compared to the background shades and hence are assigned longer codes.

We observe from the above two examples that applying Huffman coding to random photographs would identify faces or at least parts of it as being improbable events and these are assigned longer codes. This highlights the potential of Information-theoretic coding for segregating pixels into categories of the improbable intensities (which include parts of faces in the photographs) and the more probable intensities (which include the majority of the background).

Theorem 1 Symbols that are assigned longer codes contribute significant information that helps in identification.

Proof In the variable length coding techniques like Huffman and Shannon–Fano coding, the shorter codes are assigned to the symbols that are highly probable and predictable and thus carry less information since they are more or less expected to occur. The idea behind the encryption is that guessing this highly probable symbol will not give much information to the attacker hence lesser number of bits is assigned to cut the computational cost. As the length of the codeword increases, the guesswork becomes more difficult for the attacker and the symbols now pertain to useful information that must be hidden to secure the primary message content [43]. The expected value of the guesswork $E(G(W_l))$ (defined as the number of guesses for the symbol W_l till the symbol is guessed) increases proportionally with the length of the codeword l [43].

3.1 *Motivation for our problem*

We start with the assumption that it is the improbable and indistinct intensities in an image that contain the traces of emotion in a human face. Recent literature highlights the study of facial micro-expressions which are subtle changes in facial expressions when a person tries to conceal his real emotions [44]. The identification of facial intensities particular to an emotion makes the recognition task easier. The dynamic changes in facial expressions play a greater role in emotion recognition as compared to the static information in video sequences [43]. A recent work on face recognition from the videos of subjects dynamically portraying emotion through facial expressions emphasizes the need for capturing the salient spatial information in the video, which is the face itself that appears in every frame irrespective of its dynamically changing facial expression [45]. This was achieved using the 3D-Difference Theoretic Texture Features (DTTF) that relies on averaging the pixel-defined gray level difference statistics throughout the entire volume of the video block to extract the high probability facial intensities contained in every frame. The averaging procedure would subdue the effect of the intensity changes pertaining to the dynamically changing emotion and helps in recognizing the face irrespective of its emotion. In our work on facial expression analysis, on the other extreme, we seek to highlight the improbable intensities in the facial image that would indicate characteristics of the emotion being portrayed. The face with the improbable intensities highlighted would appear differently for different emotions. In collaboration with texture analysis techniques, a future emotion categorization tool is visualized. We use information-theoretic coding in a novel attempt to identify the parts of the face that are vulnerable and specific to different emotions. The vulnerable intensities are defined as those that are assigned longer codes on account of their being improbable and difficult to distinguish in terms of their occurrence frequency which is neither too low nor too high. The more obvious and predictable facial intensities do not give any clues of the emotion being portrayed.

In a cropped frontal face image the improbable intensities mostly pertain to:

i. The dilation of the eyes and the arch of the eyebrows
ii. The creases in the forehead and around the eyes
iii. The crinkling of the nose and the dilated ends of the nostrils
iv. The shape of the mouth which is the most expressive part of the face whether it is open, closed, drooping, shut tightly or stretched in a smile
v. The shadows along the sides of the face where lighting is less change with different emotions

Our aim is to locate and identify the 'difficult' intensities listed above which not only have low probabilities but also separate out last due to their indistinctiveness and lack of

proper definition with respect to the rest of the intensities in the facial image. This refines our present definition of 'vulnerable' intensities related to facial expressions as those having low and indistinct probability values and having the longest codes assigned.

4. Proposed image coding using maximum entropy based partitioning for analyzing facial expressions

In this section we describe in detail the new image coding technique for facial expression analysis using a novel level-partitioning based on the maximum entropy principle. The maximum entropy principle has been used before in applications such as image thresholding [46] to create optimal partitions of probability histograms. The central idea is that for the optimal partition, the sum of entropies of the two partitions is maximum since each of the two subsets contains equally likely members at that point. We apply this principle to create the partitions in Shannon–Fano coding which at present relies on roughly matching the sums of probabilities in the two subsets. The steps follow the order of Shannon–Fano coding in their execution and code assignment procedure; however, the partitions between symbols at each level are determined from the positive entropy spike or simply the maximum entropy among all possible partitions, as explained below with the help of relevant notations and formulae.

Shannon entropy for a complete probability distribution is defined as

$$H(\mathbf{p}) = -\sum_i p_i \log p_i. \tag{1}$$

The entropy in (1) is additive i.e. for the statistically independent case,

$$H(\mathbf{x}, \mathbf{y}) = H(\mathbf{x}) + H(\mathbf{y}). \tag{2}$$

The steps of the proposed coding algorithm for a set of symbols (image intensities quantized to K bins in our case) and their associated probabilities (derived from the image histogram) are outlined below.

Step 1: Given a list of symbols with their associated probabilities, arrange them in the decreasing order of the probabilities.

Step 2: Divide the set/subset of sorted symbols tentatively into two probability partitions **p1** and **p2** (all possible partitions are iteratively tested starting with the lone top symbol versus the rest in iteration $k = 1$ and ending with all the symbols versus the last symbol in the last iteration).

Step 3: Find the entropy values $H_k(\mathbf{p1}_N)$ and $H_k(\mathbf{p2}_N)$ corresponding to the two probability partitions **p1** and **p2** for the kth iteration, after normalizing the probabilities first so that they sum up to 1 within each partition as shown below.

$$\mathbf{p1}_N = \frac{p1}{\sum_i p1_i} \tag{3}$$

$$\mathbf{p2}_N = \frac{p2}{\sum_i p2_i} \tag{4}$$

$$H_k(\mathbf{p1}_N) = -\sum_{x \in \mathbf{p1}_N} x \log x \tag{5}$$

$$H_k(\mathbf{p2}_N) = -\sum_{y \in \mathbf{p2}_N} y \log y \tag{6}$$

Step 4: Find the weighted sum of the two (equiprobable) entropies $H_k(\mathbf{p1}_N)$and $H_k(\mathbf{p}2_N)$ to generate the entropy of the source $H_k(S)$ for the kth iteration as

$$H_k(S) = \frac{1}{2} H_k(\mathbf{p1}_N) + \frac{1}{2} H_k(\mathbf{p2}_N) \tag{7}$$

Step 5: Repeat steps 3–4 for all possible partitions k starting from the top with at least one symbol being in one partition

Step 6: Find the partition that corresponds to maximum entropy as

$$opt = \underset{\forall k}{\arg\max}\, H_k(S) \tag{8}$$

Step 7: Assign a code '0' to the first partition and a code '1' to the second partition.

Step 8: Repeat steps 2–7 recursively on all subsets of the partitions created until no more partitions are possible and all the symbols have been individually assigned codes.

We describe next two theorems which further helps in strengthening the validity of the proposed maximum entropy based partitioning and a propose a further improvisation of results by the substitution of the extensive Shannon entropy by the non-extensive entropy with Gaussian gain.

Theorem 2 Maximum entropy partitioning assigns longer codes to groups of symbols in an image that are indistinct in terms of their number of occurrences and assume a uniform distribution among themselves.

Proof The occurrence of an event such as a smile on a face is related to the co-occurrence of several low probability intensities other than the normal predictable facial intensities. To detect the closely related intensities associated with a smile such as the creases in the skin near the mouth and the contour of the lips we search for uniform probability densities in the probability graph of the facial image. Our iterative procedure described above, zeroes in on these inseparable intensities towards the end, assigning them the longest codewords. Therefore, to isolate image intensities that contribute to an event we have to find groups of image intensities which have a similar occurrence frequency. They would thus share a uniform probability

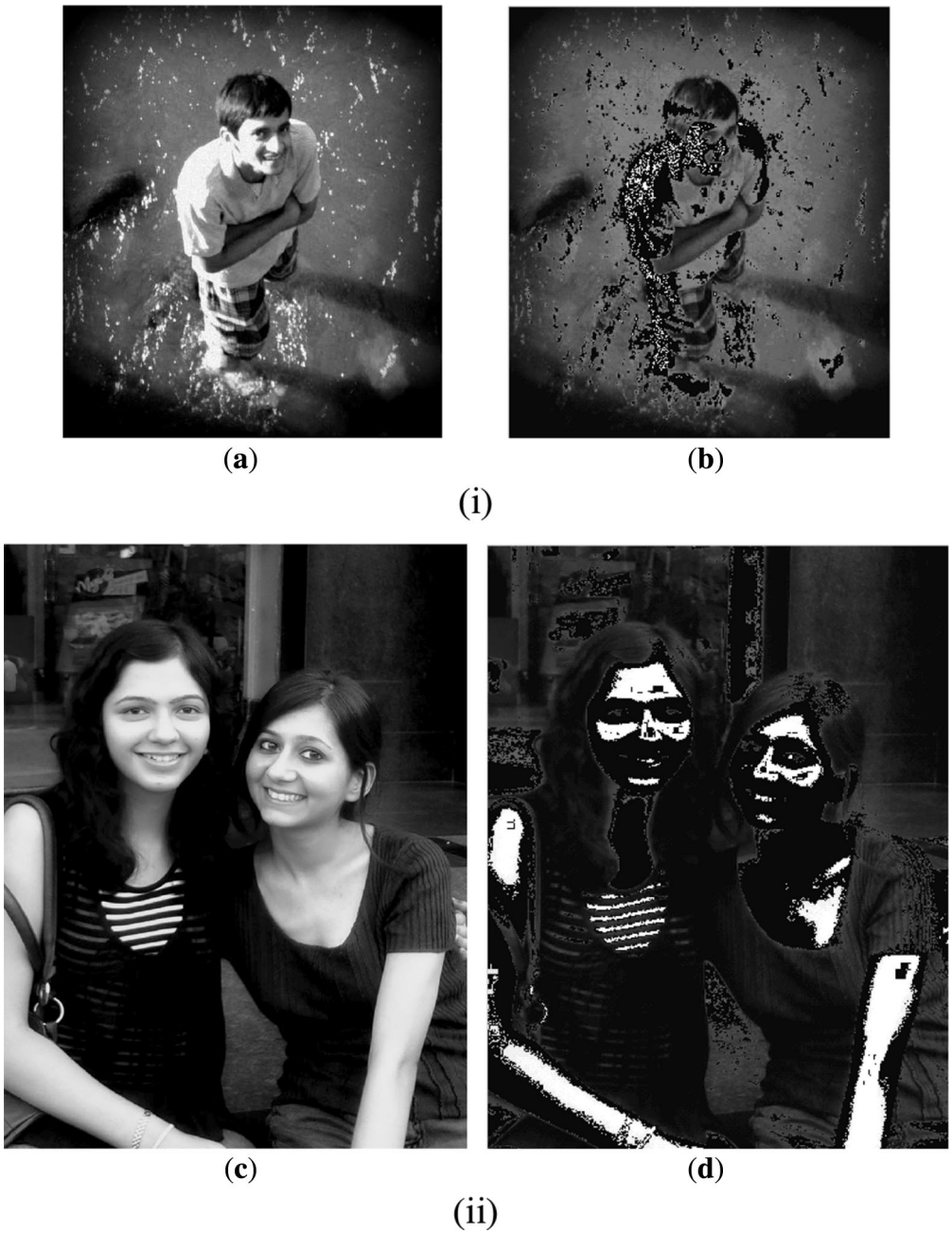

Figure 1. (i) The masked original image using Huffman coding: (**a**) Original image 1. (**b**) Reconstructed image after masking the improbable intensities by 0 (black). (ii) Highlighting the improbable intensities in the image: (**c**) Original image 2. (**d**) Reconstructed image after highlighting the improbable intensities by 1 (white).

distribution among themselves. The maximum entropy principle in general, states that the optimal probability partition is obtained at the point where the sum of entropies of the two partitions is maximum or in other words when the two partitions individually approximate uniform distributions. For instance from (7), the entropy between two sub-partitions is stretched to the maximum limit when the distributions in both partitions are uniform

$$\max H_k(S) = - \underset{p1_i \to \frac{1}{P}}{Lt} \left[0.5 \sum_{i=1}^{P} p1_i \log p1_i \right] - \underset{p2_i \to \frac{1}{Q}}{Lt} \left[0.5 \sum_{i=1}^{Q} p2_i \log p2_i \right] \quad (9)$$

or when

Sym 1	0.48	0.48	0.48	0.48	0.48	0.48	0.52	1.00
	1	*1*	*1*	*1*	*1*	*1*	*0*	
Sym 2	0.18	0.18	0.18	0.18	0.21	0.31	0.48	
	000	*000*	*000*	*000*	*01*	*00*	*1*	
Sym 3	0.13	0.13	0.13	0.13	0.18	0.21		
	001	*001*	*001*	*001*	*000*	*01*		
Sym 4	0.07	0.07	0.08	0.13	0.13			
	0100	*0100*	*011*	*010*	*001*			
Sym 5	0.06	0.06	0.07	0.08				
	0101	*0101*	*0100*	*011*				
Sym 6	0.05	0.05	0.06					
	0110	*0110*	*0101*					
Sym 7	0.022	0.03						
	01110	*0111*						
Sym 8	0.008							
	01111							

Figure 2. Example showing Huffman coding for eight symbols: Sym 1 – Sym 8 with their probabilities shown in black and the codes constructed shown in red.

Sym 1	0.48	0.48	0.48	0.48	0.48
	0	*0*	*0*	*0*	*0*
Sym 2	0.18	0.18	0.18	0.18	0.18
	1	*10*	*100*	*100*	*100*
Sym 3	0.13	0.13	0.13	0.13	0.13
	1	*10*	*101*	*101*	*101*
Sym 4	0.07	0.07	0.07	0.07	0.07
	1	*11*	*110*	*1100*	*1100*
Sym 5	0.06	0.06	0.06	0.06	0.06
	1	*11*	*110*	*1101*	*1101*
Sym 6	0.05	0.05	0.05	0.05	0.05
	1	*11*	*111*	*1110*	*1110*
Sym 7	0.022	0.022	0.022	0.022	0.022
	1	*11*	*111*	*1111*	*11110*
Sym 8	0.008	0.008	0.008	0.008	0.008
	1	*11*	*111*	*1111*	*11111*

Figure 3. Example showing Shannon–Fano coding for eight symbols: Sym 1 – Sym 8 with their probabilities shown in black and the codes constructed shown in red.

Table 1. Proposed image coding scheme using Shannon entropy based partitioning with symbol partitions shown by different color and fonts.

Symbol	Shannon entropy	Code assigned	Symbol	Shannon entropy	Code assigned	Symbol	Shannon entropy	Code assigned
0.48		*0*	0.48		*00*	0.48		*000*
0.18	1.656	*0*	**0.18**	0	*00*	**0.18**		*001*
0.13	2.132	*0*	0.13	**0.5816(max)**	*01*	0.13		*01*
0.07	**2.363(max)**	*1*	0.07		*10*	0.07		*1000*
0.06	2.327	*1*	0.06	1.182	*10*	0.06	0.6891	*1001*
0.05	2.188	*1*	0.05	1.569	*10*	*0.05*	**0.6902(max)**	*101*
0.022	2.024	*1*	0.022	**1.669(max)**	*11*	0.022		*110*
0.008	1.519	*1*	0.008	1.314	*11*	0.008		*111*

$$\underset{\max}{H_k(S)} \rightarrow \log P + \log Q. \tag{10}$$

In the special case when the probability density function (pdf) of the image is more uniform than its partitions, we proceed by partitioning the lowest probability from others and repeating the procedure on the remaining probabilities.

Theorem 3 The non-extensive entropy with Gaussian gain is more suitable than the extensive Shannon entropy for the proposed maximum entropy based partitioning of symbols

Table 2. Proposed image coding scheme using non-extensive entropy based partitioning with symbol partitions shown by different color and fonts.

Symbol	Non-extensive entropy	Code assigned	Symbol	Non-extensive entropy	Code assigned	Symbol	Non-extensive entropy	Code assigned
0.48		*0*	0.48		*00*	0.48		*00*
0.18	1.308	*0*	**0.18**	**0.7358(max)**	*01*	**0.18**		*010*
0.13	1.612	*0*	**0.13**	0.6817	*01*	**0.13**		*011*
0.07	**1.724 (max)**	*1*	0.07		*10*	0.07		*1010*
0.06	1.718	*1*	0.06	1.2492	*10*	0.06	1.1427	*1011*
0.05	1.641	*1*	0.05	1.5528	*10*	*0.05*	**1.1438(max)**	*100*
0.022	1.559	*1*	**0.022**	**1.5664(max)**	*11*	**0.022**		*110*
0.008	1.258	*1*	**0.008**	1.2876	*11*	**0.008**		*111*

Table 3. Coding of the intensities of the *Happy* image of *S052* using various methods.

Sorted probabilities from histogram	Symbol	Huffman code	Shannon–Fano code	Proposed method using non-extensive entropy partitioning	Proposed method using Shannon entropy partitioning
0.2318	11	00	00	000	0000
0.1573	10	100	010	001	0001
0.1365	8	101	011	010	0010
0.1362	9	110	100	011	0011
0.1210	7	111	101	1000	0100
0.0966	6	011	110	1001	0101
0.0626	5	0100	1110	101	011
0.0268	4	01011	11110	1100	100
0.0163	3	010100	111110	1101	101
0.0129	2	0101000	1111110	1110	110
0.0020	1	0101001	1111111	1111	111

Table 4. Coding of the intensities of the *Surprise* image of *S052* using various methods.

Sorted probabilities from histogram	Symbol	Huffman code	Shannon–Fano code	Proposed method using non-extensive entropy partitioning	Proposed method using Shannon entropy partitioning
0.1984	11	10	00	000	0000
0.1874	10	11	010	001	0001
0.1700	9	001	011	010	001
0.1461	8	010	100	011	010
0.0833	7	0001	101	1000	011
0.0758	6	0110	1100	1001	100
0.0518	5	0111	1101	101	1010
0.0495	4	00000	1110	1100	1011
0.0243	3	000010	11110	1101	1100
0.0109	2	00000110	111110	1110	1101
0.0026	1	00000111	111111	1111	111

Proof The non-extensive entropy with Gaussian gain [47] is defined as

$$H(P) = \sum_{i=1}^{n} p_i e^{-p_i^2}. \tag{11}$$

It was originally introduced as an identifier of regular textures. It is adept at representing the sparse probabilities in images. It was proved superior in performance to other forms of entropy such as: Renyi, Shannon, Pal & Pal, Tsallis entropies for texture categorization experiments that use entropy as a single feature. It is especially good at detecting regularity in sparsity due to its single-sided Gaussian information gain function $e^{-p_i^2}$ which highlights the contribution of the low probabilities lying in the bell of the Gaussian curve. This is well suited for our experiments where we are searching through improbable intensities for

Table 5. Coding of the intensities of the *Sad* image of *S052* using various methods.

Sorted probabilities from histogram	Symbol	Huffman code	Shannon–Fano code	Proposed method using non-extensive entropy partitioning	Proposed method using Shannon entropy partitioning
0.3091	11	00	00	000	000
0.1796	10	010	01	001	0010
0.1050	9	100	100	010	0011
0.1005	7	101	1010	011	0100
0.0965	8	110	1011	1000	0101
0.0933	6	111	110	1001	0110
0.0588	5	0110	1110	1010	0111
0.0290	4	01110	11110	1011	100
0.0153	3	011110	111110	1100	101
0.0108	2	0111110	1111110	1101	110
0.0022	1	0111111	1111111	111	111

Table 6. Coding of the intensities of the *Anger* image of *S052* using various methods.

Sorted probabilities from histogram	Symbol	Huffman code	Shannon–Fano code	Proposed method using non-extensive entropy partitioning	Proposed method using Shannon entropy partitioning
0.3918	11	1	00	000	000
0.1742	10	001	01	001	001
0.1089	9	011	100	0100	0100
0.1019	8	0000	101	0101	0101
0.0881	7	0001	110	011	011
0.0509	6	0101	1110	1000	1000
0.0428	5	01000	11110	1001	1001
0.0200	4	010011	111110	101	101
0.0121	3	0100100	1111110	1100	1100
0.0085	2	01001010	11111110	1101	1101
0.0007	1	01001011	11111111	111	111

the occurrence of uniform distributions. The sum of non-extensive entropies, in a subsequent work on crowd motion monitoring [48], indicated anomalies by positive spikes, a feature attributed to the non-additive nature of the non-extensive entropy with Gaussian gain. Additional experiments on the dynamic growth of the hidden layer in the Multi-Layer Perceptron neural network, identify the occurrence of anomalic training inputs in the process of incremental learning by positive entropy spikes [49]. In applications to image processing, uniform distributions within an image were localized by mean-shift clustering using the maximum non-extensive entropy of the mode-probabilities [50]. In this work, we expect to utilize the non-additivity of the sum of non-extensive entropies of the two partitions, to indicate to us which is the optimal partition by a positive entropy spike.

The maximum non-extensive entropy is achieved when

$$\underset{\max}{H_k(S)} = \underset{p1_i \to \frac{1}{P}}{Lt}\left[0.5\sum_{i=1}^{P} p1_i e^{-p1_i^2}\right] + \underset{p2_i \to \frac{1}{Q}}{Lt}\left[0.5\sum_{i=1}^{Q} p2_i e^{-p2_i^2}\right] \tag{12}$$

or when

$$\underset{\max}{H_k(S)} \to e^{-\left(\frac{1}{P}\right)^2} + e^{-\left(\frac{1}{Q}\right)^2}. \tag{13}$$

Comparing the two entropies, the logarithmic sum in (10) roughly takes into account the noise in both partitions and gives a partition that is globally optimum for the whole image. The exponential sum in (13) on the other hand gathers the uniform densities only in one partition and accumulates all other intensities including noise in the second partition, producing a positive spike for this combination. Any small addition to a uniform density that disturbs its uniformity is amplified exponentially and that combination is rejected as having lower entropy. Therefore the non-extensive entropy is more useful to us in our quest for localizing uniform densities accurately in the probability graph.

4.1 *Automated computation of the threshold for code-length using maximum entropy partitioning*

We extend the maximum entropy principle for automatically computing the threshold for code-length *t_len*, in order to create the binary mask explained in section 3.

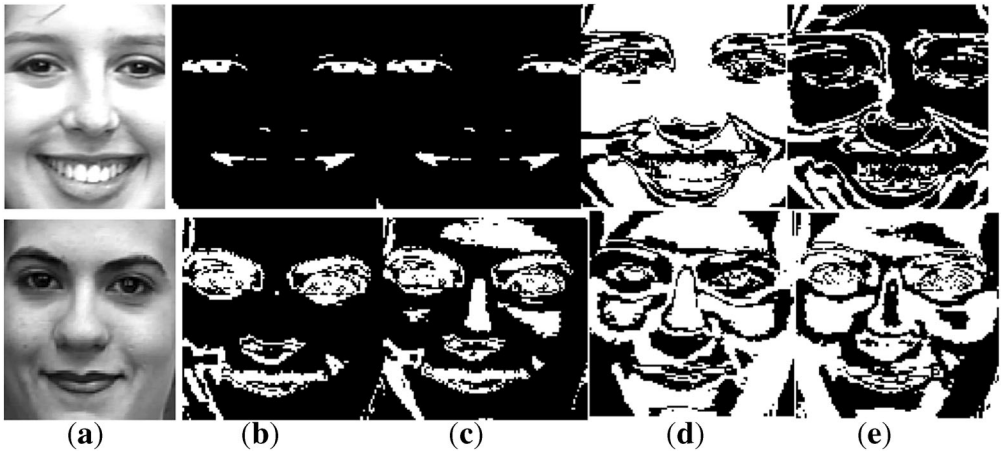

Figure 4. Intensities related to the *Happy* emotion (row-wise from top to bottom) shown in white in a black background, identified using different coding techniques, (shown here for two subjects *Top row*: Subject *S052*, *Bottom row*: Subject *S130*). (**a**) Cropped original images, (**b**) Huffman coding, (**c**) Shannon–Fano coding, (**d**) proposed method using maximum (Shannon) entropy partitions and (**e**) proposed method using maximum (non-extensive) entropy partitions.

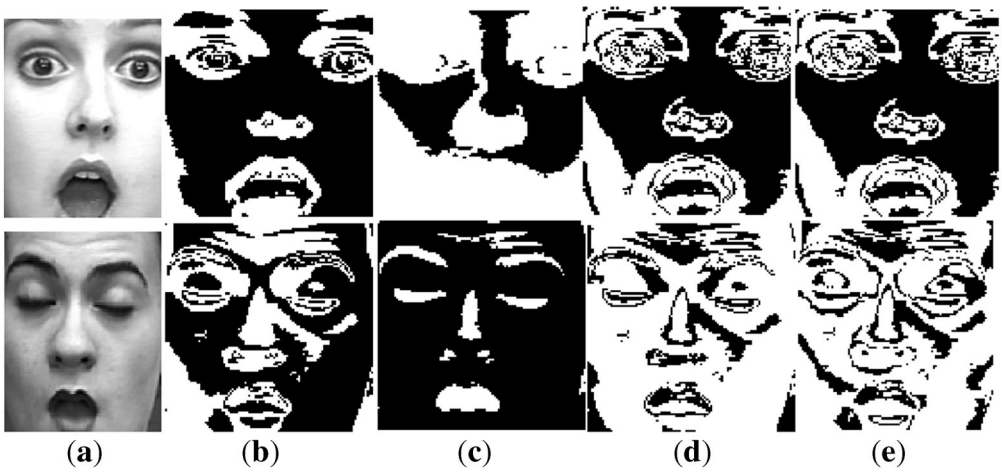

Figure 5. Intensities related to the *Surprise* emotion (row-wise from top to bottom) shown in white in a black background, identified using different coding techniques, (shown here for two subjects *Top row*: Subject *S052*, *Bottom row*: Subject *S130*). (**a**) Cropped original images, (**b**) Huffman coding, (**c**) Shannon–Fano coding, (**d**) proposed method using maximum (Shannon) entropy partitions and (**e**) proposed method using maximum (non-extensive) entropy partitions.

The steps for automated computation of the code-length threshold are detailed below:

1. For the K codes constructed by any image coding scheme for K symbols, enlist the code-lengths associated with each symbol/intensity
2. Map the code-length to each pixel position in the original image by closest bin matching with pixel intensity
3. Construct the probability histogram of the resulting code-length matrix
4. To find the optimal partition of symbols/intensities of this probability histogram do:
5. Set the partition point $k = 1$
6. Create partitions of symbols from Symbol 1 to k (Partition 1) and Symbol $k + 1$ to K (Partition 2)
7. Find the non-extensive entropy with Gaussian gain within each partition using (11), after first normalizing the probabilities in each partition so that they sum to one
8. Find the weighted sum of entropies of the two partitions using (7)
9. Increment k by 1 and repeat steps 6–9 until $k = K - 1$
10. Find the value of k at which maximum entropy is achieved using (8). Let this value be called *opt*

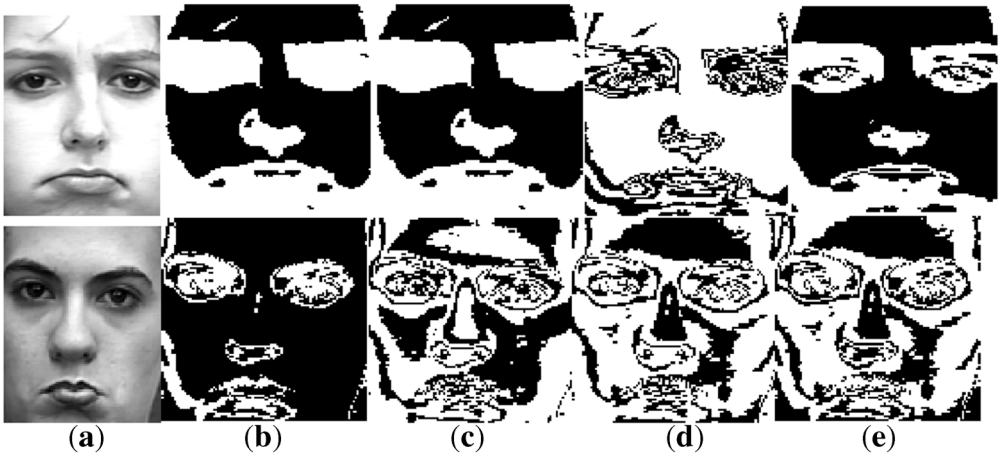

Figure 6. Intensities related to the *Sad* emotion (row-wise from top to bottom) shown in white in a black background, identified using different coding techniques, (shown here for two subjects *Top row*: Subject *S052*, *Bottom row*: Subject *S130*). (**a**) Cropped original images, (**b**) Huffman coding, (**c**) Shannon–Fano coding, (**d**) proposed method using maximum (Shannon) entropy partitions and (**e**) proposed method using maximum (non-extensive) entropy partitions.

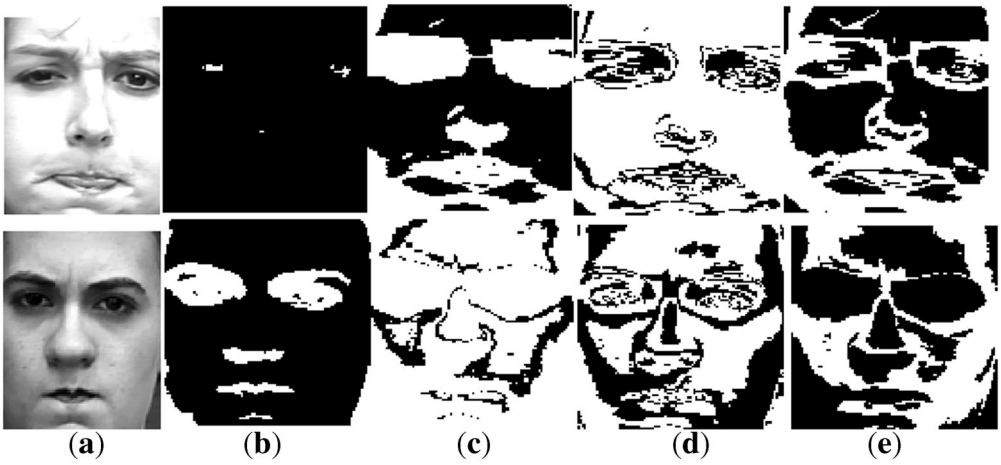

Figure 7. Intensities related to the *Anger* emotion (row-wise from top to bottom) shown in white in a black background, identified using different coding techniques, (shown here for two subjects *Top row*: Subject *S052*, *Bottom row*: Subject *S130*). (**a**) Cropped original images, (**b**) Huffman coding, (**c**) Shannon–Fano coding, (**d**) proposed method using maximum (Shannon) entropy partitions and (**e**) proposed method using maximum (non-extensive) entropy partitions.

Table 7. Evaluation of the image coding results in terms of the *average code-length* for various encoding techniques for different emotions of the two subjects *S052* and *S130* (proposed method shown in gray).

Encoding scheme	S052-Happy	S130-Happy	S052-Surprise	S130-Surprise	S052-Sad	S130-Sad	S052-Anger	S130-Anger
Huffman	2.9894	3.0750	3.0525	2.9813	2.9023	3.0627	2.6945	2.9939
Shannon–Fano	2.9894	3.0709	3.0665	2.9936	2.9179	3.0627	2.7228	3.0214
Non-extensive entropy based partitioning	3.2748	3.2489	3.2474	3.5295	3.3035	3.3401	2.8142	3.1360
Shannon entropy based partitioning	3.8810	3.4968	3.5202	3.5502	3.6359	3.7359	3.3258	3.4685

11. The threshold is decided as $t_len = opt$, i.e. all the (longer) code-lengths in the second partition indicate the symbols of interest (in our case, the image intensities that pertain to emotion)
12. Referring to the code-length matrix constructed in step 3, all the pixels satisfying the criterion of longer code-lengths in step 11 are indicated by 1 (white) in the binary mask and the remaining pixels by 0 (black)

Table 8. Evaluation of the binary masks created by measuring the *average information* (*Shannon entropy*) for various encoding techniques for different emotions of the two subjects *S052* and *S130* (proposed method shown in gray).

Encoding scheme	S052-Happy	S130-Happy	S052-Surprise	S130-Surprise	S052-Sad	S130-Sad	S052-Anger	S130-Anger
Huffman	0.2839	0.3351	0.6931	0.2186	0.2785	0.4392	0.2178	0.3733
Shannon–Fano	0.2839	0.4241	0.1065	0.4573	0.6859	0.5585	0.3364	0.5343
Non-extensive entropy based partitioning	0.5263	0.6031	0.4998	0.6909	0.5689	0.6743	0.5659	0.5343
Shannon entropy based partitioning	0.2839	0.6823	0.6723	0.6921	0.6921	0.4368	0.5973	0.6740

(a)

	Happy	Surprise	Sad	Anger
Happy	**1**	0	1	0
Surprise	0	**1**	0	1
Sad	0	1	**1**	0
Anger	1	0	0	**1**

(b)

	Happy	Surprise	Sad	Anger
Happy	**1**	1	0	0
Surprise	1	**1**	0	0
Sad	0	1	**1**	0
Anger	0	1	0	**1**

(c)

	Happy	Surprise	Sad	Anger
Happy	**1**	0	1	0
Surprise	0	**1**	1	0
Sad	0	1	**1**	0
Anger	0	0	1	**1**

(d)

	Happy	Surprise	Sad	Anger
Happy	**2**	0	0	0
Surprise	1	**1**	0	0
Sad	1	0	**1**	0
Anger	0	0	0	**2**

(e)

	Happy	Surprise	Sad	Anger
Happy	**1**	0	1	0
Surprise	0	**1**	1	0
Sad	1	0	**1**	0
Anger	0	0	1	**1**

(f)

	Happy	Surprise	Sad	Anger
Happy	**1**	0	0	1
Surprise	0	**1**	0	1
Sad	0	0	**1**	1
Anger	0	0	1	**1**

(g)

	Happy	Surprise	Sad	Anger
Happy	**1**	1	0	0
Surprise	1	**1**	0	0
Sad	0	0	**1**	1
Anger	0	1	0	**1**

(h)

	Happy	Surprise	Sad	Anger
Happy	**1**	0	1	0
Surprise	0	**1**	1	0
Sad	1	0	**1**	0
Anger	0	0	1	**1**

Figure 8. Fuzzy clustering of the DTTF texture cues (results shown in terms of confusion matrices) extracted from the result images of different methods. (**a**) Huffman coding, (**b**) Shannon–Fano coding. (**c**) proposed method using maximum (Shannon) entropy partitions, (**d**) proposed method using maximum (non-extensive) entropy partitions methods, (**e**) cropped mouth image [53], (**f**) 3×3 grid partitioning of original cropped image [27], (**g**) cropped eye and mouth canny output [55], and (**h**) 6×7 weighted grid partitioning of original image [56].

5. Experimental results and discussions

The experiments are performed on MATLAB 7.9 platform on an Intel Pentium IV processor. The codes constructed using Huffman, Shannon–Fano coding and the proposed maximum entropy based partitioning (for both Shannon entropy and the non-extensive entropy with Gaussian gain) are compared for their coding performance and their ability to identify the gray-level facial intensities associated with different emotions. Figure 2 and figure 3 demonstrate the Huffman and Shannon–Fano code construction for a synthetic sample set of eight symbols $K = 8$ arranged in the decreasing order of their probabilities. In both these coding schemes, we observe that all the lower rung probability intensity levels without exception are assigned longer codes, some of them being very long. These intensity levels when highlighted are of no consequence in a facial image since they are very low in number and may not indicate any useful information regarding the facial expression. The codes constructed by the proposed maximum entropy based

partitioning are shown for Shannon entropy in table 1 and for the non-extensive entropy with Gaussian gain in table 2, with all stages of coding shown including the maximum entropy point at each stage used to generate the partitions. It is noted from both tables 1 and 2 that the maximum entropy based partitioning assigns relatively longer codes to the indistinct intensity levels having probabilities 0.07 and 0.06 which are in the middle of the range of intensities, as opposed to the conventional encoding shown in figures 2 and 3. The non-extensive entropy based partitioning method is further able to distinguish the probability of 0.48 (highest probability) from the subset of {0.18,0.13} as rightly belonging to two groups in table 2, while Shannon entropy is unable to discern that, and clubs {0.48, 0.18} together as seen from table 1. Compared to the Shannon entropy induced partitions, we observe that the non-extensive entropy partitions are closer to uniform distributions interpreting the maximum entropy point correctly. The proposed method overall focuses on the 'improbable' intensities that are difficult to distinguish from their peers in terms of their frequency of occurrence, rather than the lowest probabilities, since these are more likely to reflect on emotions due to their subtle and imprecise nature.

We next implement our image coding scheme on four different sample images of facial expressions (*Happy*, *Surprise*, *Sad*, *Anger*) of the subjects *S052* and *S130* of the Cohn-Kanade facial expression dataset [2]. The gray level intensities are contained in 11 bins of the histogram $K = 11$ for the ease of depiction of values in tables 3, 4, 5 and 6. We determine the gray-level intensities that are indicative of emotions by using the information-theoretic coding techniques: Huffman, Shannon–Fano and the proposed maximum entropy partitioning (using both the entropies) as per procedures outlined in sections 3 and 4. The threshold for code-length *t_len* is selected in an automatic manner by maximum (non-extensive) entropy partitioning, for all the four image coding schemes, as discussed in section 4. The binary facial mask with the improbable intensities (code-length > *t_len*) highlighted are visually depicted in figures 4, 5, 6 and 7 for all the four image coding methods, with the codes constructed shown in tables 3, 4, 5 and 6 respectively. While the Huffman and Shannon–Fano codes predictably form a tree or pyramid type structure, as observed from tables 3, 4, 5 and 6, the new image coding scheme though more compact and less code-length efficient assumes an unpredictable coding pattern with the middle intensities assigned longer codes. The proposed coding is sufficiently efficient in terms of average code length: $L = \sum_{j=1}^{K=11} p_j l_j$, $j = 1, 2, \ldots, 11$, where l_j is the code-length of the jth symbol and p_j is the probability of occurrence of the jth symbol, though not nearly as code-length efficient as the Huffman and Shannon–Fano codes as shown in table 7. The non-extensive entropy based partitioning is more code-length efficient than Shannon entropy based partitioning as observed from the code-lengths in table 7 and comparable to that of Huffman and Shannon–Fano code-lengths. The average information or Shannon entropy of the binary mask B containing the selected intensities pertaining to emotion is computed from the normalized probability distribution of the highlighted features as $-\sum_{h\in B} p_{hN} \log p_{hN}$, where $\sum_{h\in B} p_{hN} = 1$, and the results are summarized in table 8. These results indicate that the proposed entropy based partitioning contributes to higher average information than either Huffman or Shannon–Fano codes due to the code-assignment procedure which assigns longer codes to mid-level probabilities than to the lowest probabilities. The significance of the segmented information is thus higher for maximum entropy based partitioning as deduced from table 8. The binary masks containing the segmented improbable facial intensities in figures 4, 5, 6 and 7 show visually different results for the two subjects due to the contrast between the subtlety of the emotion being displayed by subject *S130* (bottom row of all figures) and the highly intense emotions displayed by the subject *S052* (top row of all figures). A texture analysis of the facial binary mask is required to measure the binary pattern to check for similarities between the masks for the same facial expression of the two subjects. The difference theoretic texture features or DTTF texture cues [51] are computed from all the binary masks in figures 4, 5, 6 and 7 and clustered for the four emotions using the Fuzzy c-means (FCM) algorithm [52]. The DTTF is a low dimensional feature set superior to LBP, LBPV, filter banks for affine-invariant texture classification. Also it gives high accuracies with distance classifiers and hence is suitable for distance-based clustering algorithms. The clustering results shown as confusion matrices in figure 8 indicate the highest clustering accuracy for the proposed non-extensive entropy based maximum entropy partitioning. It is the only method which clusters the *Happy* and *Anger* facial expressions of the two subjects correctly, a fact also corroborated from the segmentations in figures 4(e) and 7(e) which show the same pattern despite a change of intensity of emotions for the two subjects. We also compare our results with four benchmark methods of facial expression recognition namely, (i) cropped mouth image [53] (ii) 3×3 grid partitioning of original cropped image [54] (iii) cropped eye and mouth canny output [55], (iv) 6×7 weighted grid partitioning of original image [56]. The clustering results of any comparison method do not show the two subjects clubbed into one cluster for any one emotion due to the highly different nature of emotion intensity portrayed by the two subjects for all emotions.

While the Huffman and Shannon–Fano coding do not show any emotionally significant intensities in figures 4–7 (b, c) the proposed entropy based partitioning especially using non-extensive entropy correctly identifies all traces of emotions. The segmented face highlighting the facial features shows distinct results in all four cases of facial expressions and could be used for categorizing emotions which forms our future work.

6. conclusions

In this paper, we propose a new variable length coding especially for identifying the improbable image intensities that help in decoding facial expressions. The new image coding scheme assigns longer codes to 'improbable and indistinct' intensities which are more likely to represent emotion in a facial image than the intensities with distinct probability values (very low and very high). The resultant coding though not as code-length efficient as Huffman or Shannon–Fano, identifies the vulnerable facial intensities much better. These intensities are used as a binary pattern for emotion categorization with successful results as proved by the experimentation on sample facial expressions from a benchmark dataset and comparison with state of the art methods. The non-extensive entropy with Gaussian gain is proved superior to the extensive Shannon entropy for the proposed maximum entropy based partitioning.

References

[1] De la Torre Fernando and Jeffrey F Cohn 2011 Facial expression analysis. In: *Visual analysis of humans*, pp. 377–409. Springer London

[2] Kanade T, Cohn J F and Tian Y 2000 Comprehensive database for facial expression analysis. In: *Proceedings of International Conference on Automatic Face and Gesture Recognition*, pp. 46–53

[3] Zwakhalen Sandra M G, Jan P H Hamers, Huda H Abu-Saad and Martijn P F Berger 2006 Pain in elderly people with severe dementia: a systematic review of behavioural pain assessment tools. *BMC Geriatr.* 6(1): 3a

[4.] Izard Carroll E et al 1983 Changes in facial expressions of 2-to 19-month-old infants following acute pain. *Dev. Psychol.* 19(3): 418

[5] Edwards Jane, Henry J Jackson and Philippa E Pattison 2002 Emotion recognition via facial expression and affective prosody in schizophrenia: a methodological review. *Clin. Psychol. Rev.* 22(6): 789–832

[6] Prkachin Kenneth M 1992 The consistency of facial expressions of pain: a comparison across modalities. *Pain* 51(3): 297–306

[7] Schwartz Gary E, Paul L Fair, Patricia Salt, Michel R Mandel and Gerald L Klerman 1976 Facial expression and imagery in depression: an electromyographic study. *Psychosomatic Med.* 38(5): 337–347

[8] Picard Rosalind W 2000 Toward computers that recognize and respond to user emotion. *IBM Syst. J.* 39(3.4): 705–719

[9] Bartlett Marian Stewart, Gwen Littlewort, Ian Fasel and Javier R Movellan 2003 Real time face detection and facial expression recognition: development and applications to human computer interaction. In: *CVPRW'03, Conference on Comput.er Vision and Pattern Recognition Workshop 2003*, vol. 5, pp. 53–53

[10] Fong Terrence, Illah Nourbakhsh and Kerstin Dautenhahn 2003 A survey of socially interactive robots. *Robotics Autonom. Syst.* 42(3): 143–166

[11] Scheirer Jocelyn, Raul Fernandez and Rosalind W Picard 1999 Expression glasses: a wearable device for facial expression recognition. In: *CHI'99 Extended Abstracts on Human Factors in Computing Systems*, pp. 262–263. ACM

[12] Lyons Michael J and Nobuji Tetsutani 2001 Facing the music: a facial action controlled musical interface. In: *CHI'01 extended abstracts on Human factors in computing systems*, pp. 309–310. ACM

[13] Den Uyl M J and Van Kuilenburg H 2005 The FaceReader: online facial expression recognition. In: *Proceedings of Measuring Behavior*, vol. 30

[14] Oliver Nuria, Alex Pentland and François Bérard 2000 LAFTER: a real-time face and lips tracker with facial expression recognition. *Pattern Recognit.* 33(8): 1369–1382

[15] Boucher Jerry D and Gary E Carlson 1980 Recognition of facial expression in three cultures. *J. Cross-Cultural Psychol.* 11(3): 263–280

[16] Tranel Daniel, Antonio R Damasio and Hanna Damasio 1988 Intact recognition of facial expression, gender, and age in patients with impaired recognition of face identity. *Neurology* 38(5): 690–690

[17] Cohen Ira, Nicu Sebe, Ashutosh Garg, Lawrence S Chen and Thomas S Huang 2003 Facial expression recognition from video sequences: temporal and static modeling. *Comput. Vis. Image Understand.* 91(1): 160–187

[18] Hills Peter J and Michael Pake J 2013 Eye-tracking the own-race bias in face recognition: revealing the perceptual and socio-cognitive mechanisms. *Cognition* 129(3): 586–597

[19] Lienhart Rainer and Jochen Maydt 2002 An extended set of haar-like features for rapid object detection. In: *Proceedings of International Conference on Image Processing. 2002*. vol. 1. IEEE

[20] Magalhães Filipe et al 2013 Compressive sensing based face detection without explicit image reconstruction using support vector machines. *Image analysis and recognition*. Springer Berlin Heidelberg, pp. 758–765

[21] Reisfeld Daniel and Yehezkel Yeshurun 1992 Robust detection of facial features by generalized symmetry. In: *International Conference on Pattern Recognition*, pp. 117–117. IEEE Computer Society Press

[22] Roth Dan, Ming-Hsuan Yang and Narendra Ahuja 2000 A SNoW-based face detector. *Urbana* 51: 61801

[23] Susan Seba and Pooja Kadyan 2013 A supervised fuzzy eye pair detection algorithm. In: *5th International Conference on Computational Intelligence and Communication Networks (CICN), 2013*, pp. 306–310. IEEE

[24] Zhang Lun et al 2007 Face detection based on multi-block lbp representation. *Advances in biometrics*. Springer Berlin Heidelberg, pp. 11–18

[25] Viola Paul and Michael J Jones 2004 Robust real-time face detection. *Int. J. Comput. Vis.* 57(2): 137–154

[26] Ojala T, Pietikaenen M, Maenepae T 2002 Multi-resolution gray scale and rotation invariant texture classification with LBP. *IEEE Trans. Pattern Anal. Mach. Intell.* 24(7): 971–987

[27] Zhao G and Matti Pietikäinen 2007 Dynamic texture recognition using local binary patterns with application to facial expressions. *IEEE Trans. Pattern Anal. Mach. Intell.* 29(6): 915–928

[28] Hernández Benjamín, Gustavo Olague, Riad Hammoud, Leonardo Trujillo and Eva Romero 2007 Visual learning of

texture descriptors for facial expression recognition in thermal imagery. *Comput. Vis. Image Understand.* 106(2): 258–269

[29] Liao Shu, Wei Fan, Albert CS Chung and Dit-Yan Yeung 2006 Facial expression recognition using advanced local binary patterns, tsallis entropies and global appearance features. In: *IEEE International Conference on Image Processing, 2006* pp. 665–668

[30] Lyons Michael, Shigeru Akamatsu, Miyuki Kamachi and Jiro Gyoba 1998 Coding facial expressions with gabor wavelets. In: *Proceedings of Third IEEE International Conference on Automatic Face and Gesture Recognition, 1998*, pp. 200–205

[31] Manjunath Bangalore S and Wei-Ying Ma 1996 Texture features for browsing and retrieval of image data. *IEEE Trans. Pattern Anal. Mach. Intell.* 18(8): 837–842

[32] Seba Susan and Gitin Kakkar 2015 Decoding facial expressions using a new normalized similarity index. In *2015 Annual IEEE India Conference (INDICON)*, pp. 1–6. IEEE

[33] Milborrow Stephen and Fred Nicolls 2008 Locating facial features with an extended active shape model. In: *Computer Vision–ECCV 2008*, pp. 504–513. Springer Berlin Heidelberg

[34] Huffman David A 1952 A method for the construction of minimum redundancy codes. *Proc. IRE* 40(9): 1098–1101

[35] Fano Robert M and Wintringham W T 1961 Transmission of information. *Phys. Today* 14: 56

[36] Shannon C E 1948 A mathematical theory of communication. *Bell Syst. Tech. J.* 27: 379–423

[37] Chanda Bhabatosh and Dwijesh Dutta Majumder 2004 *Digital image processing and analysis*. PHI Learning Pvt. Ltd

[38] Jeon Byeung-woo, Jechang Jeong and Ju-ha Park 1996 *Apparatus for variable-length coding and variable-length-decoding using a plurality of Huffman coding tables*. U.S. Patent 5,528,628, issued June 18

[39] Takishima Yasuhiro, Masahiro Wada, and Hitomi Murakami 1995 Reversible variable length codes. *IEEE Trans. Commun.* 43(234): 158–162

[40] Zhou Jiantao, Zhiqin Liang, Yan Chen and Oscar C Au 2007 Security analysis of multimedia encryption schemes based on multiple Huffman table. *Signal Process. Lett. IEEE* 14(3): 201–204

[41] Nag Amitava, Sushanta Biswas, Debasree Sarkar and Partha Pratim Sarkar 2011 A novel technique for image steganography based on DWT and Huffman encoding. *Int. J. Comput. Sci. Security* 4(6): 497–610

[42] Al-Laham Mohammed and Ibrahiem MM El Emary 2007 Comparative study between various algorithms of data compression techniques. *Int. J. Comput. Sci. Netw. Security* 7(4): 281

[43] Christiansen Mark M et al 2013 Brute force searching, the typical set and Guesswork. *IEEE International Symposium on Information Theory Proceedings (ISIT), 2013*

[44] Xiaohua Huang, Guoying Zhao, Xiaopeng Hong, Wenming Zheng, and Matti Pietikäinen 2016 Spontaneous facial micro-expression analysis using spatiotemporal completed local quantized patterns. *Neurocomputing* 175: 564–578

[45] Seba Susan and Roni Chakre 2016 3D-difference theoretic texture features for dynamic face recognition. In *2016 International conference on computational techniques in information and communication technologies (ICCTICT)*, pp. 227–232. IEEE

[46] Pal Nikhil R and Sankar K Pal 1989 Entropic thresholding. *Signal Process.* 16(2): 97–108

[47] Susan Seba and Madasu Hanmandlu 2013a A non-extensive entropy feature and its application to texture classification. *Neurocomputing* 120: 214–225

[48] Seba Susan and Madasu Hanmandlu 2015 Unsupervised detection of nonlinearity in motion using weighted average of non-extensive entropies. *SIViP* 9(3): 511–525

[49] Susan S and Dwivedi M 2014 Dynamic growth of hidden-layer neurons using the non-extensive entropy. In *2014 Fourth international conference on communication systems and network technologies (CSNT)*, 7 Apr 2014, pp. 491–495. IEEE

[50] Seba Susan and Ankit Kumar 2016 Auto-segmentation using mean-shift and entropy analysis. In: *2016 3rd International conference on computing for sustainable global development (INDIACom)*, pp. 292–296. IEEE

[51] Susan Seba and Madasu Hanmandlu 2013 cDifference theoretic feature set for scale-, illumination-and rotation-invariant texture classification. *IET Image Process.* 7(8): 725–732

[52] Bezdek J C 1981 *Pattern recognition with fuzzy objective function algorithms.* New York: Plenum Press

[53] Raheja Jagdish Lal, Radhey Shyam, Jatin Gupta, Umesh Kumar and Bhanu Prasad P 2010 Facial gesture identification using lip contours. In: *Second International Conference on Machine Learning and Computing (ICMLC), 2010*, pp. 3–7. IEEE

[54] Engin Avci 2007 An expert system based on wavelet neural network adaptive norm entropy for scale invariant texture classification. *Expert Syst. Appl.* 32: 919–926

[55] Filko Damir and Goran Martinovic 2013 Emotion recognition system by a neural network based facial expression analysis. *Automatika–J. Control Meas. Electron. Comput. Commun.* 54(2): 263–272

[56] Shan Caifeng, Shaogang Gong and Peter W McOwan 2009 Facial expression recognition based on local binary patterns: a comprehensive study. *Image Vis. Comput.* 27(6): 803–816

Accepted Manuscript

Title: Inducing half-metallicity with enhanced stability in zigzag graphene nanoribbons via fluorine passivation

Author: Neeraj K. Jaiswal Neha Tyagi Amit Kumar Pankaj Srivastava

PII: S0169-4332(16)32316-9
DOI: http://dx.doi.org/doi:10.1016/j.apsusc.2016.10.178
Reference: APSUSC 34272

To appear in: *APSUSC*

Received date: 27-6-2016
Revised date: 3-10-2016
Accepted date: 27-10-2016

Please cite this article as: Neeraj K. Jaiswal, Neha Tyagi, Amit Kumar, Pankaj Srivastava, Inducing half-metallicity with enhanced stability in zigzag graphene nanoribbons via fluorine passivation, *<![CDATA[Applied Surface Science]]>* (2016), http://dx.doi.org/10.1016/j.apsusc.2016.10.178

This is a PDF file of an unedited manuscript that has been accepted for publication. As a service to our customers we are providing this early version of the manuscript. The manuscript will undergo copyediting, typesetting, and review of the resulting proof before it is published in its final form. Please note that during the production process errors may be discovered which could affect the content, and all legal disclaimers that apply to the journal pertain.

ACCEPTED MANUSCRIPT

Inducing half-metallicity with enhanced stability in zigzag graphene nanoribbons via fluorine passivation

Neeraj K. Jaiswal[a,*], Neha Tyagi[b], Amit Kumar[a], Pankaj Srivastava[c]

[a] *Discipline of Physics, Indian Institute of Information Technology Design & Manufacturing, Jabalpur-482005, INDIA.*
[b] *Department of Applied Physics, Delhi Technological University, Delhi-110042, INDIA.*
[c] *Nanomaterials Research Group, ABV-Indian Institute of Information Technology & Management, Gwalior-474015, INDIA.*

Abstract

Half metals are the primary ingredients for the realization of novel spintronic devices. In the present work, by employing density functional theory based first-principles calculation, we predict half metallic bahavior in fluorine passivated zigzag graphene nanoribbons (F-ZGNR). Four different structures have been investigated viz. one edge F passivated ZGNR (F-ZGNR-1), both edges F passivated ZGNR (F-ZGNR-2), F passivation on alternate sites in first configuration (alt-1) and F passivation on alternate sites in second configuration (alt-2). Interestingly, it is noticed that F passivation is analogous to H passivation (pristine), however, F-ZGNR are reckoned energetically more stable than pristine ones. An spin induced band gap is noticed for all F-ZGNR irrespective of their widths although its magnitude is slightly less than the pristine counterparts. With an external transverse electric field, ribbons undergo semiconducting to half metallic transformation. The observed half metallic character with enhanced stability present F-ZGNR as a better candidate than pristine ZGNR towards the realization of upcoming spintronic devices.

Keywords: `Graphene nanoribbon, fluorine, electronic structure, half-metal`
2010 MSC: 73.22.Pr, 31.15.E-, 71.20.-b, 85.75.-d

1. Introduction

Since from inception of the idea for beyond Si electronic devices, graphene has become a ray of hope for the future electronic and sensing devices [1, 2, 3, 4]. However, other 2-dimensional (2-D) materials have also been investigated [5, 6, 7] but the dominance of graphene is still maintained due to its exotic

☆Fully documented templates are available in the elsarticle package on CTAN.
*Corresponding author
Email address: `neerajkjaiswal@gmail.com` (Neeraj K. Jaiswal)

ACCEPTED MANUSCRIPT

physical properties [8, 9, 10, 11]. Graphene has also been regarded as an ideal material for sensing applications [12, 13, 14, 15]. Furthermore, nanoribbons (thin 1-D counterparts of graphene), exhibit interesting electronic properties due to presence of edges where edge C atom is bonded with only two neighbouring atoms. Therefore, an additional bond is lying vacant at each of the edge C atoms. The presence of these additional bonds (the so called dangling bonds) play a crucial role to determine the electronic properties of the ribbon. It is known that ribbons with zigzag edges, henceforth to be referred as zigzag graphene nanoribbons (ZGNR), have magnetic ground state whereas the armchair graphene nanoribbons (AGNR) are nonmagnetic semiconductors when their edges are terminated via H atoms [16, 17, 18]. Several reports are available which reveal that the electronic properties of GNR can be tailored via chemical edge functionalizations [19, 20, 21, 22].

Owing to its potential for replacing Si in future electronic devices, various efforts have been made to synthesise mono as well as few layered graphene, its nanoribbons with controlled edge shapes as well as various other derivatives to meet the expectations of industry towards device fabrication [23, 24, 25, 26, 27]. Withers et al., synthesized fluorinated graphene via two step mechanical exfoliation technique and found that electronic properties of graphene are dependent upon the degree of fluorination [28]. Despite of these efforts, producing graphene in bulk quantity is still challenging and one of the major obstacle for the realization of graphene based devices. Jeon et al. [29] reported the synthesis of graphene flakes with scalable quantity in the halogen rich environment using simple ball milling process. In this method, halogen atoms react with the edges of the graphene flakes. Thus, halogens act as a natural passivating element to the edge C atoms of graphene samples in this method. As the output is quite higher, it could be envisioned as a viable way to produce graphene commercially for various technological applications. To use GNR prepared by this method for the device fabrication, it is crucial to understand the physics of halogen interaction with graphene edges and its impact on the structural and electronic properties of graphene/GNR. Till now, only few efforts have been made to examine the effect of halogen functionalization on graphene [30, 31, 32]. Karlický et al., [33] have presented a nice overview of the halogenated graphenes. However, a complete understanding of halogen passivation GNR as widely studied for H passivation is still unavailable. Therefore, in the present work, we investigated the effect of fluorine (F) passivation on the electronic and spintronic properties of ZGNR.

2. Methodology

We study the effect of F passivation at the edges of ZGNR to reveal their spin dependent electronic properties. The present investigations have been performed by employing density functional theory (DFT) based first principles calculations. We used Atomistix ToolKit Virtual Nanolab (ATK-VNL) which is the further advancement of TranSiesta code [34]. Our considered structures of F passivated ZGNR (F-ZGNR) are one edge F passivated ZGNR (F-ZGNR-1),

Accepted Manuscript

ACCEPTED MANUSCRIPT

both edges F passivated ZGNR (F-ZGNR-2), F passivation on alternate sites in first configuration (alt-1) and F passivation on alternate sites in second configuration (alt-2) as shown in Fig. (1). To account the effect of ribbon size, we considered ZGNR having width N_z = 4, 6, 8. The widths are defined as per the convention of previous literature, i.e. number of C-C pairs across the ribbon [16]. All the ribbons were periodic along Z-axis whereas X and Y axes were confined. The Brillouin zone has been sampled in Monkhorst-Pack scheme with a grid of $1 \times 1 \times 50$ k-points and centred at Γ. The exchange correlation contribution was treated using generalized gradient approximation (GGA) in Perdew-Burke-Ernzerhof (PBE) form [35]. All calculations were performed using normconserving pseudopotential. The wavefunction was expanded with double zeta polarized basis set and the mesh cut off energy was chosen equal to 70 Rydberg. The geometry optimization was carried out in a self consistent manner without enforcing any constraint on the considered structures. During the optimization process, all the atoms were allowed to make changes in their position towards attaining a minimum energy configuration. Pulay mixer algorithm was used for optimization and the tolerance of convergence for self-consistent iteration loop over the total energy was taken as 1×10^{-5} Rydberg. The optimized geometry was recognized with a convergence criteria based upon forces on individual atom less than 0.05 eV/Å. All the nanoribbons under investigation were kept isolated from their periodic replica using a vacuum region of 10 Å in the non-periodic (X and Y) directions.

3. Results and Discussion

3.1. Structural Stabilities

We have investigated the structural stabilities and spin dependent electronic properties of F-ZGNR considering various possible structures as shown in Fig. (1). For the comparison basis, we have also studied the pristine (H-passivated) nanoribbons. It is noticed that after optimization, passivating F atom takes in-plane position with the ribbon and the optimized C-F bond length varies from 1.32 to 1.35 Å. First of all, we compared the structural stabilities of considered structures on the basis of binding energy (BE) analysis. We found that all considered F passivated ZGNR (F-ZGNR) are relatively more stable as compared to pristine nanoribbons. F-ZGNR-2 are found to be energetically most stable configuration followed by alt-2, alt-1 and F-ZGNR-1 structures. Interestingly, pristine (H-ZGNR) which are the only widely investigated nanoribbons till date, are found to be less stable as compared to considered family of F-ZGNR. Further, the BE difference (varying from ∼0.4 to 0.23 eV) between pristine and F-ZGNR, is sufficiently larger than the room temperature thermal excitation energy (∼0.025 eV). This shows that the observed energetic stability would survive at the normal room temperature as well. Therefore, being more stable, F-ZGNR could be more promising building blocks for the future electronic/spintronic devices. Moreover, all the F-ZGNR prefer to be settled in magnetic ground state similar to that of pristine nanoribbons reported previously [16]. The most stable ground state observed here is antiferromagnetic

ACCEPTED MANUSCRIPT

(AFM) one for all the structures under investigation. The electronic configuration of F is similar to that of H since both are lacking one electron to obtain the status of an inert gas. Therefore, the passivation of ZGNR by F is similar to that by H and both result in the similar magnetic (AFM) ground state.

To examine the origin of the observed AFM ground state of F-ZGNR, we computed spin compensatory density of states (DOS) as depicted in Fig. (2). It is noticed that all the structure are metallic with a sharp peak lying exactly at the Fermi level. Further, the characteristic 1-D behavior of ribbons is also reflected in the DOS profiles. The existence of sharp electron density peaks at the Fermi level is responsible for the observed AFM ground state in F-ZGNR. It is due to total energy difference between magnetic and nonmagnetic states which is referred as the magnetic stabilization (ΔE). The similar splitting of edge states near the Fermi level also accounts for the AFM ground state of the pristine ZGNR [16]. The calculated BE, ΔE, Fermi energy (E_F) and the spin induced band gap (E_g) are presented in Table 1. The perusal of Table (1) reveals that E_F goes down as a result of F passivation. It suggests that F passivation takes place via charge transfer from the edge C to the passivating F atoms which in turn is analogous to the hole doping of GNR [36]. Further, the enhanced stability of F-ZGNR as compared to pristine GNR is due to more charge transfer between C and F than that of C and H. Recently, F passivated armchair boron nitride nanoribbons were also found to be more stable as compared to H passivated ribbons [37] which agrees with our present findings.

Table 1: The calculated binding energy (BE), magnetic stabilization (ΔE), Fermi energy (E_F) and the spin induced band gap (E_g) as a function of ribbon width for considered structures.

Width (N_z)	Configration	B.E.(eV)	ΔE (meV)	E_F (eV)	E_g (eV)
4	Pristine	-6.60	60	-3.72	0.639
	F-ZGNR-1	-6.84	32	-3.82	0.464
	F-ZGNR-2	-7.08	40	-3.93	0.527
	alt-1	-6.91	110	-3.92	0.591
	alt-2	-6.92	110	-3.92	0.593
6	Pristine	-6.59	70	-3.77	0.555
	F-ZGNR-1	-6.83	49	-3.85	0.441
	F-ZGNR-2	-7.08	50	-3.92	0.480
	alt-1	-6.90	130	-3.92	0.525
	alt-2	-6.91	140	-3.92	0.527
8	Pristine	-6.59	70	-3.79	0.478
	F-ZGNR-1	-6.83	60	-3.86	0.427
	F-ZGNR-2	-7.09	60	-3.93	0.423
	alt-1	-6.90	140	-3.93	0.458
	alt-2	-6.91	140	-3.93	0.459

ACCEPTED MANUSCRIPT

3.2. Electronic Properties

After studying the structural stabilities, we next examined the electronic properties of considered F-ZGNR. Since the electronic properties are adequately independent of ribbon width, we selected ribbons of width N_z=8 as the representative candidate for all considered F-ZGNR. First, we computed spin compensated electronic band structures as depicted in Fig. (3). It is revealed that the peculiar edge states which are characteristic of pristine ZGNR, still prevails in F-ZGNR due to similar electronic configuration of H and F. The observed band structures of F-ZGNR-2 are identical to that of pristine ribbon [Fig. (3)]. This also confirms that F passivation is analogous to H passivation of ZGNR. The highest valence band and lowest conduction band stick together at the Fermi level near the Z point. Further, the edge states are more localized in alt-1 and alt-2 configurations. These localized degenerate electronic bands are responsible for the sharp density peaks at the Fermi level [Fig. (2)]. The origin of these peaks has been traced in p-orbital contributions from edge C and passivating F atoms as confirmed by partial density of states (PDOS). To be concise, PDOS have been depicted only for F-ZGNR-2 [Fig. 4].

In order to observe the effect of spin polarization, we also calculated spin polarized electronic band structures as depicted in Fig. (5). It is noticed that inclusion of spin results into opening of a direct band gap for all the considered structures. However, the position of band gap opening (k-value) is different depending upon the different configurations of F-ZGNR. For pristine, F-ZGNR-1 and F-ZGNR-2, the gap opening is shifted towards the Z point of Brillouin zone 5(a)-(c) whereas for alt-1 and alt-2 structures [Fig. 5(d),(e)], the opening of band gap is noticed in the middle of Γ and Z point. The opening of band gap is due to splitting of edge states in opposite directions i.e. highest valence band (HVB) shifts downward whereas the lowest conduction band (LCB) is pushed upward. Further, the degeneracy of opposite spin (spin up and spin down) electrons is still preserved for all structures except for F-ZGNR-1 particularly near Z point [Fig. 5(b)]. The broken spin degeneracy for this configuration is due to dissimilar passivating atoms and hence unequal charge transfer at opposite edges of the ribbon. Owing to this broken degeneracy, the magnitude of spin assisted band gap is larger (smaller) for spin down (up) electrons at the Z point. For a further verification of the observed spin degeneracy, we also calculated spin polarized DOS as presented in Fig. (6). The unavailability of electronic states across Fermi level confirms the semiconducting behavior as suggested by spin polarized band structures. Moreover, the observed DOS peaks exhibit mirror symmetry (with respect to Fermi Level) for spin up and spin down electrons which is consistent with the corresponding degenerate band structures. On the other hand, an exception has been noticed in the mirror symmetry of DOS for F-ZGNR-1 particularly in the vicinity of Fermi level which is due to broken degeneracy of opposite spins (near Z point) in this configuration.

To obtain more in-depth information about the splitting of electronic states near the Z point in the vicinity of Fermi level, we also investigate the Bloch functions of the HVB and LCB. Since the splitting mechanism is same in the considered family of F-ZGNR, we have shown Bloch functions selectively for

Accepted Manuscript

ACCEPTED MANUSCRIPT

F-ZGNR-2 in Fig. (7). The present Bloch functions have been plotted at Z point where the maximum splitting has been noticed. It is revealed that Bloch functions are localized at Z point [Fig. 7(a)] which in turn supports the localization of edge states at Fermi level towards Z point [Fig. 3]. Further, it can be observed that in AFM state, the electronic states of spin up and spin down electrons are localized at opposite edges of the ribbon [Fig. 7(b)] which also explains the observed magnetic stabilization and splitting of electronic states.

3.2.1. Effect of electric field

As the present ribbons exhibit AFM ground state, the external electric field may cause shifting of spin up and spin down electronic states in opposite directions as reported by Son et. al., [38]. If it happens, the possibility is there to turn the ribbons half-metallic in nature i.e. metallic for one (up or down) type of spin and semiconducting/insulating for other type of spin. To further probe in this direction, we have also examined the electronic properties of F-ZGNR under the influence of external transverse electric field. Schematic model of the applied field has been depicted for F-ZGNR-2 in Fig. (8). It is observed that electric field tend to weaken the degeneracy between opposite spin states. Moreover, the field also pushes spin up states towards Fermi level and spin down states away from Fermi level. As a result, the electronic band gap decreases (increases) for spin up (spin down) electrons. If the field is continued to increase, a critical field is reached where the ribbons become metallic for spin up electrons whereas semiconducting/insulating for spin down electrons as shown in Fig. (9). It is possible due to localization of spin up and spin down states on the opposite edges of the ribbon [Fig. (7)]. Owing to this, the electric field widens the band gap for one (down) type of spin whereas suppressing for other (up) flavour of spin [38]. Perusal of Fig. (9) and (10) reveals the possibility of turning F-ZGNR into half metals with spin up as conducting channel and spin down as semiconducting/insulating channel. All the ribbons under investigation can be tuned to half-metallic behavior irrespective of their width or the configuration. Moreover, the effective conduction channel (spin up or spin down) may be selected depending upon the polarity of applied field.

The variation of electronic band gap as a function of electric field is depicted in Fig. (11). It is revealed that the magnitude of critical field required to make the structures half-metallic is $\sim 0.3V/\mathring{A}$ except for F-ZGNR-1 which becomes half-metallic at slightly higher ($0.35V/\mathring{A}$) electric field. This is due to unequal charge transfer at the opposite edges since in this configuration, one edge is passivated by H and other edge with F. The electro-negativity difference between H and F causes unequal charge transfer from edge C to passivating (H/F) atoms. Owing to this, an electrostatic potential difference is originated in this configuration between opposite edges of ribbon as explained by Kan et al., [39]. A fraction of external electric field is invested to overcome the effect of this induced potential. Therefore, it requires slightly higher electric field to exhibit half-metallicity in F-ZGNR-1. To comment on the size effects on the observed half-metallicity, electronic structures of F-ZGNR-2 having width upto $N_z = 20$ have been investigated under external electric field. The variation of

ACCEPTED MANUSCRIPT

critical electric field versus ribbon width has been plotted in Fig. 12(a) for F-ZGNR-2. It is revealed that magnitude of critical field is inversely proportional to the ribbon width. Further, the value of band gap for insulating (spin down) channel in F-ZGNR-2 with $N_z = 16$ [Fig. 12(b)] is sufficiently larger ($\sim$0.39 eV) than that of thermal excitation energy (0.025 eV) at room temperature. Recently, the potential of fluorinated graphene for room temperature spintronic devices has also been confirmed experimentally by Makarova et al., [40]. Moreover, site selective fluorination of graphene has been achieved by focused ion beam irradiation [41] as well as via laser irradiation [42]. All these recent experimental advancements support that present structures can play a vital role in spintronic applications.

Present values of critical field to make ribbons half metallic, are higher than that of previously reported values by Son et. al., [38]. This is due to the fact that we have used GGA exchange correlation functional instead of local density approximation (LDA). Since the underestimation of E_g is larger in LDA (as used by Son et. al.,), the magnitude of spin induced gap is larger in our findings which obviously demands for comparatively higher magnitude of electric field towards the closure of band gap. Although, other methods have also been adopted for realising half-metallicity in GNR like unequal charge transfer at opposite edges, selective doping of particular impurities etc. [39, 43, 44, 45], however, present structures are expected to be more viable for spintronic applications. This is because the observed half metallicity in present structures is independent of ribbon width and the way of passivating ribbon edges by F. Furthermore, manipulating electric field is comparatively easier than controlling doping sites to achieve spin polarization/half metallicity in GNR.

4. Conclusion

In summary, we have investigated the structural stability and spin dependent electronic properties of F-ZGNR incorporating first-principle calculations based on DFT. A total of four configurations namely F-ZGNR-1, F-ZGNR-2, alt-1, alt-2 were proposed and examined in detail and the findings were compared with that of pristine ribbons. It is revealed that F passivation is analogous to H passivation of the ribbons with zigzag edges. F passivation enhances the structural stability of ZGNR keeping its electronic properties intact as compared to pristine ZGNR. The characteristic edge states of ZGNR are preserved upon F passivation, however, the spin induced band gap is slightly reduced in F-ZGNR than that of pristine ribbons. Electric field induced half-metallicity has been noticed in all considered structures independent of their widths. The observed half metallic character and greater stability makes the proposed F-ZGNR structures a potential competitor of pristine ZGNR for realizing novel spintronic devices.

ACCEPTED MANUSCRIPT

Acknowledgements

NKJ is thankful to Science and Engineering Research Board, Department of Science and Technology (DST) Government of India for providing financial support through DST Young Scientist research project grant number SB/FTP/PS-101/2014. Authors also acknowledge Computational Nanoscience and Technology Laboratory at ABV-Indian Institute of Information Technology & Management, Gwalior for providing computational facilities.

References

[1] C. Soldano, A. Mahmood, E. Dujardin, Production, properties and potential of graphene, Carbon 48 (2010) 2127 –50.

[2] Y. J. Park, S.-K. Lee, M.-S. Kim, H. Kim, J.-H. Ahn, Graphene-based conformal devices, ACS Nano 8 (2014) 7655–62.

[3] Y. An, K. Wang, Z. Yang, Z. Liu, G. Jia, Z. Jiao, T. Wang, G. Xu, Negative differential resistance and rectification effects in step-like graphene nanoribbons, Org. Electron. 17 (2015) 262–269.

[4] N. K. Jaiswal, G. Kovačević, B. Pivac, Reconstructed graphene nanoribbon as a sensor for nitrogen based molecules, Appl. Surf. Sci. 357 (2015) 55–59.

[5] N. Pournaghavi, M. Esmaeilzadeh, S. Ahmadi, M. Farokhnezhad, Electrically controllable spin conductance of zigzag silicene nanoribbons in the presence of anti-ferromagnetic exchange field, Solid State Commun. 226 (2016) 33–38.

[6] B. Van den Broek, M. Houssa, E. Scalise, G. Pourtois, V. V. Afanas'ev, A. Stesmans, First principle electronic functionalization of silicene and germanene by adatom chemisorption, Appl. Surf. Sci. 291 (2014) 104–108.

[7] P. Srivastava, N. K. Jaiswal, V. Sharma, Adsorption of $COCl_2$ gas molecule on armchair boron nitride nanoribbons for nano sensor applications, Microelectron. Eng. 146 (2015) 62–67.

[8] L. Ma, J. M. Zhang, K. W. Xu, V. Ji, A first-principles study on gas sensing properties of graphene and Pd-doped graphene, Appl. Surf. Sci. 343 (2015) 121–27.

[9] Z. Jiang, Y. Song, Band gap oscillation and novel transport property in ultrathin chiral graphene nanoribbons, Physica B 464 (2015) 61–67.

[10] T. S. Li, C. T. Hsieh, S. P. Yang, S. C. Chang, Ballistic transport of bilayer graphene nanoribbons in a spatially modulated magnetic field, Solid State Commun. 206 (2015) 6–11.

ACCEPTED MANUSCRIPT

[11] D. Wang, Z. Zhang, J. Zhang, X. Deng, Z. Fan, G. Tang, Electronic and magnetic properties of zigzag-edged hexagonal graphene ring nanojunctions, Corbon 94 (2015) 996–1002.

[12] F. Schedin, A. K. Geim, S. V. Morozov, E. W. Hill, P. Blake, M. I. Katsnelson, K. S. Novoselov, Detection of individual gas molecules adsorbed on graphene, Nat. Mater. 6 (2007) 652–55.

[13] R. Chowdhury, S. Adhikari, P. Rees, S. P. Wilks, F. Scarpa, Graphene-based biosensor using transport properties, Phys. Rev. B 83 (2011) 045401–1–045401–8.

[14] Y. Wang, L. Zhang, N. Hu, Y. Wang, Y. Zhang, Z. Zhou, Y. Liu, S. Shen, C. Peng, Ammonia gas sensors based on chemically reduced graphene oxide sheets self-assembled on Au electrodes, Nanoscale Res. Lett. 9 (2014) 251–1–251–12.

[15] S. S. Varghese, S. Lonkar, K. K. Singh, S. Swaminathan, A. Abdala, Recent advances in graphene based gas sensors, Sens. Actuators B 218 (2015) 160–183.

[16] L. Pisani, J. A. Chan, B. Montanari, N. M. Harrison, Electronic structure and magnetic properties of graphitic ribbons, Phys. Rev. B 75 (2007) 064418–1–064418–9.

[17] M. Fujita, K. Wakabayashi, K. Nakada, K. Kusakabe, Peculiar localized state at zigzag graphite edge, J. Phys. Soc. Jpn. 65 (1996) 1920–23.

[18] N. K. Jaiswal, P. Srivastava, First principles calculations of armchair graphene nanoribbons interacting with Cu atoms, Physica E 44 (2011) 75–79.

[19] A. Ramasubramaniam, Electronic structure of oxygen-terminated zigzag graphene nanoribbons: A hybrid density functional theory study, Phys. Rev. B 81 (2010) 245413–1–245413–6.

[20] Y. Wang, C. Cao, H. P. Cheng, Role of edge states in metal-terminated graphene nanoribbons, Phys. Rev. B 82 (2010) 205429–1–205429–5.

[21] L. Li, R. Qin, H. Li, L. Yu, Q. Liu, G. Luo, Z. Gao, J. Lu, Functionalized graphene for High performance two-dimensional spintronic devices, ACS Nano 5 (2011) 2601–10.

[22] F. J. Martin-Martinez, S. Fias, G. V. Lier, F. D. Proft, P. Geerlings, Tuning aromaticity patterns and electronic properties of armchair graphene nanoribbons with chemical edge functionalisation, Phys. Chem. Chem. Phys. 15 (2013) 12637–1–12637–11.

[23] Z. S. Wu, W. Ren, L. Gao, B. Liu, J. Zhao, H. M. Cheng, Efficient synthesis of graphene nanoribbons sonochemically cut from graphene sheets, Nano Res. 3 (2010) 16–22.

Accepted Manuscript

ACCEPTED MANUSCRIPT

[24] P. Nemes-Incze, L. Tapasztó, G. Z. Magda, Z. Osváth, G. Dobrik, X. Jin, C. Hwang, L. P. Biró, Graphene nanoribbons with zigzag and armchair edges prepared byscanning tunneling microscope lithography on gold substrates, Appl. Surf. Scie. 291 (2014) 48–52.

[25] A. Konishi, Y. Hirao, H. Kurata, T. Kubo, Investigating the edge state of graphene nanoribbons by a chemical approach: Synthesis and magnetic properties of zigzag-edged nanographene molecules , Solid State Commun. 175-176 (2013) 62–70.

[26] T. Kato, R. Hatakeyama, Site and alignment-controlled growth of graphene nanoribbons from nickel nanobars, Nat. Nanotech. 7 (2012) 651–56.

[27] D. Geng, B. Wu, Y. Guo, L. Huang, Y. Xue, J. Chen, G. Yu, L. Jiang, Uniform hexagonal graphene flakes and films grown on liquid copper surface, PNAS 109 (2012) 7992–96.

[28] F. Withers, S. Russo, M. Dubois, M. F. Craciun, Tuning the electronic transport properties of graphene through functionalisation with fluorine, Nanoscale Res. Lett. 6 (2011) 526–1–526–11.

[29] I.-Y. Jeon, H.-J. Choi, M. Choi, J.-M. Seo, S.-M. Jung, M.-J. Kim, S. Zhang, L. Zhang, Z. Xia, L. Dai, N. Park, J.-B. Baek, Facile, scalable synthesis of edge-halogenated graphene nanoplatelets as efficient metal-free eletrocatalysts for oxygen reduction reaction, Sci. Rep. 3 (2013) 1810–1–1810–7.

[30] A. Natan, M. C. Hersam, T. Seideman, Insights into graphene functionalization by single atom doping, Nanotechnol. 24 (2013) 505715–1–505715–7.

[31] J. T. Robinson, J. S. Burgess, C. E. Junkermeier, S. C. Badescu, T. L. Reinecke, F. K. Perkins, M. K. Zalalutdniov, J. W. Baldwin, J. C. Culbertson, P. E. Sheehan, E. S. Snow, Properties of Fluorinated Graphene Films, Nano Lett. 10 (2010) 3001–05.

[32] C. Xu, P. A. Brown, J. Lu, K. L. Shuford, Electronic properties of halogen-adsorbed graphene, J. Phys. Chem. C 119 (2015) 17271–77.

[33] F. Karlický, K. K. R. Datta, M. Otyepka, R. Zbořil, Halogenated graphenes: rapidly growing family of graphene derivatives, ACS Nano 7 (2013) 6434–64.

[34] M. Brandbyge, J. L. Mozos, P. Ordejón, J. Taylor, K. Stokbro, Density-functional method for nonequilibrium electron transport, Phys. Rev. B 65 (2002) 165401–1–165401–17.

[35] J. P. Perdew, K. Burke, M. Ernzerhof, Generalized gradient approximation made simple, Phys. Rev. Lett. 77 (1996) 3865–1–3865–4.

Accepted Manuscript

ACCEPTED MANUSCRIPT

[36] G. Giovannetti, P. A. Khomyakov, G. Brocks, V. M. Karpan, J. v. d. Brink, P. J. Kelly, Doping graphene with metal contacts, Phys. Rev. Lett. 101 (2008) 026803–1–026803–4.

[37] H. M. Rai, S. K. Saxena, V. Mishra, R. Late, R. Kumar, P. R. Sagdeo, N. K. Jaiswal, P. Srivastava, Possibility of spin-polarized transport in edge fluorinated armchair boron nitride nanoribbons, RSC Adv. 6 (2016) 11014–22.

[38] Y. W. Son, M. L. Cohen, S. G. Louie, Half-metallic graphene nanoribbons, Nature 444 (2006) 347–49.

[39] E.-j. Kan, Z. Li, J. Yang, J. G. Hou, Half-metallicity in edge-modified zigzag graphene nanoribbons, J. Am. Chem. Soc. 130 (2008) 4224–25.

[40] T. L. Makarova, A. L. Shelankov, A. A. Zyrianova, A. I. Veinger, T. V. Tisnek, E. Lähderanta, A. I. Shames, A. V. Okotrub, L. G. Bulusheva, G. N. Chekhova, D. V. Pinakov, I. P. Asanov, Z. Šljivančanin, Edge state magnetism in zigzag-interfaced graphene via spin susceptibility measurements, Sci. Rep. 5 (2015) 13382–1–13382–8.

[41] H. Li, L. Daukiya, S. Haldar, A. Lindblad, B. Sanyal, O. Eriksson, D. Aubel, S. Hajjar-Garreau, L. Simon, K. Leifer, Site-selective local fluorination of graphene induced by focused ion beam irradiation, Sci. Rep. 6 (2016) 19719–1–19719–7.

[42] W. H. Lee, J. W. Suk, H. Chou, J. Lee, Y. Hao, Y. Wu, R. Piner, D. Akinwande, K. S. Kim, R. S. Rouff, Selective-area fluorination of graphene with fluoropolymer and laser irradiation, Nano Lett. 12 (2012) 2374–78.

[43] M. Wu, X. Wu, Y. Gao, X. C. Zeng, Materials design of half-metallic graphene and graphene nanoribbons, Appl. Phys. Lett. 94 (2009) 223111–1–223111–3.

[44] S. L. Yan, M. Q. Long, X. J. Zhang, H. Xu, The effects of spin-filter and negative differential resistance on Fe-substituted zigzag graphene nanoribbons, Phys. Lett. A 378 (2014) 960–65.

[45] F. Zou, L. Zhu, K. Yao, Perfect spin filtering effect and negative differential behaviour in phosphorus-doped zigzag graphene nanoribbons, Sci. Rep. 5 (2015) 15966–1–15966–10.

Accepted Manuscript

ACCEPTED MANUSCRIPT

List of Figures

1 The schematics of defining ribbon width and the ball-stick models of considered F-ZGNR for (a) Pristine (b) F-ZGNR-1 (c) F-ZGNR-2 (d) alt-1 and (e) alt-2 configurations. Rectangles represent the supercell used. The white, grey and green spheres represent H, C and F atoms respectively. 14

2 The spin compensated density of states (DOS) for ribbons of width $N_z = 8$ in (a) Pristine (b) F-ZGNR-1 (c) F-ZGNR-2 (d) alt-1 and (e) alt-2 configurations. The Fermi level is set at 0 eV as shown by dotted vertical line. 15

3 The spin compensated electronic band structures ($N_z = 8$) for (a) Pristine (b) F-ZGNR-1 (c) F-ZGNR-2 (d) alt-1 and (e) alt-2 configurations. The Fermi level is set at 0 eV as shown by dotted horizontal line. 16

4 The partial density of states (PDOS) for F-ZGNR-2 ($N_z = 8$) exhibiting the contribution of (a) C-p and (b) F-p orbital. The Fermi level is set at 0 eV as shown by vertical dotted line. 17

5 The spin polarized electronic band structures ($N_z = 8$) for (a) Pristine (b) F-ZGNR-1 (c) F-ZGNR-2 (d) alt-1 and (e) alt-2 configurations. The Fermi level is set at 0 eV as shown by dotted horizontal line. The preserved degeneracy of spin up and spin down states is noticed in all ribbons except for ZGNR-1. 18

6 The spin polarized DOS for ribbons with $N_z = 8$ in (a) Pristine (b) F-ZGNR-1 (c) F-ZGNR-2 (d) alt-1 and (e) alt-2 configurations. The Fermi level is set at 0 eV as shown by vertical dotted line. 19

7 The Bloch functions of F-ZGNR-2 ($N_z = 8$) for highest valence band (HVB) and lowest conduction band (LCB) in (a) non magnetic state and (b) AFM state. The HVB-Up (LCB-Up) and HVB-Down (LCB-Down) represent the contributions of spin up and spin down electrons for HVB (LCB) respectively. 20

8 The schematic model of external electric field applied on F-ZGNR-2. The electric field exists in the plane of the ribbon and parallel to the Y axis while the periodicity of ribbon is maintained along Z axis. 21

9 The spin polarized electronic band structures for width $N_z = 8$ under the influence of external electric field for (a) Pristine (b) F-ZGNR-1 (c) F-ZGNR-2 (d) alt-1 and (e) alt-2 configurations. The Fermi level is set at 0 eV as shown by horizontal dotted line. 22

10 The spin polarized DOS for width $N_z = 8$ under the effect of external electric field in (a) Pristine (b) F-ZGNR-1 (c) F-ZGNR-2 (d) alt-1 and (e) alt-2 configurations. The Fermi level is set at 0 eV as shown by vertical dotted line. 23

ACCEPTED MANUSCRIPT

11 The variation of spin dependent band gap for gap narrowing (spin up) channel ($N_z = 8$) in various configurations as mentioned therein. 24
12 The variation of (a) critical electric field required to induce half-metallicity as a function of ribbon width and (b) band gaps for gap narrowing (spin up) and gap opening (spin down) electrons as a function of external electric field for F-ZGNR-2 with $N_z = 16$. 25

Accepted Manuscript

ACCEPTED MANUSCRIPT

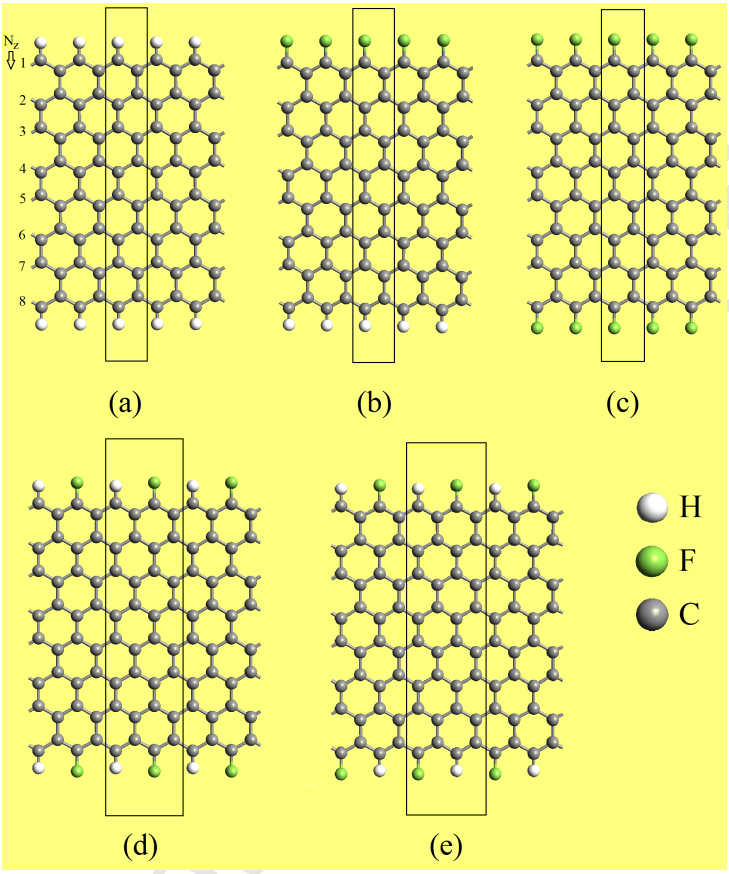

Figure 1: The schematics of defining ribbon width and the ball-stick models of considered F-ZGNR for (a) Pristine (b) F-ZGNR-1 (c) F-ZGNR-2 (d) alt-1 and (e) alt-2 configurations. Rectangles represent the supercell used. The white, grey and green spheres represent H, C and F atoms respectively.

ACCEPTED MANUSCRIPT

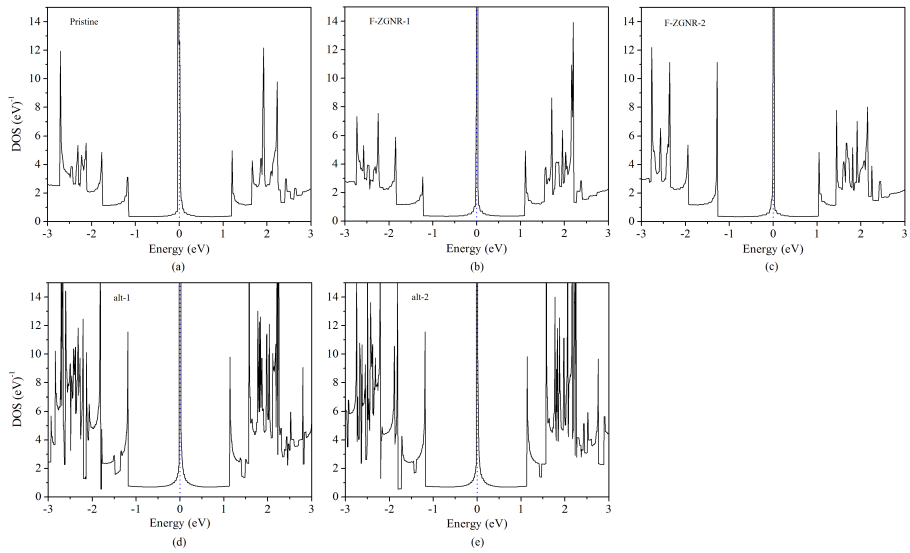

Figure 2: The spin compensated density of states (DOS) for ribbons of width $N_z = 8$ in (a) Pristine (b) F-ZGNR-1 (c) F-ZGNR-2 (d) alt-1 and (e) alt-2 configurations. The Fermi level is set at 0 eV as shown by dotted vertical line.

Accepted Manuscript

ACCEPTED MANUSCRIPT

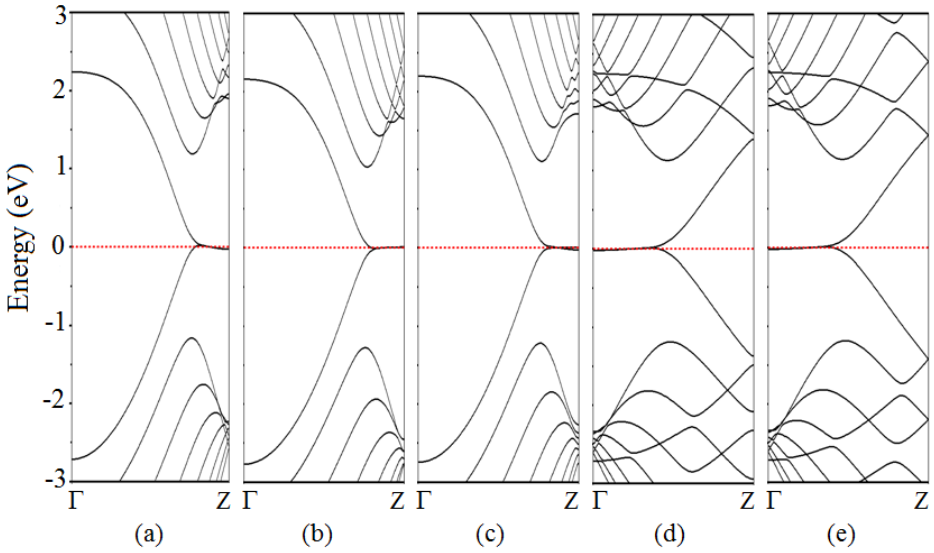

Figure 3: The spin compensated electronic band structures ($N_z = 8$) for (a) Pristine (b) F-ZGNR-1 (c) F-ZGNR-2 (d) alt-1 and (e) alt-2 configurations. The Fermi level is set at 0 eV as shown by dotted horizontal line.

Accepted Manuscript

ACCEPTED MANUSCRIPT

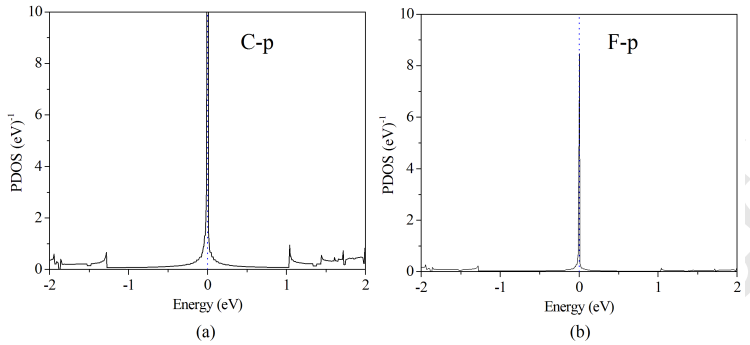

Figure 4: The partial density of states (PDOS) for F-ZGNR-2 ($N_z = 8$) exhibiting the contribution of (a) C-p and (b) F-p orbital. The Fermi level is set at 0 eV as shown by vertical dotted line.

Accepted Manuscript

ACCEPTED MANUSCRIPT

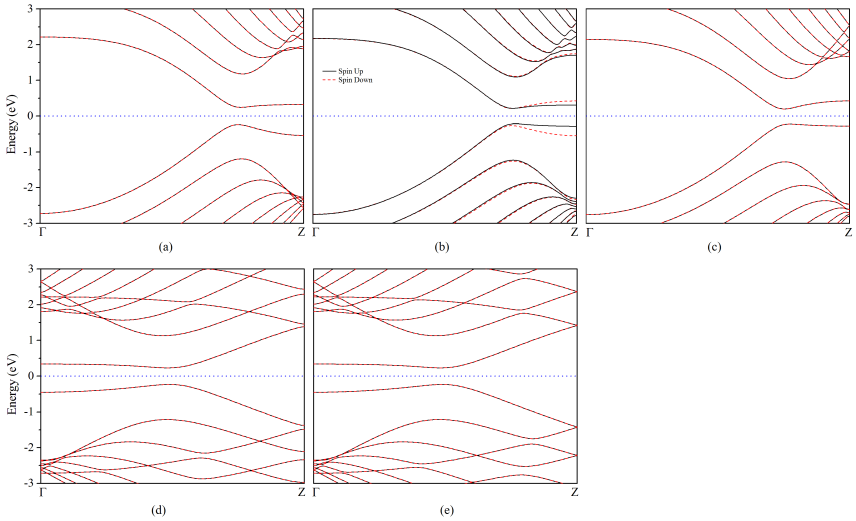

Figure 5: The spin polarized electronic band structures ($N_z = 8$) for (a) Pristine (b) F-ZGNR-1 (c) F-ZGNR-2 (d) alt-1 and (e) alt-2 configurations. The Fermi level is set at 0 eV as shown by dotted horizontal line. The preserved degeneracy of spin up and spin down states is noticed in all ribbons except for ZGNR-1.

Accepted Manuscript

ACCEPTED MANUSCRIPT

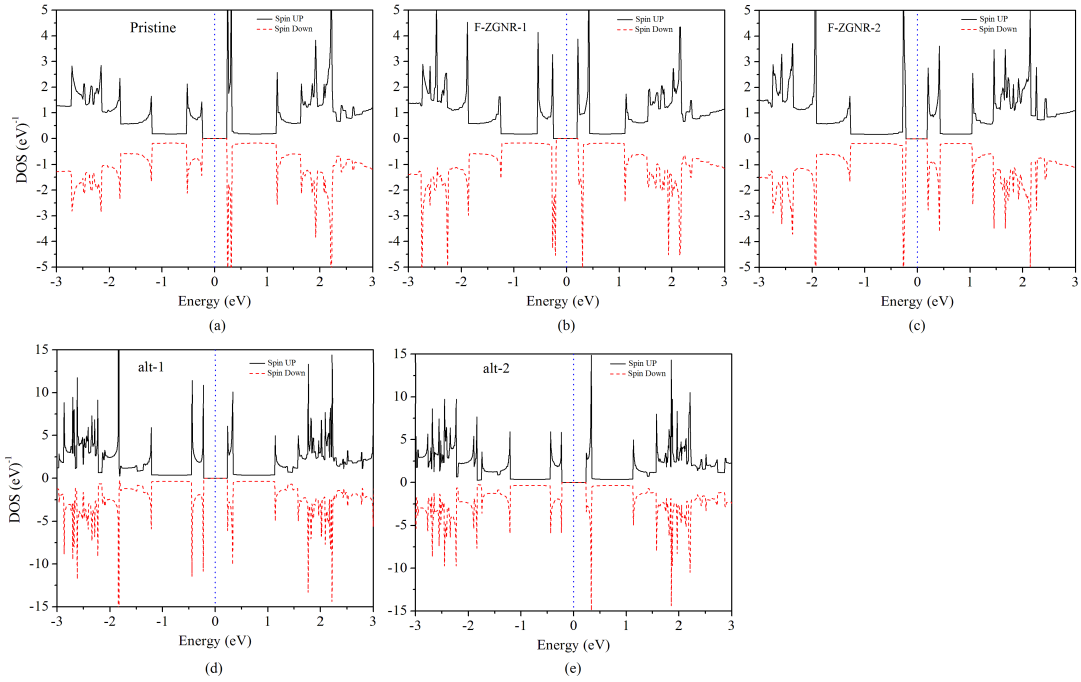

Figure 6: The spin polarized DOS for ribbons with $N_z = 8$ in (a) Pristine (b) F-ZGNR-1 (c) F-ZGNR-2 (d) alt-1 and (e) alt-2 configurations. The Fermi level is set at 0 eV as shown by vertical dotted line.

Accepted

ACCEPTED MANUSCRIPT

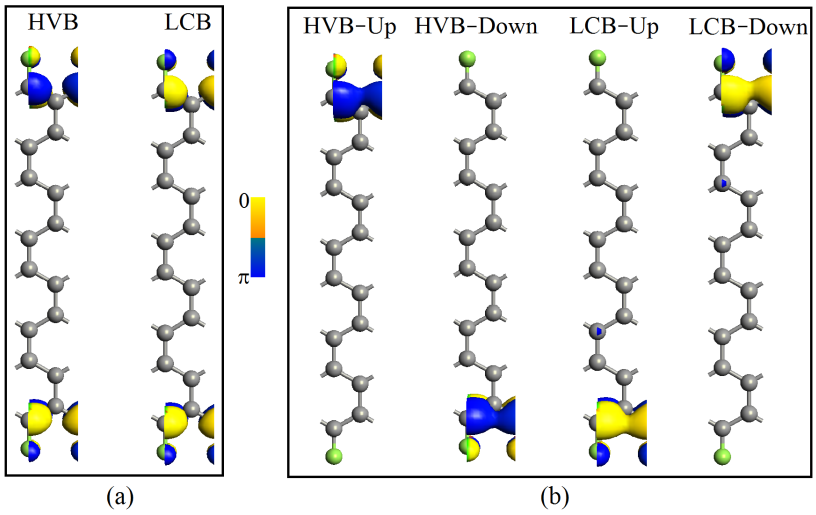

Figure 7: The Bloch functions of F-ZGNR-2 ($N_z = 8$) for highest valence band (HVB) and lowest conduction band (LCB) in (a) non magnetic state and (b) AFM state. The HVB-Up (LCB-Up) and HVB-Down (LCB-Down) represent the contributions of spin up and spin down electrons for HVB (LCB) respectively.

Accepted Manuscript

ACCEPTED MANUSCRIPT

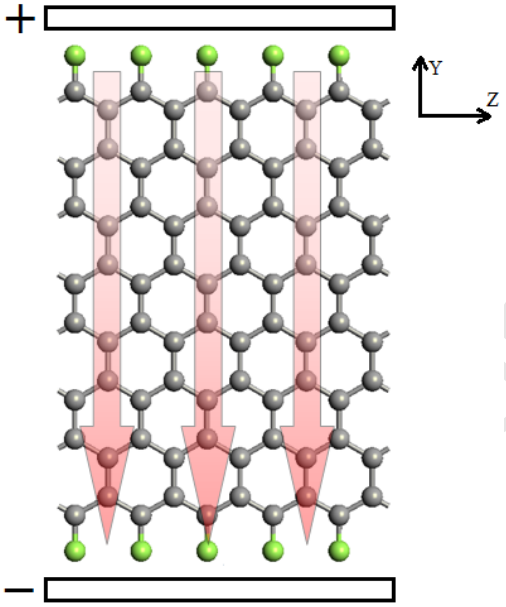

Figure 8: The schematic model of external electric field applied on F-ZGNR-2. The electric field exists in the plane of the ribbon and parallel to the Y axis while the periodicity of ribbon is maintained along Z axis.

Accepted Manuscript

ACCEPTED MANUSCRIPT

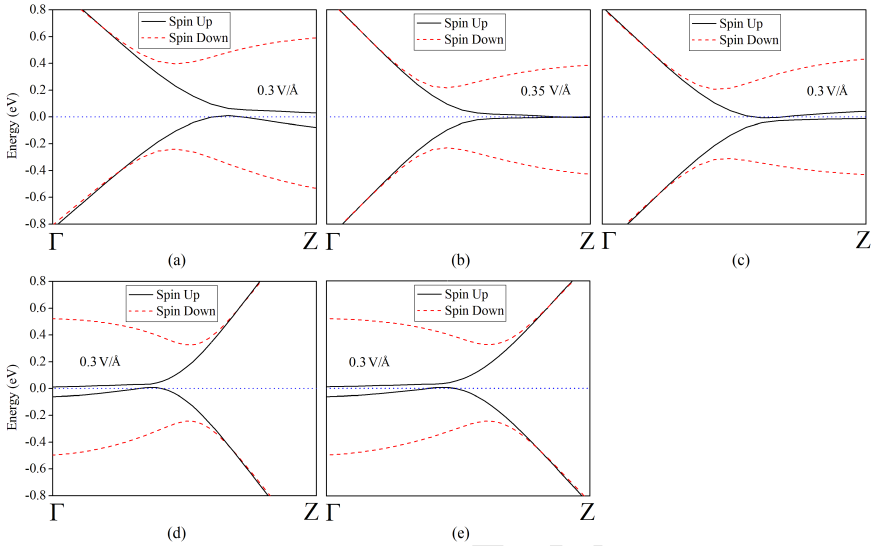

Figure 9: The spin polarized electronic band structures for width $N_z = 8$ under the influence of external electric field for (a) Pristine (b) F-ZGNR-1 (c) F-ZGNR-2 (d) alt-1 and (e) alt-2 configurations. The Fermi level is set at 0 eV as shown by horizontal dotted line.

Accepted Manuscript

ACCEPTED MANUSCRIPT

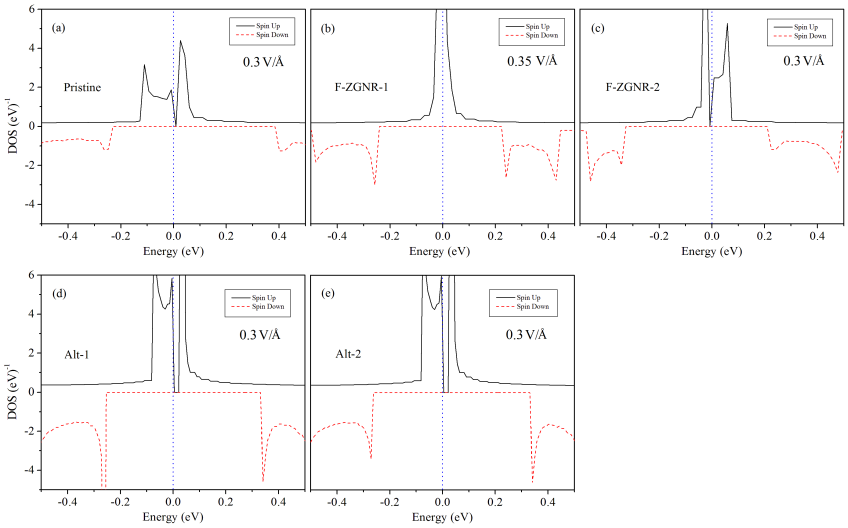

Figure 10: The spin polarized DOS for width $N_z = 8$ under the effect of external electric field in (a) Pristine (b) F-ZGNR-1 (c) F-ZGNR-2 (d) alt-1 and (e) alt-2 configurations. The Fermi level is set at 0 eV as shown by vertical dotted line.

Accepted Manuscript

ACCEPTED MANUSCRIPT

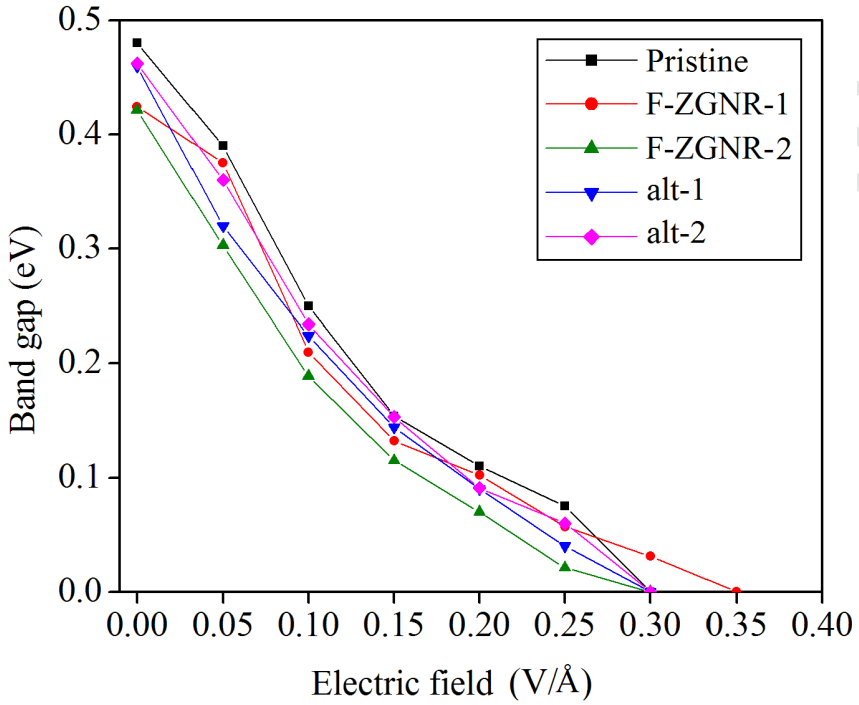

Figure 11: The variation of spin dependent band gap for gap narrowing (spin up) channel ($N_z = 8$) in various configurations as mentioned therein.

Accepted Manuscript

ACCEPTED MANUSCRIPT

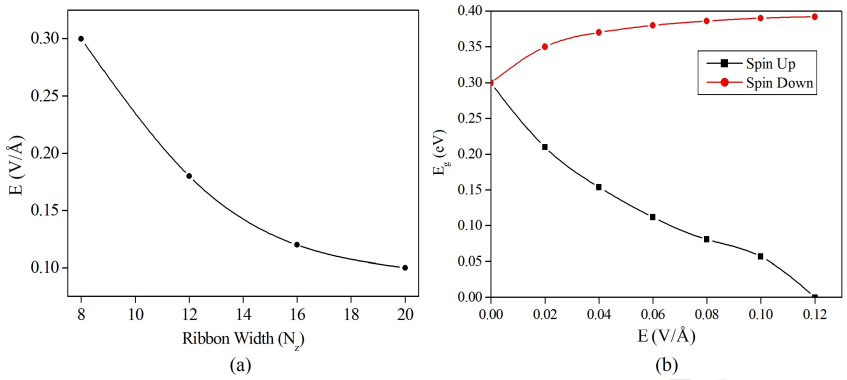

Figure 12: The variation of (a) critical electric field required to induce half-metallicity as a function of ribbon width and (b) band gaps for gap narrowing (spin up) and gap opening (spin down) electrons as a function of external electric field for F-ZGNR-2 with $N_z = 16$.

Accepted Manuscript

ACCEPTED MANUSCRIPT

Graphical Abstract

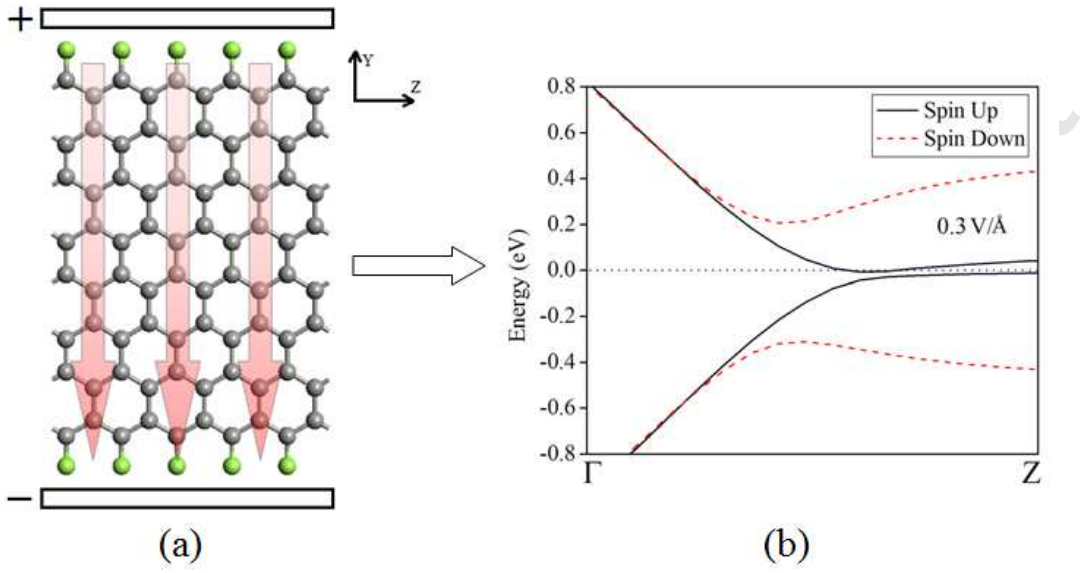

Fig.: (a) Both edges Fluorine passivated ZGNR under the external electric field and (b) induced half metallicity in the corresponding band structure at 0.3 V/Å.

Research Highlights

- F passivated zigzag graphene nanoribbon (F-ZGNR) are more favorable than pristine ones.
- External electric field induces half metallicity in F-ZGNR.
- The observed half metallicity is independent of ribbon widths.
- Enhanced stability makes F-ZGNR preferable over pristine ribbon.

Accepted Manuscript

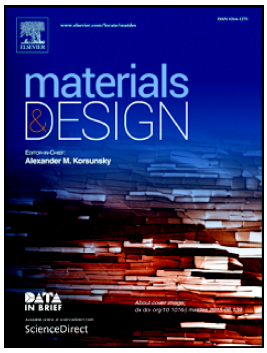

Influence of 100MeV Au+8 ion on photovoltaic response of BiFeO3/BaTiO3 multilayer structures

Savita Sharma, Monika Tomar, Ashok Kumar, Fouran Singh, Nitin K. Puri, Vinay Gupta

PII: S0264-1275(16)31398-3
DOI: doi: 10.1016/j.matdes.2016.11.011
Reference: JMADE 2447

To appear in: *Materials & Design*

Received date: 22 July 2016
Revised date: 2 November 2016
Accepted date: 3 November 2016

Please cite this article as: Savita Sharma, Monika Tomar, Ashok Kumar, Fouran Singh, Nitin K. Puri, Vinay Gupta , Influence of 100MeV Au+8 ion on photovoltaic response of BiFeO3/BaTiO3 multilayer structures. The address for the corresponding author was captured as affiliation for all authors. Please check if appropriate. Jmade(2016), doi: 10.1016/j.matdes.2016.11.011

This is a PDF file of an unedited manuscript that has been accepted for publication. As a service to our customers we are providing this early version of the manuscript. The manuscript will undergo copyediting, typesetting, and review of the resulting proof before it is published in its final form. Please note that during the production process errors may be discovered which could affect the content, and all legal disclaimers that apply to the journal pertain.

ACCEPTED MANUSCRIPT

Influence of 100 MeV Au^{+8} ion on photovoltaic response of $BiFeO_3/BaTiO_3$ multilayer structures

Savita Sharma[1,4], Monika Tomar[2], Ashok Kumar[5] , Fouran Singh[3], Nitin K. Puri[4] and Vinay Gupta[1*]

[1]Department of Physics and Astrophysics, University of Delhi, Delhi-110007, INDIA,

[2]Physics Department, Miranda House, University of Delhi, Delhi-110007, INDIA,

[3]Inter University Accelerator Centre, Aruna Asaf Ali Marg, New Delhi-110067, INDIA,

[4]Department of Applied Physics, Delhi Technological University, Delhi-110042, INDIA

[5]CSIR-National Physical Laboratory, Dr. K.S .Krishnan Marg, Delhi, INDIA

ACCEPTED MANUSCRIPT

ACCEPTED MANUSCRIPT

Abstract

This work presents the swift heavy ion (SHI) irradiation induced possible modifications in structural strain and surface morphology of ($BiFeO_3$)BFO/($BaTiO_3$)BTO multilayer structures prepared by chemical solution deposition technique. Furthermore, the role of structural defects (induced due to irradiation) on the ferroelectric property and photovoltaic response of BFO/BTO multilayer structures having different number of layers has been studied. Significant modifications in the morphological and ferroelectric properties of BFO/BTO (two, four and six layers) multilayer structures due to induced structural defects were observed after SHI irradiation performed using 100 MeV Au^{+8} ion with ion fluence of ~ 1×10^{12}, $1x10^{13}$ and 3×10^{13} ions/cm^2. Ferroelectric photovoltaic response decreases with increase in ion fluence from $1x10^{12}$ to $1x10^{13}$ ions/cm^2 along with change in open circuit voltage from 0.41 V to 0.23 V, short circuit current density from 5.177 μA/cm^2 to 1.71 μA/cm^2 and I_{on}/I_{off} ratio from 33.02 to 13.02. This study on effect of SHI irradiation on multilayer ferroelectric photovoltaic cell is important to understand the possible application of BFO/BTO multilayer photovoltaic cells in the regions susceptible to radiations. Furthermore, the study of perovskite solar cell performance in the presence of SHI radiation, is essentially required for the development of durable solar energy harvesters.

Keywords : Irradiation, photovoltaic, fluence, ferroelectric.

ACCEPTED MANUSCRIPT

1. Introduction

Energetic ion beams play a significant role in modifying the properties of materials [1-3]. The change in material properties strongly depend on the ion energy, fluence and ion species. Low energy ions having energy up to a few hundred keV available from ion implanters are mainly used in semiconductors for modification of surface and interface and hence the functional properties. The ion beams interact with material in the form of elastic and inelastic scattering of the particles resulting in the excitation and ionization of the atoms. However, it may also trigger a nuclear reaction leading to a disturbance in the structure of matter, which is referred to as radiation damage. The ions entering into a solid having velocity similar to the Bohr velocity of electron (2.18×10^8 m/s), lose their energy while passing through the material either by (a) displacing atoms (of the sample) by elastic collisions where energy transfer takes place directly to target atoms, which is called as the nuclear stopping or nuclear energy loss or (b) exciting the atoms by inelastic collisions between the incoming ions and electrons of the target atoms, which is known as electronic stopping or electronic energy loss [4]. The nuclear energy loss (S_n) is significant at low energies, whereas electronic energy loss (S_e) is dominant at high energies. The heavy ions with very high energies, generally in the range of a few tens of Mega electron volts (MeV) to Giga electron volts (GeV) where the electronic energy loss (S_e) dominates, are called as the swift heavy ions (SHI). SHI generated

ACCEPTED MANUSCRIPT

electronic excitation not only results in the displacement of the lattice atoms, but may also lead to various structural defects [4]. SHI also plays a major role in synthesis and material modification. The passage of SHI involves very rapidly developing processes, which are difficult to observe during or immediately after their occurrence. Hence, a number of modifications can occur in the material including creation of defects, defect annealing, amorphization, crystallization, crystalline-to-crystalline phase transition etc. This is due to the fast energy transfer during the electronic excitation confined to a narrow cylindrical region along the path of the heavy ion beam [5].

Extensive research is in progress for the last two decades, adhering to the SHI induced changes in structural and physical properties of magnetic insulators like ferrites [6-7]. Enormous radiations like low energy ions, high energy ions, fast neutrons etc. are capable of inducing certain crystallographic and magnetic changes in bulk ferrite samples such as spinels, garnets and hexa-ferrites [8-10]. There are reports on the study of material modifications related to surface properties of manganite films and interface behavior due to SHI irradiation. The reports give an insight for better understanding of the localized strain in the films and creation of controlled defects in the lattice [11-14]. Majority of the reports showed that SHI irradiation deteriorates the transport properties and crystallinity of manganite films [12-15]. Considerable efforts have been made to study the effect of SHI irradiation on the property of PLD-grown

ACCEPTED MANUSCRIPT

manganite films, however, limited work is reported on its effect on the multiferroic thin films and their photovoltaic applications [12-14,16]. Therefore, an attempt has been made towards the establishment of BFO/BTO multilayer structure as a renewable source of energy in space where normal detectors are vulnerable to exposure of energetic ions. Significance of the present work is the sustenance of Photovoltaic properties of the prepared multilayer structures post ion beam irradiation.

Based on the reported literature, the effect of SHI irradiation on the structural, electrical and ferroelectric properties of CSD grown BFO/BTO multilayer structures has been studied in the present work. The selection of highly energetic 100 MeV Au^{+8} ions was made by varying the fluence from $1x10^{12}$ to $3x10^{13}$ ions/cm^2, and the results are presented in the following sections.

2. Experimental details

BFO/BTO multilayer structures having 2, 4 and 6 alternating layers of BTO and BFO, were deposited onto Pt/Ti coated passivated silicon (Pt/Si) substrates by CSD technique (Deposition details as described in previous reports) [17]. The total thickness of the BFO/BTO structure was maintained as 350 nm and thickness of the individual layer was approximately 175 nm, 88 nm and 60 nm for 2, 4 and 6 layer BFO/BTO structures respectively . All BFO/BTO multilayer samples, of size,

ACCEPTED MANUSCRIPT

$2\times1cm^2$, were irradiated with 100 MeV Ag^{+8} ions with varying fluence of 1×10^{12}, 1×10^{13} and 3×10^{13} ions/cm^2, using 15 UD Tandem Accelerator facility at Inter University Accelerator Centre (IUAC), New Delhi. The experimental parameters used for irradiation of samples have been tabulated in Table 1. Ion beam was focused onto a spot of ~ 1mm diameter and was continuously scanned over the complete area of the film using a magnetic scanner, to ensure uniform irradiation. Irradiation was performed at low angle with respect to the ion beam direction, to avoid channeling effect.

The electronic energy loss (S_e) and nuclear energy loss (S_n) for BFO and BTO thin films have been calculated using Stopping and Range of Ions in Matter (SRIM) simulation program [18]. The projectile range of 100 MeV Ag^{+8} ions (ion fluencies ~ 1×10^{12} , 1×10^{13} and 3×10^{13} ions/cm^2) has also been calculated. The calculated values of S_e, S_n and projectile range have been tabulated in Table 2. The calculated value of projectile range was found to be very large as compared to the thicknesses of thin film/multilayer samples (15-20 μm), ensuring that all the ions striking the sample, completely pass through thin film. According to thermal spike model, highly energetic ions, on passing through a thin multilayer multiferroic sample, deposit their energy on to the material resulting in large electronic excitation, and are expected to modify the properties of irradiated samples [19].

ACCEPTED MANUSCRIPT

Structural and microstructural properties of the pristine and irradiated BFO/BTO multilayer samples were studied using XRD (θ-2θ) and atomic force microscopy (AFM) measurements respectively. Optical properties were studied by UV-Visible spectrophotometer (Make: Perkin Elmer, Model: Lambda 35) in 1100 to 190 nm range of wavelength. For electrical measurement, Au circular top electrodes (200 μm diameter) were deposited on to surface of sample using magnetron sputtering technique. P-E hysteresis loop measurements were carried out using Radiant technologies precession ferroelectric loop tracer. Ferroelectric-Photovoltaic (FE-PV) measurements have been carried out using Keithley 4200 semiconductor characterization unit.

3. Results and discussion

3.1 Structural studies: X-ray diffraction (XRD)

The important properties of the ferroelectric materials are determined by their structure. The crystal symmetry and related strains of these materials have a strong influence on their switching behavior. The structural studies help in establishing a relation between the crystallographic symmetry and ferroelectric switching capability of a material, which in turn plays an important role in its ferroelectric photovoltaic response. Therefore in the following section structural properties of BFO/BTO multilayer structures have been studied in detail.

TED MANUSCRIPT

ACCEPTED MANUSCRIPT

Figures 1 (a), (b) and (c) show the XRD patterns of irradiated BFO/BTO multilayer structures having 2, 4 and 6 layers, respectively. XRD patterns obtained for the as prepared pristine BFO/BTO multilayer structures having 2, 4 and 6 layers are also included in the figures for comparison. XRD patterns of the irradiated BFO/BTO multilayer samples show (110) oriented growth of the BTO thin film (Figure 1). No significant change in the crystalline structure of BFO/BTO multilayer was observed after Au^{8+} irradiation with different fluence (Figure 1). However, the appearance of new XRD peaks (broad and low intensity) at all fluences (1×10^{12} and 1×10^{13} and 3×10^{13} ions cm^{-2}*)* indicates the formation of some impurity phase (related to $Bi_2Fe_4O_9$) in the BFO/BTO multilayer structures (Figure 1). It has been reported that $BiFeO_3$ is unstable at high temperatures and rapidly decomposes into parasitic phases like $Bi_2Fe_4O_9$ or Fe_2O_3 [20].The formation of $Bi_2Fe_4O_9$ secondary phase in the present case for irradiated BFO/BTO multilayer samples may be due to the increased temperature in the material medium during the passage of 100 MeV Ag^{+8} ions. The obtained result, thus, supports the applicability of "Thermal spike model" of ion-matter interaction for prepared BFO/BTO samples.

The (110) peak shows a shift towards the lower angle at a fluence of $1x10^{13}$ ions/cm^2 for all prepared samples, (Figure 1) depicting the introduction of strain as a result of irradiation. At highest fluence of $3x10^{13}$ ions/cm^2, (110) peak shifts towards the higher angle showing relaxation of strain. The values of lattice parameters (a, c), c/a

ACCEPTED MANUSCRIPT

distortion ratio and strain induced along 'c' axis at varying fluences for all prepared multilayer structures having 2, 4 and 6 layers are summarized in Table 3, 4 and 5 respectively. The stress modulus in the BFO/BTO multilayer structures is obtained using equation: stress = $|(c_o-c)|/c_o$ in %, where "c" is the respective lattice constant of BFO or BTO in deposited multilayer film and "c_o" is the corresponding bulk value. Values of crystallite size along the dominant plane, calculated from the Debye Scherrer formula [21] for all the films are tabulated in Table 6. The crystallite size for all the multilayers is seen to be decreasing with increasing the fluence of SHI (Table 6).

The variation in c/a distortion ratio in both BFO and BTO thin films in the pristine and irradiated (a) two layer (b) four layer and (c) six layer multilayer structures as a function of fluence from $1x10^{12}$ to $3x10^{13}$ ions/cm^2 shows an oscillating behavior with consecutive depositions of BTO and BFO layers. The large lattice distortion observed for multilayer structure at lowest fluence $1x10^{12}$ ions/cm^2 is expected to result in improved ferroelectric property than at higher fluences and hence in corresponding ferroelectric photovoltaic response.

ACCEPTED MANUSCRIPT

3.2 Surface morphology : Atomic force microscopy (AFM)

The surface morphology and grain size play an important role in defining the electrical properties of oxide thin films, thus it is necessary to systematically study the effect of irradiation on the surface morphology and grain size of the BFO/BTO multilayer structures.

Modifications in the surface morphology were observed using AFM (2D) images of different multilayer (2, 4 and 6 layers) BFO/BTO structures before and after irradiation, respectively with various ion fluences ($1x10^{12}$, $1x10^{13}$ and $3x10^{13}$ ions/cm^2) are shown in Figure 2 (a), (b) and (c). Particle fragmentation and agglomeration into bigger grains occurs with the increase in fluence from 1×10^{12} to 3×10^{13} ions/cm^2. With increase in fluence, the spread of energy lost by the SHI is relatively large, thus promotes bigger grain growth.

It may be seen from the AFM images (Figures 2 (a), (b) and (c)) that the small sized crystallites coalesce with increase in ion fluence in all the samples making bigger globular structures. Values of root mean square (rms) surface roughness (RSR) increase with ion fluence and are listed in Table 6.

ACCEPTED MANUSCRIPT

3.3 Optical studies: UV visible spectroscopy

UV visible spectroscopy is an efficient technique to determine the optical properties of any sample which includes film thickness, refractive index, band gap, color and the reflectance properties in general. Here, the band gap of the pristine and irradiated BFO/BTO multilayer structures have been calculated to check the application of BFO/BTO multilayer structures towards photovoltaic effect in visible region. Also, the effect of ion beam irradiation on the optical properties of prepared samples have been examined.

Figure 3 (a, b and c) shows the effect of the increasing fluence of irradiation on the optical transmission of BFO/BTO multilayer structures. The average transmittance is seen to be decreasing in the visible region with increase in fluence for all the prepared (2, 4 and 6 layers) BFO/BTO multilayer structures (Figures 3 (a), (b) and (c)). Pristine sample of 2 layer BFO/BTO structure had 65% transmittance in the visible region, which decreased upto 59% upon ion irradiation at a fluence of $3x10^{13}$ ions/cm^2 (Figure 3 (a)). The decrease in transmittance of BFO/BTO multilayer structures after irradiation may be due to increased optical scattering caused by increase in the surface roughness of film as demonstrated by the AFM images (Figure 2).

It can be observed clearly from Figure 3 that the band edge shifted towards the higher wavelength upon ion irradiation with increase in ion fluence, in all the

ACCEPTED MANUSCRIPT

BFO/BTO multilayer structures. Shift towards the higher wavelength is due to the formation of defect states producing localized states near the band edges in the forbidden gap. This modification is attributed to the simultaneous lowering of the conduction band edge and uplifting of the valence band edge due to induced defects in the material, post ion irradiation. The Transmittance in the visible region and effect of ion fluencies on pristine and irradiated BFO/BTO multilayer structures have been listed in Table 7.

3.4 Ferroelectric (P - E loop)

For understanding the ferroelectric behavior of pristine and irradiated BFO/BTO multilayer films, room temperature P – E hysteresis loops for 2, 4 and 6 layered structures were obtained at 1 kHz frequency, and are shown in Figures 5 (a), (b) and (c) respectively. All multilayer structures show well defined and saturated PE hysteresis loops without ion irradiation. It can be seen that, all the BFO/BTO multilayer samples exhibit stable P - E loops at low ion fluence upto $1x10^{13}$ ions/cm^2, whereas, for higher fluence ($3x10^{13}$ ions/cm^2), the leakage current increases. The polarization decreases with increase in ion fluence in all the multilayer structures (Figure 5 (a) to (c)).

The degradation in hysteresis loops may be correlated with the formation of oxygen vacancies in the multilayer sample due to ion irradiation, resulting in enhanced

ACCEPTED MANUSCRIPT

conductivity. The increase in defects upon ion irradiation can be seen from the large value of rms roughness along with the onset of impurity phases (from XRD analysis) in the BFO/BTO multilayer structure. The $3x10^{13}$ ions/cm^2 irradiated samples exhibit negligible polarization and lossy PE hysteresis loops; or in other words, the ferroelectric property of a material is highly compromised (Figure 5). For ion beam with high fluence, the passage of highly energetic ions for longer duration creates more defects in the multilayer sample, which increases the leakage current. Values of saturation polarization and remnant polarization for all the multilayer structures before and after irradiation are included in Table 8. The values of P_s obtained for irradiated BFO/BTO multilayer structures are comparatively lower than those reported for BFO films grown on highly conducting Pt/Ti/SiO_2/Si and other substrates [22-25]. A decrease in the value of saturation and remnant polarization has been observed for all multilayer samples upon ion irradiation with increasing fluence.

Hence, it may be inferred that the ion irradiation degrades the ferroelectric properties of the BFO/BTO multilayer structures and at fluence of the order of $3x10^{13}$ ions/cm^2, the multilayer structure completely loses its ferroelectric behavior. Furthermore, amongst all the multilayer structures prepared, the 6 layered BFO/BTO structure exhibits maximum polarization, which is least

ACCEPTED MANUSCRIPT

degraded even after ion irradiation, i.e. the ferroelectric properties of 6 layer structure are superior to 2 and 4 layered systems, both before and after irradiation (Table 8). Hence, for studying the ferroelectric photovoltaic response, 6 layered structures irradiated with SHI of $1x10^{12}$ and $1x10^{13}$ ions/cm^2 fluence have been used. The results are discussed in the subsequent sections.

3.5 Photovoltaic studies

The photovoltaic (PV) measurements of 6-layered BFO/BTO multilayer structures irradiated at $1x10^{12}$ and $1x10^{13}$ ions/cm^2 fluence were studied in MFM configuration with Au circular dots (200 μm diameter and 40 nm thin) as the top electrodes. Figure 5 (a) represents the fluence dependent J-V plots of six layered BFO/BTO pristine structure and irradiated structures, measured at room temperature under dark conditions. Figure 5 (b) shows the corresponding plots of *J* versus *V* under illumination conditions (λ = 405 nm). It can be noted that the dark current (J_{dark}) increases significantly from 6 nA/cm^2 to 1.12 μA/cm^2 even after irradiation. However, it may be seen from Figure 5 (b), that both the irradiated samples show degraded photovoltaic response with low value of open circuit voltage and short circuit current.

ACCEPTED MANUSCRIPT

Photovoltaic response characteristics of six-layered pristine and irradiated BFO/BTO structures at zero bias have been tabulated in Table 9. The dark current (J_{dark}) was found to increase significantly after irradiation and increases further with increase in fluence from $1x10^{12}$ to $1x10^{13}$ ions/cm^2 as shown in Figure 5 (a). The short circuit photocurrent density, J_{sc}, was found to decrease with increase in fluence from $1x10^{12}$ to $1x10^{13}$ ions/cm^2 in the six layer BTO/BTO structure (Figure 5 (b)). The value of open circuit photo voltage, V_{oc}, is also found to decrease from 0.41 V to 0.23 V with increasing fluence. The observed results indicate that after irradiation, ferroelectric-photovoltaic response of multilayer PV cell degraded. The decrease in FE-PV response with increase in fluence from $1x10^{12}$ to $1x10^{13}$ ions/cm^2 is in accordance with the ferroelectric PE hysteresis loops obtained in previous section for the six layer BFO/BTO structure (Figure 4). It may be recalled that, simultaneous increase in dark current (J_{dark}) (Figure 5 (a)) and decrease in photocurrent (J_{sc}) results in poor $J_{on/off}$ ratio (13.02) (Table 9) of the BFO/BTO irradiated samples as compared to pristine sample (2.955×10^3). It is important to point out that with increase in fluence up to $3x10^{13}$ ions/cm^2, ferroelectric loops (Figure 4) become completely lossy and therefore no significant ferroelectric-photovoltaic response was obtained in the corresponding six layered BFO/BTO sample. Figure 5 (c) shows the repeatability of experiments measuring photocurrent density for BFO/BTO six layer identical samples at different ion beam fluence. Sixteen identical samples (6

ACCEPTED MANUSCRIPT

layers BFO/BTO thin film structure) were prepared for irradiation. Each batch constituted of 4 identical samples irradiated with same fluence. The photovoltaic response of each sample was studied to ensure repeatability of data. The variation in photocurrent density is found to be less than ± 5% at each fluence.

Time-dependent variation of photocurrent density (*J*) for Au^{+8} irradiated BFO/BTO multilayer structures at $1x10^{12}$ and $1x10^{13}$ ions/cm^2 fluences with repeated exposure to light are shown in Figures 6 (a). For comparison, time-dependent variation of photocurrent density (*J*) for pristine BFO/BTO six layer structure is shown in Figure 6 (b). Both irradiated samples show increase in the photo current density under illumination of violet laser light (405 nm) of intensity 160 $mWcm^{-2}$ on the sample surface with respect to the dark current (Figure 6 (a)). But it can be seen clearly from Figure 6 (a), that with increase in Au^{+8} ion fluence from $1x10^{12}$ to $1x10^{13}$ ions/cm^2 the photocurrent density decreases from 5.17 $\mu A/cm^2$ to 1.71 $\mu A/cm^2$, owing to the increased defects and degraded ferroelectric properties, as discussed earlier. Furthermore, the obtained photo-response is not well saturated under light illumination (Figure 6 (a)) which is also related to the degraded ferroelectric properties of the BFO/BTO multilayer structure post ion irradiation.

The current study is dedicated towards the establishment of BFO/BTO multilayer structure as a renewable source of energy in space where normal detectors are vulnerable to exposure of energetic ions. The present report is also a holistic study

ACCEPTED MANUSCRIPT

of Ferroelectric Photovoltaic sensors and transducers when subjected to adverse conditions (fusion/fission reactors). Most important aspect of the present work is the sustenance of Photovoltaic properties of the prepared multilayer structures post ion beam irradiation. The obtained response in irradiated structures is superior to those reported by other workers for bare thin film Photovoltaic sensors [26-27]. Thus, the present work is encouraging for the application of BFO/BTO multilayer Photovoltaic sensors in areas susceptible to energetic radiations.

4. Conclusions

Significant modifications in the morphological and ferroelectric properties of BFO/BTO (two, four and six layers) multilayer structures due to induced structural defects were observed after SHI irradiation performed using 100 MeV Au^{+8} ion with ion fluence of ~ 1×10^{12}, $1x10^{13}$ and 3×10^{13} ions/cm^2. XRD studies confirm a continuous decrease in crystallite size with increase in fluence from $1x10^{12}$ to $3x10^{13}$ ions/cm^2 for all prepared BFO/BTO multilayer structures. Microstructural investigations using AFM, shows formation of agglomerated globular grain morphology in BFO/BTO structures after irradiation. Depending on ion fluences and number of layers in multilayer structures, defects are created and fragmentation and agglomeration effect is observed which results in decrease in grain size and increase in surface roughness.

ACCEPTED MANUSCRIPT

All multilayer BFO/BTO structures after irradiation exhibit degradation in ferroelectric behaviour with increase in ion fluence and at a fluence of $3x10^{13}$ ions/cm^2, ferroelectricity diminished, giving completely lossy P-E loops. Further, ferroelectric-photovoltaic effect have been studied in six layered BFO/BTO multilayer structure irradiated at different fluences. Ferroelectric photovoltaic response also degraded with increase in ion fluence from $1x10^{12}$ to $1x10^{13}$ ions/cm^2 with decrease in open circuit voltage from 0.41 V to 0.23 V, short circuit current density from 5.177 μA/cm^2 to 1.71 μA/cm^2 and I_{on}/I_{off} ratio from 33.02 to 13.02. This irradiation of BFO/BTO multilayer PV cell degraded the PV response due to overall poor ferroelectric property in comparison to the pristine multilayer sample. The study of the effect of SHI irradiation on multilayer ferroelectric photovoltaic cell is important to understand the possibility of application of photovoltaic cell in regions susceptible to high radiation. Hence, it is essentially required to study the effect of SHI irradiation on multilayered BFO/BTO structure for photovoltaic applications. Further, irradiation studies on similar multilayer structures and PV devices will help in engineering the properties of pervoskite materials for other device applications.

ACCEPTED MANUSCRIPT

ACKNOWLEDGMENTS

The authors are thankful to the pelletron group of IUAC, New Delhi for providing good quality scanned beam during irradiation. Authors are also thankful to Nanoscale Research Facility (NRF) for providing AFM facility at Indian Institute of Technology (IIT), New Delhi. The authors wish to thank the University of Delhi for financial support along with providing XRD facility and one of the authors (SS) is thankful to Delhi Technological University (DTU) for teaching assistantship.

ACCEPTED MANUSCRIPT

ACCEPTED MANUSCRIPT

References

1. A. M. Vredenberg, A. Polman, P. A. Stolk, E. Snolesand, L. M. Brongersma, Proceedings of 11th International Conference on Ion Beam Modification of Materials Amsterdam, North Holland, Amsterdam, (1998).
2. S. Klaumuenzer, N. Stolterfoht, Proceedings of the International Conference on Swift Heavy Ions in Matter, North Holland, Berlin, May (1998).
3. D. K. Avasthi, D. Kanjilal, Proceedings of the International Conference on Swift Heavy Ions in Materials Engineering and Characterization, New Delhi, North Holland, Amsterdam, October (1998).
4. D. Kanjilal, Swift heavy ion-induced modification and track formation in materials Current Science, 80 (2001) 12.
5. P. Mohanty, V. P. Singh, N. C. Mishra, S. Ojha, D. Kanjilal, C. Rath, Evolution of structural and magnetic properties of Co-doped TiO2 thin films irradiated with 100 MeV Ag7+ ions, J. Physics D: Applied Physics, 47 (2014) 315001.
6. S. Ghosh, S. A. Khan, V. Ganesan, S. Kundu, R. Bhattacharya, Study of 200MeV Ag^{15+} ion induced amorphisation in nickel ferrite thin films, Nuclear Instruments and Methods in Physics Research B, 244 (2006) 34–39.
7. S. R. Shinde, A. Bhagwat, S. I. Patil, S. B. Ogale, G. K. Mehta, M. K. Singh, R. S. Katiyar, Phonon anomalies near the magnetic phase transitions in

ACCEPTED MANUSCRIPT

$BiFeO_3$ thin films with rhombohedral R_{3c} symmetry, J. Appl. Phys., 109 (2011) 07D916.

8. F. Studer, A. Meftah, F. Brisard, J. M. Costantini, M. Hage-Ali, J. P. Stoquert, M. Toulemonde, Swift heavy ions in magnetic insulators: A damage-cross-section velocity effect, Physical Review B, 48 (1993) 920.
9. S. Kumar, R. S. Chauhan, S. A. Khan, W. Bolse, D. K. Avasthi, Nuclear Instruments and Methods in Physics Research Section B: Beam Interactions with Materials and Atoms, 244 (2006) 194-197.
10. R. Kumar, S. K. Sharma, A. Dogra, V. V. Siva Kumar, S. N. Dolia, A. Gupta, M. Knobel, M. Singh, Magnetic Study of Nanocrystalline Ferrites and the Effect of Swift Heavy Ion Irradiation, Hyperfine interactions, 160 (2005) 143-156.
11. R. N. Parmar, J. H. Markna, D. G. Kuberkar, R. Kumar, D. S. Rana, C. Bagve, S. K. Vivas, Swift-heavy-ion-irradiation-induced enhancement in electrical conductivity of chemical solution deposited $La_{0.7}Ba_{0.3}MnO_3$ thin films, Appl. Phys. Lett., 89 (2006)1–3 202506.
12. S. B. Ogale, K. Ghosh, G. Y. Gu and G. K. Mehta, Influence of 90 MeV oxygen ion induced disorder on the magnetotransport in epitaxial $La_{0.7}Ca_{0.3}MnO_3$ thin films, J. Appl. Phys., 84(11) (1998) 6255 - 6261.

ACCEPTED MANUSCRIPT

13. J. Y. Lee, Sk.F. Ahmed, M. H. Park, S. k. Ha, J. K. Park, J. H. Yun, S. J. Ahn, K. R. Lee, W. J. Choi, M. W. Moon, C. W. Yang, Self-assembled Cu(In,Ga)Se_2 nanocrystals formed by Ar ion beam irradiation, Solar Energy Mater. & Solar Cells, 105 (2012) 119–124.

14. R. Sathyamoorthy, S. Chandramohan, P. Sudhagar, D. Kanjilal, D. Kabiraj, K. Asokan, K. P. Vijayakumar, Effect of 80 MeV oxygen ion beam irradiation on the properties of CdTe thin films, J. Mater. Sci., 42 (2007) 6982–6988.

15. B. L. Belevtsev, V. B. Krasovitsky, V. V. Bobkov, D. G. Naugle, K. D. D. Rathnayaka, A. Parasiris, Influence of high-energy electron irradiation on the transport properties of $La_{1-x}Ca_xMnO_3$ films (x≈1/3), Eur. Phys. J. B, 15 (2000) 461–468

16. J. H. Markna, R. N. Parmar, D. G. Kuberkar, R. Kumar, D. S. Rana, S. K. Malik, Thickness dependent swift heavy ion irradiation effects on electronic transport of $La_{0.5}Pr_{0.2}Ba_{0.}MnO_3$ thin films**,** Appl. Phys. Lett., 88 (2006) 1–3 152503.

17. S. Sharma, M. Tomar, A. Kumar, N. K. Puri and V. Gupta, Energy harvesting and systems, **(**2016) DOI: 10.1515/ehs-2016-0001.

18. F. Ziegler, J. P. Biersack, M. D. Ziegler, Program SRIM, 2008.

ACCEPTED MANUSCRIPT

19. M. Toulemonde, Swift heavy ions in magnetic insulators: A damage-cross-section velocity effect Swift heavy ions in magnetic insulators: A damage-cross-section velocity effect, Physical Review B, 48 (1993) 920.

20. G. Catalan, J. F. Scott, Physics and Applications of Bismuth Ferrite, Adv. Mater., 21 (2009) 2463.

21. B.D. Cullity, S. R. Stock, Elements of X-ray diffraction, Prentice Hall, Inc. New Jersey (2001).

22. J. M. Park, G. Fumiya, K. Takeshi, O. Masanori, Preparation and characterization of $BiFeO_3$ thin films deposited on ITO substrates by using pulsed laser deposition, Journal of the Korean Physical Society, 59 (2011) 2537-2541.

23. W. Dong, Y. Guo, G. Bing, L. Hongyan, H. Li, L. Hezhou, Enhanced photovoltaic properties in polycrystalline $BiFeO_3$ thin films with rhombohedral perovskite structure deposited on fluorine doped tin oxide substrates, Materials Letters, 88 (2012) 140–142.

24. R. Guo, L. You , Y. Zhou, Z. S. Lim, X. Zou , L. Chen, R. Ramesh, J. Wang, Non-volatile memory based on the ferroelectric photovoltaic effect Nature Communications, 4 (2013) 1990. DOI: 10.1038/ncomms2990.

ACCEPTED MANUSCRIPT

25. Surbhi Gupta, Monika Tomar, Vinay Gupta, Ferroelectric photovoltaic properties of Ce and Mn codoped $BiFeO_3$ thin film, Journal of Applied Physics, 115 (2014) 014102.

26. R. K. Katiyar, P. Misra, S. Sahoo, G. Morell, R. S. Katiyar, Enhanced photoresponse in $BiFeO_3/SrRuO_3$ heterostructure, Journal of Alloys and Compounds, 609 (2014) 168–172.

27. R. K. Katiyar, A. Kumar, G. Morell, J. F. Scott, R. S. Katiyar, Photovoltaic effect in a wide-area semiconductor-ferroelectric device, Applied Physics Letters, 99 (2011) 092906.

ACCEPTED MANUSCRIPT

ACCEPTED MANUSCRIPT

Table 1: *Experimental parameters used for irradiation of samples at IUAC, New Delhi.*

Selected ion bean parameters	Used
Pelletron	15UD@IUAC New Delhi
Ion bean	Au^{8+}
Fluence	$1x10^{12}$, $1x10^{13}$, $3x10^{13}$ ions/cm^2
Energy	100 MeV
Current	1 pnA

ACCEPTED MANUSCRIPT

ACCEPTED MANUSCRIPT

Table 2: *Calculated value S_e, S_n and projectile range.*

Thin films	S_e(eV/Å)	S_n(eV/Å)	Projectile Range (μm)
BFO	1.266×10^3	3.172×10^1	14.64
BTO	9.558×10^2	1.955×10^1	19.63

ACCEPTED MANUSCRIPT

ACCEPTED MANUSCRIPT

Table 3: *Lattice parameters "a" and "c", c/a distortion ratio and stress modulus along c-axis in BFO/BTO two layers structure after irradiation at varying fluencies.*

	BTO				**BFO**			
	Lattice parameter		**Stress modulus**	**c/a distortion ratio**	**Lattice parameter**		**Stress modulus**	**c/a distortion ratio**
	a (Å)	**c (Å)**			**a (Å)**	**c (Å)**		
Bulk	3.999	4.033	---	1.0085	5.876	13.867	---	2.3599
$1x10^{12}$ ions/cm^2	3.981	4.019	0.002	1.009	5.523	13.567	0.0216	2.45645
$1x10^{13}$ ions/cm^2	3.975	3.989	0.010	1.003	5.525	13.571	0.0213	2.45628
$3x10^{13}$ ions/cm^2	3.978	3.998	0.008	1.005	5.526	13.573	0.0212	2.45620
Pristine	3.989	4.028	0.124	1.009	5.520	13.563	2.192	2.4570

ACCEPTED MANUSCRIPT

ACCEPTED MANUSCRIPT

Table 4: *Lattice parameters "a" and "c", c/a distortion ratio and stress modulus along c-axis in BFO/BTO four layers structure after irradiation at varying fluencies.*

	BTO				**BFO**			
	Lattice parameter		**Stress modulus**	**c/a distortion ratio**	**Lattice parameter**		**Stress modulus**	**c/a distortion ratio**
	a (Å)	**c (Å)**			**a (Å)**	**c (Å)**		
Bulk	3.999	4.033	---	1.0085	5.876	13.867	---	2.3599
$1x10^{12}$ions/cm^2	4.225	4.047	0.003	0.9578	5.521	13.579	0.0207	2.45951
$1x10^{13}$ ions/cm^2	4.199	4.027	0.002	0.9590	5.520	13.574	0.0211	2.45905
$3x10^{13}$ ions/cm^2	4.207	4.027	0.001	0.9572	5.511	13.585	0.0203	2.46506
Pristine	4.229	4.051	0.446	0.9579	5.523	13.582	2.055	2.4591

ACCEPTED MANUSCRIPT

ACCEPTED MANUSCRIPT

Table 5: *Lattice parameters "a" and "c", c/a distortion ratio and stress modulus along c-axis in BFO/BTO six layers structure after irradiation at varying fluencies.*

	BTO				**BFO**			
	Lattice parameter		**Stress modulus**	**c/a distortion ratio**	**Lattice parameter**		**Stress modulus**	**c/a distortion ratio**
	a (Å)	**c (Å)**			**a (Å)**	**c (Å)**		
Bulk	3.999	4.033	---	1.0085	5.876	13.867	---	2.3599
$1x10^{12}$ ions/cm^2	4.249	4.070	0.010	0.957	5.527	13.600	0.0192	2.46064
$1x10^{13}$ ions/cm^2	4.220	3.995	0.009	0.946	5.526	13.597	0.0194	2.46055
$3x10^{13}$ ions/cm^2	4.269	4.090	0.014	0.958	5.525	13.595	0.0196	2.46063
Pristine	4.252	4.079	1.140	0.9586	5.528	13.603	1.903	2.4607

ACCEPTED MANUSCRIPT

ACCEPTED MANUSCRIPT

Table 6: *Values of grain size and roughness for 2, 4 and 6 layered BFO/BTO structure.*

Samples	2 layers BFO/BTO		4 layers BFO/BTO		6 layers BFO/BTO	
	Crystallite size (nm)	**Roughness (nm)**	**Crystallite size (nm)**	**Roughness (nm)**	**Crystallite size (nm)**	**Roughness (nm)**
Pristine	25	4.3	28	8.71	29	14.7
$1x10^{12}$ ions/cm^2	22	9.1	18	10.3	26	15.2
$1x10^{13}$ ions/cm^2	20	14.5	17	15.4	24	18.7
$3x10^{13}$ ions/cm^2	19	15.4	16	18.8	15	30.3

ACCEPTED MANUSCRIPT

ACCEPTED MANUSCRIPT

Table 7: *Values of % Transmission in the visible region (λ = 686 nm) and effect of ion fluencies on pristine and irradiated BFO/BTO multilayer structures.*

Samples	**% Transmission (λ = 686 nm)**		
	2 layers	**4 layers**	**6 layers**
Pristine	64	62	60
$1x10^{12}$ions/cm^2	62	60	58
$1x10^{13}$ ions/cm^2	61	58	55
$3x10^{13}$ ions/cm^2	59	57	45

ACCEPTED MANUSCRIPT

ACCEPTED MANUSCRIPT

Table 8: *Values of saturation polarization (P_s) and remnant polarization (P_r) for different layered BFO/BTO structure after ion irradiation with various fluence.*

Samples	**2 layers**		**4 layers**		**6 layers**	
	Ps (μC/cm^2)	2Pr (μC/cm^2)	Ps (μC/cm^2)	2Pr (μC/cm^2)	Ps (μC/cm^2)	2Pr (μC/cm^2)
Pristine	23.77	19.33	47.50	40.56	95.85	108.12
1x10^{12} ions/cm^2	10.06	9.66	25.54	13.62	57.93	24.72
1x10^{13} ions/cm^2	3.91	2.41	13.23	4.38	29.55	20.13
3x10^{13} ions/cm^2	--	--	--	--	--	--

ACCEPTED MANUSCRIPT

ACCEPTED MANUSCRIPT

Table 9: *Photovoltaic response characteristics of irradiated BFO/BTO six layered structures at varying fluence at zero bias*

Fluence (ions/cm^2)	**J_{dark} (μA/cm^2) (at 2V)**	**J_{sc} (μA/cm^2)**	**V_{oc} (V)**	**I_{on}/I_{off}**
Pristine	0.006	17.73	1.806	2.955 x 10^3
1x10^{12}	0.75	5.17	0.41	33.02
1x10^{13}	1.12	1.71	0.23	13.02

ACCEPTED MANUSCRIPT

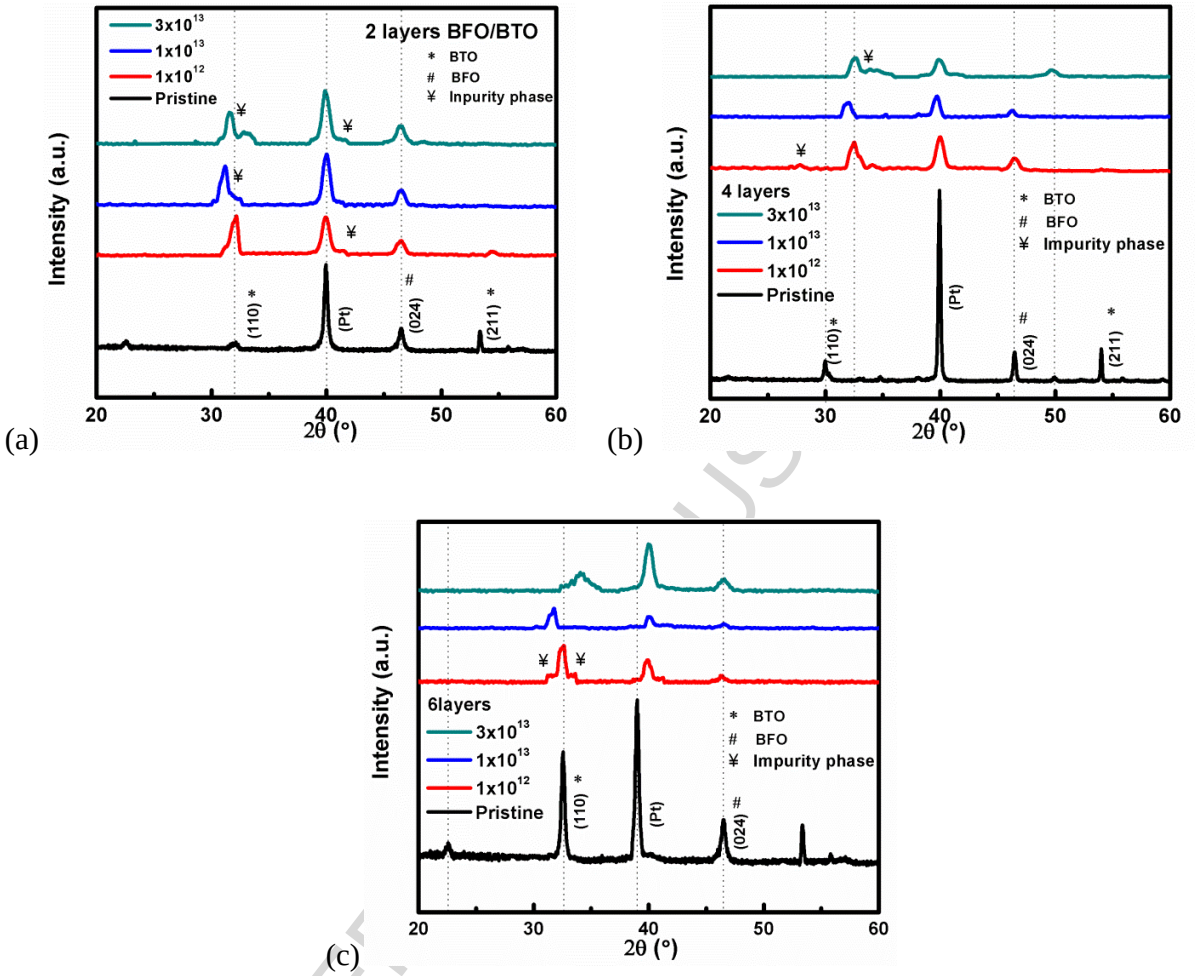

Figure 1: *XRD patterns of bare and irradiated (a) 2 layers (b) 4 layers and (c) 6 layers BFO/BTO multilayer structures.*

ACCEPTED MANUSCRIPT

2 layers

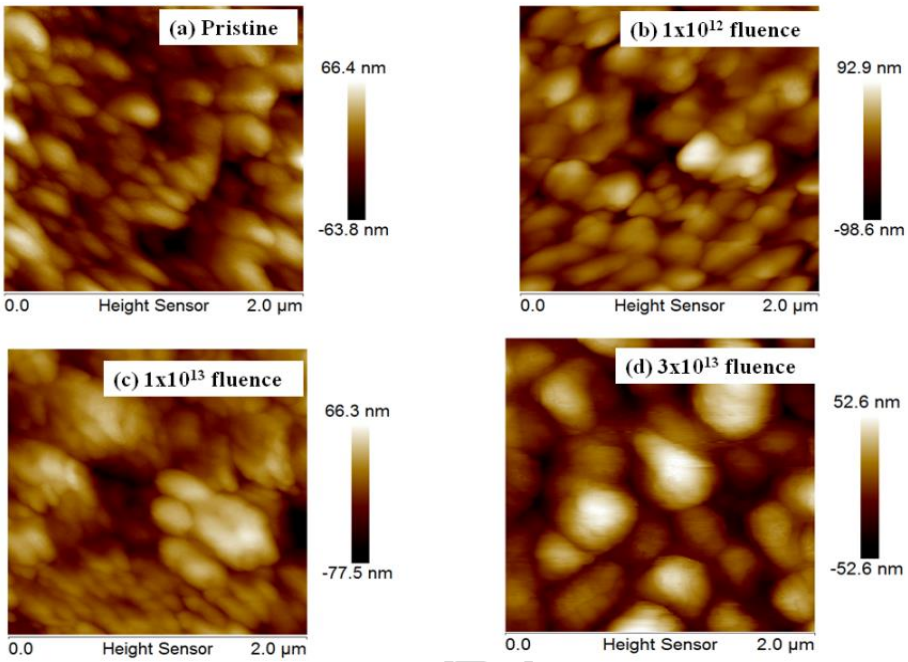

(a)

4 layers

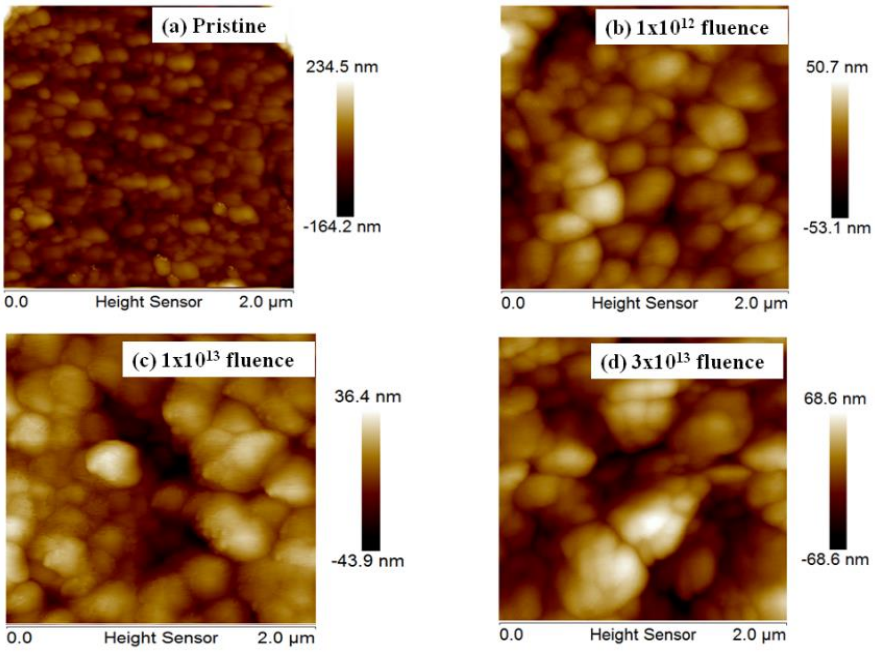

(b)

ACCEPTED MANUSCRIPT

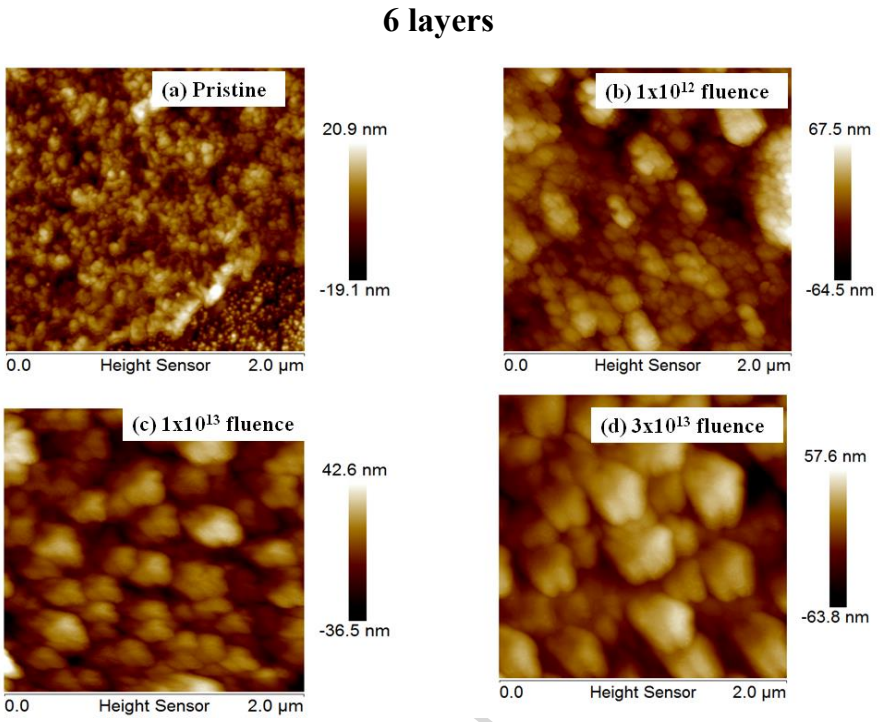

Figure 2: *Surface morphology of pristine and irradiated (a) 2 layers,(b) 4 layers and (c) 6 layers BFO/BTO structures.*

ACCEPTED MANUSCRIPT

ACCEPTED MANUSCRIPT

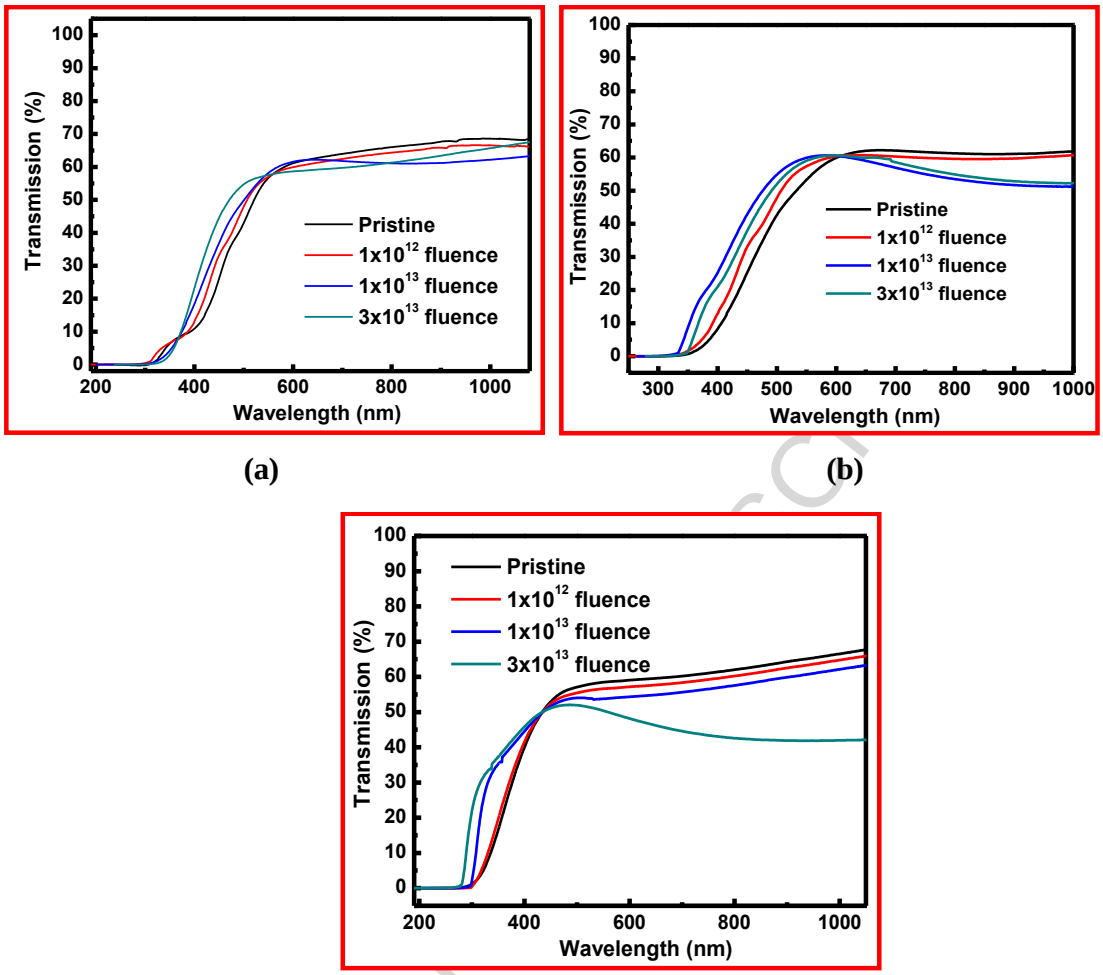

Figure 3:*Uv-visible transmittance spectra of pristine and irradiated (a) 2 layers (b) 4 layers and (c) 6 layers BFO/BTO multilayer structures.*

ACCEPTED MANUSCRIPT

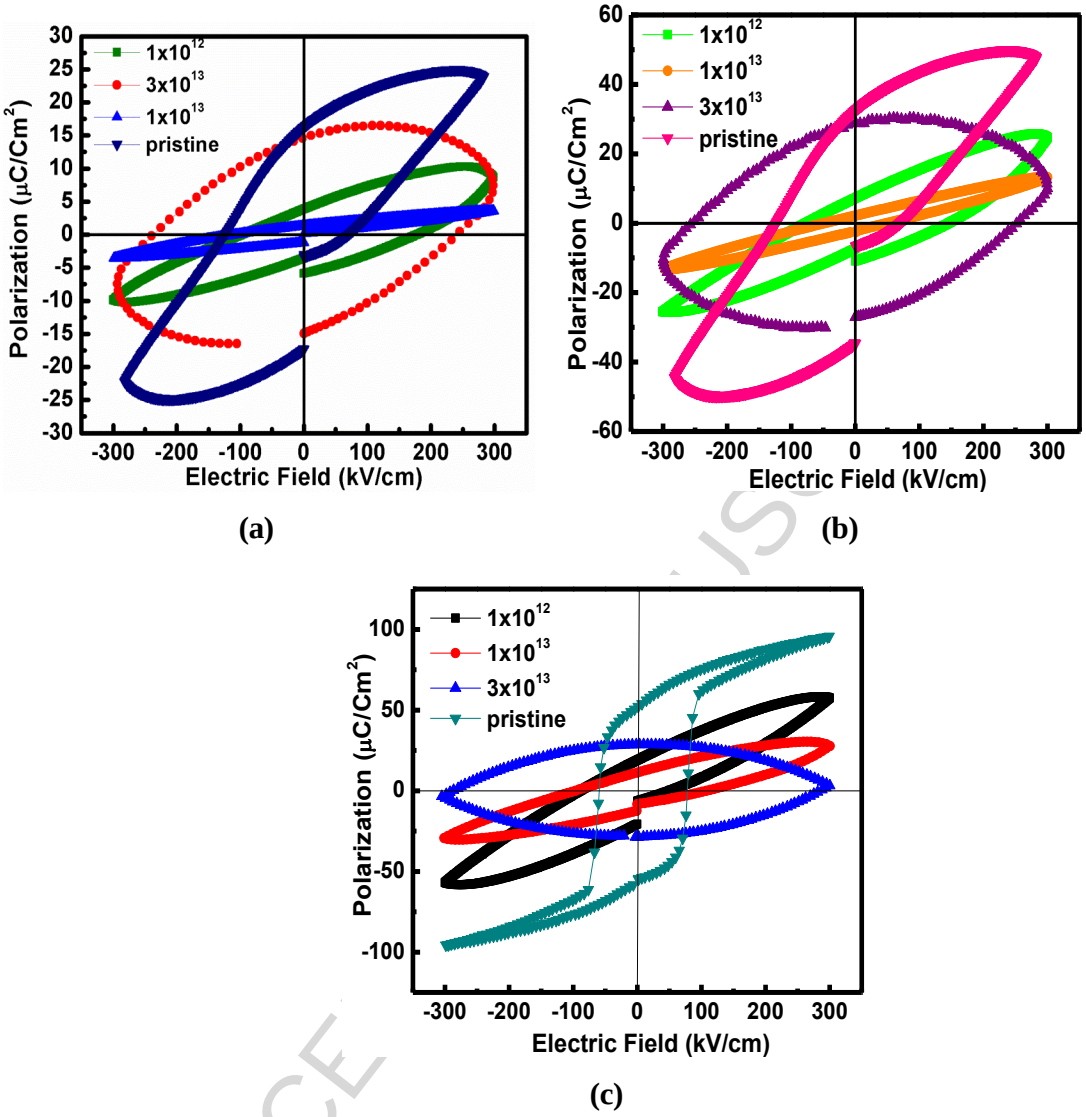

Figure 4: *P - E hysteresis loop of pristine and irradiated (a) 2 layers, (b) 4 layers and (c) 6 layers BFO/BTO structures.*

ACCEPTED MANUSCRIPT

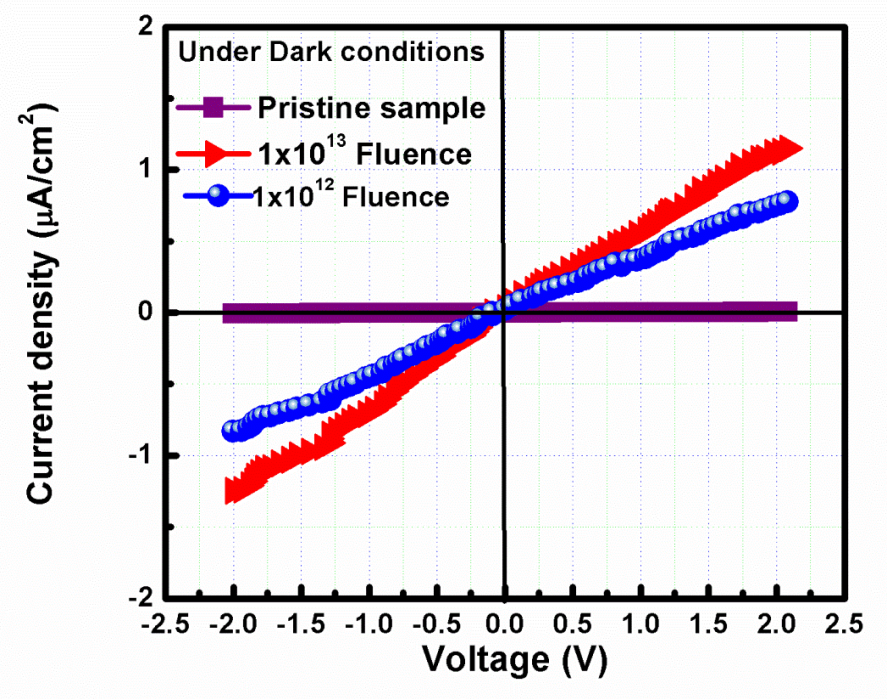

(a)

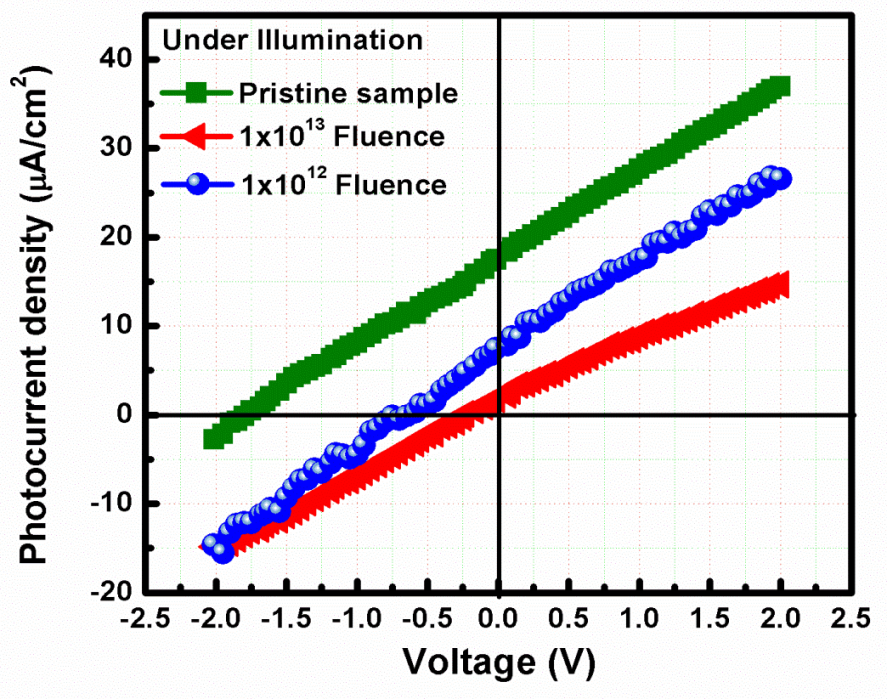

(b)

ACCEPTED MANUSCRIPT

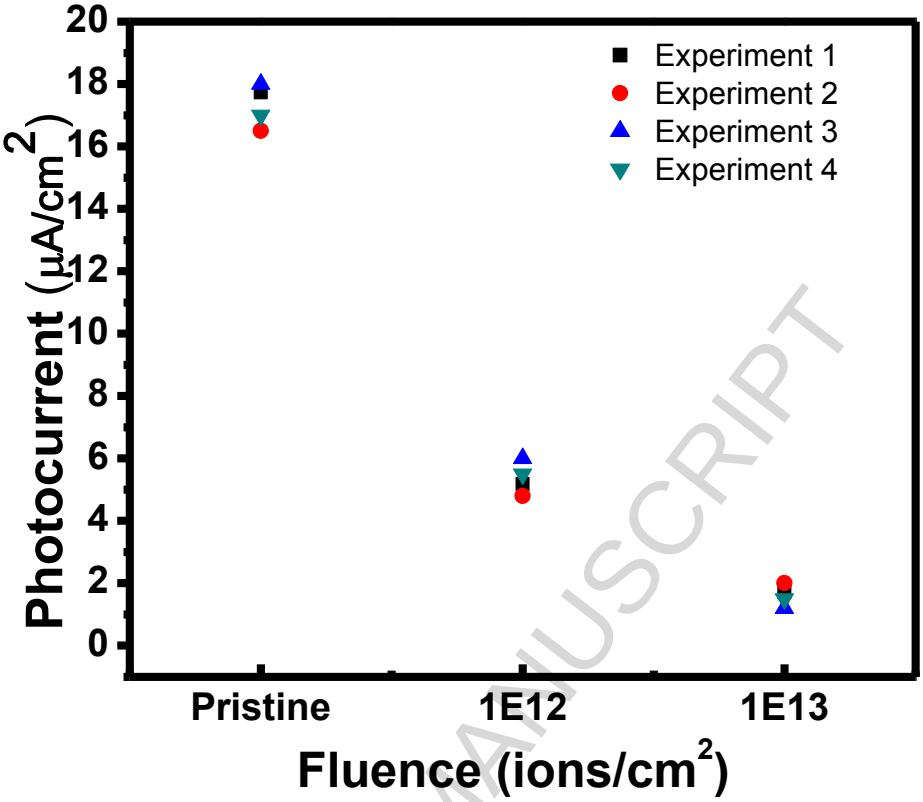

(c)

Figure 5: *J-V curves obtained for the BFO/BTO six layer structure irradiated with different fluences (a) under dark conditions, and (b) under light illumination (λ = 405 nm and intensity = 160 mW/cm^2) showing short circuit photocurrent density and open circuit photo voltage. (c) Repeatability of the experiments measuring photocurrent density for BFO/BTO six layer identical samples at different ion beam fluence.*

ACCEPTED MANUSCRIPT

ACCEPTED MANUSCRIPT

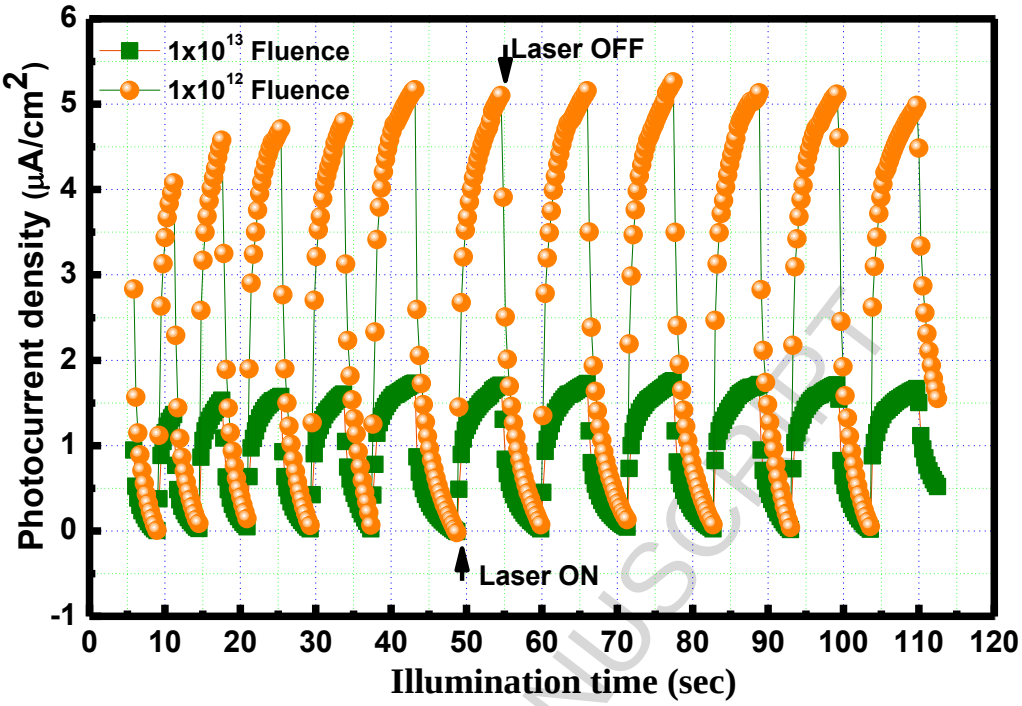

(a)

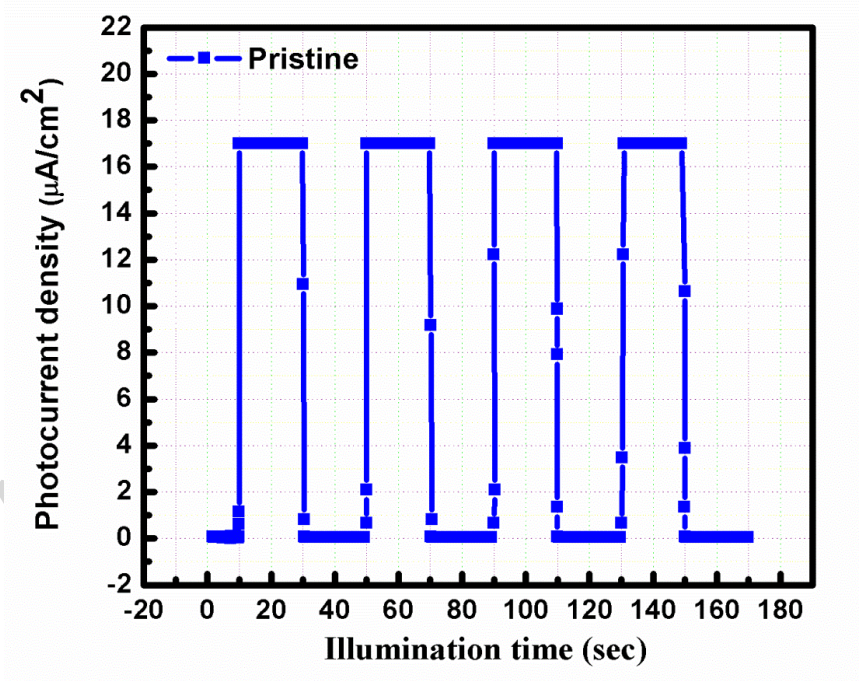

(b)

Figure 6: *Transient response curves of short circuit photocurrent density of six layered BFO/BTO structure (a) irradiated at different fluencies (b) without irradiation when laser beam is switched on and off at regular intervals of 20s.*

ACCEPTED MANUSCRIPT

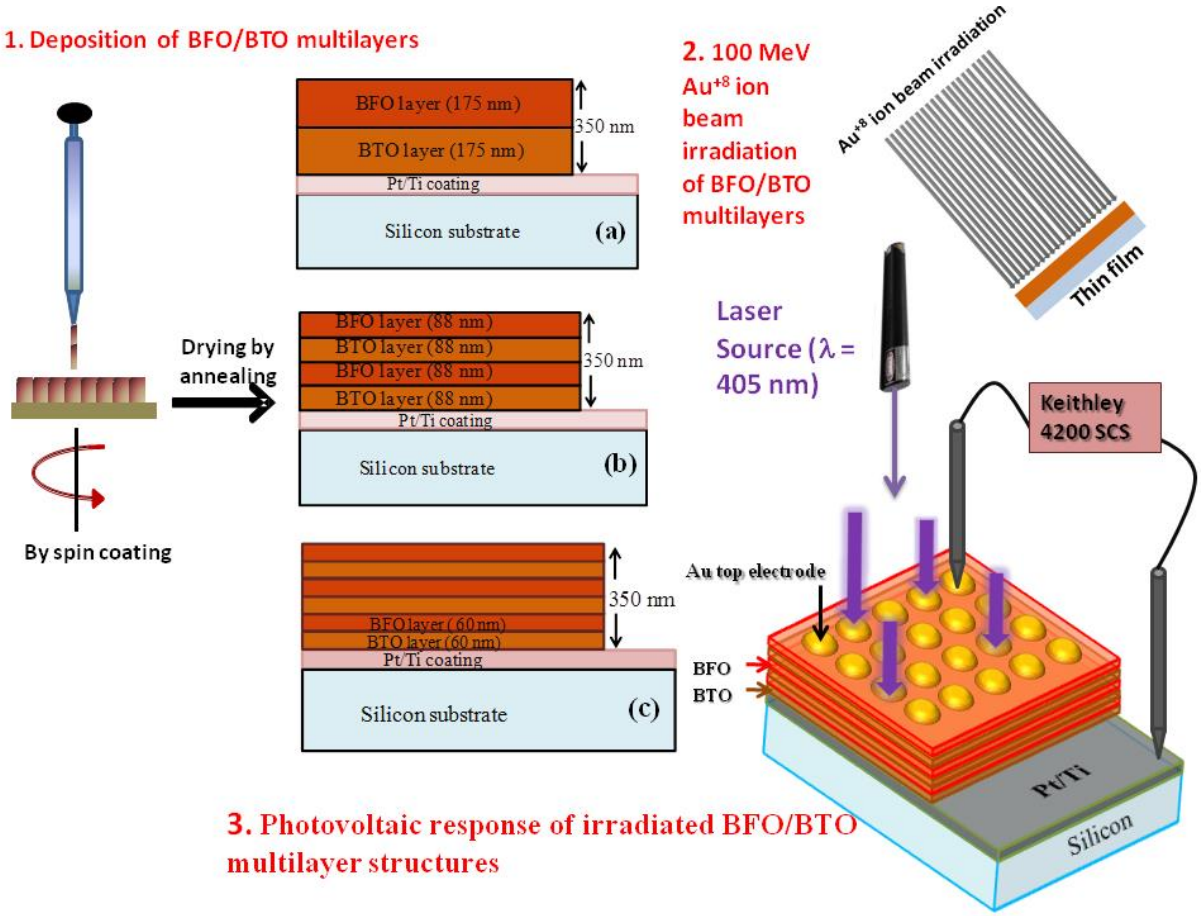

Graphical abstract

ACCEPTED

ACCEPTED MANUSCRIPT

Highlights

- BFO/BTO multilayers of varying layer number deposited on Pt/Si using CSD technique
- 100 MeV Au^{+8} irradiation performed at fluences 1×10^{12}, $1x10^{13}$ and 3×10^{13} ions/cm^2
- Irradiation effects on Photovoltaic response studied in MFM capacitor configuration
- Photovoltaic response sustained in multilayer structures post ion beam irradiation

ACCEPTED

Decision Science Letters 6 (2017) 117–136

Contents lists available at GrowingScience

Decision Science Letters

homepage: www.GrowingScience.com/dsl

MCDM based evaluation and ranking of commercial off-the-shelf using fuzzy based matrix method

Rakesh Garg[a*], R. K. Sharma[b], Kapil Sharma[c] and R. K. Garg[d]

[a, b]*Department of Computer Science & Engineering, Al-Falah School of Engineering & Technology, Faridabad, Haryana, India*
[c]*Department of Computer Science and Engineering, Delhi Technological University, Delhi, India*
[d]*Department of Mechanical Engineering, Deenbandhu Chhotu Ram University of Science and Technology, Murthal, Haryana, India*

C H R O N I C L E

Article history:
Received June 25, 2016
Received in revised format:
October 22, 2016
Accepted November 10, 2016
Available online
November 11 2016

Keywords:
Commercial Off-the-Shelf (COTS)
Matrix method
Selection criteria
CBSE

A B S T R A C T

In today's scenario, software has become an essential component in all kinds of systems. The size and the complexity of the software increases with a corresponding increase in its functionality, hence leads to the development of the modular software systems. Software developers emphasize on the concept of component based software engineering (CBSE) for the development of modular software systems. The CBSE concept consists of dividing the software into a number of modules; selecting Commercial Off-the-Shelf (COTS) for each module; and finally integrating the modules to develop the final software system. The selection of COTS for any module plays a vital role in software development. To address the problem of selection of COTS, a framework for ranking and selection of various COTS components for any software system based on expert opinion elicitation and fuzzy-based matrix methodology is proposed in this research paper. The selection problem is modeled as a multi-criteria decision making (MCDM) problem. The evaluation criteria are identified through extensive literature study and the COTS components are ranked based on these identified and selected evaluation criteria using the proposed methods according to the value of a permanent function of their criteria matrices. The methodology is explained through an example and is validated by comparing with an existing method.

© 2017 Growing Science Ltd. All rights reserved.

1. Introduction

The concept of CBSE which has a great influence on the software development primarily concerned with the integration of a number of COTS components in the desired system. COTS are usually the reusable software products that are developed for specific use by the various vendors and can be used without any modification for the development of a new system. CBSE approach can reduce the software complexity by decomposing the large software project into small functional or logical pieces that are

* Corresponding author. Tel.: +91-9416907980
E-mail address: rkgarg06@gmail.com (R. Garg)

© 2017 Growing Science Ltd. All rights reserved.
doi: 10.5267/j.dsl.2016.11.002

more manageable with the aim of reassembling them to get the desired system. Here, instead of building the whole software from a scratch, a new system can be assembled and constructed by the use of COTS components provided by different vendors in the market. The COTS based software development has five main phases as shown in Fig. 1 (Oberndorf, 1997).

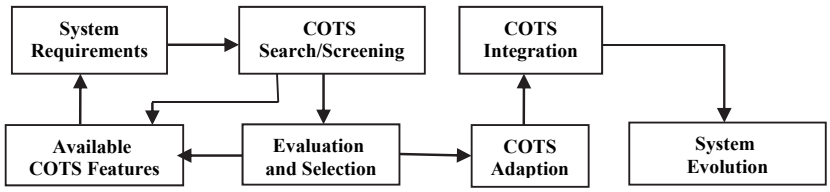

Fig. 1. COTS-based software development process

The need for rapid software development and requirement of cost, time and effort reduction has increased the usage of COTS components (Alves & Finkelstein, 2003). COTS are defined as the software pieces that can be further reused by the software developers to build the new software systems (Firesmith, 2005; Vigder et al., 1996). Gupta et al. (2012) described the COTS products that are available for purchase, lease or license to the general public. The COTS products are ready made and can be used by the software developers "as it is" and can be easily installed and incorporated with the existing system components. The use of COTS products provides many potential benefits as: (i) Reduction in development cost (ii) Reduction in development time and effort (iii) Improved quality of target software. In spite of many potential benefits, some disadvantages are also associated with the COTS products as (i) Incomplete knowledge of inner working code (ii) Compatibility issues (iii) Unavailability of correct and complete specifications. The COTS component selection involves a number of functional and non-functional criteria. Further, the importance of each evaluation criteria is different and also may vary under different requirements. The nature of the evaluation criteria is always conflicting and imprecise. Hence, there arises a need to develop a method which is efficient for optimal selection and ranking of the COTS components considering the conflicting and imprecise nature of the mutually interacting evaluation criteria. To resolve this problem, the present research paper proposes a fuzzy based matrix method for ranking and selection of COTS components. It is a hybrid method comprising fuzzy logics and matrix methods. Fuzzy logics are used to accommodate the conflicting and imprecise nature of evaluation criteria and vagueness of mind. Key elements in fuzzy logics are linguistic variables or fuzzy numbers rather that integers, (Zadeh, 1965). The matrix method is capable to model multi-criteria decision problems in the form of matrices and then matrices are converted into a single numerical value through its determinant or permanent. The main purpose of performing this empirical research is to improve the understanding of the COTS selection and evaluation process that may have a great influence on the software development. Though the matrix method has already been used for solution of MCDM problems of another area, however, this hybrid approach is being applied for the first time for ranking and selection of COTS. The method is validated by comparing with other existing methods.

The rest of the paper is structured as follows: in section 2, a review of COTS selection and the evaluation problem with the various COTS evaluation criteria and existing COTS selection approaches is provided. Section 3 explains the proposed fuzzy matrix method (FMM). Ranking procedure and empirical study are given in section 4. Results are provided in section 5 whereas a comparison of FMM proposed in this research with other existing methods is given in section 6. The research work is concluded in section 7.

2. Previous Related Work

COTS selection for a particular application from the large number of available COTS components in the market has become a challenging task for the software developers because the improper selection of COTS may lead either development of poor quality software or its complete failure to perform desired tasks. Various considerations such as software design, software functionality and economics

need to be considered before a suitable COTS component is selected for the development of the desired software. So, the research on COTS selection has very important theoretical and practical meaning, whether COTS selection is of rational concern for the better software development. Therefore, the available literature is revealed for selection criteria identified and used by various researchers in the past, methods and techniques developed for COTS evaluation and selection and other general issues relevant to the present research problem.

2.1 COTS evaluation criteria

Bertoa and Vallecillo (2002) proposed a quality model for the component based software development (CBSD) based on ISO 9126, that defines a set of quality attributes as Functionality, Reliability, Usability, Efficiency, Maintainability and Portability, etc. and their associated metrics for the effective selection and evaluation of COTS components. Wanyama and Homayoun (2005) found that the COTS selection is a complex multi-criteria decision making (MCDM) problem characterized by uncertainty, complexity, multiple stakeholders and multiple objectives. In the contemporary work Yang et al. (2005) present vendor dependence as a major factor in COTS selection.

Huan-Jyh Shyur (2006) identified cost, supplier's support, technological risk, closeness of fit to a company's business, ease of implementation, flexibility to easy change of business and system integration (CO, SS, TR, FB, EI, FC, SI) as the potential criteria for COTS selection. Neubauer and Stummer (2007) solved the problem of COTS selection by categorizing the different COTS selection factors, mainly in 4-groups, namely (i) functional criteria; (ii) quality criteria (defect rate, performance, usability, security, etc.); (iii) strategic criteria (cost, available time etc.) and (iv) domain and architectural criteria.

Table 1
Description of 4-major groups of COTS evaluation criteria

Quality Characteristics	Quality characteristic is a set of properties of a software product or cots component by which its quality can be described and evaluated. In the past, many researchers have introduced various quality models such as ISO 9126, ISO 14598 etc. for the assessment of the software product quality. The attributes which are considered by various researchers in their quality model are functionality, reliability, usability, efficiency, maintainability, and portability.
Technology Factors	Technology factors are concerned with the technology opted during the development of any component provided by any vendor.
Domain and Architectural Factors	Domain and Architectural factors describe the scope, applicability and the basic structure of the components.
Strategic Factors	Strategic factors are those non-functional requirements that are directly related to the component providers and the organizational policies such as vendor capabilities, business issues and the cost.

Wanyama and Far (2008) addressed the problem of COTS selection using reliability, maintainability, security, portability, compatibility, vendor ability, initial product price, initial hardware price, implementation costs, training costs, license conditions as selection criteria. Suleiman (2008) considered system integration interface, functionality aspects, COTS vendor maturity, conformity to system environment (consistency between system requirements, hardware, software application systems and COTS component infrastructure), budget, time, vendor support as selection criteria. Ibrahim et al. (2009) proposed the selection criteria for the COTS component such as usability, security, functionality, performance, recoverability and impact. Ravichandran et al. (2013) listed a large number of COTS selection attributes such as reliability, stability, portability, consistency, completeness, interface and structural complexity, understandability of software documents, security, usability, accuracy, compatibility, performance, serviceability and customizability. Baharom et al. (2012) introduced vendor characteristics such as vendor stability, vendor reputation, vendor supportability and organization characteristics as system platform, development environment, culture and financial

characteristic for COTS component selection. Gupta et al. (2013, 2011) used quality, cost, probability of failure on demand, average number of invocations, number of lines of code, execution time, delivery time and quality characteristics as selection criteria. The COTS selection criteria are generally into four major groups, namely quality characteristics, technology factors, domain and architectural factors and strategic factors. The brief description of these four groups is provided in Table 1. The details of these selection criteria and the corresponding researchers are summarized in Table 2.

Table 2
Summary of COTS evaluation criteria/sub-criteria

Criteria	Sub-criteria	Researchers
Quality Characteristics	Quality, Functionality, Accuracy, Adaptability, Compliance, Conformance, Customizability, Efficiency, Installability, Interoperability, Maintainability, Maturity, Operability, Recoverability, Reliability, Replace-ability, Reusability, Serviceability, Stability, Suitability, Testability, Understandability	Jung and Choi (1999), Neubauer and Stummer (2007), Gupta et al. (2012-13), Leung and Leung (2002), Beetoa and Valliecillo (2002), Sassi et al. (2006), Mohamed et al. (2007), Basem Suleiman (2008), Kwong et al. (2010), Ibrahim et al. (2011), Gupta et al. (2013), Ravichandran et al. (2012), Wanyama and H. Far (2008), Ibrahim et al. (2009), Cortellssa et al. (2006), Tang et al. (2011), Iribrane and Vallecillo (2002).
Technological Factors	Closeness of Fit, Cohesion, Compatibility, Line of Code, POF on Demand, Technological Risk, No. of Invocations, Coupling	Huan-Jyh Shyur (2006), Mohamed et al. (2007), Rao and Rajesh (2009), Kwong et al. (2010), Indumati et al. (2011), Wanyama and H. Far (2008), Ibrahim et al. (2009), Tang et al. (2011), Ravichandran et al. (2012), Gupta et al. (2012), Rao and Rajesh (2009).
Domain and Architectural Factors	Time Behavior, Resource Behavior, Ease of Implementation, Interface Complexity, Impact, Environment, Flexibility, Consistency, Completeness	Gupta et al. (2013), Huan-Jyh Shyur (2006), Rao and Rajesh (2009), Wanyama and Homayoun (2005), Carvallo et al. (2006), Neubauer and Stummer (2007), Ravichandran et al. (2012), Ibrahim et al. (2011), Baharom et al. (2012), Yang et al. (2005), Kaur and Mann (2010).
Strategic Factors	Vendor Stability, Schedule, Multi-Objectives, Execution Time, Delivery Time, Cost	Basem Suleiman (2008), Baharom et al. (2012), Yang et al. (2005), Wanyama and Homayoun (2005), Gupta et al. (2012), Cortellssa et al. (2006), Neubauer and Stummer (2007), Jung and Choi (1999), Huan-Jyh Shyur (2006), Wanyama and H. Far (2008), Basem Suleiman (2008), Rao and Rajesh (2009), Kaur and Mann (2010), Indumati et al. (2011), Gupta et al. (2013).

2.2 COTS Selection methods

In the component based software development, the selection of appropriate COTS products is of great importance. Many precision-based methods for COTS selection have been developed. J. Kontio (1995) proposed the OTSO approach for the COTS selection and evaluation with the help of AHP (Analytical Hierarchical Process) and WSM (Weighted Score Method). Morisio and Tsukios (1997) introduced a two-phase model "Isuware" based on multi-criteria decision making approach to the evaluation of COTS components Lichota et al. (1997) proposed PRISM (Portable, Reusable, Integrated software modules) based on progressive filtering comprising of two parts as formation of generic component architecture and product evaluation process (PEP) for the COTS selection. Tran and Liu (1997) proposed a waterfall stylistic approach CISD for the identification and evaluation of COTS components and then their integration into the system for the software development. Maiden and Ncube (1998) proposes a new process PORE (Procurement-Oriented Requirements Engineering) to address the lack of guidance for acquiring requirements to enable evaluation of commercial off-the-shelf (COTS) software. Kunda and Brooks (1999) presented STACE (Social-Technical Approach to COTS

evaluation) comprising of non-technical issues as social, human and organizational characteristics, political and economic factors and customer participation. Alves and Castro (2001) presented a systematic, repeatable and requirement oriented procedure CRE (COTS-Based Requirement Engineering) for evaluation and selection of COTS based on the non-functional requirements such as performance and security. Cavanaugh and Polen (2002) developed CEP (Comparative Evaluation Technique) as the modification in OTSO method. Tello and Perez (2002) proposed BAREMO (Balanced Reuse Model) as an application of AHP (Analytical Hierarchal Process) for selecting the appropriate COTS component for the software development. Gregor et al. (2002) developed STORYBOARD approach for the COTS selection by focusing on the understanding of customer's requirements with the use of use cases and screen captures. Burgues et al. (2002) proposed CS (Combined Selection), a two level (Local and Global) approach for the selection of multiple COTS component in COTS intensive Systems.

Bohem et al. (2003) presented a risk-driven approach Win-Win approach based on classical software development spiral model. Erol and Ferrel (2003) proposed a fuzzy QFD (Quality Function Deployment) based approach for the COTS component selection. Chung and Kooper (2004) produced a well-disciplined and systematic approach CARE (COTS-Aware Requirement Engineering) for the COTS component selection. Grau et al. (2004) develop a system named as DesCOTS for the effective evaluation of COTS components by considering various attributes of the software quality model. Cortellessa et al. (2006) introduced CODER framework for the COTS component selection composed of a UML case tool, a model builder and a model solver. Huan-Jyh Shyur (2006) developed a framework for the COTS selection by combining two different approaches mainly ANP and TOPSIS.

Mohamed et al. (2007) proposed a decision support system MiHOS (Miss-match Handling aware COTS selection) for the COTS component selection by handling miss-match between the COTS and the requirements. Sheng and Wang (2008) proposed an evaluation approach for COTS based on gap theory. Kwong et al. (2010) provide an optimization model for component selection by the use of GA (Genetic Algorithm). Ibrahim et al. (2009) proposed a hybrid model UnHOS (Uncertainty Handling in COTS Selection) by combining AHP (Analytical Hierarchical Process) and BBN (Bayesian Belief Network) followed by the sensitivity analysis for the COTS component selection. Ravichandran et al. (2013) adopted Neuro-fuzzy approach and presented an effective methodology ANFIS for the COTS component selection. Sarkar (2012) provided a comprehensive framework ACT (Architecture Centric Tradeoff) for the COTS selection, implementation and governance by focusing on benefits to the customer organization and system Integrator. Gupta et al. (2013, 2011) has developed a systematic and interactive Fuzzy Optimization framework for the solution of bi-objective fuzzy COTS selection. Kaur and Singh (2014) used PROMETHEE whereas Nazir et al. (2014) used Analytic Network Process approach for the selection of COTS. A brief description about the various COTS selection methods is summarized in Table 3.

Table 3
Existing COTS selection approaches

Approach	Year	Researchers	Approach	Year	Researchers
OTSO	1995	J. Kontio	FUZZY QFD	2003	Ferrel-Jr
IUSWARE	1997	Morisio and Tsoupis	CARE	2004	Chung and Kooper
PRISM	1997	Lichota et al.	DESCOTS	2004	Grau et al.
CISD	1997	Tran and Liu	CODER	2006	Cortellessa et al.
PORE	1998	Maiden and Ncube	ANP+MODIFIED TOPSIS	2006	Huan-Jyh-Shyur
STACE	1999	Kunda and Brooks	MIHOS	2007	Mohammed et al.
CRE	2001	Alves and Castro	GAP THEORY	2008	Sheng and Wang
CEP	2002	Cavavaugh and Polen	GA	2010	Kwong et al.
PECA	2002	Doreda et al.	UNHOS	2011	Ibrahim et al.
BAREMO	2002	Tello and Parez	ANFIS	2012	Ravichandran et al.
STORYBOARD	2002	Gergor et al.	FMP	2012	Gupta et al.
CS	2002	Butges et al.	ACT	2012	Subhankar Sarkar
WIN-WIN	2003	Bohem et al.	FMOP	2013	Gupta et al.

3. Methodology Adopted

In this paper, a multi criteria decision making approach combining fuzzy set theory and matrix method is proposed for optimal evaluation and ranking of COTS components based on a number of conflicting evaluation criteria. Optimal refers to the best under given circumstances of certain parameters or restrictions. Here, the optimal selection refers to an appropriate selection of COTS candidates for a particular application from a group of viable and potential COTS candidates based on pre-identified evaluation criteria considered in this study. The concept of optimal selection is explained with the help of following example in its simplest form.

Example: A class consists of 60 students. The top ten students, in accordance to their academic merit, are S_1, S_2, S_3… S9, S_{10}. Five students are to be selected to represent the institute for a competitive event considering the sole criteria of academic merit. In general, top five students, i.e. S_1, S_2, S_3, S_4 and S_5 will be selected. If, say, two students S_2 and S_4 are not available due to ill health or any other family engagements/problems for participation, then the selection will comprise S_1, S_3, S_5, S_6 and S_7 students. It is called as optimal selection. However, in this case, only one criteria, i.e. academic merit is considered and if more numbers of criteria e.g., academic merit, medical fitness, physical health, decision making, team management, etc. are to be considered for selection; it will become more complex and hence need to be modeled as an MCDM problem.

The matrix method has already been used for the ranking of software engineering metrics (Garg et al., 2013) and power plants (Dahiya et al., 2007). This hybrid methodology takes the advantage of both fuzzy set theory to accommodate impreciseness and vagueness and matrix method for calculation of single numerical index called permanent for ranking of COTS components. A brief introduction to basic concepts of fuzzy logics, algebraic operations, triangular fuzzy numbers, linguistic variables, and matrix operations is presented in this section.

3.1. Fuzzy Set Theory

Fuzzy set theory is referred as an extension of classical set theory where the elements of set have varying degree of membership. Any logic that is based on two values either true or false seems to be inadequate while describing human reasoning. In contrast, fuzzy logic can use the whole interval between true (1) and false (0). Simply it can be stated that fuzzy logic is derived from FST to deal approximations rather than precision. Fuzzy logic is a form of many valued logics where the truth values of variables fall between 0 and 1 and are considered to be "fuzzy". It does not happen in case of Boolean algebra/logic in which the truth values are either 1 or 0, often called "crisp" values/score. The values 0 and 1 are the extreme values in case of fuzzy logic and it also takes the in-between values, for example, the result of a comparison between two things could be not "tall" or "short" but " 0.38 of tallness." It means more number of truth values, depending on fuzzy scale, will lie between extreme values. In case where linguistic variables are used, these in-between values are expressed by specific (membership) functions. Zadeh (1965) introduced initially the fuzzy set theory by considering the problem of fuzziness of the data. Fuzzy set theory basically provides a better way to solve the various problems having some uncertainty in them. Mathematical operations can easily be applied to fuzzy sets (Dubois & Prade, 1979).

3.2 Triangular fuzzy numbers

Triangular fuzzy numbers (TFN) are used as membership functions, corresponding to the elements in a set, as shown in Fig. 2. TFN is most accepted among the various shapes of fuzzy numbers and also most widely used because of its capability to represent uncertain information. The use of the triangular fuzzy numbers is intuitively easy for the decision makers to use and calculate. A fuzzy number is a triangular fuzzy number if its membership function can be denoted as follows:

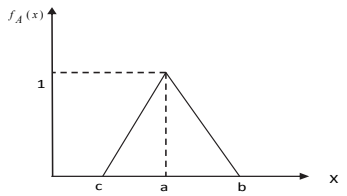

Fig. 2. Membership function of a triangular fuzzy number

$$f_A(x) = \begin{cases} \frac{(x-c)}{(a-c)}, & c \le x \le a \\ \frac{(b-x)}{(b-a)}, & a \le x \le b \\ 0, & otherwise \end{cases} \quad (1)$$

where *a, b* and *c* are real numbers and $c = a = b$. To calculate membership functions for different operations, Zadeh's extension principle can be used. Only addition and multiplication are used here. Defining triangular fuzzy numbers A_1 and A_2 by the triplets as $A_1 = (c_1, a_1, b_1)$ and $A_2 = (c_2, a_2, b_2)$, addition and multiplication operations of A_1 and A_2 can be expressed as follows:
Addition: if $\oplus$ denotes addition.

$$A_1 \oplus A_2 : (c_1, a_1, b_1) \oplus (c_2, a_2, b_2) = (c_1 + c_2, a_1 + a_2, b_1 + b_2) \quad (2)$$

Multiplication: if $\otimes$ denotes multiplication.

$$A_1 \otimes A_2 : (c_1, a_1, b_1) \otimes (c_2, a_2, b_2) = (c_1 \times c_2, a_1 \times a_2, b_1 \times b_2), \quad c_1 \ge 0, c_2 \ge 0 \quad (3)$$

3.3 Linguistic terms of triangular fuzzy numbers

Fuzzy set theory is primarily concerned with quantifying the uncertainty in human thoughts and perceptions, where linguistic terms can be properly represented by the approximate reasoning of fuzzy set theory. The weights of various criteria and the rating values of COTS components are considered as linguistic terms throughout this paper. A linguistic term can be defined as a variable whose values are words or sentences in natural language. In this research paper, a seven point fuzzy scale is used to evaluate the weights using linguistic terms such as extremely more important (EMI), very more important (VMI), more important (MI), important (I), less important (LI), very less important (VLI) and extremely less important (ELI). To determine the suitability of different COTS versus different evaluation criteria, the rating values in a seven point fuzzy scale can be accessed by linguistic terms such as very high (VH), high (H), above average (AA), average (A), below average (BA), low (L) and very low (VL). The seven point fuzzy scale is shown in Fig. 3.

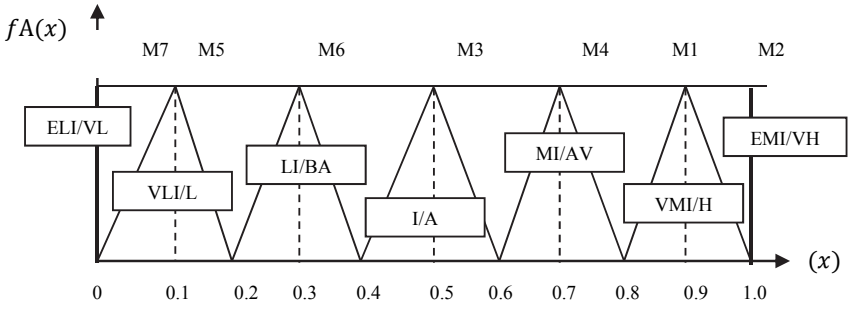

Fig. 3. Seven point fuzzy scale

The linguistic variable along-with their corresponding membership functions and crisp scores for a seven point fuzzy scale are given in Table 4.

Table 4
Linguistic terms representation using triangular fuzzy numbers

Qualitative measures of evaluation criteria/sub-criteria (Linguistic Term)	Fuzzy numbers	Membership function $\mu(x)$	Right Utility Value $\mu_R(M_1)$	Left Utility Value $\mu_L(M_1)$	Crisp Value $\mu_T(M_1)$
Very Low/ Extremely Less Important	$M_1(0, 0, 0)$	$\mu_{M_1}(x) = 1, x = 0$	0	1	0
Low/ Very Less Important	M_2 (0, 0. 1, 0. 2)	$\mu_{M_2}(x) = \begin{cases} (x-0)/(0,1)\ 0 \le x \le 0.1 \\ (0.2-x)/(0,1)\ 0.1 \le x \le 0.2 \end{cases}$	0.1818	0.9091	0.1364
Below Average/ Less Important	M_3 (0.2, 0.3, 0.4)	$\mu_{M_3}(x) = \begin{cases} (x-0.2)/(0,1)\ 0.2 \le x \le 0.3 \\ (0.4-x)/(0,1)\ 0.3 \le x \le 0.4 \end{cases}$	0.3636	0.7273	0.3182
Average/ Important	M_4(0.4, 0.5, 0.6)	$\mu_{M_4}(x) = \begin{cases} (x-0.4)/(0,1)\ 0.4 \le x \le 0.5 \\ (0.6-x)/(0,1)\ 0.5 \le x \le 0.6 \end{cases}$	0.5455	0.5455	0.5
Above Average/ More Important	M_5(0.6, 0.7, 0.8)	$\mu_{M_5}(x) = \begin{cases} (x-0.6)/(0,1)\ 0.6 \le x \le 0.7 \\ (0.8-x)/(0,1)\ 0.7 \le x \le 0.8 \end{cases}$	0.7273	0.3636	0.6818
High/ Very More Important	M_6(0.8, 0.9, 1)	$\mu_{M_6}(x) = \begin{cases} (x-0.8)/(0,1)\ 0.8 \le x \le 0.9 \\ (1-x)/(0,1)\ 0.9 \le x \le 1 \end{cases}$	0.9091	0.1818	0.8636
Very high/ Extremely More Important	M_7 (1, 1, 1)	$\mu_{M_7}(x) = 1, \quad x = 1$	1	0	1

3.4 Fuzzy algorithm for COTS ranking problem

A systematic approach to the COTS ranking problem, based on fuzzy set theory and multi-criteria decision analysis, is described in this section. Various methods have been proposed to aggregate the expert's opinions such as mean, median, max, min and mixed operators. In this study, the mean operator was used to aggregate the assessments of experts. For COTS ranking problem, there is a group of 'n' experts (E1, E2, . . . ,En), who evaluate the weights of k criteria (C_1, C_2, . . . ,C_k) and the ratings of m COTS components (A_1, A_2, . . . ,A_m), under each of these k criteria. Let W_{te} (t = 1, 2,. . . , k; e = 1, 2,. . . , n) be the weight given to C_t by expert Ee. Let R_{ite} (i = 1, 2,. . . , m; t = 1, 2,. . . ,k; e = 1, 2,. . . , n) be the rating assigned to COTS A_i by expert Ee under criterion C_t. W_t and R_{it} are defined as follows:

$$W_t = \left(\frac{1}{n}\right) \otimes (W_{t1} \oplus W_{t2} \oplus \ldots \oplus W_{tn}) = \frac{1}{n}\sum_{e=1}^{n} W_{te} \tag{4}$$

$$R_{it} = \left(\frac{1}{n}\right) \otimes (R_{it1} \oplus R_{it2} \oplus \cdots \oplus R_{itn}) = \frac{1}{n}\sum_{e=1}^{n} R_{ite} \tag{5}$$

where W_t is the average weight of criterion C_t and R_{it} is the aggregated rating of COTS components A_i under criterion C_t.

3.5 Conversion of fuzzy numbers to crisp scores

As the aggregated assessments are represented as triangular fuzzy numbers, there is a requirement of a conversion mechanism to convert these fuzzy triangular numbers to a single numeric value known as crisp value/scores. In this paper, the maximizing set and minimizing set methods (Chen, 1985) are applied. If $F_i(i = 1,2,...,m)$ be the fuzzy ratings of m COTS components. Chen (1985) defined the maximizing set $M = \{(x, f_M(x)) \mid x \in \Re\}$ with

$$f_M(x) = \begin{cases} \dfrac{(x - x_{min})}{(x_{max} - x_{min})}, & x_{min} \le x \le x_{max} \\ 0, & otherwise \end{cases} \tag{6}$$

and, minimizing set $G = \{(x, f_G(x)) \mid x \in \Re\}$ with

$$f_G(x) = \begin{cases} \dfrac{(x - x_{max})}{(x_{min} - x_{max})}, & x_{min} \le x \le x_{max} \\ 0, & otherwise \end{cases} \tag{7}$$

where $x_{\min} = \inf S,\ x_{\max} = \sup S,\ S = \cup_{i=1}^{m} F_i, F_i = \{x \mid f_{F_i}(x) > 0\},\ \ i = 1, 2, ...m.$

Further, the right utility value $U_M(F_i)$ and the left utility value $U_G(F_i)$ for COTS metric 'i' are defined as:

$$U_M(F_i) = \sup(f_{F_i}(x) \cap f_M(x)), \quad i = 1, 2, ...m \tag{8}$$

$$U_G(F_i) = \sup(f_{F_i}(x) \cap f_G(x)), \quad i = 1, 2, ...m \tag{9}$$

And, the total utility value $U_T(F_i)$ of alternative 'i' are defined as:

$$U_T(F_i) = \frac{U_M(F_i) + 1 - U_G(F_i)}{2} \tag{10}$$

3.6 Matrix Method

COTS components are characterized by multiple criteria, which need to be converted into a single number index. This single number index will be used to rank the COTS. This value for each COTS component is obtained using the concept of matrices. The crisp scores of the aggregated assessments i.e. ratings of the COTS components and the relative aggregated weights of all evaluation criteria are stored in a matrix known as 'Criteria Matrix' having size n x n corresponding to n criteria. The diagonal elements (a_{ii}'s or a_i's) and the off-diagonal elements (a_{ij}'s) of this matrix give the aggregated ratings of different COTS versus different ranking criteria and the relative aggregated weights of different evaluation criteria, respectively. Thus, the criteria matrix is a combination of two matrices namely 'COTS Rating Matrix and 'Criteria Weight Matrix'.

Criteria Weight Matrix: The Criteria Weight Matrix is formed by considering aggregated weights of different criteria. The off diagonal elements of this matrix show the aggregated weights of the criteria e.g. the element (a_{ij}) of this matrix will give the relative importance weight of j^{th} criteria in respect of i^{th} criteria. All diagonal elements of this matrix are zero because there is no significance of comparing a criterion with respect to itself. Mathematically a_{ij} = weight of j^{th} criteria/ weight of i^{th} criteria-

$$\begin{bmatrix} 0 & a_{12} & a_{13} & \cdots & a_{1n} \\ a_{21} & 0 & a_{23} & \cdots & a_{2n} \\ \vdots & & & & \\ a_{n1} & a_{n2} & a_{n3} & \cdots & 0 \end{bmatrix}$$

COTS Rating Matrix: This matrix is formed on the basis of deterministic values (crisp values) of the aggregated ratings of the COTS matrices versus different ranking criteria. This is a diagonal matrix whose elements (a_{ii}'s or a_i's) represent the aggregated ratings of different COTS components versus different evaluation criteria.

$$\begin{bmatrix} a_{11} & 0 & 0 & \cdots & 0 \\ 0 & a_{22} & 0 & \cdots & 0 \\ \vdots & & & & \\ 0 & 0 & 0 & \cdots & a_{nn} \end{bmatrix}$$

Criteria Matrix: The criteria matrix is formed by combining the criteria rating matrix and weight matrix. The criteria matrix is a complete representation of the COTS selection system which considers the performance ratings of the COTS for each evaluation criteria as well as the relative importance of the various evaluation criteria under considerations in an integrated manner. Thus the 'Criteria Matrix' corresponding to 'n' criteria, in general, is written as:

$$\begin{bmatrix} a_{11} & a_{12} & a_{13} & \cdots & a_{1n} \\ a_{21} & a_{22} & a_{23} & \cdots & a_{2n} \\ \vdots & & & & \\ a_{n1} & a_{n2} & a_{n3} & \cdots & a_{nn} \end{bmatrix}$$

3.7 Permanent Function Representation

In order to compare and rank the various COTS candidates, it is necessary to have a single numerical index for each criteria matrix and the permanent function representation is the method to convert the criteria matrix into the single numerical index. Since, no negative value appears in the permanent function representation and hence there is no chance of loss of any information contained in criteria matrix. Variable Permanent Function (VPF) is a standard matrix function that is used in combinatorial mathematics. It is a powerful tool for multi-criteria based evaluation and ranking of the systems in some specific order. VPF is similar to the determinant of a matrix with a difference that no negative term appears in it. Further, computer software is developed to determine the value of the Permanent of the 'Criteria Matrix'. The algorithm is:

$(A)\, P \leftarrow 0;\ X_i \leftarrow a_{in} - \frac{1}{2} \sum_{i,j=1}^{n} a_{ij};\ \text{sgn} \leftarrow -1$

$(B)\text{sgn} \leftarrow -\text{sgn};\ P \leftarrow \text{sgn},$

Get next subset of $(1, 2, ..., n-1)$ *from NEXSUB*;

if empty, go to (C) *and if* j *was deleted, then* :

$z \leftarrow -1$; *otherwise,* $z \leftarrow 1$;

$x_i \leftarrow x_i + z\, a_{ij}\ (i = 1, 2, ..., n)$

$(C)\, P \leftarrow P.x_i\ (i = 1, 2, ..., n);\ p \leftarrow p + p$

if more subsets remain, to (B); $Permanant \leftarrow 2(-1)^{n-1}\, p$; *EXIT*.

ALGORITHM NEXSUB
(A)[*First entry*] $m \leftarrow 1;\ j \leftarrow 1;\ z \leftarrow 1;$ *exit*.
(B)[*Later entry*] $m \leftarrow m + 1;\ x \leftarrow m;\ j \leftarrow 0;$

$(C)\ j \leftarrow j + 1;\ x \leftarrow \frac{x}{2};$ *if* x *is an integer, to* (C).

$(D)\ z \leftarrow (-1)^{\frac{x+1}{2}};$ *if* $= 2^n$, *final exit*; *EXIT*.

4. Procedure for COTS Components Ranking

4.1 COTS Components Searching and Screening

Initially, a search process is performed to find the suitable COTS components based on the availability of the documentation that describes it, the familiarity of the community and its domain of applicability. An assumption is made that the COTS components actually considered fulfill all functional requirements of the target system.

4.2 Formation of Evaluation team

In the existing COTS selection and evaluation literature, the data that can be used for ranking of pre-selected COTS component are unattainable, due to lack of maturity in this field. So, the reliance on the expert's opinion was the optimal approach to the problem of collecting selection and evaluation data for COTS components. The first step is to form a team of experts who represent a wide variety of experiences as is obtained in universities/consulting firms, software companies, or government agencies demonstrated by publications, hands on experience and managing research in the area of component based software engineering related to the issues under study and should also be versatile enough to address these issues. Some of the experts have been both in academia and in company. Members of the software companies may have better insight into the issues of this study, whereas academia may have better measures of knowledge in experimental development and it is at the edge of technological advances. For this research, finally a team of ten experts was formed deliberately. All experts have more than 20 years experience in the area of component based software engineering. Out of these ten experts, six are from software industries, three from academics, and one of the software research laboratories.

4.3 Selection of Evaluation criteria

COTS components can be compared with the mean of several attributes, named as evaluation criteria. In this study, the evaluation criteria are categorized into four major categories as Quality, Technology, Strategic and Domain & Architectural factors. Each of the evaluation criteria relates to some particular aspects of the measure considered important to the objectives of the study. In this study, we choose the strategic factors criteria for the selection and ranking of COTS components as shown in Fig. 4.

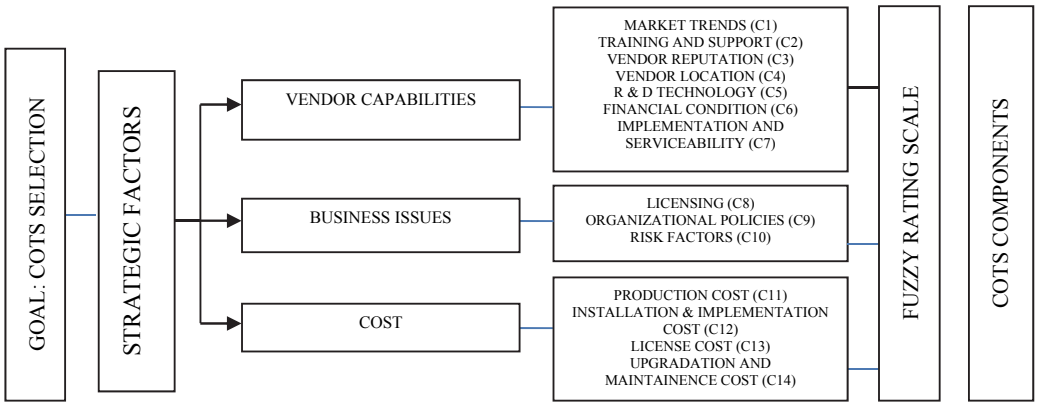

Fig. 4. COTS selection criterion

Strategic factors alone are considered in the present research work because all other criteria/factors are functionally required and hence must be fulfilled. Moreover, the strategic factors are the most common overlooked issue in the available literature. The available budget is very important which forces to consider the 'cost' criteria. Further, these criteria 'vendor capabilities' and 'business issues' play a vital role, even after the selection has been made. The brief description of the evaluation criteria considered in this study is provided in the Table 5.

Table 5
Definitions of Criteria/Sub-criteria

Evaluation Criteria/Sub-criteria	Description/Definition
Vendor Capabilities	
Market Trends	'Market Trends' deals with the concept that whether any particular vendor is going to develop cots according to the present user requirements in the market.
Training and Support	Whether the vendor provides some sort of training to learn the functionality of COTS provided by him?
Vendor Reputation	Vendor Reputation represents what the marketplace as a whole thinks of the vendor or manufacturer. If a vendor is well thought of, it is said to have a good reputation, if it is poorly regarded, its reputation is poor.
Vendor Location	Vendor location is referred as the locality or place where the vendor is located.
R & D Technology	R&D technology refers to the technological capabilities of the vendor.
Financial Condition	Financial condition deals with the financial position of the vendor in the market, i.e. "How much the vendor is financially strong"?
Implementation & Serviceability	Implementation and Serviceability are the property which represents the support of the implementation and further use of COTS provided by the vendor.
Business Issues	
Licensing Arrangements	An End User License Agreement (EULA) is a legal contract between a software application author or publisher and the user of that application.
Organizational Policies	An organizational policy is a formal document describing the organization's position on a particular aspect of compliance with regulations, standards, and guidelines.
Risk factors	How much risk is involved if the particular COTS component is used?
Cost	
Production Cost	The cost for the system at the time system fulfilling its expectations.
Installation & Implementation Cost	The cost incurred to make the system available for use.
License Cost	The cost for the permit from vendor to install the system.
Upgradation & Maintenance Cost	The cost incurred during the useful period of the system.

4.4 COTS evaluation of the fuzzy based matrix method

In the proposed methodology, the importance of the evaluation criteria and the performance ratings of the COTS components are assigned into linguistic variables by the experts. The linguistic variables are then converted into corresponding fuzzy numbers, triangular in nature, and then into crisp scores. The 'Criteria matrix' for each component is obtained using the aggregated average weights of the evaluation criteria and the performance ratings of the respective COTS component. The permanent value of each matrix is then determined in order to rank various alternate COTS components in ascending/descending order of merit. The COTS component having the highest value of the VPF is ranked at number 1, the next as number 2, and so on.

4.5 An Empirical Study

Databases are used to maintain internal records that support many business activities. With the rapid changes in computer technology and the decline of hardware costs, many applications are becoming database management systems. The database management system is specialized software which embodies the technology and the knowledge developed in the past several decades from where the supremacy of the databases is derived. A DBMS is a dominating tool which is capable to handle even very huge data, to control it efficiently and to store it for long periods of times. In this case study, the developed method is applied to select the best DBMS candidate to develop a website of an online store. The complete procedure is illustrated in the following steps:

4.5.1 COTS Candidates: Selection and Performance Rating

To select the COTS candidates related to database management system for the development of a website of an online store, initially the most popular and widely used websites were visited, namely: www.flashline.com; www.jars.com and www.componentsource.com. A number of possible DBMS COTS candidates were identified. The identified COTS candidates are then screened on the basis of the version, availability and compatibility etc. The candidates with obsolete version and no longer available in the open market are omitted. The potential COTS candidates are then shortlisted after brainstorming with the evaluation team of ten evaluators/experts. These evaluators are from the fields of information technology, database experts and academic researchers who are specialized in database system in various reputed industries and academic institutions and are termed as "Experts". The COTS candidates finally selected in this research are: (1) Oracle; (2) SQL Express; (3) MYSQL; (4) MS-Access and (5) Postgreys.

4.5.2 Data Collection

The questionnaire is considered to be the best way of collection of data in survey researches which are exploratory in nature. Since, no secondary data are available in the open literature and hence questionnaires are used to collect primary data. Two questionnaires were prepared. The first questionnaire is related to estimating the weights of the COTS evaluation criteria and the second questionnaire is used to get the performance ratings of the COTS components based on each evaluation criteria. The weights and ratings are obtained on a seven point fuzzy scale. The questionnaires are designed in three parts:

- The first part of each questionnaire contains a covering letter which explains the purpose of the research study and statement of confidentiality.
- Second part consists of demographic details e.g. name of the organization, field of expertise (software development, software design, software purchasing and procurement, etc.); length of experience, qualification and designation, etc. of the respondent expert/evaluator which are necessary to establish his credibility and suitability for the research work to be undertaken.
- Third part of the questionnaire consists of assigning weights to the evaluation criteria/performance ratings of the COTS components on a predetermined seven point fuzzy scale.

Two separate questionnaires were designed. The first questionnaire is used to get the weights of the identified evaluation criteria from the experts. Here, the weight of evaluation criteria means the level of importance of that criterion in the selection of any COTS component for the development of particular software. Since, all evaluation criteria are not equally important, it is necessary to find out their own importance. Ten experts were asked to rate the level of importance of each selection criterion considered in this study on a 7-point fuzzy scale in linguistic terms, namely: Extremely More Important (EMI), Very More Important (VMI), More Important (MI), Important (I), Less Important (LI), Very Less Important (VLI) and Extremely Less Important (ELI). The following principles are followed in assigning the weights to the criteria/sub-criteria:

- 'Extremely More Important' a linguistic term is assigned if the criterion is of greatest importance, whereas the linguistic term 'Extremely Less Important' is assigned if the criterion is of least importance. The in-between linguistic term is assigned based on the comparative importance of the criteria.

All questions are completely independent and sample questions are given in the Appendix. The weights of the criteria assigned by the experts in linguistic terms on a seven point fuzzy scale are given in Table 6.

Table 6
Criteria weights assigned by the Experts in linguistic terms on a 7-point fuzzy scale

	Criterion/Sub-Criterion	E1	E2	E3	E4	E5	E6	E7	E8	E9	E10
	Strategic Factors										
	Vendor Capabilities										
C1	Market Trends	I	LI	VMI	I	I	MI	LI	LI	I	MI
C2	Training and Support	MI	LI	I	I	I	MI	MI	MI	LI	I
C3	Vendor Reputation	MI	I	MI	LI	LI	I	MI	I	I	LI
C4	Vendor Location	I	I	MI	I	I	I	LI	MI	LI	I
C5	R & D Technology	I	I	LI	I	I	LI	MI	LI	LI	LI
C6	Financial Condition	VMI	MI	MI	I	I	MI	VMI	MI	MI	I
C7	Implementation and Serviceability	MI	MI	VMI	I	I	I	I	MI	VMI	MI
	Business Issues										
C8	Licensing Arrangements	VMI	VMI	I	MI	MI	I	VMI	MI	I	I
C9	Organizational Policies	EMI	MI	VMI	MI	MI	MI	EMI	MI	VMI	MI
C10	Risk factors	VMI	VMI	MI	VMI	VMI	VMI	MI	VMI	MI	MI
	Cost										
C11	Production Cost	MI	MI	EMI	VMI	MI	VMI	VMI	MI	I	MI
C12	Installation and Implementation Cost	VMI	MI	MI	I	MI	I	VMI	MI	I	I
C13	License Cost	VMI	I	LI	I	I	MI	LI	LI	I	I
C14	Upgradation and Maintenance Cost	MI	I	VMI	I	MI	MI	I	VMI	VMI	I

These linguistic terms are converted into TFNs in accordance to Table 4. The TFNs of all the ten experts are then aggregated and averaged arithmetically i.e. simple arithmetic mean is calculated using Eqs. (4-5). The TFN corresponding to the arithmetic mean is then converted into a single numeric value known as crisp value using Eqs. (5-10). For example: the crisp value for the importance of the criterion 'Market Trends' is calculated as given in Table 7.

Table 7
Crisp value calculation

Expert	Linguistic Term	TFN	Aggregation of TFN	Arithmetic Mean TFN
E1	I	0.4, 0.5, 0.6	(0.4+0.2+0.8+0.4+0.4+0.6+0.2+0.2+0.4+0.6,	= (4.2, 5.2, 6.2)/10
E2	LI	0.2, 0.3, 0.4	0.5+0.3+0.9+0.5+0.5+0.7+0.3+0.3+0.5+0.7,	= (4.2/10, 5.2/10, 6.2/10)
E3	VMI	0.8, 0.9, 1	0.6+0.4+1.0+0.6+0.6+0.8+0.4+0.4+0.6+0.8)	= (0.42, 0.52, 0.62)
E4	I	0.4, 0.5, 0.6	= (4.2, 5.2, 6.2)	
E5	I	0.4, 0.5, 0.6		
E6	MI	0.6, 0.7, 0.8		
E7	LI	0.2, 0.3, 0.4		
E8	LI	0.2, 0.3, 0.4		
E9	I	0.4, 0.5, 0.6		
E10	MI	0.6, 0.7, 0.8		

The arithmetic mean TFN is then converted into crisp value using Eqs. (6-10). The corresponding crisp values for the importance of all 14 criteria are obtained in the same manner. The weight of each criterion

is determined by normalizing the importance in such a way that the total weight of all evaluation criteria is unity. The weights (local and global weights) of all criteria are so calculated and given in Table 8.

Table 8
Weights (Local and Global) for evaluation criteria

S. No.	Criterion/Sub-Criterion	Local Weight	Global Weight	S. No.	Criterion/Sub-Criterion	Local Weight	Global Weight
	Vendor Capabilities	-	0.4415		**Business Issues**	-	0.2605
C1	Market Trends	0.1367	0.06035	C8	Licensing Arrangements	0.2967	0.07729
C2	Training and Support	0.1415	0.06247	C9	Organizational Policies	0.3496	0.09107
C3	Vendor Reputation	0.1319	0.05823	C10	Risk factors	0.3837	0.09995
C4	Vendor Location	0.1319	0.05823		**Cost**	-	0.2980
C5	R & D Technology	0.1127	0.04975	C11	Production Cost	0.2931	0.08734
C6	Financial Condition	0.1751	0.07730	C12	Installation & Implementation Cost	0.2522	0.07515
C7	Implementation & Serviceability	0.1703	0.07518	C13	License Cost	0.1954	0.05822
				C14	Upgradation & Maintenance Cost	0.2593	0.07727

The second questionnaire is used to get the performance ratings of five potential COTS components, namely (i) Oracle (ii) SQL-Express (iii) MYSQL (iv) Ms-Access (v) Postgreys, undertaken to be ranked in the present research paper. The experts are asked to rate the performance of each COTS component, one by one, against each evaluation criteria on a 7-point fuzzy scale containing linguistic terms as: Very High; High; Above Average; Average; Below Average; Low and Very Low. The following principle is followed while assigning the values:

- 'Very High' a linguistic term is assigned if the performance of any COTS component is maximum among all of that evaluation criteria for a particular application, whereas the linguistic term 'Very low' is assigned if the performance is at the lowest possible level. The in-between linguistic term is assigned based on the comparative performance. In case of sub-criteria under 'Cost', the linguistic terms are assigned in reverse order, e.g. linguistic term 'Very High' is assigned if the cost of that COTS component is minimum and 'Very low', if the cost is maximum.

The linguistic terms assigned by the experts for performance ratings of all five DBMS COTS against each selection criterion are given in Table 9.

Table 9
Linguistic assessments for COTS components

COTS/ Criterion	Experts	C1	C2	C3	C4	C5	C6	C7	C8	C9	C10	C11	C12	C13	C14
Oracle	E1	AA	BA	H	AA	BA	AA	AA	BA	BA	H	BA	BA	BA	BA
	E2	AA	L	H	BA	AA	BA	AA	BA	BA	AA	BA	L	BA	BA
	E3	A	BA	AA	L	A	BA	A	BA	L	H	BA	L	BA	BA
	E4	A	BA	AA	A	AA	L	A	A	L	H	L	BA	BA	BA
	E5	A	L	H	BA	BA	VL	AA	L	L	H	L	BA	BA	L
	E6	AA	VL	BA	A	A	BA	AA	L	BA	AA	BA	L	BA	L
	E7	AA	BA	AA	BA	AA	BA	AA	A	VL	AA	BA	L	BA	VL
	E8	AA	L	A	L	AA	BA	A	BA	BA	A	L	BA	L	L
	E9	A	A	H	A	A	L	BA	A	BA	AA	BA	BA	A	BA
	E10	A	BA	A	BA	AA	L	A	BA	BA	AA	A	L	VL	BA
SQL Express	E1	AA	BA	H	A	AA	BA	AA	BA	BA	H	BA	BA	BA	BA
	E2	A	BA	H	BA	AA	BA	A	BA	BA	H	BA	L	BA	BA
	E3	AA	A	H	AA	AA	A	AA	A	A	AA	A	A	BA	A
	E4	AA	A	AA	H	AA	A	AA	AA	A	A	A	BA	BA	BA
	E5	A	A	AA	A	AA	BA	A	BA	A	A	A	BA	A	BA
	E6	AA	AA	H	AA	H	BA	AA	A	BA	A	BA	A	BA	BA
	E7	A	AA	H	H	AA	AA	A	AA	A	BA	AA	BA	L	A
	E8	A	AA	AA	H	H	BA	AA	A	A	A	A	A	A	A
	E9	AA	H	AA	AA	H	AA	H	BA	AA	BA	A	BA	BA	BA
	E10	AA	A	AA	H	AA	A	H	BA	A	A	AA	A	BA	A

Table 9 (Continued)
Linguistic assessments for COTS components

COTS/ Criterion	Experts	C1	C2	C3	C4	C5	C6	C7	C8	C9	C10	C11	C12	C13	C14
MYSQL	E1	VH	H	H	A	H	VH	H	H	BA	A	VH	VH	VH	AA
	E2	H	VH	H	AA	H	H	AA	H	A	AA	VH	H	H	H
	E3	H	H	AA	AA	AA	H	AA	AA	AA	AA	H	H	H	AA
	E4	AA	H	H	A	H	VH	H	AA	A	H	VH	VH	H	H
	E5	H	AA	AA	AA	AA	H	AA	H	AA	AA	H	H	VH	AA
	E6	AA	AA	A	AA	AA	AA	H	AA	AA	H	VH	H	H	H
	E7	VH	VH	H	AA	H	H	H	H	A	H	VH	VH	VH	H
	E8	AA	AA	AA	A	H	VH	H	AA	A	AA	VH	VH	H	VH
	E9	H	VH	H	AA	H	H	AA	H	A	AA	VH	H	VH	H
	E10	H	H	H	AA	H	H	AA	H	A	H	AA	VH	VH	H
Ms-Access	E1	L	BA	BA	BA	BA	BA	A	A	A	H	BA	BA	BA	BA
	E2	BA	BA	AA	A	BA	A	A	BA	BA	AA	A	A	BA	BA
	E3	A	A	A	A	A	A	AA	A	A	AA	A	BA	A	BA
	E4	A	BA	A	AA	A	BA	A	A	A	AA	A	A	A	A
	E5	A	BA	AA	A	BA	A	A	A	BA	A	BA	A	BA	A
	E6	L	A	BA	BA	L	BA	BA	A	BA	AA	A	BA	A	A
	E7	BA	L	BA	BA	A	A	A	BA	BA	A	BA	L	BA	A
	E8	A	A	A	AA	L	BA	BA	L	BA	A	L	BA	A	A
	E9	BA	BA	A	A	BA	A	A	BA	A	AA	A	BA	A	BA
	E10	A	BA	BA	AA	L	BA	BA	A	BA	A	BA	L	BA	BA
Postgreys	E1	VH	H	H	A	H	VH	H	H	BA	A	VH	VH	VH	AA
	E2	H	H	H	AA	VH	VH	AA	AA	BA	A	VH	H	VH	H
	E3	AA	H	AA	AA	H	H	H	H	L	AA	H	AA	H	AA
	E4	H	AA	H	H	VH	AA	H	AA	A	AA	VH	H	VH	H
	E5	AA	AA	A	AA	AA	H	AA	H	BA	AA	VH	H	VH	H
	E6	VH	H	H	A	H	VH	H	H	BA	A	H	VH	VH	AA
	E7	H	H	H	AA	H	VH	AA	AA	A	A	VH	AA	H	H
	E8	AA	H	AA	AA	H	H	H	H	L	AA	VH	VH	H	H
	E9	H	AA	AA	H	VH	AA	H	AA	A	AA	VH	H	VH	H
	E10	AA	H	A	A	AA	H	AA	H	A	AA	VH	H	VH	H

Then, performance ratings assigned by the experts are converted into triangular fuzzy numbers and crisp values through aggregation and arithmetic averaging as explained in the above paragraph. The values, so obtained, are given in Table 10.

Table 10
Crisp values of DBMS COTS components

Criterion/ Sub-Criterion		ORACLE	SQL EXPRESS	MYSQL	MS-ACCESS	POSTGREYS
Strategic Factors		0.3864	0.5079	0.7960	0.4246	0.7600
Vendor Capability		0.4675	0.6042	0.7935	0.4117	0.7928
C1	Market Trends	0.5909	0.6091	0.8363	0.3727	0.8182
C2	Training and Support	0.2500	0.5545	0.8500	0.3546	0.8091
C3	Vendor Reputation	0.7000	0.7727	0.7727	0.4636	0.7363
C4	Vendor Location	0.3364	0.6818	0.6273	0.5000	0.6454
C5	R & D Technology	0.5909	0.7363	0.8091	0.3182	0.8682
C6	Financial Condition	0.2318	0.4636	0.8863	0.4091	0.8818
C7	Implementation and Serviceability	0.5727	0.6636	0.7727	0.4636	0.7909
Business Issues		0.4349	0.4879	0.6879	0.4758	0.5848
C8	Licensing Arrangements	0.3364	0.4455	0.7909	0.4091	0.7909
C9	Organizational Policies	0.2318	0.4636	0.5364	0.3909	0.3546
C10	Risk Factors	0.7363	0.5545	0.7363	0.6273	0.6091
Cost		0.2568	0.3955	0.9068	0.3864	0.9023
C11	Production cost	0.2818	0.4818	0.9409	0.3909	0.9727
C12	Installation and Implementation cost	0.2273	0.3727	0.9318	0.3364	0.8682
C13	License Cost	0.2864	0.3364	0.9318	0.4091	0.9591
C14	Upgradation and Maintenance Cost	0.2318	0.3909	0.8227	0.4091	0.8091

The ‘Criteria Matrices’ are formed for each of the COTS components and the value of the Permanent of each such ‘Criteria Matrix’ is determined and given as under:

$$[POSTGREYS] = \begin{bmatrix} 0.8182 & 1.035113 & 0.964887 & 0.964887 & 0.824433 & 1.280907 & 1.245794 \\ 0.966078 & 0.8091 & 0.932155 & 0.932155 & 0.796466 & 1.237456 & 1.203534 \\ 1.036391 & 1.072782 & 0.7363 & 1 & 0.854435 & 1.327521 & 1.29113 \\ 1.036391 & 1.072782 & 1 & 0.6454 & 0.854435 & 1.327521 & 1.29113 \\ 1.212955 & 1.255546 & 1.170364 & 1.170364 & 0.8682 & 1.553682 & 1.511091 \\ 0.780697 & 0.80811 & 0.753284 & 0.753284 & 0.643632 & 0.8818 & 0.972587 \\ 0.802701 & 0.830887 & 0.774516 & 0.774516 & 0.661773 & 1.028186 & 0.7909 \end{bmatrix}$$

$$[ORACLE] = \begin{bmatrix} 0.5909 & 1.035113 & 0.964887 & 0.964887 & 0.824433 & 1.280907 & 1.245794 \\ 0.966078 & 0.25 & 0.932155 & 0.932155 & 0.796466 & 1.237456 & 1.203534 \\ 1.036391 & 1.072782 & 0.7 & 1 & 0.854435 & 1.327521 & 1.29113 \\ 1.036391 & 1.072782 & 1 & 0.3364 & 0.854435 & 1.327521 & 1.29113 \\ 1.212955 & 1.255546 & 1.170364 & 1.170364 & 0.5909 & 1.553682 & 1.511091 \\ 0.780697 & 0.80811 & 0.753284 & 0.753284 & 0.643632 & 0.2318 & 0.972587 \\ 0.802701 & 0.830887 & 0.774516 & 0.774516 & 0.661773 & 1.028186 & 0.5727 \end{bmatrix}$$

$$[SQLEXPRESS] = \begin{bmatrix} 0.6091 & 1.035113 & 0.964887 & 0.964887 & 0.824433 & 1.280907 & 1.245794 \\ 0.966078 & 0.5545 & 0.932155 & 0.932155 & 0.796466 & 1.237456 & 1.203534 \\ 1.036391 & 1.072782 & 0.7727 & 1 & 0.854435 & 1.327521 & 1.29113 \\ 1.036391 & 1.072782 & 1 & 0.6818 & 0.854435 & 1.327521 & 1.29113 \\ 1.212955 & 1.255546 & 1.170364 & 1.170364 & 0.7363 & 1.553682 & 1.511091 \\ 0.780697 & 0.80811 & 0.753284 & 0.753284 & 0.643632 & 0.4636 & 0.972587 \\ 0.802701 & 0.830887 & 0.774516 & 0.774516 & 0.661773 & 1.028186 & 0.6636 \end{bmatrix}$$

$$[MYSQL] = \begin{bmatrix} 0.8363 & 1.035113 & 0.964887 & 0.964887 & 0.824433 & 1.280907 & 1.245794 \\ 0.966078 & 0.85 & 0.932155 & 0.932155 & 0.796466 & 1.237456 & 1.203534 \\ 1.036391 & 1.072782 & 0.7727 & 1 & 0.854435 & 1.327521 & 1.29113 \\ 1.036391 & 1.072782 & 1 & 0.6273 & 0.854435 & 1.327521 & 1.29113 \\ 1.212955 & 1.255546 & 1.170364 & 1.170364 & 0.8091 & 1.553682 & 1.511091 \\ 0.780697 & 0.80811 & 0.753284 & 0.753284 & 0.643632 & 0.8863 & 0.972587 \\ 0.802701 & 0.830887 & 0.774516 & 0.774516 & 0.661773 & 1.028186 & 0.7727 \end{bmatrix}$$

$$[MS-ACCESS] = \begin{bmatrix} 0.3727 & 1.035113 & 0.964887 & 0.964887 & 0.824433 & 1.280907 & 1.245794 \\ 0.966078 & 0.3546 & 0.932155 & 0.932155 & 0.796466 & 1.237456 & 1.203534 \\ 1.036391 & 1.072782 & 0.4636 & 1 & 0.854435 & 1.327521 & 1.29113 \\ 1.036391 & 1.072782 & 1 & 0.5 & 0.854435 & 1.327521 & 1.29113 \\ 1.212955 & 1.255546 & 1.170364 & 1.170364 & 0.3182 & 1.553682 & 1.511091 \\ 0.780697 & 0.80811 & 0.753284 & 0.753284 & 0.643632 & 0.4091 & 0.972587 \\ 0.802701 & 0.830887 & 0.774516 & 0.774516 & 0.661773 & 1.028186 & 0.4636 \end{bmatrix}$$

Finally, the ranking values of all five COTS components and their respective rankings are obtained and presented in Table 11.

Table 11
Ranking values and ranks of COTS components using the Fuzzy Matrix method

COTS Components	Vendor Capabilities		Business Issues		Cost		Strategic Concerns	
	Ranking Values	**Rank**	**Ranking Values**	**Rank**	**Ranking Values**	**Rank**	**Ranking Values**	**Rank**
ORACLE	2951.624	4	3.3619	5	11.4531	5	3.2114	5
SQL EXPRESS	3514.206	3	3.5781	3	13.1198	3	3.6471	3
MYSQL	4097.519	1	4.37	1	21.8555	2	4.8832	1
MS-ACCESS	2797.631	5	3.5276	4	13.0069	4	3.3496	4
POSTGREYS	4095.037	2	3.9254	2	22.5906	1	4.6982	2

In order to validate the methodology and the results obtained, the present COTS component selection problem using the same datasets is solved using Distance based Approach (DBA) proposed by Kumar and Garg (2010). The results so obtained are given in Table 12.

Table 12
Overall Ranking of DBMS COTS Component using DBA

COTS Components	Vendor Capabilities		Business Issues		Cost		Strategic Concerns	
	Composite Distance	**Rank**	**Composite Distance**	**Rank**	**Composite Distance**	**Rank**	**Composite Distance**	**Rank**
ORACLE	4.69127	4	3.36158	5	4.337614	5	3.725443	5
SQL EXPRESS	2.432702	3	2.816597	4	3.477869	3	2.700875	3
MYSQL	0.487837	2	0	1	0.4568	2	0	1
MS-ACCESS	5.590946	5	2.538834	3	3.528409	4	3.423775	4
POSTGREYS	0.421601	1	2.229029	2	0.19439	1	1.011105	2

The comparison shows that the results obtained using the proposed method, i.e. the fuzzy matrix and DBA are same for the evaluation criteria – cost and strategic concerns. In case of evaluation criteria, namely 'Vendor Capabilities' and 'Business Issues' a minor difference in the rankings of two COTS components is observed. In case of fuzzy matrix method MYSQL is ranked at #1 followed by POSTGREYS whereas the Postgreys are ranked at #1 followed by MYSQL using DBA method. The reason is quite obvious that there is a negligible difference in the ranking values (4097.519 and 4095.037) of these two components using the fuzzy matrix method. The same pattern is observed in the ranking values, SQL Express and MS-Access components. It is thus evident that the fuzzy matrix method is validated.

5 Results

According to the methodology adopted in this empirical study, the higher the value of permanent implies better ranking. The comparative rankings of all five COTS components based on vendor capabilities, Business issues and cost individually as well as taken altogether is given in Fig. 5. It is depicted that MYSQL has been ranked first on the basis of vendor capabilities, Business issues and cost as evaluation criteria and is followed by Postgreys and SQL Express ranked at 2 and 3 and are top three DBMS cots components. Oracle is ranked at five based on Business issues and cost whereas

ranked at four based on vendor capabilities which shows the least use of this component. MYSQL is ranked at #1 based on strategic concern, i.e. considering all three evaluation criteria, namely vendor capabilities, Business issues and cost collectively, and is followed by Postgreys whereas Oracle is ranked at the last. Hence, Postgreys can be termed as an optimal COTS selection for this kind of problem considering all constraints inspite the fact that MS Access is a better option in terms of 'cost' than Postgreys.

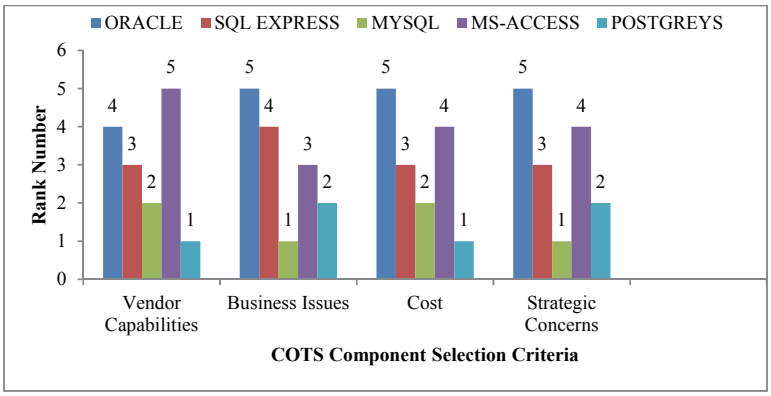

Fig. 5. Comparative rankings of COTS components

6 Conclusions

This paper addresses the issue of ranking the COTS using the state-of-art knowledge in the field of component based software engineering by applying fuzzy based matrix methodology. A set of evaluation criteria is identified; their weights and ratings are taken from various experts in linguistic terms. The following conclusions can be drawn from the study:

- As the triangular fuzzy numbers concept of fuzzy set theory is used in this study, the data collection, calculation and result interpretation become very easier for the experts due to the fact that FST is capable to accommodate the vagueness of mind and imprecise nature of the evaluation criteria.
- Interdependencies of the evaluation criteria have given a due consideration in the proposed methodology. The non-diagonal elements of the criteria matrix represent the interdependencies of the evaluation criteria which influence the value of the permanent function which is used to rank the alternate COTS components.
- A computer based decision support system (DSS) is developed for ranking of COTS on the basis of various evaluation criteria which is very user-friendly and do not require much technical knowledge. Once a complete database is prepared in terms of evaluation criteria/sub-criteria to be considered and the COTS components, the DSS may be used to rank the COTS components.

In terms of future work, it is necessary to rank the COTS components based on all four groups of evaluation criteria which includes both functional and non-functional requirements. Further, in case of large software systems, COTS components which are mutually dependent, should not be evaluated individually as single and local evaluation and selection may lead to sub-optimal solution from a global perspective.

Acknowledgement

The authors would like to thank the anonymous referees for constructive comments on earlier version of this paper.

References

Alves, C., & Castro, J. (2001, October). CRE: A systematic method for COTS components selection. In *XV Brazilian Symposium on Software Engineering (SBES)*. Rio de Janeiro, Brazil.

Alves, C., & Finkelstein, A. (2003). Investigating conflicts in COTS decision-making. *International Journal of Software Engineering and Knowledge Engineering*, *13*(05), 473-493.

Bertoa, M. F., & Vallecillo, A. (2002). Quality attributes for COTS components. *I+ D Computacion, 1* (2), 128-143.

Boehm, B., Port, D., & Yang, Y. (2003, May). WinWin spiral approach to developing COTS-based applications. In *EDSER-5 5 th International Workshop on Economic-Driven Software Engineering Research* (p. 57).

Burgués, X., Estay, C., Franch, X., Pastor, J. A., & Quer, C. (2002). Combined selection of COTS components. In *COTS-Based Software Systems* (pp. 54-64). Springer Berlin Heidelberg.

Cavanaugh, B. P., & Polen, S.M. (2002). Add decision to your COTS selection process. *The Journal of Defense Software Engineering*, 21-25.

Chen, S. H. (1985). Ranking fuzzy numbers with maximizing set and minimizing set. *Fuzzy sets and Systems*, *17*(2), 113-129.

Chung, L., & Cooper, K. Matching, ranking, and selecting COTS components: A COTS-aware requirements engineering approach.

Cortellessa, V., Marinelli, F., & Potena, P. (2006). Automated selection of software components based on cost/reliability tradeoff. In *Software Architecture* (pp. 66-81). Springer Berlin Heidelberg.

Dahiya, S., Jain, D. K., Kumar, A., Garg, R. K., & Gupta, V. K. (2007). Power quality evaluation in deregulated power system using matrix method.*International Journal of Global Energy Issues*, *28*(1), 1-10.

Dubois, D., & Prade, H. (1979). Fuzzy real algebra: some results. *Fuzzy sets and systems*, *2*(4), 327-348.

Erol, I., & Ferrell, W. G. (2003). A methodology for selection problems with multiple, conflicting objectives and both qualitative and quantitative criteria.*International Journal of Production Economics*, *86*(3), 187-199.

Fauziah Baharom, Feras Tarawnch, Jamaiah Hj. Yahaya, Azida Zainol, Nurnasran Puteh, Haslina Mohd, Norida Muhd Darus, Zaharin Marzuki Matt, Azman Yasin. (July, 2012). The Vendor and User Organizations Characterstics for COTS Softwre evaluation and Selection. Malaysia : Knowledge Management International Conference,

Firesmith, D. (2005). Achieving Quality Requirements with Reused Software Components: Challenges to Successful Reuse. *MPEC'05*.

Garg, R. K., Sharma, K., Nagpal, C. K., Garg, R., Garg, R., & Kumar, R. (2013). Ranking of software engineering metrics by fuzzy-based matrix methodology. *Software Testing, Verification and Reliability*, *23*(2), 149-168.

Grau, G., Carvallo, J. P., Franch, X., & Quer, C. (2004, August). DesCOTS: a software system for selecting COTS components. In *Euromicro Conference, 2004. Proceedings. 30th* (pp. 118-126). IEEE.

Gregor, S., Hutson, J., & Oresky, C. (2002). Storyboard process to assist in requirements verification and adaptation to capabilities inherent in COTS. In*COTS-Based Software Systems* (pp. 132-141). Springer Berlin Heidelberg.

Gupta, P., Mehlawat, M. K., & Verma, S. (2012). COTS selection using fuzzy interactive approach. *Optimization Letters*, *6*(2), 273-289.

Gupta, P., Pham, H., Mehlawat, M. K., & Verma, S. (2013). A fuzzy optimization framework for COTS products selection of modular software systems. *International Journal of Fuzzy Systems*, *15*(2), 91-109.

Gupta, P., Verma, S., & Mehlawat, M. K. (2011). A membership function approach for cost-reliability trade-off of COTS selection in fuzzy environment. *International Journal of Reliability, Quality and Safety Engineering*, *18*(06), 573-595.

Ibrahim, H., Far, B. H., & Eberlein, A. (2009, April). Tradeoff and Sensitivity Analysis of a Hybrid Model for Ranking Commercial Off-the-Shelf Products. In *Engineering of Computer Based Systems, 2009. ECBS 2009. 16th Annual IEEE International Conference and Workshop on the* (pp. 119-127). IEEE.

Kaur, K., & Singh, H. (2014). Quantifying COTS Components Selection using Multi Criteria Decision Analysis Method-PROMETHEE. *Global Journal of Computer Science and Technology*, *14*(2).

Kontio, J. (1995). OTSO: a systematic process for reusable software component selection.

Kumar, R., & Garg, R. K. (2010). Optimal selection of robots by using distance based approach method. *Robotics and Computer-Integrated Manufacturing*, *26*(5), 500-506.

Kunda, D., & Brooks, L. (1999, April). Applying social-technical approach for COTS selection. In *Proceedings of the 4th UKAIS Conference* (pp. 552-565).

Kwong, C. K., Mu, L. F., Tang, J. F., & Luo, X. G. (2010). Optimization of software components selection for component-based software system development. *Computers & Industrial Engineering*, *58*(4), 618-624.

Lichota, R. W., Vesprini, R. L., & Swanson, B. (1997, June). PRISM Product Examination Process for component based development. In *Assessment of Software Tools and Technologies, 1997., Proceedings Fifth International Symposium on* (pp. 61-69). IEEE.

Lozano-Tello, A., & Gómez-Pérez, A. (2002, July). BAREMO: how to choose the appropriate software component using the analytic hierarchy process. In*Proceedings of the 14th international conference on Software engineering and knowledge engineering* (pp. 781-788). ACM.

Maiden, N. A., & Ncube, C. (1998). Acquiring COTS software selection requirements. *Software, IEEE*, *15*(2), 46-56.

Mohamed, A., Ruhe, G., & Eberlein, A. (2007, February). Decision support for handling mismatches between COTS products and system requirements. In *Commercial-off-the-Shelf (COTS)-Based Software Systems, 2007. ICCBSS'07. Sixth International IEEE Conference on* (pp. 63-72). IEEE.

Morisio, M., & Tsoukiàs, A. (1997, June). IusWare: a methodology for the evaluation and selection of software products. In *Software Engineering. IEE Proceedings*-Vol. 144, No. 3, pp. 162-174). IET.

Nazir, S., Anwar, S., Khan, S. A., Shahzad, S., Ali, M., Amin, R., ... & Cosmas, J. (2014, December). Software component selection based on quality criteria using the analytic network process. In *Abstract and Applied Analysis* (Vol. 2014). Hindawi Publishing Corporation.

Neubauer, T., & Stummer, C. (2007, January). Interactive decision support for multiobjective COTS selection. In *System Sciences, 2007. HICSS 2007. 40th Annual Hawaii Int. Conf. on* (pp. 283b-283b). IEEE.

Oberndorf, P. A. (1997, June). Facilitating component-based software engineering: COTS and open systems. In *Assessment of Software Tools and Technologies, 1997., Proceedings Fifth International Symposium on* (pp. 143-148). IEEE.

Ravichandran, K. S., Sekar, K. R., & Suresh, P. (2013). A novel approach for optimal grouping of reusable software components for component based software development systems. *International Journal of Software Engineering and Knowledge Engineering*, *23*(07), 895-912.

Sarkar, Subhankar, (2012) Archiectecture centric Tradeoff: A Decision Support Method for COTS Selection and Life Cycle Management.International Conference on Software Engineering Advances.

Shyur, H. J. (2006). COTS evaluation using modified TOPSIS and ANP. *Applied mathematics and computation*, *177*(1), 251-259.

Suleiman, B. (2008, March). Commercial-off-the-shelf software development framework. In *Software Engineering, 2008. ASWEC 2008. 19th Australian Conference on* (pp. 690-695). IEEE.

Tran, V., & Liu, D. B. (1997, June). A procurement-centric model for engineering component-based software systems. In *Assessment of Software Tools and Technologies, 1997., Proceedings Fifth International Symposium on* (pp. 70-79). IEEE.

Vigder, M., Gentleman, W. M., & Dean, J. (1996). COTS Software Integration: State of the art.

Wang, B., & Sheng, J. (2008, December). Extending FCD Process to Support COTS Selection. In *Computer Science and Software Engineering, 2008 International Conference on* (Vol. 2, pp. 139-142). IEEE.

Wanyama, T., & Far, B. (2008). An empirical study to compare three methods for selecting COTS software components. *International Journal of Computing and ICT Research*, *2*(1), 34-46.

Wanyama, T., & Far, B. H. (2005, May). Towards providing decision support for COTS selection. In *Electrical and Computer Engineering, 2005. Canadian Conference on* (pp. 908-911). IEEE.

Yang, X., Dong, J., & Ghafoor, M. A. (2005, May). Prioritized selecting COTS vendor in cots-based software development process. In *Electrical and Computer Engineering, 2005. Canadian Conference on* (pp. 1939-1945). IEEE.

Zadeh, L. A. (1965). Fuzzy sets. *Information and Control*, *8*(3), 338-353.

Appendix

Sample Questions

Questionnaire - I

Q-1 What is the level of importance of 'Market Trends' for selection of DBMS COTS for the development of a website of an online store?

- Extremely More Important
- Very More Important
- More Important
- Important
- Less Important
- Very Less Important
- Extremely Less Important

Questionnaire - II

Q-2 To what extent the organizational policies are followed by the vendor of the COTS component "Oracle".

- Very High
- High
- Above Average
- Average
- Below Average
- Low
- Very Low

Q-3 What is the level of 'R & D Technology' being adopted by the vendor of "MYSQL?

- Very High
- High
- Above Average
- Average
- Below Average
- Low
- Very Low

Q-4 How you rate the COTS component "Postgreys" for its 'Upgradation and Maintenance Cost'?

- Very High
- High
- Above Average
- Average
- Below Average
- Low
- Very Low

Note: Please choose only one option in each question.

© 2016 by the authors; licensee Growing Science, Canada. This is an open access article distributed under the terms and conditions of the Creative Commons Attribution (CC-BY) license (http://creativecommons.org/licenses/by/4.0/).

Volume 4, Issue 2 (2016) 463-468 ISSN 2347 - 3258
International Journal of Advance Research and Innovation

Modeling and Microstructure Study of Thermally Evaporated Nano film Thickness of Gold

Shailendra Kumar Gaur, R. S. Mishra*
Department of Mechanical Engineering, Delhi Technological University, Delhi, India

Article Info

Article history:
Received 25 January 2016
Received in revised form
20 February 2016
Accepted 28 February 2016
Available online 15 March 2016

Keywords
Physical Vapor Deposition,
Modeling,
Film Thickness Simulation,
Thin Film Deposition,
Vacuum

Abstract

The paper represents the modeling of nano scale gold film thickness deposited by thermal evaporation process. Gold is evaporated from a resistively heated boat at a temperature of 1900 K onto a surface held on a fixed surface. The incident molecular flux onto the silicon surface is 7.86×10^{19} ($1/m^2sec$). The thickness varies between 78 nm and 80 nm across the sample after 60 s of deposition, with radial symmetry about the midpoint of the source. The film thickness, mass deposited on the substrate and mass transfer rate on silicon substrates with time dependent model using BDF solver is calculated. The SEM micrographs shows the smooth and uniformly distributed nano scale gold film on silicon and the average grain size of gold is 15-30 nm. The XRD analysis shows the polycrystalline face centered cubic (fcc) structure in preferential (111) plane. Deposited gold film thickness measured from Dektek surface profiler at different points on the substrate surface

1. Introduction

PVD is used for metals while dielectrics can be deposited using specialized equipments. It rely on thermal energy supplied to the crucible or boat to evaporate atoms. Evaporated atoms travel through the evacuated space between the source and the sample and stick to the sample. Few, if any, chemical reactions occur due to low pressure can force a reaction by flowing a gas near the crucible. Physical methods produce the atoms that deposit on the substrate by evaporation and sputtering. Sometimes called vacuum deposition because the process is usually done in an evacuated chamber Surface reactions usually occur very rapidly and there is very little rearrangement of the surface atoms after sticking. Thickness uniformity and shadowing by surface topography, and step coverage are issues. Ali Moarrefzadeh et al. [1] discussed that Physical vapor deposition (PVD) includes a wide range of vacuum coating processes in which material is physically taken out from a source by evaporation or sputtering, transported through a vacuum or partial vacuum by the energy of the vapor particles, and condensed as a film on the surfaces of appropriately placed parts or substrates. A group of very versatile coating processes in which a material is converted to its vapor phases in a vacuum chamber and condensed onto a substrate surface as a very thin film(upto 1 μm thickness). The deposition of thin film layers from the vapor phase is done through several methods. We study and analyze the physical vapor deposition (PVD) techniques and equipments that are in common use in the large scale production of coatings that find uses in the optical, display, decorative, tribological, and energy-generating /saving industries. Evaporating materials are classified as dielectric compounds, metals, alloys, or mixtures. The same evaporant material can exhibit different optical, electrical, and mechanical properties depending on the deposition process. Titanium oxide is a unique example of a metal oxide compound that, depending on deposition process parameters, can be made into film layers that are: transparent, electrically conductive, chemically reactive to light and bio- agents, chemically inert, or exhibit spectrally selectively absorption. The dependent parameters are starting composition, oxidation state, and crystalline structure and packing density. PVD techniques used generally are basically two in nature: thermal evaporation by resistively heating or by using an electron- beam heating, and sputtering, a no thermal process. P.S.Raghupathi et.al. [2] and Haichuan Mu et.al. [3] discussed that the thermal evaporation deposition rate influence the structural, electrical & optical properties of thin film deposited like in case of Indium-tin-oxide(ITO).Alterations and accompaniments are made to the basic PVD techniques to permit different coating materials and substrate types to be included additions designed to alter the growth nano-structure or composition of the film through control of the dependent variables listed above include bombardment of the growing film by high energy inert- or and reactive ions, substrate heating, atmosphere composition and partial pressure, rate, and vapor incidence angle.

***Corresponding Author,**
E-mail address: professor_rsmishra@yahoo.co.in
All rights reserved: http://www.ijari.org

2. Literature Review

The nanoscale gold film thickness has found newer capabilities in different fields of science & technology such as coating glasses/mica to change their properties and many coloured optical coding for biological assays. Gold nanometer thick film is being used to enhance electro luminescence and quantum efficiency in light emitting diodes. Besides signal amplification, nanometer thick gold film evoluted new types of new sensors that are capable of detecting very small amounts of analyses such as chemical vapors in the scale of few ppm. Adeleh Granmayeh Rad et al [4] discussed the usage of gold nano film is in making advanced dyes and pigments. Sometimes gold nano film has been used to dye textiles, support to supply clean energy (by solar cell) and high density data storage (flash memories and discs). Gold nanoscale film quality of non-toxic and biocompatibility both in vivo and in vitro environments makes useful in bio-medical applications.

The unique properties of gold nanoscale structured materials supply good opportunity for coordinating biological identification events with electronic signal transduction and for making an evolution of bioelectronics devices with newer features. Gold in nanoscales have been found for potential candidates to support in photo-thermal therapy and radiotherapy. Optical and electronic properties of gold can be utilized to improve the contrast in molecular imaging for the detection of cancer initially. Gold-based technologies also help to facilitate a ultimate needle-free delivery system, a technique that used gold and permitted vaccines to be supplied through the skin producing use of the fact that small particles can go through gaps between cells while large ones cannot. Gold nanoscale- based technologies give solution to some of environmentally great issues, such as ecofriendly production methods, pollution control and water purification. No doubt gold is really one of the non- reactive metals, and it is resistant to oxidation**.** Ragini Raj Singh et al. [5] discussed gold is also used in Photovoltaic HgCdTe Mid wavelength Infra-red detector to make ohmic contacts to find out the passivation characterstics of CdS/HgCdTe structure using C-V measurements. Wenjun Zhou et.al [6] discussed the Chemical vapour deposition (CVD) generally uses a gas-phase precursor, often a halide or hydride of the element to be deposited. In the case of MOCVD, an organometallic gas is used. Commercial techniques often use very low pressures of precursor gas. The chamber is first evacuated to a vacuum of around 5m torr and substrate temperature fixed to 350°C. Now evaporator is resistively heated to a temperature of about 160°Cto start volatilization of the precursor. The deposited precursor then thermally decomposes into pure gold by a reaction above 300°C. The thickness of the gold film can be controlled by adjusting the amount of precursor, the temperature of the deposition chamber, and the location of the samples to be coated relative to the inlet of the evaporator into the deposition chamber. Generally gold precursor is thermally stable between 150 and 300 °C. Keewah Chan et al [7] discussed that gold can be deposited on silicon or quartz by rf sputtering by using DC sputter coating system. The rf power can of several hundred watt, substrate temperature about 300 °C with a vacuum of 1mbar order or better for time depending upon the thickness required, say for nanometer thickness 1 hour. Carl E. Larson et al. [8] discussed that gold deposition of high purity gold onto various substrates from dimethyl-2fl- pentandionato gold (III), Me2Au (acac), by localized, laser- induced (photothermal) chemical vapor deposition. CVD of gold from dimethyl-(1,1,1-trifluoro-2,4-pentandionato) gold (III) and dimethyl-(1,1,1,5,5,5-hexafluoro-2,4- pentandionato) gold(III),Me2Au(tfac) and Me2Au(hfac) complex can be done in a stainless steel vacuum chamber evacuated by a turbomolecular/diffusion/cryo pump to a base pressure of < 10 -6 torr. A flow of argon or nitrogen carrier gas through a Pyrex vessel containing the gold complex at room temperature is used to deliver the organogold precursor into the chamber through stainless steel lines. Chamber vacuum and carrier gas flow rate could be varied independently. Deposition proceeds on a substrate placed in the chamber in the flow path of the carrier gas and heated by a copper block heater with temperature controller. Miroslav Gojo et al [9] discussed that gold can be deposited in a thermostatically controlled electode cells in a electrodeposition Cell has two openings, one for thermometer another for nitrogen inlet for purging the oxygen out of the electrolyte keeping pH value 5 to 7 and each silicon wafer piece coated and alloyed with gold as working electrode, filled with chosen electrolyte warmed upto a given temperature and purged with nitrogen. Gold deposited by electrochemical method has higher purity, lower permeability and good adhesion to the substrate. Anne-Felicie Lamic-Humblot et al[10] discussed that gold can be very easily deposited at ambient pressure and in distilled water with magnetic rod stirring , followed by thermal treatment from tetrachloroauric acid and urea. T. Donnely et.al.[11] discussed that gold on nano scale can be deposited on Si and sapphire by pulse laser deposition(PLD) by Nd : laser operating at 1064, 20Hz and pulse length of 6 nano sec used in a vacuum. The PLD deposited gold nano scale film is characterized and below 5 nm equivalent thickness AFM confirms the nano particles while optical measurement shows surface plasmon resonance shifts to longer wavelengths with increasing thickness. X.Zhang et.al.[12] discussed that gold film deposited on a quartz crystal ablated by excimer laser and found that ablation rate is more than two order higher than surface vaporization model prediction. Also this ablation rate strictly dependent on gas pressure. Anna Schaub et.al [13] discussed that gold deposited by vacuum evaporation on glass substrate without heating glass and with heated glass. Further characterization is done of those deposited films i.e. without heated glass, without heated glass followed by annealing at 300 °C and heated glass, finding that heating during evaporation results in decrease in roughness and morphology changes with heating and annealing conditions. Behrang Moazzez et.al.[14] stated that the good adhesion gold on electronic device such as sensors, MEMS etc. making surface can be improved by applying gold deposition step on SU-8 photo resist prior to UV exposure but after the pre-bake step of SU-8 processing. Maxime Gougis et al. [15] discussed the gold deposition by pulse laser ablation on carbon nano-tube electrode but with in presence of oxygen and confirmed the non oxide formation by characterization. C. Celed´on et.al.[16] discussed that the surface roughness affects on the energy straggling associated to the energy loss distributions of protons transmitted through a self supported metallic thin foil. Hartmann Hieber and Karin Pape [17] discussed the ageing of gold stating that degradation under thermal and electrical fault and in contaminated conditions is very low that is why gold is better than other metallization. Adam Proszynski et al [18] discussed that stress is developed during vacuum evaporation of gold nanometer film which can be reduced by post annealing process and further characterized the film for confirmation. Thin tin oxide deposited surface is very useful in industries due to their properties such as n-type Semi-conductor character, high optical transmission in visible range, high reflectivity; in the infra-red as well as good chemical resistance. Thus they can be used to form transparent and chemically stable thermal barriers.

3. Research Gap Identified

A lot of research work has been done on the evolution of gold film deposited on nanoscale or higher thickness by different deposition process through different heating sources (resistively, sputtering, E-beam, magnetron, radio frequency) in different baskets/crucibles at different temperatures and modeled mostly with direct simulation monte carlo. Also these methods solve in the volumes of the modeled and geometries. Number densities found to be not accurate and precise. Ineligible simulation for the accurate modeling of low pressure, low velocity gas flows in complex geometries. These studies subjected to statistical scatter. Moreover, these could not completely explained free molecular flow interface and applied direct simulation monte carlo (dsmc) computes the trajectories of large numbers of randomized particles through the system, but introduces statistical noise to the modeling process and also the method is slower. Moreover, present work emphasis on the thermal and mass transfer of thermal evaporation process as well as structural analysis of deposited thin films leading to better optimization of thermal evaporation process and development of suitable electronic device fabrication applications.

4. Experimental Details

Generally during thermal evaporation of gold island films were prepared using a laboratory thermal evaporation setup as shown in figure 1 working at residual vacuum of (2.5 - 4) × 10^{-6} mbar. The deposition setup was equipped with the two-stage vacuum system based on the diffusion pump (oil based), turbomolecular or cryopump along with rotary vane pump or rotary screw pump (oil free). In case of oil based pumps the ultimate vacuum achieved in the system depends upon the vapor pressure of the oil used in pumps, generally Silicone based oils are used to achieve vacuum of 1.0 x 10^{-6} or higher order in the chamber. Thermal evaporation system consists of multi turret to resistively heat molybdenum boat or tungsten filament/basket into source material (gold, tin or indium) is kept, radiant heater, quartz crystal assembly. To measure the film thickness during process as well as rate of deposition, it consists of digital thickness monitor (DTM) which is basically a piezoelectric transducer. It consists of quartz crystal of standard 6MHz frequency with crystal assembly and digital monitor .This frequency of crystal decreases with damped oscillation during deposition with time and for this crystal oscillator is attached with crystal assembly as shown in figure 3.3. This quartz crystal needs regular cleaning with certain chemical depending upon the evaporant (source) material. Furthur this thickness of deposited film can be measured with dektek surface profilometer. To measure the rotary pump and turbo molecular pump vacuum thermal evaporation system consists of pirani gauge and penning gauge with gauge head. For initial pre-heating of source material (gold) to remove oxides etc a source shutter is provided in the system. A liquid nitrogen trap is provided inside the thermal evaporation of system to get more fine and fast vacuum in the system as well as acts as a barrier in oil diffusion pump for hot oil vapor not going into the vacuum chamber. Sometimes high discharge Ar gas plasma substrate cleaning can be done at vacuum of 5 x 10^{-3} mbar, if needed. The films were deposited on the silicon substrates cleaned in the ultrasound bath in isopropyl alcohol and drained by a compressed air flux. During the deposition, all substrates were kept at room temperature i.e no substrate heating or cooling. Gold film evaporated at residual vacuum from tungsten filament/molybdenum boat at temperature of 2000°K

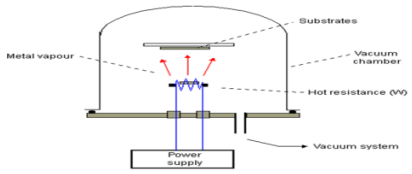

Fig: 2. Vacuum coating process diagram

Vapor pressure varies depending upon the source temperature and is different for different materials, for suitability standard plot [31] is provided from which depending upon source material vapor pressure is selected.

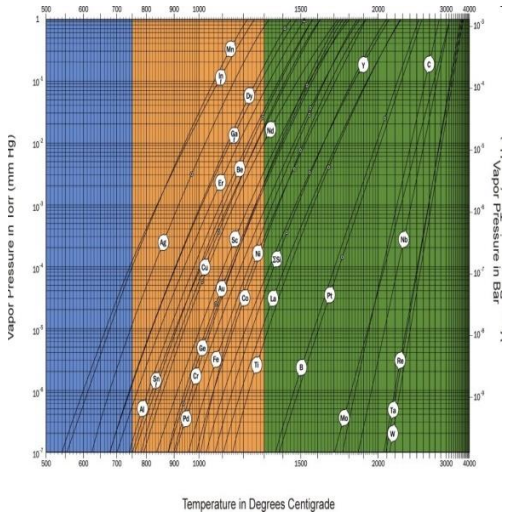

5. Model Description

General description of the model is presented in figure 4 where pressure gas flow low in vacuum system i.e molecular flow and it can be seen that the model inputs are ambient temperature, evaporate temperature, vapor pressure, molecular weight, density of gold, neglecting the substrate surface temperature. The Free Molecular Flow interface uses the angular coefficient method to model flows with Knudsen numbers Kn >10. This physics interface avoids solving the physics in the volumes of the modeled geometries, and requires meshing only of the surfaces. Completely diffuse scattering (total accommodation) and emission are assumed at all surfaces in the geometry, and flow is computed by integrating the flux arriving at a surface from all other surfaces in its line-of-sight. This means that the dependent variables exist only on the surfaces of the geometry, and the solution process is much faster than the direct simulation monte carlo(DSMC) method. Furthermore, it is not subject to statistical scatter. Number densities are reconstructed using a method included in the free molecular flow interface. The Molecular flow module is designed to offer previously unavailable simulation capabilities for the accurate modeling of low pressure, low velocity gas flows in complex geometries. It is

ideal for the simulation of vacuum systems including those used in semiconductor processing, particle accelerators and mass spectrometers. Small channel applications (e.g. shale gas exploration and flow in nanoporous materials) can also be addressed. The Molecular Flow Module uses a fast angular coefficient method to simulate steady-state free molecular flows. We can model isothermal and non-isothermal molecular flows, and automatically calculate the heat flux contribution from the gas molecules. The discrete velocity method is also included in the module for the simulation of transitional flows. Historically, flows in this regime have been modeled by the direct simulation monte carlo (DSMC) method. This computes the trajectories of large numbers of randomized particles through the system, but introduces statistical noise to the modeling process. For low velocity flows, such as those encountered in vacuum systems, the noise introduced by DSMC renders the simulations unfeasible. COMSOL uses alternative approaches: employing a discrete velocity method for transitional flows (using a Lattice Boltzmann velocity quadrature) and the angular coefficient method for molecular flows. Using the input parameters, the model computes the thickness of gold deposited, mass deposited on the surface of substrate, mass transfer rate and mass loss by using COMSOL software. The following wall conditions are inbuilt in COMSOL software:

- wall
- outgassing wall
- adsorption/desorption
- deposition

In adsorption/desorption boundry condition, sticking coefficient can be defined along with other condition. Gold, tin and indium is placed in resistively heated tungstun/molybdenum boat which is having very high melting point of 3420^{o}C. Substrate is one quarter of a 4″ wafer mounted on stationary support on top of tungsten boat depending upon the mean free path and Langumuire-Kundsen relation. A screen is placed to cover the substrate, if more than one source is used.

6. Results & Discussion

In table 1 various input parameter required for the gold model are given to compute the molecular flow in vacuum system. Generally, the ambient temperature is fixed based on the experimental setup or experimental conditions but the evaporation temperature can be varied as per the thickness or mass transfer to be deposited on the substrate by considering the vapor pressure, to make fast the mass transfer keeping the good adhesion with uniformity on the substrate surface.

Table: 1. Input parameter for the gold model

Name	Expression	Value	Description
Tamb	293.15[K]	293.2 K	Ambient temperature
Tevap	1900[K]	1900 K	Evaporation temperature
pvap	100[Pa]	100.00 Pa	Vapor pressure of gold
Mn0	197[g/mol]	0.1970 kg/mol	Molecular weight of gold
Rho0	19.3 gc/m^3	1.930E 4 kg/m^3	Density of Gold

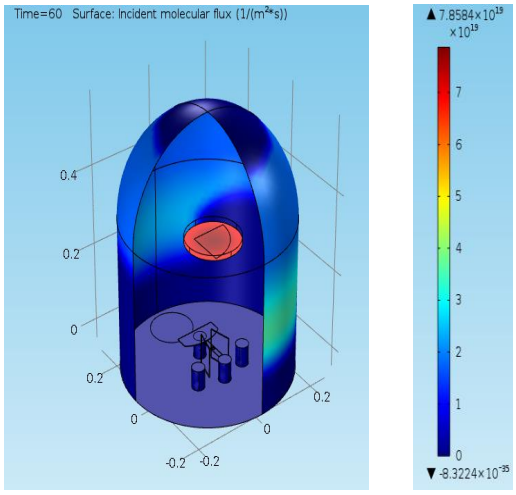

Fig: 3. Molecular flux after 60 sec

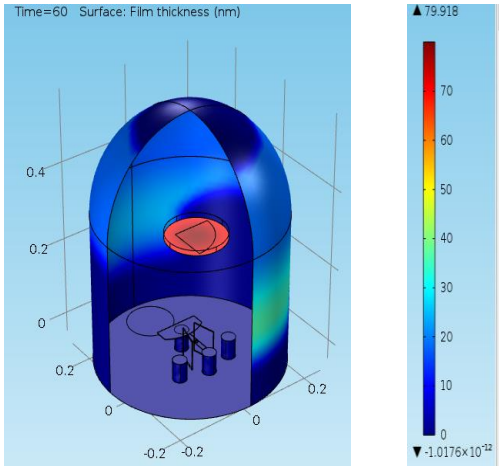

Fig: 4. Surface film thicknes

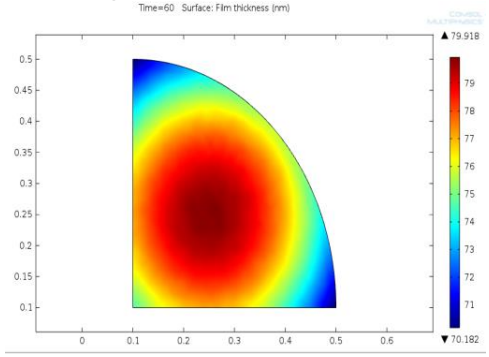

Fig: 5. Film Thickness Variation on Substrate Surface

Figure 3 shows the flux of gold molecules on the surfaces of the model. This constant molecular flux 7.858 x 10^{19} (1/m^{2}s) determines the thickness of gold deposited shown in figure

4. In figure 5, it is obvious the film

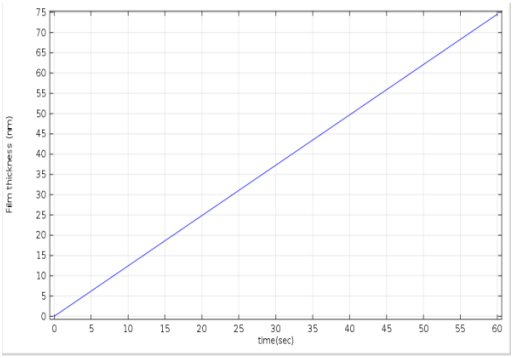

Fig: 6. film thickness after 60 sec

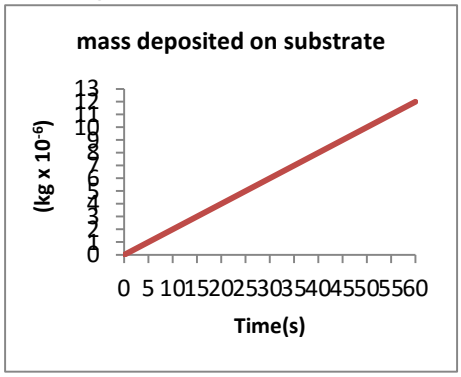

Fig-7(a) Variation of mass deposited on substrate with time

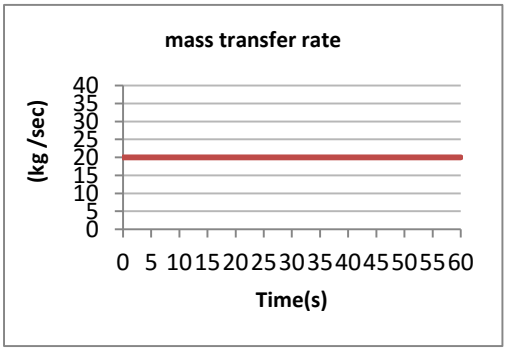

Fig: 7. Mass Transfer rate in Kg/sec

thickness is maximum in the centre of substrate positioned directly on vertically centre of tungsten boat/source, greater than 79.9 nm after 60 seconds of thermal evaporation process. This thickness decreases radialy outwards surface of the substrate 70 nmIn figure 6. based the molecular flux deposited on substrate , graph shows the gold deposited thickness after 60 seconds from initial condition of zero second. It is clear from graph that the film thickness varies linearly with time. In figure 7 graph is plotted with time for mass (kg x 10^{-6}) deposited on the surface of substrate and shows that as mass deposited on substrate is 12 x10^{-6}) which increases with time as in the case of figure 8 since the depositing thickness with time adds mass also on the substrate. In figure 10 mass transfer rate (kg/sec x 10^{-8}) is plotted for 60 seconds and is a straight constant abscissa parallel line showing 20 x 10^{-8} kg/sec. Only the flux is required to compute the deposition rate, but in this instance, since most of the computational time is used to compute the view factors, solving the time dependent problem adds little additional time to the solution process. Using a time dependent model also allows for more advanced extensions of the model, for example, re-evaporation of gold from hot surface close to the evaporative source could be included

Figure 8. mass deposited on substrate surface

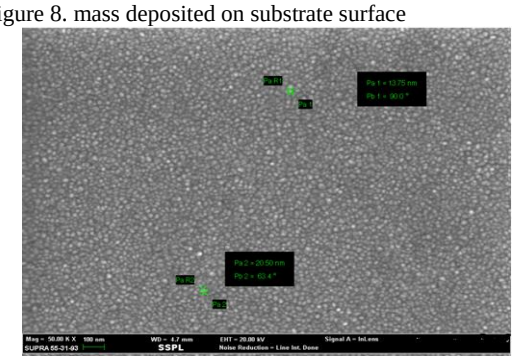

Fig: 8. SEM micrograph of gold at 50 KX Magnification

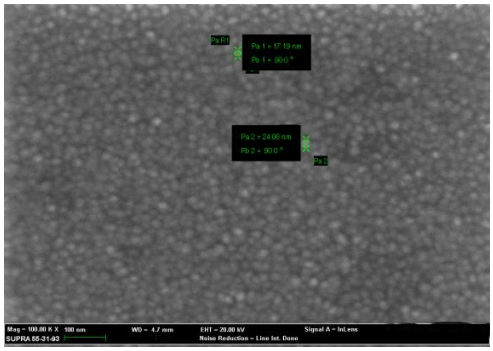

Fig: 9. SEM micrograph of gold at 100KX magnification

Figure 9 &10 shows that gold SEM micrographs at 50KX & 100KX magnification which is very uniform and smooth and average grain size of gold is 15-30 nm across the grain boundary. Figure 11 shows the XRD analysis of gold and shows the polycrystalline face centered cubic structure with preferential (111) plane.

Measurement of deposited film thickness for gold 800 Å from Dektek surface profiler & comparison with thickness value given by Digital thickness monitor (DTM), a piezoelectric transducer is shown in figure 14. From the measurement results shows that in gold film thickness variation 5-15%. This variation in thickness is obvious since the locations of quartz crystal and substrate are different inside the vacuum chamber & this variation can be minimized by keeping them close together

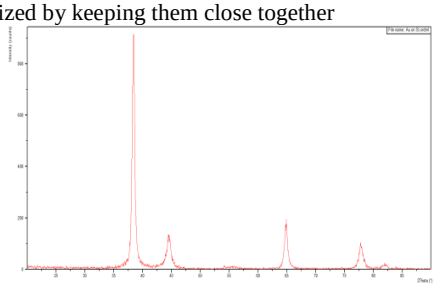

Fig: 11. XRD analysis of gold on silicon

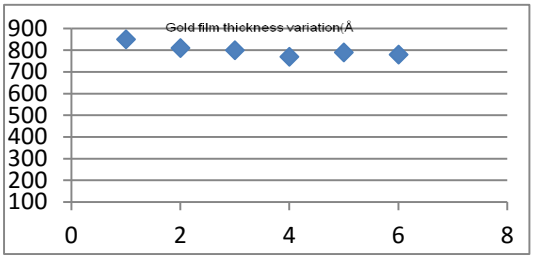

Fig: 12. Measurement of gold film thickness at 6 points by dektek

7. Conclusion

For Optimized methods for fast and accurate simulations, gases at low pressures cannot be modeled using conventional computational fluid dynamics tools or DSMC method. That is due to the fact that kinetic effects become important as the mean free path of the gas molecules becomes comparable to the length scale of the flow. Coatings of gold having good uniformity & appropriate thickness have been produced on stationary, non-rotated, flat substrates using a vacuum thermal evaporation technique that incorporates the use of a resistively heated tungsten/molybdenum boat. Thus this work presents the thermal evaporation of gold on silicon with thickness of 78-80 nm. The mass deposition of gold for 60 sec is 12 $x10^{-6}$ kg and mass transfer rate is 20 x 10^{-8} kg/sec. Gold is polycrystalline with fcc structure with preferential (111) plane. The average grain size is 15-30 nm with good, smooth and better dispersion on silicon. From above measurements it is concluded that variation in thickness in general is 5-15% from the value given by DTM (piezoelectric transducer). This variation in thickness is obvious since the positions of substrate and quartz crystal are at different locations in the vacuum chamber.

References

[1] Ali Moarrefzadeh et.al., Simulation and Modeling of Physical Vapor Deposition (PVD) Process, Wseas Transactions on Applied and Theoretical Mechanics, 7(2), 2012

[2] P. S. Raghupathi, Joseph George, C. S. Menon, The Effect of Deposition Rate on Electrical, Optical and Structural Properties of ITO Thin Films, E-Journal of Chemistry, 2(3), 2005, 171-177

[3] Haichuan Mu, Hui Shen, David Klotzkin, Dependence of film morphology on deposition rate in ITO/TPD/Alq_3/Al organic luminescence diode, Journal of Solid-State Electronics, 48, 2004, 2085–2088

[4] Adeleh Granmayeh Rada, Hamed Abbasib,Mohammad Hossein Afzalib, Gold Nanoparticles: Synthesising, Characterizing and Reviewing Novel Application in Recent Years Physics Procedia, 22, 2011, 203 – 208

[5] Ragini Raj Singh, et.al, Investigation of passivation processes for HgCdTe/CdS structure for infrared application, 10, 2006, 235–240

[6] Wenjun Zhou et al. , Effective Permittivity of Ultrathin Chemical Vapor Deposited Gold Films on Optical Fibers at Infrared Wavelengths, J. Phys. Chem. C, 118, 2014, 670−678

[7] Keewah Chan et al., Formation of gold nanoparticles in silicon suboxide films prepared by plasma enhanced chemical vapour deposition, journal of thin solid films, 519, 2011, 4952-4957

[8] Carl E. Larson et al.,Chemical Vapor deposition of Gold, IBM Almaden Research Center, San Jose, California 95120, 1986

[9] Miroslav Gojo et al., Electrochemical Deposition of Gold in Citrate Solution Containing Thallium Polja~eka, Acta Chim. Slov. 2008, 55, 330–337

[10] Anne-Felicie Lamic-Humblot, et.al, An easy way to obtain thin film on silica glass substrate by chemical method, 539, 2013, 151–153

[11] T. Donnelly, S. Krishinamurthy, K. Carney, N. McEvovy, J. G. Lunney, Pulsed laser deposition of Nanoparticles of film Au, Journal of Applied Surface Science, 254, 2007, 1303–1306

[12] X. Zhang, X. Zhang, S. S. Chu, J. R. Ho, C. P. Grigoropoulos, Excimer laser ablation of thin gold fims on a quartz crystal microbalance at various agron background pressures, Journal of applied physics A, 64, 1997, 545-552

[13] Anna Schaub, Petr Slepicka, Irena Kasparkova, Petr Malinsky, Gold Nanolayer and Nanocluster coatings induced by heat treatment and evaporation technique, Springer Open Journal, Nanoscale Research letters 2013, 8, 249

[14] Behrang Moazzez, Stacey M. O'Brien and Erika F. Merschrod S., Improved Adhesion of Gold Thin Films Evaporated on Polymer Resin: Applications for Sensing Surfaces and MEMS, Journal of Sensors, 13, 2013, 7021-7032

[15] Maxime Gougis, Antonio Pereira, Dongling Ma1 and Mohamed Mohamedi, Oxygen Gas Assisted Laser Deposition of Gold Thin Films: Electrooxidation of Glucose, International Journal of Electrochemical Science, 9, 2014, 3588-3601

[16] C. Celed´on, M. Flores, P. H¨aberle , J. E. Vald´es, Surface Roughness of Thin Gold Films and its Effects on the Proton Energy Loss Straggling, Brazilian Journal of Physics, 36(3B), 2006, 956-959

[17] Hartmann Hieber, Karin Pape, Ageing of Thin Gold Films, Gold Bull., 1982, 15, (3)

[18] Adam Proszkynski, Dariusz Chocyk, Grzegorz Gladyszewski, Stress modification in gold metal thin films during thermal annealing, Optica Applicata, XXXIX(4), 2009, 705-710

[19] Authur K.Burak Ucer, Vacuum evaporation, www.users.wfu.edu

Novel 4-terminal Perovskite/SiC-based Rear Contact Silicon Tandem Solar Cell With 27.6 % PCE

Rahul Pandey, Apurva Jain, and Rishu Chaujar

Microelectronics Research Laboratory, Department of Engineering Physics, Delhi Technological University, Bawana Road, Delhi-110042, India

***Abstract* — In this work, a novel 4-terminal perovskite / SiC-based rear contact silicon tandem device has been proposed for long-term cost reduction and higher efficiency. The novel tandem device proposed in this work shows ultra-high power conversion efficiency (PCE) of 27.6 % and 22.7 % with 300 µm and 10 µm thick rear contact Si solar cell, respectively. The realistic TCAD simulation has been performed for Methylammonium lead triiodide perovskite cell. To simulate and predict the realistic behavior of the device, all the fundamental recombination mechanisms have been included in $CH_3NH_3PbI_3$ film during the simulation. The perovskite device which is used as top cell shows PCE of 19.9% which is almost equivalent to experimentally available record efficiency of 20.1%. The charge carrier decay constants for $CH_3NH_3PbI_3$ used in the simulation have been obtained from experimentally available data.**

***Index Terms* — perovskite, SiC, silicon, simulation, solar cell tandem.**

I. Introduction

The crystalline silicon solar cells have dominated the photovoltaics market with 90% current market share. The peak efficiency of c-Si solar cells has reached 25.6%, asymptotically approaching the practical limit of 29.4% with the improvement being very marginal in the last 15 years. For photovoltaic devices to completely replace the conventional energy sources, the solar modules must achieve high efficiency at low cost. Organo-metal halide perovskite solar cells have garnered much attention in this regard. Due to their high absorption coefficient, long charge carrier diffusion lengths, suitable band gap, high photovoltage, and ambipolar charge transport, the perovskite solar cells have recently reached a certified efficiency of 20.1% [1]. With the rapid progress in perovskite-based solar cell device performance, critical studies i.e. device simulation considering the impact of the various recombination mechanisms on photovoltaic device parameters are lagging in any of the literature available till date. In this work, we use the Silvaco ATLAS device simulator to carry out simulations of the methylammonium lead triiodide perovskite solar cell. For obtaining more realistic results, all the fundamental recombination mechanisms have been incorporated in the perovskite layer with the help of SRH (first order), optical recombination (second order) and Auger (third order) recombintaion models. Model parameters used in the simulation have been obtained from experimentally available data as reported in [2-3]. Further, the impact of film thickness and charge carrier decay constant on device performance has also been studied. The simulation work reported here achieves 19.9% PCE, which is in good agreement with the available experimental result [1].

Moreover, novel perovskite/ SiC-based silicon solar cell has also been proposed for ultra-high efficiencies and low-cost solar modules. The high-efficiency SiC-based Si solar cells were combined with the high band gap perovskite top cell to form a tandem cell. Tandem cells split the spectrum and are optimized to each part of it. These cells minimize the amount of thermalization by using multiple absorptions. 27.6 % and 22.7% efficient tandem cell have been realized in this work using SiC-based 300µm and 10µm thick rear contact silicon solar cell as bottom subcell. In the simulation, the rear electrode for perovskite cell is assumed to be transparent to maximize the absorption in bottom Si solar cell. SiC has been used as a surface passivating layer for the bottom rear contact silicon solar cell. Previous work shows that presence of SiC at the front surface creates a positive electric field and hence decreases the minority carrier (holes) concentration at the interface. This further results in lower interface recombination rate [4-6]. Previous work shows that SiC/SiO_2 based layer is a good candidate for antireflective (AR) coating against Si_3N_4, which is commonly preferred as an AR coating layer [7]. SiC based antireflective passivation layer has also been discussed in [8]. Material parameters for perovskite top subcell has been obtained from experimentally available data reported in [9] and the optical properties from [10, 11].

II. Methods

Simulation methods enable us to examine the fundamental physical phenomena taking place in photovoltaic (PV) devices, thereby allowing to make reliable predictions about the most favorable conditions for operation. Fig. 1(a) shows the perovskite device used in the simulation. The device consists of a methylammonium lead iodide ($CH_3NH_3PbI_3$) layer sandwiched between compact TiO_2 and 2,2',7,7'-tetrakis(N,N'-di-p-methoxyphenylamine)-9,9' spirobifluorene (Spiro-MeOTAD). The compact TiO_2 is N-type with a doping density of 5×10^{19} cm^{-3}, whereas $CH_3NH_3PbI_3$ and Spiro-MeOTAD are P-type with a doping density of 2.14×10^{17} cm^{-3} and 3×10^{18} cm^{-3} respectively. Further, work function: -4.4 eV and -5.1 eV have been used to form contacts from compact

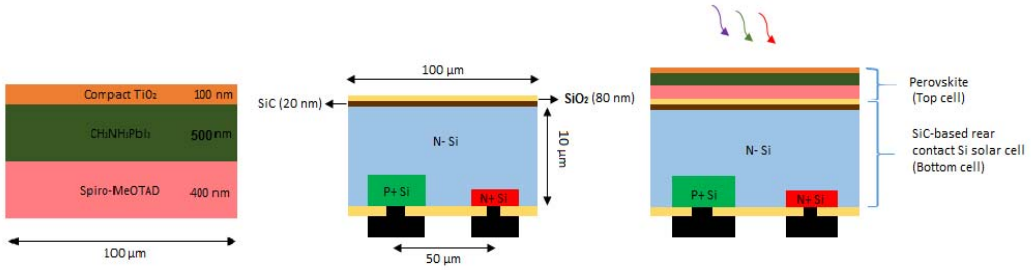

(a) (b) (c)

Fig. 1. Simulated device structures: (a) Perovskite solar cell, (b) 10 µm thick SiC based rear contact silicon solar cell, and (c) a 4 terminal perovskite/silicon tandem

TiO_2 and Spiro-MeOTAD, respectively. Further, for silicon bottom cell as shown in Fig.1 (b), (50-µm-wide pitch, 46-µm-wide P+, and 30-µm-wide N+) was used. The substrate was n-type, with doping density (3 x 10^{15} cm^{-3}). P+ region was doped with boron (4 × 10^{20} cm^{-3}, depth of 300 nm). N+ region was doped with phosphorus (1 × 10^{20} cm^{-3}, depth of 100 nm). All the materials and models parameter used in the simulation have been obtained from experimentally available data, and the simulator is calibrated accordingly. To get the current density-voltage curve under illumination, the standard AM 1.5 solar spectrum has been used. The perovskite cell is simulated with the help of SRH, Auger, and radiative recombination models to obtain realistic device performance results. A 4-terminal Perovskite/SiC-based silicon cell tandem solar cell was also simulated as shown in Fig.1 (c). Radiative recombination model is omitted for silicon solar cell since it is an indirect band gap semiconductor. Tandem cell is simulated with two different thickness of bottom silicon solar cell i.e. 300 µm and 10 µm thick SiC- based rear contact silicon solar cell.

III. RESULTS

Firstly, the impact of the thickness of the perovskite layer on device characteristics is examined as shown in Fig. 2(a-b). Substantial improvement in short circuit current (J_{SC}) has been observed up to the thickness of 500 nm. However, the enhancement is not significant for the thickness beyond 500 nm, as shown in Fig. 2 (a-b). The result also shows a slight decrease in the open circuit voltage (V_{OC}), which is attributed to the increased carrier recombination in the thicker film, as shown in Fig. 2b. Further, three current density-voltage (J-V) curves has also been obtained with different second and third order recombination rate constants denoted as B and C.

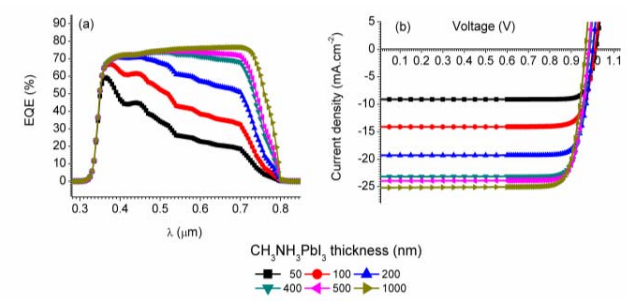

Fig. 2. Impact of perovskite layer thickness on optical and electrical behavior of the device: (a) EQE, and (b) J-V

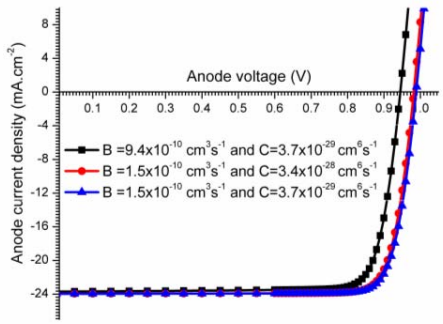

Fig. 3. J-V curve based on different carrier decay constants as reported experimentally in [2-3].

The carrier lifetime 10^{-6} has been used for SRH recombination model. The square and circle symbolled J-V curves are based on experimental carrier decay constants reported by [2] and [3], respectively. The triangular J-V curve is obtained for optimum performance by selecting the smaller values of both the constants. The PCEs of 18.7%, 19.9%, 20.1% are obtained in black, red and blue curves respectively. The photovoltaic parameters have been summarized in Table.1 for different carrier recombination rate constants. Thus, the incorporation of recombination models results in a better agreement between simulation and experimental results. A power conversion efficiency of 19.9% has been achieved with perovskite solar cells in the above section. Further, for achieving greater efficiencies, a new perovskite/SiC-based rear contact silicon-based tandem device has been proposed. The perovskite cell being used as the top cell and the silicon cell being used as the bottom cell. The tandem cell splits the solar spectrum for attaining ultrahigh efficiency. The rear electrode of the perovskite cell is assumed to be transparent in the simulation for allowing efficient absorption by the bottom cell. The four-terminal tandem device achieves PCEs of 22.7% and 27.6% with 10-micron and 300-micron thick silicon bottom subcell, respectively. The carrier lifetime 10^{-5} s has been used for the thinner device since longer diffusion lengths are not required. Therefore, the quality of silicon used for bottom cell remains immaterial. The 300 µm thick device however, requires longer charge carrier diffusion lengths. Therefore, the thicker device has been simulated with a carrier lifetime of 10^{-3} s. The simulations for the novel tandem cell achieved higher efficiencies than individual PV cells as tabulated in Table.2. In

TABLE 1
PHOTOVOLTAIC PARAMETERS OF PEROVSKITE SOLAR CELL: CHARGE CARRIER DECAY CONSTANT HAS BEEN OBTAINED FROM EXPERIMENTALLY AVAILABLE DATA FROM [2, 3]

Charge Carrier Decay Constants		Photovoltaic Parameters			
2nd order, A ($cm^3\ s^{-1}$)	3rd order, B ($cm^6\ s^{-1}$)	J_{SC} ($mA.cm^{-2}$)	V_{OC} (V)	FF (%)	PCE (%)
9.4×10^{-10}	3.7×10^{-29}	23.69	0.94	83.6	18.72
1.5×10^{-10}	3.4×10^{-28}	23.95	0.98	84.7	19.92
1.5×10^{-10}	3.7×10^{-29}	23.97	0.98	84.7	20.08

TABLE 2
PHOTOVOLTAIC PARAMETERS OF THE 4 TERMINAL PEROVSKITE / SiC-BASED SILICON TANDEM SOLAR CELL

Solar cells	J_{SC} ($mA.cm^{-2}$)	V_{OC} (mV)	FF (%)	PCE (%)
Perovskite top subcell	23.95	982	84.7	19.9
Silicon bottom cell 10 micron (stand-alone)	26.03	662	82.3	14.2
Silicon bottom cell 10 micron bottom subcell	5.59	606	81.8	2.8
Silicon bottom cell 300 micron (stand-alone)	34.63	688	82.9	19.7
Silicon bottom cell 300 micron bottom subcell	14.53	649	82.3	7.7
4-terminal using 10 micron thick Si bottom subcell				19.9+2.8=22.7
4-terminal using 300 micron thick Si bottom subcell				19.9+7.7=27.6

previous work, calibrated software program has been written in the Silvaco ATLAS device simulator as the results already published [12]. The same device has been incorporated in tandem configuration by replacing the AR coating with the SiC-based front surface, and SiO_2 has been used as an insulation layer between top subcell and bottom subcell. The performance of SiC passivated device without perovskite filter on the top has also been obtained for comparisons. Detailed photovoltaic parameters for tandem cells have been summarized in Table 2.

VI. Conclusion

A novel ultra-high 27.6% efficient perovskite/ SiC-based silicon tandem solar cell device design has been proposed and analyzed with the help of Silvaco ATLAS device simulator. The impact of perovskite layer thickness and recombination have been obtained on the performance of perovskite top subcell. SiC-based passivated rear contact silicon device has been used as bottom subcell.

Acknowledgement

The authors would like to thank Microelectronics Research Lab, Department of Engineering Physics, Delhi Technological University to carry out this work. Rahul Pandey (JRF) acknowledge UGC, Govt. of India for providing fellowship.

References

[1] W. S. Yang, J. H. Noh, N. J. Jeon, Y. C. Kim, S. Ryu, J. Seo, and S. Il Seok, "High-performance photovoltaic perovskite layers fabricated through intramolecular exchange," *Science.*, no. May, p. science.aaa9272, 2015.

[2] C. Wehrenfennig, G. E. Eperon, M. B. Johnston, H. J. Snaith, and L. M. Herz, "High Charge Carrier Mobilities and Lifetimes in Organolead Trihalide Perovskites," *Adv. Mater.*, vol. 26, no. 10, pp. 1584–1589, Mar. 2014.

[3] Y. Yang, M. Yang, Z. Li, R. Crisp, K. Zhu, M.C. Beard, Comparison of Recombination Dynamics in CH 3 NH 3 PbBr 3 and CH 3 NH 3 PbI 3 Perovskite Films: Influence of Exciton Binding Energy, J. Phys. Chem. Lett. 6 (2015) acs.jpclett.5b02290. doi:10.1021/acs.jpclett.5b02290.

[4] R. Pandey and R. Chaujar, "Novel SiC Encapsulated Coaxial Silicon Nanowire Solar Cell for Optimal Photovoltaic Performance" *IEEE PVSC 42nd*, June 14-19, New Orleans, USA.

[5] R. Pandey and R. Chaujar, "Front Surface Passivation Scheme for Back-Contact Back-Junction (BC-BJ) Silicon Solar Cell", (Accepted), *Adv. Sci. Lett.,* 2015 ISSN: 1936-6612 (Print): EISSN: 1936-7317 (Online)

[6] R. Pandey and R. Chaujar, "Rear contact SiGe solar cell with SiC passivated front surface for > 90-percent external quantum efficiency and improved power conversion efficiency," *Sol. Energy*, vol. 135, pp. 242–252, 2016.

[7] R. Pandey and R. Chaujar, "Novel back-contact back-junction SiGe (BC-BJ SiGe) solar cell for improved power conversion efficiency", *Microsystem Technologies,* DOI: 10.1007/s00542-015-2552-1. Available:

http://link.springer.com/article/10.1007%2Fs00542-015-2552-1#page-1.
[8] S. Allen and Y. Awad, “Silicon carbide-based antireflective coating,” US Pat. App. 12/994,973, 2009.
[9] F. Liu, J. Zhu, J. Wei, Y. Li, M. Lv, S. Yang, B. Zhang, J. Yao, and S. Dai, “Numerical simulation: Toward the design of high-efficiency planar perovskite solar cells,” *Appl. Phys. Lett.*, vol. 104, no. 2014, p. 253508, 2014.
[10] A. M. A. Leguy, Y. Hu, M. Campoy-Quiles, M. I. Alonso, O. J. Weber, P. Azarhoosh, M. van Schilfgaarde, M. T. Weller, T. Bein, J. Nelson, P. Docampo, and P. R. F. Barnes, “Reversible Hydration of CH 3 NH 3 PbI 3 in Films, Single Crystals, and Solar Cells,” *Chem. Mater.*, vol. 27, no. 9, pp. 3397–3407, May 2015.
[11] M. Filipič, P. Löper, B. Niesen, S. De Wolf, J. Krč, C. Ballif, and M. Topič, “CH(3)NH(3)PbI(3) perovskite / silicon tandem solar cells: characterization based optical simulations.,” *Opt. Express*, vol. 23, no. 7, pp. A263–78, Apr. 2015.
[12] R. Pandey and R. Chaujar, “Rear contact solar cell with ZrO_2 nano structured front surface for efficient light trapping and enhanced surface passivation,” in 2015 IEEE 42nd Photovoltaic Specialist Conference (PVSC), 2015, pp. 1–5.

Ontology Based Framework for Reverse Engineering of Conventional Softwares

MPS Bhatia
Division of Computer Engineering,
Netaji Subhas Institute Of Technology
Delhi- 78, India
Email Id: mpsbhatia@nsit.ac.in

Akshi Kumar
Department of Computer Engineering
Delhi Technological University, DTU
Delhi - 42, India
Email Id: akshi.kumar@gmail.com

Rohit Beniwal
Division of Computer Engineering,
Netaji Subhas Institute Of Technology
Delhi- 78, India
Email Id: rohitbeniwal@yahoo.co.in

Abstract— **Incontemporary years, integration among research areas of semantic web technologies and software engineering took place due to the reason of developers being present at different virtual, cultural, and geographical locations. Due to this amalgamation, a new collaborated field has emerged known as Semantic Web Enabled Software Engineering. This field presents researchers ample opportunities to probe issues and challenges, which are originated due to their amalgamation.Among such issues, one is the reverse engineering of conventional softwares using ontologies. This research paper presents a framework and discusses the implementation approach to resolve to the above issue.**

Keyword— Conventional Software,Ontology, Reverse Engineering, Semantic Web, Software Engineering

NOMENCLATURE

API- Application Programming Interface
IT- Information Technology
N3- Notation 3
OWL- Web Ontology Language
SE- Software Engineering
SW- Semantic Web
RDF- Resource Description Framework
SPARQL- SimpleProtocol and RDF Query Language
RDFS- Resource Description Framework Schema
UML- Unified Modified Language

I. INTRODUCTION

Nowadays, due to global competitiveness, every organization wants to reduce it expenditure on Information Technology (IT)operations.Therefore, offshoring IT services is a very common phenomenon.Also, in offshore projectsthere is high probability that thedevelopment, support & maintenance teams are located at different geographical, virtual, and cultural locations. For example, when Merck (the UnitedStates of America based pharmaceutical company) hasoffshored its IT work to HCL Technologies (an Indian based IT services company) to look after for various development, support & maintenance activities, the HCL Technologies gottheir teams distributed geographically and virtually at various locations of India and United States of America to support their day to day IT activities and eachsuch team belongs to different cultural background.Consider another similar example where British Airways (the United Kingdom based flag carrier airline organization)has also offshored its IT operations to NIIT Technologies (an Indian based global IT solutions organization) to handle their complex and expensive business, the NIIT Technologies has deployed its several teams across various locations of United Kingdom and India to support their all IT activities. Again these teams belong to different culture and geographical locations.Therefore, in situations where IT workingteams belong to different locations, they possessdiversified information,knowledge & skills and sharing them becomes a key challenge. In the absence of any proper sharing mechanism, the developmentleads to generation of inconsistent information.This inconsistency further results into the development of undesired software [1],[2].

Also, when various development, support & maintenance activitiestook place, itgenerates a lot of information involving numerous participants [3]. Reusing already available information further saves the human effort in various development, support & maintenance activities [4]. Due to this overall scenario, reusing and sharing IT information turns out to be a key operative challenge.

The above challenge leads to the integration between research fields of Semantic Web (SW) technologies & Software Engineering (SE)[5],[6],[7] because "Semantic Web provides a common framework that allows data to be shared and reused across application, enterprise, and community boundaries" [8]. On the other hand Software Engineering is "the application of a systematic, disciplined, quantifiable approach to the development, operation, and maintenance of software, and the study of these approaches; that is, the application of engineering to software" [9]. This integration opened new avenues for researchers to look after various issues & challenges that got generated due to amalgamation of SW & SE. Among such issues, one is reverse engineering of conventional softwares using ontologies.

"Reverse engineering, also called back engineering, is the processes of extracting knowledge or design information from anything man-made and re-producing it or reproducing anything based on the extracted information" [10]. Hence, reverse engineering plays a crucial role in understanding the software system during various support & maintenance activities in the absence of any updated documentation. Ontologies, which are "formal and explicit specification of

978-9-3805-4421-2/16/$31.00 ©2016 IEEE

shared conceptualization" [11], and Semantic Web techniques such as RDF, RDFS, SPARQL, etc. have been used to improve various software engineering processes [5],[6],[7],[12].However, reverse engineering of conventional softwares using ontologies is yet to be examined. Therefore, this research paper address the above particular issue and presents a framework as well as an implementation approach for reverse engineering of conventional softwares using ontologies.

The rest of the paper is organised as follows: section II provides a talkabout related work; section III discusses the proposed framework followed bysection IV which elaborates the implementation approach. Section V concludes and provides direction for future work.

II. CURRENT APPROACH

Legacy systems are generally old-fashioned systems, although, still in use instead of availability of upgraded versions. For e.g. old server operating systems from supplier such as Microsoft, IBM, Hewlett- Packard, Unisys, etc. are legacy systems which are still in use.These systems tendto become problematic because of various compatibility issues and security concerns. These systems undergo many changes done by different vendors or developers. Keeping updates of all documents is generally ignored resulting in loss of important internal structural knowledge. In this above situation, there is no proper documentation or the documentation is highly unstructured or the structure has been highly degraded through a sequence of various maintenance activities. Recovering such important structural knowledge or information can provide great help in understanding and maintaining the software system. The various activities associated with reverse engineering include redocumentation, recovery of design knowledge at the desired level of abstraction, identifying components that can be reused, identifying modules that require restructuring, understanding high level system description, and recovering various business rules. The various levels of reverse engineering include recovery at low, intermediary, and at high level of abstraction which meansredocumentation at implementation, design, and at specification level.

In this regard,Bouchihaet al. [13] proposed reverse engineering approach for web applications based on the domain ontology. Their approach generated aUnified Modelling Language(UML) conceptual schema modelling the web application.Benslimaneet al. [14] also provided an ontology-based reverse engineering approach for maintaining web applications. They also generated a conceptual schema of web application using a set of transformation rules from given domain ontology. Although many literature available but all of them focuses on ontology based reverse engineering of web applicationswhereas the scope of using semantic web especially ontologies in reverse engineering of conventional softwares is yetnot examined.

III. FRAMEWORK

Reverse engineering is a process offinding critical, unknown, and hidden information about a software system. It helps in better understanding and maintenance of software system. It furtherenriches and improves the operation and maintenance phase. Thus, we propose a semantic-web enabled reverse engineering approach.The framework of the approach is divided into three phases namely development phase, alignment phase, and reverse engineering phase.

A. Development Phase

This phase comprisestwosteps. In the beginning step, we develop a pattern ontology, which will contain library of patterns that are commonly used to create the software system. It consists of various patterns such as design pattern, workflow pattern, and usability pattern [5]. In the next step, we will develop a software architecture ontology, "which models architecture- related concepts, such as architectural styles, components that are required in each architectural style, and their interactions" [5]and an object oriented design ontology, which consists UML design concepts for our existing software. "It defines the vocabulary for describing object-oriented software designs" [5].

B. Alignment Phase

In this step, we alignsoftware architecture and object- oriented design ontologies with pattern ontology in order toknow similarities between them.

C. Reverse Engineering Phase

If any similarity is established in alignment phase, we will be able to detect the way software system was developed from pattern ontology. In this finalphase, with the information acquired in the last phase, we will use a semantic reasoner on the matching part of pattern ontology to deduce new logical inferences. This step by step procedure of reverse engineering is depicted by the following figure

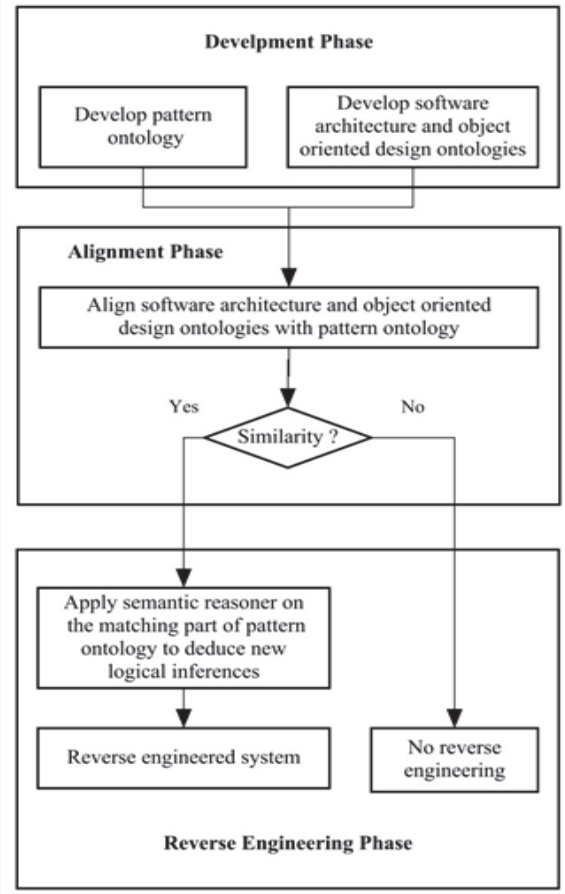

Fig.1.Reverse Engineering of conventional softwares using ontologies

IV. IMPLEMENTATION APPROACH

In this section we elaborate the implementation approach for all the phases of framework, which are as follows:

A. For Development Phase

Pattern, software architecture, and object oriented design ontologies can be created using suitable ontology editor tool depending upon its features and limitations. "There are more than one hundred eighty ontology editor tools available in the market. A large no. of tools can be downloaded from AI^3 [Adaptiva Information, Adaptiva Innovation, Adaptiva Infrastructure] on www.mkbergman.com" [15], [16].

B. For Alignment Phase

PARIS, KitAMO, Alignment API, BLOOM, Optima etc. are among the few current active tools that can be used for alignment of software architecture and object oriented design ontologies with pattern ontology."PARIS is a system for the automatic alignment of RDF ontologies. PARIS aligns not only instances, but also relations and classes. Alignments at the instance level cross-fertilize with alignments at the schema level" [17]. "KitAMO is a tool for evaluating ontology alignment strategies and their combinations. It supports the study, evaluation and comparison of alignment strategies and their combinations based on their performance and the quality of their alignments on test cases" [17]."The Alignment API is an API and implementation for expressing and sharing ontology alignments" [17]."Blooms is a tool for ontology matching. It utilizes information from Wikipedia category hierarchy and from the web to identify subclass relationship between entities" [17]."Optima is a state of the art general purpose tool for performing ontology alignment. It automatically identifies and matches relevant concepts between ontologies. The tool is supported by an intuitive user interface that facilitates the visualization and analysis of ontologies in N3, RDF and OWL and the alignment results. This is an open source ontology alignment frame work. Optima is also available as a plugin to Protégé ontology editor" [17]. Information about various ontology mapping and alignment tools is available on [17].

C. For Reverse Engineering Phase

Semantic reasoner is used on the axioms of matching part of pattern ontology to deduce new logical inferences. "Choosing a particular semantic reasoner depends upon its compatibility with ontology editor tools and its native profile and semantics. Information about various reasoners is available in OWL implementation notes at w3 website". [16],[18].

V. CONCLUSION AND FUTURE WORK

In this research paper, we described ontology based framework as well as an implementation approach for reverse engineering of conventional softwares. Hence, as an expected deliverable from this research goal is to generate unknown and hidden knowledge, which emerged undocumented as software systems are maintained or have evolved. As a potential direction of future work, we intend to evaluate our approach using a case study.

REFERENCES

[1]. M.P.S. Bhatia, R. Beniwal and A. Kumar, "An ontology based framework for automatic detection and updation of requirement specifications." In Contemporary Computing and Informatics (IC3I), 2014 International Conference on, pp. 238-242. IEEE, 2014.

[2]. N. Wadhera, R. Beniwal, and A.Kushwaha"mobileDBMS A Client-Server RDBMS for Mobile Devices using Bluetooth Technology." International Journal of Applied Engineering Research10, no. 13,pp. 33165-33169, 2015.

[3]. Bhatega and K. Sharma. "Secure cancelable fingerprint key generation." In Power India International Conference (PIICON), 2014 6th IEEE, pp. 1-4. IEEE, 2014.

[4]. S. Dhall, SK. Pal, and K. Sharma. "Improvised block cipher customized for multimedia security." In Power India International Conference (PIICON), 2014 6th IEEE, pp. 1-5. IEEE, 2014.

[5]. Y Zhao, J Dong and T Peng, "Ontology classification for semantic-web-based software engineering," Services Computing, IEEE Transactions on Services Computing, Vol. 2, No. 4, pp. 303-317, 2009.

[6]. M.P.S Bhatia, A Kumar, and R Beniwal, "Ontologies for Software Engineering: Past, Present, and Future," Unpublished.

[7]. D Gašević, N Kaviani and M Milanović. "Ontologies and software engineering." In Handbook on Ontologies, pp. 593-615. Springer Berlin Heidelberg, 2009.
[8]. W3C Semantic Web: http://www.w3.org/2001/sw.
[9]. IEEE Standard Glossary of Software Engineering Terminology-Description, 1990. http://ieeexplore.ieee.org/servlet/opac?punumber=2238.(Last accessed date: October, 2015)
[10]. Eilam. Reversing: secrets of reverse engineering. John Wiley & Sons, 2011.
[11]. R. Studer, R. Benjamins, and D. Fensel, "Knowledge engineering: Principles and methods," Data & Knowledge Engineering 25, no.1, pp. 161–198, 1998.
[12]. M.P.S. Bhatia, A. Kumar, and R. Beniwal, "Ontology Based Framework for Automatic Software's Documentation." In Computing for Sustainable Global Development, 2015 2nd International Conference on, pp. 725-728. IEEE. 2015.
[13]. Bouchiha, M. Malki, and SM. Benslimane, "Ontology based web application reverse-engineering approach." INFOCOMP journal of Computer Science 6, no. 1, pp. 37-46, 2007.
[14]. S. Mohamed Benslimane, M. Malki, and D. Bouchiha. "Maintaining web application: an ontology-based reverse engineering approach." International Journal of Web Information Systems 5, no. 4, pp. 495-517, 2009.
[15]. AI3 [Adaptiva Information, Adaptiva Innovation, Adaptiva Infrastructure]: http://www.mkbergman.com/904/listing-of-185-ontology-building-tools/ (Last accessed date: October, 2015)
[16]. M.P.S. Bhatia, R. Beniwal and A. Kumar. "Ontology based Framework for Ambiguity Detection in SRS," Unpublished.
[17]. 50 Ontology Mapping and Alignment Tools: http://www.mkbergman.com/1769/50-ontology-mapping-and-alignment-tools(Last accessed date: October, 2015)
[18]. OWL/Implementations: http://www.w3.org/2001/sw/wiki/OWL/Implementations (Last accessed date: October, 2015)

Optimized Sentiment Analysis Tool
A sentiment analysis tool to study cognitive inclinations

Nayonika Sharma
Department of Information Technology
Guru Gobind Singh Indraprastha University
New Delhi, INDIA
Email ID: nayonikaa@gmail.com

Chetna Sharma
Department of Information Technology
Guru Gobind Singh Indraprastha University
New Delhi, INDIA
Email ID: chetnasharma_93@yahoo.com

Dr. S. Indu
Department of Electronics and Communication
Delhi Technological University
Delhi, INDIA
Email ID: s.indu@dce.ac.in

Priyanka Chugh
Department of Information Technology
Guru Gobind Singh Indraprastha University
New Delhi, INDIA
Email ID: Shivankachugh84@gmail.com

Abstract— **Sentiment Analysis also known as Opinion Mining deals with studying the cognitive inclinations of people. It pertains to automating the process of decoding the sentiment behind a notion and to develop a better understanding of the views being presented. Sentiment Analysis is not only used on social media, it has deepened its roots in sociology, psychology, business reviews and even in analyzing the performance of a particular company. The need for a sentiment analysis tool is strengthened hence. Moving forth with this in mind we had first done a 4 month long research on the various types of sentiment analysis tools and their associated pros and cons. By elevating the pros and eradicating the cons, we developed a sentiment analysis tool in the latter four months. The scale of the tool had been escalated to a never before reached level. The tool also incorporated many other features which had never been amalgamated before into one optimized sentiment analysis tool.**

Keywords— Optimized Sentiment Analysis Tool; Cognitive Inclination

I. INTRODUCTION

Internet is a vast virtual space where expressing and sharing an individual's opinions, concerning any facet of life, has implications for marketing and communication alike. [1]This implies that all and every sentiment put forth on social media or any public platform bare huge importance.

The Internet, as a result has caused a huge content growth and has made a huge volume of information accessible. [2]This availability of information has caused a surge of sentiment analysis tools in the market. By collection of opinions, companies can strategize for marketing and products improvement. [3]It can also benefit the customers while purchasing and analyzing various products. Taking the implementation forward there is an essential domain of financial markets, they are considered to be intricate and to be volatile. [4]It has been observed that whenever the social opinion about a certain matter is positive, it is reflected in the stock market prices as they rise. However, it has also been witnessed that the criticism of a commodity or subject results in a decrease in the stock market prices of the commodity. There are various tools which have been built over the past years to analyze the sentiments associated with social media informal texts. These tools employ various techniques ranging from existing systems developed in academic settings, commercial API-based tools, and even a few algorithms available in the NLP literature. [5] We have implemented a sentiment tool which multi facedly deals with the various kinds of emotions depicted on social media. The tool encompasses a plethora of sentiment analysis. It covers the direct detection of sentiment using a vivacious list of keywords containing about 2481 marked words. It also includes analysis of conjunctions when they appear in a statement, various emotions and interjections, emphatic words. It also covers negation tagging being an essential part in determining the opinion of the statement. Finally it analyzes the sentiment as put forth by the symbols, as these symbols have the ability to transform the meaning of the statement and also play a vital role in detecting sarcasm in a sentence.

II. METHODOLOGY USED

A. Direct Sentiment Detection

In case of direct sentiment detection, a word or sentence is directly given a polarity by associating it with the corresponding polarity in the database. In order to compute the sentiment of a word, the word is first allocated a polarity in the database prior to the analysis and this figure is put forth in order to give the result. Secondly, in order to compute the sentiment of a sentence, every word in the sentence is first allocated a digit, which is its polarity; all the polarities obtained therein are added and divided by the number of words in the sentence to compute the sentiment. It should be noted here, that while calculating the sentiment score of a sentence it is of prime and utmost importance to let go of the stop-words. This step needs to be the first step in calculating the sentiment score of a statement. As the stop-words can make the process of sentiment analysis more tedious and tiresome, also these stop-

978-9-3805-4421-2/16/$31.00 ©2016 IEEE

words can also change the sentiment score in an undesirable manner; they should be done away with before we put the texts to the analysis procedure.

Usually, Polarity classification is said to allot a piece of text, an opinion on a single issue, classifying it largely as one of the two opposing sentiment. [6] In this tool, however, we have a scale of +10 to -10 to assign a relative polarity to a given textual snippet. Acquiring the polarity of words and phrases is considered an active line of research in sentiment analysis [7] In the development process of this tool, the lexicon to assign polarity to the text have been manually created with 2481 of the most frequently words used. Albeit most researchers have focused on assigning sentiments to documents, certain others have focused on more explicit tasks such as finding the sentiments of words, subjective expressions, subjective sentences and topics. [8]This intrinsic analysis, by analyzing the textual snippets at a fine grained level help in escalating the quality of sentiment detection at a very minute level. We have implemented the analysis of words and sentence both; this tool can help a lot of researches in the coming times.

B. Analysing Conjunctions

It has been observed that the sentence structure has a vital role in sentiment determination, and conjunctions play a major role in defining the sentence structure. [9] A conjunction is said to be a word that links words, phrases, or clauses, and it can also be used to indicate the relationship amongst the notions expressed in a clause and the notions expressed in rest of the sentence.[11] The presence of this part of speech can alter the intent of the speaker completely, if used in a specific manner. We have paid substantial importance in putting our tool to detect the sentiments wherein conjunctions are involved. While analyzing a statement with conjunctions, we divided the sentence into the corresponding number of parts as are the number of joining words in the text, then we allocate a score to each constituent snippet and add the scores hence obtained, the resultant figure is divided by the constituent snippets to obtain the total sentiment score of the sentence. Conjunctions can be broadly classified into two broad categories: Coordinative conjunctions and Adversative conjunctions. [10] The coordinative conjunctions put across the same opinion as all the composed snippets; however the adversative conjunctions on the contrary put forth a different if not opposite opinion as conveyed by the other constituent snippets. It is important that such conjunctions are differently handled. As one conjunction has the ability to alter the complete polarity of the given statement. In our tool, we have paid substantive importance to the conjunctions analysis process. The role of full syntactic parsing is extremely crucial in order to appropriately extract sentiment, as the local structures obtained by a shallow parser do not always prove to be reliable. [11]

C. Emoticons and Interjections

The most vital purpose of sentiment analysis is to understand and decode the emotion as conveyed by the texts under study. An effective method to decipher the interjections plays a very pivotal role in sentiment analysis. As interjections, is a part of speech which has the ability to convey the essence of the mood of the speaker in a word or two at maximum, once decrypted can make the task of sentiment analysis a lot easier. Our methodology to track the sentiment relies critically on pursuing the reference frequencies of adjectives with affirmative and destructive implications. [12]

For example, a sentence which contains the word "wowwwwwwww!" shall essentially convey a very ecstatic emotion; it could also be sarcastic, which we shall later analyze. This is in contrast to "wow", which can have different connotations as well. In our tool we have given careful importance to emoticons as well. The easiest of all mechanisms to detect the polarity (i.e., positive and negative affect) of a message is based on the emoticons it contains. [13] The entire emotion no matter how complex it might be to decipher it when words are involved becomes extremely easy to decode when emoticons are present in the text. Analyzing the emoticons is a very important part of sentiment analysis but it is often ignored in major sentiment analysis tools. Our tool has given weight to the emoticons involved in a statement as well. Thus incurring a feature which is absent in many others of its counterparts. The following figure depicts the segrregation of various emoticons in three broad categories: Positive, Negative and Neutral. The positive emoticons are the ones which are assosciated with a sentiment score of more than 0 (1 to 10), the negative emoticons are the ones which are assosciated with a sentiment score of less than 0(-10 to -1) . And the neutral emoticons are associated with a sentiment score of 0. These emoticons have the ability to suffice the essence of the mood of the speaker in symbols appropriately and in a fairly concise manner and hence these are one of the most optimum medium to put across ones sentiment. Therefore, there decoding process becomes of even more grave importance and need.

Emoticons and their variations

Emoticon	Polarity	Symbols
	Positive	:) :] :} :o) :o] :o} :-] :-) :-} =) =] =} =^] =^) =^} :B :-D :-B :^D :^B =B =^B =^D :') :'] :'} =') ='] ='} <3 ^.^ ^-^ ^_^ ^^ :* =* :-* ;) ;] ;} :-p :-P :-b :^p :^P :^b =P =p \o\ /o/ :P :p :b =b =^p =^P =^b \o/
	Negative	D: D= D-: D^: D^= :(:[:{ :o(:o[:^(:^[:^{ =^(=^{ >=(>=[>={ >=(>:-{ >:-[>:-(>=^[>:-(:-[:-(=(=[={ =^[>:-=(>=[>=^(:'(:'[:'{ ='{ ='(='[=\ :\ =/ :/ =$ o.O O_o Oo :$:-{ >:-{ >=^{ :o{
	Neutral	:| =| :-| >.< >< >_< :o :O =O :@ =@ :^o :^@ -.- -.-' -_- -_-' :x =X :# =# :-x :-@ :-# :^x :^#

Fig. 1. emoticons used

D. EmphaticWords

The role of emphatic words is crucial in escalating or deescalating the polarity obtained of a specific word or sentence. These emphatic words generally precede or succeed the word or group of words whose intensity they aggravate or degrade. The emphatic words draw the line between for example, a "very good" and a "good" in a sentence. These emphatic words have been carefully analyzed in our tool. We have used these words to increase the polarity of words used in a normal connotations. On encountering an emphatic word the polarity which had been previously obtained is changed and is either decreased or increased on the basis of the score of the word. It should be noted here that, if a word is positive, then on addition of an emphatic word. Its polarity becomes more positive and affirmative. However, if the word being analyzed is negative, as and when it encounters an emphatic word the polarity of the statement or textual snippet being analyzed is made more negative and deleterious. For example on encountering "very" a score of -6 becomes -10 and 6 becomes 7.

We have also given a scale to these emphatic words, i.e. an emphatic word very is less polar in comparison to the emphatic word "excellent", this is reflective in the sentiment scores which we have annotated with them.

E. Negation Tagging

Negations are the kinds of words which completely alter the meaning of words or sentence when used along with them or in them. The process of decoding these negations and assigning a sentiment score to it is termed as Negation Tagging. It is a very communal linguistic construction which has a deep effect onpolarity and therefore, needs to be taken into consideration in sentiment analysis[14] Negations as are commonly perceived does not only deal with the words like (not,neither,nor) but negation can also be conveyed by other lexical units in various languages and argots. In order to perform the conventional negation tagging we have applied a scaling algorithm , which interprets the opposite of the sentiment initially conveyed without the negative tag. For example, "I am not dissappointed by your performance" , which shall have a polarity of (-9) without the negation is changed to (7), which has its association with the impressed. Similarly, the negation tagging in our tool is performed by scaling in comaprison to the conventional approach wherein the score is only negated.Some examples of such lexical units are: valence shifters, connectors or modals. Negations are difficult to detetct, especially when lexical units are involved.Forexample in a sentence where valence shifter are involved, " The government is givng the nation less of good days and more of bad days" , this sentence can be interpreted as a neutral one usually but this sentence has a negative polarity, this is reflective of the mamoth task which are involved in the case of negation tagging. Our tool has been carefully employed with efficient mechanism to tag the negtions and alter the polarity when such a lexicon is encountered in a piece of text. An important feature which most of the analysis tools employ is to negate the polarity obtained without taking into account the negation word for sentiment analysis. This tool has incorporated the process of scaling in contrast to the conventional approach , which magnifies the performance of the tool by multitudes in comparison to its counterparts.

III. COMPARISON WITH OTHER TOOLS

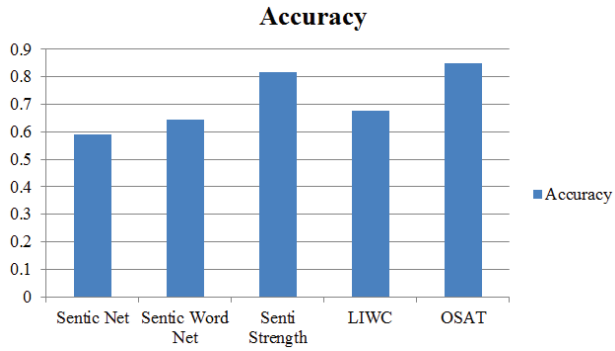

Fig. 2. Accuraracy measures of tools

The above graph shows the comparison of OSAT with the prevelent sentiment analysis tools in the industry. During the development of our tool, we had come across various tools which have implemented sentiment analysis. Our tool has implemented a sentiment score of +10 to -10, previously the highest score implemented was +5 to -5 in the case of SentiStrength [15]. This is reflected in the increased precision figure, second only to Sentic Net which gives a detailed document of analysis.

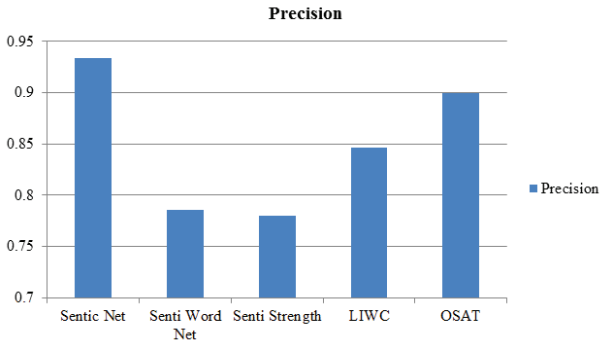

Fig. 3. precision measures of tools

We have also associated an emotion with every sentiment score which has never been done before. This is indicted in the above graph, which has ultimately led to increased accuracy levels for OSAT. The role of conjunctions has also been highlighted in our tool. We have implemented both Coordinative and Adversative Conjunctions in our tool. As mentioned afore, emoticons and interjections convey very well and in a concise manner, the opinion present in the text snippet being analyzed. This tool has also employed a mechanism to study emoticons and interjections. Emphatic words have the capability of altering the sentiment score obtained by a huge margin,

therefore, it becomes very important to bring them into consideration. This tool has brought the analysis of these emphatic words under its purview. An efficient method to analyze such words is yet to be seen. Negation Tagging has been the most crucial part of this tool, this domain of sentiment analysis has often been left untouched by most sentiment analysis due to the complexities involved in its execution. We have carefully implemented Negation Tagging in both direct and indirect form.

IV. ACKNOWLEDGMENT

In conclusion, we would like to put forth a sentiment analysis tool which brings together five of the most important and complex features of sentiment analysis in a highly efficient manner. This tool has covered about 2500 of the most common words used in the english language to depict ones emotions. This tool has also employed other data sets for stop words and sentiment score. The tool is a highly professional and useful one, which can be employed to study the data and sentiments across platforms in order to analyze people's opinion for various purposes.

REFERENCES

[1]. Federico Neri, Carlo Aliprandi, Federico Capeci, Montserrat Cuadros, Tomas By, "Sentiment Analysis on Social Media".IEEE Conference on Advances in Social Network Analysis and Mining, 2012.

[2]. J. Bollen, H. Mao, and X.-J. Zeng, "Twitter mood predicts the stock market", Journal of Computational Science (2, 1), pp. 1–8, 2011.

[3]. Thelwall, M., Buckley, K., Paltoglou, G. Cai, D., & Kappas, A. "Sentiment strength detection in short informal text." Journal of the american society for information science and technology, 61(12), 2544–2558, 2010

[4]. Mostafa Karamibekr, Ali A. Ghorbani "Sentiment analysis of social issues" International Conference on Social Informatics (SocialInformatics). 2012

[5]. Lotfi A. Zadeh, "Fuzzy logic = computing with words", IEEE Transactions on Fuzzy Systems, 2, 103-111, 1996

[6]. Calvo, R. A. & Ceccatto, H. A. "Intelligent document classification", Intelligent Data Analysis, 4(5),411–420, 2000

[7]. Choi, Y., Cardie, C., Riloff, E., & Patwardhan, S., "Identifying sources of opinions with conditional random fields and extraction patterns" Conference on empirical methods in natural language processing (EMNLP 2005), October 6–8, 2005 (pp. 355–362). Vancouver, B.C., Canada, 2005.

[8]. Church, K. W. & Hanks, P., "Word association norms, mutual information and lexicography", 27th annual meeting of the Association for Computational Linguistics (ACL), June 26–29, 1989 (pp. 76–83). Vancouver, B.C., 1989.

[9]. Derks, D., Bos, A. E. R., and Grumbkow, J. V. 2008. "Emoticons and online message interpretation", Soc. Sci. Comput. Rev., 26(3), 379-388, 2008

[10]. Gamon, M., "Sentiment classification on customer feedback data: noisy data, large feature vectors,and the role of linguistic analysis" 20th international conference on computationallinguistics (COLING 2004), August 23 – 27, 2004 (pp. 841–847). Geneva, Switzerland, 2004

[11]. Thelwall, M., Buckley, K., Paltoglou, G., Cai, D., Kappas, A., "Sentiment strength detection in short informal text", Journal of the American Society forInformation Science and Technology, 61(12), pp.2544-2558, 2010.

[12]. Hiroshi, K., Tetsuya, N., & Hideo, W., "Deeper sentiment analysis using machine translationtechnology.", 20th international conference on computational linguistics (COLING 2004),August 23 – 27, 2004 (pp. 494–500). Geneva, Switzerland, 2004.

[13]. Ishibuchi, H.,Nakashima, T., &Kuroda, T., "Ahybrid fuzzy gbml algorithmfor designing compact fuzzy rule-based classification systems.", 9th IEEE International Conference on Fuzzy Systems, 2(706–711), 2000.

[14]. K¨onig, A. C. & Brill, E., "Reducing the human overhead in text categorization", 12th ACM SIGKDD conference on knowledge discovery and data mining, August 20–23, 2006 (pp. 598–603).Philadelphia, Pennsylvania,USA, 2006.

[15]. Miller, George, and Walter Charles, "Contextual correlates of semantic similarity", 6:1-28, Language and Cognitive Processes, 1991

[16]. Pang, B. & Lee, L., "Seeing stars: exploiting class relationships for sentiment categorization with respect to rating scales", 43rd annual meeting of the Association for Computational Linguistics (ACL), June 25–30 , 2005 (pp. 115–124), 2005.

[17]. Sebastiani, F., "Machine learning in automated text categorization" ACMComputing Surveys, 34(1),1–47, 2002.

[18]. Yi, J., Nasukawa, T., Niblack,W., & Bunescu, R., "Sentiment analyzer: extracting sentiments about a given topic using natural language processing techniques", 3rd IEEE international conference on data mining (ICDM 2003), November 19–22, 2003 (pp. 427–434). Florida, USA, 2003.

[19]. L. Zhou and P. Chaovalit, "Ontology-supported polarity mining", Journal of the ASIS&T (59, 1), 2008,pp. 98–110, 2008.

[20]. D. Delen and M. D. Crossland, "Seeding the survey and analysis of research literature with text mining, Expert Systems with Applications (34, 3), pp. 1707–1720, 2008.

[21]. Fangtao Li, Minlie Huang, Xiaoyan Zhu, "Sentiment analysis with global topics and local dependency," in press.

[22]. Michael Siering "Boom or ruin – does it make a difference? using text mining and sentiment analysis to support intraday investment Decisions", in press.

[23]. Ahmed Abbasi, Ammar Hassan, Milan Dhar, "Benchmarking twitter sentiment analysis tools," in press.

[24]. Theresa Wilson, Janyce Wiebe, Paul Hoffmann, Recognizing Contextual Polarity, "An exploration of features for phrase-level sentiment analysis", unpublished.

[25]. Rudy Prabowo, Mike Thelwall, "Sentiment analysis: a combined approach", in press.

[26]. Ritesh Agarwal, T. V. Prabhakar, Sugato Chakrabarty, "I know what you feel": Analyzing the Role of Conjunctions in Automatic Sentiment Analysis", in press.

[27]. Fangtao Li, Minlie Huang, Xiaoyan Zhu, "Sentiment analysis with global topics and local dependency", unpublished.

[28]. Arun Meena and T.V. Prabhakar, "Sentence level sentiment analysis in the presence of conjuncts using linguistic analysis", in press.

[29]. Erik Cambria, Björn Schuller, Yunqing Xia, Catherine Havasi, "New avenues in opinion mining and sentiment analysis", in press.

[30]. Pollyanna Gonçalves, Matheus Araújo, Fabrício Benevenuto, Meeyoung Cha, "Comparing and combining sentiment analysis methods", in press.

[31]. G.Vinodhini , RM.Chandrasekaran, "Sentiment analysis and opinion mining: a survey" , in press.

[32]. Oren Tsur, Dmitry Davidov, Ari Rappoport, "ICWSM – a great catchy name: semi-supervised recognition of sarcastic sentences in online product reviews",in press.

Performance of Static Sink in Wireless Sensor Networks when Implementing Geographic Routing

PriyankaChugh(Shivanka)
Department of Information Technology
Maharaja Surajmal Institute of Technology
New Delhi, India
Email Id: shivankachugh84@gmail.com

Dr. S. Indu
Department of Electronics and Communication
Delhi Technological University
Delhi, India
Email Id: s.indu@dce.ac.in

Anupam Joshi
Department of Information Technology
Guru Gobind Singh Indraprastha University
Maharaja Surajmal Institute of Technology
New Delhi, India
Email Id: anupam.msit@gmail.com

Abhinav Singh
Department of Information Technology
Guru Gobind Singh Indraprastha University
Maharaja Surajmal Institute of Technology
New Delhi, India
Email Id: ab.msit1@gmail.com

Rahul Rajpal
Department of Information Technology
Guru Gobind Singh Indraprastha University
Maharaja Surajmal Institute of Technology
New Delhi, India
Email Id: rahul.rajpal.in@ieee.org

***Abstract* – Wireless sensor networks comprise of small devices called sensor nodes. Routing protocols are used in wireless sensor networks to ensure reliable multi-hop/multi-path communication. Among various routing protocols available, geographic routing is one of the most capable routing methods for wireless sensor networks due to its scalability and simplicity. The main aim of our research is to analyze static sink in geographical routing and observe its performance under various parameters such as Path Loss Exponent, Reliability, System Lifetime, Lifetime Threshold , Initial Battery Capacity etc. through extensive simulations and graphical representations. We have also highlighted problems associated with the concerned protocols.We finally conclude our research by mentioning parameter specific effects on a sensor network. We leave a future scope for analyzing mobile sink protocols through simulation, taking into consideration various parameters.**

Keywords– Compass Routing; Geographic Routing; Lifetime; LOOP problem; Lost Link problem; NFP; Reliability.

NOMENCLATURE

WSN – Wireless Sensor Network

NFP – Nearest with Forward Progress

LLNK – Lost Link Problem

GPS – Global Positioning System

I. INTRODUCTION

Recent advancements and developments in the area of wireless technology have provided us with better and low cost sensor devices and have hence, diversified the applications of wireless sensor networks. These Sensor networks have provided solutions to many problems in the areas of infrastructure, disaster management, military sensing, traffic management etc. and have become one of the most fascinating areas of research in the past few years. [1][2]

A wireless sensor network comprises of a large number of sensor nodes deployed in an ad hoc manner in the area of concern or somewhere nearby. The network also contains a *Sink* that receives the data collected by the sensor nodes for analysis. An unrestrained deployment of sensors, result in an unknown and unusual topology, which can be problematic. There are various factors that govern the design of a sensor network, like geographic area, production costs, hardware constraints, power consumption, scalability, fault tolerance, transmission media, storage capacity etc. [3]

Every sensor network should be reliable and functional for as long as possible because usually the sensor nodes are spread over large geographical areas and in hostile environments, where frequent human interference is not possible. As Reliability is the key concern, there are various ways to increase reliability, but each one of them comes with certain drawbacks and constraints (cost being the most common factor). Reliability is also dependent on the functionality of the sink. Sensor networks can have either a static sink or a mobile sink. A mobile sink moves in the area where the sensors are deployed, to collect data, and the static one is a fixed node serving as the destination. The main aim of our paper is to analyze scenarios with a static sink, through extensive simulations of widely used approach called geographic routing (Compass, NFP) and to show how various factors and parameters affect the functioning of the whole network. The

978-9-3805-4421-2/16/$31.00 ©2016 IEEE

rest of the paper is organized as follows: Section 2 summarizes geographic routing and its concepts with a static sink. The sub sections, 2.1, 2.2 and 2.3 analyze the routing protocols, the problems with the routing protocols and the parameters respectively. Section 3 shows results and graphs based on simulations of the concerned protocol. We conclude our paper with section 4.

II. GEOGRAPHIC ROUTING WITH A STATIC SINK

As described in the introduction, a *Sink* that receives the data collected by the sensor nodes for analysis. This section analyzes the various parameters related to the network, and geographical routing, NFP in a scenario with a static sink. Geographical routing takes location into consideration (using GPS) for devising aproficient route to the destination. This routing is apposite to sensor networks, where data aggregation is a helpfulway to decrease the number of transmissions directed to the base station by eliminating redundancy among packets from the diverse sources. Geographic routing has great scalability and simplicity and can also support mobility of nodes.

Also, in thisrouting, only locations are shared between the nodes, which reduce the overhead too. [4]

A The routing Protocols

In a typical WSN setup, the main energy consumer is the communication element of each node. In practice, multi-hop communication is requisite for data transmission, from source to the sink node.There's a widely used greedy forwarding strategy which considers distance instead of progress, i.e. one node sends packets to the neighbour that is closest to the destination, but there are various problems associated with it.If signal strength is a fixed parameter, sending the packet to a neighbour, far away in the border area of transmission range leads to a greater probability of packet loss due tonode mobility and signal attenuation.

So by varying signal strength to the desired level, for nearest neighbours, the probability of message failure due to collision can be reduced significantly. *Nearest with forward progress (NFP)* transmits packet to the nearest neighbour of the sender which is closer to the destination (See Fig.1).

(Note: *To have higher signal strength, a larger battery capacity is required.The battery capacity also has to be kept fixed, and the whole setup should be economic, as Increasing it may lead to a higher cost.*)

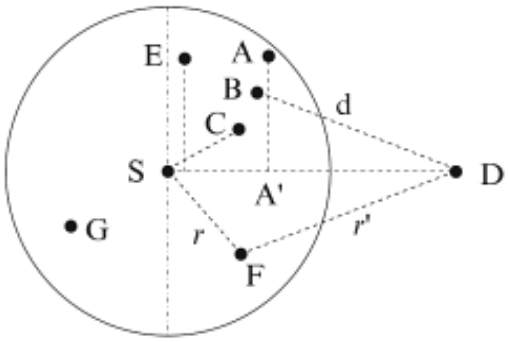

Fig. 1. Sensor Network Scenario

The distance between a node S and the projection A' of a neighbor node A onto the line connecting S and destination D is defined as progress.Here, Node A is neighbour of node S with most forward progress, B has least distance to D and C is closest in direction to D, Node E is the nearest neighbour with forward progress.Neighbors having positive progress are termedas nodes in forward direction. In the figure above, the neighbors A, B, C, E, and F are in forward direction. The G node however, is said to be in the backward direction. Direction-based methods use the deviation (angle between next hop, current, and destination node) from the line that connectsthe destination andcurrent sender. [5][6]

Compass routing is a direction based method, and itselects the neighbor closest to the straight line between sender and destination.

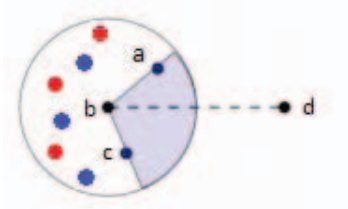

Fig. 2. Sensor Network Scenario

Let's say, *b* has to relay data to the next node, and it uses the compass routing scheme, so it will select the neighbor closestto the straight line between*u* and *d,* i.e. either angle *abd* or angle *cbd*. Also, if there is a case where the angles are the same in both, clockwise and counter clockwise cases, then the node having the smallest distance to the destination is selected. This kind of compass scheme is called the greedy compass algorithm.[7]

In real time/ live scenarios, the sensor nodes save their location marked through GPS and further use it for calculations of angles and distances using simple formulas. The location of the node is saved in terms of coordinates (X and Y).

B Problems with these Protocols

The chief energy consumer is the communication unit of each sensor node. Multi-hop communication is essential for sending data from source to sink nodes. Consequently, the energy

expenditure increases with communication distance.Communication distance can be reduced bydeploying multiple static sinksand by programmingeach sensor node such that they route the data to the nearest sink.

However, a bigissue with multiple static sinks is that theposition of their deploymenthas to be decided, inside the monitored region so that the data relaying load can be balanced amongst the nodes.This can be regarded as a very well-known problem called ''*facility location problem*'' where for a given number of facilities and customers the optimal position for the placement of the facilities has to be known, so that all facilities are equally burdened. However, even if we assume location-optimal deployment of static sinks, the nodes closer to the sink will have a rather rapid energy dissipation.[8][9]

These protocols also have node mobility induced errors known as LLNK and LOOP problem. These problems occur due to inaccurate location information and mobility of nodes. Loop problem causes formation of loops in message transmission, while in lost link problem, a node that is no longer there at the specified position, as the neighbour, is still mentioned in the routing table as the nearest neighbour. [10]

III. CONCERNED PARAMETERS

We have analyzed the effect of various parameters on the whole network and how they vary with changes in other parameters. We've taken into account, parameters like, Sink Position, Reliability, System Lifetime, Lifetime Threshold, Sensor Numbers, Transmission time etc. Sink Position, is a simulator specific parameter where we specify the position of the sink as X and Y coordinates. Reliability tells us about how reliable a network is, in terms of its functioning. System Lifetime is defined as the time for the first node or a percentage of nodes to die (run out of power) and is specified in seconds. [11] Lifetime Threshold is defined as the initial energy that the nodes possesses and varies from 0.1 to 1.0. Sensor numbers tell us about the number of sensors present in the topology, while the transmission time is defined as the time taken by a node to transmit data.

IV. SIMULATIONS AND GRAPHS

Through extensive simulations we have analyzed the effect of specific parameters on the sensor network and how variations in these parameters change the performance and what their consequences are. We have used an indigenous Java based simulator that uses the NFP algorithm.This simulator takes into consideration various factors and parameters mentioned in section 3.We have used graphs to explain the effect of these parameters on each other.

A System Lifetime vs. Lifetime Threshold

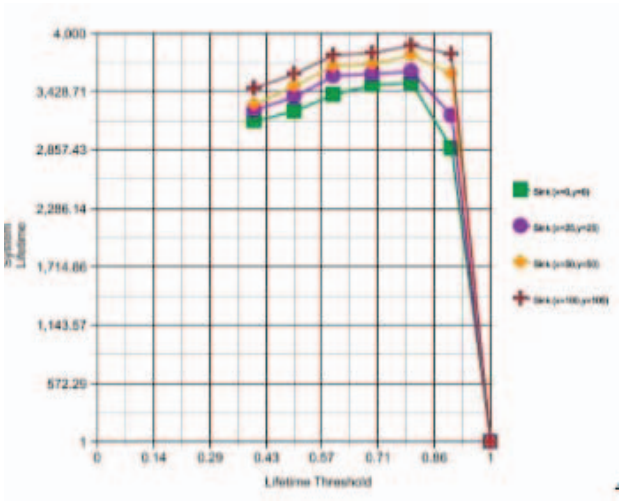

Fig. 3. System Lifetime vs. Lifetime Threshold

This graph shows how System Lifetime and Lifetime threshold (described in Section 3) vary with each other. We have taken 4 scenarios, where the position of sink is different in each case. As we increase the lifetime threshold, the system lifetime also increases slowly and fluctuates between 3400 and 3900. We can clearly see how different positions of the sink in the network result in different system lifetimes, the highest being in case of 100, 100(X & Y).When we further increase the Lifetime threshold to the extreme value, i.e. 1, the System Lifetime becomes zero, as that would be an ideal case. Hence, with a steady increase in the lifetime threshold, the system lifetime also increases till a specific point, with fluctuations.

B Lifetime Threshold vs. Reliability

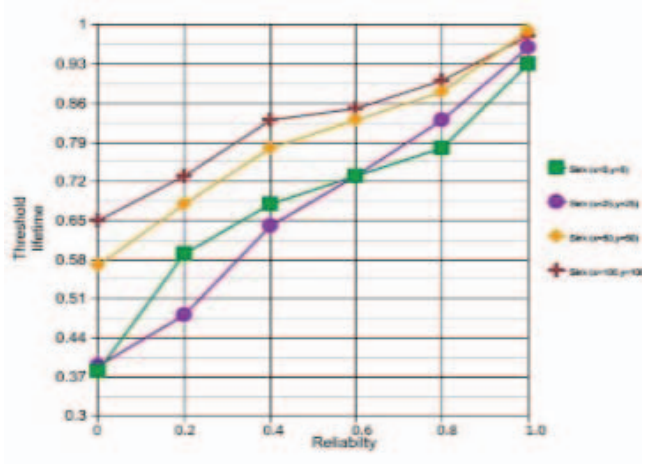

Fig. 4. Lifetime Threshold vs. Reliability

This graph shows how Lifetime Threshold varies with reliability. These terms have been defined in section 3 of the paper. We have taken 4 scenarios, where the position of sink is different in each case. With increase in Lifetime threshold the reliability grows considerably. In the 4 different scenarios, of 4 different positions, the growth in the case of sink position (100,100), is the least, while that in the case of (25, 25) is the most. These coordinates specify the position of the sink within the network. As the lifetime threshold approaches to value 1, the reliability also escalates till 1 (ideal case). Hence we can say that the reliability increases with increase in lifetime threshold, however the increase is subjective to the position of the sink.

C Number of Sensors vs. Reliability

This graph (Fig. 5) shows how reliability is related to sensor numbers. The reliability for the least number of sensors (50) is the lowest, but as the number of sensors increase, the reliability goes up and then fluctuates between 0.55 and 0.59 for numbers greater than 150. We can say that, if we further increase the sensor numbers, there won't be any significant change in the reliability. Less number of sensors would make the network less reliable, however if we keep increasing the number, the reliability won't change much after a particular point.

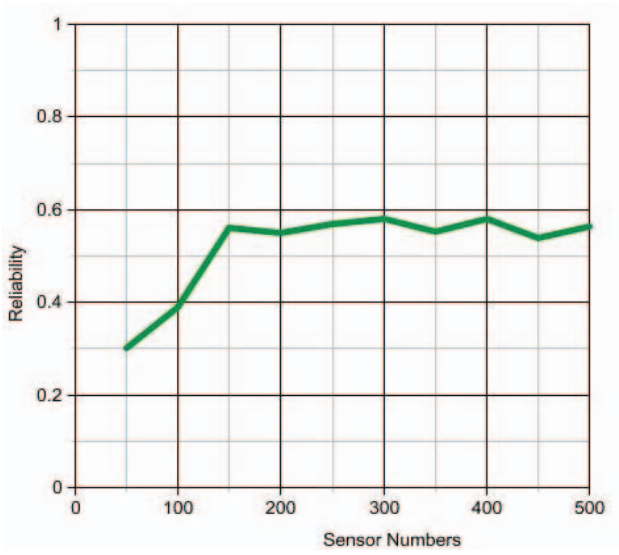

Fig. 5. Number of Sensors vs. Reliability

D System Lifetime vs. Transmission Time

This graph shows how System Lifetime and Transmission Time (described in section 3) vary with each other. As transmission time increases, the system lifetime drops.

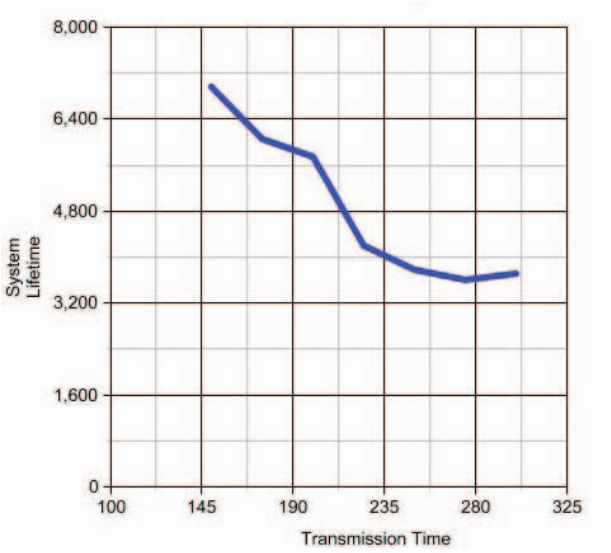

Fig. 6. System Lifetime vs. Transmission Time

When the transmission time approaches values near 250 and further, the system lifetime becomes somewhat stable (between 3600 and 3800). We haven't considered very large values of transmission time because they would lead to a sensor network with slow transmission and hence it would make the network less reliable. We can conclude by saying that larger transmission time makes the network (system) lifetime small and also makes it less reliable.

V. CONCLUSION AND FUTURE SCOPE

In this paper we have extensively compared various parameters related to a sensor network in a scenario of geographical routing that has a static sink.Geographic routing is a suitable routing method due to its simplicity and scalability. Our graphs and results demonstrate how the parameters considered vary with each other and what the consequences of variations of these parameters are. The paper describes various aspects of a network with a static sink, however it does not tell about the possibilities and improvements after introduction of a mobile sink. We aim to collect supplementary information in future, about mobile sinks in geographical routing, further analyze and study the trends in it. We also aim to target various issues and problems incurred during the mobility of a sink and also to build a more refined mobility scheme that can make wireless sensor networks more efficient and reliable.

REFERENCES

[1]. Majid I. Khan, Wilfried N. Gansterer, Guenter Haring , "Static vs. mobile sink: The influence of basic parameters on energy efficiency in wireless sensor networks",*Computer Communications 36 (2013) 965–978*

[2]. Vivek Katiyar, Narottam Chand, Naveen Chauhan, "Recent advances and future trends in Wireless Sensor Networks", *International Journal Of Applied Engineering Research*,Dindigul,Volume 1, No 3, 2010

[3]. Ian F. Akyildiz, Weilian Su, YogeshSankarasubramaniam, and ErdalCayirci Georgia Institute of Technology, "A Survey on Sensor Networks", *IEEE communications Magazine 2002*
[4]. Rama Sundari Battula, O. S. Khanna – "Geographic Routing Protocols for Wireless Sensor Networks: A Review", *International Journal of Engineering and Innovative Technology (IJEIT),*Volume 2, Issue 12, June 2013
[5]. [Hannes Frey, Stefan Ruhrup, and Ivan Stojmenovic – *Routing in Wireless Sensor Networks*
[6]. Sudip Misra, Issac Woungang, Subhas Chandra Misra - *Guide to wireless sensor networks*
[7]. Samir Medjiah**,** Toufik Ahmed, Francine Krief, "AGEM: Adaptive Greedy-Compass Energy-aware Multipath Routing Protocol for WMSNs, *7th IEEE Consumer Communications and Networking Conference (CCNC),* 2010, Las Vegas : United States (2010)
[8]. Denis Krivitski , Assaf Schuster , and Ran Wolff – "A Local Facility Location Algorithm for Sensor Networks", *In DCOSS '05, Conference 2005*
[9]. Christian Frank and Kay Romer, "Distributed Facility Location Algorithms for Flexible Configuration of Wireless Sensor Networks", *Third IEEE International Conference, DCOSS 2007,* Santa Fe, NM, USA, June 18-20, 2007.
[10]. D.ArockiaNancy, P.Anbumani, "GRGPS – Geographic Routing based on Greedy Perimeter Stateless Position for Multi- Hop Mobile Ad-hoc Networks", *International Journal of Emerging Trends & Technology in Computer Science (IJETTCS)*, Volume 2, Issue 2, March – April 2013.
[11]. Kewei Sha and Weisong Shi, "Modeling the Lifetime of Wireless Sensor Networks", *Sensor Letters* Vol.3, 1–10, 2005

Sensors and Actuators B 243 (2017) 59–63

Contents lists available at ScienceDirect

Sensors and Actuators B: Chemical

journal homepage: www.elsevier.com/locate/snb

Photoacoustic sensor for trace detection of post-blast explosive and hazardous molecules

Ramesh C. Sharma*, Subodh Kumar, Surya Gautam, Saurabh Gupta, Hari B. Srivastava

Laser Science and Technology Centre, DRDO, Delhi, 110054, India

ARTICLE INFO

Article history:
Received 14 May 2016
Received in revised form 24 October 2016
Accepted 24 November 2016
Available online 24 November 2016

Keywords:
Quantum cascade laser
Laser photoacoustic sensor
Laser spectroscopy
Trace detection
Post-blast explosive

ABSTRACT

The development of a sensor based on laser photoacoustic spectroscopic technique for detection of nanogram quantity of hazardous molecules, drugs and post-blast explosive is discussed. Traces of explosive and hazardous molecules on nanogram scales collected by swiping small pieces of paper on the contaminated surfaces have been detected. The Photoacoustic cell used in the sensor is of T type. The cell is designed using COMSOL software and developed with a compatible sensitive microphone. The photoacoustic signal is detected via indirect method. Sample kept in the cell was not in direct contact of the microphone. Indirect photoacoustic experiments have been done in closed cell. Tunable quantum cascade laser having tunability in the wavelength range of 7–9 μm (wavenumber 1400–1100 cm^{-1}) was used in the experiments. A phase sensitive data acquisition system has also been developed. The developed sensor is capable to identify traces of explosives up to the order of ppb level in post blast materials.

© 2016 Published by Elsevier B.V.

1. Introduction

As a result of invention of quantum cascade lasers (QCL) [1], laser absorption spectroscopy (LAS) in the mid-infrared is rapidly becoming a viable alternative to other analytical methods such as FTIR for trace-gas spectroscopy. The QCL is a new type of mid-IR tunable semiconductor laser based on intersubband transitions in a multiple quantum well heterostructure, designed by means of band-structure engineering grown by molecular beam epitaxy [MBE]. Recently, the QCL has attracted much attention due to its room temperature operation and its superior output power and mode quality as compared to that of lead salt diode lasers [2]. Many vapor phase chemical direct photoacoustic sensors based on QCL have been demonstrated [3]. The transduction displacement has been studied using the photoacoustic spectroscopy [4]. Laser photoacoustic spectroscopy has been used for trace detection of vapor, gas and aerosols [5–8]. Photoacoustic spectroscopy has also been utilized for detection of explosives and other remote sensing applications [9,10].

In present work, a photoacoustic laser spectrometer system with QCL emission in the mid-infrared range has been developed. A high quality factor resonant photoacoustic cell was used in the system. For the first time (to the best of our knowledge), a resonant cell catering to solid powder, liquid, thin film and vapor on adsorbed surfaces has been developed. The system is also capable to detect the samples taken on paper by swiping through the contaminated surfaces (sample quantity in nanogram). The resonant frequency of the photoacoustic cell was 25 kHz. The detection limit of the system was estimated to be of the order of nanogram for molecules of TATP and plastic explosive. With the developed system, we have been able to detect explosives (including Plastic explosives) and gun powder which are very challenging to detect otherwise. In the present scenario, the system has potential applications in ensuring homeland security by way of forensic investigation of traces of explosives and onsite post blast examinations of explosive materials.

2. Acoustics of the photoacoustic cell

The photoacoustic (PA) cell performs three functions: keeping the sample confined, providing a structure to connect the various components of the sensor, and increasing the photoacoustic signal. To maximize the later function, the acoustic properties of the PA cell need to be considered carefully. There are several approaches of cell design for influencing the PA signal: acoustic resonance, acoustic filters, buffer volumes, differential cell designs and multi-pass etc. Acoustic resonance is the most important of these, and the most complex to design.

* Corresponding author.
E-mail addresses: ramehsharma@lastec.drdo.in, rameshsmarma06@yahoo.com (R.C. Sharma).

http://dx.doi.org/10.1016/j.snb.2016.11.133
0925-4005/© 2016 Published by Elsevier B.V.

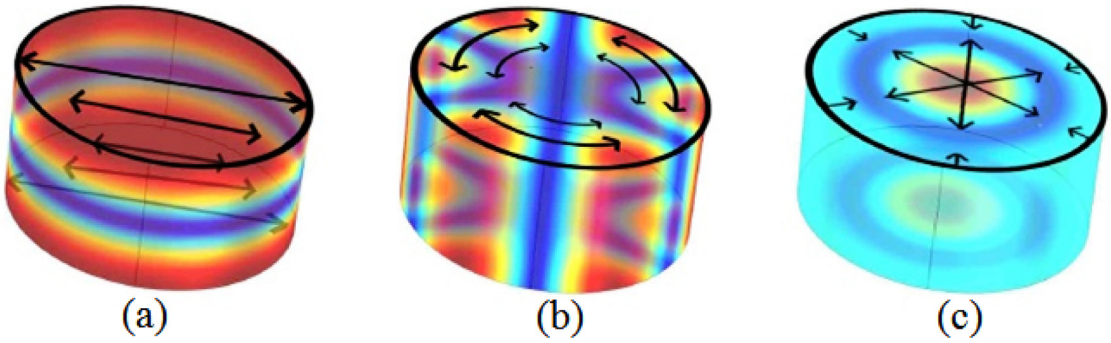

Fig. 1. Acoustic resonance modes in a cylindrical cell (a) longitudinal, (b) azimuthal and (c) radial.

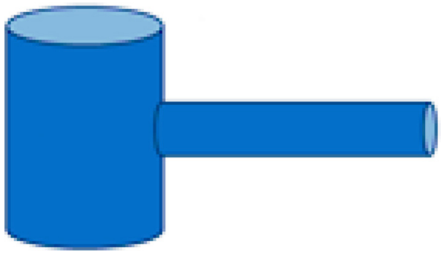

Fig. 2. T-shaped Photoacoustic cell geometry.

2.1. Acoustic resonance

As described before, designing the cell with acoustic resonance in mind allows the cell to function as an acoustic amplifier. The higher is the Q-value (quality factor), the lower the concentrations of material that can be detected in the cell. In a cylindrical cell, resonance can occur along three axes: longitudinal, azimuthal and radial resonance as displayed in Fig. 1. The resonance frequencies in a cylindrical cell can be estimated with the following equation:

$$f_{jmq} = \frac{c}{2}\sqrt{\left(\alpha_{jm}/R\right)^2 + \left(q/L\right)^2}. \quad (1)$$

Here, R and L are the radius and length of the cylinder, the indices *j, m* and *q* (non-negative integers) refer to the eigenvalues of the radial, azimuthal, and longitudinal modes, respectively, and α_{jm} is the j^{th} zero of the derivative of the m^{th} Bessel function divided by π. It is possible to choose the modes which are effectively excited and detected, depending on placement of the laser and the microphone.

2.2. Design of photoacoustic (PA) cell geometry

In contrast to other spectroscopic techniques, a specialty of the photoacoustic spectroscopy is that one can take advantage of acoustic resonances of the sample cell to enhance the signal. The photoacoustic signal and hence the sensitivity gets enhanced considerably due to the formation of standing waves in the PA cell generated by the constructive interference of the sound waves. The widely used geometry of sample cells is cylindrical, however, Miklós *et al.* have investigated a large number of other cell shapes in gas phase, direct photoacoustic method [11]. Wolff et al. have introduced the so called T-type photoacoustic for samples in vapor and gaseous phases [12]. The possibility of independent optimization of key parameters affecting sound generation and signal enhancement in T-type cell (Fig. 2) gives an edge to the cell in comparison to the cylindrical cell. In our experiments, PA cell is designed and developed for indirect photoacoustic method to detect samples on a piece of paper swiped on the suspected surfaces, liquid adsorbed on surfaces and samples in powder & liquid forms.

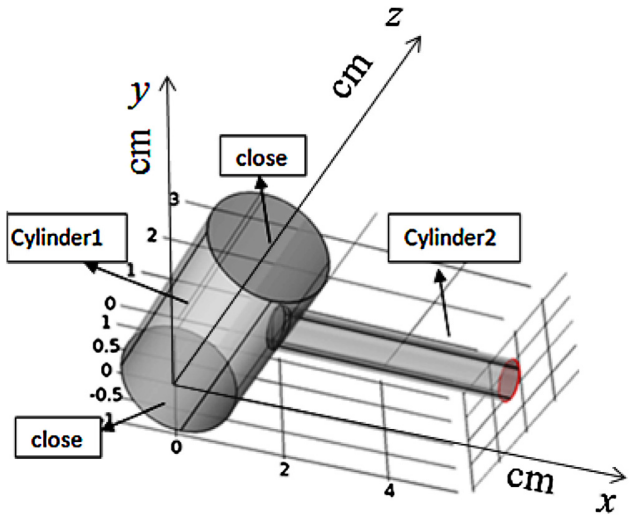

Fig. 3. Dimensions of the designed T type resonant photoacoustic cell.

2.3. Simulation of T type photoacoustic cell

The acoustic chambers are modeled in 3D in COMSOL, by adding or joining simple geometrical shapes, mostly cylinders. The structures are filled with air from the COMSOL Materials Library. The material properties used are ρ(air density)and *c* (sound velocity in air).The surfaces of the cylinders are considered sound hard walls, which mean the normal component of the acceleration at the surface is zero. Because the inside of the cylinder has zero dipole charge and has constant fluid density, the normal derivative of the pressure is also zero:

$$\frac{dp}{dt} = 0 \quad (2)$$

If the end of a cylinder is left open, this surface is modeled as a sound soft wall where the acoustic pressure is zero ($p = 0$). Two cases are possible for designing the T cell; both end closed and one end open. In our design, we have considered cell with both the ends closed. The geometry and dimensions of the designed cell are shown in Fig. 3.The dimensions of the PA cell have been worked out using COMSOL software program and are shown in Table 1.

Resonant frequencies of T type PA cell were calculated using the COMSOL sofware program. The resonant frequency spectrum is shown in Fig. 4. The decsrete dominent resonant frequencies of the PA cell were found to be 500 Hz, 4.0 kHz, 10 kHz, 15 kHz, 25 kHz, 40 kHz. The bandwidth was narrow (few Hz) at each resonant frequency.The ampltude of average pressure is the maximum at resonant frequency of 25 kHz.

Table 1
Dimensions of T type Resonant Photoacoustic cell.

Sl. No.	Description	Value (in cm)
1	Radius of Cylinder 1	1.06
2	Height of Cylinder 1	3.87
3	Radius of Cylinder 2	0.38
4	Length of Cylinder 2	4.42

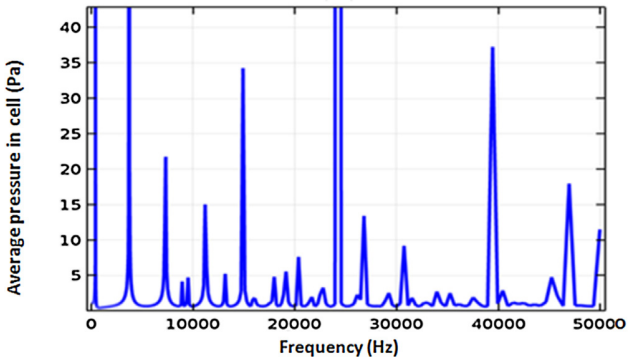

Fig. 4. Calculated resonant frequency spectrum of the designed photoacoustic cell.

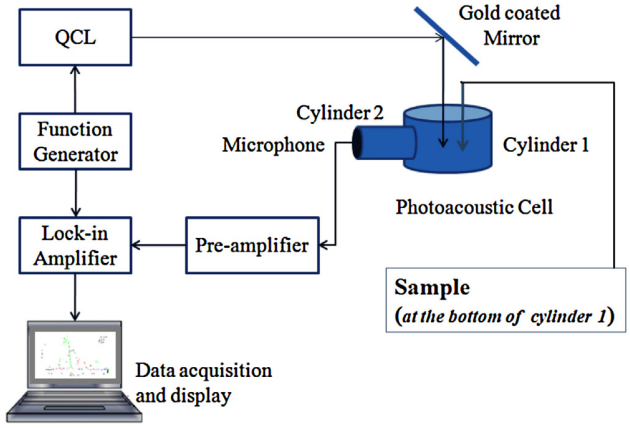

Fig. 5. Schematic of Experimental set up for trace detection based on laser photoacoustic spectroscopy.

3. Experimental

The schematic diagram of the experimental setup is shown in Fig. 5. The laser source and the acoustic detector are situated away from the target sample. The samples were kept at the bottom of cylinder 1 of the PA cell and the microphone was integrated to the far end of cylinder 2 of the PA cell, so that there was no direct contact between sample and microphone. The samples setting procedure was as follows: The top lid (Mid IR transmission window) of the cylinder 1 of the photoacoustic cell used to be opened to introduce the sample. From the top opening, samples were placed at the bottom of the cylinder 1 using a spatula (powdered sample) or a micropipette (liquid sample). For the samples adsorbed on surfaces, small piece of paper (~1 cm x 1 cm) or steel plates were used. For collecting the samples, the pieces of paper or steel were swiped through the contaminated area. The commercially available pulsed tunable QCL sourced from M/s. Daylight Solutions was used. A commercially available quartz microphone having resonance frequency of 25 kHz was used. The PA cell has been fabricated for the acoustic resonance frequency maximum at 25 kHz. Acoustic wave propagates from sample cell cylinder 1 to microphone cylinder 2 through boundary layer/coupling media and through metallic connectivity

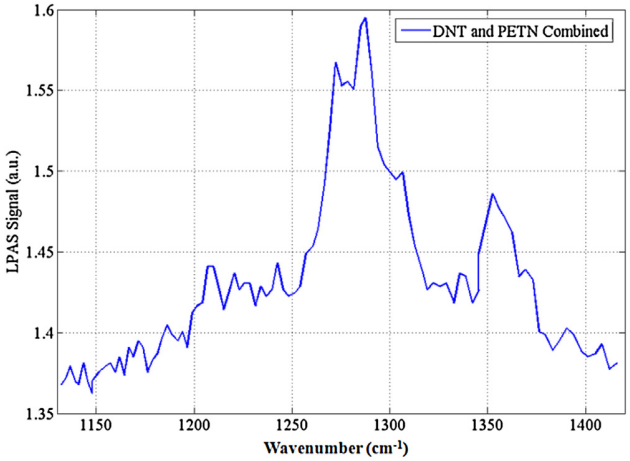

Fig. 6. Photoacoustic spectrum of mixture of PETN and DNT explosives materials in powder form and microgram quantity. The peaks 1287 cm^{-1}, 1276 cm^{-1} and 1355 cm^{-1} to DNT.

of cylinder. The cell is capable of both open and close operation. Photoacoustic signal is amplified by a pre-amplifier (based on two-stage AD829 IC) and fed to Lock-in-amplifier (Stanford Research SR 830). The signal is then processed through the electronic set-up as shown in Fig. 5. A Lab view based Graphical User Interface (GUI) based software was integrated into the PA set up for automatic operation. The experiments were conducted at ambient temperature of 25 °C. The temperature of the PA cell was the same as there was no additional temperature control mechanism provided with the cell.

4. Results and discussion

Tunable quantum cascade laser radiations were made to fall on the sample. The sample absorbs laser radiations and after absorption, the non-radiative relaxation takes place accompanied by emission of heat. Since the laser is modulated this emission of heat generates a pressure wave which comes to the boundary layer of the samples. The boundary layers were also coupled with the atmospheric air present inside the cell. This pressure wave is converted in the electrical signal by the Piezo microphone detector. We have recorded photoacoustic spectra as voltage versus wavenumbers of the tunable quantum cascade laser. The photoacoustic spectra of mixture of explosives, explosives, chemical warfare agents and drugs were recorded in the tuning range (1400–1100 cm^{-1}) of the quantum cascade laser (QCL) and are shown in Figs. 6–9. These spectra were recorded with the samples in three forms-powders, liquid and adsorbed/swiped on small pieces of paper. In the group of powdered materials, samples of explosives namely RDX, PETN and DNT were used. Their characteristic peaks in the form of Photoacoustic spectra are shown in Figs. 6–8. Fig. 6 shows the photoacoustic spectrum of mixture of explosives PETN and DNT in the powder form. The characteristic peaks of these two can easily be identified at 1287 cm^{-1}, 1276 cm^{-1} and 1355 cm^{-1} respectively. The first two belong to PETN and the last one to DNT. The Photoacoustic spectra of post-blast explosive materials (explosives mixed in soil and moisture) are depicted in Figs. 7 and 8. In Fig. 7, the graph (a) shows the baseline i.e. the spectrum of soil and moisture only. Graphs (b)–(d) show the spectra of post blast explosive materials having concentration of RDX of the order of 30 ppb, 100 ppb and 1 ppm. All the peaks of RDX (~1238, 1269 and 1320 cm^{-1}) are clearly resolved. Fig. 8 shows the Photoacoustic spectra of (a) moistened soil, (b) post-blast explosive (PETN mixed with moistened soil) and (c) PETN. The concentrations of PETN in these spectra were

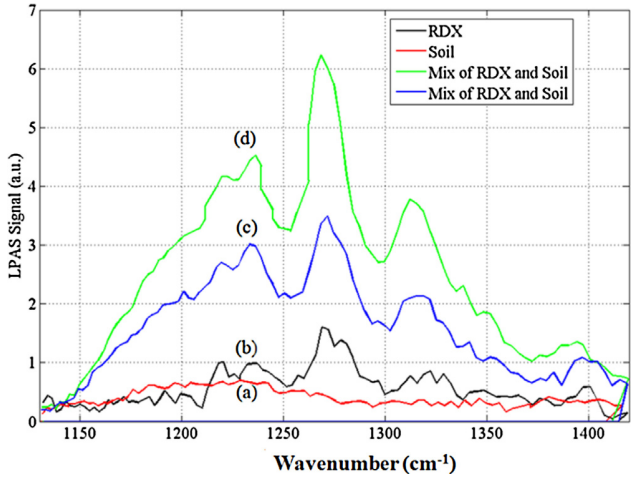

Fig. 7. Photo acoustic spectrum of (a) only moistened soil, (b) 30 ppb of RDX (c) 100 ppb of RDX and (d) 1.0 ppm of RDX mixed in post-blast material (moistened soil) in powder form. The prominent peaks are at wavenumbers around 1238, 1269 and 1320 cm^{-1}.

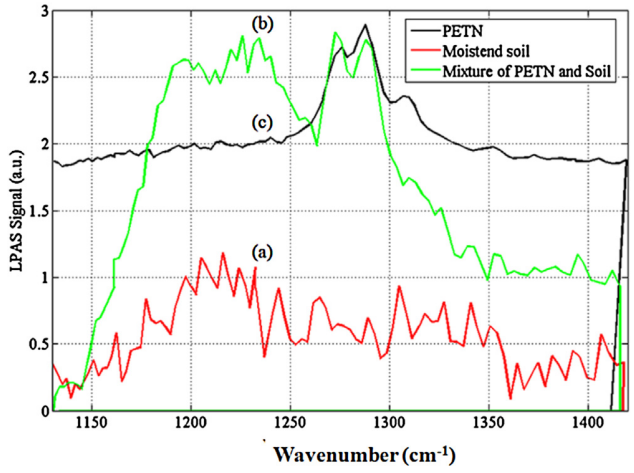

Fig. 8. Photoacoustic spectra of (a) moistened soil only, (b) 300 ppb of PETN mixed in soil and (c) pure PETN in powder form (swiped on a piece of paper).

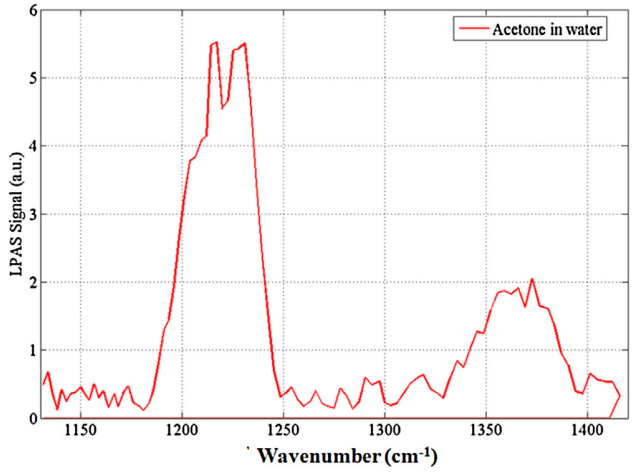

Fig. 9. Photoacoustic spectrum of 20 ppb of Acetone (Precursor of TATP) in water. The characteristic peaks are at 1217 and 1231 cm^{-1}.

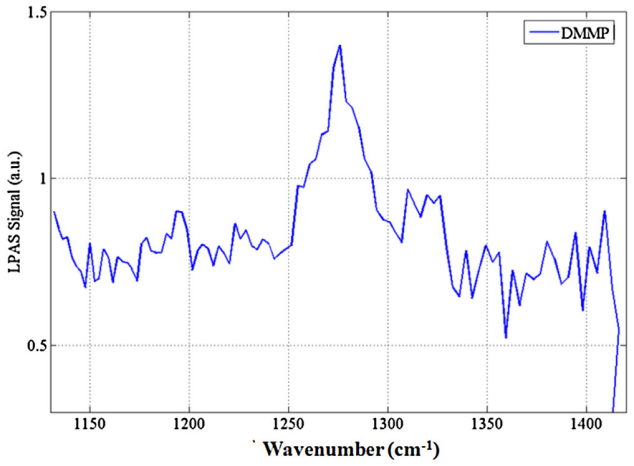

Fig. 10. Photoacoustic spectra of chemical warfare agent DMMP (simulant of Sarin) collected by swiping a piece of paper on the contaminated surface.

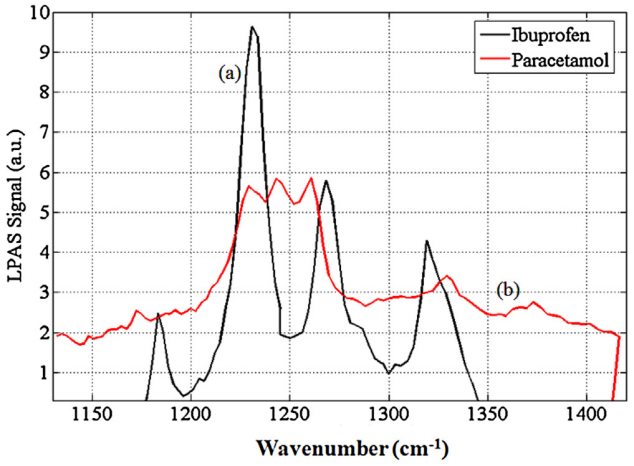

Fig. 11. Photoacoustic spectra of (a) Ibuprofen (peaks at 1230, 1268 and 1319 cm^{-1}) and (b) paracetamol (peaks at 1260, 1243 and 1229 cm^{-1}) collected by swiping a piece of paper on the contaminated surface.

nil, 300 ppb and 100 ng respectively. The prominent characteristic peaks (1287 cm^{-1} and 1276 cm^{-1}) are resolved clearly.

In the group of liquid samples, we have recorded the photoacoustic spectrum of acetone mixed in water. The acetone is a precursor of TATP explosive. Fig. 9, shows the photoacoustic spectrum of Acetone mixed in water. The prominent peaks (1217 and 1231 cm^{-1}) of Acetone can be observed precisely in the mixtures. The concentration of Acetone in the samples was of the order of 20 ppb. A liquid sample of DMMP (a simulant of Sarin) was swiped on a paper (quantity ~100 μg) for taking the photoacoustic spectrum. The spectrum of the same is shown in Fig. 10. The characteristic peak of DMMP (1276 cm^{-1}) can be identified clearly.

In another category, we have taken the photoacoustic spectra of drugs: Ibuprofen and Paracetamol. For taking photoacoustic spectra, the samples were swiped on paper. The quantities of these drugs were of the order of 10 micrograms. The photoacoustic spectra of these drugs are shown in Fig. 11. Figs. 11(a) and (b) correspond to Ibuprofen and Paracetamol respectively.

5. Conclusion

A system based on Photoacoustic spectroscopy has been developed which has unique capability to detect traces of explosives

materials, hazardous chemicals and drugs in various forms such as powder, liquid and samples adsorbed on surfaces. T-type Photoacoustic cell was design and developed for the detection of traces of explosives in the post-blast materials. All the experiments have been carried out using indirect photoacoustic spectroscopy method in T-type Photoacoustic cell at 25 kHz resonant frequency. Experimental results show that components of mixture of these materials can be identified. Explosives such as RDX, DNT, and PETN mixed with moistened soil can be identified up to nanogram level. A Precursor of TATP (Acetone) mixed in water can be detected up to the order of 20 ppb. Samples swiped on paper have also been detected. The methodology is useful for forensic applications.

Acknowledgements

Authors are thankful to Dr. Chris R Webster and Dr. Stan Sander, Jet propulsion laboratory NASA, USA for fruitful discussion for this work. Authors are also thankful to Professor J. P. Singh, MSU, USA, Professor Thomas Thundat, Alberta University, Canada and Professor S. N. Thakur, BHU, Varanasi for their valuable suggestions.

References

[1] J. Faist, C. Federico, L.S. Deborah, S. Carlo, A.L. Hutchinson, A.Y. Cho, Quantum cascade laser, Science 264 (1994) 553.
[2] F. Xie, C. Caneau, H.P. Leblanc, D.P. Caffey, L.C. Hughes, T. Day, C-en. Zah, Watt-level room temperature continuous-wave operation of Quantum cascade laser with (>10 μm), IEEE J. Sel. Top. Quantum Electron. 19 (2013) 1200407.
[3] E. Holthoff, J. Bender, P. Pellegrino, A. Fisher, Quantum cascade laser based photoacoustic spectroscopy for trace vapor detection and molecular discrimination, Sensors 10 (2010) 1986.
[4] A. Talukdar, M.F. Khan, D. Lee, S. Kim, T. Thundat, G. Koley, Piezotransistive transduction of femtoscale displacement for photoacoustic spectroscopy, Nat. Commun. 6 (2015) 7885.
[5] M.C. Phillips, T.L. Myers, M.D. Wojcik, B.D. Cannon, External cavity quantum cascade laser for quartz tuning fork photoacoustic spectroscopy of broad absorption features, Opt. Lett. 32 (2007) 1177.
[6] K. Liu, S. Zha, Q. Liu, W. Chen, X. Gao, Development of photoacoustic spectroscopy sensor for aerosol optical absorption measurement, in: Light, Energy and the Environment 2015, OSA Technical Digest, Optical Society of America, 2015, paper JTu5A.18. 10.1364/PV.2015. JTu5A.18.
[7] N.E. Glauvitz, R.A. Coutu, I.R. Medvedev, D.T. Petkie, Terahertz photoacoustic spectroscopy using an mems cantilever sensor, J. Microelectromech. Syst. 24 (2015) 216.
[8] B.A. Paldus, T.G. Spence, R.N. Zare, C. Gmachl, F. Cappasso, D.L. Sivco, J.N. Baillargeon, A.L. Hutchinson, A.Y. Cho, Photoacoustic spectroscopy using quantum-cascade lasers, Opt. Lett. 24 (1999) 178.
[9] J.S. Li, B. Yu, H. Fischer, W. Chen, A.P. Yalin, Quantum cascade laser based photoacoustic detection of explosives, Rev. Sci. Instrum. 86 (2015) 031501.
[10] T. Berer, M. Brandstetter, A. Hochreiner, G. Langer, W. Märzinger, P. Burgholzer, B. Lendl, Remote mid-infrared photoacoustic spectroscopy with a quantum cascade laser, Opt. Lett. 35 (2010) 4151.
[11] A. Miklós, P. Hess, Z. Bozóki, Application of acoustic resonators in photoacoustic trace gas analysis and metrology, Rev. Sci. Instrum. 72 (2001) 1937.
[12] M. Wolff, H.G. Groninga, B. Baumann, B. Kost, H. Harde, Resonance investigations using PAS and FEM, Acta Acustica 91 (Suppl. (1)) (2005) 99.

Biographies

Ramesh C. Sharma is currently a Senior Scientist with the Laser Science and Technology Centre, Defense Research and Development Organization, Delhi, India. He received the Ph.D. degree in experimental laser spectroscopy from BHU Varanasi, Varanasi, India, in 1995. He was a Post-Doctoral Fellow with IIT Kanpur, Kanpur, India, University of California, San Diego, USA, and Mississippi State University; Starkville, MS, USA. He has worked several years as a Research Fellow/Scientist with the University of Tokyo, Tokyo, Japan, the University of Leeds, Leeds, and the University of Manchester, Manchester, U.K. He has worked in the field of laser technology, laser spectroscopy, nonlinear optics, nanotechnology, chemical dynamics, laser plasma physics, and laser remote sensing technologies. Dr. Sharma is the Group Leader and working on remote sensing of bio and hazardous molecules using ultraviolet laser-induced fluorescence technique and quantum cascade laser photoacoustic spectroscopy. He is a Life Member of the Indian Laser Association and the Laser and Spectroscopy Society of India.

Subodh Kumar received the M.Sc. degree in physics from Patna University, Patna, India, in 1998. He is currently pursuing the Ph.D. degree in physics with the Indian Institute of Technology Delhi, Delhi. He joined the Laser Science and Technology Centre, Defense Research and Development Organization, Delhi, India, in 2001, as a Scientist. He is involved in, laser Photoacoustic spectroscopy of explosive and other hazardous materials after having brief experience in the synthesis and characterization of laser materials (glasses). His research interests also include remote sensing of bio-molecules using ultraviolet laser-induced fluorescence technique and terahertz generation by laser plasma interaction. Mr. Kumar is a Life Member of the Indian Laser Association.

Surya Kumar Gautam received the B.E degree in Electronics and Communication engineering from Delhi Technological University, India, in 2012, and M.Tech degree in Applied Optics from Indian Institute of Technological Delhi, India, in 2015. He is currently a Research Fellow in Laser Science and Technology Centre with the Defense Research and Development Organization (DRDO), Delhi, India. He is having research interest in several field of optics like laser spectroscopy, imaging and quantum optics. He is currently involved in, laser photoacoustic spectroscopy and laser induced fluorescence LIDAR techniques.

Saurabh Gupta received his B.Tech. degree in Electronics engineering from Aligarh Muslim University, Aligarh, India in year 2000 and his M.Tech. degree in VLSI Design Tools and Technology from Indian Institute of Technology, Delhi in Dec. 2001. Since then, he is working with Defense Research and Development Organization as a scientist. He is involved in development of data acquisition and system development for detection of explosives and other hazardous chemicals. His interests include development of rugged and compact systems for military use. He is a life member of IETE.

Hari B. Srivastava received the B.E. degree in electrical engineering from the University of Roorkee, Roorkee, India, in 1983, and the M.Tech. degree in electrical engineering from the Indian Institute of Technology Kanpur, Kanpur, India, in 1989. He currently the Director of the Laser Science and Technology Centre with the Defense Research and Development Organization (DRDO), Delhi, India. He is a Life Member of the Instrument Society of India and the Optical Society of India, and a member of the Computer Society of India. He has authored more than 25 research papers in various national/international technical research papers in proceedings and journals. Mr. Srivastava was a recipient of the DRDO Group Technology Award.

Prolonging Network Lifetime by Electing Suitable Cluster Head by Dynamic Weight Adjustment for Weighted Clustering Algorithm in MANET

Vijayanand Kumar
Department of Computer Sc & Engineering
Delhi Technological University
Delhi, India
vijayanand033@gmail.com

Rajesh Kumar Yadav
Department of Computer Sc & Engineering
Delhi Technological University
Delhi, India
rkyadav@dce.edu

Abstract — Mobile Ad hoc network has taken the lead in the field of wireless communication.
MANET has supported mobility, scalability and extendibility of the network over the air. Connectivity in wireless medium has several costs for communication. Costs such as life of connections, packets routing, information delay, security over the air and trusted source and receivers needs extra care in communication. Flat topology was not able to support scalability of the mobile nodes in the wireless network. To overcome this, hierarchy topology has been proposed which overcome the scalability problem. One of the hierarchy topology can be consider as clustering. Clustering of mobile nodes solves basic three problems which are (a) expanding the network (b) communication stays within the cluster so that other neighboring cluster remains unawares of the communication and (c) maintenance of routing become much easier. Clustering has mainly two processes which are (a) cluster formation and (b) cluster maintenance. Weighted clustering is one of the clustering schemes and this paper has described the constraints on weights which is fixed and not varying with the dynamics [Degree Difference Δv, Sum of Distances Dv, Mobility (Mv) and Power (Pv) of the nodes] of the mobile node in the network. Weight plays major role to select the best stable cluster head as it defines and support the dynamics of the mobile nodes. Algorithm depends on the minimum weight among the mobile nodes, which become the cluster head.

Choosing cluster head is an important task of the clustering which takes in cluster formation and also in maintenance phase as well.
This paper describes the dynamic weight adjustments by using method of soft computing. Soft computing has non-deterministic algorithm such as fuzzy logic and neural networks.
Weight based clustering algorithm shows the nature of artificial neural network with fuzzy behavior on their node dynamics. Since less computation and fast clustering is goal of any clustering based algorithm, so proposed work is intended to select the best cluster head by choosing the appropriate weights for mobile nodes with less computation overhead. Choosing and selecting intermediate weights impact overall performance in election of cluster head selection process and consequently impact the overall network stability. Weight correction model helps in prolonging network lifetime and reduce load on selected cluster head.

Keywords— Adhoc networks; Clustering, Clustering Algorithm; NS-2, Weight Based Clustering; Load balancing; Cluster Creation, Cluster Formation, Fuzzy Logic, Neural Network, Weights Adjustment in MANET.

NOMENCLATURE

WCA - Weighted Clustering Algorithm
Node Dynamic - [Δv, Dv, Mv, Pv], used with weighted clustering algorithm for cluster formation.
Weighing factors - [w_1, w_2, w_3, w_4], used with weighted clustering for cluster formation.

I. INTRODUCTION

Weighted clustering algorithm is a weight based algorithm to select best suited cluster head in the mobile adhoc network. Weighted clustering algorithm is eight step processes for cluster head election procedure [1].

Cluster Head Election Procedure:

Step 1: Find the neighbors of each node v (i.e., nodes within its transmission range) which defines its *degree*, dv, as

$$dv = |N_{(v)}| \quad (1)$$

Step2: Compute the ***degree-difference***,

$$\Delta v = |dv - \delta|, \text{ for every node } v. \quad (2)$$

Where δ is maximum nodes supported by mobile nodes for better physical layer functioning.

Step3: For every node, compute the ***sum of the distances***, Dv, with all its neighbors, as

$$Dv = \sum \{dist(v,v')\} \quad (3)$$

Step4: Compute the running average of the speed for every ***node v*** till current time T. This gives a ***measure of mobility*** and is denoted by Mv, as

978-9-3805-4421-2/16/$31.00 ©2016 IEEE

$Mv = 1/T \sum sqrt[(X_t - X_{t-1})^2+(Y_t - Y_{t-1})^2]$, *Coordinates*$(X_t, Y_t)$ *and* (X_{t-1}, Y_{t-1}) *at time t and t-1 for node v respectively* (4)

Step 5: Compute the cumulative time, *Pv*, during which a node *v* acts as a cluster head.

Step 6: Calculate the *combined weight Wv* for each node *v*,

$$Wv = w1\Delta v + w2Dv + w3Mv + w4Pv, \quad (5)$$

Where *w1, w2, w3* and *w*4 are the *weighing factors* for the corresponding system parameters

Step 7: Choose that node with the smallest *Wv* as the cluster head. All the neighbors of the chosen cluster head are no longer allowed to participate in the election procedure.

Step 8: Repeat steps 2–7 for the remaining nodes not yet selected as a cluster head or assigned to a cluster.

Minimum weight *Wv* among the nodes will be elected as cluster head in the cluster of mobile nodes. In the next section of related work, it will be analyzed that the weights associated with the **node dynamics [*Δv, Dv, Mv, Pv*]** plays important role to elect the best suited role of cluster head which must be stable in the network..

Sum of intermediate weights $[w_1, w_2, w_3, w_4]$ associated with the dynamics must satisfy below condition:

$$W1+W2+W3+W4=1 \quad (6)$$

Intermediate weights must satisfy equation 6 but distribution of intermediate weights on dynamics must be well balanced so that better cluster head election must take place.

Section II explains about the relative work based on intermediate weight distribution in piece wise which also informs that distribution of weights are not dynamic and based on the node dynamics which is most important in the network. Section III describes the proposed weight distribution model and dynamic adjustments of the weights for supporting the dynamics of mobile node and further electing best suited cluster head. Section IV deals with simulation environment and comparative results with the existing weight based clustering algorithms and the conclusion has been made in Section V.

II. RELATED WORK

This section describes the weight selection on the mobile nodes based on dynamic consideration of the network. Goal of clustering algorithm is to select the best possible cluster head which shows stability in terms of defining its dynamics. Mobile node has dynamic behavior and best clustering algorithm wins to show preferred clustering. Main issue here is that weight distribution for node dynamics consideration is static and based on assumption on the importance of the node dynamics **[*Δv, Dv, Mv, Pv*]**. It is presumption that which dynamically changing parameters need to be given priority. Weights distribution to calculate overall weights from given equation (5) is much dependent on the node dynamics. Weights here are the tuning parameters for finding overall weights so that best cluster heads can be chosen. To gain understanding the effects of tuning the weights analysis on the network variation i.e. node dynamics consideration is important.

Let's consider the below intermediate configuration shown to analyze the weight effects on cluster formation process for weighted clustering algorithm [1].

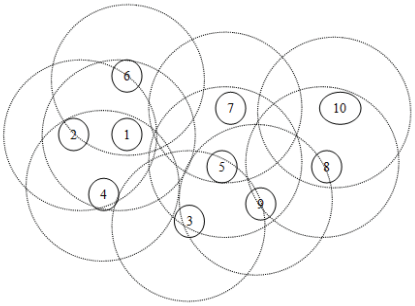

Fig1. Node Arrangements (Equal Range)

Figure 1 shows the nodes arrangements in the network with equal range. Figure 1 shows ten nodes with their ranges where maximum node supported by cluster head is 2. Cluster formation is about to take place based on the overall weight calculation.

Node_id	Pv	Mv	Dv	Δv
1	18	20	5.19	1
2	15	22	5.19	1
3	14	23	3.46	0
4	16	24	3.46	0
5	13	25	5.19	1
6	10	26	3.46	0
7	16	27	1.73	1
8	17	28	3.46	0
9	12	29	5.19	1
10	10	30	1.73	1

TABLE I. INITIAL NODE DYNAMICS (Δ= 2)

Node_id	w_1	w_2	w_3	w_4	$\mathbf{W_v}$
1	0.05	0.05	0.2	0.7	16.90
2	0.05	0.05	0.2	0.7	15.20
3	0.05	0.05	0.2	0.7	14.57
4	0.05	0.05	0.2	0.7	19.40
5	0.05	0.05	0.2	0.7	14.40
6	0.05	0.05	0.2	0.7	12.37
7	0.05	0.05	0.2	0.7	16.73
8	0.05	0.05	0.2	0.7	17.63
9	0.05	0.05	0.2	0.7	14.50
10	0.05	0.05	0.2	0.7	13.13

TABLE II. WEIGHT CALCULATION (Δ= 2)

Table 1 shows the node dynamics value of a ten mobile nodes. Table 2 has calculation of overall weight according to equation

(5).

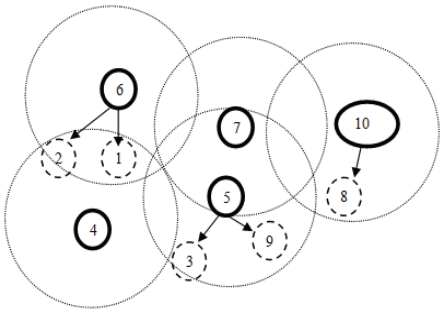

Fig 2. Cluster Formation Process Result

Figure 2 is the resultant of cluster formation process resultant from table 1 and table2 data. From table 2, Node_6 has the minimum weight and chosen as cluster head for neighboring nodes node_1 and node_2. Important observation here is that node_6 has power reduced to half of the initial (20 J) and node_1 and node_2 has still power higher than the node_6 but not elected has the cluster heads. Reason is the weighing factor [w_4] which is set higher for power. In this power has been considered as important parameter but weighing factor has shown the adverse effect. Once the power reaches to lowest threshold node_6 will trigger the cluster formation process. Possible that node_6 become dead and do not participate in cluster formation process which affects the overall network configuration or in routing of data packets.

This proves that the changes of weighing factor [w_1, w_2, w_3, w_4] are equally important as node dynamics **[Δ*v, Dv, Mv, Pv*]**.Experiment and data presented shows that tuning of weighing factor is as much important as node dynamics are. There must be some association of node dynamics with the weighing factors which can be self-adjusted or self-configured. Proposed work is related to the tuning of the weighing factors in the network dynamics which also associates itself with the node dynamics

[Δ*v, Dv, Mv, Pv*].

Mobile adhoc network must show the behavior of self-adjusting or self-configuring. Weighing factors must also self-configure with changing node dynamics in the network. Dynamic weight adjustment model is required which can sense the network's node dynamics and consequently adjust itself to support the node dynamics and help in electing the best cluster head.

III. PROPOSED WORK

This section of work demonstrates and presents the theory for distributing the weighing factors dynamically. Node dynamics **[Δ*v, Dv, Mv, Pv*]** and weighing factors must be correlated so that on changing the node dynamics, weights for each node dynamics must get self-configured. The point here is to choose the correct weight when node dynamics changes and also weighted clustering algorithm retains its original form on every cluster formation and maintenance process.

Many researchers have presented their work to choose cluster head based on fuzzy logic. Fuzzy logic has been applied on the node dynamics to select the best cluster head. Many inferences mechanism have been built to select the cluster head based on the variation of mobile nodes.

Figure 3 present the complete picture of dynamic weight adjustments model. Figure 3 has the *"**weight sets**"* corresponding to the node dynamics with defuzzified output i.e. crisp output of node dynamics. Weights need to learn or supervised itself for correct weight. Weight correction model is based on supervised learning and represent a feed forward networks. Crisp outputs for node dynamics can be consider as input to the weight set which adjusts the weights based on the input quality of crisp output.

Weighing factors must be adjusted in such a manner that equation 6 get satisfy any number of iteration. For this case there are four crisp outputs in terms of node dynamics **[Δ*v, Dv, Mv, Pv*]** and correspondingly four weighing factors.

Proposed model is not only valid for weighted clustering algorithm but it can be extended to another weight based algorithm proposed in mobile adhoc networks or in sensor networks. Weight distribution or correction model can be having "n" node dynamics and correspondingly "n" weighing factors.

Mathematically,

Node Dynamics Parameters can vary for each node:

$$1 < N_v[P_v, M_v \ldots X_n] < n,\ n \epsilon R^+ \qquad (7)$$

N_v – Node v, X_n – Node dynamics.

Associated Node Weighing Factors can vary for each node:

$$1 < w_m < n,\ n \epsilon R^+ \qquad (8)$$

w_m – weighing factor

Equation 7 and 8 generalize node dynamics and intermediate weight factors for each node in the network.

Crisp output for node dynamics are four and different sixteen combinations can be derived from the fuzzy model [14].

[Δv] – {(LOW, Difference of neighborhood nodes and Maximum supported nodes are less), (HIGH, Difference of neighborhood nodes and Maximum supported nodes are high)}

[Dv] – {(LOW, Sum of distances is less in value), (HIGH, Sum of distances is high in value)}

[Mv] – {(LOW, Relatively less mobile), (HIGH, Relatively high mobility)}

[Pv] – {(LOW, Less power consumed with respect to time), (HIGH, high power consumed with respect to time)}

This is a fuzzy approximation and totally dependent upon the membership function consideration for crisp interval i.e. there could be more possible crisp output on node dynamics. Here sixteen combinations have been formed considering that node

dynamics has only two crisp interval [LOW, HIGH].This consideration has been taken for fast processing and computation on mobile node must not take much time to make decision in fuzzy logic model.

Weight set offer different combination which suits for the combination achieved through defuzzification process. Weight set have infinite combination to offer to the crisp outputs of node dynamics.

Δv	**Dv**	**Mv**	**Pv**
HIGH	HIGH	LOW	LOW
w_1	w_2	w_3	w_4
.5	.4	.05	.05
.35	.35	.15	.15
.45	.25	.15	.15

TABLE III. MULTIPLE WEIGHTS SET FOR ONE OUTPUT

Table 3 shows different weighing factors for all crisp outputs but selecting the best weight combination comes under the learning mechanism.

Figure 4 explains the learning of best weight based on time stamp recording process for the same crisp output. For the first time when specific crisp output occurs [HIGH, HIGH, LOW, LOW] select the arbitrary weight set prepared [refer table 3].

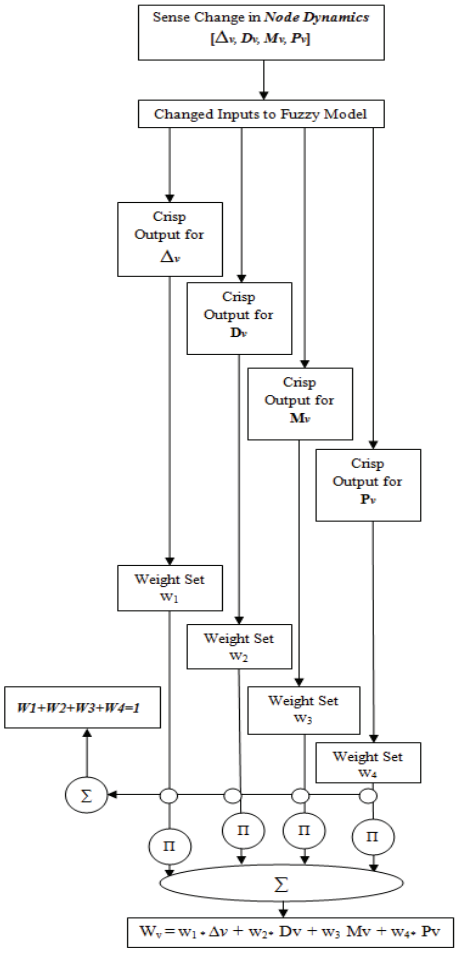

Fig 3: Weight Correction Model

Δv	Dv	Mv	Pv
LOW	LOW	LOW	LOW
LOW	LOW	LOW	HIGH
LOW	LOW	HIGH	LOW
LOW	LOW	HIGH	HIGH
LOW	HIGH	LOW	LOW
LOW	HIGH	LOW	HIGH
LOW	HIGH	HIGH	LOW
LOW	HIGH	HIGH	HIGH
HIGH	LOW	LOW	LOW
HIGH	LOW	LOW	HIGH
HIGH	LOW	HIGH	LOW
HIGH	LOW	HIGH	HIGH
HIGH	HIGH	LOW	LOW
HIGH	HIGH	LOW	HIGH
HIGH	HIGH	HIGH	LOW
HIGH	HIGH	HIGH	HIGH

Time stamp	w_1	w_2	w_3	w_4
10	.5	.4	.05	.05
25	.35	.35	.15	.15
15	.45	.25	.15	.15

Fig 4.Time Stamp recording for different weight sets

When demand of same weight set i.e. if the crisp output in the

next iteration i.e. either cluster formation or in maintenance phase demands or results the same crisp output then time stamp can be recorded for the earlier chosen arbitrary weigh set. For next iteration choose the weights which has unrecorded time stamp and process similar steps for next iteration. In figure 4 there are three weight set prepared for particular crisp output and all the weight sets has been iterated for cluster formation or cluster maintenance phase for particular node in the mobile adhoc network.

Method of recording the time stamp for the weight set is nothing but the learning for the weight set that which weight set has effectively helped the node to prolong the network lifetime. Time stamp with value "25" is supposed to be the best weighing distribution for particular mobile node and can be consider as best weighing distribution for other nodes as well. Crisp output is for particular node where node dynamics is valid for each and every node in the network.

Once the selection of best weighing distribution has been found for particular crisp output, same can be applied to all mobile nodes in the network for particular crisp output [refer table 2]. Weight set can be prepared in the cluster formation process and carried forward in cluster maintenance process. Variation can be present to the timestamp field. Once for particular network time all the timestamp can be reset and further recording of timestamp can be invoked.

Fuzzy model and weight correction model is implemented for all mobile nodes in the network so for specific crisp output weights on the mobile nodes can vary. Mobile node selects the best suited weight set for specific crisp out which helps to prolong the network lifetime.

IV. SIMULATION RESULTS

Simulation has been performed on network simulator ns-2.35. Figure 5 present the comparison between the original weight based clustering algorithm and with weight correction model. Appropriate weight set can prolong the network lifetime but it could have cost of computation. Intelligence of adding time stamp could help in learning best weight distribution. Method used to achieve network lifetime is the first mobile node which become dead in the network.

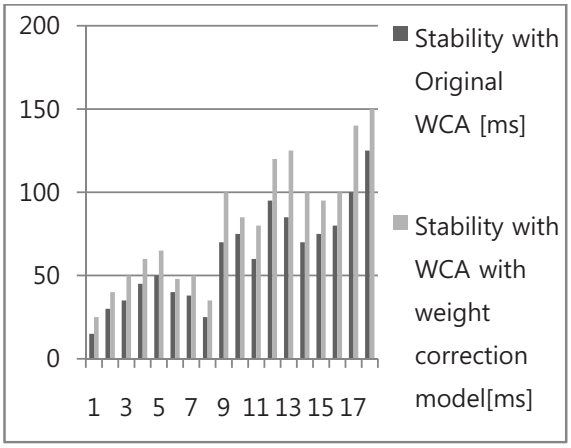

Fig 5. Stability of Network Lifetime

V. CONCLUSION

The proposed work is applicable for all mobile nodes in the network. Fuzzy model along with weight correction model must be implemented on the mobile node in order to provide best cluster head election in the MANET. Weight correction technique must be simple to deploy and less computational. In order to make simple and reduction of computation overhead, proposed method select any random option among the weight set and record the time stamp when same weight set requested for same crisp output again. For next iteration new unrecorded time stamp weight distribution has been applied to find the best weight distribution for same crisp output. After some iteration a set of recorded weights are prepared and considered as best distribution for particular crisp output. Since the distribution applied for one mobile node, other mobile node is unaware of this distribution and could have different weight distribution for same crisp output which other mobile nodes have. All mobile nodes try to reach configuration of the best weight distribution in order to provide stable network by choosing the best cluster head. Weight correction model is based on supervised learning, where time stamp is the teacher for informing the best distributed weights. Overall network combining the fuzzy model and supervised learning shows matching behavior with the feed forward supervised learning based model.

Future scope for tuning weight sets and variation of the model could take place. It is important that calculation overhead is minimal which consume less battery power. Computation for weight distribution must be intelligent and fast.

REFERENCES

[1] M Chatterjee, S K Das, D Turgut, "WCA: A Weighted Clustering Algorithm for Mobile AdHoc Networks", *IEEE Journal of Clustering Computing* Vol.5 (2),193-204, 2002.

[2] Jane Y. Yu et.al. "a Survey of clustering schemes for mobile ad hoc networks",IEEE Communications Surveys.

[3] Abdel Rahman H. Hussein et.al.,"A Load-Balancing and Weighted

Clustering algorithm in Mobile Ad-Hoc Network".

[4] D. Turgut, B. Turgut, et.al,"Optimizing clustering algorithm in mobile adhoc networks using simulated annealing," *Proc.IEEE Wireless Communication and NetworkingConference*, 2003.

[5] D. Turgut, S. K. Das, R. Elmasari, and B. Turgut,"Optimizing clustering algorithm in mobile adhoc networks using genetic algorithm approach," *Proc. 45th IEEE Global Telecommunications Conference*, 2002.

[6] Charalampos Konstantopoulos et.al. "Clustering in mobile adhoc networks through neighborhood stability-based mobility prediction",Computer Networks 52 (2008) 1797– 1824.

[7] Mohamed Aissa, Abdelfettah Belghith and Khalil Drira "New strategies and extensions in weighted clustering algorithms for mobile Ad Hoc networks" , The 4th International Conference on Ambient Systems, Networks and Technologies (ANT 2013).

[8] Mohamed Aissa, Abdelfettah Belghith"Quality of Clustering in mobile Ad Hoc networks", 5th International Conference on Ambient Systems, Networks and Technologies (ANT-2014).

[9] Yu-Xuan Wang, Forrest Sheng Bao "An Entropy-based Weighted Clustering Algorithm and Its Optimization for Ad hoc Networks" originally published on 3rd IEEE Int'l Conf. on Wireless and Mobile Computing, Networking and Communications, 2007. (WiMOB 2007)

[10] Basagni S., "Distributed clustering for ad hocnetworks,"Proceedings of International Symposium on Parallel Architectures, Algorithms and Networks, Jun. 1999, pp. 310-315.

[11] Kadri B, Mohamed A, et.al. Secured Clustering for mobile *ad hoc* networks. Int. J. Comput. Sci. Netw. Sec. 2007; 7:27–34.

[12] Wang Y, Liang T, et.al,Scalable and effective cluster based routing algorithm using node's location for mobile *adhoc* networks. Inform.Technol.J. 2008;7:958–971.

[13] Atanassov K. Intuitionistic fuzzy sets. Fuzzy Sets Syst. 1986; 20:87–96.

[14] Anitha VS, Sebastian MP. SCAM:Scenario-based clustering algorithm for mobile *ad hoc* networks. Proceedings of the 2009 13th IEEE/ACM International Symposium on Distributed Simulation and Real-Time Applications; Singapore. October 2009; pp. 97–104.

[15] Basagni S, et.al.. Localized protocols for *adhoc* Clustering and backbone formation:A performance comparison. IEEE Trans.Parall. Distrib. Sys. 2006;17:292–306.

[16] Dhurandher SK, Singh GV. Weighted-based adaptive clustering algorithm in mobile *ad hoc* networks. Proceedings of ICPWC'2005;

Quality Issues with Big data Analytics

Sangeeta
Computer Engineering Department
Delhi Technological University
New Delhi, India
Email id: Sangeeta.phogat@gmail.com

Kapil Sharma
Computer Engineering Department
Delhi Technological University
New Delhi, India
Email id: kapil@ieee.org

***Abstract*—The promise of data-driven decision-making is now being recognized broadly, and there is growing enthusiasm for the notion of ``Big Data.' 'In this paper techniques related with the big data pipelining or processing are discussed. There are number of issues related with the analytical results of the big data and the big data processing software. The major issues are included in this paper and will be helpful for the new beginners in this area of big data analytics.**

Keywords— Big Data Reliability; Big Data Analytic.

I. INTRODUCTION

Big data involves the data sets that are having the large volume, velocity and variety and it is becoming difficult to process this dataset using traditional data management tools or processing applications. The size of data in 2011 is roughly 1.8 Zettabytes.There is supporting networking infrastructure and have to manage nearly 60 times more information by year 2020.Issues of efficiency, economics and privacy need to be carefully planned when adding the big data building blocks in the already developed data and networking infrastructure. Big data is defined in terms of three ways which includes Infrastructure Perspective, Analytics perspective and from the business perspectives. In terms of infrastructure perspective Big data has been defined as data with high volume, velocity, and variety, veracity, viability, validity, value and volatility(8V) and unpredictability. The data here is very much large that current, traditional methods can't be used to process it. In terms of the analytics perspective, big data can be defined in terms of the events which are having the low probability of happening and are different from the traditional small sampled data. From the business perspective, big data are giving the opportunities of gaining the actionable intelligence. Actionable intelligence is the output of the big data software that will be directly useful for the business and other perspectives without any modifications or any production process.

These definitions are providing the important context that must be considered by the big data analysis software.

The quality of analytics system is one of its most important attributes.Organizations are trying to ensure highest quality for the systems being developed, but ensuring the same is very difficult due to the following reasons-

Increasing software size
Budget constraints
Time constraints
Shortage of skilled manpower.

The present situation requires that the organizations be equipped with techniques that enable them to improve the quality of deliverables. There are number of factors that are used to measure the system development quality and each attribute can be used to measure the product performance. These includes Reliability, Security, Usability, Availability, Correctness, Efficiency, Integrity and the testability, flexibility, Reusability and the interoperability.Reliability is one of the most important quality attributes for developed systems. In modern society there is a great impact of big data software reliability because of its vast applications in different areas affecting many millions of people directly or indirectly. So there is requirement to predict the reliability in terms of consistency of the analytical results of the big data software.

Big data are having the need of super computers, such machines can now be analyzed with the desktop computers with standard software and the modern fast developing techniques has the advantages for the development in the big data handling techniques.

The big data analytics is the procedure for examining the large amount of datasets which is having the variety, velocity and the volume of the data types that is the big data. This analysis will uncover the unknown patterns, unknown correlations and other useful information related with the business. The analytics results can be directly used for more effective marketing, new revenue opportunities and better improved customer services etc. without any processing to the analytics results. There is a need to check the quality factors associated with these analytical results.

II. LITERATURE REVIEW

Sharma in 2010 [5] proposed a new approach of Distance Based for the Optimal selection of SRGMs. This approach is useful for the optimal selection of parameters in the big data analytical results. C. E. and A. Peter gave "Research Directions for Engineering big data analytics software," in Jan/feb 2015,this article gave major factors that are helpful in learning the factors that are related with the quality of the analytical results.A group at united state gave the ways for rhe challenges and opportunities with the bigdata.L. Cai and Y. Zhu[3] gave the the Challenges of Data Quality and Data Quality Assessment in the Big Data Era. This challenges are providing the methods that can be helpful in the research in

978-9-3805-4421-2/16/$31.00 ©2016 IEEE

bigdata analytics. X. Wu, [4]X. Liu and S. Dai, The Reliability of Big Data gave the methods that are helpful in the reliability assessment of the bigdata.they used the random sampling method ,which is the statistical technique for assessing the reliability of data,other such techniques can be used.

III. PHASES IN THE PROCESSING PIPELINE

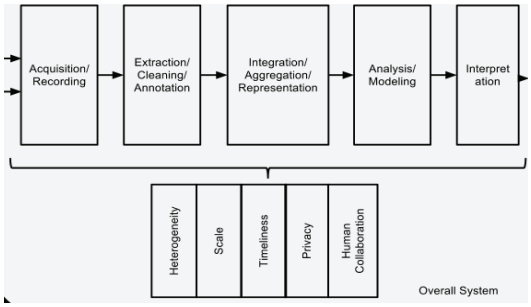

Fig-1 Major steps in the analysis of big data: big data pipeline

There are five major steps in processing of the big data, and are giving the analytical results starting from the Acquisition/recording state then doing the Extraction/Cleaning following the Integration/Aggregation and at last doing the analysis and Interpretation of the datasets. These steps are more explored as follows-

Data Acquisition and Recording -Big Data cannot be obtained directly, data have to be recorded from the data sources and need to be filtered[3].

Information Extraction /Cleaning-The information which has been collected is not in a ready to use format for analysis .This needs to be extracted using different data extraction techniques. Data cleaning considers/assumes well-understood conditions on valid data error finding models [2].

Data Integration, Aggregation, and Representation –There is a problem with today's Big Data analytics, which is the lack of correlation between database systems, which handles the data and provide queries for processing of the no SQL queries, such as data mining and statistical analyses.The bigdata needs to be properly integrated and presented.

Query Processing/Data Modeling, and Analysis -Querying and mining Big Data methods are functionally different from traditional statistical analysis which is done using the small samples. New optimal techniques and models for analysis are required to be used [6] and ranking of the techniques on particular methods is also required to be done so that optimal model and method can be selected [7].

Interpretation-Big data analyzing capability is of no use if anyone cannot understand the analysis. There should be a decision-maker, that provides the result of analysis, and he has to interpret these results.

IV. PROBLEM ENCOUNTERD WITH BIGDATA ANALYTICS

There are number of problems encountered when big data analytics is done. These are related with the Requirements specification, Security, design including the reliability and testing of the big data analysis [1].

Requirements

Specifying the details of the requirements is important for the successful construction of software. The problem of requirement can be understood if one can develop a model for functional requirements specification and verification. To show this feature of big data software, there is need to develop a model which can include the attributes like time and functional details and this can be better understood as-

$$R_i = \text{fi}\,(x_i \wedge t_i \wedge p_i)$$

where the system provides a functional feature x_i, with some time constraint t_i,and verifiable during some period p_i.

There is the necessity for the big data software to include all the above three parameters to completely define the requirement specification for such software .But all of the models are not including the constrained time and verifiable time and specify the requirement only in terms of the functional features.

Reliability

Reliability is the most difficult to achieve quality attribute. There is no direct way to check the consistency of the results of the data analytics. There are number of ways by which we can check the reliability of the data analytics result.

Random sampling is the main method for the analysis of the big data and accuracy of the random sampling completely depends on the randomness of the data. It is essential to make the analysis of the reliability for the big data. Big data provides the messiness of the data .The data samples taken will be more random and size of the samples does not matter. This messiness of the data can have the more reliable results. There is the need to analyze the reliability of these datasets [5].

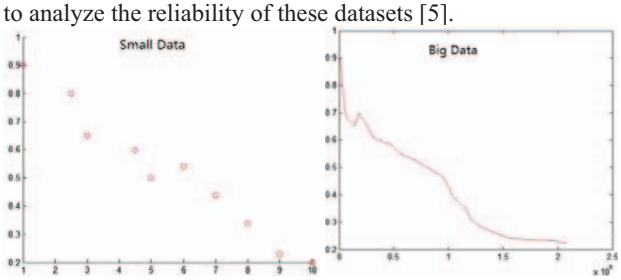

Fig-2 Graph showing the sampled data in case of small dataset and big datasets.

In case of small datasets, dataset is not random, limited amount of data is there and have the fixed point in the graph. But in case of big data, data is very random and large and is showing the curve in the graph.

Consistency of the data analytics results cannot be provided directly rather some human decisions and domain knowledge can be used to detect the inaccurate or extreme results.
The other way is to use design for reliability method in which architectural tactics are used to enhance the reliability of the big data software analytics results. As the big data software are complex there construction is complex enough as these are requiring the multiprocessing technologies as CUDA, GPUs, Map Reduce and Hadoop etc. These are requiring the high skill development during the development phase. New environments and frame-works for improving the usability of these technologies are enhancing day by day to reduce the learning curve for the big data software and involve the Spark, Mahout and Storm etc.

TABLE-SHOWING THE BEHAVIOR OF SMALL DATA SET VERSUS LARGE DATA SET

Features	Small data	Big data
1.Entropy of data	Low	High
2.Modeling Techniques	Parametric	Non-Parametric
3Effect of data size	Efficiency, Easy	Accuracy
4.Method of problem solution	Direct rules are available	Non-linear models are available

In this table comparison of the small data and big data is done showing that there are different ways by which the two datasets are handled. In both of them Entropy of data, Modeling Techniques, Effect of data size on result and Method of problem solution are different. So different methods are required to handle them.

Security-
Security is also the major concern in big data analytics. There are two types of attacks these are Execution phase attack and attacks which occur during the training. Execution phase attacks the data input streams which are added to influence the actionable intelligence and has been generated by the big data software. In case of training phase attacks malicious attackers can create data generators that affect the reliability of the big data software analytics results. Denial of service is also the problem in big data soft wares and may cause the problem of denying access to system.

Testability
Testability of the big data is also the major issue in big data analytical results. Verification techniques should be there to test the validity of the results.

Availability
Data must have the accessibility and timeliness. There is a need to check whether a data access is available or not. Availability requires that the 1) data is easily made public or easy to purchase 2) data should arrive on a given time 3)data are required to be regularly updated 4)the data interval from data collection and processing to release meets requirements. Availability incurs all these above features.

Scalability
Size of big data is a major challenge today. First Big data is having scalability in storage, as there are the increases in data density on the secondary storage devices. The current Redundant Array of Independent disks method that is in common use does not provide the level of performance and durability of the data those enterprises requires for dealing with large volumes of data. Second Data volume is increasing at high speed than computing resources and processor speeds that are available in the market areas. Techniques for the Parallel data processing that were used in the traditional approaches are not directly applied for the internal and intra node parallelism, because the architecture looks very different. As the power considerations in the future are likely to inhibit us from using all of the hardware in the system continuously, new data processing systems and techniques will be required to actively manage the power consumption of the processor. All these changes force us to rethink how data processing components are designed, built, and operated.

V. CONCLUSION

In this paper basics of big data analytics are discussed with the techniques for big data processing .The major issues related with the big data analytics software and their results are discussed in this paper. This will be helpful for the researchers having a interest in the big data analytics. Every one must support and encourage all the fundamental research towards addressing these issues if we have to achieve the promised use of Big Data.

REFERENCES

[1] C. E. a. A. Peter, "Research Directions for Engineering big data analytics software," Jan/feb 2015.

[2] B. Li, "Survey of Recent Research Progress and Issues in Big data," 2013.

[3] A. c. w. p. d. b. l. r. a. t. U. States, "Challenges and Opportunities with Big Data".

[4] L. Cai and Y. Zhu, "The Challenges of Data Quality and Data Quality Assessment in the Big Data Era".

[5] X. Wu, X. Liu and S. Dai, "The Reliability of Big Data".

[6] K. sharma, R. Garg, C. Nagpal and R.K.Garg, "Selection of Optimal Software Reliability Growth Models using a distance based Approach," *IEEE Transaction on Reliability,* pp. 266-276, 2010.

[7] R. Garg, K. Sharma, C. Nagpal, R. Garg, R. Garg, R. Kumar and Sandhaya, "Ranking of Software engineering metrics by fuzzy-based matrix methodology," *Software Testing , Verification and Reliability,* vol. 23, pp. 149-168, 2011.

Journal of Chemical and Pharmaceutical SciencesISSN: 0974-2115

Removal of Baseline Wander from ECG using CEEMD and Adaptive Morphogocial Function

Mahipal Singh Choudhry*, Rajiv Kapoor
Department of Electronics & Communication Engineering, Delhi Technological University, Delhi, India
***Corresponding author: E-Mail: msc_1976@yahoo.com**

ABSTRACT

ECG is a documentation of the electrical activities of the heart and it is used for the identification of a number of cardiac imperfections. Quite ECG signal get tainted by various kinds of artifacts, thus in order to gain proper information from them they must first be denoised. Baseline wander is one of the most common artifact in ECG. CEEMD shows better denoising performance compared to EMD and EEMD. Results also prove that morphology of an ECG signal drastically improved by using adaptive SE in morphological functions. Proposed method presents a novel approach for the filtering of baseline wander artifact of ECG by using a cascade of CEEMD and morphological functions using adaptive structuring elements. By using this novel approach for denoising of baseline wander artifact, it is ensured that the morphological information present in the ECG signal remains preserved and denoising performance is independent of heart rate and external factors. Proposed method is compared with all latest methods and results prove that proposed method provide far superior denoising and morphological results in terms of output Minimum Square Error, Output Signal to Noise Ratio and Correlation Coefficient.

KEY WORDS: ECG, Morphological Operators, EMD, EEMD, CEEMD, Baseline Wander.

1. INTRODUCTION

ECG signal is a quasi-periodic signal quantifying the electrical activities of the heart. It includes information content mostly in the 0.5-120 Hz range and is used to ascertain if a patient is suffering from any form of cardiac disorder. It primarily consists of the P wave, QRS complex and the ST segment. Any additional structures present in the ECG signify noise or cardiac defects. The diagnosis of these defects is generally performed by presence of certain morphologies in the ECG signal. Thus the morphology of an ECG signal is a crucial aspect which must not be tampered with to as large an extent as possible. However, ECG signal also captures a large amount of varying noises as well, thereby making proper diagnosis very difficult. Hence for proper diagnosis a filtering process is required to remove the constituent noise while ensuring no loss of information in terms of the morphology of the ECG signal. Baseline wander artifact is one of the most important types of noises present in ECG and it present in middle frequency region of ECG. It takes place due to the respiration of the patient, thereby making it omnipresent in all ECG signals. This artifact is often found during stress ECG in particular as patient breathing rate increases. The baseline wanders artifact result in a gradual sloping of the ST segment and a reduced R-R duration in the ECG signal. All these changes in the morphology are natural and necessary for diagnosis, however most existing denoising methods generally tend to a loss of information due to filtering. In this paper, a new technique is proposed to remove baseline wander from ECG signals by cascading of Complete Ensemble Empirical Mode Decomposition (CEEMD) and morphological operators with adaptive structuring elements (SE). The main contributions of the paper are as follows:

a) The cascading helps in overcoming inherent weaknesses that exist in using either method alone.
b) Each method preserves shape, thus a cascade of these two methods results in a strong preservation of shape of signal.
c) Further the lengths of structuring element are derived from real time ECG signal, thus making proposed filter adaptive to changes in heart rate and consequently changes of lengths of QRS and ST complexes.

This paper is divided into six sections, Section-II covers literature survey. Section-III explains background of proposed method. Proposed method is covered in Section-IV. Section-V shows the results obtained and Section-VI, follow by reference, is a summary of conclusions.

Literature Survey: Initial techniques of baseline wander denoising from ECG signals has used digital window based filters for the removal of low frequency noise from ECG but these filters introduced ripples in pass band if a sharp cut-off is opted and these ripples cause changes in the morphology of the ECG signal, which is unacceptable from a diagnosis point of view. Furthermore, inability to effectively use of Fourier Transform (FT) on ECG signal due to its non-stationary and non-linear property, implies uncertainty about exact frequency cut-offs requirement of window based filters. As an improvement upon window based filters, adaptive filters (LMS, NLMS, BLMS, etc.) were used. These filters involve dynamic tracking of the signal and estimation of noise based on difference between the tracked signal and the observed one. The problems that arise while using these filters for ECG denoising begin with requirement of pure input samples to obtain an estimate of the way the signal changes. Further issues arise due to the mean square error criterion for adaptive filters and also the fact that the reference signals are not correlated very well with the primary input. Thus even though these filters improve performance compared to simple window based filtering but there remained considerable scope for further improvement.

Recent advancements in non-linear signal analysis using wavelets have led to the extensive use of wavelets in ECG denoising. The work initially proposed by Donoho (1995), was carried forward to the field of ECG denoising and many algorithms have been built over it. Traditional wavelet approach has been found to be ineffective for the removal of baseline wander noise as confirmed by Luong (2013). To address this issue a fuzzy rule based multi wavelet technique was proposed by Ho (2008), which helped in terms of optimization of pre and post filtering choices for a particular data set.

Huang (1998), proposed a new technique, known as Empirical Mode decomposition (EMD) for analysis of non-linear non-stationary signals. This has been found to be very effective in ECG denoising and has been extensively used in several algorithms. However, most of the work using EMD has been done in relation to the removal of high frequency noises. Denoising of ECG signal using linear filtering especially Butterworth Low pass filter, gives better results when compare to direct denoising by EMD method. When EMD combined with adaptive filters, it gives better results compared to its combination with linear filters. A combination of EMD and wavelets is a very effective technique for ECG denoising. Further improvements are made upon this by Zhang (2010). In this work, he analyzes the energy of each IMF and accordingly detects the noisy IMF's and thus only the noisy IMF's are denoised using the wavelet based soft thresholding technique. All these techniques are generally applied to deal with the lower IMF's or high frequency components present in the signal and hence can't be used to deal with baseline wander.

EMD was first used in the paper by Zhi and Yu (2006), for the denoising of baseline wander. The residue signal was assumed to be an estimate of the baseline wander and this residue was removed to correct the noise signal. Further work in this field was done by Na Pan (2007). The signal was decomposed into 15 IMF's and it was considered that the last three IMF's contained mostly noise components so the baseline wander was removed by removal of last three components. The problems that arose with these works were the limited nature of tested signal and the lack of a proper system to find out number of noise effected IMFs. The major drawbacks present in EMD are its sensitivity to noise and the property of mode mixing which introduces error in the taken signal. Hence to overcome these Huang proposed a system of Ensemble Empirical Mode Decomposition (EEMD) and this was improved upon for denoising of ECG however EEMD also faced most of the same problems of EMD in terms of insufficient denoising strength on its own.

The use of Morphological operators has wide applications in image processing. Chee-Hung (1989), used morphological operators first time for denoising of biomedical signals. Building on this work, OGUZ (1992), in his paper title "A morphology based algorithm for baseline wander elimination in ECG records" used an opening operation followed by closing. The opening operations was used to extract the positive pulses such as P, R, T and U waves while the closing operation was used to remove the negative waves such as S wave. The primary drawback with this approach was the use of an ECG like but not pure ECG signal for analysis. Further the use of a disk shaped structuring element (SE) was a poor approximation for a real ECG. In another paper by Sun (2003), neonatal ECG signals were picked up for analysis. The aim of this paper was to successfully preserve the QT interval present. Opening and closing operations were used in tandem and then averaged to remove the QRS complex and leave with the QT complex. This was then fed as the structuring element for the second stage of morphological filtering. This work, while addressing the drawbacks of previous works, aims at the study of neonatal ECG signals only and need to be generalized.

A more recent approach was outlined by Zhongguo Liu (2011), here the morphologies present in the ECG signals were removed in two steps by using opening and closing operations in tandem and then taking the average. First the QRS complex is removed and then the P and T pulses are removed. Linear structuring elements are used in accordance with the available biological data. The major limitation being here that the ECG being a quasi-periodic and dynamic signal, the pulse widths are not fixed and keep on varying, hence a more adaptive structuring element are required. This problem is especially observed in the case of stress ECG's, where there is an inherent baseline drift, an upward slope in the ST interval and a clear change in the lengths of the QRS and ST segments. The major advantages however lie in the computational simplicity present in the use of morphological operators, further the ability of these operators to retain morphological information present in the signal is crucial.

It was found that EMD and Morphological functions alone has limited ECG denoising capacity so Mahipal (2016), proposed a new method for ECG baseline denoising by combining EMD with morphological functions to fetch optimum results. It is observed by them that performance of baseline denoising from ECG can be improved by using EEMD in place of EMD and by using adaptive SE for morphological operators.

Back ground:

Complete Ensemble Empirical Mode Decomposition: EMD is a method of analyzing non-linear and non-stationary signals and it is a fully adaptive and data driven technique. However, it experiences some problems such as the presence of oscillations of very dissimilar amplitude in a mode or the presence of very similar oscillations in different modes; this is known as "mode-mixing". To overcome mode mixing issues, a new method, known as Ensemble Empirical Mode Decomposition (EEMD). In EEMD, an ensemble of the original signal is taken by adding

various instances of Gaussian white noise to it. These instances are then broken down using EMD and the average over the entire ensemble is taken. Problem of mode mixing and oscillations is solved by averaging of IMFs. However EEMD also has a few problems of its own like it is computationally very expensive and due to uneven number of modes over all the ensemble, the final amplitudes associated with the IMF's is greatly reduced. Thus a more advanced technique known as Complete Ensemble Empirical Mode Decomposition (CEEMD) is used for decomposition of ECG into IMFs. In CEEMD, breakup of a signal into its constituent IMFs is performed in following manner:

a) Using EMD, decompose K realizations ($x[n] + \varepsilon\, w^k[n]$) of the base signal plus added white Gaussian noise to obtain their first modes and thereby create an ensemble of first IMFs by average over to obtain first true IMF using following formula

$$\widetilde{IMF_1}[n] = \frac{1}{K}\sum_{k=1}^{K} IMF_1^k \qquad (1)$$

b) At the first stage, the first residue is calculated by

$$r_1[n] = x[n] - \widetilde{IMF_1}[n] \qquad (2)$$

c) For the second stage of CEEMD, this residue signal is consider as base signal and create an ensemble of k realizations of the residue with Gaussian white noise, the first IMF for each element is obtained and averaged over to return second true IMF, which is written as

$$\widetilde{IMF_2}[n] = \frac{1}{K}\sum_{k=1}^{K} E_1(r_1(n) + \varepsilon_1 E_1(w^k[n])) \qquad (3)$$

d) Similar to above mentioned equation now calculate second residue. This will then form the basis for the third true IMF.

e) Continue the above mentioned steps until further decomposition is no longer possible.

f) Subtract all the obtained true IMF's to obtain the final residue.

Initial ECG signal can be considered as sum of the true IMF's and the remaining residue. Initial ECG signal is given by

$$x(n) = \sum_{i=1}^{N} c_i(n) + d \qquad (4)$$

CEEMD results in much improved computational complexity and a reduced ensemble size, further the low mode amplitude problem is not experienced due to the fact that only first mode is searched at each realization of this method. This method guarantees almost zero reconstruction error. This is very important feature of this method, which ensures that no information is lost while working with biological signals such as ECG and it prove superiority of CEEMD over EMD and EEMD for removal of baseline wander from ECG. Results also prove same conclusion regarding CEEMD.

Adaptive Morphological Operators: Mathematical morphology is a powerful process for the numerical analysis of geometric structures. It consists of numerous algorithms designed to obtain information concerning shape and size from a geometric object. Selected Structuring Element (SE) is the most important feature of these filters and by varying the shape and size of the SE, it enables to obtain information from the non-linear signal. Erosion and Dilation are the fundamental morphological operators upon which the more advanced processes and filtering techniques are based. They are

Erosion: It is used to find matches of a SE in the signal under consideration and defined as

$$f \oplus l(n) = max\big(f(n-i) + g(i)\big) \qquad (5)$$

Dilation: It is generally used to fill small pits in the signal and perform smoothing and defined as

$$f \theta l(n) = \min\big(f(n+i) - g(i)\big) \qquad (6)$$

Two important operations known as opening and closing, derived from the erosion and dilation operators, are used in proposed method and they are defined as

$$\text{Opening: } (f \circ l)(n) = (f \theta l \oplus l)(n) \qquad (7)$$

$$\text{Closing: } (f \cdot l)(n) = (f \oplus l \theta l)(n) \qquad (8)$$

Opening operation is responsible for the removal of peaks and smoothening of the contour. Closing handles removal of pits and discontinuities.

2. PROPOSED METHOD

The algorithm consists of passing the noisy signal through cascaded CEEMD and adaptive morphological filters and has following steps:-

a) Decomposition of Noisy ECG signal into constituent IMFs using CEEMD.

b) Dropping of artifactual IMFs and partial reconstruction of ECG signal for partial denoising.

c) Extraction of lengths of QRS complex and ST segment.

d) First phase of morphological filtering using QRS complex length as length of SE.

e) Second phase of morphological filtering using ST segment length as length of SE.

f) Subtraction of the remaining residual signal from partially denoised signal obtained in Step 2.

g) Calculation of performance parameters (SNR, MSE and correlation) from the output signal.

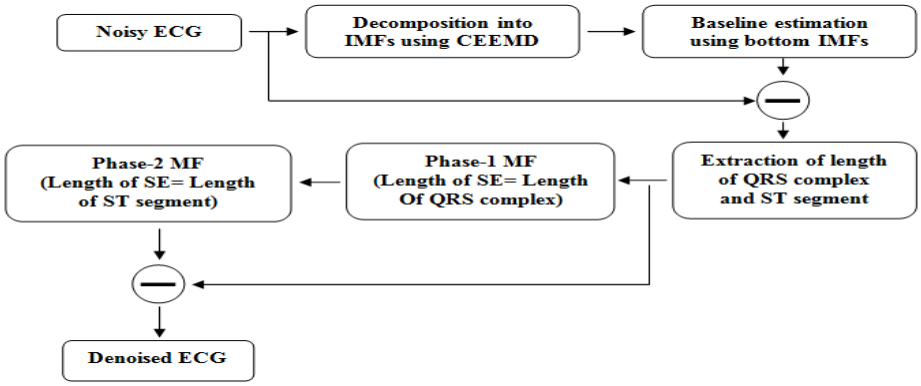

Fig.1. Proposed Methodology

Step 1: Noisy ECG is decomposed into N true IMFs using CEEMD operation

$$x_{original}\,(n) = \sum_{i=1}^{N} c_i(n) + d \qquad (9)$$

Step 2: To perform partial filtering, a set of IMFs is chosen to drop. Based on experimental data, the value of lower IMFs (m) to be discarded is obtained as

$$m = round(0.38\,N) \qquad (10)$$

This number is obtained by testing real time ECG signals with known noise added to them. Various fractions of the total number of modes are dropped and it is observed that on an average, maximum SNR and correlation are obtained using 0.38. Thus, the CEEMD filtered ECG signal is given as

$$\overline{x}_{ceemd}(n) = \sum_{i=1}^{N-m} c_i(n) \qquad (11)$$

This is partially filtered ECG signal. The aim behind partially filtering it is to ensure that no shape related information is lost.

Step 3: The morphological filters have been divided into two steps, one to remove QRS complex and other to remove ST wave. This is done because if all the features are removed at once, it may give rise to severe distortion and loss of information. Linear SEs are used because they are found to be more accurate for denoising ECG signals. A simple artifact analysis algorithm using a wavelet breakdown and identification of ECG components, is used to determine the lengths of the complexes and hence the structuring elements. It is a fully adaptive method in which position of peaks is located and then average length of complexes is obtained based on the number of samples between peaks. The length of the QRS complex is defined as the number of samples between the onset of the Q wave and the onset of the S wave. By obtaining the locations of S and T peaks, length of ST interval is calculated.

Step 4: The partially filtered ECG signal is now applied to the first morphological filter. Based on the length of a QRS complex obtained from the real time ECG signal as mentioned earlier, a linear structuring elements (SE1) of length '$l1$'is used. QRS complex removed ECG signal is given by

$$\bar{x}_{mp1}(n) = \{(\bar{x}_{ceemd} \circ l1 \cdot l1)(n) + (\bar{x}_{ceemd} \cdot l1 \circ l1)(n)\}/2 \qquad (12)$$

Step 5: The QRS complex removed ECG signal is then applied to a second morphological function to remove the ST wave. ST interval of partially filtered ECG signal is used as length of structuring elements for second morphological filter, '$l2$'. ST segment removed ECG signal is given

$$\bar{x}_{mp2}(n) = \{(\bar{x}_{mp1} \circ l2 \cdot l2)(n) + (\bar{x}_{mp1} \cdot l2 \circ l2)(n)\}/2 \qquad (13)$$

This signal does not contain any of the characteristic ECG segments. It is an estimate of the total remaining baseline noise present in the original signal.

Step 6: This obtained noise signal is subtracted from the initially denoised ECG signal to achieve the clean or denoised ECG signal, which is given by

$$x_{denoised}(n) = \bar{x}_{ceemd}(n) - \bar{x}_{mp2}(n) \qquad (14)$$

Step 7: For clean ECG output signal, performance parameters are calculated as

(i) Output Mean Square Error, $$MSE = \Sigma\left(x_{original} - x_{denoised}\right)^2 \qquad (15)$$

(ii) Output Signal to Noise Ratio, SNR (dB) $$= 10 * \log \frac{X^2_{original}}{\left(X_{original} - X_{denoised}\right)^2} \qquad (16)$$

To compare performance of proposed method, same process is carried out for testing using various combinations of cascading using EMD and EEMD also and also all three types of morphological operators, static, partially adaptive and fully adaptive.

3. RESULTS

X-axis shows number of samples and Y-axis shows amplitude of signal. Table.1 shows corresponding results of ECG baseline wander denoising method using EMD, EEMD and CEEMD.

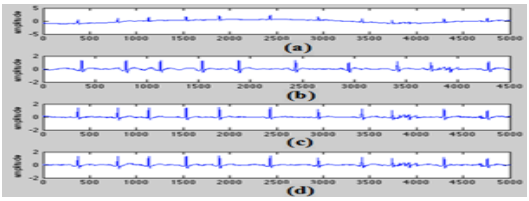

Fig.2 (a) Noisy signal (b) Denoised signal using EMD (c) Denoised signal using EEMD (d) Denoised signal using CEEMD

Table.1. Comparision of CEEMD with EMD and EEMD

Parameter	Method		
	EMD	EEMD	CEEMD
Output MSE	0.0023	0.0020	0.0018
Output SNR (Db)	24.5055	28.2483	30.3593
Correlation Coefficient	0.8825	0.9153	0.9374

(Input SNR =-16.2870 dB; Input MSE = 0.4096)

Fig.3 shows corresponding plots of denoised ECG using morphological functions with various levels of adaptiveness. X-axis shows number of samples and Y-axis shows amplitude of signal. The table.2 shows corresponding results with various levels of adaptiveness of morphological functions for ECG baseline wander denoising.

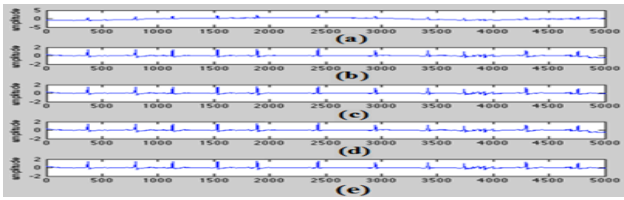

Fig.3 (a) Noisy Signal (b) Denoised signal using static morphological operators (c) Denoised signal using QRS adaptive morphological operators (d) Denoised signal using ST adaptive morphological operators (e) Denoised signal using fully adaptive morphological operators

Table.2. Comparision between different types of morphological functions (MF)

Parameter	Method			
	Case 1	Case 2	Case 3	Case 4
Output MSE	0.0027	0.0024	0.0024	0.0022
Output SNR (Db)	20.8442	23.5292	22.7893	25.6805
Correlation Coefficient	0.8732	0.9027	0.8983	0.9184

(Input SNR = -16.2870 Db; Input MSE = 0.4096)

Case 1: Static MF (SE1= 0.11Fs; SE2= 0.3 Fs)
Case 2: Partially Adaptable MF-1 (SE1 = QRS Interval; SE2 = 0.3 Fs)
Case 3: Partially Adaptable MF-2 (SE1 = 0.11Fs; SE2 = ST Segment)
Case 4: Fully Adaptable MF (SE1= QRS Interval; SE2 = ST Segment)

The filtering properties change as move from a static function, to one in which the first stage is adaptive, then one in which the second stage is adaptive and finally the fully adaptive model. As can be clearly seen, adaptability enhances the denoising property of filter with the fully adaptive filter giving the best results.

Fig.4 shows plots of denoised ECG using different cascaded combination. X-axis shows number of samples and Y-axis shows amplitude of signal. Table.3 shows corresponding results of different cascaded combinations for ECG baseline wander denoising.

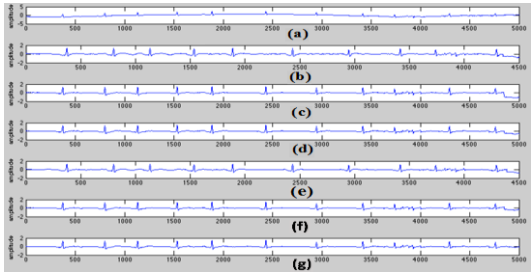

Fig.4 (a) Noisy signal (b) Denoised signal using EMD and static morphological operators (c) Denoised signal using EEMD and static morphological operators (d) Denoised signal using CEEMD and static morphological operators (e) Denoised signal using EMD and adaptive morphological operators (f) Denoised signal using EEMD and adaptive morphological operators (g) Denoised signal using CEEMD and adaptive morphological operators.

Table.3. Comparision between performances of different cascaded combinations

Parameter	Method					
	Case 1	Case 2	Case 3	Case 4	Case 5	Case 6
Output MSE	0.0022	0.0017	0.0015	0.0014	0.0012	0.0010
Output SNR (dB)	26.369	32.314	34.596	36.196	38.257	40.276
Correlation Coefficient	0.8869	0.9261	0.9427	0.9353	0.9406	0.9656

(Input SNR = -16.2870 Db; Input MSE = 0.4096)

Case 1: EMD & Static MF
Case 2: EEMD & Static MF
Case 3: CEEMD & Static MF
Case 4: EMD & Adaptive MF
Case 5: EEMD & Adaptive MF
Case 6: CEEMD & Adaptive MF

It can be clearly seen, adaptability enhances the denoising property of filter in cascaded combination also and cascaded combination of CEEMD and adaptive filter gives the best results.

4. CONCLUSION

Results clearly indicate a superior performance of the proposed denoising algorithm over all latest methods for a wide range of ECG data. The algorithm shows significantly improved results over existing methods while testing on real stress ECG signals. The main points of advantage observed are the efficiency in removal of the Baseline Wander noise coupled with the preservation of the morphology of the ECG signal. Further the ability to adapt towards changes in heart rate is another major advantage. The main contributory factors for this advantage are the nature of both of the filters applied. Future work in this area could include reduction in computation times of CEEMD. Despite the fact that a modified and faster version of EEMD is used in proposed method, there is further scope for reduction in the computation time.

REFERENCES

Alfaouri M, and Daqrouq K, Electrocardiogram (ECG) Signal denoising by Wavelet Transform thresholding, American Journal of Applied Sciences, 5 (3), 2008, 276-281.

Boudraa A.O, Cexus J-C, EMD Based signal filtering, IEEE Transactions on instrumentation and measurement, 56 (6), 2007.

Chacko A, and Ari S, Denoising of ECG signals using Empirical Mode Decomposition based technique, IEEE-International conference on Advances in Engineering, Science and Management (ICAESM -2012), 2012, 6-9.

Changnian Zhang, Xia Li, and Mengmeng Zhang, A novel ECG signal denoising method based on Hilbert Huang Transform, International Conference on Computer and Communication Technologies in Agriculture Engineering, CCTAE-2010, 2010, 284-287.

Chavan M.S, Agarwala R.A, and Uplane M.D, Application of Chebyshev Type II Digital Filter For Noise Reduction In ECG Signal, Proceedings of the 5th WSEAS Int. Conf. on Signal Processing, Computational Geometry & Artificial Vision, Malta, 2005.

Chavan M.S, Agarwala R.A, and Uplane M.D, Digital Elliptic Filter Application For Noise Reduction In ECG Signal, 4th WSEAS International Conference on Electronics, Control and Signal Processing, Miami, Florida, USA, 2005, 58-63.

Chee Hung Henry Chu and Edward J Delp, Impulsove noise suppression and background normalization of ECG signals using morphological operators, IEEE transactions in biomedical engineering, 36 (2), 1989, 262-273.

Ching-Haur Chang, Kang-Ming Chang, and Hsien-Ju Ko, Cancellation of high frequency noise in ECG signals using Adaptive filter without external reference, Proceedings of International Conference on Biomedical Engineering and Informatics, Yantai, 2010, 787-790.

Chmelka L, and Kozumpik J, Wavelet Based Wiener Filter for Electrocardiogram signal denoising, IEEE computers in cardiology, 2005, 771-774.

Donoho D.L, Denoising by soft thresholding, IEEE Trans Inform Theoy, 14 (3), 1995, 612-627.

Gurpreet Singh, Gagandeep Kaur, Vineet Kumar, ECG Denoising Using Adaptive selection of IMFs through EMD and EEMD, ICDSE, 2014.

Ho C.Y-F, Ling B.W-K, Wong T.R-L, Chan A.Y-P, Tam K.S, Fuzzy rule based multi-wavelet Electrocardiogm (ECG) denoising, Fuzzy Systems, IEEE international Conference, 2008, 1064-1068.

Huang N.E, Shen Z, Long S.R, Wu M.C, Shih H.H, Zheng Q, Yen N.C, Tung C.C, and Liu H.H, The Empirical Mode Decomposition and Hilbert Spectrum for Nonlinear and Nonstationary Time Series Analysis, Proceedings of the Royal Society London A, 454, 1998, 903–995.

Kania M, Fereniec M, Maniewski R, Wavelet Denoising for Multilead High resolution Electrocardiogram (ECG) Signals, Measurement Science Reiew, 7 (4) Section 2, 2007, 30-33.

Luong D.T, Study on the limitations of removal of Baseline noise from electro cardiography signal in measurement using wavelet analysis, IEEE, ICUFN, 2013.

Mahipal Singh Choudhry, Akshay Puri and Rajiv Kapoor, Removal of Baseline Wander from ECG signal using Cascaded Empirical Mode Decomposition and Morphological Functions, 3rd International Conference on Signal Processing and Integrated Networks (SPIN-2016), 2016.

Maria E. Torres, Marcelo A. Colominas, Gaston Schlotthauer, Patrick Flandrin, A complete ensemble empirical mode decomposition with adaptive noise, ICASSP, 2011.

Muhammad Zia Ur Rahman, Rafi Ahamed Shaik and Rama Koti Roddy D.V, Efficient sign based normalized adaptive filtering techniques for cancelation of artifacts in ECG signals: Application to wireless biotelemetry, Journal of signal processing, 91 (2), 2011, 225-239.

Na Pan, Vai Ming I, Mai Peng Un and Pun Sio Hang, Accurate removal of baseline wander in ECG using EMD, proceedings of NFSI & ICFBI 2007, China, 2007, 177-180.

Pradeep Kumar B, Balambigai S, and Asokan R, ECG denoising based on Hybrid Technique, IEEE- International conference on Advances in Engineering, Science and Management (ICAESM -2012), 2012, 285-290.

Seyfullah Halit OGUZ and Muka Hakan Asyali, A morphology based algorithm for baseline wander elimination in ECG records, International Biomedical Engineering days, 1992, 157-160.

Sun P, Wu Q.H, Weindling A.M, Finklestein A, and Ibrahim K, An improved morphological approach to background normalization of ECG signals, IEEE trnasactions on biomedical engineering, 50 (1), 2003, 117-121.

Wu Z, and Huang N.E, Ensemble empirical mode de- composition: A noise-assisted data analysis method, Advances in Adaptive Data Analysis, 1 (1), 2009, 1–41.

Yadav K.L, and Sachin Singh, Performance evaluation of different adaptive filters for ECG signal processing, International Journal On Computer Science and Engineering, 40 (5), 2010, 1880-1883.

Zhi-Dong Zhao, Yu-Quen Chen, A new method for Removal of Baseline Wander and Power Line Interference in ECG signals, Proceedings if the Fifth International Conference on Machine Learning and Cybernetics, Dalian, 2006, 4342-4347.

Zhongguo Liu, Jinliang Wang and Boqiang Liu, ECG signal denoising based on morphological filtering, 5th International conference on Bioinformatics and Biomedical Engineering, 2011.

This article has been accepted for publication in a future issue of this journal, but has not been fully edited. Content may change prior to final publication. Citation information: DOI 10.1109/TPEL.2016.2619367, IEEE Transactions on Power Electronics

Repetitive Controller for VSIs in Droop Based AC-Microgrid

Ashutosh Trivedi, *Student Member, IEEE* and Mukhtiar Singh, *Member, IEEE*

***Abstract*— A major requirement of AC-microgrid is to keep on feeding its connected load at regulated voltage and frequency which is difficult to achieve especially in inverter based microgrid. In modern distribution system, most of the loads are non-linear in nature and draw harmonic current. The variable load with the non-linear characteristics may distort the output voltage and degrade the power quality. In order to mitigate the negative impact of these disturbances on output voltage, a novel Repetitive Controller (RC) has been proposed. A mix-sensitivity based approach is used here to design the RC and comparison of performance with non-linear load is shown with conventional PI regulator. The overall microgrid system is designed and simulated with the help of various toolboxes available in MATLAB/SIMULINK. Further, a scaled hardware prototype of microgrid consisting of two voltage source inverter (VSI) is developed and controlled using RC in real time with the help of FPGA.**

Index Terms— Droop control, micro-grid, mix-sensitivity, repetitive control, FPGA.

I. Introduction

In recent years, microgrids have become the most popular way of integrating Renewable Energy Sources (RES) in distribution network [1-3]. Any type of RES can be connected to microgrid via power electronics interface [4].

A Microgrid has well defined boundaries within main electric power system (EPS), and may be operated in both grid tie mode or islanded mode. In islanded mode, microgrid is required to operate on certain control strategies that are able to share power among various sources while ensuring stable and reliable operation whereas in grid tie mode microgrid works as lumped source/load. In case of islanded mode of operation, droop control based methods have been widely reported in literature [5-7]. Such kinds of system do not require any type of communication channel to control power sharing among the various sources forming a microgrid. Therefore, these methods uses virtual droop in frequency and voltage according to their active and reactive power output. Further, voltage and current control techniques are used to regulate the output voltage under variable load demand. Therefore, the objectives of overall control are not only to achieve power sharing and regulated voltage but also to maintain output voltage with sinusoidal profile [9-11].

In modern EPS, most of the loads are non-linear in nature and inject harmonic current into the system. These current harmonics further distort the voltage waveform and consequently degrade the power quality of the overall system. The majority of voltage control scheme uses proportional plus integral (PI) controller in rotating reference frame, which fails to maintain the desired sinusoidal profile of voltage waveform especially in presence of harmonic current [11-13]. Proportional plus resonant (PR) controllers, deal with harmonic distortion to some extent. However, the strategies based on PR controllers are very complex due to adjustment of gains for different harmonic components [6], [8], [15]. A perfectly tuned PR controller may exhibit better performance but requires much more DSP resources compare to other controllers.

RC can be applied to the types of system where disturbances are periodic in nature which is shown in variety of applications [26-28]. Some of the researchers have also utilized RC based control approach for VSI in microgrid for Grid tied application. Various methodologies have been proposed to design the RC for VSI. H^{∞} and frequency adaptive RC has been applied to grid connected VSI [29]. This method uses μ-analysis to minimize H^{∞} norm to get optimal control. With this method, RC shows good performance w.r.t. conventional control. However, this kind of scheme assumes fixed grid frequency and requires exact mathematical modeling of whole microgrid/ network, which is practically not feasible where both the frequency and network configuration keep on varying in real time. This kind of problem tries to mitigate in [30], where RC with adaptive frequency has been used. However the major drawback of the proposed approach is dependent on Phased Locked Loop (PLL) performance. Here it is important to mention that the performance of PLL depends on accuracy of frequency measurement.

This paper proposes a simpler method for the RC design for VSI's. The RC based voltage and current control loops exhibit enhanced performance in comparison to conventional PI controller. It also helps in the stable operation of overall droop based microgrid comprising VSI's.

II. Control Strategy of Micro-grid

In an EPS, active and reactive power outputs from the source are function of voltage and frequency. For a completely decoupled EPS, active and reactive power depends upon either of voltage or frequency. This decoupling depends upon X/R ratio of transmission lines [6]. If lines are purely inductive, the active and reactive power transfer will depend upon the frequency and voltage magnitude respectively whereas it is opposite in the case of resistive lines. Therefore, droop control can be implemented in either of the cases but the conventional droop control may not provide stable operation and proper power sharing among different sources in case of strongly coupled system.

In this section, basic droop control method for islanded microgrid with their voltage and current control loop is discussed. The basic derivations are omitted as they are already given in [14-17].

0885-8993 (c) 2016 IEEE. Personal use is permitted, but republication/redistribution requires IEEE permission. See http://www.ieee.org/publications_standards/publications/rights/index.html for more information.

This article has been accepted for publication in a future issue of this journal, but has not been fully edited. Content may change prior to final publication. Citation information: DOI 10.1109/TPEL.2016.2619367, IEEE Transactions on Power Electronics

A. Droop Control

In microgrid, with assumption of inductive transmission line, droop method can be employed between frequency and voltage for active and reactive power transfer respectively [7], [16] [35]. Therefore,

$$\omega = \omega^* - m_f \cdot P \tag{1}$$

$$E = E^* - m_e \cdot Q \tag{2}$$

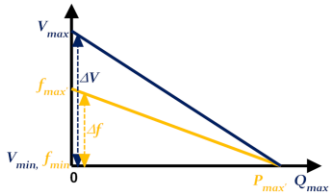

Fig.1 Droop Characteristics

Where, ω^* and E^* are nominal frequency and voltage of microgrid, m_f and m_e are the proportional droop coefficients of frequency and voltage respectively.

The frequency and voltage droop coefficient can be calculated as follows,

$$m_f = \frac{allowed\ deviation\ in\ frequency}{Inverter\ KVA\ rating} \tag{3}$$

and,

$$m_e = \frac{\min deviation\ in\ voltage\ at\ rated\ KVA}{\sqrt{(KVA\ rating^{\,2} - Active\ power^{\,2})}} \tag{4}$$

In order to prevent the violation of inverter rating, the values for voltage droop coefficient are set according to available reactive power capacity after supplying active power. Whereas, minimum value of voltage droop coefficient can be set for appropriate reactive power sharing and stable control.

B. Voltage and Current control loop

In main grid, sources need to provide only fundamental voltage as it cannot compensate the other high frequency voltage disturbance at long distance. Therefore, harmonic compensations are provided at the distribution end.

Microgrid is a small capacity grid confined to small area. It interconnects distributed resources (DR) which already have their local loads. Interconnection of DR generally improves the stability and reliability of the system. The majority of the sources are interfaced via static inverters in ac-microgrid. Inverters are inertia less system, which can give very fast response to the given command. At the same time being inertia less inverter have very short time overload capacity. Therefore, it is advantageous to use a fast controller where inverters are primary used as interconnecting interface.

Voltage and current control loops regulate the output voltage under various load disturbances within each DR. Block diagram of comprehensive voltage and current controller is shown in Fig.2 [17]. As mentioned earlier, many control techniques are applicable for this purpose but most of them do not exhibit satisfactory performance in the presence of harmonics due to non-linear loads. These harmonics can be treated as periodic disturbances in the system.

RCs are well known for the rejection of periodic disturbances as it is based on Internal Model Principle (IMP) theo-

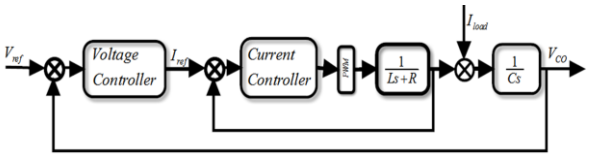

Fig.2 Voltage and Current Control Loop

ry [18]. According to this theory, a controller can reject the entire disturbances for a plant, if it incorporates an internal model of all its disturbances within itself. Internal model of periodic disturbances can be built using polynomial of high order however design of controller for such case becomes tedious due to complexity involved in the assignment of closed loop poles.

Incorporating fixed period time delay (L) in a feedback loop is another way to realize an internal model of a periodic sig-nal [19]. The controllers having such time delay consists of large number of poles on imaginary axis as shown in Fig.3 which may destabilize the system. For the stable operation, these poles must be stabilized in feedback control loop itself. However, designing such a stabilizing controller is very difficult for strictly proper plant just like microgrid [20-21].

An attenuator or a low pass filter is most commonly used in feedback loop to reduce the complexity in designing a stabilizing controller as shown in Fig.3 (a-2) [21]. This enables in shifting of close loop poles to left hand side in complex plan.

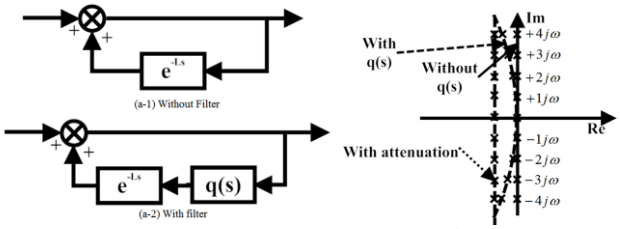

(a) Feedback Time Delay (b) Poles of the system

Fig.3 Internal Model of Feedback Time Delay

III. Design of Proposed Repetitive Controller

The proposed RC design is implemented in stationary reference frame in order to reduce the number of controllers. Hence, Clarke's transformation has been used to convert three phase (*abc*) quantity into two phases, as per following equation:

$$\begin{bmatrix} v,i_\alpha \\ v,i_b \end{bmatrix} = \frac{\sqrt{2}}{\sqrt{3}} \begin{bmatrix} 1 & -1/2 & -1/2 \\ 0 & \sqrt{3/2} & -\sqrt{3/2} \end{bmatrix} \begin{bmatrix} v,i_a \\ v,i_b \\ v,i_c \end{bmatrix} \tag{5}$$

And for inverse Clarke's transform,

$$\begin{bmatrix} v,i_a \\ v,i_b \\ v,i_c \end{bmatrix} = \begin{bmatrix} 1 & 0 \\ -1/2 & \sqrt{3/2} \\ -1/2 & -\sqrt{3/2} \end{bmatrix} \begin{bmatrix} v,i_\alpha \\ v,i_\beta \end{bmatrix} \tag{6}$$

Where, $[v,i_\alpha, v,i_\beta]^T$ and $[v,i_a, v,i_b, v,i_c]^T$ are transformed voltage and current vectors respectively.

According to [19-22], a generalized RC is of the following form:

$$C(s) = C_1(s) + C_2(s) * C_r(s) \tag{7}$$

Where, $C_1(s)$ is an Internally Stabilizing Controller (ISC)

0885-8993 (c) 2016 IEEE. Personal use is permitted, but republication/redistribution requires IEEE permission. See http://www.ieee.org/publications_standards/publications/rights/index.html for more information.

This article has been accepted for publication in a future issue of this journal, but has not been fully edited. Content may change prior to final publication. Citation information: DOI 10.1109/TPEL.2016.2619367, IEEE Transactions on Power Electronics

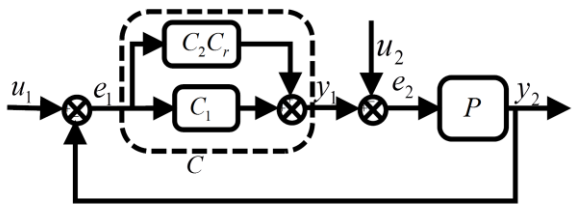

Fig.4 Unity feedback RC

and $C_2(s)$ is a pre- compensator.

Further, C_r can be defined as,

$$C_r(s) = \frac{1}{1 - q(s)e^{-Ls}} \tag{8}$$

Where, $q(s)$ is a low pass filter.

A Unity feedback RC system with plant *P* is shown in Fig.4. Here, controller $C_1(s)$ is said to be an ISC, if and only if all the transfer functions from e to u, as described by (9), are strictly Hurwitz [30-31].

$$\begin{bmatrix} e_1 \\ e_2 \end{bmatrix} = \begin{bmatrix} \frac{1}{1+PC_1} & \frac{-P}{1+PC_1} \\ \frac{C}{1+PC_1} & \frac{1}{1+PC_1} \end{bmatrix} \begin{bmatrix} u_1 \\ u_2 \end{bmatrix} \tag{9}$$

Here, u is an input vector and e is an error vector. According to [27], set of all controllers, $C_1(p)$ that stabilize $P(s)$, can be given by

$$C_1(p) = \left. \frac{X(s) + R(s) * D_P(s)}{Y(s) - R(s) * N_p(s)} \right|_{Y(s) - R(s) * N_p(s) \neq 0} \tag{10}$$

Where, $N_P(s)$ and $D_P(s)$ are the co-prime factors of plant $P(s)$, such that $P(s) = N_p(s) / D_p(s)$

and,

$$X(s) * N_p(s) + Y(s) * D_p(s) = 1 \tag{11}$$

Eq.(11) is known as Bezout's identity. In (10), $R(s)$ is a free rational function and the value of $R(s)$ are conventionally chosen to maximize the gain of $C(s)$ at the fundamental frequency but in this way the impact of the disturbance on the output increases. Therefore, the value of $R(s)$ must be chosen to ensure maximum attenuation to the disturbance and this can be achieved by mixed sensitivity optimization. For this purpose, robust design of the controller can be achieved by mixed sensitivity constraint (12),

$$\left\| \begin{bmatrix} W_1 S \\ W_2 T \end{bmatrix} \right\|_\infty \leq 1 \tag{12}$$

Where, W_1, W_2 are frequency dependent weighting functions. Now, *S* and *T* are nominal sensitivity and complimentary sensitivity functions respectively, defined by:

$$S = \frac{1}{1+PC} \quad and \quad T = \frac{PC}{1+PC} \tag{13}$$

Further, in the absence of suitable controller satisfying (12), a sub-optimal controller can be designed by minimizing (12) for a sufficiently large bandwidth. According to [27],[29], for optimal controller C, (12) can be inferred as:

$$\|W_1 S\|^2 + \|W_2 T\|^2 \ll 1 \tag{14}$$

or

$$\|W_1 S\| \ll 1 \ and \ \|W_2 T\| \quad 1 \tag{15}$$

or $$\|S\| \ll \frac{1}{W_1} \ and \ \|T\| \quad \frac{1}{W_2} \tag{16}$$

For $P = \frac{N}{D}$ and $C = \frac{X + RD}{Y - RN}$ (13) can be written as,

$$S = \frac{1}{1 + \frac{N(X + RD)}{D(Y - RN)}} \tag{17}$$

$$S = \frac{D(Y - RN)}{XN + DY} \tag{18}$$

As $XN + DY = 1$,

Therefore, from (16) and (18)

$$D(Y - RN) < \frac{1}{W_1} \tag{19}$$

or $$R > \frac{1}{N}\left(Y - \frac{1}{DW_1}\right)$$

In inequality (19), we can introduce a free rational function q_r ($\|q_r(0)\| = 1$ and $\|q_r(\infty)\| = 1$) to make R proper. However, in (13) controller can approach to infinite gain at ($\|Y - RN\|_{\omega=\omega_0} = 0$) which is damped by taking *R* as

$$R = \frac{q_r}{N_0}\left(Y - \frac{1}{DW_1}\right) \tag{20}$$

Where, $N_0 = N/N_i$ is the outer function of *N*.

Similarly, from (13) and (16), for complimentary sensitivity *T*,

$$R < \frac{1}{N_0}\left(Y - \frac{1}{D}\left(1 - \frac{1}{W_2}\right)\right) \tag{21}$$

Inequality (21) is complimentary and gives the upper bond for *R*. The weighing function W_1 is to be selected in order to shape the sensitivity function for any given perturbation bandwidth.

IV. Computation of Parameters

RC requires parameterization of stabilizing controller. The methodology for designing the RC has already been described in section-III. Now this methodology will be used to design the voltage and current controller for VSI.

A. Design of Voltage Controller

Fig.5 shows the block diagram of control system where, P_1 and P_2 are taken as *LC* - filter and load transfer functions respectively. Hence, transfer function for P_2 can be written as:

$$P_2 = \frac{K}{(L_x s + R_x)} \tag{22}$$

Where, K is load gain calculated at nominal KVA rating of VSI, L_x & R_x are transmission line parameters. The plant P_1 transfer's function is taken $(1/Cs)$. Then closed loop transfer function (P_1 & P_2) will be,

0885-8993 (c) 2016 IEEE. Personal use is permitted, but republication/redistribution requires IEEE permission. See http://www.ieee.org/publications_standards/publications/rights/index.html for more information.

This article has been accepted for publication in a future issue of this journal, but has not been fully edited. Content may change prior to final publication. Citation information: DOI 10.1109/TPEL.2016.2619367, IEEE Transactions on Power Electronics

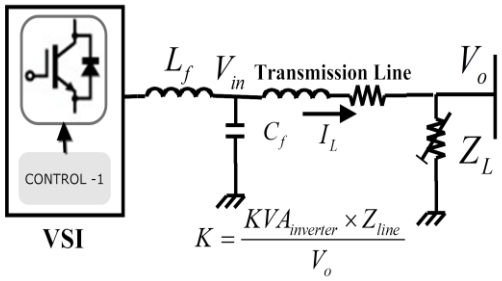

Fig.5 (a) Inverter's interface in microgrid

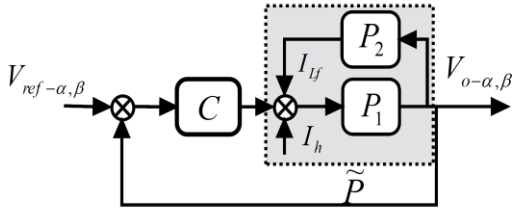

Fig.5 (b) Voltage control loop

$$P = \frac{P_1}{1 + P_1 P_2} \tag{23}$$

or

$$P = \frac{K^{'}(s+p)}{s^2 + c_1 s + c_0} \tag{24}$$

Using parameter from Table-1 in appendix, (24) gives following transfer function.

$$P = \frac{K^{'}(s+166.7)}{s^2 + 166.7s + 1.81e^8} \tag{25}$$

Where, $K^{'} = 1/C_f$ and $p = R_x / L_x$

As discussed in section- III, P can be factorized in rational function such that $P = \frac{N}{D}$, where N and D are co-prime factors [19], [24]. Weighing function W_1 shapes sensitivity, therefore, taken equal to $\frac{s+\omega}{s}$. The corresponding frequency response for sensitivity $\left(S = \left\| \frac{1}{W_1} \right\| \right)$ is shown in Fig.6(a), where ω is taken equal to the required bandwidth of controller.

Since plant is strictly proper, it has attenuation for high order frequency and therefore W_2 can be chosen as unity. The value of free variable $'R'$ is calculated by solving (20) that gives the parameter of high order ISC$\left(C_1(s)\right)$. Therefore, the designed controller further reduced by balance truncation method by calculating error bond of Hankel's singular value as:

$$\left\| C_{1V} - C_{1V} \right\|_\infty \le 2\sum_{k+1}^{n} \sigma_i \tag{26}$$

Where, k is the order of reduced controller and σ_i is the Hankel's singular values.

Hankel's singular values are calculated with separated stable and unstable parts, then transfer function corresponding to relatively higher stable value are retained in the controller.

The reduced order approximated ISC for voltage controller in 2nd and 1st order transfer function is given in (27-28).

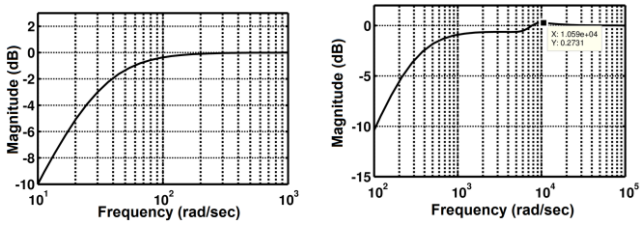

(a) (b)

Fig.6 Bode plot of (a) Sensitivity shaping function $1/W_1$ (b) System sensitivity with C_v

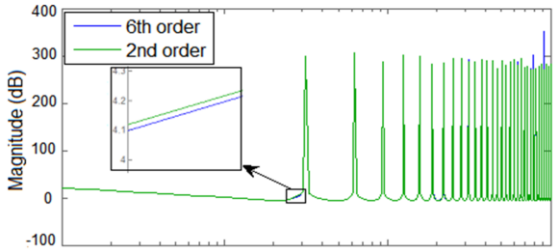

Fig.7.Frequency Response of Voltage RC

$$C_{1V}(s)^{2nd} = \frac{0.00785s^2 + 1.308s + 1.425e^6}{s^2 + 166.7s + 1.359e^{-14}} \tag{27}$$

and,

$$C_{1V}(s)^{1st} = \frac{0.00785s + 8547}{s + 8.154e^{-17}} \tag{28}$$

Fig.6 (b) shows the frequency response of sensitivity with designed controller (29). It is worthwhile to mention that system attain maximum sensitivity of 0.27dB, hence satisfying (12).

The first order low pass filter with corner frequency of 5 KHz is used in time delay loop to implement C_r. The corner frequency is chosen as per bandwidth of feedback of signals i.e. voltage and current. The bode plot of full and approximated voltage controller with unity pre-compensator ($C_2 = 1$) is shown in Fig.7. Here, it can be observable that the approximated controller is perfectly matching the characteristics of original controller with minimal error.

B. Design of Current Controller

The current controller is also designed in similar fashion as of voltage controller. Here, the plant transfer function is described by series connected filter inductance L_f and resistance R_f.

Plant transfer function for current control loop can be written as,

$$P(s) = \frac{1}{L_f s + R_f} \tag{29}$$

Where L_f and R_f are Inductance and parasitic resistance of inductor.

Now, co-prime factors of (29) is taken as, $N(s) = \frac{(1/L_f)}{(s + R_f/L_f)}$ and $D(s) = 1$.

The value of *R(s)* as calculated from (20) is further utilized in (10) in order to obtain high order controller parameters. Further, the high order controller is reduced to 2nd order with balanced truncation method as given in (30).

0885-8993 (c) 2016 IEEE. Personal use is permitted, but republication/redistribution requires IEEE permission. See http://www.ieee.org/publications_standards/publications/rights/index.html for more information.

This article has been accepted for publication in a future issue of this journal, but has not been fully edited. Content may change prior to final publication. Citation information: DOI 10.1109/TPEL.2016.2619367, IEEE Transactions on Power Electronics

$$C_{1C}(s)^{2nd} = \frac{1.005s^2 + 125.6s + 3925}{s(s+62.5)} \quad (30)$$

Frequency response of approximated current controller is shown in Fig. 8(a). The value of pre-compensator (C2) is gain set to unity for simpler configuration. Fig. 8(b) shows frequency response of inner current loop with different inverter output impedance. It shows that the loop bandwidth improve when low value of filter inductance is used. Therefore, same controller can perform better when used with high switching frequency that reduce filter inductance requirement [34]. In conventional controller, the bandwidth is limited by controller, therefore will not perform better with improved hardware configuration.

V. Hardware Description & Control

A scaled hardware prototype of microgrid has been developed to test the proposed controller. The prototype consists of two three phase VSI having batteries as a constant DC voltage source. Inverters are connected with each other through equivalent network impedance (implemented by inductance). The three phase linear and non-linear loads are connected to common bus via switch. A three phase contactor has been used as C.B. which makes/disconnects the interconnection on low voltage control signal. Each inverter has a LC-filter on its output to filter out PWM carrier frequency and its harmonic component.

The whole control system for both the VSI's is implemented within FPGA (Xilinx-ZYNQ 7000/ZEDBOARD) board as depicted in Fig.9. FPGA has various digital I/O port to connect it to external world. All the transfer functions are computed in continuous time domain and discretized by *bilinear transformation* to make them suitable for real time digital control implementation.

Since RC's always have long time delays in order to get them implemented for real time control applications and accordingly require large number of logic resource of FPGA. Therefore, in order to have optimal utilizations of logic resources, the delays are generated with dual port RAMs within FPGA. This method reduces the logic count while improving utilization of FPGA.

In addition to this, other resource optimization techniques are also critically required to implement a bigger system within single FPGA chip. Therefore, to reduce logic count for FPGA,

1) All computations are performed in Fixed Point Numbers.
2) Function blocks are shared among similar signals using signal multiplexing and overclocking.

However, above measures may decrease the control performance and increases complexity of the system in prototyping.

The whole control requires inductor current and voltage across capacitor as a feedback signal. This can be done by isolated voltage and current sensors. The voltage and current signals are measured only in two phases of each inverter so that number of sensor can be minimized. The outputs of these sensors are converted into digital signal by analog to digital converter (ADC) which are further communicate to FPGA via digital I/O port. The value of voltage and current of third phase is computed numerically inside the FPGA since it is assumed that the system is balanced. Further, all three phase quantities in a stationary reference frame ($\alpha\beta$) using *Clarke transformation* (7, 8). Further, the calculation

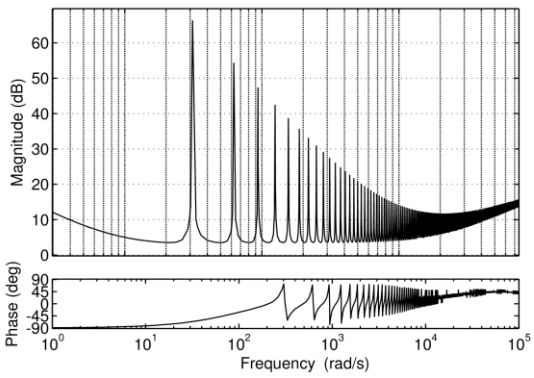

Fig. 8 (a) Frequency Response of Current RC

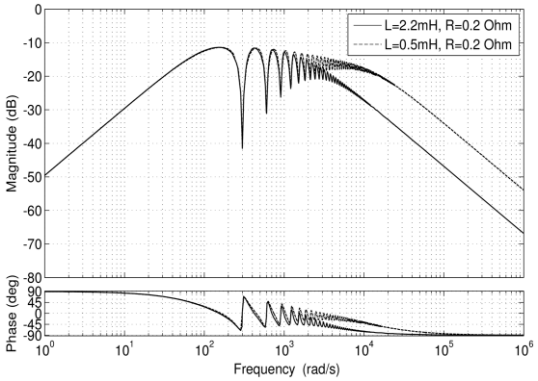

Fig. 8 (b) Frequency Response of Current RC with different filter inductance

of inverter's active (P) and reactive powers (Q) are made by equations (32-33), voltage and current quantities are converted into two phase.

$$P = \frac{\omega_c}{s+\omega_c}(V_\alpha I_\alpha + V_\beta I_\beta) \quad (31)$$

$$Q = \frac{\omega_c}{s+\omega_c}(V_\alpha I_\beta - V_\beta I_\alpha) \quad (32)$$

Where, ω_c is power filter cut off frequency in rad/sec.

The calculated values of P and Q is passed to droop controller which gives voltage (V) and rotating phase (θ) to generate three phase voltage reference. Three voltage references are then generated by *Direct Digital Synthesizer (DDS)*. *DDS* is an IP with *Xilinx design suite*, and used to generate unity sine and cosine signal with FPGA logic.

Reference voltage generated by *DDS* block is first transformed to ($\alpha\beta$) and subsequently fed to voltage and current RC. The output of RC is transformed back into three phase voltage by *Inverse Clarke transformation* and fed to the PWM block which generates six gate pulses at output.

For basic comparative study the *PI* control is implemented in similar fashion except the process of transformation of the quantities which is performed in synchronous reference frame using *park transformation* (dq) instead. The values of PI gains are calculated with root locus after the linearization.

The VHDL synthesis shows *RC* is better suited for FPGA implementation as it better utilize memory than logic slices. Same time the PI control requires an additional step of *dq*-transformation. This also reduces the logic count as well as other resources in the system.

0885-8993 (c) 2016 IEEE. Personal use is permitted, but republication/redistribution requires IEEE permission. See http://www.ieee.org/publications_standards/publications/rights/index.html for more information.

This article has been accepted for publication in a future issue of this journal, but has not been fully edited. Content may change prior to final publication. Citation information: DOI 10.1109/TPEL.2016.2619367, IEEE Transactions on Power Electronics

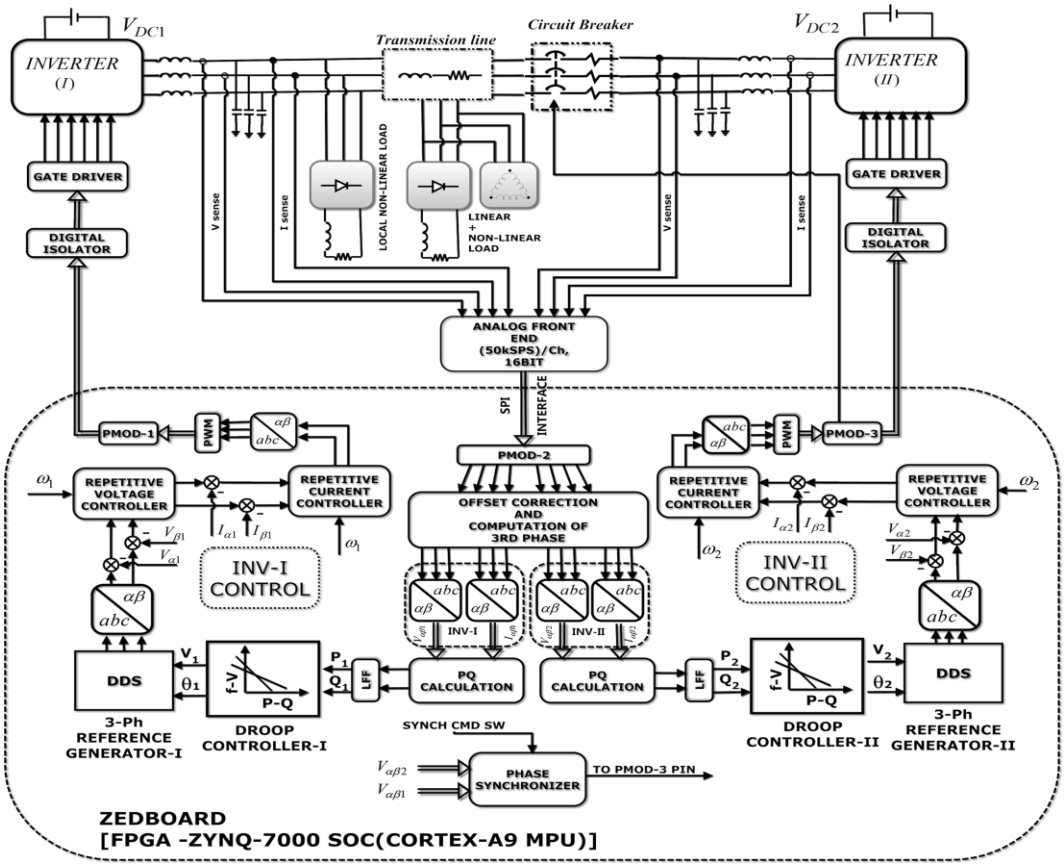

Fig.9 Interconnected VSIs in Microgrid

VI. Simulation and Experimental Results

In this section simulation and experimental studies are present in two parts. First part shows the performance of proposed RC on the basis of its reference tracking capability under linear and non-linear load condition and compared with conventional PI control. In the second part, performance of the controller is analyzed by connecting both the inverters in parallel under droop control mode to show the stable parallel operation.

A. Performance of RC with Non-Linear Load

As already discussed, the RC has an ability to minimize periodic error generated by non-linear load in the form of harmonics. A VSI serving rectified RL load has been used to test performance of the RC. The results are compared with convention-al PI controller with same system. At first, model was simulated in MATLAB/ SIMULINK to show the reference tracking capability of inverter. Phase 'A' voltage trajectory for both the controllers have been plotted in Fig.10, and it may be easily observed that the RC tracks voltage reference very much precisely in comparison of PI controller.

As evident from Fig. 10(a) that the PI controller is able to track the voltage reference in phase but unable to avoid the superimposition of harmonics on output voltage.

The above observations were also verified with scaled down experimental setup. The performance of controller were test-ed with a non-linear load at the output of the VSI, where the non-linear voltage drop across filtering inductance deforms the output voltage waveform in absence of proper control efforts. The performance of perfectly tuned PI controller is shown in Fig. 11(a) where the harmonic effect of non-linear current with THD of 29% almost deforms the output voltage with THD of 6.8%. However, this deformation in voltage waveform may be countered by a more capable voltage and current controller.

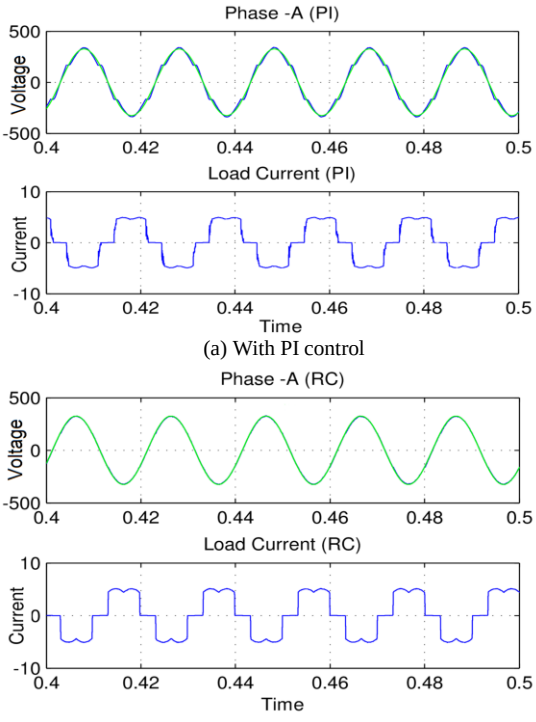

(a) With PI control

(b) With RC

Fig.10 Output Voltage, Reference Voltage and load current

In order to reduce the impact of non-linear load current on output voltage waveform, a RC and current controllers were designed and experimentally validated. The experimental results with RC are shown in Fig.12. Here, it can be easily observed that the THD in voltage waveforms are almost negligible (THD = 4.1%) despite of highly non-linear load current with THD of more than 29%.

0885-8993 (c) 2016 IEEE. Personal use is permitted, but republication/redistribution requires IEEE permission. See http://www.ieee.org/publications_standards/publications/rights/index.html for more information.

This article has been accepted for publication in a future issue of this journal, but has not been fully edited. Content may change prior to final publication. Citation information: DOI 10.1109/TPEL.2016.2619367, IEEE Transactions on Power Electronics

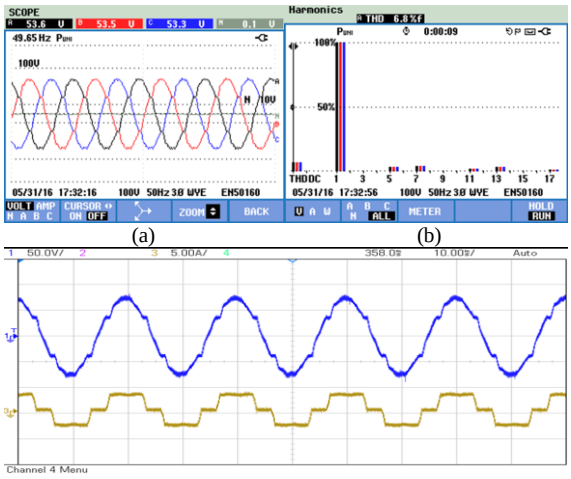

(a) (b)

(c)

Fig.11 (a) 3-Phase voltage waveform with PI control (b) Harmonics profile of voltage (6.8% THD) (c) Voltage and Non-linear load current profile

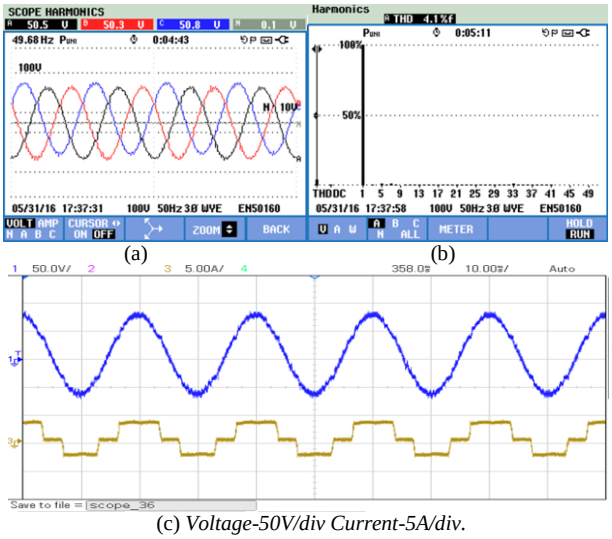

(a) (b)

(c) *Voltage-50V/div Current-5A/div.*

Fig.12 (a) Voltage waveform with RC control (b) Harmonics profile of voltage (4.1% THD) (c) Voltage and Non-linear load current

In Fig. 13 -15, the dynamic performance with step increase in a non-linear load is demonstrated. Here, it is pertinent to mention that the PI regulator shows satisfactory performance under linear load. However, the voltage waveforms deteriorate as soon as the non-linear load is applied as shown in Fig. 13. Further the voltage profile keep on deteriorating with the increase in non-linear load current.

In Fig. 14, the voltage and current profiles with RC are shown. Here, it is shown that the RC is able to handle the dynamic changes in load current without any significant on output voltage waveform. Moreover, the increase in THD level of load current has very negligible effect on output voltage profile where the THD's of voltage are kept within prescribed limit of 5%.

In Fig.15, the effect of increase in nonlinear load current on voltage waveform has been shown. Here, it can be seen that there is abrupt rise in voltage THD level with increase in non-linear load. However, the percentage change in THD of voltage w.r.t. percentage change in non-linear load current is very less in case of RC based control strategy.

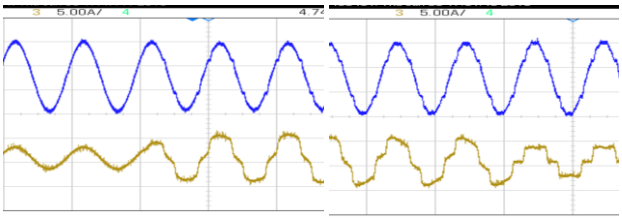

(a) *Voltage-50V/div Current-5A/div.*

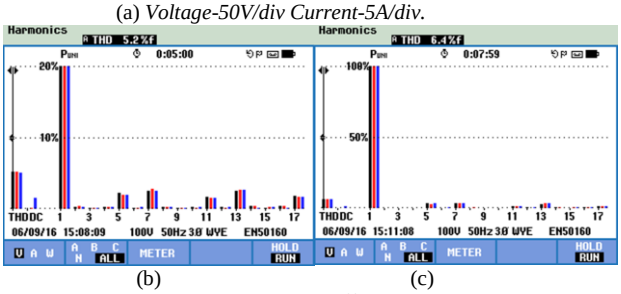

(b) (c)

Fig.13 (a) Voltage and current under different load condition with PI (b) Harmonic profile of voltage under linear plus non-linear loading (c) Harmonic profile of voltage under non-linear loading

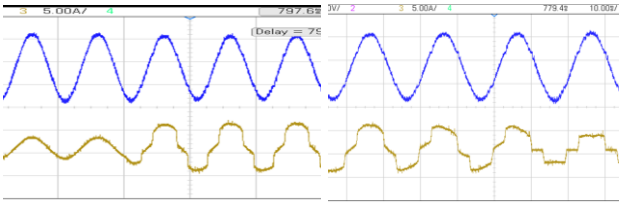

(a) *Voltage-50V/div Current-5A/div.*

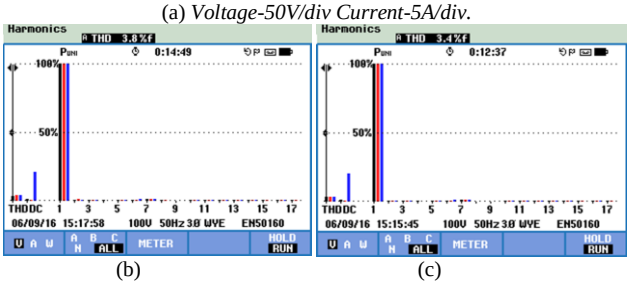

(b) (c)

Fig.14 (a) Voltage and current under different load condition with RC (b) Harmonic profile of voltage under linear plus non-linear loading (c) Harmonic profile of voltage under non-linear loading

B. Performance of RC in parallel operation

In droop based microgrid, voltage and current loop must show stability during parallel operation and maintain synchronism with remaining system. Therefore, RC was tested for parallel operation, where INV-II brought to synchronism by phase synchronizer with INV-I and then interconnected by circuit breaker immediately.

The sharing of power is in accordance with their droop coefficient as frequency droop is equal for both the inverters. When an additional load (non-linear in nature) was added to the system, both the inverters increased their power in proportional manner and dropped their frequency and voltage according to their droop coefficients.

Initially, only INV-I is connected to a resistive load which is far from inverter and INV-II is running separately at no load. When both the inverters are connected, due to droop control active power of INV-I decreased to half of its value while remaining half is shared by INV-II as shown in Fig. 16. There is small mismatch in reactive power sharing

0885-8993 (c) 2016 IEEE. Personal use is permitted, but republication/redistribution requires IEEE permission. See http://www.ieee.org/publications_standards/publications/rights/index.html for more information.

This article has been accepted for publication in a future issue of this journal, but has not been fully edited. Content may change prior to final publication. Citation information: DOI 10.1109/TPEL.2016.2619367, IEEE Transactions on Power Electronics

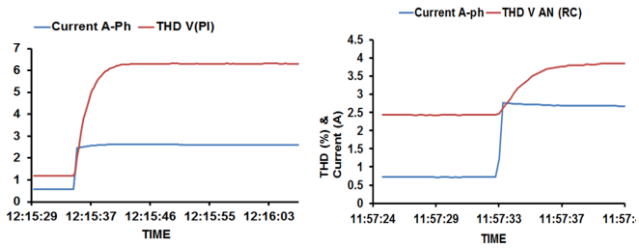

(a) PI control (b) Repetitive Control

Fig.15 THD comparison with Load Current

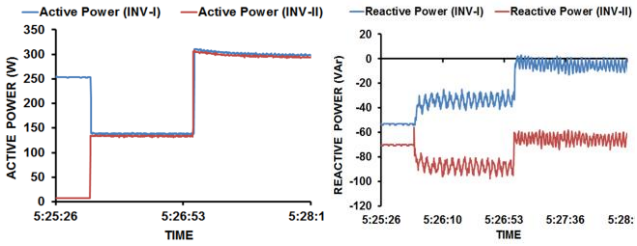

(a) (b)

Fig.16 (a) Active and (b) Reactive Power sharing of inverters

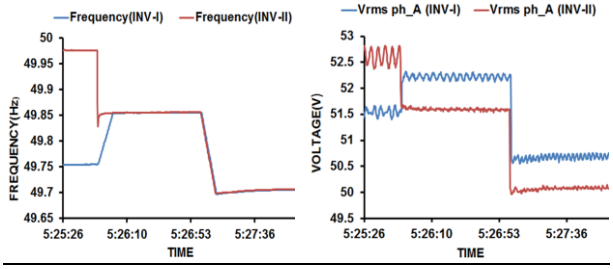

(a) (b)

Fig.17 (a) Frequency and (b) Voltage of both inverters

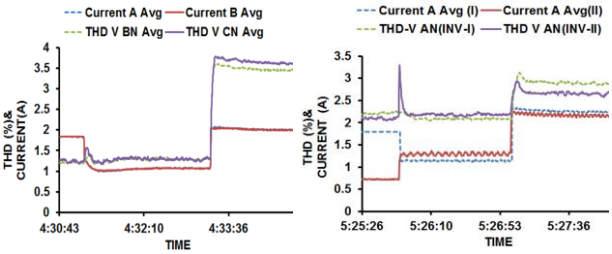

(a) PI control (b) Repetitive control

Fig. 18 THD vs Load Current diagram during parallel operation of both the inverters

which occurs probably due to difference between voltage magnitudes of the inverters at the time of interconnection.

This effect can be verified in output voltage (RMS) of inverters in Fig-17. Although, the load is connected far (as per network impedance) from inverter's terminal, the harmonics in inverter's output voltage shows a slight improvement with RC (Fig-18).

VII. Conclusion

The paper shows a new simpler RC design methodology for VSI in droop based microgrid. The simulation study as well as experimental validation has been presented. It has been demonstrated that proposed RC based control strategy shows good performance under steady state and dynamic conditions in comparison to conventional PI controller. The experimental results for parallel operation of two VSI's in microgrid have been presented where both the inverters are able to handle the linear as well as non-linear varying load demand seamlessly. It is also shown that the RC has very good control in rejecting the harmonic component on voltage waveform in comparison to its PI counterpart under highly non-linear load conditions.

Appendix

TABLE I
SYSTEM PARAMETERS

Parameters	**INV-I**	**INV-II**
DC –voltage *	160 V	158 V
PWM frequency	5kHz	6kHz
Filter Inductance and ESR	2.2mH,0.1 Ω	1.8mH,0.1Ω
Filter capacitance	25uF	25uF
Nominal Frequency	50 Hz	50 Hz
Nominal AC voltage*	54 V	54 V
Transmission line Inductance and Resistance	1.2mH,0.2 Ω	1:5mH,0.2 Ω
Droop coefficient Frequency (m_f)	1Hz/1Kw	1Hz/1Kw
Droop coefficient Voltage (m_e)	2V/QKVar**	2V/QKVAr**
Power filter cut off frequency (ω_c)	15 rad/sec	15 rad/sec
Non-linear Load, Gain K	Resistance=22 Ω (Cold) , Inductance=120 mH , 7.5	
Kpv & Kiv (PI V- controller)	0.40 / 186	0.42 / 184
Kpc & Kic (PI current controller)	0.30 / 67	0.34 / 73

**In simulation, DC voltage =760 V, and Nominal AC RMS Voltage=230V*

** $Q=\sqrt{KVA^2-Kw^2}$, *Rated KVA=1,(INV-1,INV-2)*

References

[1] C. Marnay, H. Asano, S. Papathanassiou, and G. Strbac, "Policymaking of microgrids, economic and regulatory issue of microgrid implementation," *IEEE Power & Energy magazine*, may/june 2008.

[2] M. Singh and A. Chandra, "Real-Time Implementation of ANFIS Control for Renewable Interfacing Inverter in 3P4W Distribution Network," in *IEEE Transactions on Industrial Electronics*, vol. 60, no. 1, pp. 121-128, Jan. 2013.

[3] M. Singh, V. Khadkikar, A. Chandra and R. K. Varma, "Grid Interconnection of Renewable Energy Sources at the Distribution Level With Power-Quality Improvement Features," in *IEEE Transactions on Power Delivery*, vol. 26, no. 1, pp. 307-315, Jan. 2011.

[4] C. Marnay and O. C. Bailey, "The certs microgrid and the future of the macrogrid," August 2004.

[5] H. van der Broeck et al., "A simple method for parallel operation of inverters," in Telecommunications Energy Conference, 1998. INTELEC.IEEE, Oct 1998, pp. 143–150.

[6] J. M. Guerrero, J. C. Vásquez, J. Matas, M. Castilla, and L. G. de Vicuña, "Control strategy for flexible microgrid based on parallel line-interactive ups systems," *IEEE Transactions on Industrial Electronics*, vol. 56,no. 3, pp. 726–737, March 2009.

[7] S. J. Chiang and J. M. Chang, "Parallel control of the ups inverters with frequency-dependent droop scheme." IEEE PESC'01 Conf., June 2001,pp. 957–961.

[8] J. M. Guerrero, J. Matas, L. G. de Vicuña, M. Castilla, and J. Miret,"A wireless controller to enhance dynamic performance of parallel inverters in distributed generation systems," *IEEE transactions on power electronics*, vol. 19, no. 5, September 2004.

[9] N. R. Tummuru, M. K. Mishra and S. Srinivas, "Multifunctional VSC Controlled Microgrid Using Instantaneous Symmetrical Components Theory," *in IEEE Transactions on Sustainable Energy*, vol. 5, no. 1, pp. 313-322, Jan. 2014.

[10] Y. Han, P. Shen, X. Zhao and J. M. Guerrero, "An Enhanced Power Sharing Scheme for Voltage Unbalance and Harmonics Compensation in an Islanded AC Microgrid," in *IEEE Transactions on Energy Conversion*, vol. 31, no. 3, pp. 1037-1050, Sept. 2016.

[11] J. Rocabert, A. Luna, F. Blaabjerg and P. Rodríguez, "Control of Power Converters in AC Microgrids," in *IEEE Transactions on Power Electronics*, vol. 27, no. 11, pp. 4734-4749, Nov. 2012.

[12] M. Singh and A. Chandra, "Application of Adaptive Network-Based Fuzzy Inference System for Sensorless Control of PMSG-Based Wind Turbine With Nonlinear-Load-Compensation Capabilities," in *IEEE Transactions on Power Electronics*, vol. 26, no. 1, pp. 165-175, Jan. 2011.

0885-8993 (c) 2016 IEEE. Personal use is permitted, but republication/redistribution requires IEEE permission. See http://www.ieee.org/publications_standards/publications/rights/index.html for more information.

This article has been accepted for publication in a future issue of this journal, but has not been fully edited. Content may change prior to final publication. Citation information: DOI 10.1109/TPEL.2016.2619367, IEEE Transactions on Power Electronics

[13] J. G. de Matos, F. S. F. e Silva and L. A. d. S. Ribeiro, "Power Control in AC Isolated Microgrids With Renewable Energy Sources and Energy Storage Systems," in *IEEE Transactions on Industrial Electronics*, vol. 62, no. 6, pp. 3490-3498, June 2015.
[14] J. M. Guerrero, J. C. Vasquez, J. Matas, L. G. de Vicuña, and M. Castilla, "Hierarchical control of droop-controlled ac and dc microgrids–a general approach toward standardization," *IEEE Transactions On Industrial Electronics*, vol. 58, no. 1, pp. 158–172, January 2011.
[15] J. C. Vasquez, J. M. Guerrero, M. Savaghеb, J. Eloy-Garcia, and R. Teodorescu, "Modeling, analysis, and design of stationary-reference frame droop-controlled parallel three-phase voltage source inverters,"*IEEE Transactions On Industrial Electronics*, vol. 60, no. 4, pp. 1271–1281, April 2013.
[16] A. Trivedi, D. K. Jain, and M. Singh, "A modified droop control method for parallel operation of vsi's in microgrid," in ISGT Asia. IEEE,November 2013, pp. 1–5.
[17] S. Luo et al., "A classification and evaluation of paralleling methods for power supply modules," in PESC 99, vol. 2. IEEE, 1999, pp. 901 –908.
[18] B. A. Francis and W. M. Wonham, "The internal model principle for linear multivariable regulators," J. Applied Mathematics and Optimization, vol. 2, pp. 170–194, 1975.
[19] G. Weiss, "Repetitive control systems: old and new ideas," Systems and Control in the Twenty-First Century, pp. 389–404, 1997.
[20] S. Hara, M. Nakano, Y. Yamamoto, and T. Omata, "Repetitive control system: A new type servo system for periodic exogenous signals," *IEEE Transactions on Automatic Control*, vol. 33, no. 7, pp. 659–668, July1988.
[21] K. Watanabe and K. Yamada, "Repetitive control of time-delay systems," in Declilon and Control. IEEE, December 1990, pp. 1685–1690.
[22] K. Yamada, H. Takenaga, Y. Saitou, and K. Satoh, "Proposal for simple repetitive controllers," ECTI Transactions on Electrical Eng., Electronics and Communications, vol. 6, no. 1, pp. 64–72, 2008.
[23] K. Yamada, H. Tanaka, H. Takenaga, and M. Kobayashi, "A design method for simple repetitive controllers for time-delay plants," in ECTI-CON 2008. IEEE, 2008, pp. 597–600.
[24] K. Yamada and T. Okuyama, "A parametrization for the class of all stabilizing repetitive learning controllers for linear minimum phase systems," in Proc. IEEE Conf. Systems Man and Cybernetics'99, vol. 5,1999, pp. 62–67.
[25] K. Yamada et al., "The parameterization of all robust stabilizing simple repetitive controllers," *Journal of System Design and Dynamics*, vol. 4,no. 3, pp. 457–470, 2010.
[26] X. H. Wu, S. K. Panda and J. X. Xu, "Design of a Plug-In Repetitive Control Scheme for Eliminating Supply-Side Current Harmonics of Three-Phase PWM Boost Rectifiers Under Generalized Supply Voltage Conditions," *in IEEE Transactions on Power Electronics*, vol. 25, no. 7, pp. 1800-1810, July 2010.
[27] M. Morimoto, T. Zanma, M. Ishida, G. Pipeleers and J. Swevers, "Suppression of harmonic current for IPMSM using generalized repetitive control," IECON 2010 - 36th Annual Conference on *IEEE Industrial Electronics Society*, Glendale, AZ, 2010, pp. 2270-2275.
[28] G. Pandove, A. Trivedi and M. Singh, "Repetitive control-based single-phase bidirectional rectifier with enhanced performance," in *IET Power Electronics*, vol. 9, no. 5, pp. 1029-1036, 4 20 2016.
[29] G. Weiss, Qing-Chang Zhong, T. C. Green and Jun Liang, "H∞ repetitive control of DC-AC converters in microgrids," in *IEEE Transactions on Power Electronics*, vol. 19, no. 1, pp. 219-230, Jan. 2004.
[30] D. Chen, J. Zhang and Z. Qian, "An Improved Repetitive Control Scheme for Grid-Connected Inverter With Frequency-Adaptive Capability," in *IEEE Transactions on Industrial Electronics*, vol. 60, no. 2, pp. 814-823, Feb. 2013.
[31] J. Doyal, B. Francis, and A. Tannenbaum, Feedback control theory. Macmillian Publishing Co., 1990.
[32] M. Vidyasagar, Control System Synthesis: A Factorization Approach, ser.Part-1, C. Abdallah and M. W. Spong, Eds. MIT Press, Cambridge,MA, 2011.
[33] H. Sugimoto and K. Washida, "A proposition of design method for modified repetitive control system with corrected dead time using sensitivity function shaping and its application to motor control system,"in PCC-Nagaoka '97. IEEE, 1997, pp. 619–624.
[34] A. J. Roscoe, S. J. Finney and G. M. Burt, "Tradeoffs Between AC Power Quality and DC Bus Ripple for 3-Phase 3-Wire Inverter-Connected Devices Within Microgrids," in *IEEE Transactions on Power Electronics*, vol. 26, no. 3, pp. 674-688, March 2011.
[35] J. M. Guerrero, J. Matas, L. Garcia de Vicuna, M. Castilla and J. Miret, "Decentralized Control for Parallel Operation of Distributed Generation Inverters Using Resistive Output Impedance," in *IEEE Transactions on Industrial Electronics*, vol. 54, no. 2, pp. 994-1004, April 2007.

Ashutosh Trivedi (S'15) has been pursuing his Ph.D from Delhi Technological University, Delhi. He has earlier completed his B.Tech and M.Tech in Electrical Engineering from Utter Pradesh Technical University and DCRUST, Murthal in 2008 and 2013 respectively. His field of Interest is primarily Microgrid and Renewable energy technologies.

He has worked with Everest Industries Ltd. from 2008-11 as electrical engineer and involved in many automation project within company.

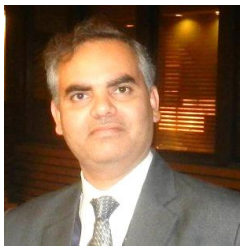

Dr. Mukhtiar Singh (M'11) is presently working as Associate Professor, Deptt. of electrical engineering, Delhi Technological University, Delhi, Since July-2012. Prior to Joining DTU, he was with dept. of electrical engineering, DCRUST, Murthal, Since july 2002.

He has completed his B. Tech and M. Tech. Degrees in electrical engineering from NIT, Kurukshetra (Erstwhile REC Kurukshetra), in 1999 and 2001, respectively. During March 2007 to Sept.-2010, he has been on study leave to pursue Ph.D from Ecole de Technologie Superieure, University of Quebec, Montreal, Canada with the financial support from Govt. of India under national overseas scholarship. He is also recipient of IEEE student scholarship for the best paper in 34Th IEEE conference on Industrial electronics, IECON-2008, held at Orlando, Florida, USA. Dr. Singh is also the winner of Researchers Merit Scholarship of University of Quebec for the three years consecutively, 2008, 2009, and 2010.

Dr. Singh is also actively involved in various activities of IEEE and presently holds the position of treasurer, IEEE PELS-IES Delhi Chapter. He had also been the General Chair of 5th and 6th IEEE power India international conference, PICON 2012 and PICON2014. He is also in the technical advisory group of leading renewable energy companies like Enercon.

0885-8993 (c) 2016 IEEE. Personal use is permitted, but republication/redistribution requires IEEE permission. See http://www.ieee.org/publications_standards/publications/rights/index.html for more information.

Renewable and Sustainable Energy Reviews 69 (2017) 188–196

Contents lists available at ScienceDirect

Renewable and Sustainable Energy Reviews

journal homepage: www.elsevier.com/locate/rser

Sensitivity and reliability models of a PV system connected to grid

Nikita Gupta[a,*], Rachana Garg[a], Parmod Kumar[b]

[a] Department of Electrical Engineering, Delhi Technological University, Delhi, India
[b] Department of Electrical Engineering, Maharaja Agrasen Institute of Technology, Delhi, India

ARTICLE INFO

Keywords:
Photovoltaic (PV) system
Sensitivity
Reliability
MTBF
Failure rate
Redundancy

ABSTRACT

With growing environmental concerns over the climate change risks associated with power generation using fossil fuels, solar power generation has emerged as one of the most rapidly growing renewable sources of electricity in the world. In recent technological advancements for improving the performance of PV system, efficiency improvement of solar PV cell and power converter stage has become a critical area of interest for researchers. Sensitivity and reliability studies of a system are important tools to evaluate the performance of the system. In this paper, sensitivity and reliability models of a grid-connected PV system are developed. Analytical relations of first order sensitivity are developed for PV cell and DC-DC converter. Further, reliability models are developed for individual components and for different configurations of PV system using Pareto analysis and logic gate representations. The main reference for electronic component reliability evaluation is MIL-HDBK-217 military handbook and MTBF calculator software by ALD. The developed models can be applied to any PV system to have a better insight.

1. Introduction

The advances in electronics and control technologies have made solar energy an economical and favorable alternative source of electric power generation. PV cell, a direct current (dc) generator, converts solar energy into electric energy. To obtain desired output voltage and current, these PV cells are configured in series and/or parallel to form a solar module which are further configured to form solar arrays [1]. The output of PV cell is sensitive to atmospheric temperature and light intensity incident on the cell, and usually varies with time of day and type of weather [2]. In order to maximize the power extraction from a PV cell, tracking of its output under varying meteorological parameters is required. Maximum power point tracking is implemented using choppers [3]. For power evacuation to ac loads, the dc output of solar arrays is further converted to ac output of desired voltage and frequency through inverters [4]. The PV systems can be broadly categorized as: grid-connected and standalone systems. In order to meet the load requirements for a grid-connected system, PV inverter is synchronized with conventional ac grid using Phase-Locked Loop (PLL) based synchronization algorithm [5–7].

Sensitivity and reliability are the performance indicators of any system. Sensitivity analysis is performed to determine the response of the system due to the parametric variations. Power available from PV system is a function of the PV cell characteristics, such as voltage and current, and converter parameters, voltage output in particular. The PV cell shows nonlinear current-voltage characteristics depending on irradiance level and the cell temperature. Also, the output of converter depends upon its designed parameters. Thus, there is a need to develop sensitivity functions of PV cell and converter output related to these parameters of interest to analyze their performances under real conditions.

Cristina and D'Amore [8,9], Indulkar et al. [10] and Kumar et al. [11] have made notable contributions in the field of sensitivity studies of conventional power systems. For nonlinear equations of PV cell, different sensitivity methods are proposed in the literature, including static sensitivity methods and dynamic trajectory sensitivity methods [12–16]. Also, the researchers have carried out the sensitivity analysis of solar cells with different point of views and with different parameters of interest.

Guo et al. [17] have proposed cat swarm optimization algorithm to estimate the unknown parameters of PV cell for sensitivity analysis. A comparative study of CSO algorithms with other existing algorithms was performed and CSO algorithms were found most effective in identifying parameters of solar cell models. Andrei et al. [18] used sensitivity study to analyze the performances of PV cells related to the different temperature and irradiance levels. The model parameters for the equivalent circuit of PV cell were derived. The accuracy of proposed method was checked with numerical values obtained from real case studies. Needleman et al. [19] had performed sensitivity studies of spectral splitters. Spectral splitters increase the amount of solar

* Corrresponding author.
E-mail address: guptanikita08@gmail.com (N. Gupta).

http://dx.doi.org/10.1016/j.rser.2016.11.031
Received 18 March 2016; Received in revised form 15 July 2016; Accepted 2 November 2016
1364-0321/ © 2016 Elsevier Ltd. All rights reserved.

spectrum absorbed for better efficiency of PV cell. Authors performed simulations on 2-D TCAD to analyze the sensitivity of PV system performance with respect to two parameters of illumination intensity viz. spectral uniformity and spatial uniformity. Ito et al. [20] conducted sensitivity analysis of very large-scale PV systems from economic and environmental viewpoints. The authors concluded that the generation cost was affected by degradation, interest ratio, depreciation period and labor cost.

Further to sensitivity analysis of a PV cell, the reliable operation of all the components of the PV system is also important. Although, PV modules operate reliably for 25–30 years, but the components experience stresses due to switching operation of devices, environment parameters and voltage levels to which devices are subjected. The reliability studies of the components for the considered time shall also be studied.

Reliability evaluation techniques can be broadly classified as analytical and simulation techniques. Analytical techniques represent the system by a mathematical model and evaluate the reliability indices whereas simulation techniques estimate the reliability indices by simulating the actual process and random behavior of the system [21–24]. Researchers have suggested several methods to improve the reliability for longer useful life of system or component, for reducing cost and failure time, etc. Peng et al. [25] had carried out studies for improvement of reliability so that maintenance cost can be reduced.

High reliability is achieved by selecting suitable converter topology of a PV system. Chan and Calleja [26] analyzed and compared the reliability of three inverter configurations of PV system, such as integrated topology, two-stage and three-stage configuration. They calculated the failure rate using MIL-HDBK 217 [27] and established that the reducing the stress factors with highest contribution to failure rate helps in improving the reliability. Graditi et al. [28] compared and analyzed the reliability aspect of three basic dc-dc converter topologies for single phase grid tied PV applications. Using graphical and mathematical analysis, they concluded that the boost converter topology has the best reliability amongst other converter topologies. Harb et al. [29] proposed a module-integrated inverter while implementing double-frequency ripple cancellation concept and found that this topology has a better reliability than those of existing topologies. They replaced a bulky and low reliable electrolytic capacitor with a highly reliable film capacitor and validated the proposed topology with simulation and experimental findings. Khelifi et al. [30] calculated reliability of two chopper configurations, viz.: parallel and cuk configurations for MPPT operation in solar PV using MIL-HDBK-217-F. Simulation results concluded that a parallel chopper in CCM (continuous-conduction mode) mode is the most reliable solution to achieve MPPT. Madkor et al. [31] in their work have studied the effect of number of inverters in PV grid-Connected system on its efficiency, reliability and cost. They found that the reliability is inversely related to the number of inverters in the system.

Researchers have also assessed and shown with experiments that improvement in even a single component of a device connected to PV system can improve the overall reliability of that device. Aldaco et al. [32,33] have assessed the reliability of push-pull DC-DC converter by derating its power transistors. Obeidat and Shuttleworth [34] discussed the reliability of 250 W PV micro inverter through failure rate calculated using MIL-HDBK-217F N2. Variation in failure rate of different configurations of micro inverter was observed for over a wide variation of temperature stress factor and voltage ratio stress factor.

Though sufficient literature exist about the sensitivity and reliability analysis in the field of solar PV, but very little research has been done on a complete PV system level. The author(s) in this paper has developed the sensitivity functions of PV cell and converter with respect to parameters of interest using first derivative of Taylor's series. The performance of the PV array is examined by using MATLAB along with Simulink toolbox, and is mapped with the sensitivity results. Also, reliability model of complete grid-connected PV system has been developed. Further, reliability studies have been performed for individual components using Pareto analysis, considering the failure rate of components of the PV system due to stresses. Logic gate representation has been used to develop the reliability models for different configurations of the complete PV system.

2. Problem formulation

In this paper the author(s) have developed sensitivity functions of PV cell with respect to temperature and irradiation. Further, the sensitivity functions of converter output voltage are developed with respect to switching frequency, inductor value, capacitor value and duty cycle. The developed sensitivity functions are used to compute the sensitivity values and to carry out sensitivity analysis.

For the intended purpose, solar PV system of 10 kW rating is considered for computation of sensitivity with respect to the parameters of interest as shown in Fig. 1.

Further to sensitivity, reliability of the PV system considering stress factors related to different components is studied. Also, the reliability models for different PV system configurations have been developed using logic gate representation.

3. Mathematical model of the PV system

The line diagram representation shown in Fig. 1 comprises of three main sections of a PV system: (1) PV array, (2) DC-DC converter and

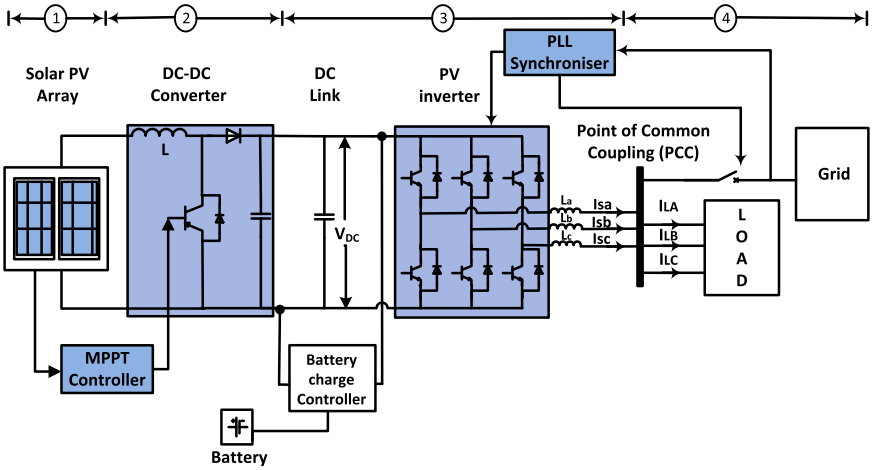

Fig. 1. Line diagram representation of the grid-connected PV system constituting four sections: (1) PV array, (2) DC-DC converter, (3) PV inverter and (4) grid interconnection of PV system.

(3) PV inverter. The design and mathematical model of each section is as follows:

3.1. PV array

A solar PV cell, an active transducer, converts the photon energy of sunlight directly into electricity. When exposed to sunlight (or other intense light source), a solar cell produces almost constant open circuit voltage depending upon the cell material while the current ($I_{PV(cell)}$) flow to connected load is proportional to light energy (photons) and is given by [1],

$$I_{PV(cell)} = I_{ph} - I_o\left[\exp\left\{\frac{q(V_{PV} + I_{PV}Rs)}{AkT}\right\} - 1\right] - \frac{V_{PV} + I_{PV}Rs}{Rp} \quad (1)$$

where k is constant, called the Boltzmann constant, q is the elementary charge (1.602×10^{-19} C), A is the diode ideality factor, R_s is the series resistance (Ω) and R_p is the shunt resistance (Ω) of solar cell. The equation for the PV array is obtained by modifying the above cell equation by inserting the indices n and m where n and m are number of cells in series and parallel respectively, and is given by

$$I_{PV(array)} = mI_{ph} - mI_o\left[\exp\left\{\frac{q(V_{PV(array)} + I_{PV(array)}Rs(\frac{n}{m}))}{nAkT}\right\} - 1\right] - \frac{V_{PV(array)} + I_{PV(array)}Rs(\frac{n}{m})}{Rp(\frac{n}{m})} \quad (2)$$

where the photocurrent I_{ph}, depends upon parameters, such as temperature and solar irradiance, and is defined by

$$I_{ph} = I_{sc}\frac{E}{E_{ref}}[1+(T - T_{ref})*k] \quad (3)$$

where E is operating irradiation, E_{ref} is PV cell reference irradiation, T_{ref} is PV cell reference temperature of 278 K, T is the PV cell operating temperature and k is constant related to temperature co-efficient due to SCC (short circuit current) of I_{SC} taken as 0.004%/°C.

Fig. 2 depicts the effect of irradiation level and temperature on Current Vs Voltage and Power Vs Voltage curve of the given PV array. The array used in simulation work has a peak capacity of 10 kW, and is designed at V_{oc} (open circuit voltage, maximum voltage that exist between the cells terminals) of 403 V and 34.5 A, I_{sc} (short circuit current, maximum current that the cell can provide).

3.2. DC-DC converter

In the designed system, DC–DC boost converter (Fig. 1) is used to obtain and regulate the required dc bus voltage. The passive elements of converter, inductor (L) and capacitor (C) are computed using the following equations [4]:

$$L = V_i(V_o - V_i)/\Delta i_f V_o \quad (4)$$

$$C = I_o D/\Delta v f \quad (5)$$

where D is the Duty cycle defined by

$$D = 1 - (V_i/V_o) \quad (6)$$

Further, V_i is the input voltage, V_o is the output voltage, Δi_i is input current ripple taken as 10% of input current, f is the switching frequency, Δv is ripple in output voltage taken as 3% of the boost converter output voltage and I_o is the output current of boost converter [4].

3.3. PV inverter

A three phase PV inverter is used to convert dc voltage to ac voltage. The single stage PV inverter consists of six IGBTs as shown in Fig. 1. In this paper, a 10 kW three phase 415 V inverter [4] is designed with 0.9 power factor load. Further, IGBTs of the inverter are designed for 1200 V, 60 A.

4. Sensitivity model

Sensitivity model provides a powerful tool for validating a designed system by studying the change in the response of the system with 1% change in any of its parameters [8,9]. Among different methods available for sensitivity calculations, partial differentiation method is the simplest, computationally better and fast. The normalized sensitivity function F with respect to parameter p can be evaluated as

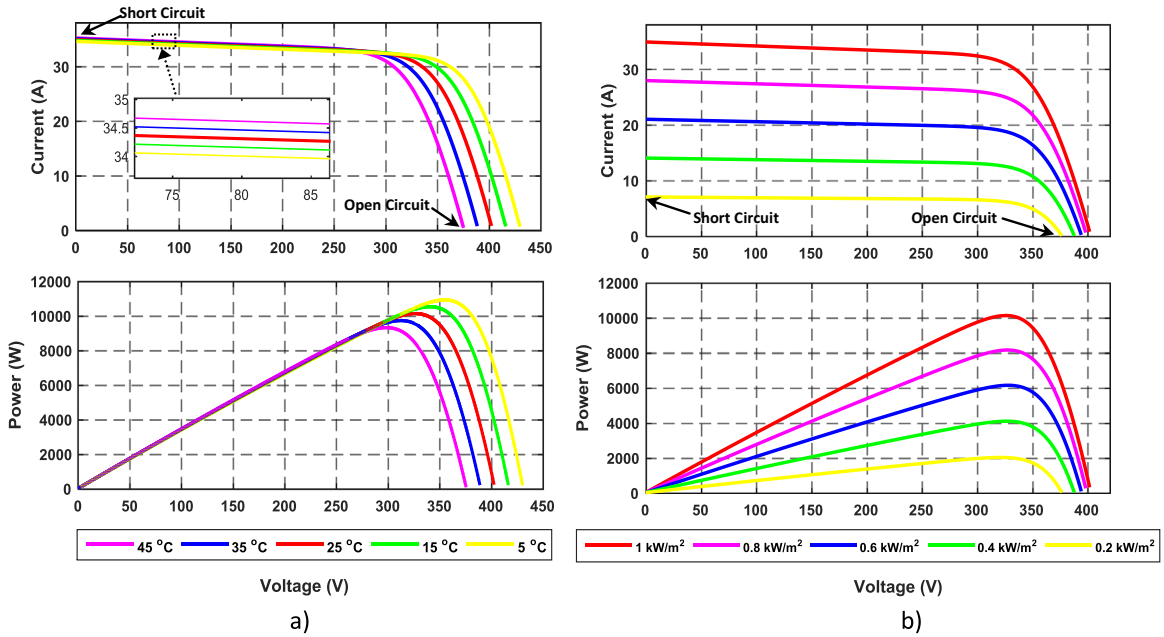

Fig. 2. Current vs voltage and power vs voltage curve of PV array used in proposed model for a) Different temperature levels b) Different irradiation level. PV cell when exposed to a higher temperature, I_{SC} increase slightly while V_{OC} fall sharply. Higher temperatures result in a decrease in the maximum power output. Further, PV cell when exposed to lower irradiation level, I_{SC} decreases sharply, while V_{OC} decreases less significantly. Decrease in irradiation level reduces the maximum power output.

Table 1
Sensitivity functions and sensitivity values of PV cell and converter parameters.

Parameters		Sensitivity functions developed	Sensitivity values using	
			Sensitivity function	Difference equation
PV cell parameter	$I_{ph} = I_{sc}\frac{E}{E_{ref}}[1+(T-T_{ref})*k]$	$\hat{S}_E^{I_{ph}} = \frac{E}{I_{ph}}*\left([1+(T-T_{ref})*k]*\frac{I_{sc}}{E_{ref}}\right)$	1.000	1.032
		$\hat{S}_T^{I_{ph}} = \frac{T}{I_{ph}}*\left(\frac{I_{sc}*k*E}{E_{ref}}\right)$	0.100	0.100
	$V_{oc} = \left(\frac{1}{\alpha}\ln\left(\frac{I_{ph}}{I_0}+1\right)\right)$	$\hat{S}_E^{V_{oc}} = \frac{E}{V_{oc}}*\left(\frac{1}{\alpha*(I_{ph}+I_0)}*\frac{\partial I_{ph}}{\partial E}\right)$	0.024	0.024
		$\hat{S}_T^{V_{oc}} = \frac{T}{V_{oc}}*\left(\frac{1}{\alpha*(I_{ph}+I_0)}*\frac{\partial I_{ph}}{\partial T}\right)$	−1.143	−1.143
	$I_{sc} = \left(\frac{I_{ph}}{1+\frac{R_s}{R_{sh}}}\right)$	$\hat{S}_E^{I_{sc}} = \frac{E}{I_{sc}}*\left(\frac{1}{1+\frac{R_s}{R_{sh}}}*\frac{\partial I_{ph}}{\partial E}\right)$	0.993	0.993
		$\hat{S}_T^{I_{sc}} = \frac{T}{I_{sc}}*\frac{\partial}{\partial T}\left(\frac{1}{1+\frac{R_s}{R_{sh}}}*\frac{\partial I_{ph}}{\partial T}\right)$	0.099	0.099
Converter parameter	$L=\left(\frac{V_{in}*(V_o-V_{in})}{\Delta i*f*V_o}\right)$	$\hat{S}_L^{V_o} = \frac{L}{V_o}*\left(\frac{\Delta i*f*V_o^2}{V_{in}^2}\right)$	0.972	0.973
	$f=\left(\frac{V_{in}*(V_o-V_{in})}{\Delta i*L*V_o}\right)$	$\hat{S}_f^{V_o} = \frac{f}{V_o}*\left(\frac{\Delta i*L*V_o^2}{V_{in}^2}\right)$	0.972	0.972
	$C=\left(\frac{I_o*(V_o-V_{in})}{V_o*f*\Delta v}\right)$	$\hat{S}_C^{V_o} = \frac{C}{V_o}*\left(\frac{f*V_o*\Delta v}{I_o-2*f*C*\Delta v}\right)$	0.556	0.55
	$D=\left(1-\frac{V_{in}}{V_o}\right)$	$\hat{S}_D^{V_o} = \frac{D}{V_o}*\left(\frac{V_{in}}{(1-D)^2}\right)$	0.960	0.960

$$\hat{S}_p^F = \frac{\partial F/F}{\partial p/p} = \left(\frac{p}{F}\right)\left(\frac{\partial F}{\partial p}\right) \tag{7}$$

If number of parameters of any function vary simultaneously, then the sensitivity of that function is computed using Jacobian matrix and is given by

$$J_{0_{P_i}}^{F} = \begin{bmatrix} \frac{\partial F1}{\partial P1} & \frac{\partial F1}{\partial P2} & \cdots & \frac{\partial F1}{\partial PN} \\ \vdots & \vdots & & \vdots \\ \frac{\partial Fu}{\partial P1} & \frac{\partial Fu}{\partial P2} & \cdots & \frac{\partial Fu}{\partial PN} \end{bmatrix} \tag{8}$$

In this paper, first term of partial differential of Taylor series is considered. This study helps in the real time performance evaluation of the system [8–11].

4.1. Sensitivity functions

Table 1 shows sensitivity functions developed with respect to parameters of interest. Further, the numerical values of sensitivity are obtained corresponding to the developed sensitivity functions. The numerical values of sensitivity functions are computed using the data presented in Appendix A. Finally, values obtained from sensitivity functions are validated with the values obtained from difference equation, changing parametric value by 1%.

From Table 1, it can be seen that the I_{sc} of PV cell increases with increase in irradiation level and temperature. The V_{oc} increases with increase in irradiation level but decreases with the increase in temperature. The same findings has been obtained from Fig. 2 also.

Sensitivity graphs for photocurrent and boost converter output voltage has been obtained from the developed sensitivity functions. Fig. 3(a) and (b) shows the calculated sensitivity values by changing each design variable from −4% to +4% in steps of 1%.

5. Reliability model of PV system

In this paper, reliability model of a PV system has been developed considering stress factors of its different components. Further, critical stress factors are identified and are improved upon to enhance the

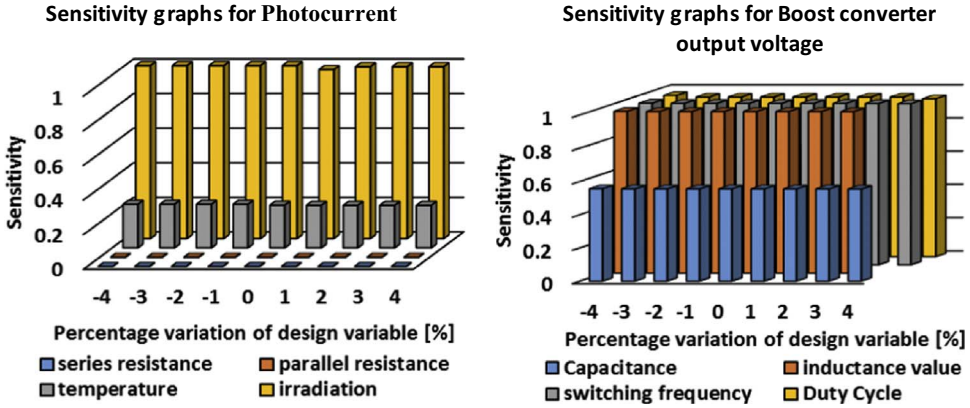

Fig. 3. Sensitivitygraphs fora) Photocurrent and b) Boost converter output voltage. Photocurrent is most sensitive to irradiation level. The output voltage of converter on the other hand is equally sensitive to inductor value and switching frequency and least sensitive to capacitor value.

Table 2
Failure rate and MTBF of electronics components of PV System, λ_b=Listed failure rate; σ=Stress factor; λ_p=Actual failure rate.

Component	Failure rate[a]	MTBF[a]
Capacitor	λ_b= 0.0007 $\sigma_t = \exp\left(-\frac{0.35}{8.617*10^{-5}}\left\{\frac{1}{T+273}-\frac{1}{298}\right\}\right)$=15.33 $\sigma_c = C^{0.23}$=1.3, σ_q = 10,σ_e = 1, σ_v = ((*applied voltage/rated voltage*)/0.6)^5 + 1 = 5.21 $\lambda_p = \lambda_b(\sigma_C*\sigma_E*\sigma_Q*\sigma_T*\sigma_V)$= **0. 1245**	8.032×10^6
Inductor/transformer	λ_b= 0.0000324 $\sigma_t = \exp\left(-\frac{0.11}{8.617*10^{-5}}\left\{\frac{1}{T_j+273}-\frac{1}{298}\right\}\right)$=2.36 σ_q = 20,σ_e = 1 $\lambda_p = \lambda_b(\sigma_e*\sigma_q*\sigma_t)$= **0. 00152**	6.578×10^8
MOSFET	λ_b=0.012 $\sigma_t = \exp\left(-1925\left\{\frac{1}{T_j+273}-\frac{1}{298}\right\}\right)$=3.63 σ_q = 8,σ_e = 1,σ_a = 10 $\lambda_p = \lambda_b(\sigma_a*\sigma_e*\sigma_q*\sigma_t)$ = **3. 48**	0.287×10^6
Diode	λ_b= 0.030 $\sigma_t = \exp\left(-3091\left\{\frac{1}{T_j+273}-\frac{1}{298}\right\}\right)$=8.004 σ_q = 8,σ_e = 1, $\sigma_s = V_S^{2.43}$=0.29 $\lambda_p = \lambda_b(\sigma_e*\sigma_q*\sigma_t*\sigma_s)$=**0. 271**	3.690×10^6

[a] Failure rate is measured in per million hours and MTBF is measured in hours.

system reliability. Lastly, logic gate representation is used to develop the reliability models for different configurations of PV system.

5.1. Component reliability analysis

Reliability of the PV System is the probability of various components performing their functions satisfactorily for the period under consideration and at their designed operating parameters. Additionally, the reliability can also be defined as probability of system's availability. The availability can further be defined as [21,22]

$$Availability = \frac{Operational\ time\ of\ PV\ system}{Operational\ time\ of\ PV\ system\ +\ DownTime}*100 = \frac{\text{mean time between failures}(MTBF)}{Mean\ cycle\ time} \quad (9)$$

where MTBF is related to failure rate (λ_p), and is given as

$$MTBF = \lambda_p^{-1} \quad (10)$$

Finally, the reliability is calculated by

$$Reliability = e^{-\lambda_p t} \quad (11)$$

Actual failure rate, λ_p is obtained by multiplying manufacturer listed failure rate (λ_b) with the associated stress factor σ_i.

Thus

$$\lambda_p = \lambda_b\left(\prod_{i=1}^{n}\sigma_i\right) \quad (12)$$

where σ_i is the product of all the stress factors applicable to a particular component of PV system. The different stress factors σ_a, σ_c, σ_e, σ_q, σ_s, σ_t *and* σ_v corresponds to device power rating, the capacitance value, operational environment, quality of component, reverse voltage index factor of diode, temperature and capacitor voltage index factor respectively. Total failure rate of a series system, λ_{system} can be computed by the summation of failure rate of all the individual components.

$$\lambda_{system} = \sum \lambda_{p(components)} \quad (13)$$

In order to compute the reliability of standalone PV System, the failure rate of PV system components due to various stress factors is considered. The stress factors are computed using MIL-HDBK-217 [27] and MTBF calculator software by ALD [35]. Failure rate and MTBF of various components are then computed from Eqs. (10)–(12) using data in Appendix A. The computed values of failure rate and MTBF of the considered components are shown in Table 2.

The failure rates of solar array, batteries, battery charger controller and controller for converter are computed from MTBF of these devices [31] using Eq. (10) and are presented in Table 3.

It can be deduced from Table 2 and Table 3 that MOSFET and battery charge controllers have got the highest failure rate. The same can be validated by performing the Pareto analysis of electrical and electronics components as shown in Fig. 4.

The values of failure rate and reliability of the standalone system, excluding controllers and drivers, are computed for one year using Table 2 and Table 3 and Eq. (13) and are given as

$\lambda_{(standalonesystem)}$=68. 1745Per million hour

$Reliability_{(standalonesystem)} = e^{-\lambda t}$=0. 55

From above result, it can be inferred that the calculated reliability of a PV standalone system is very low. Reliability improvement of the system can be achieved by reducing the failure rate of its components. To enhance the reliability, the stress factors the various components have to be identified and then minimized. In order to identify the critical stress factors, sensitivity analysis of failure rate of components

Table 3
Failure rate and MTBF of electrical components of PV system.

Components	Failure rate[a]	MTBF[a]
Solar array	33.3	3.00×10^4
Batteries	22.83	4.38×10^4
Battery charge controller	57.07	1.75×10^4
Motor	10	1.00×10^5
Controller	53.33	1.87×10^4

[a] Failure rate is measured in per million hours and MTBF is measured in hours.

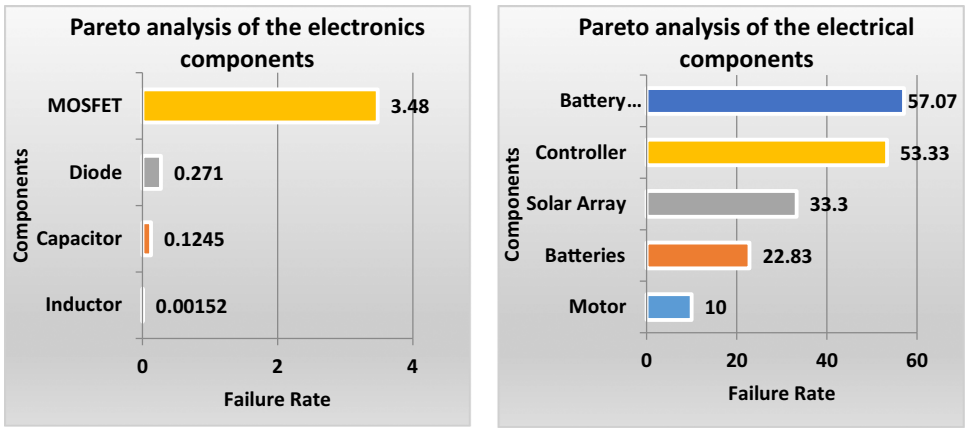

Fig. 4. Pareto analysis of the electrical and electronics components. MOSFET has the highest failure rate while inductor has minimum contribution towards system failure rate among electronics components. Motor load has the minimum percentage contribution among different electrical components.

with respect to the stress factors are performed as shown in Fig. 5. Effect of stress factors on failure rate is obtained by varying one factor at a time. Fig. 5 shows that capacitor is most sensitive to quality stress factor while diode is most sensitive to temperature stress factor.

The identified stress factors have to be minimized to improve the component reliability. Quality stress factor (σ_q) can be reduced, to an extent, by improving the packaging quality of components, as it may increase the cost of components. Also, the voltage stress factors (σ_s, σ_v) can be reduced by derating the components. The designer shall derate the components in such a way that the overall intended purpose of that system is not hampered. Further, to reduce the impact of environmental stress factor (σ_e), the components should be used in their designed environmental conditions, thus, making the system more reliable.

Considering the above factors, Table 4 shows the improved failure rate and reliability of the components and the system under consideration.

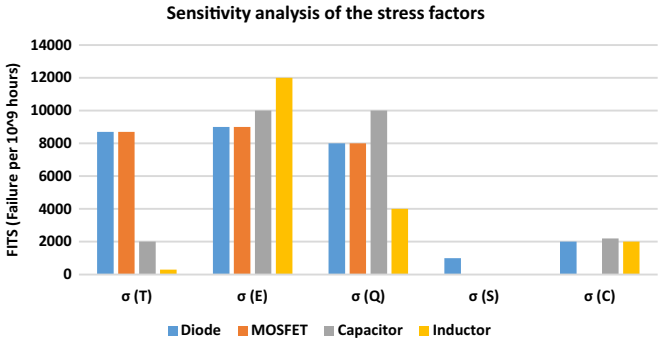

Fig. 5. Sensitivity analysis of the stress factors.

Table 4
Improved failure rate and reliability of components and standalone PV system.

Component	Failure rate*		Reliability*	
	Initial	Improved	Initial	Improved
Capacitor	0.124	0.064	0.9989	0.9994
MOSFET	3.48	1.917	0.9699	0.9833
Diode	0.271	0.103	0.9976	0.999
System(standalone)	68.174	52.63	0.55	0.63

* Failure rate measured in Per Million hours and reliability ranges from 0 to 1.

5.2. System reliability model and analysis

In the present studies, system approach model using logic gate representation is used to obtain reliability of the PV system. Logic diagrams are used for mathematical modelling to express the reliability of the system in terms of the individual component's reliability. The system may have only series components, parallel components or a combination of both. These configurations help in understanding logic relationship. Reliability of a series system, $R_s(t)$ is computed as [21,22],

$$R_s(t) = \prod_{i=1}^{k} [R_i(t)]; i=1, \ldots\ldots, n \quad (14)$$

where, $R(t)$ reliability of the system/ components [21]. Further, the reliability of the parallel system, $R_p(t)$ is defined by

$$R_p(t) = 1 - \Pi[1 - R_i(t)]; i=1, \ldots\ldots, n \quad (15)$$

PV system can be represented by three different configurations for reliability computation, namely, (i) standalone system, (ii) standalone system with battery storage and (iii) grid-connected system with battery storage. Reliability of these different configurations are evaluated using Eqs. (14) and (15). The logic gate representation of these configurations are shown in Fig. 6(a), (b) and (c) respectively.

The standalone PV system is the simplest of all and its reliability is computed by multiplying the reliability of individual components. The reliability of the standalone PV system with battery storage, R_A can be obtained by

$$R_A = (\{1-(1- R_1 * R_2)(1- R_3 * R_4)\} * R_5 * R_6 * R_{10}) \quad (16)$$

Further, reliability of the grid-connected PV system with battery storage, R_B is defined by

$$R_B = [1-(1-\{1-(1- R_1 * R_2)(1- R_3 * R_4)\} * R_5 * R_6)(1- R_8 * R_7)(1- R_9)] * R_{10} \quad (17)$$

where, R_1, R_2, R_3, R_4, R_5, R_6, R_7, R_8, R_9 and R_{10} are the reliabilities of PV array, chopper, battery, battery charger, capacitor, inverter, switch, synchronizer, grid and load respectively.

The reliability values of these systems are computed on the basis of data given in Appendix B are presented in Table 5.

It can be inferred from Table 5 that the grid-connected PV system has the highest reliability value followed by standalone PV system with battery storage and standalone PV system. Hence, grid-connected PV system with battery storage should be preferred for a higher reliability. Also, it is observed that the value of reliability of standalone PV system calculated above conforms to the value of reliability calculated using Pareto analysis.

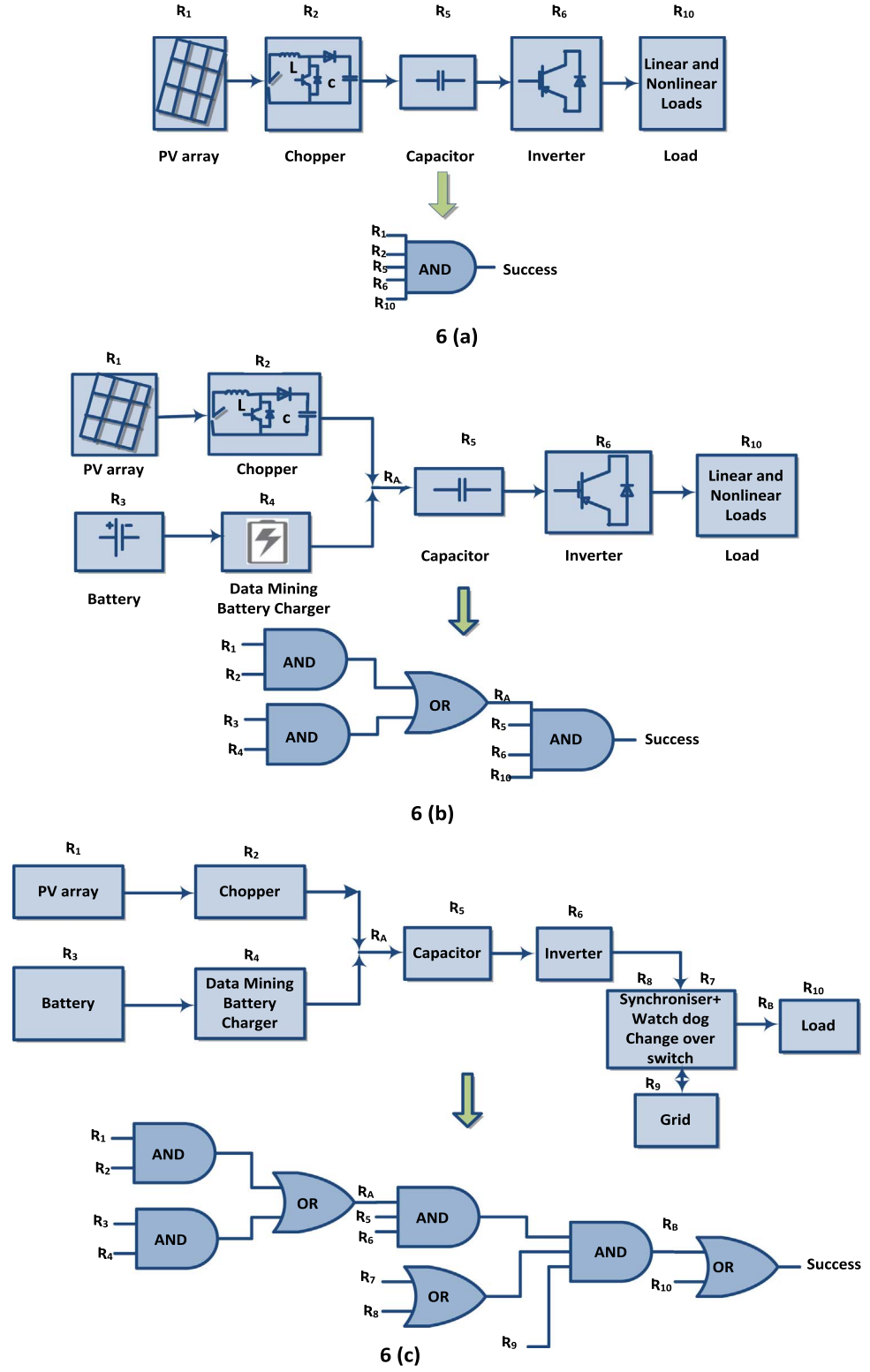

Fig. 6. Block diagram and logic gate representation of a) standalone PV system b) standalone PV system with battery storage c) grid-connected PV system with battery storage.

The reliability of standalone PV system can be increased by employing the redundancy approach considering the fact that the reliability has greater significance than cost. Redundancy involves creation of new parallel paths. In hot standby redundant system, redundant elements are continuously energized and made to perform circuit function. In cold standby redundancy, redundant elements perform only when primary elements fails. The redundancy,R_u in hot standby system is given by [21,22],

$$R_u = 2\prod_{i=1}^{n} p(a_i) - \left[\prod_{i=1}^{n} p(a_i)\right]^2 = \prod_{i=1}^{n} p(a_i)[2 - \prod_{i=1}^{n} p(a_i)] \quad (18)$$

where, $p(a_i)$ is the probability of system under consideration. The redundancy can be computed for the system under consideration using

Table 5
Reliability values for different PV system configurations.

Configuration	Reliability[a]
Standalone system	0.568
Standalone with battery storage	0.675
Grid-connected system with battery storage	0.899

[a] Reliability ranges from 0 to 1.

Table 6
Reliability values of the considered PV systems with redundancy.

Configuration	Reliability[a] with redundancy
Standalone System	0.813
Standalone with battery storage	0.894
Grid-Connected system with battery storage	0.989

[a] Reliability ranges from 0 to 1.

Eq. (18). The computed values are presented in Table 6.

From the Tables 5 and 6 it is noted that system reliability has increased when redundant standby system is considered.

6. Conclusion

In this study, the sensitivity functions of PV cell and boost converter have been developed and the numerical values has been computed for the system considered. It is found that PV cell output is most sensitive to irradiation level and Converter output is most sensitive to inductor value and switching frequency. The performance of the PV array has been examined by using MATLAB along with Simulink toolbox and is mapped with the sensitivity results. The two results conform.

The reliability studies of standalone and grid connected PV system have been carried out using Pareto analysis and logic gate representation model. Pareto analysis has been used as a tool to identify the component with highest failure rate. Also, sensitivity analysis of failure rate of these components with respect to stress factors is performed and critical stress factors are identified. Further, logic gate representation models have been developed to study reliability of both standalone and grid-connected PV system and it has been observed that grid connected system is the most reliable. Lastly, the redundancy impact on system reliability is analyzed.

These studies are intended to give a better insight to the PV system designer and its operator to predict and select the optimal operating point in dynamic situations.

Appendix A

Data for Solar PV Sunmodule SW-230:

Peak power of array=10 kW, Short circuit current of module=8.72 A, open circuit voltage of module=36.7 V, Cells per module=60, series resistance=0.325 Ω, parallel resistance=50 Ω, Module current at MPP=7.74 A, Module voltage at MPP=29.7 V. Initial Solar irradiation=1000 W/m^2 and temperature=278 K. Diode ideality factor=0.9616.

Data for DC-DC boost converter:

$D = 0.531 - 0.493, \quad L = 8.31$ mH, $C = 255$ μF, $fs = 10$ kHz

Appendix B

Data for reliability studies:

The reliability of PV array, chopper, battery, battery charger, capacitor, inverter, switch, synchronizer, grid and load are taken respectively as-

1=0. 8, 2=0. 95, 3=0. 85, 4=0. 7, 5=0. 99, 6=0. 84, 7=0. 95, 8=0. 91, 9=0. 99 and 10=0. 9

References

[1] McEvoy A, Markvart T, Castaner L. Practical handbook of photovoltaics-fundamentals and applications, 2nd ed.. Wyman Street, USA: Elsevier; 2012.

[2] Jong P, Sánchez AS, Esquerre K, Kalid RA, Torres EA Solar and wind energy production in relation to the electricity load curve and hydroelectricity in the northeast region of Brazil. Renew Sustain Energy Rev. Vol. 23; July 2013, p. 526535. ⟨http://dx.doi.org/10.1016/j.rser.2013.01.050⟩.

[3] Rub HA, Malinowski M, Al-Hadad K. Power electronics of renewable energy systems, transportation, and industrial application, 1st ed.. IEEE Press and John Wiley and Sons Publication; 2014.

[4] Erickson RW. Fundamentals of power electronics, 2nd ed.. Secaucus, NJ, USA: Kluwer Academic Publishers; 2000.

[5] Jain C, Singh B A single- phase two-stage grid interfaced SPV system with adjustable DC link voltage for VSC under non ideal grid conditions. In: IEEE International conference on power electronics, drives, and energy systems. Mumbai; 16–19 Dec 2014. ⟨http://dx.doi.org/10.1109/PEDES.2014.7041983⟩.

[6] Kim SK, Jeon JH, Cho CH. Modelling and simulation of a grid –connected PV generation system for electromagnetic transient analysis Elsevier. J Sol Energy 2009:664–78. http://dx.doi.org/10.1016/j.solener.2008.10.020.

[7] Pyo GC, Kang HW, Moon SI. A new operation for Grid-Connected PV system considering voltage regulation n distribution system. In: IEEE power and energy society general meeting - conversion and delivery of electrical energy. Pittsburgh, PA; 20–24 July 2008 .⟨http://dx.doi.org/10.1109/PES.2008.4596783⟩.

[8] D'Amore M. Sensitivity functions of corona loss on HVDC practical power lines: an introduction to optimal design. IEEE Trans PAS 1977;98(2):778–91. http://dx.doi.org/10.1109/T-PAS.1977.32391.

[9] Cristina S and D'Amore M. Sensitivity analysis of modal quantities for horizontal transmission lines. In: IEEE Canadian communications and power conference; October 18–20 1978. p. 172–5. ⟨http://dx.doi.org/10.1109/TPAS.1979.319511⟩.

[10] Indulkar CS, Kumar P, Kothari DP. Sensitivity analysis of a multi conductor transmission line. In: The proceedings of the IEEE. Vol. 70(3); March 1982. ⟨http://dx.doi.org/10.1109/PROC.1982.12290⟩.

[11] Kumar P, Garg R, Thomas MS Sensitivity analysis of corona noise interference due to EHV Lines. J Inst Eng [India]. Vol. 79. February 99 p. 182–5.

[12] Zhu XG, Fu ZH, Long XM, Xin-Li . Sensitivity analysis and more accurate solution of photovoltaic solar cell parameters. Sol Energy 2011;85:393. http://dx.doi.org/10.1016/j.solener.2010.10.022.

[13] Jakhrani AQ, Othman AL, Ragai A, Rigit H, Samo SR, Kamboh SA. Sensitivity analysis of a standalone photovoltaic system model parameters. J Appl Sci 2013. http://dx.doi.org/10.3923/jas.2013.220.231.

[14] Farghally HM, Ahmed NM, El-Madany HT, Atia DM, Fahmy FH. Design and sensitivity analysis of photovoltaic/thermal solar collector. Int J Electr Comput Electron Commun Eng 2014;8(5).

[15] Mallada UR, Leyva R, Garcés P Sensitivity analysis in boost converters optimal design. In: International conference on electrical power quality and utilization. Lisbon; 17–19 Oct. 2011. ⟨http://dx.doi.org/10.1109/EPQU.2011.6128898⟩.

[16] Praene JP, Marc O, Ennamiri H, Rakotondramiarana HT. In sensitivity analysis to optimize a solar absorption cooling system. Energy Procedia 2014;57:2636–45.

http://dx.doi.org/10.1016/j.egypro.2014.10.275.
[17] Guoa BH, Menga Z, Suna Z, Wanga L. Parameter identification and sensitivity analysis of solar cell models with cat swarm optimization algorithm. Energy Convers Manag 2016;108:520–8. http://dx.doi.org/10.1016/j.enconman.2015.11.041.
[18] Andrei H, Ivanovici T, Diaconu E, Ghita MR, Marin O, Andrei PC Analysis and experimental verification of the Sensitivity of PV cell model parameters. In: International conference on synthesis, modeling, analysis and simulation methods and applications to circuit design (SMACD). Seville; 19–21 Sept. 2012. ⟨http://dx.doi.org/10.1109/SMACD.2012.6339434⟩.
[19] Needleman DB, Mailoa JP, Brandt RE, Mangan NM, Buonassisi T. Sensitivity analysis of optical metrics for spectral splitting photovoltaic systems: a case study. IEEE J Photovolt 2015;5(5). http://dx.doi.org/10.1109/JPHOTOV.2015.2457292.
[20] Ito M, Kato K, Komoto K, Kichimi T. A sensitivity analysis of very large-scale photovoltaic power generation (VLS-PV) systems in deserts. In: IEEE conference on photovoltaic energy conference. Waikoloa; May 2006. ⟨http://dx.doi.org/10.1109/WCPEC.2006.279672⟩.
[21] Hines WH, Mountgomery DC, Goldsman DM. Probability and statistics in engineering, 4th ed.. United States of America: John Wiley and Sons Publishers; 2000.
[22] Srinath LS. Reliability engineering. New Delhi, Delhi: Affiliated East-West Press Pvt. Ltd.; 1991.
[23] Garro A, Barrara F. Reliability analysis of residential photovoltaic systems. In: International conference on renewable energies and power quality (ICREPQ'11). Spain; 13–15th April 2010.
[24] Sharma V, Chandel SS. Performance and degradation analysis for long term reliability of solar photovoltaic systems: a review. Renew Sustain Energy Rev 2013;27:753–67. http://dx.doi.org/10.1016/j.rser.2013.07.046.
[25] Zhang P, Li W, Li S, Wang Y, Xiao W. Reliability assessment of photovoltaic power systems: review of current status and future perspectives. Appl Energy 2013;104:822–33. http://dx.doi.org/10.1016/j.apenergy.2012.12.010.
[26] Chan F, Calleja H. Reliability estimation of three single-phase topologies in grid-connected PV systems. IEEE Trans Ind Electron 2011;58(7). http://dx.doi.org/10.1109/TIE.2010.2060459.
[27] Reliability Prediction of Electronic Equipment. Military handbook 217-F. Arlington, VA: Dept. Defense, Section 4; 1991.
[28] Graditi G, Colonnese D, Femia N. Efficiency and reliability comparison of DC-DC converters for single phase grid-connected photovoltaic inverters. In: SPEEDAM. PISA; 14–16 June 2010⟨http://dx.doi.org/10.1109/SPEEDAM.2010.5542235⟩.
[29] Harb S, Mirjafari M, Balog RS. Ripple-port module-integrated inverter for grid-connected PV applications. IEEE Trans Ind Appl 2013;49(6). http://dx.doi.org/10.1109/TIA.2013.2263783.
[30] Khelifi F, Nadji B, Chelali Y. Study of the reliability of static converter for photovoltaic application. Energy Procedia 2015;74:564–74. http://dx.doi.org/10.1016/j.egypro.2015.07.755.
[31] Madkor AN, Anis WR, Hafez I. The effect of numbers of inverters in photovoltaic grid-connected system on efficiency, reliability and cost. Int J Sci Technol Res 2015;4(09), [ISSN 2277-8616].
[32] De León-Aldaco SE, Calleja-Gjumlich JH, Jiménez-Grajales HR, Chan-Puc FI. Experimental assessment of derating guidelines applied to power electronics converters. J Appl Res Technol 2013;11(01). http://dx.doi.org/10.1016/S1665-6423(13)71519-0.
[33] De Le´on-Aldaco SE, Calleja H, Chan Freddy, Jim´enez-Grajales HR. Effect of the mission profile on the reliability of a power converter aimed at photovoltaic applications – a case study. IEEE Trans Power Electron 2013;28(6). http://dx.doi.org/10.1109/TPEL.2012.2222673.
[34] Obeidat F, Shuttleworth R. Reliability prediction of PV inverters based on MIL-HDBK-217F N2. In: IEEE photovoltaic specialist conference (PVSC). New Orleans, LA; 14–19 June 2015. ⟨http://dx.doi.org/10.1109/PVSC.2015.7356277⟩.
[35] MTBF calculator user guide by ALD. Available: ⟨http://aldservice.com/FreeMTBFCalculatorUserGuide.html⟩.

Hindawi Publishing Corporation
Journal of Engineering
Volume 2016, Article ID 1674343, 10 pages
http://dx.doi.org/10.1155/2016/1674343

Research Article

Single VDTA Based Dual Mode Single Input Multioutput Biquad Filter

Rajeshwari Pandey, Neeta Pandey, and Navin Singhal

Department of Electronics and Communication Engineering, Delhi Technological University, Delhi 110042, India

Correspondence should be addressed to Rajeshwari Pandey; rajeshwaripandey@gmail.com

Received 14 June 2016; Revised 9 September 2016; Accepted 3 October 2016

Academic Editor: Durga Misra

Copyright © 2016 Rajeshwari Pandey et al. This is an open access article distributed under the Creative Commons Attribution License, which permits unrestricted use, distribution, and reproduction in any medium, provided the original work is properly cited.

This paper presents a dual mode, single input multioutput (SIMO) biquad filter configuration using single voltage differencing transconductance amplifier (VDTA), three capacitors, and a grounded resistor. The proposed topology can be used to synthesize low pass (LP), high pass (HP), and band pass (BP) filter functions. It can be configured as voltage mode (VM) or current mode (CM) structure with appropriate input excitation choice. The angular frequency (ω_0) of the proposed structure can be controlled independently of quality factor (Q_0). Workability of the proposed biquad configuration is demonstrated through PSPICE simulations using 0.18 μm TSMC CMOS process parameters.

1. Introduction

The ever shrinking feature size of devices on ICs and consequential reduction of power supply voltage poses serious challenges to analog design such as reduced input common mode range, output swing, and linearity. This can be handled by operating in the current domain, as current mode circuits are designed for lower voltage swings. Therefore, over the last few decades, current mode (CM) processing has evolved as an alternative design technique [1] and has resulted in emergence of numerous active building blocks (ABBs) [2] such as differential difference current conveyor transconductance amplifier (DDCCTA) [3], current difference transconductance amplifier (CDTA) [4], current feedback operational amplifier (CFOA) [5], operational transresistance amplifier (OTRA) [6], differential input buffered transconductance amplifier (DBTA) [7], current difference buffered amplifier (CDBA) [8], current conveyor transconductance amplifier (CCTA) [9], and voltage differencing transconductance amplifier [10] which are used for realization of various signal processing and generation circuits. Among these, the voltage differencing transconductance amplifier (VDTA) is a recently introduced active element [11]. The VDTA is a voltage input current output ABB with two transconductance gain stages. It provides electronic tuning ability through its transconductance gains. Thus, the VDTA is one of the most suitable ABBs for easy and compact CMOS implementation [12] of signal processing and generating circuits.

Electronic filters are essential building block of communication and instrumentation systems. A variety of VDTA based biquadratic filters are available in literature [10–18] which can be classified as single input multioutput (SIMO) [11–14, 18], multi-input single output (MISO) [15–17], and multi-input multioutput MIMO [10] filter configurations. These filters can further be classified as voltage mode [10, 13, 17], current mode [11, 12, 14–16], and dual mode [18] structures. A detailed comparison of these structures is given in Table 1.

It may be noted from Table 1 that only a single VDTA based dual mode SIMO structure is available in literature and it uses five passive components. In this paper, a new single VDTA based SIMO-type dual mode biquad filter using four passive components is proposed. The proposed structure provides either voltage or current outputs through proper selection of input excitation. The proposed structure realizes three standard filter functions, namely, LP, HP, and BP, with independent ω_0 and Q_0 tuning feature. Proposed circuit configuration also offers low passive sensitivities. The rest of the paper is organised as follows: In Section 2, detailed circuit description is presented. The circuit behaviour in

Table 1: Comparison of the proposed work with the previously reported work.

Ref.	Number of inputs	Simultaneous outputs	Standard filter functions	VM/CM	Active blocks used	Passive components	Orthogonal tunability of ω_0 and Q_0
[10]	Two	Two	LP, HP, BP	VM	Two	Two C	No
[11]	One	Three	LP, HP, BP	CM	Two	Two C	No
[12]	One	Three	LP, HP, BP	CM	One	Two C; One R	Yes
[13]	One	Five	LP, HP, BP, NF, AP	VM	Two	Two C; Two R	Yes
[14]	One	Three	LP, HP, BP	CM	One	Two C	No
[15]	Three	One	LP, HP, BP, NF, AP	CM	Two	Two C	Yes
[16]	Three	One	LP, HP, BP, NF, AP	CM	One	Two C	No
[17]	Three	One	LP, HP, BP, NF, AP	VM	one	Two C	Yes
[18]	One	Three	LP, HP, BP	VM and CM	One	Three C; two R	Yes
Proposed work	One	Three	LP, HP, BP	VM and CM	One	Three C; one R	Yes

presence of nonidealities of VDTA has been analysed in Section 3 and deviation in filter parameters is enumerated. The functionality of the proposed filter has been confirmed through SPICE simulations using 0.18 μm TSMC CMOS process parameters and the results are presented in Section 4. Section 5 concludes the paper.

2. Circuit Description

The circuit symbol of the VDTA is shown in Figure 1 where P and N are the input terminals and Z, X_+, and X_- are the output terminals. The CMOS realization of VDTA [10] is shown in Figure 2. It consists of two transconductance (TC) stages, namely, input and output stages. The input TC stage converts the differential input voltage (V_P -V_N,) into current I_Z through first TC gain (g_{m1}) and the voltage at Z terminal (V_Z) is converted to current (I_X) through second TC gain (g_{m2}). All VDTA terminals exhibit high impedance values [10]. The port relations are given in matrix form in

$$\begin{bmatrix} I_Z \\ I_{X_+} \\ I_{X_-} \end{bmatrix} = \begin{bmatrix} g_{m1} & -g_{m1} & 0 \\ 0 & 0 & g_{m2} \\ 0 & 0 & -g_{m2} \end{bmatrix} \begin{bmatrix} V_P \\ V_N \\ V_Z \end{bmatrix}. \quad (1)$$

The TC gains, g_{m1} and g_{m2}, respectively, can be expressed as [10]

$$g_{m1} = \frac{g_1 g_2}{g_1 + g_2} + \frac{g_3 g_4}{g_3 + g_4}$$
$$g_{m2} = \frac{g_5 g_6}{g_5 + g_6} + \frac{g_7 g_8}{g_7 + g_8}, \quad (2)$$

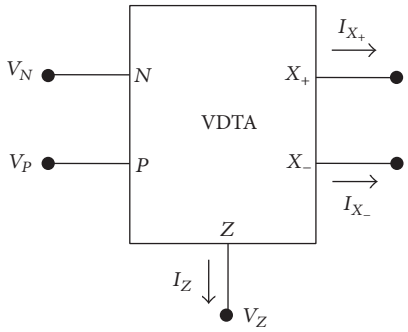

Figure 1: Circuit symbol of VDTA.

where g_i is the transconductance value of the ith transistor and is given by

$$g_i = \sqrt{\mu C_{ox} \left(\frac{W}{L}\right)_i I_{Bi}}. \quad (3)$$

In (3), μ is effective carrier mobility; C_{ox} is the gate oxide capacitance per unit area; I_{Bi} and $(W/L)_i$ represent the dc bias current and the aspect ratio of the ith MOS transistor, respectively.

The proposed dual mode SIMO filter is shown in Figure 3 which comprises of a single VDTA, three capacitors, and a resistor. With appropriate choice of input signal, it can be configured as either VM or CM structure.

2.1. The VM Configuration. The filter configuration of Figure 3 operates in VM if input current is removed ($I_{in} = 0$).

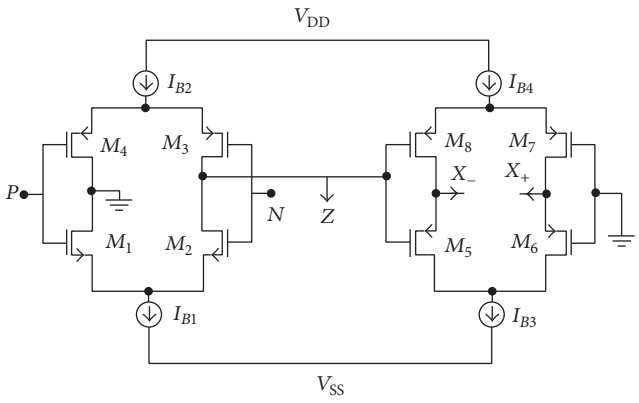

Figure 2: The CMOS realization of VDTA [10].

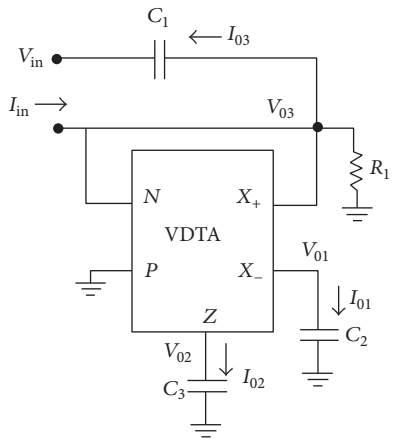

Figure 3: Proposed VM and CM mode SIMO filter.

Routine analysis of the circuit yields voltage mode transfer functions given by

$$\left.\frac{V_{01}}{V_{in}}\right|_{LP} = \frac{g_{m1}g_{m2}/C_2C_3}{\Delta}$$
$$\left.\frac{V_{02}}{V_{in}}\right|_{BP} = -\frac{(g_{m1}/C_3)\,s}{\Delta} \quad (4)$$
$$\left.\frac{V_{03}}{V_{in}}\right|_{HP} = \frac{s^2}{\Delta},$$

where

$$\Delta = s^2 + \frac{s}{R_1C_1} + \frac{g_{m1}g_{m2}}{C_1C_3}. \quad (5)$$

2.2. The CM Configuration. Removal of voltage source V_{in} ($V_{in} = 0$) in Figure 3 results in CM filter topology. Analysis of the resulting topology leads to the following transfer function:

$$\left.\frac{I_{01}}{I_{in}}\right|_{LP} = -\frac{g_{m1}g_{m2}/C_1C_3}{\Delta}$$
$$\left.\frac{I_{02}}{I_{in}}\right|_{BP} = \frac{(g_{m1}/C_1)\,s}{\Delta} \quad (6)$$
$$\left.\frac{I_{03}}{I_{in}}\right|_{HP} = -\frac{s^2}{\Delta}.$$

The angular frequency ω_0 and quality factor Q_0 for both the filter structures are given by

$$\omega_0 = \sqrt{\frac{g_{m1}g_{m2}}{C_1C_3}} \quad (7)$$

$$Q_0 = R_1\sqrt{\frac{g_{m1}g_{m2}C_1}{C_3}}. \quad (8)$$

It may be observed from (7) and (8) that the parameters ω_0 can be set to a desired value and Q_0 can be controlled through R_1 independently.

It is relevant to mention here that the voltage outputs of the proposed structure are available at high impedance, which is invariably true for all available VDTA based voltage mode structures [10, 13, 17, 18]. It is therefore suggested that either the voltage output structures should be used to drive the high input impedance circuits or the output should be taken through buffers. Further, in CM operation, current outputs are available through passive elements and would require additional ABBs for accessing current at high impedance. However, it is also applicable to all single ABB based SIMO structures [12, 14, 18]. It may also be noted that in proposed structure I_{02} can be accessed at high impedance by lifting the drain node of transistors M_1 and M_4.

The passive sensitivities of ω_0 and Q_0 of the proposed filter structures can be expressed as given by (9) and their absolute values do not exceed unity in magnitude.

$$S^{\omega_0}_{g_{m1},g_{m2}} = \frac{1}{2},$$
$$S^{\omega_0}_{C_1,C_3} = -\frac{1}{2},$$
$$S^{Q_0}_{g_{m1},g_{m2}} = \frac{1}{2},$$
$$S^{Q_0}_{C_1} = \frac{1}{2}, \quad (9)$$
$$S^{Q_0}_{C_3} = -\frac{1}{2},$$
$$S^{Q_0}_{R_1} = 1.$$

3. Nonideal Analysis

In this section, the effect of nonidealities of VDTA on the filter performance has been analysed. The nonidealities associated

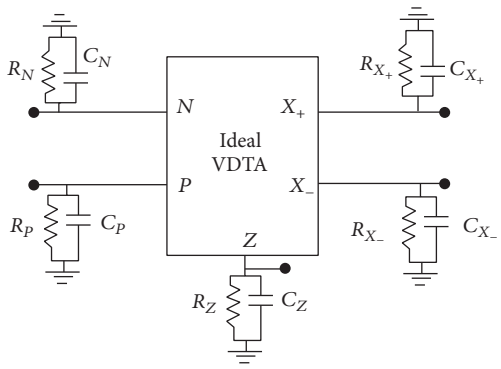

Figure 4: Nonideal model of VDTA.

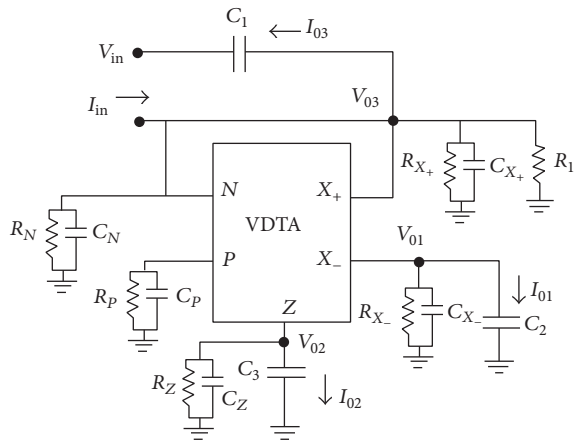

Figure 5: Nonideal filter structure.

with VDTA based circuits may be divided into two groups. The first group concerns the finite voltage tracking errors and the second results from the presence of parasitics at all the terminals of VDTA.

3.1. Nonideality due to Tracking Error. Taking the tracking errors of the VDTA into account, the port relations expressed by (1) get modified as

$$\begin{bmatrix} I_Z \\ I_{X_+} \\ I_{X_-} \end{bmatrix} = \begin{bmatrix} \beta_1 g_{m1} & -\beta_1 g_{m1} & 0 \\ 0 & 0 & \beta_2 g_{m2} \\ 0 & 0 & -\beta_2 g_{m2} \end{bmatrix} \begin{bmatrix} V_P \\ V_N \\ V_Z \end{bmatrix}, \tag{10}$$

where β_1 and β_2 are, respectively, the tracking errors for the first and second stages of the VDTA. In presence of β_1 and β_2, the new expressions for ω_0 and Q_0 can be obtained as

$$\omega_0 = \sqrt{\frac{\beta_1\beta_2 g_{m1} g_{m2}}{C_1 C_3}}$$
$$Q_0 = R_1\sqrt{\frac{\beta_1\beta_2 g_{m1} g_{m2} C_1}{C_3}}. \tag{11}$$

It is evident that the values of ω_0, and Q_0 deviate slightly from their ideal values. These changes may be accommodated by adjusting TC gains g_{m1} and g_{m2} through bias current of VDTA. However, the sensitivities of ω_0 and Q_0 with respect to β_1 and β_2 are quite low, as given by

$$S^{\omega_0}_{\beta_1,\beta_2} = S^{Q_0}_{\beta_1,\beta_2} = \frac{1}{2}. \tag{12}$$

3.2. Nonideality due to Parasitics. The nonideal model of VDTA is shown in Figure 4 wherein each terminal is characterized by finite parasitic impedance consisting of resistance in parallel with capacitance (R_P, C_P; R_N, C_N; R_Z, C_Z; R_{X_+}, C_{X_+}; $R_{X_}, C_{X_}$ for V_P, V_N, Z, and X terminals, resp.) [12]. The filter performance might deviate from ideal behaviour due to parasitics of VDTA. Thus, the filter structure of Figure 3 is to be analysed in the presence of parasitics. Using the nonideal model of VDTA, the proposed filter structure can be redrawn as shown in Figure 5.

Using routine analysis, ω_0 and Q_0 of the filter configuration of Figure 5 may be obtained as

$$\omega_0 = \sqrt{\frac{A}{B}} \tag{13}$$
$$Q_0 = \sqrt{\frac{AB}{D}}, \tag{14}$$

where

$$A = g_{m1}g_{m2} + \frac{1}{R_1R_Z} + \frac{1}{R_{X_+}R_Z} + \frac{1}{R_NR_Z} \tag{15}$$

$$B = C_1C_3 + C_ZC_3 + C_{X_+}C_Z + C_NC_Z + C_2C_{X_+} + C_2C_N, \tag{16}$$

$$D = \left(\frac{C_3}{R_Z} + \frac{C_3}{R_1} + \frac{C_2}{R_{X_+}} + \frac{C_Z}{R_1} + \frac{C_Z}{R_{X_+}} + \frac{C_Z}{R_N} + \frac{C_{X_+}}{R_Z} + \frac{C_N}{R_Z}\right)^2. \tag{17}$$

The parasitic resistances associated with all terminals are practically too large making

$$\left(\frac{1}{R_1R_Z} + \frac{1}{R_{X_+}R_Z} + \frac{1}{R_NR_Z}\right) \langle\langle g_{m1}g_{m2}. \tag{18}$$

Thus, (15) reduces to

$$A \approx g_{m1}g_{m2}. \tag{19}$$

By selecting external capacitances much larger than parasitic capacitances, (16) can be simplified as

$$B = C_3C_1 + C_Z\left(C_3 + C_{X_+}\right) + C_{X_+}\left(C_2 + C_Z\right) + C_2C_N = C_3C_1 + C_ZC_3 + C_{X_+}C_2 + C_2C_N$$
$$= C_3\left(C_1 + C_Z\right) + C_2\left(C_{X_+} + C_Z\right) \approx C_3C_1. \tag{20}$$

Table 2: List of 0.18 μm CMOS process parameters used.

NMOS	LEVEL = 7+VERSION = 3.1 TNOM = 27 TOX = 4.1E-9+XJ = 1E-7NCH = 2.3549E17 VTH0 = 0.3672292+K1 = 0.5893162 K2 = 3.053194E-3K3 = 1E-3+K3B = 1.8246765 W0 = 1E-7NLX = 1.771394E-7+DVT0W = 0 DVT1W= 0 DVT2W = 0+DVT0 = 1.2540673 DVT1 = 0.3671218DVT2 = 0.0374285+U0 = 2.3448599 UA = -1.473692E-9UB= 2.452512E-18+UC = 6.566514E-11 VSAT = 1.025312E5 A0 = 2+AGS = 0.4532362 B0= 3.222688E-7B1 = 5E-6+KETA = -0.0109204 A1= 0 A2 = 0.9744209+RDSW = 105 PRWG = 5PRWB = -0.2+WR = 1 WINT = 1.660932E-9 LINT = .520122E-8+XL = 0 XW = -1E-8DWG = -2.794177E-9+DWB = 7.839758E-9 VOFF = -0.091184 NFACTOR = 2.2684002+CIT = 0 CDSC = 2.4E-4 CDSCD = 0+CDSCB = 0 ETA0 = 3.031184E-3 ETAB = 9.427488E-6+DSUB = 0.0153239 PCLM = 0.704686 PDIBLC1 = 2435533 +PDIBLC2 = 2.76003E-3 PDIBLCB = -0.1 DROUT = 0.8035265+PSCBE1 = 4.372065E10 PSCBE2 = 2.518414E-9 PVAG = 0.0749313+DELTA = 0.01 RSH = 6.4 MOBMOD = 1+PRT = 0 UTE = -1.5 KT1 = -0.11+KT1L = 0 KT2 = 0.022 UA1= 4.31E-9+UB1 = -7.61E-18 UC1 = -5.6E-11 AT = 3.3E4 +WL = 0 WLN = 1 WW = 0+WWN = 1WWL = 0 LL = 0+LLN = 1 LW = 0 LWN = 1+LWL = 0 CAPMOD = 2 XPART = 0.5+CGDO = 8.79E-10 CGSO = 8.79E-10 CGBO = 1E-12+CJ = 9.605878E-4 PB = 0.8 MJ = 0.3831903+CJSW = .643918E-10 PBSW = 0.8 MJSW = 0.1407086+CJSWG = 3.3E-10 PBSWG = 0.8 MJSWG = 0.1407086+CF = 0 PVTH0 = -6.317463E-6 PRDSW = -.8440536+PK2 = 9.250773E-4 WKETA = 1.074587E-3 LKETA = -.453047E-3+PU0 = 4.3638022 PUA = -1.50117E-12 PUB = 0+PVSAT = 1.356677E3 PETA0 = 1.003159E-4 PKETA = -2.902589E-3
PMOS	LEVEL = 7+VERSION = 3.1 TNOM= 27 TOX = 4.1E-9+XJ = 1E-7 NCH = 4.1589E17 VTH0 = -0.38888+K1 = 0.5636481 K2 = 0.0308017 K3 = 0+K3B= 7.400372 W0 =1E-6 NLX = 1.385693E-7+DVT0W = 0DVT1W = 0 DVT2W = 0+DVT0 = 0.5846878 DVT1 = 0.2165736 DVT2 = 0.1+U0 = 3.6325808 UA = 1.459877E-9 UB = 1.18636E-21+UC = -1E-10 VSAT = 2E5 A0 = 1.7849198+AGS = 0.3754547 B0 = 3.172437E-7 B1 = 7.280105E-7+KETA = 0.0156934 A1 = 0.3222966 A2 = 0.3+RDSW = 196.7345438 PRWG = 0.5 PRWB = -0.1589203+WR = 1 WINT = 0 LINT = 2.702835E-8+XL = 0 XW = -1E-8 DWG = -2.627805E-8+DWB = 1.03876E-9 VOFF = - 0.0927458 NFACTOR = 2+CIT = 0 CDSC = 2.4E-4 CDSCD = 0+CDSCB = 0 ETA0 = 0.145648 ETAB = -0.0543017+DSUB = 0.9610783 PCLM = 2.0812378 PDIBLC1 = 7.131255E-4+PDIBLC2 = 0.0185628 PDIBLCB = -9.170788E-4 DROUT = 0+PSCBE1 = 3.206374E9 PSCBE2 = 9.279285E-10 PVAG= 15+DELTA = 0.01 RSH = 7.3 MOBMOD = 1+PRT = 0 UTE = -1.5 KT1 = -0.11+KT1L = 0 KT2 = 0.022 UA1 = .31E-9+UB1 = -7.61E-18UC1 = -5.6E-11 AT = 3.3E4 +WL = 0 WLN = 1 WW= 0+WWN = 1 WWL= 0 LL = 0 +LLN= 1LW= 0 LWN = 1+LWL = 0 CAPMOD = 2 XPART = 0.5+CGDO = 6.41E-10CGSO = 6.41E-10 CGBO = 1E-12+CJ = 1.136354E-3 PB = 0.8459606 MJ = 0.4088875+CJSW = 2.255183E-10 PBSW = 0.832695 MJSW = 0.3342249+CJSWG = 4.22E-10 PBSWG = 0.832695 MJSWG = 0.3342249 +CF = 0 PVTH0 = 4.532819E-3 PRDSW = 7.6587079+PK2 = 3.513392E-3 WKETA = 0.0251295 LKETA = -2.32504E-3+PU0 = -.4738884 PUA = -8.40745E-11 PUB = 1E-21+PVSAT = -50 PETA0 = 1E-4 PKETA = -2.114056E-3

Similarly, (17) can be simplified as

$$D = \left(\frac{C_3}{R_Z} + \frac{C_3}{R_1} + \frac{C_2}{R_{X_+}} + \frac{C_Z}{R_1} + \frac{C_Z}{R_{X_+}} + \frac{C_Z}{R_N} + \frac{C_{X_+}}{R_Z} + \frac{C_N}{R_Z}\right)^2 = \left(\frac{C_3 + C_Z + C_N}{R_1} + \frac{C_3 + C_{X_+}}{R_Z} + \frac{C_Z + C_2}{R_{X_+}} + \frac{C_Z}{R_N}\right)^2 \approx \left(\frac{C_3}{R_1} + \frac{C_3}{R_Z} + \frac{C_2}{R_{X_+}} + \frac{C_Z}{R_N}\right)^2 \approx \left(\frac{C_3}{R_1} + \frac{C_3}{R_Z} + \frac{C_2}{R_{X_+}}\right)^2 \approx \left(\frac{C_3}{R_1}\right)^2. \tag{21}$$

Substituting (19) and (20), it may thus be noted that (13) can be approximated to (7) which represents the ideal value of ω_0.

Also putting (19), (20), and (21) in (14), Q_0 may be expressed by (22) which is equal to its ideal value.

$$Q_0 \approx \sqrt{\frac{g_{m1}g_{m2}C_3C_1}{(C_3/R_1)^2}} = R_1\sqrt{\frac{g_{m1}g_{m2}C_1}{C_3}}. \tag{22}$$

It may be concluded therefore that, by selecting external capacitances much larger than parasitic capacitances, the frequency response of the proposed structure would not be affected.

4. Simulation Results

The functionality of the proposed filter is validated through SPICE simulated using 0.18 μm TSMC process parameters which have been listed in Table 2 for ready reference. First, the DC transfer characteristic of the VDTA is validated which is followed by verification of both VM and CM filter responses.

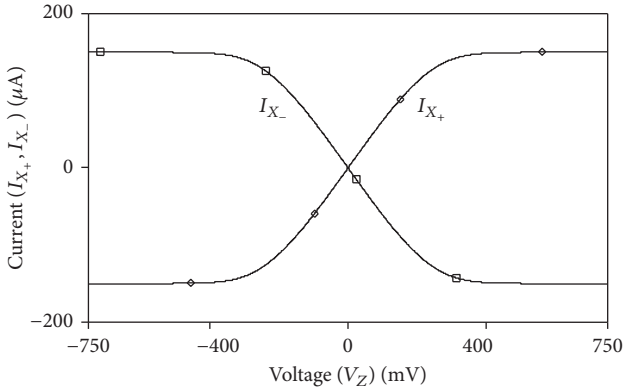

Figure 6: The DC transfer characteristics of the VDTA.

Table 3: The % frequency deviation for CM LP filter.

Capacitor value	Theoretical f_0	Simulated f_0	% frequency deviation
0.1 nF	1.01231 MHz	1.06 MHz	4.5
0.01 nF	10.1231 MHz	10.639 MHz	4.8
1 pF	101.231 MHz	108.854 MHz	7.0
0.1 pF	1.01231 GHz	886.833 MHz	12.3
0.01 pF	10.1231 GHz	2.269 GHz	77.0
1 fF	101.231 GHz	2.76 GHz	97.3

Subsequently, as a case study, the transient behaviour of BP filter (VM and CM) is studied and its total harmonic distortion (THD) variation is also observed.

4.1. The DC Transfer Characteristic. The VDTA structure shown in Figure 3 [10] with supply voltages of ±0.9 V is used for simulation. The same aspect ratios of the MOS transistors are used as given in [10]. The DC transfer characteristic of the VDTA, as shown in Figure 6, is plotted for $I_{B1} = I_{B2} = I_{B3} = I_{B4} \cong 150\,\mu$A, which resulted in $g_{m1} = g_{m2} = 636.3\,\mu$ A/V.

4.2. Frequency Response. The LP, HP, and BP filter responses for both VM and CM filter structures with $f_0 = 1$ MHz and $Q_0 = 1$ are shown in Figures 7(a) and 7(b), respectively. The passive components were chosen as $C_1 = C_2 = C_3 = 0.1$ nF and $R_1 = 1.57$ KΩ. The tuning of gain expression for low pass filter with respect to C_2 is shown in Figure 7(c).

It may be observed from (7) and (8) that f_0 can be tuned by changing either capacitance values (C_1, C_3) or the transconductances (g_{m1}, g_{m2}). The transconductance variation can be obtained through bias current adjustment. The Q_0 tuning can be accomplished through R_1 without affecting f_0. The orthogonal adjustment of f_0 and Q_0 is shown by plotting the BP responses for $f_0 = 100$ KHz, 1 MHz, and 10 MHz while keeping Q_0 fixed at 1. The responses for VM and CM structures are shown in Figures 8(a) and 8(b), respectively. Similarly, the simulation results for $Q_0 = 0.5$, 1, and 5 when f_0 remains constant at 1 MHz, for VM and CM topologies, are shown in Figures 9(a) and 9(b), respectively. It is evident from Figures 8 and 9 that f_0 and Q_0 are orthogonally tunable.

Another set of simulations have been carried out to examine frequency response limitations of the proposed structure. Low pass current mode response is used for illustration. The simulations conditions on bias currents are kept the same as reported in the beginning while the capacitor values are changed and corresponding theoretical and simulated pole frequencies are noted and listed in Table 3. It may be noted that there is a close match between theoretical and simulated pole frequencies when the values of external capacitors are chosen to be sufficiently greater than parasitic capacitances. However, a significant deviation is seen when external capacitances are selected close to parasitics (tens of fF order). Further, it is also observed that parasites limit frequency range because their pole frequencies are much lower than those for tracking errors.

4.3. Transient Response. The time domain behaviour of the VM BP filter is also studied by applying three sinusoidal frequency components: a low frequency signal of 1 MHz, a high frequency component of 100 MHz, and the third component of 10 MHz which is f_0 of the BP filter. The input signal is shown in Figure 10(a) and its frequency spectrum is depicted in Figure 10(b). The transient response of the filter and the associated frequency spectrum are shown in Figures 11(a) and 11(b), respectively. It may be noted that the frequency components other than f_0 are significantly attenuated.

To observe the transient response of CM BP filter, it is driven by an input current signal consisting of three frequency components: 1 KHz, 10 KHz, and 100 KHz. The BP filter is designed for an $f_0 = 10$ KHz. The related results are depicted in Figures 12 and 13 which clearly show that the signals outside the bandwidth of BP filter are significantly attenuated.

To check the quality of the output of BP filter, the percentage total harmonic distortion (%THD) with the sinusoidal input signal is obtained as shown in Figure 14. It is observed from Figure 14(a) that the %THD remains considerably low [19] for input signal values up to 500 mV for VM topology. Similarly, it may be noted from Figure 14(b) that the %THD is well below 7% for current signals up to 200 μA. The simulated value of power dissipation, in both VM and CM operations, is observed to be 0.54 mW.

5. Conclusion

A single VDTA based dual mode SIMO biquad which realizes LP, HP, and BP responses has been proposed in this paper. The proposed biquad is a SIMO structure and can be configured as voltage mode or current mode with appropriate input excitation selection. The angular frequency and the quality factor of the proposed configuration can be controlled in a noninteractive manner. The filter f_0 is electronically tunable. The filter structure functionality is verified through SPICE

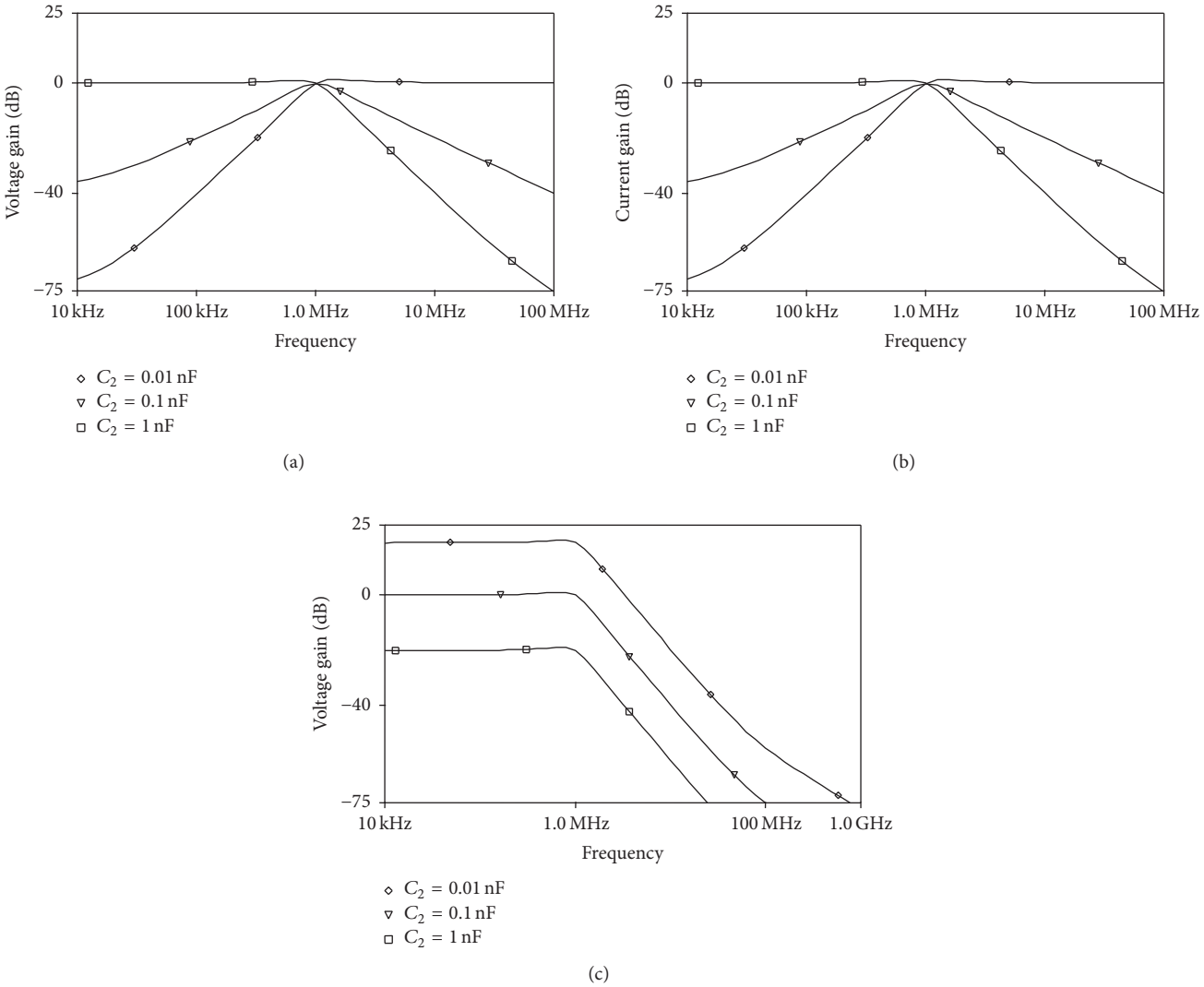

Figure 7: Frequency response at $f_0 = 1$ MHz and $Q_0 = 1$. (a) VM topology. (b) CM topology. (c) VM LP filter depicting gain tuning with C_2.

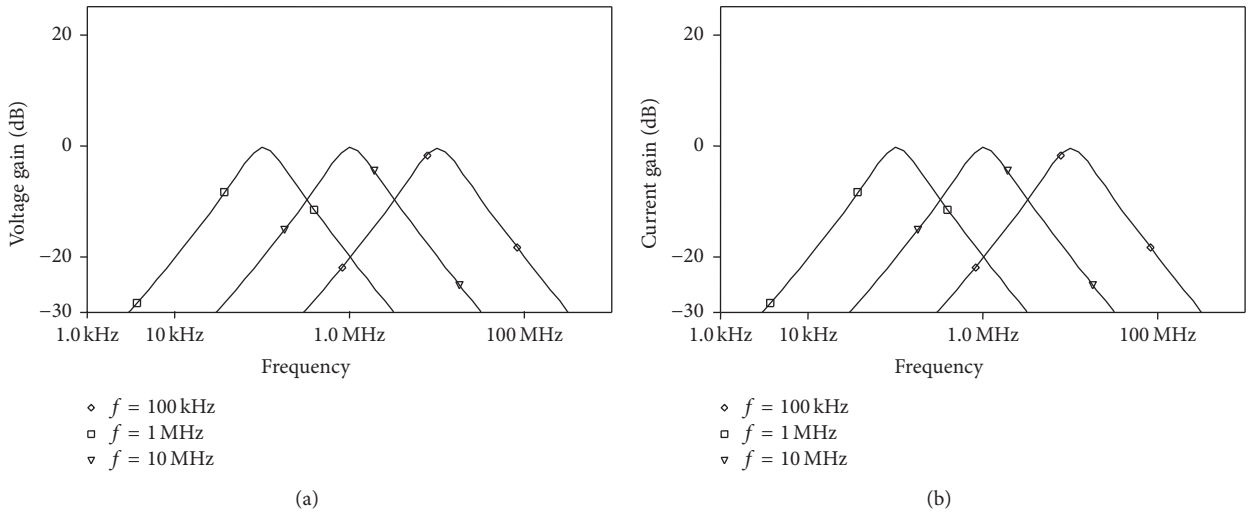

Figure 8: BP responses for $f_0 = 100$ KHz, 1 MHz, and 10 MHz keeping Q_0 fixed at 1 for (a) VM and (b) CM topology.

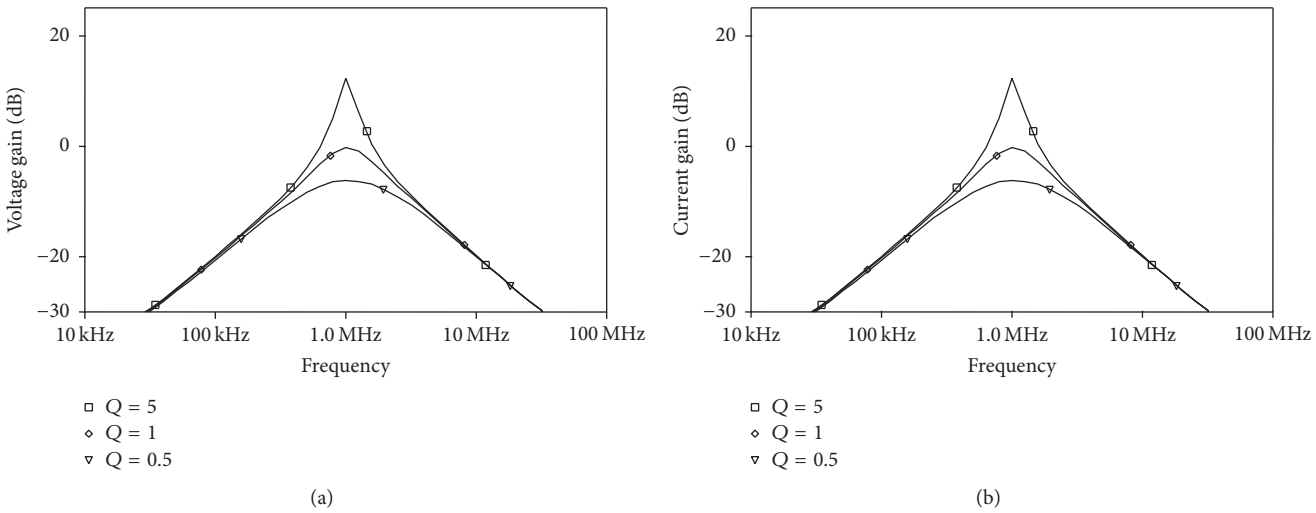

Figure 9: BP responses for $Q_0 = 0.5, 1$, and 5 with $f_0 = 1$ MHz for (a) VM and (b) CM topology.

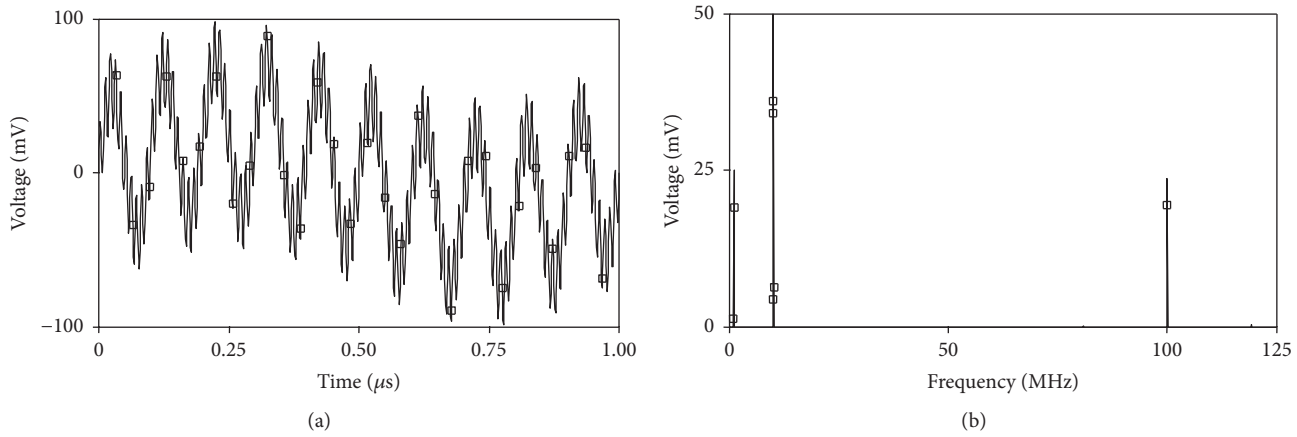

Figure 10: (a) The voltage input transient signal and (b) its frequency spectrum.

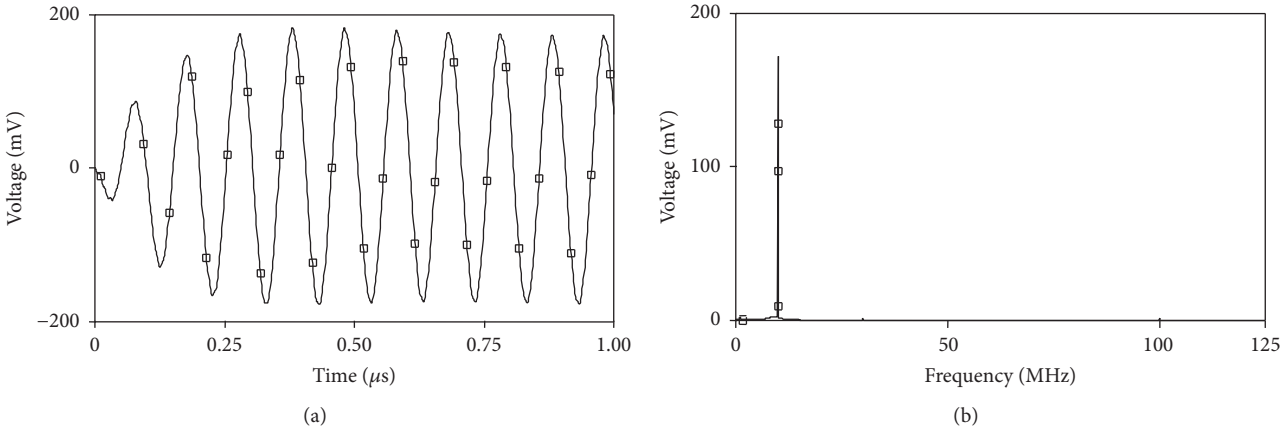

Figure 11: (a) The voltage output transient signal and (b) its frequency spectrum.

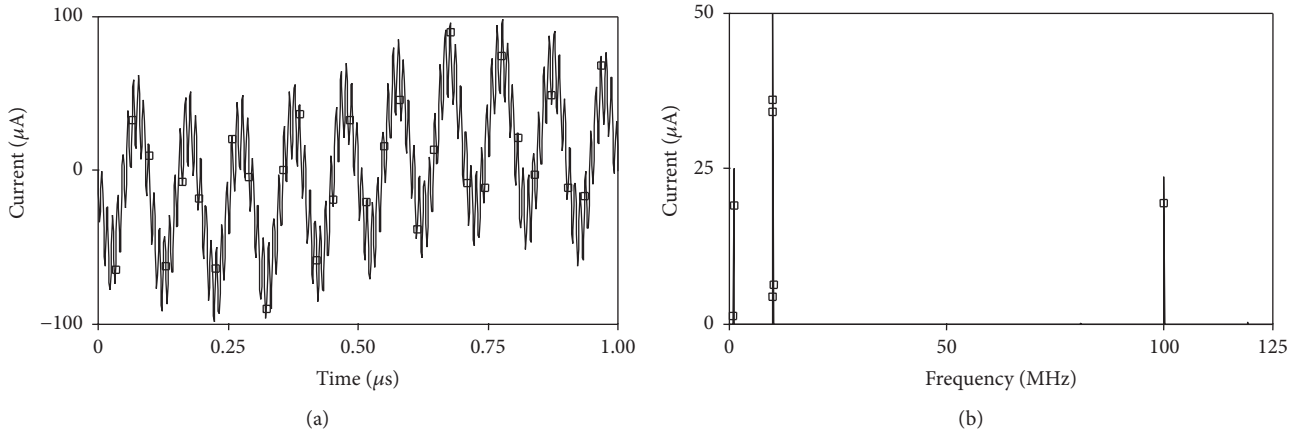

Figure 12: (a) The current input transient signal and (b) its frequency spectrum.

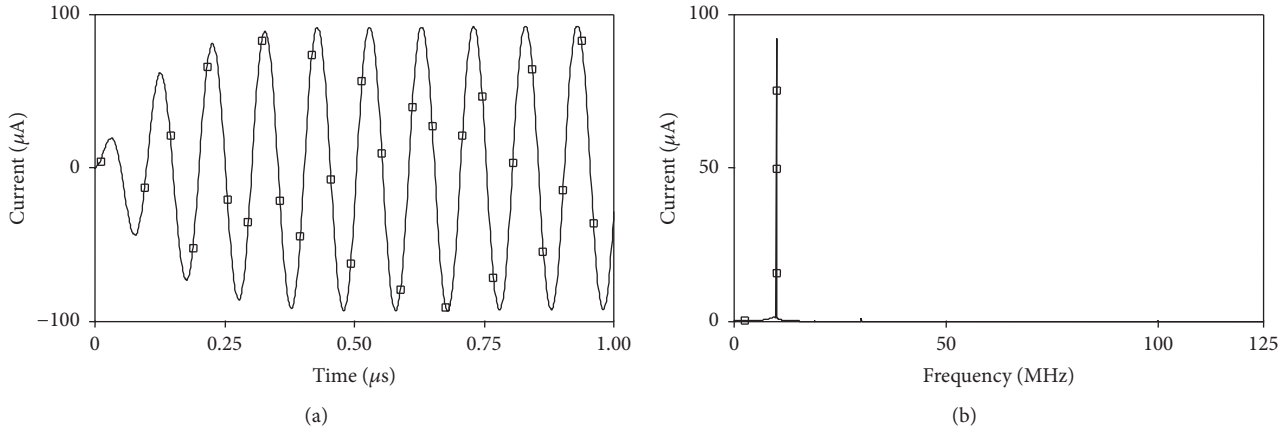

Figure 13: (a) The current output transient signal and (b) its frequency spectrum.

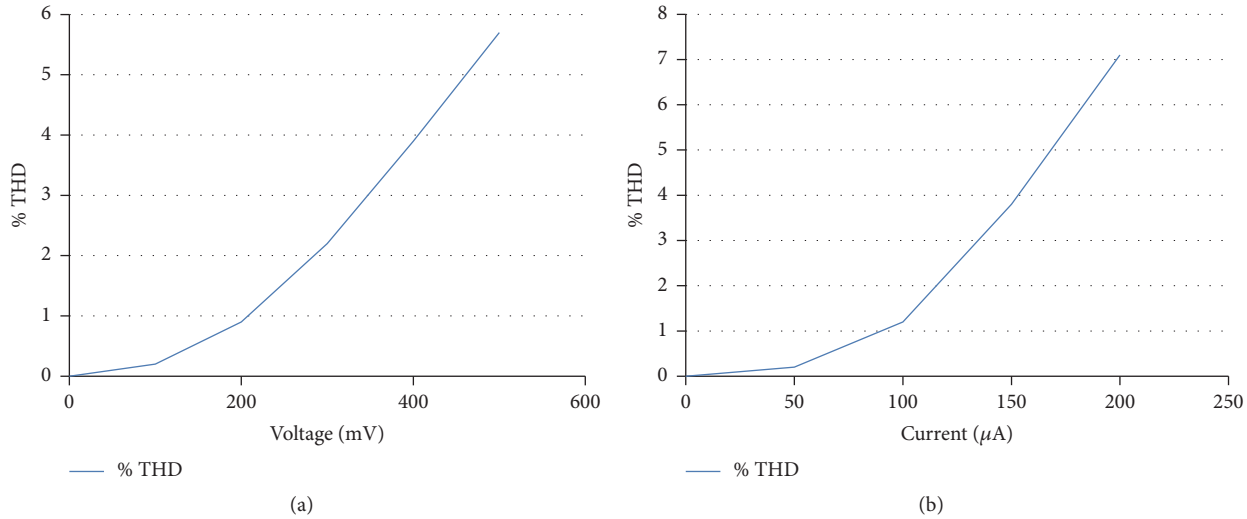

Figure 14: THD variation of BP filter against amplitude of the applied sinusoidal signal at 159 KHz (a) voltage mode and (b) current mode.

simulations and both frequency and transient responses are studied.

Competing Interests

The authors declare that they have no competing interests.

References

[1] C. Toumazau, F. J. Lidgey, and D. G. Haigh, *Analogue IC Design: The Current-mode Approach*, Peter Peregrinus Limited, London, UK, 1990.

[2] D. Biolek, R. Senani, V. Biolkova, and Z. Kolka, "Active elements for analog signal processing: classification, review, and new proposals," *Radioengineering*, vol. 17, no. 4, pp. 15–32, 2008.

[3] N. Pandey and S. K. Paul, "Differential difference current conveyor transconductance amplifier: a new analog building block for signal processing," *Journal of Electrical and Computer Engineering*, vol. 2011, Article ID 361384, 10 pages, 2011.

[4] D. Biolek, "CDTA—building block for current-mode analog signal processing," in *Proceedings of the European Conference on Circuit Theory and Design (ECCTD '03)*, vol. 3, pp. 397–400, 2003.

[5] W. Tangsrirat and W. Surakampontorn, "Single-resistance-controlled quadrature oscillator and universal biquad filter using CFOAs," *AEU—International Journal of Electronics and Communications*, vol. 63, no. 12, pp. 1080–1086, 2009.

[6] R. Pandey, N. Pandey, S. K. Paul, A. Singh, B. Sriram, and K. Trivedi, "Novel grounded inductance simulator using single OTRA," *International Journal of Circuit Theory and Applications*, vol. 42, no. 10, pp. 1069–1079, 2014.

[7] N. Herencsár, J. Koton, K. Vrba, and I. Lattenberg, "New voltage-mode universal filter and sinusoidal oscillator using only single DBTA," *International Journal of Electronics*, vol. 97, no. 4, pp. 365–379, 2010.

[8] R. Pandey, N. Pandey, T. Negi, and V. Garg, "CDBA based universal inverse filter," *ISRN Electronics*, vol. 2013, Article ID 181869, 6 pages, 2013.

[9] N. Herencsar, J. Koton, and K. Vrba, "Single CCTA-based universal biquadratic filters employing minimum components," *International Journal of Electrical and Computer Engineering*, vol. 1, no. 3, pp. 316–319, 2009.

[10] D. Biolek, M. Shaktour, V. Biolkova, and Z. Kolka, "Current-input current-output universal biquad employing two bulk-driven VDTAs," in *Proceedings of the 4th International Congress on Ultra Modern Telecommunications and Control Systems (ICUMT '12)*, pp. 484–489, IEEE, St. Petersburg, Russia, October 2012.

[11] A. Yeşil, F. Kaçar, and H. Kuntman, "New simple CMOS realization of voltage differencing transconductance amplifier and its RF filter application," *Radioengineering*, vol. 20, no. 3, pp. 632–637, 2011.

[12] D. Prasad, D. R. Bhaskar, and M. Srivastava, "Universal current-mode biquad filter using a VDTA," *Circuits and Systems*, vol. 4, pp. 29–33, 2013.

[13] J. Satansup, T. Pukkalanun, and W. Tangsrirat, "Electronically tunable single-input five-output voltage-mode universal filter using VDTAs and grounded passive elements," *Circuits, Systems, and Signal Processing*, vol. 32, no. 3, pp. 945–957, 2013.

[14] J. Satansup and W. Tangsrirat, "Single VDTA-based current-mode electronically tunable multifunction filter," in *Proceedings of the 4th International Science, Social Science, Engineering and Energy Conference*, pp. 1–8, 2012.

[15] J. Satansup, T. Pukkalanun, and W. Tangsrirat, "Electronically tunable current-mode universal filter using VDTAs and grounded capacitors," in *Proceedings of the International Multiconference of Engineers and Computer Scientists*, vol. 2, pp. 647–650, 2013.

[16] J. Satansup and W. Tangsrirat, "Compact VDTA-based current-mode electronically tunable universal filters using grounded capacitors," *Microelectronics Journal*, vol. 45, no. 6, pp. 613–618, 2014.

[17] J. Satansup and W. Tangsrirat, "VDTA based voltage-mode electronically tunable universal filter," in *Proceedings of the 27th International Technical Conference on Circuits/Systems, Computers and Communications*, pp. 1–4, July 2012.

[18] N. Singhal, R. Pandey, and N. Pandey, "Dual mode biquadratic filter using single VDTA," *International Journal of Electrical and Electronics Engineers*, vol. 6, pp. 134–139, 2014.

[19] E. S. Erdogan, R. O. Topaloglu, H. Kuntman, and O. Cicekoglu, "New current-mode special function continuous-time active filters employing only OTAs and OPAMPs," *International Journal of Electronics*, vol. 91, no. 6, pp. 345–359, 2004.

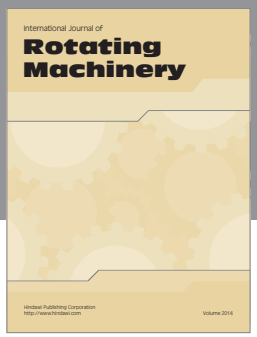

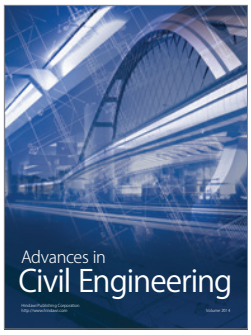

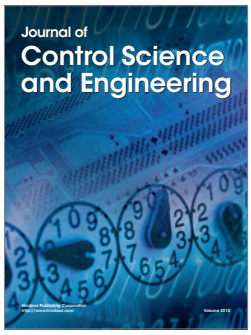

Hindawi
Submit your manuscripts at
http://www.hindawi.com

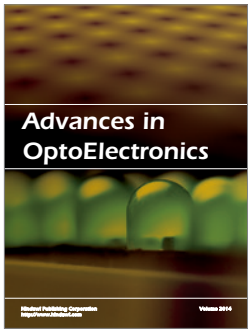

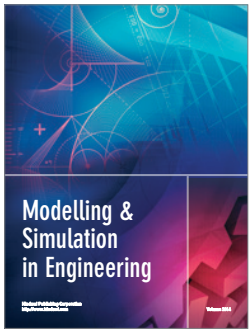

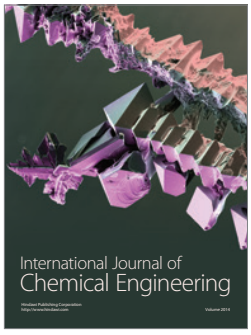

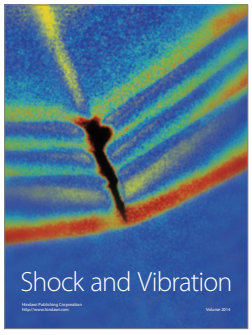

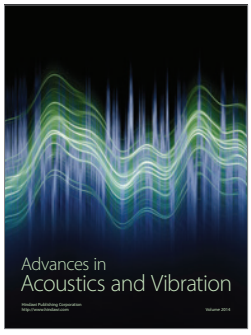

Volume 4, Issue 2 (2016) 458-462 ISSN 2347 - 3258
International Journal of Advance Research and Innovation

Skill Development in Solid Waste Management

Shubham Gupta, R. S. Mishra*
Department of Mechanical Engineering, Delhi Technological University, Delhi, India

Article Info

Article history:
Received 15 January 2016
Received in revised form
10 February 2016
Accepted 28 February 2016
Available online 15 March 2016

Keywords
Skill Development,
Solid Waste Management,
Roorkee,
Swach Bharat,
Municipal Solid Waste

Abstract

To have fast and sustainable growth power demand-supply gap can be linked only by consuming and spreading of renewable energy sources such as Solar, Wind, Biomass, Small Hydro, etc. Fossil fuels are fast depleting and pose an intolerable import bill while adding to the overall pollution. Municipal Solid Waste (MSW) has high potential of generating energy by utilizing various techniques. Training programmes are needed across India for development of skill, knowledge for effective and efficient utilization of MSW to meet rising energy demands in India.

1. Introduction

The consumption habits of modern consumer lifestyle are causing a huge worldwide waste problem. Having overfilled local landfill capacities, many first world nations are now exporting their refuse to third world countries. This is having a devastating impact on ecosystems and cultures throughout the world. Some alternative energy companies are developing new ways to recycle waste by generating electricity from landfill waste and pollution. Waste management is the "generation, prevention, characterization, monitoring, treatment, handling, reuse and residual disposition of solid wastes". There are various types of solid waste including municipal (residential, institutional, commercial), agricultural, and special (health care, household hazardous wastes, sewage sludge).The term usually relates to materials produced by human activity, and the process is generally undertaken to reduce their effect on health, the environment or aesthetics. Traditionally Landfill is used to dispose of waste generated. With the lack of space for new landfills, five technologies for waste to energy generation, namely bio-methanation, incineration, gasification/ pyrolysis, Refused Derived Fuel (RDF) and plasma arc gasification are playing an increasingly important role in waste management have been compared. Under “Swach Bharat Abhiyan” and “Ganga Bachao” program, it is necessary to develop such effective technologies which not only solves waste management problem but also provides us useful output such as electricity or cooking gas at an economical and highly efficient way. Above program also encourages the need of Shubham et al. (2015) [15] carried out optimal mixing of technology in rural area of Roorkee City, Uttarakhand and expand the energy potential and role of skill development. Skill development techniques, Programmes and workshops which can guide people, provide knowledge, and create awareness of the necessity of sanitation, methods of effective Waste Management for Rural and Urban Areas both and for all type of age people from childhood to old age.

Corresponding Author,
E-mail address: professor_rsmishra@yahoo.co.in
All rights reserved: http://www.ijari.org

2. India Energy Challenges

The key task in India is to provide safe, reliable & eco-friendly energyfor rapid economic growth in keeping mind of global threat of climate change.
The present total Indian installed capacity is 281,423 MW, which includes thermal, hydel, nuclear, renewable [13].

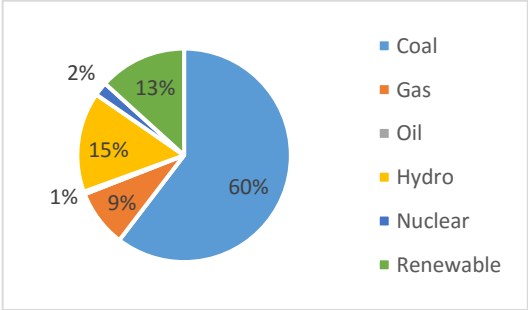

Fig: 1. Break-up of installed power generation capacity as on 30/11/2015 (Source:http://powermin.nic.in/power-sector-glance-all-india)

- At present the shortages are assessed to be in the range 2-10% in energy and 3-13% in peaking capacity from 2009-2015 [1].
- Instability of the grid is also a big challenge as on 30/31st July 2012 was a widespread grid failure across the northern and eastern regions. 600 million people were left without power or electricity for more than 6 hours those were connected to the grid.
- 45% of Rural India still don’t have access to electricity. Decentralized Solutions are necessary for the growth of electricity infrastructure.
- Over dependence on imported coal as domestic production lacks in meeting the demand and quality required.

3. Municipal Solid Waste Utilization for Generating Energy

Municipal Solid Waste, includes all new plant growth, residues and wastes, agricultural and forest residues, kitchen and city garbage, sewage etc. furthermore, To meet the

growing demand of energy, it is necessary to focus on efficient production and use of biomass resources to meet both traditional and high energy demand. The biomass production for fuel, food, fiber and fodder, requires sustainable land use and integrated planning approaches at all levels in the country. The estimated potential of various biomass resources is: Biomass energy 17,000 MW, Co-generation 8000MW and energy from waste [MSW, etc.] 1000MW. The generation of municipal solid waste (MSW) increases with socio-economic development of urban population. In an emerging economy like India, rapid population growth has further added to the intensity of waste generation. Uncontrolled dumping of wastes on the outskirts of towns and cities has created overflowing landfills, which have environmental impacts in the form of pollution to soil, groundwater, and air, and also contribute to global warming.

4. Literature Review

Dhere et.al. (2008) [1] studied the adverse impact of municipal solid waste on air and ground water due to the improper disposal of waste in Pune city. Waste material also impacts the soil quality as pointed out by Ahel et.al. (1998)[2], mainly by increasing the concentration of various hazardous elements of soil through municipal solid waste. Omofonmwan and Esiegbe (2009)[3] reported the ground water contamination due to the lechate contribution of the solid waste in metropolitan city of Nigeria. Zade and Noori (2008) [4] also described the adverse impact of solid waste in concerned areas. Mondal et.al (2010)[5] described the role of WtE to manage the solid waste problems. Therefore it appears that WtE can play an important role to minimize and manage the solid waste during the different festival and normal days at the study site and separation of the waste as Biodegradable and non-biodegradable at the point will be very helpful to manage the wastes material. Buenrostro et.al (2001)[6] classified municipal solid waste at the source that will be very useful to manage the waste especially for the developing countries.HM Zakir Hossin et.al (2014)[7] explained WTE technologies such as Biomethanation, pyrolysis and land gas recovery which can generate 186 MWh/day of electricity from 7765 Tonnes/day of waste to deal energy security problem in Bangladesh In Bangladesh 6 different corporations: Khulana City Corporation (KCC), Dhaka City Corporation (DCC), Chittagong City Corporation (CCC), Rajshahi City Corporation (RCC), Barisal City Corporation (BCC), Sylhet City Corporation (SCC) work for the collection, transportation, disposal and treatment of MSW and mentioned the composition analysis with quantity percentage of each corporation, total MSW generation in KCC, DCC, CCC, RCC, BCC, SCC was 595 Tonnes/day, 5340 Tonnes/day, 1315 Tonnes/day, 170 Tonnes/ day, 130 Tonnes/day, 215 Tonnes/day, respectively and electric power generation (KWh/day) from landfill process is 14328, 128160, 31560, 4080, 3120, 5160 respectively. Sieting Tan et.al (2014)[8] compared three WTE technologies i.e. incineration, landfill gas recovery and anaerobic digestion (AD) on environmental and economic basis which included includes transportation cost, carbon credit and sale of by-product of Taman Beringin, Malaysia landfill which can yield in 287% of increment in profit. CHG emission was checked on basis of Intergovernmental Pollution Climate Change (IPCC) guidelines. Incineration plants produced 1430 MW/day of heat and 480 MWh/day of electricity from 100 tonnes/day of waste. Hefa Cheng et.al (2007)[9]carried out methodology to study two incinerators of capacity each 250 tonnes/day having technology based on co-firing of MSW with coal in grate circulated fluidized producing 46.2 million KWh of electricity having calorific value of 3000-6700 KJ/Kg lower than developed countries of 8400-17000 KJ/Kg. In addition he calculated coal equivalent to MSW fuel ratio of 0.14, with saving of 0.2 million m3 landfill yearly. Sudhanshu Kaushik et.al (2011)[10] studied the MSW generation during Kumb Mela 2010 at famous temples of Haridwar City; Mansa Devi &Chandi Devi located at Shiwalik Foothills on seven days of Hindu festival which includes Makar sakranti, Magh Purnima, Mahashivratri, Chaitra Amavasya and Full moon days by recording observations of individual composition of MSW according to days. 7615.0 Kg of Waste was produced at Mansa Devi Site and approximately 5000 Kg of waste was produced at Chandi Devi Site. He observed that 64.7% was biodegradable waste and 12.3% was non-biodegradable at Mansa Devi hillock and at Chandi Devi hillock 62.7% of biodegradable and 10.2% of non-biodegradable. C Liamsanguan et.al (2007)[11] compared incineration, landfill & conventional power plants using Life Cycle Assessment (LCA) methodology and declared that incineration had higher advantages for global warming & photochemical ozone formation over conventional power plants but from acidification and nutrient enrichment aspect incineration was not suitable. He described landfill with gas collection and flaring systems were much favourable than incineration technology. In addition he compared conventional plant's energy content which was much higher than of Municipal Solid Waste (MSW) and also conventional power plants had higher efficiency than incineration plants. Dioxins emissions from incineration plants cause health issues. Khaiwal Ravindra et.al (2015)[12] interestingly defined complete transfer of waste to RDF plant can save 5451 tCO2 emission in Chandigarh and suggested new and better Municipal Solid Waste Management (MSWM) in which segregation of waste should be at source site only. Collection bin should be lifted every day irrespective of filled or partially filled. Special facilities of transportation during rainy season should be there to avoid rain water penetration. Carbon emission should be checked for storage, transportation, and disposal and processing site. Proper training of people involved in MSWM and their routine health check -up. Shubham et.al (2015) [14] carried out estimation of electrical energy from municipal solid waste utilizing waste to energy incineration technology of Roorkee City and suggested methods to improve the waste collection efficiency.

5. Municipal Solid Waste in Roorkee City

Roorkee is a city in Haridwar district, Uttarakhand that is spread over a flat terrain with the grand spectacle of Himalaya's ranges flanking it in the East and the North-east. It is on the banks of the Ganges canal on the national highway 58 (Delhi - Sri Badnrinath - Mana). The dominant

feature of the city is the Upper Ganges Canal which flows north-south and bisects the city. Also known for Roorkee Cantonment, one of the country's oldest, and the headquarters of Bengal Engineer Group (Bengal Sappers) since 1853. The city generates, on an average, about 250 MT of MSW per day. The major sources of MSW generation of the city are domestic, shops and commercial establishments, hotels, restaurants, dharamsalas and fruit and vegetable markets. Number of registered hotels, restaurants and dharamsalas in the city are 90, 50 and 52 respectively. In addition there are 3 fruit and vegetable markets. Out of which 1 market is excluded as it is not under Roorkee Nagar Palika Parishad [RNPP]. The MSW is composed of biodegradable (Vegetable waste, yard waste, paper waste, cotton clothes) and Non- biodegradable waste (Metal, stone, bricks, leather, plastic, Glass)

6. Scope of the Project

- Study of current Municipal Solid Waste Management (MSWM) in India.
- Study of current Municipal Solid Waste Management (MSWM) in Roorkee City.
- Estimate the Energy required by Roorkee City.
- Estimate the quantity of waste generated in Roorkee City.
- Estimate the waste generated administrative zone wise in Roorkee City.
- Theoretical Calculation of Energy potential from waste on basis of Literature Review.
- Collection of sample of wastes from landfill and city.
- Collection of water of sample from landfill near by side.
- Proximity & Ultimate Analysis of waste sample.
- Comparison of different Waste to Energy technologies i.e. Incineration, Bio-gasification, Bio-methanation, Pyrolysis.
- Calculation of potential of energy on basis of technology feasibility analysis.
- CFD simulation to improve incinerator.

7. Methods of Solid Waste Management

Studies and technologies prove that now waste is not a waste by proper assessment of chemical and physical composition suitable method of waste management can be very eco- friendly and profitable for humanity. Following are some traditional methods for solid waste management.

7.1. Recycling

Plastics& Paper are the most important recyclable material. Traditionally method follows with some rag pickers start collecting plastics and paper in early morning and at noon they washed the plastics and after drying them they sold it to a dealer. They usually work for more than 10 hours a day. This dealer sells this plastic to local plant where shredding and recycling is done. Paper is also recoverable material that ends up in the recycling industry. But in paper mills working with recyclable paper have to deal the problems of inherent impurities such as plastic, staples, stones and sand. The industry must have special processes and equipment to remove these from the paper before it is processed. Products like craft paper, card board or toilet paper are created. Paper can be recycled seven to eight times, each time, 22 trees are saved every tonne of recycled paper produced.

7.2. Composting

It is seen that in developing countries over 50% of the municipal waste is organic in nature. Organic waste usually has high moisture content and more likely suitable for composting and convert it to a rich organic fertilizer by biological natural aerobic process under controlled conditions. Various micro- organisms like bacteria, fungi etc. convert organic waste to smaller molecular substances by degradation. This process depends on various parameters such as oxygen percentage, moisture content, temperature, organic matter, micro-organism activity, etc. This technology is very traditional but recently percentage of Carbon, nitrogen, oxygen and moisture are inappropriate quantities due to pollution which greatly affects the compost. If these are not present in proper proportion then this process is greatly affected Composting method helps in the reduction of weight and volume of the organic waste.

7.3. Incineration

It is a process in which there is a controlled burning of waste at high temperature which reduces the volume as well as mass of the waste to considerable extent. This process removes water from the hazardous sludge from various industries and converts it into a non-burnable ash which can be used for various purposes like making fly ash bricks, boards, as an additive in cement industries etc. Incinerators need material like plastic, card boards etc. which have a good calorific value and these are considered as the material which mostly recyclers target and are livelihood of the rag pickers.

7.4. Land filling

Dumping of MSW is the most common and the cheapest way of waste management the Therefore around 60% of the world practices open dumping or land filling. Landfills are used for the disposal of wastes that cannot be recycled, composted, or incinerated. Landfills have been known to cause pollution in air and water and are a major source of greenhouse gases. These landfills are devoid of landfill gas (LFG) and leachate collection and treatment systems. Poor maintenance of these landfills renders them a threat to health and the environment rather than a solution to the problem of MSW management. Hence, landfilling should be used as a last resource and only when the first four components of integrated solid waste management have been exhausted.

8. Current Municipal Solid Waste Management practice in Roorkee

8.1. Collection of Municipal Solid Waste

Door to door, primary collection by engaging private sweepers. Waste is mostly collected through community bins/containers and road sweeping. Sweepers and sanitary workers engaged by the MSS sweep the streets. They accumulated the collected waste into small heaps and

subsequently loaded manually or mechanically onto the community containers/bins or directly loaded onto the solid waste transportation vehicles for onward transportation to the disposal site. Roorkee Nagar Palika Parishad (RNPP) presently utilizes the vehicles and equipment for transportation of solid waste.

8.2. Transportation of Municipal Solid Waste

RNPP maintains a low figure of vehicles for transportation and secondary collection of MSW from the various waste receptacles to the disposal sites. The vehicle contains TATA Ace, compactors, dumpers and tractor-trailers. Currently RNPP uses 10TATA Ace, 5 tractor trailer, 1 dumper and 3 compactor. These vehicles have duty for collection and transportation of waste from collection points to the landfills. Though the available transport volume is not adequate and make 4-5 trips per day per vehicle, due to operational inefficiency the available volume is not adequate even at four- five trips per day per vehicle. The situation has been worsened by poor management, no segregation & low awareness among people.

8.3. Disposal of MSW

In India, MSW from the urban areas is commonly disposed in the nearest available low-lying areas and wastelands on the outskirts of the city. Selection of these disposal sites depend solely on availability and not on scientific and socio-environmental criteria for a landfill. Open burning have highly impact on environment MSW is disposed in an uncontrolled manner and the daily cover material is not applied, although it is known that daily cover is necessary to abate odour, rodents and birds and to decrease site litter. At present RNPP disposes the solid waste of the city to one site located at the side of the national highway-74 at a distance of about 3 km from the city. In this site waste disposal is done by uncontrolled dumping village Saliar. Near Guru Ram Rai Public School which is located 500 meters from dumping site.

9. Problem Faced in Solid Waste Management by Roorkee

Today, Roorkee is experiencing the problem of solid waste management; this situation had been brought about by:

- Better and improving standard of living
- Growth of consumerism
- Population growth
- Increasing presence of substances in the municipal waste stream which are difficult to degrade/breakdown.
- Increasing industrial activities
- Poor public participation in finding solutions.
- Lack of recognition of solid waste as a problem demanding attention and action by the regulatory agencies.
- Shortage of space for disposal.

10. Waste Generated in Roorke City

Data is collected by weighing each vehicle throughout the day on weekends in each month. Then evaluated for the whole month. Variation is seen having highest in March and November.

These vehicles on average make 5 trips daily So total

MSW generated: 42.8*5 ≈ 214 MT

Table: 1. Vehicle Carrying MSW

S. No.	Vehicle Type	Amount of MSW (in MT)	Quantity of vehicles	Total (In MT)
1.	TATA Ace	1.6	10	16
2.	Tractor Trolley	2.5	5	12.5
3.	Compactor	3.1	3	9.3
4.	Dumper	5	1	5

11. Methodology

Roorkee City being under holy district Haridwar is a target place of the government to clean it under “Swach Bharat Abhiyan” and “Ganga Bachao” programme, so in order to be part of these programmes Roorkee city is selected for the work. Effective waste management has been a big challenge in most developing cities including Roorkee. Collection and sorting of municipal wastes at source in Roorkee with the hope of reducing the indiscriminate dumping of wastes has never been realized. Roorkee is also a big generation city of MSW as city comprises of Industrial Area & Colleges also. The population of Roorkee city as per the census 2011 is around 3 lakh. The study is conducted by collecting data from waste collection points of Roorkee city. The waste generation per day is around 200 tonne per day. The work represents study of current municipal solid waste management technique of Roorkee City and comparison of different Waste to Energy technologies. Relevant literature and information on the waste management practices in India was reviewed for conducting the present study. Key information was collected from the stakeholders through interviews and recorded office data for waste generation, transport and disposal. To validate or cross check the gathered information extensive field visits were made from the waste collection to the final disposal/processing sites to know the role of each element in waste management. Representative waste samples were also collected from different locations to get information about the physical composition of the waste.

12. Energy Potential

By considering Waste to Incineration technology theoretical estimation of Heat Energy is calculated by whole Roorkee city’s solid waste. Dulong’s formula needs to be applied. Heart

HV(KJ/Kg) = 338.2*C + 1442.8*(H-O/8) + 94.2*S

Where C, H, O and S are the % of these elements on dry ash free basis. Considering Literature Review taking percentage by Mass theoretical calculations are as follows:

C= 31.22, H= 8.17, O= 55.68, Sulphur very small so neglected. Applying to formulae we get Heat Energy Generated = 12260.69 kJ/kg

First, heat energy generated is used to calculate steam energy which is 70% of heat energy. Finally after steam energy calculation, net electric power generated by solid waste is calculated after accounting station service allowance and heat losses.Net electric power generation =

118582.55 kWh/day = 118.5 MWh/day. The above generated electricity is for one day and one day has 24 hours, so using this net electric power is calculated for per hour basis.

Net electric power generated = 118.5 MWh / 24h.

Net electric power generated = 4.9 MW≈ 5 MW.

13. Results and Discussion

Six objectives stated in work are accomplished by applying Dulong's formula to calculate net electricity generated. Dulong's formula is applied on WTE incineration technique. Incineration technique is chosen because it has many advantages over other techniques like the majority of wastes will burn without giving rise to noxious products of combustion (HCI, HF, SO_2 and NOx) in significant quantities, the volume and mass occupied by the waste is greatly reduced, it produces an effectively sterile ash residue etc. Total theoretical energy potential comes out to be 6 MW which is around enough for nearby rural areas. However in further work Sample will be collected from the site and proximate & ultimate analysis will done to calculate actual energy potential and CFD analysis will also be done to improve the performance of incineration plant. Further all the waste to energy technologies will be compared on technical, economic and environmental aspect. However the improper fate of solid wastes and mismanagement of sanitary system create disease supportive environment.

14. Conclusions

Due to the strong economic growth and urbanization in recent years, India faces many environmental challenges. In particular solid waste management in cities has been promoted as the big issue. Solid waste generation in Roorkee is increasing dramatically, mainly generated from households, buildings, commercial activities and other sources whose activities are similar to those of households and commercial enterprises such as wastes from offices, hotels, supermarkets, shops, institutions, and from municipal services such as street cleaning, etc. The main component of MSW is food waste which is a source of a very high potential of energy. Problems faced by this field is lack of comprehensive short and long term plan with municipal authorities to handle MSW in accordance with the MSW Rules, 2000. Majority of the municipal authorities do not have preparedness to set up waste processing and disposal facilities. There should be a proper trainings and awareness from worker to supervisor to managers to general public about effective and efficient waste management in order to accomplish "Swach Bharat" mission and target 'Zero Waste' for land filling.

References

[1] M. A. Dhere, B. P. Chandrasekhar, B. P. Pratapsingh, A. P. Dhanraj, Municipal solid waste disposal in Pune city- An analysis of air and groundwater pollution. 95(6), 2008, 773-777

[2] M. Ahel, N. Mikac, B. Cosvic, E. Prohic, V. Soukup, The impact of contamination from a municipal solid waste landfill (Zagreb, Croatia) on underlying soil. Wat. Sci. Tech., 37(8), 1998, 203-210.

[3] S. I. Omofonmwan, J. O. Eseigbe, Effect of solid waste on the quality of underground water in Benin Metropolis, Nigeria. J. Hum. Ecol. 26(2), 2009, 99-105

[4] J. G. M. Zade, R. Noori, Prediction of solid waste generation by use of artificial neural neatwork: A case study of Mashhad. Int. J. Environ. Res, 2(1), 2008, 13-22

[5] M. K. Mondal, Rashmi, B. V. Dasgupta, EIA of Municipal solid waste disposal site in Varansi using RIAM analysis. Resor. Cons. Recyc., 54(9), 2010, 541-546

[6] O. Buenrostro, G. Bocco, S. Cram, Classification of sources of municipal solid wastes in developing countries. Resor. Cons. Recyc, 32, 2001, 29-41.

[7] Q. H. H. M. Zakir Hossin, Municipal Solid waste (MSW) as a source of renewable energy in Bangladesh: Revisited. Renewable and Sustainable Energy Reviews, 2014, 35-41.

[8] H. H. Sieting Tan, Economical and environmental impact of waste-to-energy (WTE) alternatives for waste incineration, landfill and anerobic digestion. Energy procedia, 2014, 704-708.

[9] Y. Z. Hefa Cheng, Municipal Solid Waste Fueled Power Generation in China: A Case Study of Waste-to-Energy in Changchun City. Environmental Science Technology, 2007, 7509-7515

[10] P. D. Sudhanshu Kaushik, A comparitve study of solid waste generation at Mansa Devi and Chandi Devi in the Shiwalik foothills, during the KumbMela 2011

[11] S. H. C Liamsanguan, Environmental assessment of energy production from Municipal Solid Waste incineration. LCA Case Studies, 2007, 529-536.

[12] K. K. Khaiwal Ravindra, System analysis of municipal solid waste management in chandigarh and minimization for cleaner emissions. journal of Cleaner Production, 2015, 251-256.

[13] http://powermin.nic.in/power-sector-glance-all-india

[14] Shubham Gupta, R. S. Mishra, Estimation of Electrical Energy Generation from Waste to Energy using Incineration Technology, International Journal of Advance Research and Innovation, 3(4), 2015, 615-618

[15] Shubham Gupta, R. S. Mishra, Mixing of Various Renewable Energy Technologies towards Development of Village Energy Need, International Journal of Advance Research and Innovation, 3(4), 2015, 601-604

Egyptian Journal of Petroleum (2016) xxx, xxx–xxx

HOSTED BY

ELSEVIER

Egyptian Petroleum Research Institute

Egyptian Journal of Petroleum

www.elsevier.com/locate/egyjp
www.sciencedirect.com

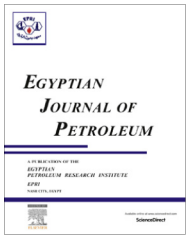

FULL LENGTH ARTICLE

Sorting of *Glossiphonia complanata* (Linnaeus, 1758) (*Rhynchobdellida*: *Glossiphoniidae*) from three aquatic plants in Tigris River within Baghdad city

Manar Dawood Salman [a], Mohammed K. Shebli [a], Mohammed Jassim Obed Alfalahi [b], Allaa M. Aenab [c,*], S.K. Singh [c]

[a] *Environment and Water Directorate – Ministry of Science and Technology, Baghdad, Iraq*
[b] *Environmental Engineer, Rasan Group Company, Erbil, Iraq*
[c] *Environmental Engineering Department, Delhi Technological University, Delhi, India*

Received 10 June 2016; revised 26 October 2016; accepted 2 November 2016

KEYWORDS

Glossiphonia complanata;
Aquatic plants;
Snails;
Feeding of *G. complanata*

Abstract The present study shows that the reason for isolation of *Glossiphonia complanata* from these aquatic plants was firstly founding of aquatic oligochaeta, snails and chironomidae that settled on aquatic plants as food. Secondly the aquatic plants itself represent favorable environment for growth and reproduction for *G. complanata* and as food for oligochaeta, chironomidae and snails. When the number of *G. complanata* increased the number of worms and snails decreased as observed. The aim of this study was to discover causes of isolation of *G. complanata*.
© 2016 Egyptian Petroleum Research Institute. Production and hosting by Elsevier B.V. This is an open access article under the CC BY-NC-ND license (http://creativecommons.org/licenses/by-nc-nd/4.0/).

1. Introduction

Glossiphonia complanata species is one of phylum Annelida, class clitellata, subclass Hirudinea, order Rhynchobdellida, family Glossiphoniidae [7,12].

This species is broad and dorso-ventrally flattened brownish color. Eyes normally are three pairs in two rows parallel with the mid dorsal line, and have small anterior sucker and broad posterior sucker [7].

This species is one of the commonest leeches in fresh water and is usually rare on a muddy substratum and found chiefly on stones and macrophytes [14,16]. Although molluscs consider its chief prey including *Bithynia tentaculata*, *Lymnaea stagnalis*, *Physa fontinalis*, *Physa heterostropha*, *Planorbarius corneus*, *Planorbis vortex* (L.), *Potamopyrgus jenkinsi* (smith), *Pisidium* spp., *Sphaerium* spp., it sucks the body fluids of aquatic oligochaetes and insect larvae, [4,5,8]. The young *G. complanata* gains its first meal by feeding on other leeches including *Erpobdella octoculata*, *Dina lineata*, *Trocheta subviridis*, *Trocheta bykowskii*, *Hirudo medicinalis*, *Haemopis sanguisuga*, *Hemiclepsis marginata*, and *Haementeria costata*, that is considered an unusual feature of feeding. The attacked leech moves violently,

* Corresponding author.
E-mail address: allaaaenab@gmail.com (A.M. Aenab).
Peer review under responsibility of Egyptian Petroleum Research Institute.

http://dx.doi.org/10.1016/j.ejpe.2016.11.001
1110-0621 © 2016 Egyptian Petroleum Research Institute. Production and hosting by Elsevier B.V.
This is an open access article under the CC BY-NC-ND license (http://creativecommons.org/licenses/by-nc-nd/4.0/).

Please cite this article in press as: M.D. Salman et al., Sorting of *Glossiphonia complanata* (Linnaeus, 1758) (*Rhynchobdellida*: *Glossiphoniidae*) from three aquatic plants in Tigris River within Baghdad city, Egypt. J. Petrol. (2016), http://dx.doi.org/10.1016/j.ejpe.2016.11.001

burrowing into sand, or trying to remove the young leeches with its posterior sucker [10,13,16].

Many aspects of the life cycle of this species were noticed from [6,11]. The parent covers eggs that are laid in soft, transparent cocoons that are attached to the substratum with its body for five to six days prior to hatching. The young *G. complanata* has left its parent, then grows to maturity, breeds and dies after about one or two years, depending upon local conditions.

2. Materials & methods

2.1. Sampling

The 20 samples of aquatic plants: *Eichhornia crassipes*, *Hydrella vorticellata* and *Phragmites australis* are collected, from different aquatic habitats inside Baghdad city on the Tigris River for a period from September 2015 to September 2016, using hand forklift to eradicate the plants.

2.2. Sorting method

The excised aquatic plants were collected in a container with water from the river and then transferred to the laboratory where they are distributed into three aquarium of ($40 \times 20 \times 20$ cm) and left for about 2–5 days to allow the invertebrates (Leech, worms, Snails and Chironomid larvae) to settle down. To ventilate water in each aquarium an air pump was used. The settled sediment on the floor of aquarium is collected with care by a dropper and transferred to Petri dishes of 10 cm diameter. Then they were sorted carefully to dislodge them without damage using a dissecting microscope. Then they were transferred to a clean Petri dish that contains a little amount of distilled water. Later on, 4% formaldehyde was added drop by drop to the dish to immobilize them, 4% formalin was added to kill the worms and larvae then preserved in 70% alcohol while the snails were sorted by hand from the plants.

2.3. Preparation of permanent slides

The preserved worms were transferred to distilled water, then transferred to a clean slide by a fine brush on which a drop of polyvinyl lacto-phenol was added and covered with a cover slip then left overnight before examining under a compound microscope (Olympus: made in japan).

2.4. Identification

The leech, Worms, Snails and Chironomids larvae were identified according to [7,3,15,1,2] respectively.

3. Results and discussion

We isolated 205 individuals of *G. complanata* from three kinds of aquatic plants, 133 individuals were isolated from *E. crassipes*, 49 individuals were isolated from *Hydrella verticillata* and 23 individuals were isolated from *Phragmites australis*. In addition to isolation of *G. complanata* from aquatic plants we isolated it from the mantle cavity of snails (*Physa acuta*, *Viviparous viviparous*, and *Lymnaea auricularia*) that settled on the same plants that represent their food.

1128 Individuals of oligochaeta 12 species were sorted from these aquatic plants belonging to the family Naididae, subfamily Naidinae (8 species), and subfamily Pristininae (2 species), family tubificidae (2 species) in addition to 3 species of Snails and Chironomid larvae (Table 1).

G. complanata was sorted from these aquatic plants because it considers aquatic plants as a refuge for hiding, when hungry or carrying young, also because of finding assemblages of aquatic oligochaeta, snails and chironomids larvae that are considered the main source of food especially snails [5,8,11], by extending a proboscis through its mouth to touch the prey then releasing digestive enzymes from the tip of the proboscis, allowing the species to suck up the fluids of the body of the prey. Generally fresh water invertebrates and especially aquatic oligochaetes are associated with these aquatic plants

Table 1 *G. complanata* and other taxa that appeared and are sorted from the aquatic plants.

Taxa		*Eichhornia crassipes*	*Hydrella verticillata*	*Phragmites australis*	Total
Naididae	*Glossiphonia complanata*	133	49	23	205
	Chaetogaster limnaei	7	8	3	18
	C. langi	4	8	3	15
	Dero dorsalis	0	79	3	82
	Stylaria fossularis	18	52	11	81
	Nais stolci	3	43	5	51
	Pristina foreli	45	64	41	150
	P. proboscidea	26	42	41	109
Tubificidae	*Limnodrilus hoffmeisteri*	0	14	1	15
	Tubifex tubifex	9	22	1	32
Molluscs	*Viviparous viviparous*	0	31	22	53
	Physa acuta	4	16	0	20
	Lymnaea auricularia	1	7	0	8
Insects	*Chironomid larvae*	200	77	12	289
	Total	450	512	166	1128

Note: The families Naididae and Tubificidae are belonging to Phylum Oligochaeta.

Please cite this article in press as: M.D. Salman et al., Sorting of *Glossiphonia complanata* (Linnaeus, 1758) (*Rhynchobdellida*: *Glossiphoniidae*) from three aquatic plants in Tigris River within Baghdad city, Egypt. J. Petrol. (2016), http://dx.doi.org/10.1016/j.ejpe.2016.11.001

because either the aquatic plants itself resemble part of the food or the microorganisms, bacteria and settled algae that are found on aquatic plants are considered as a source of food for these organisms. This result confirmed by Ref. [9] and these organisms resembles the main source of food for *G. complanata*. Considering the snails as prey was the reason for sorting leeches from it, hence when the number of leeches increase, the number of snails decrease [4].

4. Conclusion

1. *G. complanata* feed on oligochaeta (worms), chironomid larvae, snails.
2. Oligochaeta (worms), chironomid larvae, snails settled on aquatic plants for growth and reproduction.
3. *G. complanata* lives inside the mantle cavity of snails because of founding of *Dero dorsalis* (worm) to eat it as food for *G. complanata*.

Reference

[1] M.M. Ahmed, A Systematic Study on Molluscs from Arabian Gulf and Shatt Al-Arab, Iraq, Center for Arab Gulf Studies, Univ. Basrah. Iraq, 1975.
[2] A.J. Al-Marsumi, Taxonomic Study of Larvae of Subfamilies: Orthocladiinae and Chironominae (Chironomidae: Diptera) from Different Aquatic Habitat in central Iraq (M.Sc. thesis), College of Education (Ibn Al-Haithem), University of Baghdad, 1975, p. 131.
[3] R.O. Brinkhurst, A Guide for the Identification of British Aquatic Oligochaeta, 2nd ed., 1971, Scientific Publication No. 22 Biological Association.
[4] Ch. Brönmark, B. Malmqvist, Oecologia 69 (2) (1986) 268–276.
[5] R.W. Davies, R.P. Everett, Verh. Int. Verein. Theor. Angew. Limnol. 19 (1975) 2816–2817.
[6] M. de Eguileor, S. Daniel, B. Giordana, G. Lanzavechia, R. Valvassori, J. Exp. Zool. 269 (5) (1994) 389–402.
[7] J.M. Elliott, K.H. Mann, A key to the British Freshwater leeches with notes on their life cycles and ecology. Scientific Publication No. 40, Freshwater Biological Association, 1979.
[8] D.J. Klemm, Sterkiana (58) (1976) 1–50, 59, 1–20.
[9] D.M. Lodge, Aquat. Bot. 41 (1991) 195–224.
[10] T.K. McCarthy, Proc. R. Ir. Acad. 75b (1975) 401–451.
[11] K.H. Mann, J. Anim. Ecol. 26 (1957) 99–111.
[12] P. Myers, R. Espinosa, C.S. Parr, T. Jones, G.S. Hammond, T. A. Dewey, The Animal Diversity web (online) Accessed at http://animaldiversity.org2014.
[13] R.T. Sawyer, North American Freshwater Leeches, Exclusive of the Piscicolidae with a Key to All Species, Illinois boil. Monogr., 1972.
[14] A. Soós, Actazool. Hung. 15 (1969) 151–201.
[15] T. Timm, Lauterbornia 66 (2009) 1–235.
[16] J. Wilkialis, Zool. Pol. 20 (1970) 29–54.

Please cite this article in press as: M.D. Salman et al., Sorting of *Glossiphonia complanata* (Linnaeus, 1758) (*Rhynchobdellida*: *Glossiphoniidae*) from three aquatic plants in Tigris River within Baghdad city, Egypt. J. Petrol. (2016), http://dx.doi.org/10.1016/j.ejpe.2016.11.001

Study of Dangerous Voltages in Substation, Different Soil Models and Designing of Grounding System of High Voltage Substation with the help of Computer Program RPDGS Using MATLAB GUI

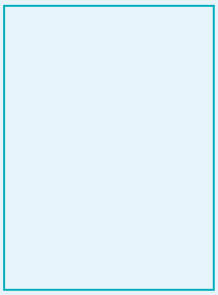
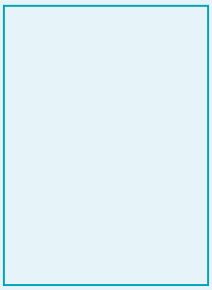
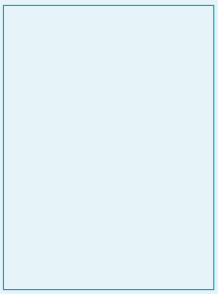
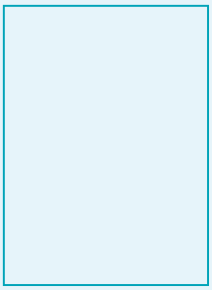

RAJESH KUMAR — *Delhi Transco Ltd.*

KAMAL BANSAL — *UPES, Dehradhun, India.*

DEVENDER K. SAINI — *UPES, Dehradhun, India.*

IPS PAUL — *HRIT, Ghaziabad*

www.IndianJournals.com
Members Copy, Not for Commercial Sale
Downloaded From IP - 14.139.251.107 on dated 27-Nov-2016

ABSTRACT

This paper presents study of dangerous voltages in substation, different soil models and maximum grid current. Further it represents a computer program named RPDGS which can be used for designing the grounding system in uniform layer as well as for two layers soil model. This program can design the grounding system for both Gas Insulated Substation (GIS) and Air Insulted Substation (AIS). This program has been developed using MATLAB GUI.

The computer program may be used for soil modelling & parametric analysis of designing of grounding system by engineers and helps in improving the design of the grounding system.

Key Words: Grounding, Resistivity, Ground Potential Rise (GPR), Touch and step Potential, Resistance, Single and Two Layers soil Model, MATLAB GUI.

1. INTRODUCTION

The grounding system in a substation is very crucial for a few reasons, all of which are related to either the protection of people and equipment and/or the optimal operation of the electrical system. These include:

1. The grounding system provides a low resistance return path for earth faults within the substation, which protects both personnel and equipment
2. For earth faults occurred in far away generation sources, a low resistance grounding grid relative to remote earth prevents dangerous ground potential rises (GPR)
3. The grounding system provides a low resistance path for voltage transients such as lightning and surges / over voltages in the system
4. Equipotential bonding of conductive objects (e.g. metallic equipments, buildings, piping etc) to the grounding system prevents the presence of dangerous voltages between objects (and earth).
5. Equipotential bonding helps prevent building up of electrostatic chare and discharge within the substation, which can cause sparks with enough energy to ignite flammable atmospheres
6. The grounding system provides a reference potential for electronic circuits and helps reduce electrical noise for electronic, instrumentation and communication systems

Earlier, the design motive was to get minimum value of earth resistance of grounding mat of substation. However, the modern design practices also focus on the importance of control of step and touch potential within allowable limits. The designing of grounding system depends on the soil resistivity model chosen for the substation soil & the design of grounding system may become inaccurate if average value of resistivity measured is taken in the design calculation especially when the variation of resistivity of different probe distance is more than 25 %. It is advisable to use two layer soil models in such cases[1,2,3]

The pictures of Gas Insulated and Air Insulated Substation are shown in Figure 1 and Figure 2 respectively.

Fig 1 : High Voltage Gas Insulated Substation

Fig. 2 : Air Insulated Substation and Grounding area with Gravel Surface

2. ACCIDENTAL GROUND CURRENT

2.1 Resistance of the Human Body

For dc and 50 Hz or 60 Hz ac currents, the human body can be approximated by a resistance. The current path typically considered from one hand to both feet or from one foot to the other one. The internal resistance of the body is approximately 300Ω, whereas values of body resistance including skin range from 500 Ω to 3000 Ω as suggested in many research. The human body resistance is decreased by damage of puncture of the skin at the point of contact.

Dalziel conducted extensive tests[1] using saltwater to wet hands and feet to determine safe let-go currents, with hands and feet wet. Values obtained using 60 Hz for men were as follows: the current was 9.0 mA, corresponding voltages were 21.0 V for hand-to-hand and 10.2 V for hand-to-feet. Hence, the ac resistance for a hand-to-hand contact is equal to 21.0/0.009 or 2330 Ω and the hand-to-feet resistance equals 10.2/0.009 or 1130 Ω, based on this experiment[1].

The following resistances, in series with the body resistance, are assumed as follows:

(a) Hand and foot contact resistances are equal to zero.

(b) Glove and shoe resistances are equal to zero.

A value of 1000 Ω represents the resistance of a human body form hand-to-feet and also from hand-to –hand, or from one foot to the other foot, is used for designing purpose i.e. RB = 1000 Ω

2.2 Current Paths through the Body

It should be remembered that the choice of a 1000 Ω resistance value relates to paths such as those between the hand and one foot or both feet, where a major part of the current passes through parts of the body containing vital organs, including the heart. It is generally agreed that current flowing from one foot to the other is far less dangerous. Also it has been revealed[1] that much higher foot-to-foot than hand-to-foot currents had to be used to produce the same current in the heart region. He stated that the ratio is as high as 25:1.

Based on these conclusions, resistance values greater than 1000 Ω could possibly be allowed where a path from one foot to the other foot is concerned. However, the following factors should be considered:

(A) A voltage between the two feet, painful but not fatal, might result in a fall that could cause a larger current flow through the chest area. The degree of this hazard would further depend on the fault duration and the possibility of another successive shock, perhaps on reclosing of the circuit.

(B) A person might be working or resting in a prone potion when a fault occurs.

It is apparent that the dangers form foot-to-foot contact is far less than from the other type. However, since deaths have occurred from case (a) above, it is a danger that should not be ignored.

2.3 Accidental Circuit Equivalents

Using the value of tolerable body current established above and the appropriate circuit constants, it is possible to determine the tolerable voltage between any two points of contact.

The following notations are used for the accidental circuit equivalent shown in Figure 3:

I_b is the body current (body is part of the accidental circuit) in A

R_A is the total effective resistance of the accidental circuit in Ω

V_A is the total effective voltage of the accidental circuit (touch or step voltage) in V

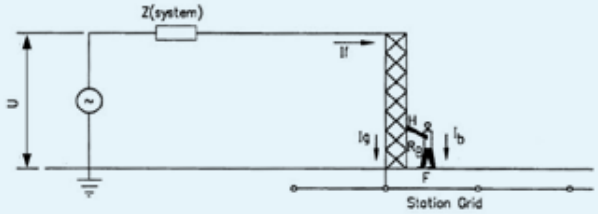

Fig. 3 : Flow of Current through the Body of Working Staff during Fault

The tolerable body current, Ib, above, is used to define the tolerable total effective voltage of the accidental circuit (touch or step voltage) i.e. the tolerable total effective voltage of the accidental circuit is that voltage that will cause the flow of a body current, I_b, equal to the tolerable body current, I_b,.

Figure 3 shows the fault current If being discharged to the ground by the grounding system of the substation and a person touching a grounded metallic structure at H. Various impedances in the circuit are shown in Figure 4 . Terminal H is a point in the system at the same potential as the grid into which the fault current flows and terminal F is the small area on the surface of the earth that is in contact with the person's two feet. The current, I_b, flows from H through the body of the person to the ground at F the Thevenin theorem allows us to represent this tow terminal (H,F) network of Figure 4 by the circuit shown in Figure 5

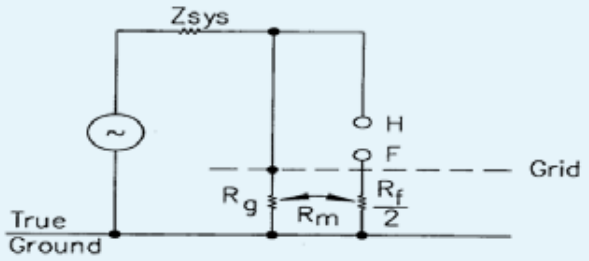

Fig. 4 : Different Resistances of Circuit for Touch Voltage

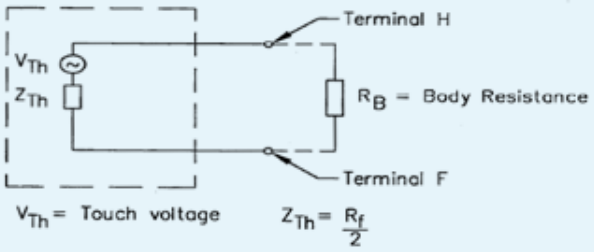

Fig. 5 : Thevenin Equivalent of Circuit of Fig 4

The Thevenin voltage V_{Th} is the voltage between terminals H and F when the person is not present. The Thevenin impedance Z_{Th} is the impedance of the system as seen from points H and F with voltage sources of the system short circuited. The current I_b, through the body of a person coming in contact with H and F is given by

$$I_b = V_{Th} / Z_{Th} + R_B) \quad ...(1)$$

Figure 6 shows the fault current If being discharged to the ground by the grounding system of the substation. The current, I_b, flows from one foot F1 through the body of the person to the other foot, F2. Terminals F1 and F2 are the areas on the surface of the earth that are in contact with the two feet, respectively. The Thevenin theorem allows us to represent this two-terminal (F1, F2) network in Figure 6. The Thevenin voltage V_{Th} is the voltage between terminals F1 and F2 when the person is not present. The Thevenin impedance Z_{Th} is the impedance of the system as ween from the terminals F1 and F2 with the voltage sources of the system short circuited.

For touch voltage accidental circuit

$$z_{Th} = R^{f}/_{2} \quad ...(2)$$

And for the step voltage accidental circuit

$$z_{Th} = 2R_f \quad ...(3)$$

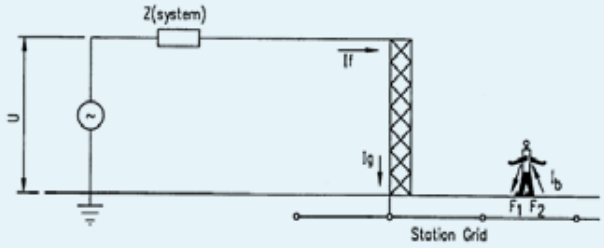

Fig. 6 : Different Resistances of Circuit for Step Voltage

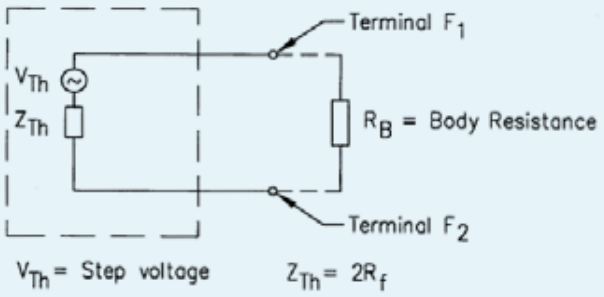

Fig. 7 : Thevenin Equivalent of Circuit of Fig 6

For the purpose of circuit analysis, the human foot is usually represented as a conducting metallic disc and the contact resistance of shoes, socks, etc., is neglected. Traditionally, the metallic disc representing the foot is taken as a circular plate with a radius of 0.08m[1]. With only slight approximation, equations for ZTh can be obtained in numerical from and expressed in terms of as follows:

$$R_f = \rho/4b \quad ...(4)$$

Where ρ = Resistivity of the soil

For touch voltage accidental circuit

$$Z_{Th} = 1.5\rho \quad ...(5)$$

For step voltage accidental circuit

$$Z_{Th} = 6.0\rho \quad ...(6)$$

The permissible total equivalent voltage (i.e., tolerable touch and step voltage), using above Equations are

$$E_{touch} = IB\ (R_B + 1.5\ \rho) \quad ...(7)$$

$$E_{step} = IB\ (R_B + 6.0\rho) \quad ...(8)$$

The equations 7 and 8 shall be changed into equation 9&10 and 11&12 respectively if we are using surface material with resistivity ρs.

The maximum tolerable voltages for step and touch scenarios can be calculated empirically from IEEE Std Section 8.3 for body weights of 50 kg and 70 kg:

www.IndianJournals.com
Members Copy, Not for Commercial Sale
Downloaded From IP - 14.139.251.107 on dated 27-Nov-2016

1. 50 kg person: $E_{touch,50} = (1000 + 1.5C_s\rho_s)\frac{0.116}{\sqrt{t_s}}$ ...(9)

2. 70 kg person: $E_{touch,70} = (1000 + 1.5C_s\rho_s)\frac{0.157}{\sqrt{t_s}}$ ...(10)

3. 50 kg person: $E_{step,50} = (1000 + 6C_s\rho_s)\frac{0.116}{\sqrt{t_s}}$ ...(11)

4. 70 kg person: $E_{step,70} = (1000 + 6C_s\rho_s)\frac{0.157}{\sqrt{t_s}}$ ...(12)

Where E_{touch} is the touch voltage limit (V)

E_{step} is the step voltage limit (V)

C_s is the surface layer derating factor (as calculated in Step 2)

ρ_s is the soil resistivity (Ω.m)

t_s is the maximum fault clearing time (s)

The choice of body weight (50 kg or 70 kg) depends on the expected weight of the personnel at the site. Typically, where women are expected to be on site, the conservative option is to choose 50 kg.

This derating factor can be approximated by an empirical formula as per IEEE Std 80 Equation 13:

$$C_s = 1 - \frac{0.09\left(1 - \frac{\rho}{\rho_s}\right)}{2h_s + 0.09} \quad ...(13)$$

Where C_s is the surface layer derating factor

ρ is the soil resistivity (Ω.m)

ρ_s is the resistivity of the surface layer material (Ω.m)

h_s is the thickness of the surface layer (m)

3. CONCEPT OF GPR AND DANGEROUS VOLTAGES IN SUBSTATION

In electrical engineering, earth potential rise (EPR) also called ground potential rise (GPR) occurs when a large current flows to earth through an earth grid impedance. The potential relative to a distant point on the Earth is highest at the point where current enters the ground, and declines with distance from the source. Ground potential rise is a concern in the design of electrical substations because the high potential may be a hazard to people or equipment[1-5].

The change of voltage over distance (potential gradient) may be so high that a person could be injured due to the voltage developed between two feet, or between the ground on which the person is standing and a metal object. Any conducting object connected to the substation earth ground, such as telephone wires, rails, fences, or metallic piping, may also be energized at the ground potential in the substation. This transferred potential is a hazard to people and equipment outside the substation.

Earth Potential Rise (EPR) is caused by electrical faults that occur at electrical substations, power plants, or high-voltage transmission lines. Short-circuit current flows through the plant structure and equipment and into the grounding electrode. The resistance of the Earth is non-zero, so current injected into the earth at the grounding electrode produces a potential rise with respect to a distant reference point. The resulting potential rise can cause hazardous voltage, many hundreds of metres away from the actual fault location. Many factors determine the level of hazard, including: available fault current, soil type, soil moisture, temperature, underlying rock layers, and clearing time to interrupt a fault.

At points outside the earth grid, the potential rise decreases. The simplest case of the potential at a distance is the analysis of a driven rod electrode in homogeneous earth. The voltage profile is given by the following equation.

$$V_r = \rho I / 2\pi rX \quad ...(14)$$

where

r_x is a point from the center of the earth grid (in meters).

V_r is the voltage at distance from the earth grid, in volts.

ρ is the resistivity of the earth, in Ω•m.

I is the earth fault current, in amperes.

This case is a simplified system; practical grounding systems are more complex than a single rod, and the soil will have varying resistivity.

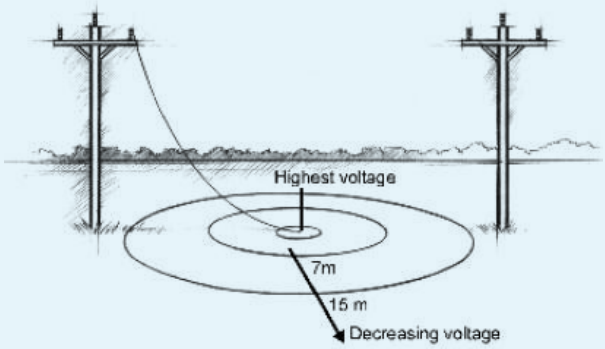

Fig. 8 : Concept of Voltage Gradient

The six dangerous voltages which are being faced in the substation are:

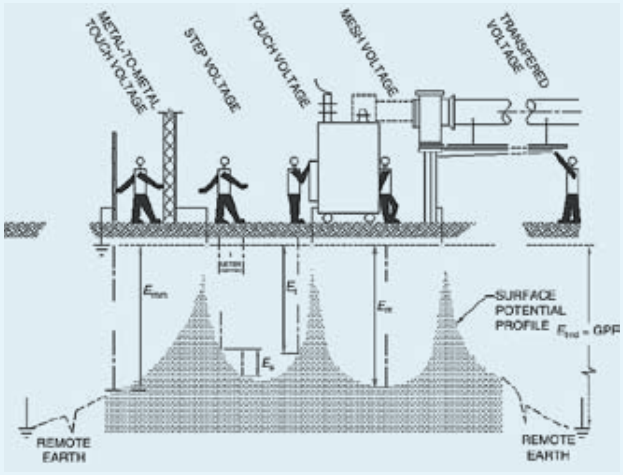

Fig. 9 : Six Dangerous Voltages in Substation

1. **Step Voltage** : The difference in surface potential experienced by a person bridging a distance of 1 m with the feet without contacting any grounded object.
2. **Touch Voltage**: The potential difference between the ground potential rise (GPR) and the surface potential at the point where a person is standing while at the same time having a hand in contact with a grounded structure.
3. **Transferred Voltage**: A special case of the touch voltage where a voltage is transferred into or out of the substation from or to a remote point external to the substation site.
4. **Mesh Voltage**: The maximum touch voltage within a mesh of a ground grid.
5. **Metal-to-Metal Touch Voltage**: The difference in potential between metallic objects or structures within the substation site that may be bridged by direct hand-to-hand or hand-to-feet contact.
6. **Ground Potential Rise (GPR)**: The maximum electrical potential that a substation grounding grid may attain relative to a distant grounding point assumed to be at the potential of remote earth. This voltage, GPR, is equal to the maximum grid current times the grid resistance.

4. FAULT CURRENT AND MAXIMUM GRID CURRENT

The maximum grid current is the worst case earth fault current that would flow via the grounding grid back to remote earth. To calculate the maximum grid current, there is need to calculate the worst case symmetrical earth fault current at the facility that would have a return path through remote earth (call this I_F).

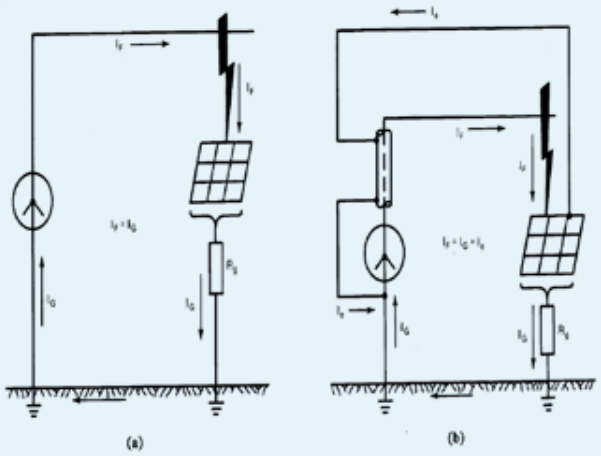

Fig. 10 : Fault Current and Max Grid Current in Substation

Current Division Factor

Not all of the earth fault current will flow back through remote earth. A portion of the earth fault current may have local return paths (e.g. local generation) or there could be alternative return paths other than remote earth (e.g. overhead earth return cables, buried pipes and cables, etc). Therefore a current division factor S_f must be applied to account for the proportion of the fault current flowing back through remote earth[1-5]. In the most conservative case, a current division factor of S_f can be applied, meaning that 100% of earth fault current flows back through remote earth.

The symmetrical grid current I_g is calculated by:

$$I_g = I_F S_f \quad ...(15)$$

Decrement Factor (S_f)

The symmetrical grid current is not the maximum grid current because of asymmetry in short circuits, namely a dc current offset. This is captured by the decrement factor as below:

$$D_f = \sqrt{1 + \frac{T_a}{t_f}\left(1 - e^{\frac{-2t_f}{T_a}}\right)} \quad ...(16)$$

Where D_f is the decrement factor

t_f is the duration of the fault (s)

T_a is the dc time offset constant

$$T_A = \frac{X}{R} \cdot \frac{1}{2\pi f}$$

Where X/R is the X/R ratio at the fault location

f is the system frequency (Hz)

OR the following table 1 can be used for D_f.

Table 1 : (IEEE 80)[1]

The maximum grid current I_G is lastly calculated by:

$$I_G = I_g D_f \quad ...(17)$$

The maximum GPR is calculated by:

$$GPR = I_G R_g \quad ...(18)$$

Where GPR is the maximum ground potential rise (V)

I_G is the maximum grid current

R_g is the grounding grid resistance

5. SUBSTATION GROUNDING SYSTEM

A typical grounding system of any high voltage substation[4] usually made of the following:

www.IndianJournals.com
Members Copy, Not for Commercial Sale
Downloaded From IP - 14.139.251.107 on dated 27-Nov-2016

(a) Grounding mat formed by copper on mild steel bars buried in the ground at a depth of about 0.6 meter in a horizontal plane (Figure.11). The crossings are welded. The grounding mat is laid for the entire substation area and sometimes this ground mat moves a few meters beyond the fencing area of the substation. The grounding rods/ electrodes are also connected to this mat along the border of the grounding mat of the substation.

(b) Earth electrodes driven vertically into the ground at several locations & are connected to the ground mat.

(c) Grounding risers are used for making interconnections between the equipment structures, equipment bodies and the grounding mat.

(d) Grounding strips of different sizes to connect the riser with the equipment body, structure and transformer neutral.

Fig. 11 : Grounding Mat of the Substation

6. UNIFORM AND TWO LAYER SOIL RESISTIVITY MODEL

Uniform soil model is rarely found in the field but average resistivity measured at different locations is considered as the resistivity for designing of grounding grid of substation and soil is taken as uniform model with this resistivity. Actually electrical engineers usually come across the following different types (Figure 12) of soil models of the substation which is obtained by soil resistivity measurement data[6-15].

Fig. 12 : Apparent Soil Resistivity versus Electrode Separation Curve

1. Curve (A) represents uniform soil resistivity model
2. Curve (B) represents two layer soil models where upper layer resistivity is low
3. Curve (C) represents three layer soil model (Low –High – Low).
4. Curve (D) represents two layer soil model where upper layer resistivity is high
5. Curve (E) represents three layer soil model which are vertically stratified.

Two layer soil model[7,8] which has an upper layer of a finite depth H, and resistivity (rho1) over a lower layer of infinite depth and resistivity (rho2) is represented by Figure 13.

Fig. 13 : Two Layer Soil Resistivity Model

7. ALGORITHM FOR DESIGNING OF GROUNDING SYSTEM OF SUBSTATION

The algorithm of the steps involved in the designing of the grounding system of Air and Gas insulted substation is given in Figure 14[1]

Fig. 14 : Algorithm for Design of Grounding System

8. USE OF RPDGS FOR DESIGNING OF GROUNDING SYSTEM

STEP 1 : First of all measure the earth resistivity of the substation soil at different locations and values

2. Fill this data in the Soil modelling module of RPDGS and we get the results as shown below[16-21] :

www.IndianJournals.com
Members Copy, Not for Commercial Sale
Downloaded From IP - 14.139.251.107 on dated 27-Nov-2016

Fig. 15 : SnapShot of Soil Modelling Module of RPDGS

STEP 2 : Input Parameters cum data for design:

INPUT DATA consist of the followings:

1. System / network data (system fault current, fault duration, and ambient temperature etc.)
2. Field data like average earth resistivity, surface layer type and resistivity and thickness of surface layer etc.
3. Grounding conductor type and constants.
4. Earth mat design parameters like duration of shock, weight of human working in the station, max grid current, no of electrodes required / to be buried and spacing of earth mat conductor (initial value) etc.

Final Step Write down all the input parameters in the program and press the design button.

The screen shot of the MATLAB GUI program for designing of grounding system as per IEEE-80 is shown[16-21] below:

Fig. 16 : SnapShot of Complete Design Module of RPDGS

7. CONCLUSION

This paper highlights the various parameters of designing of the grounding system of substations. The program named RPDGS can be proved very useful tool for accurate soil modelling and optimal designing of grounding system of HV substations. The parameters which have been found to have substantial effect on ground grid design and performance include Maximum grid current, Fault duration, Shock duration, Soil resistivity, Surface layer resistivity, Thickness of surface layer, Area occupied by the grid conductors, Depth of burial of grid, Spacing between grid conductors & No. and location of vertical ground rods .

Acknowledgement

The first author would like to express his deepest gratitude to Mr. M.K. Chaudary for inspiring me to learn more about grounding of substation. High appreciation is given to Mr. Hitesh Kumar and Mr. N.B. Soni for their invaluable advice and support. Finally the author would like to thank Mrs Krishna Arora for her blessings and Mrs Poonam Arora & Master Divyanshu Arora for their unflinching support in this work.

REFERENCES

1. IEEE Std. 80-2000, IEEE Guide for Safety in AC Substation Grounding, New York, NY: IEEE
2. IEEE: 81: 1983, IEEE Guide for Measuring Earth Resistivity, Ground Impedance, and Earth Surface Potentials of a Ground System
3. Manual on," Grounding of A C Power Systems," Publication No 302, C.B.I.P. New Delhi, Oct. 2007
4. I.S.3043-1987, Indian Standard Code of Practice for Grounding
5. IEEE 142-2007 - IEEE Recommended Practice for Grounding of Industrial and Commercial Power Systems
6. Hans R.Seedher, J.K. Arora, "Estimation of two layer soil Parameter using finite wenner Resistivity Expressive",

IEEE Transaction on Power Delivery,Vol.7 No.3, July , 1992.

7 Gary Gilbert, "Soil modelling techniques", International Journal of Materials Science and Applications. Vol. 1, No. 1, pp. 8-13., 2012.

8 M. Nessereddine, J. Rizk, M. Nagrial, A. Helleny, "Estimation of apparent soil resistivity for two - layer soil structure," International Journal Of Energy And Environment, Volume 4, Issue 4, pp.573-580, 2013.

9. Rodney Urban, Karl Mardira, Session Three:Accurate "Soil Resistivity Testing for Power System Grounding", Grounding, Lightning & Surge Protection Forum – IDC Technologies

10. Ioannis F. GONOS, Vassiliki T. Kontargyri, Ioannis A. Stathopulos, Antonios X. Moronis, Anastasios P. Sakarellos, Nikolaos I. Kolliopoulos, "Determination Of Two Layer Earth Structure Parameters" XVII International Conference on Electromagnetic Disturbances EMD'2007 ,Poland

11. Adekitan I. Aderibigbe, Fakolujo A. Olaosebikan," Alogorithm for Determining the Parameters of a Two- Layer Soil Model", World Academy of Science, Engineering and Technology International Journal of Electrical, Computer, Electronics and Communication Engineering Vol:8, No:11, 2014

12. M. Nassereddine, J. Rizk, and G. Nasserddine," Soil Resistivity Data Computations; Single and Two - Layer Soil Resistivity Structure and Its Implication on Grounding Design," World Academy of Science, Engineering and Technology Vol:7 2013

13. O.E. Gouda1, G.M. Amer, T. M.EL-Saied , "Factor Affecting the Apparent Resistivity of Multi-Layer Soil", Proceedings of the XIVth International Symposium on High Voltage Engineering,Singhua University, Beijing, China, 2005.

14. Sherif S.M. Ghoneim, kamel A. Shoush," Analytical Methods for Earth Surface Potential Calculation for Grounding Grids "International Journal of Engineering & Computer Science ,Vol:13 No:03 ,June 2013

15. Mosleh Maiet AI-Harthi, Sherif Salama Mohamed Ghoneim ," Measurement the Earth Surface Potential for Different Grounding System Configurations Using Scale Model ",International Journal of Electrical Engineering & Technology (IJEET), Vol 3, Issue 2 , July-September,pp. 405-416, 2012

16. Kaustubh A. Vyas and J.G. Jamnani, "Development of IEEE Complaint Software 'Economical Substation Grounding System Designer' Using MATLAB GUI Development Environment", International Journal on Electrical Engineering and Informatics, Vol. 4, pp. 335-346, 2012.

17. M. Soni, Abraham George, "Cost Effective Grounding Grid Design for Substation", International Journal Scientific & Engineering Research,vol.6, Issue 8, Aug 2012

18. R Kumar, K Bansal , D K Saini, I P S Paul, " Two Layer soil modeling and optimal designing of Grounding System of High Voltage Air Insulated and Gas Insulated Substation using MATLAB GUI", Water and Energy International, 2015, 88(1), pp. 21-26.

19. R Kumar , K Bansal, D K Saini, I P S Paul , "Importance and Need of Accurate Modelling of Soil of High Voltage Substation for Optimal Designing of Grounding System", IJEC 2015, 7(1), pp. 29-44

20. R Kumar, K Bansal, D K Saini , I P S Paul , " Development of Empirical Formulas and Computer Program with MATLAB GUI for Designing of Grounding System in Two Layer Soil Resistivity Model for High Voltage Air Insulated & Gas Insulated Substations" IJST, Volume 9, Issue 28, July, 2016

21. Online help of MATLAB for GUI development available at: "http://www.mathworks.in/help/techdoc/creating guis/bqz6p81.html ".

BIOGRAPHICAL DETAILS OF AUTHORS

Rajesh Kumar obtained the B. Tech. & Master of Engineering (ME) degrees in Electrical Engineering from Delhi College of Engineering, University of Delhi, India in 1999 and 2003, respectively. He is also certified Energy Manager and Auditor. He has worked in 400 KV and 220 KV Substation for more than 13 years in Delhi Transco Limited (DTL). He has also worked as Deputy Director (Transmission and Distribution) in Delhi Electricity Regulatory Commission (DERC) for 03 years and 06 months. Presently he is working in the OS department of Delhi Transco Limited (DTL). His research interests include high voltage technology, grounding system, protection system, computer application and power distribution automation

Dr Kamal Bansal is a Professor in University of Petroleum and Energy Studies, Bidholi, Dehradhun, India. He obtained his B. Tech (Electrical Engineering) degree from Malaviya Regional Engineering College, Jaipur & M. Tech (Power System) from Regional Engineering College Kurukshetra and completed his PhD in "Analysis and Redesigning of watermills for sustainable development of Uttarakhand". He is a BEE Certified Energy Auditor and professional member of Energy Institute U.K.

Dr. Devender Kumar Saini is an Assistant Professor in University of Petroleum and Energy Studies, Bidholi, Dehradhun, India. He obtained his B.Tech (Electrical Engineering) degree from LIET, Alwar, University of Rajasthan, in 2006. He obtained M.Tech. (System and control) and PhD from IIT Roorkee in 2009 and 2012 respectively.

Dr. IPS Paul obtained B.E.(Mech) from MACT, Bhopal, P.G. Diploma in Energy Management-Italy, M.B.A. from Delhi University & PhD from IIT,Delhi. He started his career as Assistant Executive Engineer in PSEB, Patiala & worked there for 3 years & 6 months. He further joined NTPC, Badarpur as a Senior Engineer / Engineer & provided his services for 3 years. He further joined NPTI(PETS) New Delhi as Deputy Director/Director & worked there for 10 years. He further joined CPRI & worked as Joint Director/ Additional Director/ Additional Director Scientist-G for 16 years. Currently, he is working as Professor M. E., DEAN-R&D at BBDIT, HRIT. He has published 19 papers at National and International levels.

International Journal of Engineering Applied Sciences and Technology, 2016
Vol. 1, Issue 11, ISSN No. 2455-2143, Pages 77-88
Published Online September-October 2016 in IJEAST (http://www.ijeast.com)

STUDY ON CHARACTERISATION OF INDIAN DAIRY WASTEWATER

Rakesh Mehrotra, A. Trivedi
Dept. of Civil Engineering, Delhi Technical University

S.K.Mazumdar
Former Professor, Delhi College of Engineering, Delhi

I. INTRODUCTION

With the growing consciousness of nutrition and health, organized efforts to enhance milk production has given rise to large scale production, processing and distribution of milk through a large number of dairies. With the objective of hiking milk production in India, a program named "Operation Flood" was started with the assistance of International agencies. To give initial thrust to dairy development activities "National Dairy Development Board." was established in 1970. Under the programme, Operation flood I (1970-80), Flood II (1980-85), Flood lIl (1985-90) significant achievements have been made and progress is on in improving per capita availability of milk and its products all round the country. To day, most of the large cities are receiving their milk supplies through large dairies. Gujrat state, for example, has well developed. dairies - mostly processing centres, some organised on co-operative lines .Anand experiment revolutionized the procurement, storage and distribution of milk. It has brought in millions of small dairy farmers all over the country into a vast network of co-operatives. There are more than 1,01000 milk co-operatives functioning in the country (Govt of India,2002)helping in production and marketing.

The dairy Industry in India has grown from an almost unorganized into a vastly complex organized industry of large magnitude during the last 45 years. India with an animal milk production of 84.5 million tonnes in 2002 and with a 4-5 % annual growth has an expected milk production of 155.2 million Tonnes in 2016-17.India has since long been ranking first in the world in terms of milk production.

India has a unique pattern of production, processing and marketing/consumption of milk, which is not comparable with any large milk producing country. Only a small part of milk produced in India is processed. The organized sector (large scale dairy plants) processes about 25-28 million tonnes annually, which is 18-20 per cent of the total production. (140)/ 3,800 LLPD of milk. Organised sector is expected to grow to 25% of total production by 2018.

In the organized sector, there are 1000+ dairies(678, March 2002) in the Co-operative/Government and private Sector which process nearly 100 million liters of milk per day (ww.thehindubusinessline.com ,27 oct / 21 Dec 2015)one single organization with brand AMUL has presently an aggregate national processing capacity of 28.0 million litres per day & expected to be 32 million litres per day by 2017. Most of the Dairy plants are in the co-operative or private sector. The processing capacity is expected to grow many fold through external investments in the future to cater to a large market in the Indian cities Besides this there are many small dairies all around the country.

Effluents are generated in dairy plants, from washing of tankers/cans/storage tanks, cleaning in place of processing equipment, floor washing, spoilage, manufacturing wastes & other wastes. Hygienic requirements of the industry result in huge amount of waste water .Nearly 2% of the milk handled in a dairy goes out as waste water & the volume of waste water generated is 2- 10 time the milk processed. The dairy effluents have a high organic content and are readily putricible resulting in high BOD & COD. Therefore dairy industry with its wide dispersal and high pollution potential requires due attention.Dairy wastes are generally dilution of milk products. The strength of the waste varies very widely depending upon the products. From literature it is seen that the dairy wastes from U.S.A has COD in the range (80-95000) mg/1 (Marshall &Harper, 1984). A typical strength from most of the western countries will be a COD of 4000 mg/l. In India, however the dairy industry COD range is much lower at (800-500)mg/l.

In view of the current Water Pollution Control regulations, the dairy industry has to comply with the norms for effluent discharge. Therefore characterization, appropriate treatment and disposal

International Journal of Engineering Applied Sciences and Technology, 2016
Vol. 1, Issue 11, ISSN No. 2455-2143, Pages 77-88
Published Online September-October 2016 in IJEAST (http://www.ijeast.com)

of Dairy effluents are an important concern. There is a considerable difference between dairy effluents of USA, Europe, rest of the world and Indian dairies, because of portfolio of dairy products produced and recycle/reuse /water conservation practices. Present Study is aimed at characterization of Indian dairy effluents.

II. MILK

2.0.1 Composition of milk

Milk fat is a complex mixture of triglycerides (98-99%) phospholipids (1-2%) and traces of sterols, carotenoids and the fat soluble vitamins A,D,E and K exists as an oil in water emulsion in small globules 2-5(μm) in the milk serum. The milk proteins. comprise two major classes, the casein and whey proteins. The caseins (80% of the total proteins) are of four major types namely α,β,k,γ caseins.The casein exists mainly as suspended agglomerates known as micelles. The micelles are a colloidal calcium phosphate complex containing all types of casein and about 7% inorganic material. Together with lactose and minerals they form the milk serum in which the milk fat globules and casein micelles are suspended. Lactose, a disaccharide molecule, is a carbohydrate comprising one molecule of glucose and one of galactose. The major salts in the the mineral component are those of calcium ,sodium, potassium and magnesium which occur as phosphates, chlorides, nitrates, and caseinates, sulphur, zinc, rubidium, silicon, bromine, aluminium, iron etc. are also present in trace quantities.A typical composition of milk in three countries is shown in table 2.0.1.1

Table2.0.1.1 Composition in % (Barnes, 1984 ; Mohan Rao *etal.,* 1972)

	USA	NEWZEALAND	INDIA
Milk fat	3.6	4.7	3.9
Protein	3.5	3.6	3.2
Lactose	4.9	5.0	5.1
Minerals	0.7	0.75	0.6
Total Solids	13.0	14.30	9.5

The variation in composition for different classes of milk is as in the following Table 2.0.1.2& 2.0.1.3

Table 2.0.1.2 ,Chemical Composition (%) of milk of different animal species (Sukumar De,1980)

Species	Water	Fat	Protein	lactose	Ash
Buffalo	84.2	6.6	3.9	5.2	0.8
Cow	86.6	4.6	3.4	4.9	0.6
Goat	86.5	4.5	3.5	4.7	0.8

Table 2.0.1.3 Composition (%)milk &bye-products in India (Mohan Rao *etal* ., 1972)

	Protein	Fat	Lactose	TS*	OS**	pH
Whole milk	3.2	3.9+	5.1	9.5	8.7	7.2
Skim milk	3.3	0.1	5.3	9.4	8.7	7.2
Butter milk	3.4	0.4	4.3	6.9	6.3	3.5
Whey	0.9	0.3	4.9	12.9	12.2	10.3

@Casein about 80 %., *Total Solids **Organic Solids +Cow Milk

International Journal of Engineering Applied Sciences and Technology, 2016
Vol. 1, Issue 11, ISSN No. 2455-2143, Pages 77-88
Published Online September-October 2016 in IJEAST (http://www.ijeast.com)

2.0.2 Milk Products

- Flavoured milk
- Whole milk & skimmed milk powder.

Indian products such as Khoa, Paneer, Curd, Srikhund, Rosgulla & milk cake etc.A variety of products can be made from milk. The most common products manufactured in India are the following

- Homogenised and pasteurised milk
- Skim milk
- Butter, Butter milk and Ghee
- Cheese
- Casein
- Toned milk

2.1 Dairy product manufacture

The milk is transferred to storage tanks which are usually insulated tanks,and refrigerated.

- Thermization:

A technique used by some large dairies, in which milk is given a mild heatCommon procedures used in manufacture of all dairy products include: (Barnes, 1984)

- Receiving of milk:

From the farm or receiving station the milk is delivered in cans or tanks, although cans are much less common to-day.

- Storage of milk:

Treatment (63-65^{o}C) for 15 sec. immediately after delivery so that it can be stored in silo tanks for four hours or even days without deterioration of quality.

- Pasteurization:

A heat treatment designed to kill non-spore-forming or vegetative pathogenic micro-organism to a level which will minimize the adverse effects on milk quality. Older plants use batch pasteurization, heating of Milk to 63°C in a vat holding for 0.5 hours. Modern plants use high temperature short time {HTST;72- 75°C for 15Sec} or ultra high temp (UHT :135-150°C For 5-3 Sec) continuous techniques.

- Clarification

It is a operation to get rid of foreign particles and sediments .Centrifugal force about 6000 g is applied for skimming the cream from the milk.

- Standardization

It is the standardization of the milk fat concentration, by separating a part of the milk, removing the cream and returning the skim milk to storage tank

- Homogenization

Process to reduce the size of milk fat globules so that they will remain dispersed instead of rising to form a cream line on the surface .

Major milk products:

Market milk:
Market milk (Also known as liquid milk or drinking milk) is a liquid product made
from whole milk, skim milk and cream and is directly used by consumers.
Cultured products:
Cultured products that are frequently manufactured include yoghurt, acidophilus milk, kefir, cultured buttermilk. Koumiss, sour milk and sour creams. The viscosity of cultured product is very high and a considerable quantity of product remains on the surface. of the processing equipment with subsequent high waste loads in rinsing and cleaning solutions. The wastes are of relatively low pH(4.5-4.7).
Butter:
Butter is essentially the fat of milk and is available in two main `categories', sweet cream butter and acidulated cream butter. Butter may also be salted or unsalted. Whey butter is manufactured from the cream separated from the whey after cheese making, The principal constituents of a normal salted butter are milk fat (80-82 %), water (15.5-17.5%), salt (1-2%) and small quantities of milk proteins, calcium, phosphorus and vitamins.
Cheese:
Cheese is the fresh or ripened product obtained after coagulation of milk or cream and on separation of whey. Cheese contains proteins, milk fat, water and minerals in varying amounts.
Dried milk:
A major method of processing milk is to remove the water to produce a powder containing 2.5-5.0% moisture. The most common method is to remove water from clarified standardized milk by evaporation followed by drying. Whole milk powder is produced by standardised whole milk, skim milk powder from the skim milk remaining after cream separation from whole milk and butter milk powder is made from the butter milk which is produced during butter making from cream.
Toned milk:
It is obtained by addition of water and skim milk powder to whole milk to bring down the fat content, while still maintaining the non fat solid concentration. Toned milk can also be composed by using Cream/ fat with appropriate quantity of skim milk/ whole milk or powder.

International Journal of Engineering Applied Sciences and Technology, 2016
Vol. 1, Issue 11, ISSN No. 2455-2143, Pages 77-88
Published Online September-October 2016 in IJEAST (http://www.ijeast.com)

2.2 PROCESS EQUIPMENT**:**

Equipments common to most processes include storage tank, processing vessels, buffer or balance tanks, heat exchanger for heating & cooling, pumps piping and associated valves, control equipment, instrumentation and equipment required for packaging, water supply and treatment, steam raising and compressed air.

2.3 UNIT OPERATIONS

Unit operations in dairy processing (Barnes, 1984)

• Transportation of fluids • Mechanical separation• Mixing •Evaporation•Heat transfer • Gas absorption.• Drying • Leaching• Distillation • Crystallization• Extraction• Filtration• Humidification • Reverse osmosis • ultrafiltration • Electrodialysis•Ion - exchange • Fluidisation• Size reduction • Settling• Enzyme reaction • Fermentation •Centrifugation

2.4 DAIRY PLANT WASTES

Dairy food plant wastes are generally dilutions of milk or milk products together with detergents, sanitizers cleaning chemical such as caustic soda, nitric acid, lubricants, washing from tank trucks and domestic wastes. The wastes are characterized by a relatively high organic concentration and high initial total oxygen demand.

2.4.1 Sources of dairy plant wastes

The process and other sources of wastes that have a significant effect on the liquid effluent from dairy plant operations include:

- Rinsing and washing of bulk tanks or cans in receiving operations.

- Rinsing of residual product remaining in or on the surfaces of all pipelines, pumps, tanks, vats, processing equipments& filling machines etc.

- Washing of all processing equipments.

- Water-milk solids mixture discharged to drain during start up, product changeover and shutdown of pasteurisers, heat exchangers, separators, clarifiers, and evaporators.

- Sludge discharge from clarifiers.

- Fines from cheese and casein operations.

- Spills and leaks due to improper equipment operation and maintenance, overflows, freezing on and incorrect handling.

- Wilful waste of unwanted by-product (e.g. whey, butter milk)or spoiled materials

- Loss in packaging operations through instrument break down and broken packs

- Lubricants from equipment, stackers, and conveyors.

- Washing from the outside of tank trucks including dirt, and farm debris.

- Dust from coal and wood fuel and spills of fuel oils.

- Powder deposits from discharges from dryers.

- Dust from coal and wood fuel and spills of fuel oils

- Ash from boilers

- Water and boiler treatment chemicals

- Chemicals from the regeneration of ion-exchanger resins.

2.4.2 Composition of dairy fluids and products

If domestic wastes are excluded, the principal contaminants of dairy wastes are milk, milk fraction and milk products. It is generally conceded that 90% of organic loading (BOD_5) in dairy processing wastes come from these materials. Estimates of the average daily equivalent quantity of milk in the wastes vary from 0.4 to 6% of the milk received at the plant. The knowledge of the composition of milk dairy fluids and dairy products and BOD/ COD.(Table, 2.4.2.1 , 2.4.2.2 are a helpful guide for determining the the typical composition of dairy waste .The BOD: COD for raw Dairy waste is mostly 0.5- 0.7. Milk and its products are organic materials and the organic waste parameters normally measured include the biochemical oxygen demand ($B.O.D_5$), chemical oxygen demand (C.O.D) and total organic carbon (T.O.C). The whole milk has a high BOD (table 2.4.2.1), therefore ,even dilute milk solutions have a marked polluting effect. The major constituents contributing to BOD of the dairy waste are lactose , milk fat , protein and lactic acid. The reported values are 0.65, 0.89, 1.03 and 0.63 kg BOD/kg respectively. The ratio of COD and TOC to BOD varies considerably with the chemical composition of the milk and wastes. Ratios established in one Dairy can not be used in another plant, values as high as 0.8 that are outside the range 0.5- 0.7 probably indicate solutions. The values that are outside the range 0.5- 0.7 probably indicate contamination by refrigerant leaks or the presence of some compound toxic to BOD test.

International Journal of Engineering Applied Sciences and Technology, 2016
Vol. 1, Issue 11, ISSN No. 2455-2143, Pages 77-88
Published Online September-October 2016 in IJEAST (http://www.ijeast.com)

Table 2.4.2.1 B.O.D. & C.O.D of some dairy fluids (EPA 1971 in Barnes, 1984)

	B.O.D (mg/l)	C.O.D. (mg/l)
Skim milk	67000	100,000
Whole milk	104000	210.000
Cream	399000	860,000
Cultured butter milk	64000	n.a.
Ice-cream	292,000	n.a.
Sweet whey	34000	75000

Table2.4.2.2 Some values of BOD / COD (Barnes, 1984)

	BOD / COD
Whole milk	0.69
Skim milk	0.63
Butter milk	0.66
Whey	0.52
Milk fat	0.79
Casein	0.46
Lactose	0.53
Whey protein	0.23
Chedder cheese	0.33-0.78
Dairy waste (raw)	0.5- 0.48 & 0.45- 0.8
Treated effluent	0.15 -0.35

2.4.3 Composition and characteristics of dairy plant wastes:

2.4.3.1 General characteristics of dairy wastewaters

Major effluents are generated in dairy plants, from washing of cans/tankers, cleaning in place of process equipment(such as pasteurizers, separators, pipelines, chillers, vats, storage tank and silos, sachet filling machines),floor washings, spillages/leakages of milk/milk products, boiler blow down , softner regeneration water & bleed from the condenser etc. Dairy processing effluents are generated in an intermittent way (because of batch operations and product changes) and the flow rates& characteristics of these effluents change significantly Section /unit wise.

Dairy industry produces different products, such as Processed milk, butter/Ghee , yogurt, ice-cream, and various types of desserts and cheese, the characteristics of these effluents also vary widely both in quantity and quality, depending on the type of system and the methods of operation used .

Significant fractions of the organic components and nutrients in dairy waste streams are derived from milk and milk products. Dairy wastewater contains milk solids, detergents, sanitizers, milk wastes, and cleaning water. It is characterized by, high concentrations of easily degradable carbohydrates(mainly lactose) and lipids as well as less biodegradable proteins- present in various forms as organic nitrogen (proteins, urea, nucleic acids) or as ions such as NH_4 , NO_3 &NO_2. Phosphorus is found mainly in inorganic forms; as orthophosphate and poly-phosphate , as well as organic forms . Concen-trations of suspended solids (SS) and volatile suspended solids (VSS) are also used to evaluate wastewater strength. Suspended solids in dairy wastewaters originate from coagulated milk, cheese curd fines or flavoring ingredients . Concentrations of selected elements, namely sodium (Na), potassium (K), calcium (Ca), magnesium (Mg), iron (Fe), cobalt (Co), nickel (Ni) and manganese (Mn), are also found. Particularly high Na concentrations point out the use of large amount of alkaline cleaners at dairy plants. The concentrations ofheavy metals, such as copper (Cu), nickel (Ni) and zinc (Zn) are also reported .

Significant variations in COD and BOD have been

International Journal of Engineering Applied Sciences and Technology, 2016
Vol. 1, Issue 11, ISSN No. 2455-2143, Pages 77-88
Published Online September-October 2016 in IJEAST (http://www.ijeast.com)

reported by various investigators of dairy wastewater. The total COD of dairy wastewater is mainly influenced by the milk, cream, or whey . The pH varies in the range of 4 –11,whereas the concentration of suspended solids (SS) varies in the range of 0.024–4.5g/l. Significant amount of nutrients, 14–830 mg/l of total nitrogen and 9-280 mg/l of total phosphorus are found.

Table 2.4.3.1 Characteristics of the Combined Wastes from a small size Dairy

	*Mohanrao &Subrahmanyam,1972	#Agarwal, 1981
Volume of Milk Processed l/d	12800	1500
Waste water Volume l/l of milk	3.6	4.7
pH	8.1	7.3-8.4
Totalsolids mg/l	2730	1600-2000
Volatilesolids mg/l	2,205	1070
Suspendedsolids mg/l	1,810	300-400
Volatilesuspended mg/l	1,660	----------
Alkalinity as $CaCO_3$ mg/l	220	----------
Volatileacids (CH_3COOH) mg/l	20	----------
COD mg/l	4510	800-1400
BOD_5 mg/l	3070	360-700
BOD rate constant /d	0.19	----------
Totalnitrogen mg/l	1080	150
Total P mg/l	110	25-30
Sulphates mg/l	45	----------
Fat mg/l	1390	----------

* Average values of 10 composite samples(dairy is primarily a pasteurisation and bottling plant) # Small dairy(Allahbad Military dairy farm)

Table 2.4.3.2 Characterisitics of the Individual Wastes from a Large Dairy (Mohanrao and Subramanyam, 1972) * A product oriented dairy processing about 360, 0001/d of milk. Flow: 6-8 liters of waste/liter of milk processed (All values except pH are expressed in mg/l)

.	Receiving & Pasteurizing unit	Cheese plant	Butter/Ghee unit	Casein plant	Combined Effluent
pH	8.2	6.7	7.1	7.7	8.0
Colour	White	White	Brown	Clear	White
Total Solids	3640	2300	3460	680	1690
VolatSolid%	77	29	72	62	67
S.S	1320	600	2240	160	690
Alk CaCO3	500	490	450	490	590
Oxygen Abs	437	483	90	09	120
BOD	1820	2150	1377	200	816
COD	2657	3188	3218	372	1340
Total N					84
Phosphate	10	12	2	5	12
O&G	690	520	1320	Nil	290
Chlorides	105	105	105	70	112
COD:BOD	1.46	1.48	2.33	1.86	1.65

Table 2.4.3.3 Characteristics of Individual Wastes) (Mohanrao and Subrahamanyam, 1972), Medium-Size Dairy * 60,0001 of Milk /d (* Mostly bottling, preparation of butter and casein from sourced milk).All,except pH, mg/l

International Journal of Engineering Applied Sciences and Technology, 2016
Vol. 1, Issue 11, ISSN No. 2455-2143, Pages 77-88
Published Online September-October 2016 in IJEAST (http://www.ijeast.com)

	ButterWashings	Rejected Milk	Milk Bottling Waste
pH	4.7	6. 6	7.8
Alkalinity(to pH 8.3	Nil	Nil	Nil
Alkalinity (pH4.50)	100	10,350	256
Total Solids	13,820	85,920	2560
Total volatilesolids	10,640	75,500	2000
Fixed Solids	3,180	10,420	560
Suspended solids	5,112	34,904	1380
Volatile S.S	4,832	33,280	1220
BOD at 37°C	10,000	62,000	620
COD	16,000	88,000	1000
Ca++	180	900	140
Mg++	12	474	49
COD:BOD	1.60	1.33	1.61

Table 2.4.3.4 Characteristics of wastewater mother dairy(Delhi) , Delhi milk scheme(Naresh kumar,1992)&UDSDairy, Ujjain (Datar & Kale ,1997)

ITEM	RAW EFFLUENT			TREATED EFFULENT		
	MOTHER DAIRY	DMS	UDS	MOTHER DAIRY	DMS	UDS
Avg. flow m^3/d	800 -900	1600-1800	600	----------		----------
.BOD_5 mg/l	1200	1000	1180	10	10	68
COD mg/l	2500	2000	2328	100	36	359
Suspended Solids mg/l	700	600	693	10-30	17	122
Dissolved Solids mg/l	1500	1200	3738	1500	----	204
pH	7.0-7.5	12	7.5	7.5-8.0	7.5-7.8	7.28
O&G mg/l	40-50	350	293	Negligible	3.0	18
Total Nitrogen mg/l	70-80	25		30-40	-	
Phosphate mg/l	10-15	30		7-8	-	

Table 2.4.3.5 Characteristics of wastewater of Five Indian Dairies

International Journal of Engineering Applied Sciences and Technology, 2016
Vol. 1, Issue 11, ISSN No. 2455-2143, Pages 77-88
Published Online September-October 2016 in IJEAST (http://www.ijeast.com)

ITEM	RAW EFFLUENT A	B	C	D	E	TREATED EFFULENT A	B	C	D	E
Avg. flow m^3/d	60	100	2000	650	480					
.BOD_5 mg/l	150	810	820	1150	1400	30	30	40	152	-
COD mg/l	400	1500	2100	2500	1700	220	250	150	385	
Susp.Solids mg/l	350	500	450	1257	450	Nil	100	60	-	
Total Solids mg/l	750	1000	1800	3750	1500	-	-	-	-	-
pH	5-9	7.7-8.	9- 6.5	9.3	7-8.5	7	5.5-9	6.5-7	7.3	-
Oil & Grease mg/l	50	400	100	130	--	10	10	10	10	-
Total " N" mg/l	-	-	-	-	160				42	-
Total PO_4 mg/l	-	-	-	-	16				30	-

Dairy A: Sri Ganga Nagar Zila Dugdh Utpadak Sehkari sangh, Hanumangarh JN;Dairy B : Udaipur Dugdh Utpadak Sehkari sangh, Udaipur;Dairy C : Sabarkantha dist Co-operative milk producers Union, Saber Dairy;Dairy D: Banglore Dairy, Housur Road;Dairy E: Feeder Balancing Dairy, Patna (Roy,B etal,1996)

Table 2..4.3.6 Combined Wastewater Characteristics of Dairy (CPCB, 1993)

Country Parameter	U.S.A	New Zealand	Milk Processing Lit	CPCB	India Integrated Dairy Lit	CPCB	India Chilling Plant Lit	CPCB
BOD_5	40- 48000	90-12400	1100	657-1016	236-1540	1634-4953	290-4926	55-5034
COD	80-95000	180-23000	2400	1341-2195	502-2290	3800-8631	520-6318	121- 6877
SS	244500	7-7200	850	538-657	160-810	89- 4953	200-618	36-899
TS	135- 8500	-	2100	--	902-1340		-	
Nitrogen	1-180	1-70	-	50.25-126.2	84-105	96.32	-	49.25-72.5
carbohydrt	250-930	-	-					
Fat	35-500	0-2100	-		-	100-6070	-	
Calcium	55-115	-	-					
Sodium	60-810				105			
Potassium	10-160							
Phosphorus	9-210	4-150	110	2.6-4.8	12	0.3-0.8	-	0.14-0.2
Chloride	48-1930				104			
Temp ^{0} C	18-55	11-72						
pH	4.4-9.4	3-13.2	7.3	6.6-6.9	7.5-8.0	5.6-6.8	3.2-7.8	2.9-10.7
O&G	-	-	150		194-601	280-2207	56-426	5-176

International Journal of Engineering Applied Sciences and Technology, 2016
Vol. 1, Issue 11, ISSN No. 2455-2143, Pages 77-88
Published Online September-October 2016 in IJEAST (http://www.ijeast.com)

Table 2.4.3.7: Characteristics of Indian dairy industry wastewaters (in mg/l, except pH)

WASTE TYPE	COD	BOD	pH	TSS	TS	**REFERENCES**
Dairy effluent, Karnataka	1900-2700	1200-1800	7.2-8.8	500-740	900-1350	Deshannavar, *et al* .,2012
Bhandara Co- operative Dairy wastewater, Mah	1400-2500	800-1000	7.1-8.2	1045-1800	1100-1600	Gotmare, *et al* .,2011
Dairy industry wastewater, TN	2100	1040	7-8	1200	2500	Arumugam *et al* .,2008
(Whey) Warna milk dairy,Kohlapur	71526	20000	4.1	22050	56782	Deshpande ,*etal.*, 2012
Aavin, TN dairy, industry washwater	2500-3300	-	6.4-7.1	630-730	1300-1400	Sathyamoorthy *etal.*, 2012
Cuddalore district Co-operative Dairy Industry Ltd Sethiyathope-TN	3786	1112	8.45	514	2451	Dhanam,2009
Jalgaon Jila Dudh utpadak Sangh mdt, Jalgaon	790-810	530-585	6.5-6.7	696-729	2532-2608	Swati Patil *etal.*, 2014
Yashodhara Milk & Food Products MIDC, Amaravti	2144	1295		680	-	Kadu *etal.*,2013
Kolhapur Zillah Sahakari DhudhUtpadak Sangh Ltd., Gokul Shirgaon, Kolhapur	1330-2100	1200	7.26-8.8	650	-	Bhavsar Swati R *etal.*,2013.
Mother Dairy,Yelahanka, Bangluru	1172	635	8.33	450	1183	Manu,*etal.*,2011
Dairy sample 2002 in Chennai	300-1630	260-490	4.5-9	20-700		Noorjahan *etal.*,2004
Kolhapur dairy, Mah	1448	672	9.9	267	5950	Shivsharan *etal.*,2013a
ShivamrutDudhMaryadit, vijaynager	1457-1599	548-650	9.52-10.06	237-262.6	1373-1876	Shivsharan *etal.*,2013b
AP dairy, Hyderabad	1500-3000	350-600	5.5-7.5	250-600	-	Sarkar *etal.*,2006
Sangam Dairy,Vadlamudi Guntur District,AP	2500	1200	6.23	145	1990	Y.Harika *etal.*,2014
Government Milk Scheme of Dairy Ind, Distt. Nagpur	1243	480		420	-	Chaiudhari *etal.*, 2010
Parag Dairy(Lucknow producers coop milk union)	2580.00	1139.00	6.93	1233	-	Singh *etal.*,2014
Shakti Dairy at Kashti Tal Shrigonda .	1400	890	8.2	-	-	Pachpute *etal.*,2014
Jaipur Dairy	741.7-754.6	309-316.6	6.3-6.6			Sharma, N *etal.*, 2013

International Journal of Engineering Applied Sciences and Technology, 2016
Vol. 1, Issue 11, ISSN No. 2455-2143, Pages 77-88
Published Online September-October 2016 in IJEAST (http://www.ijeast.com)

Pune Dairy	2332-2398	1210-1268	6.03-6.06	601.6-626.6	1964-2342	Porwal *etal.*, 2015

Table 2.4.3.8 Characteristics of International dairy industry wastewaters (composition in mg/l, except for pH){Kaushik etal.,2011+}DI: Dairy Industry; CI: Cheese Industry; YB: Yogurt and buttermilk.=_ :TS = 135–18500, R: TS = 675

Type	COD	BOD	pH	TSS	VSS	TN	TP	Cl	Fats	References
DI$^{=-}$	80–95000	40–48000	4.5–9.4	24–4500	–	15–180	12–132	48–559	–	Rico Gutierrez et al., 1991
DI^{-R}	4000	2600	8.0-11	–	635	55	35	–	400	Kasapgil et al., 1994
DI	4000	2000	–	800	–	60	–	–	–	Koyuncu et al., 2000
YB	1500	1000	7.2	191	–	63	–	–	–	Koyuncu et al., 2000
CI	4430	3000	7.32	1100	–	18	14	–	–	Monroy et al., 1995
DI	1745	–	–	400	355	75	9.1	–	–	Koyuncu et al., 2000
DI	980–7500	680–4500	–	300	–	–	–	–	–	Kolarski & Nyhuis, 1995
CI	–		4.7	2500	–	830	280	–	–	Gavala et al., 1999
DI	18045	8239	–	7175	–	329	–	593	4890	Arbeli et al. 2006
DI	2000-6000	1200–4000	8.0–11	350–1000	330–940	50–60	–	–	–	Ince, 1998a
DI	430–15200	650–6240	4.7–11	250–2750	210–890	14–90	–	–	160–1760	Passeggi et al., 2009
DI	2800	1600	–	–	–	140	30	–	–	Schwarzenbeck etal.,2005
DI	4500	2300		800		60			350	Koyuncu et al., 2000
DI	3383 ± 1345	1941± 864	7.9 ± 1.2	831± 392	746± 214	51 ± 5.7	22 ± 4.8		263± 23	Tawfik et al., 2008
DI	2500-3000	1300-1600	7.2-7.5	8000-10000	800-1000	-	-	-	20-70	Qazi et al., 2011
CI	80000-90000	53333-60000	6.0	8000-11000		600-1000	-	-	500	Kabbout et al., 2011

2.4.3.2 Characteristics **of Dairy Wastewaters in Present Study**

The nature of wastes generated by various processes operated by dairy industry reflects the overwhelming effect of the wasted milk and dairy products Characteristics. However, volume of waste water from different dairies seems to vary (2-8) times the volume of milk processed depending upon the

International Journal of Engineering Applied Sciences and Technology, 2016
Vol. 1, Issue 11, ISSN No. 2455-2143, Pages 77-88
Published Online September-October 2016 in IJEAST (http://www.ijeast.com)

process used, product made, care taken in the use of water, housekeeping and quantity of water available.

The characteristics of waste water are shown in table 2.4.3.1to 2.4.3.8. The characteristics of dairy waste water from New Zealand, U.S and India are presented in table2.4.3.6. Similarly table 2.4.3.8 details dairy waste water from all over the world.

It is found in table2.4.3.6 that there is a wide difference between the characteristics with respect to BOD, COD, S.S Close examination confirms that fat and grease content in Indian Dairy waste is high in comparison with U .S.A and New Zealand. However, the BOD and COD of Indian Dairy waste is much lower. From table 2.4.3.8, it is observed that Rico Gutierrez et al., 1991, Kolarski & Nyhuis, 1995, Arbeli et al. 2006 have reported about High strength dairy wastes with BOD:(40-48000)and COD : (80-95000). The general range for BOD and COD in case of western countries is BOD-(1000-6250) and COD-(1500-15000), which is much greater than Indian dairy Effluents.

- Among Indian dairies, from table 2.4.3.3, it is observed that the waste water characteristics vary widely for Butter washing, milk bottling and rejected milk streams. For butter washing stream COD & BOD are high because some fats and other volatile solids get washed out. Table 2.4.3.2 shows 1320 mg/l O&G in effluent, even the pH is slightly acidic. For rejected milk (curdled with acidic pH)all the constituents will be going in effluent stream, therefore the COD, BOD and Suspended solids are nearly equal to sourced milk diluted with wash water.

  There are some Integrated dairy plants producing combined effluents from sections that may include milk pasteurization, Creamery, butter/ ghee production, flavoured milk/ yogurt production, cheese production, Ice cream unit besides Indian sweet dishes. Characteristics of Combined effluents from plants with variety of products will vary with the wastes being released from specific product manufacturing.
- In the case of milk receiving, pasteurisation and milk bottling sections, the only milk loss is in cleaning/washing vessels. Therefore, the COD, BOD are 1-2 % of milk COD,BOD and remains in range of BOD- (500-3000) mg/l and COD-(1000-4500) mg/l (depending upon quantity of wash water used) this is supported with data of table 2.4.3.1-2.4.3.7. In Indian dairy industry market milk production is 80% of all the milk processing.
- Deshpande etal (2012) has reported about Cheese production unit in Kolhapur (table-2.4.3.7) discharging Whey and found BOD and COD at 20000mg/l and 71500 mg/l respectively.
- Most Indian dairies are primarily a pasteurisation and milk bottling/ packing plants with some producing cream/ butter/ghee. There is some producing skim milk powder besides producing cream/ butter/ghee. Dairy plants producing Yogurt and other milk products like Ice cream are also there. Production of Cheese is very uncomm on. However, there are some large plants which have production facility for variety of milk products

III. CONCLUSION

- Indian dairy waste water is having of BOD- (500-3000) mg/l and COD- (1000-4500) mg/l (depending upon quanity of wash water used)
- The dairy waste water from USA, Europe and New Zealand etc are stronger because of the product mix that include cheese-processing wastewater and other processed milk products.
- In India more than 80 % of the milk produced does not go to organized Dairy processing Plants .Most Indian dairies cater to production of Market milk (pasteurized milk in various grades – Full cream, standardized, Toned etc). In keeping with milk demand in times of low fresh milk production, powder milk and butter are used for milk blending to produce larger volumes of market milk. There is some Production of butter/Ghee, milk powder during milk flush seasons (when milk is surplus).
- In organized Indian dairy plants Production of Yogurt, ,lassi, butter/ ghee, Khoya, Cheese, Ice cream, sweets and other value added products is very small. The composition of effluents from such units reflect the wastes of product manufacture and could have high O&G, cream, sugar or whey contents . As milk pasteurization is the basic operation/ process that is essential in all Dairy processing plants(exceptChillingplants) there is additional pollutant load with every additional dairy product manufacture. In a typical a pasteurisation and milk bottling/ packing plants the COD is not likely to be above 2500 mg/l and the BOD not above 1500 mg/l. Whereas , in an Integrated dairy processing plant the combined effluent could reach a COD- 10000 mg/l and BOD – 5000 mg/l, depending upon product mix.

International Journal of Engineering Applied Sciences and Technology, 2016
Vol. 1, Issue 11, ISSN No. 2455-2143, Pages 77-88
Published Online September-October 2016 in IJEAST (http://www.ijeast.com)

IV. REFERENCES

Agarwal, I.C . and Suria Pandian , P.S. (1981). Removal of dairy waste organics by rotating biological contactors. *Indian Journ. Environ. Hlth*., Vol.23(1), pp. 27-40

Barnes, D., Forster, C. F. and Hrudley , S. E {eds}.(1984) *Surveys in Industrial Waste water treatment*, Vol 1, pp 296-376. Pitman Adv Publishing Ltd, London

Bhavsar, Swati R., Pujari, Vedavati R. and Diwan, V.V(2013) Potential of Phytoremediation for dairy wastewater treatment *IOSR Journal of Mechanical and Civil Engineering (IOSR-JMCE).*, vol**6**, PP: 16-23

Chaiudhari, Dipali. H. and Dhoble, R.M. (2010) Performance evaluation of effluent treatment plant of dairy industry ,*Current World Environment* .,Vol. **5(**2), 373-378

Comprehensive Industry document- Dairy Industry,(!993) *CPCB*, N Delhi

Datar, M.T and Kale, S.B. (1997). Performance of a Dairy Effluent Treatment Plant.*Indian Journ. Environ. Hlth*., Vol 39 (1), pp 52-60

De , Sukumar (1980) . Outline of Dairy Technology, Oxford Univ Press

Deshannavar, U. B., Basavaraj, R. K and. Naik, Nandini M(2012)High rate digestion of dairy industry effluent by upflow anaerobic fixed-bed reactor‖, *Journal of Chemical and Pharmaceutical Research.*, **4**(6):2895-2899

Deshpande, D.P., Patil, P.J. and Anekar S.V., (2012) . Biomethanation of Dairy Waste, *Research Journal of Chemical Sciences, ISSN 2231-606X.*,Vol. 2(4), 35-39.

Gotmare, Monali.,Dhoble, R.M and Pittule A.P(2011). Biomethanation of Dairy Waste Water Through UASB at Mesophilic Temperature Range,*IJAEST* ., Vol.8 Issue 1, 001-009

Harika ,Y and Siri ,G.Sai.(2014**)** Removal Of COD Of Dairy Effluent. ,docslide.us**,** Nov 2014

Kushwaha Jai Prakash, Srivastava Vimal Chandra & Mall Indra Deo (2011): An Overview of VariousTechnologies for the Treatment of Dairy Wastewaters, Critical Reviews in Food Science and Nutrition, 51:5, 442-452

Manu K. J., Mohana V. S. and Ganeshaiah K. N(2011)Effluent Generation by the Dairy Units: Characterization and Amelioration forIrrigation*International Journal ofResearch in Chemistry and Environment*.,Vol. 1 Issue 2 ,(173-182)

Mohanrao, G.J and Subramanyam (1972) Sources, Flows and characteristics of Dairy Waste water. *Indian Journ. Environ. Hlth* ., Vol.14(3), pp. 207-217

Pachpute A.A., Kankal S. B, Jadhav,M.V(2014**)** Use of Artificial Wetland for Treatment of Dairy Industry Waste Water for Analysis of BOD and COD *International Journal of Scientific Engineering and Research (IJSER) www.ijser.in* .,Volume 2 Issue 6, pp 38-41

Roy, B and Chaudhuri, N (1996). Appropriate Treatment Option for Dairy Waste Water in India. *Jour of IAEM*, Vol 23, No.1,pp 1-8.

Sarkar, B., Chakrabarti, P.P., Vijaykumar, A., and Kale, V. (2006). Wastewater treatment in dairy industries — possibility of reuse. *Desalination* **195**: 141–152

Sathyamoorthy, G.L. and Saseetharan, M.K(2012)Dairy Wastewater Treatment by Anaerobic Hybrid Reactor – a study on the Reactor Performance and Optimum Percentage of Inert Media Fill inside Reactor *Res. J. Chem. Environ* ., Vol.**16** (1) ,pp 51-56

Shivsharan, Vishakha Sukhadev ., Wani, Minal and Khetmalas, M. B. (2013a), Characterization of Dairy Effluents byPhysicochemical Parameters.*British Biotechnology Journal* ., 3(4):575-80.

Shivsharan, Vishakha Sukhadev ., Kulkarni S W andWani, Minal (2013b) Physicochemical Characterization Of Dairy Effluents Int. J. LifeSc. Bt & Pharm. Res. Vol.2, 2No.,pp182-191

Singh, N. B., Singh Ruchi and Imam, Mohammed Manzer (2014)Waste Water Management In Dairy Industry: Pollution Abatement And Preventive Attitudes, *International Journal of Science, Environment and technology* Vol. **3**, No 2, , 672 – 683

Survey and Evaluation of Food Recommendation Systems and Techniques

Akshi Kumar
Department of Computer Engineering,
Delhi Technological University,
New Delhi, India
akshi.kumar@gmail.com

Pulkit Tanwar
Department of Computer Engineering,
Delhi Technological University,
New Delhi, India
pulkit.tan45@gmail.com

Saurabh Nigam
Department of Computer Science &
Engineering, Maharaja Agrasen Institute
of Technology, Delhi, India
saurabhnigam999@gmail.com

***Abstract* – Recommending proper food is of paramount importance for person's sound health. It is also useful in revenue generation in restaurants by recommending varied choices of food or recommending restaurants depending on the type of food to customers. In this paper, we survey the existing food recommendation engines and compare the different recommendation algorithms – Content based filtering, collaborative filtering, hybrid techniques etc. Further, we would see the challenges and limitations of each technique.**

Keywords – Food Recommendation System, Collaborative Filtering, Content Based Filtering, Evaluation, Hybrid Techniques, Comparative study, Survey.

NOMENCLATURE

TFIDF-Term frequency-inverse document frequency
SWRL - Semantic web rule language
OWL -Web Ontology Language

I. INTRODUCTION

Recommendation systems [6] provide users with a whole lot of things to choose from. Food recommender systems are of vital importance, since they allow people to choose from a lot of choices of food. Similarly, many Food Recommendation systems are based on health benefits that provide users with proper diets that are relevant for the person's good health. Food recommendation system can also help in getting personalized restaurants recommendations based on preferences of people.
Recommendation systems help users to get the personalized choices among items and ease the gap to obtain relevant information on the internet. There are many approaches used in food recommendation system, they are as follows:

- Content-based filtering approach
- Collaborative Filtering approach
- Demographic approach
- Knowledge-based approach
- Hybrid systems

In this paper, we surveyed previous research done in the domain of recommendation systems targeting food, diet and nutrients as the core. We considered research papers on food Recommendation system till September 2015, tabulated them to find inferences. Content based filtering approach is used in many of the papers that recommend users with the choices of food considering the user's circumstances. User-User, Item-Item and Dimensionality reduction personalized collaborative filtering techniques were also used in many papers that used opinion of other people to predict and recommend rather than attributed data. A numerical statistic, TFIDF was used to for information retrieval in content based filtering system and to generate the keyword vectors. A lot of previous recommendation systems used the data mining techniques. Further we described the limitations and challenges of each recommendation technique in detail.

II. CONTENT BASED APPROACH

In recommendation systems, content based filtering is one of the important techniques. It plays an important role in recommending the users with the predictions based on user's liking and interests. The main key concept for content based filtering revolves around vector space model [1].

A numerical statistics, TFIDF can be used to generate the keywords vector. The whole collection of all the possible keywords will define a content space for the recommendation system.

We can generate a vector of item keywords for all the items in the food domain. Similarly, each user can have one or more than one taste profiles which can also be described as the vector space. We can have three ways to represent an item with keywords vectors:

(i) Count the occurrence of each item.
(ii) Providing a label 0 or 1, present or absent respectively.
(iii) TFIDF

For the user profile, we can use the positive and negative weights for ratings. To update the user profiles with new ratings, we can decay the old profile and add the new ratings in it.

For recommending items in content based filtering, the prediction is done by finding the dot product of the item vector with the profile vector. This is calculated by taking the cosine of the angle found between these vectors.

III. COLLABORATIVE FILTERING APPROACH

The first use of collaborative systems was done in 1992 in Information Tapestry [2]. The term collaborative filtering was coined by Goldberg et al. [2].They designed a system for

978-9-3805-4421-2/16/$31.00 ©2016 IEEE

filtering the electronic mails. Further, from 1994 to 1995 many automated collaborative filtering recommendation systems were developed like Grouplens Movie recommendation [3] systems, Ringo movie recommendation systems [4] and Bellcore video recommender [5]. The algorithmic framework for collaborative filtering was provided by Herlocker et al. [2]. Collaborative filtering is a widespread technique of recommendation systems, generally regarded as complement to content-based filtering systems. Collaborative filtering is used massively on the internet, used in the websites like - Amazon.com, largest book store on the internet and Yelp.com, largest food recommendation system.

Like Food recommendation systems, Collaborative filtering uses the opinion of other users to predict choices to a particular user. It works by collecting the ratings of items by the users in the food domain and match them together with the user who have the same taste or taste profiles.

Pearson correlation can be used to weight the user similarity with all the correlated neighbors and the final prediction can be found by calculating the weighted average of deviation from the neighbor's mean:

$$p_{a,i} = \bar{r}_a + \frac{\sum_{u=1}^{n}(r_{u,i} - \bar{r}_u) * w_{a,u}}{\sum_{u=1}^{n} w_{a,u}} \quad (1)$$

$p_{a,i}$describes the prediction for the user *a* for item *i*, *n* is the number of neighbors and $w_{a,u}$ is the similarity weight between the user *a* and the neighbor *u* as defined by the Pearson correlation coefficient:

$$w_{a,u} = \frac{\sum_{i=1}^{m}(r_{a,i} - \bar{r}_a) * (r_{u,i} - \bar{r}_u)}{\sigma_a * \sigma_u} \quad (2)$$

IV. DEMOGRAPHIC APPROACH

Systems using this approach recommend items on the basis of user's profile by categorizing the user to the section of the users having common characteristics (by making classes) or their personal attributes like age, language, country etc. In food recommendation this approach is highly useful as users food choices significantly depends on his/her demographic profile. For example, salads may be more popular among adults than children and certain food products would be a better choice than others of the same category due availability, economic reasons etc.

- Switching: switching is done between two or more recommendation systems depending upon the need and criteria are met.
- Mixed: using two or more systems at the same time.

In food recommendation this approach is getting very popular. For example in restaurant recommendation, on holiday's, recommendations should be restaurants that are more suitable for a user to go with his/her family or friends whereas on working days, recommendations should be restaurants that are more suitable for a user to go with his/her colleagues. Hence this system might combine content based with knowledge based approach to give reasonable recommendations.

V. KNOWLEDGE BASED APPROACH

Knowledge based recommender systems recommends items using domain knowledge about how a particular feature of an item meets a specific user requirement and therefore, determining the usefulness of an item for the user**.** They find the connection between a necessity and a potential recommendation.

Types of knowledge based recommender systems are:

- Case based system: These systems recommends on the basis of similarity using a function which calculates the closeness of user needs with the item being recommended.
- Constraint based system: These systems uses predefined knowledge dataset having clear-cut set of rules on how to relate user's requirements with the features of the items.

In food recommendation, knowledge based approach has been exploited mainly in health related situation like diets for a diabetic or a cancer patient, hence knowledge about these diseases is very important in making recommendations as wrong recommendation can be harmful for the user.

VI. HYBRID RECOMMENDER SYSTEM

Hybrid recommender systems are highly popular these days. These systems combine the approaches of some of the above mentioned system into one system. The combination is so selected that one system overcomes the disadvantages of the other systems and hence improving the overall performance of the system. Different ways by which hybridization can be attained are as follows:

- Weighted: separately using different techniques and then combining their results.
- Combination of the features: Features from various different recommendation systems are extracted and are merged to form an algorithm to be used in the new system.
- Augmentation of the features: The existing system is expanded by using its output as an input feature to another system.
- Cascading of systems: similar to augmentation of features, in this, a recommendation system enhances the results produced by another.

TABLE 1**:** AUTHOR AND THEIR TECHNIQUES USED FOR FOOD RECOMMENDATION

Sr. No.	Authors Name	Publication name and Year	Approach Used	Techniques and Algorithms Used	Dataset Used	Advantages
1.	Wubin Guo et al. [9]	IEEE, July 2007	Content Based Filtering Approach	Knowledge Based Reasoning,	Restaurant menu ratings from surveys.	Improve prediction quality.
2.	Chi-Chun Lo et al. [10]	IEEE, December 2008	Content Based Filtering Approach	TFIDF, Latent Semantic Analysis (LSA), K-Nearest Neighbour.	Restaurant menu ratings from surveys	Improve prediction quality.
3.	Yoosoo Oh et al. [11]	Springer US, July 2009	Content Based Filtering Approach	Context-awareness integration, Personalised food recommendation	Data collection using sensors.	Better recommendation quality by using sensed environmental information.
4.	AsamiYajima et al. [12]	IET, September 2009	Content Based Approach	Browsing log, Recipe Retrieval	AJINOMOTO Web recipe.	Better Recommendation quality.
5.	Yoko MINO et al. [13]	IEEE, November 2009	Content Based Approach	Recipe recommendation on the basis of nutritional balance.	AJINOMOTO Recipe Encyclopaedia.	Flexibility in the control of calorie intake depending on user's schedule.
6.	Jong-Hun Kim et al. [14]	IEEE, November 2009	Content Based Approach	Personalised diet recommendation service.	Data recorder that stores XML data of user's health.	Better recommendation based on specific diet by observing the nutrition condition of users.
7.	Jill Freyne et al. [15]	ACM, New York, USA, February 2010	Hybrid Recommendation technique	Personalised diet recommendation	Opinions of 183 users for the recipes and foods over a period of 3weeks	Accuracy in Recipe Recommendation
8.	Chang-Shing Lee et al. [16]	IEEE, February 2010	Hybrid Recommendation technique	Type 2 Fuzzy ontology model	Taiwanese Food dataset	Used Fuzzy ontology, much better than classical ontology. Effectively handled and processed uncertain data and knowledge
9.	Wahidah Husain et al. [17]	IEEE,2011	Data mining	Case based reasoning, Rule-based reasoning (CAMP,PRISM and CAMPER algorithm) and genetic algorithm	User Database, Knowledge database and Food database	High accuracy of recommendations when the data set is large
10.	M. A. El-Dosuky et al. [18]	Advanced machine learning technologies and applications :first international conference (AMLTA) 2012, Cairo Egypt, December 8-10,2012	Semantic Recommender system	Hermes framework, TFIDF, binary cosine, Jaccard.	Food database(Corpus of 300 food items) provided by United States Department of agriculture (USDA)	Proposed system had a better F-measure than existing semantic recommenders at that time.
11.	Sumedh Sawant et al. [19]	2012, Stanford University	Collaborative filtering approach	k-nearest neighbors clustering, weighted bipartite graph algorithm and their combinations	Yelp Dataset Challenge data	Compared algorithms in which "cascaded clustered multistep weighted bipartite graph projection" algorithm performed best hence improved predictions quality.
12.	Shilpa Dharkar et al. [20]	IJSER ,2012	Content Based filtering, Data mining	Decision tree algorithm(ID3 and C4.5),bagging	Content database collected from external web atmosphere	An effective web data mining solution to e-commerce for personalized diet recommendations.
13.	Achmad Arwan et al. [21]	IEEE , 2013	Domain Knowledge based recommender system	OWL,SWRL,SPARQL,JAVA SWING,JENA	Database containing data of 30 patients	Showed 73% accurate recommendations
14.	E-Seok Jo et al. [22]	International journal of advancements in computer technology(IJACT),Au	Content Based filtering approach	Termite Colony algorithm(TCA) k-means	Blogs acquired from http://kitwitobes.com/clusters/feedlis	Food recommendation based on similarity levels of blog and using TCA K-means

		gust 2013			t.text	algorithm that simulates habits of termites improved processing time of clustering
15.	Irshad Faiz et al. [23]	IEEE,2014	Knowledge- Based recommender system	modeled SHADE(semantic healthcare assistant for diet and exercise) architecture using OWL based ontology, SWRL and pellet reasoning engine	USDA and myfitnesspal	Better recommendation because of simultaneous diet and exercise suggestions
16.	Shreya B.Ahire et al. [24]	IEEE computer society,2015	Demographic and knowledge based recommender system	The Decision tree algorithm ,SWRL, OWL	Database maintaining user profiles based on health care information	Better understanding of User's query results in more accurate and relevant recommendations

VII. COMPARISON

The above mentioned system uses different kinds of data for the recommendation to occur. Content based filtering approach uses the user taste profiles and compares it with the items profile. It can integrate with the query based systems as well as case base approaches. Domain knowledge is not required. One main limitation of content based filtering is that it cannot handle inter-dependencies. Other limitations are that it suffers from ramp-up problem and plasticity.

Collaborative filtering uses the ratings for items in a particular domain and matches it with the users who share the tastes. It provides useful personalized recommendation. All the users share their opinion and ratings of each item which is used to predict items.

Advantages of collaborative filtering over content based filtering include:

(i) Potential to provide coincidental recommendations.
(ii) Potential to filter items based on taste and quality profile.
(iii) Have the support for treat items whose content is not easily inspected.

Knowledge-based recommender systems effectively use the knowledge about users and items and finds relationship on which item meets the user's requirements. One main advantage of Knowledge-based Recommendations is that they do not suffer from the ramp-up problem because its predictions do not depend on any table of user ratings. Disadvantages of Knowledge-based Recommendation are that the system gives recommendation limited to its database and this database requires Knowledge engineering. So, this database has to be updated periodically so as to match the changing user preferences.

The advantage of Demographic based Recommendation system is that it can identify different groups. This system also doesn't require any domain knowledge. Disadvantages of this system are that extra demographic information is required to be stored and processed. This system also suffers from ramp-up problem and its recommendation quality depends on large historical data.

Hybrid Recommender System integrates two or more recommendation techniques to limit the weaknesses of any individual ones and using their strengths to make system more reliable.

VIII. CONCLUSION AND FUTURE SCOPE

In this paper, we described different recommendation techniques which are being used in food recommendation systems. We have also surveyed the existing food recommendation systems with their advantages and have tabulated the results which can act as a quick reference. Further we have compared the mentioned different recommendation approaches on the basis of their advantages and disadvantages. We can draw the conclusion that many of the papers on food recommendation are based on Content based filtering approach or collaborative filtering approach. There is a clear scope of research in other recommendation system and as the hybrid recommendation system gives better system performance, further research in this direction can give better algorithms and significant improvements in recommendation system.

REFERENCES

Journal References

[1]. G. Salton, A. Wong, and C. S. Yang (1975), "A Vector Space Model for Automatic Indexing" ,*Communications of the ACM*, vol. 18, nr. 11, pages 613–620.

[2]. D. Goldberg, D. Nichols, B.M. Oki, and Terry, D. (1992). "Using Collaborative Filtering to Weave an Information Tapestry", *Communications of the ACM*, 35, pages 61—70, 1992.

[3]. Joseph A. Konstan, Bradley N. Miller, David Maltz, Jonathan L. Herlocker, Lee R. Gordon, John Riedl, GroupLens, "Applying collaborative filtering to Usenet news" , *Communications of the ACM*, v.40 n.3, p.77-87, March 1997.

[4]. Upendra Sharda and, Pattie Maes, "Social information filtering: algorithms for automating 'word of mouth'", *Proceedings of the SIGCHI Conference on Human Factors in Computing Systems*, p.210-217, May 07-11, 1995, Denver, Colorado, USA.

[5]. Will Hill, Larry Stead, Mark Rosenstein, George Furnas, "Recommending and evaluating choices in a virtual community of use", *Proceedings of the SIGCHI Conference on Human Factors in Computing Systems*, p.194-201, May 07-11, 1995, Denver, Colorado, USA.

[6]. B. Mobasher, R. Cooley and J. Srivastava Automatic, "Personalization based on web usage mining". *Communications of the ACM*, vol. 43, no. 8, pp.142 -151 2000a.
[7]. Shiva Nadi, Mohammad Hossein Saraee and Ayoub Bagheri," A Hybrid Recommender System for Dynamic Web Users", *International Journal Multimedia and Image Processing(IJMIP),* vol. 1, no. 1, 2011
[8]. D. Riecken," Personalized Views of Personalization. *"Communications of the ACM,* vol. 43, no. 8, pp.27 -28 2000.
[9]. Wubin Guo, Xianpei Hu, Kuanjiu Zhou, Lijun Sun. "An Intelligent Query System Based on Chinese Short Message Service for Restaurant Recommendation", *Sixth International Conference on the Management of Mobile Business (ICMB 2007)*, 2007, 1 page.
[10]. Chi-Chun Lo, Ding-Yuan Cheng, Chi-Hua Chen. "A Semantic Web Methodology for Situation-Aware Curative Food Service Recommendation System", .*Computer Science and Software Engineering, 2008 International Conference* on, pp.444-447, 12-14 Dec. 2008.
[11]. Yoosoo Oh, Ahyoung Choi, Woontack Woo. "U-BabSang: a context-aware food recommendation system", *J. Supercomput*, 2010, vol. 54, no. 1, pp. 61-81.
[12]. Asami Yajima, Ichiro Kobayashi. ""Easy" Cooking Recipe Recommendation Considering User's Conditions", *Proceedings of the 2009 IEEE/WIC/ACM International Joint Conference on Web Intelligence and Intelligent Agent Technology*, p.13-16, September 15-18, 2009.
[13]. Yoko MINO, Ichiro KOBAYASHI, "Recipe recommendation for a diet considering a user's schedule and the balance of nourishment", *IEEE International Conference on Intelligent Computing and Intelligent Systems*, vol. 2, pp. 383-387, 2009.
[14]. Jong-Hun Kim, Jung-Hyun Lee, Jee-Song Park, Young-Ho Lee, Kee-Wook Rim. "Design of Diet Recommendation System for Healthcare Service Based on User Information", *Fourth International Conference on Computer Sciences and Convergence Information Technology, ICCIT'09*, pp. 516-518, 24-26 Nov. 2009.
[15]. Jill Freyne, Shlomo Berkovsky, "Intelligent food planning: personalized recipe recommendation*", Proceedings of the 15th international conference on Intelligent user interfaces*, February 07-10, 2010, Hong Kong, China.
[16]. Chang Shing Lee , M. H. Wang and H. Hagras, "A type-2 fuzzy ontology and its application to personal diabetic-diet recommendation", *IEEE Trans. Fuzzy Syst.,* vol. 18, no. 2, pp.374 -395, February 2010.
[17]. Wahidah Husain, Lee Jing Wei, Sooi Li Cheng and Nasriah Zakaria. "Application of data mining techniques in a personalized Diet recommendation system for cancer patients", *Published in Humanities, Science and Engineering (CHUSER), 2011 IEEE Colloquium*, 5-6 Dec. 2011, pp. 239 – 244.
[18]. M. A. El-Dosuky, M. Z. Rashad, T. T. Hamza, A.H. EL-Bassiouny. "Food Recommendation using Ontology and Heuristics", *First International Conference, AMLTA 2012, Cairo, Egypt*, December 8-10, 2012, pp. 423-429.
[19]. Sumedh Sawant, Gina Pai, "Yelp Food recommendation System", <http://cs229.stanford.edu/proj2013/SawantPai-YelpFoodRecommendationSystem.pdf>
[20]. Shilpa Dharkar, Anand Rajavat, "Performance analysis of healthy Diet recommendation System using Web data mining", *International Journal of Scientific & Engineering Research (IJSER) Volume 3*, Issue 5, May-2012.
[21]. Achmad Arwan, Bayu Priyambadha, Riyanarto Sarno, Mohamad Sidiq, Heri Kristiantol, "Ontology and semantic matching for diabetic food recommendations", *Published in Information Technology and Electrical Engineering (ICITEE), 2013 International Conference*, Yogyakarta, 7-8 Oct. 2013, pp. 170 - 175.
[22]. E-Seok Jo, Yong-Sung Kim. "A good food restaurant recommendation system using termite clustering model", *Published in International Journal of Advancements in Computing Technology (IJACT), Advanced Institute of Convergence Information Technology (AICIT), Republic of Korea*, Volume 5 Issue 12, August, 2013, pp. 505-509.
[23]. Irshad Faiz, Hamid Mukhtar and Sharifullah khan, "An integrated approach of diet and exercise recommendations for diabetes patients", *Published in e-Health Networking, Applications and Services (Healthcom), Natal, 2014 IEEE 16th International Conference*, 15-18 Oct. 2014, pp. 537 - 542
[24]. Shreya B. Ahire, Harmeet kaur khanuja, "A personalized framework for health care recommendation", *published in Computing Communication Control and Automation (ICCUBEA), 2015 International Conference, Pune*, 26-27 Feb. 2015, pp. 442 – 445.

SWOT Analysis of Search Based Software Engineering

Abhilasha Sharma
Assistant Professor, CSE Department,
Delhi Technological University
New Delhi, India
Email Id: abhilasha_sharma@dce.ac.in

Yogita Khatri
Full Time Student, CSE Department,
Delhi Technological University
New Delhi, India
Email Id: yogitabaveja65@gmail.com

***Abstract* – Search Based Software Engineering basically involves amalgamation of software engineering, operation research and metaheuristic techniques. It is specially excelled in providing an ideally balanced solution to a SE problem involving several competing goals. This study radically highlights the SWOT Analysis of Search Based Software Engineering for taking measure of inside potency/capabilities, vulnerabilities and the probable favorable chances, obstacle/risks from the outward environment. It caters to the problem of SE and provides optimal solution to give better prospects over tools and techniques required to grow a productive, proficient and cohesive approach.**

Keywords* – *Fitness Function, Search Based Software Engineering, Software Engineering

NOMENCLATURE

SBSE Search Based Software Engineering

SE Software Engineering

SWOT Strengths, Weaknesses, Opportunities and Threats

HC Hill Climbing

I. INTRODUCTION

Different phases of software engineering are complex in nature and consist of numerous problems. Following are some of the problems of SE:

(1) What should be the optimal set of requirements which establishes equilibrium between software development budget and customer satisfaction?

(2) What should be the best way of distribution of resources to a software development project?

(3) What should be the optimum alignment of test cases (test case prioritization) to be executed for regression testing?

(4) What should be the minimum set of test cases that will award complete branch coverage?

Although, we have many classical approaches to solve these problems like linear programming, dynamic programming, but these approaches do not work well with NP-hard problems as they cover maximum range of SE problems. However, it has been found by many researchers that SBSE often gives satisfactory results when used on such problems. They may not be able to give a global optimal solution but can provide a list of near optimal solutions.

It provides an efficient way to automate software engineering tasks by applying meta-heuristic search algorithms. For applying any search algorithm to a problem, firstly, we reformulate the given problem as a search problem and then select the appropriate fitness function for guiding the search. Since all the above mentioned problems belong to different domain of software engineering and do not have any thing in common but from SBSE point of view all are essentially the optimization problems. SBSE approach has especially excelled where it is required to obtain an ideal balance between competing factors like completion of goals vs. money spend. In case of such problems there can't be a single ideal solution rather there can be many near optimal solutions that contain a perfect mix of competing factors.

As a step forward to bring clairvoyance to the use of search based techniques in software engineering, we do a SWOT analysis highlighting the alphas and omegas of the area impacting the growth and scope. The paper is structured as follows: Section 2 provides a layout of the progress graph in the area of search based software engineering. Section 3 details the rational technique of SWOT analysis which unfolds SBSE as a major thrust area to urge researchers to perceive and explore in this domain. The paper concludes all the primitive information for developers, investigators, scholars and academicians, exigent/needed to perceive, perform, and prolify the convergence of search based techniques in software engineering.

II. SBSE SO FAR

Although the title SBSE (Search Based Software Engineering) was first introduced by Harman and Jones in 2001 [1] but originally an attempt for optimization to a software engineering problem dates back to 1976 and was reported by Miller and Spooner. They have applied it in software testing. With the passage of time , the interest of researchers towards SBSE increased rapidly and since then the significant work has been reported in the fields of requirement engineering[3,4,5],

978-9-3805-4421-2/16/$31.00 ©2016 IEEE

management[6,7,8], testing[9,11,13], maintenance[10,12], design[12,14,15] etc. thus, covering entire life cycle of software engineering. A broad range of optimization algorithms have been applied in SBSE. The most commonly exercised are Hill Climbing, Simulated Annealing, Tabu Search, Genetic Algorithm and Genetic Programming.

Proportional rate of published papers in different domains of software engineering and yearly publication graph of SBSE has been represented in Fig. 1 and Fig. 2 respectively. So far the major exploration has been done in software testing as reflected from Fig. 1. However in order to apply SBSE in any domain, following four key elements [1, 2] must be satisfied.

1) *Large Search Space*: SBSE problem must have a big search space. If small, then no need to apply this.
2) *Low Computational Complexity*: Fitness function must be easy and fast to compute, so that overall complexity of the algorithm should be low.
3) *Approximate Continuity*: There must be a well defined objective for every SBSE problem that needs to be optimized.
4) *No Known Optimal Solution*: No need to apply SBSE technique, if an ideal solution to a problem is discovered previously.

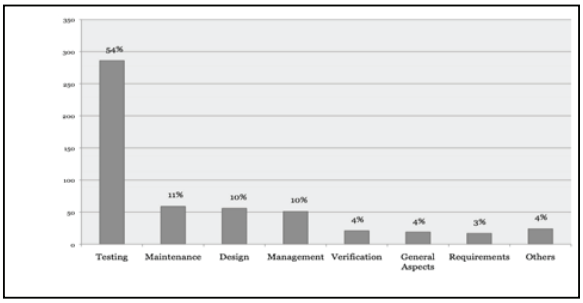

Fig 1. SBSE Application Domain Publications (Source: SBSE Repository [23])

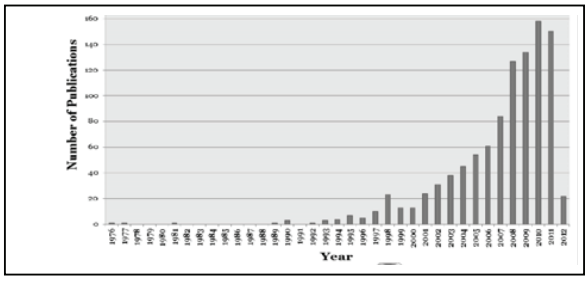

Fig 2. Yearly SBSE Publication Rate (Source : SBSE Repository [23])

III. SWOT ANALYSIS OF SBSE

SWOT analysis of SBSE represents a layout/framework to assess the internal and external elements that can have an impact on the vitality of the project, place or person .Its four factors are:

1) Strengths: Internal factors and resources that accelerates the success of SBSE.
2) Weaknesses: Internal factors and resources that give rise to the failure of SBSE.
3) Opportunities: External factors that can boost the performance rate of SBSE.
4) Threats: External factors that could imperil the SBSE.

A. Strengths

Strengths of SBSE are its vigorous characteristics that make it more advantageous over other approaches. These are as follows:

1) *Broad Domain*: SBSE has a very broad application domain. It has been implemented almost on all phases of software development, thus covering requirement analysis, design, testing, project management, and refactoring. This approach views every problem related to above fields as a search based optimization problem and remarkable improvements have been observed as compared to existing techniques.
2) *Readymade Fitness Function:* In order to apply the search based technique to a software engineering problem, one of the essential element required is the exigency of fitness function to lead the search. Many problems in software engineering have a wide variety of software matrices associated with them which can be used as a fitness function .No extra effort required to construct the fitness function. Undeviatingly, any one of the associated software matrices can be used as fitness function.
3) *Re-Coalescence*: It bridges the gap between unrelated areas of software engineering. For example, regression testing and requirement analysis are two unrelated techniques of software engineering. But both can be seen as similar problem species with respect to SBSE. The task of selection and prioritization works on similar lines for requirements as well as for test cases of regression testing. Although, the purpose of both are different, regression testing is targeted towards selecting and prioritizing test cases to have code coverage to attain high fitness where as requirement analysis is targeted towards selecting and prioritizing requirements to cover customer expectation. Such relationships give rise to new dimensions for fusion of unrelated research areas.

4) *Good Provider for Solution to NP-Hard Problems*: For the problems which are characterizes by a set of competing parameters and there exist a tradeoff between them, SBSE techniques are found to be ideal for finding out the near optimal solution representing an ideal balance between the competing factors. For example, the expenditure vs. the realization of goals.
5) *Fast and Efficient*: Most of the SBSE problems are favoured by hill climbing or simulated annealing. Since they are fast and easy to implement and thus are very efficient. Sometimes they may lead to a local optima, but can always be restarted multiple times. For problems that require quick solution, HC is a good choice as it provides a palpation of landscape structure. By applying multi-objective search algorithms we can obtain many good solutions that shows potential tradeoffs between competing targets specially when time or resources are short.
6) *Malleability through Parallelism***:** Malleability is a big milestone in software engineering. But it can be achieved because of the implicit parallel nature of SBSE techniques. For example, hill climbing can be done in parallel, each commencing with a new climb point. Genetic Algorithms can also be operated in parallel, since it's a population based technique so fitness for each candidate or individual can be calculated in parallel. Therefore, this inherent parallel nature of SBSE techniques unveils a solution to address the issue of SE malleability.
7) *Feedback and Insight:* One of the root causes of failure in software engineering is poor understanding of customer requirements, making false assumptions, thus leading to improper specification. SBSE can handle this problem as the search is guided by automatic fitness function in comparison to human based search, leads to exciting results with no deviation.

B. Weaknesses

Weaknesses of SBSE are its fragile characteristics that place it at a competitive disadvantage. These are as follows:

1) *Unfit Stopping Rule*: Two stopping rules have been used till now to terminate the search
   a) By Budget Constraint
   b) By Some Stipulated Time

   These rules are not sufficient as sometimes they give poor results. However in case of GA (since it is population based), third rule arises, which says, stop the search, when all individuals in the population have similar chromosome. But this leads to a problem of how to assess the similarity of individuals. This limitation is splattered as a challenge for SBSE researchers to come out with such metrics. Thus we are lacking with the right stopping rule.
2) *Opting Appropriate Optimization Algorithm for a Specific SBSE Problem:* It has been observed that the researchers are randomly choosing the optimization algorithm and comparing their work with random search as standard. This approach is acceptable for new domains of SE which has not yet been explored by SBSE. But the necessity is to characterize the complexity of SE problem and comparatively analyze them with that search algorithm which already produced good results for the similar problem space. This characterization will help in selection of suitable search algorithm for the problem in hand, so that already existing results can be improved.
3) *Achieving Human Competitive Results:* One of the weaknesses of SBSE is that the outcomes produced by automatic computation are not human competitive. But there are fields likes test data generation and modularization, where it would be possible to beat the human competitors. Researchers believe that growing interest in this area will definitely achieve human competitive results in near future.
4) *Choosing Suitable Parameter Setting*: Sometimes the fruitful deployment of search algorithm on a given problem bank on discovery of relevant/desired parameter settings, but the charge of finding such parameters can be huge. Sound experimental design can cut-down the cost of parameter tuning in some cases.[15]

C. Opportunities

There are certain areas under software engineering or search based approaches that are not fully excavated but on scouting leads to astonishing future prospects.[24] Following are the favorable conditions/situations leading towards attainment of SBSE goals:

1) *Theoretical Fact Fitness*: This fitness function is formulated based upon theoretical facts and is first used by Lutz [14] for the problem of hierarchical disintegration of software. It gives more fitness value to hierarchies that present the software design in more understandable way. Not much work has been done in this area but there is a great scope in using the information theory as a basis for constructing a fitness

function, because in SE, theoretical information is found in abundance.

2) *Security and Protection*: Although it is one of the very important areas of SBSE application, but limited by the search of a suitable fitness function to handle a security problem.
3) *Protocols*: Correctness of communication protocol can be checked in terms of its efficiency and security using SBSE techniques as first demonstrated by Alba and Troya [16]. They applied genetic algorithm for testing the accuracy of communication protocols. Later in 2000 and 2001, Clark and Jacob [17, 18] used genetic algorithm and simulated annealing for obtaining optimized tradeoffs between efficiency, security and cost of BAN (Burrows, Abadi, and Needham) protocols. In 2008, Ferreira et al [19] proposed particle swarm optimization technique to find network protocol errors in concurrent system. The research could be extended in handling the problems related to this domain using SBSE techniques.
4) *Scope of SBSE in Distributed Artificial Intelligence and Software Agents***:** The researchers believe that there is a great scope of SBSE application in the field of distributed artificial intelligence and software agents. A very few work has been done so far in this area. The nature of multi-agent system resembles very closely with the nature of SBSE problem. There is a population of individuals in an agent based system that communicates with each other, exchange information, leading to solve a common objective. The evolutionary algorithms like genetic algorithm, genetic programming seems a perfect choice for these agent based system. Latest work in this area [20] visualizes how agents can be tested using search based algorithms.
5) *Scope for Intermutual Optimization*: Intermutual optimization means where fitness function is based on human judgment. Outside the domain of SBSE application, huge amount of work on fitness function can be found based on human evaluation. In SE, we can make use of intermutual optimization in design problem where the constraints are subjective or not well defined. One of the possibilities is to make use of a search based technique to delve the implicit assumption in human judgment of solutions. The only problem with this approach is that, in the course of every iteration, human judgment for fitness evaluation has to be considered that can be time consuming and may create fatigue also.
6) *Scope for Non-functional Optimization*: There are some non-functional attributes like temperature, heat dissipation, power consumption that never get importance as software paradigms. But researchers have shown that these are emerging and augmented SE fields for non functional optimization over which SBSE techniques can be applied.
7) *Optimization of Source Code Analysis:* One of the important future prospects for SBSE is the optimization of source code analysis which has been an upcoming area but merely few papers pop up to take a hand in source code based SBSE. With the execution of SBSE practices, it will be possible to explore for striking features and produce a probabilistic source code analyses resulting in a very rigid optimization model of analysis.
8) *Multi-Objective Optimization***:** There are some areas where problems are multi-objective in nature , like in project planning prime concern is to complete the project well in time and with lesser cost. Optimization is required for both. This multi-objective optimization is called pareto optimality. Recent researches on SBSE have shifted to multi-objective codification from single objective codification, using pareto optimality optimization technique. There is a great scope for this new technique as many areas in SE have multi-objective problem domains.

D. Threats

Threats to SBSE are potential risks that are involved in design and execution phase. These threats may limit the ability to yield the reliable results or their generalization to a bigger population than the sample instances taken in the experiment. Some of the validity threats are as follows.

1) *Laxness in Considering Random Variation:* Search based algorithms are generally involved with generating random number. For example, the starting point of a hill climbing search is generally selected randomly and the first population for the genetic algorithm is usually generated randomly. Therefore, sometimes even iteratively running the algorithms can lead to a bad starting point selection and tend towards failure.
2) *Scarcity of Good Descriptive Stats***:** Since we have to run the algorithms several times, the data collected from them at the end must be accumulated and presented in a meaning full way to interpret the conclusions. For example, one can make use of function like standard deviation, min-max range for

the outcome observed from the experiment. However, they are not of much significance and are actually lacking in good statistical measures and hypothesis that is based on the traits of data under evaluation.

3) *Paucity of Standards for Comparison:* In SBSE, whenever a new algorithm is applied to a particular problem instance, the result of the algorithm is compared with a benchmark. Most of the time random search is used as a baseline, but it's an incorrect practice, rather the standards should be the representative of best solution known so far.
4) *Poor Choice of Fitness Function:* Many software matrices can be used as fitness function directly. Searching a solution from the search space is totally directed by the fitness function chosen as per the objective to meet. However, if not selected intelligently, can lead to a threat to its validity.
5) *Complex Environment:* The environment under which the software is developed is usually complex, because of technical and social issues involved. So when formulating a model for software related problem by simplifying some measures or making certain assumptions, one must account for its implication on practical application. Ignoring these factor can lead to validity threats. Fig. 3 summarizes all the points related to strengths, weaknesses, opportunities and threats of SBSE. .

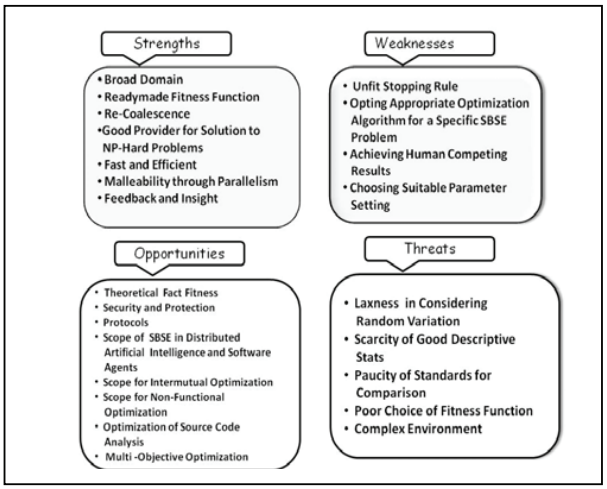

Fig.3. SWOT Analysis of SBSE

IV. CONCLUSION & FUTURE WORK

The paper presents a summary of the search based software engineering whose goal is to provide a more acceptable solution to a SE problem surrounded by various fighting factors by applying the meta heuristic approaches. SWOT analysis illustrates all the bane's & boon's within and outside the areas that impact the development and coerce for a universal and proactive approach to SBSE, which will minimizes the inaccuracies and enhance the results. Future work of SBSEs SWOT is open for the convergence of future opportunities in to present strength , to overcome with existing weaknesses and to reduce the probability and severity of threats.

REFERENCES

[1]. M. Harman and B.F. Jones, " Search-based software engineering", Journal of Information and Software Technology, Vol. 43, pp. 833-839, December 2001

[2]. M Harman and J. Clark , "Metrics are fitness functions too", International Software Metrics Symposium (METRICS 2004), pp. 58-69, 2004.

[3]. A. Bagnall, V. Rayward-Smith, and I. Whittley , "The next release problem" , Information and Software Technology, Vol. 43, No.14, December 2001.

[4]. A. Ngo-The and G. Ruhe, "Optimized resource allocation for software release planning", IEEE Transactions on Software Engineering, Vol. 35, No. 1, pp. 109-123, Jan.-Feb. 2009.

[5]. Y. Zhang, M. Harman, and S.A. Mansouri, "The multi-objective next release problem", Genetic and Evolutionary Computation Conference (GECCO 2007), ACM, page 11, 2007.

[6]. C. Burgess and M. Leey, "Can genetic programming improve software effort estimation? a comparative Evaluation", Information and Software Technology, Vol. 43, No. 14, pp. 863-873, 2001.

[7]. J. Dolado, " On the problem of the software cost function", Information and Software Technology, Vol. 43, No. 1, pp. 61-72, 2001.

[8]. C. Kirsopp, M. Shepperd, and J. Har, "Search heuristics, case-based reasoning and software project effort prediction", Proceedings of the 4th Annual conference on Genetic and evolutionary computation (GECCO '02), pp. 1367-1374, 2002.

[9]. A. Baresel, H. Sthamer, and M. Schmidt, "Fitness function design to improve evolutionary structural Testing", Proceedings of the 4th Annual conference on Genetic and evolutionary computation(GECCO '02), pp. 1329-1336, 2002.

[10]. B. S. Mitchell and S. Mancoridis, "Using heuristic search techniques to extract design abstractions from source code", Proceedings of the 4th Annual conference on Genetic and evolutionary computation (GECCO '02), pp. 1375-1382, 2002.

[11]. S.L. Rhys, S. Poulding, and J.A. Clark, "Using automated search to generate test data for matlab", Proceedings of the 11th Annual conference on Genetic and evolutionary computation (GECCO '09), pp. 1697-1704, 2009.

[12]. M. Harman, R. Hierons, and M. Proctor, "A new representation and crossover operator for search-based optimization of software modularization" Proceedings of the Genetic and Evolutionary Computation(GECCO 2002), pp. 1351-1358, July 2002

[13]. M. Claudia Figueiredo, P. Emer, and S. Regina Vergilio, "GPTesT: A testing tool based on genetic Programming", Proceedings of the 4th Annual conference on Genetic and evolutionary Computation (GECCO '02), pp. 1343-1350, 2002.

[14]. R. Lutz, "Evolving Good Hierarchical Decompositions of Complex Systems", *Journal of Systems Architecture,* Vol. 47, No. 7, pp. 613–634, 2001.

[15]. S. Poulding, P. Emberson, I. Bate, and J A. Clark, " An efficient experimental methodology for configuring search-based design algorithms", Proceedings of 10th IEEE High Assurance System Engineering Symposium (HASE'2007), pp. 53–62, 2007.

[16]. E. Alba, and J. M. Troya, " Genetic Algorithms for Protocol Validation", *Proceedings of the 4th International Conference on Parallel Problem Solving from Nature (PPSN '96)*, Springer, pp. 870–879,1996.

[17]. J. A. Clark and J. L. Jacob, "Searching for a Solution: Engineering Tradeoffs and the Evolution of Provably Secure Protocols", *Proceedings*

of the 2000 IEEE Symposium on Security and Privacy (S&P '00), IEEE, pp.82–95, 2000.
[18]. J. A. Clark and J. L. Jacob, "Protocols are Programs too: the Meta-Heuristic Search for Security Protocols", *Information and Software Technology, Vol. 43, No.* 14, pp. 891–904, 2001.
[19]. M. Ferreira, F.Chicano, E. Alba, and J. A. G´omezpulido,
[20]. "Detecting Protocol Errors using Particle Swarm Optimization with Java
[21]. Pathfinder", Proceedings of the High Performance Computing &
[22]. Simulation Conference (HPCS '08), Cyprus, pp. 319–325, 2008.
[23]. C. Nguyen, S. Miles, A. Perini, P. Tonella, M. Harman, and M. Luck, " Evolutionary Testing Autonomous Software Agents", *Proceedings of the 8th International Conference on Autonomous Agents and Multiagent Systems (AAMAS '09)*, International Foundation for Autonomous Agents and Multiagent Systems, pp. 521–528,2009.
[24]. T. Jiang, N. Gold, M. Harman and Z. Li, "Locating Dependence Structures using Search-based Slicing", *Information and Software Technology,* Vol. 50, No. 12, pp. 1189–1209, 2007.
[25]. T. Jiang, M. Harman and Y. Hassoun, "Analysis of Procedure Splitability", *Proceedings of the 15th Working Conference on Reverse Engineering (WCRE '08)*. IEEE, pp. 247–256, 2008.
[26]. Y. Zhang, M. Harman, and A. Mansouri, " The SBSE repository: A repository and analysis of authors and research articles on search based software engineering". crestweb.cs.ucl.ac.uk/resources/sbse repository
[27]. M.Harman, A. Mansouri, and Y. Zhang, "Search based software engineering: A comprehensive analysis and review of trends techniques and applications", Technical Report TR-09-03, April 2009.

Synchrophasor Based Real Time Monitoring of Grid Events in Indian Power System

K.V.S. Baba, S.R. Narasimhan, *Senior Member, IEEE*; N.L. Jain; Amandeep Singh; Rahul Shukla; Ankit Gupta
Power System Operation Corporation, New Delhi, India

***Abstract*--The availability of Synchrophasors has considerably enhanced the wide area visualization and situational awareness of power system behaviour under steady state as well in transient/dynamic conditions. The availability of Synchrophasor data at control center has become first-hand information for grid operator to view and analyze any transient phenomenon occurring in the grid. Various events that went un-noticed with Supervisory Control and Data Acquisition (SCADA) system are now being detected and analyzed, opening up a completely new era in power system monitoring and control. There is a paradigm shift in monitoring the grid after the commissioning of Synchrophasor projects. Now-a-days control centre operator first observes the signature of events through PMUs data and then refers to SCADA system for the details of the events. Since the commissioning of Synchrophasor pilot projects in India, the synchrophasor data available at the Regional & National Load Despatch Centre has been utilized for real time visualization and also for post-dispatch analysis in offline mode.**

***Index Terms*— Wide Area Measurement Systems, Phasor Measurement Units, System Operator, Low Frequency Oscillations, System Protection schemes, Supervisory Control and Data Acquisition**

I. INTRODUCTION

The Wide Area Measurement Systems have several offline applications apart from real time operations. The data made available from synchrophasors are being used in fault analysis, oscillation analysis, multiple tripping cases, Frequency Response Characteristics, analyzing weather related contingencies, HVDC related transient study etc. With the help of Synchrophasor technology, system operators are now able monitor the magnitude and angle of each phase of the three phase voltage/current, frequency, rate of change of frequency and angular separation at every few millisecond interval (say 40 milliseconds) in the Load Despatch Centre. Thus the transient / dynamic behavior of the power system can be observed in near real-time at the control centre which hitherto was possible only in offline mode in the form of substation Disturbance Records or through offline dynamic simulations performed on network models. Therefore synchrophasor applications not only enhance the system operation in real time but also provide proper feedback to planning so that mitigation measures can be taken to avoid recurrence. Measurement based techniques provide more confidence than simulation based models as far as the system operator is concerned.

II. REAL TIME APPLICATIONS

In real time operations the control room operators observe the various parameters and any variation in trend is further monitored for probable event in the grid. The paper discusses about a few interesting cases observed in real time so far in the Indian Grid.

A. Angular Separation

The control room operators constantly monitor angular difference between two extreme nodes of Indian Grid which gets refreshed at 25 samples per second. The angle difference between the nodes reflects the stress in the system, angle difference within a threshold value indicates normal situation in system operation whereas sudden rise or fall in the angular separation indicates alarm state in the Grid. This is particularly important for the Indian Grid where power flow is unidirectional for almost 3000 Km from state of Madhya Pradesh to Kerala. There was an incident of tripping of highly loaded double circuit. The trippings occurred in continuation with one circuit tripping after other. The sequential tripping was well captured by Synchrophasor angular plot. The tripping of one circuit led to the rise in loading of other parallel circuit and small rise in angle while post tripping of double circuit the angle difference increased to high value. The operator witnessed this and was able to take prompt action to contain the rising angle difference. Modifications to the System protection Schemes (SPS) are also being envisaged accordingly.

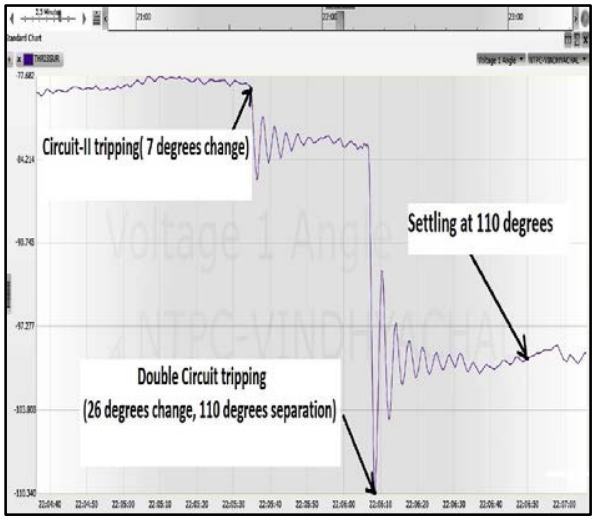

Fig. 1: Displaying Angular Separation between extreme nodes of Indian Grid

978-1-4673-8848-1/16/$31.00 ©2016 IEEE

B. Power Flow Monitoring During Auto-recloser

The power flow display of a double circuit line is constantly monitored for keeping a check on unusually high flows. The tripping of any circuit of this double circuit may pose a threat to system security. The system protection schemes have been employed to keep a check on the arising alarming situation due to contingency related to these lines. On one occasion there was an incident in which Circuit-I tripped on distance protection after failed autoreclosure attempt. This led to high power flow on other parallel circuit and power flow variation during reclaim time. The event was captured well by power flow PMU Plot and signature of failed autoreclose attempt was also observed. During single phase Autoreclose the power flow via other healthy phases decreased to two thirds of initial value and after one second when recloser attempt failed the power flow got reduced to zero. The Synchrophasor helped the real time operator to successfully identify that a sustained single phase to ground fault is present in the line. Thus the operator got prepared for the next contingency that is the second line overloading/tripping.

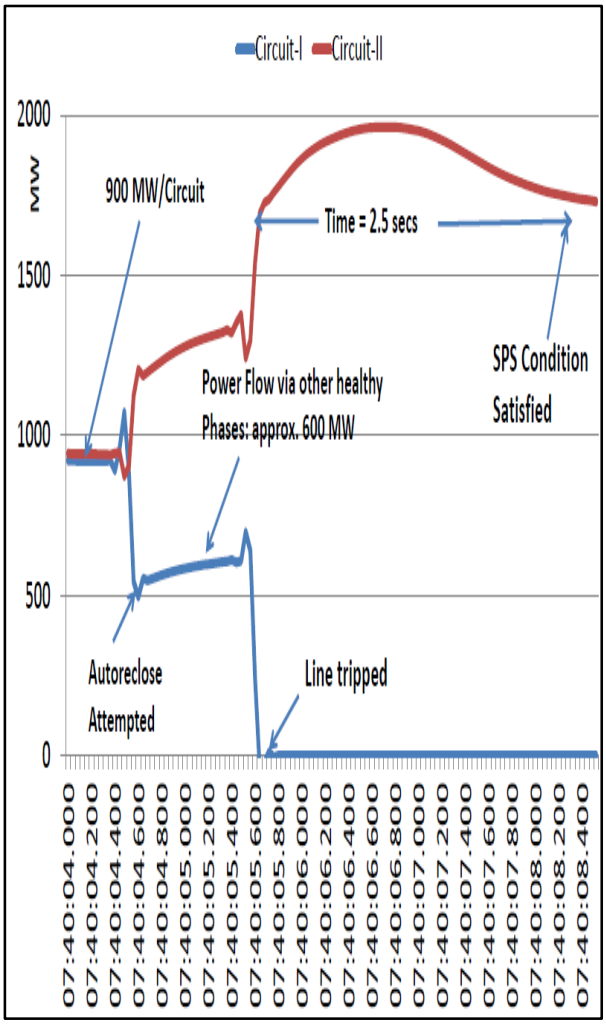

Fig 2: Displaying Line tripping post unsuccessful auto-reclose and power flow variation on other parallel line

C. HVDC Link Power Order Fluctuation Monitoring

Several PMUs are placed at HVDC stations to monitor the events related to HVDC links. In many cases the PMUs are placed at Bus sectionaliser of HVAC and HVDC buses. The PMUs measure the current flowing through Bus-Sectionaliser and thus give an indication to any tripping/contingency at HVDC station. On one occasion there was blocking of one pole of HVDC Bipole Link and post blocking there were repeated fluctuations in current plot of PMU placed at HVDC. Before The power flow on HVDC Bipole was 1225 MW and post blocking of one pole other pole went to 1250 MW for 10 secs and settled at 10 percent overload capacity. Immediately after that an anomalous power flow was observed in HVDC Bipole power flow, a sample of the same is as shown below:

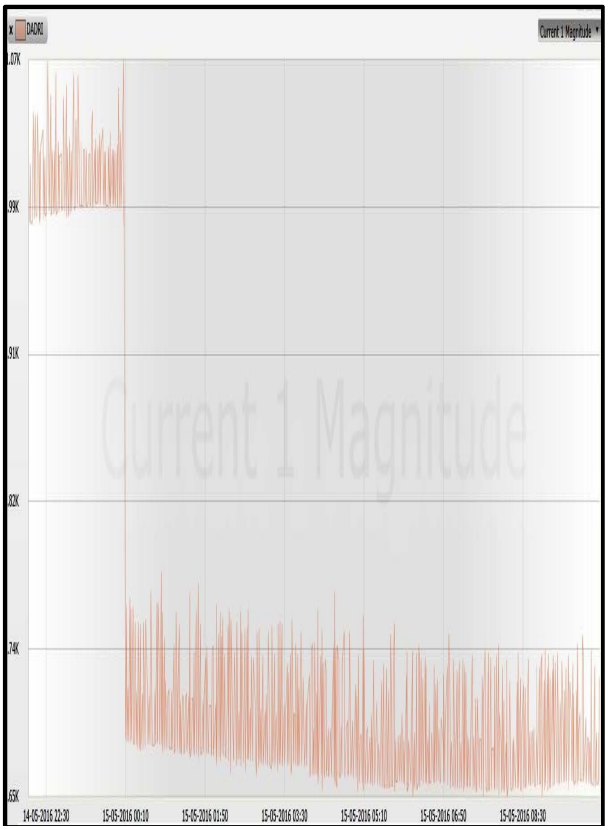

Fig 3: PMU Plot of AC current plot on one of Bus Sectionalizer at HVDC station showing anomalous flow

It was gathered that there was noisy telecommunication between the two ends of the HVDC link. As per the adopted scheme, in case of outage of one of the poles the other HVDC pole is supposed to operate at the 10% overload capacity only when the communication is through so that the remote end temperature & other details can be gathered. Due to the patchy communication link between the two poles whenever the communication link became healthy, power order used to be ramped up to 825 MW (at sending end) and when the link failed the power order was reduced to 750 MW (at sending end). This caused the rapid and irregular power changes in the power order. Once the manual over ride for reducing power order was done the pole stopped trying to move towards the overload capacity.

978-1-4673-8848-1/16/$31.00 ©2016 IEEE

D. Fault Identification Using Sequence Component Monitoring

The fault occurring on transmission lines are also captured well using synchrophasors. For every line tripping and auto-reclose the voltage and current plots capture the signature dip in voltage, however in several cases due to unbalance in voltage it becomes difficult to identify exact nature of fault. It is also important to identify whether ground is involved in the fault or not. In such cases sequence component helps in fault nature identification. On one such incident, a 400 kV line tripped after failed auto-reclose attempt by the line due to phase to ground fault. The line attempted auto-reclose before tripping and fault current was 2.8 kA. As per sequence components based fault analysis theory the sequence components during single line to ground fault should be approximately equal in magnitude and one third of fault current. In this case the sequence components were found to be approximately equal and with magnitude near 900 amps which is approximately one-third of 2.8 kA fault current. Moreover significant zero sequence component helped in identifying presence of ground in fault. This helped in prioritizing the line for early restoration by the system operator.

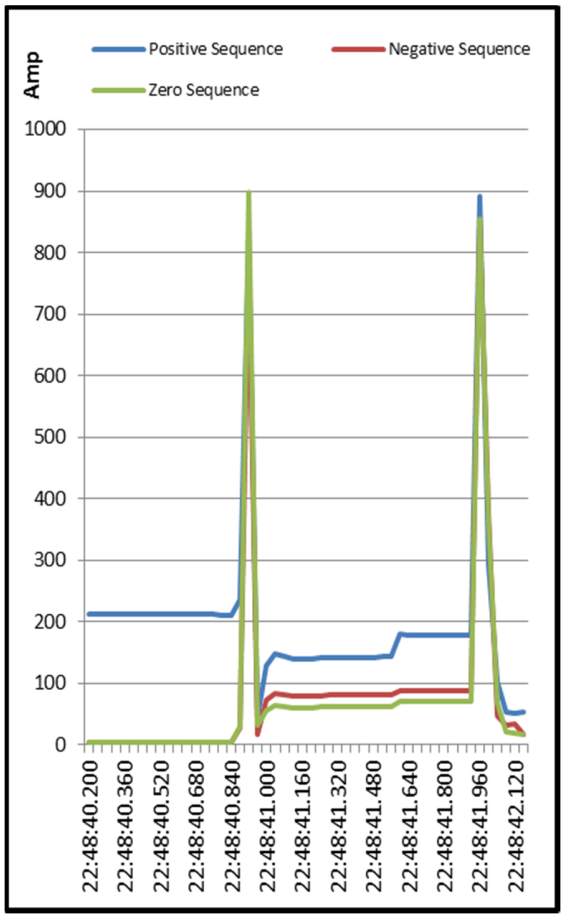

Fig. 4: Displaying Sequence Component of currents in tripping of line on single line to ground fault

E. System Protection Scheme Operation Monitoring

A single line connecting two regions is monitored using power flow plot of PMU Data. The monitored line was connecting two grids and its tripping would isolate them and so to prevent any further collapse System Protection scheme was designed which has to trip the monitored line if the current remains above the set limit for 10 seconds.

On one of the occasion the line flow has exceeded the set limit due to large generation tripping in one of the grid. During this event the circuit tripped on the SPS and isolated the two grids. In order to ensure the correct operation, Synchrophasor measurement were checked as shown in figure 5 and it was observed that the operation of SPS was as per its design. Initially the SPS got reset on two occasions due to oscillatory nature of power flow and then as the swings got damped the power remained above set limit for 10 seconds. The line tripped on SPS action and led to the separation of two regions. Thus the operator quickly identified that the two regions had desynchronized and took suitable actions in both regions to stabilize the grids for early restoration.

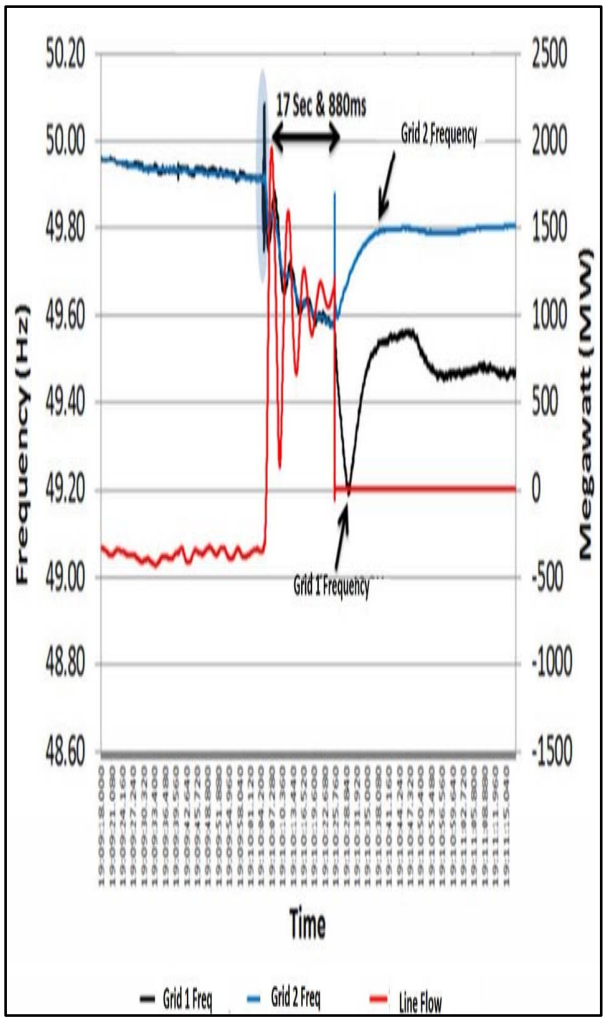

Fig 5: Displaying monitored line flow and two system frequency

978-1-4673-8848-1/16/$31.00 ©2016 IEEE

F. Monitoring Grid Restoration Post Desynchronisation

The double circuit lines which synchronize the two grids tripped at the same time leading to de-synchronization of grids. The process of restoration was monitored at control center using PMU plots of frequency and line power flow. In the process a charging attempt failed as the line could not hold from one end, this was captured by PMU. The same was captured in Fig.6 which shows sudden swing in power flow.

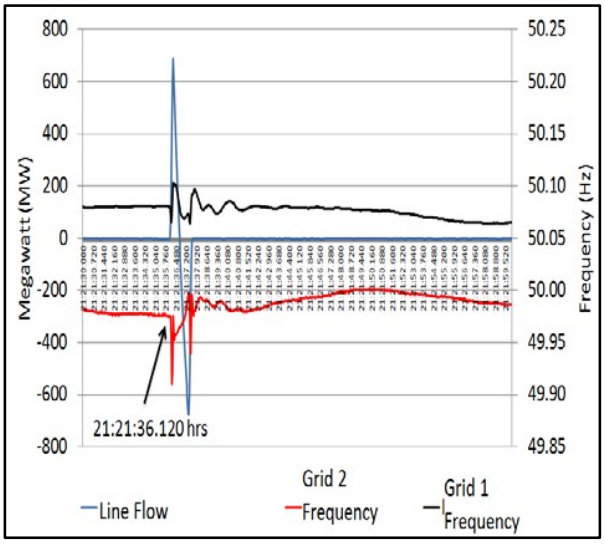

Fig 6: Displaying the power flow swing during synchronization attempt

Later both the grids were synchronized by charging the line and same was also captured well by PMU frequency plot of the stations from both the Grids. The two different frequencies and one synchronized frequency are being shown as Fig 7.

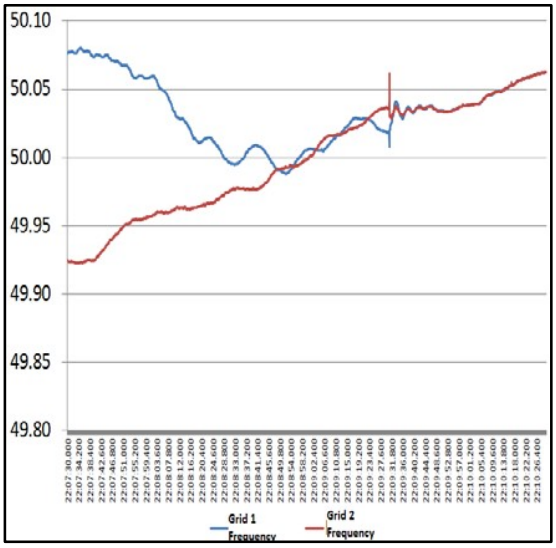

Fig 7: Displaying the different Frequency and the event of synchronization

G. Very Low Frequency Oscillation Due To Hydro Power Station

The case of oscillation arising during start stop sequence in a hydro unit has been observed in Indian Grid. This is one unique case where oscillation in Hydro units were observed by system operator, analyzed and then corrected with the help of generating station. In this case of oscillation, it was observed that while desynchronising a hydro unit from the Grid, the voltage plots of PMU located near the particular generating unit were observing the oscillation. The oscillation observed were of very low frequency nature i.e. 0.066 Hz, the oscillations were present in all three phases of voltage in the nearest PMU as shown in Fig 8. Since these oscillations were occurring repeatedly while one of the unit was being desynchronised at the particular hydro power plant. So the generating station was asked to investigate the matter further. On investigation by the generator, it was found that improper pulse from PLC while stop sequence was causing variation in reactive power thereby causing oscillations in voltage.

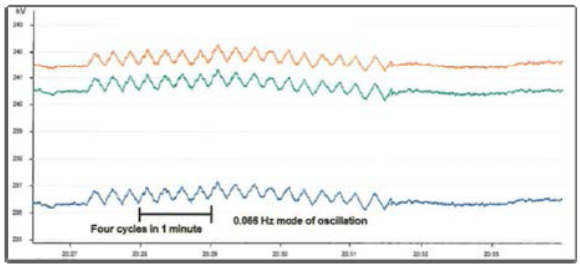

Fig 8: Oscillation in All Three Phases of Voltage

The PLC Pulse Logic was modified accordingly and the modification helped in eliminating the oscillations during the desynchronization. The situational awareness created by the Synchrophasors helped to detect and mitigate the source of oscillations in the grid.

III. CONCLUSION

Analysis of both SCADA and PMU data are being carried out in real time operations for the system to baseline its operating conditions and understanding the signature for different types of events. With the help of synchrophasors, operators are developing and improving insight of power system dynamics and identifying appropriate alerts and application settings for more accurate diagnosis of grid conditions and prediction of grid events. These are leading to recommendations for system planners on how to identify the problem areas and take steps to mitigate possible disturbances.

IV. ACKNOWLEDGMENT

The authors gratefully acknowledge the contributions of fellow colleagues. POSOCO also acknowledges the contribution of eminent experts from India and abroad whose valuable insights during the course of several years of

interaction have helped in understanding the synchrophasor based system operation in detail.

V. REFERENCES

[1] Report on Power System oscillations experienced in Indian Grid on 9th, 10th, 11th and 12th August 2014. POSOCO, India

[2] Operational Feedback on Transmission Constraints- April 2016, POSOCO.

[3] Report on Low Frequency Oscillation in Indian Power System, March 2016, POSOCO, India.

[4] Synchrophasors Initiatives in India Decmber 2013,POSOCO,India

[5] Synchrophasors Initiative in India June 2012,POSOCO,India

[6] Mukhopadhyay, P.; Seshadri, P.; Gangrekar, C.; Kumar, C.; Rai, A.B.; Reddy, N.M., "WAMS and synchrophasor experience during synchronization of large grids in India," in Signal Processing, Informatics, Communication and Energy Systems (SPICES), 2015 IEEE International Conference on , vol., no., pp.1-5, 19-21 Feb. 2015

[7] P. Kundur, Power System Stability and Control, (McGraw-Hill: New York, 1994).

[8] EPRI Power Systems Dynamics Tutorial. EPRI, Palo Alto, CA: 2009. 1016042.

VI. BIOGRAPHIES

K.V.S. Baba graduated in Electrical Engineering from JNTU College of Engineering, Kakinada, Andhra Pradesh in the year 1982. He worked in NTPC from 1984 to 1991 and subsequently joined POWERGRID. He is currently Executive Director of Power System Operation Corporation (POSOCO). He has a wide area of experience covering Power System Engineering & Feasibility, Project Management, Grid Management, Market Operations and Renewables.

S.R. Narasimhan graduated in Electrical Engineering from Delhi College of Engineering in the year 1986. He first joined Bharat Heavy Electrical Limited as an Engineer and worked there for a period of 2 years. He then joined Central Electrical Authority as an Assistant Executive Engineer in the year 1988 and subsequently joined POWERGRID in the year 1996. In the meantime he also completed his MBA in Finance from IGNOU, New Delhi. He has been a Senior Member of IEEE since 2010 and has many IEEE and CIGRE papers to his name. He is currently working as Additional General Manager in POSOCO.

N.L. Jain has graduated from Government Engineering College Jabalpur in the year 1984. He has worked in SAE (India) Pvt Limited prior to joining POWERGRID in the year 1988 He has a vast experience in Transmission Line Construction, Maintenance & Sub-Station O&M as well as Power System Operation. He is currently working as Deputy General Manager in POSOCO.

Amandeep Singh graduated in Electrical Engineering from DAV Institute of Engineering and Technology in the year 2006. He then joined POWERGRID as an Executive Trainee in the same year. He has worked in Testing & Commissioning of Sub-station Equipment and Protection System, Automation and Power System. He is currently working as Deputy Manager in POSOCO.

Rahul Shukla graduated in Electrical Engineering from HBTI, Kanpur in the year 2008. He is working in POSOCO and his area of expertise is Power System Operation, Synchrophasor Technologies and Post Fault Analysis.

Ankit Gupta graduated in Electrical Engineering from Jamia Millia Islamia University in the year 2012. He is working in POSOCO and his area of expertise is Power System Operation, Synchrophasor Technologies and Post Fault Analysis.

978-1-4673-8848-1/16/$31.00 ©2016 IEEE

Accepted Manuscript

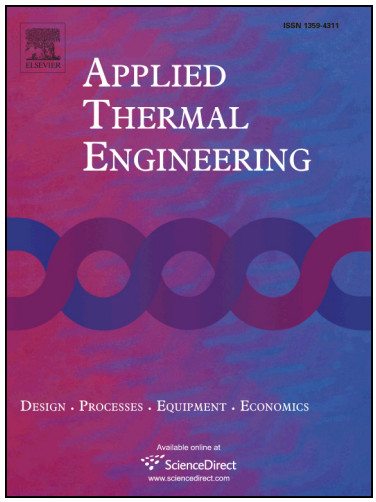

Research Paper

Thermodynamic and thermoeconomic analyses of two stage hybrid absorption compression refrigeration system

Manoj Dixit, Akhilesh Arora, S.C. Kaushik

PII: S1359-4311(16)32448-6
DOI: http://dx.doi.org/10.1016/j.applthermaleng.2016.10.206
Reference: ATE 9424

To appear in: *Applied Thermal Engineering*

Received Date: 20 May 2016
Revised Date: 14 October 2016
Accepted Date: 15 October 2016

Please cite this article as: M. Dixit, A. Arora, S.C. Kaushik, Thermodynamic and thermoeconomic analyses of two stage hybrid absorption compression refrigeration system, *Applied Thermal Engineering* (2016), doi: http://dx.doi.org/10.1016/j.applthermaleng.2016.10.206

This is a PDF file of an unedited manuscript that has been accepted for publication. As a service to our customers we are providing this early version of the manuscript. The manuscript will undergo copyediting, typesetting, and review of the resulting proof before it is published in its final form. Please note that during the production process errors may be discovered which could affect the content, and all legal disclaimers that apply to the journal pertain.

ACCEPTED MANUSCRIPT

Thermodynamic and thermoeconomic analyses of two stage hybrid absorption compression refrigeration system

Manoj Dixit[a*], Akhilesh Arora[b], S C Kaushik[a]

[a] Centre for Energy Studies, Indian Institute of Technology, New Delhi-110016, India.

[b] Mechanical Engineering Department, Delhi Technological University, Delhi - 110042, India.

*Corresponding author: Tel.:+919540660289, E-mail address: mandixdtu@gmail.com

Abstract

In this paper a two stage hybrid absorption compression refrigeration system utilizing LiBr-H_2O as working fluid is proposed. The hybrid system is compared thermodynamically with the conventional two stage absorption refrigeration system and it is found that the former can be operated at lower generator temperature and performs better than the latter. The effects of various operating parameters on thermodynamic and thermoeconomic performance indices like exergetic efficiency, area of heat exchangers and cost of the system are also studied. The heat exchangers are designed to estimate the size and cost of the system. The objective of thermoeconomic optimization is the minimization of annual cost of system, which includes investment costs and exergy fuel costs. The optimized hybrid system has COP of 0.43 and exergetic efficiency of 11.68%. The optimization results in the reduction of heat exchangers area from 79.61 m^2 to 71.96 m^2 and annual cost of operation of hybrid system by 5.2%.

ACCEPTED MANUSCRIPT

Keywords: absorption, compression, exergy, thermoeconomic, optimization, two stage cycle

1. Introduction

The energy and environmental issues associated with conventionally employed electricity driven vapor compression refrigeration (VCR) systems have paved the way for vapor absorption refrigeration (VAR) systems primarily because of latter's ability to harness renewable energy and recover waste heat without damaging the environment. However, on the performance front VAR systems lag far behind VCR systems and therefore, integration of these two technologies is looked upon as a potential alternative. This allows the retention of merits and rejection of shortcomings of both VAR and VCR technologies.

There are several studies which suggests that absorption compression hybrid refrigeration systems perform better than conventional VAR systems. Boer et al. [1] studied a hybrid absorption compression refrigeration system in which compressor was integrated between the evaporator and the absorber of a double effect VAR system. The COP of the hybrid cycle was reported to be 15-50% higher than the standard double effect VAR cycle without compressor. Kim et al. [2] reported that the generator temperature can be appreciably lowered by integrating a compressor in a triple effect vapour absorption refrigeration cycle. Zheng and Meng [3] found that the presence of a mechanical compressor between the evaporator and the absorber of a single effect VAR system can lower the required generator temperature and heat input. Kang et al. [4] found that using compressor between the evaporator and the absorber, the COP of GAX refrigeration cycle can be improved by 24% and by employing compressor between the generator and the condenser generation temperature can be lowered from 190-200°C to 164°C.

ACCEPTED MANUSCRIPT

Most of the studies on absorption compression hybrid refrigeration systems involves single/double/triple effect VAR configuration and no study, to the authors' knowledge, is available on two stage absorption compression hybrid refrigeration system. The commercially available single and double effect VAR systems require heat source of temperature greater than 100°C [5]. Therefore, a lot of thermal energy which is available below 100°C from sources like solar, geothermal, industrial waste heat etc., remains utilized and gets wasted. A two stage VAR system promises the utilization of low temperature heat sources between 60°C and 80°C [6]. Ma and Deng [7] also supports the fact that two stage VAR system is useful in recovering low temperature heat, but even in it, conventional working fluids like $LiBr/H_2O$ require heat input at 80 °C. Also, from the viewpoint of utilization of solar energy using low cost flat plate collectors, Kim and Machielsen [8] recommended the use of double stage absorption chiller. The efficiency of solar collectors increases when operates at low temperature, therefore, higher global efficiency of the solar absorption cooling system can be obtained by double stage cycle in comparison to single stage cycles [9].

Arivazhagan et al. [10] carried out theoretical study on half effect (two stage) R134a-DMAC absorption refrigeration system with low temperature heat sources for cold storages. They optimized intermediate pressure of the cycle corresponding to maximum coefficient of performance. For the baseline system, the COP varied from 0.35 to 0.46 whereas the second law efficiency was found to vary between 28% and 44%. Arivazhagan et al. [11] experimentally investigated a half effect VAR cycle using R134a-DMAC pair. The performance of the half effect VAR cycle was assessed in terms of COP, exergetic efficiency and degassing range. The system

ACCEPTED MANUSCRIPT

was able to operate at as low as -7°C evaporator temperature with generator temperatures varying from 55 to 75°C.

Domínguez-Inzunza et al. [12] studied the performance of single-effect, half-effect and double-effect in series, double-effect inverse and triple-effect absorption cooling systems operating with ammonia-lithium nitrate. The COP obtained was 0.3 for half effect systems at the lowest evaporator and generator temperatures. Crepinsek et al. [13] examined the performance of single effect and half effect absorption cycles for refrigeration temperatures below 0°C on the basis of coefficient of performance and circulation ratio.

Izquierdo et al. [14] carried out exergetic analysis of a double stage LiBr-H_2O absorption cycle driven by solar energy from flat plate solar collectors. The system attained COP of 0.37 for the condensation temperature of 50°C and the required generation temperature was about 80°C. They also concluded that the exergetic efficiency of double stage system was 22% less than that of the single effect system. Gebreslassie et al. [15] performed exergy analysis of half effect, single effect, double effect and triple effect LiBr-H_2O absorption cycles taking into account only unavoidable exergy destruction. Gomri [16] performed thermodynamic analysis based on principles of energy and exergy of a solar driven 10 kW two stage absorption cooling system. Arora et al., [17] computed the optimum parameters of half effect LiBr-H_2O absorption refrigeration system for various operating conditions on the basis of energy and exergy analyses.

Thermoeconomics, also known as exergoeconomics, couples the exergy concept of thermodynamics with the principles of economics. It is a powerful tool for design, analysis and optimization of complex thermal systems. The main motive of the exergoeconomic analysis is to strike a balance between expenses on capital cost

ACCEPTED MANUSCRIPT

and fuel (exergy) costs to minimize the net cost of the product of the system. The concepts of exergoeconomics have been applied by many researchers for the evaluation and optimization of various energy conversion systems in general and refrigeration systems in particular. Misra et al. [18, 19] carried out thermoeconomic optimization of single effect and series flow double effect LiBr-H_2O absorption refrigeration systems. Garousi Farshi et al. [20] analyzed series, parallel and reversed flow double effect absorption refrigeration systems from the viewpoint of exergoeconomics. The exergoeconomic comparison of series flow double effect and ejector integrated double effect absorption refrigeration systems was performed by Garousi Farshi et al. [21]. Similarly, many other researchers [22-24] carried out thermoeconomic analysis and optimization of vapor absorption refrigeration systems.

It is clear from the literature survey that a large amount of low temperature heat remains unused even with conventional two stage VAR system and therefore efforts are required to further lower the required generator temperature. So far only energy and exergy analyses of two stage VAR systems have been carried out but thermoeconomic analysis which is quite essential for their practical application is missing. Thus, a hybrid two stage absorption compression refrigeration cycle utilizing LiBr-H_2O is proposed in this paper. The use of compressor between the intermediate pressure generator and intermediate pressure absorber can further lower the temperature required in the generator for same thermal lift. Since the proposed cycle requires generator temperature less than conventional two stage cycle, it is one of the refrigeration cycles with lowest generation temperature. As compared to vapor compressor refrigeration (VCR) system, hybrid two stage VAR system consists of a large number of heat exchangers and thus its size and initial investment cost

ACCEPTED MANUSCRIPT

becomes much higher. Therefore, it is needed to estimate the size and cost of the hybrid two stage system.

In the present work a mathematical model of hybrid two stage absorption compression refrigeration system is developed to carry out the thermodynamic (energy and exergy) and thermoeconomic analyses. The size and cost of the system is estimated by designing the heat exchangers. In order to determine the improvement in its performance the hybrid two stage absorption compression refrigeration system is compared with the conventional two stage VAR system. The effect of important operating parameters like generator, condenser and evaporator temperatures on the system performance is studied. The further improvement in the performance and cost of the hybrid system is carried out by optimization approaches based on thermodynamic and economic aspects.

2. System description

Fig.1 shows the schematic diagram of the hybrid two stage absorption compression refrigeration system. Basically it is a two stage absorption refrigeration system in which compressor is introduced between low pressure generator (LPG) and high pressure absorber (HPA) in order to enhance the absorption process [25]. The use of compressor allows higher thermal lift or alternatively allows lower generator temperature for same thermal lift. Thus, this system works at four pressure levels as against the conventional two stage VAR system which operates at three pressure levels.

It comprises of evaporator, low pressure absorber (LPA), HPA, LPG, high pressure generator (HPG), condenser, compressor, low pressure solution heat exchanger (LPSHE), high pressure solution heat exchanger (HPSHE), low and high pressure

ACCEPTED MANUSCRIPT

pumps (LPP and HPP) and solution throttle valves ($STVs$) and refrigerant throttle valve (RTV). The condenser and HPG operate at same pressure which is the highest system pressure. The LPG operates at an intermediate pressure, HPA operates at compressor discharge pressure and the LPA and evaporator operate at same pressure which is the lowest pressure in the system.

The refrigerant, water, is circulated through the evaporator, LPA, LPG, compressor, HPA, HPG and condenser. After water vapour has condensed in the condenser, it returns to the evaporator through refrigerant throttle valve (RTV). However, the absorbent lithium bromide aqueous solution is circulated within two separate stages i.e. a low pressure (LP) stage between the LPA and the LPG, and a high pressure (HP) stage between the HPA and the HPG.

3. Thermodynamic analysis

3.1. Assumptions

For the analysis of the hybrid two stage absorption compression refrigeration system, following assumptions are made:

- All the components of the system operate under steady state conditions.
- Pressure losses in different components and connecting pipelines are neglected.
- The potential, kinetic and chemical exergies are neglected.
- The solutions are at equilibrium at the exit of the generators and the absorbers.
- Refrigerant is saturated at the exit of evaporator and condenser.
- The system operates far away from crystallization limit.
- Water is used for heating, cooling and chilling operations.

ACCEPTED MANUSCRIPT

3.2. System model

For the energy and exergy analyses of the hybrid two stage absorption compression refrigeration system, the principles of mass and material conservation, energy balance and exergy balance are applied to each component of the system. Each component is treated as a control volume with inlet and outlet streams, heat transfer and work interactions. The application of above mentioned principles is presented in the following equations.

$$\sum \dot{m}_i - \sum \dot{m}_o = 0 \quad (1)$$

$$\sum \dot{m}_i x_i - \sum \dot{m}_o x_o = 0 \quad (2)$$

$$\sum \dot{Q} - \sum \dot{W} = \sum \dot{m}_o h_o - \sum \dot{m}_i h_i \quad (3)$$

Where $\dot{Q}$ and $\dot{W}$ are heat transfer rates and work transfer rates crossing the system boundary respectively.

The first law based performance of the two stage hybrid absorption compression refrigeration system is expressed in terms of coefficient of performance (COP):

$$COP = \frac{\dot{Q}_{evap}}{\dot{Q}_{HPG}+\dot{Q}_{LPG}+\dot{W}_{p-1}+\dot{W}_{p-2}+\dot{W}_{comp}} \quad (4)$$

where $\dot{Q}_{evap}$ is the cooling output in the evaporator, $\dot{Q}_{HPG}$ and $\dot{Q}_{LPG}$ are heat input to HPG and LPG respectively and $\dot{W}_{p-1}$, $\dot{W}_{p-2}$ and $\dot{W}_{comp}$ are the electrical power consumed by low pressure side pump, high pressure side pump and compressor respectively.

The exergy is defined as the maximum possible reversible work that can be obtained by bringing the state of the system to equilibrium with that of environment. The

ACCEPTED MANUSCRIPT

exergy flow rate of stream at each operating point, considering only physical component, is calculated using eqn. (5).

$$\dot{E} = \dot{m}[(h - h_0) - T_0(s - s_0)] \quad (5)$$

The rate of exergy destruction in a component for steady state process is expressed as :

$$\dot{E}D = \sum \dot{E}_{in} - \sum \dot{E}_{out} + \sum \dot{Q}\left(1 - {}^{T_0}/_{T}\right) - \sum \dot{W} \quad (6)$$

Here, $\dot{E}_{in}$ is the exergy of stream entering the component and $\dot{E}_{out}$ is the exergy of stream exiting the component.

The exergetic efficiency for the system is given by eqn. (7).

$$\eta_{ex} = 1 - \frac{\sum \dot{E}D}{\dot{E}_{19} - \dot{E}_{20} + \dot{E}_{25} - \dot{E}_{26} + \dot{W}_{p-1} + \dot{W}_{p-2} + \dot{W}_{comp}} \quad (7)$$

The application of mass conservation, energy conservation and exergy balance to individual components of hybrid two stage absorption compression refrigeration system results in the relations shown in Table 1. The simulation procedure for calculating thermodynamic properties at various state points is briefly described in appendix.

3.3. Thermoeconomic analysis

Thermoeconomics includes exergy costing which is nothing but assignment of cost to each stream of exergy and each component. The HPG, LPG, LPA, HPA, condenser, evaporator and both the solution heat exchangers are considered as simple heat exchangers and in order to obtain the purchase cost of each component power relations of [18] are used.

$$Z_{HX} = Z_{R,HX}\left(\frac{A_{HX}}{A_R}\right)^{0.6} \quad (8)$$

ACCEPTED MANUSCRIPT

ACCEPTED MANUSCRIPT

$$Z_p = Z_{R,p}\left(\frac{\dot{W}_p}{\dot{W}_{R,p}}\right)^{0.26}\left(\frac{1-\eta_p}{\eta_p}\right)^{0.5} \quad (9)$$

$$Z_m = Z_{R,m}\left(\frac{\dot{W}_m}{\dot{W}_{R,m}}\right)^{0.87}\left(\frac{1-\eta_m}{\eta_m}\right) \quad (10)$$

The subscript 'R' represents the reference component, 'HX' for heat exchangers, 'p' for pump and 'm' for motor. Here, A_R=100 m^2, $Z_{R,p}$=\$2100 and $\dot{W}_{R,p}$=10 kW. Also, $Z_{R,m}$=\$500 and $\dot{W}_{R,m}$=10 kW.

The investment cost for compressor is given by eqn. (11) [24]

$$Z_{comp} = 7364.\dot{m}_{ref}.PR_{comp}.\left(\frac{1-\eta_{comp}}{\eta_{comp}}\right)^{0.7} \quad (11)$$

Here, $\dot{m}_{ref}$ is the mass flow rate of refrigerant and PR_{comp} is the compressor pressure ratio. The costs involved in economic analysis at different years are converted to same reference year 2016.

In order to calculate the area of heat exchanger, the eqn. (12) is used.

$$\dot{Q} = U.A.LMTD \quad (12)$$

Here, $LMTD$ is the log mean temperature difference, U is the overall heat transfer coefficient and A is the heat transfer area of the heat exchanger. The reference costs for each of the heat exchangers are given in Table 2. The overall heat transfer coefficient based on outside diameter of tube is expressed as:

$$U = \frac{1}{\left[\left(\frac{D_o}{D_i}\right)\left(\frac{1}{h_i}\right)+\left(\frac{D_o}{D_i}\right)F_i+\left(\frac{D_o}{2k}\right)ln\left(\frac{D_o}{D_i}\right)+F_o+\left(\frac{1}{h_o}\right)\right]} \quad (13)$$

Here, D_o and D_i are the outside and inside diameters of the tube, F_i and F_o are the fouling factors at inside and outside surfaces and their value is 0.09 $\mathrm{m^2\,K\,kW^{-1}}$ [26]. In order to determine the internal and external heat transfer coefficients (h_i and h_o)

ACCEPTED MANUSCRIPT

the design methodologies of [27] and [28] are followed. The generators, absorbers, condenser and evaporator are designed as shell and tube heat exchangers whereas the solution heat exchangers are considered as single pass annular heat exchangers. The material considered for all the heat exchangers is copper. The dimensioning parameters for all the heat exchangers are given in Table 2.

The annual levelized cost for a component is given by the following equation

$$\dot{Z}_k = \dot{Z}_k^{CI} + \dot{Z}_k^{OM} \quad (14)$$

Here, $\dot{Z}_k^{CI}$ is the annual levelized capital investment and $\dot{Z}_k^{OM}$ is the annual levelized operation and maintenance cost, given as [29]

$$\dot{Z}_k^{CI} = CRF.Z_k \quad (15)$$

$$\dot{Z}_k^{OM} = \emptyset.\dot{Z}_k^{CI} \quad (16)$$

Here, Z_k is the initial capital investment of equipment (\$),$\emptyset$ is a factor which takes into account the cost of maintenance and its value is taken as 0.06 [30] and the CRF, the capital recovery factor for interest rate of i_r and life span of n years is given by

$$CRF = \frac{i_r(1+i_r)^n}{(1+i_r)^n-1} \quad (17)$$

3.4. Thermoeconomic optimization

The hybrid two stage absorption compression refrigeration system is composed of a large number of components and therefore, it is imperative to perform optimization. The thermoeconomic optimization is carried out with the purpose of striking a balance between the input exergy cost and the initial investment. In order to carry out thermoeconomic optimization both thermodynamic and economic models are required as the former provides performance prediction while latter gives cost values

ACCEPTED MANUSCRIPT

for a given set of thermodynamic parameters. The objective function of the thermoeconomic optimization is given as:

$$Minimize\ C_{Total} = \sum t_{op}.c_F.\dot{E}_F + \sum \dot{Z}_k \quad (18)$$

Here, C_{Total} is the annual cost of system operation and t_{op} are annual hours of operation of the system. The first term on the right side of the above equation represents the annual cost associated with exergy fuel input to the system which includes cost of hot water and electricity. The second term takes care of annual investment and maintenance cost of the system. In the present system the decision variables which allow the minimization of the cost of system operation are temperature of HPG, LPG, HPA, LPA, condenser, evaporator, effectiveness of both solution heat exchangers, and compressor pressure ratio.

3.5. Input Parameters

The thermodynamic and thermoeconomic analyses of two stage hybrid absorption compression refrigeration system are carried out using a computer program developed in Engineering Equation Solver (EES) software [31]. The parameters considered for the base case are given in Table 3. The streams of hot water enter HPG and LPG at 70℃ and exit at 60℃. The inlet and outlet temperatures for cooling water used in condenser, HPA and LPA are 25℃ and 30℃ respectively. The water in evaporator enters at 17℃ and exits from it at 12℃. The costs of exergy input associated with hot water (c_i) and electrical work (c_{el}) are respectively taken as 15.24 $/GJ and 32 $/GJ [18]. The thermodynamic properties at each state point for the base case are shown in Table 4.

4. Results and discussion

ACCEPTED MANUSCRIPT

Once the model is developed it is used for the analysis and optimization of hybrid two stage absorption compression refrigeration system. Initially hybrid system is compared with conventional two stage refrigeration system.

Figures 2 and 3 show the variation of COP and exergetic efficiency with generator temperature for hybrid two stage (HTS) and conventional two stage (CTS) refrigeration systems. It is clear from the figures that hybrid system requires heat source of lower temperature in comparison to conventional two stage system. Fig.2 reveals that for T_{evap}=7°C and T_{cond}=35°C, HTS system attains its maximum COP (0.43) at 55°C whereas for CTS system maximum COP (0.42) is achieved at 64°C. Thus from energy point of view, hybrid system requires low temperature heat source and offers better performance. Similarly, Fig. 3 shows that the generator temperatures corresponding to maximum exergetic efficiencies are around 7-11°C lower for HTS in comparison to CTS. Also, the maximum values of exergetic efficiencies for HTS are 2-14% greater than that for CTS, for evaporator temperature variation of 4-10°C. The existence of higher exergetic efficiencies at lower generator temperature makes the hybrid system attractive candidate for the utilization of low temperature heat.

The preliminary investigation clearly shows that the hybrid two stage absorption compression refrigeration system is very promising as compared to conventional two stage refrigeration system and must be further analysed. Therefore, thermodynamic and thermoeconomic analyses of the hybrid two stage refrigeration system are performed in rest of the section.

4.1. Parametric analysis

ACCEPTED MANUSCRIPT

The proper selection of operating parameters is very important because it not only allows the system to perform better but also helps in controlling the size and cost of the system. So effects of various parameters are discussed in this section.

4.1.1. Effects of generator temperature

Figs. 4 and 5 show the effect of generator temperature on area of each heat exchanger and total heat exchange area and annual cost of plant operation and exergetic efficiency respectively. As the generator temperature ($T_g = T_{HPG} = T_{LPG}$) is increased from 52℃ to 58℃ (keeping all other parameters unchanged) the areas of HPG and LPG are found to increase from 6.80 m^2 to 15.78 m^2 and from 7.13 m^2 to 22.85 m^2 respectively on account of reduction in LMTD (54.73% for both) and overall heat transfer coefficient. The reduction in U_{HPG} is 4% and in U_{LPG} it is 31.2%. The area of HPSHE and LPSHE registers the reduction of the order of 34% and 53% respectively due to reduced thermal load ($\dot{Q}_{HPSHE}$ decreases by 8.7% and $\dot{Q}_{LPSHE}$ decreases by 32%). The total area of heat exchangers is minimum (79.25 m^2) at generator temperature of 54.3℃.

The COP (not shown in figure) and exergetic efficiency both initially increase and attain a maximum value and then decrease with the increase in T_g. Thus, there is a particular value of generator temperature at which COP as well as η_{ex} achieves maximum value. It is found that maximum value of η_{ex} is obtained at lower T_g in comparison to COP. The maximum value of COP (0.43) is achieved at generator temperature of 53.6℃ whereas the maximum value of η_{ex} is attained at T_g of 52.8℃. The annual cost of plant operation is minimized at generator temperature of 52.7℃.

ACCEPTED MANUSCRIPT

4.1.2. Effects of evaporator temperature

Fig. 6 shows the effect of evaporator temperature on the required area of heat exchangers. The increase in T_{evap} from 6℃ to 10℃, keeping other variables constant, results in increase in evaporator area. The area of evaporator is found to increase from 9.41 m^2 to 18.93 m^2 on account of reduction in LMTD of evaporator. The area of all other components except LPG reduces with the increase in evaporator temperature. The minimum value of total area of the system is 79.61 m^2 which is obtained at evaporator temperature of 8℃.

With the increase in T_{evap}, COP (Fig. 8) tends to increase from 0.42 to 0.43 and exergetic efficiency increases from 11.24% to 11.29% (Fig. 7). The increase in evaporator temperature, for fixed cooling capacity and external fluid temperatures, causes reduction in average temperature gradient between evaporator and external chilled water and thus exergy destruction reduces and exergy efficiency increases.

Thus, from the point of view of energy and exergy analyses the performance of the system is improved with increase in T_{evap}. The maximum values of exergetic efficiency and COP are attained at maximum evaporator temperature (10℃), while at this evaporator temperature the required area becomes maximum. Hence, the system with high T_{evap} is not necessarily optimum. The system operates optimally with minimum cost of plant operation at T_{evap} of 8℃ (Fig. 7).

4.1.3. Effects of condenser temperature

The effect of condenser temperature on area of heat exchangers, and annual cost and exergetic efficiency are shown in Fig. 9 and Fig. 10. The $\pm$3℃ variation in condenser temperature from its design value causes the reduction in condenser area

ACCEPTED MANUSCRIPT

from 11.7 m^2 to 4.5 m^2 due to surge in its both LMTD and overall heat transfer coefficient. The thermal load across condenser remains, however, constant. The area of HPG and LPG registers a slight decrease whereas area of LPG, LPA and LPSHE shows nominal increase with the increase in condenser temperature. The increase in T_{cond} from 32℃ to 38℃ brings SCR_h up to 4.7 from 3.5, causing increase in heat load in HPSHE which results in increase in area of HPSHE by almost 68%. The total area of the system is reduced by 6.83% and its minimum value is attained at the maximum value of condenser temperature.

The increase of 6℃ in T_{cond} causes an increase in its exergy destruction from 1.6 kW to 3.5 kW due to high thermal gradient between condenser and cooling water. Consequently, the exergetic efficiency of the system drops in from 11.44% to 11.31%, as shown in Fig. 10. It is also found in the study that with the increase in T_{cond}, the required heat input in HPG and LPG increases by 1.4% and 1.1% respectively, consequently COP of the system falls down from 0.434 to 0.417 as shown in Fig. 8.

Thus, it can be concluded that higher value of T_{cond} is advantageous from the viewpoint of area and thus initial investment cost, but its lower value is favourable from the perspective of first and second law analyses. Hence, a trade-off is made and minimum annual cost of plant operation is obtained at condenser temperature of 34.5℃.

4.1.4. Effects of absorber temperature

Fig. 11 shows the variation of heat exchangers area and total area with absorber temperature and Fig. 12 shows the effect of absorber temperature on exergetic

ACCEPTED MANUSCRIPT

efficiency and annual cost of the system. The increase in absorber temperature ($T_{abs} = T_{HPA} = T_{LPA}$) from 32℃ to 38℃ causes the thermal load at HPG, LPG, LPA, HPSHE and LPSHE to increase while keeping other variables constant. The increase in thermal load in these components is attributed to increase in the value of SCR_h (2.51 to 6.27) and SCR_l (9.20 to 19.18) with the increase in T_{abs}. The thermal load across condenser, however, remains constant.

The area of HPA and LPA drops by 41.6% and 40.1% respectively due to rise in corresponding overall heat transfer coefficient and LMTD with the increase in T_{abs}. The area of HPG increases from 9.38 m^2 to 15.80 m^2 whereas the area of LPG decreases from 14.29 m^2 to 9.58 m^2. This is because of the decrease of U_{HPG} and increase of U_{LPG}, LMTD of both the generators remains constant. The required area of HPSHE and LPSHE is increased immensely with the increase in absorber temperature due to increase in $\dot{Q}_{HPSHE}$ (154.5%) and $\dot{Q}_{LPSHE}$ (64.2%) and decrease in the corresponding product of overall heat transfer coefficient of heat transfer and LMTD. The net area is minimum (79.35 m^2) at 34.4℃.

Further, the increase in absorber temperature causes the exergy destruction in HPA and LPA to increase by 47.4% and 35.5 % respectively. The 6℃ rise in absorber temperature deteriorates the performance of the system as COP drops from 0.4325 to 0.4217 and exergetic efficiency falls down to 11.24% from 11.48%.

So, from the viewpoint of first and second law, lowest absorber temperature is recommended but it is not so from the standpoint of initial cost which is based on area of heat exchangers. Hence, a compromise is made and minimum cost is obtained at absorber temperature of 34.3℃, as shown in Fig. 12.

ACCEPTED MANUSCRIPT

4.1.5. Effects of compressor pressure ratio

Fig. 13 shows the variation of area of each heat exchanger and total area with the compressor pressure ratio (PR_{comp}) which is defined as the ratio of compressor discharge pressure to compressor suction pressure. With the increase in pressure ratio from 1.7 to 1.9, area of all heat exchangers remains constant except that of HPG, HPA and HPSHE. The increase in the areas of HPG and HPA is 0.5% and 2.1% respectively. The area of HPSHE is reduced by 37.74% and the net effect is the drop in the total required area. The increase in the compressor discharge pressure, (keeping suction pressure of compressor constant) reduces SCR_h which causes the reduction in heat loads in HPG, HPA and HPSHE and reduction in the product of overall heat transfer coefficient and LMTD of HPG and HPA. However, the trend of the product of overall heat transfer coefficient and LMTD in case of HPSHE is opposite.

Fig. 14 reveals the effect of compressor pressure ratio on exergetic efficiency as well as total annual cost of the system. The exergetic efficiency of the system decreases from 11.54% to 11.23% as compressor work input increases from 4.53 kW to 5.55 kW with the increase in PR_{comp}. However, COP shows a slight improvement and increases from 0.427 to 0.428. The overall economic consequence of increase in PR_{comp} is the rise of almost 3% of annual cost of plant operation.

4.1.6. Effects of compressor isentropic efficiency

Fig. 15 shows the variation of area of heat exchangers and Fig. 16 shows the variation of exergetic efficiency and annual cost of operation with the isentropic efficiency of compressor (η_{comp}). Keeping all the operating variables constant at

ACCEPTED MANUSCRIPT

base case condition the increase in η_{comp} from 0.7 to 0.9 results in minimal decrease in HPA area only, the area of other heat exchangers remains unaffected. Consequently, the total area is also reduced by 0.14%. The exergetic efficiency is positively affected by the increase in compressor isentropic efficiency. It registers a growth of 4% with increase in η_{comp}. The minimum annual cost of plant operation is obtained at the compressor isentropic efficiency of 0.88.

4.1.7. Effects of effectiveness of solution heat exchanger

The effectiveness of solution heat exchanger (ϵ_{SHE}) is one of the crucial decision variables which affect the hybrid two stage absorption compression refrigeration system to a great strength. The impact of effectiveness of solution heat exchangers on areas is shown in Fig. 17 whereas its influence on exergetic efficiency and cost is shown in Fig.18. For the base case its value is taken as 0.7 for both HPSHE as well as LPSHE. Keeping other design variable mentioned in Table 2 as fixed, as ϵ_{SHE} (=$\epsilon_{LPSHE} = \epsilon_{HPSHE}$) is increased from 0.6 to 0.8 the thermal load across both the solution heat exchangers is increased by 33.3%. Also, the products of overall heat transfer coefficient and LMTD for LPSHE and HPSHE are decreased by 42.85% and 31.54% respectively. Consequently, the required area of LPSHE and HPSHE is increased respectively by 133.1% and 94.9%. The area of LPG and HPG is decreased while that of HPA and LPA is increased with increase in ϵ_{SHE}. The total area of all heat exchangers registers an increase of 27.57%.

The heat input required in generators decreases with increase in effectiveness of SHEs, resulting in improvement in COP by 2.12%. The exergetic efficiency rises from 11.28% to 11.48% with the increase in ϵ_{SHE} from 0.6 to 0.8.

ACCEPTED MANUSCRIPT

Fig.18 clearly shows that annual cost of the chiller increases with the increase in solution heat exchanger effectiveness. It is increased from 16567 $/year to 17132 $/year. Hence, it is clear that higher values of ϵ_{SHE} are desirable from the standpoint of energy and exergy but from the viewpoint of area and thus economics lower values of ϵ_{SHE} are advantageous.

4.2. Results of thermoeconomic optimization

The parametric analysis clearly reveals that heat exchanger with high exergetic performance is not always optimum as overall cost of the system may be high. So, it becomes imperative to establish the optimum point of operation not only thermodynamically but also economically. The minimization of the annual cost of plant operation is the objective of the optimization. The decision variable employed here are the temperatures of HPG, LPG, HPA, LPA, condenser, evaporator, effectiveness of HPSHE and LPSHE and compressor pressure ratio. The values of decision variables are varied simultaneously within the limits used for parametric analysis. There are two cases of thermoeconomic optimization: case-1 corresponds to economic parameters of the base case and case-2 corresponds to reduced interest rate (3.5%), increased annual operation hours (6000 h) and increased life span of plant (15 years).

Table 5 and 6 provide the results of thermoeconomic optimization of two stage absorption compression hybrid refrigeration system. The optimum values of decision variables $T_{HPG}, T_{LPG}, T_{evap}, T_{cond}, T_{HPA}, T_{LPA}, PR_{comp}, \epsilon_{HPSHE}, \epsilon_{LPSHE}$ are found to be 52℃, 52℃, 8.2℃, 34.1℃, 33.1℃, 32.8℃, 1.65, 0.6 and 0.6 for case-1. The corresponding values for case-2 are 52℃, 52℃, 9.4℃, 32.4℃, 33.0℃, 32.6℃, 1.65, 0.6 and 0.6. The first and second law of thermodynamics clearly reveals that

ACCEPTED MANUSCRIPT

optimization results in improvement of COP, though marginal. The improvement in COP for case-1 (0.428 to 0.429) is lesser than in case-2 (0.428 to 0.435). The electrical COP (COP_{el}), calculated using electrical energy input only and ignoring the heat input, of the optimized system is significantly higher than the base case. The COP_{el} for case-1 is increased from 19.80 to 23.75 whereas for case-2 it is improved from 19.80 to 23.81, as given in Table 5. The exergetic performance is also observed to improve as total exergy destruction reduce through optimization for both the cases.

It is to be highlighted that the cost and size are the major hurdles in the practical implementation of the two stage absorption compression hybrid refrigeration system. They can be reduced considerably through system optimization. The total heat exchange area for case-1 is reduced from 79.61 m^2 to 71.96 m^2, resulting in reduction in initial investment cost by 6.0%, through optimization. Similarly, for cas-2, the optimization brings down heat exchange area from 79.61m^2 to 77.65 m^2. As a result, the initial capital investment in case-2 is decreased by only 2.8%. The lower reduction in initial capital cost in case-2 as compared to case-1 is compensated by greater reduction in cost of fuel exergy (hot water and electricity) in case-2 in comparison to case-1. Consequently, the annual cost of system operation is reduced by 5.2% for both the cases through thermoeconomic optimization. Table 6 provides the values of LMTD, overall heat transfer coefficient and area of all the heat exchangers for base case as well as their optimized values for case-1 and case-2.

Conclusions

In the present study hybrid two stage lithium bromide absorption compression refrigeration system is proposed. The design of heat exchangers of the system is

ACCEPTED MANUSCRIPT

carried out for air conditioning applications in order to assist the design engineer in the estimation of size and cost of the system.

The effects of important decision variables on size, performance and cost of the system are examined. The hybrid two stage absorption compression refrigeration system needs 7-10°C lower generator temperature than the conventional one. The COP and exergetic efficiency of hybrid system are better than that of the conventional system. There is a particular value of generator temperature at which COP as well as exergetic efficiency achieves maximum value. The maximum value of exergetic efficiency is obtained at lower generator temperature in comparison to maximum value of COP. The system with high evaporator temperature is not optimum as annual cost is high. Though low values of absorber and condenser temperatures are desirable from viewpoint of energy and exergy yet operating system at their high values is advantageous as this results in low overall cost of the system. The increase in compressor discharge pressure increases COP and annual cost but reduces exergetic efficiency and size of the system. The higher values of solution heat exchanger effectiveness are preferable from the standpoint of first and second law of thermodynamics but from viewpoint of size and cost, their low values are recommended.

Finally, the system is optimized with the objective of minimizing the annual cost of the system which covers both thermal and economic aspects. The optimization results in reduction of annual cost of the system by 5.2%.

Nomenclature

A	area (m^2)
COMP	compressor
COP	coefficient of performance

ACCEPTED MANUSCRIPT

CRF	capital recovery factor
CTS	conventional two stage
D	diameter (m)
$\dot{E}$	exergy flow rate (kW)
$\dot{ED}$	rate of exergy destruction (kW)
$\dot{EF}$	exergy flow rate of fuel (kW)
$\dot{EP}$	exergy flow rate of product(kW)
F	fouling factor ($m^2\ K\ kW^{-1}$)
h	specific enthalpy (kJ kg^{-1})
h_i	internal heat transfer coefficient (kW m^{-2} K^{-1})
h_o	external heat transfer coefficient (kW m^{-2} K^{-1})
HPA	high pressure absorber
HPG	high pressure generator
HPSHE	high pressure solution heat exchanger
HPSTV	high pressure solution throttle valve
HTS	hybrid two stage
i_r	rate of interest (%)
k	thermal conductivity (kW m^{-1} K^{-1})
LMTD	log mean temperature difference (°C)
LPA	low pressure absorber
LPG	low pressure generator
LPSHE	low pressure solution heat exchanger
LPSTV	low pressure solution throttle valve
$\dot{m}$	mass flow rate (kg s^{-1})

ACCEPTED MANUSCRIPT

ACCEPTED MANUSCRIPT

n	Life span of plant
p	pressure (kPa)
PR	pressure ratio
$\dot{Q}$	heat transfer rate (kW)
RTV	refrigerant throttle valve
s	specific entropy (kJ kg^{-1} K^{-1})
SCR	solution circulation ratio
STV	solution throttle valve
T	temperature (°C or K)
t_{op}	annual hours of operation (h)
U	overall heat transfer coefficient (kW m^{-2} K^{-1})
$\dot{W}$	work transfer rate (kW)
x	LiBr concentration in solution (%)
Z	Initial investment cost ($)
$\dot{Z}$	annual levelized cost ($)
Greek letters	
ϵ	Effectiveness of heat exchanger
η	efficiency
Subscripts	
0	represents dead state
1, 2, 3…	state points
abs	absorber
comp	compressor
cond	condenser

ACCEPTED MANUSCRIPT

ACCEPTED MANUSCRIPT

el	electrical
evap	evaporator
ex	exergetic
F	fuel
g	generator
h	high pressure side
i	inside
l	low pressure side
m	motor
o	outside
P	pump
she	Solution heat exchanger

Acknowledgement

The support of Ministry of New and Renewable Energy (MNRE), government of India is duly acknowledged.

Appendix

The main steps to carry out energy and exergy analyses are as follows:

- Input and assumptions:
  $T_{HPG}, T_{LPG}, T_{HPA}, T_{LPA}, T_{cond}, T_{evap}, \dot{Q}_{evap}, \epsilon_{HPSHE}, \epsilon_{LPSHE}, P_{LPG}, PR_{comp}, \eta_p, \eta_{comp}, T_{19}, T_{20}, T_{21}, T_{22}, T_{23}, T_{24}, T_{25}, T_{26}, T_{27}, T_{28}, T_{29}, T_{30}, y_{16}, y_{18}$
  (Here, y is water vapor quality)

- Calculate: P_{cond}=$P_{sat}(T_{cond})$; P_{evap}=$P_{sat}(T_{evap})$; P_{HPA}
- P_{HPG}=P_{cond}; P_{LPA}=P_{evap}

- T_1= T_{LPA}; P_1= P_{LPA}: Calculate x_1, h_1, s_1

ACCEPTED MANUSCRIPT

- x_2=x_1; P_2= P_{LPG}: Calculate T_2, h_2, s_2 and $\dot{W}_{p-2}$ (using η_p)
- Calculate T_3 and T_5 using energy balance at LPSHE and ϵ_{LPSHE}
  x_5=x_4; x_3=x_2 Calculate h_3, h_5, s_3 and s_5
- T_4= T_7= T_{LPG}; P_4= P_7= P_{LPG}: Calculate x_4, h_4, s_4, h_7, s_7
- x_6=x_5; h_6=h_5 Calculate T_6 and s_6
- P_8= P_{HPA}; Calculate T_8, h_8, s_8 and $\dot{W}_{comp}$ (using η_{comp})
- T_9= T_{HPA}; P_9= P_{HPA}: Calculate x_9, h_9, s_9
- x_{10}=x_9; P_{10}= P_{HPG}: Calculate T_{10}, h_{10}, s_{10} and $\dot{W}_{p-1}$ (using η_p)
- Calculate T_{11} and T_{13} using energy balance at HPSHE and ϵ_{HPSHE}
  x_{13}=x_{12}; x_{11}=x_{10} Calculate h_{11}, h_{13}, s_{11} and s_{13}
- T_{12}= T_{15}= T_{HPG}; P_{12}= P_{15}= P_{HPG}: Calculate x_{12}, h_{12}, s_{12}, h_{15}, s_{15}
-
- x_{14}=x_{13}; h_{14}=h_{13} Calculate T_{14} and s_{14}
- T_{16}=T_{cond} y_{16}=0, Calculate h_{16}, s_{16}
- h_{17}=h_{16}, P_{17}=P_{evap} Calculate T_{17} and s_{17}
- T_{18}=T_{evap}, y_{18}=1, Calculate h_{18} and s_{18}
- Mass and species balance to each component gives mass flow rates and LiBr concentration at each internal point of the cycle.
- Using energy relations (Table 1), energy and work interactions across each component are calculated.
- Mass flow rates of external chilled water, cooling water and hot water is calculated
- Exergy at each point is calculated state point properties (h and s) and exergy destruction rates are calculated using exergy relations of Table 1.

References

ACCEPTED MANUSCRIPT

[1] Boer, D., Valles, M., Coronas, A., 1998. Performance of double effect absorption compression cycles for air-conditioning using methanol–TEGDME and TFE–TEGDME systems as working pairs. Int. J. Refrig. 21(7), 542-555

[2] Kim, J.S., Ziegler, F., Lee, H., 2002. Simulation of the compressor-assisted triple-effect H_2O/LiBr absorption cooling cycles. Applied Thermal Engineering 22, 295-308

[3] Zheng, D., Meng, X., 2012. Ultimate refrigerating conditions, behavior turning and a thermodynamic analysis for absorption-compression hybrid refrigeration cycle. Energy Conversion and Management 56, 166-174

[4] Kang, Y.T., Hong, H., Park, K.S., 2004. Performance analysis of advanced hybrid GAX cycles: HGAX Int J Refrig. 27(4), 442–448

[5] Medrano, M., Bourouis, M., Coronas, A., 2001. Double-lift absorption refrigeration cycles driven by low–temperature heat sources using organic fluid mixtures as working pairs. Appl. Energy 68, 173–185. doi:10.1016/S0306-2619(00)00048-9

[6] Herold, K.E., Radermacher, R., Klein, S.A., 1996. Absorption chillers and heat pumps. CRC Press, USA

[7] Ma, W.B., Deng, S.M., 1996. Theoretical analysis of low-temperature hot source driven two-stage LiBr/H_2O absorption refrigeration system. International Journal of Refrigeration 19(2), 141-146

[8] Kim, D., Machielsen, C., 2002. Evaluation of air-cooled solar absorption cooling systems. In: Proc. 7th Int. Sorption Heat Pump Conf., 117−22

[9] Izquierdo, M., 2004. Crystallization as a limit to develop solar air-cooled LiBr–H2O absorption systems using low-grade heat. Sol. Energy Mater. Sol. Cells 81,

ACCEPTED MANUSCRIPT

205–216. doi:10.1016/j.solmat.2003.11.002

[10] Arivazhagan S., Murugesan S.N., Saravanan R., Renganarayanan S., 2005. Simulation studies on R134a—DMAC based half effect absorption cold storage systems Energy Conversion and Management 46, 1703–1713.

[11] Arivazhagan S., Saravanan R., Renganarayanan S., 2006. Experimental studies on HFC based two-stage half effect vapour absorption cooling system. Applied Thermal Engineering 26, 1455–1462.

[12] Domínguez-Inzunza, L. A., Hernández-Magallanes, J.A., Sandoval-Reyes, M., Rivera, Florides, G. a., Kalogirou, S. A., Tassou, S. A., Wrobel, L.C., 2014. Design and construction of a LiBr–water absorption machine. Energy Convers. Manag. 44, 2483–2508. doi:10.1016/S0196-8904(03)00006-2.

[13] Crepinsek, Z., Goricanec, D., Krope, J., 2009. Comparison of the performances of absorption refrigeration cycles. WSEAS Transactions on Heat and Mass Transfer 3(4), 65-76.

[14] Izquierdo, M., Venegas, M., García, N., Palacios, E., 2005. Exergetic analysis of a double stage LiBr–H2O thermal compressor cooled by air/water and driven by low grade heat. Energy Convers. Manag. 46, 1029–1042. doi:10.1016/j.enconman.2004.06.016.

[15] Gebreslassie, B.H., Medrano. M., Boer, D., 2010. Exergy analysis of multi-effect water-LiBr absorption systems from half to triple effect. Reneawable Energy 35, 1773-1782.

[16] Gomri, R., 2010. Solar energy to drive half-effect cooling system. Int. J. of Thermal and Environmental Engineering 1(1), 1-8.

[17] Arora, A., Dixit, M., Kaushik, S.C., 2016. Computation of optimum parameters of

ACCEPTED MANUSCRIPT

a half effect water-lithium. Journal of Thermal Engineering 2 (2), 683–692.

[18] Misra, R.D., Sahoo, P.K., Sahoo, S., Gupta, a, 2003. Thermoeconomic optimization of a single effect water / LiBr vapour absorption refrigeration system. Int. J. Refrig. 26, 158–169. doi:10.1016/S0140-7007(02)00086-5.

[19] Misra, R.D., Sahoo, P.K., Sahoo, S., Gupta, A, 2005. Thermoeconomic evaluation and optimization of a double effect H_2O/LiBr vapour absorption refrigeration system. Int. J. Refrig. 28(3), 331–343.

[20] Garousi Farshi, L., Mahmoudi, S.M.S., Rosen, M.A., Yari, M., Amidpour, M., 2013. Exergoeconomic analysis of double effect absorption refrigeration systems. Energy Convers. Manag. 65, 13–25. doi:10.1016/j.enconman.2012.07.019.

[21] Garousi Farshi, L., Mahmoudi, S.M.S., Rosen, M.A., Yari, M., Amidpour, M., 2013. Exergoeconomic analysis of double effect absorption refrigeration systems. Energy Convers. Manag. 65, 13–25. doi:10.1016/j.enconman.2012.07.019.

[22] Kizilkan O., Sencan, A., Kalogirou S.A., 2007. Thermoeconomic optimization of a LiBr absorption refrigeration system. Chem. Eng. Process 46, 1376–84.

[23] Maya, C.R., Ibarra, J.J.P., Flores, J.M.B., González, S.R.G., Covarrubias, C.M., 2012. NLP model of a LiBr H_2O absorption refrigeration system for the minimization of the annual operating cost. Applied Thermal Engineering 37,10–8.

[24] Mehr, A. S., Zare, V., Mahmoudi, S.M.S., 2013. Standard GAX versus hybrid GAX absorption refrigeration cycle: From the view point of thermoeconomics. Energy Convers. Manag. 76, 68–82. doi:10.1016/j.enconman.2013.07.016.

ACCEPTED MANUSCRIPT

[25] Bouaziz, N., BenIffa, R., Nehdi, E., Kairouani, L., 2011. Conception of an absorption refrigerating system operating at low enthalpy sources. In: Moreno-Pirajan Juan Carlos, editor. Thermodynamics - systems in equilibrium and non-equilibrium;. ISBN: 978-953-307-283-8, InTech.

[26] Howell, R.H., Sauer, H.J., Coad, W.J., 1998. Principles of HVAC, ASHRAE Refrigeration Equipment, [chapter 18.21].

[27] Bakhtiari, B., Fradette, L., Legros, R., Paris, J., 2011. A model for analysis and design of H_2O–LiBr absorption heat pumps. Energy Convers. Manag. 52, 1439–1448. doi:10.1016/j.enconman.2010.09.037.

[28] Florides, G.A., Kalogirou, S.A., Tassou, S.A., Wrobel, L.C., 2003. Design and construction of a LiBr–water absorption machine. Energy Convers Manage., 44, 2483–508.

[29] Bejan, A., Tsatsaronis, G., Moran, M., 1996. Thermal design and optimization. New York, USA: John Wiley and Sons Inc.

[30] Singh, O.K., Kaushik, S.C., 2013. Thermoeconomic evaluation and optimization of a Brayton-Rankine-Kalina combined triple power cycle. Energy Convers. Manag. 71, 32–42. doi:10.1016/j.enconman.2013.03.017.

[31] Klein, S.A., Alvarado, F., 2005. Engineering Equation Solver, Version 7.441. F Chart software, Middleton, WI.

ACCEPTED MANUSCRIPT

ACCEPTED MANUSCRIPT

List of Figures

Fig.1. Two stage hybrid absorption compression refrigeration system

Fig.2. Variation of COP with generator temperature in hybrid and conventional two stage refrigeration system

Fig. 3. Variation of exergetic efficiency with generator temperature in hybrid and conventional two stage refrigeration system

Fig. 4. Variation of heat transfer area with generator temperature

Fig. 5. Variation of annual cost and exergetic efficiency with generator temperature

Fig. 6. Variation of heat transfer area with evaporator temperature

Fig. 7. Variation of annual cost and exergetic efficiency with evaporator temperature

Fig. 8. Variation of COP with condenser temperature at various evaporator temperatures

Fig. 9. Variation of heat transfer area with condenser temperature

Fig. 10. Variation of annual cost and exergetic efficiency with condenser temperature

Fig. 11. Variation of heat transfer area with absorber temperature

Fig. 12. Variation of annual cost and exergetic efficiency with absorber temperature

Fig. 13. Variation of heat transfer area with compressor pressure ratio

Fig. 14. Variation of annual cost and exergetic efficiency with compressor pressure ratio

Fig. 15. Variation of heat transfer area with compressor efficiency

Fig. 16. Variation of annual cost and exergetic efficiency with compressor efficiency

ACCEPTED MANUSCRIPT

ACCEPTED MANUSCRIPT

Fig. 17. Variation of heat transfer area with effectiveness of solution heat exchanger

Fig. 18. Variation of annual cost and exergetic efficiency with effectiveness of solution heat exchanger

List of Tables

Table 1 Energy and exergy relations for hybrid two stage absorption compression refrigeration system

Table 2 Reference cost and dimensioning parameters for heat exchangers

Table 3 Input data for the base case

Table 4 Thermodynamic properties at various state points for base case

Table 5 Results of the thermoeconomic optimization

Table 6 Parameters of heat exchangers

ACCEPTED MANUSCRIPT

ACCEPTED MANUSCRIPT

Components	Energy relations	Exergy relations
HPG	$\dot{Q}_{HPG} + \dot{m}_{11}h_{11} = \dot{m}_{12}h_{12} + \dot{m}_{15}h_{15}$	$\dot{ED}_{HPG} = \dot{E}_{19} + \dot{E}_{11} - \dot{E}_{12} - \dot{E}_{15} - \dot{E}_{20}$
LPG	$\dot{Q}_{LPG} + \dot{m}_3 h_3 = \dot{m}_4 h_4 + \dot{m}_7 h_7$	$\dot{ED}_{LPG} = \dot{E}_{25} + \dot{E}_3 - \dot{E}_4 - \dot{E}_7 - \dot{E}_{26}$
HPA	$\dot{Q}_{HPA} + \dot{m}_9 h_9 = \dot{m}_{14}h_{14} + \dot{m}_8 h_8$	$\dot{ED}_{HPA} = \dot{E}_8 + \dot{E}_{14} + \dot{E}_{23} - \dot{E}_9 - \dot{E}_{24}$
LPA	$\dot{Q}_{LPA} + \dot{m}_1 h_1 = \dot{m}_{18}h_{18} + \dot{m}_6 h_6$	$\dot{ED}_{LPA} = \dot{E}_{18} + \dot{E}_6 + \dot{E}_{27} - \dot{E}_1 - \dot{E}_{28}$
Condenser	$\dot{Q}_{cond} = \dot{m}_{15}(h_{15} - h_{16})$	$\dot{ED}_{cond} = \dot{E}_{15} + \dot{E}_{21} - \dot{E}_{16} - \dot{E}_{22}$
Evaporator	$\dot{Q}_{evap} = \dot{m}_{18}(h_{18} - h_{17})$	$\dot{ED}_{evap} = \dot{E}_{17} + \dot{E}_{29} - \dot{E}_{18} - \dot{E}_{30}$
HPSHE	$\dot{Q}_{HPSHE} = \dot{m}_{11}(h_{11} - h_{10})$	$\dot{ED}_{HPSHE} = \dot{E}_{12} + \dot{E}_{10} - \dot{E}_{13} - \dot{E}_{11}$
LPSHE	$\dot{Q}_{LPSHE} = \dot{m}_3(h_3 - h_2)$	$\dot{ED}_{LPSHE} = \dot{E}_4 + \dot{E}_2 - \dot{E}_5 - \dot{E}_3$
COMP	$\dot{W}_{comp} = \dot{m}_8(h_{8s} - h_7)/\eta_{comp}$	$\dot{ED}_{comp} = \dot{E}_7 + \dot{W}_{comp} - \dot{E}_8$
P-1	$\dot{W}_{p-1} = \dot{m}_{10}(h_{10s} - h_9)/\eta_p$	$\dot{ED}_{p-1} = \dot{E}_9 + \dot{W}_{p-1} - \dot{E}_{10}$
P-2	$\dot{W}_{p-2} = \dot{m}_2(h_{2s} - h_1)/\eta_p$	$\dot{ED}_{p-2} = \dot{E}_1 + \dot{W}_{p-2} - \dot{E}_2$
HPSTV	$h_{14} = h_{13}$	$\dot{ED}_{HPSTV} = \dot{E}_{13} - \dot{E}_{14}$
LPSTV	$h_6 = h_5$	$\dot{ED}_{LPSTV} = \dot{E}_5 - \dot{E}_6$
RTV	$h_{17} = h_{16}$	$\dot{ED}_{RTV} = \dot{E}_{16} - \dot{E}_{17}$

ACCEPTED MANUSCRIPT

Component	**Reference cost** [14] **($)**	D_o **(mm)**	D_i **(mm)**
HPG	17500	14.97	13.57
LPG	17500	14.97	13.57
HPA	16500	14.97	13.57
LPA	16500	14.97	13.57
Condenser	8000	14.97	13.57
Evaporator	16000	14.97	13.57
$HPSHE$	12000	14.97[a]/9.50[b]	13.57[a]/8.80[b]
$LPSHE$	12000	14.97[a]/9.50[b]	13.57[a]/8.80[b]

[a] refers to outer tube, [b] refers to inner tube

ACCEPTED MANUSCRIPT

ACCEPTED MANUSCRIPT

Parameters	**value**
Cooling capacity, $\dot{Q}_{evap}$ (kW)	100
Environment pressure, P_0 (kPa)	101.3
Environment temperature, T_0 (℃)	25
HPG temperature, T_{HPG} (℃)	55
LPG temperature, T_{LPG} (℃)	55
Evaporator temperature, T_{evap} (℃)	8
Condenser temperature, T_{cond} (℃)	35
HPA temperature, T_{HPA} (℃)	35
LPA temperature, T_{LPA} (℃)	35
Effectiveness of HPSHE, ϵ_{HPSHE}	0.7
Effectiveness of LPSHE, ϵ_{LPSHE}	0.7
Compressor isentropic efficiency, η_{comp}	0.8
Pump efficiency, η_p	0.9
Compressor pressure ratio, PR_{comp}	1.8
Interest rate, i_r (%)	15
Life span of system, n (years)	10
annual operation of hours, t_{op} (hours)	5000

ACCEPTED MANUSCRIPT

ACCEPTED MANUSCRIPT

State No.	T (°C)	P (kPa)	$\dot{m}$ (kg s^{-1})	LiBr Concentration (%)	h (kJ kg^{-1})	s (kJ kg^{-1} K^{-1})
1	35	1.073	0.5304	53.46	79.31	0.2224
2	35	2	0.5304	53.46	79.32	0.2224
3	47.09	2	0.5304	53.46	104.4	0.3024
4	55	2	0.4882	58.08	136.7	0.321
5	41.04	2	0.4882	58.08	109.4	0.2359
6	41.04	1.073	0.4882	58.08	109.4	0.2359
7	55	2	0.04222	-	2603	8.95
8	118.4	3.6	0.04222	-	2723	9.012
9	35	3.6	0.1672	35.26	79.05	0.3758
10	35	5.627	0.1672	35.26	79.05	0.3758
11	43.53	5.627	0.1672	35.26	101.6	0.4479
12	55	5.627	0.125	47.18	115.5	0.4151
13	41.74	5.627	0.125	47.18	85.26	0.3213
14	41.74	3.6	0.125	47.18	85.26	0.3213
15	55	5.627	0.04222	-	2602	8.47
16	35	5.627	0.04222	-	146.6	0.505
17	8	1.073	0.04222	-	146.6	0.5231
18	8	1.073	0.04222	-	2515	8.948
19	70	600	2.565	-	293.5	0.9546
20	60	600	2.565	-	251.6	0.8309

ACCEPTED MANUSCRIPT

21	25	100	4.956	-	104.8	0.367
22	30	100	4.956	-	125.7	0.4365
23	25	100	5.373	-	104.8	0.367
24	30	100	5.373	-	125.7	0.4365
25	70	600	2.898	-	293.5	0.9546
26	60	600	2.898	-	251.6	0.8309
27	25	100	5.619	-	104.8	0.367
28	30	100	5.619	-	125.7	0.4365
29	17	100	4.779	-	71.28	0.2532
30	12	100	4.779	-	50.36	0.1804

ACCEPTED MANUSCRIPT

ACCEPTED MANUSCRIPT

Parameters	**Base case**	**Thermoeconomic optimized**	
		Case-1 (i_r=15%, n=10 years, t=5000 h)	**Case-2 (i_r=3.5%, n=15 years, t=6000 h)**
Annual cost ($/year)	16788[a]/15204[b]	15919	14418
Capital investment ($)	30614	28772	29758
Area (m^2)	79.61	71.96	77.65
COP	0.4281	0.4294	0.4352
η_{ex} (%)	11.38	11.68	11.83
$\dot{E}D$(kW)	25.66	24.81	24.47
$\dot{E}D_{HPG}$(kW)	5.14	5.77	6.40
$\dot{E}D_{LPG}$(kW)	4.64	5.67	5.86
$\dot{E}D_{HPA}$(kW)	4.77	3.75	3.58
$\dot{E}D_{LPA}$(kW)	4.76	3.82	3.92
$\dot{E}D_{cond}$(kW)	2.55	2.23	1.70
$\dot{E}D_{evap}$(kW)	2.40	2.31	1.86
$\dot{E}D_{HPSHE}$(kW)	0.11	0.10	0.09
$\dot{E}D_{LPSHE}$(kW)	0.28	0.28	0.23
$\dot{E}D_{comp}$(kW)	0.78	0.67	0.67
$\dot{E}D_{RTV}$(kW)	0.23	0.21	0.16

ACCEPTED MANUSCRIPT

ACCEPTED MANUSCRIPT

SCR_l	12.56	11.50	10.41
SCR_h	3.96	3.78	3.22
$\dot{Q}_{HPG}$ (kW)	107.3	107.5	106.6
$\dot{Q}_{LPG}$ (kW)	121.3	121.1	119.0
$\dot{Q}_{HPA}$ (kW)	112.4	111.8	110.9
$\dot{Q}_{LPA}$ (kW)	117.5	117.7	115.6
$\dot{Q}_{cond}$ (kW)	103.7	103.4	103.3
$\dot{Q}_{evap}$ (kW)	100	100	100
$\dot{Q}_{HPSHE}$ (kW)	3.8	3.2	2.4
$\dot{Q}_{LPSHE}$ (kW)	13.3	11.0	9.1
$\dot{W}_{comp}$ (kW)	5.05	4.21	4.20

ACCEPTED MANUSCRIPT

ACCEPTED MANUSCRIPT

Parameters		**Base case**	**Thermoeconomic optimization**	
		(i_r=15%, n=10 years, t=5000 h)	**Case-1** (i_r=15%, n=10 years, t=5000 h)	**Case-2** (i_r=3.5%, n=15 years, t=6000 h)
	HPG	9.10	12.33	12.33
	LPG	9.10	12.33	12.33
	HPA	10.84	9.58	8.72
LMTD	LPA	10.51	9.07	8.95
(K)	COND	7.21	6.25	4.48
	EVAP	6.17	5.92	4.62
	HPSHE	8.89	9.94	10.88
	LPSHE	6.93	8.47	8.66
	HPG	1.25	1.25	1.23
	LPG	1.13	1.13	1.01
	HPA	1.11	1.12	1.09
U	LPA	1.17	1.17	1.16
($kW\ m^{-2}K^{-1}$)	COND	2.23	2.22	2.22
	EVAP	1.31	1.31	1.32
	HPSHE	0.12	0.13	0.13
	LPSHE	0.13	0.12	0.12

ACCEPTED MANUSCRIPT

	HPG	9.46	6.95	7.05
	LPG	11.79	8.67	9.55
	HPA	9.65	10.82	12.04
A	LPA	9.86	11.43	11.50
(m^2)	COND	6.46	7.44	10.37
	EVAP	12.42	12.91	16.41
	HPSHE	3.28	2.51	1.70
	LPSHE	16.69	11.23	9.03

ACCEPTED MANUSCRIPT

ACCEPTED MANUSCRIPT

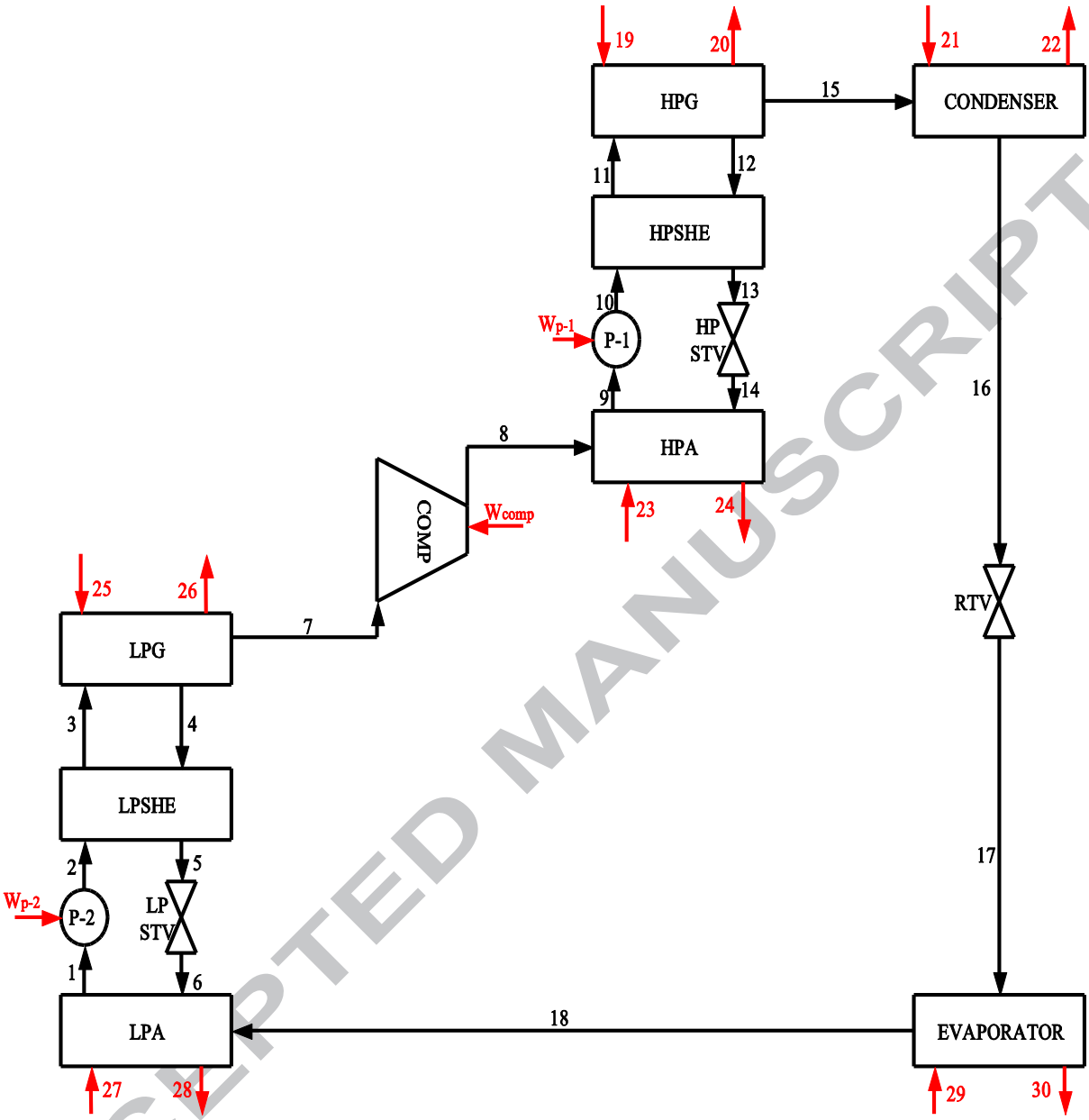

ACCEPTED MANUSCRIPT

ACCEPTED MANUSCRIPT

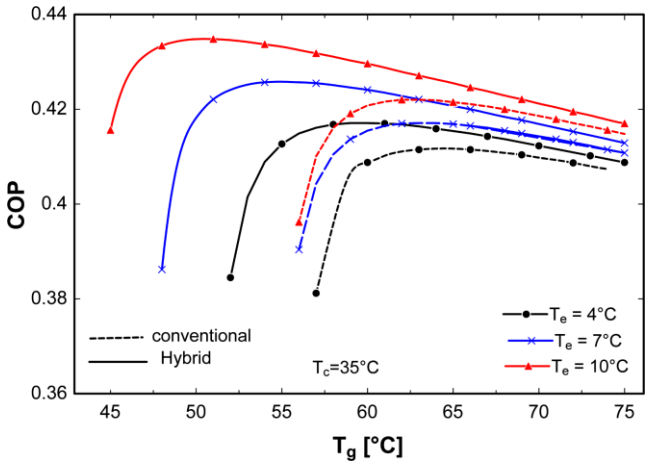

ACCEPTED MANUSCRIPT

ACCEPTED MANUSCRIPT

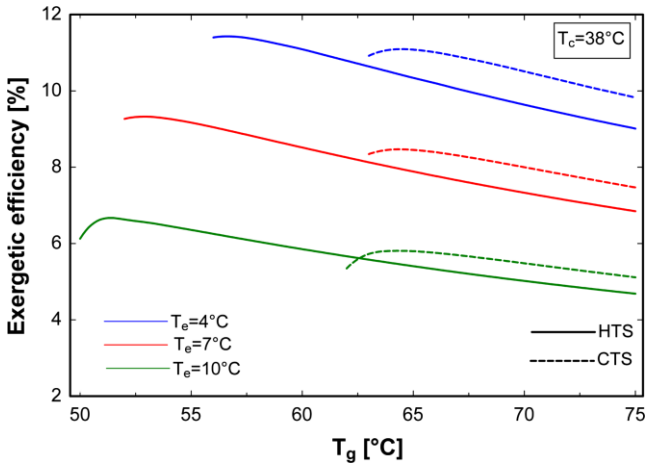

ACCEPTED MANUSCRIPT

ACCEPTED MANUSCRIPT

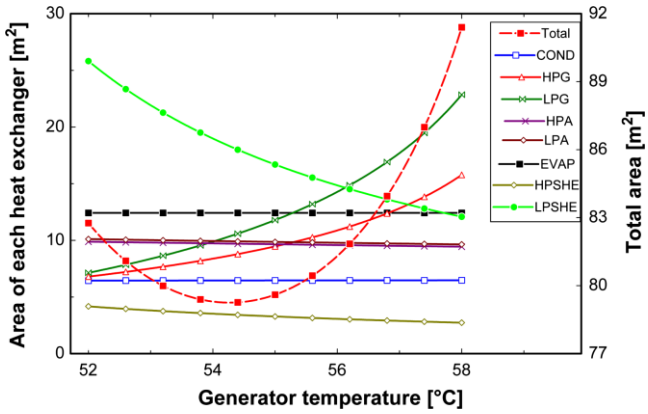

ACCEPTED MANUSCRIPT

ACCEPTED MANUSCRIPT

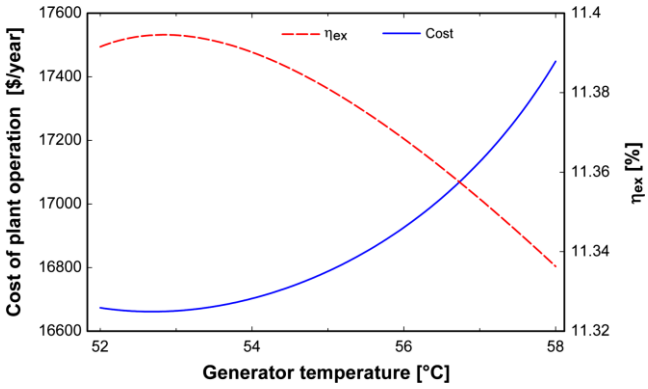

ACCEPTED MANUSCRIPT

ACCEPTED MANUSCRIPT

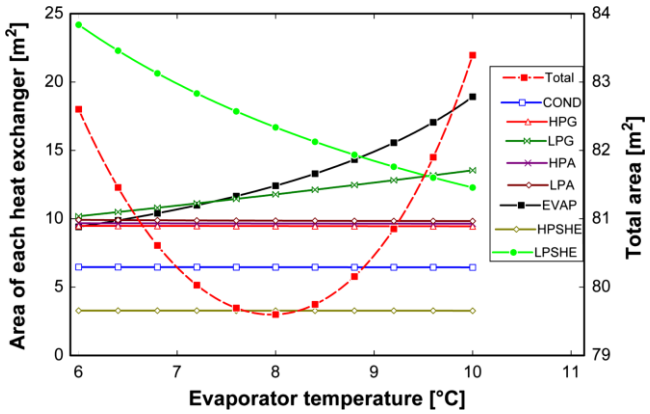

ACCEPTED MANUSCRIPT

ACCEPTED MANUSCRIPT

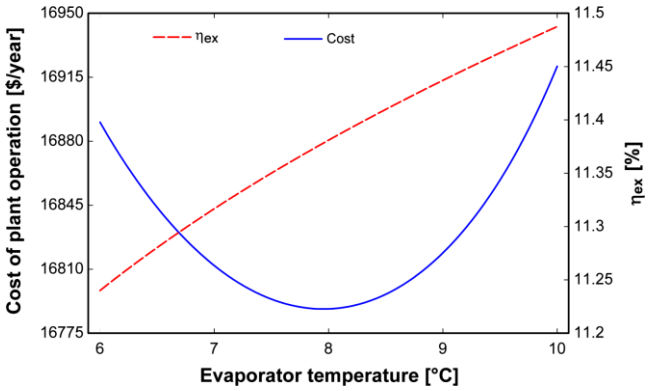

ACCEPTED MANUSCRIPT

ACCEPTED MANUSCRIPT

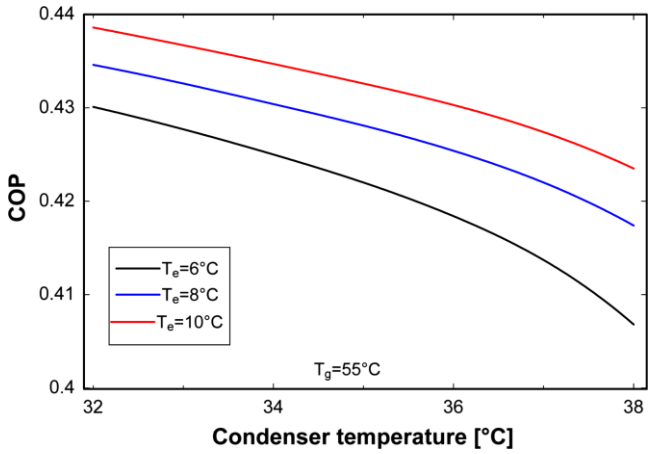

ACCEPTED MANUSCRIPT

ACCEPTED MANUSCRIPT

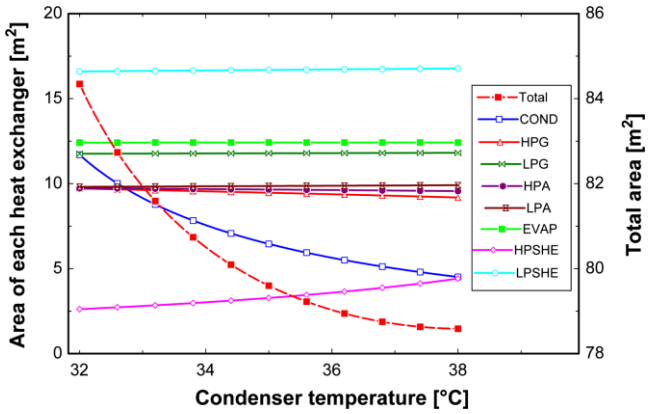

ACCEPTED MANUSCRIPT

ACCEPTED MANUSCRIPT

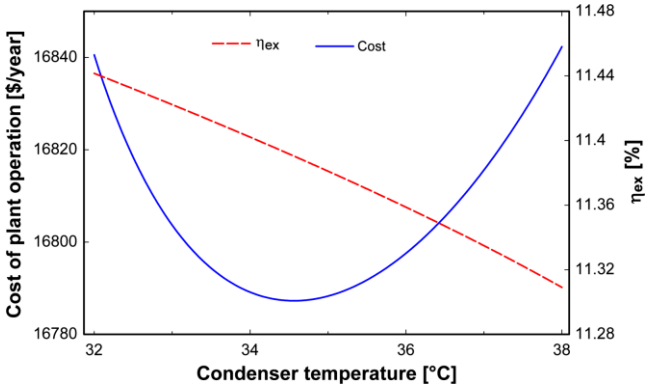

ACCEPTED MANUSCRIPT

ACCEPTED MANUSCRIPT

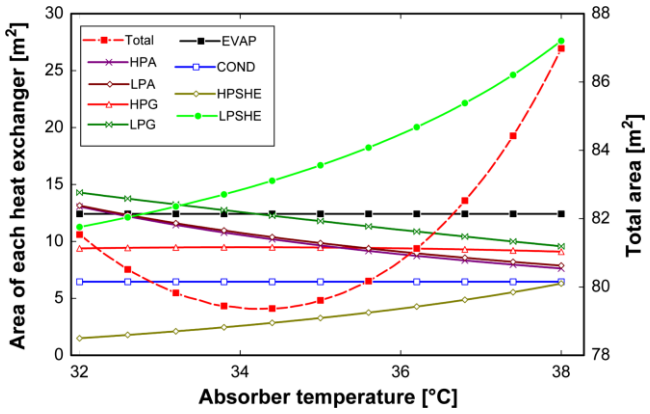

ACCEPTED MANUSCRIPT

ACCEPTED MANUSCRIPT

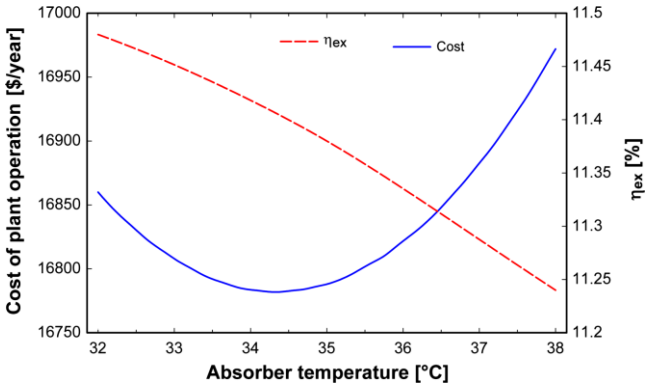

ACCEPTED MANUSCRIPT

ACCEPTED MANUSCRIPT

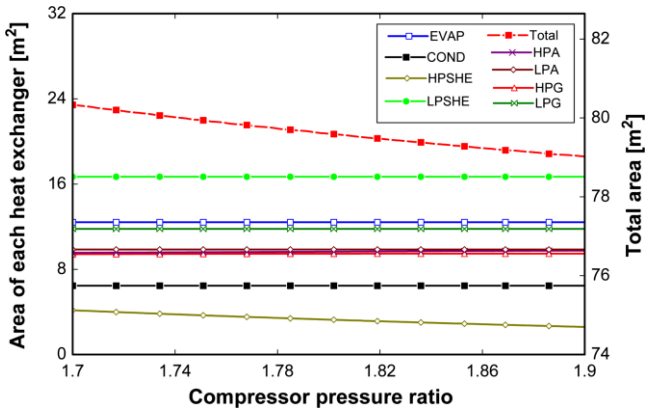

ACCEPTED MANUSCRIPT

ACCEPTED MANUSCRIPT

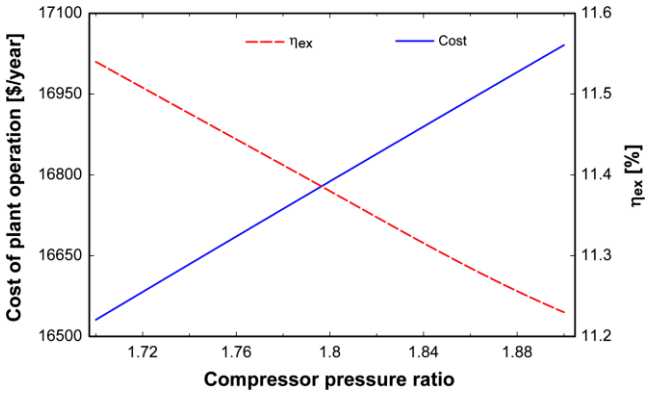

ACCEPTED MANUSCRIPT

ACCEPTED MANUSCRIPT

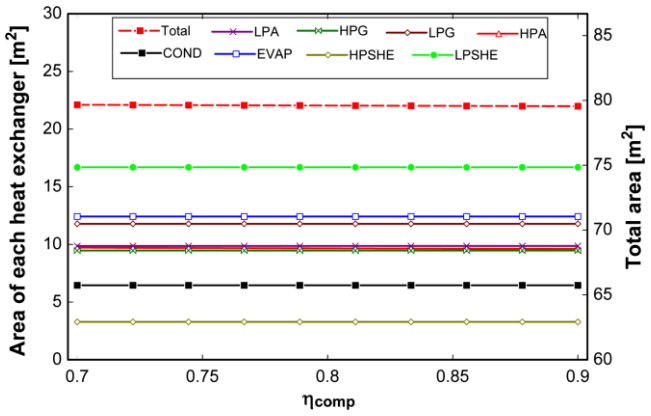

ACCEPTED MANUSCRIPT

ACCEPTED MANUSCRIPT

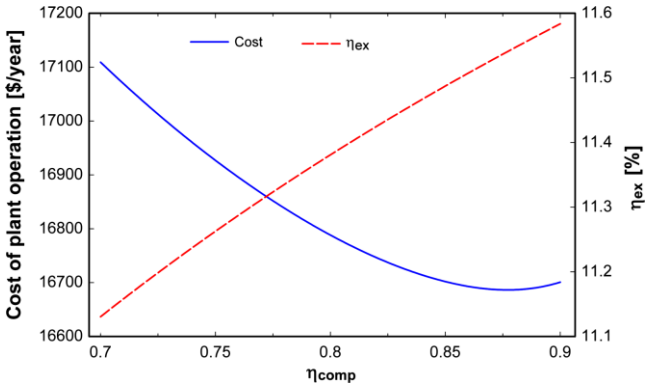

ACCEPTED MANUSCRIPT

ACCEPTED MANUSCRIPT

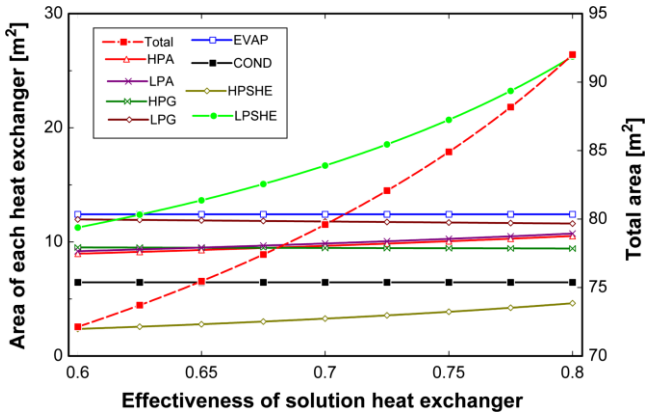

ACCEPTED MANUSCRIPT

ACCEPTED MANUSCRIPT

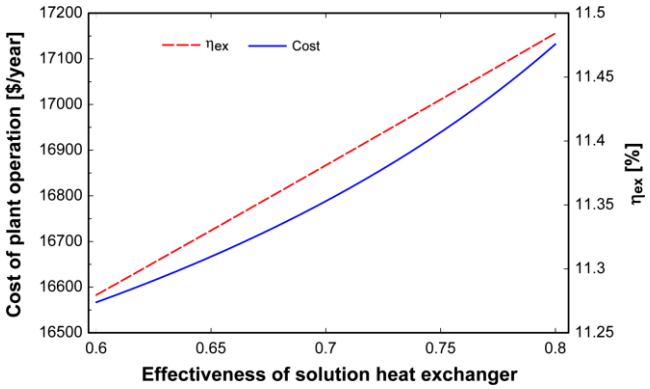

ACCEPTED MANUSCRIPT

ACCEPTED MANUSCRIPT

Highlights

- Hybrid absorption compression refrigeration system employing LiBr-H_2O is proposed.
- It requires lower generator temperature than conventional two stage system.
- Parametric analysis is performed to investigate the effects of operating variables.
- The size and cost of the hybrid system are estimated.
- Thermoeconomic optimization is done to minimize total annual plant operation cost.

ACCEPTED MANUSCRIPT

Tuning of Software Cost Drivers using BAT Algorithm

Sanchi Girotra
Department of Computer Engineering, Delhi Technological University, Delhi, INDIA
Email ID: sanchi,girotra@gmail.com

Kapil Sharma
Department of Computer Engineering, Delhi Technological University, Delhi, INDIA
Email ID: kapil@ieee.org

***Abstract* – Software effort estimation is an important process in software development as it predicts the no. of resources required to build the project. Lack of its accuracy and precision will impact timely delivery of project and its budget. There are numerous methods to estimate software effort. COCOMO II has been employed because of its wide acceptance as an industry standard and its applicability at diverse stages of software Engineering. And Accuracy in COCOMO II software effort estimation is highly dependent on its input parameters such as size of project, coefficients and cost drivers. Thus small changes in these parameters bring huge differences in Effort estimation. In this paper, we used Nature Inspired - Meta Heuristic Bat Algorithm to fine tune values of 15 cost drivers, which can effectively reduce error (MMRE) in effort estimation. It has been validated using NASA 93 dataset and its results are found better than COCOMO and genetic algorithm.**

Keywords – Bat Algorithm; COCOMO II; Cost Drivers; MMRE; MRE; NASA 93 Dataset; Software Effort Estimation

NOMENCLATURE

BA: Bat Algorithm

COCOMO: Constructive Cost Model

MMRE: Mean Magnitude of Relative Errors

I. INTRODUCTION

During the initial phase of requirement analysis, project managers are confronted with a crucial activity of providing the amount of effort required for the development of a project. And it's over or under estimation can impact bid proposals, budgeting and deadlines of software project delivery thus accuracy and precision in the estimates of effort is necessary.

There are several methods and models to estimate effort. Among them, Constructive Cost Model (COCOMO) is the commonly accepted and used model due to its applicability in diverse stages of software Engineering. Furthermore there are various effort optimization techniques based on COCOMO (Shepperd & Schofield, 2000), (Huang, Ho, Ren, & Capretz, 2007), (Choudhary, 2010; M, P, & M, 2010).

But accuracy in COCOMO effort estimation highly depends on the input parameters such as size of project, coefficients and values of cost driver's thus small miscalculations in values of input parameters can bring huge differences in Effort estimation. In order to handle this uncertainty of input parameters, numerous methods are being proposed to fine tune COCOMO coefficients(a,b,c,d) (Aljahdali & Sheta, 2010), (Kaushik & Chauhan, 2012), (M, et al., 2010), (Sehra, Brar, & Kaur, 2011), (Singh & Sahoo, 2011). Some have optimized parameters by combining COCOMO with heuristic algorithms like PSO (Prasad & Hari, 2010), swarm intelligence (Manikavelan & Ponnuswamy, 2011), genetic (Galinina, Burceva, & Parshutin, 2012), Tabu search (Kaur & Sindhu, 2014), simulated annealing (Kundu & Sethi, 2012), bat algorithm (Gupta & Sharma, 2015) etc.

In this paper, swarm intelligence based Meta-heuristic bat algorithm is used to search continuous valued COCOMO cost drivers (15) which can effectively improve the effort estimation. In the problem search space of bat is:

$$6^{15} = 470184984576$$

Here, total no of cost drivers are 15 and each having value within 6 given ratings.

The outline of this paper is as follows. Section II provides literature review on BA and COCOMO II. Section III revisits Bat Algorithm. Section IV provides more detailed explanation of COCOMO II followed by demonstration of how bat algorithm can be used to fine tune Software Cost Drivers. Section VI provides simulation dataset and results. Section VII presents the conclusion and future scope.

II. LITERATURE REVIEW

In 2010, X.-S. Yang (2010) proposed Bat Algorithm (BA), which is a Meta-heuristic algorithm for continuous problem optimization. From then many enhanced versions of BA have been proposed which resulted in better performance than original algorithm. Like Abdel Raouf, Abdel Baset, and El henawy (2014) used Chaotic variables in BA for solving integer programming problems, Jr., Fister, and Yang (2013) hybridized BA by using differential evolution strategy, Nakamura, et al. (2012) solved feature selection problem using discrete BA, U., Huang, Wang, and Chen (2012) improved BA exploration by considering Doppler Effect in echo, Xin-She (2011) extended bat algorithm to solve multi objective optimisation problems, Yılmaz, Kucuksille, and Cengiz (2014) used different frequency for different dimension in BA. Moreover, many researchers have also

978-9-3805-4421-2/16/$31.00 ©2016 IEEE

united BA with other algorithms to solve optimization problems like Lemma and Bin Mohd Hashim (2011) used BA for Training fuzzy models, Komarasamy and Wahi (2012) combined BA with K-Medoid (KM) clustering algorithm to fulfill the problem of initialization cluster centroid of K mediod, G. Wang and Guo (2013) combined BA with Harmony Search for Global Numerical Optimization Nawi, Rehman, and Khan (2014) combined with Back-propagation neural network (BPNN) algorithm to solve the local minima problem in gradient descent trajectory and to increase the convergence rate.

And due to the problem independent nature of meta heuristic algorithms, BA has successfully provided optimized solutions of various problems like Feature Selection (Nakamura, et al., 2012), economic generator dispatch (Ramesh, Mohan, & Reddy, 2013), software development effort estimation (Gupta & Sharma, 2015), Brushless DC Wheel Motor design optimization problem (Bora, Coelho, & Lebensztajn, 2012), Phishing website detection and optimization (Damodaram & Valarmathi, 2012), hybrid flow shop scheduling problems (Marichelvam & Prabaharam, 2012), topology optimization (X. S. Yang, Karamanoglu, & Fong, 2012), test effort estimation (Srivastava, et al., 2014) etc.

III. BAT ALGORITHM

Bat Algorithms is swarm intelligence based meta-heuristic optimization algorithm proposed by Yang [1] in 2010. BA finds the solution in the search space by exploiting the echolocation behavior of bats in which they locate their prey by emitting a short - loud ultrasonic sound pulse and listen for the echo that reflect back from the surrounding objects then they use the time interval from the discharge of sound pulse to the receiving of the echo and the time difference between of their two ears and also the loudness variations (signal intensity) of the echo's to get a view about surrounding and prey size.

In addition to this, BA uses a dynamic approach for exploitation (local search) and exploration (global search) to improve the solution. Like the variations in pulse emission rates r and loudness $A0$ controls exploration and exploitation in BA.

In this algorithm, the bat behaviour of finding the best location is captured to optimize the fitness function of the problem to be solved. It consists of the following steps:-

- Initialization of Bat Population -Initially, N bats are randomly spread over the search space as they have no idea where the prey is located thus population is randomly generated for each dimension d with default values for frequency, velocity, pulse emission rate and loudness.

$$x_{ij} = x_{\min j} + rand(0,1)\,(x_{\max j} - x_{\min j}) \qquad (0)$$

Where i = 1, 2 … N, j = 1, 2… d, $x_{\min j}$ and $x_{\max j}$ are lower and upper boundaries for dimension *j* respectively.

- Steps to update Frequency, Velocity and Solution -In the iterations of BA, each bat in the population emits sound pulses of random frequency dispersed between $[fmin, fmax]$ and this frequency controls the speed and new position of bat using below equations:

$$f_i = f_{\min} + (f_{\max} - f_{\min})\beta \qquad (0)$$

$$v_i^t = v_i^{t-1} + (x_i^{t-1} - x^*) f_i \qquad (0)$$

$$x_i^t = x_i^{t-1} + v_i^t \qquad (0)$$

Where β denotes a randomly generated number with in the interval [0, 1] and x^* is the current global best solution which is found after comparing all the solutions. Upper and lower bounds of frequency are selected such that it is comparable to the size of search space of that variable.

- Local search -Then each bat performs Random walk in order to exploit a position around the best solution.

$$x_{new} = x_{old} + \varepsilon A^t \qquad (0)$$

Here x_{old} is selected best solution from current best solutions, ε denotes a random number within the interval [-1, 1], while A^t is the average loudness of all the bats at this time.

- Steps to update Loudness and Pulse Emission Rate -

If new solution is improved than previous solution i.e. as the bat approach their prey, loudness of emitted sound pulse decreases and pulse emission rate increases so loudness and pulse rate needs to be updated using below equations:

$$A_i^{t+1} = \alpha A_i^t \qquad (0)$$

$$r_i^{t+1} = r_i^0 (1 - e^{-\gamma t}) \qquad (0)$$

Where α and γ are constants. r_i^0 & A_i^0 consist of random values and $r_i^0 \in [0, 1]$ and $A_i^0 \in [1, 2]$

Find the current best solution -Find the current best bat by comparing last best fitness value with improved bat fitness. If it is better than update the current best bat solution.

After all the iterations, the current best bat improves and acts as the solution to the problem.

IV. COCOMO II MODEL

The Constructive Cost Model (COCOMO) uses regression based techniques for software effort/cost estimation. It is given by Barry W. Boehm in 1981 which is also called as COCOMO 81. COCOMO 81 is said to be the most recognized, best documented and it reflects most software development practices on that time.

The major problem with COCOMO I was, it does not support modern software building processes like desktop development,

code reusability, rapid-development, object-oriented approaches etc. Therefore in 1997, Boehm developed the COCOMO II for estimating today's software development projects.

COCOMO was defined for three forms of software development:-

- Basic COCOMO computes software development effort for projects that can be developed by small teams of two or three members.
- Intermediate COCOMO provides more accurate estimates by taking into account software development environment through 15 cost drivers.
- Detailed COCOMO is the extension of intermediate COCOMO with use of specific cost drivers for each step of software life cycle.

The COCOMO software cost model measures effort in calendar months required per person (PM).
Intermediate COCOMO Equation is given as :

$$Effort(Person-month) = a \times [LOC]^b \times (EM1 \times EM2 \times EM3 \times \ldots \times EM15) \quad (1)$$

Here, the coefficient "a" is known as productivity coefficient and the coefficient "b" is the scale factor. They apply on different classes of projects as given in Table I.

TABLE I. MODES OF COCOMO

Software Project	Project Size	a	b
Organic	Less than 50 KLOC	3.2	1.05
Semi-detached	50 – 300 KLOC	3	1.12
Embedded	Over 300 KLOC	2.8	1.2

EM_i - are effort multipliers (Cost drivers) which have total of six levels of rating: Very Low, Low, Nominal, High, Very High, and Extra High. Each rating has a corresponding value depending on the degree to which the factor can influence productivity as shown in Table II.

TABLE II. RATING OF COCOMO COST DRIVERS

Cost Drivers	Rating					
	Very Low	Low	Nominal	High	Very High	Extra High
Analysts Capability (acap)	1.46	1.19	1	0.86	0.71	-
Programmers Capability (pcap)	1.42.	1.17	1	0.86	0.7	-
Application Experience (aexp)	1.29	1.13	1	0.91	0.82	-
Modern Programing Practices (modp)	1.24.	1.1	1	0.91	0.82	-
Use of Software Tools (tool)	1.24	1.1	1	0.91	0.83	-
Virtual Machine Experience (vexp)	1.21	1.1	1	0.9	-	-
Language Experience (lexp)	1.14	1.07	1	0.95	-	-
Schedule Constraint (sced)	1.23	1.08	1	1.04	1.1	-
Main Memory Constraint (stor)	-	-	1	1.06	1.21	1.56
Database Size (data)	-	0.94	1	1.08	1.16	-
Time Constraint For CPU (time)	-	-	1	1.11	1.3	1.66
Turnaround Time (turn)	-	0.87	1	1.07	1.15	-
Machine Volatility (virt)	-	0.87	1	1.15	1.3	-
Required Software Reliability (rely)	0.75	0.88	1	1.15	1.4	-
Process Complexity (cplx)	0.7	0.85	1	1.15	1.3	1.65

This effort multiplier belongs to three groups as shown in Table III.

TABLE III. GROUPING OF EFFORT MULTIPLIERS

Increase these to decrease effort	acap, pcap, aexp, modp, tool, vexp, lexp
	sced
Decrease these to decrease effort	stor, data, time, turn, virt, cplx, rely

V. TUNING OF SOFTWARE COST DRIVERS USING BAT ALGORITHM

A. Dataset

The proposed algorithm is tested on 93 NASA projects from different centers from 1971 to 1987.This dataset consist of development mode, 15 cost drivers and size of each project in kilo source line of code and actual effort. The proposed algorithm is executed separately for each project mode - embedded (21), organic (3), semidetached (69).

B. Working Steps

The main steps to optimize/tune Intermediate COCOMO cost drivers (15) such that calculated efforts approximate to actual efforts for NASA 93 project Dataset is shown in Fig. 1. Thus, BA solves the problem of finding tuned values (from one of 6 level rating) of these 15 Effort multipliers EM1, EM_2, and EM_3 … EM_{15} that minimize the following equations:

$$MRE_{ij} = \frac{ActualEffort_j - EstimatedEffort_{ij}}{ActualEffort_j} \quad (2)$$

$$MMRE_i = \frac{1}{n}\sum_{j=1}^{n} MRE_{ij} \quad (3)$$

MMRE is used as evaluation criteria for assessment of proposed algorithm. MMRE is calculated as average of the Magnitude of Relative Errors MRE's of each 93 projects**.**
The main steps include:

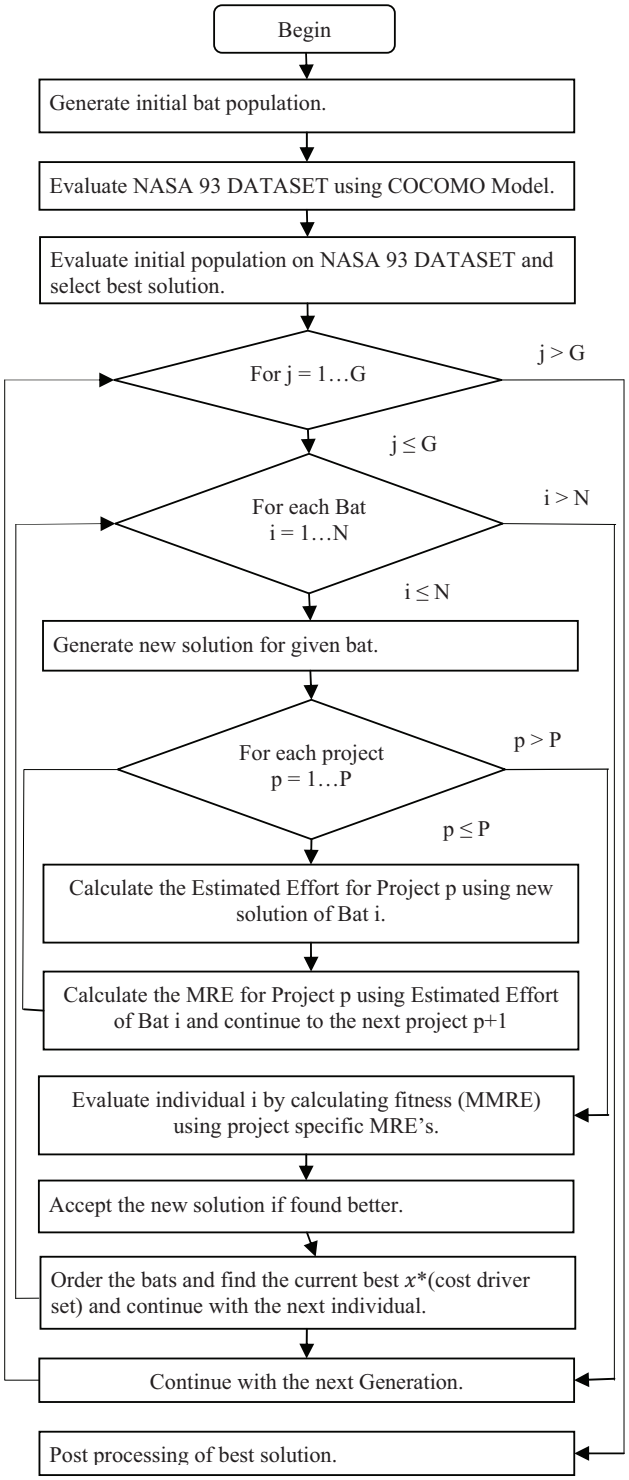

Fig. 1. Proposed method of COCOMO Cost Drivers Tuning.

1. Generate Initial Bat Population - Population of N bats is generated randomly for each dimension d. Here, each bat will have 15 dimensions (cost drivers). Then each bat is given default velocity v_i (i=1, 2, 3... N), pulse rate ri, loudness A_i and pulse frequency $f_i \in [f_{min}, f_{max}]$. And each bat represents potential tuned cost drivers to the problem.
2. Evaluate NASA 93 Dataset using COCOMO Model - Calculate MRE for each 93 projects in NASA dataset using Eq. (9) where $ActualEffort_i$ is given and $EstimatedEffort_i$ is COCOMO calculated effort using Eq. (8). Then overall fitness (MMRE) is calculated using Eq. (10).
3. Evaluate initial population on NASA 93 Dataset and select best solution -For each bat in population, fitness (MMRE) is calculated by taking average of MRE's for each NASA project. Then best bat is selected from them having min. fitness i.e. min. MMRE.
4. Generate new solution for each bat i in generation j, either by exploration or exploitation using Eqn. 4 and 5 respectively and adjust them with 6 available ratings.
5. Evaluate the fitness (MMRE) of newly generated individual of bat.
6. Accept the new cost drivers, if its fitness is less than from old solution.
7. Order the bats(x) according to fitness function and find the current best bat x*.
8. Repeat step 4 to 7 for each individual in generation j.
9. After the N generations, final x* would act as the optimized cost drivers for NASA 93 Project dataset.
10. Post process the result.

This algorithm is implemented using Java as have various inbuilt method like random generator which makes coding easy.

VI. RESULT ANALYSIS

In the experiment, the tuning i.e. the appropriate selection from 6 level ratings (vl, l, n, h, vh, xh) for each of 15 COCOMO model cost drivers were performed using the proposed algorithm. And since each of the three classes of COCOMO model has its own values for coefficients (a, b), therefore experiments were performed separately for each mode using corresponding dataset. And Bat algorithm parameters (no. of bats, no. of generations, f_{min}, f_{max}, pulse rate, amplitude) were taken based on experimental results by changing them.

The proposed algorithm is validated with NASA 93 dataset and results were compared with COCOMO and genetic algorithm generated MMRE. Table IV shows the MMRE using Genetic algorithm, COCOMO and proposed algorithm for different project modes. And Fig, 2 illustrate that the proposed algorithm generates smaller MMRE than COCOMO and Genetic Algorithm. The final tuned Cost Drivers Set (rely, data, cplx, time, stor, virt, turn, acap, aexp, pcap, vexp, lexp, modp, tool, sced) for NASA 93 projects are: Organic (0.75,

1.16, 0.7, 1.0, 1.56, 0.87, 0.87, 0.71, 0.82, 0.7, 0.9, 0.95, 0.82, 0.83, and 1.1), Semi-detached (1.4, 0.94, 1.0, 1.66, 1.21, 1.3, 0.87, 0.71, 0.82, 0.7, 0.9, 0.95, 0.82, 0.83, 1.1), Embedded (0.75, 0.94, 1.65, 1.0, 1.56, 1.15, 0.87, 0.71, 0.82, 0.7, 0.9, 0.95, 0.82,0.83,1.1).

TABLE IV. MMRE OF NASA 93 PROJECT DATASET

	MMRE for Genetic method	MMRE for COCOMO	MMRE for Proposed Bat method
Embedded	0.72	0.82	0.7902
Organic	0.8	0.876	0.4622
Semidetached	0.51	0.51	0.4403

VII. CONCLUSION AND FUTURE WORK

In this paper, we addressed the problem of inaccurate and ambiguous selection of cost driver values which results in inaccurate effort estimation thus small change in selection of COCOMO cost drivers can bring significant improvements in the MMRE. The proposed algorithm produced tuned values of the cost drivers, which are good enough to improve the MMRE of the projects thus gives nearly accurate software effort estimation. Furthermore, this model is validated on NASA 93 dataset and obtained MMRE are compared with current COCOMO II model cost drivers and Genetic Algorithm and proposed algorithm provides good estimation results as compared to them. In the future other strategies can be incorporated to further improve the MMRE like considering of order of cost drivers, combining other software engineering methods which can be tested on other datasets as well.

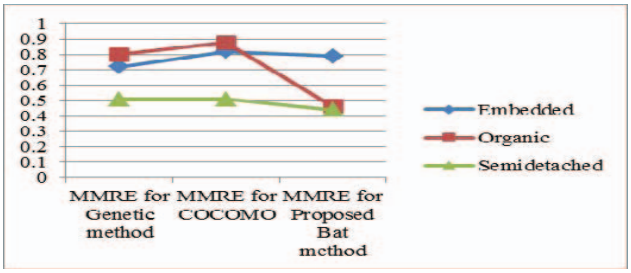

Fig. 2. Comparison of MMRE for NASA 93 Dataset.

REFERENCES

[1]. Abdel Raouf, O., Abdel Baset, M., & El henawy, I. (2014), "An Improved Chaotic Bat Algorithm for Solving Integer Programming Problems", *International Journal of Modern Education and Computer Science, 6*, 18-24.

[2]. Aljahdali, S., & Sheta, A. F. (2010). "Software Effort Estimation by Tuning COOC"MO Model Parameters Using Differential Evolution", In *2010 IEEE/ACS International Conference on Computer Systems and Applications (AICCSA)* (pp. 1283-1289). Hammamet: IEEE.

[3]. Bora, T. C., Coelho, L. S., & Lebensztajn, L. (2012), "Bat-inspired optimization approach for the brushless DC wheel motor problem. In *IEEE Transactions on Magnetics",* (Vol. 48, pp. 947-950): IEEE.

[4]. Choudhary, K. (2010). GA Based Optimization of Software Development Effort Estimation. *International Journal of Computer Science and Technology, 1*, 38-40.

[5]. Damodaram, R., & Valarmathi, M. L. (2012), "Phishing website detection and optimization using modified bat algorithm" *International Journal of Engineering Research and Applications, 2*, 870–876.

[6]. Galinina, A., Burceva, O., & Parshutin, S. (2012), "The Optimization of COCOMO Model Coefficients Using Genetic Algorithms", *Information Technology and Management Science, 15*.

[7]. Gupta, N., & Sharma, K. (2015), "Optimizing intermediate COCOMO model using BAT algorithm", In *2015 2nd International Conference on "Computing for Sustainable Global Development" (INDIACom)* (pp. 1649 - 1653). New Delhi, India IEEE

[8]. Huang, X., Ho, D., Ren, J., & Capretz, L. F. (2007), "Improving the COCOMO model using a neuro-fuzzy approach", *Applied Soft Computing, 7*, 29-40.

[9]. Jr., I. F., Fister, D. s., & Yang, X.-S. (2013), "A Hybrid Bat Algorithm".

[10]. Kaur, J., & Sindhu, R. (2014), "Parameter Estimation of COCOMO II using Tabu Search", *International Journal of Computer Science and Information Technologies,, 5*.

[11]. Kaushik, A., & Chauhan, A. (2012), "COCOMO Estimates Using Neural Networks", *International Journal of Intelligent Systems and Applications, 9*, 22-28.

[12]. Komarasamy, G., & Wahi, A. (2012), "An optimized K-means clustering technique using bat algorithm", *European Journal Scientific Research, 84*, 263-273.

[13]. Kundu, A., & Sethi, V. (2012),"Parameter Estimation of COCOMO II using Simulated Annealing", *International Journal of Science and Research (IJSR), 3*, 1-5.

[14]. Lemma, T. A., & Bin Mohd Hashim, F. (2011),"Use of fuzzy systems and bat algorithm for exergy modelling in a gas turbine generator" In *IEEE Colloquium on Humanities, Science and Engineering (CHUSER'2011)* (pp. 305–310). Penang: IEEE.

[15]. M, A., P, K., & M, H. (2010), "Software Cost Estimation using Fuzzy logic", *ACM SIGSOFT Software Engineering Notes, 35*, 1-7.

[16]. Manikavelan, D., & Ponnuswamy, D. R. (2011), "Optimized Software Cost Estimation using Swarm Optimization", *International Journal of Computer Science and Technology (IJCST), 2*, 465-468.

[17]. Marichelvam, M. K., & Prabaharam, T. (2012),"A bat algorithm for realistic hybrid flowshop schedulihng problems to minimize makespan and mean flow time", *ICTACT Journal on Soft Computing, 3*, 428–433.

[18]. Nakamura, R. Y. M., Pereira, L. A. M., Costa, K. A., Rodrigues, D., Papa, J. P., & Yang, X. S. (2012), "BBA: A binary bat algorithm for feature selection" In *25th SIBGRAPI Conference on Graphics, Patterns and Images (SIBGRAPI),* (pp. 291-297): IEEE Publication.

[19]. Nawi, N. M., Rehman, M. Z., & Khan, A. (2014),"A New Bat Based Back-Propagation (BAT-BP) Algorithm", In *Advances in Systems Science*.

[20]. Prasad, R. P. V. G., & Hari, C. V. M. K. (2010), "Software effort estimation using Particle Swarm Optimization with inertia weight",*International journal of software Engineering, 2*, 87 - 96.

[21]. Ramesh, B., Mohan, V. C. J., & Reddy, V. C. V. (2013),"Application of bat algorithm for combined economic load and emission dispatch", *International Journal of Electricl Engineering and Telecommunications, 2*, 1–9.

[22]. Saji, Y., Riffi, M. E., & Ahiod, B. (2014),"Discrete bat-inspired algorithm for travelling salesman problem", In *2014 Second World Conference Complex Systems (WCCS)* (pp. 28 - 31). Agadir: IEEE.

[23]. Sehra, S. K., Brar, Y. S., & Kaur, N. (2011),"Soft Computing Techniques for Software project Effort Estimation", *International Journal of Advanced Computer and Mathematical Sciences, 2*, 162-167.

[24]. Shepperd, M., & Schofield, C. (2000),"Estimating software project effort using analogies", *IEEE Transaction on Software Engineering, 23*, 736-743.

[25]. Singh, J., & Sahoo, B. (2011),"Software Effort Estimation with Different Artificial Neural Network", In *2nd National Conference on Computing, Communication and Sensor Network* (Vol. 2, pp. 13-17).

[26]. Srivastava, P. R., Bidwai, A., Khan, A., Rathore, K., Sharma, R., & Yang, X. S. (2014),"An empirical study of test effort estimation based on bat algorithm",*International Journal of Bio-Inspired Computation, 6*, 57-70.

[27]. U., G. L. I., Huang, H., Wang, S., & Chen, Z. (2012), "An Improved Bat Algorithm with Doppler Effect for Stochastic Optimization", *International Journal of Digital Content Technology and its Applications, 6*, 326-336.

[28]. Wang, G., & Guo, L. (2013),"A novel hybrid bat algorithm with harmony search for global numerical optimization",*Journal of Applied Mathematics, 2013*, 1–21.
[29]. Xin-She , Y. (2011),"Bat algorithm for multi-objective optimisation", *Internal Journal of Bio-Inspired Computation, 3*, 267-274.
[30]. Yang, X.-S. (2010),"A New Metaheuristic Bat-Inspired Algorithm", *Studies in Computational Intelligence, Springer Berlin*, 65-74.
[31]. Yang, X. S., Karamanoglu, M., & Fong, S. (2012),"Bat aglorithm for topology optimization in microelectronic applications", In *IEEE International Conference on Future Generation Communication Technology (FGCT2012)* (pp. 150–155). London.
[32]. Yilmaz, S., & Kucuksille, E. U. (2013),"Improved Bat Algorithm (IBA) on Continuous Optimization Problem", *Lecture Notes on Software Engineering*, 279-283.Yılmaz, S., Kucuksille, E. U., & Cengiz, Y. (2014),"Modified Bat Algorithm",*Electronics and Electrical Engineering, 20*.

Using Cell Division for Text to Image Encryption

Vaishnavikannan

Student
Delhi technological university
kannan.vaishnavi25@gmail.com

Smita Jhajharia

Guest Faculty
Delhi technological university
smitasingh0819@gmail.com

***Abstract*-- Protection of data has always been an issue and newer encryption methods are a constant need. Our paper provides a novel text encryption technique that encrypts a text message into an image using the concept of cell division thatoccurs in cellular organisms. Cell division, that includes the meiotic and the mitotic division, leads to the distribution of genetic material between two daughter cells. We draw a parallel between the cell division and encryption to achieve a high level of security. Our method works in three main stages - the mitotic phase, the meiotic phase and the image formation phase. Encrypted message is obtained in the form of an image. The results are passable. As per our knowledge, no prior work similar to our approach has been done.**

Keywords-Encryption; DNA; Cell Division; Meiosis; Mitosis;Cryptography

I. INTRODUCTION

Cryptography is the art and study of techniques for secret writing and message hiding[1].Cryptography includes algorithms, techniques and protocols for the encryption of a plain text message and its secure transmission over a networkwithout any time delay and protected from any intruder,to prevent misuse and further vulnerability[2]. Cryptography can be used for confidentiality (i.e. making the message inaccessible to any unauthorized user or intruders), integrity (to ensure that the message has not been changed and is received in its original form and not modified),authenticity (the receiver should be able to verify he message arrivedand the path travelled by it), non repudiation (i.e.to confirm the receival of a message and of the sender sending it) and to limit the availability, validity or recipient in time or space.*Encryption* is the act of making a message un-intelligible by mystifying it. Our paper discusses a new technique of text encryption inspired by the mechanism of cell division in multi-celled organisms.

A. Cell division

The cell cycle is the series of events that take place in a cell leading to its division and duplication(or replication). The cell division involves two basic types of divisions-*Mitotic* and *Meitotic*.

The steps in the two divisions are explained as follows-

B. Mitotic Division

1.The chromosomal material untangles during the chromatin condensation to form 'n' single stranded chromosomes (i.e.their monad form). DNA replication occurs and the chromosomes obtain their dyad form characterized by two strands called chromatids joined together at the centriole.

2.Small disc-shaped structures called kinetochores provide to be the sites of attachment for the spindle fibers. The spindle fibersattach to the chromosomes, to move the chromosomes move towards the center of the cell.

*3.*The chromosomes split and chromatids separate,to move towards opposite poles.

*4.*The two poles of the cell form two different daughter cells. This step accomplishes the segregation of duplicated chromosomes into different daughter nuclei.

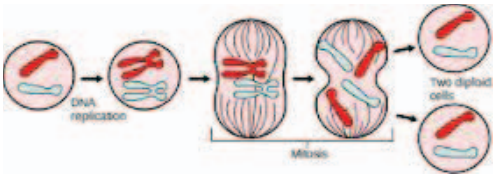

Fig.1. Mitosis cell division

C. Meiosis

There are two phases to this cell division -

Meiosis 1

1.The chromosomes start by replicating.

2. Identical chromosomes start pairing up. Such paired chromosomes are called homologous chromosomes.

3.Crossing over of genetic material occurs between non-sister chromatids of the two pairs of homologous chromosomes.

4.Centromeres attach to the spindle fibers and move to the center of the cell.

5.The homologous chromosomes separate and move to separate daughter cells.

Meiosis 2

1.The chromosomes in the daughter cell (obtained above , after meiosis 1) attach to spindle fibres and move to the center.

2.The chromatids of the double stranded chromosomes seperate and move to different daughtercells.

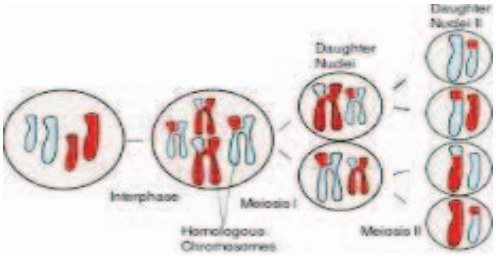

Fig.2. Meiosis cell division

II. LITERATURE SURVEY

Many papers on genetic and DNA based encryption were studied and analyzed to learn about the previous attempts made in this field. One of the paper,[3],uses pixel displacement to encrypt an image. The R,G,B values are shifted and interchanged with the boundaries of the image, providing an suitable results.[4] Proposes a DNA encryption scheme uses matrix manipulations and a key generation scheme. The algorithm works in two parts. The first part involves matrix operations whereas the second makes use of data reshaping and DNA operations. Genetic algorithm was the basis for [5] which segments its images into a number of regions depending on the intensity and entropy measure. The security of the algorithm can be attributed to the Variable key length. [6] Proposes an efficient image encryption technique that uses chaotic functions, DNA sequences and genetic algorithm. The algorithm generates DNA masks that are used for encryption. The algorithm is shown to be resistant to a variety of attacks like the differential and plaintext attack. The concept data to image encryption using meiosis,fertilization, translation and mutation also form the basis of [7]. The algorithm proceeds in two phases to encode data and images. An encryption algorithm that encrypts data in blocks is given in [8]. The data is first encrypted using AE and then an equivalent color code is obtained. The final output is given in the form of image.A similar approach of text to image conversion can be seen in [9].

III. APPROACH

Both the sender and the receiver maintain a database of images to be used for the encryption process. Depending on the time of the day, an image is chosen to be encrypted with the message.

R,G,Bvalues of the image are extracted.

The three obtained vectors are divided into equal '*n*' number of "chromosomes" to obtain a total of *3n* chromosomes ('n' from R, G and B each).

Three vectors, each from R, G, and B is chosen and XOR'edwith each other, reducing *3n* to *n*.

Encode the above vectors to DNA sequences. The coding scheme followed is - 00-A, 01-T, 10-G and 11-C.

A. MITOTIC PHASE

Step 1.The *n* chromosomes are replicated by DNA replication scheme (as shown in fig3) to obtain 2n chromosomes. The replication is as follows

- The replicating is such that the chromosome number 1 replicates to form the chromosome number *n*+1.
- An A in the original chromosome is replicated as a T in the replicated chromosome, a T as A , a G as a C and a G as a C (as in fig.3).
- The centromere values are the same in both the cells and are copied as such during replication. So, even in the replicated chromosome the values at the centromere are same as the values in the centromere of the original.

Step2.Replication can lead to four different types of chromosomes depending on the position of the centromere joining the two chromosomes – *Metacentric Chromosomes*(having chromosomes at the centre and equal length of two sections), *Sub metacentric Chromosomes (*slightly off centre, leading to small asymmetry in the length of the two sections),*Acrocentric Chromosomes*(a severely off centromere, one section is really long compared to the other),*Telocentric Chromosomes*(centromere at one end).

The chromosomes produced can exhibit the above four conditions. However, metacentric condition is the highest probable, whereas telocentric the lowest

Step 3. All the *2n* chromosomes are again converted to binary vectors using decimal to binary conversion.

Step 4.The spindle attachment is implemented as a XOR with the message sequence.

Step 5.Two Kinetochore points are chosen. The sequence between these two points are XOR'ed with the message (in binary) .

Step 6.The above *2n* chromosomes are now to be divided equally to obtain two daughter cells with *n* chromosomes each.

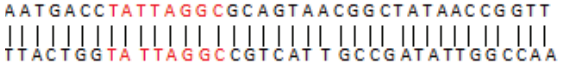

Fig.3. Replication of DNA with centromere at position 8 to 15.

Step 7. The chromosomes are randomly divided so that n chromosomes are passed to both the daughter cells. However, the i^{th} chromosome should not go to the same cell as the chromosome number $(n+i)$. This is because; the chromosome $(n+i)$ is the genetic replica of the i^{th} chromosome and should be passed to different daughter cells, to ensure that both cells contain identical information.

Step 8. The 2 cells containing 'n' chromosomes are converted to an image,using the text to image conversion phase (sec III C) (Fig 6b and 6c). These two images are concatenated to obtain a single image (Fig 6d), which is further passed on for meiotic phase.

B. MEIOTIC PHASE

The image is again converted to 'n' chromosomes, following the same procedure mentioned before.

Step 9. DNA encoding takes place as in step (1b). Replication takes place to obtain $2n$ chromosomes as in Step 1.

Meiosis 1

Step 10.The meiotic process is characterized chromosome crossover. The $2n$ chromosomes (obtained in step 9) are such that the i^{th} and the $(n+i)^{th}$ chromosome are joined at the centromere and form one pair of chromosome. For e.g, for a total of 46 chromosomes, the 1st and the 47th chromosome form a pair and the 24th and the 70th chromosome form a pair. This chromosome pair is crossovered with the pair formed by $(n/2+i)$ and $n+(n/2+i)^{th}$ chromosome. The crossover can be one-point, two-point or multi-point. Crossover takes place to introduce gene recombination (fig 4).

Fig.4.Crossing over in meiosis 1 of homologous chromosomes.

Step 11.The chromosomes are now equally divided to obtain two cells. However this time the i^{th}chromosome goes to the same cell as the $(n+i)^{th}$ chromosome and to the opposite cell of the $(n/2+i)$ and $n+(n/2+i)^{th}$ chromosome. The daughter cells are again, obtained as images (Fig 6e and 6f).

Meiosis 2

Step 12.The above-obtained two daughter cells are further divided such that they each produce two daughter cells.The chromosomal division is such that chromosomes from one pair go to different cells. The two divisions should yield 4 daughter cells, obtained as images (Fig 6g, 6h, 6i and 6j) using the text to image conversion phase, with n chromosomes each. Again, concatenation occurs to give a final image (Fig 6k). The process is repeated, with the initial image taken to be the final image obtained above ,till desired characteristics are obtained.

C. TEXT TO IMAGE CONVERSION

This phase takes the generated chromatids of meiosis phase of both the daughter cells and converts them into an image. The steps followed are as given-

Step1. Choose an initial key$M$(<253).

Step 2. Add or subtract the bits of the first block from M and obtain $m1$,$m2$ and $m3$ for that block. E.g. if the bits are 010 and M=132, then $m1$ can be M+/- 1 i.e. 131 or 133,$m2$ can be M+/- 0 i.e. 132 and $m3$= M+/- 1 i.e. 131 or 133. The combination of ($m1$,$m2$, $m3$) form the values the corresponding pixel. Note that if the bit is X it is always treated as a 0 value. If any value of m_i comes out to be 254, 255 or 256 take them as 0, 1 and 2 respectively i.e. the calculation of m and M is cyclic.

Step 3. Obtain M values for the next block as (M_i=M+$z$and M_j=M-z ,where z is the decimal value of the previous block). Let n different values for Mbe generated. If any $M_i \mp 0/1 = M_k$ then the values M_i, and M_k values of M cannot be used for encryption and therefore, need to be discarded. Different bits of the block can be encrypted with different valid values of M. Repeat steps for the other blocks.

Step 4. Generate all the pixels till the end of the bit stream. Use these pixel values to form your image. Once the image is obtained it can be further encrypted to provide better security.

Example -

1. Consider the bit stream 11001
   110 01x
   Let M=126
2. The pixel values for the first block 110 is obtained as follows –
   1 -> M+/- 1 = 125 or 127
   1->M+/- 1 = 125 or 127
   0->M+/- 0 = 126
   The first pixel values are say, (125,127,126) .
3. For the next block, the M values are M+/- D where D is the decimal value of the next block , in this case = 2. Therefore $M1$= 123 +2 = 125 and $M2$=123 – 2= 121 and $M3$=126.
4. The second block is processed as

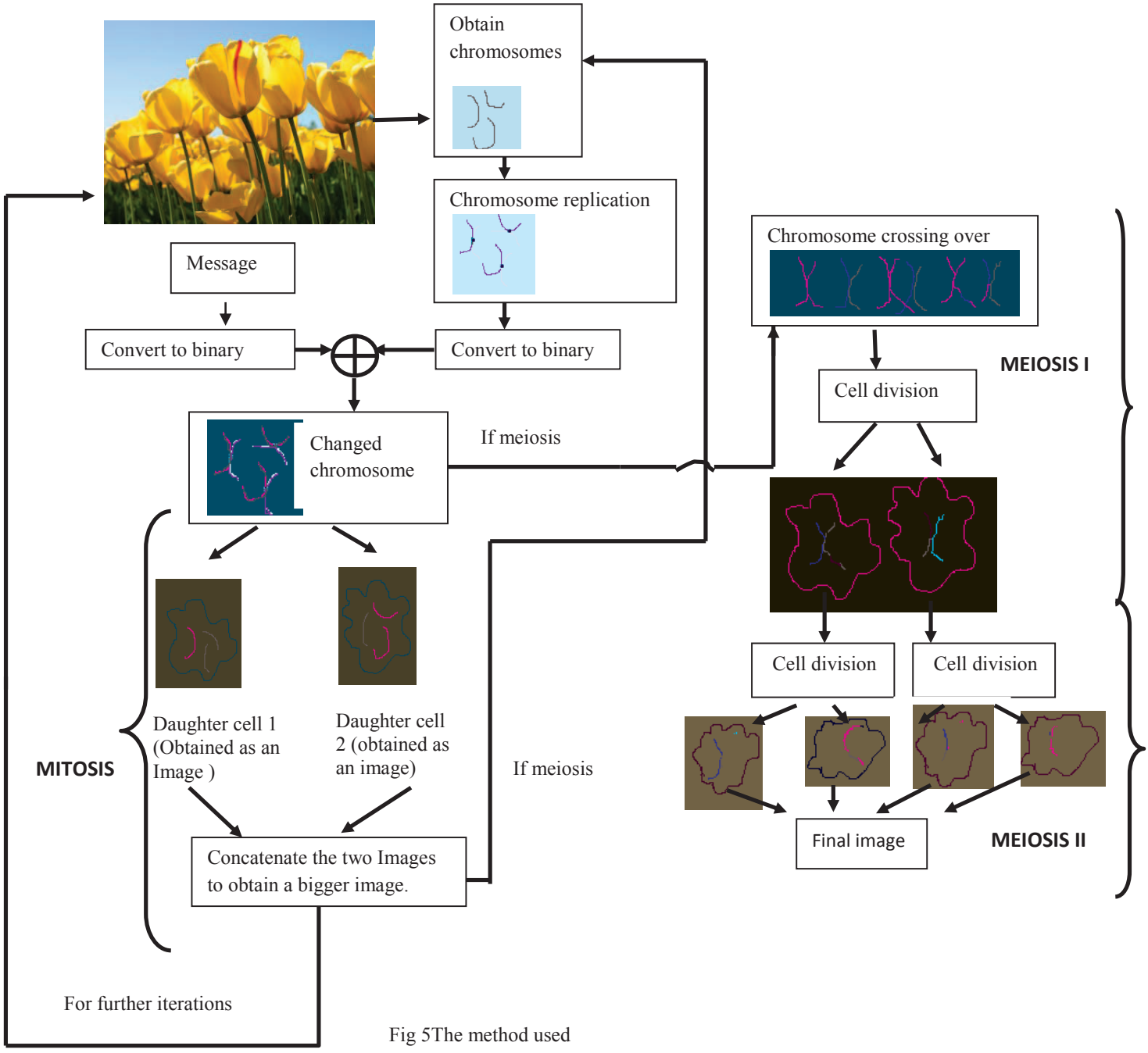

Fig 5The method used

0-> 125+/- 0 =125 or 121 +/- 0 =121 or 123+/- 0= 123 , 1-> 125 +/- 1= 124 or 126 or 123+/- 1= 122 or 124 or 123+/-1 = 122 or 124.

5. However, since *M1*-1=*M2*+1, we reject both *M1* and *M2* and the values generated by them.
6. Therefore the second pixel values can be (123,122, 123).

IV. MUTATION

Mutation is the process in living organisms that introduces changes in the DNA sequence, resulting in introduction of variation to the population. The Normal anomalies that occur during cell division may be summarized as follows-

1. *Down's and klinefelter's syndrome*- Theseare marked by the presence of an extra X or Y chromosome in the chromosome set. These anomalies can be introduced by unequal division of chromosome or passing one extra copy of a chromosome to one of the daughter cells. The extra gene can be a replica of any of the 'n' genes, chosen randomly.
2. *Error in chromosome replication* – An A in the

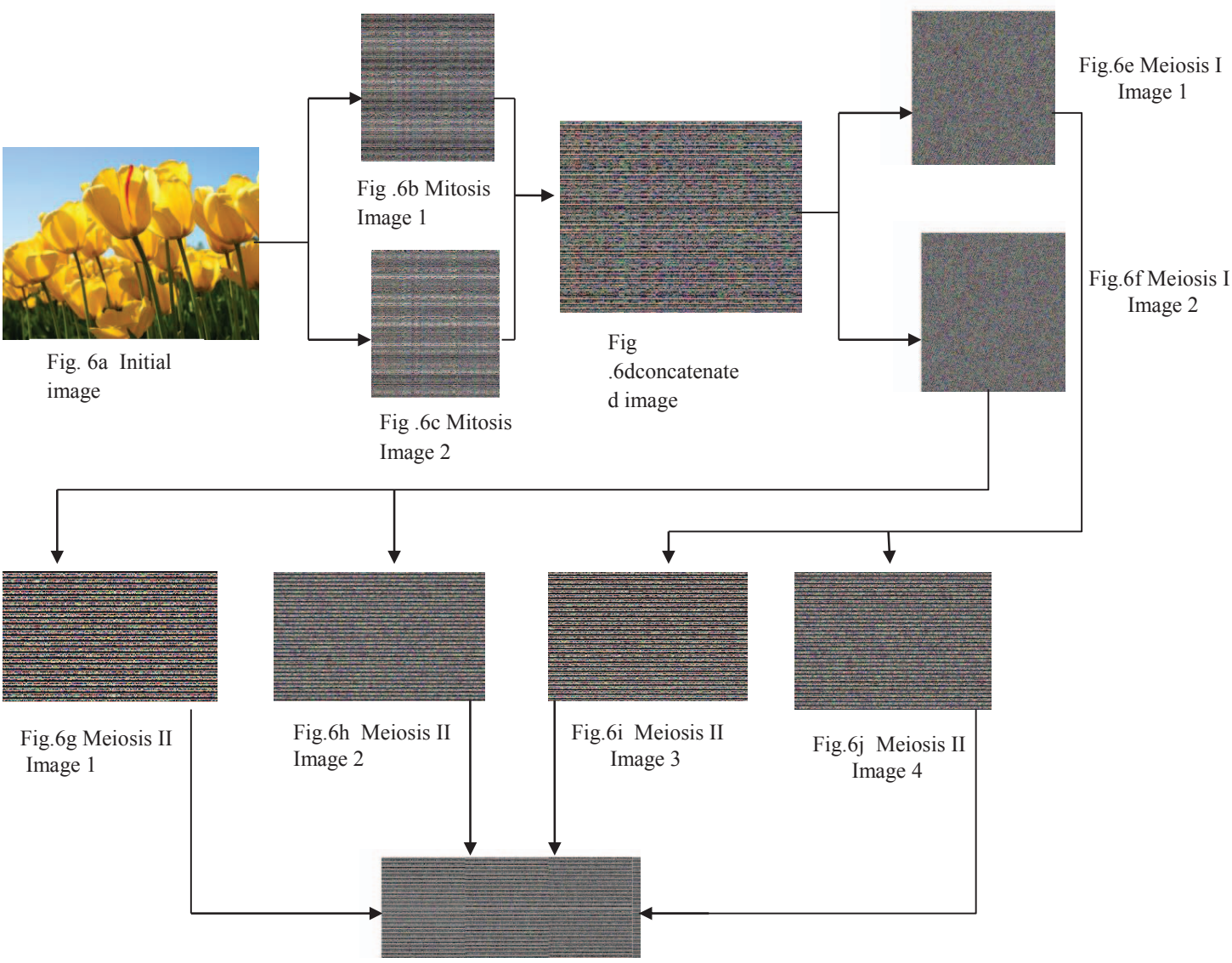

Fig.6 images obtained after encryption at various stages

Chromosome, instead of the defined T.

3. *Trisomy 21*- Trisomy 21 results when the 21st chromosome fails to separate during division. One of the daughter cells is produced with an extra chromosome 21; this cell thus has 24 chromosomes.

Translocation –An extra copy of the 21st chromosome may also be caused due to a Robertsonian translocation . The long arm of chromosome 21 attaches to another chromosome often the 14thchromosome. Thepercentage of occurrence is however, as low as in 2-4% case.

Mutation can be introduced with a probability given by

$$P = \frac{\text{length of chromosome} * \text{mutation rate}}{1000}$$

Where, mutation rate can be taken as 0.05.

V. ADVANTAGES

Our method has the following advantages-

1. The encryption strength depends on the size of the image used and is independent of the message length. Larger the image used, more are the number of chromosomes and bigger is the output image.
2. The image can be lossless compressed for transmission, saving space and bandwidth.
3. No specific keys are used. However the permutation used for the random division of chromosomes among daughter cells or the initial values of M can be hidden in the pixel values or by using steganography techniques.
4. The final image itself can be encrypted using a different image encryption technique for increased security.

VI. RESULTS

The output image was tested for randomness using the chi square test.

Chi square test- the chi square test is used to test the output for significant distance between the observed and expected values. For a binary image, the chi square test determines takes into account the relative frequency of 1's and 0's. the chi square test also gives a good estimate of the randomness in a given data set, i.e. output image pixel values in our case. The test was performed using MATLAB 2013 and a value of 5.39 was observed.

The images obtained after encryption with the message are given in Fig6.and the histograms are as in Fig7. The plaintext was taken to be "CRYPTOGRAPHY".

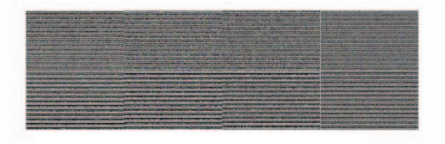

Fig.7a Final Image

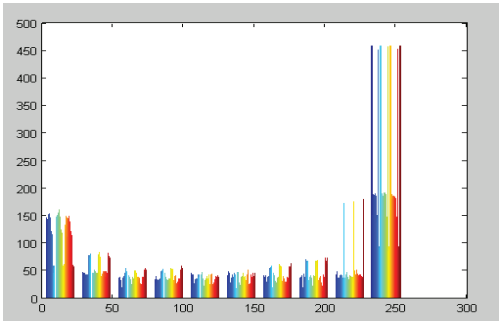

Fig.7b Histogram of final image

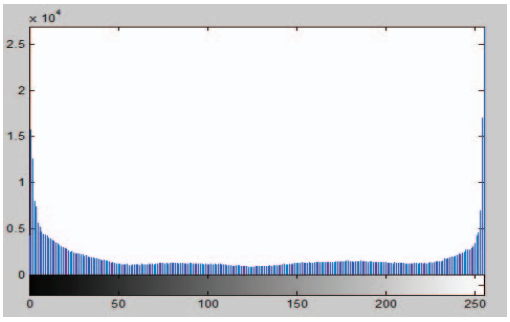

Fig.7c Histogram of final gray scale image

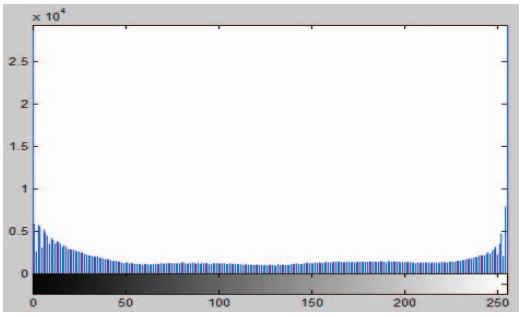

Fig7d Histogram of red component

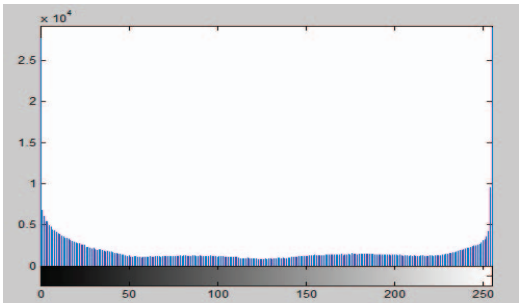

Fig.7e Histogram of green component

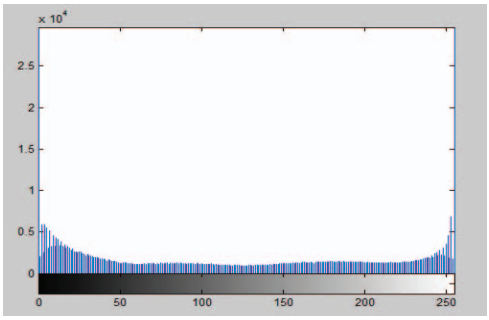

Fig.7f Histogram of blue component

Fig.7 Histogram of final image

VII. CONCLUSION

The paper introduces a new encryption algorithm. The results of the conducted chi-square test prove the randomness of the output image and hence the algorithms fit as a potential encryption scheme.

REFERENCES

[1]"Review Paper on Cryptography", VaishnaviKannan and Smita Jhajharia, IJSET.

[2]http://math.colorado.edu/~hiba/crypto/cryptanalysis.html

[3] "cryptographic technique for image encryption based on the rgb pixel displacement" , quistkester ,ieee 2012

[4] "A DNA Encryption Technique Based on Matrix Manipulation and Secure key Generation Scheme", TusharMandge

[5] "An Adaptive Encryption Based Genetic Algorithms For Medical Images",*AhmedMahmood,* 2013 IEEE International workshop On Machine Learning For Signal Processing

[6] algorithm for enhanced image security using DNA and genetic algorithms by saranya IEEE 2015

[7] "Formulation of an Encryption Algorithm on the Basis of Molecular Genetics and Image Patterns" M Prashant, R Siddharth and Rajeev Kumar

[8] "A Novel Text to Image Encryption Technique by AES Rijndael Algorithm with Color CodeConversion", Shanthi ,International Journal of Engineering Trends and Technology (IJETT) – Volume 13– Jul 2014.

[9] "An Enhanced Text to Image Encryption Technique using RGB Substitution and AES", Sourabh Singh, International Journal of Engineering Trends and Technology (IJETT) - Volume4Issue5-May2013